

Wolfgang Kollmann

Navier–Stokes Turbulence

Theory and Analysis

Navier–Stokes Turbulence

Wolfgang Kollmann

Navier–Stokes Turbulence

Theory and Analysis



Springer

Wolfgang Kollmann
Department of Mechanical Engineering
University of California Davis
Davis, CA, USA

ISBN 978-3-030-31868-0 ISBN 978-3-030-31869-7 (eBook)
<https://doi.org/10.1007/978-3-030-31869-7>

© Springer Nature Switzerland AG 2019

This work is subject to copyright. All rights are reserved by the Publisher, whether the whole or part of the material is concerned, specifically the rights of translation, reprinting, reuse of illustrations, recitation, broadcasting, reproduction on microfilms or in any other physical way, and transmission or information storage and retrieval, electronic adaptation, computer software, or by similar or dissimilar methodology now known or hereafter developed.

The use of general descriptive names, registered names, trademarks, service marks, etc. in this publication does not imply, even in the absence of a specific statement, that such names are exempt from the relevant protective laws and regulations and therefore free for general use.

The publisher, the authors and the editors are safe to assume that the advice and information in this book are believed to be true and accurate at the date of publication. Neither the publisher nor the authors or the editors give a warranty, expressed or implied, with respect to the material contained herein or for any errors or omissions that may have been made. The publisher remains neutral with regard to jurisdictional claims in published maps and institutional affiliations.

This Springer imprint is published by the registered company Springer Nature Switzerland AG
The registered company address is: Gewerbestrasse 11, 6330 Cham, Switzerland

Preface

The subject of the book is the theoretical treatment of fully developed turbulence in fluids governed by the Navier–Stokes equations. The investigation begins with a collection of properties of turbulent flows of Newtonian fluids observed in experiments and direct numerical simulations. The main purpose of this assembly is to condense them to a working definition of turbulence. Then the variables for the complete description of turbulence based on Navier–Stokes dynamics are established and the equations governing them are derived within the framework of classical mechanics.

The phenomenon of turbulence is analysed with the tools of probability theory. The fundamental difficulty encountered in this approach is the fact that countably infinite systems of equations or functions of infinitely many variables appear, which cannot be truncated without arbitrary measures to generate solvable systems. It is, however, possible to derive a single, linear equation for the characteristic functional containing all relevant information on a turbulent flow. This equation, derived by E. Hopf more than 50 years ago, is central to the treatment of turbulent flows in this book. It contains functional operations that require careful and detailed consideration for their proper use. The basic operations of differentiation and integration of functionals are reviewed and examples relevant to turbulent flows are constructed to illustrate their application. The equation for the characteristic functional in the spatial description contains the effects of convection as second variational derivatives, whose trace is a generalized Laplacian. There have been several variants of the infinite-dimensional Laplacian developed for different purposes, two of those definitions are considered in detail. These are the generalized and the Lévy-Laplacian. The relations of convection, expressed in terms of the characteristic functional, to the generalized Hessian and the generalized Laplacian operators are explored.

The Hopf fde for turbulent flows of an incompressible fluid in statistical steady state is analysed with the aid of a solenoidal ONS basis for a compact flow domain with a combination of homogeneous and periodic boundary conditions. The arguments of the characteristic functional are represented in the solenoidal basis as divergence-free vector fields thus allowing elimination of the pressure gradient in the Hopf equation. Basis projection of the argument fields and the projection of the

Hopf fde onto finite-dimensional subspaces is central to the numerical treatment of turbulent flow through pipes. It is shown to produce linear, second-order standard pdes. The example of pipe flow with periodic entrance and exit conditions is the vehicle to develop and illustrate the general theory.

Two aspects of turbulence theory require the geometric and limit properties of the n -dimensional ball in Euclidian space as the dimension n goes to infinity, first, the definition and evaluation of the standard and the Lévy-Laplacian; second, the formulation of integrals in infinite-dimensional spaces.

The properties of the n -dimensional ball in Euclidian space are summarized in Sect. 23.11 of Appendix A.

The properties of turbulence measures and the associated characteristic functional are discussed at an elementary level in Chap. 6. Methods of construction of measures in infinite-dimensional spaces are presented and illustrated with examples. The Hopf and Lewis–Kraichnan equations (Vishik et al. [1, 2], Lewis and Kraichnan [3], Dopazo and O’Brien [4]) governing the evolution of characteristic functionals are derived in several versions. Furthermore, variants of these equations are established using various local and global mappings and a general mapping equation is derived.

The indeterminate pdes (partial differential equations) for finite-dimensional Pdfs play an important role in the practical treatment of turbulence, they are deduced using the (coarse-grained) Dirac pseudo-function leading to the well-known Lundgren–Monin–Novikov hierarchy. The properties of the terms representing convection, frictional effects and external volume forces are established and examples are constructed to illustrate their properties. Furthermore, examples for the closure of these pdes are presented and the shortcomings of various arbitrary assumptions necessary to construct a solvable system of equations are discussed.

Homogeneous turbulence is discussed in the light of the hypotheses of Kolmogorov and Onsager and recent experimental results leading to modifications of the theory due to internal intermittency. The notion of structures in turbulent flow fields and their classification is analysed in the spatial and material descriptions. Several examples are discussed in detail.

Wall bounded flows are of prime importance for theoretical and a variety of practical reasons. Thus, particular examples (pipe flow and plane channel flow) are chosen to illustrate theoretical difficulties and, briefly in Appendices C and D, simple engineering approaches for dealing with this phenomenon are presented.

The emphasis is placed on fully developed turbulence for incompressible fluids, but some aspects of compressible fluids are also included in Sects. 2.1, 2.1.2, 2.5.3, while stability and transitional phenomena are not covered, since they deserve a volume on their own and there is an enormous amount of literature on these subjects available [5–9], Chap. 9 and references therein.

References

1. Vishik, M.J.: Analytic solutions of Hopf's equation corresponding to quasilinear parabolic equations or to the Navier-Stokes system. *Sel. Math. Sov.* **5**, 45–75 (1986)
2. Vishik, M.J., Fursikov, A.V.: Mathematical Problems of Statistical Hydromechanics. Kluwer Academic Publ., Dordrecht (1988)
3. Lewis, R.M., Kraichnan, R.H.: A space-time functional formalism for turbulence. *Comm. Pure Appl. Math.* **XV**, 397–411 (1962)
4. Dopazo, C., O'Brien, E.E.: Functional formulation of nonisothermal turbulent reactive flows. *Phys. Fluids* **17**, 1968–1975 (1974)
5. Schlichting, H.: Boundary Layer Theory. McGraw-Hill (1987)
6. Ruelle, D., Takens F.: On the nature of turbulence. *Comm. Math. Phys.* **20**, 167–192 (1971)
7. Pomeau, Y., Manneville, P.: Intermittent transition to turbulence in dissipative dynamical systems. *Comm. Math. Phys.* **74**, 189–197 (1980)
8. Andereck, C.D., Liu, S.S., Swinney, H.L.: Flow regimes between independently rotating cylinders. *JFM* **164**, 155–183 (1986)
9. Schmid, P.J., Henningson, D.S.: Stability and Transition in Shear Flows. Springer Verlag (2001)

Acknowledgements

It is a pleasure to acknowledge many fruitful discussions with J. J. Chattot (MAE Department, University of California, Davis), M. S. Chong (MAE Department, University of Melbourne, Australia), J. Janicka (EKT, TU-Darmstadt, Germany), M. Oberlack (Department of Mechanical Engineering, TU-Darmstadt, Germany), B. A. Younis (Civil and Environmental Engineering, UCD) and M. D. White (Dayton, Ohio). I am particularly indebted to Florian Ries (Department of Mechanical Engineering, TU-Darmstadt) for providing DNS data for the pipe flow and to Thomas O. Kollmann (Davis) for help with graphics applications.

Contents

1	Introduction	1
1.1	Notation	10
	References	14
2	Navier–Stokes Equations	17
2.1	Spatial/Eulerian Description	18
2.1.1	Incompressible Fluids	19
2.1.2	Compressible Fluids	21
2.1.3	Symmetries of the Euler and Navier–Stokes pdes	22
2.2	Fundamental Properties of the Solutions for a Single Incompressible Fluid	28
2.3	Rotation and Vorticity in the Spatial Description	33
2.3.1	Beltrami and Trkalian Vector Fields	35
2.3.2	Vorticity pde for Compressible Fluids	35
2.4	Lamb Vector Dynamics for Incompressible Fluids	37
2.5	Material/Lagrangean Description	40
2.5.1	Piola Transform $\pi_{\alpha\beta}$	41
2.5.2	Incompressible Fluids	41
2.5.3	Compressible Fluids	42
2.6	Rotation and Vorticity in the Material Description	44
2.6.1	Divergence of the Material Vorticity	45
2.6.2	Material Vorticity in Plane Flows	46
2.6.3	Frozen Vector Fields	47
2.7	Velocity Gradient Tensor in the Spatial Description	49
2.8	Problems for this Chapter	50
	References	52
3	Basic Properties of Turbulent Flows	55
3.1	Working Definition of Turbulence	63
3.2	Asymptotic Properties of Turbulent Flows	66

3.3	Number of Degrees of Freedom of the Turbulence Attractor for Maintained Turbulence	67
3.4	Problems for this Chapter	69
	References	71
4	Flow Domains and Bases	73
4.1	Homogeneous Turbulence Domain \mathcal{D}_{ht}	74
4.2	Periodic Pipe Flow Domain \mathcal{D}	75
4.2.1	Schauder Basis for Scalar Fields	76
4.2.2	Schauder Basis for Vector Fields with Non-zero and Zero Dilatation	77
4.3	Open and Noncompact Domains	80
4.3.1	Semi-infinite Pipe: $z_0 = 0$ and $z_1 = \infty$	80
4.3.2	Boundary Layer Domain \mathcal{D}_{bl}	82
4.3.3	Free Shear Layer Domain \mathcal{D}_{fs}	85
4.4	Problems for this Chapter: Flow Domains and Bases	88
	References	91
5	Phase and Test Function Spaces	93
5.1	Solution Sets	93
5.2	Phase Space for the Turbulence Measure: Incompressible Fluids and Homogeneous Boundary Conditions	94
5.3	Phase Space: Noncompact Domains	96
5.4	Argument/Test Function Space for Characteristic Functionals	97
5.5	Example for a Nuclear Space	98
	References	99
6	Probability Measure and Characteristic Functional	101
6.1	Elementary Properties of the Turbulence Measure	102
6.2	Turbulence Measure for Incompressible Fluids	104
6.3	Construction of Measures as Limits of Cylinder Measures	105
6.3.1	Cylinder Measures	105
6.3.2	Kolmogorov Extension Theorem	106
6.3.3	Examples of Measures in Function Spaces	108
6.3.4	Wiener Measure	108
6.4	Problems for this Chapter	112
	References	112
7	Functional Differential Equations	115
7.1	Elliptic fdes	115
7.2	Parabolic fdes	116
7.3	Problems for this Chapter	117
	Reference	117

8 Characteristic Functionals for Incompressible Turbulent Flows	119
8.1 Bochner–Minlos Theorem	121
References	121
9 Fdes for the Characteristic Functionals	123
9.1 Elementary Properties of the Characteristic Functional	124
9.2 The Hopf fde for the Spatial Characteristic Functional	124
9.2.1 The Pressure Gradient in the Spatial Description	127
9.2.2 Green’s Function for Periodic Pipe Flow	131
9.2.3 The Hopf fde Version I: Non-random External Force	137
9.2.4 The Hopf Equation Version IX: Stochastic External Force	137
9.2.5 The Hopf Equation II: Homogeneous Dirichlet Conditions	138
9.2.6 Spectral Version of the Hopf fde I	139
9.2.7 Convection as Diffusion in Hilbert Space	140
9.3 The Lewis–Kraichnan Equation for the Space–Time Functional	141
9.3.1 Lewis–Kraichnan fde Version I	142
9.3.2 Lewis–Kraichnan fde Version II	143
9.3.3 Variational Derivatives of a Gaussian Characteristic Functional	146
9.4 Definitions of Laplacians	148
9.4.1 Variational and Standard Laplacians	148
9.4.2 Lévy–Laplacian	150
9.4.3 The Laplacians Applied to a Gaussian Characteristic Functional	153
9.5 Fde for the Characteristic Functional in the Material Description	156
9.5.1 Gateaux Derivative of Velocity with Respect to the External Force	159
9.6 Problems for this Chapter	160
References	161
10 Solution of Hopf-Type Equations in the Spatial Description	163
10.1 Steady-State Solutions	164
10.2 fde in Cartesian Coordinates	165
10.3 fde in Cylindrical Coordinates	166
10.4 Steady-State Solutions for Periodic Pipe Flow	167
10.4.1 Steady-State fde in a Solenoidal ONS Basis \mathcal{B}_e for \mathcal{N}	169
10.5 Variational Hessian and the pde for θ_N	172

10.6	Boundary Conditions	175
10.7	Problems for this Chapter	176
	References	177
11	Finite-Dimensional Characteristic Functions, Pdfs and Cdfs Based on the Dirac Distribution	179
11.1	The Role of the Pressure	181
11.2	Transport Equation for the Multipoint Cdf F_{4N}	183
11.3	Cdf Equation in Terms of Conditional Fluxes	196
11.4	Pdf Equation in Terms of Conditional Expectations	196
11.5	Problems for this Chapter	199
	References	201
12	Properties and Construction of Mappings	203
12.1	Elementary Properties of Mappings	204
12.2	Bijective Mappings for Probability Measures	205
12.2.1	Bijective Mappings for Characteristic Functionals	206
12.3	Construction of Mappings	207
12.4	Local and Global Mappings	209
12.4.1	Construction of Global Maps	211
12.4.2	Construction of Local Maps	214
12.5	Problems for this Chapter	215
	References	215
13	$\mathcal{M}_1(1)$: Single Scalar in Homogeneous Turbulence	217
13.1	The CCK Method	217
13.1.1	Single, Bounded Scalar in Homogeneous Turbulence	218
13.1.2	Mapping Equation for a Single Scalar	221
13.1.3	Solution of the Mapping pde for a Single Scalar	226
13.1.4	Initial Values for Mapping $\mathcal{X}(\eta; 0)$	229
13.2	Mapping Method for the Characteristic Function	234
13.2.1	Transport pde for the Image $\theta[\theta_G]$	238
13.3	Problems for this Chapter	245
	References	246
14	$\mathcal{M}_1(N)$: Mappings for Velocity–Scalar and Position–Scalar Pdfs	249
14.1	Single-Point Mapping Equation for Homogeneous Turbulence	249
14.1.1	Time-Dependent Reference Measures	254
14.2	Multipoint Mapping Method in the Spatial Description	255
14.3	Multipoint Mapping Method in the Material Description	259

14.4	Mapping Method for Two-Point Pdfs in the Material Description	263
14.5	A Pdf Reduction Property for Multidimensional Mappings	265
14.6	Summary	266
	References	267
15	Integral Transforms and Spectra	269
15.1	Fourier Transform (FT)	269
15.2	Fourier Transformed Navier–Stokes Equations	270
	References	274
16	Intermittency	277
16.1	External Intermittency	277
16.2	Internal Intermittency	280
16.2.1	The Intermittency Generating Function of Wilczek et al. [15]	280
16.3	Problems for this Chapter	282
	References	282
17	Equilibrium Theory of Kolmogorov and Onsager	285
17.1	Energy Cascade	285
17.2	Basic Assumptions of Kolmogorov–Onsager Theory	288
17.3	Remarks	292
	References	293
18	Homogeneous Turbulence	295
18.1	Homogeneous and Isotropic Turbulence	295
18.2	Problems for this Chapter	297
	Reference	297
19	Length and Time Scales	299
19.1	Dissipative Range of Scales (Kolmogorov Range)	303
19.2	Scale Relations	303
19.3	Taylor’s Length Scale	304
19.4	Macroscales	305
	References	306
20	The Structure of Turbulent Flows	307
20.1	Transforms	308
20.2	Definition and Classification of Flow Structures	308
20.3	Characteristic Scales	308
20.4	Spatial/Eulerian Structures	309
20.4.1	Line-Type Structures	309
20.4.2	Surface-Type Structures	310
20.4.3	Volume-Type Structures	312

20.5	Material/Lagrangean Structures	313
20.5.1	Vortex Rings	314
20.5.2	Chaplygin–Lamb Dipole	319
20.5.3	Hill’s Vortex as Solution of the Bragg–Hawthorne pde	322
20.6	Large-Scale Motion in Jupiter’s Atmosphere	325
20.7	Problems for this Chapter	327
	References	329
21	Wall-Bounded Turbulent Flows	333
21.1	Statistical Description of Turbulent Flows	334
21.1.1	Moment Equations Derived from the Navier–Stokes pdes	336
21.1.2	Moment Equations Derived from the Leray Version of the Navier–Stokes pdes	338
21.2	Pipe Flow	343
21.2.1	(iii.2) Numerical Aspects	344
21.2.2	(iii.3), (iv.1) Theoretical Aspects	346
21.2.3	Fully Developed Turbulent Flow Through Circular Pipes	347
21.3	DNS Examples	348
21.3.1	Turbulent Pipe Flow	349
21.3.2	Compressible Boundary Layer Flows	353
21.4	Problems for this Chapter	355
	References	356
22	The Limit of Infinite Reynolds Number for Incompressible Fluids	359
22.1	A Bounded Vector Field Derived From Vorticity	362
22.2	The Kolmogorov–Onsager Conjecture	364
22.2.1	Experimental and Numerical Evidence	365
22.2.2	Analysis	366
22.2.3	Weierstrass Function	369
22.3	Duchon–Robert Distribution	371
22.4	The Physical Limit: Extrapolation of Smits’ Formula for Pipe Flow	372
22.4.1	Existence of a Physical Limit	375
22.5	The Mathematical Limit	375
22.5.1	Hopf fde for the Limit (ii) of Infinite Reynolds Number	376
22.6	Problems for this Chapter	378
	References	379

23 Appendix A: Mathematical Tools	381
23.1 Compactness	381
23.2 Limits	381
23.3 Caratheodory, Hausdorff and Box Dimensions	382
23.4 Chaos	384
23.5 Levi-Civita Symbol	384
23.6 Multi-index Notation	385
23.7 Function Spaces	386
23.8 Schauder Bases	390
23.9 Ergodicity	390
23.10 Leray–Stokes Operator	392
23.11 n -Sphere and n -Ball	394
23.12 Differentiation of Functionals and Measures	395
23.12.1 Lebesgue Integral	405
23.13 Examples	417
23.14 Problems for Sect. 23.14	418
23.15 Spherical Coordinates in R^n	419
23.16 Applications of Spherical Coordinates	421
23.16.1 Integrand x_k	421
23.16.2 Integrand x_k^2	422
23.16.3 Integrand $x_k x_l$ for $k \neq l$	423
23.16.4 Surface Average of an Analytic Function Over the n -Sphere	424
23.17 Integration in Infinite-Dimensional Spaces	428
23.17.1 Properties of n -Sphere and n -Ball as $n \rightarrow \infty$	428
23.17.2 Limit $n \rightarrow \infty$ of Lebesgue/Riemann Surface Area and Volume	429
23.18 Gaussian Measures	433
23.18.1 Example: Lebesgue/Riemann and Gaussian Volumes of an n -Ball for $n > 2$	434
23.18.2 Gaussian Measure on the Space of Infinite Sequences	438
23.18.3 Characteristic Functional	441
23.19 Lagrangean and Eulerian Statistics	442
23.20 Problems for Sects. 23.17 to 23.20	444
References	445
24 Appendix B: Example for a Measure on a Ball in Hilbert Space	447
Reference	449
25 Appendix C: Scalar and Vector Bases for Periodic Pipe Flow	451
25.1 Modified Jacobi Polynomials $\mathcal{P}_n^{a,b}(r)$	452
25.2 Orthonormalization of the Modified Polynomials $\mathcal{P}_n^{a,b}(r)$	454

25.3	Test Function Space \mathcal{N}_p : Scalar Fields	454
25.4	Projected Functionals	455
25.5	Bases for the Test Function Space \mathcal{N}_p	456
25.6	Discrete Fourier Transform w.r.t. the Angular Coordinate	457
25.7	Scalar Parity Conditions for Azimuthal Wavenumbers $k \geq 0$	458
25.7.1	Design Requirements for the Scalar Basis Functions	459
25.7.2	Construction of Scalar Basis Functions	459
25.8	Radial Modes for Homogeneous Dirichlet Conditions	460
25.9	Representation of Scalar Fields	463
25.10	Function Spaces: Vector Fields	467
25.11	Bases in Phase \mathcal{V}_p and the Test Function \mathcal{N}_p Spaces	467
25.12	Vector Parity Conditions for Azimuthal Wavenumbers $k \geq 0$	468
25.13	Design Requirements for the Vector Basis Functions	469
25.14	Representation of a Vector Field	470
25.15	Construction of the Vector Modes for Homogeneous Dirichlet Conditions	472
25.16	Radial Shape Function	473
25.17	(i) Construction of a General Vector Basis	476
25.18	Divergence of the Basis	477
25.18.1	Numerical Test Functions: Non-zero Divergence	478
25.19	(ii) Construction of a Solenoidal Vector Basis	480
25.20	Solenoidal Vector Basis for Doubly Periodic Flow Fields, First Method	480
25.20.1	Modes $k = m = 0$	481
25.20.2	Modes $k > 0, m = 0$	482
25.20.3	Axial Modes $m \neq 0$	483
25.20.4	Radial Derivative	485
25.20.5	Incomplete Orthonormality of the Solenoidal Vector Components	486
25.21	Solenoidal Vector Basis for Doubly Periodic Flow Fields, Second Method	490
25.21.1	Jacobi–Fourier Space	492
25.21.2	Modified Vector Potential Set Up in Jacobi–Fourier Form	492
25.22	Gram–Schmidt Orthonormalization	494
	References	506
26	Appendix D: Green’s Function for Periodic Pipe Flow	507
26.1	Domain of Definition	507
26.2	Function Spaces: Scalar Fields	509

26.3	Poisson pde for the Disturbance Pressure	510
26.4	Fourier Transform of the Poisson pde	511
26.4.1	Parity Conditions for the Modal Form of Scalar Fields	515
26.5	Representation of the Pressure	516
26.6	Solution of the BVP for the Complementary Pressure p_h	517
26.7	Green's Theorem and its Application	524
26.8	Solution of the Poisson pde for the Disturbance Pressure	536
26.9	Leray Version of the Navier–Stokes pdes	537
	References	539
27	Appendix E: Semi-empirical Treatment of Simple Wall-Bounded Flows	541
27.1	Exact Moment pdes for Fully Developed Turbulent Channel Flow	541
27.1.1	The Closure Problem	548
27.1.2	Empirical Mean Velocity Profiles: The Nickels Interpolant	554
	References	557
28	Appendix F: Solutions to Problems	559
	References	709
	Bibliography	713
	Index	715

Abbreviation

FT	Fourier Transform
FFT	Fast Fourier Transform
FTS	Finite Time Singularity
dA	Surface differential in R^n
dv	Volume differential in R^n
$d\mu$	Measure differential
Re	Reynolds number
Fr	Froude number
Gr	Grashof number
Kn	Knudsen number
Ma	Mach number
Pr	Prandtl number
Ro	Roshko number
Sc	Schmidt number
Str	Strouhal number
qk	quasi-Keplerian flows
CCK	Chen, Chen and Kraichnan
CTR	Center for Turbulence Research
DNS	Direct Numerical Simulation
LES	Large Eddy Simulation
ode	ordinary differential equation
pde	partial differential equation
fde	functional differential equation
LCS	Lagrangean Coherent Structure
BVP	boundary value problem
IVP	initial value problem
IBVP	initial-boundary value problem
LMN	Lundgren-Monin-Novikov hierarchy
$\Gamma(x)$	Gamma function
Γ	Circulation

OS	O(rthogonal) S(ystem)
ONS	O(rtho)-N(ormalized) S(ystem)
Cdf	Cumulative distribution function
pdf	Probability density function
POD	Proper Orthogonal Decomposition
SI	International System of Units
v_{4N4N}	Conditioning set
C_N	Conditioning set
C_i	Conditioning set
mTF	Maintained turbulent flow
uTF	Unsteady turbulent flow
w.r.t	with respect to
$\hat{\cdot}$ (hat)	Fourier transformed variable
$\tilde{\cdot}$ (tilde)	dimensional quantity (SI system)
$\bar{\cdot}$ (overbar) or \cdot^* (asterisk)	complex conjugate

List of Figures

Fig. 2.1	Flux $\mathbf{n} \cdot \mathbf{B}$ through an open surface $\mathcal{S}(\tau)$ bounded by an unknotted, closed line $\mathcal{C}(\tau)$ in a 3-d flow field, p denotes a Lagrangean line parameter	48
Fig. 3.1	Visualization of a low Mach number turbulent round jet (Bradshaw et al. [1])	56
Fig. 3.2	Visualization of a supersonic, turbulent round jet (Oertel [2]) at a Mach number $M = 1.8$, slightly underexpanded showing the diamond-shaped pattern of oblique shock waves.	56
Fig. 4.1	Level surfaces of the real part of the Cartesian basis function vector component $v_x^{n,a,k,m} = f_r^{n,a,k,m} \cos(\theta) - f_\theta^{n,a,k,m} \sin(\theta)$ for $q_n^k(r)$ with $a = 2$ (25.80) and $s_n^k(r)$ with $a = 2$ (25.78) satisfying the zero divergence condition shown in $0 \leq z \leq 0.6\pi/L$ (the modes are periodic in $z \in [0, 2\pi/L]$), the radial index $n = 2$, the azimuthal wavenumber $k = 3$ and the axial wavenumbers $m = -4$ (left graph) and $m = 4$ (right graph). The level values are colour coded as indicated on the left upper corner of the graphs.	78
Fig. 4.2	Level surfaces of the real part of the Cartesian basis function vector component $v_y^{n,a,k,m} = f_r^{n,a,k,m} \sin(\theta) + f_\theta^{n,a,k,m} \cos(\theta)$ for $q_n^k(r)$ with $a = 2$ (25.80) and $s_n^k(r)$ with $a = 2$ (25.78) satisfying the zero divergence condition shown in the axial range $0 \leq z \leq 0.6\pi/L$, the radial index $n = 2$, the azimuthal wavenumber $k = 3$ and the axial wavenumbers $m = -4$ (left graph) and $m = 4$ (right graph). The level values are colour coded as indicated on the left upper side of the graphs	79
Fig. 4.3	Level surfaces of the real part of the Cartesian basis function vector component $f_z^{n,a,k,m}(r, \theta, z)$ for $q_n^k(r)$ with $a = 2$ satisfying the zero divergence condition shown in $0 \leq z \leq 0.6\pi/L$, $n = 2$, $k = 3$ and for $m = -4$ (left graph)	

Fig. 4.4	and $m = 4$ (right graph). The level values are colour coded as indicated on the left upper side of the graphs.....	79
Fig. 4.5	Laguerre functions $l_n^\alpha(x)$ as defined by (4.18) for $\alpha = 0$ (left graph) and $\alpha = 2$ (right graph) and $n = 1$ (full line), $n = 3$ (dashed line), $n = 7$ (dot-dashed line), $n = 11$ (long dashed line), $n = 15$ (dot-dot-dashed line) for the construction of orthogonal bases suitable for the flow through semi-infinite pipes.....	81
Fig. 4.6	B-splines $b_j^k(x)$ for $k = 4$ and $j = -k, \dots, 1$ near the left boundary of the domain $[0, 1]$ with equally spaced distinct knot points x_j	85
Fig. 4.7	Hermite functions (4.29) $\Psi_n(x) = (2^n n! \sqrt{\pi})^{-\frac{1}{2}} \exp(-\frac{x^2}{2}) H_n(x)$ for $n = 0$ (grey), $n = 1$ (green), $n = 2$ (blue), $n = 7$ (magenta), $n = 30$ (black).....	86
Fig. 10.1	Lateral mode (modified Jacobi polynomial, $\alpha = \beta = 1$) $R_n(\eta(x_1))$ of basis functions suitable for mixing layers for $n = 1$ (red line), $n = 2$ (green), $n = 5$ (blue) and $n = 10$ (black) as function of $x_1 = x_1^0 \operatorname{arctanh}(\eta)$, the inverse of the mapping $\eta(x_1) = \tanh(\frac{x_1}{x_1^0})$. The reference length for the mapping $\eta(x_1) = \tanh(\frac{x_1}{x_1^0})$ is $x_1^0 = 1.0$	88
Fig. 11.1	The coefficient $C_z^{k,n,m}$ (10.24) for $k = m = 0$ as function of the radial mode index n w.r.t. the solenoidal basis \mathcal{B}_e constructed in Sect. 4.2 for the periodic pipe flow example. The blue squares are the real (identically zero) and the red circles the imaginary part of $\mathbf{e}^{k,n,m}(r, \theta, z)$, which is for $k = m = 0$ the radial shape function $\chi_e^{k,n,m}(r)$	174
Fig. 11.2	Pure convection in physical-velocity space of the Pdf $f(v : x, t)$ for $t = 0.0$ (left graph, initial condition), and at $t = 0.3$ in the right graph. It appears as rotation around the origin without change of shape	188
Fig. 11.3	Pure convection in physical-velocity space of the Pdf $f(v : x, t)$ for time $t = 0.3$ as iso-line plot. Convection appears as counterclockwise rotation around the origin in the first quadrant of the $v - x$ plane without change of shape of the Pdf	188
	Pure diffusion in scalar space $\mathcal{R}_\Phi = [0, 1]$ of the Cdf $F(\varphi : x, t)$ in the left graph and the Pdf $f(\varphi; x, t)$ in the right graph for $t = 0.0$ (initial condition, black line) and $t = 0.1$ (red line). The product of Schmidt and Reynolds number was set to $ScRe = 1.0$. Note that the graphs are solution of the hyperbolic pde (11.36) with a model for the flux term, they show the reduction of width corresponding to time inverse diffusion	190

Fig. 11.4	Pure diffusion in velocity space $\mathcal{S} = R^2$ of the Pdf $f(v : \mathbf{x}, t)$ in the left graph at $t = 0.06$, at $t = 0.36$ in the middle graph and at $t = 0.54$ (end of simulation) in the right graph. The time derivative of f is colour coded with red signalling increase and blue decrease. Note that the graphs are solution of the hyperbolic pde (11.38) with an arbitrary but consistent model for the flux term, they show the reduction of width corresponding to time inverse diffusion	193
Fig. 11.5	Pure sink effect on Cdf (left graph) and Pdf (right graph): $t = 0.0$ (black line), $t = 0.17$ (light blue line), $t = 0.3$ (red line). The sink $Q(\varphi)$ is shown in Fig. 11.6, note that $Q(\varphi) = 0$ for $\varphi = 0, 1$. The effect of the sink on the Pdf is distortion and motion to smaller mean value	194
Fig. 11.6	Sink term $Q(\varphi)$ in Pdf equation (11.42)	195
Fig. 13.1	Mapping $\mathcal{X}(t, \eta)$ (black lines) and its Jacobian $J(t, \eta)$ (red lines) for two time instances $t = 0$ (dot-dashed lines) and $t > 0$ computed as solution of equation (13.28). The unit interval on the vertical axis is the scalar space \mathcal{R}_Φ , and the horizontal η axis is the domain of definition of the Gaussian reference Pdf f_G	219
Fig. 13.2	Bijective mapping $\mathbf{Y}(t, \mathbf{x}) : \mathcal{D} \rightarrow \hat{\mathcal{D}}$ of the physical domain of definition \mathcal{D} onto the reference domain of definition $\hat{\mathcal{D}} = R^3$ to complete the closure in the spatial description, Eq. (13.16) in Sect. 13.1	223
Fig. 13.3	Numerical solution of the mapping equation (13.23) for increasing times $t = 0.08$ (black), $t = 0.56$ (red), $t = 0.88$ (blue), $t = 1.2$ (light blue), 1.6 (green) for the Jacobian $J(y, t)$ (left graph) and the mapping $\mathcal{X}(y, t)$ (right graph) in homogeneous turbulence. The image domain of $\mathcal{X}(\eta; t)$ is $\mathcal{R}_\Phi = [0, 1]$	229
Fig. 13.4	Pdf $f(x; t)$ computed via (13.28) using the solution of the mapping Eq. (13.23) for increasing times from $t = 0.08$ (black line) to $t = 1.6$ (green line) in homogeneous turbulence, colour coding as in Fig. 13.3. The black line at $t = 0.08$ is close to the initial Pdf	230
Fig. 13.5	Initial mapping $\mathcal{X}(\eta; 0)$ (right graph, $y = \eta$, the dashed line is the initial Jacobian J) computed numerically as solution of the ode (13.33) with the beta function Pdfs $f(\mathcal{X}(\eta; 0); 0)$ (left graph, $\phi = \varphi = \mathcal{X}(\eta; 0)$) with $N = 2$ specified as input. The exponents of the beta function are $\alpha = (3, 11)$ and $\beta = (12, 3)$ and weights $w_1 = 0.5$, $w_2 = 1 - w_1$	231
Fig. 13.6	Mapping $\mathcal{X}(\varphi; t)$ (upper left graph), Pdf $f(\mathcal{X}(\eta; t); t)$ (upper right graph), the real part of the characteristic function $\theta(\varphi; 0)$ (lower left graph) and the imaginary part (lower right graph)	

at time $t = 1.6$. The times shown in the upper two graphs are indicated by colour: $t = 0.08$ (black), $t = 0.56$ (red), $t = 0.88$ (blue), $t = 1.2$ (green), $t = 1.6$ (magenta)	236
Fig. 13.7 The Pdf $f(\mathcal{X}(\eta; t); t)$ (left graph) and the Jacobian $J(\eta; t)$ (right graph) generated by the solution of the mapping pde (13.61) for $t = 0.067$ (red/green), $t = 0.405$ (green/blue), $t = 0.74$ (dark blue/red), $t = 1.07$ (blue/dark blue), $t = 1.35$ (black)	243
Fig. 13.8 Real part of the complex mapping function $Z(k, k', \eta; t)$ depicted as function of the wavenumber variable k and the coordinate η for $k' = 0$ in the upper graphs and for $k' = 3.2$ in the lower graphs. The left graphs are the initial state and the right graphs at the later time $t = 1.35$	243
Fig. 13.9 Imaginary part of the complex mapping function $Z(k, k', \eta; t)$ depicted as colour-coded scalar field on the surface of the real part in Fig. 13.8 as function of the wavenumber k and the coordinate η for $k' = 0$ in the upper graphs and for $k' = 3.2$ in the lower graphs. The left graphs are the initial state and the right graphs at time $t = 1.35$	244
Fig. 17.1 Energy spectrum (logarithmic scale left, linear scale right graph) as function of the dimensionless wavenumber k according to Domaradski and Rogallo [1] at low Reynolds numbers ($R_\lambda = 13.6$ based on the Taylor scale) for isotropic and homogeneous turbulence. The full line is the Ling and Huang model spectrum (17.10) [4], the symbols are the DNS results at four different times normalized by $2\lambda(t)\langle u^2 \rangle$, and $\lambda(t)$ is the time-dependent Taylor length scale	287
Fig. 17.2 DNS computed spectral transfer function $T(k)$ (17.6) (solid line), the energy dissipation rate $-2vk^2E(k)$ (broken line) and $\partial E/\partial t$ (dotted line) according to Domaradski and Rogallo [1]	288
Fig. 17.3 Energy and dissipation rate spectra for homogeneous and isotropic turbulence	291
Fig. 19.1 Energy flow through the spectrum for homogeneous and isotropic turbulence	302
Fig. 19.2 Two-point correlation and definition of a macroscale	305
Fig. 20.1 Isolines of the azimuthal vorticity component $\tilde{\Omega}_\theta$ in the plane $\theta = 0$ at time $t = 6.007$ (left graph) and $t = 9.0$ (right graph). Full lines are positive and dashed lines negative values, equally spaced. Vorticity of the opposite sign generated by the start-up near the entrance has been entrained into both rings (labelled start-up) [52]	316

Fig. 20.2	Colour-coded distribution of enstrophy (red denotes high and blue low values) in the plane $z = 3.0$ at time $t = 14.0$ [52]. The plane cuts through four vortex tubes generated in the wake of the rings by the stretching effect of the rings	316
Fig. 20.3	Two views of two vector surfaces generated by vorticity by integrating vorticity starting from circles in forward (yellow/pink surfaces) and backward (grey/green surfaces) direction at time $t = 14.0$ for the simulation of two vortex rings [52]. The two disjoint circles serving as starting point for the forward and backward integration along the vorticity field are visible in the right graph as the bounding line separating differently coloured surfaces.	317
Fig. 20.4	Isosurface of enstrophy $ \omega = 2.744$ (max $e = 11.629$) at time $t = 14.0$ (end of simulation). The positive z -axis is the direction of propagation of the vortex rings	317
Fig. 20.5	Enstrophy level surface (red lines are vector lines for the vorticity in wake of the rings) after vortex ring collision for the Reynolds number $Re_\Gamma = 2701.82$ (20.19) at $t = 14.1$ [17]. The experimental result is in Fig. 28.12 Appendix F for comparison	318
Fig. 20.6	Streamlines (left graph) given by (20.31) inside and (20.23) outside the cylinder and vorticity (right graph) in the cylinder $0 \leq r \leq a$ for $a = 1.0$, $v_0 = 1.0$ for the Chaplygin–Lamb dipole with $\lambda = 0$ (symmetric case), dashed lines indicate negative values	321
Fig. 20.7	Streamlines (left graph) given by (20.32) inside and (20.23) outside the cylinder and vorticity ω (right graph) in the cylinder $0 \leq r \leq a$ for the Chaplygin–Lamb dipole with $\frac{\lambda}{av_0} = 0.5$ (asymmetric case, the blue line is the positive x -axis through the origin)	321
Fig. 20.8	Streamlines for Hill’s vortex assuming potential flow outside the sphere \mathcal{D} (Eq. 20.41, left graph) and potential flow everywhere (right graph), the flow is the result of a doublet at the origin plus parallel flow from the right. Note that the flow outside the bubble is the same in both cases.	324
Fig. 20.9	Streamlines inside the Hill’s vortex for $\alpha = 10$, $\lambda = 1$, $c = 0.2$. All lines are confined to the sphere with radius $R = 0.449470878$	325
Fig. 20.10	Swirling clouds in the dynamic North Temperate Belt of Jupiter taken by the NASA spacecraft Juno from 7000 km distance on October, 29. 2018. The white blobs are anticyclonic storms. It is noticeable that they contain more small-scale turbulence structures than the surrounding atmosphere	326

Fig. 20.11	Swirling cloudscape in Jupiter's atmosphere taken by the NASA spacecraft Juno from 11,350 km distance on May, 23. 2018	327
Fig. 21.1	Materially invariant, compact flow domain $\mathcal{D}(\tau)$ for the DNS simulation of pipe flow at times $\tau = 0$ (black, initial domain $\mathcal{D}(0) = \{0 \leq r \leq 0.5, 0 \leq \theta \leq 2\pi, 0 \leq z \leq L\}$), $\tau = 2$ (red), $\tau = 20$ (blue). The domain $\mathcal{D}(\tau)$ is constructed as materially invariant in laminar Hagen–Poiseuille flow (21.31) for ease of computation and for the sole purpose of illustration. The fluid is incompressible implying invariant volume, a property shared by laminar and turbulent flows	346
Fig. 21.2	Flow domain \mathcal{D} for the DNS simulation of turbulent pipe flow, the length of the pipe is $30D$. The Newtonian fluid is incompressible	349
Fig. 21.3	Hairpin structure near a fixed wall boundary, Adrian and Marusic [37], reproduced with permission. The induced velocity moves fluid from the wall towards the centre of the pipe. See Fig. 21.9 for numerically computed hairpin structures	350
Fig. 21.4	Colour-coded enstrophy distribution in plane through the axis in the axial range of length $3.5D$ out of the total $L = 12D$. Data provided by F. Ries, TU-Darmstadt 2018.	351
Fig. 21.5	Instantaneous kinetic energy in a plane through the coordinate axis $r = 0$ for the DNS simulation of turbulent pipe flow, data provided by F. Ries, TU-Darmstadt 2018.	352
Fig. 21.6	Level surfaces of Q variable (21.33) colour coded with the axial velocity in DNS simulation of turbulent pipe flow domain of length $12D$, data provided by F. Ries, TU-Darmstadt 2018	353
Fig. 21.7	Detail of the Q -surface in Fig. 21.6 with the axial velocity colour coded. A yellow coloured hairpin vortex is visible left of the centre of the figure. The main flow direction is from left to right	353
Fig. 21.8	Detail of the Q -surface in Fig. 21.6 with the dynamic pressure colour coded	354
Fig. 21.9	Hairpin structure in the late stage of transition according to the DNS simulation of Tian et al. [42] observed in a compressible boundary layer. The structures are defined as level surfaces of $\Omega = 0.5$, (21.37). The lambda vortices upstream of the hairpins at lower left corner show the earlier stages of the development	355

Fig. 22.1	Normalized dissipation rate (22.19) $D(\epsilon) = C_\epsilon^u$ (length scale l computed as the area under the autocorrelation function) and $D(\epsilon) = C_\epsilon^p$ (l determined from the spectrum) for a number of shear flows according to Pearson et al. [20]	366
Fig. 22.2	Partial sums of the Weierstrass function $W(x)$ (22.33) for two Hölder exponents $\alpha = 1/3$ (left graph) and $\alpha = 0.95$ (right graph). The red line refers to $N = 32$ and the black dot-dashed line $N = 2$	370
Fig. 22.3	Partial sums of the bounded field (22.11) defined by the derivative of the Weierstrass function (22.33) $b(x) = dW/dx/[1 + (dW/dx)^2]^{\frac{1}{2}}$ for two Hölder exponents $\alpha = 1/3$ (left graph) and $\alpha = 0.95$ (right graph). The black line refers to $N = 3$ and the red dot-dashed line $N = 2$. Note, that $-1 \leq b(x) \leq 1$ holds for the presentation of the singular derivative dW/dx	370
Fig. 22.4	Friction coefficient for smooth pipes as function of Reynolds number (semi-logarithmic scale left and logarithmic scale right figure) for the Prandtl correlation (22.44) (dot-dashed line), the Smits correlation (22.47) (dashed line) and the Smits correlation accounting for the near-wall velocity (22.48) (full line). The limit of f for $Re \rightarrow \infty$ is zero for all extrapolated experimental correlations	374
Fig. 23.1	Integrand of (23.90) leading to the recursive relation (23.93) for several values of the dimension n , which is indicated on the lines. The dimension $n = 2$ produces a circle (green line), all other dimensions result in non-circular graphs. The dot-dashed lines indicate the locations of diagonal points $(1/\sqrt{n}, \dots, 1/\sqrt{n})$, $(-1/\sqrt{n}, \dots, -1/\sqrt{n})$ as function of dimension n , the limit $n \rightarrow \infty$ is $x = 0$ and $f(x) = e^{-0.5}$. The limit $n \rightarrow \infty$ of the integrand is zero except unity at $x = 0$; therefore, the integral is zero for the limit	407
Fig. 23.2	Surface area $A(1)$ (left graph) and volume $V(1)$ of the n -ball as function of dimension n in linear scale.	432
Fig. 23.3	Volume of the n -sphere $V_n(1)$ (full line) and the volume of the n -cube $C_n(\frac{2}{\sqrt{n}})$ with sidelength $\frac{2}{\sqrt{n}}$ (dot-dashed line) as function of the dimension n in logarithmic scale (left graph) and the shape of 2-d spheres for various L_p norms (values of p are indicated on curves) in the right graph. The 2-d balls for $p < 1$ are not convex	432
Fig. 23.4	Shape of the unit sphere in R^3 for L_p -norms with $p = 0.5$ (left graph) and $p = 3.0$ (right graph). The balls for $p < 1$ are not convex	433

Fig. 23.5	Two views of the Gaussian volume $I_N^G(\rho)$ of N -balls as function of the normalized dimension $N / \max N$ ($\max N = 400$) and the normalized radius $\rho / \max \rho$ ($\max \rho = 20$). Colour coding of $I_N^G(\rho)$: red corresponds to unity, blue to zero. Note that for finite dimension N exists a radius $R(N)$, such that the Gaussian volume is close to unity for given accuracy. The radius $R(N)$ varies asymptotically as $R(N) \approx N^{\frac{1}{2}}$ (Eq. (23.184)) as evident in the graphs.	436
Fig. 23.6	The volume of the unit ball as function of dimension measured with the aid of Riemann/Lebesgue integration (black line) and Gaussian integration (red line) shown in linear scale (left graph) and log-scale (right graph).	437
Fig. 23.7	Gaussian volumes of a N -ball as function of the radius, dimensions N as indicated on the lines.	437
Fig. 25.1	Normalized standard Jacobi polynomials $P_n^{a,b}(x)$ (25.2) (left graph), $x \in [-1, 1]$ and normalized, modified polynomials $\mathcal{P}_n^{a,b}(r)$ (25.6), $r \in [0, 1]$ (right graph) for Jacobi parameters $a = 1.25$, $b = 0.75$ and $n = 0, 1, 2, 3, 20$ as indicated in the graphs. The basis functions are constructed by modifying the symmetric polynomials $\mathcal{P}_n^{a,b}(r)$ to satisfy divergence, parity and boundary conditions, see Figs. 25.2 to 25.5 in Sect. 25.5 of Appendix C and 25.12	453
Fig. 25.2	Radial shape functions $q_{k,n}^{a,b(k)}(r)$ (25.37) for the scalar modes and Jacobi parameters $a = 2$, $b(k) = k$ are illustrated for several radial mode indices. The shape functions for two azimuthal wavenumbers are shown, $k = 0$ in the left graph and $k = 5$ in the right graph. Both design requirements (S1) and (S2) are satisfied and the derivative at the outer boundary is non-zero. The radial mode indices n are indicated by the numbers in the graphs	462
Fig. 25.3	Radial shape functions $s_{k,n}^{a,b(k)}(r) = (1 - r^2)q_{k,n}^{a,b(k)}(r)$ (25.106) for the radial vector component modes for the Jacobi parameters $a = 2$, $b(k) = k - 1 $. The azimuthal wavenumber $k = 1$ (left graph) and $k = 6$ (right graph) for comparison with Fig. 25.2. The divergence of the vector modes is non-zero. Note that the derivative at the outer boundary is zero. The radial mode indices n are indicated by numbers	463
Fig. 25.4	Cross section $z = 0$ of the real part of the basis modes $f_{k,n,m}^{k,n,m}(r, \theta, z)$ in Jacobi–Fourier form for the radial index $n = 0$ (modified Jacobi polynomial) and the azimuthal wavenumber $k = 4$ (Fourier polynomial, left graph)	

and $n = 4$, $k = 4$ (right graph), the axial wavenumber is $m = 0$. The red circle indicates the boundary of the flow domain \mathcal{D}	464
Fig. 25.5 Colour-coded level surfaces of the real (left graph) and imaginary (right graph) part of the scalar mode $f^{k,n,m}(r, \theta, z)$ in Jacobi–Fourier form for the radial index $n = 2$, azimuthal wavenumber $k = 4$, axial wavenumber $m = 2$	465
Fig. 25.6 Maximum norm of the difference between test function $F_x \equiv y(r, \theta, z)$ with $\mathcal{H}(z) = \cos(m_0 z)$ (25.51) (single term $A_{1,1,1} = 1$) and the finite-dimensional projection $F_n \equiv y^{N_r, N_\theta, N_z}$ (25.41) of its representation in the base $\{f^{k,n,m}(r, \theta, z)\}$ (25.32) as function of $P = N \equiv \max(N_r, N_\theta, N_z)$, a scalar mode $f^{2,4,2}(r, \theta, z)$ is presented in Fig. 25.5 in terms of colour-coded level surfaces.	466
Fig. 25.7 Colour-coded level surfaces of the 3-d radial (left graph) and azimuthal (right graph) numerical test vector components (disturbances). They satisfy the parity conditions (25.25) for all azimuthal wavenumbers k	479
Fig. 25.8 Maximum norm of the difference between the test vector components v_r, v_θ, v_z in cylindrical coordinates (25.105) (shown in Fig. 25.7 as colour-coded level surfaces for the radial and azimuthal components) and the finite-dimensional projections v_r^P, v_θ^P, v_z^P (25.41) of its representation in the vector base $f_\alpha^{k,n,m}(r, \theta, z), \alpha = r, \theta, z$ (25.94) as function of $P \equiv \max(N_r, N_\theta, N_z)$ (v_r - red triangles, v_θ - green squares, v_z - blue circles)	479
Fig. 25.9 Radial shape functions for the vector components modes $\chi_\alpha^{k,n,m}(r), \alpha = r, \theta, z$ in Jacobi–Fourier form (radial modes: real part in upper left, azimuthal modes: imaginary part in upper right, axial modes: imaginary part in lower graph) set up in Sect. 25.19 of Appendix C for the axial wavenumber $m = 2$ and the azimuthal wavenumber $k = 0$. The divergence of all vector modes is zero, but the modes are not orthonormalized. The radial mode indices n are indicated by numbers	485
Fig. 25.10 Radial shape functions for the vector components modes $\chi_\alpha^{k,n,m}(r), \alpha = r, \theta, z$ in Jacobi–Fourier form (radial modes: real part in upper left, azimuthal modes: imaginary part in upper right, axial modes: imaginary part in lower graph)	

- set up in Sect. 25.19 of Appendix C for the axial wavenumber $m = 2$ and the azimuthal wavenumber $k = 5$. The divergence of all vector modes is zero, but the modes are not orthonormalized. The radial mode indices n are indicated by numbers. 486
- Fig. 25.11 Curl of a complex velocity mode $\mathbf{f}^{k,n,m}$ (25.70) in Jacobi–Fourier form (left graph) compared to the curl of a vector potential mode $\mathbf{A}^{k,n,m}$ (25.148) based on the shape function (25.146) (right graph) for $n = 2, k = 3, m = 5$ as function of r for $\theta = z = 0.0$. Real parts are the full lines and dash-dotted lines are the imaginary parts; colours signify the components: black—radial, blue—azimuthal and red—axial. The radial component of the curl of the velocity mode in the left graph is zero at the boundary $r = 1$, since the vector mode $\mathbf{f}^{k,n,m}$ is zero at the boundary. The curl Ω of the vector potential mode $\mathbf{A}^{k,n,m}$ in the right graph satisfies the boundary condition for all components. 492
- Fig. 25.12 Solenoidal, ONS, radial shape functions $\chi_x^{e,k,n,m}(r)$ in Jacobi–Fourier form resulting from the Gram–Schmidt orthonormalization of the curl of the vector potential with radial shape functions $\chi_x^{A,n,k}(r), \alpha = r, \theta, z$, Eq. (25.148). The radial mode indices are $n = 0, 2, 4, 8, 16$ as indicated on the lines, the azimuthal wavenumber $k = 6$ and the axial wavenumber $m = 2$ are fixed. The real parts are in the left and the imaginary parts in the right column. The shape functions for the radial component are in the first, the shape functions for the azimuthal component in the second and the third row contains the functions for the axial component. 497
- Fig. 25.13 Solenoidal, non-ONS, radial shape functions $\chi_x^{G,k,n,m}(r)$ (25.158) for the vector component modes constructed as curl of the vector potential \mathbf{A} for comparison with the ONS modes in Fig. 25.12. The radial mode indices are $n = 0, 2, 4, 8, 16$ as indicated on the lines, the azimuthal wavenumber $k = 6$ and the axial wavenumber $m = 2$ are fixed. The real parts are in the left and the imaginary parts in the right column except for the axial component in the third row, which has only the imaginary part non-zero. The shape functions for the radial component are in the first, the shape functions for the azimuthal component in the second and the third row contains the functions for the axial component. 498
- Fig. 25.14 Radial shape functions $\chi_r^{e,k,n,m}(r)$ according to (25.161) for a solenoidal, radial ONS mode $\mathbf{e}^{n,k,m}(r, \theta, z)$ (real part: upper

graph, imaginary part: lower graph) for the radial index $n = 0$ after Gram–Schmidt orthonormalization as function of r (x-axis) and the azimuthal wavenumber k (y-axis) at the axial wavenumber $m = 2$	499
Fig. 25.15 Radial shape functions $\chi_r^{n,k,n,m}(r)$ according to (25.161) for a solenoidal, radial ONS mode $\mathbf{e}^{n,k,m}(r, \theta, z)$ (real part: upper graph, imaginary part: lower graph) for the radial index $n = 16$ after Gram–Schmidt orthonormalization as function of r (x-axis) and the azimuthal wavenumber k (y-axis) at the axial wavenumber $m = 2$. The basis functions are orthogonal and divergence free to machine accuracy	500
Fig. 25.16 Vector lines of the complex-valued, Gram–Schmidt orthonormalized and solenoidal ONS vector mode $\mathbf{e}^{n,k,m}(r, \theta, z)$ (25.163) (constructed in Jacobi–Fourier form) in the cross section $0 \leq r \leq 1$, $0 \leq \theta \leq 2\pi$ at $z = 0$ for the radial index $n = 0$, the azimuthal wavenumber $k = 3$, axial wavenumber $m = 1$. Shown are the vector lines for real part of the ONS mode $\mathbf{e}^{n,k,m}(r, \theta, z)$ in the left graph and the imaginary part in the right graph	501
Fig. 25.17 Vector lines of the complex-valued, Gram–Schmidt orthonormalized and solenoidal ONS vector mode $\mathbf{e}^{n,k,m}(r, \theta, z)$ (25.163) (constructed in Jacobi–Fourier form) in the cross section $0 \leq r \leq 1$, $0 \leq \theta \leq 2\pi$ at $z = 0$ for the radial index $n = 3$, the azimuthal wavenumber $k = 3$, axial wavenumber $m = 1$. Shown are the vector lines for real part of the ONS mode $\mathbf{e}^{n,k,m}(r, \theta, z)$ in the left and the imaginary part in the right graph.	501
Fig. 25.18 Streamlines of the real-valued, Gram–Schmidt orthonormalized and solenoidal ONS vector mode $\mathbf{e}^{n,k,m}(r, \theta, z)$ (25.163) in Jacobi–Fourier form transformed back to physical space using FFT are depicted in the cross section $0 \leq r \leq 1$, $0 \leq \theta \leq 2\pi$ at $z = 0$ and for the radial index $n = 0$, the azimuthal wavenumber $k = 1$, axial wavenumber $m = 1$ in the upper left graph, for $n = 1$, $k = 1$, $m = 1$ in the upper right graph and for $n = 1$, $k = 1$, $m = 3$ in the lower graph.	503
Fig. 25.19 Streamlines of the real-valued, Gram–Schmidt orthonormalized and solenoidal ONS vector mode $\mathbf{e}^{n,k,m}(r, \theta, z)$ (25.163) in Jacobi–Fourier form transformed back to physical space using FFT are depicted in the plane $0 \leq r \leq 1$, $0 \leq z \leq 2.5$ at $\theta = 0$ and for the radial index $n = 1$, the azimuthal wavenumber $k = 0$ (left graph) and $k = 1$ (right graph), the axial wavenumber $m = 3$	504

Fig. 25.20	Streamlines of the real-valued, Gram–Schmidt orthonormalized and solenoidal ONS vector mode $\mathbf{e}^{n,k,m}(r, \theta, z)$ (25.163) constructed in Jacobi–Fourier form and transformed back to physical space using FFT in the cross section $0 \leq r \leq 1$, $0 \leq \theta \leq 2\pi$ at $z = 0$ for the radial index $n = 0$, the azimuthal wavenumber $k = 3$, axial wavenumber $m = 1$ corresponding to Fig. 25.16. The lower graph shows the vector lines for $n = 3$ in physical space corresponding to Fig. 25.17	504
Fig. 25.21	Contour colours/lines of the Cartesian components y_x (left graph) and y_y (right graph) for the test field (25.169) in the cross section $z = 0.087664$ and $N = 16$ modes w.r.t. the solenoidal ONS basis \mathcal{B}_e for the periodic pipe flow example	505
Fig. 26.1	Cross section at $\theta = \pi/2$ of the test field $f(r, \theta, \zeta)$ for the harmonic pressure $p_h(r, \theta, \zeta)$, negative values of r are defined as radial coordinates for $\theta + \pi$. The test field provides the Neumann boundary values shown in Fig. 26.3.	520
Fig. 26.2	Level surfaces of the test field for the level values: $f = 1.1191$ yellow, $f = 0.0707$ green, $f = -0.61305$ blue	520
Fig. 26.3	Doubly periodic Neumann boundary values $dp_h/dr(\theta, \zeta)$ at the boundary $\partial\mathcal{D} = \{(r, \theta, \zeta)\} : r = 1$ provided by the test field f for the harmonic pressure p_h . The azimuthal variable is denoted by $s \equiv r\theta$, $0 \leq s \leq 2\pi$ for $r = 1$	521
Fig. 26.4	Axial–radial section at $\theta = \pi/2$ of the solution p_h (26.72) of the BVP for the Laplacian pde with non-homogeneous boundary conditions in Fig. 26.3 for the complementary pressure p_h . Compare p_h with the test field f in Fig. 26.1	521
Fig. 26.5	Maximum error of the complementary pressure gradient on the outer boundary as function of the number of Fourier modes N for an analytic test field	523
Fig. 26.6	Modified Bessel functions of the first kind $I_k(x)$ (left graph) and the second kind $K_k(x)$ (right graph) for the azimuthal wavenumbers $k = 0, \dots, 4$	528
Fig. 26.7	Normalized modal 1-d Green’s functions $G_{k,m}(r, \rho)/\ G_{k,m}\ $ (26.120) as function of the radial location r (x-axis) and the jump location ρ (y-axis) for $k = 3$, $m = 0$ (left graph, $\ G_{k,m}\ = 0.333333$) and $G_{k,m}^\rho(r, \rho)/\ G_{k,m}\ $ for $k = 3$, $m = 4$ (right graph, $\ G_{k,m}\ = 0.212878$)	533

- Fig. 26.8 Radial profiles of the modal 1-d Green's functions $G_{k,m}(r, \rho)$ (26.120) at $\rho = 0.4$ for $m = 4$ and several k (right graph) and $k = 3$ and several m (left graph). Note that the modes $G_{0,m}(r, \rho)$ satisfy the homogeneous Neumann condition at $r = 0$, due to the parity condition (26.45), as seen as the top red line in the right graph. 533
- Fig. 26.9 Test example for $m = 4$ and $k = 3$: Right-hand side function $R(r) = -\mathcal{L}f(r)$ with Sturm–Liouville operator defined by (26.29) (left graph). Test function $f(r)$ (26.129) (black line) and the disturbance pressure $p_h + p_G$ (26.72), (26.127) (red, dash-dotted line) are shown in the right graph 534
- Fig. 26.10 Test example for $m = 4$ and $k = 3$: Difference between test function $f(r)$ and numerically computed disturbance pressure $p = p_h + p_G$ (26.72). The maximum norm of the error is $\|error(r, \rho)\| = 3.713e-04$ 534
- Fig. 26.11 Test function results in the plane $\theta = 0(r > 0)/\pi(r < 0)$ for the application of the linear functional (26.76) for the harmonic pressure (upper graph) and the linear functional (26.128) for the Green's function pressure (lower graph). The disturbance pressure p is the sum of harmonic p_h and Green's function pressure p_G , the difference between p and the test function is the absolute error 535
- Fig. 26.12 Radial profiles at $\theta = 0.0$, $z/L = 1.346$ (left graph) and $\theta = 0.0$, $z/L = 2.244$ (right graph). The test function $f(r, \theta, \zeta)$ is the black, the disturbance pressure $p(r, \theta, \zeta) = p_h(r, \theta, \zeta) + p_G(r, \theta, \zeta)$ the red dash-dotted, the Green's function pressure $p_G(r, \theta, \zeta)$ the blue and the harmonic pressure $p_h(r, \theta, \zeta)$ the green line. The maximum norm of the error $e(r, \theta, \zeta) \equiv |f(r, \theta, \zeta) - p(r, \theta, \zeta)|$ is $\|e\| = 8.25e-04$, the difference between test function and computed disturbance pressure is not discernible. 536
- Fig. 27.1 Mean velocity $\langle u \rangle(2y/h)$, $0 \leq y \leq h/2$ in linear (left graph) and semi-logarithmic scale (right graph) as function of y^+ for turbulent channel flow according to the DNS simulation data of Moser et al. [6]. The Reynolds number based on the wall shear velocity u^* (27.15) and the channel half-width δ is $Re_\tau = 590$. The right graph shows the mean velocity in semi-logarithmic scale and the exact solution $u^+ = y^+$ valid in the viscous sublayer as dot-dashed line 542

Fig. 27.2	Mean pressure $\langle p \rangle(x, 2y/h) - p_w(x)$ (left graph, where p_w is the mean wall pressure) and near-wall variation (right graph) as function of y^+ for turbulent channel flow according to the DNS simulation data of Moser et al. [6]. The Reynolds number based on the wall shear velocity u^* (27.15) and the channel half-width δ is $Re_\tau = 590$	542
Fig. 27.3	Normal stress component profiles, $\langle u^2 \rangle(2y/h)$ (full line), $\langle v^2 \rangle(2y/h)$ (dot-dashed line), $\langle w^2 \rangle(2y/h)$ (dashed line), for turbulent channel flow according to the DNS data of Moser et al. [6]. The Reynolds number based on the wall shear velocity u^* (27.15) and the channel half-width δ is $Re_\tau = 590$. The right graph shows the near-wall variation as function of y^+	545
Fig. 27.4	The Reynolds shear stress $-\langle uv \rangle(x, 2y/h)$ and the total shear stress $-\langle uv \rangle + \frac{1}{Re} \frac{\partial \langle U \rangle}{\partial y}$ (dot-dashed line) for turbulent channel flow according to the DNS data of Moser et al. [6] for $Re_\tau = 590$. The right graph shows the near-wall variation as function of y^+	545
Fig. 27.5	Mixing length in the near-wall layer of a fully developed turbulent channel flow with the van Driest wall correction	551
Fig. 27.6	Mean velocity in the near-wall layer of a fully developed turbulent channel flow ($Re = 10,000$) according to the mixing length model with the van Driest wall correction (27.43) in linear scale	553
Fig. 27.7	Mean velocity in the near-wall layer of a fully developed turbulent channel flow ($Re = 10,000$) according to the mixing length model with the van Driest wall correction (27.43) in semi-logarithmic scale. The dashed line is the law of the wall (27.47) and the dot-dashed line is the logarithmic profile (27.50)	554
Fig. 27.8	Mean velocity for a fully developed turbulent boundary layer according to the Nickels correlation (27.56) in semi-logarithmic scale. The pressure gradient parameter is for the left/right graph $p_x = 0.002 / -0.002$ and the wake parameter $b = 2.0$ is the same for both graphs ($v = 10^{-5} \text{ m}^2/\text{s}$, $\delta = 0.05 \text{ m}$, $u^* = 0.1 \text{ m/s}$ in both graphs). The dot-dashed line is the law of the wall (27.47), and the dashed line is the logarithmic profile (27.50)	557
Fig. 28.1	Maximum norm of the error $e(P)$ in representing the test function $f(x) = \sin(k\pi x)$ on $[-1, 1]$ for $k = 1$ (left graph) and $k = 16$ (right graph), P denotes the number of terms in the partial sums for the expansion with the Jacobi parameters $\alpha = \beta = 0$	586

- Fig. 28.2 Test function $f(x) = \sin(k\pi x)$ (black dot-dashed line) and partial sum $f_{b24}(x) = \sum_{n=0}^P c_n P_n^{x,\beta}(x)$ ($P = 24$, full red line) for $k = 16$ on $[-1, 1]$. The error for $P = 24$ is of order unity, for $P \geq 80$ it is reduced to machine accuracy as the right graph in Fig. 28.1 indicates 587
- Fig. 28.3 Coordinates of the test function $f(x)$ (red symbols, left graph) with respect to the Hermite function basis and the maximum norm of the error $e(N)$ (right graph) in representing the test function $f(x) = \frac{\cos(kx)}{\sqrt{2\pi\sigma^2}} \exp(-\frac{1}{2\sigma^2}(x - x_0)^2)$ with $k = 4$, $x_0 = 0$, $\sigma = 0.5$ on $R^1 = [-\infty, \infty]$, N denotes the number of terms in the partial sums for the expansion (4.33) 588
- Fig. 28.4 Test function $f(x) \in C_R^\infty \cap L_{R^1}^2$ (red line) and the approximation $f_N(x) = \sum_{i=0}^N c_i \Psi_i^x$ for $N = 20$ terms (black dot-dashed line) using the Hermite function basis. The difference between test function and approximation is not discernible for $N > 80$ as the right graph in Fig. 28.3 indicates 588
- Fig. 28.5 Semi-logarithmic plot of the functional integral with respect to the Wiener measure $I \equiv \int_C \exp\left\{\lambda \int_0^1 dx w(x) f^2(x)\right\} d\mu_w(f)$ for $w(x) = 1$ as function of λ , $0 \leq \lambda < \pi^2/4$ 602
- Fig. 28.6 Solutions of the Sturm–Liouville ode determining the functional integral for $v = 0.01$ ($\lambda = 0.2499$, green line), $v = 0.10253$ ($\lambda = 0.23948$, red line), $v = 0.14465$ ($\lambda = 0.22907$, black line) and $v = 0.17702$ ($\lambda = 0.21866$, blue line). Note that $f_\lambda(0) \neq 0$ holds for $\lambda < \lambda_0$ 604
- Fig. 28.7 The functional Wiener integral $I(\alpha, \lambda) = \int_C \exp\left(\lambda \int_0^1 dx w(x) f^2(x)\right) d\mu_w(f)$ as function of $\lambda < \frac{1}{4}$ for several, equally spaced values of α , starting with $\alpha = 0.01$ (red line) and down to $\alpha = 0.91$ (black line) 604
- Fig. 28.8 Shape functions $\chi_z^{e,k,0,0}(r)$ for the radial mode index $n = 0$, the axial wavenumber $m = 0$ and the azimuthal wavenumbers $k = 0, 1, 2$. The components are indicated by $\alpha = r$ (black), $\alpha = \theta$ (red) and $\alpha = z$ (blue), real parts are full and imaginary parts are dot-dashed lines. The upper left graph is for the azimuthal wavenumber $k = 0$ (the selected mode), the upper

right for $k = 1$ and the lower graph for $k = 2$ illustrating the parity conditions, Sect. 25.12, Appendix C, which require for $k = 1$ that the axial values satisfy $\chi_r^{e,1,0,0}(0) + i\chi_\theta^{e,1,0,0}(0) = 0$ as the upper right graph verifies	630
Fig. 28.9 Shape functions $\chi_z^{e,k,0,0}(r)$ for the axial wavenumber $m = 0$ and all azimuthal wavenumbers k for a given level of projection ($N = P = 72$). The components are indicated by $\alpha = r$ (imaginary part, black, the shape function $\chi_r^{e,0,0,0}$ is zero), $\alpha = \theta$ (real part, red) and $\alpha = z$ (imaginary part, blue). The upper left graph is for the radial component, the upper right for azimuthal and the lower graph for the axial component. Wavenumbers $k = 0, 1, 2$ are indicated, the higher wavenumbers are increasingly crowded to the outer boundary $r = 1$	631
Fig. 28.10 Coefficient $a_{k,n,m}^{l,o,q,r,s,t}$ as function of r (azimuthal wavenumber) and s (radial mode index) for $o = 2$, $t = 1$, $k = 1$, $n = 2$, $m = 1$ in the pde (10.21), real part in the left and imaginary part in the right graph. The truncation level is $N = 12$	634
Fig. 28.11 Coefficient $a_{k,n,m}^{l,o,q,r,s,t}$ as function of r (azimuthal wavenumber) and s (radial mode index) for $o = 2$, $t = 1$, $k = 3$, $n = 5$, $m = 1$ in the pde (10.21), real part in the left and imaginary part in the right graph. The truncation level is $N = 12$	635
Fig. 28.12 Pdf mapped by the solution of the ode: $t = 0$ dash-dotted line (log-normal Pdf), image Pdf at $t = 0.1$ as dashed line and image Pdf at $t = 0.2$ as full line for $C = 1.0$, initial mean value $\langle y \rangle = 0.1$ and variance $\sigma = 0.5$. Obviously, the ode generates a reduction of variance with zero as asymptotic limit	635
Fig. 28.13 Gaussian error function (black line) and its complement (red line)	657
Fig. 28.14 Solution $X(\eta; t)$ of the mapping pde (13.23) for $t = 0.01$ (dashed line, close the initial condition), $t = 0.01$ (blue line), $t = 0.2$ (red line) and $t = 0.3$ (black line)	659
Fig. 28.15 Jacobian $J(\eta; t)$ of the mapping pde (13.23) for $t = 0.2$ (black line), $t = 0.3$ (red line), $t = 0.4$ (light blue line), $t = 0.5$ (blue line) and $t = 1.0$ (magenta line). The initial condition consists of two Dirac pseudo-functions at $\eta = 0$ and $\eta = 1$	661
Fig. 28.16 The Pdf $f(\varphi; t)$ of the mapping pde (13.23) for $t = 0.2$ (red), $t = 0.3$ (green), $t = 0.4$ (blue), $t = 0.5$ (pink), $t = 0.6$ (black), $t = 0.7$ (brown), $t = 0.8$ (red) and $t = 1.0$ (grey). The initial Pdf consists of two Dirac pseudo-functions at $\varphi = 0$ and $\varphi = 1$	662

Fig. 28.17	Jacobian $J(t, \eta)$ (left graph) at $t = 0$ (black line), $t = 0.5767$ (light blue line), $t = 1.0573$ (green line), $t = 1.538$ (red line), $t = 2.0186$ (brown line) and the associated mapping $X(t, \eta)$ (right graph) at the same times. The solutions were obtained with $nBasis = 400$ Hermite function modes	666
Fig. 28.18	Pdf $f(t, \varphi)$, $\varphi = X(t, \eta)$ (upper graph) at $t = 0$ (black line), $t = 0.5767$ (light blue line), $t = 1.0573$ (green line), $t = 1.538$ (red line), $t = 2.0186$ (brown line) and coefficients $A_n(t)$ (2) of the Hermite basis functions, computed as solutions to the system of Eq. (4), for the Jacobian $J(\eta; t)$ shown in the left graph of Fig. 28.17 as function of the radial mode index n for $t = 0$ (black squares, the values for $n = 0$, $A_0(0) = 0.599341$ and $n = 2$, $A_2(0) = -0.114256$ are outside the graph) and $t = 2.5$ (red circles). The numerical solutions were obtained with the spectral range $n(\text{Basis}) = 400$ Hermite function modes	667
Fig. 28.19	Vorticity profiles at $x = 0$ for three values of λ as indicated on the lines	677
Fig. 28.20	Visualization of the Nickels vortex ring collision experiment ([46], reproduced with permission) for the initial Reynolds number $Re = 1000$. Vortex reconnection is in progress leading to a larger number of small rings compared to $Re = 1000$ in the left graph. The trailing vortex sheet, indicated by the spokes inside the ring in the left graph, undergoes a different instability forming radial tubes. Vortex reconnection is completed in the right graph and the small rings have suffered considerable distortion. The trailing vortex sheet is barely recognizable	678
Fig. 28.21	Intrinsic vector lines in the $Q - R$ invariant plane, the line for $c = 0$ with the cusp singularity at the origin is shown in red. Note that the standard form of the cusp singularity $x^2 = y^3$ is obtained for $x = \frac{R}{2}$ and $y = -\frac{Q}{3}$	681
Fig. 28.22	Pathline for the Shilnikov system with $P = 0.5 < P_c$ and details near the critical points in the upper right and lower graphs	685
Fig. 28.23	Time histories for the material coordinates $\Phi_1(\tau)$ (left graph) and $\Phi_1(\tau)$ and $\Phi_3(\tau)$ (red line) for $P = 0.5 < P_c$ for the Shilnikov system	685
Fig. 28.24	Pathline for the Shilnikov system and $P = 0.8 < P_c$ and details near the critical points in the upper right and lower graphs	686
Fig. 28.25	Time history of the material coordinates $\Phi_1(\tau)$ and $\Phi_3(\tau)$ (red line) for the Shilnikov system with $P = 0.8 > P_c$. The time history of $\Phi_2(\tau)$ is similar to Φ_1 but out of phase	686

Fig. 28.26	Azimuthal velocity profile (v_θ black, $\frac{v_\theta}{r}$ red line, left graph) and enstrophy $(r, z) = \frac{1}{2} \sqrt{\Omega_r^2 + \Omega_z^2}$ (black line) and the vorticity components $\frac{1}{2} \Omega_r(r, z)$ (red), $\frac{1}{2} \Omega_z(r, z)$ (blue) for the Townsend model eddy in the right graph. All profiles are at $z = 0.25$	690
Fig. 28.27	Profiles of the rhs vectors $Q_A(r, 0)$ due to the rate of deformation in black, $Q_S(r, 0)$ due to the rate of strain in red and $p_W(r, 0)$ due to vorticity in blue (left graph) and the pressure profiles $p[Q_A](r, 0)$ black, $p[Q_S](r, 0)$ red and $p[Q_W](r, 0)$ blue line (right graph) for the Townsend model eddy. All profiles are at $z = 0$	691
Fig. 28.28	Volume integral $V_n^p(1)$ of the unit ball as function of dimension n for several values of p (23.18) as indicated	704
Fig. 28.29	Volume integral $V_n^p(1)$ of the unit ball in R^n as function of dimension n and the norm exponent p (23.18)	705
Fig. 28.30	Generalized balls (23.118) for $p_1 = 0.2, p_2 = 1.5, p_3 = 2$ (left graph) and $p_1 = 0.2, p_2 = 0.5, p_3 = 2$ (right graph)	705
Fig. 28.31	Volume of generalized balls (23.118) $V(0.2, p_2, 2)$ as function of p_2	706

Chapter 1

Introduction



Any fluid consists of elementary particles and molecular compounds. The first step in the analysis of flow phenomena is the decision on the range of physical conditions measured by temperature, pressure and chemical composition to be considered and then the fundamental approach for their mathematical description can be selected. There are two ways to do this:

- (i) The fluid and possible constraining boundaries are sets of discrete entities (atoms, molecules, electrons, charged particles, etc.), hence statistical methods are required leading to master equations or the Boltzmann equation for gases at low density, see, for instance, Chap. 5 in Van Kampen [1] for further development.
- (ii) The fluid and possible constraining boundaries are regarded as continua, i.e. the following hypothesis holds:

Continuum hypothesis: All variables describing the static and dynamic behaviour of the fluid vary continuously with respect to space and time except on sets of measure zero.

It is necessary to establish criteria and to define a computable parameter to decide the applicability of the fundamental approach (i) or (ii). To begin with, the notion of zero measure needs to be explained. The notion of a measure is a precise generalization of volume, area, length and is not restricted to integer dimension [2]. Sets of measure zero are in particular surfaces in R^3 , lines in R^2 , points in R^1 and more complicated subsets of a flow domain that may arise in the analysis of turbulent flows, i.e. fractal sets with noninteger geometric dimension, [3, 4]. The continuum hypothesis is an idealization and it is, therefore, necessary to establish a criterium for its application. The Knudsen number, defined by

$$Kn \equiv \frac{\tilde{l}}{\tilde{L}} \quad (1.1)$$

where tilde indicates dimensional quantities, as the ratio of the (microscopic) mean free path \tilde{l} over the (macroscopic) length scale of the flow \tilde{L} , is the parameter that provides the quantitative information for the applicability of the continuum hypothesis

(see Karniadakis et al. [5] for details). The mean free path \tilde{l} is the statistical average of the distance travelled by particles between collisions. The scale \tilde{L} of a flow is a macroscopic distance over which a change of order unity of a flow variable is observed (such as, for instance, the diameter in pipe flow). The commonly accepted range for the continuum hypothesis is $Kn < 10^{-2}$. The range of thermodynamic conditions considered in this book is centred around properties of earth's atmosphere for macroscopic systems with speeds of fluid motion of the order of the speed of sound or less. Hence, the continuum hypothesis (ii) is adopted throughout the book.

Most flow phenomena encountered in nature and in myriad technical devices are called turbulent based upon simple observations. From an observer's point of view, it seems intuitively clear, what turbulence is, but it is surprisingly difficult to come up with a mathematically precise definition of turbulence. Visualizations of turbulent flows, as presented in Fig. 2 for a subsonic round jet (Bradshaw, Ferris and Johnson [6]) and Fig. 3 for a supersonic round jet (Oertel [7]), show a fundamental property: Highly complicated and apparently random distributions of flow variables in space (and time) common to incompressible and compressible turbulence. The figures also indicate important differences between subsonic, nearly incompressible and supersonic, compressible turbulent flows. Compressible flows allow the formation, interaction and propagation of waves that may emerge as expansion waves or shock waves, whereas flows of incompressible fluids do not support this type of motion. These elementary observations indicate that it is necessary to compile the properties of turbulent flows and then to extract from them a definition of turbulence.

It will be argued in Sect. 3.1 that apparent randomness is insufficient to define turbulence. It should be noted first that turbulence is a flow property and not a material property of the fluid, i.e. there is no such thing as a turbulent fluid. The investigation of the transition processes from predictable laminar flow to an apparently unpredictable turbulent flow showed (Schmid and Henningson in [8] Chap. 9 provide extensive details on transition phenomena) that the nonlinearity of the underlying equations is responsible for the creation of an asymptotically chaotic state and is, therefore, at the core of the problem. However, not every nonlinear set of differential equations has chaotic solutions and the appearance of such solutions for the Navier–Stokes pdes depends on the structure of the pdes and the values of characteristic dimensionless parameters such as the Reynolds number for momentum transport and the Peclet, Prandtl, Schmidt numbers for the transport of scalars such as temperature, enthalpy, entropy, mass fractions, etc. Furthermore, the particular structure of the nonlinearity is obviously not invariant under nonlinear transformations unless it is a symmetry of the Navier–Stokes equations. This becomes clear when the transformation between material and spatial description is established in Sect. 2.5, where it is shown that the nonlinear convective terms in the spatial description are absent in the material description, but terms linear in the spatial description emerge as nonlinear in the material description. The nonlinearity of the material version of the Navier–Stokes pdes is concentrated in the deformation gradient appearing in the coefficients of velocity derivatives. Certain components of the deformation gradient maybe singular on the stable/unstable manifold of critical points of the velocity field [9]. This fact raises two interesting questions:

(i) whether nonlinear, invertible transformations can be constructed that produce linear pdes in the image variables, hence would the pdes in image space be nonchaotic and this type of transformation would have to reflect the chaotic nature of the turbulent flow; and

(ii) whether the stochastic properties of the solutions depend on the description, i.e. the choice of independent and dependent variables, and, therefore, the structure of the associated pdes. The physics of turbulence does not ‘know’ anything about the mathematical tools employed to describe and analyse it, but the same physical phenomenon may appear in different form or not at all with respect to different sets of variables, unless the transformation generates a symmetry (covered briefly in Sect. 2.1.3), examples for the former are presented in Sect. 2.6 of [10]. Furthermore, one could ask whether there exists an optimal (in the sense of ease of analysis, a notion to be defined) choice of variables. These aspects are briefly discussed in Sect. 23.19 of Appendix A.

The pure IVP (Initial Value Problem) for the nonlinear Burgers pde, Woyczyński [11], is a well-known example for the transformation of a nonlinear pde to a linear one. The flow domain is the plane spanned by the real line $\mathcal{D} = \mathbb{R}^1 \equiv (-\infty, \infty)$ times the time interval $[0, \infty)$. The solution $u(t, x)$ of the IVP for the Burgers pde

$$\frac{\partial u}{\partial t} + u \frac{\partial u}{\partial x} = \frac{1}{2Re} \frac{\partial^2 u}{\partial x^2} \quad (1.2)$$

(all variables are dimensionless, $Re > 0$ is just a parameter) with initial condition $u(0, x) = u_0(x)$, $u_0(x) \in \Omega \equiv L^2_{\mathbb{R}^1} \cap C_{\mathbb{R}^1}^\infty$, maps the space of all possible states of a system called phase space (or sample space) Ω into itself. It shares type, order and nonlinearity with the Navier–Stokes momentum balances, but not dimensionality of the flow domain \mathcal{D} and it lacks the pressure gradient term as there is no mass balance to be enforced. The main tool for the solution of the pure IVP is the Hopf–Cole transformation

$$\Psi(x, t) = \exp(Re \int_x^\infty dx' u(x', t)) \quad (1.3)$$

It transforms the Burgers equation (1.2) into the linear heat equation for the image variable $\Psi(x, t)$. The solution of the pure initial value problem for the heat equation is explicitly known and transforming this solution back to $u(x, t)$ provides the analytic solution to the IVP for the nonlinear Burgers equation (the detailed derivation can be found in the solution of Problem (9.1) in Appendix F, Chap. 28)

$$u(x, t) = \frac{\int_{-\infty}^\infty d\zeta \frac{(x-\zeta)}{t} \exp\{Re[\int_\zeta^\infty dy u(y, 0) - \frac{(x-\zeta)^2}{2t}]\}}{\int_{-\infty}^\infty d\zeta \exp\{Re[\int_\zeta^\infty dy u(y, 0) - \frac{(x-\zeta)^2}{2t}]\}} \quad (1.4)$$

However, the nonlinear Burgers pde is not a 1-d model equation for turbulence [12], since neither the Hopf–Cole transformation to the linear heat pde nor the image pde are chaotic. Therefore, it does not possess chaotic solutions developing from an

initially non-random state, unless the initial condition is randomly chosen and/or a stochastic external force is added to the right side of (1.2).

However, it has an interesting asymptotic property, as the solution of the IVP develops discontinuities, Woyczyński [11] Sect. 3.3. This is relevant for turbulent flows with respect to the limit of infinite Reynolds numbers and their relation to the regularity of the solutions of the Euler equations. The hypotheses proposed by Kolmogorov and Onsager (Chap. 17) are based on the dissipation rate in the spatial description defined by

$$\tilde{\epsilon} \equiv 2\tilde{\nu}\tilde{s}_{\alpha\beta}\tilde{s}_{\alpha\beta} \geq 0 \quad (1.5)$$

where $\tilde{s}_{\alpha\beta}$ denotes (tilde indicates dimensional variables) the rate of strain (2.53), $\langle \tilde{\epsilon} \rangle$ possessing a non-zero limit value as $\tilde{\nu} \rightarrow 0/Re \rightarrow \infty$, which in turn would imply singularities of the second order (kinetic energy remains bounded but enstrophy (3.16) blows up, the Beale, Kato and Majda theorem (3.15) in Chap. 3 provides some information on possible blow-ups) in the vorticity and strain fields. The formation, existence and the nature of these singularities is an open question so far, further discussion can be found in Sect. 22.2 on the Kolmogorov–Onsager hypotheses. Onsager’s [13] arguments that the turbulent velocity field emerges as Hölder continuous with an exponent less than one as the Reynolds number approaches infinity, leads to a testable property analysed in the same Sect. 22.2 (Hölder continuity is briefly discussed in Sect. 23.7 of Appendix A).

Unfortunately, no invertible transformation has been found so far to transform the Navier–Stokes pdes to a linear system. Such a transformation would have to reflect for $Re \gg 1$ the chaotic properties of solutions of the Navier–Stokes system, hence can be expected to have complicated, non-analytic structure. Nevertheless, these examples point to the important role of mappings in the analysis of turbulent flows, which will be taken up later in Chap. 12.

The main part of the book is devoted to the theoretical analysis of fully developed turbulent flows based on probability theory and statistics (Lumley [14], Frisch [15], Sect. 3.4, Tsinober [16], Chap. 3). The theoretical treatment of turbulent flows in the literature contains notions that seem intuitively clear, such as turbulence itself, eddy, cascade, scale, etc., but they are loosely or not uniquely or not at all defined. Intuition is not a reliable argument, hence definitions are suggested in the present book to put the discussion on a firm basis, see Sect. 3.1 and Chap. 19. Of course, they are open to criticism and modification.

There are at present several approaches available for this analysis, they are listed below. The basic idea common to the majority of them is to treat turbulence as stochastic phenomenon. Lacking a rigorous theory addressing existence and regularity of the solutions of the Navier–Stokes pdes, the assumption of a stochastic nature of turbulence is unavoidable.

The first step in the analysis of turbulence is to compile a set of properties, which are regarded as characteristic for turbulent flows, and then to deduce from them a tentative definition of turbulence. This is done in Sect. 2.2. The properties of turbulence measures and the associated characteristic functional are the central part of the book and they are discussed in detail. The construction of bases in the function

spaces relevant to turbulence is developed for a particular flow to show explicitly the design of a vector basis spanning phase and test function spaces. Then methods of defining measures in infinite-dimensional spaces are presented and illustrated with examples. The Hopf and Lewis–Kraichnan equations (Vishik et al. [17, 18], Lewis and Kraichnan [19], Dopazo and O’Brien [20]) governing the evolution of characteristic functionals are derived in several versions. Furthermore, variants of these equations are established using various local and global mappings and a general mapping equation is derived. Methods for the solution of the functional differential equations are outlined for the spacial case of steady state in Chap. 10.

The material discussed in the following sections is at times abstract and an effort has been made to construct examples, frequently in the guise of exercise problems, relevant to turbulence to justify, explain and illustrate the approach. Literature references are provided frequently to guide the reader to relevant material too voluminous to be included in the book. The example of turbulent flows through straight pipes with circular cross section occupies a central position among the particular flows considered in the book, because pipe flow, like all turbulent flows bounded by walls, poses theoretical questions of fundamental nature still awaiting resolution. Necessary mathematical tools for the description and analysis of turbulence are collected in Appendix A, Chap. 23. The main approaches to analyse and predict turbulent flows are the following:

DNS approach

The numerical solution of the Navier–Stokes pdes is the direct and clean approach to computing the properties of individual sample fields of turbulent flows. This has been advocated by J. von Neumann as early as 1949 (quoted by Frisch in Sect. 9.2 of [15]) to enable analytical attacks of the problem. However, the obstacles to the application of DNS to flows at high Reynolds numbers and complex domains as encountered in engineering and astrophysical applications and to the statistical aspects of turbulence are still formidable, only flows in simple domains at low Reynolds numbers have been successfully computed. Illuminating examples for the use of DNS are the mixing layer simulations of Rogers and Moser [21], the channel flow simulations of Lee and Moser [22] Hoyas and Jimenez [23], the simulations of highly turbulent Taylor–Couette flow of Ostillia-Monico et al. [24] and the prediction of instabilities, transition to turbulence and the fully turbulent flow for the conditions of the pipe flow experiment of Osborne Reynolds by Wu, Moin, Adrian and Baltzer [25]. DNS has contributed significantly to the investigation of the non-unique laminar–turbulent transition phenomena as summarized by Barkley for pipe flow, [26]. DNS results will be discussed throughout the book, but numerical methods appropriate for DNS will not be covered, since there are many excellent sources available, for instance, the publications of the CTR (Center for Turbulence Research) at Stanford University, California.

Moment approach

Statistical moments of the various scalar, vector and tensor fields describing a realization of a turbulent flow are the essential variables in the moment approach, moments of order one and two are the main interest in many scientific and industrial applications. The transport equations for them are derived without difficulty in principle, but the system of equations increases rapidly in complexity with the order of the moments nor does it terminate at a finite level, thus posing the well-known closure problem for statistical moments. This property of the moment equations has lead to the development of semi-empirical schemes to construct finite systems of solvable equations (called turbulence models) to capture some features of turbulent flows relevant to various applications. However, they still lack a theoretical basis and rigorous error estimates. The moment approach will not be discussed at great length in the present book, except for a brief discussion of turbulence near wall boundaries in Appendix E, Chap. 27 to illustrate the various arguments and experimental data applied for the design of a turbulence model. Detailed accounts and critical analysis of the various closure assumptions and a wealth of applications can be found in the literature, for instance, in Sagaut and Cambron [27] (incompressible and compressible, homogeneous turbulence), Pope [28], Poinsot and Veynante [29] (both with emphasis on reacting flows), Oberlack [30] (symmetry analysis and its application to turbulence modelling), Fox [31] (covers both moment and Pdf methods for chemical engineering applications), Davidson [32] (non-reacting flows), Garnier et al. [33] (Large Eddy Simulations of compressible flows), Leschziner [34] (RANS models, hybrid RANS-LES closures and advanced LES with embedded RANS patches) are excellent sources. Certain families of turbulent flows still pose serious difficulties for the development of closure models as Jakirlic et al. [35] document with the simulation of rotating and swirling flows.

Pdf/Cdf approach

The statistical properties of the various fields describing turbulence at a finite number of selected points in the flow domain are determined by the probability density function (Pdf) or, more generally, the cumulative distribution function (Cdf), i.e. the underlying probability measure μ called turbulence measure in the following. The equations for finite-dimensional Pdfs/Cdfs are easily derived from first principles, Novikov [36], Lundgren [37], they are called L(undgren)M(onin)N(ovikov) hierarchy. They are nonlinear integro-differential equations containing additional unknown terms, hence posing a closure problem. There is at any level of description only a single equation in the LMN hierarchy for a Pdf/Cdf, which is a function of an increasing number of independent variables in contrast to the single-point moment method, where the number of equations is increasing with the level of decription, but the number of independent variables remains unchanged.

Statistical moments follow from Pdfs by integration over all probabilistic independent variables (an independent variable is called probabilistic if the Pdf integrates to a non-negative number less than or equal to unity with respect to it, the integral over all probabilistic variables is unity). Consider the Pdf f_n of the velocity \mathbf{v} at time t and n points \mathbf{x}_j , $j = 1, \dots, n$ in the flow domain

$$f_n(\mathbf{u}_1, \dots, \mathbf{u}_n; \mathbf{x}_1, \dots, \mathbf{x}_n, t) \prod_{j=1}^n d\mathbf{u}_j = \mu\{\mathbf{u}_1 \leq \mathbf{v}(t, \mathbf{x}_1) \leq \mathbf{u}_1 + d\mathbf{u}_1, \dots, \mathbf{u}_n \leq \mathbf{v}(t, \mathbf{x}_n) \leq \mathbf{u}_n + d\mathbf{u}_n\} \quad (1.6)$$

where μ denotes the turbulence measure; it is the set function in a measure space $(\Omega, \mathcal{A}, \mu)$ as explained in Chap. 10. The multipoint correlation at time t is then computed by Riemann/Lebesgue integration

$$\langle \mathbf{v}(t, \mathbf{x}_1), \dots, \mathbf{v}(t, \mathbf{x}_n) \rangle = \int_{R^3} \dots \int_{R^3} \mathbf{u}_1 \dots \mathbf{u}_n f_n(\mathbf{u}_1, \dots, \mathbf{u}_n; \mathbf{x}_1, \dots, \mathbf{x}_n, t) \prod_{j=1}^n d\mathbf{u}_j \quad (1.7)$$

If there exists a finite radius r and a constant $0 < K < \infty$ independent of n , such that

$$|\langle \mathbf{v}(t, \mathbf{x}_1), \dots, \mathbf{v}(t, \mathbf{x}_n) \rangle| \leq K V_{3n}(r) \quad (1.8)$$

holds, where $V_{3n}(r)$ is the $3n$ -dimensional volume of the ball with radius r , then the limit of $V_{3n}(r)$ for $n \rightarrow \infty$ is zero, this is discussed in detail in Sects. 23.11 and 23.17. This indicates that the integration domains, being subsets of appropriate function spaces, and integration in infinite-dimensional spaces deserve attention, since the limit of (1.8) is a source of concern, if multipoint Pdf/Cdfs are contemplated for the analysis of turbulent flows by letting the number of probabilistic variables grow to infinity, see also Novikov [38] Chap. 4.

Statistical multipoint moments are multi-dimensional integrals according to the definition (1.7). If for the radius $0 < r < \infty$ of an enclosing sphere a constant K exists, the resulting values approach zero with dimension as the example of the volume $V_{3n}(r)$ (23.95) and surface area (23.115) of the sphere $S_{3n-1}(r)$ embedded in R^{3n} shows, whose limit is zero as the dimension $n \rightarrow \infty$. The underlying reason for this is the non-existence of the Riemann integral in infinite-dimensional spaces (see, for instance, Kuo [39]). However, there are sophisticated methods for the integration of special classes of functionals in infinite-dimensional spaces. These matters are discussed in Sects. 23.12 and 23.17 of Appendix A, Chap. 23. The usage of Pdf/Cdf methods, in particular for turbulent combustion applications, has been limited to moderate dimensions of the scalar-velocity phase space for the just outlined reasons.

Characteristic function/functional approach

The Fourier transform of a Pdf is the characteristic function, hence provides an approach equivalent to the Pdf/Cdf method. The main difference to the Pdf/Cdf method is its relation to statistical moments, which follow from the characteristic function by differentiation w.r.t. the argument/test function at the origin. Furthermore, the characteristic function can be extended to infinitely many variables [40], since differentiation is well defined (in the sense of Frechét/ Gateaux as discussed in Sects. 23.12 and 23.12 of Appendix A) in contrast to integration. The transport equation for the characteristic function at finitely many points is nonlinear and non-closed. However, in the proper limit as the number of variables goes to infinity, the resulting equations for the spatial (and material) and space–time characteristic functionals are linear and closed. They are the celebrated Hopf and Lewis–Kraichnan functional differential equations (fdes). Several versions of the Hopf and Lewis–Kraichnan equations will be derived and their properties discussed in detail below, Sects. 9.2 and 9.3.

The approach centred around the characteristic function or functional is much less developed than the moment and Pdf methods, but it has found application in the context of the latter methods for the construction of closure models for particular terms in moment and Pdf equations, as championed by Lumley [14]. Development of the characteristic function(al) approach can be expected to generate new insights into the asymptotic state of turbulence and the closure problem, in fact Chaps. 5–10 constitute the core of the book.

Mapping approach

An alternative to Pdf/Cdf methods is the mapping approach. The idea, due to Kraichnan [41], is to establish an equation for the mapping of the argument and/or image space formed by the independent and/or dependent variables of the Pdf/Cdf or characteristic function onto the argument space of a known reference Pdf/Cdf or characteristic function. The reference Pdf/Cdf is usually a Gaussian for several theoretical reasons to be discussed later. One of the advantages of the mapping method is the possibility to build the asymptotic limit, consistent with the laws of probability theory, explicitly into a mapping equation, Pope [42], Pierce and Moin [43] or to construct non-Gaussian random fields, Rosales and Meneveau [44]. The mapping approach can be extended to infinitely many variables resulting in a functional mapping equation. A detailed discussion of this limit and related matters is given in Chap. 12.

The turbulence problem

Turbulence poses fundamental and practical problems awaiting solution.

At the core of the practical problem is the difficulty to solve an infinite system of nonlinear, partial, integro-differential equations, which arise, for instance, in the moment approach, or solving differential equations in infinite-dimensional spaces, which appear in the characteristic functional approach.

The fundamental problems are

(i) the formation of singularities and the depletion of nonlinearity in turbulent flows at high Reynolds numbers and

(ii) the existence of the turbulence measure and its relation to Gaussian measures.

There is strong evidence (see Tsinober [16], for a review of the experimental data) that the turbulence measure, if it exists (see Chap. 4 in [18] for existence of solutions for the characteristic functional), is non-Gaussian with certain marginal properties close to but not exactly Gaussian, it is not known whether it is continuous or singular with respect to a Gaussian reference measure. This question has been pursued for a long time, see, for instance, Hopf [45], Batchelor [46], Frisch [15], Schumacher et al. [47], Tsinober [16], Wilczek et al. [48] and further references therein.

The Clay Mathematical Institute [49] recognized the existence and smoothness of the solutions of the Navier–Stokes equations for incompressible fluids in R^3 as one of the unsolved millennium problems. It is specified in the prize conditions that a solution is regarded as smooth, if it is infinitely often differentiable and square integrable in R^3 . So far, the prize remains unclaimed.

Plan of the book

The first section of the book reviews the Navier–Stokes equations in spatial and material description and presents the fundamental properties of the solutions to lay the groundwork for the following chapters with the emphasis placed on turbulent flows of a single incompressible, Newtonian fluid. The subsequent Chaps. 4–9 are the main chapters of the book. The phase space, as the space of all possible states of a turbulent flow fields, is constructed for the motion of incompressible fluids. The notions of probability measure and characteristic functional are defined and methods for their construction are discussed based on theorems by Kolmogorov and Minlos. Chapter 9 is devoted to the development of the linear and closed equations for the spatial and spatial–temporal characteristic functionals of turbulent flows of an incompressible fluid. The general formulation of the equations governing the characteristic functional is specialized to the finite-dimensional case in Chap. 11. Sections 12–14.3 are devoted to the mapping idea as alternative to moment and Pdf/characteristic function methods.

Integral transform methods are discussed in Chap. 15 to prepare the analysis of homogeneous turbulence. Chap. 16 is devoted to the notion of external and internal intermittency. Homogeneous turbulence is discussed in Chaps. 17 and 18 based on the theories of Kolmogorov and Onsager followed by Chap. 19 on length and time scales and scale relations. Structural properties of turbulent flows are introduced in Chap. 20 within the spatial and material description. A brief discussion of wall-bounded flows covering the periodic pipe flow and boundary layers is given in Chap. 21. The limit of infinite Reynolds number is investigated in Chap. 22 in terms of the characteristic functional for turbulence in incompressible fluids. The relation between statistics given in the spatial and material descriptions is analysed in Sect. 23.19 within the context of characteristic functionals and turbulence measures.

Appendices A to E contain mathematical tools, scalar and vector bases for periodic pipe flow and the detailed derivation of the Green’s function for it, the Leray version

of the Navier–Stokes pdes and a semi-empirical treatment of simple wall-bounded flows. Examples are an integral part of the book containing details, too lengthy for the main text, special cases and applications and references for further directions for investigation. The last Appendix F contains the solutions of the problems posed at the end of the individual chapters.

1.1 Notation

Notational uniformity and convenience require a few conventions. Two separate notions of dimension will be employed: The physical dimension and geometric dimensions (Lebesgue covering dimension and its extensions, cardinality, linear topological, fractal dimension, etc.). The physical dimension is only used in the statement of basic physical laws, dimensional variables, measured with an agreed-upon system of units (the international system of units called SI, are denoted with tilde throughout the book except in Sect. 2.1.3 covering symmetry transformations. However, the analysis of physical processes and the solution of associated equations is always done using dimensionless variables to enable the application of various abstract transformations (such as Fourier and Laplace transforms) and norms such as Sobolev norms. The equations contain as a result dimensionless parameters such as the Reynolds, Prandtl, Froude, Schmidt, Peclet, Mach, Grashof, etc., numbers. They are defined in the appropriate sections below as indicated in the list of abbreviations.

Cartesian coordinate systems will be employed unless explicitly stated otherwise. The index notation for Cartesian tensors together with the summation convention applying to Greek but not Latin subscripts will be used throughout the book. Multi-index notation is summarized in Sect. 23.6 of Appendix A. Vectors and tensors are also denoted symbolically by boldface. Complex conjugate variables are denoted with an asterisk except in Sects. 5.5 and 22.2.2, where it is denoted by overline due to the length of complex expressions.

The volume differentials are denoted by $d\mathcal{V}(\tau, \mathbf{X})$ in the material and by $d\nu(t, \mathbf{x})$ in the spatial description, the independent variables time τ , label \mathbf{X} (material/Lagrangean description) and time t , observer position \mathbf{x} (spatial/Eulerian description), respectively, are introduced below in Sects. 2.1 and 2.5. Overline signifies filtering (except Sect. 2.1.3) or coarse-graining defined as volume integral with a kernel/ weight/ filter function, applied in Chap. 22 and Sect. 22.2.2.

Integration appears in various forms throughout the text, ranging from one-dimensional to countable infinite-dimensional integrals. The integration over two and higher dimensional domains will be denoted with a single integral sign, the dimensionality will be clear from the context. Fourier-transformed variables/fields are denoted with hats, i.e. $\hat{f}(\mathbf{k}) = \mathcal{F}f(\mathbf{x})$ and $f(\mathbf{x}) = \mathcal{F}^{-1}\hat{f}(\mathbf{k})$, where \mathcal{F} and \mathcal{F}^{-1} are the Fourier transform operator and its inverse as defined in Sect. 15.1.

The term Lagrangean is spelled differently from the common usage Lagrangian to avoid modifying, unnecessarily, the last name of Joseph-Louis Lagrange. A list of common abbreviations is provided below.

Functionals are denoted in general by $F[\mathbf{y}; \mathbf{x}, t, \dots]$ and by $\theta[\mathbf{y}; \mathbf{x}, t, \dots]$ for the special case of characteristic functionals, where $\mathbf{y}(t, \mathbf{x}) \in \mathcal{H}(\mathcal{D})$ is a vector field defined on $[0, T] \times \mathcal{D}$ and an element of a Banach or Hilbert space $\mathcal{H}(\mathcal{D})$. The semicolon separates the argument field from parametric dependence on location \mathbf{x} , time t and other parameters. There is some confusion in the literature how to denote variational/Fréchet/Gateaux derivatives, a closer look is, therefore, called for.

Proper notation for variational derivatives

Characteristic functionals are the main theme of the book; hence, all considerations are done with this in mind. Functional derivatives in the spatial description are denoted by

$$\frac{\delta \theta}{\delta y_\alpha} [\mathbf{y}, \mathbf{w}; t, \mathbf{x}] \text{ or } \frac{\delta \theta}{\delta y_\alpha(\mathbf{x})} [\mathbf{y}, \mathbf{w}; t]$$

to emphasize the dependence on location \mathbf{x} in the flow domain \mathcal{D} generated by the variational derivatives. Functional derivatives in the material description are denoted analogously by

$$\frac{\delta \theta}{\delta Y_\alpha} [\mathbf{Y}, \mathbf{W}; \tau, \mathbf{X}] \text{ or } \frac{\delta \theta}{\delta Y_\alpha(\mathbf{X})} [\mathbf{Y}, \mathbf{W}; \tau]$$

where \mathbf{X} is the location in the initial flow domain $\mathcal{D}(0)$ serving as identifying label of a material point, and τ time, definitions are given in Sect. 2.5. This notation is not arbitrary, but justified by the dimensional analysis in the next section.

An elementary analysis of the first Gateaux derivative of complex-valued characteristic functionals is carried out for this purpose, further details can be found in Sect. 23.12. For characteristic functionals that are Gateaux and Fréchet differentiable, the derivatives agree and so do the results of the dimensional analysis. Generalization to higher derivatives is straightforward.

First Gateaux derivative

Consider the real locally convex vector spaces X and Y and the linear topological vector space \mathcal{T} of operators $T \in \mathcal{T} : X \rightarrow Y$, let $T \in \mathcal{T}$ have the domain of definition $\mathcal{D}(T) = \Omega \subset \mathcal{T}$. If the limit $DT[u](w) = \lim_{\epsilon \rightarrow 0} \frac{1}{\epsilon} \{T[u + \epsilon w] - T[u]\}$ exists for $u \in X$ and $u + \epsilon w \in X$ for some interval containing $\epsilon = 0$, then is $DT[u](w)$ called the Gateaux differential of the operator T at the vector u in the direction w . The Gateaux derivative in Banach spaces with scalar product (v, w) can be deduced from the representation (23.46)

$$DT[u](w) = (w, \frac{\delta T}{\delta u})$$

of the Gateaux differential $DT[u](w)$. Assuming that all variables have a physical dimension and denoting it with brackets, as, for instance, velocity

$$[\mathbf{v}] = \frac{L}{T}$$

where the physical dimension is length L and T time, it follows from the definition of the spatial characteristic functional (9.1), defined as functional integral with respect to the turbulence measure μ and called expectation operator $\langle \cdot \rangle$

$$\theta[\mathbf{y}(\mathbf{x}); t] \equiv \langle \exp[i(\mathbf{y}, \mathbf{v})] \rangle, \quad \mathbf{y} \in \mathcal{N}, \quad \mathbf{v} \in X, \quad \mathbf{x} \in \mathcal{D}$$

that it must be dimensionless due to the normalization of probability measures. The scalar product for the present (spatial) case of incompressible flows is defined by (25.43)

$$(\mathbf{y}, \mathbf{v}) \equiv \int_{\mathcal{D}} d\mathbf{x} \mathbf{y}(\mathbf{x}) \cdot \mathbf{v}(t, \mathbf{x})$$

where $\mathbf{y}(\mathbf{x})$ is element of a nuclear space (see Gelfand and Vilenkin [50] and Sect. 5.4 for definition of nuclear spaces) of test functions $\mathcal{N} = \{\mathbf{y} \in C_{\mathcal{D}}^{\infty} : \mathbf{y}(\mathbf{x}) = 0, \mathbf{x} \in \partial\mathcal{D}\}$ and the realization $\mathbf{v}(t, \mathbf{x})$ is element of the phase space X .

The argument of the exponential function in (9.1) must be dimensionless. There are several possibilities to arrange this:

(1) Redefine the scalar product (25.43) as

$$(\mathbf{y}, \mathbf{v}) \equiv \int_{\mathcal{D}} d\mathbf{x} w(\mathbf{x}) \mathbf{y}(\mathbf{x}) \cdot \mathbf{v}(t, \mathbf{x}) \quad (1.9)$$

where $w(\mathbf{x}) \geq 0$ denotes a weight function such that $\int_{\mathcal{D}} d\mathbf{x} w(\mathbf{x}) = 1$ holds, the dimension of w is thus $[w] = L^{-3}$. Obviously, this works only for bounded domains or integration with respect to measures other than the Lebesgue measure in R^n such as Gaussian. The dimension of the test functions is then

$$[\mathbf{y}] = \frac{1}{[\mathbf{v}]}$$

whatever the dimension of the realizations \mathbf{v} is.

(2) Define the elements $\mathbf{y} \in \mathcal{N}$ by dividing with the volume \mathcal{V} , hence

$$[\mathbf{y}] = \frac{1}{\mathcal{V}[\mathbf{v}]}$$

where $\mathbf{v} \in X$. This works under the same restriction as in (1).

(3) Redefine the elements $\mathbf{y} \in \mathcal{N}$ and the realizations $\mathbf{v} \in X$ as

$$\mathbf{v} \Leftarrow \frac{1}{\mathcal{V}^{\frac{1}{2}}} \mathbf{v}, \quad \mathbf{y} \Leftarrow \frac{1}{\mathcal{V}^{\frac{1}{2}}} \mathbf{y}$$

This works under the same restriction as in (1). It follows now from the definition (23.45) of the Gateaux differential and the choice (1) for the integration defining the scalar product that it is also dimensionless

$$[D\Theta[\mathbf{y}](\mathbf{w})] = [\Theta(\mathbf{y})]$$

and it follows from the definition (23.46) of the first Gateaux derivative that its physical dimension is

$$[\frac{\delta\Theta}{\delta y_\alpha(\mathbf{x})}] = \frac{1}{[y_\alpha]} = [v_\alpha]$$

for $\alpha = 1, 2, 3$ in a Cartesian coordinate system. This result is consistent with the first Gateaux derivative of the characteristic functional at the origin $\mathbf{y} = 0$ of the test function space, which is the mean field up to a dimensionless constant. If the flow domain \mathcal{D} is subset of the d -dimensional Euclidean space, the physical dimension of the first Gateaux derivative is unaffected by the dimension of the flow domain.

Summary

The dimensional analysis of the previous section suggests that the scalar product should be dimensionless (1.9) and the first Gateaux/Fréchet derivatives of characteristic functionals should be denoted by

$$\frac{\delta\Theta}{\delta y_\alpha(\mathbf{x})} \text{ or } \frac{\delta\Theta}{\delta y_\alpha}[\mathbf{y}; \mathbf{x}] \text{ but not } \frac{\delta\Theta}{\delta y_\alpha(\mathbf{x})d\mathbf{x}}$$

to avoid dimensional inconsistency. The example of the linear, dimensionless functional $\Theta[y]$, defined in the space of continuous scalars $X = \{y(\mathbf{x}) : \mathbf{x} \in \mathcal{D}\}$ as the nuclear space \mathcal{N} of argument/test functions

$$\Theta[y] \equiv (K, y) = \frac{1}{\mathcal{V}} \int_{\mathcal{D}} d\mathbf{x}' K(\mathbf{x}') y(\mathbf{x}')$$

with continuous $K(\mathbf{x})$ and dimension $[K] = \frac{1}{[y]}$, illustrates this fact. A simple computation shows that the Gateaux differential is according to (23.45) $D\Theta[y] = (K, w)$. Hence, the Gateaux derivative is a standard function of location in \mathcal{D} according to (23.46)

$$\frac{\delta\Theta}{\delta y(\mathbf{x})}[\mathbf{y}; \mathbf{x}] = K(\mathbf{x})$$

independent of field argument $y(\mathbf{x})$ and the direction $w(\mathbf{x})$.

Triple sums appearing in certain projection techniques are abbreviated as shown below

$$\sum_{k,n,m}^N \equiv \sum_{k=0}^{\frac{1}{2}N_\theta} \sum_{n=0}^{N_r} \sum_{m=-\frac{1}{2}N_z}^{\frac{1}{2}N_z}$$

$$\sum_{k,n,m} \equiv \sum_{k=0}^{\infty} \sum_{n=0}^{\infty} \sum_{m=-\infty}^{\infty}$$

The index definitions and limits for the storage of the Fourier kernels are consistent with 2-d FFT transforms as defined by Rogallo [51] incorporating the condition that the inverse Fourier transforms are real. The number of Fourier modes N_θ and N_z must be even and the number of terms in the triple sums is given by (10.18).

References

1. Van Kampen, N.G.: Stochastic Processes in Physics and Chemistry, 3rd edn. Elsevier, Amsterdam, The Netherlands (2007)
2. Bogachev, V.I.: Measure Theory, vol. 1. Springer, New York (2006)
3. Berge, P., Pomeau, Y., Vidal, C.: Order within Chaos: Towards a Deterministic Approach to Turbulence. Wiley, New York (1984)
4. Mandelbrot, B.B.: Fractals and Chaos: The Mandelbrot Set and Beyond. Springer, New York (2004)
5. Karniadakis, G., Beskok, A., Aluru, N.: Microflows and Nanoflows. Springer, New York (2000)
6. Bradshaw, P., Ferriss, D.H., Johnson, R.F.: Turbulence in the noise-producing region of a circular jet. *JFM* **19**, 591–624 (1964)
7. Oertel Sr., H.: Modern developments in shock tube research. *Shock Tube Research Soc. Japan*, 488–495 (1975)
8. Schmid, P.J., Henningson, D.S.: Stability and Transition in Shear Flows. Springer (2001)
9. Wiggins, S.: Introduction to Applied Nonlinear Dynamical Systems and Chaos. Springer, New York (2003)
10. Kollmann, W.: Fluid Mechanics in Spatial and Material Description. University Readers, San Diego (2011)
11. Woyczyński, W.A.: Burgers-KPZ Turbulence: Goettingen Lectures. Lecture Notes in Math, vol. 1700. Springer, Berlin (1999)
12. Kraichnan, R.H.: Lagrangian history statistical theory for Burgers' equation. *Phys. Fluids* **II**, 265–277 (1968)
13. Onsager, L.: Statistical hydrodynamics. *Nuovo Cimento* **6**(Suppl.), 279–287 (1949)
14. Lumley, J.L.: Stochastic tools in Turbulence. Academic Press (1970)
15. Frisch, U.: Turbulence: The Legacy of A.N. Kolmogorov. Cambridge University Press (1995)
16. Tsinober, A.: An Informal Conceptual Introduction to Turbulence, 2nd edn. Springer, Dordrecht (2009)
17. Vishik, M.J.: Analytic solutions of Hopf's equation corresponding to quasilinear parabolic equations or to the Navier-Stokes system. *Sel. Math. Sov.* **5**, 45–75 (1986)
18. Vishik, M.J., Fursikov, A.V.: Mathematical Problems of Statistical Hydromechanics. Kluwer Academic Publication, Dordrecht (1988)
19. Lewis, R.M., Kraichnan, R.H.: A Space-time functional formalism for turbulence. *Comm. Pure Applied Math.* **XV**, 397–411 (1962)
20. Dopazo, C., O'Brien, E.E.: Functional formulation of nonisothermal turbulent reactive flows. *Phys. Fluids* **17**, 1968–1975 (1974)

21. Rogers, M.M., Moser, R.D.: Direct simulation of a self-similar turbulent mixing layer. *Phys. Fluids* **6**, 903–923 (1994)
22. Lee, M., Moser, R.D.: Direct numerical simulation of turbulent channel flow up to $Re_\tau = 5200$. *JFM* **774**, 395–415 (2015)
23. Hoyas, S., Jimenez, J.: Scaling of velocity fluctuations in turbulent channels up to $Re_\tau = 2000$. *Phys. Fluids* **18**, 011702 (2006)
24. Ostilla-Monico, R., Verzicco, R., Grossmann, S., Lohse, D.: The near-wall region of highly turbulent Taylor-Couette flow. *JFM* **788**, 95–117 (2016)
25. Wu, X., Moin, P., Adrian, R.J., Baltzer, J.R.: Osborne Reynolds pipe flow: direct simulation from laminar through gradual transition to fully developed turbulence. In: *Proceedings of the National Academy of Sciences of the United States of America*, vol. 112 (26), pp. 7920–7924 (2015)
26. Barkley, D.: Theoretical perspective on the route to turbulence in a pipe. *JFM* **803**, P1–1 (2016)
27. Sagaut, P., Cambon, C.: *Homogeneous Turbulence Dynamics*. Cambridge University Press, New York (2008)
28. Pope, S.B.: *Turbulent Flows*. Cambridge University Press, Cambridge, U.K. (2001)
29. Poinsot, T., Veynante, D.: *Theoretical and Numerical Combustion*. R.T. Edwards, Philadelphia, PA (2001)
30. Oberlack, M., Busse, F.H.: *Theories of Turbulence*. Springer, New York (2002)
31. Fox, R.O.: *Computational Models for Turbulent Reacting Flows*. Cambridge University Press, U.K. (2003)
32. Davidson, P.A.: *Turbulence*. Oxford University Press, Oxford, U.K. (2004)
33. Garnier, E., Adams, N., Sagaut, P.: *Large Eddy Simulation for Compressible Flows*. Springer, New York (2009)
34. Leschziner, M.: *Statistical Turbulence Modelling for Fluid Dynamics - Demystified*. Imperial College Press, London (2015)
35. Jakirlic, S., Hanjalic, K., Tropea, C.: Modeling rotating and swirling turbulent flows: a perpetual challenge. *AIAA J.* **40**, 1984–1996 (2002)
36. Novikov, E.A.: Functionals and the Random-force method in turbulence theory. *Sov. Phys. JETP* **20**, 1290–1294 (1965)
37. Lundgren, T.S.: Distribution functions in the statistical theory of turbulence. *Phys. Fluids* **10**, 969–975 (1967)
38. Novikov, E.A.: Random-force method in turbulence theory. *Sov. Phys. JETP* **17**, 1449–1454 (1963)
39. Kuo, H.-H.: *Gaussian Measures in Banach Spaces*. Lecture Notes in Mathematics, vol. 463. Springer, Berlin (1975)
40. Hosokawa, I.: A functional treatise on statistical hydromechanics with random force action. *J. Phys. Soc. Jpn* **25**, 271–278 (1968)
41. Kraichnan, R.H.: Models for intermittency in hydrodynamic turbulence. *Phys. Rev. Lett.* **65**, 575 (1990)
42. Pope, S.B.: Mapping closures for turbulent mixing and reaction. *Theoret. Computat. Fluid Dyn.* **2**, 255–270 (1991)
43. Pierce, C.D., Moin, P.: Progress-variable approach for large-eddy simulation of non-premixed turbulent combustion. *JFM* **504**, 73–97 (2004)
44. Rosales, C., Meneveau, C.: A minimal multiscale Lagrangian map approach to synthesize non-Gaussian turbulent vector fields. *Phys. Fluids* **18**, 075104 (2006)
45. Hopf, E.: Remarks on the functional-analytic approach to turbulence. *Proc. Symp. Appl. Math.* XIII, 157–163 (1962)
46. Batchelor, G.K.: *The Theory of Homogeneous Turbulence*. Cambridge University Press (1967)
47. Schumacher, J., Sreenivasan, K.R., Yakhot, V.: Asymptotic exponents from low-Reynolds-number flows. *New J. Phys.* **9**, 1–19 (2007)
48. Wilczek, M., Daitche, A., Friedrich, R.: On the velocity distribution in homogenous isotropic turbulence: correlations and deviations from Gaussianity. *JFM* **676**, 191–217 (2011)

49. www.claymath.org/millennium/
50. Gelfand, I.M., Vilenkin, N.Y.: Generalized Functions, vol. 4. Academic Press, New York (1964)
51. Rogallo, R.S.: Numerical Experiments in Homogeneous Turbulence (1981). NASA-TM-81315

Chapter 2

Navier–Stokes Equations



The dynamics of the Newtonian fluids considered here are determined by the laws of classical mechanics, a selection of references for the derivation of the fundamental pdes from these laws are Lamb [1], Landau and Lifshitz [2], Serrin [3], Majda and Bertozzi [4], Wu et al. [5]. The description and analysis of fully developed turbulent flows is the central theme. Turbulence in superfluids, i.e. liquid helium below the λ -temperature $T = 2.17\text{ K}$ at atmospheric pressure, exhibits properties similar to turbulence in classical Newtonian fluids for vanishing viscosity, but are also subject to quantum-mechanical phenomena that do not have counterparts in classical fluid mechanics. Turbulence in superfluids, called quantum turbulence, is beyond the scope of this book, the current status of experiment and theory can be found in the literature (Guénault [6], Vinen [7], Donnelly [8], Skrbek [9]).

The mathematical expression of the laws of classical mechanics governing the motion of fluids is the set of Navier–Stokes equations plus appropriate initial and boundary conditions. The Navier–Stokes equations in the spatial description for incompressible and compressible fluids are introduced first plus a short discussion of the fundamental properties of the solutions. Then the same system is considered in the material description and the transformation of the Navier–Stokes equations from spatial to material description and vice versa is shown to be governed by the Lagrangean position field $\Phi(\tau, \mathbf{X})$, defined as the position of a material point Φ at time τ and identified by its position \mathbf{X} at the reference time zero, it is discussed briefly in Sect. 2.5. A detailed account of spatial and material descriptions and the relation between them can be found in references [5, 10], reference [11] by Bennett is devoted entirely to fluid mechanics in the material description and geophysical applications.

Rotation plays an important role in the description, interpretation and investigation of turbulent flows. For this reason, vorticity as measure of rotation at a material point in a flow field is defined in spatial and material descriptions and elementary properties are established in the present chapter for later use.

The velocity gradient tensor (rate of deformation) is an important tool for the investigation of the small scale phenomena in turbulent flows. Hence, a brief introduction containing definition and transport pde are included in Sect. 2.7.

2.1 Spatial/Eulerian Description

The independent variables in the spatial or Eulerian description are time \tilde{t} and observer position $\tilde{\mathbf{x}}$ (tilde signifies dimensional quantities). Let $\mathcal{D} \subset \mathbb{R}^3$ denote the flow field containing a single compressible Newtonian fluid and let $\partial\mathcal{D}$ denote its boundary subject to mild restrictions, as stated in the chapter on kinematics in [10]. Any sufficiently smooth (a field is called sufficiently smooth, if it is three times continuously differentiable in \mathcal{D} , Serrin [3]) velocity field $\tilde{\mathbf{v}}(t, \mathbf{x})$ defined in $\mathcal{D} \cup \partial\mathcal{D}$ is considered a possible instantaneous state of the fluid provided that mass

$$\frac{\partial \tilde{\rho}}{\partial \tilde{t}} + \frac{\partial}{\partial \tilde{x}_\alpha} (\tilde{\rho} \tilde{v}_\alpha) = 0 \quad (2.1)$$

and momentum balances

$$\tilde{\rho} \left(\frac{\partial \tilde{v}_\alpha}{\partial \tilde{t}} + \tilde{v}_\beta \frac{\partial \tilde{v}_\alpha}{\partial \tilde{x}_\beta} \right) = - \frac{\partial \tilde{p}}{\partial \tilde{x}_\alpha} + \frac{\partial \tilde{\tau}_{\alpha\beta}}{\partial \tilde{x}_\beta} + \tilde{\rho} \tilde{g}_\alpha \quad (2.2)$$

are satisfied, where \tilde{p} is the pressure, $\tilde{\tau}_{\alpha\beta}$ the viscous stress tensor and \tilde{g}_α is the external force per unit volume. Two cases for the external force field will be discussed: The constant field (the gravitational field being the main example) and stochastic fields dependent on location and time (random forcing). The left-hand side of the momentum balance can be expressed in terms of the substantial time derivative (dimensional/non-dimensional)

$$\frac{D}{D\tilde{t}} \equiv \frac{\partial}{\partial \tilde{t}} + \tilde{\mathbf{v}} \cdot \tilde{\nabla}, \quad \frac{D}{Dt} \equiv \frac{\partial}{\partial t} + \mathbf{v} \cdot \nabla \quad (2.3)$$

with respect to the vector field $\tilde{\mathbf{v}}$, it is the material time derivative in the spatial description. Newtonian fluids obey the constitutive relation

$$\tilde{\tau}_{\alpha\beta} = 2\tilde{\mu}(\tilde{s}_{\alpha\beta} - \frac{1}{3}\delta_{\alpha\beta}\tilde{s}_{\gamma\gamma}) \quad (2.4)$$

where $\tilde{\mu} = \tilde{\rho}\tilde{\nu}$ denotes the dynamic viscosity in SI units and $\tilde{s}_{\alpha\beta}$ the strain rate

$$\tilde{s}_{\alpha\beta} \equiv \frac{1}{2} \left(\frac{\partial \tilde{v}_\alpha}{\partial \tilde{x}_\beta} + \frac{\partial \tilde{v}_\beta}{\partial \tilde{x}_\alpha} \right) \quad (2.5)$$

with trace $\tilde{s}_{\gamma\gamma} = \tilde{\nabla} \cdot \tilde{\mathbf{v}}$ being the divergence of velocity. Mass and momentum balances are incomplete for compressible fluids and the energy balance plus thermodynamic state relations must be added to close the Navier–Stokes system. This is done in Sect. 2.1.2 after consideration of the incompressible case in Sect. 2.1.1.

2.1.1 Incompressible Fluids

The special case of a single, incompressible fluid with constant viscosity reduces mass balance (2.1) in dimensionless (assuming that the reference values are available) form to

$$\frac{\partial v_\alpha}{\partial x_\alpha} = 0 \quad (2.6)$$

and momentum balances for Newtonian fluids to

$$\frac{\partial v_\alpha}{\partial t} + v_\beta \frac{\partial v_\alpha}{\partial x_\beta} = - \frac{\partial P}{\partial x_\alpha} + \frac{1}{Re} \frac{\partial^2 v_\alpha}{\partial x_\beta \partial x_\beta} + \frac{1}{Fr} g_\alpha \quad (2.7)$$

where the dimensionless coefficients are the inverse of Reynolds (2.8) and Froude (22.2) numbers, P denotes the ratio of pressure and the constant density for convenience. The pressure in flows of an incompressible fluid has no physical meaning in contrast to compressible flows (where it is linked to density via an equation of state), since it is just a Lagrange multiplier to enforce the incompressibility constraint (2.6). For some flows in simple domains, the gradient of a base pressure P_0 can be identified that maintains the turbulent flow in a statistical steady state by balancing in the average the loss of kinetic energy with the work done by the base pressure gradient. Under special circumstances, it can be related to the shear stress at the wall boundary, see Sect. 27.1 Eq. (27.19) for the plane channel flow.

Assuming a base pressure P_0 can be defined, the pressure gradient is then $\nabla P(t, \mathbf{x}) = \nabla P_0 + \nabla p$, the gradient of the base pressure is a known constant as for the periodic pipe flow and $p(t, \mathbf{x})$ is the disturbance pressure is part of the set of unknowns. The version of the Navier–Stokes system (2.6) and (2.7) is formally closed, i.e. the number of equations is equal to the number of unknowns. It is assumed in the present and the following sections that appropriate reference values (scales) for length, velocity and viscosity can be found such that the equations can be transformed to the dimensionless form (2.6) and (2.7) given above. It is essential and advantageous to cast the Navier–Stokes equations in dimensionless form, generating dimensionless coefficients Reynolds Re (2.8) and Froude Fr (defined by (22.2) in Chap. 22) numbers, the most important coefficient being the Reynolds number Re , replacing viscosity according to $\tilde{\nu} \rightarrow 1/Re$. It is defined by

$$Re \equiv \frac{\tilde{\rho}_0 \tilde{U} \tilde{D}}{\tilde{\mu}} \quad (2.8)$$

as the ratio of convective/inertial to viscous forces. The reference values are \tilde{U} and \tilde{D} being velocity and length scales, $\tilde{\rho}_0$ is the reference density and $\tilde{\mu}$ the reference value of the dynamic viscosity. For example, the reference length and velocity for pipe flow can be chosen as the pipe diameter \tilde{D} and the bulk velocity \tilde{U} given by the volume flow rate (for turbulent flows the statistical expectation for it) divided by the cross-sectional area. Other reference quantities suiting particular classes of flows

can be introduced (see, for instance, Cantwell [12] for an advanced treatment based on Lie groups and outlined in Sect. 2.1.3).

The conditions for the field \mathbf{v} on the boundary $\partial\mathcal{D}$ and in the flow field \mathcal{D} at $t = 0$ are prescribed to complete the IBVP (Initial Boundary Value Problem). The set of all possible states of the turbulent flow are embedded in a suitable linear vector space called phase space Ω , a point in the phase space represents the instantaneous state of a (laminar or transitional or turbulent) flow, it is for a single, incompressible fluid a vector field $\mathbf{v}(\mathbf{x})$ or in the general case $\mathbf{v}(t, \mathbf{x})$, for compressible fluids and mixtures further scalar fields must be included. The phase space is discussed in detail below in Chap. 5. The differential system (2.6), (2.7) and the boundary conditions determine the time rate of change of a phase $\partial\mathbf{v}/\partial t$ as function of the phase $\mathbf{v}(t, \mathbf{x})$, boundary conditions for the pressure are required for the elimination of $p(t, \mathbf{x})$ in the incompressible case. This elimination of p can be achieved with the aid of a Green's function as elaborated in Appendix D, Chap. 26 and, as an example, the Green's function for pipe flow periodic in axial direction is explicitly constructed. The result of the elimination of the pressure p from mass and momentum balances is called Leray version of the Navier–Stokes pdes [4] as given in Sect. 26.9, pdes (26.131), (26.132), (26.133) for periodic pipe flow in cylindrical coordinates.

The Navier–Stokes equations are very difficult to analyse for three major reasons (Landau and Lifshitz [2], Gallavotti [13], Wu et al. [5], Tsinober [14])

- (1) Nonlinearity, which depends on the description (choice of independent variables);
- (2) Non-locality, which becomes apparent for flows of an incompressible fluid, if the pressure is eliminated with the aid of the Leray–Stokes operator (Sect. 23.10 in Appendix A) or a Green's function;
- (3) Non-integrability, the IBVP has no closed-form solution for Reynolds numbers in the turbulent regime.

Euler equations

The Euler equations are the mass and momentum balances for an inviscid fluid, i.e. $\nu = 0/Re = \infty$ in dimensionless form.

$$\frac{\partial v_\alpha}{\partial x_\alpha} = 0, \quad \frac{\partial v_\alpha}{\partial t} + v_\beta \frac{\partial v_\alpha}{\partial x_\beta} = -\frac{\partial p}{\partial x_\alpha} + \frac{1}{Fr} g_\alpha \quad (2.9)$$

They are a system of nonlinear first-order pdes, thus requiring fewer boundary conditions than the Navier–Stokes equations. The dimensionless Euler equations do not contain the Reynolds number, but a subset of solutions of the Euler pdes can be regarded as solutions of the Navier–Stokes pdes in the limit $Re \rightarrow \infty$. However, this limit is a delicate operation, since it is linked to the regularity of the Navier–Stokes solutions (an open problem for 3-d flows at $Re \gg 1$) and the change of type of the momentum balances, see the Duchon–Robert distribution in Sect. 22.3 for the explicit contribution of singularities of the second kind to dissipation in the energy equation. The Euler pdes possess elementary singular solutions, for instance, line

vortex and vortex sheet constructed for aerodynamic applications, but the existence of singular solutions developing from smooth initial data is an open question.

2.1.2 Compressible Fluids

The Navier–Stokes equations for a single, compressible, ideal gas (2.1) and (2.2) must be complemented with the energy balance and appropriate thermodynamic state relations in order to obtain a formally complete system of equations. The energy balance for the enthalpy per unit mass \tilde{h}

$$\tilde{h} \equiv \tilde{u} + \frac{\tilde{p}}{\tilde{\rho}} \quad (2.10)$$

where \tilde{u} denotes the internal energy per unit mass, can be stated in dimensional form as follows:

$$\tilde{\rho} \frac{D\tilde{h}}{D\tilde{t}} = \frac{\partial}{\partial \tilde{x}_\alpha} (\tilde{k} \frac{\partial \tilde{T}}{\partial \tilde{x}_\alpha}) + \frac{D\tilde{p}}{D\tilde{t}} + \tilde{\Phi} \quad (2.11)$$

where the dissipation function is defined by

$$\tilde{\Phi} \equiv \tilde{\tau}_{\alpha\beta} \frac{\partial \tilde{v}_\alpha}{\partial \tilde{x}_\beta} \quad (2.12)$$

This scalar can be shown to be non-negative for Newtonian fluids consistent with the second law of thermodynamics. The relations for a pure and simple substance

$$\begin{aligned} d\tilde{h} &= \tilde{c}_p(\tilde{T})d\tilde{T} + \frac{1}{\tilde{\rho}^2} [\tilde{\rho} + \tilde{T}(\frac{\partial \tilde{\rho}}{\partial \tilde{T}})_p]d\tilde{\rho} \\ d\tilde{u} &= \tilde{c}_v(\tilde{T})d\tilde{T} - \frac{1}{\tilde{\rho}^2} [\tilde{T}(\frac{\partial \tilde{\rho}}{\partial \tilde{T}})_\rho - \tilde{\rho}]d\tilde{\rho} \end{aligned} \quad (2.13)$$

(\tilde{c}_p , \tilde{c}_v are the specific heats) reduce for ideal gases to

$$\tilde{p} = \tilde{\rho} \tilde{R} \tilde{T} \quad (2.14)$$

(\tilde{R} is the gas constant) to

$$d\tilde{h} = \tilde{c}_p(\tilde{T})d\tilde{T}, \quad d\tilde{u} = \tilde{c}_v(\tilde{T})d\tilde{T} \quad (2.15)$$

They are useful to reformulate the energy balance (2.11) in terms of temperature or other relevant variables. The system of Eqs. (2.1), (2.2), (2.11), (2.13), (2.14) is formally closed, hence solvable for suitable initial and boundary conditions. The

Navier–Stokes system for multicomponent reacting mixtures must be extended to keep track of the thermodynamic state and composition, see Poinsot and Veynante [15] for a detailed treatment. The dimensionless version of the compressible Navier–Stokes system involves several new dimensionless coefficients such as the Mach

$$Ma \equiv \frac{\tilde{U}}{\tilde{a}} \quad (2.16)$$

as the ratio of the velocity scale \tilde{U} to the speed of sound \tilde{a} ($a^2 = \gamma \tilde{R} \tilde{T}$ for an ideal gas), determined locally or at a reference state and the Prandtl

$$Pr \equiv \frac{\tilde{c}_p \tilde{\mu}}{\tilde{k}} \quad (2.17)$$

(ratio of dynamic viscosity times specific heat to thermal conductivity), Damköhler (ratio of flow time scale to chemical time scale, ratio of reaction rate to convective mass transport rate, ratio of reaction rate to diffusive mass transfer rate) numbers.

2.1.3 Symmetries of the Euler and Navier–Stokes pdes

The basic system of dimensional (the tilde signifying dimensional quantities is not used in the present section to unclutter the equations) equations in the spatial description (2.6), (2.7) and the material description (2.85), (2.86) in Sect. 2.5.2 can be transformed to a new system in various ways. Among all possible transformations, the class of transformations that do not change the form of the equations play a special role; they are called symmetry transformations or simply symmetries of the system, Frisch [16], Sect. 2.2, Oberlack [17], Oberlack et al. [18]. It should be noted that the transformation of the Navier–Stokes pdes from the spatial description to the material description (Sect. 2.5) does not qualify as symmetry transformation, in fact preimage and image equations are quite different.

The tools for the computation of all symmetries of a system of equations are established in the theory of transformation groups for transformations that depend continuously on a parameter. The theory was originated by Sophus Lie in the nineteenth century, see Cantwell [12] for historical details. A brief outline of the Lie group approach is presented for the computation of symmetries of differential equations.

A group is a set of objects that is equipped with a binary operation \circ and satisfies four axioms. Hence, transformation groups $G_T \equiv \{T_\epsilon : \mathbf{x}^* = T_\epsilon \mathbf{x} = \Phi(\mathbf{x}, \epsilon), \mathbf{x}, \mathbf{x}^* \in R^n\}$ must satisfy the axioms:

- (G.1) The group operation is closed, $T_{\epsilon_3} = T_{\epsilon_1} \circ T_{\epsilon_2} \in G_T$.
- (G.2) There exists a unit element $T_0 \in G_T$, $T_0 \circ T_\epsilon = T_\epsilon \circ T_0 = T_\epsilon$.

(G.3) There exists an inverse transformation T_ϵ^{-1} for each $T_\epsilon \in G_T$, $T_\epsilon^{-1} \circ T_\epsilon = T_\epsilon \circ T_\epsilon^{-1} = T_0$.

(G.4) The group operation is associative, $T_{\epsilon_1} \circ (T_{\epsilon_2} \circ T_{\epsilon_3}) = (T_{\epsilon_1} \circ T_{\epsilon_2}) \circ T_{\epsilon_3}$.

The task of determining all symmetries of a system of differential equations was made accessible by the first and second theorem of Lie [17, 19], Chap. 1.8. The first theorem implies that it is sufficient to determine the differentials of the group transformations thus constructing a solvable set of linear equations. Oberlack et al. [18] present a detailed explanation of the Lie group approach for systems of differential equations, which is the source for the following development for incompressible fluids and the spatial description. This requires some preparations to properly formulate the method.

Derivatives and definition of symmetry

The system of M differential equations is written in general form

$$\mathbf{F}(\mathbf{x}, \mathbf{y}, \mathbf{y}^{(1)}, \mathbf{y}^{(2)}, \dots, \mathbf{y}^{(p)}) = 0 \quad (2.18)$$

where $\mathbf{x} \in R^n$, $\mathbf{y}(\mathbf{x}) \in R^M$, \mathbf{F} is M -dimensional, $p \geq 0$ is the order of the system and $\mathbf{y}^{(|\alpha|)}$, $|\alpha| = 1, \dots, p$ denotes the set of $|\alpha|$ th-derivatives

$$y_{k;\alpha_1, \alpha_2, \dots, \alpha_n} \equiv \frac{\partial^{|\alpha|} y_k}{\partial^{\alpha_1} x_1 \partial^{\alpha_2} x_2 \dots \partial^{\alpha_n} x_n}, \quad 1 \leq k \leq M, \quad 1 \leq |\alpha| \leq p \quad (2.19)$$

according to (23.14) and (23.16) in Appendix A, Chap. 23, $\alpha = \{\alpha_1, \alpha_2, \dots, \alpha_n\} \in N_0^n$, $\alpha_k \geq 0$ and integer, (N_0^n is the set of n -dimensional arrays of non-negative and finite integers) is a multi-index of order $|\alpha| = \sum_{k=1}^n \alpha_k$. For multi-indices $\alpha, \beta \in N_0^n$ and $\mathbf{x} = (x_1, x_2, \dots, x_n) \in R^n$ many operations can be defined for multi-indices analogous to single indices, details are given in Appendix A, Sect. 23.6.

Consider a scalar function $G(\mathbf{x}, \mathbf{y}, \mathbf{y}^{(1)}, \mathbf{y}^{(2)}, \dots, \mathbf{y}^{(p)})$ of $\mathbf{x} \in R^n$, $\mathbf{y} \in R^M$ and the derivatives $y_{k,\alpha_1\alpha_2\dots\alpha_n}$ for $k = 1, \dots, M$ and $|\alpha| \leq p$, then is the total derivative with respect to x_i , $i = 1, \dots, n$ defined by

$$\frac{\mathcal{D}G}{\mathcal{D}x_i} = \frac{\partial G}{\partial x_i} + \sum_{k=1}^M y_{k,i} \frac{\partial G}{\partial y_k} + \sum_{k=1}^M \sum_{j=1}^n y_{k,ij} \frac{\partial G}{\partial y_{k,j}} + \dots + \sum_{k=1}^M \sum_{j_1=1}^n \dots \sum_{j_n=1}^n y_{k,i,j_1\dots j_n} \frac{\partial G}{\partial y_{k,j_1\dots j_n}} \quad (2.20)$$

where the summation convention was not applied to show the proper limits of the sums. Note that the partial derivative $\partial/\partial x_i$ of $G(\mathbf{x}, \mathbf{y}(\mathbf{x}), \dots)$ with G depending on \mathbf{x} explicitly and not only via \mathbf{y} and its derivatives, requires, that all independent variables x_m , y_k , $y_{k,j}$, \dots , $y_{k,j_1\dots j_n} \neq x_i$ are held constant, whereas the total derivative $\mathcal{D}/\mathcal{D}x_i$ must be computed regarding the $y_{k,j_1\dots j_m}(\mathbf{x})$, $m = 1, \dots, p$ as function of \mathbf{x} using implicit differentiation. A simple example $G(\mathbf{x}, \mathbf{y}, \dots) \equiv y_m$ should clarify the role of explicit dependence, where G does not explicitly depend on \mathbf{x}

$$\frac{\mathcal{D}G}{\mathcal{D}x_i} = \frac{\partial G}{\partial x_i} + y_{k,i} \frac{\partial G}{\partial y_k} + y_{k,ij} \frac{\partial G}{\partial y_{k,j}} + \cdots + y_{k,ij_1 \cdots j_n} \frac{\partial G}{\partial y_{k,j_1 \cdots j_n}} = y_{m,i}$$

therefore, $\frac{\partial G}{\partial x_i} = 0$ and $y_{k,i} \frac{\partial G}{\partial y_k} = y_{k,i} \delta_{mk}$ and all higher terms are zero.

The total first derivative operator is thus

$$\frac{\mathcal{D}}{\mathcal{D}x_i} = \frac{\partial}{\partial x_i} + y_{k,i} \frac{\partial}{\partial y_k} + y_{k,ij} \frac{\partial}{\partial y_{k,j}} + \cdots + y_{k,ij_1 \cdots j_n} \frac{\partial}{\partial y_{k,j_1 \cdots j_n}} \quad (2.21)$$

with the summation convention restored, where $\sum_{k=1}^n j_k = p$ is the order of the operator.

The example $G(\mathbf{y}) = y_m$ leads to

$$y_{m,i} = \frac{\mathcal{D}y_m}{\mathcal{D}x_i}, \quad y_{m,ij} = \frac{\mathcal{D}y_{m,i}}{\mathcal{D}x_j}, \quad y_{m,ijk} = \frac{\mathcal{D}y_{m,ij}}{\mathcal{D}x_k}, \dots$$

since $G(\mathbf{y})$ does not explicitly depend on $\mathbf{x}, \mathbf{y}_{,ij}$ and higher derivatives.

Consider now local or point transformations depending continuously on a parameter ϵ ,

$$\mathbf{x}^* = \Phi(\mathbf{x}, \mathbf{y}, \epsilon), \quad \mathbf{y}^* = \Psi(\mathbf{x}, \mathbf{y}, \epsilon) \quad (2.22)$$

with Φ and Ψ at least p -times continuously differentiable, that map the system of differential equations to the transformed system

$$\mathbf{F}^*(\mathbf{x}^*, \mathbf{y}^*, \mathbf{y}^{*(1)}, \mathbf{y}^{*(2)}, \dots, \mathbf{y}^{*(p)}) = 0 \quad (2.23)$$

Definition: A transformation, which leaves the form of the equations unchanged, is called symmetry transformation or symmetry

$$\mathbf{F}^*(\mathbf{x}^*, \mathbf{y}^*, \mathbf{y}^{*(1)}, \mathbf{y}^{*(2)}, \dots, \mathbf{y}^{*(p)}) = \mathbf{F}(\mathbf{x}, \mathbf{y}, \mathbf{y}^{(1)}, \mathbf{y}^{(2)}, \dots, \mathbf{y}^{(p)}) \quad (2.24)$$

if the transformed variables are renamed as the original variables.

The definitions of partial and total derivatives carry over to the transformed variables, i.e.

$$y_{m,i}^* = \frac{\mathcal{D}^* y_m^*}{\mathcal{D}^* x_i^*}, \quad y_{m,ij}^* = \frac{\mathcal{D}^* y_{m,i}^*}{\mathcal{D}^* x_j^*}, \quad y_{m,ijk}^* = \frac{\mathcal{D}^* y_{m,ij}^*}{\mathcal{D}^* x_k^*}, \dots \quad (2.25)$$

The derivatives of the preimage variables $\mathbf{x}, \mathbf{y}, \dots$ can be expressed in terms of the image variables $\mathbf{x}^*, \mathbf{y}^*, \dots$ according to the transformation (2.22) and the chain rule

$$\frac{\mathcal{D}}{\mathcal{D}x_i} = \frac{\mathcal{D}\Phi_m}{\mathcal{D}x_i} \frac{\mathcal{D}^*}{\mathcal{D}^* x_m^*} \quad (2.26)$$

hence

$$\frac{\mathcal{D}\Psi_k}{\mathcal{D}x_i} = y_{k,m}^* \frac{\mathcal{D}\Phi_m}{\mathcal{D}x_i} \quad (2.27)$$

is obtained using (2.25).

Infinitesimal transformations

Smooth and invertible symmetry transformations (2.22) are considered, rearranged such that $\epsilon = 0$ is the identity transformation $\mathbf{x}^* = \Phi(\mathbf{x}, \mathbf{y}, 0) = \mathbf{x}, \mathbf{y}^* = \Psi(\mathbf{x}, \mathbf{y}, 0) = \mathbf{y}$. The Taylor series expansion with respect to $\epsilon = 0$ is then

$$\mathbf{x}^* = \mathbf{x} + \xi\epsilon + O(\epsilon^2), \quad \mathbf{y}^* = \mathbf{y} + \eta\epsilon + O(\epsilon^2)$$

where the infinitesimals are defined by

$$\xi(\mathbf{x}, \mathbf{y}) \equiv \frac{\partial \Phi}{\partial \epsilon}(\mathbf{x}, \mathbf{y}, 0), \quad \eta(\mathbf{x}, \mathbf{y}) \equiv \frac{\partial \Psi}{\partial \epsilon}(\mathbf{x}, \mathbf{y}, 0) \quad (2.28)$$

The analysis of differential equations requires the extension (called prolongation) of the infinitesimals to derivatives $\zeta_{m; j_1 j_2 \dots}$ (the semicolon in subscript does not indicate derivation but component of ζ via derivatives of y_m)

$$y_{m,i}^* = y_{m,i} + \zeta_{m;i} \epsilon + O(\epsilon^2), \quad y_{m,ij}^* = y_{m,ij} + \zeta_{m;ij} \epsilon + O(\epsilon^2), \quad \dots \quad (2.29)$$

The transformation (2.27) determines the infinitesimals $\zeta_{m; j_1 j_2 \dots}$ as follows. Expanding in Taylor series $\Phi_m = x_m^* = x_m + \xi_m \epsilon + O(\epsilon^2)$, $\Psi_k = y_k^* = y_k + \eta_k \epsilon + O(\epsilon^2)$ and $y_{k,m}^* = y_{k,m} + \zeta_{k;m} \epsilon + O(\epsilon^2)$ with respect to ϵ according to (2.25) and (2.27) leads to

$$\frac{\mathcal{D}}{\mathcal{D}x_i}(y_k + \eta_k \epsilon + O(\epsilon^2)) = (y_{k,m} + \zeta_{k;m} \epsilon + O(\epsilon^2)) \frac{\mathcal{D}}{\mathcal{D}x_i}(x_m + \xi_m \epsilon + O(\epsilon^2)) \quad (2.30)$$

Collecting the zeroth and first powers of ϵ produces the relations

$$\frac{\mathcal{D}y_k}{\mathcal{D}x_i} = y_{k,m} \frac{\mathcal{D}x_m}{\mathcal{D}x_i}$$

and

$$\frac{\mathcal{D}\eta_k}{\mathcal{D}x_i} = \zeta_{k;m} \frac{\mathcal{D}x_m}{\mathcal{D}x_i} + y_{k,m} \frac{\mathcal{D}\xi_m}{\mathcal{D}x_i}$$

Since $\frac{\mathcal{D}x_m}{\mathcal{D}x_i} = \delta_{m,i}$ holds, the recursive relation

$$\zeta_{k;i} = \frac{\mathcal{D}\eta_k}{\mathcal{D}x_i} - y_{k,m} \frac{\mathcal{D}\xi_m}{\mathcal{D}x_i} \quad (2.31)$$

for $\zeta_{k;i}$ is arrived at. This type of recursion can be generalized (see Oberlack et al. [18])

$$\zeta_{k;i_1 i_2 \dots i_s} = \frac{\mathcal{D}}{\mathcal{D}x_i} \zeta_{k;i_1 i_2 \dots i_{s-1}} - y_{k,m i_1 i_2 \dots i_{s-1}} \frac{\mathcal{D}\xi_m}{\mathcal{D}x_i}, \quad s > 1 \quad (2.32)$$

for the computation of higher order infinitesimals.

Invariance of differential equations

The transformed system of differential equations (2.23) can be expanded in Taylor series

$$\mathbf{F}(\mathbf{x}, \mathbf{y}, \mathbf{y}^{(1)}, \mathbf{y}^{(2)}, \dots, \mathbf{y}^{(p)}) + \epsilon X^{(p)} \mathbf{F}(\mathbf{x}, \mathbf{y}, \mathbf{y}^{(1)}, \mathbf{y}^{(2)}, \dots, \mathbf{y}^{(p)}) + O(\epsilon^2) = 0 \quad (2.33)$$

where $p > 0$ is the highest derivative in the system. The prolongation operator $X^{(p)}$ of the generator $X = \xi_i \frac{\partial}{\partial x_i} + \eta_i \frac{\partial}{\partial y_i}$ follows from the Taylor series expansions in (2.33)

$$X^{(p)} \equiv \xi_i \frac{\partial}{\partial x_i} + \eta_i \frac{\partial}{\partial y_i} + \zeta_{i;j} \frac{\partial}{\partial y_{i,j}} + \dots + \zeta_{i;j_1 j_2 \dots j_p} \frac{\partial}{\partial y_{i,j_1 j_2 \dots j_p}} \quad (2.34)$$

Since $\mathbf{F}(\mathbf{x}, \mathbf{y}, \mathbf{y}^{(1)}, \mathbf{y}^{(2)}, \dots, \mathbf{y}^{(p)}) = 0$ and $\mathbf{F}^*(\mathbf{x}^*, \mathbf{y}^*, \mathbf{y}^{*(1)}, \mathbf{y}^{*(2)}, \dots, \mathbf{y}^{*(p)}) = 0$ and since Lie's first theorem implies that only terms of order ϵ need to be considered, it follows that

$$\boxed{X^{(p)} \mathbf{F}|_{\mathbf{F}=0} = 0} \quad (2.35)$$

determines the symmetry transformations of the system $\mathbf{F} = 0$. The details of the computation of all symmetries for the linear, second-order pde describing heat conduction in R^1 are illustrated in Problem (2.4) with solution provided in Appendix F, Chap. 28.

The infinitesimals can be represented by a sum of different irreducible operators that are elements of a linear vector space. This is also illustrated in the solution to the IBVP of the heat pde in Problem (2.4) in Appendix F, Chap. 28 and applied to the Euler and Navier–Stokes equations below.

Symmetries of the Euler pdes

The Euler equations in the spatial description for an incompressible fluid (Eq. (2.6), (2.7) with $\nu = 0$) possess ten symmetries (Oberlack [17] Sect. 3.1, Cantwell [12] Chap. 11. These symmetries are presented as irreducible operators)

$$X_1 = \frac{\partial}{\partial t}$$

$$X_2 = x_\alpha \frac{\partial}{\partial x_\alpha} + v_\alpha \frac{\partial}{\partial v_\alpha} + 2p \frac{\partial}{\partial p}$$

$$\begin{aligned}
X_3 &= t \frac{\partial}{\partial t} - v_\alpha \frac{\partial}{\partial v_\alpha} - 2p \frac{\partial}{\partial p} \\
X_4 &= -x_2 \frac{\partial}{\partial x_1} + x_1 \frac{\partial}{\partial x_2} - v_2 \frac{\partial}{\partial v_1} + v_1 \frac{\partial}{\partial v_2} \\
X_5 &= -x_3 \frac{\partial}{\partial x_2} + x_2 \frac{\partial}{\partial x_3} - v_3 \frac{\partial}{\partial v_2} + v_2 \frac{\partial}{\partial v_3} \\
X_6 &= -x_1 \frac{\partial}{\partial x_3} + x_3 \frac{\partial}{\partial x_1} - v_1 \frac{\partial}{\partial v_3} + v_3 \frac{\partial}{\partial v_1} \\
X_7 &= f_1(t) \frac{\partial}{\partial x_1} + \frac{df_1}{dt} \frac{\partial}{\partial v_1} - x_1 \frac{d^2 f_1}{dt^2} \frac{\partial}{\partial p} \\
X_8 &= f_2(t) \frac{\partial}{\partial x_2} + \frac{df_2}{dt} \frac{\partial}{\partial v_2} - x_2 \frac{d^2 f_2}{dt^2} \frac{\partial}{\partial p} \\
X_9 &= f_3(t) \frac{\partial}{\partial x_3} + \frac{df_3}{dt} \frac{\partial}{\partial v_3} - x_3 \frac{d^2 f_3}{dt^2} \frac{\partial}{\partial p} \\
X_{10} &= f_4(t) \frac{\partial}{\partial p}
\end{aligned} \tag{2.36}$$

where $f_1(t)$, $f_2(t)$, $f_3(t)$ are twice continuously differentiable functions and $f_4(t)$ an arbitrary function of t . Any linear combination of the X_i generates an invariant transformation of the Euler pdes.

Symmetries of the Navier–Stokes pdes

The symmetries for the Navier–Stokes equation ($\nu > 0$) are established letting viscosity ν vary (Oberlack [17])

$$\begin{aligned}
X_1 &= g_1(\nu) \frac{\partial}{\partial t} \\
X_2 &= g_2(\nu) \left\{ x_\alpha \frac{\partial}{\partial x_\alpha} + v_\alpha \frac{\partial}{\partial v_\alpha} + 2p \frac{\partial}{\partial p} \right\} \\
X_3 &= g_3(\nu) \left\{ t \frac{\partial}{\partial t} - v_\alpha \frac{\partial}{\partial v_\alpha} - 2p \frac{\partial}{\partial p} \right\} \\
X_4 &= g_4(\nu) \left\{ -x_2 \frac{\partial}{\partial x_1} + x_1 \frac{\partial}{\partial x_2} - v_2 \frac{\partial}{\partial v_1} + v_1 \frac{\partial}{\partial v_2} \right\} \\
X_5 &= g_5(\nu) \left\{ -x_3 \frac{\partial}{\partial x_2} + x_2 \frac{\partial}{\partial x_3} - v_3 \frac{\partial}{\partial v_2} + v_2 \frac{\partial}{\partial v_3} \right\}
\end{aligned}$$

$$\begin{aligned}
X_6 &= g_6(\nu) \left\{ -x_1 \frac{\partial}{\partial x_3} + x_3 \frac{\partial}{\partial x_1} - v_1 \frac{\partial}{\partial v_3} + v_3 \frac{\partial}{\partial v_1} \right\} \\
X_7 &= g_7(t, \nu) \frac{\partial}{\partial x_1} + \frac{dg_7}{dt}(t, \nu) \frac{\partial}{\partial v_1} - x_1 \frac{d^2 g_7}{dt^2}(t, \nu) \frac{\partial}{\partial p} \\
X_8 &= g_8(t, \nu) \frac{\partial}{\partial x_2} + \frac{dg_8}{dt}(t, \nu) \frac{\partial}{\partial v_2} - x_2 \frac{d^2 g_8}{dt^2}(t, \nu) \frac{\partial}{\partial p} \\
X_9 &= g_9(t, \nu) \frac{\partial}{\partial x_3} + \frac{dg_9}{dt}(t, \nu) \frac{\partial}{\partial v_3} - x_3 \frac{d^2 g_9}{dt^2}(t, \nu) \frac{\partial}{\partial p} \\
X_{10} &= g_{10}(t, \nu) \frac{\partial}{\partial p}
\end{aligned} \tag{2.37}$$

Any linear combination of the X_i generates an invariant transformation of the Navier–Stokes system. An example for the computation of all symmetries is provided in the solution to Problem (2.5) in Appendix F, Chap. 28.

2.2 Fundamental Properties of the Solutions for a Single Incompressible Fluid

It is assumed in the present section that appropriate reference values for the variables exist and the dimensionless version (2.6) and (2.7) is thus well defined with positive and finite Reynolds (2.8) and Froude (22.2) numbers. Initial and boundary conditions in dimensionless form must be specified for the Navier–Stokes system of Eqs. (2.6), (2.7) to obtain a solvable problem. Consider a compact (bounded and closed) flow domain \mathcal{D} with sufficiently smooth (a uniquely defined unit normal vector exists nearly everywhere) boundary $\partial\mathcal{D}$ and set up the initial condition

$$v_\alpha(0, \mathbf{x}) = v_\alpha^0(\mathbf{x}) \text{ for } \mathbf{x} \in \mathcal{D} \tag{2.38}$$

where $v_\alpha^0(\mathbf{x})$ is a prescribed vector satisfying the constraint (2.6), whose norm and smoothness properties play a fundamental role in existence and uniqueness of the solution. The boundary conditions prescribed on $\partial\mathcal{D}$ are of Dirichlet type

$$v_\alpha(t, \mathbf{x}) = v_\alpha^b(t, \mathbf{x}) \text{ for } \mathbf{x} \in \partial\mathcal{D} \text{ and } t \geq 0 \tag{2.39}$$

The fundamental questions concerning the solutions of this initial/boundary value problem (IBVP) are:

- (i) Existence of a solution;
- (ii) Uniqueness of the solution;
- (iii) Smoothness (or regularity) of the solutions.

The Navier–Stokes equations have been subject of research for more than a century, see Serrin [3], Von Wahl [20], Constantin and Foias [21], Kreiss and Lorenz [22], Sohr [23], Constantin [24] for the mathematical analysis and further development. However, there remain several fundamental questions still open for the case of $3 - d$ flows at $Re \gg 1$, which are, unfortunately, relevant for the investigation of turbulence.

An initial/boundary value problem that can be proved to satisfy all three conditions is called well posed. The nonlinearity of the Navier–Stokes equations (2.6), (2.7) has precluded complete proofs of all three conditions in 3-d for all Reynolds numbers and initial energies (see the problem statement for the millennium prize of the Clay Institute [25]). The existence of a solution (i) for the special case of homogeneous boundary conditions $v_\alpha^b = 0$ and zero external volume forces $g_\alpha = 0$ will be discussed briefly.

The solution $\mathbf{v}(t, \mathbf{x})$ of the Navier–Stokes equations is called strong if it is twice differentiable in the classical sense and satisfies mass (2.6) and momentum (2.7) balances on the open domain $\mathcal{D} \subset \mathbb{R}^n$, $n = 2, 3$. The notion of a solution can be generalized to weak solution defined below as introduced by J. Leray [3] in 1933. It is relevant to the analysis to high Reynolds number turbulence, see Eyink [26], Duchon and Robert [27], who constructed a term in the energy equation representing dissipation due to lack of smoothness (Sect. 22.3), and to computational methods in fluid mechanics for the construction of approximate solutions, see Spalart [28]). Furthermore, it is an important tool for the analysis of the existence and regularity properties of solutions of the Navier–Stokes equations [23, 29].

Definition: A vector function $v_\alpha(t, \mathbf{x})$ is called *weak solution* of the initial/boundary value problem for the Navier–Stokes equations (2.6), (2.7) in the space–time domain $[0, \infty) \times \mathcal{D}$ if $v_\alpha \in V$ (defined below) and if

$$\int_0^\infty dt \{(v_\alpha, \frac{\partial u_\alpha}{\partial t}) + \frac{1}{Re} (v_\alpha, \Delta u_\alpha) + (v_\alpha, v_\beta \frac{\partial u_\alpha}{\partial x_\beta})\} = -(v_\alpha^0, u_\alpha^0) \quad (2.40)$$

holds for all test vectors $u_\alpha(t, \mathbf{x}) \in L_{0,\sigma}^\infty([0, \infty) \times \mathcal{D})$ (see Sect. 23.7 in Appendix A for definitions and notation of function spaces) and for all initial conditions $v_\alpha^0(\mathbf{x}) \in W$ (the space W is defined below, note that $u_\alpha^0(\mathbf{x}) = u_\alpha(0, \mathbf{x})$) and $L_{0,\sigma}^\infty([0, \infty) \times \mathcal{D})$ denotes the space of all infinitely often differentiable test vectors u_α , which have compact support (set of all points \mathbf{x} , where u_α is non-zero) in $[0, \infty) \times \mathcal{D}$ and which have zero divergence (called solenoidal vector fields). The parenthesis denotes the L^2 -scalar product

$$(\mathbf{v}, \mathbf{u}) \equiv \int_{\mathcal{D}} d\mathbf{x} \mathbf{v}(t, \mathbf{x}) \cdot \mathbf{u}(t, \mathbf{x})$$

as defined by (23.19) in Appendix A, Sect. 23.7. The scalar product induces the L^2 -norm

$$\|\mathbf{u}\|_{L^2(\mathcal{D})} \equiv (\mathbf{u}, \mathbf{u})^{\frac{1}{2}} \quad (2.41)$$

The Hilbert space V is defined as the set of all vector functions $\mathbf{v}(\mathbf{x}, t)$ that satisfy the conditions:

(V.1) For each $T > 0$, $0 < T < \infty$ the vector function $\mathbf{v}(t, \mathbf{x})$ is in the closure of $L_{0,\sigma}^\infty([0, \infty) \times \mathcal{D})$ with respect to the Sobolev norm (23.21) (Sect. 23.7, Appendix A) for $m = 1$, $p = 2$

$$\|\mathbf{v}\|_{1,2,\mathcal{D}}^2(t) = \sum_{|\alpha| \leq 1} \|\partial^\alpha \mathbf{v}(t, \mathbf{x})\|_{L^2(\mathcal{D})}^2 \quad (2.42)$$

where $\|\mathbf{v}\|_{L^2(\mathcal{D})}^2 \equiv (v_\alpha, v_\alpha)$ is the associated L^2 -norm (23.18) for $p = 2$. Note that closure means that the convergent limits of functions from $L_{0,\sigma}^\infty([0, \infty) \times \mathcal{D})$ with convergence measured using the Sobolev norm (2.42) are included in V .

(V.2) The norm $\|\mathbf{v}\|_{1,2,\mathcal{D}}(t)$ is uniformly bounded in time.

The initial conditions are restricted by the condition that $\mathbf{v}^0 \in W$. The space W is defined as the closure D_0 of the space C^∞ of infinitely often differentiable vector fields $\mathbf{v}^0(\mathbf{x})$, which have zero divergence and compact support in \mathcal{D} , under the norm $\|\mathbf{v}^0\|$ defined by (2.41).

The notion of weak solutions lead to two fundamental results concerning the existence of solutions for the initial/boundary value problem for (2.6) and (2.7).

Theorem 2.1 (Hopf [30]) *For any initial velocity field $\mathbf{v}^0 \in W$ there exists a weak solution $\mathbf{v} \in V$ of the initial/boundary value problem (2.6)–(2.39). Moreover*

$$\|\mathbf{v}\|_{L^2(\mathcal{D})}^2 + 2 \int_0^T dt \|\mathbf{v}\|_{1,2,\mathcal{D}}^2(t) \leq \|\mathbf{v}^0\|_{L^2(\mathcal{D})}^2 \quad (2.43)$$

and

$$\lim_{t \rightarrow 0} \|\mathbf{v} - \mathbf{v}^0\|_{L^2} = 0 \quad (2.44)$$

hold. The proof can be found in the original paper by Hopf (1950) [30].

The solutions, whose existence is insured by Theorem 2.1, are not necessarily differentiable (in the classical sense) vector fields. Furthermore, no information on uniqueness is contained in this theorem. It should be noted that the initial velocity field is not necessarily smooth since it is only required to be the limit of test fields with respect to the norm (2.41). The space of initial fields can be made smaller by using a stricter norm that includes integrals over derivatives (such as the Sobolev norm (2.42)). This leads to the second theorem.

Theorem 2.2 (Kiselev and Ladyzhenskaya [31]) *Let the dimension of the flow be $n = 2$ or $n = 3$, then for any initial velocity field $v_\alpha^0 \in W^2$ there exists a weak*

solution $v_\alpha \in V$ of the initial/boundary value problem (2.6), (2.7) with homogeneous boundary values (2.39) and a time interval $[0, T)$, $T > 0$, such that $|\frac{\partial v_\alpha}{\partial x_\beta}|$ and $|\frac{\partial v_\alpha}{\partial t}|$ are uniformly bounded in the interval $0 \leq t \leq T$. The length T of the time interval depends only on the Reynolds number and on bounds for the initial velocity field. In case of $n = 2$ (two-dimensional flows), Theorem 2.3 gives a complete answer for $T = \infty$. In case of $n = 3$ this holds only if the norm of the initial velocity field is small enough as Theorem 2.4 indicates.

The space of initial velocity fields is for Theorem 2.2 restricted by the Sobolev norm

$$\|\mathbf{v}\|_{2,2,\mathcal{D}}^2(t) = \sum_{|\alpha| \leq 2} \|\partial^\alpha \mathbf{v}(t, \mathbf{x})\|_{L^2(\mathcal{D})}^2 \quad (2.45)$$

with $m = 2$, $p = 2$. This norm is much more selective in deciding which sequences from D_0 are convergent and are, therefore, elements of W^2 .

The second theorem shows explicitly that turbulent flow fields, which are always three-dimensional, as argued later in property (T.4) in Chap. 3 summarizing the defining properties of turbulence, and whose initial norm is usually not small, cannot be guaranteed to possess smooth solutions for all time. This result is indicative that singularities of the second kind as defined by Beale, Kato and Majda in theorem (3.15) in Chap. 3 and the Kolmogorov - Onsager hypotheses (Chap. 17) play an important role in guiding any rigorous approach to turbulence. Note that Theorem 2.2 says that the solution, if it exists, has square-integrable first derivatives, whereas Theorem 2.1 makes no statement concerning derivatives.

The properties of the solutions of the Navier-Stokes equations have received considerable attention over the last decades and a review of the relevant results can be found, for instance, in Von Wahl [20] (1985), Constantin and Foias [21] (1988), Sohr [23]. Two recently proved theorems, showing the fundamental difference between 2-d and 3-d flows with respect to existence and regularity, are briefly discussed.

Two-dimensional viscous flows

The IVP for homogeneous Dirichlet conditions for two-dimensional flows, in contrast to 3-d flows, always has a strong solution. The mathematical theory of artificial, two-dimensional turbulence has received recently considerable attention and progress on the existence and regularity of the solutions of the 2-d Navier-Stokes pdes with stochastic forcing has been reported by Kuksin and Shirikyan [32]. In fact, the following theorem (Sohr [23], Chap. 4) holds for any admissible domain $\mathcal{D} \subset \mathbb{R}^2$ with boundary $\partial\mathcal{D}$, the time interval $0 < T \leq \infty$, initial velocity $\mathbf{v}^0(\mathbf{x}) \in L_\sigma^2(\mathcal{D})$ and homogeneous Dirichlet boundary condition $\mathbf{v}(\mathbf{x}) = 0$ on $\partial\mathcal{D}$ and external force $f_\alpha = f_\alpha^0 + \frac{\partial F_{\alpha\beta}}{\partial x_\beta}$ with

$$\mathbf{f}^0 \in L_{loc}^1([0, T); L^2(\mathcal{D})^n), \quad \mathbf{F} \in L_{loc}^2([0, T); L^2(\mathcal{D})^{n^2})$$

where $n = 2$ is the dimension of the domain \mathcal{D} .

Theorem 2.3 *There exists a uniquely determined weak solution*

$$\mathbf{v}(t, \mathbf{x}) \in L_{loc}^\infty([0, T); L_\sigma^2(\mathcal{D}) \cap L_{loc}^2([0, T); W_{0,\sigma}^{1,2}(\mathcal{D})) \quad (2.46)$$

of the $2 - d$ Navier–Stokes equations with initial condition $\mathbf{v}^0(\mathbf{x})$ and external force \mathbf{f} . The solution satisfies the Serrin uniqueness condition [33]

$$\mathbf{v}(t, \mathbf{x}) \in L_{loc}^4([0, T); L^4(\mathcal{D})^2) \quad (2.47)$$

and is, therefore, also a strong solution. The proof can be found in Sohr [23], Chap. 4, Kuksin and Shirikyan [32], Chap. 2. The conclusion is that the IBVP for the $2 - d$ Navier–Stokes system is well posed.

Recent results for three-dimensional viscous flows

However, the existence of smooth solution of three-dimensional flows for arbitrary Reynolds numbers and large initial data is still an open question, in particular asymptotic regularity remains a serious obstacle to a rigorous theory of turbulence. The following theorem for homogeneous Dirichlet IBVPs summarizes the present state of affairs.

Theorem 2.4 *Let $\mathcal{D} \subset \mathbb{R}^3$ be an admissible domain with boundary $\partial\mathcal{D}$, the time interval $0 < T \leq \infty$, initial velocity $\mathbf{v}^0(\mathbf{x}) \in L_\sigma^2(\mathcal{D})$ and homogeneous Dirichlet boundary condition $\mathbf{v}(\mathbf{x}) = 0$ on $\partial\mathcal{D}$ and external force $f_\alpha = f_\alpha^0 + \frac{\partial F_{\alpha\beta}}{\partial x_\beta}$ with*

$$\mathbf{f}^0 \in L^{\frac{4}{3}}([0, T); L^2(\mathcal{D})^n), \quad \mathbf{F} \in L^4([0, T); L^2(\mathcal{D})^{n^2})$$

where $n = 3$ is the dimension of the domain \mathcal{D} . Then there exists a constant $K > 0$ independent of \mathcal{D} , \mathbf{v}^0 , \mathbf{f} , T and Re with the following property: Choose T' with $0 < T' \leq T$

$$\|\mathbf{f}^0\|_{2, \frac{4}{3}; T'} + Re^{\frac{1}{2}} \|\mathbf{F}\|_{2, 4; T'} + \|(I - e^{-2T'A})A^{\frac{1}{4}}\mathbf{v}^0\|_2^{\frac{1}{8}} \|A^{\frac{1}{4}}\mathbf{v}^0\|_2^{\frac{7}{8}} \leq K Re^{-(1+\frac{1}{4})}$$

such that in the time interval $[0, T')$ exists a uniquely determined strong solution

$$\mathbf{v}(t, \mathbf{x}) \in L_{loc}^\infty([0, T); L_\sigma^2(\mathcal{D}) \cap L_{loc}^2([0, T); W_{0,\sigma}^{1,2}(\mathcal{D})) \quad (2.48)$$

of the Navier–Stokes pdes with initial condition $\mathbf{v}^0(\mathbf{x})$, external force $\mathbf{f}(t, \mathbf{x})$ satisfying the Serrin condition (2.47). The proof for this theorem can be found in Sohr [23], Chap. 4.2. Note that the theorem is valid for homogeneous Dirichlet problems, the case of non-homogeneous IBVP for domains with entrance and exit sections, i.e. noncompact domains with exit sections at infinity, has received some attention (see Pileckas [34] for the mathematical treatment of open domains with entrance and exit sections) due to their importance in many applications.

These theorems involve a number of function spaces defined in Sect. 23.7 of Appendix A, Chap. 23. The Leray–Stokes operator A is defined in Sect. 23.10 in Appendix A.

Well-posedness assumption

The state of affairs concerning the well-posedness conditions (i) to (iii) for the Navier–Stokes equations (2.6), (2.7) reflected in the four theorems stated above makes an assumption necessary:

The IBVPs for the Navier–Stokes equations are well posed for all finite Reynolds numbers and initial energies.

This assumption implies that the solution of the Navier–Stokes equations (2.6), (2.7) with appropriate boundary and initial conditions at time t is determined for $Re < \infty$ by the operator $T_t(Re)$

$$v_\alpha(t, \mathbf{x}) = T_t(Re)v_\alpha(0, \mathbf{x}) \quad (2.49)$$

with unique inverse $T_{-t}(Re)$ (Temam [35] Introduction, sec.3, also Vishik and Fur-sikov [36] Chap. IV who need it to prove uniqueness of statistical solutions). The operators T_t satisfy the semi-group identity

$$T_t \circ T_s = T_{t+s}$$

used by Vishik [37] to study the asymptotic properties of evolution equations. The assumption is correct for $2 - d$ flows (Theorem 2.3), but unproven for fully $3 - d$ flows at high Reynolds numbers and arbitrary initial energy (Theorem 2.4). There is some indication that the assumption does not hold for the limit $Re \rightarrow \infty$ as the velocity field may emerge as Hölder continuous with a positive exponent less than unity and as a consequence the formation of singularities for vorticity and the strain rate (Sect. 22.2.2), but there is no rigorous proof for it. Hopefully, the future will affirm this assumption for $Re < \infty$ and make it redundant. Obviously, a theory based on this assumption is correct conditional upon its validity.

2.3 Rotation and Vorticity in the Spatial Description

Rotation measured by vorticity plays an important role in turbulent flows. The rate of deformation tensor can be split into a symmetric and an antisymmetric part

$$\frac{\partial v_\alpha}{\partial x_\beta} = \frac{1}{2} \left(\frac{\partial v_\alpha}{\partial x_\beta} + \frac{\partial v_\beta}{\partial x_\alpha} \right) + \frac{1}{2} \left(\frac{\partial v_\alpha}{\partial x_\beta} - \frac{\partial v_\beta}{\partial x_\alpha} \right) \quad (2.50)$$

valid for any dimension. However, the three-dimensional case is special, because the number of independent elements in the skew-symmetric part ($\frac{1}{2}n(n-1)$) is equal to the dimension (n) itself for $n = 3$ only. It follows for $n = 3$ that the entries of the skew-symmetric matrix can be rearranged in a pseudo-vector (or axial vector) with the aid of the Levi-Civita symbol $\epsilon_{\alpha\beta\gamma}$ defined by (23.13) in Appendix A Sect. 23.5. This vector is called vorticity and it is defined as the curl of velocity

$$\omega_\alpha(\mathbf{x}, t) \equiv \epsilon_{\alpha\beta\gamma} \frac{\partial v_\gamma}{\partial x_\beta} \quad \text{or} \quad \boldsymbol{\omega} \equiv \nabla \times \mathbf{v} \quad (2.51)$$

where $\epsilon_{\alpha\beta\gamma}$ is the Levi-Civita symbol. Vorticity has zero divergence for compressible and incompressible fluids due to an elementary kinematic relation. An elementary property of $\epsilon_{\alpha\beta\gamma}$ leads to

$$\frac{\partial v_\alpha}{\partial x_\beta} = s_{\alpha\beta} - \frac{1}{2} \epsilon_{\alpha\beta\gamma} \omega_\gamma \quad (2.52)$$

relating vorticity to the rate of deformation and the rate of strain,

$$s_{\alpha\beta} = \frac{1}{2} \left(\frac{\partial v_\alpha}{\partial x_\beta} + \frac{\partial v_\beta}{\partial x_\alpha} \right) \quad (2.53)$$

valid for three dimensions only. It is worth noting that for plane flows vorticity has only one non-zero component, hence cannot be represented as pseudo-vector in R^2 . Important vector fields related to vorticity are the Lamb vector

$$\mathbf{L} \equiv \boldsymbol{\omega} \times \mathbf{v} \quad (2.54)$$

and the flexion vector

$$\mathbf{f} \equiv \nabla \times \mathbf{L} \quad (2.55)$$

The properties of Lamb and flexion vectors are discussed in Sect. 2.4.

The velocity field induced by a given vorticity distribution can be established using basic vector calculus relations for solenoidal (zero divergence) vector fields. The Biot–Savart law ([5], Chap. 3.2, [10], Chap. 5.4) emerges for Cartesian coordinates in the form

$$v_\alpha(t, \mathbf{x}) = -\frac{1}{4\pi} \int_{\mathcal{D}} d\nu(\mathbf{y}) \epsilon_{\alpha\beta\gamma} \frac{(x_\beta - y_\beta) \omega_\gamma(t, \mathbf{y})}{|\mathbf{x} - \mathbf{y}|^3} \quad (2.56)$$

This is the velocity induced by a vorticity distribution with compact support in R^3 .

2.3.1 Beltrami and Trkalian Vector Fields

Let \mathcal{L} be a linear differential operator defined for differentiable vectors on the flow domain. The linear operator \mathcal{L} in R^n possesses non-zero eigenvector fields \mathbf{v}

$$\mathcal{L}\mathbf{v} = \lambda\mathbf{v} \quad (2.57)$$

if a parameter $\lambda \neq 0$ exists satisfying this relation. For the curl operator $\mathcal{L} \equiv \nabla \times$, the eigenvectors are a special case of Beltrami vectors, defined by

$$\mathbf{v} \times (\nabla \times \mathbf{v}) = 0 \quad (2.58)$$

i.e. vectors that are parallel to their curl.

If the eigenvalue λ in (2.57) is non-zero, the eigenvectors are solenoidal and called Trkalian vectors. This is not necessarily true for Beltrami vectors (2.58), since the proportionality factor λ in $\nabla \times \mathbf{v} = \lambda(\mathbf{x})\mathbf{v}$ may vary with location.

The eigenproblem for the curl is related to the eigenproblem for the Laplacian. This follows from the vector calculus relation

$$\nabla \times (\nabla \times \mathbf{v}) = -\Delta\mathbf{v} + \nabla(\nabla \cdot \mathbf{v}) \quad (2.59)$$

applied to solenoidal vector fields \mathbf{v}

$$\nabla \times (\nabla \times \mathbf{v}) = -\Delta\mathbf{v} \quad (2.60)$$

Taking the curl of (2.57) and using (2.60) leads to the eigenproblem

$$-\Delta\mathbf{v} = \lambda^2\mathbf{v} \quad (2.61)$$

for the Laplacian. Therefore, the set of the solution of (2.61) contains the solutions of the eigenproblem (2.57) for the curl. The solution to the eigenproblem for the curl in simple domains can be found in the literature, for instance, for cylindrical domains in Morse [38].

2.3.2 Vorticity pde for Compressible Fluids

The transport equation for vorticity is easily derived; it follows from the momentum balance (2.2) for compressible fluids by applying the curl to it and using mass balance (2.1). The result is in dimensionless form

$$\rho \frac{D}{Dt} \left(\frac{\omega_\alpha}{\rho} \right) = \omega_\beta s_{\alpha\beta} + \frac{1}{\rho^2} \epsilon_{\alpha\beta\gamma} \frac{\partial \rho}{\partial x_\beta} \frac{\partial p}{\partial x_\gamma} + \epsilon_{\alpha\beta\gamma} \frac{\partial}{\partial x_\beta} \left(\frac{1}{\rho} \frac{\partial \tau_{\gamma\delta}}{\partial x_\delta} \right) + \epsilon_{\alpha\beta\gamma} \frac{1}{Fr} \frac{\partial g_\beta}{\partial x_\gamma} \quad (2.62)$$

(detailed derivation in the solution to Problem 2.1, Chap. 28), the stress–strain relation for Newtonian fluids is given by (2.4), (2.5). The vorticity pde (2.62) is then for incompressible, Newtonian fluids reduced to

$$\frac{D\omega_\alpha}{Dt} = \omega_\beta s_{\alpha\beta} + \frac{1}{Re} \frac{\partial^2 \omega_\alpha}{\partial x_\beta \partial x_\beta} + \epsilon_{\alpha\beta\gamma} \frac{1}{Fr} \frac{\partial g_\gamma}{\partial x_\beta} \quad (2.63)$$

in dimensionless form, where the Reynolds number is defined by (2.8) and the Froude number by (22.2). The external force field $\mathbf{g}(t, \mathbf{x})$ is in general nonconservative, i.e. has a rotational part, hence $\nabla \times \mathbf{g}$ is then non-zero. This situation is encountered in MHD flows of an electrically conducting fluid exposed to the rotational part of the Lorentz force, see Wu et al. [5] Chap. 4.1 for details on the electromagnetic force field.

The transport equation for inviscid compressible fluids and volume forces being the gradient of a potential Φ ($\nabla \times \mathbf{g} = -\nabla \times \nabla \Phi = 0$) follows at once from (2.62)

$$\rho^2 \frac{D}{Dt} \left(\frac{\omega_\alpha}{\rho} \right) = \rho s_{\alpha\beta} \omega_\beta + \epsilon_{\alpha\beta\gamma} \frac{1}{\rho} \frac{\partial \rho}{\partial x_\beta} \frac{\partial p}{\partial x_\gamma} \quad (2.64)$$

in dimensional form. Consider now barotropic fluids, defined by the condition, that the pressure is a local function of density, i.e. $p(\mathbf{x}) = p(\rho(\mathbf{x}))$, hence are density and pressure gradients parallel and $\int \frac{dp}{\rho}$ is integrable. The transport equation for vorticity (2.64) is, therefore, for barotropic and inviscid fluids reduced to

$$\frac{D}{Dt} \left(\frac{\omega_\alpha}{\rho} \right) = \frac{\omega_\beta}{\rho} s_{\alpha\beta} \quad (2.65)$$

This pde implies a theorem due to Helmholtz:

The vorticity of a material point remains zero for non-singular flows of an inviscid and barotropic fluids, if it was zero initially.

The vorticity equation (2.65) can be solved in the material description, if the velocity field is specified. The elementary split

$$\frac{\partial v_\alpha}{\partial x_\beta} = s_{\alpha,\beta} - \frac{1}{2} \epsilon_{\alpha\beta\gamma} \omega_\gamma \quad (2.66)$$

holds for flows of compressible and incompressible fluids, hence

$$\frac{D}{Dt} \left(\frac{\omega_\alpha}{\rho} \right) = \frac{\omega_\beta}{\rho} \frac{\partial v_\alpha}{\partial x_\beta} \quad (2.67)$$

also holds. Transformation of (2.67) to the material description, discussed in the next Sect. 2.5, i.e. $\Omega_\alpha(\tau, \mathbf{X}) = \omega_\alpha(t, \mathbf{x})$ and $R(\tau, \mathbf{X}) = \rho(t, \mathbf{x})$ for $t = \tau$ and $\mathbf{x} = \Phi(\tau, \mathbf{X})$, where $\Phi(\tau, \mathbf{X})$ is the position of the material at time τ , which was at \mathbf{X} at time zero, leads to

$$\frac{\partial}{\partial \tau} \left(\frac{\Omega_\alpha}{R} \right) = \frac{\Omega_\beta}{R} \frac{1}{2J} \epsilon_{\beta\zeta\gamma} \epsilon_{\delta\eta\omega} \frac{\partial \Phi_\zeta}{\partial X_\eta} \frac{\partial \Phi_\gamma}{\partial X_\omega} \frac{\partial V_\alpha}{\partial X_\delta} \quad (2.68)$$

The solution of this pde is given by

$$\frac{\Omega_\alpha(\tau, \mathbf{X})}{R(\tau, \mathbf{X})} = \frac{\Omega_\beta(0, \mathbf{X})}{R(0, \mathbf{X})} \frac{\partial \Phi_\alpha}{\partial X_\beta}(\tau, \mathbf{X}) \quad (2.69)$$

as can be verified by differentiation (see the solution of Problem 2.2 in Appendix F, Chap. 28). This result shows that the change of vorticity at a given material point for barotropic and inviscid fluids is solely due to the deformation gradient $F_{\alpha\beta}(\tau, \mathbf{X})$ defined in Eq. (2.82) below in Sect. 2.5. This equation will be applied occasionally for the analysis of turbulent flows under the special conditions of barotropic, inviscid fluids.

2.4 Lamb Vector Dynamics for Incompressible Fluids

The Lamb vector, defined the vector product of velocity and its curl by (2.54) $L_\alpha \equiv \epsilon_{\alpha\beta\gamma} \omega_\beta v_\gamma$, has several useful properties for the analysis and interpretation of turbulent flows. It can be shown to be part of the convective acceleration by applying the definition (2.54) to the momentum balance. The momentum balance (2.7) can be reformulated in terms of vorticity

$$\frac{Dv_\alpha}{Dt} = -\frac{\partial p}{\partial x_\alpha} - \frac{1}{Re} \epsilon_{\alpha\beta\gamma} \frac{\partial \omega_\gamma}{\partial x_\beta} + \frac{1}{Fr} g_\alpha \quad (2.70)$$

This version of the momentum balance shows that viscosity has no influence on momentum transport, if vorticity is zero. Furthermore, the use of vector identities produces the seemingly paradoxical property that the resultant viscous force acting on a material point in the flow field can be expressed in terms of vorticity despite the fact that vorticity (as a measure of rotation) does not produce viscous stress. However, regions with constant non-zero vorticity do not contribute to the viscous force. The viscous term in (2.70) is apparently the curl of vorticity, which is called flexion vector (2.55) (Truesdell [39], 1954). The vorticity pde (2.63)

$$\frac{D\omega_\alpha}{Dt} = \omega_\beta \frac{\partial v_\alpha}{\partial x_\beta} + \frac{1}{Re} \frac{\partial^2 \omega_\alpha}{\partial x_\beta \partial x_\beta} + \epsilon_{\alpha\beta\gamma} \frac{1}{Fr} \frac{\partial g_\gamma}{\partial x_\beta}$$

is also required for the derivation of the transport pde for the Lamb vector according to (2.54)

$$\frac{D\mathbf{L}}{Dt} = \frac{D\boldsymbol{\omega}}{Dt} \times \mathbf{v} + \boldsymbol{\omega} \times \frac{D\mathbf{v}}{Dt}$$

The pde for the Lamb vector emerges then in the form

$$\frac{D\mathbf{L}}{Dt} = -\boldsymbol{\omega} \times \nabla p + \mathbf{v} \times (\boldsymbol{\omega} \cdot \mathbf{s}) + \frac{1}{Re} \nabla^2 \mathbf{L} + \frac{1}{Fr} \left(\nabla \times \mathbf{g} \times \mathbf{v} + \boldsymbol{\omega} \times \mathbf{g} \right) \quad (2.71)$$

The external volume force may possess a Helmholtz representation with non-zero rotational contribution. The special case of potential force fields is considered in the next section.

Potential volume forces

If the volume force g_α has a potential $\Phi(t, \mathbf{x})$

$$g_\alpha = -\frac{\partial \Phi}{\partial x_\alpha}$$

which holds, for instance, if the external force is gravity, the dimensionless momentum balance emerges in the form

$$\frac{\partial v_\alpha}{\partial t} = L_\alpha - \frac{\partial}{\partial x_\alpha} \left(\frac{1}{2} v_\beta v_\beta + p + \frac{1}{Fr} \Phi \right) - \frac{1}{Re} \epsilon_{\alpha\beta\gamma} \frac{\partial \omega_\gamma}{\partial x_\beta} \quad (2.72)$$

and the vorticity pde (2.70) is reduced to

$$\frac{D\omega_\alpha}{Dt} = \omega_\beta \frac{\partial v_\alpha}{\partial x_\beta} + \frac{1}{Re} \frac{\partial^2 \omega_\alpha}{\partial x_\beta \partial x_\beta} \quad (2.73)$$

The acceleration in the Lamb–Gromeka form (2.72) is split into three contributions: The local term on the left side, the Lamb vector and the gradient of the kinetic energy, which is combined with the pressure and the potential of the volume force. If vorticity is zero, it follows from the Stokes theorem that velocity has also a potential and (2.72) leads to a Bernoulli theorem (see Truesdell [39] for proofs). The Lamb vector in the momentum balance represents the rotational part of the convective acceleration in the sense that the curl of the convective acceleration is equal to the curl of the Lamb vector. The Lamb vector furnishes a geometric interpretation of the case of steady inviscid flow with non-zero vorticity. The momentum balance (2.72) emerges then in the form

$$\frac{\partial H}{\partial x_\alpha} = L_\alpha \quad (2.74)$$

which can be interpreted as follows: The gradient of the Bernoulli function

$$H \equiv P_t + \frac{1}{Fr} \Phi, \quad P_t \equiv p + \frac{1}{2} v_\alpha v_\alpha \quad (2.75)$$

is in the direction normal to the surface formed by streamlines and vortex lines. This surface has the Lamb vector as normal vector and is called Lamb surface. The scalar product of (2.74) with velocity vanishes, since velocity is orthogonal to the Lamb vector. It follows that the gradient of the Bernoulli function H has only one non-zero component normal to the Lamb surface and the result is obtained that H is constant for points on the Lamb surface. Hence, the Bernoulli function H is constant along streamlines for steady inviscid vortical flows, but its value depends in general on the particular Lamb surface chosen.

The evolution of the Lamb vector for unsteady flows is governed by

$$\frac{D\mathbf{L}}{Dt} = -\boldsymbol{\omega} \times \nabla p + \mathbf{v} \times (\boldsymbol{\omega} \cdot \mathbf{s}) + \frac{1}{Re} \nabla^2 \mathbf{L} + \frac{1}{Fr} \boldsymbol{\omega} \times \mathbf{g} \quad (2.76)$$

where \mathbf{s} denotes the rate of strain defined by (2.53). The Lamb vector is created or destroyed by four distinct processes. The first source term is the cross product of vorticity and the pressure gradient. It is zero if these two vectors are aligned and it is always present in plane flows since vorticity is orthogonal to the plane of the flow and the pressure gradient is always in this plane. The second source is analogous to the vortex stretching term in the vorticity equation. It is easy to show that it is zero for plane flows and that it produces exponential growth in three-dimensional flows, if the Lamb vector is aligned with the eigenvector of the rate of strain tensor associated with the middle (positive) eigenvalue. The third term is viscous diffusion of the Lamb vector and the fourth is the external force acting on the fluid.

The divergence of the Lamb vector

$$\frac{\partial L_\alpha}{\partial x_\alpha} = \omega_\alpha \omega_\alpha - \frac{\partial v_\alpha}{\partial x_\beta} \frac{\partial v_\alpha}{\partial x_\beta} + \frac{\partial^2}{\partial x_\alpha \partial x_\alpha} \left(\frac{1}{2} v_\beta v_\beta \right) \quad (2.77)$$

is non-zero even for solenoidal velocity fields in contrast to vorticity. The example of linear Couette flow $v_1 = Ax_2$, $v_2 = v_3 = 0$ generates the divergence $\nabla \cdot \mathbf{L} = A^2$, where the Lamb vector is oriented in the positive x_2 direction $L_\alpha = \delta_{\alpha,2} A^2 x_2$ pointing away from the x_1 -axis. The Lamb vector field can be interpreted as the flow (in a generalized sense regarding the Lamb vector as velocity) generated by a uniform distribution of sources with strength A^2 . The source points on the x_1 -axis are obviously unstable critical points.

Structures bounded by surfaces that move relative to the fluid are of a general nature, which may be described in either the spatial or material picture. The appearance of large structures of rolling vortex shape observed by Brown and Roshko [40] in plane mixing layers of two fluids with different densities provided an example for such structures. They are characterized by a dimensionless parameter called Roshko number

$$Ro \equiv \frac{fL^2}{\nu} = Str \cdot Re \quad (2.78)$$

where f is a frequency relevant to the structures, such as observed in vortex shedding,

$$Str \equiv \frac{fL}{U} \quad (2.79)$$

denotes the Strouhal number and Re the Reynolds number (2.8).

2.5 Material/Lagrangean Description

The independent variables in the material or Lagrangean description are time τ and the label variable \mathbf{X} uniquely identifying a material point (defined as a point moving with the velocity at its location), which is usually defined as the position at a reference time, say zero. The dependent variables such as position Φ , velocity \mathbf{V} , etc., are denoted either by capital letters or by specifying the independent variables, to distinguish them from their spatial counterparts. The initial position is in the flow domain $\mathcal{D}(\tau)$ at time $\tau = 0$, the flow domain may move and deform as time evolves, and hence the transformation between flow domains at different times is desirable. The transformation between spatial and material description

$$t = \tau, \mathbf{x} = \Phi(\tau, \mathbf{X}), \Leftrightarrow \tau = t, \mathbf{X} = \Phi^*(t, \mathbf{x}) \quad (2.80)$$

is furnished by the Lagrangean position field $\Phi(\tau, \mathbf{X})$, which is defined as the position of a material point at time τ that was at \mathbf{X} at time zero. $\Phi(\tau, \mathbf{X})$ is the solution of the system of odes (called pathline equations)

$$\frac{d\Phi}{d\tau} = \mathbf{v}(t(\tau), \mathbf{x}(\tau, \Phi)), \Phi(0, \mathbf{X}) = \mathbf{X} \in \mathcal{D}(0) \quad (2.81)$$

provided the right-hand side vector $\mathbf{v}(t, \mathbf{x})$, for instance, as solution of the Navier–Stokes equations, is specified (\mathbf{v} denotes velocity in the spatial description, for details consult the first chapter of [10]). Alternatively, the Lagrangean position field can be computed directly as solution of the Navier–Stokes equations in the material description given below (2.85), (2.86). The transformation of statistical information from the material to the spatial description and vice versa is discussed from the mathematical point of view by Constantin [41] and in Sect. 23.19 of Appendix A.

The position field $\Phi_\alpha(\tau, \mathbf{X})$ is for fixed time τ a diffeomorphism of $\mathcal{D}(0)$ onto $\mathcal{D}(\tau)$ called flow map. It has a unique inverse $\Phi^*(t, \mathbf{x})$, if the Jacobian J of the transformation is positive. This can be shown to be true as long as the spatial divergence of velocity exists and remains bounded in a suitable norm, but fails if singularities of the second order emerge (property T.4 in Chap. 3) in the flow. The partial derivatives of the position field form a second-order tensor called deformation gradient,

$$F_{\alpha\beta}(\tau, \mathbf{X}) = \frac{\partial\Phi_\beta}{\partial X_\alpha}, \quad F_{\alpha\beta}(0, \mathbf{X}) = \delta_{\alpha\beta} \quad (2.82)$$

The Jacobian J of the mapping generated by the position field Φ is the determinant of the deformation gradient $F_{\alpha\beta}(\tau, \mathbf{X})$. The transformation of derivatives in the spatial description to the material description can be carried out using the relations established in the first chapter of [10] and they lead to the Navier–Stokes system for fluids with constant density in the material description.

2.5.1 Piola Transform $\pi_{\alpha\beta}$

The Piola transformation maps vectors and tensors between spatial—Eulerian and material—Lagrangean description in continuum mechanics: Consider a materially invariant subdomain with Lipschitz continuous boundary $\partial\mathcal{D}$ and a tensor flux field $\mathbf{T}(\tau, \mathbf{X})$, then is the Piola transformation defined by the invariance of the tensor flux

$$\int_{\partial\mathcal{D}(0)} dA(0)\mathbf{T}(0, \mathbf{X}) \cdot \mathbf{n}(0, \mathbf{X}) = \int_{\partial\mathcal{D}(\tau)} dA(\tau)\mathbf{T}(\tau, \mathbf{X}) \cdot \mathbf{n}(\tau, \mathbf{X})$$

Ciarlet [42] proves that the multiplication of a tensor of order one or higher with the second-order tensor $J^{-1}F_{\alpha\beta}$ is the explicit expression for the Piola transform. It is denoted by $\pi_{\alpha\beta}$ in the continuum mechanics literature (Ciarlet [42]). Furthermore, it is invertible, if the Lagrangean deformation gradient $F_{\alpha\beta}$ is non-singular, i.e. $J = F \neq 0$,

$$\pi_{\alpha\beta} = \frac{1}{J}F_{\alpha\beta} \Leftrightarrow \pi_{\alpha\beta}^{-1} = JF_{\alpha\beta}^{-1} \quad (2.83)$$

For example, the inverse Piola transform relates the (vector) surface differential at time zero to the differential at the later time τ according to (see [10], Chap. 2.12 for proof)

$$dA_\alpha(u, v, 0) = \pi_{\gamma\alpha}^{-1}dA_\gamma(u, v, \tau) \quad (2.84)$$

where u, v are surface parameters. Similar relations hold for the stress tensor given in the next section, further details can be found in [10].

2.5.2 Incompressible Fluids

Mass balance appears as $J = 1$, where J is the Jacobian of the transformation, or explicitly (Monin and Yaglom [43], Chap. 9, Tsinober [14], Chap. 13.5)

$$\frac{1}{6}\epsilon_{\alpha\beta\gamma}\epsilon_{\delta\eta\omega}F_{\alpha\delta}F_{\beta\eta}F_{\gamma\omega} = 1 \quad (2.85)$$

and momentum balance as

$$\frac{\partial^2 \Phi_\alpha}{\partial \tau^2} = -\frac{1}{2R} \epsilon_{\alpha\beta\gamma} \epsilon_{\delta\eta\omega} F_{\beta\eta} F_{\gamma\omega} \frac{\partial P}{\partial X_\delta} + \frac{1}{2Re} \epsilon_{\theta\beta\gamma} \epsilon_{\delta\eta\omega} F_{\zeta\eta} F_{\phi\omega} \frac{\partial}{\partial X_\delta} (F_{\zeta\beta} F_{\phi\gamma} \frac{\partial^2 \Phi_\alpha}{\partial X_\theta \partial \tau}) + \frac{1}{Fr} G_\alpha \quad (2.86)$$

where $F_{\alpha\beta}$ is the Lagrangean deformation gradient (2.82), $R(\tau, \mathbf{X})$ denotes density (capital of the Greek letter ρ) and $G_\alpha(\tau, \mathbf{X})$ the external force per unit volume in the material description. The Levi-Civita symbol $\epsilon_{\alpha\beta\gamma}$ used frequently in the following shares most properties with third-order tensors, except it does not transform properly under an odd number of reflection of a coordinate axis (Sect. 23.5, see Pope [44] Appendix A.4 for details). It is evident from the comparison of the same Navier–Stokes system with two different options for the independent variables that the structure of nonlinearity of the momentum balance in the material description is quite different from the spatial description and linear terms in one description can be nonlinear in the other description. For instance, the nonlinear convection terms are present in the spatial, but absent in the material description.

The Navier–Stokes system for an incompressible fluid set up in the material description in terms of Lagrangean position Φ and pressure P fields can be regarded as the equations determining a measure-preserving mapping $\Phi(\tau, \mathbf{X}) : \mathcal{A}(0) \rightarrow \mathcal{A}(\tau)$ of any measurable subset $\mathcal{A}(0)$ of the flow domain at time $\tau = 0$ onto the image set in the flow domain at a later time. The smoothness of this mapping is guaranteed only for a time interval depending on the initial velocity norm and the Reynolds number (Theorem 2.4 in Sect. 2.2, VonWahl [20], Sohr [23]), the asymptotic properties are unknown at this time. The role of the pressure in this system is to preserve the measure of any measurable subset of the flow domain.

2.5.3 Compressible Fluids

For flows of compressible fluids, the system of equations consisting of mass and momentum balances is incomplete and, after completion with energy balance and state relations (called compressible Navier–Stokes equations), the mapping is not measure preserving due to expansion and compression phenomena changing density. Mass balance in the material description

$$R(\tau, \mathbf{X}) J(\tau, \mathbf{X}) = R(0, \mathbf{X}) \quad (2.87)$$

relates density R at time τ to density at the reference time zero for a specified material point \mathbf{X} , the Jacobian $J = \det(F_{\alpha\beta})$ being the scale factor. Expansion and compression phenomena produce values of the Jacobian J different from unity, hence violate measure preservation.

It is advantageous for the formulation of momentum and energy balance to introduce the (first) Piola–Kirchhoff stress tensor $\Sigma_{\alpha\gamma}^{(1)}$ defined by [10, 42]

$$\Sigma_{\alpha\beta}^{(1)} \equiv F\sigma_{\alpha\gamma}F_{\beta\gamma}^{-1} \quad (2.88)$$

where $\sigma_{\alpha\gamma}$ is the total stress tensor $\sigma_{\alpha\beta}(\tau, \mathbf{X}) = -p(\tau, \mathbf{X})\delta_{\alpha\beta} + \tau_{\alpha\beta}(\tau, \mathbf{X})$ and $F_{\beta\gamma}^{-1}$ denotes the inverse of the Lagrangean deformation gradient $F_{\beta\gamma}$ defined by (2.82). The relation between the spatial (Cauchy) stress tensor $\sigma_{\alpha\gamma}$ and the (first) Piola–Kirchhoff tensor $\Sigma_{\alpha\beta}^{(1)}$ is the Piola transformation $\pi_{\alpha\beta}^{-1}$ (defined above, Eq. (2.83)) $\Sigma_{\alpha\beta}^{(1)} = \pi_{\beta\gamma}^{-1}\sigma_{\alpha\gamma}$, where $\sigma_{\alpha\gamma}(t, \mathbf{x})$ is the stress tensor in the spatial description, whereas $F(\tau, \mathbf{X})$ and $F_{\beta\gamma}^{-1}(\tau, \mathbf{X})$ are in the material description. It follows that the first Piola–Kirchhoff stress tensor is a function of time and the current location \mathbf{x} and the initial location \mathbf{X} , hence a two-point tensor. Computing the differential force acting on the surface differential at time zero and using (2.84) $\Sigma_{\alpha\beta}^{(1)}dA_{\beta}(u, v, 0) = \sigma_{\alpha\gamma}(\mathbf{x}, t)dA_{\gamma}(u, v, \tau)$ is arrived at. It follows that the first Piola–Kirchhoff stress tensor relates the forces in the current configuration at time τ to areas in the reference configuration at time zero. A detailed discussion of the Piola–Kirchhoff stress tensors can be found in reference [10].

The strong form of the momentum balance in the material description follows from the integral formulation for a materially invariant domain using standard arguments (see [10] for details) in the form

$$R(0, \mathbf{X}) \frac{\partial^2 \Phi_{\alpha}}{\partial \tau^2} = \frac{\partial}{\partial X_{\gamma}}[J(T_{\alpha\beta} - \delta_{\alpha\beta}p)F_{\gamma\beta}^{-1}] + R(0, \mathbf{X})G_{\alpha} \quad (2.89)$$

It indicates that the momentum balance would be linear, if density was constant and the viscous part of the Piola–Kirchhoff stress tensor $J T_{\alpha\beta} F_{\gamma\beta}^{-1}$ defined by (2.88) (note that $T_{\alpha\beta}(\tau, \mathbf{X}) = \tau_{\alpha\beta}(t(\tau), \mathbf{x}(\tau, \mathbf{X}))$ is the spatial viscous stress $\tau_{\alpha\beta}$ transformed to the material description according to (2.80)) was a linear and local function of the Lagrangean displacement field. The first condition is satisfied by incompressible fluids (implying $J = 1$), but the second is in general, except for trivial flows, not satisfied.

The local or strong form of the energy balance in the material description can be obtained by standard arguments from the integral formulation using the Gauss divergence theorem. The result can be given for the total, specific energy composed of specific internal, kinetic and potential energy $e(\tau, \mathbf{X}) = u(\tau, \mathbf{X}) + \frac{1}{2}V_{\alpha}(\tau, \mathbf{X})V_{\alpha}(\tau, \mathbf{X}) - \Phi_{\alpha}(\tau, \mathbf{X})G_{\alpha}$ in the two-time form

$$\rho(0, \mathbf{X}) \frac{\partial e}{\partial \tau}(\tau, \mathbf{X}) = -\frac{\partial j_{\beta}^{(1)}}{\partial X_{\beta}}(\tau, \mathbf{X}) + \frac{\partial}{\partial X_{\beta}}\left(\Sigma_{\beta\alpha}^{(1)}(\tau, \mathbf{X}) \frac{\partial \Phi_{\alpha}}{\partial \tau}(\tau, \mathbf{X})\right) \quad (2.90)$$

containing the material heat flux vector defined by

$$j_\alpha^{(1)}(\tau, \mathbf{X}) = J F_{\alpha\beta}^{-1} j_\beta(\tau, \mathbf{X}) \quad (2.91)$$

and the first Piola–Kirchhoff stress tensor (2.88). The notion of flux is understood as the amount of a physical property (scalar, vector or tensor) moving through an integrable and orientable surface. The transported property is in slight misuse of terminology called flux density or flux vector.

The thermodynamic relations (2.14), (2.13) are local, hence do not change their form after transformation to the material description. The Navier–Stokes equations for a single, compressible Newtonian fluid in the material description are thus given by mass balance (2.87), momentum balance (2.89), energy balance (2.90) and the thermodynamic relations (2.14), (2.13). This system of equations is closed as for the spatial description.

The transformation between spatial and material description (2.80) furnished by the Lagrangean position field $\Phi(\mathbf{X}, \tau)$ is not a symmetry transformation as discussed in Sect. 2.1.3. In fact, the Navier–Stokes pdes are quite different in spatial (2.6), (2.7) and material (2.85), (2.86) description as the inspection of the nonlinearities shows. The nonlinearity of the pdes is clearly not an invariant as the transformation to the material description verifies. The convective nonlinearity in the spatial description of the momentum balance (2.7) vanishes by transformation to the material description (2.86), but the pressure gradient and the linear viscous terms become highly nonlinear images of their linear counterparts.

2.6 Rotation and Vorticity in the Material Description

Vorticity defined as the curl of velocity in the spatial description in Sect. 2.3 has a counterpart in the material description (Truesdell [39] Chap. VIII sec. 84, Casey and Naghdi [45], Bennett [11] Sect. 3.7, [5] Appendix A.4.2). The definition of the material vorticity Ω_α^0 (called Beltrami vorticity by some authors) associated with the spatial form (2.51) is in the material description [45] given in mixed formulation ($\omega_\beta(\mathbf{x}, t)$ is the spatial vorticity) by

$$\Omega_\alpha^0(\mathbf{X}, \tau) \equiv J F_{\alpha\beta}^{-1}(\Phi(\mathbf{X}, \tau), \tau) \omega_\beta(\Phi(\mathbf{X}, \tau), \tau) \quad (2.92)$$

It reduces to $\Omega_\alpha^0(0, \mathbf{X}) = \omega_\alpha(0, \mathbf{x})$ at the reference time $\tau = 0$, since $J(0, \mathbf{X}) = 1$ and $F_{\alpha\beta}(0, \mathbf{X}) = \delta_{\alpha\beta}$ hold and noting that the observer position $\mathbf{x} = \Phi(\mathbf{X}, \tau), t = \tau$ is the transformation of the position of a material point $\Phi(\mathbf{X}, \tau)$ to the spatial description furnished by the Lagrangean position field, which is the solution of the pathline odes (2.81). The definition (2.92) can be recast in strictly material form

$$\Omega_\alpha^0(\mathbf{X}, \tau) = \epsilon_{\beta\gamma\delta} F_{\alpha\beta}^{-1} F_{\eta\gamma}^{-1} \frac{\partial V_\delta}{\partial X_\eta} \quad (2.93)$$

where $V_\delta(\tau, \mathbf{X}) = v_\delta(t, \mathbf{x})$ and $\mathbf{x} = \Phi(\tau, \mathbf{X})$, $t = \tau$

$$\frac{\partial}{\partial x_\alpha} = F_{\beta\alpha}^{-1} \frac{\partial}{\partial X_\beta} \quad (2.94)$$

established in [10], Sect. 2.4.1 was used. Setting time $\tau = 0$ recovers the spatial definition of vorticity .

The multiplication of a tensor of order one or higher with the second-order tensor $J^{-1}F_{\alpha\beta}$ is called Piola transform $\pi_{\alpha\beta}$ as defined at the beginning of the present Sect. 2.5. The Piola transform (2.83) can be inverted, if the Lagrangean deformation gradient $F_{\alpha\beta}$ has a non-zero determinant $J = F \neq 0$. The spatial vorticity ω_α is under this condition $J(\tau, \mathbf{X}) > 0$ related to the material version according to the Piola transformation by

$$\omega_\alpha(\mathbf{x}, t) = J^{-1}F_{\alpha\beta}(\Phi^*(\mathbf{x}, t), t)\Omega_\beta^0(\Phi^*(\mathbf{x}, t), t) \quad (2.95)$$

where $\mathbf{X} = \Phi^*(\mathbf{x}, t)$, $\tau = t$ is the inverse transformation from spatial to material description (see Sect. 2.1 for details). The material vorticity Ω_α^0 is, therefore, the inverse Piola transform (2.83) of its spatial counterpart ω_α .

2.6.1 Divergence of the Material Vorticity

The material vorticity $\Omega_\alpha^0(\mathbf{X}, \tau)$ can be shown to satisfy the kinematic condition

$$\frac{\partial}{\partial X_\alpha} \Omega_\alpha^0(\mathbf{X}, \tau) = 0 \quad (2.96)$$

analogous to the zero divergence property of the spatial vorticity. It can be derived as follows. Applying the divergence operation with respect to the initial position \mathbf{X} to the definition (2.92) leads to

$$\frac{\partial}{\partial X_\alpha} \Omega_\alpha^0 = \frac{\partial}{\partial X_\alpha} (J F_{\alpha\beta}^{-1} \omega_\beta) = \omega_\beta \frac{\partial}{\partial X_\alpha} (J F_{\alpha\beta}^{-1}) + J F_{\alpha\beta}^{-1} \frac{\partial \omega_\beta}{\partial X_\alpha} \quad (2.97)$$

The first term on the right side can be evaluated using (25.128)

$$J \frac{\partial X_\alpha}{\partial x_\beta} = \frac{1}{2} \epsilon_{\beta\gamma\zeta} \epsilon_{\alpha\eta\omega} \frac{\partial \Phi_\gamma}{\partial X_\eta} \frac{\partial \Phi_\zeta}{\partial X_\omega} \quad (2.98)$$

hence

$$\frac{\partial}{\partial X_\alpha} (J F_{\alpha\beta}^{-1}) = \frac{1}{2} \epsilon_{\beta\gamma\zeta} \epsilon_{\alpha\eta\omega} \left(\frac{\partial^2 \Phi_\gamma}{\partial X_\alpha \partial X_\eta} \frac{\partial \Phi_\zeta}{\partial X_\omega} + \frac{\partial \Phi_\gamma}{\partial X_\eta} \frac{\partial^2 \Phi_\zeta}{\partial X_\alpha \partial X_\omega} \right) \quad (2.99)$$

Renaming subscripts and using the properties of the Levi-Civita symbol $\epsilon_{\alpha\beta\gamma}$ results in

$$\frac{\partial}{\partial X_\alpha} (J F_{\alpha\beta}^{-1}) = \epsilon_{\beta\gamma\eta} \epsilon_{\alpha\eta\omega} \frac{\partial^2 \Phi_\gamma}{\partial X_\alpha \partial X_\eta} \frac{\partial \Phi_\zeta}{\partial X_\omega} = 0 \quad (2.100)$$

The expression on the right side is zero since the second derivative is symmetric with respect to the subscripts α and η but the Levi-Civita symbol $\epsilon_{\alpha\eta\omega}$ is antisymmetric, hence all terms cancel. It follows that the divergence of the material vorticity is

$$\frac{\partial}{\partial X_\alpha} \Omega_\alpha^0 = J F_{\alpha\beta}^{-1} \frac{\partial \omega_\beta}{\partial X_\alpha} \quad (2.101)$$

which is according to (2.94) (see Sect. 2.4.1 in [10]) given by

$$\frac{\partial \Omega_\alpha^0}{\partial X_\alpha} = J \frac{\partial \omega_\beta}{\partial x_\beta} = 0 \quad (2.102)$$

The right side is zero since the spatial vorticity has zero divergence for kinematic reasons and the claim is proved for incompressible and compressible fluids. Further kinematic properties of vorticity in the material description can be found in Casey and Naghdi [45] and Wu et al. [5] Appendix A.4.2.

2.6.2 Material Vorticity in Plane Flows

The relation between material and spatial vorticity is particularly simple for plane flows. Let the flow be in the $x_1 - x_2$ plane, then is the spatial vorticity $\omega_\alpha = \omega(t, x_1, x_2) \delta_{\alpha 3}$ in the direction normal to the plane of the flow. The Lagrangean deformation gradient emerges as (note that $\Phi_\alpha(\tau, X_1, X_2)$ for $\alpha = 1, 2$ and $\Phi_3 = X_3$ hold for plane flows)

$$\mathbf{F} = \begin{pmatrix} \frac{\partial \Phi_1}{\partial X_1} & \frac{\partial \Phi_1}{\partial X_2} & 0 \\ \frac{\partial \Phi_2}{\partial X_1} & \frac{\partial \Phi_2}{\partial X_2} & 0 \\ 0 & 0 & 1 \end{pmatrix} \quad (2.103)$$

with inverse

$$\mathbf{F}^{-1} = \begin{pmatrix} \frac{\partial \Phi_1^*}{\partial x_1} & \frac{\partial \Phi_1^*}{\partial x_2} & 0 \\ \frac{\partial \Phi_2^*}{\partial x_1} & \frac{\partial \Phi_2^*}{\partial x_2} & 0 \\ 0 & 0 & 1 \end{pmatrix} \quad (2.104)$$

It follows from (2.92) that the material vorticity Ω_α^0 has only one non-zero component as its spatial counterpart

$$\Omega_\alpha^0(\mathbf{X}, \tau) = J F_{\alpha 3}^{-1}(\Phi(\mathbf{X}, \tau), \tau) \omega_3(\Phi(\mathbf{X}, \tau), \tau) \rightarrow \Omega_3^0 = J \omega_3 \quad (2.105)$$

If the plane flow is incompressible $J = 1$ it follows that $\Omega_3^0 = \omega_3$ holds. Material and spatial vorticity are thus the same for incompressible, plane flows. For plane flows of a compressible fluid, the mass balance in the material description (2.87) implies that the difference between spatial and material vorticities is proportional to the density ratio at the material point \mathbf{X}

$$\Omega_3^0(\tau, \mathbf{X}) = \frac{R(\tau, \mathbf{X})}{R(0, \mathbf{X})} \omega_3(t, \mathbf{x}) \quad (2.106)$$

(note that $R(\tau, \mathbf{X})$ denotes density in the material description). This result is stated in mixed formulation, where $t = \tau$ and $\mathbf{x} = \Phi(\tau, \mathbf{X})$ is the transformation rule for spatial and material descriptions. It is seen from this relation that plane combustion flows may produce significant deviations between spatial and material vorticities near stoichiometric conditions (i.e. high temperature regions). Consider a material point \mathbf{X} that started in the cold, unreacted mixture and arrives at time τ in the flame zone. The density $R(\tau, \mathbf{X})$ in the flame is in the absence of shock waves significantly smaller than in the cold region, hence is the material vorticity $\Omega_3^0(\tau, \mathbf{X})$ in the flame significantly smaller than the Eulerian vorticity $\omega_3(t, \mathbf{x})$ at the location $\mathbf{x} = \Phi(\tau, \mathbf{X})$ and time $t = \tau$.

2.6.3 Frozen Vector Fields

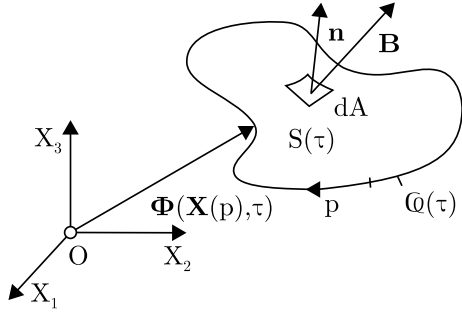
Vector fields transported by and interacting with another vector field formally called velocity play an important role for the dynamics of ideal fluids and magnetohydrodynamics (Vladimirov and Moffatt [5, 46]). An important example is vorticity in flows of ideal fluids, it can be shown to be a frozen vector field as long as it is non-singular. Frozen vector fields are thus defined and their transport pdes derived in the spatial and material descriptions.

Solenoidal fields, i.e. $\nabla \cdot \mathbf{v} = 0$, $\nabla \cdot \mathbf{B} = 0$, are considered, where the vector field transported by the velocity field \mathbf{v} is denoted by \mathbf{B} . Let \mathcal{S} be an open, orientable surface with finite area spanned by the closed, rectifiable, unknotted line $\partial\mathcal{S} = \mathcal{C}$ (called admissible circuit) as sketched in Fig.2.1. The flux through the surface \mathcal{S} is defined by

$$F(\mathbf{B}, \mathcal{C}) \equiv \int_{\mathcal{S}} dA \mathbf{n} \cdot \mathbf{B} \quad (2.107)$$

where \mathbf{n} is the unit normal vector (which can be chosen in a unique way, since the surface is orientable). A frozen vector field is defined in the material description by

Fig. 2.1 Flux $\mathbf{n} \cdot \mathbf{B}$ through an open surface $S(\tau)$ bounded by an unknotted, closed line $C(\tau)$ in a 3-d flow field, p denotes a Lagrangean line parameter



Definition: The vector field \mathbf{B} is frozen with respect to the velocity field \mathbf{v} iff the flux of \mathbf{B} through any admissible, materially invariant circuit is independent of time, i.e.

$$\frac{\partial}{\partial \tau} F(\mathbf{B}, \mathcal{C}) = 0 \quad (2.108)$$

holds for all admissible circuits \mathcal{C} .

The transport pde in the spatial/Eulerian description for the frozen vector field follows from the definition (proof in [10] Sect. 2.16.2) in the form

$$\frac{\partial B_\alpha}{\partial t} + v_\beta \frac{\partial B_\alpha}{\partial x_\beta} = B_\beta \frac{\partial v_\alpha}{\partial x_\beta} \quad (2.109)$$

It suggests the definition of the frozen field operator L_v (Vladimirov and Moffatt [46])

$$L_v \mathbf{B} \equiv \frac{D \mathbf{B}}{D t} - (\mathbf{B} \cdot \nabla) \mathbf{v} \quad (2.110)$$

hence $L_v \mathbf{B} = 0$ for \mathbf{B} frozen and vice versa. In the material description, it emerges in the form (proof in [10] Sect. 2.16.3)

$$\frac{\partial B_\alpha}{\partial \tau} = \frac{1}{2} \epsilon_{\beta\gamma\zeta} \epsilon_{\delta\eta\omega} F_{\gamma\eta} F_{\zeta\omega} B_\beta \frac{\partial V_\alpha}{\partial X_\delta} \quad (2.111)$$

where

$$F_{\alpha\beta} \equiv \delta_{\alpha\beta} + \int_0^\tau d\tau' \frac{\partial V_\alpha}{\partial X_\beta}(\tau', \mathbf{X}) \quad (2.112)$$

is the deformation gradient disguised as functional of the Lagrangean velocity, expressing the time rate of change following a material point in terms of velocity $\mathbf{V}(\tau, \mathbf{X})$ and the frozen vector field $\mathbf{B}(\tau, \mathbf{X})$. This is the material/Lagrangean counterpart of the spatial pde (2.109) for a frozen vector field.

A frozen vector field is not materially invariant locally (at a chosen material point \mathbf{X}), it can change its (vector invariant) length and its orientation as the flow evolves, but it cannot spread into material regions, where it was zero initially. The topological properties of the support (the hull of the set of material points where the frozen field is non-zero) of a frozen vector field cannot change with time as long as the fields remain smooth. This does not hold if singularities appear.

2.7 Velocity Gradient Tensor in the Spatial Description

The velocity gradient (or rate of deformation) tensor is defined in the spatial description by

$$A_{\alpha\beta}(t, \mathbf{x}) \equiv \frac{\partial v_\alpha}{\partial x_\beta} \quad (2.113)$$

It has three invariants, one of which is the trace $A_{\alpha\alpha}$ being zero for incompressible fluids, the remaining non-zero invariants are defined by

$$Q \equiv -\frac{1}{2} A_{\alpha\beta} A_{\beta\alpha} \quad (2.114)$$

$$R \equiv -\frac{1}{3} A_{\alpha\beta} A_{\beta\gamma} A_{\gamma\alpha} \quad (2.115)$$

The transport pde for the velocity gradient tensor is obtained without difficulty by manipulating the Navier–Stokes pdes (2.1), (2.2) resulting for incompressible fluids in the transport pde

$$\frac{\partial A_{\alpha\beta}}{\partial t} + v_\gamma \frac{\partial A_{\alpha\beta}}{\partial x_\gamma} = -A_{\alpha\gamma} A_{\gamma\beta} - P_{\alpha\beta} + \frac{1}{Re} \frac{\partial^2 A_{\alpha\beta}}{\partial x_\gamma \partial x_\gamma} + \frac{\partial g_\alpha}{\partial x_\beta} \quad (2.116)$$

where $g_\alpha(t, \mathbf{x})$ denotes a solenoidal external force field. The pressure Hessian is defined by

$$P_{\alpha\beta} \equiv \frac{\partial^2 p}{\partial x_\alpha \partial x_\beta} \quad (2.117)$$

If the second derivatives are continuous in an open neighbourhood $U \subset \mathbb{R}^3$, then is the Hessian matrix symmetric in U , since the order of differentiations does not matter. The Hessian is an important tool for the analysis of critical points of manifolds in Morse theory [47].

The trace of $P_{\alpha\beta}$ is the (standard) Laplacian of the pressure, hence

$$\Delta P = -A_{\alpha\beta} A_{\beta\alpha} \quad (2.118)$$

holds for incompressible fluids. Equation (2.116) can be given in the form [48]

$$\frac{DA_{\alpha\beta}}{Dt} = -(A_{\alpha\gamma}A_{\gamma\beta} - \frac{1}{3}\delta_{\alpha\beta}A_{\gamma\delta}A_{\delta\gamma}) + H_{\alpha\beta}^P + H_{\alpha\beta}^\nu + \frac{\partial g_\alpha}{\partial x_\beta} \quad (2.119)$$

using the substantial derivative and the abbreviations

$$H_{\alpha\beta}^P \equiv -(P_{\alpha\beta} - \frac{1}{3}\delta_{\alpha\beta}\Delta P) \quad (2.120)$$

for the traceless pressure Hessian and

$$H_{\alpha\beta}^\nu \equiv \frac{1}{Re} \frac{\partial^2 A_{\alpha\beta}}{\partial x_\gamma \partial x_\gamma} \quad (2.121)$$

for the viscous terms. This version (2.119) of the transport pde for $A_{\alpha\beta}$ suggests an intrinsic and closed set of equations in the material description, i.e. a system of odes valid along pathlines and amenable to analytic solution, called restricted Euler system

$$\frac{DA_{\alpha\beta}}{Dt} = -(A_{\alpha\gamma}A_{\gamma\beta} - \frac{1}{3}\delta_{\alpha\beta}A_{\gamma\delta}A_{\delta\gamma}) \quad (2.122)$$

if the sum of the pressure term $H_{\alpha\beta}^P$, the viscous term $H_{\alpha\beta}^\nu$ and the external force $\frac{\partial g_\alpha}{\partial x_\beta}$ is neglected. It is called the homogeneous case of (2.119).

The velocity gradient (or rate of deformation) tensor $A_{\alpha\beta}$ governed by the general pde (2.116) is subject to convection, self-amplification/attenuation, the pressure Hessian $P_{\alpha\beta}$, viscous effects and external forces. It has been the subject of intensive research (Vieillefosse [49, 50], Cantwell [51], Gibbon et al. [52], Wilczek and Meneveau [53], Meneveau [48] and references therein), since it contains information on the smallest scales of a turbulent flow as can be seen in the structure of the Fourier-transformed velocity gradient tensor.

2.8 Problems for this Chapter

Problem 2.1 Derive the dimensional vorticity pde (2.62) for a single, compressible Newtonian fluid using Cartesian coordinates.

Problem 2.2 Verify that (2.69) is the solution of the vorticity pde (2.65) in $\mathcal{D} = R^3$ for inviscid and barotropic fluids.

Problem 2.3 Consider the flow of an inviscid, incompressible fluid with non-zero vorticity governed by the Euler pdes in $\mathcal{D} = R^3$, let the vorticity be specified initially as a smooth vector field $\Omega_\alpha(0, \mathbf{X}) \in L^2_{\mathcal{D}}$, then establish the equation for the

Lagrangian position field $\Phi_\alpha(\tau, \mathbf{X})$ in terms of vorticity $\Omega_\alpha(0, \mathbf{X})$ at the reference time.

Problem 2.4 Consider the flow of an incompressible, Newtonian fluid. Define the Lamb vector by Eq. (2.54) $\mathbf{L} \equiv \boldsymbol{\omega} \times \mathbf{v}$, where $\boldsymbol{\omega} \equiv \nabla \times \mathbf{v}$ denotes the vorticity vector.

2.4.1 Show that the convective acceleration is the sum of the Lamb vector and the gradient of a scalar field.

2.4.2 Compute the Lamb vector, the flexion vector (2.55) $\mathbf{f} \equiv \nabla \times \boldsymbol{\omega}$ and the divergence of the Lamb vector for an unidirectional parallel flow

$$v_\alpha = U(x_2, t)\delta_{\alpha,1}$$

in Cartesian coordinates.

2.4.3 Establish the transport pde for the Lamb vector and its divergence.

Problem 2.5 Determine the symmetries of the heat pde

$$\frac{\partial T}{\partial t} - \frac{\partial^2 T}{\partial x^2} = 0$$

defined on $\mathcal{D} = [0, \infty] \times \mathbb{R}^1$.

2.5.1 Change the notation to $x \rightarrow x_1$, $t \rightarrow x_2$, $T \rightarrow y_1$ and determine the prolonged operator $X^{(2)}$ and the condition for symmetry transformations.

2.5.2 Compute the total derivatives determining the infinitesimals appearing in the condition for symmetry transformations.

2.5.3 Establish the equations for the infinitesimals.

2.5.5 Solve the equations for the infinitesimals.

2.5.6 Choose a set of values for the parameters and compute the global transformation.

Problem 2.6 Integrate the Euler pdes (2.9)

$$\frac{\partial v_\alpha}{\partial x_\alpha} = 0$$

$$\frac{\partial v_\alpha}{\partial t} + v_\beta \frac{\partial v_\alpha}{\partial x_\beta} = - \frac{\partial p}{\partial x_\alpha}$$

governing the motion of an incompressible, inviscid fluid, along a pathline (Weber's equation).

2.6.1 Write the Euler pdes in mixed spatial/material description.

2.6.2 Transform to strictly material form.

2.6.3 Reformulate the momentum balance using (2.94) such that integration along a pathline starting at \mathbf{X} becomes possible.

References

1. Lamb, H.: *Hydrodynamics*. 3rd ed. Cambridge University Press (1906)
2. Landau, L.D., Lifshitz, E.M.: *Fluid Mechanics*. Pergamon Press, Oxford, U.K. (1956)
3. Serrin, J.: The initial value problem for the Navier–Stokes equations. In: Langer, R. (ed.) *Nonlinear Problems, Symp. Proc.*, University of Wisconsin Press, p. 69 (1963)
4. Majda, A.J., Bertozzi, A.L.: *Vorticity and Incompressible Flow*. Cambridge University Press, Cambridge, U.K. (2002)
5. Wu, J.-Z., Ma, H.-Y., Zhou, M.-D.: *Vorticity and Vortex Dynamics*. Springer, Berlin (2006)
6. Guénault, A.M.: *Basic Superfluids*. Taylor & Francis, London, U.K. (2003)
7. Vinen, W.F.: Superfluid turbulence: experiments, physical principles, and outstanding problems. In: Smits, A.J. (ed.) *IUTAM Symposium on Reynolds Number Scaling in Turbulent Flow*, pp. 101–108. Kluwer Academic Publishers, Dordrecht (2004)
8. Donnelly, R.J.: Background on Superfluid turbulence. In: Smits, A.J. (ed.) *IUTAM Symposium on Reynolds Number Scaling in Turbulent Flow*, pp. 92–100. Kluwer Academic Publishers, Dordrecht (2004)
9. Skrbek, L.: Quantum turbulence. *J. Phys. Conf. Ser.* **318**, 012004 (2011)
10. Kollmann, W.: *Fluid Mechanics in Spatial and Material Description*. University Readers, San Diego (2011)
11. Bennett, A.: *Lagrangian Fluid Dynamics*. Cambridge University Press, Cambridge, U.K. (2006)
12. Cantwell, B.J.: *Introduction to Symmetry Analysis*. Cambridge University Press, U.K. (2002)
13. Gallavotti, G.: *Foundations of Fluid Dynamics*. Springer, Berlin (2002)
14. Tsinoberry, A.: *An Informal Conceptual Introduction to Turbulence*, 2nd edn. Springer, Dordrecht (2009)
15. Poinsot, T., Veynante, D.: *Theoretical and Numerical Combustion*. R.T. Edwards, Philadelphia, PA (2001)
16. Frisch, U.: *Turbulence: The Legacy of A.N. Kolmogorov*. Cambridge University Press (1995)
17. Oberlack, M.: *Symmetrie, Invarianz und Selbstähnlichkeit in der Turbulenz*. Shaker, Aachen, Germany (2000)
18. Oberlack, M., Waclawczyk, M., Rosteck, A., Avsarkisov, V.: Symmetries and their importance for statistical turbulence theory. *Bull. JSME* **2**, 1–72 (2015)
19. Duistermaat, J.J., Kolk, J.A.C.: *Lie Groups*. Springer, Berlin (2000)
20. Von Wahl, W.: *The Equations of Navier–Stokes and Abstract Parabolic Equations*. Vieweg, Braunschweig (1985)
21. Constantin, P., Foias, C.: *Navier–Stokes Equations*. University of Chicago Press (1988)
22. Kreiss, H.O., Lorentz, J.: *Initial-Boundary Value Problems and the Navier–Stokes Equations*. Academic Press (1989)
23. Sohr, H.S.: *The Navier–Stokes Equations*. Springer, Basel (2001)
24. Constantin, P.: Euler Equations, Navier–Stokes equations and turbulence. In: *Mathematical Foundation of Turbulent Viscous Flows*. Lecture Notes in Mathematics, vol. 1871, pp. 1–43 (2006)
25. www.claymath.org/millennium/
26. Eyink, G.L.: Energy dissipation without viscosity in ideal hydrodynamics: fourier analysis and local energy transfer. *Physica D* **78**, 222–240 (1994)
27. Duchon, J., Robert, R.: Inertial energy dissipation for weak solutions of incompressible Euler and Navier–Stokes equations. *Nonlinearity* **13**, 249–255 (2000)
28. Spalart, P.R.: *Numerical Simulation of Boundary Layers. Part 1. Weak Formulation and Numerical Method*, NASA TM-88222 (1986)
29. Seregin, G.: *Lecture Notes on Regularity Theory for the Navier–Stokes Equations*. World Scientific, New Jersey (2015)
30. Hopf, E.: Über die Anfangswertaufgabe für die hydrodynamischen Grundgleichungen. *Math. Nachrichten* **4**, 213–231 (1950)

31. Kiselev, A.A., Ladyshenskaya, O.A.: On existence and uniqueness of the solution of the non-stationary problem for a viscous incompressible fluid. *Izvestiya Akad. Nauk SSSR* **21**, 655 (1957)
32. Kuksin, S., Shirikyan, A.: Mathematics of two-dimensional turbulence, Cambridge Tracts in Mathematics, vol. 194. Cambridge University Press, U.K. (2012)
33. Serrin, J.: On the interior regularity of weak solutions of the Navier-Stokes equations. *Arch. Rat. Mech. Anal.* **9**, 187–196 (1962)
34. Pileckas, K.: Navier-Stokes system in domains with cylindrical outlets to infinity. In: Friedlander, S., Serre, D. (eds.) *Handbook of Mathematical Fluid Dynamics*, vol. 4, North Holland, pp. 447–647 (2007)
35. Temam, R.: *Infinite Dimensional Dynamical Systems in Mechanics and Physics*. Springer, New York (1988)
36. Vishik, M.J., Fursikov, A.V.: *Mathematical Problems of Statistical Hydromechanics*. Kluwer Academic Publication, Dordrecht (1988)
37. Vishik, M.J.: *Asymptotic Behaviour of Solutions of Evolutionary Equations*. Cambridge University Press, Lezioni Lincee (1992)
38. Morse, E.C.: Eigenfunctions of the curl in cylindrical geometry. *J. Math. Phys.* **46**, 113511-1–113511-13 (2005)
39. Truesdell, C.A.: *The Kinematics of Vorticity*. Indiana University Press, Bloomington, Indiana (1954)
40. Brown, G.L., Roshko, A.: On density effects and large structure in turbulent mixing layers. *JFM* **64**, 775–816 (1974)
41. Constantin, P.: *Analysis of Hydrodynamic Models*. CBMS-NSF Regional Conference Series in Applied Mathematics (2017)
42. Ciarlet, P.G.: *Mathematical Elasticity: Three-dimensional Elasticity*, vol. 1. Elsevier Sci. Pub, Amsterdam, The Netherlands (1988)
43. Monin, A.S., Yaglom, A.M.: *Statistical Fluid Mechanics: Mechanics of Turbulence*, vol. 1. The MIT Press, Cambridge Mass (1975)
44. Pope, S.B.: *Turbulent Flows*. Cambridge University Press, Cambridge, U.K. (2001)
45. Casey, J., Naghdi, P.M.: On the lagrangian description of vorticity. *Arch. Rational Mech. Anal.* **115**, 1–14 (1991)
46. Vladimirov, V.A., Moffatt, H.K.: On general transformations and variational principles for the magnetohydrodynamics of ideal fluids. Part 1. Fundamental principles. *JFM* **283**, 125–139 (2001)
47. Milnor, J.: *Morse Theory*. Princeton University Press (1963)
48. Meneveau, C.: Lagrangian dynamics and models of the velocity gradient tensor in turbulent flows. *Annua. Rev. Fluid Mech.* **43**, 219–245 (2011)
49. Vieillefosse, P.: Local interaction between vorticity and shear in a perfect incompressible fluid. *J. Phys. France* **43**, 837–842 (1982)
50. Vieillefosse, P.: Internal motion of a small element of fluid in an inviscid flow. *Physica A* **125**, 150–162 (1984)
51. Cantwell, B.J.: Exact solution of a restricted Euler equation for the velocity gradient tensor. *Phys. Fluids A* **4**, 782–793 (1992)
52. Gibbon, J.D., Galanti, B. and Kerr, R.M.: Stretching and compression of vorticity in the 3D euler equations. In: Hunt, J.C.R., Vassilicos, J.C. (eds.) *Turbulence Structure and Vortex Dynamics*. Cambridge University Press (2000)
53. Wilczek, M., Meneveau, C.: Pressure Hessian and viscous contributions to velocity gradient statistics based on Gaussian random fields. *JFM* **756**, 191–225 (2014)

Chapter 3

Basic Properties of Turbulent Flows



Turbulent flows possess several properties observed in and deduced from experiments and direct numerical simulation (DNS) of the Navier–Stokes equations, which set them apart from three-dimensional and unsteady laminar flows. They will be compiled for later reference and a brief discussion will be given. At the end of the section, a working definition of turbulence is proposed, which is deduced from these properties. Only Newtonian fluids and the idealization of an inviscid fluid will be considered. The spatial description is used throughout this section.

(T.1) Turbulent motion is chaotic and random

Consider the flow of a gaseous or liquid Newtonian fluid described by a set of variables $\Phi_\alpha(\mathbf{x}, t)$, which may be scalars, vectors or tensors, and governed by the Navier–Stokes system of nonlinear pdes. Consider a thought experiment, where initial and boundary conditions are known with small but finite accuracy. The variables Φ_α are now ideally measured without error at a position \mathbf{x} and at a time t . If the flow is turbulent, it is not possible by repetition of the experiment to obtain the same values for the variables $\Phi_\alpha(\mathbf{x}, t)$ at the fixed position \mathbf{x} and a chosen time t with an accuracy commensurate to the initial value. This is in contrast to laminar flows, where the repetition of the experiment produces results within the error of the initial and boundary conditions. If the values of Φ_α in turbulent flow are recorded for a large number of experiments, they scatter significantly and it follows that the Φ_α do not possess reproducible values at \mathbf{x} and t for finite accuracy of the initial and boundary conditions. Note that this does not imply that the solution of the Navier–Stokes equations is not unique, a question which is unfortunately still open for 3-d flows. It is observed that the level (intensity) of these fluctuations is several orders of magnitude larger than the level of the thermal fluctuations of the fluid in the ranges of temperature and pressure encountered in most applications and in the atmosphere near the surface of the earth (Figs. 3.1 and 3.2).

The apparent randomness of turbulent flows is not induced by random boundary conditions or stochastic coefficients in the equations, but the sensitivity of the solution of the Navier–Stokes equations to the initial conditions for a certain range of values of dimensionless parameters such as the Reynolds number. This property is inherent

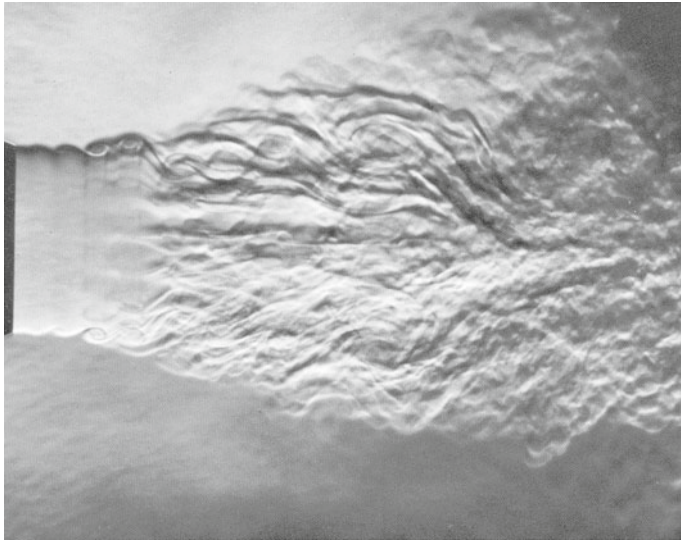


Fig. 3.1 Visualization of a low Mach number turbulent round jet (Bradshaw et al. [1])

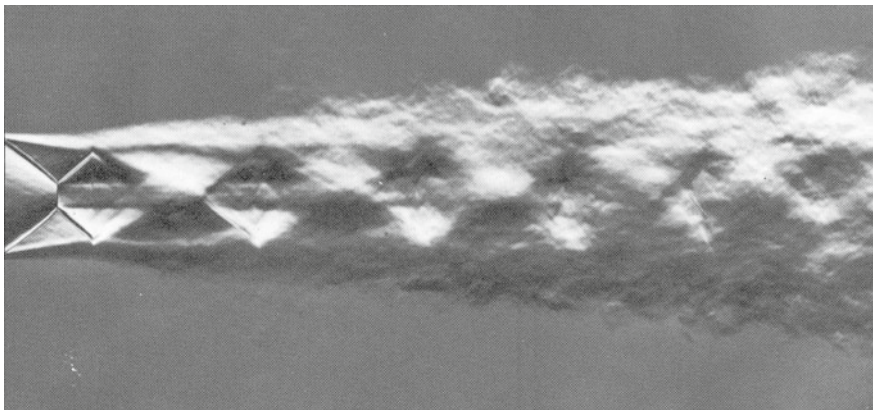


Fig. 3.2 Visualization of a supersonic, turbulent round jet (Oertel [2]) at a Mach number $M = 1.8$, slightly underexpanded showing the diamond-shaped pattern of oblique shock waves

in the nonlinearity of the Navier–Stokes equations, as no linear and non-singular system of equations displays this sensitivity towards initial conditions. Chaos in low-dimensional dynamical systems can be defined by the properties (Hasselblatt and Katok [3]):

- (i) Sensitive dependence on initial conditions.
- (ii) topological mixing; A continuous map $T_t : \Omega \rightarrow \Omega$ of a topological space Ω onto itself is topologically mixing, if there exists an integer $N > 0$ such that for two open sets $A, B \subset \Omega$ $T_n(A) \cap B \neq \emptyset$ for $n > N$ applications of the map T_t .

(iii) periodic orbits must be dense. Periodic solutions (orbits) of the system are dense in phase space Ω if every point is approached arbitrarily close by the solutions.

The phase space for turbulent flows (Chap. 5) is an infinite-dimensional Banach space, an element (point) in the phase space is a 3-d vector field evolving in time according to the Navier–Stokes equations. The distance between two points is measured with the norm of the Banach space, hence condition (iii) can be applied to the phase space of turbulent flows.

Apparent randomness can also be found in the guise of arbitrariness of the limit values of conditionally convergent series. An example for this is the alternating harmonic series

$$\sum_{k=1}^{\infty} \frac{(-1)^{k+1}}{k} \quad (3.1)$$

which is convergent according to the Leibniz test, but whose limit value depends crucially on the way the partial sums are arranged, in fact any limit value can be obtained (Riemann series theorem, Rudin [4]). The limit value is usually given as $\ln 2$, which is the value for $x = 1$ of the Mercator series for the natural logarithm

$$\ln(1+x) = \sum_{k=1}^{\infty} \frac{(-1)^{k+1}}{k} x^k \quad (3.2)$$

This series is absolutely convergent for $0 < x < 1$ and conditionally convergent for $x = 1$. If the positive and negative terms in the alternating harmonic series (3.1) for $x = 1$ are summed separately, the result is infinity minus infinity, hence indeterminate. Choosing an arbitrary, but finite limit value, say $a \neq \ln 2 > 0$, the partial sums can be arranged by selecting enough terms for partial sums just above the chosen limit value and then partial sums just below it, alternating this construction and the limit will be a , Klauder [5] Sect. 1.3. It is clear that for conditionally convergent series the result depends not only on the terms of the series but also on the way the terms for the partial sums are arranged. For absolutely convergent series the limit is independent of the arrangement of the terms in the partial sums. The summation of a conditionally convergent series can be arranged with the aid of an index map $I(k)$, $k = 1, \dots, \infty$

$$S_I \equiv \sum_{k=1}^{\infty} \frac{(-1)^{I(k)+1}}{I(k)}$$

with the identity map $I(k) = k$ generating the natural logarithm of two for the present example. The value of the series $-\infty < S_I < \infty$ is then determined by the index map, hence by the coefficients and their arrangement. The latter is regarded as an elementary structural property of a conditionally convergent series.

The dependence of the limit of an alternating, conditionally convergent series on the ordering of the terms according to the Riemann series theorem suggests a possible scenario for the formation of a singularity. Let the terms in the series be the

coefficients of a functional expansion of vorticity in a turbulent flow and let sum of the positive terms and the sum of the negative terms be infinite, then it is conceivable that the temporal evolution of the coefficients is such that the negative (or positive) terms are diminished and asymptotically an infinite subset of them vanishes. The conditionally convergent series becomes asymptotically divergent and a singularity is created without any individual term becoming unbounded.

The notion of conditional convergence can be generalized to Hilbert and Banach spaces as weak convergence, Vishik and Fursikov [6], Temam [7], Rudin [8]. Consider a Hilbert space H with scalar product (x, y) , weak convergence is then defined for $x_n, x \in H$ by

$$x_n \xrightarrow{w} x \iff (x_n, y) \rightarrow (x, y) \forall y \in W \quad (3.3)$$

It is, of course, possible to artificially introduce randomness via stochastic momentum sources or boundary values, but these do not qualify as criterium for turbulence. However, stochastic momentum sources are a popular computational device to create homogeneous, non-decaying turbulence on the computer (Davidson [9], Sagaut and Cambon [10]).

Summary

The notion of conditionally convergent series and weakly convergent functionals can be imagined as a mechanism to generate non-uniqueness and singularities. Considering the expansion of a turbulent field variable (scalar, velocity, etc.) at a fixed point \mathbf{x} , let the expansion of the field variable $\Phi(t, \mathbf{x})$ at \mathbf{x}

$$\Phi(t, \mathbf{x}) = \sum_{n=0}^{\infty} \Phi_n(t) \Psi_n(\mathbf{x})$$

w.r.t. an ONS basis $\mathcal{B} = \{\Psi_n, n = 0, 1, 2, \dots\}$ be weakly convergent. As the flow evolves in time, the basis remains unchanged, but the coefficients change. It is conceivable that a new state at \mathbf{x} is a rearrangement of the previous coefficients. The result would be a different limit value solely due to the rearrangement or even a singularity if infinitely many positive or negative terms are eliminated. This property is taken into account for Schauder bases spanning Banach or Hilbert spaces by requiring that the basis vectors are ordered.

(T.2) Turbulent motion is vortical

Rotation measured by vorticity plays an important role in turbulent flows, since irrotational flows cannot become chaotic. Vorticity in the spatial/Eulerian description is defined by Eq. (2.51) as the curl of velocity, hence a solenoidal vector field. Observations show that turbulent flows exhibit a high level of vorticity fluctuations. It is possible to create random fluctuations of velocity which are irrotational ($\omega_\alpha = 0$ everywhere in the flow domain \mathcal{D}) by random movement of a bounding surface, for instance. However, the flow created in such a way does not depend sensitively on the initial and boundary conditions and is, therefore, not considered turbulent. This

can be seen for incompressible Newtonian fluids as follows. The condition of zero vorticity $\omega_\alpha(\mathbf{x}, t) = 0$ for all $\mathbf{x} \in \mathcal{D}$ and mass balance (2.6) $\nabla \cdot \mathbf{v} = 0$ imply that there exists a potential $\Psi(\mathbf{x}, t)$, such that

$$v_\alpha = -\frac{\partial \Psi}{\partial x_\alpha} \quad (3.4)$$

holds and consequently

$$\Delta \Psi = 0 \quad (3.5)$$

plus boundary conditions of Dirichlet or Neumann type, determines Ψ in \mathcal{D} . The important fact is now that the equation governing this type of flow is linear with linear boundary conditions. The solution of the Laplace equation for the potential is uniquely determined and depends smoothly on the boundary conditions. The temporal evolution of the flow is completely specified by the evolution of the boundary conditions and it follows that two solutions that are close initially measured with an appropriate norm remain so for all time. No sensitivity with respect to initial conditions is observed. Conversely, if the boundary conditions are non-random with respect to finite accuracy, the flow remains non-random in this sense in contrast to vortical flows, which can become random with respect to non-random initial and boundary conditions known to finite accuracy. It follows that the latter property requires non-zero vorticity.

(T.3) Turbulent motion is dissipative

Flows bounded by fixed or moving walls require non-zero viscosity in order to satisfy the no-slip boundary condition that the fluid velocity is equal to the wall velocity at the wall. In laminar flows at high Reynolds numbers the zone, where the viscous shear stresses are significant, is limited to a thin layer next to the boundary with the no-slip condition, or the viscous region originates at a no-slip boundary such as the backward-facing step. It is a region of small volume and large surface area with known or at least predictable location. In turbulent flows, on the other hand, the regions with large vorticity and dissipation rates are characterized by small volume and large surface area of the bounding iso-surface, but the geometrical properties and the location of these regions are fluctuating and thus not known a priori. Therefore, it is evident that the observation of vorticity and dissipation rate above a specified non-zero level at a fixed point in the flow field leads to a signal that is highly intermittent (intermittency is defined in Chap. 16). There is considerable evidence that the regions, where high values of vorticity and dissipation are concentrated, are not space filling [11, 12]. Hence, it can be argued that for maintained turbulence in the limit of infinite Reynolds numbers the region of large values of vorticity (and dissipation rate) has zero volume and infinite surface area with fractal dimension between two and three (Mandelbrot [13, 14], Sreenivasan and Meneveau [11] and references therein). Due to the work performed in these regions by the viscous stresses, the internal energy of the fluid is increased at the expense of the kinetic energy contained in the fluctuating turbulent

motion. If no energy is supplied by external volume forces or via the boundaries of the flow domain (by maintaining a pressure gradient in a pipe flow, for instance) to make up for the kinetic energy converted to internal energy, the turbulence is observed to decay.

The relation between vorticity and viscosity can be elucidated by considering the dimensionless mass and momentum balances for an incompressible Newtonian fluid. The definition of vorticity shows that its components are the skew-symmetric part (called rotation or spin tensor $R_{\alpha\beta}$) of the deformation rate tensor

$$2R_{\alpha\beta} \equiv \frac{\partial v_\alpha}{\partial x_\beta} - \frac{\partial v_\beta}{\partial x_\alpha} = \epsilon_{\alpha\beta\gamma}\omega_\gamma \quad (3.6)$$

The momentum balance

$$\frac{\partial v_\alpha}{\partial t} + v_\beta \frac{\partial v_\alpha}{\partial x_\beta} = -\frac{\partial p}{\partial x_\alpha} + \frac{1}{Re} \Delta v_\alpha - \frac{1}{Fr} \frac{\partial \Psi}{\partial x_\alpha} \quad (3.7)$$

(the pressure is actually p/ρ and Ψ denotes the potential of an external force field, the Froude number (22.2) is $Fr \equiv \frac{\tilde{U}^2}{\tilde{\rho}\tilde{g}\tilde{L}}$ with \tilde{g} being a characteristic value of $\nabla\Psi$) appears then in the vortical form as (called incompressible Crocco–Vazsonyi equation, Wu et al. [15], Sect. 2.4)

$$\frac{\partial v_\alpha}{\partial t} + \frac{1}{2} \frac{\partial}{\partial x_\alpha} (v_\beta v_\beta) = -\frac{\partial p}{\partial x_\alpha} + \epsilon_{\alpha\beta\gamma} (v_\beta \omega_\gamma - \frac{1}{Re} \frac{\partial \omega_\gamma}{\partial x_\beta}) - \frac{1}{Fr} \frac{\partial \Psi}{\partial x_\alpha} \quad (3.8)$$

It follows at once from this version of the momentum balance that irrotational flow implies the Bernoulli equation (see Truesdell [16] for proof)

$$\frac{\partial v_\alpha}{\partial t} + \frac{\partial H}{\partial x_\alpha} = 0 \quad (3.9)$$

where H denotes the Bernoulli function $H = \frac{1}{2}v_\beta v_\beta + p + \frac{1}{Fr}\Psi$ as defined by (2.75). It is evident by inspection of the Crocco–Vazsonyi version of momentum balance (3.8) that viscosity has no effect on momentum transport, if vorticity is zero.

Comment on the Crocco–Vazsonyi form of momentum balance

The Crocco–Vazsonyi version of the dimensional momentum balance and the Crocco relation for flows of a compressible fluid can be established easily. They are the key to the analysis of acoustic phenomena in turbulent flows. The momentum balance for compressible fluids (2.2)

$$\frac{\partial}{\partial t} (\tilde{\rho}\tilde{v}_\alpha) + \frac{\partial}{\partial x_\beta} (\tilde{\rho}\tilde{v}_\alpha v_\beta) + \frac{\partial \tilde{p}}{\partial \tilde{x}_\alpha} - \frac{\partial \tilde{\tau}_{\alpha\beta}}{\partial \tilde{x}_\beta} - \tilde{\rho}\tilde{g}_\alpha = 0$$

can be recast using the Gibbs relation ([17] Sect. 4.3.5)

$$\tilde{T}d\tilde{s} = d\tilde{h} - \frac{d\tilde{p}}{\tilde{\rho}}, \quad \tilde{T}\frac{\partial\tilde{s}}{\partial\tilde{x}_\alpha} = \frac{\partial\tilde{h}}{\partial\tilde{x}_\alpha} - \frac{1}{\tilde{\rho}}\frac{\partial\tilde{p}}{\partial\tilde{x}_\alpha} \quad (3.10)$$

resulting in

$$\frac{\partial\tilde{v}_\alpha}{\partial\tilde{t}} = \tilde{L}_\alpha - \frac{\partial\tilde{\Phi}}{\partial\tilde{x}_\alpha} - \tilde{\nu}(\epsilon_{\alpha\beta\gamma}\frac{\partial\tilde{\omega}_\gamma}{\partial\tilde{x}_\beta} - \frac{4}{3}\frac{\partial\tilde{\Theta}}{\partial\tilde{x}_\alpha}) + \tilde{T}\frac{\partial\tilde{s}}{\partial\tilde{x}_\alpha} \quad (3.11)$$

for compressible fluids, where \tilde{L}_α is the Lamb vector (2.54) $\tilde{L}_\alpha \equiv \epsilon_{\alpha\beta\gamma}\tilde{v}_\gamma\tilde{\omega}_\beta$ (discussed in Sect. 2.4) and Θ is the dilatation (divergence of velocity)

$$\tilde{\Theta} \equiv \frac{\partial\tilde{v}_\alpha}{\partial\tilde{x}_\alpha} \quad (3.12)$$

The term $\tilde{H} = \tilde{h} + \frac{1}{2}\tilde{v}_\alpha\tilde{v}_\alpha + \tilde{\Psi}$ is a scalar field called Bernoulli function consisting of the total enthalpy $\tilde{h} + \frac{1}{2}\tilde{v}_\alpha\tilde{v}_\alpha$ and the potential $\tilde{\Psi}$ of the external force. The momentum balance (3.11) is called the Crocco–Vazsonyi equation for compressible flows.

The special case of homentropic flow of an inviscid fluid follows from (3.11) at once

$$\frac{\partial\tilde{v}_\alpha}{\partial\tilde{t}} = \tilde{L}_\alpha - \frac{\partial\tilde{\Phi}}{\partial\tilde{x}_\alpha} \quad (3.13)$$

For steady flows, the Crocco relation follows

$$\frac{\partial\tilde{H}}{\partial\tilde{x}_\alpha} = \tilde{L}_\alpha \quad (3.14)$$

The Bernoulli function \tilde{H} is, as for incompressible fluids, constant on surfaces, which have the Lamb vector as normal vector. However, as for flows of an incompressible fluids, such surfaces may not exist as, for instance, in irrotational or Beltrami flows (Beltrami flows are defined as flows with velocity and vorticity being parallel, equation (2.58) in Sect. 2.3.1, also Wu et al. [15], Sect. 3.1.1). It is evident that the Bernoulli function is constant throughout the flow field for Beltrami flows or flows where either velocity or vorticity or, trivially, both are zero.

(T.4) Turbulent motion is three-dimensional

The property (T.1) implies that magnitude and direction of vectors (such as velocity and vorticity) are random. However, it does not follow from (T.1) that the randomness created by the nonlinearities of the Navier–Stokes system must be three-dimensional. The three-dimensional character of turbulent flows is due to two facts, first, 2-d shear flows such as the flat plate boundary layer are, for sufficiently high Reynolds numbers, unstable with respect to 3-d disturbances and, second, the phenomenon of

vortex stretching is absent in 2-d flows. Two-dimensional flows lack this fundamental mechanism, as is shown below, that is able to increase or decrease locally the amount of vorticity and, possibly, create a singularity in finite time from smooth initial data. To see this, the vorticity transport equation (2.62) must be considered. For two-dimensional flows, it follows from the fact that velocity and vorticity are orthogonal that the term

$$\omega_\beta \frac{\partial v_\alpha}{\partial x_\beta} = 0$$

is identically zero. A closer look at this term reveals that it is for 3-d flows responsible for the increase or decrease of a vorticity component due to turning and stretching or compression. For this reason, it is called vortex stretching term and its absence in two-dimensional flows shows that vorticity is then only convected and diffused for incompressible fluids.

There is some evidence from numerical simulations of inviscid flows that the vortex stretching term may generate a singularity of second order in finite time starting from smooth initial conditions, but the results are still inconclusive, see Gibbon [18], Kerr [19, 20] for careful analysis and lucid discussion. Singularities are termed first order, if a velocity norm (kinetic energy) becomes unbounded and second order, if the velocity norm stays bounded, but a vorticity/ensrophy norm (i.e. the time integral of the L^∞ norm, theorem below) goes to infinity. Beale, Kato and Majda [21] proved the theorem

Theorem *There exists a global solution of the 3d Euler equations $\mathbf{v}(t, \mathbf{x}) \in C([0, \infty]; H^s) \cap C^1([0, \infty]; H^{s-1})$ for $s \geq 3$ if*

$$\int_0^T dt' \|\omega\|_{L^\infty(\mathcal{D})}(t') < \infty \quad (3.15)$$

holds for every $T > 0$.

Note that $C^a([0, \infty]; H^s)$ denotes the space of vector fields $\mathbf{v}(t, \mathbf{x})$ continuously differentiable w.r.t. time up to order a in the time interval $[0, \infty]$ and w.r.t. to location \mathbf{x} the vector field \mathbf{v} is element of the Sobolev space $H^s = W_p^s$ (see Sect. 23.7 and Adams [22] for details on Sobolev spaces) for $p = 2$, thus H^s is also a Hilbert space.

Hence, if the solution of the Euler equations becomes singular under the assumptions of the theorem, it must be a singularity of second order. Bustamante and Kerr [23] and Hou and Li [24] present a possible flow configuration for a second-order singularity according to (3.15) as result of their accurate numerical solution of the Euler equations. The structure emerging during the interaction of two antiparallel vortex tubes has locally the form of two flattened vortex sheets with enstrophy

$$e^2 \equiv \omega_\alpha \omega_\alpha \quad (3.16)$$

maxima growing in time. However, computational solutions must be terminated at some stage, since the resolution deteriorates, and, unfortunately, no definitive answer can be obtained numerically for the asymptotic nature of the solution.

The situation is less clear for the case of finite Reynolds numbers, where vortex stretching may lead to rapid growth of local vorticity due to stretching, but viscous effects tend to dampen this growth at small scales. No final answer to the question of existence of singularities for the 3-d Navier–Stokes system can be given at present. Theoretical estimates of (second-order) singular sets (Caffarelli et al. [25])

$$\Sigma(t) \equiv \{\mathbf{x} \in \mathcal{D}(t) : \|\mathbf{v}\| < \infty, \|\nabla \times \mathbf{v}(t, \mathbf{x})\| = \infty\} \quad (3.17)$$

in suitable weak solutions (defined in [25]) of the Navier–Stokes equations show that their Hausdorff measure is zero and their Hausdorff dimension (Sect. 23.3 in Appendix A) at most 5/3 (see Sect. 23.3 for definitions). The Hausdorff dimension is in general noninteger, hence fractal, and regarded by Mandelbrot [13, 14] as a defining property of turbulence. The dimension is regarded as measure of complexity of the singular sets, but very little is known of the topological and geometric properties of singular sets [20].

For compressible flows, there appears a new term in the vorticity equation (2.62) not present in the incompressible case, that is, the cross product of the gradients of density and pressure. It is particularly important in combustion flows, where the density may vary by an order of magnitude due to the heat release of the combustion reactions and the gradients of pressure and density are not parallel.

(T.5) Turbulent motion is unsteady

This is again a consequence of (T.1), the apparent randomness of the turbulent flow field. If there was such a thing as a steady and random flow field, the repeated observation of flow quantities at a fixed location and at different times would produce the same result. Such a flow would not be considered turbulent since the apparent randomness would be solely due to the randomly chosen boundary conditions.

(T.6) Turbulent motion is diffusive

Turbulent flows show enhanced transport of mass, momentum and scalar properties due to the random movement of fluid material points. This increased turbulent or effective diffusivity leads to rapid spreading of properties transported with the fluid material. It is several orders of magnitude larger than the corresponding molecular diffusivity.

3.1 Working Definition of Turbulence

Various definitions of turbulence have been suggested over the last and the present century. von Karman [26] and Taylor [27] in the 1930s put forward the following definition of turbulence distilled from experimental observations:

Turbulence is an irregular motion which in general makes its appearance in fluids, gaseous or liquid, when they flow past solid surfaces or even when neighbouring streams of the same fluid flow past or over one another.

Hinze, in his book on turbulence [28] (1975, 2nd ed.), offered another definition:

Turbulent fluid motion is an irregular condition of the flow in which the various quantities show a random variation with time and space coordinates, so that statistically distinct average values can be discerned.

None of these definitions offers a precise characterization of turbulent flow in the sense of predicting, on the basis of specific flow conditions, when turbulence will or will not occur. It seems likely that this lack of precision has at least to some extent contributed to the inability to solve the turbulence problem: if one does not know what turbulence is or under what circumstances it occurs, it is rather unlikely that one can say much of anything about it in a quantitative sense.

Chapman and Tobak [29] have described the evolution of our understanding of turbulence in terms of three overlapping areas:

- (i) statistical,
- (ii) structural, and
- (iii) deterministic.

A more precise definition of turbulence based on these three areas was proposed by Chapman and Tobak [29]

Turbulence is any chaotic solution to the 3-d Navier–Stokes equations that is sensitive to initial data and which occurs as a result of successive instabilities of laminar flows as a bifurcation parameter is increased through a succession of values.

It contains the notions of chaotic solutions of the Navier–Stokes pdes and bifurcation parameters, which still have to be defined. Kolmogorov explained turbulence as characterized by the minimal attractor dimension growing with a positive power of the Reynolds number. Ruelle and Takens [30], Ruelle [31] connected transition to turbulence with the appearance of a global attractor with sensitive dependence on the initial conditions.

Finally, definitions of turbulence are suggested based on the properties observed in experiments and direct numerical solutions of the Navier–Stokes equations. Corrsin [32] was one of the more recent scientists to put forward such a definition. It can be stated as follows for flows of an incompressible fluid:

Incompressible turbulence is defined as a spatially complex distribution of vorticity, which is advected in chaotic manner according to the transport equation for vorticity (2.62)

$$\tilde{\rho} \frac{D}{Dt} \left(\frac{\tilde{\omega}_\alpha}{\tilde{\rho}} \right) = \tilde{\omega}_\beta \frac{\partial \tilde{v}_\alpha}{\partial \tilde{x}_\beta} + \frac{1}{\tilde{\rho}^2} \epsilon_{\alpha\beta\gamma} \frac{\partial \tilde{\rho}}{\partial \tilde{x}_\beta} \frac{\partial \tilde{p}}{\partial \tilde{x}_\gamma} + \tilde{\rho} \epsilon_{\alpha\beta\gamma} \frac{\partial}{\partial \tilde{x}_\gamma} \left(\frac{1}{\tilde{\rho}} \frac{\partial \tilde{\tau}_{\beta\delta}}{\partial \tilde{x}_\delta} \right) + \epsilon_{\alpha\beta\gamma} \frac{\partial \tilde{g}_\beta}{\partial \tilde{x}_\gamma}$$

where

$$\frac{D}{D\tilde{t}} \equiv \frac{\partial}{\partial \tilde{t}} + \tilde{v}_\beta \frac{\partial}{\partial \tilde{x}_\beta} \quad (3.18)$$

denotes the material derivative in the spatial description and g_β is the external volume force with non-zero rotational part. The vorticity field is random in space and time and exhibits a wide and continuous distribution of length and time scales.

The pde for vorticity ω_α follows from mass and momentum balances and its definition $\omega_\alpha = \epsilon_{\alpha\beta\gamma} \frac{\partial v_\gamma}{\partial x_\beta}$ in Cartesian coordinates (the summation convection applies to repeated Greek subscripts, $\epsilon_{\alpha\beta\gamma}$ is the Levi-Civita symbol). The vorticity field is random in space and time and exhibits a wide and continuous distribution of length and time scales.

Length and time scales will be defined once the statistical properties of turbulent flows have been established in sections below. The present definition incorporates the essential points of Corrsin's definition and can be stated for compressible and incompressible turbulence in the form:

A flow is called **turbulent** iff it is

- (TF.1): apparently random and remains random after removal of all external sources of randomness;
- (TF.2): vortical;
- (TF.3): has a wide and continuous distribution of length and time scales.

This definition allows to distinguish between turbulent and non-turbulent flows at a given instant in time, but not for a single realization. Randomness is interpreted as sensitive dependence on initial conditions. Vortical means $||\omega|| \gg 0$ with respect to the L_2 -norm. The property (TF.3) implies that turbulent flows possess a mechanism for spreading energy to the available range of length scales and to the available physical space, chaotic systems do not necessarily have this property. The nonlinear convective terms in the momentum balance in the spatial description provide this mechanism for the velocity field, convective and vortex stretching terms do this for vorticity. The Navier–Stokes equations can be derived as well in the material description resulting in equations of different structure. The convective term is then absent and the question arises, which mechanisms are responsible for spreading energy over available scales and physical dimensions. They are the pressure gradient and the viscous terms, both proportional to the deformation gradient and nonlinear. Turbulent flows are classified for later use as

- (mTF) Maintained turbulent flows, including statistical steady state;
- (uTF) Unsteady turbulent flows.

Maintained turbulent flows are defined as flows for which a finite time $0 \leq t_m < \infty$ exists, such that the defining properties of turbulence are for $t_m \leq t$ either invariant with respect to time or approach smoothly a unique turbulent asymptotic state, an example for maintained turbulence is steady-state turbulence. Maintained turbulent flows possess, therefore, an asymptotic state that is not laminar.

Unsteady turbulence is defined as turbulence for which no finite t_m exists, important examples for the unsteady case are turbulence in the cylinder of an internal combustion engine and decaying turbulence. An asymptotic state may not exist, may not be unique or may be laminar flow. The notion of uniqueness refers to the turbulence measure / characteristic functional, but see the discussion in the next section.

3.2 Asymptotic Properties of Turbulent Flows

Low-dimensional dynamical systems are chaotic, if they possess an asymptotic property called axiom A attractor (Ruelle [31], Wiggins [33] Chap. 30), one of the axioms is the condition of sensitive dependence on initial conditions, the others being, that the dimension is larger than two and the dimension of the attractor is fractal. The notion of attractor can be extended to the phase space of maintained turbulent flows (mTF) as follows. The assumption put forward in Sect. 2.2 states that the solution operator T_t of IVP for the Navier–Stokes is well defined. Based on this assumption and the notion of chaos, introduced in property (T.1) above, the definition of a turbulent attractor [34] is proposed.

Turbulent Attractor: The subset A of the phase space Ω is called turbulent attractor iff

- (TA.1) A is invariant under the action of the flow $T_t A = A$.
- (TA.2) A has fractal dimension.
- (TA.3) A possesses a domain of attraction $A \subset B$, $B - A$ is not empty, such that every point in B ends up in A under the action of the solution operator $\mathbf{X} \implies \lim_{t \rightarrow \infty} T_t \mathbf{X} \in A, \forall \mathbf{X} \in B$.

It is known that maintained turbulent flows possess attractor dimensions proportional to a power of the Reynolds number [34] and show pre-fractal properties for finite time intervals, Mandelbrot [14] defines (maintained) turbulence by its fractal properties. This aspect of maintained turbulence is discussed in the next section.

The definition of turbulence (TF.1) to (TF.3) just introduced makes no statement on the uniqueness of the asymptotic state or how to measure it by means of appropriate topological and geometric properties of the attractor representing turbulent flow (Eden et al. [35], Chepyzhov and Vishik [36]). It is conceivable that these properties depend on the ergodicity (definition in Sect. 23.9) of turbulence, i.e. the phase space Ω does not consist of disjoint subsets, and/or the routes to turbulence, as suggested by the different transition paths to fully developed, maintained turbulence starting from a laminar flow as observed, for instance, in the Taylor–Couette flow (Andereck et al. [37], Ostilla-Monico et al. [38]), mixing layers (Brown and Roshko [39]), wake flows (Castro [40]), boundary layers (Barkley [41]). It is important to notice that experiments and stability theory have shown that there are at least two simple shear flows that are linearly stable for all Reynolds numbers: Plane Couette and pipe flow,

see Schmid and Henningson [42] for detailed stability analysis of both flows. The transition to turbulence is subcritical for these flows, since linear stability analysis does not provide a criterium for transition and nonlinear methods must be applied. A well-known example for the nonlinear approach is the transition to turbulence in straight circular pipes discussed in Sect. 21.2.2, see also Ostilla-Monico et al. [38] for DNS of turbulent Taylor–Couette flow.

Furthermore, rotating flows, with angular velocity $v_\theta(r)$ decreasing and the specific angular momentum $r v_\theta(r)$ increasing in radially outward direction called qK (quasi-Keplerian) flows show peculiar stability properties. They maintain stability even for finite disturbances at very large Reynolds numbers ($Re > 10^6$), Balbus [43], Lopez and Avila [44] (DNS of a Taylor–Couette flow with $\Omega_i > \Omega_o$ and $r_i^2 \Omega_i < r_o^2 \Omega_o$, Ω_i , r_i and Ω_o , r_o are angular speed and radius at inner and outer cylinder), a phenomenon unexplained so far but the DNS results point to stability w.r.t. finite disturbances. These examples indicate that the structure of the strange attractor (defined in Sect. 3.2) for turbulent shear flow possesses pathlines that do not mix with the rest of the attractor. Thus, it is not certain that ergodicity is always satisfied.

The answer to the question of attractor uniqueness for 3-d flows is so far unknown. However, Feigenbaum [45] argued that the route to chaos is universal for nonlinear systems. The properties of turbulent flows hold asymptotically for flows maintained by external energy sources, decaying turbulence (such as unforced homogeneous turbulence) have the origin of phase space Ω as trivial asymptotic attractor.

The theory to be discussed in the following chapters is based on the Navier–Stokes equations, which are not an exact description of fluid motion occurring in nature. They lose their validity at very low density, very high speeds and, generally speaking, in flows characterized by very small length and time scales. The theory of turbulence based on the Navier–Stokes equations should, therefore, be called Navier–Stokes turbulence, since it is the theory of chaotic solutions of this system of equations (Temam [7]). Thus, it cannot be expected that the limit properties of Navier–Stokes turbulence (for instance, as the Reynolds number approaches infinity) are necessarily in agreement with asymptotics deduced from experimental observations.

3.3 Number of Degrees of Freedom of the Turbulence Attractor for Maintained Turbulence

Notions of degrees of freedom are introduced for the analysis of turbulent flows. The heuristic definition of degrees of freedom due to Landau and Lifshitz [46, 47] is applicable to the d -dimensional flow domain \mathcal{D} . Let $\tilde{\lambda} > 0$ be the smallest length scale of the flow, then divide \mathcal{D} into boxes of sidelength $\tilde{\lambda}$. The number N of degrees of freedom is the number of boxes needed to fill the domain.

An abstract definition of the number of degree of freedom is the topological dimension of the attractor in the phase space of a turbulent flow discussed in Sect. 5.2. The attractor dimension need not be integer for turbulent flows according to

(TA.2), hence a more general notion of dimension must be employed, as explained in Sect. 23.3 of Appendix A.

The hypotheses of Kolmogorov and Onsager, discussed below in Chap. 17, can be applied to roughly estimate the number of degrees of freedom of the turbulence attractor for maintained turbulence at high Reynolds numbers. Turbulence at $Re \gg 1$ and far away from wall boundaries and supplied with energy with a statistically mean rate, is assumed to be dissipated with the same rate $\tilde{\epsilon} > 0$ that becomes independent of the Reynolds number and the turbulence locally isotropic as $Re \rightarrow \infty$. The fundamental properties that the dissipation rate $\tilde{\epsilon} > 0$ becomes independent of the Reynolds number as $Re \rightarrow \infty$ and local isotropy have so far not been derived from the Navier–Stokes equations; hence, they must be regarded as hypotheses.

A simple dimensional argument (Landau and Lifshitz [46], Chap. 32, Tran [48]) can be used to estimate the number of degrees of freedom n in a volume of linear extent $\tilde{L} \gg \tilde{\eta}$. In Chap. 18, it is shown using dimensional arguments that the length scale of the viscous range of the velocity spectrum is the Kolmogorov scale (19.8)

$$\tilde{\eta} = \left(\frac{\tilde{\nu}^3}{\tilde{\epsilon}} \right)^{\frac{1}{4}}$$

determined by the kinematic viscosity $\tilde{\nu}$ and the statistical expectation $\tilde{\epsilon}$ of the dissipation rate. If turbulence in such a volume is homogeneous and isotropic and consists of vortical structures of volume $\tilde{\eta}^3 = (\frac{\tilde{\nu}^3}{\tilde{\epsilon}})^{\frac{3}{4}}$ filling the available space, then is their number in the volume of linear size \tilde{L} given by

$$\left(\frac{\tilde{L}}{\tilde{\eta}} \right)^3 \approx \frac{\tilde{L}^3 \tilde{\epsilon}^{\frac{3}{4}}}{\tilde{\nu}^{\frac{9}{4}}} \quad (3.19)$$

The Reynolds number, determined by the length scale $\tilde{L} \gg \tilde{\eta}$ and the velocity scale $(\tilde{L}\tilde{\epsilon})^{\frac{1}{3}}$ proportional to the dissipation rate $\tilde{\epsilon} > 0$ and viscosity $\tilde{\nu}$

$$Re = \frac{\tilde{L}^{\frac{4}{3}} \tilde{\epsilon}^{\frac{1}{3}}}{\tilde{\nu}} \quad (3.20)$$

Thus, a rough estimate for the number of vortical structures N , i.e. the number of Landau–Lifshitz degrees of freedom, in the subset with linear extent \tilde{L} follows as

$$N \equiv \left(\frac{\tilde{L}}{\tilde{\eta}} \right)^3 \approx Re^{\frac{9}{4}} \quad (3.21)$$

This estimate was obtained by dimensional arguments and the Kolmogorov–Onsager assumptions for turbulence at $Re \gg 1$, the Navier–Stokes equations did not enter the derivation.

Attempts to establish the estimate for the number of degrees of freedom for 3-d turbulence from first principles are not possible as long as the question of smoothness

of the solutions of the Navier–Stokes equations is not settled and assumptions on the solution operator are necessary to proceed. There have been a number of attempts to start with the Navier–Stokes equations [34, 48, 49], but it was found that the fundamental hypothesis of Kolmogorov that the dissipation rate becomes independent of the Reynolds number as $Re \rightarrow \infty$ had to be retained. The situation is different for 2-d flows, the dimension of the attractor can be established rigorously, see Constantin et al. [50] for periodic flows and uniform external force.

3.4 Problems for this Chapter

Problem 3.1 Derive the pde for the dimensionless mean kinetic energy $k \equiv \frac{1}{2} \langle v'_\alpha v'_\alpha \rangle$ assuming a viscous, incompressible Newtonian fluid. Identify production, viscous destruction and the total turbulent flux terms.

Problem 3.2 Derive the pde for the dimensionless mean enstrophy $\langle e^2 \rangle$ defined by (3.16) in homogeneous turbulence for an incompressible Newtonian fluid with constant viscosity $\tilde{\nu} > 0$, i.e. $0 < Re < \infty$.

Problem 3.3 Consider the pde for the mean enstrophy obtained in the previous problem.

(3.3.1) Solve the pde assuming that the vortex stretching term has the form

$$\langle \omega_\alpha \omega_\beta \frac{\partial v_\alpha}{\partial x_\beta} \rangle \approx A e^{\frac{3}{2}}$$

where $A > 0$ is a constant and the initial value $e(0) > 0$ is known.

(3.3.2) Determine the pde for $\langle e^2 \rangle$ for 2-d ($v_3 = 0$) homogeneous turbulent flow. Solve the pde for the cases

$$\frac{1}{Re} \langle \frac{\partial \omega_\alpha}{\partial x_\beta} \frac{\partial \omega_\alpha}{\partial x_\beta} \rangle \approx 0$$

and

$$\frac{1}{Re} \langle \frac{\partial \omega_\alpha}{\partial x_\beta} \frac{\partial \omega_\alpha}{\partial x_\beta} \rangle \approx B \frac{\langle e^2 \rangle}{\tau}$$

where $B > 0$ and $\tau > 0$ are constants and the initial value $\langle e^2 \rangle(0)$ is known.

Problem 3.4 This problem is devoted to the analysis of the dynamics of vorticity in flows of an inviscid and incompressible fluid. The vortex stretching term in the transport pde for vorticity is analysed following Gibbon et al. [51]. All derivations should be done in the spatial description except in part (3), all transport equations

should be set up in terms of the substantial time derivative. Consider the Euler equations, i.e. the Navier–Stokes pdes (2.6) and (2.7) for an inviscid, incompressible fluid

$$\frac{Dv_\alpha}{Dt} = -\frac{\partial p}{\partial x_\alpha}, \quad \frac{\partial v_\alpha}{\partial x_\alpha} = 0$$

(3.4.1) Derive the vorticity transport equation from the Euler equations. Show that can be written in terms of the rate of strain tensor

$$s_{\alpha\beta} \equiv \frac{1}{2} \left(\frac{\partial v_\alpha}{\partial x_\beta} + \frac{\partial v_\beta}{\partial x_\alpha} \right)$$

The vector field called vortex stretching term is defined as

$$s_\alpha \equiv \omega_\beta \frac{\partial v_\alpha}{\partial x_\beta}$$

Express it in terms of the rate of strain tensor $s_{\alpha\beta}$.

(3.4.2) Derive the transport equation for enstrophy (3.16). Define the vorticity stretch factor $\alpha(t, \mathbf{x})$ by

$$\alpha(t, \mathbf{x}) \equiv \frac{\omega_\alpha s_{\alpha\beta} \omega_\beta}{e^2}$$

and express the right side of the enstrophy pde in terms of α .

(3.4.3) Let the vorticity stretch factor $\alpha(t, \mathbf{x})$ be a given scalar field, then transform the enstrophy equation to the material description and solve it for the initial condition $e(0, \mathbf{X}) = e_0(\mathbf{X})$, where $\mathbf{X} \in \mathcal{D}(0) = \mathbb{R}^3$.

(3.4.4) Derive the transport equation for the stretch vector field $\sigma_\alpha \equiv \omega_\beta \frac{\partial v_\alpha}{\partial x_\beta}$ (Ohkitani's equation, [51]). Introduce the pressure Hessian (2.117)

$$P_{\alpha\beta} \equiv \frac{\partial^2 p}{\partial x_\alpha \partial x_\beta}$$

into the transport pde.

(3.4.5) Show that the second substantial time derivative of vorticity is proportional to the pressure Hessian.

(3.4.6) Define the vector field $\delta_\alpha(t, \mathbf{x}) \equiv \epsilon_{\alpha\beta\gamma} \omega_\beta s_{\gamma\delta} \omega_\delta$ and derive its transport pde. Show that the right-hand side is proportional to the pressure Hessian.

(3.4.7) Redefine the stretch vector field

$$\chi_\alpha(t, \mathbf{x}) \equiv \frac{1}{e^2} \epsilon_{\alpha\beta\gamma} \omega_\beta s_{\gamma\delta} \omega_\delta$$

where

$$\alpha(t, \mathbf{x}) = \frac{1}{e^2} \omega_\alpha s_{\alpha\beta} \omega_\beta$$

is the vorticity stretch factor defined in (2) above, and the analogous fields replacing the rate of strain with the pressure Hessian

$$\chi_\alpha^p(t, \mathbf{x}) \equiv \frac{1}{e^2} \epsilon_{\alpha\beta\gamma} \omega_\beta P_{\gamma\delta} \omega_\delta, \quad \alpha^p(t, \mathbf{x}) \equiv \frac{1}{e^2} \omega_\alpha P_{\alpha\beta} \omega_\beta$$

Derive the transport equations for the stretch factor α and the stretch vector χ_α .

References

1. Bradshaw, P., Ferriss, D.H., Johnson, R.F.: Turbulence in the noise-producing region of a circular jet. *JFM* **19**, 591–624 (1964)
2. Oertel Sr., H.: Modern developments in shock tube research. *Shock Tube Research Soc. Japan*, 488–495 (1975)
3. Hasselblatt, B., Katok, A.: *A First Course in Dynamics: With a Panaorama of Recent Developments*. Cambridge University Press (2003)
4. Rudin, W.: *Principles of Mathematical Analysis*, 3rd edn. McGraw-Hill, Auckland N.Z (1976)
5. Klauder, J.R.: *A Modern Approach to Functional Integration*. Birkhaeuser/Springer, New York (2010)
6. Vishik, M.J., Fursikov, A.V.: *Mathematical Problems of Statistical Hydromechanics*. Kluwer Academic Publication, Dordrecht (1988)
7. Temam, R.: *Infinite Dimensional Dynamical Systems in Mechanics and Physics*. Springer, New York (1988)
8. Rudin, W.: *Functional Analysis*, 2nd edn. McGraw-Hill Education (Asia), Singapore (2005)
9. Davidson, P.A.: *Turbulence*. Oxford University Press, Oxford, U.K. (2004)
10. Sagaut, P., Cambiron, C.: *Homogeneous Turbulence Dynamics*. Cambridge University Press, New York (2008)
11. Sreenivasan, K.R., Meneveau, C.: The fractal facets of turbulence. *JFM* **173**, 357–386 (1986)
12. Procaccia, I., Brandenburg, A., Jensen, M.H., Vincent, A.: The fractal dimension of iso-vorticity structures in 3-dimensional turbulence. *Europhys. Lett.* **19**, 183–187 (1992)
13. Mandelbrot, B.B.: *Comment on Coherent Structures in Fluids, Fractals, and the Fractal Structure of Flow Singularities*. *Turbulence and Chaotic Phenomena in Fluids, IUTAM*. Elsevier Science Publication, North Holland (1984)
14. Mandelbrot, B.B.: *Fractals and Chaos: The Mandelbrot set and beyond*. Springer, New York (2004)
15. Wu, J.-Z., Ma, H.-Y., Zhou, M.-D.: *Vorticity and Vortex Dynamics*. Springer, Berlin (2006)
16. Truesdell, C.A.: *The Kinematics of Vorticity*. Indiana University Press, Bloomington, Indiana (1954)
17. Bejan, A.: *Advanced Engineering Thermodynamics*, 3rd edn. John Wiley & Sons Inc., Hoboken, New Jersey (2006)
18. Gibbon, J.D.: The three-dimensional Euler equations: where do we stand? *Physica D* **237**, 1894–1904 (2008)
19. Kerr, R.M.: The role of singularities in turbulence. In: Kida, S. (ed.) *Unstable and Turbulent Motion in Fluids*. World Scientific Publishing, Singapore
20. Kerr, R.M.: A new role for vorticity and singular dynamics in turbulence. In: Debnath, L. (ed.) *Nonlinear Instability Analysis*, vol. II, pp. 15–68. WIT Press, Southampton U.K. (2001)
21. Beale, J.T., Kato, T., Majda, A.J.: Remarks on the breakdown of smooth solutions for the 3d Euler equations. *Comm. Math. Phys.* **94**, 61–66 (1984)
22. Adams, R.A.: *Sobolev Spaces*. Academic Press, New York (1975)

23. Bustamante, M.D., Kerr, R.M.: 3D Euler about a 2D symmetry plane. *Physica D* **237**, 1912–1920 (2008)
24. Hou, T.Y., Li, R.: Blowup or no blowup ? The interplay between theory and numerics. *Physica D* **237**, 1937–1944 (2008)
25. Caffarelli, L., Kohn, R., Nirenberg, L.: Partial regularity of suitable weak solutions of the Navier-Stokes equations. *Comm. Pure Appl. Math.* **35**, 771–831 (1982)
26. von Karman, T.: On the statistical theory of turbulence. *Proc. Nat. Acad. Sci.* **23**, Washington, 98 (1937)
27. Taylor, G.I.: Statistical theory of turbulence. *Proc. Roy. Soc. London* **151**, 421–478 (1935)
28. Hinze, J.O.: Turbulence: An introduction to its Mechanism and Theory, 2nd edn. McGraw-Hill (1975)
29. Chapman, G.T. and Tobak, M.: Observations, theoretical Ideas and Modeling of Turbulent Flows—Past, Present and Future. In: Dwoyer et al. (eds.) *Theoretical Approaches to Turbulence*, pp. 19–49. Springer, New York (1985)
30. Ruelle, D., Takens, F.: On the nature of turbulence. *Comm. Math. Phys.* **20**, 167–192 (1971)
31. Ruelle, D.: Elements of Differentiable Dynamics and Bifurcation Theory. Academic Press (1989)
32. Corrsin, S.: Theories of turbulent dispersion. In *Mecanique de la Turbulence*. CNRS publ. **108**, 27–52 (1962)
33. Wiggins, S.: Introduction to Applied Nonlinear Dynamical Systems and Chaos. Springer, New York (2003)
34. Constantin, P., Foias, C., Temam, R.: Attractors representing turbulent flows. *Memoirs Am. Math. Soc.* **314** (1985). Am Math. Soc., Providence R.I.
35. Eden, A., Foias, C., Nicolaenko, B., Temam, R.: Exponential Attractors for Dissipative Evolution Equations. Wiley, New York (1994)
36. Chepyzhov, V.V., Vishik, M.I.: Attractors for Equations of Mathematical Physics. Americal Math. Soc, Providence, Rhode Island (2002)
37. Andereck, C.D., Liu, S.S., Swinney, H.L.: Flow regimes between independently rotating cylinders. *JFM* **164**, 155–183 (1986)
38. Ostilla-Monico, R., Verzicco, R., Grossmann, S., Lohse, D.: The near-wall region of highly turbulent Taylor-Couette flow. *JFM* **788**, 95–117 (2016)
39. Brown, G.L., Roshko, A.: On density effects and large structure in turbulent mixing layers. *JFM* **64**, 775–816 (1974)
40. Castro, I.P.: Dissipative distinctions. *JFM* **788**, 1–4 (2016)
41. Barkley, D.: Theoretical perspective on the route to turbulence in a pipe. *JFM* **803**, P1–1 (2016)
42. Schmid, P.J., Henningson, D.S.: Stability and Transition in Shear Flows. Springer (2001)
43. Balbus, S.A.: When is high Reynolds number shear flow not turbulent? *JFM* **824**, 1–4 (2017)
44. Lopez, J.M., Avila, M.: Boundary-layer turbulence in experiments on quasi-Keplerian flows. *JFM* **817**, 21–34 (2017)
45. Feigenbaum, M.: The transition to aperiodic behaviour in turbulent systems. *Comm. Math. Phys.* **77**, 65–86 (1980)
46. Landau, L.D., Lifshitz, E.M.: Fluid Mechanics. Pergamon Press, Oxford, U.K. (1956)
47. Robinson, J.C.: Parametrization of global attractors, experimental observations, and turbulence. *JFM* **578**, 495–507 (2007)
48. Tran, C.V.: The number of degrees of freedom of three-dimensional Navier-Stokes turbulence. *Phys. Fluids* **21**, 125103-1 (7) (2009)
49. Constantin, P., Foias, C., Manley, O.P., Temam, R.: Determining modes and fractal dimension of turbulent flows. *JFM* **150**, 427 (1985)
50. Constantin, P., Foias, C., Temam, R.: On the dimension of the attractor in two-dimensional turbulence. *Physica D* **30**, 284–296 (1988)
51. Gibbon, J.D., Galanti, B., Kerr, R.M.: Stretching and compression of vorticity in the 3D euler equations. In: Hunt, J.C.R., Vassilicos, J.C. (eds.) *Turbulence Structure and Vortex Dynamics*. Cambridge University Press (2000)

Chapter 4

Flow Domains and Bases



A set of simple flow domains \mathcal{D} relevant to turbulent flows and Schauder bases (Sect. 23.8 in Appendix A) for the phase space Ω of functions defined on a domain \mathcal{D} of particular structure and its dual space \mathcal{N} called test function space are introduced for later use. A fundamental tool for operations in Banach and Hilbert spaces is the notion of a Schauder basis. Note that Schauder bases $\mathcal{B}(\mathcal{D})$ are defined for Banach and Hilbert spaces in Sect. 23.8 as follows: Let Ω be a Banach space of vector functions $\mathbf{v}(\mathbf{x})$ defined on the domain \mathcal{D} , a Schauder basis \mathcal{B} is an ordered sequence $\{\mathbf{f}^k(\mathbf{x}), k = 0, 1, \dots, \infty\}$ of elements of Ω , such that for every $\mathbf{v} \in \Omega$, there exists a unique sequence of numbers $a_n, n = 0, \dots, \infty$, so that

$$\mathbf{v}(\mathbf{x}) = \sum_{k=0}^{\infty} a_k \mathbf{f}^k(\mathbf{x}), \quad a_k = (\mathbf{v}, \frac{\mathbf{f}^k}{\|\mathbf{f}^k\|_{\Omega}}) = \frac{1}{\|\mathbf{f}^k\|_{\Omega}} \int_{\mathcal{D}} d\nu w(\mathbf{x}) v_{\alpha}(\mathbf{x}) f_{\alpha}^k(\mathbf{x})$$

where $w(\mathbf{x})$ denotes the weight function required for the orthogonality

$$\|\mathbf{f}^k\|_{\Omega}^2 = \delta_{k,m} \int_{\mathcal{D}} d\nu w(\mathbf{x}) f_{\alpha}^m(\mathbf{x}) f_{\alpha}^k(\mathbf{x}) = \delta_{k,m} (\mathbf{f}^m, \mathbf{f}^k)$$

of the basis functions. The convergence is understood with respect to the norm topology,

$$\lim_{n \rightarrow \infty} \|\mathbf{v}(\mathbf{x}) - \sum_{k=0}^n a_k \mathbf{f}^k(\mathbf{x})\|_{\Omega} = 0$$

as indicated by the subscript.

The infinite sequence of orthogonal, normalized basis functions can be thought of as complete set of ‘unit vectors’ analogous to the orthonormal unit vectors $\mathbf{e}^k, k = 1, \dots, n$ in Euclidean space R^n . An element $\mathbf{v} \in R^n$ can be represented uniquely as linear combination of (orthogonal) unit vectors

$$\mathbf{v} = \sum_{k=0}^n a_k \mathbf{e}^k, \quad \mathbf{e}^k \mathbf{e}^m = \delta_{k,m}$$

and an element of a separable Hilbert function space can be represented as convergent series using the basis functions. The phase space Ω need not be specified completely at this point (this is done later in Chap. 5), it is only assumed to be a separable Hilbert space with the set of infinitely often differentiable scalar/vector fields as dense subset. Bases for scalar and vector fields are conveniently constructed with the aid of families of special, orthogonal functions, the relevant references for this aspect are Abramovitz and Stegun [1] Chap. 22 and Olver et al. [2] Sect. 18.3. Domains and scalar bases are discussed for several elementary flows, the case of periodic flow through a pipe is covered in more detail and includes detailed material for the design of solenoidal vector bases.

The first case to be considered is the turbulent flow in a periodic cube as approximation of homogeneous turbulence. The second case is a pipe flow domain periodic in axial direction, hence topologically equivalent to a torus. The bases for the phase and test function spaces on this domain are developed in detail in Appendix C, Chap. 25. It poses several difficulties and illustrates the method for the construction of bases. The results are summarized below (tilded symbols indicate dimensional variables in the present section). The third class of flows are defined in open domains with at least one entrance and one exit section.

4.1 Homogeneous Turbulence Domain \mathcal{D}_{ht}

The flow domain for homogeneous turbulence is the full Euclidean space

$$\mathcal{D}_{ht}(\infty) \equiv \mathbb{R}^3 \quad (4.1)$$

However, this definition poses a few obstacles (Batchelor [3]) to the application of Fourier transforms (Sect. 15.1) to homogeneous flow fields. Functions defined on an infinite or semi-infinite domain are not square integrable, for instance, the total kinetic energy of fluctuations would be infinite. Hence, the range of flows is restricted to periodic in all three directions with periodicity interval as large as possible, but finite to include as large a range of scales as possible. The compact domain

$$\mathcal{D}_{ht}(S) \equiv \{\mathbf{x} : -\frac{S}{2} \leq x_\alpha \leq \frac{S}{2}, \alpha = 1, 2, 3\} \quad (4.2)$$

with sidelength a multiple of $S = 2\pi$, is the usual choice.

A Schauder basis for $L^2_{\mathcal{D}}$ is defined in the compact \mathcal{D}_{ht} by

$$\mathcal{B}(\mathcal{D}_{ht}) = \{\exp(i\mathbf{k} \cdot \mathbf{x}), \mathbf{k} \in N^3\} \quad (4.3)$$

The basis functions are orthogonal in \mathcal{D}_{ht} and can be normalized. Elements $f(\mathbf{x})$ of $L^2_{\mathcal{D}}$ can be expanded $f(\mathbf{x}) = \sum_{i,j,k}^{\infty} (f(\mathbf{x}), \exp(i\mathbf{k} \cdot \mathbf{x})) \exp(i\mathbf{k} \cdot \mathbf{x})$ convergent in the L^2 -norm but not necessarily pointwise.

4.2 Periodic Pipe Flow Domain \mathcal{D}

The flow through straight pipes with uniform cross section poses fundamental questions concerning the behaviour of turbulence near fixed walls (Robinson [4], Smits and Zagarola [5], Smits [6], McKeon et al. [7]), in particular as function of the Reynolds number in the asymptotic limit $Re \rightarrow \infty$, it also has numerous practical applications. The Reynolds number for pipes with circular cross section is usually defined by (2.8) $Re \equiv \frac{\tilde{R}\tilde{U}}{\tilde{\nu}}$, where \tilde{R} denotes a cross-sectional length scale such as the pipe radius, \tilde{U} the bulk velocity (volume flow rate divided by the cross-sectional area) and $\tilde{\nu}$ the kinematic viscosity. The limit $Re \rightarrow \infty$ is of great interest for fundamental reasons. The question of the existence of a smooth wall and turbulence properties, such as the value of the friction factor, in this limit will be investigated later in Chap. 22 based on extrapolation of experimental evidence at high but finite Reynolds numbers as presented by McKeon et al. [7].

A geometrically simple class of compact domains in cylindrical coordinates is defined by the straight pipe with uniform circular cross section $\mathcal{D}(\tilde{R}, \tilde{z}_0, \tilde{z}_1) \equiv \{(\tilde{r}, \theta, \tilde{z}) : 0 \leq \tilde{r} \leq \tilde{R}, 0 \leq \theta \leq 2\pi, \tilde{z}_0 \leq \tilde{z} \leq \tilde{z}_1\}$, where \tilde{R} is the pipe radius, θ the azimuthal coordinate and \tilde{z} the axial coordinate in a cylindrical coordinate system (r, θ, z) with the origin located at the centre of the entrance boundary. The axial and radial coordinates are made dimensionless with the pipe radius \tilde{R} , hence

$$\mathcal{D}(z_0, z_1) = \{(r, \theta, z) : 0 \leq r \leq 1, 0 \leq \theta \leq 2\pi, z_0 \leq z \leq z_1\} \quad (4.4)$$

is the dimensionless flow domain. The flow domain is noncompact, if the value for z at the exit section z_1 is unbounded (semi-infinite pipe), and/or the entrance section is also at (negative) infinity (infinite pipe), then are the values of integral quantities (L_2 norm, etc.) not bounded and special precautions must be taken. One way to avoid this situation is the restriction of the class of flows to periodic with respect to the axial coordinate z with period $2\pi L$. The flow domain \mathcal{D} is in this case topologically equivalent to a torus and the boundary $\partial\mathcal{D}$ of the domain is a single closed surface.

Scalar, vector and tensor fields in cylindrical coordinates must satisfy parity (or pole) conditions near the axis $r = 0$ to guarantee non-singular, smooth variation. These parity conditions link the radial variation to the azimuthal wavenumber k and can be specified (see Boyd [8], Kollmann [9] for details and proofs, summary in Sects. 25.7 and 25.12) in Appendix C as follows. It is convenient to transform scalar and vector fields to Fourier space with respect to the azimuthal coordinate θ (dependence on z and t is not indicated).

$$\Phi(r, \theta) = \sum_{n,k} \hat{\Phi}^{n,k}(r) \exp(ik\theta), \quad v_\alpha(r, \theta) = \sum_{n,k} \hat{v}_\alpha^{n,k}(r) \exp(ik\theta) \quad (4.5)$$

and formulate the parity conditions for the complex-valued Fourier amplitudes $\hat{\Phi}^{n,k}(r), \hat{v}_\alpha^{n,k}(r)$. The parity conditions for scalar and vector fields are summarized in Sect. 25.12 of Appendix D. Scalar and vector basis functions for the periodic flow through straight pipes with circular cross section are then constructed in Chap. 25 of Appendix D. Three cases are summarized; details are given in Appendix B: bases for scalar fields, bases for general vector fields with non-zero dilatation and bases for solenoidal vector fields.

4.2.1 Schauder Basis for Scalar Fields

A scalar fields such as pressure $p(t, \mathbf{x})$ is represented according to Sect. 25.9 with respect to the base

$$\mathcal{B}(\mathcal{D}) = \{f^{k,n,m}(r, \theta, z), 0 \leq n \leq \infty, 0 \leq k \leq \infty, -\infty \leq m \leq \infty\}$$

by

$$p(t, \mathbf{x}) = \sum_{k,n,m} \hat{p}_n^{k,m}(t) f^{k,n,m}(r, \theta, z) \quad (4.6)$$

The base function is constructed as product of Fourier and modified Jacobi modes

$$f^{k,n,m}(r, \theta, z) = h_k(\theta) q_n^k(r) h_m(z)$$

where the normalized Fourier modes are defined by $\langle h_k(\theta) \rangle = \frac{1}{\sqrt{2\pi}} \exp(ik\theta)$ Eq. (25.16) and $\langle h_m(z) \rangle = \frac{1}{\sqrt{2\pi}} \exp(imz)$ Eq. (25.30). The radial modes are set up in terms of modified Jacobi polynomials $Q_n^{0,k}(r)$ (25.6)

$$q_n^k(r) \equiv q_n^{0,k}(r) = r^k (1 - r^2) Q_n^{0,k}(r) \quad (4.7)$$

satisfying the homogeneous Dirichlet condition on the outer boundary $\partial\mathcal{D}$ and the parity conditions, Sect. 25.7 in Appendix C. The weight function $\omega(r)$ (25.79) emerges in the form $\omega(r) = 2r$. The coordinates (coefficients) $\hat{p}_n^{k,m}(t)$ are at most a function of time and are complex valued since the Fourier modes $h_k(\theta)$ (25.16) and $h_m(z)$ (25.30) are written in complex form. The properties of the scalar Schauder basis such as orthonormalization and numerical verification with the aid of analytic test fields can be found in Appendix B, Sect. 25.7.2.

It is important to realize that the dynamics and interaction of modes are dependent on the type of modes/basis being used (Fourier, wavelet, orthonormalized polynomials, POD, etc.). Mathematically all bases are equivalent, but physically the situation

is quite different. Nonlinear terms such as the convective terms require mode interaction, which is different in different bases, Tsinober [10]. It is crucial to construct a basis that represents the physical quantity of interest (energy, enstrophy, etc.) and associated interaction phenomena efficiently, i.e. with a minimal number of modes.

4.2.2 Schauder Basis for Vector Fields with Non-zero and Zero Dilatation

Eliminating the zero divergence condition (Sect. 25.13), i.e. the design requirement (V1), allows the construction of a family of orthogonal vector basis functions $f_{\gamma}^{n,a,k,m}(r, \theta, z)$, $\gamma = r, \theta, z$ given by

$$f_{\gamma}^{k,n,m}(r, \theta, z) = h_k(\theta) \chi_{\gamma}^{n,k}(r) h_m(z), \quad \gamma = r, \theta, z \quad (4.8)$$

with Fourier modes (25.16) and (25.30). The radial modes are given by (25.93)

$$\chi_r^{n,k}(r) = q_n^{|k-1|}(r) \quad (4.9)$$

$$\chi_{\theta}^{n,k}(r) = i \chi_r^{n,k}(r) \quad (4.10)$$

$$\chi_z^{n,k}(r) = q_n^k(r) \quad (4.11)$$

where the Jacobi parameter a is set to either zero for the present case (basis of scalar fields and general vector fields in Sect. 25.8) or $a = 2$ for certain components of the solenoidal vector basis constructed in Sect. 25.15 to insure the common form of the weight function (25.79).

The basis vectors for the present case of compressible flows satisfy the parity (Sect. 25.12) and boundary condition, but not the zero divergence condition (V1). Orthogonality of the individual vector components leads to

$$\begin{aligned} (f_{\gamma}^{k,n,m}, f_{\gamma}^{*,n',k',m'}) &= \delta_{k,k'} \delta_{m,m'} \int_0^1 dr w^a(r) \chi_{\gamma}^{n,k}(r) \chi_{\gamma}^{*,n',k}(r) \\ &= \delta_{k,k'} \delta_{m,m'} \delta_{n,n'} \sum_{\gamma=r,\theta,z} \frac{\Gamma(n+a+1) \Gamma(n+b(\gamma)+1)}{2(2n+a+b(\gamma)+1) n! \Gamma(n+a+b(\gamma)+1)} \end{aligned} \quad (4.12)$$

where Γ denotes the Gamma function at discrete arguments, $\Gamma(n+1) = n!$. The Jacobi parameter b depends on the wavenumber k

$$b(\gamma) = \begin{cases} |k-1| & \text{for } \gamma = r, \theta \\ k & \text{for } \gamma = z \end{cases}$$

follows from (25.40) with the appropriate choice of weight function (4.13)

$$w^a(r) = (1 - r^2)^{a-2} \quad (4.13)$$

The Jacobi parameter is $a = 2$ for the present case, the weight function $w^a(r) = \omega(r)$ (25.79) is thus the same for scalar and vector fields.

Partially orthogonal basis for solenoidal vector fields

The family $\{f_{\alpha}^{n,a,k,m}(r, \theta, z), \alpha = r, \theta, z\}$ defined in Sect. 25.19 of Appendix C is only orthonormal for the radial component, but not for the azimuthal and axial component with respect to the radial direction due to the zero divergence condition (25.66) imposed on the basis functions. To illustrate the solenoidal basis functions, the level surfaces for the Cartesian velocity components are shown in Figs. 4.1, 4.2 and 4.3. The radial variation of the solenoidal basis modes $f_r^{k,n,m}(r, \theta, z), f_{\theta}^{k,n,m}(r, \theta, z), f_z^{k,n,m}(r, \theta, z)$ is shown in figures in Appendix D. Figures 25.9 and 25.10 show the modes for the azimuthal $k = 0, 5$ and the axial wavenumber $m = 2$ and the radial indices $n = 0, 2, 4, 6, 8$ (as indicated in the graphs) at the azimuthal $\theta = 0$ and the axial $z = 1$ location. The radial basis functions and their radial derivative are both zero at the outer boundary as required by mass balance and the homogenous Dirichlet condition at $r = 1$, whereas the azimuthal and axial basis functions in right and lower graphs satisfy the boundary condition only. Furthermore, it is evident that the modes satisfy the parity conditions at the coordinate axis $r = 0$.

The fact that the basis functions are not orthogonal implies that the coordinates are determined by a linear system of equations, as shown in Sects. 25.20.6 and 25.20.6.

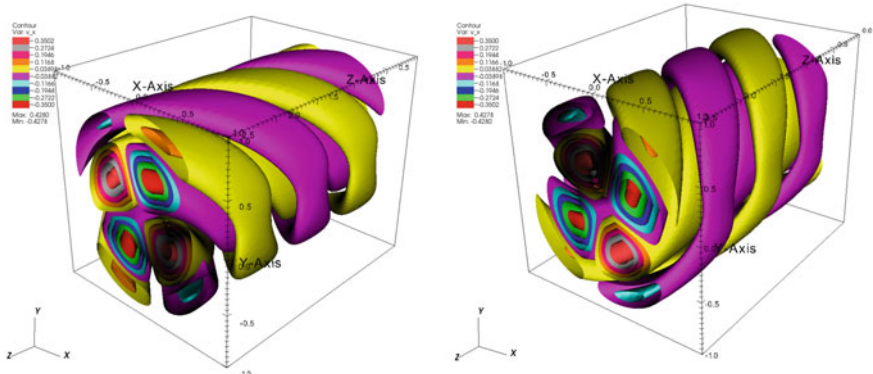


Fig. 4.1 Level surfaces of the real part of the Cartesian basis function vector component $v_x^{n,a,k,m} = f_r^{n,a,k,m} \cos(\theta) - f_{\theta}^{n,a,k,m} \sin(\theta)$ for $q_n^k(r)$ with $a = 2$ (25.80) and $s_n^k(r)$ with $a = 2$ (25.78) satisfying the zero divergence condition shown in $0 \leq z \leq 0.6\pi/L$ (the modes are periodic in $z \in [0, 2\pi/L]$), the radial index $n = 2$, the azimuthal wavenumber $k = 3$ and the axial wavenumbers $m = -4$ (left graph) and $m = 4$ (right graph). The level values are colour coded as indicated on the left upper corner of the graphs

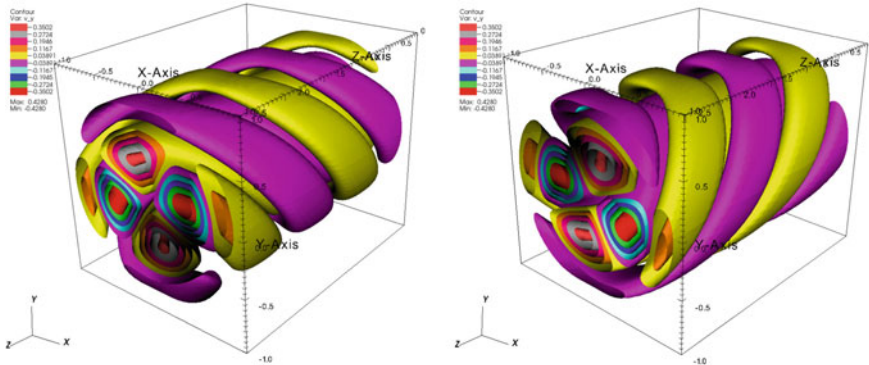


Fig. 4.2 Level surfaces of the real part of the Cartesian basis function vector component $v_y^{n,a,k,m} = f_r^{n,a,k,m} \sin(\theta) + f_\theta^{n,a,k,m} \cos(\theta)$ for $q_n^k(r)$ with $a = 2$ (25.80) and $s_n^k(r)$ with $a = 2$ (25.78) satisfying the zero divergence condition shown in the axial range $0 \leq z \leq 0.6\pi/L$, the radial index $n = 2$, the azimuthal wavenumber $k = 3$ and the axial wavenumbers $m = -4$ (left graph) and $m = 4$ (right graph). The level values are colour coded as indicated on the left upper side of the graphs

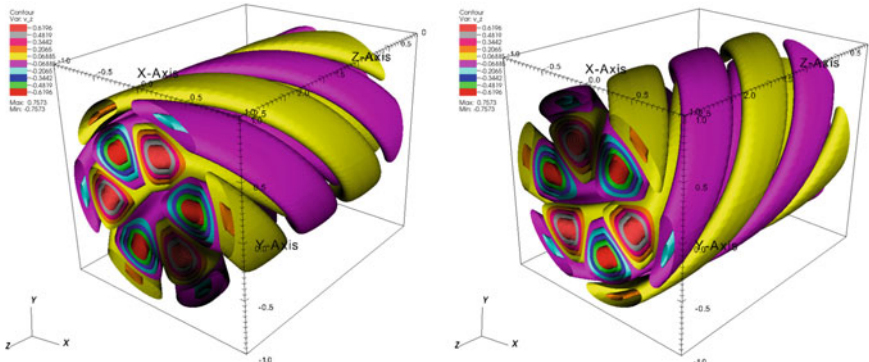


Fig. 4.3 Level surfaces of the real part of the Cartesian basis function vector component $f_z^{n,a,k,m}(r, \theta, z)$ for $q_n^k(r)$ with $a = 2$ satisfying the zero divergence condition shown in $0 \leq z \leq 0.6\pi/L$, $n = 2$, $k = 3$ and for $m = -4$ (left graph) and $m = 4$ (right graph). The level values are colour coded as indicated on the left upper side of the graphs

This is acceptable for the finite-dimensional projections, but does not work for the limit $N \rightarrow \infty$, since the determinant of this linear system grows over all bounds. It follows that the present basis is not suitable for the representation of solenoidal vector fields in infinite-dimensional Hilbert spaces.

Gram–Schmidt orthonormalized basis

A different method to construct an ONS basis for the phase Ω and argument \mathcal{N} spaces is the numerically stabilized Gram–Schmidt procedure. This construction is explained within the context of the periodic pipe flow in Sect. 25.22. It relies on

the design of a suitable vector potential satisfying boundary and pole conditions, application of the curl to insure zero divergence and subsequent orthonormalization.

4.3 Open and Noncompact Domains

Boundary layers, mixing layers, jets and wakes are ubiquitous in a variety of applications. The domains for this type of flows are open, because there is at least one intake and/or at least one exit sections. This implies that the flow field must satisfy an additional constraint, namely, the global mass balance

$$\int_{\mathcal{D}} d\nu \nabla \cdot (\rho \mathbf{v}) = \int_{\partial\mathcal{D}} dA \mathbf{n} \cdot \mathbf{v} = 0 \quad (4.14)$$

where \mathbf{n} denotes the unit normal vector pointing outward.

The presence of open sections requires special consideration since the conditions at exit sections are not known. One way to deal with this problem is to extend the exit sections cylindrically to infinity. Equation (4.14) provides then an integral constraint for those sections as indicated by Pileckas [11]. The existence of solutions for open domains depends crucially on the constraint (4.14), see Pileckas [11] for existence and regularity theorems using the tools of functional analysis.

4.3.1 Semi-infinite Pipe: $z_0 = 0$ and $z_1 = \infty$

The case of flow through a finite pipe with axial periodicity, hence unphysical boundary conditions, is unsatisfactory for several reasons. In particular, it does not allow representation of flow developing from laminar to turbulent. Hence, a second case with explicitly stated entrance boundary conditions is considered in the form of the noncompact, dimensionless domain $\mathcal{D} \equiv \{(r, \theta, z) : 0 \leq r \leq 1, 0 \leq \theta \leq 2\pi, 0 \leq z \leq \infty\}$, where \tilde{R} is the pipe radius and $\tilde{r} = r\tilde{R}$, $\tilde{z} = z\tilde{R}$ (tildes indicate dimensional variables).

The construction of a base \mathcal{B} in $C_{\mathcal{D}}^\infty \cap L_{\mathcal{D}}^2$ is complicated by the fact that polynomials are not square integrable due to the infinite length of the pipe. This is easily fixed by using Laguerre functions instead of polynomials, defined below in Eq. (4.18), as products of polynomials and rapidly decaying exponentials. The Laguerre functions $l_n^\alpha(x)$ are based on the Laguerre polynomials $L_n^{(\alpha)}(x)$, $x \in [0, \infty)$ ([1], Chap. 22 and [2], Sect. 18.3), they are a suitable choice for the semi-infinite pipe flow domain. They are explicitly given by

$$L_n^{(\alpha)}(x) = \sum_{j=0}^n \frac{(-1)^j}{n!} \binom{n+\alpha}{n-j} x^j \quad (4.15)$$

and they are orthogonal with respect to the weight function

$$w_\alpha(x) = x^\alpha \exp(-x) \quad (4.16)$$

where $\alpha > -1$. The orthogonality relation is according to [2] Chap. 18

$$\int_0^\infty dx w_\alpha(x) L_n^{(\alpha)}(x) L_m^{(\alpha)}(x) = \frac{\Gamma(n + \alpha + 1)}{\Gamma(n + 1)} \delta_{nm} \quad (4.17)$$

The Laguerre functions

$$l_n^\alpha(x) \equiv \left(\frac{\Gamma(n + 1)}{\Gamma(n + \alpha + 1)} \right)^{\frac{1}{2}} \sqrt{w_\alpha(x)} L_n^{(\alpha)}(x) \quad (4.18)$$

are then square integrable in the semi-infinite pipe domain and form an ONS since

$$\int_0^\infty dx l_n^\alpha(x) l_m^\alpha(x) = \delta_{nm} \quad (4.19)$$

holds. They are plotted for $\alpha = 0$ (left graph) and $\alpha = 2$ (right graph) and selected values of n are presented in Fig. 4.4. It is evident that modifications/transformations of the Laguerre functions are called for to satisfy the parity and outer boundary conditions as discussed in the previous section for the axially periodic case.

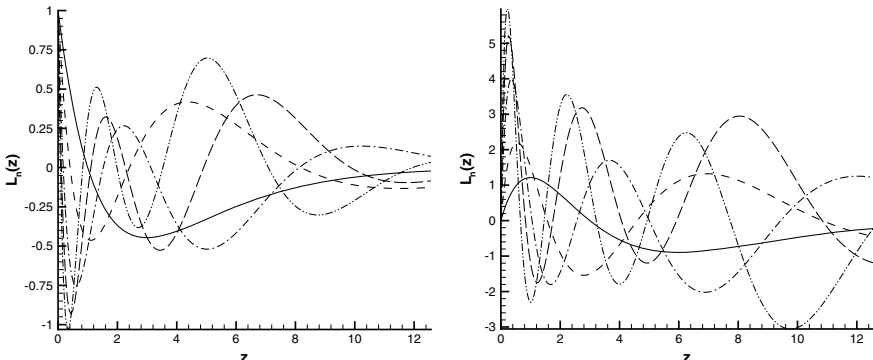


Fig. 4.4 Laguerre functions $l_n^\alpha(x)$ as defined by (4.18) for $\alpha = 0$ (left graph) and $\alpha = 2$ (right graph) and $n = 1$ (full line), $n = 3$ (dashed line), $n = 7$ (dot-dashed line), $n = 11$ (long dashed line), $n = 15$ (dot-dot-dashed line) for the construction of orthogonal bases suitable for the flow through semi-infinite pipes

4.3.2 Boundary Layer Domain \mathcal{D}_{bl}

Boundary layers pose, like the flow through pipes in the previous section, the fundamental question of turbulence modified by the presence of a wall. The simplest possible domain for this type of flow is the (noncompact) half-space

$$\mathcal{D}_{bl}(H) \equiv \{(x_1, x_2, x_3) : -\infty < x_1 < \infty, 0 \leq x_2 \leq H, -\infty < x_3 < \infty\} \quad (4.20)$$

with $0 < H \leq \infty$. It is admissible to let $H = \infty$; hence, the domain is then the half-space bounded by the $x_1 - x_3$ -plane forming the fixed wall boundary. A noncompact domain with an entrance section is defined by

$$\mathcal{D}_{bl}(H) \equiv \{(x_1, x_2, x_3) : 0 \leq x_1 < \infty, 0 \leq x_2 \leq H, -\infty < x_3 < \infty\} \quad (4.21)$$

If fluid is entering the flow domain through an entrance section an exit section must exist to maintain global mass balance. For $H = \infty$ the domain is the first quarter of R^3 .

The construction of a basis $\mathcal{B}(\mathcal{D}_{bl})$ in the phase space Ω is considered for $H < \infty$ and Cartesian coordinates. The boundary $\partial\mathcal{D} = \bigcup_{i=1}^4 \partial\mathcal{D}_i$ consists of the wall $\partial\mathcal{D}_1 = \{(x_1, 0, x_3) : 0 \leq x_1 < \infty, -\infty < x_3 < \infty\}$, the entrance boundary $\partial\mathcal{D}_2 = \{(0, x_2, x_3) : 0 < x_2 < H, -\infty < x_3 < \infty\}$, the upper boundary $\partial\mathcal{D}_3 = \{(x_1, H, x_3) : 0 \leq x_1 < \infty, -\infty < x_3 < \infty\}$ and the exit boundary $\partial\mathcal{D}_4 = \{(\infty, x_2, x_3) : 0 \leq x_2 \leq H, -\infty < x_3 < \infty\}$. Functions defined on an infinite or semi-infinite domain are not necessarily square integrable, for instance, the total kinetic energy of fluctuations could be infinite. The basis elements for $0 < H < \infty$ and constant are designed as tensor products of modes in the individual coordinate directions. The basis elements $f^{k,n,m}(\mathbf{x}) = s_k(x_1)q_n(x_2)h_m(x_3)$, where $h_m(x_3) = \frac{1}{\sqrt{2\pi}} \exp(imx_3)$ is the lateral Fourier mode with wavenumber m , for scalar fields such pressure satisfying appropriate boundary conditions on $\partial\mathcal{D}$, are then

$$p(t, \mathbf{x}) = \sum_{k,n,m} \tilde{p}^{k,n,m}(t) f^{k,n,m}(\mathbf{x}) = \lim_{N_i, i=1,2,3 \rightarrow \infty} p^{N_1, N_2, N_3}(t, \mathbf{x}) \quad (4.22)$$

The finite-dimensional projections are defined by

$$p^{N_1, N_2, N_3}(t, \mathbf{x}) \equiv \sum_{k=0}^{N_1} \sum_{n=0}^{N_2} \sum_{m=-\frac{N_3}{2}}^{\frac{N_3}{2}-1} \tilde{p}^{k,n,m}(t) s_k(x_1) q_n(x_2) h_m(x_3) \quad (4.23)$$

with respect to the scalar, orthonormal basis $\{f^{k,n,m}(\mathbf{x})\}$ completely specified below. The coefficients $\tilde{p}^{k,n,m}(t)$ must satisfy a relation such as (25.34) to insure that the pressure field is real-valued.

Longitudinal modes $s_k(x_1)$

The Laguerre functions (4.18), [2], Sect. 18.3,

$$s_k(x_1) \equiv l_k^{(\alpha)}(x_1) = \sum_{j=0}^k \frac{(-1)^j}{k!} \binom{k+\alpha}{k-j} x_1^j$$

are one of several ONSystems for the semi-infinite interval of definition, a few functions are shown in Fig. 4.4. They are orthonormal according to (4.19) for $\alpha > -1$.

Wall-normal modes $q_n(x_2)$

The direction normal to the wall boundary can be represented with the aid of ONS polynomial bases defined on the interval $[0, H]$. The basis functions can be classified into local and global functions.

(1) Global basis functions: There is a rich variety of ONSystems available [2]. The Chebyshev polynomial base is a possible choice, since it has several advantageous properties. The Chebyshev polynomials of the first $T_n(y)$ and second $U_n(y)$ kind

$$T_n(\cos \theta) = \cos(n\theta), \quad U_n(\cos \theta) = \frac{\sin((n+1)\theta)}{\sin \theta}, \quad y = \cos \theta \quad (4.24)$$

are defined on the symmetric interval $[-1, 1]$ with weight function $w(y) = (1 - y^2)^{-\frac{1}{2}}$, $y \equiv -1 + \frac{2x_1}{H}$. The ONS relation is thus

$$\int_{-1}^1 dy w(y) T_n(y) T_m(y) = \delta_{n,m}, \quad n, m \geq 0 \quad (4.25)$$

An exhaustive collection of properties such as differentiation, integration, interrelations, etc., can be found in [2], numerical example applications in Trefethen [12].

Jacobi polynomials are another popular choice as expansion functions on compact intervals. The classical Jacobi polynomials $P_n^{a,b}(x)$ (Abramowitz and Stegun [1], Chap. 22 and Olver et al. [2], Chap. 18) are defined on the interval $[-1, 1]$ (25.2), Sect. 25.8. They are orthogonal (25.4)

$$\int_{-1}^1 dx w^{a,b}(x) P_n^{a,b}(x) P_l^{a,b}(x) = \delta_{n,l} 2^{a+b+1} \frac{\Gamma(n+a+1)\Gamma(n+b+1)}{(2n+a+b+1)\Gamma(n+1)\Gamma(n+a+b+1)}$$

with weight function (25.3) $w^{a,b}(x) = (1-x)^a(1+x)^b$ and $a, b > -1$. Details can be found in Sect. 25.8 of Appendix C.

(2) Local basis functions: Extensive research on DNS methods lead to sophisticated numerical approaches for the solution of IBVP's for the Navier–Stokes pdes. A promising method employs a B-spline basis for one or more directions, see Loulou et al. [13] for the application to pipe flow DNS and review by Botella and Shariff [14].

Individual B-splines of order k are defined on a limited support of $k + 1$ subintervals $[y_i, y_{i+1}]$, y being a linear transform of x_2 , of $[0, H] = \bigcup_{i=0}^N [y_i, y_{i+1}]$ with $N + 1$ knots, the subintervals must be contiguous and non-overlapping. The B-splines are polynomials of order k on each set of support intervals with C^m , $0 \leq m \leq k - 2$, regularity at the breakpoints x_j , de Boer [15]. Multiple knots are defined at each end point to enable the enforcement of boundary conditions, i.e. $-k \leq j \leq N + k$. The lateral variation of the scalar field is then represented by the lateral mode

$$q_k(x_2; \alpha_k^{-k}, \dots, \alpha_k^{N+k}) = \sum_{j=-k}^{N+k} \alpha_k^j b_j^k(y(x_2)) \quad (4.26)$$

where $b_j^k(y)$ denotes the B-spline defined on its support of subintervals $[y_j, y_{j+1}]$. Figure 4.5 shows the B-splines $b_j^k(x)$ for $k = 4$ near the left boundary of $[0, 1]$, the support consists of $k + 1$ intervals in the inner part of the domain. It illustrates the treatment of boundary conditions using multiple node points $-k \leq j < 0$. The lateral mode for Dirichlet conditions at $x_2 = 0$, boundary value $p_0(t, 0)$, and $x_2 = H$, boundary value $p_1(t, H)$, emerges in the form

$$q_k(x_2; \alpha_k^{-k+1}, \dots, \alpha_k^{N+k-1}) = p_0(t, 0) b_{-k}^k(y(x_2)) + \sum_{j=-k+1}^{N+k-1} \alpha_k^j b_j^k(y(x_2)) + p_1(t, H) b_{N+k}^k(y(x_2))$$

Neumann and Robin type boundary conditions can be handled as easily. Further details on the recursive relations for the B-splines, related expressions and application to Galerkin methods can be found in Botella and Shariff [14]. However, the basis

$$\{q_k(x_2; \alpha_k^{-k+1}, \dots, \alpha_k^{N+k-1}) : \alpha_k^{-k+1}, \dots, \alpha_k^{N+k-1} \in (-\infty, \infty), 0 < N < \infty\}$$

for $k > 0$ fixed is well suited for numerical applications, but it is not orthonormal, since the $k + 1$ intervals of definition for individual B-splines overlap for $k > 0$ (as seen in Fig. 4.5) and the coefficient matrix for orthogonalization is, therefore, not sparse. This makes the application of B-spline bases to the solution of functional pdes difficult.

Lateral modes $h_m(x_3)$

The lateral extent of the flow domain is $(-\infty, \infty)$ with the associated difficulty of Fourier transformation of functions that are not in $L^2_{(-\infty, \infty)}$. This inconvenience is avoided by replacing the lateral extent with a bounded interval $[-\frac{1}{2}S \leq x_3 \leq \frac{S}{2}]$ and requiring periodicity with respect to x_3 . The lateral part of the basis functions is, therefore, $h_m(x_3) = \frac{1}{\sqrt{2\pi}} \exp(imx_3)$ and

$$f^{k,n,m}(\mathbf{x}) = s(x_1)q(x_2) \exp(imx_3), \quad -\frac{S}{2} \leq x_3 \leq \frac{S}{2} \quad (4.27)$$

with S being a (large) multiple of 2π .

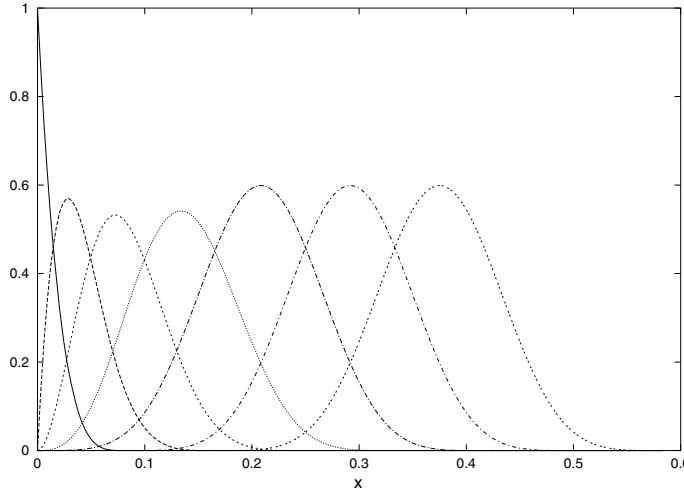


Fig. 4.5 B-splines $b_j^k(x)$ for $k = 4$ and $j = -k, \dots, 1$ near the left boundary of the domain $[0, 1]$ with equally spaced distinct knot points x_j

4.3.3 Free Shear Layer Domain \mathcal{D}_{fs}

The flow domain for free shear layers such as jets, wakes, mixing layers is a suitable half-space. These flows have a well-defined entrance section (i.e. the velocity is known); hence, the noncompact domain is defined as

$$\mathcal{D}_{fs}(H) \equiv \{(x_1, x_2, x_3) : -\infty < x_1, x_2 < \infty, 0 \leq x_3, 0 < \infty\} \quad (4.28)$$

with the x_3 -direction being the main flow orientation. The choice of coordinate system depends on the geometric properties of the entrance section.

The case of plane mixing layers is considered to illustrate approaches for the construction of bases for noncompact domains in Cartesian coordinates. There are two ways to deal with semi-infinite or infinite range of the basis functions: Either construct basis functions decaying rapidly as infinity is approached or design mappings for $[0, \infty) \rightarrow [0, 1)$ or $(-\infty, \infty) \rightarrow (-1, 1)$.

Direct approach

The Hilbert space $\mathcal{H} = L^2_{R^1}$ has a an orthonormal basis defined by the set of Hermite functions ([2], Chap. 18)

$$\Psi_n(x) = (2^n n! \sqrt{\pi})^{-\frac{1}{2}} \exp(-\frac{x^2}{2}) H_n(x) \quad (4.29)$$

for $n = 0, 1, 2, \dots, \infty$, where $H_n(x)$ denotes the n^{th} Hermite polynomial (physicist's version)

$$H_n(x) = (-1)^n \exp(x^2) \frac{d^n}{dx^n} \exp(-x^2) \quad (4.30)$$

Several Hermite functions $\Psi_n(x)$ are shown in Fig. 4.6 for $n = 0, 1, 2, 7, 30$ indicating that the $\Psi_n(x)$ are symmetric for n even and antisymmetric for n odd. The first derivative relation

$$\frac{d\Psi_n}{dx} = \begin{cases} -\sqrt{\frac{1}{2}(n+1)}\Psi_{n+1}(x) + \sqrt{\frac{1}{2}n}\Psi_{n-1}(x) & \text{for } n > 0 \\ -\sqrt{\frac{1}{2}(n+1)}\Psi_{n+1}(x) & \text{for } n = 0 \end{cases} \quad (4.31)$$

and the recursive relation

$$x\Psi_n(x) = \begin{cases} \sqrt{\frac{1}{2}(n+1)}\Psi_{n+1}(x) + \sqrt{\frac{1}{2}n}\Psi_{n-1}(x) & \text{for } n > 0 \\ \sqrt{\frac{1}{2}(n+1)}\Psi_{n+1}(x) & \text{for } n = 0 \end{cases} \quad (4.32)$$

are noted for later use, for proof see the solution to Problem (13.3) in Appendix F. Higher derivatives can easily be obtained from it. An element $y(x) \in \mathcal{H}$ is thus represented by a convergent series

$$y(x) = \sum_{j=0}^{\infty} y_j \Psi_j(x) \quad (4.33)$$

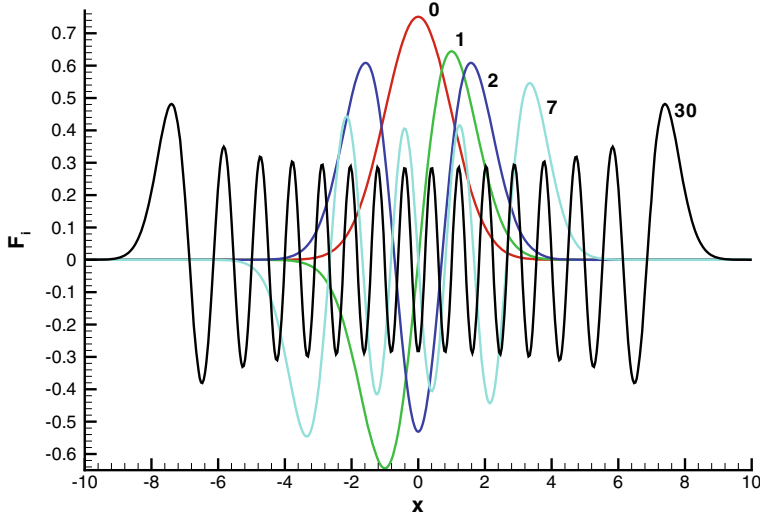


Fig. 4.6 Hermite functions (4.29) $\Psi_n(x) = (2^n n! \sqrt{\pi})^{-\frac{1}{2}} \exp(-\frac{x^2}{2}) H_n(x)$ for $n = 0$ (grey), $n = 1$ (green), $n = 2$ (blue), $n = 7$ (magenta), $n = 30$ (black)

with inverse relation

$$y_j = (y, \Psi_j), j = 0, 1, 2, \dots, \infty \quad (4.34)$$

with $\{y_0, y_1, \dots, y_\infty\}$ element of the space l^2 of infinite sequences with norm

$$\|y\|^2 = \sum_{j=0}^{\infty} |y_j|^2$$

equal to the norm (22.18) defined in L^2 . The representation (4.33) and its inverse (4.34) generate thus an isomorphism of L^2 and l^2 . The convergence of the Hermite function basis is illustrated in Problem 4.2 at the end of the present section with solution in Chap. 28, Appendix F.

Mapping approach for semi-infinite domains

Spalart et al. [16] constructed basis functions for the Galerkin method to solve the Navier–Stokes pdes, which provides examples applicable to mixing layers and wakes for the basis spanning the phase space. They employ the mapping method for boundary and mixing layers. An example for a mapping for one of the lateral directions, say x_1 , is

$$\eta \equiv \tanh\left(\frac{x_1}{x_1^0}\right) : (-\infty, \infty) \rightarrow (-1, 1)$$

where x_1^0 is an appropriate length scale (estimated shear layer thickness). The basis functions are then set up in tensor product form

$$f^{k,n,m}(\mathbf{x}) = R_k(\eta(x_1))q_n(x_2)r_m(x_3) \quad (4.35)$$

The modes $R_k(\eta(x_1))$ can be constructed with the aid of orthogonal polynomials as function of the image variable η . The numerical method of Spalart et al. [16] employs Jacobi polynomials $P_n^{\alpha,\beta}$ (see [2] Chap. 18)

$$R_k(\eta) = (1 - \eta^2)P_k^{\alpha,\beta}(\eta) \quad (4.36)$$

with $\alpha = \beta = 1$ ensuring $f^{k,n,m}(x_1, x_2, x_3)$ vanishes for $|x_1| \rightarrow \infty$. It is straightforward to verify the orthogonality relation

$$\int_{-\infty}^{\infty} dx_1 R_k(\eta(x_1)) R_m(\eta(x_1)) = \delta_{k,m} x_1^0 \frac{8(k+1)}{(2k+3)(k+2)} \quad (4.37)$$

Spalart et al. [16] discuss in detail the numerical properties of the Galerkin solver for the Navier–Stokes pdes employing the modified Jacobi polynomials R_n (4.36) for one of the lateral directions and Fourier modes in the other two directions

$$q_n(x_2)r_m(x_3) = \exp[i(nx_2 + mx_3)] \quad (4.38)$$

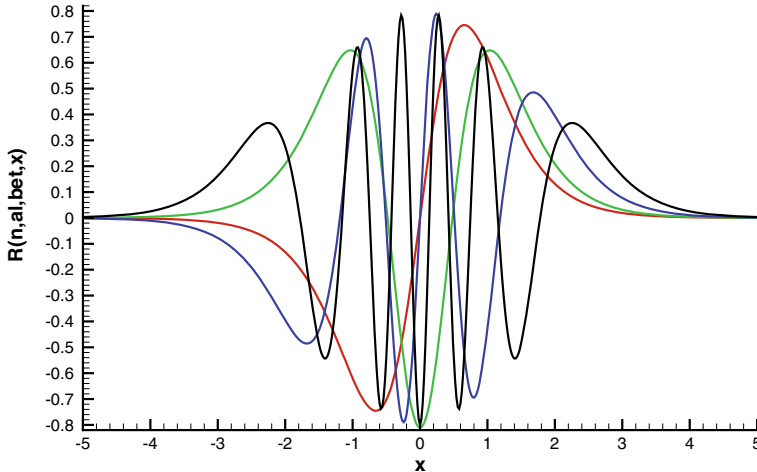


Fig. 4.7 Lateral mode (modified Jacobi polynomial, $\alpha = \beta = 1$) $R_n(\eta(x_1))$ of basis functions suitable for mixing layers for $n = 1$ (red line), $n = 2$ (green), $n = 5$ (blue) and $n = 10$ (black) as function of $x_1 = x_1^0 \operatorname{arctanh}(\eta)$, the inverse of the mapping $\eta(x_1) = \tanh(\frac{x_1}{x_1^0})$. The reference length for the mapping $\eta(x_1) = \tanh(\frac{x_1}{x_1^0})$ is $x_1^0 = 1.0$

Rogers and Moser [17] simulated the temporal mixing layer with this method and present accurate DNS results. Figure 4.7 shows several lateral modes for the basis functions with $n = 1, 2, 5, 10$ as indicated by colour. The modes decay rapidly for $|x_1| \rightarrow \infty$ as required for integrability, this also illustrated in Problem 4.2 with solution in Appendix F.

The choice for the modes $q_n(x_2)$ in the second lateral and $r_m(x_3)$ the longitudinal directions is guided by the physics of the flow. The mixing layer is statistically plane as single-point moments are not dependent on x_2 ; hence, periodicity with respect to a sufficiently large interval is an interesting case avoiding velocity fields with infinite energy.

4.4 Problems for this Chapter: Flow Domains and Bases

Problem 4.1 The Jacobi orthogonal polynomials $P_n^{\alpha,\beta}(x)$, which are the solutions of the ode

$$(1-x^2) \frac{d^2 P_n^{\alpha,\beta}}{dx^2} + [\beta - \alpha - (\alpha + \beta + 2)x] \frac{d P_n^{\alpha,\beta}}{dx} + n(n + \alpha + \beta + 1) P_n^{\alpha,\beta} = 0$$

are related to the Sturm–Liouville ode, which in turn appears in the construction of basis functions and the evaluation of certain functional integrals. Hence, clarify this

relation by determining the eigenvalues and eigenfunctions of the Sturm–Liouville operator (6.35)

$$\mathcal{L} \equiv \frac{1}{w(x)} \left[\frac{d}{dx} \left(p(x) \frac{d}{dx} \right) - q(x) \right]$$

defined on the interval $[-1, 1]$ for $p(x) = (1-x)^{\alpha+1}(1+x)^{\beta+1}$, $q(x) = 0$ and weight function $w(x) = (1-x)^\alpha(1+x)^\beta$. Assume $\alpha, \beta > -1$.

(4.1.1) Show that the Sturm–Liouville operator is self-adjoint, i.e. $(\mathcal{L}u, v) = (u, \mathcal{L}v)$ holds with respect to the scalar product

$$(u, v) \equiv \int_{-1}^1 dx w(x) u(x) v(x)$$

for $u(x), v(x) \in C_{[-1,1]}^2$.

(4.1.2) Verify that the Jacobi polynomials are eigenfunctions of the Sturm–Liouville operator for the specified coefficients.

(4.1.3) Expand the test function $f(x) = \sin(\pi kx)$ for $k = 1$ and $k = 16$ in terms of the Jacobi basis $\{P_n^{\alpha,\beta}, n = 0, 1, 2, \dots\}$ for $\alpha = \beta = 0$ fixed. Compute and plot the error

$$e(N) \equiv |f(x) - \sum_{i=0}^N c_i P_i^{\alpha,\beta}|$$

as function of N and the test function $f(x)$ together with partial sums of the expansion.

Problem 4.2 The Hermite functions (Sect. 4.3.3) are a basis for the space $\Omega = C_{R^1}^\infty \cap L_{R^1}^2$ of functions defined on the unbounded domain R^1 . Determine the coordinates c_i with respect to the basis $\{\Psi_n(x) : n = 0, 1, \dots, \infty\}$ of the test function

$$f(x) = \frac{\cos(kx)}{\sqrt{2\pi\sigma^2}} \exp\left(-\frac{1}{2\sigma^2}(x - x_0)^2\right)$$

for $k = 4$, $x_0 = 0.0$ and $\sigma = 0.5$ as defined in Eq. (4.33) of Sect. 4.3.3. Compute the maximum norm of the error

$$e(N) \equiv |f(x) - \sum_{i=0}^N c_i \Psi_i^x|$$

as function of N . Plot the coefficients c_i , the error $e(N)$ and the test function compared to the approximation for $N = 20$ terms.

Problem 4.3 Solve the BVPs for the Poisson pdes

$$\epsilon_{\delta\eta\alpha} \frac{\partial \omega_\alpha}{\partial x_\eta} = \frac{\partial^2 v_\eta}{\partial x_\delta \partial x_\eta} - \frac{\partial^2 v_\delta}{\partial x_\eta \partial x_\eta}$$

or in symbolic notation

$$\nabla \times \boldsymbol{\omega} = \nabla(\nabla \cdot \mathbf{v}) - \Delta \mathbf{v}$$

for the disturbance velocity for a doubly periodic flow in a cubic domain \mathcal{D} in Cartesian coordinates. The domain is defined by

$$\mathcal{D} \equiv \{(x_1, x_2, x_3) : 0 \leq x_1 \leq 2\pi L_1, -L_2 \leq x_2 \leq L_2, -\pi L_3 \leq x_3 \leq \pi L_3\}$$

with x_1 and x_3 as periodic directions. Velocity is the sum of the disturbance field $\mathbf{v}(\mathbf{x})$ periodic with respect to x_1 and x_3 and a basic/mean field

$$V_\alpha(x_1, x_2, x_3) = \delta_{\alpha,1} V_1(x_2) + v_\alpha(x_1, x_2, x_3)$$

The basic field $V_1(x_2)$ is assumed known, for instance, constructed analytically using the Gaussian error function. Assume an incompressible fluid.

(4.3.1) Fourier transform the Poisson pde to set up the BVP for the odes governing the complex-valued Fourier modes $\tilde{v}_\alpha^{k,m}(x_2, t)$, where k and m are the wavenumbers corresponding to x_1 and x_3 .

(4.3.2) Solve the BVP for the Fourier modes.

Problem 4.4 Let $\Omega = \{\mathbf{v}(\mathbf{x}) \in L^2_{\mathcal{D}} \cap C^2_{\mathcal{D}}\}$ be the phase space for the compact flow domain $\mathcal{D} \subset \mathbb{R}^3$ with n.e. smooth boundary $\partial\mathcal{D}$, Ω is then Hilbert space w.r.t.

$$\|\mathbf{v}\|^2 = (\mathbf{v} \cdot \mathbf{v})$$

and scalar product

$$(\mathbf{v}, \mathbf{w}) \equiv \int_{\mathcal{D}} d\nu v_\alpha(\mathbf{x}) w_\alpha(\mathbf{x})$$

(Cartesian coordinates), let $F[\mathbf{v}] : \Omega \rightarrow \mathbb{R}^1$ be a linear functional defined by

$$F[\mathbf{v}] \equiv \int_{\mathcal{D}} d\nu K_\alpha(\mathbf{x}) v_\alpha(\mathbf{x})$$

for $K_\alpha(\mathbf{x}) \in \Omega$.

- (4.4.1): Compute the first Gateaux derivative of the functional $F[\mathbf{v}]$ w.r.t. $\mathbf{v}(\mathbf{x})$.
 (4.4.2): Compute the first Gateaux derivative of (4.4.1) w.r.t. the ONS vector basis $\mathcal{B} \equiv \{\mathbf{f}^k(\mathbf{x}), k = 1, \dots, \infty\}$.
 (4.4.3): Compute the second Gateaux derivative w.r.t. $\mathbf{v}(\mathbf{x})$.

Hint: Consult Sect. 23.12.

References

1. Abramowitz, M., Stegun, I.A.: Handbook of Mathematical Functions. Dover, New York (1972)
2. Olver, F.W., Lozier, D.W., Boisvert, R.F., Clark, C.W.: NIST Handbook of Mathematical Functions. Cambridge University Press, U.K. (2010)
3. Batchelor, G.K.: The Theory of Homogeneous Turbulence. Cambridge University Press (1967)
4. Robinson, S.K.: Coherent motions in the turbulent boundary layer. *Ann. Rev. Fluid Mech.* **23**, 601–639 (1991)
5. Zagarola, M.V., Smits, A.J.: Mean-flow scaling of turbulent pipe flow. *JFM* **373**, 33–79 (1998)
6. Smits, A.J. (ed.): IUTAM Symposium on Reynolds Number Scaling in Turbulent Flow. Kluwer Academic Publishers, Dordrecht (2004)
7. McKeon, B.J., Swanson, C.J., Zagarola, M.V., Donnelly, R.J., Smits, A.J.: Friction factors for smooth pipe flow. *JFM* **511**, 41–44 (2004)
8. Boyd, J.P.: Chebyshev and Fourier Spectral Methods. Dover Publ. Inc., Mineola, New York (2001)
9. Kollmann, W.: Simulation of vorticity dominated flows using a hybrid approach: i formulation. *Comput. Fluids* **36**, 1638–1647 (2007)
10. Tsinuber, A.: Vortex Stretching versus Production of Strain/Dissipation. In: Hunt, J.C.R., Vasilicos, J.C. (eds.) Turbulence Structure and Vortex Dynamics. Cambridge University Press, Cambridge U.K. (2000)
11. Pileckas, K.: Navier-Stokes system in domains with cylindrical outlets to infinity. In: Friedlander, S., Serre, D. (eds.) Handbook of Mathematical Fluid Dynamics, vol. 4, North Holland, pp. 447–647 (2007)
12. Trefethen, L.N.: Spectral Methods in MATLAB. SIAM (2000). Philadelphia
13. Loulou, P., Moser, R.D., Mansour, N.N., Cantwell, B.J.: Direct Numerical Simulation of Incompressible Pipe Flow Using a B-spline Spectral Method, p. 110436. NASA Techn. Memor (1997)
14. Botella, O., Shariff, K.: B-spline methods in fluid dynamics. *Int. J. Comput. Fluid Dyn.* **17**, 133–149 (2003)
15. de Boer, C.: A Practical Guide to Splines, rev edn. Springer, New York (2001)
16. Spalart, P.R., Moser, R.D., Rogers, M.M.: Spectral methods for the navier- stokes equations with one infinite and two periodic directions. *J. Comput. Phys.* **96**, 297–324 (1991)
17. Rogers, M.M., Moser, R.D.: Direct simulation of a self-similar turbulent mixing layer. *Phys. Fluids* **6**, 903–923 (1994)

Chapter 5

Phase and Test Function Spaces



The state of a flow can be represented as a point or a pathline in an appropriately set up function space, called phase space and denoted by Ω , which contains all possible flow states for all times. Function spaces are the necessary tool for construction of the phase space of a turbulent flow. The most important spaces are defined and briefly discussed in Appendix A, Sect. 23.7.

The union of a strange attractor A and its basin of attraction B (defining properties TA.1, TA.2, TA.3 in Sect. 3.2) of a turbulent flow is not a linear space due to the nonlinearity and non-locality of the equations generating it. Hence, $A \cup B$ must be embedded in a suitable linear function space, $A \cup B \subset \Omega$. However, the design of the phase space Ω is hampered by the lack of regularity theorems for the 3-d solutions of the Navier–Stokes equations at high Reynolds numbers in the turbulent regime ([1, 2] and Sect. 2.2). Hence, function spaces are constructed assuming certain regularity properties, which are able to support strange attractors and thus serve as possible candidates for a phase space.

5.1 Solution Sets

The possible solutions $v_\alpha(t, \mathbf{x})$ of a well-posed IBVP for the Navier–Stokes Eqs. (2.6) and (2.7) governing the motion of a single, incompressible, Newtonian fluid are either point sets or orbits in the associated phase space Ω containing the strange attractor A . The phase space Ω depends on the choice of definition of a point:

(i) If the complete time history is regarded as an abstract point $\mathbf{v}(t, \mathbf{x})$, the flow domain is $[0, \infty) \times \mathcal{D}$ and the phase space is the point set

$$\Omega_T = \{v_\alpha(t, \mathbf{x}) : t \in [0, T], \mathbf{x} \in \mathcal{D}\} \quad (5.1)$$

Each solution of the Navier–Stokes equation, started with suitable initial data, is a single point in this phase space.

(ii) The second option is the space of vector fields $u_\alpha(\mathbf{x}) = v_\alpha(t, \mathbf{x})$ with flow domain \mathcal{D} denoted by

$$\Omega(t) = \{u_\alpha(\mathbf{x}) : \mathbf{x} \in \mathcal{D}\}, \quad t \in [0, T] \quad (5.2)$$

the temporal evolution of the flow field generates a line in this space: The operator T_t , defined by (2.49), generates a continuous sequence of points $\mathbf{u}(\mathbf{x})$ in phase space called orbit $\{T_t \mathbf{u}^0 : 0 \leq t \leq T\}$ analogous to the orbit in R^3 of a point mass under the influence of an external force in Newtonian mechanics. The geometric properties of the pathline depend on the smoothness of the solution of the Navier–Stokes pdes, which are not completely known for $Re \gg 1$, as discussed in Sect. 2.2. Hence, this operator T_t maps the phase space Ω onto itself. If the flow is truly (and asymptotically) turbulent according to the definition (mTF) of maintained turbulence in Sect. 3.1 and $T = \infty$ is allowed, the orbit will eventually be caught in a subset A of Ω called a strange attractor.

In general, the asymptotic state of a flow of a viscous, Newtonian fluid at $Re \gg 1$ may be roughly classified as follows:

(AS1) A single fixed point, if the turbulence decays asymptotically to the origin, or the flow remains laminar. There is some evidence that the latter is possible as there are shear flows (plane Couette and pipe flow, [3]) that remain linearly stable for all Reynolds numbers and there are particular rotating flows (quasi-Keplerian flows, [4]) that are nonlinearly stable for very high Reynolds numbers. This calls into question the ergodicity of turbulent shear flows.

(AS2) An oscillatory motion in a limit cycle.

(AS3) A quasi-periodic motion on a torus.

(AS4) An irregular set of points A called strange attractor.

It is this strange attractor A and its basin of attraction B that contain the essential properties of the turbulent flow. A particular phase space is considered in the next section. Note that all scalar and vector fields in the following must be dimensionless for various norms (for instance, Sobolev norms) to make sense.

5.2 Phase Space for the Turbulence Measure: Incompressible Fluids and Homogeneous Boundary Conditions

The (second option) phase space Ω of the incompressible Navier–Stokes equations can be constructed with the aid of a sequence of function spaces (Vishik [5], Vishik and Fursikov [6], Chap. I, Sect. 4). Let the compact flow domain $\mathcal{D} \subset R^3$ with smooth and orientable boundary $\partial\mathcal{D}$, that encloses the flow domain, be defined with homogeneous boundary conditions $\mathbf{v}(\mathbf{x}, t) = 0, t \in [0, \infty), \mathbf{x} \in \partial\mathcal{D}$, then is the phase space Ω constructed as follows:

The space of infinitely often differentiable and solenoidal vector fields (dimension $d = 2, 3$)

$$\mathcal{V} \equiv \{\mathbf{v}(\mathbf{x}) \in (C_0^\infty(\mathcal{D}))^d : \nabla \cdot \mathbf{v} = 0\} \quad (5.3)$$

$(\mathbf{v}(\mathbf{x}) \in (C_0^\infty(\mathcal{D}))^d$ indicates that all components of \mathbf{v} are in C_0^∞) defined on the flow domain \mathcal{D} with boundary $\partial\mathcal{D}$ is the basic building block for the phase space Ω ($C_0^\infty(\mathcal{D})$ denotes the space of infinitely often differentiable vector fields that vanish outside a compact subset of \mathcal{D}). \mathcal{V} is equipped with the norm

$$\|\mathbf{v}\|_{\mathcal{V}} = \text{ess sup}_{\mathbf{x} \in \mathcal{D}} |\mathbf{v}(\mathbf{x})| < \infty \quad (5.4)$$

where ess sup denotes the essential supremum, it is equal to the lower bound of all constants C such that the set $\{\mathbf{x} : |\mathbf{v}(\mathbf{x})| > C\}$ has the Lebesgue measure zero (see Sect. 23.12.1 for the Lebesgue integral). The normed space \mathcal{V} is a Banach, but not a Hilbert space, since no scalar product can be defined.

Several function spaces are now constructed by closure, i.e. all limit points (vector fields in the present context) with respect to a particular norm are added to the space. The Hilbert space

$$\mathcal{H}^0 \equiv \text{Closure of } \mathcal{V} \text{ in } (L_2(\mathcal{D}))^d \quad (5.5)$$

is the space \mathcal{V} with all limit points of all sequences convergent with respect to the norm

$$\|\mathbf{v}\|_{L_2} = \left(\int_{\mathcal{D}} d\nu |\mathbf{v}(\mathbf{x})|^2 \right)^{\frac{1}{2}} \quad (5.6)$$

are added. The Hilbert spaces

$$\mathcal{H}^k \equiv \text{Closure of } \mathcal{V} \text{ in } (H^k(\mathcal{D}))^d \quad (5.7)$$

(k integer, $d = 2, 3$) are the spaces \mathcal{V} with all limit points of all sequences convergent with respect to the norm

$$\|\mathbf{v}\|_{H^k} = \left(\int_{\mathcal{D}} d\nu \sum_{|\alpha| \leq k} |\partial^\alpha \mathbf{v}(\mathbf{x})|^2 \right)^{\frac{1}{2}} < \infty \quad (5.8)$$

For $k = 1$, the Sobolev space $H^1 \equiv W_p^1$, $p = 2$ is obtained as explained in Appendix A, Sect. 23.7, the multi-index differential operator ∂^α is defined in Eq. (23.14) of Appendix A.

The Hilbert space

$$\mathcal{H}^2(\mathcal{D}) \equiv \mathcal{H}^1 \cap (H^2(\mathcal{D}))^d \quad (5.9)$$

is the intersection of \mathcal{H}^1 and H^2 , where the Sobolev space $H^2 = W_2^2$ is defined analogously to H^1 .

Finally the Hilbert space Ω

$$\Omega = \mathcal{H}^{1,2} \equiv \{\mathbf{v}(\mathbf{x}, t) \in L_2(0, \infty, \mathcal{H}^2) : \frac{\partial \mathbf{v}}{\partial t} \in L_2(0, \infty, \mathcal{H}^0)\} \quad (5.10)$$

where $0, \infty$ refers to the time interval, is the phase space of incompressible turbulence in a compact domain \mathcal{D} with boundary $\partial\mathcal{D}$ and homogeneous boundary conditions. It is a separable Hilbert space, hence possess orthonormal bases.

The vector fields $\mathbf{v} \in (L_2(\mathcal{D}))^d$ can be projected onto the Hilbert space \mathcal{H}^0 by means of the orthogonal projection operator π

$$\pi : \mathbf{v} \in (L_2(\mathcal{D}))^d \rightarrow \mathcal{H}^0 \quad (5.11)$$

The Navier–Stokes equations for incompressible fluids emerge then in the equivalent form as

$$\frac{\partial v_\alpha}{\partial t} + \pi \left(v_\beta \frac{\partial v_\alpha}{\partial x_\beta} \right) = \frac{\partial}{\partial x_\beta} \left(\frac{\tau_{\alpha\beta}}{\rho} \right) + g_\alpha \quad (5.12)$$

For proof see Vishik and Fursikov [6], Chap. I, Theorem 4.1. The projection operator π can be constructed for geometrically simple domains with the aid of Green's functions as discussed in Sect. 9.2.1, the example of pipe flow periodic in axial direction is presented in detail in Appendix D, Sect. 26.

5.3 Phase Space: Noncompact Domains

Flow domains with entrance and/or exit sections, hence non-homogeneous Dirichlet boundary conditions for velocity, require a separate set up of the phase space. The construction of solenoidal vector fields is a non-trivial matter for flow domains with complicated boundary, hence a modified phase space can be set up starting with

$$\mathcal{V} = (C_0^\infty(\mathcal{D}))^d \quad (5.13)$$

instead of $\mathcal{V} \equiv \{\mathbf{v}(\mathbf{x}) \in (C_0^\infty(\mathcal{D}))^d : \nabla \cdot \mathbf{v} = 0\}$ and the Hilbert spaces $\mathcal{H}^0, \mathcal{H}^1, \mathcal{H}^2, \Omega$ constructed as above. The Navier–Stokes equations in the original or a mathematically equivalent form and containing the pressure gradient must be used in this case. Flow domains with boundary conditions different from the present homogeneous conditions require a new set up of the phase space, see Pileckas [7] for ideas to deal with open and/or noncompact domains.

Summary

The construction of a phase space Ω for a particular class of flow domains \mathcal{D} and turbulent flows of a viscous, Newtonian fluid in it, is tentative for two reasons, namely, the lack of regularity theorems for the Navier–Stokes pdes in $d = 3$ dimensions at

high Re -numbers, Sect. 2.2, and the possible existence of singularities of the second kind for $Re \rightarrow \infty$ as suggested by the Kolmogorov–Onsager hypotheses discussed in Chap. 17. The present construction may have to be revisited in the light of future research.

5.4 Argument/Test Function Space for Characteristic Functionals

The argument fields $y(\mathbf{x})$ of characteristic functionals $\theta[y(\cdot)]$ are defined on the flow domain \mathcal{D} as elements of a nuclear vector space denoted by \mathcal{N} . A nuclear space is defined by Gelfand and Vilenkin ([8], Chap. 3.2) as follows. Consider a Hilbert space H of functions $v(\mathbf{x})$ defined on the domain \mathcal{D} with countable infinite dimension, then a sequence of Hilbert spaces H_n is constructed by defining a sequence of scalar products $(\cdot, \cdot)_n$ and completing H with respect to the norm

$$\|v\|_n \equiv \sqrt{(v, v)_n} \quad (5.14)$$

to generate H_n . The elements of H are then an everywhere dense set in each H_n . The scalar products are arranged, such that for $m \leq n$ $(y, y)_m \leq (y, y)_n$ holds. Then the mapping $v^{(n)} \rightarrow v^{(m)}$ ($v^{(n)}$ and $v^{(m)}$ denote the element $v \in H$ as elements of H_n and H_m) of an everywhere dense set in H_n onto an everywhere dense set in H_m is continuous. Thus, this mapping can be extended to a continuous linear operator T_m^n , which maps H_n onto an everywhere dense subset of H_m .

Definition: A countable infinite Hilbert space H is nuclear, if for any m there is an n such that the mapping $T_m^n : H_n \rightarrow H_m$ has the form

$$T_m^n v = \sum_{k=1}^{\infty} \lambda_k (v, f^k) g^k, \quad v \in H_n \quad (5.15)$$

where $\{f^k(\mathbf{x}) \in H_n, k = 1, \dots, \infty\}$ and $\{g^k(\mathbf{x}) \in H_m, k = 1, \dots, \infty\}$ are ONS bases in H_n and H_m , respectively, and the $\lambda_k > 0$ with $\sum_{k=1}^{\infty} \lambda_k$ convergent.

This rather complicated definition is now illustrated with an example relevant to the flow through a straight, circular pipe.

5.5 Example for a Nuclear Space

Introducing cylindrical coordinates for the domain $\mathcal{D} = \{(r, x, z) : 0 \leq r \leq 1, -\pi \leq x \leq \pi, 0 \leq z \leq L\}$ implies that scalar and vector fields are periodic with respect to the angular coordinate x . Hence, the space $K(a)$ ($a = \pi$ for the present example) of infinitely often differentiable functions $v(x)$ periodic with period $2a$ and equipped with the norm

$$\|v\|_n^2 = \sum_{k=0}^n \int_{-a}^a dx v^{(k)}(x) \overline{v^{(k)}(x)}$$

where the overline denotes complex conjugate, is a countably infinite Hilbert space. The functions

$$f^k(x) = \exp(\pi k \frac{x}{a}), \quad 0 \leq k \leq \infty$$

form a non-normalized basis in $K(a)$ with respect to every scalar product

$$(g, h)_n = \sum_{k=0}^n \int_{-a}^a dx g^{(k)}(x) \overline{h^{(k)}(x)}$$

The completion of $K(a)$ with respect to the norm $\|g\|_{n+2}$ generates an embedding operator of $K_{n+2}(a)$ into $K_n(a)$ that is positive definite and has finite trace

$$\sum_{k=-\infty}^{\infty} \frac{\|g_k\|_n}{\|g_k\|_{n+2}} < \infty$$

This implies that $K(a)$ is nuclear.

Comments

Nuclear spaces are topological vector spaces with many of the useful properties of finite-dimensional vector spaces. The topology on nuclear spaces can be defined by a family of seminorms, whose unit balls decrease rapidly in size. Vector spaces whose elements are ‘smooth’ in some sense tend to be nuclear spaces; a typical example of a nuclear space is the set of smooth functions on a compact manifold.

All finite-dimensional vector spaces are nuclear, because every operator on a finite-dimensional vector space is nuclear. There are no Banach spaces that are nuclear, except for the finite-dimensional ones. In practice a sort of converse to this is often true: if a ‘naturally occurring’ topological vector space is not a Banach space, then there is a good chance that it is nuclear.

References

1. Serrin, J.: On the interior regularity of weak solutions of the Navier-Stokes equations. *Arch. Rat. Mech. Anal.* **9**, 187–196 (1962)
2. Kuksin, S., Shirikyan, A.: Mathematics of Two-dimensional Turbulence, Cambridge Tracts in Mathematics, vol. 194. Cambridge University Press, U.K. (2012)
3. Schmid, P.J., Henningson, D.S.: Stability and Transition in Shear Flows. Springer (2001)
4. Lopez, J.M., Avila, M.: Boundary-layer turbulence in experiments on quasi-Keplerian flows. *JFM* **817**, 21–34 (2017)
5. Vishik, M.J.: Analytic solutions of Hopf's equation corresponding to quasilinear parabolic equations or to the Navier-Stokes system. *Sel. Math. Sov.* **5**, 45–75 (1986)
6. Vishik, M.J., Fursikov, A.V.: Mathematical Problems of Statistical Hydromechanics. Kluwer Academic Publication, Dordrecht (1988)
7. Pileckas, K.: Navier-Stokes system in domains with cylindrical outlets to infinity. In: Friedlander, S., Serre, D., (eds.) *Handbook of Mathematical Fluid Dynamics*, vol. 4, North Holland, pp. 447–647 (2007)
8. Gelfand, I.M., Vilenkin, N.Y.: Generalized Functions, vol. 4. Academic Press, New York (1964)

Chapter 6

Probability Measure and Characteristic Functional



The variables for the complete description of the statistical properties of turbulence in incompressible Newtonian fluids and the associated equations governing them are set up and their fundamental properties, such as mathematical type, linearity/nonlinearity, solvability, etc., are discussed in the present section.

The central role is played by the turbulence measure $\mu(t, \mathbf{v})$, or, mathematically equivalent, the characteristic functional $\theta[\mathbf{y}; \mathbf{x}, t, \dots]$,

$$\theta[\mathbf{y}] \equiv \int_{\Omega} d\mu(\mathbf{v}) \exp[i(\mathbf{y}, \mathbf{v})], \quad \mathbf{y} \in \mathcal{N} \quad (6.1)$$

where $0 \leq t < \infty$ and (\cdot, \cdot) denotes the scalar product defined on the product space $\mathcal{N} \times \Omega$. The argument functions $\mathbf{v} \in \Omega$ and the test functions $\mathbf{y} \in \mathcal{N}$ are elements of suitable function spaces introduced in Sects. 5.2 and 5.4. Inspecting this definition, it becomes clear that (6.1) requires three notions to be established:

- (i) the phase space Ω , Sect. 5.2;
- (ii) the argument/test function space \mathcal{N} , Sect. 5.4;
- (iii) the construction of a measure on Banach/ Hilbert spaces and functional integration.

It remains to discuss the third point.

The probability measure μ determines the cumulative distribution function (Cdf), defined as

$$F_N(\mathbf{y}) \equiv \mu_N\{\mathbf{Y} \leq \mathbf{y}\} \quad (6.2)$$

for a N -dimensional random vector \mathbf{Y} . The finite-dimensional case is treated in detail in Chap. 11 with emphasis on the transport pdes for Cdf and Pdf.

It is sufficient for certain applications to construct the measure differential $d\mu(\mathbf{v})$, $\mathbf{v} \in \Omega$ to enable the integration over the phase space Ω instead of completely specifying the turbulence measure in terms of σ -algebra and the set function (measure) μ , as suggested by Cartier and DeWitt-Morette [1], DeWitt-Morette et al. [2], Cartier et al. [3] specifically for quantum physics.

The emphasis is placed presently on the characteristic functional $\theta[\mathbf{y}]$ for two elementary reasons:

(1) The relations of the statistical moments to the characteristic functional (9.6) are differential; hence, no functional integration is involved.

(2) The extension of the finite-dimensional case to the infinite-dimensional one is straightforward in contrast to Cdf/Pdfs, since differentiation generalizes easily to the infinite-dimensional case as variational or Fréchet or Gateaux derivatives, see Sect. 23.12 in Appendix A.

On the other hand, the relation of statistical moments to Cdf/Pdfs is of integral form (1.7), hence runs into the well-known difficulty that integrals of a bounded function over a compact domain in R^n approaches zero as the dimension n goes to infinity, see the brief presentation of the Cdf/Pdf and characteristic functional approaches in the Introduction, Chap. 1. This explains the choice of the characteristic functional as vehicle for the analysis of turbulent flows.

6.1 Elementary Properties of the Turbulence Measure

To appreciate the fundamental importance of the turbulence measure $\mu(t, \mathbf{w})$ or, mathematically equivalent, the characteristic functional $\theta[\mathbf{y}; \mathbf{x}, t, \dots]$, expectations such as the mean velocity field, local and non-local correlations of arbitrary order, etc., are shown to be computable without making any assumptions. Consider the set of solutions of the Navier–Stokes equations generated by the initial velocity fields $\mathbf{v}^0(\mathbf{x}), \mathbf{x} \in \mathcal{D}$ selected randomly according to the probability measure $\mu_0(\mathbf{v}^0)$ defined for the Borel sets in the function space \mathcal{H}^0 of initial velocity fields. There are two ways to determine the turbulence measure for $t \geq 0$:

(i) Compute the solution operator $T_t(Re)$ (2.49) of the IVP of the Navier–Stokes equations. This approach has been so far the domain of DNS (Direct Numerical Simulation), where individual orbits of finite length in phase space are determined by numerical means. However, no investigation of the asymptotic properties for maintained turbulence such as attractor measure and dimension can be carried out numerically for obvious reasons.

For the sake of argument, suppose the solution operator is known and the measure space $(\Omega, \mathcal{A}_0, \mu_0)$ of initial fields is specified, then is the turbulence measure at time $t \geq 0$ also known

$$\mu(t, B) = \mu_0(T_{-t}B), \quad B \in \mathcal{A}, \quad B_0 = T_{-t}B \in \mathcal{A}_0 \quad (6.3)$$

as image or push-forward of the measure μ_0 of initial fields with T_t as invertible mapping, i.e. $v_\alpha(t, \mathbf{x}) = T_t(Re)v_\alpha(0, \mathbf{x})$. To recognize the amount of information contained in the solution operator T_t , consider the example of the flow along a fixed wall boundary, where the flow is initially laminar. The initial measure μ_0 is then without loss of generality Gaussian with arbitrarily small but non-zero variance to trigger the effect of the sensitive dependence of the flow on the initial conditions.

The solution operator T_t develops the flow and thus the measure μ according to (6.3) through transition to a turbulent state. This indicates that the solution operator must possess asymptotically a highly complex structure nearly impossible to compute directly.

The expectation operator, denoted by angular brackets, is defined by

$$\langle \cdot \rangle \equiv \int_{\Omega} d\mu(\mathbf{v}) \cdot \quad (6.4)$$

The dot indicates the argument functional defined on the phase space Ω . The integral in (6.4) with respect to the turbulence measure μ is a functional integral over the phase space Ω of the Navier–Stokes pdes. Functional integration is a delicate, non-standard operation, since it cannot be constructed as straightforward extension of the standard Riemann/Lebesgue integral (see De Witt et al. [2], Simon [4], Cartier et al. [3], Klauder [5] for a discussion from the physicists point of view). An example for a measure differential for a functional integral is given by the Gaussian measure differential (23.208) in Sect. 23.18.2 of Appendix A. The mean velocity field is then according to (6.4)

$$\langle v_{\alpha} \rangle(t, \mathbf{x}) \equiv \int_{\Omega} d\mu(\mathbf{v}) v_{\alpha}(\mathbf{x}) \quad (6.5)$$

The generalization to higher order and spatial multipoint moments is straightforward.

(ii) Compute the solution $\theta[\mathbf{y}; t]$ of the IVP for the Hopf functional differential equation (fde). Then follow statistical moments from the solution, such as the mean velocity field $\langle \mathbf{v}(t, \mathbf{x}) \rangle$, by Gateaux /Fréchet differentiation of the characteristic functional $\theta[\mathbf{y}; t]$ at the origin $\mathbf{y} = 0$. No closure assumptions enter the computation at any stage. Suppose the characteristic functional has been determined, then follows the mean velocity field by differentiation according to (6.4), (9.1) in Sect. 9.2 and (23.46) in Appendix A

$$\frac{\delta \theta}{\delta y_{\alpha}}[\mathbf{y}; t, \mathbf{x}] = i \int_{\Omega} d\mu(\mathbf{v}) v_{\alpha}(\mathbf{x}) \exp[i(\mathbf{y}, \mathbf{v})] \quad (6.6)$$

The Gateaux derivative at the origin $\mathbf{y} = 0$ of the argument/test function space \mathcal{N} (Sect. 5.4) is then

$$\langle v_{\alpha} \rangle(t, \mathbf{x}) \equiv \int_{\Omega} d\mu(\mathbf{v}) v_{\alpha}(\mathbf{x}) = -i \frac{\delta \theta}{\delta y_{\alpha}}[0; t, \mathbf{x}] \quad (6.7)$$

The dependence on time of the mean velocity $\langle v_{\alpha}(t, \mathbf{x}) \rangle$ enters the result via the time dependence of the turbulence measure/characteristic functional. The generalization to higher order and spatial multipoint moments is straightforward.

The construction of measures and characteristic functionals is developed using fundamental theorems of Kolmogorov and Bochner–Minlos. They are discussed in the following sections to provide the basis for the derivation of several variants of the functional equation governing the evolution of the spatial $\theta[\mathbf{y}; t]$ and material $\theta[\mathbf{Y}; \tau]$ characteristic functionals.

A later Chap. 12 is devoted to local and global mappings of the domain of definition and the image space of the characteristic function/functional for finite and infinite dimensions. The aim is to prepare the ground for approximation methods for the solution of the fundamental equations for the characteristic functional and mappings.

6.2 Turbulence Measure for Incompressible Fluids

The definition of a measure on a function space follows the general definition of a measure on abstract sets ([6] Chap. II, [7] Chap. I). Let Ω be a non-empty set (sample space) and \mathcal{A} a set of subsets of Ω . The set of subsets \mathcal{A} is a σ -algebra iff the following conditions are satisfied:

(i) $\omega \in \mathcal{A}$ implies $\Omega - \omega \in \mathcal{A}$.

(ii) $\omega_i \in \mathcal{A}$, $i = 1, 2, 3, \dots$ implies $\bigcup_{i=1}^{\infty} \omega_i \in \mathcal{A}$.

The properties of a σ -algebra allow the definition of set non-negative functions called measures. The turbulence measure is a member of the subclass of real-valued, normalized measures, which are called probability measures. A set function $\mu(\omega)$ is a probability measure iff it satisfies the conditions:

(i) $\mu(\omega) \geq 0$ for all $\omega \in \mathcal{A}$.

(ii) $\mu\left(\bigcup_{i=1}^{\infty} \omega_i\right) = \sum_{i=1}^{\infty} \mu(\omega_i)$ for all countably infinite, pairwise disjoint sequences $\{\omega_i \in \mathcal{A} : i = 1, \dots, \infty, \omega_i \cap \omega_j = 0, i \neq j\}$.

(iii) $\mu(\Omega) = 1$.

The triple $(\Omega, \mathcal{A}, \mu)$ is then called a normalized measure or probability space. If the set Ω possesses a topology generated by a metric, then is the Borel σ -algebra \mathcal{A} defined as the minimal σ -algebra containing all open and closed sets of Ω .

The construction of measures on function spaces is aided by the Kolmogorov extension theorem in Sect. 6.3.2. The Hopf equation requires, either in version (9.46) the specification of the probability measure of the initial condition, or in version (9.40) the specification of the initial characteristic functional, which can be constructed directly or obtained from the initial measure via Fourier transform (9.1).

6.3 Construction of Measures as Limits of Cylinder Measures

The construction of measures on function spaces is a delicate matter, since the spaces are infinite-dimensional, where the dimension of such spaces is defined as the cardinality of a base. It relies on basic results from measure theory (see for instance Shilov [8], Dalecky and Fomin [7], Bogachev [9]) and the Kolmogorov extension theorem (Yamasaki [10]) stating the conditions that a sequence of cylinder measures converges to a measure).

Vishik and Fursikov [6] Chap. II provide the necessary background. Consider two function spaces $\Omega_i, i = 1, 2$ with σ -algebras $\mathcal{A}_i, i = 1, 2$ and a measure μ_1 on Ω_1 and a measurable mapping $T_t : \Omega_1 \rightarrow \Omega_2$, then is a measure $\mu_2 = T_t \mu_1$ defined on Ω_2 by

$$\mu_2(\omega) = T_t \mu_1(\omega) = \mu_1(T_{-t}\omega), \forall \omega \in \mathcal{A}_2, t \geq 0 \quad (6.8)$$

Lemma 2.4 in Chap. II [6] asserts that integrable functionals $\theta[\mathbf{v}]$ can be evaluated according to

$$\int \theta[\mathbf{v}] \mu_2(d\mathbf{v}) = \int \theta(T_t \mathbf{v}^0) \mu_1(d\mathbf{v}^0) \quad (6.9)$$

where \mathbf{v}^0 denotes the preimage of \mathbf{v} .

6.3.1 Cylinder Measures

Consider a locally convex space Ω (a topological vector space, in which the origin has a local base of absolutely convex absorbing sets, [11]) with the dual space Ω^* (the space of all bounded linear functionals defined on Ω , [11], see Sect. 23.7 in Appendix A). The value of a linear functional $l \in \Omega^*$ at $\mathbf{v} \in \Omega$ is denoted by $l(\mathbf{v})$. The Riesz representation theorem (see Conway [11] Chap. I.3, Kreyszig [12] Chap. 4.4 for proof) implies that there exists a $K(\mathbf{x}, \mathbf{x}') \in \Omega$ such, that $l(\mathbf{v})$ can be written in the form

$$l[\mathbf{v}(\cdot)] = \int_{\mathcal{D}} d\nu K(\mathbf{x}, \mathbf{x}') \mathbf{v}(\mathbf{x}') \quad (6.10)$$

where the integral is over the (flow) domain $\mathcal{D} \subset \mathbb{R}^3$. Let $N > 0$ be integer, then are cylinder sets C_N defined by

$$C_N \equiv \{x \in \Omega : (\varphi_1(x), \dots, \varphi_N) \in \mathcal{A}_N, \varphi_k \in \Omega^*, k = 1, \dots, N\} \quad (6.11)$$

where \mathcal{A}_N is a base of C_N [13].

For separable Hilbert spaces Ω , a countably infinite orthonormalized system (abbreviated by ONS) $\mathcal{B} \equiv \{\mathbf{f}_i(\mathbf{x}), i = 1, \dots, \infty\}$ can be constructed. Finite-dimensional subspaces Ω_m are spanned by $\{\mathbf{f}_i, i = 1, \dots, m\}$ and the orthogonal projection $P_m : \Omega \rightarrow \Omega_m$ is defined by

$$P_m \omega = \sum_{i=1}^m \omega_i \mathbf{f}_i, \quad \forall \omega \in \Omega \quad (6.12)$$

where $\omega = \sum_{i=1}^{\infty} \omega_i \mathbf{f}_i$ with coefficients $\omega_i = (\omega, \mathbf{e}_i)$ computed as scalar product. The orthogonal complement Ω_m^\perp of Ω_m is then defined by

$$\Omega_m \oplus \Omega_m^\perp = \Omega \quad (6.13)$$

A cylinder set is then given by

$$C = \omega \oplus \Omega_m^\perp, \quad \omega \in \mathcal{A}(\Omega_m) \quad (6.14)$$

where $\mathcal{A}(\Omega_m)$ is the algebra of subsets of Ω_m and ω is called the base of the cylinder set $C \subset \Omega$. The smallest σ -algebra of Ω containing $\mathcal{A}(\Omega_m)$ is denoted by $\mathcal{A}^m(\Omega)$ and the σ -algebra $\mathcal{A}(\Omega)$ is then the minimal σ -algebra containing $\bigcup_{i=1}^{\infty} \mathcal{A}^m$ (see Skorohod [14] for proof). The measure of the cylinder set C in Ω is

$$\mu(C) = \mu_m(\omega), \quad C \in \omega \oplus \Omega_m^\perp, \quad \omega \in \mathcal{A}(\Omega_m) \quad (6.15)$$

i.e. the m -dimensional measure of the cylinder base ω .

6.3.2 Kolmogorov Extension Theorem

Kolmogorov's theorem (Yamasaki [10], Chap. 2, Bogachev [15] Appendix Sect. A.3, Theorem A.3.21) provides the tool to construct probability measures from finite-dimensional projections.

Assume that a sample space Ω is specified, then the problem of constructing a probability measure on it requires two steps: First, a σ -algebra \mathcal{A} must be defined, and, second, a non-negative, normalized set function μ called probability must be specified. The construction of the σ -algebra is trivial for finite Ω , where usually the set of all subsets is chosen. The situation is different for sample spaces Ω that contain infinitely many elementary events (discrete sets or continuous sets). The set of all subsets is too large for many problems, since it contains a rich variety of sets of zero measure (events that have zero probability of occurrence but are by no means impossible) and sets that cannot be measured at all. Hence, a smaller σ -

algebra must be constructed suitable for the problem considered. The first step in such a construction is often the design of a finite algebra $\tilde{\mathcal{A}}$ of combined events, which satisfies the conditions

$$A, B \in \tilde{\mathcal{A}} \implies A \cup B \in \tilde{\mathcal{A}} \quad (6.16)$$

$$A \in \tilde{\mathcal{A}} \implies \bar{A} \in \tilde{\mathcal{A}}, \emptyset \in \tilde{\mathcal{A}} \quad (6.17)$$

and the construction of a finitely additive set function $\tilde{\mu}$ constrained by

$$\tilde{\mu}(\Omega) = 1 \quad (6.18)$$

$$\tilde{\mu}(\emptyset) = 0 \quad (6.19)$$

$$\tilde{\mu}\left(\bigcup_{i=1}^n A_i\right) = \sum_{i=1}^n \tilde{\mu}(A_i) \quad (6.20)$$

where $A_i \cap A_j = \emptyset$ for $i \neq j$ and $n < \infty$. The question arises then whether the finite algebra and the finite measure can be extended to the infinite case and thus complete the construction of a σ -algebra and the associated probability measure μ . The answer is given by Kolmogorov's extension theorem stated below.

Theorem (Kolmogorov): Let $\tilde{\mathcal{A}}$ be a set algebra of subsets of Ω , let $\tilde{\mu}$ be a finitely additive set function defined on $\tilde{\mathcal{A}}$ satisfying the conditions given above, then it is possible to construct a σ -additive measure μ defined on the σ -algebra \mathcal{A} , which is defined as the smallest σ -algebra containing $\tilde{\mathcal{A}}$. If for any sequence of sets $A_i \in \tilde{\mathcal{A}}$ such that $A_{i+1} \subset A_i$ and

$$\bigcap_{i=1}^{\infty} A_i = \emptyset \quad (6.21)$$

the condition

$$\lim_{i \rightarrow \infty} \tilde{\mu}(A_i) = 0 \quad (6.22)$$

holds, the σ -additive measure μ exists.

The measure thus created is unique and satisfies

$$\mu(A) = \tilde{\mu}(A) \quad (6.23)$$

for all $A \in \tilde{\mathcal{A}}$. The proof can be found in Bogachev [15] Appendix A.3, Theorem A.3.21.

The compatibility condition (6.22) may be difficult to apply. For separable Hilbert spaces, it can be replaced by the condition

$$\sup_m \int_{\Omega_m} \|\mathbf{v}\|_{(m)}^\gamma \mu_m(d\mathbf{v}) < \infty \quad (6.24)$$

If a $\gamma > 0$ exists, the cylinder measures are extendable to a σ -additive measure defined on $\mathcal{A}(\Omega)$ (Lemma 3.4 in Chap. II [15]). The finite-dimensional measure μ_m on $\mathcal{A}_m(\Omega_m)$ defines the measure $\mu^m(\omega \oplus \Omega_m^\perp) = \mu_m(\omega)$, $\forall \omega \oplus \Omega_m^\perp \in \mathcal{A}^m(\Omega)$. Furthermore, $\|\cdot\|_{(m)}$ is the restriction of $\|\cdot\|$ on Ω_m .

6.3.3 Examples of Measures in Function Spaces

The construction of measures on infinite-dimensional spaces is quite involved; hence, several examples are presented (Vishik and Fursikov [6]) to illustrate methods for the construction of such measures on infinite-dimensional function spaces, one of them is the well-known Wiener measure on a space of continuous functions.

The δ measure

The δ -measure is defined by

$$\delta(\mathbf{v}^0, \omega) = \begin{cases} 1 & \text{for } \mathbf{v}^0 \in \omega, \forall \omega \in \mathcal{A}(\Omega) \\ 0 & \text{otherwise} \end{cases} \quad (6.25)$$

where Ω is a metric space and $\mathcal{A}(\Omega)$ the Borel σ -algebra.

Measure constructed on a ball

An elaborate example for the construction of a measure is presented in Appendix B, Chap. 24.

6.3.4 Wiener Measure

The Wiener process is a continuous-time stochastic process with stationary, independent, Gaussian distributed increments. It is applied in a wide variety of fields, in particular in turbulence theory as stochastic forcing process [16, 17] and the closure of Pdf equations and their solution, see Pope [18]. The associated measure is introduced here to illustrate the construction of measures in a particular function space.

Consider the domain $\mathcal{D} = [0, 1]$ and the space C of continuous functions $f(x) : \mathcal{D} \rightarrow \mathbb{R}^1$ defined on it, C_0 is the subspace of functions $f(0) = 0$. The space C is equipped with the norm

$$\|f\| = \sup_{x \in \mathcal{D}} |f(x)| \quad (6.26)$$

making C a Banach space with metric

$$d(f, g) = \|f - g\| \quad (6.27)$$

generating the uniform topology on \mathcal{D} and making C a separable and complete space (called Polish space). The Wiener measure on C_0 is constructed with the aid of the Kolmogorov extension theorem in Sect. (6.3.2). A function $f(x) \in C_0$ is discretized as polygon $f(x) \leftarrow \{f(x_i) : x_i = i\Delta x, i = 1, \dots, N\}, N\Delta x = 1$. The values of a sample function $y = f(x)$ are distributed according to the Gaussian Pdf

$$P(y; x) = \frac{1}{4\pi D x} \exp\left(-\frac{y^2}{4Dx}\right) \quad (6.28)$$

Rescaling the independent variables such that $D = \frac{1}{4}$ holds, the probability μ_w for the event $\{a_1 < f(x_1) < b_1\}$ is

$$\mu_w(\{a_1 < f(x_1) < b_1\}) = \frac{1}{(\pi x_1)^{\frac{1}{2}}} \int_{a_1}^{b_1} dy_1 \exp\left(-\frac{y_1^2}{x_1}\right) \quad (6.29)$$

The Wiener measure is defined by the property that the events $\{a_i < f(x_i) < b_i\}$ and $\{a_j < f(x_j) < b_j\}$ are statistically independent for all $j \neq i$, i.e. the Wiener measure is Gaussian. It follows then that

$$\mu_w(\bigcap_{i=1}^N \{a_i < f(x_i) < b_i\}) = \frac{1}{(\pi \Delta x)^{\frac{N}{2}}} \int_{a_1}^{b_1} \cdots \int_{a_N}^{b_N} dy_1 \cdots dy_N \exp\left[-\frac{y_1^2}{x_1} - \sum_{i=2}^N \frac{(y_{i+1} - y_i)^2}{\Delta x}\right] \quad (6.30)$$

holds. The Wiener measure of a functional $F[f]$, $f(x) \in C_0$ is then the functional integral

$$\int_C F[f(x)] d\mu_w(f) =$$

$$\lim_{N \rightarrow \infty} \frac{1}{(\pi \Delta x)^{\frac{N}{2}}} \int_{a_1}^{b_1} \cdots \int_{a_N}^{b_N} dy_1 \cdots dy_N F(y_1, \dots, y_N) \exp\left[-\frac{y_1^2}{x_1} - \sum_{i=2}^N \frac{(y_{i+1} - y_i)^2}{\Delta x}\right] \quad (6.31)$$

where $F(y_1, \dots, y_N)$ is the value of the functional $F[f(x)]$ at the polygon $\{f(x_i) : x_i = i\Delta x, i = 1, \dots, N\}$. The expression under the limit in (6.31) contains two factors that approach zero and infinity, hence an indeterminate product. The integral over the Wiener measure can be recast in the form

$$\int_C F[f(x)]d\mu_w(f) = \frac{1}{N} \int_{-\infty}^{\infty} \cdots \int_{-\infty}^{\infty} F[f(x)] \prod_{x=0}^1 \exp \left[- \int_{x=0}^1 dx \left(\frac{df}{dx} \right)^2 \right] df(x) \quad (6.32)$$

The factor $1/N$ is a normalization factor determined by the condition

$$\int_C d\mu_w(f) = 1 \quad (6.33)$$

The integral in the exponent is the limit

$$\int_{x=0}^1 dx \left(\frac{df}{dx} \right)^2 = \lim_{\Delta x \rightarrow 0} \sum_{i=1}^N \left(\frac{f(x + \Delta x) - f(x_i)}{\Delta x} \right)^2 \Delta x \quad (6.34)$$

The computation of Wiener integrals is difficult, in some cases it can be related to differential equations as shown below and the problems at the end of the current section.

The Wiener integral theorems of Cameron and Martin

Cameron and Martin [19, 20] obtained explicit results for a certain class of Wiener integrals. These integrals turn out to be related to the Sturm–Liouville ode for the determinant of an infinite-dimensional matrix and require a few elementary properties of the eigenvalue theory for this ode. The linear Sturm–Liouville operator $\tilde{\mathcal{L}}$ (Hartmann [21], Chap. XI.4, Duffy [22], Chap. 2.3) is defined by

$$\tilde{\mathcal{L}} \equiv \frac{d}{dx} p(x) \frac{d}{dx} + q(x) \quad (6.35)$$

where $w(x) > 0$, $p(x) > 0$ in $[0, 1]$, $w(x)$, $p(x)$, $q(x)$ are at least continuous. The Sturm–Liouville eigenvalue problem on the unit interval is then

$$-\tilde{\mathcal{L}}f(x) = \lambda w(x)f(x) \quad (6.36)$$

defined on $\mathcal{D} = [0, 1]$ (see also Appendix D, Sect. 26.4 for an application of the Sturm–Liouville ode in a different context) with homogeneous boundary conditions $f(0) = 0$, $\frac{df}{dx}(1) = 0$. The coefficients $w(x) > 0$, $p(x) > 0$, $q(x)$ are continuous, λ is the eigenvalue. The following properties of the Sturm–Liouville eigenvalue problem are relevant to the evaluation of the Wiener integrals:

- (a) The eigenvalues λ_n are real, countable, ordered $\lambda_1 < \lambda_2 < \dots$ with smallest eigenvalue λ_1 .
- (b) For each eigenvalue λ_n exists an eigenfunction $\Phi_n(x)$ with $n - 1$ zeros in \mathcal{D} .
- (c) The eigenfunctions are orthogonal with respect to the scalar product

$$\langle \Phi_n, \Phi_m \rangle \equiv \int_0^1 dx w(x) \Phi_n(x) \Phi_m(x) \quad (6.37)$$

hence

$$\langle \Phi_n, \Phi_m \rangle = \delta_{n,m} \quad (6.38)$$

(d) The set of eigenfunctions is complete in C .

The relation of the particular class (6.39) and (6.40) of Wiener integrals to ordinary differential equations is explicitly shown in the solution of problem (6.1) in Appendix F, Sect. 28.

Consider now the space C of continuous functions defined on the unit interval \mathcal{D} . Cameron and Martin [20] prove the following theorems.

Theorem 6.1 *Let $g(x) \in L_2(\mathcal{D})$, $w(x) > 0 \in C$, let λ_1 be the smallest eigenvalue of the Sturm–Liouville EVP for $p(x) = 1$, $q(x) = 0$, let $f_\lambda(x)$ be any non-trivial solution of the Sturm–Liouville ode (6.36) with boundary condition $\frac{df}{dx}(1) = 0$ for $\lambda < \lambda_1$. Then is the Wiener integral given by*

$$\int_C \exp\left(\lambda \int_0^1 dx w(x) f^2(x)\right) d\mu_w(f) = \left(\frac{f_\lambda(1)}{f_\lambda(0)}\right)^{\frac{1}{2}} \quad (6.39)$$

For proof see [20]. Note that a solution of the Sturm–Liouville ode satisfying $\frac{df}{dx}(1) = 0$ is positive at $x = 0$ for $\lambda < \lambda_0$.

A generalization is stated in the next theorem

Theorem 6.2 *Let $g(x) \in L_2(\mathcal{D})$, $w(x) > 0 \in C$, let λ_1 be the smallest eigenvalue of the Sturm–Liouville EVP for $p(x) = 1$, $q(x) = 0$, let $f_\lambda(x)$ be any non-trivial solution of the Sturm–Liouville ode (6.36) with boundary condition $\frac{df}{dx}(1) = 0$ for $\lambda < \lambda_1$ and let $F[u]$, $u \in (-\infty, \infty)$ be Lebesgue integrable. Then is the Wiener integral given by*

$$\int_C \exp\left(\lambda \int_0^1 dx w(x) f^2(x)\right) F\left[\int_0^1 dx w(x) f(x)\right] d\mu_w(f) = \left(\frac{f_\lambda(1)}{\pi f_\lambda(0)}\right)^{\frac{1}{2}} \int_{-\infty}^{\infty} du F(bu) \exp(-u^2) \quad (6.40)$$

where

$$b^2 = \int_0^1 dx \left[\frac{1}{f_\lambda(x)} \int_x^1 dy g(y) f_\lambda(y) \right]^2 \quad (6.41)$$

provided $F(bu) \exp(-u^2) \in L_1(-\infty, \infty)$ holds. For a detailed proof see [20]. Note that the integral (6.40) requires $f_\lambda(0) > 0$, which is true for $\lambda < \lambda_1$, but not for $\lambda > \lambda_n$ for $n \geq 1$ according to property (b).

6.4 Problems for this Chapter

Problem 6.1 Compute the Wiener integral of the functional

$$F[f(x)] = \exp\{\lambda \int_0^1 dy w(y) f^2(y)\} \quad (6.42)$$

directly (without using the Cameron–Martin theorems), where λ is a real number and $w(x) > 0$, $x \in [0, 1]$, over the space C_0 of continuous functions $f(x)$, $x \in [0, 1]$ with respect to the Wiener measure.

6.1.1 Use the definition of the Wiener integral (6.31) and the relation

$$\int_{-\infty}^{\infty} \cdots \int_{-\infty}^{\infty} dx_1 \cdots dx_N \exp\left(-\sum_{i=1}^N \sum_{j=1}^N a_{i,j} x_i x_j\right) = \pi^{\frac{N}{2}} [\det(a_{i,j})]^{-\frac{1}{2}} \quad (6.43)$$

valid for positive definite matrices $a_{i,j}$ to derive a recursive relation for the determinant of $a_{i,j}$. Establish the ode and the boundary conditions for $N \rightarrow \infty$.

6.1.2 Solve the ode for $w(x) = 1$, compute the value of the functional integral and plot it as function of λ .

Problem 6.2 Compute the Wiener integral (6.39) for $p(x) = 1$, $q(x) = 0$ and $w(x) = (x + \alpha)^{-2}$, where $0 < \alpha < \infty$ is assumed. Plot the solution of the associated Sturm–Liouville ode for several values of λ and the functional integral as function of λ for several values of α .

References

1. Cartier, P., DeWitt-Morette, C.: A new perspective on functional integration. *J. Math. Phys.* **36**, 2137–2340 (1995)
2. DeWitt-Morette, C., Cartier, P., Folacci, A.: *Functional Integration*. Plenum Press, New York, London (1997)
3. Cartier, P., DeWitt-Morette, C.: *Functional Integration: Action and Symmetries*. Cambridge University Press, Cambridge U.K (2006)
4. Simon, B.: *Functional Integration and Quantum Physics*. AMS Chelsea Publication, Providence, Rhode Island (2004)
5. Klauder, J.R.: *A Modern Approach to Functional Integration*. Birkhaeuser/Springer, New York (2010)
6. Vishik, M.J., Fursikov, A.V.: *Mathematical Problems of Statistical Hydromechanics*. Kluwer Academic Publication, Dordrecht (1988)
7. Dalecky, Y.L., Fomin, S.V.: *Measures and Differential Equations in Infinite-Dimensional Space*. Kluwer Academic Publication, Dordrecht (1991)
8. Shilov, G.E., Gurevich, B.L.: *Integral, Measure and Derivative: A Unified Approach*. Prentice Hall Inc., Englewood Cliffs (1966)

9. Bogachev, V.I.: Measure Theory, vol. 1. Springer, New York (2006)
10. Yamasaki, Y.: Measures on Infinite Dimensional Spaces. World Scientific, Singapore (1985)
11. Conway, J.: A Course in Functional Analysis. Springer, New York (1990)
12. Kreyszig, E.: Introductory Functional Analysis with Applications. Wiley, New York (1989)
13. Minlos, R.A.: Cylinder sets. In: Hazewinkel, M. (ed.) Encyclopdia of Mathematics. Springer, New York (2001)
14. Skorohod, A.V.: Integration in Hilbert Space. Springer, New York (1974)
15. Bogachev, V.I.: Gaussian Measures, Mathematical surveys and monographs, p. 62. American Mathematical Society (1998)
16. Sagaut, P., Cambron, C.: Homogeneous Turbulence Dynamics. Cambridge University Press, New York (2008)
17. Kuksin, S., Shirikyan, A.: Mathematics of Two-dimensional Turbulence, Cambridge Tracts in Mathematics, vol. 194. Cambridge University Press, U.K. (2012)
18. Pope, S.B.: Turbulent Flows. Cambridge University Press, Cambridge, U.K. (2001)
19. Cameron, R.H., Martin, W.T.: Transformations of Wiener integrals under a general class of linear transformations. *Trans. Am. Math. Soc.* **58**, 184–219 (1945)
20. Cameron, R.H., Martin, W.T.: Evaluation of various Wiener integrals by use of certain Sturm-Liouville differential equations. *Bull. Am. Math. Soc.* **51**, 73–90 (1945)
21. Hartmann, P.: Ordinary Differential Equations. SIAM, Philadelphia (2002)
22. Duffy, D.G.: Green's Functions with Applications. Chapman & Hall/CRC, Boca Raton, Florida (2001)

Chapter 7

Functional Differential Equations



Equations determining a functional and involving variational derivatives are called functional differential equations (abbreviated by fde, list in Chap. 1). Definitions and elementary properties of such equations are discussed to prepare the subsequent development on fdes. Two types of such equations are considered: elliptic and parabolic fdes.

Let $\mathcal{D} \subset \mathbb{R}^d$ be a domain with dimension $d \geq 2$ and let spaces of scalar and vector fields defined on \mathcal{D} . The particular structure of these scalar and vector spaces will be specified below.

7.1 Elliptic fdes

Let X and Y be Banach spaces of scalar fields defined on \mathcal{D} and let $A : X \rightarrow Y$ be a linear operator and A^* its adjoint. $\mathcal{U}(A) = C^\infty(\mathcal{D}) \subset X$ denotes the domain of definition of A and $\mathcal{R}(A) = C^\infty(\mathcal{D}) \subset Y$ its range of values. The set $\ker A \equiv \{x \in X : Ax = 0\}$ is called null space or kernel of the operator A . The linear differential operator $A : C^\infty(\mathcal{D}) \rightarrow C^\infty(\mathcal{D})$ has the form

$$Au = \sum_{|\alpha| \leq r} a_\alpha D^\alpha u \quad (7.1)$$

where $a_\alpha(x) \in C^\infty(\mathcal{D})$ and $u(x) \in \mathcal{U}$, the order $r \geq 0$ of the operator is assumed integer and finite. The individual differential operators are defined by

$$D_k \equiv \frac{1}{i} \frac{\partial}{\partial x_k} \quad (7.2)$$

for $k = 1, \dots, d$, α denotes the multi-index $\alpha = \alpha_1 \alpha_2 \cdots \alpha_d$ such that $\partial^\alpha = \partial_1^{\alpha_1} \cdots \partial_d^{\alpha_d}$ and $|\alpha| = \sum_{k=1}^d \alpha_k$, see Sect. 23.6 for definitions and elementary properties. The symbol $p(x, \zeta)$ of the differential operator A is defined by

$$p(x, \zeta) \equiv \sum_{|\alpha|=r} a_\alpha(x) \zeta^\alpha \quad (7.3)$$

It depends only on the highest derivatives of order r .

The linear differential operator A is elliptic iff the symbol $p(x, \zeta) \neq 0$ for all $x \in \mathcal{D}$ and $\zeta \in \mathbb{R}^d - 0$.

The main examples for elliptic fdes are equations containing the generalized $A \equiv \Delta_0$ or the Lévy-Laplacian $A \equiv \Delta_L$, defined in Sect. 9.4.2, in particular the Lévy-Laplacian and Lévy-Poisson fdes. For twice differentiable functionals the Lévy-Laplacian emerges as limit

$$\Delta_L \theta[\mathbf{y}] = \lim_{n \rightarrow \infty} \frac{1}{n} \sum_{k=1}^n \frac{\partial^2 \theta_n}{\partial^2 y_k}(y_1, \dots, y_n)$$

according to Eq. (9.86). It is easy to check that the symbol $p(x, \zeta) = \frac{1}{n} \sum_{k=1}^n \zeta_i^2$ is uniformly positive for all n , hence is the Lévy-Laplacian elliptic.

7.2 Parabolic fdes

Let the differentiable functional $\Theta[f(\cdot); t]$ be also a function of a variable $0 \leq t < \infty$. A fde is called parabolic if it has the form

$$\frac{\partial \Theta}{\partial t} = A \Theta \quad (7.4)$$

where A is an elliptic operator (see Dalecky and Fomin [1], Chap. IV, 1.3). Operators of the form

$$A[\theta] \equiv (y_\alpha, \mathcal{L}_\beta \frac{\delta^2 \theta}{\delta y_\alpha(\mathbf{x}) \delta y_\beta(\mathbf{x}')}) \quad (7.5)$$

where $\mathbf{y} \in \mathcal{N}$ and \mathcal{L}_β is a linear operator acting on $\mathbf{x}, \mathbf{x}' \in \mathcal{D}$, containing a variational Hessian are of particular interest for the investigation of the Hopf fde.

7.3 Problems for this Chapter

Problem 7.1 Consider the space of continuous functions $C = \{f(x), x \in [0, 1]\}$ defined on the domain $\mathcal{D} = [0, 1]$. Solve the IVP for the functional differential equation

$$\frac{\delta F[f]}{\delta f(x)} = b(x)f(x)^n F[f]$$

where $n > 0$ is integer, for the functional $F[f] : C \rightarrow R^1$.

Problem 7.2 Consider the space of twice continuously differentiable functions $C^2 = \{f(x), x \in [0, 1]\}$. Solve the functional differential equation

$$\frac{\delta F[f]}{\delta f(x)} = \left[-\frac{d^2 f}{dx^2} + cf(x) + gf^3(x) \right] F[f]$$

where c, g are constants, for the functional $F[f] : C \rightarrow R^1$.

Reference

1. Dalecky, YuL, Fomin, S.V.: Measures and Differential Equations in Infinite-Dimensional Space. Kluwer Academic Publication, Dordrecht (1991)

Chapter 8

Characteristic Functionals

for Incompressible Turbulent Flows



The Fourier transform of a finite-dimensional Pdf is the characteristic function, hence contains probabilistic information equivalent to the Pdf/Cdf. The main difference to the Pdfs is its relation to statistical moments, which follow from the characteristic function by differentiation at the origin of the argument space \mathcal{N} . Furthermore, the characteristic function can be extended to infinitely many variables [1], since differentiation is well defined (in the sense of Frechét/ Gateaux, Sect. 23.12). This property will be exploited to establish the equation governing turbulent motion on the functional level. The characteristic functional will be derived for two levels of generality:

(CS-1) Space–time functional $\Theta[\mathbf{y}]$ [2] with $\mathbf{y}(t, \mathbf{x})$ denoting the vector field regarded as the argument corresponding to velocity; the argument field \mathbf{y} is in a nuclear space \mathcal{N} discussed in Sect. 5.4 and to be specified below in Sect. 9.3 on the Lewis–Kraichnan approach.

(CS-2) The spatial functional $\theta[\mathbf{y}; t]$ with $\mathbf{y}(\mathbf{x})$ denoting the three-dimensional argument field associated with velocity at time t , which contains the statistical information on spatial but not temporal distributions. The time evolution is represented by an orbit in the function space. The Bochner–Minlos theorem provides conditions for a functional defined on a nuclear space (a topological vector space with many properties of finite-dimensional spaces [3]) to be a characteristic functional.

The exact equations describing turbulence in terms of the characteristic functional are established below following the work of Hopf [4] and Kolmogorov [5], further extended by Monin and Yaglom vol. I [6], Sect. 3.4 and vol. II [7], Chap. 10, Stanisic [8] Chap. 12 and Vishik and Fursikov [5]. One of the remarkable properties of the fde for the characteristic functional is its linearity, in particular, convection emerges in the Hopf equation (see (9.40) or (9.46) derived and discussed in detail below) for the spatial characteristic functional defined by (9.1) of a turbulent flow as second variational derivative (9.53)

$$\begin{aligned} \frac{\delta^2}{\delta y_\alpha(\mathbf{x}) \delta y_\beta(\mathbf{x})} \theta[\mathbf{y}(\cdot); t] &= \left\{ \frac{\delta^2}{\delta y_\alpha(\mathbf{x}) \delta y_\beta(\mathbf{x})} - \frac{1}{3} \delta_{\alpha\beta} \frac{\delta^2}{\delta y_\gamma(\mathbf{x}) \delta y_\gamma(\mathbf{x})} \right\} \theta[\mathbf{y}(\cdot); t] \\ &+ \frac{1}{3} \delta_{\alpha\beta} \frac{\delta^2}{\delta y_\gamma(\mathbf{x}) \delta y_\gamma(\mathbf{x})} \theta[\mathbf{y}(\cdot); t] \end{aligned}$$

whose trace is related to the generalized Laplacian Δ_0 . The generalized Laplacian acting on an open domain in the Hilbert space \mathcal{N} (test function space) is defined (9.77) as the trace of the Hessian formed by the second Fréchet derivatives, provided the derivative and the limit $\mathbf{x}' \rightarrow \mathbf{x}$ exist,

$$\Delta_0 \theta = \text{tr} \left(\frac{\delta^2}{\delta y_\alpha(\mathbf{x}) \delta y_\beta(\mathbf{x}')} \theta[\mathbf{y}(\cdot); t] \right)$$

It is a trace-class operator, Gross [9], Cannarso and DaPrato [10], discussed in Sect. 9.4.

A different Laplacian with a wider domain of definition than the generalized one is the Lévy-Laplacian. The Lévy-Laplacian Δ_L [11] is defined as the limit involving the mean value (23.83)

$$\Delta_L \theta[\mathbf{y}^0] = 2 \lim_{\rho \rightarrow 0} \frac{1}{\rho^2} \{ \mathcal{M}_{(\mathbf{y}^0, \rho)} \theta[\mathbf{y}] - \theta[\mathbf{y}^0] \}$$

($\mathbf{y}^0 \in \mathcal{N}$, $\mathbf{y}^0 = [y_1^0, \dots, y_n^0]$ is an n -vector, ρ denotes the radius of the n -ball) of the projection of a functional onto a finite-dimensional subspace and integrated over the surface of an n -ball (23.83)

$$M_n \theta[\mathbf{y}] \equiv \frac{1}{\Omega_n(\mathbf{y}^0, \rho)} \int_{S_n(\mathbf{y}^0, \rho)} d\sigma_n \theta_n(\mathbf{y}_n)$$

where $d\sigma_n$ is the area differential in n -dimensional space and $\theta_n(\mathbf{y}_n) = \theta[P_n \mathbf{y}]$, P_n is the linear operator projecting \mathbf{y} onto the subspace spanned by n basis functions. The denominator Ω_n is the surface area of the n -ball with radius ρ centred at \mathbf{y}^0 . It is well known and established in Chap. 23 that the limit $n \rightarrow \infty$ of the surface area Ω_n and the enclosed volume are zero for any finite radius ρ . This implies that the denominator approaches zero for any finite $\rho \geq 0$ raising the question, what the relation between the limits $\Omega_n(\rho) \rightarrow 0$ and $\rho \rightarrow 0$ is. The integration of a function over the surface of a ball in three-dimensional space is conceptually simple as the integral over a compact and smooth surface with finite area. This is completely different for the limit of infinite dimension, where the surface of the infinite-dimensional ball is not (sequentially) compact and possesses infinitely many limit points at the centre \mathbf{y}^0 of the ball. The volume and surface area (the Riemann measure) of the infinite-dimensional ball are both zero for finite radius. For this reason, the limit $n \rightarrow \infty$ will be analysed in Chap. 23 in Sect. 23.17.2 to gain better understanding of the term representing convection in the Hopf equation.

8.1 Bochner–Minlos Theorem

The Bochner–Minlos theorem (Klauder [12], Sect. 3.6, Simon [13], Theorem 2.2) gives the conditions for a functional defined on a nuclear space to be characteristic functional of random process or random field.

Theorem (Bochner–Minlos) *Let $\Theta[\mathbf{y}]$ be a functional defined on a nuclear space \mathcal{N} satisfying the conditions*

$$\Theta[0] = 1 \quad (8.1)$$

$$|\Theta[\mathbf{y}]| \leq 1 \quad (8.2)$$

$$\sum_{p,q=1}^N \Theta[\mathbf{y}_p - \mathbf{y}_q] \geq 0, \quad N < \infty \quad (8.3)$$

$$\Theta[\mathbf{y}] \text{ is continuous for all } \mathbf{y} \in \mathcal{N} \quad (8.4)$$

then is Θ characteristic functional of a measure μ . The \mathbf{y}_p denotes the p -dimensional projection of \mathbf{y} . The support of this measure is limited to the generalized functions in the topological dual \mathcal{N}' to the given space \mathcal{N} . See [12, 14] for proof and further details.

References

1. Hosokawa, I.: A functional treatise on statistical hydromechanics with random force action. *J. Physical Soc. Jpn* **25**, 271–278 (1968)
2. Lewis, R.M., Kraichnan, R.H.: A Space-Time Functional Formalism for Turbulence. *Comm. Pure Appl. Math.* **XV**, 397–411 (1962)
3. Conway, J.: *A Course in Functional Analysis*. Springer, New York (1990)
4. Hopf, E.: Statistical hydromechanics and functional calculus. *J. Rat. Mech. Anal.* **1**, 87–123 (1952)
5. Vishik, M.J., Fursikov, A.V.: *Mathematical Problems of Statistical Hydromechanics*. Kluwer Academic Publication, Dordrecht (1988)
6. Monin, A.S., Yaglom, A.M.: *Statistical Fluid Mechanics: Mechanics of Turbulence*, vol. 1. The MIT Press, Cambridge Mass (1975)
7. Monin, A.S., Yaglom, A.M.: *Statistical Fluid Mechanics: Mechanics of Turbulence*, vol. 2. The MIT Press, Cambridge Mass (1975)
8. Stanisic, M.M.: *The Mathematical Theory of Turbulence*. Springer, New York (1988)
9. Gross, L.: Potential theory on hilbert space. *J. Funct. Anal.* **1**, 123–181 (1967)
10. Cannarsa, P., DaPrato, G.: Potential Theory in Hilbert Spaces. *Proc. p. 54. Symposia Appl. Math* (1998)
11. Feller, M.N.: *The Lévy-Laplacian*. Cambridge University Press (2005)
12. Klauder, J.R.: *A Modern Approach to Functional Integration*. Birkhaeuser/Springer, New York (2010)
13. Simon, B.: *Functional Integration and Quantum Physics*. AMS Chelsea Publication, Providence, Rhode Island (2004)
14. Gelfand, I.M., Vilenkin, N.Y.: *Generalized Functions*, vol. 4. Academic Press, New York (1964)

Chapter 9

Fdes for the Characteristic Functionals



The characteristic functionals associated with measures that determine completely the statistical properties of turbulence for an incompressible fluid were introduced in the previous section. The spatial characteristic functionals for incompressible (as defined in [1], Chap. 10) and compressible flows are discussed first and several versions of the Hopf equation are derived in the present section. Then the complete space–time description of incompressible and compressible turbulent flows based on the space–time characteristic functional is introduced and the elementary properties of the Lewis–Kraichnan equation [2] are established in Sect. 9.3. The characteristic functional for incompressible turbulence is defined as functional integral with respect to the turbulence measure μ and this integration is called expectation operator (6.4). This definition makes sense, if the functional integral is properly defined, [3–5], see Sect. 23.17 in Appendix A for details.

The spatial characteristic functional θ is thus defined by

$$\theta[\mathbf{y}(\mathbf{x}); t] \equiv \langle \exp[i(\mathbf{y}, \mathbf{v})] \rangle, \quad \mathbf{y} \in \mathcal{N}, \quad \mathbf{v} \in \Omega, \quad \mathbf{x} \in \mathcal{D} \quad (9.1)$$

The scalar product $(\mathbf{y}, \mathbf{v}) : \mathcal{N} \times \Omega \rightarrow \mathbb{R}^1$ for the present spatial case of incompressible flows is defined by

$$(\mathbf{y}, \mathbf{v}) \equiv \int_{\mathcal{D}} d\nu(\mathbf{x}) \mathbf{y}(\mathbf{x}) \cdot \mathbf{v}(t, \mathbf{x}) \quad (9.2)$$

where $\mathbf{y}(\mathbf{x})$ is element of a nuclear space of test functions $\mathcal{N} = \{\mathbf{y} \in C_{\mathcal{D}}^{\infty} : \mathbf{y}(\mathbf{x}) = 0, \mathbf{x} \in \partial\mathcal{D}\}$ and the realization $\mathbf{v}(t, \mathbf{x})$ is element of the phase space Ω . The measure differential is $d\nu = d\mathbf{x}w(\mathbf{x})$ with $w(\mathbf{x}) \geq 0$ being a weight function integrating to unity. The dependence of θ on time is due to the realization \mathbf{v} being time-dependent according to the Navier–Stokes equations and possibly the turbulence measure μ being a function of time. It is assumed in the following that the characteristic functionals are twice Gateaux/Fréchet differentiable (see Sect. 23.12 for differentiation of functionals).

9.1 Elementary Properties of the Characteristic Functional

The elementary properties of the characteristic functional can be deduced from the definition (9.1) as expectation of the Fourier kernel. The characteristic functional is complex-valued and satisfies

$$|\theta[\mathbf{y}(\mathbf{x}); t]| \equiv |\langle \exp[i(\mathbf{y}, \mathbf{v})] \rangle| \leq 1 \quad (9.3)$$

since $|\exp[i(\mathbf{y}, \mathbf{v})]| \leq 1$ and $\int_{\Omega} d\mu(\mathbf{v}) = 1$. Setting the argument (test) field \mathbf{y} to zero leads to

$$\theta[0; t] = 1 \quad (9.4)$$

The characteristic functional is positive definite according to

$$\sum_{i=1}^N \sum_{k=1}^N \theta[\mathbf{y}^i - \mathbf{y}^k] c_i c_k^* \geq 0 \quad (9.5)$$

for $\mathbf{y}^i \in \mathcal{N}$, $i = 1, \dots, N$ for $N \geq 1$ and complex numbers c_i (asterisk denotes complex conjugate). The conditions for a functional to be characteristic functional of a stochastic process are laid down in Bochner's theorem, as explained in Sect. 8.1. The statistical moments can be computed by functional differentiation of the characteristic functional at the origin, since it follows from the definition (9.1), that

$$\langle v_{\alpha}^{n_1}(\mathbf{x}^1) v_{\beta}^{n_2}(\mathbf{x}^2) \cdots v_{\gamma}^{n_N}(\mathbf{x}^N) \rangle = (-i)^{\sum_{i=1}^N n_i} \frac{\delta^{\sum_{i=1}^N n_i} \theta}{\delta y_{\alpha}^{n_1}(\mathbf{x}^1) \cdots \delta y_{\gamma}^{n_N}(\mathbf{x}^N)} \Big|_{\mathbf{y}=0} \quad (9.6)$$

holds for any number $N > 0$ of points in the flow field \mathcal{D} and non-negative integer exponents n_i , $i = 1, \dots, N$. It is clear that the single-time statistics of a turbulent flow are thus computable without further assumptions, once the characteristic functional $\theta[\mathbf{y}; t]$ has been determined. Therefore, the next step is to establish equations and formulate IVPs governing the characteristic functional. The elimination of the pressure gradient term in the momentum balance with the aid of a Green's function will be applied to construct two versions of the fundamental equation for the characteristic functional $\theta[\mathbf{y}; t]$. The flow through a straight circular pipe is discussed in detail as an example for this step.

9.2 The Hopf fde for the Spatial Characteristic Functional

The temporal evolution of the characteristic functional $\theta[\mathbf{y}; t]$, $\mathbf{y} \in \mathcal{N}$ is determined by the Navier–Stokes equations. Several versions of the dynamical equation for θ will be derived and their properties discussed. It should be noted that the terminology

for the solutions of these fdes is not uniform in the literature, for instance, Vishik and Fursikov [6] call a family of measures $\mu(\omega, t)$, ω is a measurable subset of the phase space Ω and t denotes time, generated by the solution $\theta[\mathbf{y}; t]$ of the Hopf fde *spatial statistical solution*, but this terminology will not be used in the following.

The first version of the Hopf equation in the spatial description and Cartesian coordinates in the flow domain \mathcal{D} can be established for the characteristic functional without explicit appearance of functional integrals in the result. It is assumed that reference values for all variables can be found; thus, the Reynolds and Froude numbers can be defined according to (2.8), (22.2) and the variables in mass and momentum balances are thus dimensionless. Furthermore, the scalar product (\mathbf{y}, \mathbf{v}) in the definition (9.1) of the characteristic functional is then dimensionless, i.e. a pure number appropriate for the definition of various norms (L^2 , Sobolev, etc.), the construction of bases and the application of integral transforms.

Consider the velocity $\mathbf{v}(t, \mathbf{x}) \in \Omega$ being the solution of the Navier–Stokes pdes exposed to a solenoidal external force field $g_\alpha(t, \mathbf{x})$, which is specified as non-random field, and a (dimensionless) test function $\mathbf{y}(\mathbf{x}) \in \mathcal{N}$, then can the time derivative

$$\frac{\partial}{\partial t} \exp[i(\mathbf{y}, \mathbf{v})] = -i(\mathbf{y}, \exp[i(\mathbf{y}, \mathbf{v})]) \left[\frac{\partial}{\partial x_\beta} (v_\alpha v_\beta) + \frac{\partial p}{\partial x_\alpha} - \frac{1}{Re} \frac{\partial^2 v_\alpha}{\partial x_\beta \partial x_\beta} - \frac{1}{Fr} g_\alpha + \frac{\partial P_0}{\partial x_\alpha} \right] \quad (9.7)$$

be evaluated using mass (2.6) and momentum (9.17) balances and elementary properties of the characteristic functional. At time $t = 0$ the state of the turbulent flow is specified by the probability measure $\mu_0(\mathbf{v})$, where $\mathbf{v}(0, \mathbf{x})$ is an element of the phase space Ω . The expectation of (9.7) is by definition the functional integral over the initial measure

$$\begin{aligned} \frac{\partial}{\partial t} \int_{\Omega} \mu_0(d\mathbf{v}(0, \mathbf{x})) \exp[i(\mathbf{y}, \mathbf{v})] = \\ -i(\mathbf{y}, \int_{\Omega} \mu_0(d\mathbf{v}(0, \mathbf{x})) \exp[i(\mathbf{y}, \mathbf{v})]) \left[\frac{\partial}{\partial x_\beta} (v_\alpha v_\beta) + \frac{\partial p}{\partial x_\alpha} - \frac{1}{Re} \frac{\partial^2 v_\alpha}{\partial x_\beta \partial x_\beta} - \frac{1}{Fr} g_\alpha + \frac{\partial P_0}{\partial x_\alpha} \right] \end{aligned} \quad (9.8)$$

where the fact that the initial measure is independent of time was exploited. The assumption on the solutions of the Navier–Stokes equations put forward in Sect. 2.2 implies that the solution operator T_t in the spatial description, mapping the solution at time zero to the solution at the later time according to $\mathbf{v}(t, \mathbf{x}) = T_t \mathbf{v}(0, \mathbf{x})$, is at least a homeomorphism, hence a measurable mapping of Ω onto itself. Lemma 2.4 in [6] Sect. 2.2 asserts then, that

$$\mu(t, \omega) = \mu(0, T_{-t}\omega), \quad \forall \omega \in \mathcal{A}(t) \quad (9.9)$$

holds, where $\mathcal{A}(t)$ denotes the Borel σ -algebra of subsets of the phase space Ω at time t and $T_{-t}\omega \in \mathcal{A}(0)$. Applying this lemma to the equation for the characteristic functional leads to

$$\begin{aligned} \frac{\partial \theta}{\partial t}[\mathbf{y}; t] = & -i(y_\alpha, \int_{\Omega} \mu(d\mathbf{v}(t, \mathbf{x})) \exp[i(\mathbf{y}, \mathbf{v}(t, \mathbf{x}))]) [\frac{\partial}{\partial x_\beta}(v_\alpha v_\beta) \\ & + \frac{\partial p}{\partial x_\alpha} - \frac{1}{Re} \frac{\partial^2 v_\alpha}{\partial x_\beta \partial x_\beta} - \frac{1}{Fr} g_\alpha + \frac{\partial P_0}{\partial x_\alpha}]] \end{aligned} \quad (9.10)$$

The external force field $g_\alpha(t, \mathbf{x})$ and the base pressure gradient ∇P_0 are assumed known, solenoidal and non-random. The extension to stochastic forcing is discussed below, see also Novikov [7, 8], Hosokawa [9], and the associated fde is established in Sect. 9.2.4. The next step in the derivation of the fde is to express the right side in terms of the characteristic functional $\theta[\mathbf{y}; t]$ starting with convection. The version of the Hopf fde for cylindrical coordinates in the flow domain \mathcal{D} is given as solution for Problem (10.2), Appendix F.

Convection

The convective part of acceleration appears in the spatial description as divergence of a quadratically nonlinear term in the momentum balance (2.7). The characteristic functional does not depend on location $\mathbf{x} \in \mathcal{D}$, hence functional differentiation is necessary to enable differentiation with respect to location and to generate the correct coefficients in (9.10) reflecting convection. Inspection of equation (9.8) indicates that second functional derivatives are required to produce the convective term. The first Gateaux differential (23.45) (see Sect. 23.12 in Appendix A) of the characteristic functional

$$\delta\theta[\mathbf{y}; t](\mathbf{w}) = \lim_{\epsilon \rightarrow 0} \frac{1}{\epsilon} \{ \theta[\mathbf{y} + \epsilon \mathbf{w}; t] - \theta[\mathbf{y}; t] \} \quad (9.11)$$

can be evaluated producing

$$\delta\theta[\mathbf{y}; t](\mathbf{w}) = (w_\alpha(\mathbf{x}), i \int_{\Omega} d\mu(t, \mathbf{v}) v_\alpha(t, \mathbf{x}) \exp[i(\mathbf{y}, \mathbf{v})]) \quad (9.12)$$

containing the first variational or Gateaux derivative according to (23.46)

$$\delta\theta[\mathbf{y}; t](\mathbf{w}) = (w_\alpha, \frac{\delta\theta}{\delta y_\alpha}) \quad (9.13)$$

Comparison with (9.12) for the differential leads to the preliminary result (showing both notations for the functional derivatives)

$$\frac{\delta\theta}{\delta y_\alpha(\mathbf{x})}[\mathbf{y}; t] = \frac{\delta\theta}{\delta y_\alpha}[\mathbf{y}; t, \mathbf{x}] = i \int_{\Omega} d\mu(t, \mathbf{v}) v_\alpha(t, \mathbf{x}) \exp[i(\mathbf{y}, \mathbf{v})] \quad (9.14)$$

depending parametrically on the location $\mathbf{x} \in \mathcal{D}$. The characteristic functional is twice differentiable; hence, the same procedure can be applied to the first derivative

$$\delta \frac{\delta \theta}{\delta y_\alpha(\mathbf{x}')}[\mathbf{y}; t, \mathbf{x}](\mathbf{w}) = \lim_{\epsilon \rightarrow 0} \frac{1}{\epsilon} \{ \frac{\delta \theta}{\delta y_\alpha(\mathbf{x}')}[\mathbf{y} + \epsilon \mathbf{w}; t, \mathbf{x}] - \frac{\delta \theta}{\delta y_\alpha(\mathbf{x}')}[\mathbf{y}; t, \mathbf{x}] \}$$

leading to the functional Hessian of the characteristic functional

$$\frac{\delta^2 \theta}{\delta y_\alpha(\mathbf{x}) \delta y_\beta(\mathbf{x}')}[\mathbf{y}; t] = \frac{\delta^2 \theta}{\delta y_\alpha \delta y_\beta}[\mathbf{y}; t, \mathbf{x}, \mathbf{x}'] = - \int_{\Omega} d\mu(t, \mathbf{v}) v_\alpha(t, \mathbf{x}) v_\beta(t, \mathbf{x}') \exp[i(\mathbf{y}, \mathbf{v})] \quad (9.15)$$

The convective term emerges thus in the form

$$-i(y_\alpha, \int_{\Omega} \mu(d\mathbf{v}) \exp[i(\mathbf{y}, \mathbf{v})] \frac{\partial}{\partial x_\beta} (v_\alpha v_\beta)) = i(y_\alpha, \frac{\partial}{\partial x_\beta} \lim_{\mathbf{x}' \rightarrow \mathbf{x}} \frac{\delta^2 \theta}{\delta y_\alpha \delta y_\beta}[\mathbf{y}; t, \mathbf{x}, \mathbf{x}']) \quad (9.16)$$

provided the limit exists. This equation is a remarkable result, since it expresses nonlinear convection in the momentum balance as linear second derivative Hessian of the characteristic functional without the creation of an additional unknown, thanks to the linearity of (9.16) with respect to $\theta[\mathbf{y}]$, in contrast to any approach based on statistical moments.

It is important to notice that the second functional derivative in Eq. (9.16) emerges as distribution on $\mathcal{D} \times \mathcal{D}$ for the limit $\mathbf{x}' \rightarrow \mathbf{x}$, since it maps a pair of functions $\mathbf{y}(\mathbf{x}), \mathbf{y}(\mathbf{x}')$ onto a complex number. The example of the standard Laplacian (defined in Sect. 9.4) applied to a Gaussian characteristic functional in Sect. 9.4.3 indicates (Inoue, [10], Chap. 2) this property. The spatial derivative is then interpreted as generalized derivative of a distribution, see Rudin [11] for relevant details on derivatives of distributions.

9.2.1 The Pressure Gradient in the Spatial Description

The pressure gradient has the function to enforce mass balance (2.6) in the momentum balance (2.7), expressed as the condition of zero divergence for the motion of incompressible fluids. The pressure gradient is written as sum of base and disturbance pressure contributions $\nabla P = \nabla P_0 + \nabla p$ with ∇P_0 a known constant vector, if no base pressure is available, $\nabla P_0 = 0$. The momentum balance (2.7) is then in slightly more general form

$$\frac{\partial v_\alpha}{\partial t} + v_\beta \frac{\partial v_\alpha}{\partial x_\beta} = -\frac{\partial p}{\partial x_\alpha} + \frac{1}{Re} \frac{\partial^2 v_\alpha}{\partial x_\beta \partial x_\beta} + \frac{1}{Fr} g_\alpha - \frac{\partial P_0}{\partial x_\alpha} \quad (9.17)$$

where the unknowns are velocity $\mathbf{v}(t, \mathbf{x})$ and the disturbance pressure $p(t, \mathbf{x})$.

The functional associated with the disturbance pressure is defined by

$$\Pi[\mathbf{y}; t, \mathbf{x}, \mathbf{g}] \equiv \langle p[\mathbf{v}; t, \mathbf{x}, \mathbf{g}] \exp[i(\mathbf{y}(\mathbf{x}), \mathbf{v}(t, \mathbf{x}))] \rangle, \quad (\mathbf{y}, \mathbf{v}) : \mathcal{N} \times \Omega \rightarrow \mathbb{R}^1, \quad \mathbf{x} \in \mathcal{D} \quad (9.18)$$

where the angular brackets denote statistical expectation. The notation $p[\mathbf{v}; t, \mathbf{x}, \mathbf{g}]$ indicates non-local dependence on velocity, to be determined below with the aid of a Green's function, and the external force and parametric dependence on time, location in the flow field. The external force \mathbf{g} is assumed solenoidal and non-random, if it is uniform as in case of gravity it is simply a parameter for the characteristic functional. The case of stochastic forces is more involved and considered in Sect. 9.2.2.

The pde for the (disturbance) pressure p follows for incompressible fluids from mass (2.6) and momentum (9.17) balances as Poisson pde

$$-\Delta p = R(t, \mathbf{x}), \quad R \equiv \frac{\partial^2}{\partial x_\alpha \partial x_\beta} (v_\alpha v_\beta) \quad (9.19)$$

Note that the external force does not appear in $R(t, \mathbf{x})$, since it is assumed solenoidal, neither does the gradient of the base pressure as it is constant. Considering compact flow domains \mathcal{D} with boundary $\partial\mathcal{D}$, then is the BVP for the pressure pde (9.19) completed by specifying non-homogeneous Neumann boundary conditions

$$n_\alpha \frac{\partial p}{\partial x_\alpha} = h(t, \mathbf{x}), \quad \mathbf{x} \in \partial\mathcal{D} \quad (9.20)$$

using the momentum balance (9.17) normal to the boundary (n_α denotes the unit vector pointing outward). The pure Neumann BVP requires an additional condition, such as $\int_{\mathcal{D}} dv p(t, \mathbf{x}) = 0$, to achieve uniqueness of the solution.

The fundamental solution valid in \mathcal{D} with boundary $\partial\mathcal{D}$ to this linear elliptic pde can be represented as volume integral with the product of Green's function $G(\mathbf{x}, \mathbf{x}')$ and the right-hand side R (9.19) as integrand plus a surface integral containing the Neumann boundary values $h(\mathbf{x})$

$$p(t, \mathbf{x}) = \int_{\mathcal{D}} dv(\mathbf{x}') G(\mathbf{x}, \mathbf{x}') \frac{\partial^2}{\partial x'_\alpha \partial x'_\beta} (v_\alpha v_\beta)(t, \mathbf{x}') + \int_{\partial\mathcal{D}} dA(\mathbf{x}') h(\mathbf{x}') G(\mathbf{x}, \mathbf{x}') + C \quad (9.21)$$

where C is an arbitrary constant. The boundary values $h(\mathbf{x})$ for the pressure follow from the momentum balance (2.7) normal to the boundary $\partial\mathcal{D}$

$$h(\mathbf{x}') = n_\alpha \left(\frac{1}{Re} \frac{\partial^2 v_\alpha}{\partial x'_\beta \partial x'_\beta} + \frac{1}{Fr} g_\alpha - \frac{\partial P_0}{\partial x_\alpha} - \frac{\partial v_\alpha^b}{\partial t} - v_\beta^b \frac{\partial v_\alpha^b}{\partial x'_\beta} \right) \quad (9.22)$$

as momentum flux, note that velocity on the boundary \mathbf{v}^b is specified, hence are the last two terms, being the acceleration on the boundary, a known entity.

The construction of a Green's function for the Poisson pde with non-homogeneous Neumann boundary conditions is a non-trivial matter and the derivation of the proper boundary conditions and the tedious construction of the associated Green's function for a particular compact domain is banned to Appendix D, Sect. 26. In special cases with periodicity in one or more directions, the solution of the BVP for the pressure can be significantly simplified with the help of discrete Fourier transform, see [12–14].

The main result of Appendix C for the periodic pipe flow is the representation of the pressure as sum of up to three contributions (26.50). It follows from the fact that the Poisson pde (26.11) is linear with linear non-homogeneous Neumann boundary conditions (26.18) that the solution of the BVP can be constructed as a combination of two linear BVPs:

(1) The complementary or harmonic solution $p_h(t, \mathbf{x})$ of the Laplace pde with non-homogeneous boundary conditions (26.48)

$$-\Delta p_h = 0, \quad \mathbf{n} \cdot \nabla p_h = h(t, \mathbf{x})$$

(2) The solution p_G (called Green's function pressure) of the (non-homogeneous) Poisson pde (26.49) with homogeneous boundary conditions

$$-\Delta p_G = R(r, \theta, \zeta), \quad \mathbf{n} \cdot \nabla p_G = 0, \quad \zeta \equiv \frac{z}{L}$$

The solution of this BVP can be expressed in terms of a Green's function as shown in Appendix D. The total pressure P is, therefore, given in cylindrical coordinates by the linear combination (26.50)

$$P(r, \theta, \zeta) = P_0(\zeta) + p_h(r, \theta, \zeta) + p_G(r, \theta, \zeta)$$

where p_h satisfies the non-homogeneous boundary conditions $h(\theta, \zeta) \neq 0$ with $R(r, \theta, \zeta) = 0$ and p_G satisfies the homogeneous boundary conditions $h = 0$ with $R(r, \theta, \zeta) \neq 0$. The sum of harmonic and Green's function pressure is called disturbance pressure,

$$p(r, \theta, \zeta) \equiv p_h(r, \theta, \zeta) + p_G(r, \theta, \zeta) \quad (9.23)$$

(3) In some cases, such as the periodic pipe flow with details in Appendix D, is it possible to identify a particular direction, where a base pressure P_0 can be defined, which is independent of the other two directions. The gradient of the base pressure $P_0(\zeta)$ in case of the pipe flow is then constant, hence solenoidal and periodic in axial direction, and provides the momentum source to keep the pipe flow going. It is the first contribution $P_0(\zeta)$, if it exists, in the representation (26.50) of the pressure and is considered an external parameter imposed by conditions outside the flow domain.

The pressure gradient functional

The gradient of the disturbance pressure is according to the previous section recognized as functional of the velocity. It is advantageous to establish the pressure

gradient functional in the spatial description and then transform it to the material description, if desired, instead of computing the pressure functional and to transform the spatial gradient and the functional to the material description. This will be pursued in Sect. 9.5, where the Hopf fde in the material description is derived. The starting point for the computation of the gradient functional in the spatial description is the relation

$$\begin{aligned} \int_{\Omega} \mu(d\mathbf{v}(t, \mathbf{x})) \exp[i(\mathbf{y}, \mathbf{v}(t, \mathbf{x}))] \frac{\partial p}{\partial x_{\alpha}} &= \frac{\partial}{\partial x_{\alpha}} \int_{\Omega} \mu(d\mathbf{v}(t, \mathbf{x})) \exp[i(\mathbf{y}, \mathbf{v}(t, \mathbf{x}))] \\ &\left\{ \int_{\mathcal{D}} dv(\mathbf{x}') G(\mathbf{x}, \mathbf{x}') \frac{\partial^2}{\partial x'_{\alpha} \partial x'_{\beta}} (v_{\alpha} v_{\beta})(t, \mathbf{x}') + \int_{\partial\mathcal{D}} dA(\mathbf{x}') n_{\alpha} h_{\alpha} G(\mathbf{x}, \mathbf{x}') \right\} \quad (9.24) \end{aligned}$$

The contribution of the gradient of the disturbance pressure to the functional equation (9.10) can be evaluated with the aid of (9.14) and (9.15) as follows:

$$-i(y_{\alpha}(\mathbf{x}), \int_{\Omega} \mu(d\mathbf{v}(t, \mathbf{x})) \exp[i(\mathbf{y}, \mathbf{v}(t, \mathbf{x}))] \frac{\partial p}{\partial x_{\alpha}}) = (y_{\alpha}(\mathbf{x}), i\Pi_{\alpha}[\mathbf{y}; t, \mathbf{x}]) \quad (9.25)$$

with the pressure gradient functional defined by

$$\begin{aligned} \Pi_{\alpha}[\mathbf{y}; t, \mathbf{x}] &\equiv \int_{\mathcal{D}} dv(\mathbf{x}') \frac{\partial G}{\partial x_{\alpha}}(\mathbf{x}, \mathbf{x}') \frac{\partial^2}{\partial x'_{\gamma} \partial x'_{\beta}} \frac{\delta^2 \theta}{\delta y_{\gamma} \delta y_{\beta}}[\mathbf{y}; t, \mathbf{x}', \mathbf{x}'] \\ &+ \int_{\partial\mathcal{D}} dA(\mathbf{x}') \frac{\partial G}{\partial x_{\alpha}}(\mathbf{x}, \mathbf{x}') n_{\gamma}(\mathbf{x}') \left\{ i \frac{1}{Re} \frac{\partial^2}{\partial x'_{\beta} \partial x'_{\beta}} \frac{\delta \theta}{\delta y_{\gamma}}[\mathbf{y}; t, \mathbf{x}'] + \frac{\partial}{\partial x'_{\beta}} \frac{\delta^2 \theta}{\delta y_{\beta} \delta y_{\gamma}}[\mathbf{y}; t, \mathbf{x}', \mathbf{x}'] \right. \\ &\left. + (g_{\gamma}(t, \mathbf{x}') - \frac{\partial P_0}{\partial x_{\alpha}} - \frac{\partial v_{\gamma}^b}{\partial t}(t, \mathbf{x}')) \theta[\mathbf{y}; t] \right\} \quad (9.26) \end{aligned}$$

The Green's function appears in the volume and surface integrals, only the latter contains the external force as part of the time derivative of the boundary values for velocity $v_{\gamma}^b(t, \mathbf{x})$.

Green's functions are not easy to compute, an example relevant to pipe flow is provided in Sect. 9.2.2 with computational details given in Appendix D, Chap. 26. However, the representation of the pressure in terms of a Green's function allows easy application of functional (Gateaux/Fréchet) differentiation and the computation of spatial derivatives generating the pressure gradient functional (9.26) as shown above.

9.2.2 Green's Function for Periodic Pipe Flow

The flow domain \mathcal{D} for periodic pipe flow (see Sect. 26.1 in Appendix D for details) $\mathcal{D} \subset \mathbb{R}^3$ is defined as straight cylinder with circular cross section by $\mathcal{D} \equiv \{(r, \theta, z) : 0 \leq r \leq 1, 0 \leq \theta \leq 2\pi, 0 \leq z \leq 2\pi L\}$, where cylindrical coordinates are chosen for convenience and denoted by r (radius), θ (azimuthal angle, not to be mistaken for the characteristic functional), \tilde{z} or $\zeta = \frac{\tilde{z}}{L}$ (axial coordinate). The origin of the coordinate system is, for instance, at the centre of the left/entrance boundary, the axial extent of the cylindrical domain is assumed to be $2\pi L$, $L \gg 1$ and integer, all variables are dimensionless. This domain \mathcal{D} is fixed in the spatial description. The Poisson pde for the disturbance pressure has the form of a linear, elliptic pde (9.19) in cylindrical coordinates with the Laplace operator given by (26.13). The Laplace operator in cylindrical coordinates contains singular coefficients and kinematic conditions at $r = 0$ must be observed to generate smooth solutions, they are discussed in Sect. 25.12 of Appendix D.

The Green's function [15] is the fundamental solution $G(\mathbf{x}|\mathbf{x}')$ of

$$-\Delta G = \frac{1}{r} \delta(r - r') \delta(\theta - \theta') \delta(z - z')$$

(the Laplacian applies to \mathbf{x}) valid in \mathcal{D} with boundary $\partial\mathcal{D}$ to the linear elliptic pde (9.19). However, the computation of the 3-d Green's function may result in series expansions that converge very slowly, Duffy [15]. Therefore, it is advantageous to exploit the periodicity in azimuthal and axial directions to reduce the Poisson pde for the Green's function to a Sturm–Liouville ode (26.33) for complex-valued coefficients of Fourier modes. The associated 1-d modal Green's function $G_{k,m}(r, \rho)$ for the azimuthal wavenumber k and the axial wavenumber m emerges in closed form, Eq. (26.120) and Figs. 26.7 and 26.8, the computational details can be found in Appendix D. The representation of the pressure (26.50) $p(r, \theta, \zeta) = P_0(\zeta) + \mathcal{P}_h(r, \theta, \zeta) + \mathcal{P}_G(r, \theta, \zeta)$ is then given by a basic pressure P_0 (irrelevant for incompressible fluids) with constant gradient and two linear functionals.

The first (called harmonic pressure p_h) is according to (26.76) in Chap. 26 computed as

$$\begin{aligned} p_h(t, \mathbf{x}) &= \mathcal{P}_h(r, \theta, \zeta | \frac{1}{Re} \frac{\partial^2 v_r}{\partial r^2} (\mathbf{x} \in \partial\mathcal{D})) \equiv \sum_{k=-\infty}^{\infty}' \frac{r^k}{k} \mathcal{F}(k, 0 | \frac{1}{Re} \frac{\partial^2 v_r}{\partial r^2} (\mathbf{x} \in \partial\mathcal{D})) \exp(ik\theta) \\ &+ \sum_{k=-\infty}^{\infty} \sum_{m=-\infty}^{\infty}' \frac{2I_k(\beta r)}{\beta[I_{k-1}(\beta) + I_{k+1}(\beta)]} \mathcal{F}(k, m | \frac{1}{Re} \frac{\partial^2 v_r}{\partial r^2} (\mathbf{x} \in \partial\mathcal{D})) \exp[i(k\theta + m\zeta)] \end{aligned}$$

where k, m are the azimuthal and axial wavenumbers, $\beta(m)$ is defined by (26.22), \mathcal{F} denotes the 2-d Fourier transform operator (Sect. 15.1), the prime on the sums

indicates that terms with $k = 0$ or $m = 0/\beta = 0$ in the denominator must be omitted, I_k , K_k denote modified Bessel function of first and second kind.

The second functional, called Green's function pressure p_G , Eq. (26.128) in Chap. 26, is given by

$$p_G(t, \mathbf{x}) = \mathcal{P}_G(r, \theta, \zeta | R(\mathbf{x})) \equiv \mathcal{F}^{-1}(\theta, \zeta | \int_0^1 d\rho \rho \mathcal{F}(k, m | R(\mathbf{x}) G_{k,m}(\rho, r)))$$

for $\mathbf{x} \in \mathcal{D}$, where the Green's functions are defined in Appendix D, Chap. 26 equations (26.33) and (26.119). The first functional \mathcal{P}_h (26.76) is derived from a surface integral reflecting the influence of the viscous stress on the pipe wall, while the second \mathcal{P}_G (26.128) follows from a volume integral, which depends on the right-hand side $R(\mathbf{x})$ of the Poisson pde (26.12).

Application of these representation of harmonic and Green's function pressure leads to the Leray version of the Navier–Stokes pdes as shown in Sect. 26.9 (Eqs. 26.131, 26.132, 26.133) of Appendix D. Test functions for p are used in Appendix D to verify the exponential convergence rate for the representation of the disturbance pressure.

The viscous term

The viscous term in (9.8) follows at once from the first Gateaux derivative (9.14) in the form

$$i(\mathbf{y}, \int_{\Omega} \mu(d\mathbf{v}(t, \mathbf{x})) \exp[i(\mathbf{y}, \mathbf{v}(t, \mathbf{x}))] \frac{1}{Re} \frac{\partial^2 v_{\alpha}}{\partial x_{\beta} \partial x_{\beta}}) = -\frac{1}{Re} (\mathbf{y}, \frac{\partial^2}{\partial x_{\beta} \partial x_{\beta}} \frac{\delta \theta}{\delta y_{\alpha}} [\mathbf{y}; t, \mathbf{x}]) \quad (9.27)$$

The kinematic viscosity $\tilde{\nu}$ determining the Reynolds number (2.8) is assumed constant for the present case of turbulent flows of an incompressible fluid without significant variation of temperature.

The external volume force

The external volume force field is not part of the solution and must be specified either directly or indirectly by generating the equations determining it to set up a proper IBVP. The solenoidal external force is considered for two cases,

(1) non-random external force field such as the uniform gravitational force, and

(2) random external force fields. This case is of considerable interest for theoretical studies of regularity of Navier–Stokes solutions [16] and for numerical simulations of turbulent flows [13].

The case (1) is straightforward and considered first.

(1) The non-random external force

The case of solenoidal and non-random external force fields $g_{\alpha}(t, \mathbf{x})$ can be evaluated at once

$$i(y_\alpha, \int_{\Omega} \mu(d\mathbf{v}(t, \mathbf{x}))(g_\alpha(\mathbf{x}) - \frac{\partial P_0}{\partial x_\alpha}) \exp[i(\mathbf{y}, \mathbf{v}(t, \mathbf{x}))]) = i(y_\alpha, (g_\alpha - \frac{\partial P_0}{\partial x_\alpha})\theta[\mathbf{y}; t]) \quad (9.28)$$

(where the known base pressure gradient has been included) since $g_\alpha(t, \mathbf{x})$ is independent of velocity $\mathbf{v}(t, \mathbf{x})$ and the argument field (test function) $\mathbf{y}(\mathbf{x})$, hence unaffected by the integration over the turbulence measure μ . Furthermore, if the force field g_α is uniform, then

$$i(y_\alpha, \int_{\Omega} \mu(d\mathbf{v}(t, \mathbf{x}))g_\alpha \exp[i(\mathbf{y}(\mathbf{x}), \mathbf{v}(t, \mathbf{x}))]) = i(g_\alpha - \frac{\partial P_0}{\partial x_\alpha})(y_\alpha, \theta[\mathbf{y}; t]) \quad (9.29)$$

emerges as explicit representation of the external force term.

(2) The stochastic external force field

The case of stochastic external force fields $g_\alpha(\mathbf{x}, t)$ requires more work, [2, 7, 9]. The phase space must be extended to include velocity and external force vector spaces as product space (Hosokawa [9])

$$\Omega_2 \equiv \Omega\{\mathbf{v}(t, \mathbf{x}) : 0 \leq t < \infty, \mathbf{x} \in \mathcal{D}\} \times \Omega_f\{\mathbf{g}(t, \mathbf{x}) : 0 \leq t < \infty, \mathbf{x} \in \mathcal{D}\}$$

Ω_2 is the space of elementary events, together with \mathcal{A}_2 as the σ -algebra of combined events, analogously, \mathcal{N}_2 is the extended test function space and μ_2 be the probability measure.

The characteristic functional is then defined as Fourier transform of the product measure μ_2 according to (6.1) by

$$\theta_2[\mathbf{y}(\cdot)] \equiv \int_{\Omega_2} d\mu_2(\mathbf{q}) \exp[i(\mathbf{y}_2, \mathbf{q})], \quad (\mathbf{y}_2, \mathbf{q}) : \mathcal{N}_2 \times \Omega_2 \rightarrow \mathbb{R}^1 \quad (9.30)$$

The argument $\mathbf{q}(t, \mathbf{x})$ of the functional integral and the test vector $\mathbf{y}_2(\mathbf{x})$ are augmented vector fields

$$\mathbf{q}(t, \mathbf{x}) \equiv [\mathbf{v}(t, \mathbf{x}), \mathbf{g}(t, \mathbf{x})]^T, \quad \mathbf{y}_2(\mathbf{x}) \equiv [\mathbf{y}(\mathbf{x}), \mathbf{y}_f(\mathbf{x})]^T \quad (9.31)$$

consisting of velocity and external force fields; the associated test function $\mathbf{y}_2(\mathbf{x})$ is thus a six-dimensional vector field. If velocity and external force are statistically independent $\mu_2(\mathbf{q}; t) = \mu(\mathbf{v}; t)\mu_f(\mathbf{g}; t)$ holds, with $\mu(\mathbf{v})$ and $\mu_f(\mathbf{g})$ being the probability measures for velocity and external force fields, the characteristic functionals would be the convolution of the individual functionals. However, the definition of the characteristic functional and the convolution depend on the proper definition of functional integration for them to make sense, a matter that will be postponed until Sect. 23.17.

In general, velocity and external force are correlated, but they are independent initially, hence

$$\mu_2(\mathbf{q}; 0) = \mu(\mathbf{v}; 0)\mu_f(\mathbf{g}; 0) \quad (9.32)$$

holds, and the correlations build up as time progresses. Therefore, the characteristic functional for velocity and external force can be computed as iterated functional integral with respect to the initial product measure

$$\theta_2[\mathbf{y}, \mathbf{y}_f; t] = \int_{\Omega} d\mu(\mathbf{v}; 0) \int_{\Omega_f} d\mu_f(\mathbf{g}; 0) \exp[i(\mathbf{y}, T_t \mathbf{v}(0)) + i(\mathbf{y}_f, G_t \mathbf{g}(0))] \quad (9.33)$$

where T_t denotes the solution operator (2.49) of the Navier–Stokes pdes, $\mathbf{v}(t, \mathbf{x}) = T_t[\mathbf{g}; Re]\mathbf{v}(0, \mathbf{x})$, and G_t the (so far unspecified) propagator for the external force, $\mathbf{g}(t, \mathbf{x}) = G_t[\mathbf{g}(0, \mathbf{x})]$, both push-forward of the initial velocity and initial external force. If the measure for the external force is time-invariant, G_t generates the identity map. The solution operator $T_t[\mathbf{g}; Re]$ depends for $t > 0$ on the external force according to momentum balance (9.17), hence velocity and external force become correlated as time progresses and the right-hand side of (9.33) ceases to be the product of integrals. The time derivative of the exponential function in $\theta_2[\mathbf{y}_2; t]$ is evaluated analogously to (9.7)

$$\begin{aligned} \frac{\partial}{\partial t} \exp[i(\mathbf{y}, T_t[\mathbf{g}]\mathbf{v}(0)) + i(\mathbf{y}_f, G_t \mathbf{g}(0))] = \\ i \exp[i(\mathbf{y}, T_t[\mathbf{g}]\mathbf{v}(0)) + i(\mathbf{y}_f, G_t \mathbf{g}(0))] [\frac{\partial}{\partial t}(\mathbf{y}, T_t[\mathbf{g}]\mathbf{v}(0)) + \frac{\partial}{\partial t}(\mathbf{y}_f, G_t \mathbf{g}(0))] \end{aligned}$$

and, using the momentum balance (2.7) (and Cartesian coordinates for convenience),

$$\begin{aligned} \frac{\partial}{\partial t} \exp[i(\mathbf{y}, T_t[\mathbf{g}]\mathbf{v}) + i(\mathbf{y}_f, G_t \mathbf{g})] = \\ -i \exp[i(\mathbf{y}_f, G_t \mathbf{g})] (\mathbf{y}_\alpha, \exp[i(\mathbf{y}, T_t[\mathbf{g}]\mathbf{v})]) [\frac{\partial}{\partial x_\beta} (v_\alpha v_\beta) + \frac{\partial p}{\partial x_\alpha} - \frac{1}{Re} \frac{\partial^2 v_\alpha}{\partial x_\beta \partial x_\beta} - \frac{1}{Fr} g_\alpha + \frac{\partial P_0}{\partial x_\alpha}] \\ + i \exp[i(\mathbf{y}, T_t[\mathbf{g}]\mathbf{v})] (\mathbf{y}_{f\alpha}, \exp[i(\mathbf{y}_f, G_t \mathbf{g})] \frac{\partial g_\alpha}{\partial t}) \end{aligned} \quad (9.34)$$

follows. The time derivative of the extended characteristic function is then set up for the conditions of flow considered (the details for the periodic pipe flow are given as solutions to Problems 10.1–10.3) to explicitly show the dependence on the externally imposed pressure gradient and the external force field

$$\begin{aligned} \frac{\partial \theta_2}{\partial t}[\mathbf{y}_2; t] = \int_{\Omega} d\mu(\mathbf{v}; 0) \int_{\Omega_f} d\mu_f(\mathbf{g}; 0) \\ \left\{ -i \exp[i(\mathbf{y}_f, G_t \mathbf{g})] (\mathbf{y}_\alpha, \exp[i(\mathbf{y}, T_t[\mathbf{g}]\mathbf{v})]) [\frac{\partial}{\partial x_\beta} (v_\alpha v_\beta) + \frac{\partial p}{\partial x_\alpha} - \frac{1}{Re} \frac{\partial^2 v_\alpha}{\partial x_\beta \partial x_\beta} - \frac{1}{Fr} g_\alpha + \frac{\partial P_0}{\partial x_\alpha}] \right. \\ \left. + i \exp[i(\mathbf{y}, T_t[\mathbf{g}]\mathbf{v})] (\mathbf{y}_{f\alpha}, \exp[i(\mathbf{y}_f, G_t \mathbf{g})] \frac{\partial g_\alpha}{\partial t}) \right\} \end{aligned} \quad (9.35)$$

keeping the cumbersome notation $T_t[\mathbf{g}]$ to signal dependency on the external force. Note that the total pressure $P(t, \mathbf{x})$ is interpreted as the sum of three contributions (26.50), hence is the gradient also a sum

$$\frac{\partial P}{\partial x_\alpha} = \frac{\partial P_0}{\partial x_\alpha} + \frac{\partial p}{\partial x_\alpha}$$

valid generally including the periodic pipe flow, where ∇P_0 is the externally imposed pressure gradient acting solely along the pipe axis and $\nabla p = \nabla p_h + \nabla p_G$ is the gradient of the disturbance pressure, see (26.76) and (26.128) in Appendix D for the explicit representation as functionals of the velocity field. The details for the pressure gradient, the convective and viscous terms are summarized in the next three subsections, they can be skipped at first reading to continue with Sect. 9.2.3.

The extended pressure gradient term

The pressure gradient functional appears for the extended phase space and probability measure analogously to (9.25) as

$$-i(y_{x,\alpha}(\mathbf{x}), \int_{\Omega_2} \mu_2(d\mathbf{v}(t, \mathbf{x})) \exp[i(\mathbf{y}, \mathbf{v}(t, \mathbf{x})) + i(\mathbf{y}_f, \mathbf{g})] \frac{\partial p}{\partial x_\alpha}) = (y_{x,\alpha}(\mathbf{x}), i\Pi_{x,\alpha}[\mathbf{y}_2; t, \mathbf{x}]) \quad (9.36)$$

defining the pressure gradient functional $\Pi_{x,\alpha}[\mathbf{y}_2; t, \mathbf{x}]$. The gradient of the disturbance pressure is a functional of the velocity and the external force fields as evident in (9.24). The external force is contained in the surface integral

$$\begin{aligned} & -i(y_{x,\alpha}(\mathbf{x}), \int_{\Omega_2} \mu_2(d\mathbf{v}(t, \mathbf{x})) \exp[i(\mathbf{y}, \mathbf{v}(t, \mathbf{x})) + i(\mathbf{y}_f, \mathbf{g})] \int_{\partial\mathcal{D}} dA(\mathbf{x}') \frac{\partial G}{\partial x_\alpha} n_\gamma(\mathbf{x}') g_\gamma(t, \mathbf{x}')) = \\ & -i(y_{x,\alpha}(\mathbf{x}), \int_{\partial\mathcal{D}} dA(\mathbf{x}') \frac{\partial G}{\partial x_\alpha} n_\gamma(\mathbf{x}') \int_{\Omega} d\mu(\mathbf{v}; 0) \int_{\Omega_f} d\mu_f(\mathbf{g}; 0) \exp[i(\mathbf{y}_f, G_t \mathbf{g}) + i(\mathbf{y}, T_t[\mathbf{g}]\mathbf{v})] g_\gamma(t, \mathbf{x}')) \end{aligned}$$

Observing that

$$i \int_{\Omega} d\mu(\mathbf{v}; 0) \int_{\Omega_f} d\mu_f(\mathbf{g}; 0) \exp[i(\mathbf{y}_f, G_t \mathbf{g}) + i(\mathbf{y}, T_t[\mathbf{g}]\mathbf{v})] g_\gamma(t, \mathbf{x}) = \frac{\delta\theta_2}{\delta y_{f,\gamma}}[\mathbf{y}, \mathbf{y}_f; t, \mathbf{x}]$$

holds, the surface integral emerges in the form

$$\begin{aligned} & -i(y_{x,\alpha}(\mathbf{x}), \int_{\Omega_2} \mu_2(d\mathbf{v}(t, \mathbf{x})) \exp[i(\mathbf{y}, \mathbf{v}(t, \mathbf{x})) + i(\mathbf{y}_f, \mathbf{g})] \int_{\partial\mathcal{D}} dA(\mathbf{x}') \frac{\partial G}{\partial x_\alpha} n_\gamma(\mathbf{x}') g_\gamma(t, \mathbf{x}')) = \\ & -(y_{x,\alpha}(\mathbf{x}), \int_{\partial\mathcal{D}} dA(\mathbf{x}') \frac{\partial G}{\partial x_\alpha} n_\gamma(\mathbf{x}') \frac{\delta\theta_2}{\delta y_{f,\gamma}}[\mathbf{y}, \mathbf{y}_f; t, \mathbf{x}']) \end{aligned}$$

The pressure gradient functional is now according to (9.36) defined by

$$\Pi_{x,\alpha}[\mathbf{y}; t, \mathbf{x}] \equiv - \int_{\Omega_2} \mu_2(d\mathbf{v}(t, \mathbf{x})) \exp[i(\mathbf{y}, \mathbf{v}(t, \mathbf{x})) + i(\mathbf{y}_f, \mathbf{g})] \frac{\partial p}{\partial x_\alpha}$$

and substituting the gradient of the disturbance pressure

$$\begin{aligned} \Pi_{x,\alpha}[\mathbf{y}; t, \mathbf{x}] &= \int_{\mathcal{D}} dv(\mathbf{x}') \frac{\partial G}{\partial x_\alpha}(\mathbf{x}, \mathbf{x}') \frac{\partial^2}{\partial x'_\gamma \partial x'_\beta} \frac{\delta^2 \theta_2}{\delta y_\gamma \delta y_\beta}[\mathbf{y}; t, \mathbf{x}', \mathbf{x}'] \\ &+ \int_{\partial\mathcal{D}} dA(\mathbf{x}') \frac{\partial G}{\partial x_\alpha}(\mathbf{x}, \mathbf{x}') n_\gamma(\mathbf{x}') \left\{ i \frac{1}{Re} \frac{\partial^2}{\partial x'_\beta \partial x'_\beta} \frac{\delta \theta}{\delta y_\gamma}[\mathbf{y}; t, \mathbf{x}'] + \frac{\partial}{\partial x'_\beta} \frac{\delta^2 \theta_2}{\delta y_\beta \delta y_\gamma}[\mathbf{y}; t, \mathbf{x}', \mathbf{x}'] \right. \\ &\quad \left. + (g_\gamma(t, \mathbf{x}') - \frac{\partial P_0}{\partial x_\alpha} - \frac{\partial v_\gamma^b}{\partial t}(t, \mathbf{x}')) \theta[\mathbf{y}; t] \right\} \end{aligned} \quad (9.37)$$

is obtained.

The extended convective term

The convective terms are now evaluated as before (9.16)

$$\begin{aligned} -i(y_\alpha, \int_{\Omega} d\mu(\mathbf{v}; 0) \int_{\Omega_f} d\mu_f(\mathbf{g}; 0) \exp[i(\mathbf{y}_f, G_t \mathbf{g}) + i(\mathbf{y}, T_t[\mathbf{g}] \mathbf{v})] \frac{\partial}{\partial x_\beta} (v_\alpha v_\beta)) = \\ i(y_\alpha, \frac{\partial}{\partial x_\beta} \lim_{\mathbf{x}' \rightarrow \mathbf{x}} \frac{\delta^2 \theta_2}{\delta y_\alpha \delta y_\beta}[\mathbf{y}; t, \mathbf{x}, \mathbf{x}']) \end{aligned} \quad (9.38)$$

The extended viscous term

The viscous stress term is analogous to (9.27)

$$\begin{aligned} i(y_\alpha, \int_{\Omega} d\mu(\mathbf{v}; 0) \int_{\Omega_f} d\mu_f(\mathbf{g}; 0) \exp[i(\mathbf{y}_f, G_t \mathbf{g}) + i(\mathbf{y}, T_t[\mathbf{g}] \mathbf{v})] \frac{1}{Re} \frac{\partial^2 v_\alpha}{\partial x_\beta \partial x_\beta}) = \\ - \frac{1}{Re} (y_\alpha, \frac{\partial^2}{\partial x_\beta \partial x_\beta} \frac{\delta \theta_2}{\delta y_\alpha}[\mathbf{y}_2; t, \mathbf{x}]) \end{aligned} \quad (9.39)$$

This concludes the preparation for the Hopf fde subject to stochastic external forces in the next sections.

9.2.3 The Hopf fde Version I: Non-random External Force

Collecting the results for convection (9.16), pressure gradient functional $\Pi_\alpha[\mathbf{v}, \mathbf{g}; t, \mathbf{x}]$ (9.25) and (9.26), the viscous term (9.27) and the external force term (9.28), the equation for the characteristic functional can be assembled

$$\begin{aligned} \frac{\partial}{\partial t} \theta[\mathbf{y}; t] = \int_{\mathcal{D}} d\mathbf{x} y_\alpha(\mathbf{x}) \left\{ i \frac{\partial}{\partial x_\beta} \lim_{\mathbf{x}' \rightarrow \mathbf{x}} \frac{\delta^2 \theta}{\delta y_\beta(\mathbf{x}') \delta y_\alpha(\mathbf{x})} [\mathbf{y}; t] + i \Pi_\alpha[\mathbf{y}, \mathbf{g}; t, \mathbf{x}] + \frac{1}{Re} \frac{\partial^2}{\partial x_\beta \partial x_\beta} \frac{\delta \theta}{\delta y_\alpha} [\mathbf{y}; t, \mathbf{x}] \right. \\ \left. + i \left(\frac{1}{Fr} g_\alpha(\mathbf{x}) - \frac{\partial P_0}{\partial x_\alpha} \right) \theta[\mathbf{y}; t] \right\} \end{aligned} \quad (9.40)$$

The time rate of change of the characteristic functional is determined by scalar product of the test (argument) function and the expectation of the time rate of linear momentum. A special version for this equation is considered in Sect. 9.2.5, where the vector fields in the phase space Ω satisfy the additional constraints of zero divergence and homogenous Dirichlet boundary conditions. The present version of the Hopf fde is for Cartesian coordinates in the flow domain \mathcal{D} , the case of cylindrical coordinates is presented as the solution to Problem (10.2) in Appendix F.

The analysis of fde (9.40) and its solvability has been attempted by several authors since the groundbreaking paper by Hopf [17]. Vishik and Fursikov defined the notion of space–time statistical solutions of the Hopf fde as a probability measure on the phase space and proved solvability, see Theorem 1.1 in Chap. V in [6]. Janocha et al. [18] started the symmetry analysis of the Hopf fde with the aid of Lie transformation group theory.

The effect of the non-random, uniform external force is illustrated in the solution to Problem (10.1) in Appendix F, Chap. 28. It is shown that for a Gaussian initial condition the sole effect of the external force is to change the mean field linearly in time, the rate of change is the integrated argument field $\mathbf{y}(\mathbf{x})$. If the non-random external force \mathbf{g} is a function of location $\mathbf{x} \in \mathcal{D}$, the rate of change is the scalar product (\mathbf{g}, \mathbf{y}) .

9.2.4 The Hopf Equation Version Ix: Stochastic External Force

Collecting the results for convection (9.38), pressure gradient functional $\Pi_{x,\alpha}[\mathbf{v}, \mathbf{g}; t, \mathbf{x}]$ (9.36) and (9.37), the viscous term (9.39) and the external force terms, the equation for the characteristic functional $\theta_2[\mathbf{y}, \mathbf{y}_f; t]$ defined by (9.33) can be assembled

$$\frac{\partial}{\partial t} \theta_2 = (y_\alpha(\mathbf{x}), \mathcal{L}_\alpha \theta_2) + (y_\alpha, \mathcal{L}_\alpha^b \theta_2) + i (y_{f,\alpha}, \mathcal{L}_\alpha^c \theta_2)$$

(9.41)

The individual contributions to the right-hand side are defined by

$$\mathcal{L}_\alpha \theta_2 \equiv i \frac{\partial}{\partial x_\beta} \frac{\delta^2 \theta_2}{\delta y_\beta(\mathbf{x}) \delta y_\alpha(\mathbf{x}')} + \frac{1}{Re} \frac{\partial^2}{\partial x_\beta \partial x_\beta} \frac{\delta \theta_2}{\delta y_\alpha(\mathbf{x})} - i \frac{\partial P_0}{\partial x_\alpha} \theta_2 + \frac{1}{Fr} \frac{\delta \theta_2}{\delta y_{f,\alpha}(\mathbf{x})} \quad (9.42)$$

and the boundary value part generated by the Green's function $G(\mathbf{x}, \mathbf{x}')$ expressing the gradient of the disturbance pressure as functional of velocity (9.21) is

$$\begin{aligned} \mathcal{L}_\alpha^b \theta_2 &\equiv \int_{\mathcal{D}} d\mathbf{x}' \frac{\partial G}{\partial x_\alpha}(\mathbf{x}, \mathbf{x}') \frac{\partial^2}{\partial x'_\beta \partial x'_\gamma} \frac{\delta^2 \theta_2}{\delta y_\beta(\mathbf{x}') \delta y_\gamma(\mathbf{x}'')} \\ &+ \int_{\partial\mathcal{D}} dA(\mathbf{x}') \frac{\partial G}{\partial x_\alpha}(\mathbf{x}, \mathbf{x}') n_\beta(\mathbf{x}') \left[-\frac{1}{Re} \frac{\partial^2}{\partial x'_\gamma \partial x'_\gamma} \frac{\delta \theta_2}{\delta y_\beta(\mathbf{x}')} - \frac{1}{Fr} \frac{\delta \theta_2}{\delta y_{f,\beta}(\mathbf{x}')} + \left(\frac{\partial P_0}{\partial x_\beta} + \frac{Dv_\beta^b}{Dt} \right) \theta_2[\mathbf{y}, \mathbf{y}_f; t] \right] \end{aligned} \quad (9.43)$$

and the external force contribution is

$$\mathcal{L}_\alpha^e \theta_2 \equiv \int_{\Omega} d\mu(\mathbf{v}; 0) \int_{\Omega_f} d\mu_f(\mathbf{g}; 0) \exp[i(\mathbf{y}_f, G_t \mathbf{g}) + i(\mathbf{y}, T_t[\mathbf{g}] \mathbf{v})] \frac{\partial}{\partial t} G_t g_\alpha(0) \quad (9.44)$$

where $\mathbf{g}(t, \mathbf{x}) = G_t[\mathbf{g}(0, \mathbf{x})]$ propagates the external force at time zero to the current time. The stochastic evolution of the external force $\frac{\partial}{\partial t} G_t g_\alpha(0)$ is not specified at this point, since it is determined by the particularities of the problem considered. A classification of external forces is presented by Kuksin and Shirikyan [16] applied to the analysis of 2-d turbulence. This rather complicated fde is linear as its counterpart driven by non-random external forces in the previous section. Novikov [7, 8] discusses the special case of Gaussian external forces.

9.2.5 The Hopf Equation II: Homogeneous Dirichlet Conditions

The case of flows of an incompressible fluid in a domain \mathcal{D} with boundary $\partial\mathcal{D}$ and homogeneous Dirichlet boundary conditions allows a second version of the Hopf fde that does not contain the pressure functional [1]. It is a consequence of mass balance (2.6), i.e. the condition that velocity field is solenoidal for incompressible fluids. An example for a solenoidal base is given in Sect. 4.2 with details in Sect. 25.19 of Appendix C. Then

$$(\mathbf{v}, \nabla \varphi) = 0 \quad (9.45)$$

holds for all velocity fields and differentiable scalars $\varphi(\mathbf{x})$. The space of argument fields $\mathbf{y}(\mathbf{x})$ can be restricted to solenoidal vector fields $\nabla \cdot \mathbf{y} = 0$, it follows from the solenoidal property that $(\mathbf{y}, \nabla p) = 0$ holds and the characteristic functional is,

therefore, invariant with respect to gradient fields. The Hopf equation (9.40) is then reduced to

$$\boxed{\frac{\partial}{\partial t}\theta[\mathbf{y}; t] = \int_{\mathcal{D}} d\mathbf{x} y_\alpha(\mathbf{x}) \left\{ i \frac{\partial}{\partial x_\beta} \frac{\delta^2 \theta}{\delta y_\beta \delta y_\alpha}[\mathbf{y}; t, \mathbf{x}, \mathbf{x}] + \frac{1}{Re} \frac{\partial^2}{\partial x_\beta \partial x_\beta} \frac{\delta \theta}{\delta y_\alpha}[\mathbf{y}; t, \mathbf{x}] \right\}} \quad (9.46)$$

where $\nabla \cdot \mathbf{y} = 0$ must be satisfied for all $\mathbf{y} \in \mathcal{N}$ (see [1], Chap. 28.1 for further details).

9.2.6 Spectral Version of the Hopf fde I

The Hopf fde I can be formulated for realization and argument fields, defined in $\mathcal{D} = R^3$, transformed to Fourier space. This is particularly useful for the analysis of homogeneous turbulence in Fourier space.

The Fourier-transformed Navier–Stokes pdes are reduced for incompressible fluids to a system of odes (15.18) for the velocity amplitudes $\hat{\mathbf{v}}(t, \mathbf{k})$, the number of odes depends on the spectral range. The characteristic functional θ_F in wavenumber space is thus defined by

$$\theta_F[\hat{\mathbf{y}}(\mathbf{k}); t] = \theta[\mathcal{F}^{-1}\hat{\mathbf{y}}(\mathbf{k}); t] \equiv \langle \exp[i(\mathcal{F}^{-1}\hat{\mathbf{y}}, \mathcal{F}^{-1}\hat{\mathbf{v}})] \rangle \quad (9.47)$$

where $\hat{\mathbf{y}} = \mathcal{F}\mathbf{y} \in \mathcal{N}_F$, $\hat{\mathbf{v}} = \mathcal{F}\mathbf{v} \in \Omega_F$, $\mathbf{k} \in R^3$ (the Fourier transform operator \mathcal{F} is defined by (15.2) in Sect. 15.1). The phase space Ω_F is the Fourier transform of phase space Ω and the space of test/argument functions \mathcal{N}_F is the dual of Ω_F (the dual of a real vector space Ω is the space Ω^* of all real linear maps $\Omega \rightarrow R^1$). The scalar product for the present spatial case of incompressible flows is defined on the product space $\mathcal{N}_F \times \Omega_F$ by

$$(\hat{\mathbf{y}}, \hat{\mathbf{v}}) \equiv \int_{\hat{\mathcal{D}}} d\mathbf{k} \hat{\mathbf{y}}(\mathbf{k}) \cdot \hat{\mathbf{v}}^*(t, \mathbf{k}) \quad (9.48)$$

where $\hat{\mathbf{y}}(\mathbf{k})$ is element of the complex nuclear space of test functions \mathcal{N}_F and the complex-valued Fourier transform $\hat{\mathbf{v}}(t, \mathbf{k})$ of a realization $\mathbf{v}(t, \mathbf{x})$ is element of the complex phase space Ω_F .

$$\frac{d}{dt} \exp[i(\hat{\mathbf{y}}, \hat{\mathbf{v}})] = -i(\hat{\mathbf{y}}, \exp[i(\hat{\mathbf{y}}, \hat{\mathbf{v}})])[-ik_\beta P_{\alpha\gamma} \hat{v}_\beta * \hat{v}_\gamma(t, \mathbf{k}) - \frac{1}{Re} k^2 \hat{v}_\alpha(t, \mathbf{k})] \quad (9.49)$$

The linear viscous term is evaluated as first Gateaux derivative

$$\langle \hat{v}_\alpha(t, \mathbf{k}) \exp[i(\hat{\mathbf{y}}, \hat{\mathbf{v}})] \rangle = -i \frac{\delta \theta}{\delta \hat{y}_\alpha(\mathbf{k})} \quad (9.50)$$

The nonlinear convolution (15.3) term representing convection and pressure gradient effects appears as

$$\langle \exp[i(\hat{\mathbf{y}}, \hat{\mathbf{v}})] \hat{v}_\beta * \hat{v}_\gamma(t, \mathbf{k}) \rangle = - \int d\mathbf{k}' \frac{\delta^2 \theta}{\delta \hat{y}_\beta(\mathbf{k} - \mathbf{k}') \delta \hat{y}_\gamma(\mathbf{k}')} \quad (9.51)$$

The Hopf fde for the characteristic functional of flows in the 3-d domain $\mathcal{D} = \mathbb{R}^3$ emerges then as

$$\frac{d\theta}{dt} = (\hat{y}_\alpha(\mathbf{k}), k_\beta P_{\alpha\gamma} \int d\mathbf{k}' \frac{\delta^2 \theta}{\delta \hat{y}_\beta(\mathbf{k} - \mathbf{k}') \delta \hat{y}_\gamma(\mathbf{k}')} - \frac{k^2}{Re} \frac{\delta \theta}{\delta \hat{y}_\alpha(\mathbf{k})}) \quad (9.52)$$

where the scalar product is defined by (9.48) as integral over the wavenumber space $\hat{\mathbb{R}}^3 = \hat{\mathcal{D}}$. This approach to turbulence theory was initiated by Hopf in 1952 [17] and continued by Lumley in Monin and Yaglom vol. II [1], Chap. 10, Vishik and Fursikov [6] and others. The solution of the IVP for the fde (9.52) can be computed if an initial condition is specified. The characteristic functional (9.47) at time zero must be consistent with mass balance, i.e. the condition that the initial velocity fields must be orthogonal to the wavenumber vector \mathbf{k} according to (15.9). This can be achieved with the aid of the projection operator (15.19). Let the initial data be given as randomly selected argument field $\hat{v}_\alpha(\mathbf{k})$, the projected field $P_{\alpha\beta}(\mathbf{k})\hat{v}_\beta(\mathbf{k})$ satisfies mass balance (15.9) and the characteristic functional at $t = 0$ is then set up in the form $\theta[P_{\alpha\beta}\hat{v}_\beta; 0]$.

9.2.7 Convection as Diffusion in Hilbert Space

The Hopf fde (9.40) for the spatial characteristic functional of turbulent flows, established first in [17], contains the effect of convection as a second variational derivative Hessian, which in turn contains the standard Laplacian as trace. The characteristic functional θ of an incompressible turbulent flow defined in a flow domain \mathcal{D} for the time interval $[0, \infty)$ is formally given by Eq. (9.1) (see also [1], Chap. 10). Recent progress in the theory of the Laplacian in infinite-dimensional spaces [19–21] suggests that the convective term in the Hopf fde (see derivation in Sect. 9.2.3, [1], Chap. 10) for the characteristic functional θ may be accessible to further analysis.

The convective term $\frac{\partial}{\partial x_\beta} \left(\frac{\delta^2}{\delta y_\beta \delta y_\alpha} \theta[\mathbf{y}; t, \mathbf{x}, \mathbf{x}] \right)$ is the functional Hessian containing second variational derivatives of the characteristic functional θ . It can be recast in the form

$$\frac{\delta^2 \theta}{\delta y_\beta \delta y_\alpha}[\mathbf{y}; t, \mathbf{x}, \mathbf{x}] = \left[\frac{\delta^2 \theta}{\delta y_\beta \delta y_\alpha}[\mathbf{y}; t, \mathbf{x}, \mathbf{x}] - \frac{1}{3} \delta_{\alpha\beta} \frac{\delta^2 \theta}{\delta y_\gamma \delta y_\gamma}[\mathbf{y}; t, \mathbf{x}, \mathbf{x}] \right] + \frac{1}{3} \delta_{\alpha\beta} \frac{\delta^2 \theta}{\delta y_\gamma \delta y_\gamma}[\mathbf{y}; t, \mathbf{x}, \mathbf{x}] \quad (9.53)$$

where the operator in the brackets is traceless and the last term is related to the generalized or standard Laplacian. The relation of the convective term to the Laplacian will be explored in detail in Sects. 9.4.1 (standard Laplacian) and 9.4.2 (Lévy-Laplacian) below.

9.3 The Lewis–Kraichnan Equation for the Space–Time Functional

Lewis and Kraichnan [2] established the equation for the space–time functional $\Theta[\mathbf{y}(t, \mathbf{x})]$ in the spatial description defined by

$$\Theta[\mathbf{y}] = \langle \exp[i(\mathbf{y}, \mathbf{v})] \rangle \equiv \int_{\tilde{\Omega}} d\mu(\mathbf{v}) \exp[i(\mathbf{y}, \mathbf{v})] \quad (9.54)$$

where $\mathbf{v}(t', \mathbf{x}') \in \tilde{\Omega}$ with $\tilde{\Omega}$ (5.1) being the phase space and $\mathbf{y}(t', \mathbf{x}')$ denoting the vector field defined on space–time $\mathcal{D} \times [0, \infty)$ and element of a suitable nuclear vector space \mathcal{N} of test functions. The scalar product is now defined by

$$(\mathbf{y}, \mathbf{v}) \equiv \int_0^\infty dt' \int_{\mathcal{D}(t')} d\mathbf{v}(\mathbf{x}') \mathbf{y}(t', \mathbf{x}') \cdot \mathbf{v}(t', \mathbf{x}') \quad (9.55)$$

The characteristic functional Θ depends on the argument field $\mathbf{y}(t', \mathbf{x}')$, but not on time t or location \mathbf{x} . The space of test functions is defined as the space of smooth vector fields $\mathcal{N} = \{\mathbf{y}(t', \mathbf{x}') \in C_{\mathcal{D} \times [0, \infty)}^\infty : \mathbf{y}(t', \mathbf{x}') = 0, \mathbf{x}' \in \partial\mathcal{D}, 0 \leq t' < \infty\}$ vanishing on the boundary. The space–time definition of the characteristic functional is suitable for the transformation between spatial and material descriptions, this is pursued in Sect. 9.5, where the fde for the material description is derived.

The first Gateaux derivative of the characteristic functional Θ is according to Sect. 23.12

$$\frac{\delta \Theta}{\delta y_\alpha}[\mathbf{y}; t, \mathbf{x}] = \langle i v_\alpha(t, \mathbf{x}) \exp[i(\mathbf{y}, \mathbf{v})] \rangle \quad (9.56)$$

and likewise for the second derivative. The derivatives depend parametrically on time t and location \mathbf{x} ; hence, the derivatives with respect to time and location can be computed, i.e.

$$\frac{\partial}{\partial t} \frac{\delta \Theta}{\delta y_\alpha}[\mathbf{y}; t, \mathbf{x}] = \langle i \frac{\partial v_\alpha}{\partial t}(t, \mathbf{x}) \exp[i(\mathbf{y}, \mathbf{v})] \rangle \quad (9.57)$$

allowing the introduction of the Navier–Stokes equations (2.6), (2.7). The result is the Lewis–Kraichnan equation (only the parameters time and location indicated)

$$\frac{\partial}{\partial t} \frac{\delta \Theta}{\delta y_\alpha}(t, \mathbf{x}) = i \frac{\partial}{\partial x_\beta} \frac{\delta^2 \Theta}{\delta y_\beta \delta y_\alpha}(t, \mathbf{x}) + \frac{1}{Re} \frac{\partial^2}{\partial x_\beta \partial x_\beta} \frac{\delta \Theta}{\delta y_\alpha}(t, \mathbf{x}) - i \frac{\partial \Pi}{\partial x_\alpha} + i g_\alpha \Theta \quad (9.58)$$

for the first Gateaux derivative of the space–time characteristic functional $\Theta[\mathbf{y}]$. The pressure term is defined by

$$\Pi[\mathbf{y}; t, \mathbf{x}, \mathbf{g}] \equiv \langle p(t, \mathbf{x}) \exp i(\mathbf{y}, \mathbf{v}) \rangle \quad (9.59)$$

The Lewis–Kraichnan equation (9.58) is incomplete, since the relation of the pressure functional Π to the argument/test field \mathbf{y} is not yet established. This can be accomplished for incompressible fluids in several ways.

9.3.1 Lewis–Kraichnan fde Version I

The first method is based on the Leray version of the Navier–Stokes equations, which can be obtained from the standard formulation (2.6) and (2.7) with the aid of Green’s theorem (Majda and Bertozzi [22] Chap. 1.8). The Green’s function G is the fundamental solution of the Poisson pde and must satisfy non-homogeneous Neumann conditions on the boundary $\partial\mathcal{D}$, an example for the construction of the boundary condition and the associated Green’s function for compact domains with periodic in and outflow boundary conditions is given in Appendix D, Chap. 26. The pressure is for compact domains represented in Cartesian coordinates as

$$p(t, \mathbf{x}) = \int_{\mathcal{D}} dv(\mathbf{x}') G(\mathbf{x}, \mathbf{x}') \frac{\partial^2}{\partial x'_\alpha \partial x'_\beta} (v_\alpha v_\beta) + \int_{\partial\mathcal{D}} dA(\mathbf{x}') n_\alpha [p(\mathbf{x}') \frac{\partial G(\mathbf{x}, \mathbf{x}')}{\partial x'_\alpha} - G(\mathbf{x}, \mathbf{x}') \frac{\partial p}{\partial x'_\alpha}] \quad (9.60)$$

The Leray version emerges as integro-differential equation for the velocity

$$\begin{aligned} \frac{\partial v_\alpha}{\partial t} + v_\beta \frac{\partial v_\alpha}{\partial x_\beta} &= \frac{1}{Re} \frac{\partial^2 v_\alpha}{\partial x_\beta \partial x_\beta} + g_\alpha \\ - \frac{1}{\rho} \int_{\mathcal{D}} dv(\mathbf{x}') \frac{\partial G}{\partial x_\alpha}(\mathbf{x}, \mathbf{x}') \frac{\partial^2}{\partial x'_\beta \partial x'_\gamma} (v_\beta v_\gamma)(t, \mathbf{x}') + \frac{1}{\rho} \int_{\partial\mathcal{D}} dA(\mathbf{x}') n_\beta h_\beta(t, \mathbf{x}') \frac{\partial G}{\partial x_\alpha}(\mathbf{x}, \mathbf{x}') \end{aligned} \quad (9.61)$$

The number of pdes is reduced by one as mass balance is eliminated. It is straightforward to prove with the aid of the energy method that the divergence of velocity remains zero if it was zero initially. The associated version of the Lewis–Kraichnan equation follows from (9.59) and (9.60)

$$\Pi(t, \mathbf{x}) = - \int_{\mathcal{D}} dv(\mathbf{x}') G(\mathbf{x}, \mathbf{x}') \frac{\partial^2}{\partial x'_\alpha \partial x'_\beta} \frac{\delta^2 \Theta}{\delta y_\alpha \delta y_\beta}[\mathbf{y}; t, \mathbf{x}', \mathbf{x}'] - \int_{\partial\mathcal{D}} dA(\mathbf{x}') n_\alpha \langle h_\alpha \exp i(\mathbf{v}, \mathbf{y}) \rangle \quad (9.62)$$

The boundary term on the right side can be explicitly stated if the boundary conditions for velocity are specified. For instance, Dirichlet conditions $\mathbf{v}(t, \mathbf{x}') = \mathbf{v}^b(t, \mathbf{x}')$, $\mathbf{x}' \in \partial\mathcal{D}(t)$ lead to

$$\begin{aligned} \int_{\partial\mathcal{D}} dA(\mathbf{x}') n_\alpha \langle h_\alpha \exp i(\mathbf{v}, \mathbf{y}) \rangle &= \int_{\partial\mathcal{D}} dA(\mathbf{x}') n_\alpha \left\{ -\frac{1}{Re} \frac{\partial^2}{\partial x'_\beta \partial x'_\beta} \frac{\delta\Theta}{\delta y_\alpha} [\mathbf{y}; t, \mathbf{x}'] \right. \\ &\quad \left. + (g_\alpha - \frac{\partial v_\alpha^b}{\partial t}) \Theta[\mathbf{y}] - i v_\beta^b \frac{\partial}{\partial x'_\beta} \frac{\delta\Theta}{\delta y_\alpha} [\mathbf{y}; t, \mathbf{x}'] \right\} \end{aligned} \quad (9.63)$$

The Lewis–Kraichnan equation is obtained using (9.61) and (9.62)

$$\begin{aligned} \frac{\partial}{\partial t} \frac{\delta\Theta}{\delta y_\alpha} [\mathbf{y}; t, \mathbf{x}] &= i \frac{\partial}{\partial x_\beta} \frac{\delta^2\Theta}{\delta y_\beta \delta y_\alpha} [\mathbf{y}; t, \mathbf{x}, \mathbf{x}] + \frac{1}{Re} \frac{\partial^2}{\partial x_\beta \partial x_\beta} \frac{\delta\Theta}{\delta y_\alpha} [\mathbf{y}; t, \mathbf{x}] + i g_\alpha \Theta[\mathbf{y}] \\ &+ i \frac{\partial}{\partial x_\alpha} \left[\int_{\mathcal{D}} dv(\mathbf{x}') G(\mathbf{x}, \mathbf{x}') \frac{\partial^2}{\partial x'_\alpha \partial x'_\beta} \frac{\delta^2\Theta}{\delta y_\alpha \delta y_\beta} [\mathbf{y}; t, \mathbf{x}', \mathbf{x}'] + \int_{\partial\mathcal{D}} dA(\mathbf{x}') n_\alpha \langle h_\alpha \exp i(\mathbf{v}, \mathbf{y}) \rangle \right] \end{aligned} \quad (9.64)$$

The equation is complete once the boundary conditions for velocity have been specified in terms of h_α . The example of Dirichlet conditions for velocity above shows that the Lewis–Kraichnan equation is then linear and closed, i.e. it does not contain additional unknowns.

9.3.2 Lewis–Kraichnan fde Version II

The second method relies on a modification of the space of test functions \mathcal{N} . Requiring the test functions to be solenoidal, i.e.

$$\frac{\partial \hat{y}_\alpha}{\partial x_\alpha} = 0 \quad (9.65)$$

The solenoidal test functions $\hat{y}_\alpha(t, \mathbf{x})$ are elements of the linear subspace $\hat{W} \subset \mathcal{N}$. The Lewis–Kraichnan equation emerges now as orthogonality condition

$$(\hat{y}_\alpha(t, \mathbf{x}), \frac{\partial}{\partial t} \frac{\delta\Theta}{\delta y_\alpha} [\mathbf{y}; t, \mathbf{x}] - i \frac{\partial}{\partial x_\beta} \frac{\delta^2\Theta}{\delta y_\beta \delta y_\alpha} [\mathbf{y}; t, \mathbf{x}] - \frac{1}{Re} \frac{\partial^2}{\partial x_\beta \partial x_\beta} \frac{\delta\Theta}{\delta y_\alpha} [\mathbf{y}; t, \mathbf{x}] - i g_\alpha \Theta[\mathbf{y}]) = 0$$

for all $\hat{y}_\alpha \in \hat{W}$. The pressure term is eliminated due to

$$(\hat{y}_\alpha, \frac{\partial \Pi}{\partial x_\alpha}) = \int_0^\infty dt \int_{\mathcal{D}(t)} dv(\mathbf{x}) \frac{\partial}{\partial x_\alpha} (\hat{y}_\alpha(t, \mathbf{x}) \Pi[\mathbf{y}; t, \mathbf{x}]) = \int_0^\infty dt \int_{\partial \mathcal{D}(t)} dA(\mathbf{x}) n_\alpha \hat{y}_\alpha(t, \mathbf{x}) \Pi[\mathbf{y}; t, \mathbf{x}] = 0 \quad (9.67)$$

(n_α denotes the unit vector orthogonal to $\partial \mathcal{D}$ pointing outward), where the divergence theorem and $\hat{\mathbf{y}}(t, \mathbf{x}) = 0$, $\mathbf{x} \in \partial \mathcal{D}(t)$ were applied. Arsenev [23, 24] discusses turbulence measures defined on a suitable Banach space and obtains the Lewis–Kraichnan fde (9.66), Foias [25, 26] provides a detailed functional analysis of Hopf-type fdes.

Summary

The derivation of the Hopf fde generated a general association of nonlinear terms in the pdes that govern the motion of a Newtonian fluid, with terms in the linear Hopf fde, which governs the evolution of the characteristic functional. This association is summarized in Table 9.1 to show the relation between a particular nonlinearity, in the form of products of velocity components, in the pdes and the order of Gateaux/Fréchet derivative in the Hopf fde.

The nonlinear convection and pressure gradient (functional of velocity) terms in the momentum balance generates a linear second-order derivative term in the Hopf pde, whereas the linear viscous term in the pde is associated with a linear, first-order derivative in the Hopf fde. Gateaux/Fréchet differentiation produces dependence on location in the flow field for functionals of exponential type as exemplified in Definition 6.1; hence, differentiation with respect to location of variational derivatives can be applied. It follows that spatial and variational (Gateaux/Fréchet) derivatives do not commute since

$$\frac{\partial}{\partial x_\alpha} \theta[\mathbf{y}; t] = 0$$

but

$$\frac{\partial}{\partial x_\alpha} \frac{\delta \theta}{\delta y_\alpha(\mathbf{x})} \neq 0$$

Spatial derivatives appear in the same form in pde (mass and momentum balances) and fde (Hopf equation). The associations in the table above explain the fact that the Hopf fde and its variants are linear in $\theta[\mathbf{y}; t]$. The association of nonlinear terms with the order of the variational derivatives depends on the choice of independent

Table 9.1 Order of nonlinearity in the Navier–Stokes pdes and variational differentiation in the Hopf fde in the spatial description

Nonlinearity order	Momentum pde term in (2.7)	Variational derivative order	Hopf fde term in (9.40)
2	$\frac{\partial}{\partial x_\beta} (v_\alpha v_\beta)$	2	$i \frac{\partial}{\partial x_\beta} \frac{\delta^2 \theta}{\delta y_\alpha \delta y_\beta}$
1	$\frac{\partial^2 v_\alpha}{\partial x_\beta \partial x_\beta}$	1	$-\frac{\partial^2}{\partial x_\beta \partial x_\beta} \frac{\delta \theta}{\delta y_\alpha}$

variables in the Navier–Stokes pdes, or more generally on the transformation applied to them, as the material version in Sect. 9.5 indicates.

The versions of the Hopf fde in the spatial description derived in the previous sections contain Gateaux/ Fréchet derivatives with the terms representing convection appearing as Hessian formed by the second variational derivatives of the characteristic functional. The trace of this Hessian may emerge as distribution on $\mathcal{D} \times \mathcal{D}$ as the limit $\mathbf{x}' \rightarrow \mathbf{x}$ is carried out (end of Sect. 9.2) and it is a possible version of the Laplacian extended to infinite dimension. This needs further investigation to clarify the properties of the variational Hessian. Hence, variants of the Laplacian are analysed in the next section to establish fundamental properties of the Hessian representing convection in the Hopf fde.

The transformation of the Navier–Stokes pdes to the material description generates nonlinear terms from linear ones and vice versa. For instance, the linear spatial gradient in the spatial description transforms to a nonlinear term in the material description composed of the material gradient multiplied with components of the deformation gradient or its inverse (2.82) according to (2.94)

$$\frac{\partial}{\partial x_\alpha} = F_{\beta\alpha}^{-1} \frac{\partial}{\partial X_\beta} = \frac{1}{2J} \epsilon_{\alpha\beta\gamma} \epsilon_{\delta\eta\omega} F_{\eta\beta} F_{\omega\gamma} \frac{\partial}{\partial X_\delta}$$

The second Gateaux derivative of the $\theta[\mathbf{y}; \tau]$ generates the Hessian analogue to (9.15)

$$\frac{\delta^2 \theta}{\delta y_\alpha(\mathbf{X}) \delta y_\beta(\mathbf{X}')} [\mathbf{y}; \tau] = - \int_{\Omega} d\mu(\tau, \Phi) \Phi_\alpha(\tau, \mathbf{X}) \Phi_\beta(\tau, \mathbf{X}') \exp[i(\mathbf{y}, \Phi)]$$

that can be recast as

$$\begin{aligned} \frac{\partial^2}{\partial X_\gamma \partial X'_\omega} \left(\frac{\delta^2 \theta}{\delta y_\alpha(\mathbf{X}) \delta y_\beta(\mathbf{X}')} [\mathbf{y}; \tau] \right) &= - \int_{\Omega} d\mu(\tau, \Phi) \frac{\partial}{\partial X_\gamma} \Phi_\alpha(\tau, \mathbf{X}) \frac{\partial}{\partial X'_\omega} \Phi_\beta(\tau, \mathbf{X}') \exp[i(\mathbf{y}, \Phi)] \\ &= - \int_{\Omega} d\mu(\tau, \Phi) F_{\alpha\gamma}(\tau, \mathbf{X}) F_{\beta\omega}(\tau, \mathbf{X}') \exp[i(\mathbf{y}, \Phi)] \end{aligned}$$

emerging in terms of the deformation gradient $F_{\alpha\beta}(\tau, \mathbf{X})$, which is due to the transformation of derivatives in physical space (2.94) to the material description. Further manipulations may be necessary to construct a desired combination of terms in the Hopf or Lewis–Kraichnan fde. The order of the variational derivatives depends thus on the nonlinearity, i.e. the number of factors resulting from the transformation of the Navier–Stokes pdes to the material description.

Comments

- (i) It is very difficult to prove existence, regularity and uniqueness for the solutions of the nonlinear Navier–Stokes pdes for all Reynolds numbers and initial energies as discussed in Sect. 2.2. On the other hand, the fdes obtained in the present section

for the characteristic functional are linear, thus raising the expectation, that existence and uniqueness proofs (see, for instance, Theorem 1.1 in Chap. V in [6]) are possible.

(ii) The Hopf and Lewis–Kraichnan fdes and their variants raise a fundamental question: Turbulence is apparently a chaotic phenomenon governed by nonlinear pdes, but the fdes, even their projections generated by cylinder functions as arguments of the characteristic functional, governing the statistics of turbulent flows are linear, then how is it possible for them to describe a chaotic phenomenon? A few possible conjectures come to mind:

(ii.1) The convective second-order nonlinear term generates the negative, second-order Gateaux/ Fréchet derivative Hessian in the Hopf fde as illustrated in the table above. The trace of this Hessian is related to the generalized Laplacian describing diffusion in scalar and velocity argument space, if it is well behaved and smoother than a distribution, hence mode interaction would be reflected by linear diffusion on the functional level. The coefficients of this Hessian are not constant, but vary with location in phase/test function space, hence changing the type of the equation. The trace of the Hessian may be stable or unstable depending on the sign of these coefficients, hence able to create chaos via instability.

(ii.2) It may be contained in the structure of the basis spanning the phase space Ω and the test function space \mathcal{N} being non-orthogonal, hence implying mode interaction. An example for a non-orthogonal vector basis is given in Chap. 25 of Appendix D for a periodic pipe flow. However, methods for the orthonormalization exist creating expansion functions consisting of linear combinations of modes. Furthermore, this implies that the instability is basis dependent, an unlikely result.

These possibilities indicate interesting lines of further research. It should be noted, that the idea for converting a nonlinear set of equations to a linear one is to change the level of description such that dependent variables become independent ones. The next section takes a closer look at the operators that represent convection in the elevated formulation, i.e. the definitions of Laplacians in infinite-dimensional spaces and their particular appearance in suitable bases.

(iii) Construction of an ONS basis in phase and argument spaces allows the transformation of the Hopf fde to an infinite system of odes. Truncation of this system produces a finite set of odes thus producing a connection to dynamical systems theory. This may holds some promise, but has not been pursued so far (however, see Jimenez [27] for a change in attitude w.r.t. the probabilistic approach and dynamical system theory).

9.3.3 *Variational Derivatives of a Gaussian Characteristic Functional*

The computation of statistical moments is important for myriad applications, they can be computed either according to (9.6) as variational derivatives at the origin of the characteristic functional or by integration w.r.t. the turbulence measure. Therefore,

as analytic example for the former approach, the variational derivatives of a non-degenerate Gaussian characteristic functional at the origin relevant for this purpose are established first without recourse to a basis and then w.r.t. an ordered Schauder basis. The Gateaux definition of variational derivatives are applied, the result is identical to the Fréchet definition if both exist.

The first Gateaux derivative follows from the definition (23.45) of the variational differential

$$\delta\theta[y, w] = \left(\frac{\delta\theta}{\delta y(\mathbf{x})}, w \right) = \left(\left[-\frac{1}{2}(K + K^*) \circ y + ia\theta \right] \theta, w \right) \quad (9.68)$$

where K^* is the adjoint operator

$$(K \circ w, y) = (w, K^* \circ y), \quad y, w \in \mathcal{H} \quad (9.69)$$

of the correlation operator. It emerges in the form analogous to the standard derivative of an exponential function

$$\frac{\delta\theta}{\delta y}[y; \mathbf{x}] = \left[-\frac{1}{2}(K + K^*) \circ y(\mathbf{x}) + ia(\mathbf{x}) \right] \theta[y] \quad (9.70)$$

independent of the direction $w(\mathbf{x})$. The first derivative is a functional of $y(\cdot) \in \mathcal{H}$ and a standard function of the location $\mathbf{x} \in \mathcal{D}$.

The same steps can be carried out to determine the second Gateaux derivative, however, the direction field $w(\mathbf{x})$ must be restricted to the nullspace of the correlation operator $(K + K^*)(\mathbf{x}, \mathbf{x}')$ to avoid singular contributions to the second variational derivatives. The differential of the first Gateaux derivative is then

$$\delta \frac{\delta\theta}{\delta y}[y, w; \mathbf{x}] = \lim_{\epsilon \rightarrow 0} \frac{1}{\epsilon} \left\{ \frac{\delta\theta}{\delta y}[y + \epsilon w; \mathbf{x}] - \frac{\delta\theta}{\delta y}[y; \mathbf{x}] \right\} \quad (9.71)$$

and using (9.70)

$$\begin{aligned} \delta \frac{\delta\theta}{\delta y}[y, w; \mathbf{x}] &= \lim_{\epsilon \rightarrow 0} \frac{1}{\epsilon} \left\{ \left[-\frac{1}{2}(K + K^*) \circ (y(\mathbf{x}) + \epsilon w(\mathbf{x})) + ia(\mathbf{x}) \right] \theta[y + \epsilon w] \right. \\ &\quad \left. - \left[-\frac{1}{2}(K + K^*) \circ y(\mathbf{x}) + ia(\mathbf{x}) \right] \theta[y] \right\} \end{aligned} \quad (9.72)$$

is obtained. It can be evaluated in the form

$$\begin{aligned} \delta \frac{\delta\theta}{\delta y}[y, w; \mathbf{x}] &= \left[-\frac{1}{2}(K + K^*) \circ y(\mathbf{x}) + ia(\mathbf{x}) \right] \left[\left(-\frac{1}{2}(K + K^*) \circ y(\mathbf{x}') + ia(\mathbf{x}') \right) \theta[y], w(\mathbf{x}') \right] \\ &\quad - \frac{1}{2}(K + K^*) \circ w(\mathbf{x}) \theta[y] \end{aligned} \quad (9.73)$$

The last term on the right side $\frac{1}{2}(K + K^*) \circ w(\mathbf{x})$ is zero, as $w(\mathbf{x})$ is in the nullspace of the operator $K + K^*$, leading to the desired result

$$\frac{\delta^2 \theta}{\delta y^2}[y; \mathbf{x}, \mathbf{x}'] = [-\frac{1}{2}(K + K^*) \circ y(\mathbf{x}) + ia(\mathbf{x})][-\frac{1}{2}(K + K^*) \circ y(\mathbf{x}') + ia(\mathbf{x}')] \theta[y] \quad (9.74)$$

for the second variational/Gateaux derivative. If the direction field $w(\mathbf{x})$ is not in the nullspace of $K + K^*$, a singular contribution to the second Gateaux derivative

$$\begin{aligned} \frac{\delta^2 \theta}{\delta y^2}[y; \mathbf{x}, \mathbf{x}'] = & [-\frac{1}{2}(K + K^*) \circ y(\mathbf{x}) + ia(\mathbf{x})][-\frac{1}{2}(K + K^*) \circ y(\mathbf{x}') + ia(\mathbf{x}')] \theta[y] \\ & + \delta(\mathbf{x} - \mathbf{x}')[-\frac{1}{2}(K + K^*) \circ w(\mathbf{x}')] \theta[y] \end{aligned} \quad (9.75)$$

appears due to (23.46). The limit $\mathbf{x}' \rightarrow \mathbf{x}$ for $\frac{\delta^2 \theta}{\delta y^2}[y; \mathbf{x}, \mathbf{x}']$ is not defined for $(K + K^*) \circ w \neq 0$.

9.4 Definitions of Laplacians

The fdes governing turbulent flow derived above for the spatial description, such as Eqs. (9.40) and (9.64), contain convection and pressure gradient as second functional derivative of the characteristic functional. The trace of these terms is a variational Laplacian acting on the characteristic functional, hence deserving a closer look to clarify its definition and determine its properties and contribution to the dynamics of the characteristic functional.

There exist several definitions of second-order, infinite-dimensional, elliptic differential operators, see Feller [21] Chap. 1. for definitions. Two Laplace operators are considered in detail with the investigation of the Hopf fde in mind.

The variational derivatives (Gateaux or Fréchet derivatives) are now recast in proper form w.r.t. a solenoidal, ordered Schauder vector basis

$$\mathcal{B}_e = \{e_\alpha^{n,k,m}(r, \theta, z) = h_k(\theta) \chi_\alpha^{e,n,k,m}(r) h_m(z), \alpha = r, \theta, z, \nabla \cdot \mathbf{e}^{n,k,m} = 0\}$$

spanning the Hilbert space \mathcal{N} being the domain of definition of the class of differentiable functionals. Specifically, the functionals $\theta[y(\mathbf{x})]$ map the space of argument/test fields $\theta[\mathbf{y}] : \mathcal{N} \rightarrow C$ with C denoting the complex plane.

9.4.1 Variational and Standard Laplacians

The variational (also called Volterra Laplacian [21]) Laplacian Δ is defined on a vector Hilbert space $H = \{\mathbf{u}(\mathbf{x}), \mathbf{x} \in \mathcal{D}\}$ of countably infinite dimension (Gross [19], Dalecky and Fomin [20], Cannarsa and DaPrato [28]) as trace of a variational Hessian

$$H_{\alpha\beta}[u; \mathbf{x}, \mathbf{x}'] \equiv \frac{\delta^2 F}{\delta u_\alpha(\mathbf{x}) \delta u_\beta(\mathbf{x}')} \quad (9.76)$$

(Cartesian coordinates in \mathcal{D}) according to

$$\Delta F[\mathbf{u}; \mathbf{x}] \equiv \text{tr} \left(H_{\alpha\beta}[\mathbf{u}; \mathbf{x}, \mathbf{x}'] \right) \quad (9.77)$$

where $\delta/\delta u_\alpha(\mathbf{x})$ denotes the Fréchet derivative at location $\mathbf{x} \in \mathcal{D}$, the trace refers to \mathbf{x}' approaching \mathbf{x} and summation over the vector components α . The function space H is in the context of the Hopf fde (Sect. 5.4) the nuclear vector space \mathcal{N} containing the argument (test) vector functions of the characteristic functional $\theta[\mathbf{y}]$.

Let the function space \mathcal{N} be a Hilbert space, then it is always possible to equip it with an ordered ONS (Schauder) basis, such as \mathcal{B}_e (10.16) for the periodic pipe flow, and the variational Hessian can be evaluated w.r.t. this basis as

$$H_{\alpha\beta}[\mathbf{u}; \mathbf{x}, \mathbf{x}'] = \sum_{n,k,m} \sum_{n',k',m'} e_\alpha^{n,k,m}(\mathbf{x}) e_\beta^{n',k',m'}(\mathbf{x}') H_{n,k,m,n',k',m'}^0(y_{0,0,0}, \cdot) \quad (9.78)$$

The functional F is regarded as function of the coordinates/expansion coefficients $y_{n,k,m}$ via the representation $\mathbf{u}(\mathbf{x}) = \sum_{n,k,m} y_{n,k,m} \mathbf{e}^{n,k,m}(\mathbf{x})$ of the argument field.

The standard Hessian $H_{n,n'}^0(y_0, \dots)$ in (9.78) is defined by

$$H_{n,n'}^0(y_0, \dots) = \frac{\partial^2 F}{\partial y_n \partial y_{n'}}(y_0, \dots) \quad (9.79)$$

where n and n' are multi-indices representing n, k, m , the sums are triple sums, etc., and the functional $F[\mathbf{u}(\cdot)] = F(y_0, \dots)$

$$F(y_0, \dots) \equiv F \left[\sum_{n=0}^{\infty} y_n \mathbf{e}^n(\mathbf{x}) \right], \quad f_n(y_0, \dots, y_n) = F \left[\sum_{k=0}^n y_k \mathbf{e}^k(\mathbf{x}) \right] \quad (9.80)$$

is now regarded as standard function of infinitely many variables y_n . Truncation of the argument fields to a finite number of basis terms projects the functional F onto a cylinder function f_n of $3(n+1)$ variables y_k .

The cylinder functions $f_n(y_1, \dots, y_n)$ are projections of the functional $F[\mathbf{y}(\cdot)]$ onto standard functions, the necessary formulae for this purpose are collected in Sect. 23.12 following Courant, [29], Smirnov [30], Wang [31], Folland [32], Guzman [33], Lerner [34]. The limit of volume and surface area (Riemann/Lebesgue) of balls as the dimension approaches infinity enters the computation of Lévy-Laplacians in the next section, they are established in Sect. 23.17.

Summary

The variational Laplacian is according to (9.77) in terms of an ONS basis given by

$$\Delta F[\mathbf{y}; \mathbf{x}] = \sum_n \sum_{n'} e_\alpha^n(\mathbf{x}) e_\alpha^{n'}(\mathbf{x}) \frac{\partial^2 F}{\partial y_n \partial y_{n'}}(y_0, \dots) \quad (9.81)$$

where $\mathbf{y}(\mathbf{x}) = \sum_n y_n \mathbf{e}^n(\mathbf{x})$, n, n' are multi-indices, is the representation w.r.t. the basis \mathcal{B}_e . The variational Laplacian (9.81) is build up with the standard Hessian $H_{n,n'}^0(y_0, \dots)$ (9.79). The standard Laplacian Δ_0 in turn is defined as the trace of the standard Hessian

$$\Delta_0 F[\mathbf{u}] = \lim_{n \rightarrow \infty} \sum_{k=0}^n \frac{\partial^2 f_n}{\partial^2 y_k}(y_0, \dots, y_n) \quad (9.82)$$

provided the limit exists. The standard Laplacian defined by (9.82) is a straightforward generalization of the Laplacian acting on differentiable functions of finitely many variables, see Gross [19], Dalecky and Fomin [20] for more details.

9.4.2 Lévy-Laplacian

The Lévy-Laplacian Δ_L [21] is constructed as ratio of surface integrals and will be shown to possess a wider domain of definition than the variational Laplacian Δ . Let H be a real Hilbert space with countably infinite dimension and $F[\mathbf{y}] : H \rightarrow C$, $\mathbf{y}(\mathbf{x}) \in H$, $\mathbf{x} \in \mathcal{D} \subset R^3$, then is the formulation of the Lévy-Laplacian Δ_L , used in the present context, following Feller [21]

$$\Delta_L F[\mathbf{y}^0] = 2 \lim_{\rho \rightarrow 0} \frac{1}{\rho^2} \{ \mathcal{M}_{(\mathbf{y}^0, \rho)} F[\mathbf{y}] - F[\mathbf{y}^0] \} \quad (9.83)$$

valid at $\mathbf{y}^0 \in H$ for a (not necessarily differentiable) functional $F[\mathbf{y}(\cdot)]$. The term $\mathcal{M}_{(\mathbf{y}^0, \rho)}$ in (9.83) denotes the mean value of the functional F over the Hilbert sphere $S_\infty(\mathbf{y}^0, \rho) \equiv \{\mathbf{y} \in H : \|\mathbf{y} - \mathbf{y}^0\|_H^2 = \rho^2\}$ centred at $\mathbf{y}^0 \in H$ with radius ρ . The computation of the mean value requires the integration of cylinder functions over the surface of spheres $S_n(\mathbf{y}^0, \rho) \in R^n$ centred at \mathbf{y}^0 with radius ρ and the letting the dimension n approach infinity.

$$\mathcal{M}_{(\mathbf{y}^0, \rho)} F[\mathbf{y}] = \lim_{n \rightarrow \infty} M_{(n, \mathbf{y}^0, \rho)} F[\mathbf{y}] \quad (9.84)$$

The surface average

$$M_{(n, \mathbf{y}^0, \rho)} F[\mathbf{y}] = \frac{\int_{S_n(\mathbf{y}^0, \rho)} f_n(y_1, \dots, y_n) d\sigma_n}{\int_{S_n(\mathbf{y}^0, \rho)} d\sigma_n} = \frac{\Gamma(\frac{n}{2})}{2\pi^{\frac{n}{2}} \rho^{n-1}} \int_{S_n(\mathbf{y}^0, \rho)} f_n(y_1, \dots, y_n) d\sigma_n \quad (9.85)$$

is the ratio of $n - 1$ -dimensional surface integrals. It should be noted that for bounded cylinder functions f_n with compact support, as defined above in Eq. (9.80), the limit $n \rightarrow \infty$ of the ratio of surface integrals is a delicate operation, since the ratio is zero over zero, hence indeterminate and requiring an ordered basis and explicit analysis. This is due to the fact that the surface area of any sphere with finite radius appearing in numerator and denominator vanishes for $n \rightarrow \infty$, since the surface integral for bounded cylinder functions is bounded by a constant times the surface area of a sphere. The geometry of compact sets in infinite-dimensional spaces has counter-intuitive properties that are briefly discussed in Appendix A, Sect. 23.17.1.

The Lévy-Laplacian in terms of a Schauder basis

Construct an ONS basis $\mathcal{B} = \{\mathbf{e}^k(\mathbf{x}) \in H, k = 0, \dots, \infty\}, \mathbf{x} \in \mathcal{D} \subset \mathbb{R}^3$ in the Hilbert space H , i.e. $(\mathbf{e}^n, \mathbf{e}^k) = \delta_{n,k}$ (n and k are multi-indices), and let the functional $F[\mathbf{y}(\cdot)]$ be twice differentiable. Several properties of differentiable functionals and mean values are established first to shorten the derivations of the Laplacian expressions with respect to a particular basis.

Let $S_n(\mathbf{y}^0, \rho)$ be the sphere in \mathbb{R}^n with radius ρ and surface area $\mathcal{A}_n(\rho)$ centred at $\mathbf{y}^0 \in \mathbb{R}^n$, define spherical coordinates in \mathbb{R}^n according to Sect. 23.15 with centre at \mathbf{y}^0 . Then the following integrals (23.144), (23.153), (23.159) over spheres centred at the origin $\mathbf{y}^0 = 0$ can be computed, the details of the computation using spherical coordinates in \mathbb{R}^n can be found in Appendix A, Sect. 23.15. Furthermore, the results for the volume of the n -ball $V_n(\rho) = \rho^n V_n(1)$, $V_n(1) = \pi^{\frac{n}{2}} / \Gamma(\frac{n}{2} + 1)$ and the surface area $\mathcal{A}(\rho, n)$ established in Appendix A, Sects. 23.12.1 and 23.12.1, will be applied in the following. Finally, it is essential to project a functional $F[\mathbf{u}(\cdot)]$ onto a standard cylinder function $f_n(\mathbf{y}_0, \dots, \mathbf{y}_n)$ of n variables according to (9.80).

The Lévy-Laplacian defined by (9.83)

$$\Delta_L F[\mathbf{y}^0] = 2 \lim_{\rho \rightarrow 0} \frac{1}{\rho^2} \{ \mathcal{M}_{(\mathbf{y}^0, \rho)} F[\mathbf{y}] - F[\mathbf{y}^0] \} = 2 \lim_{\rho \rightarrow 0} \frac{1}{\rho^2} \lim_{n \rightarrow \infty} [M_{(n, \mathbf{y}^0, \rho)}(F[\mathbf{y}]) - f_n(y_1^0, \dots, y_n^0)]$$

is build up using the limit of mean values of the functional $F[\mathbf{y}(\cdot)]$ (9.85)

$$M_{(n, \mathbf{y}^0, \rho)}(F[\mathbf{y}]) = \frac{1}{\mathcal{A}_n(1) \rho^{n-1}} \int_{S_n(\mathbf{y}^0, \rho)} d\sigma f_n(y_1, \dots, y_n)$$

over spheres in \mathbb{R}^n , where the cylinder functions are $f_n(y_1, \dots, y_n) \equiv F[\sum_{k=1}^n y_k f^k(\mathbf{x})]$, $y_k = (\mathbf{y}, \mathbf{e}^k)$, $\mathcal{A}_n(\rho) = \rho^{n-1} \mathcal{A}_n(1)$ and the surface area of the unit sphere being $\mathcal{A}_n(1) = 2\pi^{\frac{n}{2}} / \Gamma(\frac{n}{2})$ according to Appendix A. It is important to notice that the Lévy-Laplacian is a limit of ratios M_n of surface integrals.

Feller [21] Sect. 1.1 proves the following lemma for scalar argument fields $y(\mathbf{x})$, that is straightforward to extend to vector argument fields and quite helpful for the computation of the Lévy-Laplacian.

Lemma: Let the functional $F[y(\cdot)]$ be twice differentiable at $y^0(\mathbf{x}) \in H$ and the Lévy-Laplacian exist and let $\mathcal{B} = \{f^k(\mathbf{x}) \in H, k = 1, \dots, \infty\}$ be an ONS basis for the Hilbert space H . Then holds

$$\Delta_L F(y^0) = \lim_{n \rightarrow \infty} \frac{1}{n} \sum_{k=1}^n \frac{\partial^2 f_n}{\partial y_k^2}(\mathbf{y}^0) \quad (9.86)$$

where $f_n(y_1, \dots, y_n) \equiv F[\sum_{k=1}^n y_k f^k(\mathbf{x})]$ and $y_k = (y, f^k)$ for $y(\mathbf{x}) \in H$.

Proof: The differentiability of $F[y(\cdot)]$ implies that $f_n(y_1, \dots, y_n)$ is also differentiable, hence

$$f(y_1, \dots, y_n) = f(y_1^0, \dots, y_n^0) + \sum_{k=1}^n (y_k - y_k^0) \frac{\partial f_n}{\partial y_k} + \frac{1}{2} \sum_{k=1}^n \sum_{m=1}^n (y_k - y_k^0)(y_m - y_m^0) \frac{\partial^2 f_n}{\partial y_k \partial y_m} + r_n$$

holds with $O(r_n) = \rho^p$, $p > 2$. The Lévy-Laplacian is then

$$\begin{aligned} \Delta_L F(y^0) &= 2 \lim_{\rho \rightarrow 0} \frac{1}{\rho^2} \lim_{n \rightarrow \infty} \left[\frac{1}{\mathcal{A}_n(1)\rho^{n-1}} \int_{S_n(\mathbf{y}^0, \rho)} d\sigma [f(y_1^0, \dots, y_n^0) \right. \\ &\quad \left. + \sum_{k=1}^n (y_k - y_k^0) \frac{\partial f_n}{\partial y_k} + \frac{1}{2} \sum_{k=1}^n \sum_{m=1}^n (y_k - y_k^0)(y_m - y_m^0) \frac{\partial^2 f_n}{\partial y_k \partial y_m} + r_n] - f_n(y_1^0, \dots, y_n^0) \right] \end{aligned}$$

and defining $x_k \equiv y_k - y_k^0$, $k = 1, \dots, n$ the integration is shifted to spheres centred at the origin

$$\Delta_L F(y^0) = 2 \lim_{\rho \rightarrow 0} \frac{1}{\rho^2} \lim_{n \rightarrow \infty} \frac{1}{\mathcal{A}_n(1)\rho^{n-1}} \int_{S_n(0, \rho)} d\sigma \left[\sum_{k=1}^n x_k \frac{\partial f_n}{\partial y_k}(\mathbf{y}^0) + \frac{1}{2} \sum_{k=1}^n \sum_{m=1}^n x_k x_m \frac{\partial^2 f_n}{\partial y_k \partial y_m}(\mathbf{y}^0) + r_n \right]$$

The first integral on the right side is according to (23.144)

$$\frac{1}{\mathcal{A}_n(1)\rho^{n-1}} \int_{S_n(0, \rho)} d\sigma \sum_{k=1}^n x_k \frac{\partial f_n}{\partial y_k}(\mathbf{y}^0) = 0$$

and (23.153), (23.159) lead to

$$\begin{aligned} \frac{1}{\mathcal{A}_n(1)\rho^{n-1}} \int_{S_n(0,\rho)} d\sigma \frac{1}{2} \sum_{k=1}^n \sum_{m=1}^n x_k x_m \frac{\partial^2 f_n}{\partial y_k \partial y_m}(\mathbf{y}^0) &= \frac{1}{2} \frac{\pi^{\frac{n}{2}} \rho^{n+1}}{\Gamma(\frac{n}{2} + 1)} \frac{\Gamma(\frac{n}{2})}{2\pi^{\frac{n}{2}} \rho^{n-1}} \sum_{k=1}^n \frac{\partial^2 f_n}{\partial^2 y_k}(\mathbf{y}^0) \\ &= \frac{\rho^2}{2n} \sum_{k=1}^n \frac{\partial^2 f_n}{\partial^2 y_k}(\mathbf{y}^0) \end{aligned}$$

Thus

$$\Delta_L F[y^0(\cdot)] = \lim_{n \rightarrow \infty} \left[\frac{1}{n} \sum_{k=1}^n \frac{\partial^2 f_n}{\partial^2 y_k}(\mathbf{y}^0) + 2 \lim_{\rho \rightarrow 0} \frac{1}{\rho^2} \frac{1}{\mathcal{A}_n(1)\rho^{n-1}} \int_{S_n(0,\rho)} d\sigma r_n \right]$$

is obtained. The integral containing the remainder r_n vanishes as $\rho \rightarrow 0$, hence

$$\Delta_L F[y^0(\cdot)] = \lim_{n \rightarrow \infty} \frac{1}{n} \sum_{k=1}^n \frac{\partial^2 f_n}{\partial^2 y_k}(\mathbf{y}^0)$$

emerges, and the proof is complete. Note that the Lévy-Laplacian does not involve variational derivatives. Examples for the computation of variational derivatives and the application of the Laplacians just defined to the Gaussian characteristic functional are discussed in the next section.

9.4.3 The Laplacians Applied to a Gaussian Characteristic Functional

The Gaussian characteristic functional provides an instructive example for the explicit application of the Laplacian operators introduced in the previous sections. The characteristic functional for Gaussian fields is explicitly known, hence allows analytic evaluation of the Laplacians introduced above. Consider a domain of definition $\mathcal{D} \subset \mathbb{R}^1$ and the Hilbert space $\mathcal{H} = L_2(\mathcal{D})$ of square-integrable functions $y(x)$ defined on \mathcal{D} . The Gaussian characteristic functional is explicitly given by (Bogachev [35], Chap. 2)

$$\theta_G[y] = \exp\left\{-\frac{1}{2}(K \circ y, y) + i(a, y)\right\} \quad (9.87)$$

where $y(x) \in \mathcal{H}$ is the scalar argument function defined over the domain \mathcal{D} and taken from the Hilbert space \mathcal{H} with scalar product (\cdot, \cdot) , K is a positive operator of trace class in \mathcal{H} called correlation operator of the Gaussian measure (23.208) with mean field $a(x) \in \mathcal{H}$.

An operator A defined on a separable Hilbert space with basis $\mathcal{B} = \{e_k(\mathbf{x}), k \in [1, \infty)\}$ is positive iff $(Ay, y) \geq 0, \forall y \in \mathcal{H}$, it is a trace-class or nuclear operator (definitions in Appendix A, Sects. 23.1, 23.7, 23.9), if it is compact and the trace

$$tr(A) \equiv \sum_{k=1}^{\infty} (Ae_k, e_k) < \infty \quad (9.88)$$

exists and is absolutely convergent, i.e. the trace of $|A|$ is bounded

$$tr(|A|) \equiv \sum_k ((A^* A)^{\frac{1}{2}} e_k, e_k) < \infty \quad (9.89)$$

where A^* is the adjoint operator (9.69), i.e. $(Aw, y) = (w, A^*y)$ holds for all $w, y \in \mathcal{H}$, and thus the trace is independent of the basis.

The correlation operator K serves also as tool to construct a Gaussian measure on \mathcal{H} as needed later in Sect. 23.18.2. Denoting by λ_k the eigenvalues of $K^{-\frac{1}{2}}$, the Gaussian measure differential emerges as

$$\mu_G(dy) = \lim_{N \rightarrow \infty} \prod_{k=1}^N \frac{\lambda_k}{\sqrt{2\pi}} \exp\left(-\frac{1}{2} \lambda_k^2 y_k^2\right) dy_k$$

The design of measure differentials is not without pitfalls as discussed in Klauder [5], Cartier and deWitt-Morette [3], see Sect. 23.17 for the justification of the Gaussian differential.

Construction of the correlation operator K

The correlation operator K is constructed by choosing an absolutely convergent series of coefficients K_k and two ONS bases for \mathcal{H} as follows: Let $\{e^k, k = 1, \dots, \infty\}$, and $\{f^k, k = 1, \dots, \infty\}$ be ONS bases spanning \mathcal{H} , then is the convergent series $K_k, k = 1, \dots, \infty$ chosen, i.e.

$$\sum_{k=1}^{\infty} K_k < \infty \quad (9.90)$$

The correlation operator is then constructed as the nuclear (Sect. 23.7) or trace-class operator K in the form

$$K \circ y(x) = \sum_{k=1}^{\infty} K_k (e^k, y) f^k(x) \quad (9.91)$$

The ONS basis $\{f^k(x), k = 1, \dots, \infty\}$ controls the non-isotropic properties of the Gaussian measure. The trace of the correlation operator is then

$$tr K = \sum_{k=1}^{\infty} (e^k, K e^k) = \sum_{k=1}^{\infty} K_k \quad (9.92)$$

absolutely convergent and the value is independent of the base $\{e^k, k = 1, \dots, \infty\}$.

The variational Laplacian Δ applied to a Gaussian characteristic functional

The application of the variational Laplacian requires the second Gateaux/Fréchet derivative, which can be computed according to (23.53) leading to (9.74). Computing the trace according to (9.77) requires $\mathbf{x} = \mathbf{x}'$ and

$$\Delta \theta_G[y(.); \mathbf{x}] = [-\frac{1}{2}(K + K^*) \circ y(\mathbf{x}) + ia(\mathbf{x})]^2 \theta_G[y] \quad (9.93)$$

is obtained. It is valid for $(K + K^*) \circ w = 0$.

The Lévy-Laplacian Δ_L applied to a Gaussian characteristic functional

The Lévy-Laplacian follows then with the aid of (26.13) for scalar arguments $y(\mathbf{x})$ ($m = 1$)

$$\begin{aligned} \Delta_L \theta_G[y(.); \mathbf{x}] &= \int_{\mathcal{D}} dv(\mathbf{x}') [-\frac{1}{2}(K + K^*) \circ y(\mathbf{x}) + ia(\mathbf{x})] [-\frac{1}{2}(K + K^*) \circ y(\mathbf{x}') + ia(\mathbf{x}')] \theta_G[y] \\ &\quad - \frac{1}{2}(K + K^*) \circ \theta_G[y] \end{aligned} \quad (9.94)$$

without any restriction on the direction field $w(\mathbf{x})$. The comparison of the Laplacians applied to a Gaussian characteristic functional indicates that the variational Laplacian Δ_0 leads to a non-singular result only if $(K + K^*) \circ w = 0$, whereas the Lévy-Laplacian Δ_L produces a well behaved functional for any admissible $w(\mathbf{x})$. This concludes the examples illustrating the application of the standard and Lévy-Laplacian to a characteristic functional of exponential type.

Summary

The expressions for the standard and the Lévy-Laplacian in Hilbert spaces H with an ONS basis show the fundamental difference between them:

The standard Laplacian Δ_0 emerges in the form (9.82) as

$$\Delta_0 F[y^0(.)] = \lim_{n \rightarrow \infty} \sum_{k=1}^n \frac{\partial^2 f_n}{\partial y_k^2}(\mathbf{y}^0)$$

where $y^0(\mathbf{x}) \in \mathcal{N}$ and $\mathbf{y}^0 = [y_1^0, \dots, y_n^0]^{-1}$ denotes the n -vector of expansion coefficients.

The Lévy-Laplacian is according to the lemma given by (9.86)

$$\Delta_L F[y^0(.)] = \lim_{n \rightarrow \infty} \frac{1}{n} \sum_{k=1}^n \frac{\partial^2 f_n}{\partial y_k^2}(\mathbf{y}^0)$$

The comparison of the two versions of the infinite-dimensional Laplacian shows that the domain of definition of the standard Laplacian Δ_0 is a genuine subset of the domain of the Lévy-Laplacian Δ_L , since the convergence of the sum in (9.82) implies convergence in (9.83), but the reverse is obviously not true. The reason for this can be traced to the definition of the Lévy-Laplacian as limit of surface averages (9.85) without variational derivatives creating the factor $1/n$ in (9.86). Analytic examples for the application of Δ and Δ_L to the Gaussian characteristic functional are given above. They show that the variational Laplacian Δ leads to a singular contribution unless the direction fields $\mathbf{w}(\mathbf{x})$ are restricted to the nullspace of the correlation operator $K + K^*$, whereas the Lévy-Laplacian applied to a Gaussian characteristic functional produces a non-singular result. The Hopf fde (9.40) and its variants in the spatial description contain the variational Hessian (9.76), whose trace is the standard Laplacian. This Hessian is absent in the Hopf fde for the material description as shown in the next section.

9.5 Fde for the Characteristic Functional in the Material Description

The structure of the fde for the characteristic functional depends on the choice of independent variables for the Navier–Stokes pdes. This will be demonstrated for the material description under the assumption, that the flow domain \mathcal{D} is invariant w.r.t. the transformation between spatial t, \mathbf{x} and material τ, Φ descriptions, [36]. The transformation (Sect. 2.5)

$$\tau = t, \quad \mathbf{X}(t, \mathbf{x}) = \Phi^{-1}(t, \mathbf{x})$$

where $\Phi^{-1}(t, \mathbf{x})$ is the inverse position field (also called the back-to-labels map), i.e. $\mathbf{x} = \Phi(\tau, \mathbf{X})$ solved for \mathbf{X} in terms of $t = \tau$ and \mathbf{x} , is then one-to-one and differentiable, which holds in particular for the example of the periodic pipe flow. The general case of open systems is much more complicated, since material points may leave and enter the flow domain, see Kraichnan [37] and Constantin and Iyer [38] for a detailed treatment.

The standard material or Lagrangean description of fluid motion has been introduced in Sect. 2.5 by defining time τ and the label variable $\mathbf{X} \in \mathcal{D}(0)$, the position of a material point at the reference time zero, as the set of four independent variables plus the reference time, which is not indicated, since it does not vary in the standard formulation (for the generalized formulation see Kraichnan [37], Bennett [39]). The phase space Ω_M consists then of all possible position (vector) fields $\Phi(\tau, \mathbf{X})$ in the materially invariant flow domain $\mathcal{D}(\tau)$, which may move and change its shape. Specifically, for chosen time τ , the vector field $\Phi_\alpha(\tau, \mathbf{X}), \mathbf{X} \in \mathcal{D}(0)$ is an element of the phase space Ω_M . The phase space is a separable Hilbert space with scalar product

$$(\Phi, \Psi) = \int_{\mathcal{D}(0)} d\mathcal{V}(\mathbf{X}) \Phi_\alpha(\tau, \mathbf{X}) \Psi_\alpha(\tau, \mathbf{X}) : \Omega_M \times \Omega_M \rightarrow R^1 \quad (9.95)$$

where the integration is over the label domain (flow domain at reference time zero) $\mathcal{D}(0) \subset R^3$. The example of the flow through a circular pipe with artificial periodicity w.r.t. the axial direction has the advantage that material points $\mathbf{X} \in \mathcal{D}(0)$ never leave the flow domain, thus $\mathcal{D}(\tau) = \mathcal{D}(0)$ holds; the flow domain is topologically equivalent to a torus.

The characteristic functional for the Hopf fde is defined in the material description by

$$\theta[\mathbf{y}(\mathbf{X}); \tau] \equiv \langle \exp[i(\mathbf{y}, \Phi)] \rangle, \quad \mathbf{y} \in \mathcal{N}_M, \quad \Phi \in \Omega_M, \quad \mathbf{X} \in \mathcal{D}(0)$$

$$(\mathbf{y}, \Phi) : \mathcal{N}_M \times \Omega_M \rightarrow R^1 \quad (9.96)$$

The independent variable field $\mathbf{y}(\mathbf{X})$ is in the present case associated with the position field $\Phi(\tau, \mathbf{X})$ in contrast to the spatial description, where $\mathbf{y}(\mathbf{x})$ is the counterpart of velocity $\mathbf{v}(t, \mathbf{x})$. The position field $\Phi_\alpha(\tau, \mathbf{X}) \in \mathcal{D}(\tau)$ denotes for specified time τ and label \mathbf{X} the location of a material point, the phase space $\Omega_M(\tau)$ contains the (Lagrangian) position fields $\Phi_\alpha(\tau, \mathbf{X})$ at all times $\tau \geq 0$ and the nuclear space \mathcal{N}_M containing the test/argument fields $y_\alpha(\mathbf{X})$ is associated with the phase space Ω_M via Fourier transformation as seen in Eq. (9.96).

The derivation of the Hopf-type fde for $\theta[\mathbf{y}; \tau]$ requires the Navier–Stokes pdes in the material description formulated in terms of position $\Phi_\alpha(\tau, \mathbf{X})$ and pressure $P(\tau, \mathbf{X})$, as has been done in Sect. 2.5. Mass balance (2.85) for incompressible fluids states, that the Jacobian (denoted by F or J), defined as the determinant of the deformation gradient $F_{\alpha\beta}$ (2.82)

$$F_{\alpha\beta}(\tau, \mathbf{X}) = \frac{\partial \Phi_\beta}{\partial X_\alpha}$$

satisfies $F = J = 1$. Momentum balance emerges as, Eq. (2.86) in Sect. 2.5.2,

$$\begin{aligned} \frac{\partial^2 \Phi_\alpha}{\partial \tau^2} &= -\frac{1}{2} \epsilon_{\alpha\beta\gamma} \epsilon_{\delta\eta\omega} F_{\beta\eta} F_{\gamma\omega} \frac{\partial P}{\partial X_\delta} [\Phi, \frac{\partial \Phi}{\partial \tau}; \tau, \mathbf{X}] + \frac{1}{2Re} \epsilon_{\theta\beta\gamma} \epsilon_{\delta\eta\omega} F_{\zeta\eta} F_{\phi\omega} \frac{\partial}{\partial X_\delta} \left(F_{\zeta\beta} F_{\phi\gamma} \frac{\partial^2 \Phi_\alpha}{\partial \tau \partial X_\theta} \right) \\ &\quad + \frac{1}{Fr} G_\alpha(\tau, \mathbf{X}, \omega) \end{aligned} \quad (9.97)$$

where Fr denotes the Froude number (22.2) and density $R(\tau, \mathbf{X}) = R(0, \mathbf{X}) = \rho$ (R is the capital of the Greek ρ) is a positive constant included in the pressure $P \leftarrow \frac{1}{R} P$. The external force G_α is now a stochastic field $\omega \in \Omega_f$ (ω is the sample variable and Ω_f the sample space for the external force).

The pressure requires reformulation to obtain the correct form in the material description. It is assumed that the flow domain is fixed, i.e. $\mathcal{D} = \mathcal{D}(0)$, to be able to use the results from Sect. 9.2.1 on the pressure gradient. Keeping the flow domain fixed implies, that the equations derived in the following hold only for a subset of

material points \mathbf{X} , that remain $\Phi(\tau, \mathbf{X}) \in \mathcal{D}(0)$ for a given time interval $0 \leq \tau \leq T$. However, this subset is identical with the flow domain for all time for closed domains, i.e. velocity is zero on $\partial\mathcal{D}$ or open domains with artificial periodicity replacing non-homogeneous boundary conditions thus generating a toroidal domain. The general case of moving and deforming flow domains can be handled with the same approach, but is rather complicated, see Constantin and Iyer [38].

Suppose the Green's function $G(\mathbf{x}, \mathbf{x}')$ has been computed, then is the pressure gradient in the spatial description determined by the solution of the Poisson pde (9.19) with non-homogeneous Neumann boundary conditions, Eq. (9.20)

$$\frac{\partial p}{\partial x_\alpha}(t, \mathbf{x}) = \int_{\mathcal{D}} dv(\mathbf{x}') \frac{\partial G}{\partial x_\alpha}(\mathbf{x}, \mathbf{x}') \frac{\partial^2}{\partial x'_\beta \partial x'_\gamma} (v_\beta v_\gamma)(t, \mathbf{x}') + \int_{\partial\mathcal{D}} dA_\alpha(\mathbf{x}') h_\alpha(\mathbf{x}') \frac{\partial G}{\partial x_\alpha}(\mathbf{x}, \mathbf{x}')$$

where the Neumann boundary values are according to (9.22)

$$h_\alpha(\mathbf{x}') = \frac{1}{Re} \frac{\partial^2 v_\alpha}{\partial x'_\beta \partial x'_\beta} + \frac{1}{Fr} G_\alpha - \frac{Dv_\alpha}{Dt}$$

with n_α denoting the unit vector normal to $\partial\mathcal{D}$ pointing outward. This result is transformed to the material description resulting in the pressure functional (the pressure functional is explicitly computed for the pipe flow example in the spatial description, Eq. (26.130) in Sect. 26.6)

$$P[\Phi, \mathbf{V}; \tau, \mathbf{X}] = P_0(\zeta) + \mathcal{P}_h(r, \theta, \zeta) + \mathcal{P}_G(r, \theta, \zeta) \quad (9.98)$$

with terms and coordinates explained in Sect. 9.2.2, at this point only the fact, that pressure depends in integral form on position and velocity fields is relevant.

The fde for the characteristic functional $\theta[\mathbf{y}; \tau, \mathbf{X}]$ in the material description emerges then in the implicit form

$$\begin{aligned} \frac{\partial^2}{\partial \tau^2} \theta[\mathbf{y}; \tau] &= \int_{\mathcal{D}(0)} d\mathcal{V}(\mathbf{X}) y_\alpha(\mathbf{X}) \left\{ \frac{i}{2R} \epsilon_{\alpha\beta\gamma} \epsilon_{\delta\eta\omega} F_{\beta\eta} F_{\gamma\omega} \frac{\partial P}{\partial X_\delta}[\mathbf{y}; \tau, \mathbf{X}] \right. \\ &\quad \left. + \frac{1}{2Re} \epsilon_{\theta\beta\gamma} \epsilon_{\delta\eta\omega} F_{\zeta\eta} F_{\phi\omega} \frac{\partial}{\partial X_\delta} \left(F_{\zeta\beta} F_{\phi\gamma} \frac{\partial}{\partial X_\theta} \right) \frac{\delta \theta}{\delta y_\alpha}[\mathbf{y}; \tau, \mathbf{X}] + i \frac{1}{Fr} G_\alpha(\tau, \mathbf{X}, \omega) \theta[\mathbf{y}; \tau] \right\} \end{aligned} \quad (9.99)$$

using the same steps as for the spatial description in Sect. 9.2.3, where $\mathbf{X} \in \mathcal{D}(0)$ is now the label or identifying variable being element of the flow domain at the reference time $\tau = 0$ and playing the role of the observer position in the spatial description. It is worth noting that the convective terms appearing in the spatial description as second functional derivatives (functional Hessian) is absent, but the second time derivative

appears on the left side in the material description. Note that the pressure gradient is computed w.r.t. the label variable \mathbf{X} and not the observer position $\mathbf{x} = \Phi(\tau, \mathbf{X})$. To obtain an explicit version requires the substitution of the pressure gradient functional with the aid of the Green's functional. The viscous term in the Navier–Stokes momentum balance transformed to the material description (2.86) leads to fourth-order variational derivatives in the fde for the characteristic functional. It is easy to see that this would introduce second and fourth-order variational derivatives, thus making fde hyperbolic. The functional formulation allows the computation of non-local derivatives as illustrated in the next section establishing the dependence of velocity on the external force.

9.5.1 Gateaux Derivative of Velocity with Respect to the External Force

Momentum balance in the material description (9.97) has, written in terms of velocity, the form

$$\frac{\partial V_\alpha}{\partial \tau} = A_\alpha[\Phi, \mathbf{V}] + \frac{1}{Fr} G_\alpha(\tau, \mathbf{X}, \omega) \quad (9.100)$$

constrained by mass balance $J \equiv \det(\mathbf{F}) = F = 1$, where the momentum functional A_α is indirectly defined by momentum balance (9.97) and the pressure functional (9.98). Velocity V_α is independent of the external force at time $\tau = 0$ (initial value), but depends on it for $\tau > 0$ via (9.100), hence is the functional A_α dependent on G_α for $\tau > 0$, but not for $\tau = 0$. Integration with respect to time τ of the momentum balance (9.100) along a pathline $\Phi(\tau, \mathbf{X})$ starting at the label \mathbf{X} leads to

$$V_\alpha[\mathbf{G}(.); \tau, \mathbf{X}] = V_\alpha(0, \mathbf{X}) + \int_0^\tau d\tau' A_\alpha[\Phi, \mathbf{V}[\mathbf{G}]; \tau', \mathbf{X}] + \int_0^\tau d\tau' \frac{1}{Fr} G_\alpha(\tau', \mathbf{X}, \omega) \quad (9.101)$$

This representation allows the computation of the Gateaux derivative of the velocity with respect to the external force. The Gateaux differential is according to (23.45)

$$\delta V_\alpha[\mathbf{G}(.)](\mathbf{w}) = \lim_{\epsilon \rightarrow 0} \frac{1}{\epsilon} \{ V_\alpha[\mathbf{G} + \epsilon \mathbf{w}] - V_\alpha[\mathbf{G}] \}$$

hence

$$\begin{aligned} \delta V_\alpha[\mathbf{G}(.)](\mathbf{w}) &= \lim_{\epsilon \rightarrow 0} \frac{1}{\epsilon} \{ \int_0^\tau d\tau' (A_\alpha[\Phi, \mathbf{V}[\mathbf{G} + \epsilon \mathbf{w}]; \tau', \mathbf{X}] - A_\alpha[\Phi, \mathbf{V}[\mathbf{G}]; \tau', \mathbf{X}]) \\ &\quad + \epsilon \delta_{\alpha\beta} \int_0^\tau d\tau' \int_{\mathcal{D}(\tau')} d\mathbf{v}(\mathbf{X}') w_\beta(\mathbf{X}') \delta(\mathbf{X}' - \mathbf{X}) \} \end{aligned}$$

The first integral can be evaluated using functional Taylor series (23.78), hence

$$\delta V_\alpha[\mathbf{G}(\cdot)](\mathbf{w}) = \int_{\mathcal{D}(\tau')} d\mathcal{V}(\mathbf{X}') w_\beta(\mathbf{X}') \delta(\mathbf{X}' - \mathbf{X}) \left[\int_0^\tau d\tau' \frac{\delta A_\alpha}{\delta G_\beta} [\Phi, \mathbf{V}[\mathbf{G}]; \tau', \mathbf{X}'] + \delta_{\alpha\beta} \int_0^\tau d\tau' \right]$$

is obtained and the derivative follows then from (23.46)

$$\delta V_\alpha[G_\beta](\mathbf{w}) = (w_\beta, \frac{\delta V_\alpha}{\delta G_\beta})$$

as

$$\frac{\delta V_\alpha}{\delta G_\beta}[\mathbf{G}; \tau, \mathbf{X}, \mathbf{X}'] = \int_0^\tau d\tau' \frac{\delta A_\alpha}{\delta G_\beta} [\Phi, \mathbf{V}[\mathbf{G}]; \tau', \mathbf{X}, \mathbf{X}'] + \delta(\mathbf{X}' - \mathbf{X}) \delta_{\alpha\beta} \tau$$

by inspection. The Gateaux derivative of velocity w.r.t. the external force is determined by the pathline integral of the momentum functional plus a singular Dirac contribution.

9.6 Problems for this Chapter

Problem 9.1 Solve the pure IVP for the Burgers pde (1.2) with initial condition $u(0, x) = u_0(x) \in L^2_{\mathcal{D}} \cap C_{\mathcal{D}}^\infty$, $\mathcal{D} = (-\infty, \infty)$, using the Hopf–Cole transformation (1.3) as indicated in Sect. 1.

Problem 9.2 Derive the Hopf fde for the characteristic functional $\theta[y; t]$ for the pure IVP of the Burgers pde (1.2). Use the result obtained in Problem (9.1) to establish the solution operator and its inverse.

Problem 9.3 Solve the Hopf fde for the Burgers pde using the solution operator established in Problem (9.2). The initial condition is the characteristic functional $\theta[y; 0]$ for Gaussian stochastic fields with zero mean.

9.3.1: Specify the initial condition for Gaussian random fields in terms of the covariance function $R(x, x') \equiv \langle u(0, x)u(0, x') \rangle$ and zero mean. Assume that the covariance function is a function of $|x - x'|$ and work out the special case $R(x, x') = \sigma_0^2 \delta(x - x')$, $\sigma_0 > 0$ ($R(x, x')$ is delta correlated).

9.3.2: Construct a basis in $L^2_{\mathcal{D}}$ using Hermite functions (physicists version) $\Psi_n(x)$ (4.29) as defined in (4.30) according to ([40], Chap. 18).

9.3.3: Adapt the initial condition to the Hermite basis.

9.3.4: Adapt the fde obtained in Problem (9.2) to the basis constructed in Sect. 9.3.2.

9.3.5: Solve the fde (9.2) using the relation (6.3) for the measure μ at times zero and $t > 0$ assuming that the solution operator generates a bijective map of l^2 , isomorphic to $L^2_{\mathcal{D}}$, onto itself.

Problem 9.4 Consider an analytic functional $R[y]$ defined on the phase space $\Omega = \{y(\mathbf{x}) \in L^2_{R^3}\}, \mathbf{x} \in R^3$ and Gaussian stochastic fields $f_i(t, \mathbf{x})$ with zero mean and positive definite correlation tensor defined by

$$K_{i,j}(t, t', \mathbf{x}, \mathbf{x}') \equiv \langle f_i(t, \mathbf{x}) f_j(t', \mathbf{x}') \rangle$$

Prove the relation

$$\langle f_i(t, \mathbf{x}) R[f] \rangle = \int_{R^3} dt \int_{R^3} dv K_{i,j}(t, t', \mathbf{x}, \mathbf{x}') \langle \frac{\delta R}{\delta f}[f; t', \mathbf{x}'] \rangle$$

for homogeneous Gaussian fields in isotropic turbulence.

References

1. Monin, A.S., Yaglom, A.M.: Statistical Fluid Mechanics: Mechanics of Turbulence, vol. 2. The MIT Press, Cambridge Mass (1975)
2. Lewis, R.M., Kraichnan, R.H.: A Space-Time Functional Formalism for Turbulence. Comm. Pure Appl. Math. **XV**, 397–411 (1962)
3. Cartier, P., DeWitt-Morette, C.: Functional Integration: Action and Symmetries. Cambridge University Press, Cambridge U.K (2006)
4. Simon, B.: Functional Integration and Quantum Physics. AMS Chelsea Publication, Rhode Island (2004)
5. Klauder, J.R.: A Modern Approach to Functional Integration. Birkhaeuser/Springer, New York (2010)
6. Vishik, M.J., Fursikov, A.V.: Mathematical Problems of Statistical Hydromechanics. Kluwer Academic Publication, Dordrecht (1988)
7. Novikov, E.A.: Random-force method in turbulence theory. Sov. Phys. JETP **17**, 1449–1454 (1963)
8. Novikov, E.A.: Functionals and the random-force method in turbulence theory. Sov. Phys. JETP **20**, 1290–1294 (1965)
9. Hosokawa, I.: A functional treatise on statistical hydromechanics with random force action. J. Phys. Soc. Jpn **25**, 271–278 (1968)
10. Inoue, A.: Strong and classical solutions of the Hopf equation—an example of functional derivative equation of second order. Tohoku Math. J. **39**, 115–144 (1987)
11. Rudin, W.: Functional Analysis, 2nd edn. McGraw-Hill Education (Asia), Singapore (2005)
12. Spalart, P.R., Moser, R.D., Rogers, M.M.: Spectral methods for the navier-stokes equations with one infinite and two periodic directions. J. Comput. Phys. **96**, 297–324 (1991)
13. Rogers, M.M., Moser, R.D.: Direct simulation of a self-similar turbulent mixing layer. Phys. Fluids **6**, 903–923 (1994)
14. Moser, R.D., Kim, J., Mansour, N.N.: DNS of turbulent channel flow. Phys. Fluids **11**, 943–945 (1999)

15. Duffy, D.G.: Green's Functions with Applications. Chapman & Hall/CRC, Boca Raton, Florida (2001)
16. Kuksin, S., Shirikyan, A.: Mathematics of Two-dimensional Turbulence, Cambridge Tracts in Mathematics, vol. 194. Cambridge University Press, U.K. (2012)
17. Hopf, E.: Statistical hydromechanics and functional calculus. *J. Rat. Mech. Anal.* **1**, 87–123 (1952)
18. Janocha, D.D., Waclawcyk, M., Oberlack, M.: Lie symmetry analysis of the Hopf functional-differential equation. *Symmetry* **7**, 1536–1566 (2015)
19. Gross, L.: Potential theory on hilbert space. *J. Funct. Anal.* **1**, 123–181 (1967)
20. Dalecky, Y.L., Fomin, S.V.: Measures and Differential Equations in Infinite-Dimensional Space. Kluwer Academic Publication, Dordrecht (1991)
21. Feller, M.N.: The Lévy-Laplacian. Cambridge University Press (2005)
22. Majda, A.J., Bertozzi, A.L.: Vorticity and Incompressible Flow. Cambridge University Press, Cambridge, U.K. (2002)
23. Arsenev, A.A.: Construction of a turbulence measure for the system of Navier-Stokes equations. *Math. USSR Sb.* **30**, 179–186 (1976)
24. Arsenev, A.A.: On statistical solutions of the Navier-Stokes system of equations. *Math. USSR Sb.* **38**, 31–45 (1981)
25. Foias, C.: Statistical study of Navier-Stokes equations, I. *Rend. Sem. Matem. Padova* **48**, 219–348 (1972)
26. Foias, C.: Statistical study of Navier-Stokes equations, II. *Rend. Sem. Matem. Padova* **49**, 9–123 (1973)
27. Jimenez, J.: Coherent structures in wall-bounded turbulence. *JFM* **842**, P1-1-P1-100 (2018)
28. Cannarsa, P., DaPrato, G.: Potential theory in hilbert spaces. In: Proceedings, p. 54. *Symposia Appl. Math* (1998)
29. Courant, R.: Differential & Integral Calculus. vol. II, Blackie & Sons Ltd, London (1962)
30. Smirnov, V.I.: A Course of Higher Mathematics. vol. II, Pergamon Press, Oxford (1964)
31. Wang, X.: Volumes of generalized unit balls. *Math. Mag.* **78**, 390–395 (2005)
32. Folland, G.B.: How to integrate a polynomial over a sphere. *Am. Math. Month.* **108**, 446–448 (2001)
33. Guzman, A.: Derivatives and Integrals of Multivariable Functions. Birkhäuser Boston (2003)
34. Lerner, N.: A Course on Integration Theory. Birkhäuser/Springer Basel (2014)
35. Bogachev, V.I.: Gaussian Measures, p. 62. American Mathematical Society, Mathematical surveys and monographs vol (1998)
36. Kollmann, W.: Fluid Mechanics in Spatial and Material Description. University Readers, San Diego (2011)
37. Kraichnan, R.H.: Lagrangian history closure for turbulence. *Phys. Fluids* **8**, 575–598 (1968)
38. Constantin, P., Iyer, G.: A stochastic-Lagrangian approach to the Navier-Stokes equations in domains with boundary. *Ann. Appl. Prob.* **21**, 1466–1492 (2011)
39. Bennett, A.: Lagrangian Fluid Dynamics. Cambridge University Press, Cambridge, U.K. (2006)
40. Olver, F.W., Lozier, D.W., Boisvert, R.F., Clark, C.W.: NIST Handbook of Mathematical Functions. Cambridge University Press, U.K. (2010)

Chapter 10

Solution of Hopf-Type Equations in the Spatial Description



The assumption that the IBVP for the Navier–Stokes pdes governing the motion of incompressible fluids is well posed (2.49) leads to a formal solution of Hopf-type fdes, [1–3]. The assumption implies the existence of the solution operator T_t : $v_\alpha(t, \mathbf{x}) = T_t v_\alpha(0, \mathbf{x})$ with unique inverse T_{-t} . The solution operator T_t furnishes then a bijective mapping of the phase space Ω onto itself as long as T_t is defined and uniquely invertible, hence

$$\mu(t, B) = \mu_0(T_{-t}B), \quad B \in \mathcal{A}, \quad T_{-t}B \in \mathcal{A}_0 \quad (10.1)$$

holds (Vishik [1]), where B is a measurable subset of the phase space Ω , i.e. an element of the σ -algebra \mathcal{A} of events at time $\tau \geq 0$. The phase space is thus a measure space $(\Omega, \mathcal{A}, \mu)$. Accordingly, the characteristic functional satisfies

$$\theta[y; t] = \int_{\Omega} d\mu(t, u) \exp[i(y, u)] = \int_{\Omega} d\mu(0, u) \exp[i(y, T_t(u))] \quad (10.2)$$

with $y(\mathbf{x}) \in \mathcal{N}$ being an element of the test function space \mathcal{N} , Chap. 5. The initial measure $\mu_0(B)$, $B \in \mathcal{A}_0$ is set up as limit of cylinder measures or explicitly in terms of the initial characteristic functional, thus completing the IVP for the spatial Hopf fde (9.40). The fundamental difficulty with this approach is the determination of the solution operator T_t . An example, where it is explicitly known (but non-chaotic), is provided in problem (9.1) in the previous Chap. 9 with detailed solution in Appendix F, Chap. 28. However, it is virtually impossible to compute the solution operator T_t for the Navier–Stokes pdes for Reynolds numbers $Re \gg 1$ relevant for turbulent flows, hence, an attempt is made to solve the Hopf fde directly.

10.1 Steady-State Solutions

The earliest attempt to obtain a solution of the Hopf fde for steady state was due to Hopf and Titt [4] for $\mathcal{D} = R^3$. They considered turbulent flow with zero mean velocity formulated in terms of the Hopf fde in spectral argument fields, Eq. (9.52) in Sect. 9.2.6. The Hopf fde for infinite Reynolds number is according to Hopf and Titt reduced to

$$(\hat{y}_\alpha(\mathbf{k}), k_\beta(\delta_{\alpha\gamma} - \frac{k_\alpha k_\gamma}{k^2}) \int d\mathbf{k}' \frac{\delta^2 \theta}{\delta \hat{y}_\beta(\mathbf{k} - \mathbf{k}') \delta \hat{y}_\gamma(\mathbf{k}')}) = 0 \quad (10.3)$$

tacitly assuming that no singularities appear and, therefore, no external forcing is necessary to maintain steady state. However, the authors did not succeed in constructing a solution for the inviscid case essentially due to the possible emergence of singularities of the second kind (the Duchon–Robert distribution in Sect. 22.3 is a possible way to formulate singularities). This question remains open until the present; it is discussed in Chap. 22 in the light of the Kolmogorov–Onsager hypotheses.

Fully developed turbulence in statistical steady state is an important case covering many turbulent shear flows of interest for a variety of applications. Consider the turbulent flow in a domain \mathcal{D} with boundary $\partial\mathcal{D}$. The necessary condition for statistically steady state is that the conversion of kinetic energy into internal energy is balanced by the energy supplied by external forces and/or boundary conditions providing the influx of energy. The set up of the Hopf fde for this case is greatly simplified, if the space \mathcal{N} of argument vector fields $\mathbf{y}(\mathbf{x})$ is restricted to solenoidal fields. This case is relevant for turbulent flows of an incompressible fluid and pursued further in this section. The test (argument) fields $\mathbf{y}(\mathbf{x})$ are then elements of a nuclear space of solenoidal vector fields denoted by

$$\mathcal{N} = \{\mathbf{y} \in C_D^\infty : \nabla \cdot \mathbf{y} = 0, \mathbf{y}(\mathbf{x}) = 0, \mathbf{x} \in \partial\mathcal{D}\} \quad (10.4)$$

This has an elementary, but very important consequence as spatial gradient terms in the Hopf fde can be shown to vanish. The pressure gradient term is specified according to Sect. 9.2.2 as sum of two contributions $\nabla P = \nabla P_0 + \nabla p$, where the basic pressure gradient ∇P_0 is an external parameter presumably known and $p(\mathbf{x}, t)$ is the disturbance pressure to be eliminated with the aid of a Green's function. The example of the pipe flow periodic in axial direction has the basic pressure gradient as one of the driving agents providing the flow with the energy supply to keep it steady in the mean. Note that the basic pressure would not be periodic, but linear in axial direction; hence, the gradient of the basic pressure is periodic and thus the appropriate term to which the divergence theorem is not applied. Specifically, the divergence theorem implies

$$\int_{\mathcal{D}} d\nu(\mathbf{x}) \mathbf{y}(\mathbf{x}) \cdot \nabla p = - \int_{\mathcal{D}} d\nu(\mathbf{x}) (\nabla \cdot \mathbf{y}) p(\mathbf{x}) = 0$$

thus eliminating the disturbance pressure term from the fde for the characteristic functional.

10.2 fde in Cartesian Coordinates

The Hopf equation (9.46) is then reduced to the fde

$$\frac{\partial}{\partial t} \theta[\mathbf{y}; t] = \int_{\mathcal{D}} d\nu(\mathbf{x}) y_\alpha(\mathbf{x}) \left\{ i \frac{\partial}{\partial x_\beta} \frac{\delta^2 \theta}{\delta y_\beta \delta y_\alpha} [\mathbf{y}; t, \mathbf{x}, \mathbf{x}] + \frac{1}{Re} \frac{\partial^2}{\partial x_\beta \partial x_\beta} \frac{\delta \theta}{\delta y_\alpha} [\mathbf{y}; t, \mathbf{x}] + i \mathcal{F}_\alpha \theta[\mathbf{y}; t] \right\}$$

defined on the domain $\mathcal{D}_\infty \equiv \mathcal{N} \times [0, T]$, Fr denotes the Froude number (22.2) and

$$\mathcal{F}_\alpha \equiv \frac{1}{Fr} g_\alpha(\mathbf{x}) - \frac{\partial P_0}{\partial x_\alpha}$$

is the net external forcing term consisting of a volume force (such as gravity) and the basic pressure gradient. Thus, the steady-state version amounts to an orthogonality condition

$$\int_{\mathcal{D}} d\nu(\mathbf{x}) y_\alpha(\mathbf{x}) \left\{ \frac{\partial}{\partial x_\beta} \left[\left(i \frac{\delta}{\delta y_\beta} + \frac{1}{Re} \frac{\partial}{\partial x_\beta} \right) \frac{\delta \theta}{\delta y_\alpha} [\mathbf{y}; \mathbf{x}] \right] + i \mathcal{F}_\alpha \theta[\mathbf{y}; t] \right\} = 0, \quad \forall \mathbf{y} \in \mathcal{N} \quad (10.5)$$

The volume (measure) differential $d\nu = d\mathbf{x} w((\mathbf{x}))$ contains in general a weight function $w(\mathbf{x})$, which can be designed to take advantage of a particular basis spanning \mathcal{N} , see Sect. 25.20 or 25.21 for details. Since this orthogonality condition holds for all test fields \mathbf{y} in \mathcal{N} , the system of equations

$$\frac{\partial}{\partial x_\beta} \left\{ \left(i \frac{\delta}{\delta y_\beta} + \frac{1}{Re} \frac{\partial}{\partial x_\beta} \right) \frac{\delta \theta}{\delta y_\alpha} [\mathbf{y}; \mathbf{x}] \right\} + i \mathcal{F}_\alpha \theta[\mathbf{y}] = 0 \quad (10.6)$$

follows, $\alpha = 1, 2, 3$.

It is noteworthy that a non-zero external force in this equation is necessary to insure the existence of a non-trivial steady-state solution $\theta[\mathbf{y}]$. Suppose the force term \mathcal{F}_α is zero, then implies Eq. (10.6) that the expression in the brackets is independent of location \mathbf{x} , hence a complex-valued functional $c[\mathbf{y}]$

$$\left(i \frac{\delta}{\delta y_\beta} + \frac{1}{Re} \frac{\partial}{\partial x_\beta} \right) \frac{\delta \theta}{\delta y_\alpha} [\mathbf{y}; \mathbf{x}] = c[\mathbf{y}]$$

appears on the right side as first integral of (10.6). This fde for the vector functional

$$M_\alpha[\mathbf{y}; \mathbf{x}] \equiv \frac{\delta \theta}{\delta y_\alpha} [\mathbf{y}; \mathbf{x}]$$

is linear and first order

$$\left(i \frac{\delta}{\delta y_\beta} + \frac{1}{Re} \frac{\partial}{\partial x_\beta} \right) M_\alpha[\mathbf{y}; \mathbf{x}] = c[\mathbf{y}]$$

The left side of this equation must be independent of location \mathbf{x} , but M_α depends on \mathbf{x} as Gateaux derivative. Hence, $M_\alpha = 0$ and $c = 0$ is the only solution and $\theta[\mathbf{y}]$ would be a linear functional violating the condition $|\theta| \leq 1$. Therefore, no steady state exists.

The net external force per unit volume \mathcal{F}_α is set to a non-zero, constant vector for the discussion of the simplest possible case. The extension to stochastic forcing for the Hopf fde is more intricate, it is considered in Sect. 9.2. The next section develops in detail the idea of Shen and Wray for a particular turbulent shear flow in a compact flow domain.

10.3 fde in Cylindrical Coordinates

Cylindrical coordinates for the flow domain \mathcal{D} do not pose any new difficulties, but lead to lengthier derivations; hence, they are presented as problems at the end of the chapter with solutions in Appendix F. The solution to Problem (10.2) produces the Hopf fde

$$\begin{aligned} \frac{\partial \theta}{\partial t}[\mathbf{y}; t] = & -i[(y_r, \mathcal{F}_r)_c + (y_r, \mathcal{F}_r)_\nu + (y_\theta, \mathcal{F}_\theta)_c + (y_\theta, \mathcal{F}_\theta)_\nu + (y_z, \mathcal{F}_z)_c + (y_z, \mathcal{F}_z)_\nu] + \\ & i[(y_r, \Pi_r) + (y_\theta, \Pi_\theta) + (y_z, \Pi_z)] + \frac{i}{Fr}[(y_r, G_r \theta[\mathbf{y}]) + (y_\theta, G_\theta \theta[\mathbf{y}]) \\ & + (y_z, G_z \theta[\mathbf{y}])] - i(y_z, \frac{\partial P_0}{\partial z} \theta[\mathbf{y}]) \end{aligned} \quad (10.7)$$

in cylindrical coordinates. The convective contributions $(y_r, \mathcal{F}_r)_c$ emerge for the radial component in the form

$$\begin{aligned} -i(y_r, \mathcal{F}_r)_c = & i \left\{ (y_r, \frac{\partial}{\partial r} \lim_{\mathbf{x}' \rightarrow \mathbf{x}} \frac{\delta^2 \theta}{\delta y_r(\mathbf{x}') \delta y_r(\mathbf{x})}[\mathbf{y}; t]) + (y_r, \frac{\partial}{\partial z} \lim_{\mathbf{x}' \rightarrow \mathbf{x}} \frac{\delta^2 \theta}{\delta y_r(\mathbf{x}') \delta y_z(\mathbf{x})}[\mathbf{y}; t]) + \right. \\ & (y_r, \frac{1}{r} \frac{\partial}{\partial \theta} \lim_{\mathbf{x}' \rightarrow \mathbf{x}} \frac{\delta^2 \theta}{\delta y_r(\mathbf{x}') \delta y_\theta(\mathbf{x})}[\mathbf{y}; t]) + (y_r, \frac{1}{r} (\lim_{\mathbf{x}' \rightarrow \mathbf{x}} \{ \frac{\delta^2 \theta}{\delta y_r(\mathbf{x}') \delta y_r(\mathbf{x})}[\mathbf{y}; t] \right. \\ & \left. \left. - \frac{\delta^2 \theta}{\delta y_\theta(\mathbf{x}') \delta y_\theta(\mathbf{x})}[\mathbf{y}; t] \}) \right\} \end{aligned} \quad (10.8)$$

and likewise $(y_\theta, \mathcal{F}_\theta)_c$ and $(y_z, \mathcal{F}_z)_c$ as given in the solution for Problem (10.2) in Appendix F.

The viscous term $-i(y_r, \mathcal{F}_r)_\nu$ is given in the solution for Problem (10.2) as the convective terms

$$\begin{aligned} -i(y_r, \mathcal{F}_r)_\nu = \\ \frac{1}{Re} \left\{ (y_r, \frac{\partial}{\partial r} (\frac{1}{r} \frac{\partial}{\partial r} (r \frac{\delta\theta}{\delta y_r(\mathbf{x})}))) + (y_r, \frac{1}{r^2} \frac{\partial^2}{\partial \theta^2} \frac{\delta\theta}{\delta y_r(\mathbf{x})}) + (y_r, \frac{\partial^2}{\partial z^2} \frac{\delta\theta}{\delta y_r(\mathbf{x})}) - (y_r, \frac{2}{r^2} \frac{\partial}{\partial \theta} \frac{\delta\theta}{\delta y_\theta(\mathbf{x})}) \right\} \end{aligned} \quad (10.9)$$

and likewise for the azimuthal and axial components. The singularities at the coordinate axis $r = 0$ are evaluated with the aid of the parity conditions, set up in Sect. 25.12. If the argument /test function space \mathcal{N}_p is solenoidal, the pressure terms can be shown to vanish, and if the external force is constant, Hopf fde is reduced to

$$\begin{aligned} \frac{\partial \theta}{\partial t} [\mathbf{y}; t] = -i[(y_r, \mathcal{F}_r)_c + (y_r, \mathcal{F}_r)_\nu + (y_\theta, \mathcal{F}_\theta)_c + (y_\theta, \mathcal{F}_\theta)_\nu + (y_z, \mathcal{F}_z)_c + (y_z, \mathcal{F}_z)_\nu] + \\ + \frac{i}{Fr} [G_r(y_r, \theta[\mathbf{y}]) + G_\theta(y_\theta, \theta[\mathbf{y}]) + (G_z - \frac{\partial P_0}{\partial z})(y_z, \theta[\mathbf{y}])] \end{aligned} \quad (10.10)$$

This fde is used in the next section for the treatment of steady-state solutions.

10.4 Steady-State Solutions for Periodic Pipe Flow

The idea of Shen and Wray [5] to reduce the Hopf fde for solenoidal arguments $\mathbf{y}(\mathbf{x} :) \nabla \cdot \mathbf{y} = 0$ to the steady state and to solve the resulting variational hyperbolic equation, is applied with minor modifications to the turbulent flow of an incompressible fluid through circular pipes assuming periodicity in axial direction. This task will be carried out first in general form, the application to the periodic pipe flow with cylindrical coordinates for the flow domain is presented in a series of Problems in Sect. 10.7 with solutions in Appendix F containing the lengthy details of the derivations.

First, the representation of the pressure (26.50) $P(r, \theta, \zeta) = P_0(\zeta) + p(r, \theta, \zeta)$, where $\zeta = \frac{x_3}{L}$, contains the disturbance pressure $p(r, \theta, \zeta) \equiv p_h(r, \theta, \zeta) + p_G(r, \theta, \zeta)$. The gradient is then $\nabla P(\mathbf{x}) = \nabla P_0 + \nabla[p_h(\mathbf{x}) + p_G(\mathbf{x})]$, where ∇P_0 is a constant vector in ζ -direction and thus periodic in this direction, since $P_0(\zeta)$ is a linear function of the axial coordinate established in Sect. 26.3 in Appendix D. The pressure gradient is, therefore, a sum of a non-zero constant vector, which is an externally controlled parameter setting the mass flow rate through \mathcal{D} , plus a disturbance gradient, that is a combination of volume and surface integrals as shown in Sect. 26.6 for the pipe flow domain, Eqs. (26.76) and (26.130).

Thus, the momentum balance (2.7) in the spatial description can be formulated using the representation of the pressure gradient as sum of two contributions, where the balance (28.9) for the axial direction

$$\frac{\partial v_z}{\partial t} + T_z(\mathbf{v}) = -\frac{1}{\rho} \frac{\partial p}{\partial z} + \frac{1}{Re} \left[\frac{1}{r} \frac{\partial}{\partial r} \left(r \frac{\partial v_z}{\partial r} \right) + \frac{1}{r^2} \frac{\partial^2 v_z}{\partial \theta^2} + \frac{\partial^2 v_z}{\partial z^2} \right] + \frac{1}{Fr} G_z - \frac{\partial P_0}{\partial z} \quad (10.11)$$

contains both pressure gradient terms, where the gradient of the disturbance pressure $p \equiv p_h + p_G$ is defined by

$$\nabla p = \mathbf{P}[\mathbf{v}] \equiv \nabla(p_h + p_G) \quad (10.12)$$

as vector functional \mathbf{P} of velocity, explicit functionals for the harmonic and the Green's function parts of the disturbance pressure are given in Appendix D, Eqs. (26.76) and (26.128) for the example of periodic flow through a straight, circular pipe. However, the gradient of the disturbance pressure is not be needed in the present section as it will be eliminated by constructing a solenoidal Schauder basis.

The gradient of P_0 is constant and non-zero; it supplies the kinetic energy to balance the loss due to dissipation. Observing, that the momentum balance (10.11) is identical to (2.7) except the additional constant term ∇P_0 appears, it is evident that the idea of Shen and Wray can be applied using the same solenoidal test function space \mathcal{N} (10.4), thus eliminating the gradient of the disturbance pressure. The Hopf fde (9.40) for the characteristic functional is then reduced to the orthogonality condition

$$\int_{\mathcal{D}} r dr d\theta dz [y_r(\mathbf{x}) \cdot \mathcal{L}_r(\theta) + y_\theta(\mathbf{x}) \cdot \mathcal{L}_\theta(\theta) + y_z(\mathbf{x}) \cdot \mathcal{L}_z(\theta)] = 0, \quad \forall \mathbf{y} \in \mathcal{N} \quad (10.13)$$

in cylindrical coordinates. The linear vector operator \mathcal{L}_α is in Cartesian coordinates

$$\mathcal{L}_\alpha(\theta) \equiv \frac{\partial}{\partial x_\beta} \left[\left(i \frac{\delta}{\delta y_\beta} + \frac{1}{Re} \frac{\partial}{\partial x_\beta} \right) \frac{\delta \theta}{\delta y_\alpha} [\mathbf{y}; \mathbf{x}] \right] - i \frac{\partial P_0}{\partial x_\alpha} \theta[\mathbf{y}] \quad (10.14)$$

applied to the characteristic functional $\theta[\mathbf{y}]$ is evaluated by (10.14) in several forms. The first version is solving (10.13) exploiting the ONS property of a suitable basis in \mathcal{N} .

Second, partial integration w.r.t. \mathbf{x} is applied to the orthogonality condition (10.13) to reduce the order of spatial differentiation acting on the characteristic functional as follows:

$$i \left(\frac{\partial y_\alpha}{\partial x_\beta}, \frac{\delta^2 \theta}{\delta y_\alpha(\mathbf{x}) \delta y_\beta(\mathbf{x})} [\mathbf{y}] \right) + \frac{1}{Re} \left(\frac{\partial y_\alpha}{\partial x_\beta}, \frac{\partial}{\partial x_\beta} \frac{\delta \theta}{\delta y_\alpha(\mathbf{x})} [\mathbf{y}] \right) + i \frac{\partial P_0}{\partial x_\alpha} (y_\alpha, \theta[\mathbf{y}]) = 0 \quad (10.15)$$

where $\mathbf{y} = 0$ on $\partial\mathcal{D}$ was used. The second Gateaux derivative is computed according to (23.45) producing a function of two different locations \mathbf{x} and \mathbf{x}' and then the limit $\mathbf{x}' \rightarrow \mathbf{x}$ is evaluated.

Equation (10.15) and its variants determine the class of steady-state characteristic functionals $\theta[\mathbf{y}]$. This fde valid for statistically steady states of the turbulent flow through a straight, circular pipe is now investigated in the next section w.r.t. a

solenoidal Schauder basis constructed for \mathcal{N} . This fde is, however, not an equation as (10.6) for the first Gateaux derivative, but for θ itself due to the presence of the last and crucial term in (10.6) and requires, therefore, a solution strategy different from the one proposed by Shen and Wray [5].

10.4.1 Steady-State fde in a Solenoidal ONS Basis \mathcal{B}_e for \mathcal{N}

The construction of a solenoidal basis for the periodic pipe flow is contained in Sect. 25.21, Appendix C. The present (second) method for this construction is based on the kinematic property that the divergence of a curl of a vector potential is identically zero as explained in Sect. 25.21.2. The result is the solenoidal ONS basis in cylindrical coordinates

$$\mathcal{B}_e = \{e_\alpha^{k,n,m}(r, \theta, z) = h_k(\theta) \chi_\alpha^{e,k,n,m}(r) h_m(z), \alpha = r, \theta, z\} \quad (10.16)$$

with the radial shape functions $\chi_\alpha^{e,k,n,m}(r)$, $\alpha = r, \theta, z$ set up in (25.164) and the Fourier coefficients defined in (15.2). Figures 25.12 and 25.15 in Appendix C illustrate some properties of the solenoidal vector modes constructed as the Gram-Schmidt orthonormalized curl of properly designed vector potentials.

The nuclear test function space \mathcal{N} leads to a sequence of pdes for the projected characteristic functional θ_N of increasing dimension defined below (25.14). This sequence is derived and the boundary conditions are set up in the present section to generate a solvable BVP for the projected characteristic functional using the second variant (10.15) of the steady-state Hopf fde. Let $\mathcal{B}_e = \{\mathbf{e}^{k,n,m}(r, \theta, z), k \in [0, N/2], n \in [0, N], m \in [-\frac{1}{2}N, \frac{1}{2}N], N \rightarrow \infty\}$ be a solenoidal Schauder basis for the test function space \mathcal{N} , i.e. any element in \mathcal{N} is represented by

$$\mathbf{y}(\mathbf{x}) = \sum_{k=0}^{\infty} \sum_{n=0}^{\infty} \sum_{m=-\infty}^{\infty} y_{k,n,m} \mathbf{e}^{k,n,m}(r, \theta, z), \quad \nabla \cdot \mathbf{y} = 0 \quad (10.17)$$

where $y_{k,n,m} \equiv (\mathbf{y}, \mathbf{e}^{k,n,m})$ denotes the coordinates /expansion coefficients w.r.t. the basis \mathcal{B}_e for \mathcal{N} , which is a Hilbert space w.r.t. the L^2 norm (22.18). It is isomorphic to the space l^2 of infinite sequences, since $\|\mathbf{y}\|_{L^2}^2 = \sum_{k,n,m}^{\infty} |y_{k,n,m}|^2$ holds.

Projected characteristic functionals

The projection $\theta_N(\mathbf{y})$ of the characteristic functional onto an Euclidean space with finite dimension

$$M(N) = \left(\frac{1}{2}N_\theta + 1\right)(N_r + 1)(N_z + 1) \quad (10.18)$$

(the Fourier mode count is according to the FFT storage of Rogallo [6] incorporating the condition that the inverse Fourier transforms are real) is defined in Sect. 25.4 of Appendix C by

$$\theta_N(y_{k,n,m} : 0 \leq k \leq \frac{1}{2}N, 0 \leq n \leq N, -\frac{1}{2}N \leq m \leq \frac{1}{2}N) \equiv \theta\left[\sum_{k=0}^{N/2} \sum_{n=0}^N \sum_{m=-N/2}^{N/2} y_{k,n,m} \mathbf{e}^{k,n,m}(\mathbf{x})\right]$$

The projected characteristic functional is a standard function θ_N of $M(N)$ (10.18) independent variables $y_{k,n,m}$ appearing in the representation of the projected argument field

$$\mathbf{y}(\mathbf{x}) = \sum_{k,n,m}^N y_{k,n,m} \mathbf{e}^{k,n,m}(\mathbf{x}) \quad (10.19)$$

which can be regarded as the Cartesian coordinates in $R^{M(N)}$. The actual number of non-zero arguments $y_{k,n,m}$ of θ_N may be smaller than the upper limit $M(N)$ (10.18), estimated for the periodic pipe flow as about half of $M(N)$. It has the limit

$$\theta[\mathbf{y}] = \lim_{N \rightarrow \infty} \theta_N(y_{0,0,-\frac{1}{2}N}, \dots, y_{\frac{1}{2}N,N,\frac{1}{2}N}) \quad (10.20)$$

since \mathcal{B}_e is a Schauder basis for \mathcal{N} . Note that the $\theta[\mathbf{y}(\mathbf{x}); t]$ is a functional of the argument/test field $\mathbf{y}(\mathbf{x}) \in \mathcal{N}_e$ and a function of time t , but it does not vary with location $\mathbf{x} \in \mathcal{D}$, whereas the variational derivatives are also functions of one or more than one locations in \mathcal{D} .

Suppose the projected characteristic function $\theta_N(y_{k,n,m})$ has been computed, then is the value of the characteristic functional $\theta[\mathbf{y}] = \theta_N(y_{k,n,m})$ for argument fields

$$\mathbf{y} = \sum_{k=0}^{N/2} \sum_{n=0}^N \sum_{m=-\frac{1}{2}N}^{\frac{1}{2}N} y_{k,n,m} \mathbf{e}^{k,n,m}(\mathbf{x})$$

Let \mathbf{y} be an arbitrary element of \mathcal{N} represented by (10.17), then is $\theta_N(y_{k,n,m})$ an approximation of $\theta[\mathbf{y}]$ generated by truncating the representation of \mathbf{y} according to (10.19). This property is a possible starting point for an error analysis.

Gaussian example

The independence of location is illustrated with the Gaussian functional $\theta_G[\mathbf{y}; t] = \exp\{-\frac{1}{2}(\mathbf{K} \cdot \mathbf{y}, \mathbf{y}) + i(\mathbf{a}, \mathbf{y})\}$ (9.87) w.r.t. the basis \mathcal{B}_e , where $\mathbf{y}(\mathbf{x}) \in \mathcal{N}$ and \mathbf{K} denotes the correlation operator (9.91) and $\mathbf{a}(\mathbf{x})$ the mean vector field. The operator $\mathbf{K}(\mathbf{x}, \mathbf{x}')$ is represented in the basis \mathcal{B}_e by

$$K_{\alpha\beta}(\mathbf{x}, \mathbf{x}') = \sum_{k,n,m} \sum_{o,p,q} K_{k,n,m}^{o,p,q} e_{\alpha}^{k,n,m}(\mathbf{x}) e_{\beta}^{o,p,q}(\mathbf{x}')$$

The application to $\mathbf{y}(\mathbf{x})$ is computed by

$$K_{\alpha\beta}(\mathbf{x}, \mathbf{x}') y_\alpha(\mathbf{x}) = \sum_{k,n,m} \sum_{o,p,q} K_{k,n,m}^{o,p,q} y_{k,n,m} e_\beta^{o,p,q}(\mathbf{x}')$$

and the scalar product $(\mathbf{K} \cdot \mathbf{y}, \mathbf{y})$ emerges then as double sum

$$(\mathbf{K} \cdot \mathbf{y}, \mathbf{y}) = \sum_{k,n,m} \sum_{o,p,q} K_{k,n,m}^{o,p,q} y_{k,n,m} y_{o,p,q}$$

leading to

$$\theta_G[\mathbf{y}] = \exp\left\{i \sum_{k,n,m} a_{k,n,m} y_{k,n,m} - \frac{1}{2} \sum_{k,n,m} \sum_{o,p,q} K_{k,n,m}^{o,p,q} y_{k,n,m} y_{o,p,q}\right\}$$

as representation of the Gaussian characteristic functional w.r.t. the basis \mathcal{B}_e . The terms $K_{k,n,m}^{o,p,q}$ and $y_{k,n,m}$ do not depend on location $\mathbf{x} \in \mathcal{D}$, hence any spatial derivative of $\theta[\mathbf{y}]$ is zero. However, they are functionals of the argument fields $\mathbf{y}(\mathbf{x}) = \sum_{k,n,m} y_{k,n,m} \mathbf{e}^{k,n,m}(\mathbf{x})$ via the definition of the coefficients $y_{k,n,m} = (\mathbf{y}, \mathbf{e}^{k,n,m})$.

Derivatives of the projected characteristic functionals

The next step is to evaluate the derivatives in the fde (10.15) with respect to the basis vectors in \mathcal{B}_e . The first Gateaux derivative is according to (23.45) for $M(N)$ -dimensional argument fields $\mathbf{y}(\mathbf{x}) = \sum_{k,n,m} y_{k,n,m} \mathbf{e}^{k,n,m}(\mathbf{x})$ expressed as partial derivatives of θ_N w.r.t. the coefficients $y_{k,n,m}$

$$\frac{\delta \theta}{\delta y_\alpha(\mathbf{x})} = \sum_{k,n,m} \frac{\partial \theta_N}{\partial y_{k,n,m}} (y_{0,0,-\frac{1}{2}N}, \dots, y_{\frac{1}{2}N,N,\frac{1}{2}N}) e_\alpha^{k,n,m}(\mathbf{x})$$

see Eq. (23.50) in Sect. 23.12 and Sect. 23.12 for details on variational differentiation. The partial derivatives of θ_N are like θ_N itself independent of location $\mathbf{x} \in \mathcal{D}$, the dependence of the variational derivative on \mathbf{x} is explicitly given by the basis modes as factors. This holds for variational derivatives of any order.

The second Gateaux derivative is computed according to the definition (23.45) of Gateaux differentials in Sect. 23.12

$$\delta^2 \theta = \lim_{\epsilon \rightarrow 0} \frac{1}{\epsilon} \left\{ \frac{\delta \theta}{\delta y_\alpha} [\mathbf{y} + \epsilon \mathbf{w}; \mathbf{x}] - \frac{\delta \theta}{\delta y_\alpha} [\mathbf{y}; \mathbf{x}] \right\}$$

where $\mathbf{y}, \mathbf{w} \in \mathcal{N}$, $w_{k,n,m} = (w_\alpha, e_\alpha^{k,n,m})$, and then the limit $\mathbf{x}' \rightarrow \mathbf{x}$ can be computed. The projected characteristic functional is defined by (25.14)

$$\frac{\delta \theta}{\delta y_\alpha(\mathbf{x})} [\mathbf{y} + \epsilon \mathbf{w}; \mathbf{x}] = \sum_{k,n,m} \frac{\partial \theta_N}{\partial y_{k,n,m}} (y_{0,0,-\frac{1}{2}N} + \epsilon w_{0,0,-\frac{1}{2}N}, \dots, y_{\frac{1}{2}N,N,\frac{1}{2}N} + \epsilon w_{\frac{1}{2}N,N,\frac{1}{2}N}) e_\alpha^{k,n,m}(\mathbf{x})$$

The pde governing it is derived below.

Gaussian derivative example

The example of the Gaussian characteristic functional represented w.r.t. the basis \mathcal{B}_e obtained above (10.16) can be used to demonstrate the structure of a variational derivative and illustrate the dependence of the first Gateaux derivative on location $\mathbf{x} \in \mathcal{D}$. The first Gateaux derivative w.r.t. the basis \mathcal{B}_e has been obtained in the previous section

$$\frac{\delta \theta_G}{\delta y_\alpha(\mathbf{x})} = \sum_{k,n,m} \frac{\partial \theta_G}{\partial y_{k,n,m}} (y_{0,0,-\frac{1}{2}N}, \dots) e_\alpha^{k,n,m}(\mathbf{x})$$

The partial derivatives w.r.t. $y_{k,n,m}$ can be evaluated using the representation given above

$$\frac{\partial \theta_G}{\partial y_{k,n,m}} = \{ia_{k,n,m} - \frac{1}{2} \sum_{l,o,p} (K_{k,n,m}^{l,o,p} + K_{l,o,p}^{k,n,m}) y_{l,o,p}\} \theta[\mathbf{y}]$$

The partial derivative is obviously independent of location and the dependence of the Gateaux derivative on location is explicitly given by the factor $e^{k,n,m}(\mathbf{x})$. The same property is also observed for higher derivatives.

10.5 Variational Hessian and the pde for θ_N

The variational Hessian emerges for the finite-dimensional arguments (10.19) by applying the Gateaux derivatives established above to the fde (10.15) and evaluating the second variational derivative term group. The resulting Hessian

$$\frac{\delta^2 \theta}{\delta y_\alpha(\mathbf{x}) \delta y_\beta(\mathbf{x}')} = \sum_{l,o,p} \sum_{k,n,m} \frac{\partial^2 \theta_N}{\partial y_{m,l,p} \partial y_{k,n,m}} (y_{0,0,-\frac{1}{2}N}, \dots, y_{\frac{1}{2}N,N,\frac{1}{2}N}) e_\alpha^{k,n,m}(\mathbf{x}) e_\beta^{l,o,p}(\mathbf{x}')$$

shows explicitly the dependence on locations, which allows straightforward evaluation of the limit $\mathbf{x}' \rightarrow \mathbf{x}$. The spatial derivatives in the fde (10.15) are thus easy to compute as they apply to the basis functions, which allow analytic evaluation of derivatives. The fde (10.15) appears for finite-dimensional arguments now as

$$i \sum_{k,n,m} \sum_{l,o,p} A_{k,n,m}^{l,o,p} \frac{\partial^2 \theta_N}{\partial y_{k,n,m} \partial y_{l,o,p}} + \frac{1}{Re} \sum_{k,n,m} B_{k,n,m} \frac{\partial \theta_N}{\partial y_{k,n,m}} - iC \theta_N = 0 \quad (10.21)$$

where $\theta_N(y_{0,0,-\frac{1}{2}N}, \dots, y_{\frac{1}{2}N,N,\frac{1}{2}N})$ is a standard, complex-valued function of $M(N)$ (10.18) real variables $y_{k,n,m}$.

The characteristic functional $\theta[\mathbf{y}; t]$ is the limit, if it exists, of the characteristic functions θ_N as $M(N) \rightarrow \infty$. Inspection of this linear second-order pde shows the role reversal of convection and viscous effects: The convective term is represented by the second derivatives in the N -dimensional Hessian, whereas viscous effects are contained in the first derivative terms. The zero-derivative term contains the control parameter $\partial P_0 / \partial z < 0$ that maintains the flow. Note that for laminar flow the well-known Poiseuille's law [7] relates the volume flow rate \dot{Q} to the axial pressure gradient, for turbulent flows the Darcy friction factor $f(Re, \frac{d}{D})$, where d denotes roughness height and D the pipe diameter, appears

$$-\frac{\partial P_0}{\partial z} = \frac{8\rho f(Re, \frac{d}{D}) \dot{Q}^2}{\pi^2 D^5}$$

that so far cannot be computed from first principles, but is empirically determined (Moody chart [7]). However, for the present case of statistically steady pipe flow, the basic pressure gradient is an externally controlled parameter and is not computed as part of the solution.

The coefficients of (10.21) are complex, the entries of the $M(N) \times M(N)$ matrix $A_{k,n,m}^{o,l,p}$ are defined by

$$A_{k,n,m}^{o,l,p}(y_{0,0,-\frac{1}{2}N}, \dots, y_{\frac{1}{2}N,N,\frac{1}{2}N}) \equiv (\nabla_\beta^c y_\alpha, e_\alpha^{k,n,m} e_\beta^{o,l,p}) = \sum_{r,s,t} y_{r,s,t} (\nabla_\beta^c e_\alpha^{r,s,t}, e_\alpha^{k,n,m} e_\beta^{o,l,p}) \quad (10.22)$$

where the gradient in cylindrical coordinates is denoted by $\nabla^c \equiv [\frac{\partial}{\partial r}, \frac{1}{r} \frac{\partial}{\partial \theta}, \frac{\partial}{\partial z}]^{-1}$ retaining the summation convention. The $M(N)$ vector $B_{k,n,m}$ is defined by

$$B_{k,n,m}(y_{0,0,-\frac{1}{2}N}, \dots, y_{\frac{1}{2}N,N,\frac{1}{2}N}) \equiv (\nabla_\beta^c y_\alpha, \nabla_\beta^c e_\alpha^{k,n,m}) = \sum_{r,s,t} y_{r,s,t} (\nabla_\beta^c e_\alpha^{r,s,t}, \nabla_\beta^c e_\alpha^{k,n,m}) \quad (10.23)$$

and the scalar coefficient is

$$C(y_{0,0,-\frac{1}{2}N}, \dots, y_{\frac{1}{2}N,N,\frac{1}{2}N}) \equiv \sum_{r,s,t} y_{r,s,t} (e_\alpha^{r,s,t}, \nabla_\alpha^c P_0) \quad (10.24)$$

where the basis vectors are solenoidal, i.e. $\nabla \cdot \mathbf{e}^{k,n,m} = 0$, $\forall k, n, m$. The result is a linear, second-order pde for θ_N with coefficients being functions of $y_{0,0,-\frac{1}{2}N}, \dots, y_{\frac{1}{2}N,N,\frac{1}{2}N} \in R^M$. The type of this pde depends on the $M \times M$ coefficient matrix $A_{k,n,m}^{o,l,p}(y_{0,0,-\frac{1}{2}N}, \dots, y_{\frac{1}{2}N,N,\frac{1}{2}N})$ computed using the solenoidal basis \mathcal{B}_e spanning the space \mathcal{N} . The dependence of the solution on the location in the flow field \mathcal{D} is given by the particular properties of the basis.

An example for the dependence of the complex-valued coefficients $C_\alpha^{k,n,m} = (e_\alpha^{n,k,m}, h)$, where $h(\mathbf{x}) = 1$, on the radial mode index n appearing in Eq. (10.24), if written in the form

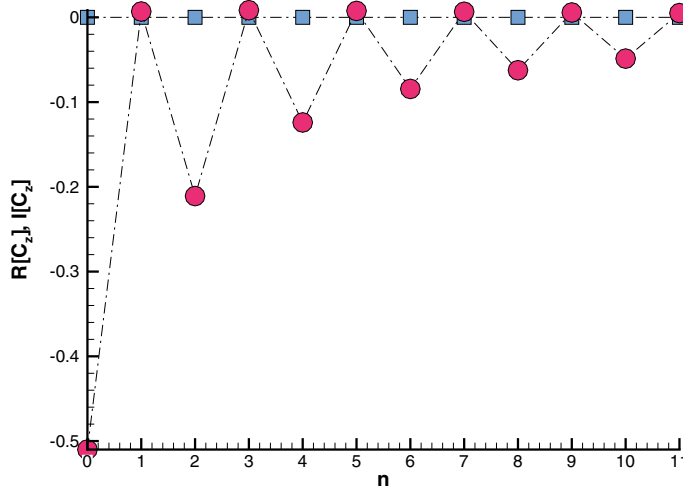


Fig. 10.1 The coefficient $C_z^{k,n,m}$ (10.24) for $k = m = 0$ as function of the radial mode index n w.r.t. the solenoidal basis \mathcal{B}_e constructed in Sect. 4.2 for the periodic pipe flow example. The blue squares are the real (identically zero) and the red circles the imaginary part of $\mathbf{e}^{k,n,m}(r, \theta, z)$, which is for $k = m = 0$ the radial shape function $\chi_e^{k,n,m}(r)$

$$C(y_{0,0,-\frac{1}{2}N}, \dots, y_{\frac{1}{2}N,N,\frac{1}{2}N}) = \frac{\partial P_0}{\partial x_\alpha} \sum_{n,k,m} C_\alpha^{k,n,m} y_{n,k,m}, \quad \alpha = r, \theta, z$$

for constant basic pressure gradient, is shown in Fig. 10.1. Note that for the periodic pipe flow example the $C_z^{k,n,m}(r)$ in the figure is only non-zero for $\alpha = z$ and $k = m = 0$, since the scalar product includes integration over θ and z over intervals, which are integer multiples of 2π . The variation of the coefficients $C_z^{k,n,m}(r)$ with the radial index n is solely due to the structure of the ONS basis functions in \mathcal{B}_e . The basis functions satisfy $\nabla \cdot \mathbf{e}_\alpha^{k,n,m} = 0$, hence mass balance is automatically taken into account. The coefficient C appears for the periodic pipe flow example as

$$C(y_{0,n,0}) = \frac{\partial P_0}{\partial z} \sum_{n=0}^N C_z^{0,n,0} y_{0,n,0}.$$

It is proportional to the externally controlled basic pressure gradient and necessary to maintain steady state. The equation (10.21) determining $\theta_N(y_{k,n,m})$ is a linear second-order pde with convection emerging as Hessian acting in the space $R^{M(N)}$ on θ_N , thus spreading the modes $y_{0,n,0}$ excited by the basic pressure gradient via the coefficient C to all of $R^{M(N)}$. Further computational details for the periodic pipe flow example can be found in the solutions to Problems 10.1 to 10.4 in Appendix F.

10.6 Boundary Conditions

The formulation of the boundary conditions for the projected characteristic functional (25.14) as function of the coordinates $y_{k,n,m}$ in \mathcal{N} depends on the properties of the chosen solenoidal basis \mathcal{B}_e . The basis vectors $\mathbf{e}^{k,n,m}(\mathbf{x})$ satisfy mass balance (they are solenoidal) and homogeneous boundary conditions in the flow domain \mathcal{D} being a subset of \mathbb{R}^3 . The domain of definition for $\theta_N(y_{0,0,-\frac{1}{2}N}, \dots, y_{\frac{1}{2}N,N,\frac{1}{2}N})$ is $\mathbb{R}^{M(N)}$. Hence, the conditions for $\theta_N(y_{0,0,-\frac{1}{2}N}, \dots, y_{r,s,t}, \dots, y_{\frac{1}{2}N,N,\frac{1}{2}N})$ must be derived from the Bochner–Minlos theorem in Sect. 8.1 to insure that the solution of (10.15) is a characteristic function. The first part of the theorem requires

$$\theta_N(0, \dots, 0) = 1 \quad (10.25)$$

and the second part

$$\lim_{y_{r,s,t} \rightarrow \infty} \theta_N(y_{0,0,-\frac{1}{2}N}, \dots, y_{r,s,t}, \dots, y_{\frac{1}{2}N,N,\frac{1}{2}N}) = 0, \quad 0 \leq r \leq \frac{1}{2}N, \\ 0 \leq s \leq N, -\frac{1}{2}N \leq t \leq \frac{1}{2}N \rightarrow \theta_N \in L^2_{M(N)} \quad (10.26)$$

The third part of the Bochner–Minlos theorem has to be checked a posteriori.

Summary:

The turbulent flow in a straight, circular pipe periodic in axial direction possesses a steady-state solution driven by the axial pressure gradient, which is an externally controlled parameter. This steady state is the solution (first integral) of the Hopf fde (9.40) with the base pressure gradient appearing explicitly as source term in (10.15). The phase space Ω and the argument space \mathcal{N} are both solenoidal vector spaces. Since they are Hilbert spaces, they can be equipped with solenoidal vector bases such as \mathcal{B}_e constructed in Appendix C. The introduction of a solenoidal vector basis in phase space Ω and its dual \mathcal{N}_e is crucial as it produces a linear pde (10.21) without the (disturbance) pressure gradient term for the $M(N)$ -dimensional projection of the characteristic functional $\theta[\mathbf{y}]$ onto a characteristic function $\theta_N(y_{0,0,-\frac{1}{2}N}, \dots, y_{\frac{1}{2}N,N,\frac{1}{2}N})$ of $M(N)$ (10.18) variables. They are defined as the coefficients $y_{k,n,m}$ of the basis vector functions $\mathbf{e}^{k,n,m}(\mathbf{x})$ analogous to the Cartesian coordinates in Euclidean space. The nonlinear convective term in the Navier–Stokes pdes induces in this formulation a linear, second-order, variational Hessian in the Hopf fde and a linear, second-order partial differential Hessian in its projection onto a finite-dimensional space. Thus, convection emerges as diffusion in the argument space \mathcal{N} of the Hopf fde and consequently the pde for the finite-dimensional projection θ_N .

10.7 Problems for this Chapter

Problem 10.1 Solve the fde for the characteristic functional $\theta[\mathbf{y}(\cdot); t]$

$$\frac{\partial}{\partial t} \theta[\mathbf{y}; t] = i \int_{\mathcal{D}} d\mathbf{x} y_\alpha(\mathbf{x}) \left(\frac{1}{Fr} g_\alpha(\mathbf{x}) - \frac{\partial P_0}{\partial x_\alpha} \right) \theta[\mathbf{y}; t]$$

governed by the truncated Hopf fde (9.40) driven solely by a constant external force

$$F_\alpha \equiv \frac{1}{Fr} g_\alpha - \frac{\partial P_0}{\partial x_\alpha}$$

The initial functional is the Gaussian

$$\theta_G[\mathbf{y}; t] = \exp\left\{-\frac{1}{2}(\mathbf{K} \cdot \mathbf{y}, \mathbf{y}) + i(\mathbf{a}, \mathbf{y})\right\}$$

with correlation operator \mathbf{K} and zero mean $\mathbf{a} = 0$.

10.1.1: Solve the IVP for the fde governing $\theta[\mathbf{y}]$ with Gaussian initial condition.

10.1.2: Show that the characteristic functional remains Gaussian and evaluate the effect of the external force on it.

Problem 10.2 Transform the Hopf fde (9.40) to cylindrical coordinates in \mathcal{D} . The explicit form of the pressure gradient term as functional of the velocity is not required. Hint: Consult Sect. 9.2.

Problem 10.3 Apply the conditions of steady state and solenoidal vector fields \mathbf{y} to the Hopf fde for cylindrical coordinates in the flow domain \mathcal{D} obtained in the previous Problem (10.2).

10.3.1 Specialize the result to constant \mathbf{G} and $\frac{\partial P_0}{\partial z}$.

10.3.2 Show that the scalar product of two modes in \mathcal{B}_e is reduced to an integral w.r.t. the radial coordinate.

Hint: Consult Sect. 9.2.

Problem 10.4 Consider the flow through a straight, circular pipe periodic in axial direction. A solenoidal ONS basis \mathcal{B}_e was constructed in Sect. 25.21 spanning the test function space \mathcal{N} for the characteristic functional $\theta[\mathbf{y}; t]$, $\mathbf{y} \in \mathcal{N}$. Solve the BVP for the projected characteristic functional $\theta_N(y_{0,0,-\frac{1}{2}N}, \dots, y_{\frac{1}{2}N,N,\frac{1}{2}N})$ introduced in Sect. 10.4 w.r.t. the basis \mathcal{B}_e .

10.4.1 Apply the pde (10.21) to the single mode $N = 0$, set up the boundary condition and solve it for $y \geq 0$.

10.4.2 Compute the coefficients $a_{k,n,m}^{l,o,q,r,s,t}$ in $A_{k,n,m}^{r,s,t} = \sum_{l,o,q} y_{l,o,q} a_{k,n,m}^{l,o,q,r,s,t}$ and $C_z^{0,n,0}$ in $C(y_{0,n,0}) = \frac{\partial P_0}{\partial z} \sum_{n=0}^N C_z^{0,n,0} y_{0,n,0}$ the pde (10.21) for several modes, say $N = 2$ and plot the results.

Hint: Consult Chap. 25 in Appendix C.

References

1. Vishik, M.J.: Analytic solutions of Hopf's equation corresponding to quasilinear parabolic equations or to the Navier-Stokes system. *Sel. Math. Sov.* **5**, 45–75 (1986)
2. Inoue, A.: Strong and classical solutions of the Hopf equation—an example of functional derivative equation of second order. *Tohoku Math. J.* **39**, 115–144 (1987)
3. Vishik, M.J., Fursikov, A.V.: Mathematical Problems of Statistical Hydromechanics. Kluwer Academic Publication, Dordrecht (1988)
4. Hopf, E., Titt, E.W.: On certain special solutions of the Φ -equation of statistical hydrodynamics. *J. Math. Mech.* **2**, 587–591 (1953)
5. Shen, H.H., Wray, A.A.: Stationary turbulent closure via the Hopf functional equation. *J. Stat. Phys.* **65**, 33–52 (1991)
6. Rogallo, R.S.: Numerical Experiments in Homogeneous Turbulence (1981). NASA-TM-81315
7. White, F.M.: Fluid Mechanics, , 6th edn. McGraw Hill (2008)

Chapter 11

Finite-Dimensional Characteristic Functions, Pdfs and Cdfs Based on the Dirac Distribution



Transport pdes for characteristic functions, Pdfs and Cdfs (LMN hierarchy) can be obtained inductively without recourse to the machinery of characteristic functionals using the notions of step function and its distributional derivative called the Dirac pseudo-function (Novikov [1], Lundgren, [2], Kollmann [3], Pope [4], Fox [5]). The pdes in the spatial description for the Cdf and Pdf are derived in the present chapter for turbulent flows of an incompressible fluid plus passive scalars to analyse to role of convection, molecular transport and the pressure. The molecular transport properties are for convenience simplified in such a way that the kinematic viscosity has the same value as the diffusivity $\tilde{\nu} = \tilde{D}$

$$Sc \equiv \frac{\tilde{\mu}}{\tilde{\rho}\tilde{D}} \quad (11.1)$$

(i.e. Prandtl/Schmidt number Sc is unity) for the passive scalar field. All equations are given in dimensionless form assuming the existence of suitable reference values.

The case of compressible and reacting mixtures is not considered in the present section, since it has been studied extensively and detailed expositions can be found in the literature, Pope [4] Chap. 12, Poinsot et al. [6], Fox [5] Chap. 6 and references therein.

The starting point are the basic differential equations set up in the spatial/Eulerian (see Sect. 2.1.1 for definitions) or material/Lagrangean (Sect. 2.5.2) description in a Cartesian system of coordinates, the spatial description is preferred for the analysis of phenomena driven by spatial derivatives since spatial derivatives in the material description are highly nonlinear expressions. Mass and momentum balances for incompressible fluids are thus given by (2.6) and (2.7)

$$\frac{\partial v_\alpha}{\partial x_\alpha} = 0, \quad \frac{\partial v_\alpha}{\partial t} + v_\beta \frac{\partial v_\alpha}{\partial x_\beta} = -\frac{1}{\rho} \frac{\partial p}{\partial x_\alpha} + \frac{1}{Re} \frac{\partial^2 v_\alpha}{\partial x_\beta \partial x_\beta}$$

A passive scalar obeys the generic equation

$$\frac{\partial \Phi}{\partial t} + v_\beta \frac{\partial \Phi}{\partial x_\beta} = Q(\Phi) + \frac{1}{ScRe} \frac{\partial^2 \Phi}{\partial x_\beta \partial x_\beta} \quad (11.2)$$

with $\tilde{D} = \tilde{\nu}$, hence $Sc = 1$, for convenience. The flow domain is denoted by \mathcal{D} and its boundary by $\partial\mathcal{D}$. Consider now N distinct, fixed points $\mathbf{x}^{(i)} \in \mathcal{D}$ and a common instant t . First, the cumulative distribution function (Cdf) and then two equivalent versions of the pde for the probability density function (Pdf) of the values of velocity and scalar at those N points in the flow domain and the same time t , will be established.

The N -point Cdf F_{4N} is derived from first principles. For this purpose, the course-grained Cdf \hat{F}_{4N} is defined with the aid of the Heaviside step function $H(x - x_0)$

$$\hat{F}_{4N} \equiv \prod_{i=1}^N H(\varphi_i - \Phi(\mathbf{x}^{(i)}, t))H(v_i - v(\mathbf{x}^{(i)}, t)) \quad (11.3)$$

where $N \geq 1$ indicates the number of points in the flow field, H denotes the standard step or Heaviside function

$$H(x) \equiv \begin{cases} 1 & \text{for } x \geq 0 \\ 0 & \text{for } x < 0 \end{cases} \quad (11.4)$$

The step function of a vector argument is for Cartesian coordinates the product of the step functions of the individual components. Derivatives of the course-grained Cdf are defined as distributional or weak derivatives, see Gelfand and Shilov [7] for theorems and proofs.

It is easy to show that the expectation of the course-grained Cdf \hat{F}_{4N} is the Cdf F_{4N}

$$\langle \hat{F}_{4N} \rangle = F_{4N}(v_1, \dots, v_N, \varphi_1, \dots, \varphi_N; \mathbf{x}^{(1)}, \dots, \mathbf{x}^{(N)}, t) \quad (11.5)$$

of the variables $v(\mathbf{x}^{(i)}, 1)$, $\Phi(\mathbf{x}^{(i)}, t)$ at the N points in the flow field (the semicolon separates the probabilistic variables from parameters location and time).

The necessary tools for the derivation of the transport pdes are the spatial and temporal derivatives of the step function \hat{F}_{4N} . Implicit differentiation leads to

$$\frac{\partial \hat{F}_{4N}}{\partial t} = - \sum_{i=1}^N \left\{ \frac{\partial v_\alpha}{\partial t}(\mathbf{x}^{(i)}, t) \frac{\partial \hat{F}_{4N}}{\partial v_\alpha^i} + \frac{\partial \Phi}{\partial t}(\mathbf{x}^{(i)}, t) \frac{\partial \hat{F}_{4N}}{\partial \varphi_i} \right\} \quad (11.6)$$

and

$$\frac{\partial \hat{F}_{4N}}{\partial x_\alpha^{(j)}} = - \frac{\partial v_\beta}{\partial x_\alpha^{(j)}}(\mathbf{x}^{(j)}, t) \frac{\partial \hat{F}_{4N}}{\partial v_\beta^j} - \frac{\partial \Phi}{\partial x_\alpha^{(j)}}(\mathbf{x}^{(j)}, t) \frac{\partial \hat{F}_{4N}}{\partial \varphi_j} \quad (11.7)$$

where the summation convention applies to Greek subscripts. The key to the analysis is the time derivative (11.6) as it allows to connect the derivative of the coarse-grained Cdf and ultimately the Cdf with the Navier–Stokes pdes. The pressure plays a particular role that is discussed first.

11.1 The Role of the Pressure

The pressure gradient appearing in the momentum balance (2.7) for incompressible fluids insures that mass balance remains satisfied as the flow evolves in time. The pde for the pressure $p(\mathbf{x}, t)$ can be obtained from mass and momentum balances in a few simple steps resulting in a Neumann BVP for the Poisson pde (9.19)

$$-\Delta p = \frac{\partial v_\alpha}{\partial x_\beta} \frac{\partial v_\beta}{\partial x_\alpha}$$

(the constant density is set to $\rho = 1$) with boundary conditions

$$n_\alpha \frac{\partial p}{\partial x_\alpha} = h(\mathbf{v}) \quad (11.8)$$

where \mathbf{n} denotes the unit normal vector on $\partial\mathcal{D}$ pointing outward. The boundary value h is according to (9.22)

$$h(\mathbf{v}) = n_\alpha \left[\frac{1}{Re} \frac{\partial^2 v_\alpha}{\partial x_\beta \partial x_\beta} - \frac{\partial v_\alpha}{\partial t} - v_\beta \frac{\partial v_\alpha}{\partial x_\beta} \right]$$

computed on $\partial\mathcal{D}$ using the momentum balance in the direction normal to it.

The elimination of the pressure is complete, if an explicit solution of this BVP can be found expressing p in terms of the velocity field for a specified flow domain \mathcal{D} with boundary $\partial\mathcal{D}$. Theoretically, this can be achieved with the aid of Green's functions, but is practically successful only for simple geometries, see Duffy [8] for numerous examples including compact flow domains and associated boundaries with Dirichlet, Neumann and Robin conditions.

The solution of the BVP for the Poisson pde for $p(\mathbf{x}, t)$ can be given in the form (9.21) obtained in Sect. 9.2.3

$$p(t, \mathbf{x}) = \int_{\mathcal{D}} d\nu(\mathbf{y}) G(\mathbf{x}, \mathbf{y}) \frac{\partial^2}{\partial y_\alpha \partial y_\beta} (v_\alpha v_\beta)(t, \mathbf{y}) + \int_{\partial\mathcal{D}} dA(\mathbf{y}) h(\mathbf{y}) G(\mathbf{x}, \mathbf{y}) + C \quad (11.9)$$

where C is an arbitrary constant. The Green's function $G(\mathbf{x}, \mathbf{y})$ is the solution of

$$-\Delta_{\mathbf{x}} G(\mathbf{x}, \mathbf{y}) = \delta(\mathbf{x} - \mathbf{y})$$

with homogeneous Neumann boundary conditions

$$\mathbf{n} \cdot \nabla_{\mathbf{x}} G(\mathbf{x}, \mathbf{y}) = 0$$

where \mathbf{n} denotes the unit normal vector pointing outward. It follows from this solution that the pressure depends in functional form on velocity, it depends on time in autonomous form via velocity and it depends on location \mathbf{x} parametrically. It is shown in the next section that the Green's function allows computation of the time derivative of the pressure and Gateaux/Fréchet derivatives with respect to velocity.

Pressure derivatives

The solution (11.9) of the Poisson pde for the pressure allows computation of derivatives of the pressure that would not be accessible otherwise in explicit form. The pressure is properly denoted by $p(\mathbf{x}, t) = p[\mathbf{v}(\cdot, t); \mathbf{x}]$, where the arguments before the semicolon indicate non-local, i.e. functional, dependence and the variables after it signify local (parametric) dependence. The representation (11.9) of the pressure indicates that time derivatives act on velocity, whereas spatial derivatives act on the Green's function. The time rate of change of the pressure at the location \mathbf{x} and time t is then

$$\frac{\partial p}{\partial t} = \dot{p}[\mathbf{v}(\cdot, t), \frac{\partial \mathbf{v}}{\partial t}(\cdot, t); \mathbf{x}] \quad (11.10)$$

where \dot{p} emerges as

$$\dot{p}[\mathbf{v}, \frac{\partial \mathbf{v}}{\partial t}; \mathbf{x}] = \int_{\mathcal{D}} d\nu(\mathbf{y}) G(\mathbf{x}, \mathbf{y}) \frac{\partial^3}{\partial y_\alpha \partial y_\beta \partial t} (v_\alpha v_\beta)(t, \mathbf{y}) + \int_{\partial \mathcal{D}} dA(\mathbf{y}) \frac{\partial h}{\partial t}(\mathbf{y}) G(\mathbf{x}, \mathbf{y}) \quad (11.11)$$

depending on the third, mixed derivative of the velocity product in the volume integral and on the time derivatives of the boundary value on the surface integral. Likewise, spatial derivatives of the pressure can be evaluated as they act on the Green's function.

The Gateaux/Fréchet derivative of pressure with respect to velocity requires a way to express the surface integral as a volume integral. The explicit form of the Neumann boundary values (9.22)

$$h(\mathbf{y}) = n_\alpha h_\alpha, \quad h_\alpha = \frac{1}{Re} \frac{\partial^2 v_\alpha}{\partial y_\beta \partial y_\beta} - \frac{\partial v_\alpha}{\partial t} - v_\beta \frac{\partial v_\alpha}{\partial y_\beta}$$

where $n_\alpha(\mathbf{x}, \partial \mathcal{D})$ is the unit normal vector depending on the structure of the domain boundary $\partial \mathcal{D}$, allows evaluation of the functional derivative with the aid of the Gauss theorem for pure Neumann boundary conditions. The surface integral is then converted into a volume integral according to

$$\int_{\partial \mathcal{D}} dA(\mathbf{y}) n_\alpha h_\alpha(\mathbf{y}) G(\mathbf{x}, \mathbf{y}) = \int_{\mathcal{D}} d\nu(\mathbf{y}) \frac{\partial}{\partial y_\alpha} \left[G(\mathbf{x}, \mathbf{y}) \left(\frac{1}{Re} \frac{\partial^2 v_\alpha}{\partial y_\beta \partial y_\beta} - \frac{\partial v_\alpha}{\partial t} - v_\beta \frac{\partial v_\alpha}{\partial y_\beta} \right) \right] \quad (11.12)$$

Both terms in (11.9) have now the form of volume integrals, hence

$$\begin{aligned} p[\mathbf{v}(., t), \frac{\partial \mathbf{v}}{\partial t}; \mathbf{x}] = \\ \int_{\mathcal{D}} d\nu(\mathbf{y}) \left\{ G(\mathbf{x}, \mathbf{y}) \frac{\partial^2}{\partial y_\alpha \partial y_\beta} (v_\alpha v_\beta) + \frac{\partial}{\partial y_\alpha} \left[G(\mathbf{x}, \mathbf{y}) \left(\frac{1}{Re} \frac{\partial^2 v_\alpha}{\partial y_\beta \partial y_\beta} - \frac{\partial v_\alpha}{\partial t} - v_\beta \frac{\partial v_\alpha}{\partial y_\beta} \right) \right] \right\} \end{aligned} \quad (11.13)$$

where the arbitrary constant was set to zero. The Gateaux differential can readily be computed without difficulty according to definition (23.45) in Sect. 23.12 in Appendix A and converted to standard form (23.46) containing the desired functional derivative.

The example $\mathcal{D} = R^3$ (domain without boundary) is much simpler due to the absence of the surface integral. The Green's function is well known

$$G(\mathbf{x}, \mathbf{y}) = -\frac{1}{4\pi|\mathbf{x} - \mathbf{y}|} \quad (11.14)$$

and the Gateaux derivative of the pressure is

$$\frac{\delta p}{\delta v_\alpha(\mathbf{y}, t)} [\mathbf{v}(., t); \mathbf{x}] = 2 \frac{\partial^2 G(\mathbf{x}, \mathbf{y})}{\partial y_\alpha \partial y_\beta} v_\beta(\mathbf{y}, t) \quad (11.15)$$

and finally

$$\frac{\delta p}{\delta v_\alpha(\mathbf{y}, t)} [\mathbf{v}(., t); \mathbf{x}] = \frac{1}{2\pi} \left\{ \frac{v_\alpha(\mathbf{y}, t)}{|\mathbf{x} - \mathbf{y}|^3} - 3 \frac{(x_\alpha - y_\alpha)(x_\beta - y_\beta)v_\beta(\mathbf{y}, t)}{|\mathbf{x} - \mathbf{y}|^5} \right\} \quad (11.16)$$

This derivative represents the change of pressure at location \mathbf{x} due to a change of the velocity \mathbf{v} at location \mathbf{y} at the same time t . It is singular at $\mathbf{x} = \mathbf{y}$ due to the particular form of the Green's function (11.14).

Another example for the first Gateaux derivative with argument functions defined in compact domains \mathcal{D} with conditions for pressure and velocity specified on the boundary $\partial\mathcal{D}$ is posed as Problem (11.3) with detailed solution in Chap. 28.

11.2 Transport Equation for the Multipoint Cdf F_{4N}

Consider the Navier–Stokes system plus the pde for a single passive scalar at N distinct locations $\mathbf{x}^{(i)}$ in the flow field \mathcal{D} , hence there are $4N$ interdependent stochastic processes $\mathbf{v}(\mathbf{x}^{(i)}, t)$, $\Phi(\mathbf{x}^{(i)}, t)$ to be analysed at $3N$ Cartesian locations $\mathbf{x}^{(i)}$. The transport equation for the coarse-grained Cdf \hat{F}_{4N} (11.3) follows from the standard differentiation rules (11.6) and (11.7) and the Navier–Stokes system (2.6) and (2.7)

plus the generic scalar pde (11.2). The preliminary result for the coarse-grained Cdf is the equation

$$\begin{aligned} \frac{\partial \hat{F}_{4N}}{\partial t} + \sum_{i=1}^N v_\alpha(\mathbf{x}^{(i)}, t) \frac{\partial \hat{F}_{4N}}{\partial x_\alpha^{(i)}} + \sum_{i=1}^N \left\{ \frac{1}{ScRe} \Delta^{(i)} \Phi \frac{\partial \hat{F}_{4N}}{\partial \varphi_i} + \frac{1}{Re} \Delta^{(i)} v_\alpha \frac{\partial \hat{F}_{4N}}{\partial v_\alpha^i} \right\} \\ + \sum_{i=1}^N \left\{ Q(\Phi_i) \frac{\partial \hat{F}_{4N}}{\partial \varphi_i} - \frac{\partial}{\partial x_\alpha^{(i)}} p[\mathbf{v}(\cdot, t); \mathbf{x}] \frac{\partial \hat{F}_{4N}}{\partial v_\alpha^i} \right\} = 0 \end{aligned} \quad (11.17)$$

This equation can be viewed as the condition that the value of the Cdf \hat{F}_{4N} remains constant with time for points in phase space (the product of N copies of the product of flow domain, scalar space and velocity spaces), which move with the velocity $(v_\alpha(\mathbf{x}^{(i)}, t), \frac{1}{ScRe} \Delta^{(i)} \Phi + Q(\Phi), \frac{1}{Re} \Delta^{(i)} v_\alpha - \partial p / \partial x_\alpha)$. Hence, it can be interpreted as a generalized mass balance for the set $\mathbf{x}^{(i)}, \varphi^i, \mathbf{v}^{(i)}, i = 1, \dots, N$ of independent variables.

It is convenient to define sets of conditions for velocities and scalars at N locations by

$$\mathcal{V}_{4N} \equiv \{\mathbf{v}(\mathbf{x}^{(1)}, t) = \mathbf{v}^{(1)}, \dots, \mathbf{v}(\mathbf{x}^{(N)}, t) = \mathbf{v}^{(N)}, \Phi(\mathbf{x}^{(1)}, t) = \varphi_1, \dots, \Phi(\mathbf{x}^{(N)}, t) = \varphi_N\} \quad (11.18)$$

and for the single passive scalar at N locations

$$\mathcal{C}_N \equiv \{\Phi(\mathbf{x}^{(1)}, t) = \varphi_1, \dots, \Phi(\mathbf{x}^{(N)}, t) = \varphi_N\} \quad (11.19)$$

and for the scalar Φ at a single location ($\mathbf{x}^{(1)} = \mathbf{x}, \varphi_1 = \varphi$)

$$\mathcal{C}_i \equiv \{\Phi(\mathbf{x}^{(i)}, t) = \varphi\}, i = 1, \dots, N \quad (11.20)$$

to unclutter the transport pdes discussed in the present chapter.

Preliminary form of the transport equation for the Cdf F_{4N}

Averaging of the transport equation for coarse-grained Cdf \hat{F}_{4N} leads at once to the equation for the Cdf F_N according to (11.5). This preliminary version has the form of a balance equation for the Cdf $F_{4N}(\mathbf{v}(\mathbf{x}^{(i)}, t), \Phi(\mathbf{x}^{(i)}, t); \mathbf{x}^{(i)}, i = 1, \dots, N)$

$$\begin{aligned} \frac{\partial F_{4N}}{\partial t} + \sum_{i=1}^N \langle v_\alpha(\mathbf{x}^{(i)}, t) \frac{\partial \hat{F}_{4N}}{\partial x_\alpha^{(i)}} \rangle + \sum_{i=1}^N \left\{ \frac{1}{ScRe} \langle \Delta^{(i)} \Phi \frac{\partial \hat{F}_{4N}}{\partial \varphi_i} \rangle + \frac{1}{Re} \langle \Delta^{(i)} v_\alpha \frac{\partial \hat{F}_{4N}}{\partial v_\alpha^i} \rangle \right\} \\ + \sum_{i=1}^N \left\{ \langle Q(\Phi_i) \frac{\partial \hat{F}_{4N}}{\partial \varphi_i} \rangle - \langle \frac{\partial}{\partial x_\alpha^{(i)}} p[\mathbf{v}(\cdot, t); \mathbf{x}] \frac{\partial \hat{F}_{4N}}{\partial v_\alpha^i} \rangle \right\} = 0 \end{aligned} \quad (11.21)$$

where Sc denotes a Prandtl/Schmidt number. All expectations appearing in this equation need to be evaluated to provide expressions containing explicitly the Cdf F_k

instead of the coarse-grained version. If $k \leq N$ the term is called closed, due to the elementary reduction property of Cdfs and Pdfs (14.53), otherwise it is called non-closed, since it represents an additional unknown.

The terms in the preliminary pde for the N -point Cdf are now analysed in detail to gain an understanding for their role and importance in the evolution of the Cdf and the associated Pdf. Elementary examples are constructed to illustrate the effect of the individual terms.

Flux in physical space

The flux $F(\mathbf{j}, \mathcal{S})$ is defined as the amount of a physical property $G(\mathbf{x}, t)$ (scalar, vector or tensor) moving through an integrable, orientable surface \mathcal{S} with finite area. The surface is either closed, i.e. its boundary $\partial\mathcal{S}$ is empty, or open being spanned by the closed, rectifiable, unknotted line $\partial\mathcal{S} = \mathcal{C}$ (called circuit)

$$F(\mathbf{j}, \mathcal{S}) = \int_{\mathcal{S}} dA \mathbf{n} \cdot \mathbf{j} \quad (11.22)$$

where \mathbf{n} denotes the unit vector normal (outward if $\partial\mathcal{S}$ is empty) to \mathcal{S} and $\mathbf{j}(\mathbf{x}, t)$ the flux vector field, i.e. the amount of G transported per unit time and per unit surface area. This notion of flux is generalized to N distinct locations in the flow domain \mathcal{D} . Distinct implies that there exist disjoint, non-empty neighbourhoods $U^{(i)} \subset \mathbb{R}^3$ for each location $\mathbf{x}^{(i)}$, $U^{(i)} \cap U^{(j)} = \emptyset$ for $\forall j \neq i$. The flux F in physical space for the multipoint case follows from the application of mass balance at a point $\mathbf{x} \in U^{(i)}$

$$\langle v_{\alpha}(\mathbf{x}, t) \frac{\partial \hat{F}_{4N}}{\partial x_{\alpha}} \rangle = \frac{\partial}{\partial x_{\alpha}} \langle v_{\alpha}(\mathbf{x}, t) \hat{F}_{4N} \rangle \quad (11.23)$$

and integration over a ball centred at $\mathbf{x}^{(i)}$ according to (11.22). Application of the divergence theorem and the definition (6.4) of the angular brackets results in the flux vector field at $\mathbf{x} = \mathbf{x}^{(i)}$ (using the simplified notation $\mathbf{v}^i \equiv \mathbf{v}(\mathbf{x}^{(i)}, t)$, etc.)

$$j_{\alpha}^{(i)}(\mathbf{x}^{(i)}, t) = \langle v_{\alpha}^i \hat{F}_{4N} \rangle$$

hence is the flux vector field

$$j_{\alpha}^{(i)}(\mathbf{x}^{(i)}, t) = \int_{-\infty}^{\infty} d\Phi^1 \cdots \int_{-\infty}^{\infty} d\mathbf{v}^N v_{\alpha}^i \hat{F}_{4N} f_{4N}(\mathbf{v}^1, \dots, \Phi^N; \mathbf{x}^{(1)}, \dots, \mathbf{x}^{(N)}, t) \quad (11.24)$$

where f_{4N} is the joint Pdf of $\mathbf{v}^1, \dots, \Phi^N$ at the associated locations $\mathbf{x}^{(1)}, \dots, \mathbf{x}^{(N)}$. The definition (11.3) of the coarse-grained Cdf \hat{F}_{4N} implies

$$\langle v_\alpha^i \hat{F}_{4N} \rangle = \int_{-\infty}^{\varphi^1} d\Phi^1 \cdots \int_{-\infty}^{v^N} d\mathbf{v}^N v_\alpha^i f_{4N}(\mathbf{v}^1, \dots, \Phi^N; \mathbf{x}^{(1)}, \dots, \mathbf{x}^{(N)}, t) \quad (11.25)$$

Note that the upper limits φ^1, \dots, v^N of the integrals are probabilistic variables, thus do not depend on location or time, this dependence is contained in the Pdf $f_{4N}(\dots; \mathbf{x}^{(1)}, \dots, \mathbf{x}^{(N)}, t)$. The relation

$$f_{4N} = \frac{\partial^{4N} F_{4N}}{\partial v_1^1 \cdots \partial \Phi^N} \quad (11.26)$$

holds nearly everywhere since the Cdf F_{4N} is monotonic, hence leads to

$$\langle v_\alpha(\mathbf{x}^{(i)}, t) \hat{F}_{4N} \rangle = \int_{-\infty}^{\varphi^1} d\Phi^1 \cdots \int_{-\infty}^{v^N} d\mathbf{v}^N v_\alpha^i \frac{\partial^{4N} F_{4N}}{\partial v_1^1 \cdots \partial \Phi^N}(\mathbf{v}^1, \dots, \Phi_N; \mathbf{x}^{(1)}, \dots, \mathbf{x}^{(N)}, t) \quad (11.27)$$

and partial integration results in

$$\langle v_\alpha(\mathbf{x}^{(i)}, t) \hat{F}_{4N} \rangle = v_\alpha^i F_{4N} - d \int_{-\infty}^{v_\alpha^i} dv_\alpha^i F_{4N} \quad (11.28)$$

where $\frac{\partial v_\alpha^i}{\partial v_\alpha^i} = d$ (d is the dimension of the velocity space R^d) explains the factor of the integral. It is consistent with the corresponding expression in the Pdf equation in Sect. 11.4, since differentiation produces

$$\frac{\partial}{\partial v_\alpha^i} \langle v_\alpha(\mathbf{x}^{(i)}, t) \hat{F}_{4N} \rangle = \frac{\partial}{\partial v_\alpha^i} (v_\alpha^i F_{4N}) - d F_{4N} = v_\alpha^i f_{4N} \quad (11.29)$$

Remarkably, the result for the flux in physical space is closed as it does not generate additional unknowns.

Example: pure convection

A simple 1d-example is now constructed to illustrate the properties of the flux in physical space in the absence of all other effects. The pde for the Cdf $F(v; x, t)$ for the values v of the 1-d velocity $v(x, t)$ follows then from (11.21) and (11.28)

$$\frac{\partial F}{\partial t} + v \frac{\partial F}{\partial x} - \int_{-\infty}^v dv' \frac{\partial F}{\partial x}(v'; x, t) = 0$$

where the factor $\partial v_\alpha / \partial v_\alpha = d = 1$ in front of the integral in (11.28) is unity since the example is one-dimensional. The initial condition is set as Gaussian $F(v; x, 0) =$

$F_0(x)$, the boundary conditions are $\lim_{x \rightarrow -\infty} F(v; x, t) = 0$ and $\lim_{x \rightarrow \infty} F(v; x, t) = 1$. The solution of this IBVP is, however, rather awkward due to the presence of the integral. Differentiation with respect to v produces the pure IVP for the associated Pdf $f(v; x, t) = \partial F/\partial v$

$$\frac{\partial f}{\partial t} + v \frac{\partial f}{\partial x}(v; x, t) = 0$$

with initial condition

$$f(v; x, 0) = f_0(x) \equiv \frac{\partial F_0}{\partial x}(x) \in L^2_{(-\infty, \infty)}$$

while the boundary conditions are replaced by $f(x, t) \in L^2_{(-\infty, \infty)}$. The pde for the Pdf $f(v; x, t)$ has a simple interpretation, the values of $f(v; x, t)$ travelling with velocity v remain unchanged. The solution of this first order, hyperbolic, linear pde is straightforward

$$f(v; x, t) = f_0(x - vt)$$

The solution for the Cdf $F(v; x, t) = \int_{-\infty}^v dv' f(v'; x, t)$ follows from it by integration

$$F(v; x, t) = F_0(x - vt)$$

The solution for the Pdf $f(x, t)$ in the $v - x$ plane is plotted in Fig. 11.1 for two times and in Fig. 11.2 at $t = 0.3$ as iso-line plot. The left graph in Fig. 11.1 depicts the initial condition, where the Pdf $f(v, x, 0)$ is uniform with respect to v . The right graph shows the solution $f(v; x, t)$ at time $t = 0.3$. This motion appears in the $v - x$ plane as counterclockwise rotation around the origin during the time interval $t \in [0, \infty)$ from the angle zero at $t = 0$ to $-\pi/2$ at $t = \infty$ as Fig. 11.2 indicates. The iso-line plot of the Pdf $f(v; x, t)$ at $t = 0.3$ in Fig. 11.2 shows the invariance of the shape w.r.t. v .

Diffusive flux in scalar space

The concept of flux can be adapted to the scalar space by analogy to the physical space flux introduced in the previous section. The scalar space $\mathcal{R}_\Phi \subset \mathbb{R}^N$ is defined as the set of all realizable values φ_i of $\Phi(\mathbf{x}^{(i)}, t)$, $i = 1, \dots, N$. It follows from this definition that the straight connecting line of two realizable states representing pure mixing must be in \mathcal{S} , hence \mathcal{S} is convex. The scalar variables are bounded, which implies that \mathcal{S} is compact. The bounding surface $\partial\mathcal{S}$ of the scalar space can be quite complicated, as examples from turbulent combustion (which imposes a number of additional constraints on the scalar space) show, but it must contain a finite volume, hence is the bounding surface orientable.

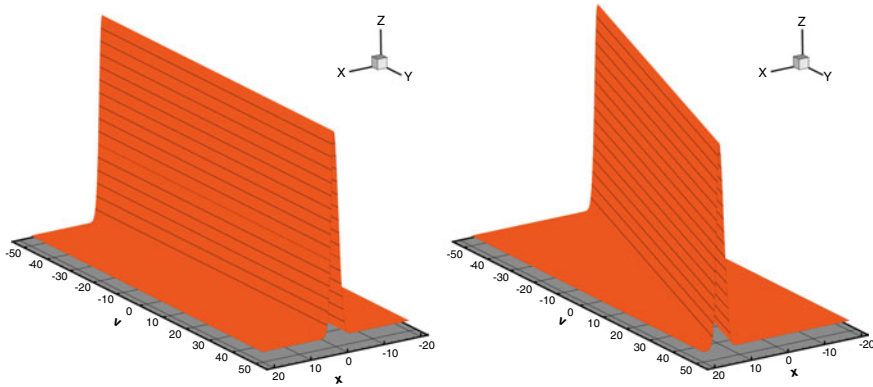


Fig. 11.1 Pure convection in physical-velocity space of the Pdf $f(v : x, t)$ for $t = 0.0$ (left graph, initial condition), and at $t = 0.3$ in the right graph. It appears as rotation around the origin without change of shape

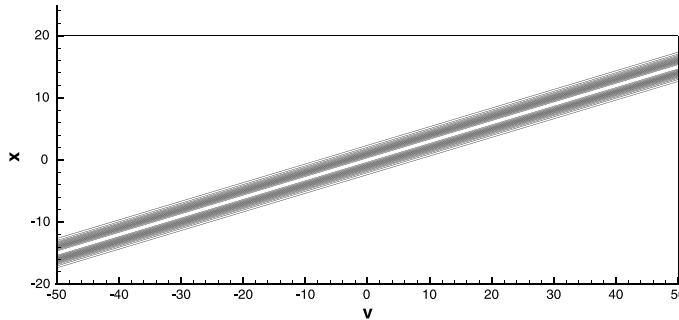


Fig. 11.2 Pure convection in physical-velocity space of the Pdf $f(v : x, t)$ for time $t = 0.3$ as isolevel plot. Convection appears as counterclockwise rotation around the origin in the first quadrant of the $v - x$ plane without change of shape of the Pdf

The divergence with respect to the scalar space variables $\varphi_i, i = 1, \dots, N$ of the diffusive flux term is according to (11.21) given by

$$\sum_{i=1}^N \frac{1}{Sc_i Re} \frac{\partial}{\partial \varphi_i} \langle \Delta^{(i)} \Phi \hat{F}_{4N} \rangle$$

which contains the flux vector field

$$\frac{1}{Sc_i Re} \langle \Delta^{(i)} \Phi \hat{F}_{4N+1} \rangle =$$

$$\frac{1}{Sc_i Re} \int_S d\Phi^1 \dots \int_{R^3 N} d\mathbf{v}^N \int_{-\infty}^{\infty} d(\Delta^{(i)} \Phi) \Delta^{(i)} \Phi \prod_{j=1}^N H(\varphi_j - \Phi^j) H(\mathbf{v}^j - \mathbf{v}^j) f_{4N+1}(\mathcal{V}_{4N}, \Delta^{(i)} \Phi, t) \quad (11.30)$$

The conditional Pdf f_c defined by

$$f_c(\Delta^{(i)}\Phi|\mathcal{V}_{4N}) = \frac{f_{4N+1}(\mathcal{V}_{4N}, \Delta^{(i)}\Phi)}{f_{4N}(\mathcal{V}_{4N})} \quad (11.31)$$

is now introduced, where the set of conditions is defined in (11.18). Note that the dimension of the joint Pdf in (11.31) is $4N + 1$ is due to N variables φ^i plus $3N$ velocity variables $\mathbf{v}(\mathbf{x}^{(i)}, t)$ plus a single variable $\Delta\Phi(\mathbf{x}^{(i)}, t)$ for each $i = 1, \dots, N$. This fact has serious consequences rendering the resulting pde indeterminate. The introduction of the conditional Pdf leads to

$$\langle \Delta^{(i)}\Phi \hat{F}_N \rangle = \int_{-\infty}^{\varphi_1} d\Phi^1 \cdots \int_{-\infty}^{\mathbf{v}^N} d\mathbf{v}^N \langle \Delta^{(i)}\Phi | \mathcal{V}_{4N} \rangle \frac{\partial^{4N} F_N}{\partial \varphi_1 \cdots \partial \mathbf{v}^N} \quad (11.32)$$

as final result (the scalar variables are set to zero outside \mathcal{S} to simplify the notation). A new unknown, the conditional expectation $\langle \Delta^{(i)}\Phi | \mathcal{V}_{4N} \rangle$, appears and the flux in scalar space is, therefore, non-closed. Consistency with the Pdf equation follows at once from the equation above by differentiation. It is important to notice the fundamental difference between the cases $N = 1$ and $N > 1$. The term actually appearing in the transport equation for the Cdf is $\frac{\partial}{\partial \varphi_i} \langle \Delta^{(i)}\Phi \hat{F}_N \rangle$, which is for $N = 1$ obviously a differential term

$$\frac{\partial}{\partial \varphi_i} \langle \Delta^{(i)}\Phi \hat{F}_1 \rangle = \frac{\partial}{\partial \varphi_i} \int_{-\infty}^{\varphi_i} d\Phi^i \langle \Delta^{(i)}\Phi | \mathcal{C}_N \rangle \frac{\partial F_1}{\partial \varphi_i} \quad (11.33)$$

given by (see Pope [9])

$$\frac{\partial}{\partial \varphi_i} \langle \Delta^{(i)}\Phi \hat{F}_1 \rangle = \langle \Delta^{(i)}\Phi | \mathcal{C}_N \rangle \frac{\partial F_1}{\partial \varphi_i} \quad (11.34)$$

whereas for $N > 1$ the integral character is preserved since the single derivative removes only one of the integrals.

Example: pure diffusion in scalar space

A simple 1-d example ($N = 1$) with $\mathcal{S} = [0, 1]$ is now constructed to illustrate the effect of the flux $\langle \Delta\Phi | \mathcal{C}_1 \rangle$ in scalar space \mathcal{R}_Φ on the evolution of the Cdf in the absence of all other effects. The pde for the Cdf $F(\varphi; x, t)$ for the values φ of the 1-d scalar $\Phi(x, t)$ follows then from (11.21) and (11.34)

$$\frac{\partial F}{\partial t} + \frac{1}{ScRe} \langle \Delta\Phi | \mathcal{C}_1 \rangle \frac{\partial F}{\partial \varphi} = 0 \quad (11.35)$$

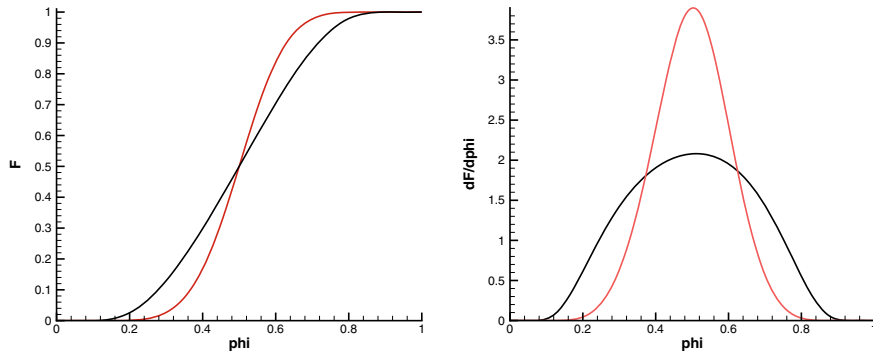


Fig. 11.3 Pure diffusion in scalar space $\mathcal{R}_\Phi = [0, 1]$ of the Cdf $F(\varphi : x, t)$ in the left graph and the Pdf $f(\varphi : x, t)$ in the right graph for $t = 0.0$ (initial condition, black line) and $t = 0.1$ (red line). The product of Schmidt and Reynolds number was set to $ScRe = 1.0$. Note that the graphs are solution of the hyperbolic pde (11.36) with a model for the flux term, they show the reduction of width corresponding to time inverse diffusion

where (11.19) is simplified to $\mathcal{C}_1 = \{\Phi(\mathbf{x}, t) = \varphi\}$. Differentiation produces the pde for the Pdf $f(\varphi; \mathbf{x}, t)$

$$\frac{\partial f}{\partial t} + \frac{1}{ScRe} \frac{\partial}{\partial \varphi} (\langle \Delta \Phi | \mathcal{C}_1 \rangle f) = 0 \quad (11.36)$$

The closure problem appears at this point, since the flux $\frac{1}{ScRe} \langle \Delta \Phi | \mathcal{C}_1 \rangle$ is not computable in terms of the Cdf $F(\varphi; x, t)$ or the Pdf $f(\varphi; x, t) = \frac{\partial F}{\partial \varphi}$. To construct an example for the flux, the interpretation of it as velocity in scalar space reducing the width of the Pdf is taken into account. Hence, the 1-d flux vector

$$\frac{1}{ScRe} \langle \Delta \Phi | \mathcal{C}_1 \rangle = \sin(\pi(2\varphi - 1))$$

is an interesting, but arbitrary choice. The boundary conditions for the pde are

$$F(0; x, t) = 0, \quad F(1; x, t) = 1$$

The initial condition $F(\varphi; x, 0) \in C_S^\infty$ with mean value $\langle \Phi \rangle = 0$ is analytically constructed and shown in the left graph of Fig. 11.3 as black line.

The pde (11.35) for the Cdf $F(\varphi; x, t)$ was solved numerically using a fourth-order uniform discretization of the scalar space $[0, 1]$ and a fourth-order Runge–Kutta time integrator. The Cdf in the left graph at time $t = 0.1$ for $ScRe = 1$ (red line) and the Pdf in the right graph shows the expected reduction in width. The asymptotic limit for the Cdf $F(\varphi; x, t)$ is in the absence of other effects the step function (11.4), the associated Pdf $f(\varphi; x, t)$ is the Dirac pseudo-function $\delta(\varphi - \langle \Phi \rangle)$. The present

example indicates that it is easy to design conditional flux vectors acting in scalar space, which have the effect to reduce the width of Cdf and Pdf.

Viscous flux in velocity space

The concept of flux can be adapted to the velocity space $\mathcal{V} = R^{3N}$ by analogy to the physical space flux introduced in Sect. 11.2. Furthermore, the viscous flux in velocity space is the analogue of the diffusive flux in scalar space $\mathcal{R}_\Phi \subset R^N$. It follows from (11.5) that

$$\frac{1}{Re} \langle \Delta^{(i)} v_\alpha \hat{F}_{4N} \rangle = \int_{-\infty}^{\varphi_1} d\Phi^1 \cdots \int_{-\infty}^{v^N} d\mathbf{v}^N \frac{1}{Re} \langle \Delta^{(i)} v_\alpha | \mathcal{V}_{4N} \rangle \frac{\partial^{4N} F_{4N}}{\partial \Phi^1 \cdots \partial \mathbf{v}^N} \quad (11.37)$$

holds. The flux in velocity space is non-closed due to the conditional moment $\frac{1}{Re} \langle \Delta^{(i)} v_\alpha | \mathcal{V}_{4N} \rangle$, which is not computable with the aid of the Cdf F_{4N} or the Pdf f_{4N} . It is consistent with the Pdf equation as can be verified by differentiation.

Example: viscous momentum diffusion in velocity space

A simple 3-d example for $N = 1$ with $\mathcal{V} = R^3$ is now constructed to illustrate the effect of the flux $\frac{1}{Re} \langle \Delta^{(i)} v_\alpha | \mathcal{V}_3 \rangle$ on the evolution of Cdf and Pdf. The pde for the Cdf for pure viscous diffusion in velocity space follows from (11.21) and (11.37)

$$\frac{\partial F_4}{\partial t}(\varphi, \mathbf{v}; t) + \frac{1}{Re} \frac{\partial}{\partial v_\alpha} \int_{-\infty}^{\varphi} d\Phi \int_{-\infty}^{\mathbf{v}} d\mathbf{v} \langle \Delta v_\alpha | \mathcal{V}_4 \rangle \frac{\partial^4 F_4}{\partial \Phi \partial \mathbf{v}} = 0$$

with boundary conditions $\lim F^4(\varphi, \mathbf{v}; t) = 0$ for $\varphi \rightarrow -\infty$ or $v_\alpha \rightarrow -\infty$ for $1 \leq \alpha \leq 3$ and $\lim F^4(\varphi, \mathbf{v}; t) = 1$ if all probabilistic variables approach ∞ . It is more convenient to solve the pure IVP for the associated pde governing the evolution of the Pdf

$$\frac{\partial f_4}{\partial t}(\varphi, \mathbf{v}; t) + \frac{1}{Re} \frac{\partial}{\partial v_\alpha} (\langle \Delta v_\alpha | \mathcal{V}_4 \rangle f_4) = 0$$

since the Pdf is in $L^2_{R^3}$ and the boundary conditions are replaced by $f(\varphi, \mathbf{v}) \in L^2_{R^3}$. Integration with respect to the scalar φ leads finally to

$$\frac{\partial f_3}{\partial t}(\mathbf{v}; t) + \frac{1}{Re} \frac{\partial}{\partial v_\alpha} (\langle \Delta v_\alpha | \mathcal{V}_3 \rangle f_3) = 0 \quad (11.38)$$

The closure problem appears at this point, since the flux $\frac{1}{Re} \langle \Delta v_\alpha | \mathcal{V}_3 \rangle$ is not computable in terms of the Cdf $F(\mathbf{v}; t)$ or the Pdf $f(\mathbf{A}; t) = \frac{\partial^3 F}{\partial v_1 \partial v_2 \partial v_3}$. To construct an example for the flux, the interpretation of it as convection in velocity space R^3 reducing the width of the Pdf is taken as guide. Hence, the 3-d vector

$$\frac{1}{Re} \langle \Delta v_\alpha | \mathcal{V}_3 \rangle = A(v_\alpha - \langle v_\alpha \rangle) \exp(-R|\mathbf{v} - \langle \mathbf{v} \rangle|) \quad (11.39)$$

with spatial decay rate $R > 0$ is an interesting, but arbitrary choice for the conditional flux vector. It is mathematically consistent with the exact term, but cannot claim quantitative physical correctness.

The IVP for the hyperbolic pde (11.38) with (11.39) can be solved numerically with standard methods for the Pdf $f(\mathbf{v}; \mathbf{x}, t)$. The results for the 2-d case governed by the hyperbolic pde

$$\frac{\partial f_2}{\partial t}(\mathbf{v}; t) + \frac{\partial}{\partial v_1} [A(v_1 - \langle v_1 \rangle) \exp(-R|\mathbf{v} - \langle \mathbf{v} \rangle|) f_2] + \frac{\partial}{\partial v_2} [A(v_2 - \langle v_2 \rangle) \exp(-R|\mathbf{v} - \langle \mathbf{v} \rangle|) f_2] = 0$$

in a truncated domain \mathcal{D} with homogeneous Dirichlet boundary conditions are shown in Fig. 11.4 ($A = 2$, $R = 0.1$ in Eq. (11.39), the initial Pdf is a linear combination of 2-d Gaussians

$$f_2(\mathbf{v}; \mathbf{x}, 0) = w f_G(\mathbf{v}; \cdot) + (1 - w) f_G(\mathbf{v}; \cdot)$$

where the dot indicates the parameters location, variances and correlation coefficients for two individual Gaussians

$$f_G(v_1, v_2; \langle \mathbf{v} \rangle, \sigma_1, \sigma_2, \rho) = \frac{1}{2\pi\sigma_1\sigma_2\sqrt{1-\rho^2}} \exp\left\{-\frac{1}{2(1-\rho^2)}\left[\frac{(v_1 - \langle v_1 \rangle)^2}{\sigma_1^2} + \frac{(v_2 - \langle v_2 \rangle)^2}{\sigma_2^2} - 2\rho\frac{(v_1 - \langle v_1 \rangle)(v_2 - \langle v_2 \rangle)}{\sigma_1\sigma_2}\right]\right\}$$

located at $(1, 0.7)$ with variances $(1.2, 1.3)$ and correlation coefficient $\rho_1 = 0.2$ and at $(-1.6, -1.1)$, $(1.5, 1.7)$, $\rho_2 = 0.5$). Comparing the graphs of the Pdf at time $t = 0.01$ with $t = 0.36$ and $t = 0.54$ in Fig. 11.4, it becomes evident, that the flux model (11.39) reduces the width and builds up the Pdf near the mean vector without affecting it as indicated by the colour coding of $\frac{\partial f}{\partial t}(\mathbf{A}; t)$ with red signalling increase and blue decrease.

Source flux in scalar space

The source term $Q(\Phi, \mathbf{v})$ is assumed to be a local function of the scalar $\Phi(\mathbf{x}^{(i)}, t)$ and the velocity $\mathbf{v}(\mathbf{x}^{(i)}, t)$. It follows from (11.5) that

$$\langle Q \hat{F}_{4N} \rangle = \int_{-\infty}^{\varphi_1} d\Phi^1 \cdots \int_{-\infty}^{\mathbf{v}^N} d\mathbf{v}^N Q(\Phi^i, \mathbf{v}^i) \frac{\partial^{4N} F_{4N}}{\partial \Phi^1 \cdots \partial \mathbf{v}^N} \quad (11.40)$$

holds. This expression can be simplified, if the source term Q depends only on Φ^i and \mathbf{v}^i , because partial integration removes the dependence with respect to all the other variables. It follows that

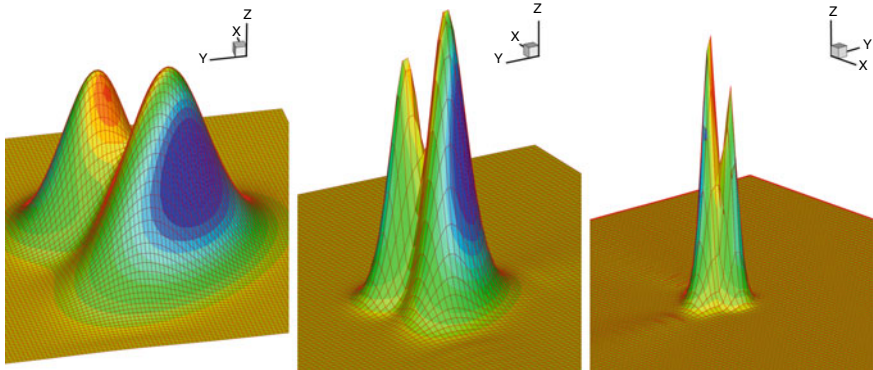


Fig. 11.4 Pure diffusion in velocity space $S = R^2$ of the Pdf $f(\mathbf{v} : \mathbf{x}, t)$ in the left graph at $t = 0.06$, at $t = 0.36$ in the middle graph and at $t = 0.54$ (end of simulation) in the right graph. The time derivative of f is colour coded with red signalling increase and blue decrease. Note that the graphs are solution of the hyperbolic pde (11.38) with an arbitrary but consistent model for the flux term, they show the reduction of width corresponding to time inverse diffusion

$$\langle Q \hat{F}_{4N} \rangle = \int_{-\infty}^{\varphi_i} d\Phi^i \int_{-\infty}^{v^i} d\mathbf{v}^i Q(\Phi^i, \mathbf{v}^i) \frac{\partial^4 F_{4N}}{\partial \Phi^i \partial \mathbf{v}^i} \quad (11.41)$$

holds, which is a closed term. For the special case that the source Q depends solely on the i^{th} -scalar Φ^i and not on velocity, the term appearing in the Cdf equation is further simplified to

$$\frac{\partial}{\partial \varphi_i} \langle Q \hat{F}_{4N} \rangle = Q(\varphi_i) \frac{\partial F_{4N}}{\partial \varphi_i} \quad (11.42)$$

Consistency with the Pdf equation (11.50) established below becomes evident by differentiation of (11.42).

Example: source flux in scalar space

The 1-d scalar space $\mathcal{R}_\Phi = [0, 1]$ is used for the example of pure source flux, the example for the source is a β -function $Q(\varphi) = AG(\varphi; \alpha_S, \beta_S)$

$$G(\varphi; \alpha, \beta) = \frac{\Gamma(\alpha + \beta)}{\Gamma(\alpha)\Gamma(\beta)} \varphi^{(\alpha-1)}(1 - \varphi)^{(\beta-1)}$$

($A = -0.3$, $\alpha_S = 9$, $\beta_S = 2$, Γ denotes the Gamma function, NIST handbook [10]). The Cdf equation (11.21) is then reduced to

$$\frac{\partial F}{\partial t}(\varphi; t) + Q(\varphi) \frac{\partial \hat{F}}{\partial \varphi}(\varphi; t) = 0$$

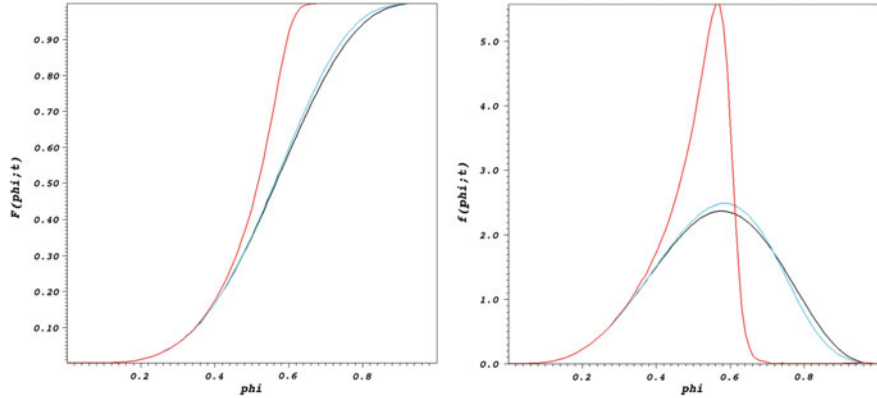


Fig. 11.5 Pure sink effect on Cdf (left graph) and Pdf (right graph): $t = 0.0$ (black line), $t = 0.17$ (light blue line), $t = 0.3$ (red line). The sink $Q(\varphi)$ is shown in Fig. 11.6, note that $Q(\varphi) = 0$ for $\varphi = 0, 1$. The effect of the sink on the Pdf is distortion and motion to smaller mean value

and the associated Pdf equation is

$$\frac{\partial f}{\partial t}(\varphi; t) + \frac{\partial}{\partial \varphi}[Q(\varphi)f(\varphi; t)] = 0$$

The IVP is defined by the boundary conditions $f(0; t) = f(1, t) = 0$ and the initial condition $f(\varphi; 0) = f_0(\varphi)$ (black lines in Fig. 11.5). The results in Fig. 11.5 for the destructive source (sink) term in Fig. 11.6 show that the effect of a source term on Cdf and Pdf is convection in scalar space. The scalar space is bounded and this implies that velocity, i.e. the source term, cannot be non-zero and constant as the Cdf/Pdf would spread outside the domain. The source is thus non-uniform and its convection is dependent on location in scalar space. This generates strong gradients and ultimately discontinuities for Cdf and Pdf. The initial Pdf is a linear combination of β -functions in the form $f(\varphi; 0) = wG(\varphi; \alpha_1, \beta_1) + (1 - w)G(\varphi; \alpha_2, \beta_2)$ with $w = 0.95$ and $\alpha = (4, 7)$, $\beta = (3, 4)$.

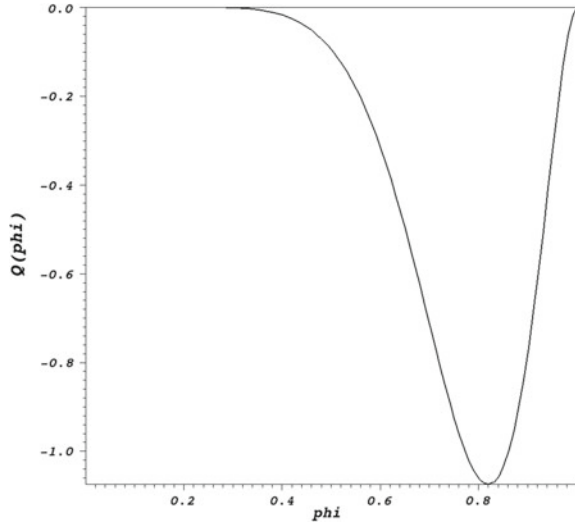
Pressure flux in velocity space

It is shown in Sect. 11.1, with the aid of the Green's function (9.21) leading to the representation of the pressure (11.9), that the pressure gradient term in (11.21)

$$\langle \frac{\partial p}{\partial x_\alpha^{(i)}} \hat{F}_{4N} \rangle = \int_{-\infty}^{\varphi_1} d\Phi^1 \dots \int_{-\infty}^{v^N} d\mathbf{v}^N \langle \frac{\partial p}{\partial x_\alpha^{(i)}} | \mathcal{V}_{4N} \rangle \frac{\partial^{4N} F_{4N}}{\partial \Phi^1 \dots \partial \mathbf{v}^N} \quad (11.43)$$

has non-local character. To represent the non-local properties, a compact notation is introduced. The $4N$ variables are abbreviated by $\xi^{(i)} \equiv \{\Phi^1(\mathbf{x}^{(i)}), \mathbf{v}^1(\mathbf{x}^{(i)}), \dots,$

Fig. 11.6 Sink term $Q(\varphi)$ in Pdf equation (11.42)



$\Phi^N(\mathbf{x}^{(i)}), \mathbf{v}^N(\mathbf{x}^{(i)})\}$ and the possible values by $\omega^{(i)} \equiv \{\varphi_1^{(i)}, \dots, \varphi_N^{(i)}\}$ and the integral is denoted by

$$\int_{-\infty}^{\omega^{(i)}} d\xi^{(i)} \equiv \int_{-\infty}^{\varphi_1} d\Phi^1 \cdots \int_{-\infty}^{\varphi_N} d\mathbf{v}^N$$

where the variables $\xi^{(i)}$ are associated with the location $\mathbf{x}^{(i)}$. Furthermore, the pressure gradient term (11.43) is written in general form as

$$\langle \frac{\partial p}{\partial x_\alpha^{(i)}} \hat{F}_{4N} \rangle = \int_{-\infty}^{\omega^{(i)}} d\xi^{(i)} \int_{-\infty}^{\omega} d\xi \langle \frac{\partial p}{\partial x_\alpha^{(i)}} | \mathcal{V}_{4N} \rangle \frac{\partial^{8N} F_{8N}}{\partial \xi^{(i)} \partial \xi} \quad (11.44)$$

where $\xi = \{\Phi^1(\mathbf{y}), \dots\}$ and $\omega = \{\varphi_1, \dots\}$ are associated with a location \mathbf{y} different from $\mathbf{x}^{(i)}$. If the conditional expectation of the pressure gradient is known as function of $\xi^{(i)}$, the general form (11.44) is immediately reduced to (11.43). The general form allows substitution of the pressure gradient (11.9) resulting in

$$\begin{aligned} \langle \frac{\partial p}{\partial x_\alpha^{(i)}} \hat{F}_{4N} \rangle &= \int_{\mathcal{D}} d\nu(\mathbf{y}) \int_{-\infty}^{\omega^{(i)}} d\xi^{(i)} \int_{-\infty}^{\omega} d\xi \frac{\partial}{\partial x_\alpha^{(i)}} G(\mathbf{x}^{(i)}, \mathbf{y}) \frac{\partial^2}{\partial y_\beta \partial y_\gamma} \langle v_\beta v_\gamma | \mathcal{V}_{4N} \rangle \frac{\partial^{8N} F_{8N}}{\partial \xi^{(i)} \partial \xi} \\ &+ \int_{\partial\mathcal{D}} dA(\mathbf{y}) \int_{-\infty}^{\omega^{(i)}} d\xi^{(i)} \int_{-\infty}^{\omega} d\xi \frac{\partial}{\partial x_\alpha^{(i)}} G(\mathbf{x}^{(i)}, \mathbf{y}) \langle h(\mathbf{y}) | \mathcal{V}_{4N} \rangle \frac{\partial^{8N} F_{8N}}{\partial \xi^{(i)} \partial \xi} \end{aligned} \quad (11.45)$$

where the boundary values h are given by (9.22). The appearance of F_{8N} indicates statistical interdependence of $\xi^{(i)}$ and ξ .

11.3 Cdf Equation in Terms of Conditional Fluxes

The expressions (11.37) to (11.43) can be used to obtain a new version of the transport equation for the Cdf F_{4N}

$$\begin{aligned}
 \frac{\partial F_{4N}}{\partial t} + \sum_{i=1}^N \{ v_\alpha^i \frac{\partial F_{4N}}{\partial x_\alpha^{(i)}} - \int_{-\infty}^{v_\alpha^i} dv_\alpha^i \frac{\partial F_{4N}}{\partial x_\alpha^{(i)}} \} + \sum_{i=1}^N \{ \frac{1}{ScRe} \frac{\partial}{\partial \varphi_i} \int_{-\infty}^{\varphi_1} d\Phi^1 \dots \int_{-\infty}^{v^N} d\mathbf{v}^N \langle \Delta^{(i)} \Phi | \mathcal{V}_{4N} \rangle \frac{\partial^{4N} F_{4N}}{\partial \Phi^1 \dots \partial \mathbf{v}^N} \\
 + \frac{1}{Re} \frac{\partial}{\partial v_\alpha^i} \int_{-\infty}^{\varphi_1} d\Phi^1 \dots \int_{-\infty}^{v^N} d\mathbf{v}^N \langle \Delta^{(i)} v_\alpha | \mathcal{V}_{4N} \rangle \frac{\partial^{4N} F_{4N}}{\partial \Phi^1 \dots \partial \mathbf{v}^N} \} \\
 + \sum_{i=1}^N \{ \frac{\partial}{\partial \varphi_i} \int_{-\infty}^{\varphi_i} d\Phi^i \int_{-\infty}^{v^i} d\mathbf{v}^i Q(\Phi^i, \mathbf{v}^i) \frac{\partial^4 F_{4N}}{\partial \Phi^i \partial \mathbf{v}^i} - \frac{\partial}{\partial v_\alpha^i} \int_{-\infty}^{\varphi_1} d\Phi^1 \dots \int_{-\infty}^{v^N} d\mathbf{v}^N \langle \frac{\partial p}{\partial x_\alpha^{(i)}} | \mathcal{V}_{4N} \rangle \frac{\partial^{4N} F_{4N}}{\partial \Phi^1 \dots \partial \mathbf{v}^N} \} = 0
 \end{aligned} \tag{11.46}$$

This version is not suitable for the limit $N \rightarrow \infty$, since it contains the N -dimensional Lebesgue measure for which no useful limit exists. However, the transport equation (11.46) has for $N < \infty$ several noteworthy properties. First, it should be noted, that the special case of a single scalar in homogeneous turbulence with source $Q(\Phi)$ allows simplification. It follows that the Cdf for the single scalar is governed by

$$\frac{\partial F}{\partial t} + \{ \frac{1}{ScRe} \langle \Delta \Phi | \Phi = \varphi \rangle + Q(\varphi) \} \frac{\partial F}{\partial \varphi} = 0 \tag{11.47}$$

which does not contain an integral with respect to the scalar value φ . The hyperbolic equation (11.47) expresses the fact that the value of the Cdf remains constant for points moving with the velocity $\frac{1}{ScRe} \langle \Delta \Phi | \Phi = \varphi \rangle + Q(\varphi)$. The conclusion is reached that the structure of the Cdf equation for $N = 1$ and $N > 1$ is fundamentally different and methods developed for $N = 1$ cannot be expected to carry over to $N > 1$ without major modifications.

11.4 Pdf Equation in Terms of Conditional Expectations

The transport equation for the Cdf can be used to obtain the equation for the Pdf f_N by differentiation according to

$$f_{4N} = \frac{\partial^{4N} F_{4N}}{\partial v_1^1 \dots \partial \varphi_N} \tag{11.48}$$

The definition (11.3) of \hat{F}_{4N} implies that f_{4N} is also given by

$$f_{4N} = \langle \hat{f}_{4N} \rangle = \langle \prod_{i=1}^N \delta(\varphi_i - \Phi(\mathbf{x}^{(i)}, t)) \delta(v_i - \mathbf{v}(\mathbf{x}^{(i)}, t)) \rangle \quad (11.49)$$

since the derivative of the step function is the Dirac pseudo-function, as originally introduced by Lundgren [2]. The pde governing the Pdf f_N emerges then as

$$\begin{aligned} \frac{\partial f_{4N}}{\partial t} + \sum_{i=1}^N v_\alpha^i \frac{\partial f_{4N}}{\partial x_\alpha^{(i)}} + \sum_{i=1}^N \left\{ \frac{\partial}{\partial \varphi_i} \left[\left\langle \frac{1}{ScRe} \Delta^{(i)} \Phi \middle| \mathcal{V}_{4N} \right\rangle + \frac{\partial}{\partial v_\alpha^i} \left(\frac{1}{Re} \langle \Delta^{(i)} v_\alpha \middle| \mathcal{V}_{4N} \rangle f_{4N} \right) \right] \right. \\ \left. + \sum_{i=1}^N \left\{ \frac{\partial}{\partial \varphi_i} [Q(\Phi^i, \mathbf{v}^i) f_{4N}] - \frac{\partial}{\partial v_\alpha^i} \left[\left\langle \frac{\partial p}{\partial x_\alpha^{(i)}} \middle| \mathcal{V}_{4N} \right\rangle f_{4N} \right] \right\} \right\} = 0 \end{aligned} \quad (11.50)$$

where the abbreviations (11.18)–(11.20) for conditioning events were used to shorten the equation. It is formally of local (non-integral) character in scalar-velocity space. It reduces for a single scalar to the well-known equation

$$\frac{\partial f}{\partial t} + \langle v_\alpha | \mathcal{C}_1 \rangle \frac{\partial f}{\partial x_\alpha} + \frac{\partial}{\partial \varphi} \left\{ \left[\frac{1}{ScRe} \langle \Delta \Phi | \mathcal{C}_1 \rangle + Q(\varphi) \right] f \right\} = 0 \quad (11.51)$$

which can be regarded as the condition, that the divergence of a flux in the phase space spanned by time and the scalar space is zero. Equation (11.51) and its generalization to higher dimensions (11.50) can be regarded as balance equations equivalent to mass balance in higher dimensions. The coefficients of f_N can be interpreted as velocity components and f_{4N} will remain non-negative and its integral unity.

An alternative version of the LMN hierarchy can be established by differentiating f_{4N} (11.49) with respect to time as suggested by Lundgren [2]. The main difference to (11.50) is the structure of the diffusive and viscous terms.

$$\begin{aligned} \frac{\partial f_N}{\partial t} + \frac{\partial}{\partial x_\beta} (v_\beta f_N) - \frac{\partial}{\partial x_\beta} \left(\mu \frac{\partial f_N}{\partial x_\beta} \right) - \frac{\partial}{\partial v_\alpha} \left(\left\langle \frac{\partial p}{\partial x_\alpha} \middle| \mathcal{V}_N \right\rangle f_N \right) + g_\alpha \frac{\partial f_N}{\partial v_\alpha} + \sum_{i=1}^n \frac{\partial}{\partial \varphi_i} [Q_i(\varphi_1, \dots, \varphi_n) f_N] \\ + \frac{\partial^2}{\partial v_\alpha \partial v_\gamma} \left(\langle \epsilon_{\alpha\gamma} | \mathcal{V}_N \rangle f_N \right) + \sum_{i=1}^n \frac{\partial^2}{\partial v_\alpha \partial \varphi_i} \left(\langle \epsilon_{\alpha i} | \mathcal{V}_N \rangle f_N \right) + \sum_{i=1}^n \sum_{j=1}^n \frac{\partial^2}{\partial \varphi_i \partial \varphi_j} \left(\langle \epsilon_{ij} | \mathcal{V}_N \rangle f_N \right) = 0 \end{aligned} \quad (11.52)$$

where the dissipation rates are defined by

$$\epsilon_{\alpha\gamma} \equiv \frac{1}{Re} \frac{\partial v_\alpha}{\partial x_\beta} \frac{\partial v_\gamma}{\partial x_\beta}, \quad \epsilon_{ij} \equiv \frac{1}{Re} \frac{\partial \Phi_i}{\partial x_\beta} \frac{\partial \Phi_j}{\partial x_\beta}, \quad \epsilon_{\alpha i} \equiv \frac{1}{ScRe} \frac{\partial v_\alpha}{\partial x_\beta} \frac{\partial \Phi_i}{\partial x_\beta} \quad (11.53)$$

using the assumption $Sc_i = 1, \forall i$ introduced at the beginning of the current section. The single scalar version emerges now in the form

$$\frac{\partial f}{\partial t} + \langle v_\alpha | \mathcal{C}_1 \rangle \frac{\partial f}{\partial x_\alpha} + \frac{\partial}{\partial \varphi} [Q(\varphi) f] = \frac{\partial}{\partial x_\alpha} \left(\frac{1}{ScRe} \frac{\partial f}{\partial x_\alpha} \right) - \frac{\partial^2}{\partial \varphi^2} (\langle \epsilon_\Phi | \mathcal{C}_1 \rangle f) \quad (11.54)$$

where the conditional dissipation rate for a single scalar is defined by

$$\langle \epsilon_\Phi | \mathcal{C}_1 \rangle = \left\langle \frac{1}{ScRe} \nabla \Phi \cdot \nabla \Phi | \mathcal{C}_1 \right\rangle \quad (11.55)$$

The important conclusion that can be drawn from this pde is the fact the diffusive terms consist of a spatial term and a term acting in scalar space with negative diffusivity. It is well known that the latter term is unconditionally unstable for numerical methods of solution.

Example: steady-state 1-d Pdf in homogenous turbulence

The interaction of source terms with the viscous-diffusive terms can be illuminated in the special case of maintained homogeneous turbulence. The Pdf equation (11.50) integrated over the velocity space emerges then in the form

$$\frac{\partial}{\partial t} (f) + \sum_{j=1}^n \frac{\partial}{\partial \varphi_j} (Q_j(\varphi_1, \dots, \varphi_l) f) = - \sum_{j=1}^n \sum_{k=1}^n \frac{\partial^2}{\partial \varphi_j \partial \varphi_k} (\langle \epsilon_{jk} | \mathcal{C} \rangle f) \quad (11.56)$$

where the condition is defined by (11.18) $\mathcal{C} \equiv \{\mathbf{v}(\mathbf{x}^{(1)}, t) = \mathbf{v}^{(1)}, \Phi_1(\mathbf{x}^{(1)}, t) = \varphi_1^{(1)}, \dots, \Phi_N(\mathbf{x}^{(1)}, t) = \varphi_N^{(1)}\}$. The case of a single scalar variable ($N = 1$) is of particular interest. Integration over the scalar interval $(-\infty, \varphi)$ leads to

$$\frac{\partial}{\partial t} (F) + Q(\varphi) f + \frac{\partial}{\partial \varphi} \{ \langle \epsilon_{11} | \mathcal{C}(\simeq) \rangle f \} = 0 \quad (11.57)$$

where F is the distribution function associated with the Pdf f . For statistically stationary turbulence, it follows that the Pdf $f(\varphi)$ is governed by

$$Q(\varphi) f(\varphi) + \frac{d}{d\varphi} \{ \langle \epsilon_{11} | \mathcal{C} \rangle f(\varphi) \} = 0 \quad (11.58)$$

This ode can be solved easily for the Pdf $f(\varphi)$ and

$$f(\varphi) = N \langle \epsilon_{11} | \mathcal{C} \rangle^{-1} \exp \left\{ - \int_{-\infty}^{\varphi} d\varphi' \frac{Q(\varphi')}{\langle \epsilon_{11} | \mathcal{C}(\varphi') \rangle} \right\} \quad (11.59)$$

is obtained as general solution. The constant N is determined by the normalization requirement

$$N^{-1} = \int_{-\infty}^{\infty} d\varphi \langle \epsilon_{11} | \mathcal{C} \rangle^{-1} \exp \left\{ - \int_{-\infty}^{\varphi} d\varphi' \frac{Q(\varphi')}{\langle \epsilon_{11} | \mathcal{C}(\varphi') \rangle} \right\} \quad (11.60)$$

This solution has several interesting properties.

(1) The influence of turbulence on the scalar Pdf $f(\varphi)$ is contained in the conditional expectation of the scalar dissipation rate $\langle \epsilon_{11} | \mathcal{C}(\varphi) \rangle$. Scaling arguments based on Kolmogorov's hypotheses applied to scalar fluctuations suggest that ϵ_{11} and φ should be statistically independent for sufficiently high Reynolds numbers.

(2) If this statistical independence was correct, it would follow that the Pdf $f(\varphi)$ is essentially determined by the source $Q(\varphi)$ and the dissipation rate $\langle \epsilon_{11} \rangle$ would be controlling its width.

(3) A source $Q(\varphi)$ linear in φ leads to the Gaussian Pdf. This can only be correct for an unbounded variable φ . For bounded variables such as temperature or mass fractions, it follows for the linear source Q that ϵ_{11} must be correlated with φ in order to create a Pdf restricted to the range of φ . This holds even in the limit of infinite Reynolds number.

Summary

The approach for the derivation of the transport pdes for CDfs and Pdfs using the Dirac pseudo-function is an alternative to the derivation from the fde for the characteristic functional in this chapter. The main result discussed in the present section is the structure of the diffusive term in the Pdf pde, which turns out to possess a negative diffusivity with respect to the velocity–scalar space, whereas the diffusivity in physical space is positive. The diffusive term acting in physical space is unfortunately negligible except near fixed wall boundaries. Problem 11.2 illustrates the properties of the diffusive term in scalar space and presents a closure model to make the numerical solution of the Pdf pde possible. An alternative approach for the diffusion in scalar space is presented in the next section.

11.5 Problems for this Chapter

Problem 11.1 A random variable $Y(t)$ defined on \mathbb{R}^1 is specified by the Pdf

$$f_Y(t) = \frac{1}{2} \exp(-|t|)$$

Compute the characteristic function $\theta(\zeta)$ and all statistical moments using θ .

Problem 11.2 Consider the random variable $\epsilon > 0$ such that

$$\Phi = \ln\left(\frac{\epsilon}{\epsilon_0}\right)$$

is Gaussian with mean $\langle \Phi \rangle$ and variance $0 < \sigma^2 < \infty$, $0 < \epsilon_0 < \infty$ is a reference value.

11.2.1 Compute the Pdf $f(\epsilon)$ of ϵ .

11.2.2 Determine the moments $\langle \epsilon^n \rangle$ for $n > 0$ and integer as function of $\langle \Phi \rangle$, σ and n .

11.2.3 Set $\epsilon_0 = \langle \epsilon \rangle$ and compute the ratio $\frac{\langle \epsilon^n \rangle}{\langle \epsilon \rangle^n}$.

11.2.4 Let

$$\frac{\langle \epsilon^2 \rangle}{\langle \epsilon \rangle^2} = A \left(\frac{L}{r} \right)^\mu$$

where A, L, μ are positive constants, $r > 0$ is a parameter. Establish the dependence of $\langle \epsilon^n \rangle / \langle \epsilon \rangle^n$ on $A, L/r, \mu$ and n .

Problem 11.3 Consider the dynamics of a passive scalar $0 \leq \Phi(t, \mathbf{x}) \leq 1$ in a turbulent flow. Specialize the transport pde (11.52) for the Pdf $f_N(\varphi_1, \dots, \varphi_N)$ of N scalars to the Pdf $f(\varphi)$ for a single scalar Φ and show that, the diffusive term in scalar space has negative diffusivity. You may assume that the scalar sources depend locally on the scalars only $Q(\varphi(1), \dots, \varphi^{(N)})$ and not on velocity. The following model expression for the diffusive term in scalar space (Curl [11]) is suggested

$$-\frac{\partial^2}{\partial \varphi^2} \left(\frac{1}{ScRe} \nabla \Phi \cdot \nabla \Phi \delta(\Phi(t, \mathbf{x}) - \varphi) \right) \approx \frac{c}{\tau} \left[4 \int_0^\varphi d\varphi' f(\varphi + \varphi') f(\varphi - \varphi') - f(\varphi) \right]$$

to mimic the effect of the diffusive term, where the time scale $\tau > 0$ is independent of Φ and c is a positive constant. Show that this expression

11.3.1 leaves normalization and mean unchanged;

11.3.2 reduces the variance.

Problem 11.4 Compute the Gateaux derivative with respect to $v_\alpha(\mathbf{x}, t)$ of the pressure represented in terms of the Green's function as shown in Sect. 11.1 for non-homogeneous Neumann conditions for the pressure and homogeneous Dirichlet boundary conditions for the momentum balances. Specialize the Gateaux derivative to harmonic directions.

Problem 11.5 Consider the turbulent flow of an incompressible Newtonian fluid in a compact domain \mathcal{D} and the special case of homogeneous, isotropic turbulence in $\mathcal{D} = \mathbb{R}^3$. The dynamics of the velocity gradient tensor (or rate of deformation) (2.113)

$$A_{\alpha\beta}(t, \mathbf{x}) \equiv \frac{\partial v_\alpha}{\partial x_\beta}$$

in the spatial description are to be analysed. The pde for $A_{\alpha\beta}$ has been derived in Sect. 2.7, Eq. (2.116)

$$\frac{\partial A_{\alpha\beta}}{\partial t} + v_\gamma \frac{\partial A_{\alpha\beta}}{\partial x_\gamma} = -A_{\alpha\gamma} A_{\gamma\beta} - P_{\alpha\beta} + \frac{1}{Re} \frac{\partial^2 A_{\alpha\beta}}{\partial x_\gamma \partial x_\gamma}$$

where external forces are absent. It contains the pressure Hessian (2.117)

$$P_{\alpha\beta} \equiv \frac{\partial^2 p}{\partial x_\alpha \partial x_\beta}$$

Carry out the following steps:

11.5.1 Decompose the pressure Hessian into a traceless and a nonzero trace contribution in terms of the velocity gradient tensor and compute the traceless part with the aid of a Green's function for a compact domain with Neumann boundary conditions for the pressure and the domain $\mathcal{D} = R^3$.

Hint: Consult Appendix D, Chap. 26, for the construction of Green's functions.

11.5.2 Decompose the velocity gradient tensor into a symmetric $S_{\alpha\beta}$ and antisymmetric part $W_{\alpha\beta}$. Derive the transport pdes for both.

11.5.3 Establish the pde for the Pdf $f(\mathbf{a}; \mathbf{x}, t)$ for the values $a_{\alpha\beta}$ of the velocity gradient tensor $A_{\alpha\beta}$ at a single point $\mathbf{x} \in \mathcal{D} = R^3$ for homogeneous, isotropic turbulence using the approach of this chapter.

References

1. Novikov, E.A.: Functionals and the random-force method in turbulence theory. Sov. Phys. JETP **20**, 1290–1294 (1965)
2. Lundgren, T.S.: Distribution functions in the statistical theory of turbulence. Phys. Fluids **10**, 969–975 (1967)
3. Kollmann, W.: The pdf approach to turbulent flow. Theoret. Comput. Fluid Dyn. **1**, 249–285 (1990)
4. Pope, S.B.: Turbulent Flows. Cambridge University Press, Cambridge, U.K. (2001)
5. Fox, R.O.: Computational Models for Turbulent Reacting Flows. Cambridge University Press, U.K. (2003)
6. Poinsot, T., Veynante, D.: Theoretical and Numerical Combustion. R.T. Edwards, Philadelphia, PA (2001)
7. Gelfand, I.M., Shilov, G.E.: Generalized Functions, vol. 1. Academic Press, New York (1964)
8. Duffy, D.G.: Green's Functions with Applications. Chapman & Hall/CRC, Boca Raton, Florida (2001)
9. Pope, S.B.: Mapping closures for turbulent mixing and reaction. Theoret. Computat. Fluid Dyn. **2**, 255–270 (1991)
10. Olver, F.W., Lozier, D.W., Boisvert, R.F., Clark, C.W.: NIST Handbook of Mathematical Functions. Cambridge University Press, U.K. (2010)
11. Curl, R.L.: Dispersed phase mixing: part i. Theory and effects in simple reactors. AIChE J. **9**, 175–181 (1963)

Chapter 12

Properties and Construction of Mappings



The idea of Chen et al. [1], abbreviated by CCK to apply mappings as tool to construct a closed form of the Pdf equations and to devise methods for their numerical solution (Kraichnan [2], Feng [3], Pope [4]) proved very successful for the case of a single scalar variable in homogeneous and non-homogeneous turbulence, in particular turbulent combustion, Pope [5], Valiño et al. [6]. This goal is achieved by avoiding the Pdf equation altogether and solving the mapping equation instead, recovering the Pdf via a local relation involving the Jacobian of the mapping. This approach overcomes the difficulty encountered in equations governing the evolution of Pdfs, where the effect of molecular diffusion is to reduce the width of the Pdf via a second derivative term with negative diffusivity. The resulting pde in this case is numerically always unstable and alternatives are essential, the mapping method discussed in the present section is one of them.

However, it is not clear how powerful this approach is for the case of more than one variable (Pope [5]) or for different formulations of the statistical equations governing turbulent flows. It will be shown in the present section that the idea of mappings can be put on a general footing and equations determining the mapping can be established. Hence, the horizon is opened to the idea of mappings as a way to treat turbulence. In particular, a closer look to the multidimensional case in spatial and material description and the passage to infinitely many (probabilistic) variables is warranted.

The rigorous theory of fully developed turbulence on the functional level requires the determination of the probability measure (called turbulence measure) or the characteristic functional governing the dynamics of turbulent flows. This probability measure μ is defined on a Borel σ -algebra of a function space Ω , termed phase space, that contains the set of all realizable flow fields. It can be constructed as a measure relative to a Gaussian measure μ_G or other suitable reference measures, if the fundamental condition stated in Sect. 12.2 is satisfied, that the unknown turbulence measure is continuous w.r.t. the reference measure. It follows then that the probability measure μ can be regarded as the image of a Gaussian reference measure μ_G . The underlying mapping contains, therefore, the essential information on turbulence. Therefore, turbulence can be viewed as the mapping of appropriately defined function

spaces and the structure of those function spaces and the mapping relating them deserve attention.

The notion of mapping can be formulated as relation between function spaces and a general equation for such a mapping will be derived in this section. It is worth noting that the mapping equation for a single variable governed by the linear diffusion equation and taken at a single point is linear (Chen et al. [1] and Pope [5]), but not exact. It will be shown in Chap. 13 that this is due to the (closure) requirement that the single-point statistics of the image of the Gaussian random fields is equal to the single-point statistics of the unknown turbulent fields. The extension of this idea to multivariables and multipoint Pdfs/characteristic functions and the passage to the functional level requires some preparations. This will be done in the present section. The closure of Pdf equations is the vehicle to develop mapping methods and to explore their power.

It is well known that the Lebesgue measure has no extension to infinitely many variables, hence there is no obvious extension of the Cdf and Pdf equations (derived in the next chapter) to the functional level, since it contains multidimensional integrals, whose limit for infinitely many variables is either not defined or zero. The equation for the characteristic function on the other hand can be (at least formally) extended to the functional level. It follows that the characteristic function as the Fourier transform of the Pdf is the appropriate starting point for the development of mapping methods for the multidimensional case. Furthermore, it is possible to set up explicitly the Gaussian measure for infinitely many variables in terms of its characteristic functional and there exists a well-defined equation for the characteristic functional of the turbulence measure, Hopf [7]. It is possible to properly define measures relative to a Gaussian measure (Skorohod [8]). If the turbulence measure is defined in such a way, all that is left to determine is the distortion of the Gaussian measure necessary to produce the turbulence measure. This distortion must be nonlinear, since turbulence is a non-Gaussian phenomenon (Tsinober [9]) and linear transformations of Gaussian processes are Gaussian. The distortion is nothing but a mapping of the function spaces relating the Gaussian fields and the turbulence fields.

The present section is organized as follows. First, the fundamental properties and classification of mappings are introduced. Then the CCK approach applied to the one-dimensional case of a single, bounded scalar field in homogeneous turbulence is developed in detail. The CCK approach is then generalized to deal with the pde for the characteristic function and higher dimensional problems in spatial and material description.

12.1 Elementary Properties of Mappings

Mappings between spaces with a minimum of structure are considered in the present chapter to lay the foundations for the following development. Consider two non-empty sets A, B and a mapping $\mathcal{X} : A \rightarrow B$, then is the mapping called

injective iff $\forall x, y \in A : \mathcal{X}(x) = \mathcal{X}(y) \rightarrow x = y$ and $\forall x, y \in A : x \neq y \rightarrow \mathcal{X}(x) \neq \mathcal{X}(y)$ it is called

surjective iff $\forall y \in B$: there is $x \in A$: $y = \mathcal{X}(x)$ and a map \mathcal{X} is

bijective iff it is injective and surjective, i.e. it is one-to-one and onto.

Bijective mappings allow comparison of sets, for instance, two sets A, B have the same cardinality iff there exists a bijective mapping $\mathcal{X} : A \leftrightarrow B$. If the sets contain a finite number of elements, cardinality is simply the number of elements.

12.2 Bijective Mappings for Probability Measures

Specifically, let $\Omega_i, i = 1, 2$ be two sets equipped with a topology, specified by Borel σ -algebras $\mathcal{A}_i(\Omega_i), i = 1, 2$ and probability measures $\mu_i : \mathcal{A}_i \rightarrow [0, 1], i = 1, 2$, let $\mathcal{X} : \Omega_1 \rightarrow \Omega_2$ be a bijective mapping of Ω_1 onto Ω_2 , then is the mapping $\mathcal{X}(\mathcal{A}_1, \mathcal{A}_2)$ -measurable if $\mathcal{X}^{-1}\omega \in \mathcal{A}_1 \forall \omega \in \mathcal{A}_2$. If $\Omega_i, i = 1, 2$ are metric spaces, the mapping is simply called measurable (see, for instance, Vishik and Fursikov [10], Chap. II). Let $\mu_1 \equiv \mu_G$ be the known reference measure (for instance, a Gaussian) and $\mu_2 \equiv \mu_T$ the unknown turbulence measure, then the mapping approach can be successful, if the fundamental property:

The turbulence measure μ_T is continuous with respect to the reference measure μ_G is satisfied. It can be checked and hopefully proved, once sufficient properties of the turbulence measure have been rigorously established.

$$\begin{array}{ccc} \mathcal{A}_1 & \xrightarrow{\mu_G \text{ (Gaussian)}} & [0, 1] \\ \mathcal{X} \downarrow & & \downarrow Z \\ \mathcal{A}_2 & \xrightarrow{\mu_T \text{ (Turbulence)}} & [0, 1] \end{array} \quad (12.1)$$

The commutative diagram for the mapping method formulated for the probability measures $\mu_i, i = 1, 2$ is shown in (12.1). If such a mapping has been computed, then is the probability of an event in \mathcal{A}_T given by the mapping and the reference measure according to

$$\mu_T(A) = \mu_G(\mathcal{X}^{-1}(A)), \quad \forall A \in \mathcal{A}_T \quad (12.2)$$

The assumption insures that $\mathcal{X}^{-1}(A) \in \mathcal{A}_G$ holds. The mapping $\mathcal{X} : \mathcal{A}_1 \rightarrow \mathcal{A}_2$ induces a bijective mapping $Z : [0, 1] \rightarrow [0, 1]$ of the unit interval.

The notion of a mapping can be exploited for the development of turbulence theory and the purpose of closure of equations determining finite-dimensional Pdfs and characteristic functions in two distinct ways:

Method $\mathcal{M}_0(d)$

The mapping $\mathcal{X} : \mathcal{A}_1 \rightarrow \mathcal{A}_2$ is known and either the image measure μ_2 or the preimage measure μ_1 are specified. The prime example for this case is the linear map

provided by Fourier transform, which can be extended to functionals (Klauder [11], Sect. 3.8, [12]). The argument d in $\mathcal{M}_0(d)$ denotes the dimension of the argument space.

Method $\mathcal{M}_1(d)$

The mapping is unknown and either the original or the image measure is known. The prime example for this case is Kraichnan's method (originally proposed for one-dimensional image and preimage domains, CCK [1]), which is based on the well-known relation between mapped and original Pdf depending on a single variable φ

$$f(\varphi) = \frac{f_G(\eta)}{J(\eta, t)}, \quad J(\eta, t) \equiv \left| \frac{d\mathcal{X}}{d\eta} \right|, \quad \eta = \mathcal{X}^{-1}(\varphi, t) \quad (12.3)$$

where $\varphi = \mathcal{X}(\eta, t)$, J is the Jacobian (i.e. the determinant of the Jacobian matrix $\partial\mathcal{X}_\beta/\partial\eta_\alpha$ for $d > 1$) and $f_G(\eta)$ is the Gaussian reference Pdf. The extension of this method to the multidimensional case and to functionals is not trivial, it is discussed in Chap. 14.

12.2.1 Bijective Mappings for Characteristic Functionals

Let $\mathcal{N}_i, i = 1, 2$ be two nuclear vector spaces (see Sect. 5.4, Gelfand and Vilenkin [13]), let $\mathcal{X} : \mathcal{N}_1 \rightarrow \mathcal{N}_2$ be a bijective, continuous mapping of the argument space \mathcal{N}_1 onto \mathcal{N}_2 . Let $\theta[\Phi]$, $\Phi \in \mathcal{N}_1$ be a characteristic functional defined on \mathcal{N}_1 , then is its image

$$\theta_{\mathcal{X}}[\Psi] = \theta[\mathcal{X}^{-1}(\Psi)] \quad (12.4)$$

for $\Psi \in \mathcal{N}_2$. The mapping \mathcal{X} must satisfy additional constraints, such that the image of a characteristic functional is also a characteristic functional. The Bochner–Minlos theorem (Sect. 8.1) provides the conditions:

(1) The mapping must have the origin as fixed point, hence $\theta_{\mathcal{X}}[\Psi] = 1$ for $\Psi = 0$ holds.

(2) Since $|\theta[\Phi]| \leq 1$, it follows at once from (12.4) that this holds for the image $\theta_{\mathcal{X}}[\Psi]$.

(3) Since $\sum_{p,q=1}^N \theta[\Phi_p - \Phi_q] \geq 0$, $\Phi_p, \Phi_q \in \mathcal{N}_1$, $N < \infty$, $\sum_{p,q=1}^N \theta_{\mathcal{X}}[\Psi_p - \Psi_q] = \sum_{p,q=1}^N \theta[\mathcal{X}^{-1}(\Psi_p) - \mathcal{X}^{-1}(\Psi_q)] \geq 0$, $\Psi_p, \Psi_q \in \mathcal{N}_2$, $N < \infty$.

(4) Continuity of $\theta_{\mathcal{X}}$ follows from the continuity of the mapping.

It is clear that the essential constraint on continuous, bijective mappings \mathcal{X} is that the origin is fixed point. The 1-dimensional case is developed first in Sect. 13.2.

12.3 Construction of Mappings

The construction of a mapping between function spaces can be daunting task and it is instructive to consider first several examples to classify mappings and to illustrate their properties.

Non-local example

Fourier transformation,

$$\mathcal{F}[\Phi(\mathbf{x})] = \Psi(\mathbf{z}) : L^2(R^3) \rightarrow L^2(R^3)$$

provides an example for the mapping of the space L^2 of square-integrable functions defined in R^3 onto itself

$$\mathcal{F}[\Phi(\mathbf{x})] = \frac{1}{(2\pi)^3} \int_{R^3} d\mathbf{x} \exp(i\mathbf{x} \cdot \mathbf{z}) \Phi(\mathbf{x}) \quad (12.5)$$

where $\mathbf{x}, \mathbf{z} \in R^3$ and $\Phi(\mathbf{x}) \in L^2(R^3)$, real and imaginary parts of $\Psi(\mathbf{z})$ are also in $L^2(R^3)$. The value of the image field Ψ at a location $\mathbf{z} \in R^3$ depends on the values of the argument field Φ at all locations $\mathbf{x} \in R^3$, hence has the mapping induced by Fourier transformation functional (or non-local or integral) character. Mappings of this type are denoted by

$$\Psi(\mathbf{z}, t) = \mathcal{X}[\Phi(\cdot); \mathbf{z}, t] \quad (12.6)$$

using brackets to indicate the functional character, where \mathcal{X} is the general notation for the mapping and the semicolon separates functional/probabilistic arguments from parameters.

Local example

Another example is provided by the function

$$\Psi(\mathbf{x}) = \exp(\Phi(\mathbf{x})), \quad \mathbf{x} \in R^3 \quad (12.7)$$

which is real-valued and has local character. Locations in argument and image fields are identical and a change of the argument field $\Phi(\hat{\mathbf{x}})$ at a location $\hat{\mathbf{x}} \neq \mathbf{x}$ has no influence on the value of the image field at \mathbf{x} .

Generally, local mappings $\mathcal{X} : L^2(\mathcal{D}) \rightarrow L^2(\mathcal{D})$ are denoted by

$$\Psi(\hat{\mathbf{x}}, t) = \mathcal{X}(\Phi(\mathbf{Y}(\mathbf{x}, t), \hat{\mathbf{x}}, t)) \quad (12.8)$$

with bijective spatial mapping $\mathbf{Y}(\mathbf{x}, t)$

$$\hat{\mathbf{x}} = \mathbf{Y}(\mathbf{x}, t) : R^3 \rightarrow R^3 \quad (12.9)$$

using parenthesis for the arguments as for standard functions. For the example of a linear spatial mapping, $\mathbf{Y}(\mathbf{x}, t)$ emerges in Cartesian coordinates as matrix multiplication $\hat{x}_\alpha = Y_{\alpha\beta}x_\beta$.

The computational effort for functional and local mapping can be expected to be widely different. To see this, consider the n -dimensional case and compare a function mapping $\mathcal{X}[\Phi_1, \dots, \Phi_n] : R^n \rightarrow R^n$ with the Pdf $f_n(\varphi_1, \dots, \varphi_n) : R^n \rightarrow [0, 1]$, which indicates that the image domains are vastly different in dimension for $n \gg 1$. This implies that the computational effort for the function mapping may be significantly larger than for the probability density function. However, the Gaussian characteristic functional can be set up explicitly and the notion of the determinant can be extended to countably infinite many variables (see Skorohod [8], Klauder [11]), thus offering an avenue for theoretical investigations.

Example for a measure-preserving global mapping

This example determines a measure (volume) preserving mapping of subsets of R^3 as solution of an IBVP of a system of nonlinear pdes. The IBVP is set up for the turbulent flow of an incompressible fluid described in material/Lagrangean variables. Hence, the measure-preserving example is not constructed explicitly, but it is the solution of the Navier–Stokes system plus suitable initial and boundary conditions. The basic laws (mass and momentum balances) governing the motion of an incompressible fluid are transformed to the material description for the Lagrangean position field $\Phi_\alpha(\tau, \mathbf{X})$ and the pressure $P(\tau, \mathbf{X})$, where τ denotes time and \mathbf{X} the identifying label (position at the reference time), Sect. 2.5. The pdes determining the mapping of the materially invariant flow domain $\mathcal{D}(0)$ at a reference time zero onto the domain $\mathcal{D}(\tau)$ at a later time emerge then as follows. Mass balance turns out to be an algebraic constraint (2.85)

$$\frac{1}{6}\epsilon_{\alpha\beta\gamma}\epsilon_{\delta\eta\omega}F_{\alpha\delta}F_{\beta\eta}F_{\gamma\omega} = 1$$

where the left side is the Jacobian $J(\tau, \mathbf{X})$, Sect. 2.5 or [14] Sect. 2.5. Momentum balances (2.86) are a nonlinear system of pdes

$$\frac{\partial^2\Phi_\alpha}{\partial\tau^2} = -\frac{1}{2}\epsilon_{\alpha\beta\gamma}\epsilon_{\delta\eta\omega}F_{\beta\eta}F_{\gamma\omega}\frac{\partial P}{\partial X_\delta} + \frac{1}{2Re}\epsilon_{\theta\beta\gamma}\epsilon_{\delta\eta\omega}F_{\zeta\eta}F_{\phi\omega}\frac{\partial}{\partial X_\delta}\left(F_{\zeta\beta}F_{\phi\gamma}\frac{\partial^2\Phi_\alpha}{\partial X_\theta\partial\tau}\right) + G_\alpha$$

where P is the pressure divided by the constant density R for incompressible fluids and

$$F_{\alpha\beta}(\mathbf{X}, \tau) = \frac{\partial\Phi_\beta}{\partial X_\alpha}$$

denotes the Lagrangean deformation gradient, as defined in [14], Sect. 2.9. The solution $\Phi(\tau, \mathbf{X})$ for $\tau \geq 0$, $\mathbf{X} \in \mathcal{D}(0)$ of this version of the Navier–Stokes equations generates a bijective global mapping $\Phi(\tau, \mathbf{X}) : \mathcal{D}(0) \rightarrow \mathcal{D}(\tau)$ of the initial flow domain onto the domain at a later time, that is a diffeomorphism as long as the smoothness of the solution of the Navier–Stokes equations is insured, see Von Wahl [15], Seregin [16] for a detailed discussion of the regularity of solutions of the Navier–

Stokes pdes. Therefore, flows of an incompressible fluid generate a measure (volume) preserving diffeomorphism due to the particular form of mass balance. Compressible fluids are subject to compression and expansion events changing density, hence is the mapping generated by the Lagrangean position field no more measure preserving. This concludes the measure-preserving example.

The measure-preserving mapping generated by the Lagrangean position field $\Phi_\alpha(\tau, \mathbf{X})$ is, however, fundamentally different from the mapping employed by Chen et al. [1], who map the phase space Ω spanned by the solutions of the Navier–Stokes equations onto a reference space equipped with a Gaussian measure. The mapping method suggested by Chen et al. [1] (CCK) is reviewed in Chap. 13 and numerical solutions of the mapping equation are presented for the one-dimensional case. It is shown that it corresponds to a convolution of the mapping with the characteristic function and the mapping equation for it is derived. The multidimensional case is then tackled in Sect. 14.5.

12.4 Local and Global Mappings

The aim of this chapter is to summarize the essential properties of mappings of a separable Hilbert space $\hat{H} = \{\hat{\Phi}(\hat{\mathbf{x}}) | \hat{\mathbf{x}} \in \hat{\mathcal{D}}\}$ with scalar product $(\hat{\Phi}, \hat{\Psi})_{\hat{H}}$

$$(\hat{\Phi}, \hat{\Psi})_{\hat{H}} = \int_{\hat{\mathcal{D}}} d\nu \hat{\Phi}(\hat{\mathbf{x}}) \hat{\Psi}(\hat{\mathbf{x}}) \quad (12.10)$$

into another separable Hilbert space H with scalar product $(\Phi, \Psi)_H$

$$(\Phi, \Psi)_H = \int_{\mathcal{D}} d\nu \Phi(\mathbf{x}) \Psi(\mathbf{x}) \quad (12.11)$$

(separable means that the space has a countably infinite basis, the hat indicates domain of definition or preimage). The elements of \hat{H} are called reference or argument fields (of the characteristic functional, for instance) and the elements of H are the image fields, the space H is also called codomain or target space. The notation for the scalar products indicates that the spatial domains $\hat{\mathcal{D}} \in \mathbb{R}^3$ and $\mathcal{D} \subset \mathbb{R}^3$ are not necessarily identical. It is convenient for differential operations to define a bijective spatial mapping $\mathbf{Y}(t) : \hat{\mathcal{D}} \rightarrow \mathcal{D}$ with inverse mapping $\mathbf{Y}^{-1}(t) : \mathcal{D} \rightarrow \hat{\mathcal{D}}$, which is at least once continuously differentiable, further regularity conditions may be imposed at a later stage.

The basic set of requirements for mapping methods can be one of the following:

(i) The statistics of the image fields agree at least at one or several points with the turbulence fields. If they agree on all points of the flow domain \mathcal{D} an exact solution of

the Hopf fde (see Vishik and Fursikov [10]) is obtained (this aspect will be discussed in Sect. 12.4.1).

(ii) Schauder bases are constructed for preimage and image spaces and projections to finite-dimensional spaces are established by restricting the preimage and image spaces to a finite number of coordinates w.r.t. the bases (this approach will be discussed in Sect. 10.4).

Generally, the mapping $\mathcal{X} : \hat{H}(\hat{\mathcal{D}}) \rightarrow H(\mathcal{D})$, $\mathcal{D} = \mathbf{Y}(t)\hat{\mathcal{D}}$ will be time-dependent and chaotic, because the image fields must be time-dependent in order to accommodate the rapidly changing properties of turbulent flows. The mapping is denoted by $\Phi(\mathbf{x}, t) = \mathcal{X}[\hat{\Phi}(.); \mathbf{x}, t]$, $\mathbf{x} \in \mathcal{D}(t)$, where the semicolon separates argument /test fields from parameters (time, location in the flow domain, Reynolds number, etc.).

The argument field $\hat{\Phi}(\hat{\mathbf{x}}) \in \hat{H}$ and the values of the parameters, location $\hat{\mathbf{x}} = \mathbf{Y}(t, \mathbf{x})$, $\mathbf{x} = \mathbf{Y}^{-1}(t, \hat{\mathbf{x}})$, $\hat{\mathbf{x}} \in \hat{\mathcal{D}}$, $\mathbf{x} \in \mathcal{D}$ and time $t \geq 0$, determine uniquely the image field $\Phi(t, \mathbf{x}) \in H(\mathcal{D})$. The argument field and the location \mathbf{x} in the flow domain $\mathcal{D}(t)$ and time t can be varied independently. This can be seen as follows. Consider the shifted argument field $\hat{\Phi}(\hat{\mathbf{z}}) + \epsilon h_\delta(\hat{\mathbf{z}} - \mathbf{Y}(t, \mathbf{x}))$, where $\hat{\mathbf{z}} \in \hat{\mathcal{D}}$ and $h_\delta \in \hat{H}$, $\epsilon > 0$ and

$$h_\delta(\hat{\mathbf{z}} - \mathbf{Y}(t, \mathbf{x})) = \begin{cases} \geq 0 & \text{for } |\hat{\mathbf{z}} - \mathbf{Y}(t, \mathbf{x})| \leq \delta > 0 \\ 0 & \text{otherwise} \end{cases} \quad (12.12)$$

where

$$\int_{R^3} d\hat{\mathbf{z}} h_\delta(\hat{\mathbf{z}} - \mathbf{Y}(t, \mathbf{x})) = 1, \quad \mathbf{x} \in \mathcal{D}(t) \quad (12.13)$$

is a filter function with compact support. The image fields at the location $\mathbf{x} = \mathbf{Y}^{-1}(t, \hat{\mathbf{x}})$ and the time t are denoted by $\Phi(\mathbf{x}, t) = \mathcal{X}[\hat{\Phi}(.); \mathbf{x}, t]$ and $\Phi_h(\mathbf{x}, t, \epsilon) = \mathcal{X}[\hat{\Phi}(. + \epsilon h_\delta(.); \mathbf{x}, t)]$. Two cases are now possible:

(i) $\Phi_h(\mathbf{x}, t, \epsilon) \neq \Phi(\mathbf{x}, t)$ for nearly all $\hat{\mathbf{x}} \in \hat{\mathcal{D}}$ and $\epsilon > 0$. The value of the image field at a given location $\mathbf{x} = \mathbf{Y}^{-1}(\hat{\mathbf{x}}, t) \in \mathcal{D}(t)$ depends on the values of the argument field at nearly all locations $\hat{\mathbf{x}} \in \hat{\mathcal{D}}$. This implies that \mathcal{X} depends on $\hat{\Phi}(.)$ in integral/functional fashion.

(ii) There exists a subset $\hat{\mathcal{D}}_o \subset \hat{\mathcal{D}}$ such that $\Phi_h(\mathbf{x}, t) = \Phi(\mathbf{x}, t)$ holds for $\hat{\mathbf{x}} \in \hat{\mathcal{D}}_o$ and $\mu_3(\hat{\mathcal{D}} - \hat{\mathcal{D}}_o) < C\delta^3$ with $C < \infty$ as $\delta \rightarrow 0$ for all $\mathbf{x} \in \mathcal{D}(t)$. This implies the existence of a relation $\hat{\mathbf{x}} = \mathbf{Y}(\mathbf{x}, t)$, such that the mapping \mathcal{X} is local (12.8), i.e.

$$\Phi(\mathbf{x}, t) = \mathcal{X}(\hat{\Phi}(\mathbf{Y}(\mathbf{x}, t)); \mathbf{x}, t), \quad \mathbf{x} \in \mathcal{D}(t) \quad (12.14)$$

The special case of a local mapping $\Phi(\mathbf{x}, t) = \mathcal{X}(\hat{\Phi}(\mathbf{Y}(\mathbf{x}, t)); t)$ is called \mathbf{x} -autonomous and $\Phi(\mathbf{x}, t) = \mathcal{X}(\hat{\Phi}(\mathbf{Y}(\mathbf{x}, t)))$ is called fully autonomous.

Example: Pure stretching map

Let the spatial map \mathbf{Y}^{-1} be defined as pure stretching in Cartesian coordinates: $i\mathbf{Y}_{\alpha\beta}^{-1}(t) = st\delta_{\alpha\beta}$ ($\mathbf{Y}^{-1} : \hat{\mathcal{D}} \rightarrow \mathcal{D}$ denotes the inverse map) and $x_\alpha = Y_{\alpha\beta}^{-1}\hat{x}_\beta = st\hat{x}_\alpha$

with stretching rate $s > 0$ and constant, furthermore, let the Hilbert space $\hat{H}(\hat{\mathcal{D}})$ be spanned by an ONS basis $\hat{\mathcal{B}} \equiv \{\hat{f}^{k,n,m}(\hat{\mathbf{x}}), k, n, m = \dots, \hat{\mathbf{x}} \in \hat{\mathcal{D}}(t)\}$, hence

$$\hat{\Phi}(\hat{\mathbf{x}}) = \sum_{k,n,m} \hat{\varphi}_{k,n,m} \hat{f}^{k,n,m}(\hat{\mathbf{x}})$$

The scalar product (12.10) for $\hat{\Phi}, \hat{\Psi} \in \hat{H}(\hat{\mathcal{D}})$ transforms to \mathcal{D} according to

$$(\hat{\Phi}, \hat{\Psi})_{\hat{H}} = \int_{\hat{\mathcal{D}}} \hat{d}\nu \hat{\Phi}(\hat{\mathbf{x}}) \hat{\Psi}(\hat{\mathbf{x}}) = \int_{\mathcal{D}} d\nu J(t, \mathbf{x}) \hat{\Phi}(\mathbf{Y} \cdot \mathbf{x}) \hat{\Psi}(\mathbf{Y} \cdot \mathbf{x}) = \int_{\mathcal{D}} d\nu J(t, \mathbf{x}) \Phi(\mathbf{x}) \Psi(\mathbf{x})$$

where the Jacobian $J(t, \mathbf{x})$ is the determinant of the Jacobian (also called Hessian) matrix

$$J_{\alpha\beta}(t, \mathbf{x}) = \frac{\partial x_{\beta}}{\partial \hat{x}_{\alpha}}(t, \mathbf{Y}(t, \mathbf{x}))$$

The Jacobian for the pure stretching map is then the determinant of $J_{\alpha\beta} = st\delta_{\alpha\beta}$,

$$J(t) = (st)^3$$

independent of location $\hat{\mathbf{x}}$. The effect of the spatial map on the scalar product is thus

$$(\hat{\Phi}, \hat{\Psi})_{\hat{H}} = (st)^3 \int_{\mathcal{D}} d\nu \hat{\Phi}(\mathbf{Y} \cdot \mathbf{x}) \hat{\Psi}(\mathbf{Y} \cdot \mathbf{x}) = (st)^3 (\Phi, \Psi)_H$$

Translating this result to the bases for \hat{H} and H is seen that the pure stretching map \mathbf{Y}^{-1} does not change orthogonality, but only the normalization. Nonlinear mappings, however, will destroy the ONS property of a basis.

12.4.1 Construction of Global Maps

Global maps are characterized by the property that the change of the argument field in a neighbourhood of a point $\hat{\mathbf{x}}_o$ in the preimage $\hat{\mathcal{D}}$ leads to a change of the value of the image field at a location $\mathbf{x} \neq \mathbf{Y}^{-1}(\hat{\mathbf{x}}_o, t) \in \mathcal{D}$. This is recognized as functional dependence; therefore, it must be possible to express the mapping \mathcal{X} in terms of a functional. It can be achieved with a special construction, which defines a particular class of global mappings.

Consider an arbitrary Gateaux/Fréchet differentiable functional

$$\Lambda[\hat{\Phi}] : \hat{H}(\hat{\mathcal{D}}) \rightarrow \mathbb{R}^1 \quad (12.15)$$

The value $\Lambda[\hat{\Phi}]$ is then independent of location in the flow domain $\hat{\mathcal{D}}$ and derivatives with respect to location $\hat{\mathbf{x}}$ obviously vanish. The Gateaux / Fréchet differentiability of Λ in \hat{H} implies

$$\left(\frac{\delta \Lambda}{\delta \hat{\Phi}(\hat{\mathbf{x}})}, h \right) = \lim_{\epsilon \rightarrow 0} \frac{\partial}{\partial \epsilon} \Lambda[\hat{\Phi} + \epsilon h] \quad (12.16)$$

for argument fields $\hat{\Phi}, h \in \hat{H}$. This expression is justified by the Riesz–Markov–Kakutani representation theorem [17], which states that for any positive linear functional mapping a locally compact Hausdorff space $\hat{H}(\hat{\mathcal{D}})$ into R^1 : $\hat{\Phi} \in \hat{H} \rightarrow \lim_{\epsilon \rightarrow 0} \frac{\partial}{\partial \epsilon} \Lambda[\hat{\Phi} + \epsilon h] \in R^1$, there exists a unique regular Borel measure μ on $\hat{\mathcal{D}}$, such that

$$\lim_{\epsilon \rightarrow 0} \frac{\partial}{\partial \epsilon} \Lambda[\hat{\Phi} + \epsilon h] = \int_{\hat{\mathcal{D}}} \frac{\delta \Lambda}{\delta \hat{\Phi}(\hat{\mathbf{x}})} h(\hat{\mathbf{x}}) d\mu(\hat{\mathbf{x}})$$

holds for all continuous functionals $\Lambda[\hat{\Phi}(\cdot)]$. The first Fréchet derivative of Λ is then a function of the location $\hat{\mathbf{x}} \in \hat{\mathcal{D}}$. It follows from this representation that

$$\mathcal{X}[\hat{\Phi}(\cdot); \mathbf{x}] \equiv \frac{\delta \Lambda}{\delta \hat{\Phi}(\mathbf{Y}(t, \mathbf{x}))}, \quad \hat{\Phi} \in \hat{H} \quad (12.17)$$

defines a mapping of the argument/preimage space \hat{H} into some function space $H(\hat{\mathcal{D}})$. The definition of the mapping (12.17) produces for a specified argument field $\hat{\Phi}(\cdot) \in \hat{H}(\hat{\mathcal{D}})$ and location $\hat{\mathbf{x}} = \mathbf{Y}(t, \mathbf{x}) \in \hat{\mathcal{D}} \subset R^3$ (generated by the increment $h(\hat{\mathbf{x}} - \mathbf{x}) \equiv \delta(\hat{\mathbf{x}} - \mathbf{x})$) a scalar field $\mathcal{X}[\hat{\Phi}(\cdot); \hat{\mathbf{x}}]$, whose smoothness properties are inherited from the continuously differentiable functional Λ .

Example

It is straightforward to construct an example for the functional Λ

$$\Lambda[\hat{\Phi}(\cdot); t] = \int_{\hat{\mathcal{D}}} \hat{d}\nu \int_{\hat{\mathcal{D}}} d\nu' K_{\alpha\beta}(\hat{\mathbf{x}}, \mathbf{x}', t) \hat{\Phi}(\hat{\mathbf{x}}) \hat{\Phi}(\mathbf{x}')$$

with continuously differentiable and symmetric kernel, $K_{\alpha\beta}(\hat{\mathbf{x}}, \mathbf{x}', t) = K_{\beta\alpha}(\mathbf{x}', \hat{\mathbf{x}}, t)$, suitable for the design of a mapping. For convenience, the spatial map \mathbf{Y} is assumed to be the identity. The first Gateaux derivative is then

$$\begin{aligned} \left(\frac{\delta \Lambda}{\delta \hat{\Phi}(\hat{\mathbf{x}})}, h \right) &= \lim_{\epsilon \rightarrow 0} \frac{d}{d\epsilon} \Lambda[\hat{\Phi}(\cdot) + \epsilon h(\cdot); t] \\ &= \lim_{\epsilon \rightarrow 0} \frac{d}{d\epsilon} \int_{\hat{\mathcal{D}}} \hat{d}\nu \int_{\hat{\mathcal{D}}} d\nu' K_{\alpha\beta}(\hat{\mathbf{x}}, \mathbf{x}', t) (\hat{\Phi}(\hat{\mathbf{x}}) + \epsilon h(\hat{\mathbf{x}})) (\hat{\Phi}(\mathbf{x}') + \epsilon h(\mathbf{x}')) \end{aligned}$$

The limit can be computed leading to

$$\left(\frac{\delta \Lambda}{\delta \hat{\Phi}(\hat{\mathbf{x}})}, h \right) = \int_{\hat{\mathcal{D}}} \hat{d}\nu \int_{\hat{\mathcal{D}}} d\nu' K_{\alpha\beta}(\hat{\mathbf{x}}, \mathbf{x}', t) \left\{ \hat{\Phi}(\hat{\mathbf{x}})h(\mathbf{x}') + \hat{\Phi}(\mathbf{x}')h(\hat{\mathbf{x}}) \right\}$$

and

$$\left(\frac{\delta \Lambda}{\delta \hat{\Phi}(\hat{\mathbf{x}})}, h \right) = 2 \int_{\hat{\mathcal{D}}} \hat{d}\nu \int_{\hat{\mathcal{D}}} d\nu' K_{\alpha\beta}(\hat{\mathbf{x}}, \mathbf{x}', t) \hat{\Phi}(\hat{\mathbf{x}})h(\mathbf{x}')$$

The first Gateaux derivative emerges then in the form

$$\mathcal{X}[\hat{\Phi}(.); \mathbf{x}', t] \equiv \frac{\delta \Lambda}{\delta \hat{\Phi}(\mathbf{x}')} [\hat{\Phi}(0); \mathbf{x}', t] = 2 \int_{\hat{\mathcal{D}}} \hat{d}\nu K_{\alpha\beta}(\hat{\mathbf{x}}, \mathbf{x}', t) \hat{\Phi}(\hat{\mathbf{x}})$$

Defining a global mapping according to (12.17), shows that, for the example mapping, the resulting scalar field inherits for fixed argument field $\hat{\Phi}(\hat{\mathbf{x}})$ the regularity w.r.t. location \mathbf{x}' from the kernel K , i.e. the properties of the chosen functional. This concludes the example for the construction of a global mapping.

Domain mapping $\mathbf{Y}(t, \mathbf{x})$

As indicated above, a second step can be added to the design of global mappings, which are constructed as variational derivative of a functional. It is convenient for the construction of closure for the mapping equation (as will be shown in the next section) to define a mapping of the flow domains $\mathbf{Y}(\mathbf{x}, t) : \hat{\mathcal{D}}(t) \rightarrow \mathcal{D}(t)$, which is bijective, local and sufficiently smooth. Then the location $\hat{\mathbf{x}}$ in $\hat{\mathcal{D}}(t)$ can be expressed in terms of the location $\mathbf{x} \in \mathcal{D}$ by

$$\hat{\mathbf{x}} = \mathbf{Y}(t, \mathbf{x}) \quad (12.18)$$

If the functional Λ is defined in such a way that the fields generated by its Fréchet derivative are always contained in a space $H(\hat{\mathcal{D}})$ and combining the derivative with the mapping $\mathbf{Y}(\mathbf{x}, t)$ of the domains a mapping can finally be defined by

$$\mathcal{X}[\hat{\Phi}(.); \mathbf{x}, t] \equiv \frac{\delta \Lambda[\hat{\Phi}(.)]}{\delta \hat{\Phi}(\mathbf{Y}(\mathbf{x}, t))} : \hat{\mathcal{D}} \rightarrow H(\mathcal{D})$$

(12.19)

The spatial domains for the turbulent scalar field and the Gaussian reference field need not be identical, thus a mapping \mathbf{Y} relating the two is necessary.

Transport equation for global maps

The mapping \mathcal{X} defined by Eq. (12.17) is governed by the dynamics of the argument/test fields $\hat{\Phi}(\hat{\mathbf{x}}, t)$ defined in $\hat{\mathcal{D}} = \mathbf{Y}\mathcal{D}$. Let the argument/test fields be solutions of

$$\frac{\partial \hat{\Phi}}{\partial t} = \hat{R}(\hat{\Phi}(t, \hat{\mathbf{x}}), t, \hat{\mathbf{x}}) \quad (12.20)$$

with suitable initial and boundary conditions. Then is the time rate of change of the mapping

$$\boxed{\frac{\partial \mathcal{X}}{\partial t}[\hat{\Phi}(.); \mathbf{x}, \mathbf{x}', t] = \frac{\delta \mathcal{X}[\hat{\Phi}; \mathbf{x}, t]}{\delta \hat{\Phi}(\mathbf{Y}(\mathbf{x}', t))} \{\hat{\mathbf{R}}(\hat{\Phi}, \mathbf{x}', t) + \frac{\partial \mathbf{Y}}{\partial t} \cdot \nabla \hat{\Phi}\}} \quad (12.21)$$

the general form of the mapping equation. The solution of the IVP for this fde requires an initial mapping $\mathcal{X}[\hat{\Phi}(.); \mathbf{x}, 0]$ and the specification of the spatial map \mathbf{Y} . Let \mathbf{Y} be set up such that $\mathbf{Y}(0)$ is the identity map and the initial mapping $\mathcal{X}[\hat{\Phi}; \hat{\mathbf{x}}, 0]$ is also the identity map, then is the IVP completely specified. More generally, mapping equations are discussed below in Sect. 14.1 for finite-dimensional Pdf/Cdfs.

12.4.2 Construction of Local Maps

The value $\Phi(\mathbf{x}, t)$ of the image field depends on the value of the argument field $\hat{\Phi}$ at a unique location $\hat{\mathbf{x}} = \mathbf{Y}(\mathbf{x}, t)$, $\mathbf{x} \in \mathcal{D}$ determined by the domain mapping $\mathbf{Y} : \mathcal{D} \rightarrow \hat{\mathcal{D}} = \mathbb{R}^3$. If the argument field is modified at any other location no change of $\Phi(\mathbf{x}, t)$ is observed. Hence is

$$\Phi(\mathbf{x}, t) = \mathcal{X}(\hat{\Phi}(\mathbf{Y}(\mathbf{x}, t); t)) \quad (12.22)$$

a strictly, \mathbf{x} -autonomous, local map. Construction of local maps is thus reduced to the design of standard, implicit functions.

Differentiation of the image field can be carried out using the rules of standard calculus. For instance, the time derivative emerges as

$$\frac{\partial \Phi}{\partial t}(\mathbf{x}, t) = \frac{\partial \mathcal{X}}{\partial \hat{\Phi}} \frac{\partial \hat{\Phi}}{\partial Y_\alpha} \frac{\partial Y_\alpha}{\partial t} + \frac{\partial \mathcal{X}}{\partial t} \quad (12.23)$$

and likewise for the spatial derivative

$$\frac{\partial \Phi}{\partial x_\alpha}(\mathbf{x}, t) = \frac{\partial \mathcal{X}}{\partial \hat{\Phi}} \frac{\partial \hat{\Phi}}{\partial Y_\beta} \frac{\partial Y_\beta}{\partial x_\alpha} \quad (12.24)$$

Higher derivatives follow from repeated application of these operations.

12.5 Problems for this Chapter

Problem 12.1 The initial value problem (IVP) for the ode

$$\frac{dY}{dt} = -CY^2$$

with C being a positive constant and initial condition $Y(0) = Y_0 \geq 0$ generates a mapping $Y(t) : Y(0) \rightarrow \mathbb{R}^1$.

12.1.1 Compute the solution of the IVP.

12.1.2 Let the initial value Y_0 be a random variable with Pdf $f_Y(y; 0)$, determine the Pdf of $Y(t)$ for $t \geq 0$.

12.1.3 Determine the asymptotic Pdf $f_Y(y; \infty)$.

Problem 12.2 Derive the single label Pdf equation for position $\Phi_\alpha(\tau, \mathbf{X})$ in the material description. Use the coarse-grained Pdf

$$\hat{f} \equiv \prod_{\alpha=1}^3 \delta(\Phi_\alpha(\tau, \mathbf{X}) - q_\alpha)$$

and the Navier–Stokes pdes (2.85), (2.86) in the material description to follow the procedure in Chap. 11.

References

1. Chen, H., Chen, S., Kraichnan, R.H.: Probability distribution of a stochastically advected scalar field. *Phys. Rev. Lett.* **62**, 2657 (1989)
2. Kraichnan, R.H.: Models for Intermittency in Hydrodynamic Turbulence. *Phys. Rev. Lett.* **65**, 575 (1990)
3. Feng, G.: Mapping closure and non-Gaussianity of the scalar probability density functions in isotropic turbulence. *Phys. Fluids A* **3**, 2438–2444 (1991)
4. Pope, S.B.: *Turbulent Flows*. Cambridge University Press, Cambridge, U.K. (2001)
5. Pope, S.B.: Mapping closures for turbulent mixing and reaction. *Theoret. Computat. Fluid Dyn.* **2**, 255–270 (1991)
6. Valiño, L., Ros, J., Dopazo, C.: Monte-Carlo implementation and analytic solution of an inert-scalar turbulent-mixing test problem using a mapping closure. *Phys. Fluids A* **3**, 2191 (1991)
7. Hopf, E.: Statistical hydromechanics and functional calculus. *J. Rat. Mech. Anal.* **1**, 87–123 (1952)
8. Skorohod, A.V.: *Integration in Hilbert Space*. Springer, New York (1974)
9. Tsinaber, A.: *An Informal Conceptual Introduction to Turbulence*, 2nd edn. Springer, Dordrecht (2009)
10. Vishik, M.J., Fursikov, A.V.: *Mathematical Problems of Statistical Hydromechanics*. Kluwer Academic Publication, Dordrecht (1988)
11. Klauder, J.R.: *A Modern Approach to Functional Integration*. Birkhaeuser/Springer, New York (2010)

12. Vakhania, N.N., Tariedladze, V.I., Chobanyan, S.A.: Probability Distributions on Banach Spaces. D. Reidel Publishing Comp, Dordrecht (1987)
13. Gelfand, I.M., Vilenkin, N.Y.: Generalized Functions, vol. 4. Academic Press, New York (1964)
14. Kollmann, W.: Fluid Mechanics in Spatial and Material Description. University Readers, San Diego (2011)
15. Von Wahl, W.: The Equations of Navier-Stokes and Abstract Parabolic Equations. Vieweg, Braunschweig (1985)
16. Seregin, G.: Lecture Notes on Regularity Theory for the Navier-Stokes Equations. World Scientific, New Jersey (2015)
17. Rudin, W.: Functional Analysis, 2nd edn. McGraw-Hill Education (Asia), Singapore (2005)

Chapter 13

$\mathcal{M}_1(1)$: Single Scalar in Homogeneous Turbulence



The equations resulting from the treatment of marginal statistics are necessarily indeterminate, hence require additional information to obtain a solvable system of equations, a non-rigorous operation called closure. This holds also for the mapping equations, which are considered in the present section for homogeneous turbulence. The single scalar case is a convenient approach to introduce and explain mapping methods in elementary form [1], the velocity and multi-scalar, non-homogeneous cases are much more complex and discussed in the following section.

13.1 The CCK Method

The CCK mapping method developed by Chen et al. [2] has several distinct advantages over the previously constructed closure models for the Pdf equation, in particular, it offers a new way of treating diffusion in scalar space (see Chap. 12 in Pope, [3] for alternatives). It produces the Gaussian Pdf as asymptotic limit for decaying turbulence and agrees very well with DNS results for pure mixing, i.e. $Q = 0$ in Eq. (13.1), in homogeneous turbulence. The derivation of the mapping equation will be reviewed, and its variant for the characteristic function will be established in the present section.

The starting point for the CCK (Chen et al. [2]) method is Eq. (11.50) established in Sect. 11.4 governing the Pdf $f(\varphi; \mathbf{x}, t)$ for the values φ of a single scalar $\Phi(\mathbf{x}, t)$ transported by a turbulent flow field. For the 1-d/single scalar case, it is reduced to

$$\frac{\partial f}{\partial t} + \langle v_\alpha \rangle \frac{\partial f}{\partial x_\alpha} + \frac{\partial}{\partial \varphi} (Qf) = -\frac{\partial}{\partial x_\alpha} (\langle v'_\alpha | \Phi(\mathbf{x}, t) = \varphi \rangle f) - \frac{1}{Pe} \frac{\partial}{\partial \varphi} (\langle \Delta \Phi | \Phi = \varphi \rangle f) \quad (13.1)$$

where $\mathbf{x} \in \mathcal{D}$ with boundary $\partial\mathcal{D}$ and $Pe = Re Sch$ is the product of Reynolds and Schmidt or Reynolds and Prandtl numbers called Peclet number. This equation contains additional unknowns in the present form as conditional expectations $\langle v'_\alpha | \Phi(\mathbf{x}, t) = \varphi \rangle$ of velocity and the scalar diffusion term $\frac{1}{Pe} \langle \Delta \Phi | \Phi = \varphi \rangle$, the map-

ping method deals with the latter. The theory is developed for homogeneous turbulence, where the velocity correlation obviously drops out and no domain boundaries are present.

13.1.1 Single, Bounded Scalar in Homogeneous Turbulence

Consider the case of a single, bounded scalar $0 \leq \Phi(\mathbf{x}, t) \leq 1$ in homogeneous turbulence, defined by the translational invariance of all statistical properties, whence

$$\frac{\partial f}{\partial t} + \frac{\partial}{\partial \varphi}(F_\varphi f) = 0 \quad (13.2)$$

follows from (13.1). The term

$$F_\varphi \equiv Q + \frac{1}{P_e} \langle \Delta \Phi | \Phi(\mathbf{x}, t) = \varphi \rangle \quad (13.3)$$

the Pdf Eq. (13.1) is acting as flux in the scalar space $\mathcal{R}_\Phi \equiv \{\varphi = \Phi(\mathbf{x}, t) : \mathbf{x} \in \mathcal{D}, 0 \leq t < \infty\} = [0, 1]$ analogous to velocity in physical space. The pde for the corresponding Cdf is

$$\frac{\partial F}{\partial t} + F_\varphi \frac{\partial F}{\partial \varphi} = 0 \quad (13.4)$$

governing the dynamics of the the marginal turbulence measure μ according to $F(\varphi, \mathbf{x}, t) = \mu\{-\infty \leq \Phi(\mathbf{x}, t) \leq \varphi\}$, where μ in general is the set function in a measure space $(\Omega, \mathcal{A}, \mu)$ as explained in Chap. 10. The pde (13.4) for Pdf $f(\varphi; t) = \partial F / \partial \varphi$ has an elementary interpretation; it is the material invariance of the values of the Cdf $F(\varphi; \mathbf{x}, t)$ at any point moving with the formal velocity F_φ in the scalar space \mathcal{R}_Φ . The probabilistic argument (or scalar space variable) $\varphi \in \mathcal{R}_\Phi$ of Pdf and Cdf covers the range of values the scalar Φ can assume at any time t at any point \mathbf{x} in the flow field. For convenience, let the scalar Φ be normalized and the scalar space is then the unit interval, $\mathcal{R}_\Phi = [0, 1]$.

A local, \mathbf{x} -autonomous mapping $\mathcal{X}(\eta; t)$ for homogeneous turbulence is statistically governed by the reference measure μ_G and the marginal turbulence measure μ , respectively,

$$\mathcal{X}(\eta; t) : \mathcal{R}_G = \mathbb{R}^d \rightarrow \mathcal{R}_\Phi \quad (13.5)$$

($d = 1$ for the single scalar case), i.e. $\varphi = \mathcal{X}(\eta; t)$, $\varphi \in \mathcal{R}_\Phi$, $\eta = G(\hat{\mathbf{x}}) \in \mathcal{R}_G$. It is subject to two conditions:

(C1) The value of the Cdf F at the image value $\mathcal{X}(\eta; t)$ is equal to the value of the standard Gaussian Cdf F_G at the argument variable η

$$F(\mathcal{X}(\eta; t)) = F_G(\eta) \quad (13.6)$$

This requires the fundamental assumption stated in Sect. 12.2 to hold.

(C2) The mapping is monotonically increasing

$$\mathcal{X}(\eta_1; t) < \mathcal{X}(\eta_2; t) \text{ for } \eta_1 < \eta_2 \quad (13.7)$$

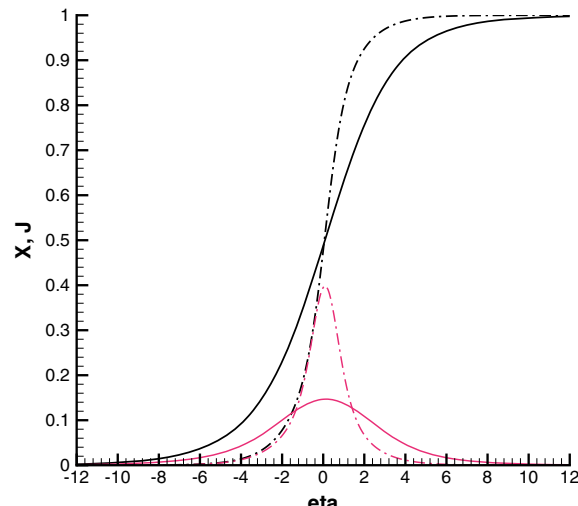
insuring the existence of a unique inverse mapping $\eta = \mathcal{X}^{-1}(\varphi; t)$. The condition (C2) is a direct consequence of the monotonicity of the Cdfs.

Mapping the domain of definition \mathcal{R}_Φ of the single-point Cdf implies that the value of the scalar $\Phi(\mathbf{x}, t)$ is the image of the reference variable $G(\hat{\mathbf{x}})$ ranging in $\mathcal{R}_G = \mathbb{R}^1$. Hence, the mapping \mathcal{X} is in general dependent on time t and in the non-homogeneous case on the location \mathbf{x} in the flow field \mathcal{D} . The first condition (13.6) requires the Gaussian reference field $G(\hat{\mathbf{x}})$, such that $\hat{\mathbf{x}} = \mathbf{Y}(t, \mathbf{x})$ and

$$F_G(\eta) = \mu_G\{G \leq \eta\} \quad (13.8)$$

hold. An example for \mathcal{X} mapping \mathbb{R}^1 onto the scalar space $\mathcal{R}_\Phi = \{0, 1\}$ and its Jacobian J is shown in Fig. 13.1. The mapping remains monotonically increasing and the effect of the diffusive term in the pde (13.23) is to spread the Jacobian like a melting ice cream cone. The evolution of the mapping is such that the neighbourhood of the origin becomes closer to linear with decreasing slope, and the Pdf approaches thus a Gaussian according to (13.28).

Fig. 13.1 Mapping $\mathcal{X}(t, \eta)$ (black lines) and its Jacobian $J(t, \eta)$ (red lines) for two time instances $t = 0$ (dot-dashed lines) and $t > 0$ (solid lines) computed as solution of equation (13.28). The unit interval on the vertical axis is the scalar space \mathcal{R}_Φ , and the horizontal η axis is the domain of definition of the Gaussian reference Pdf f_G



Correlation operator for scalars in homogeneous and isotropic turbulence

The Gaussian reference variable $G(\cdot)$ is now extended to a homogeneous Gaussian random scalar field $G(\hat{\mathbf{x}})$ in homogeneous and isotropic turbulence. The Gaussian random variable is then simply the Gaussian field $G(\hat{\mathbf{x}})$ at a specified location $\hat{\mathbf{x}} \equiv \mathbf{Y}(\mathbf{x}, t) \in R^3$. Note that this extension and thus the relation $\mathbf{Y}(\mathbf{x}, t)$ to the location \mathbf{x} in the flow field is completely arbitrary, and the mapping \mathbf{X} does not determine this relation between the locations \mathbf{x} of the image variable $\Phi(\mathbf{x}, t)$ and the location $\hat{\mathbf{x}}$ of the reference field $G(\hat{\mathbf{x}})$.

A homogeneous Gaussian scalar field is completely specified by the mean value $\langle G \rangle$, the variance $\sigma^2 = \langle (G - \langle G \rangle)^2 \rangle$ and the spatial correlation coefficient $\rho(r)$ (see [4] Sect. 5.7 for details), which is defined by

$$\rho(\mathbf{x}, \mathbf{r}) \equiv \frac{C(\mathbf{x}, \mathbf{r})}{\sqrt{\sigma^2(\mathbf{x})\sigma^2(\mathbf{x} + \mathbf{r})}}$$

where $C(\mathbf{x}, \mathbf{r}) = \langle (G(\mathbf{x}) - \langle G(\mathbf{x}) \rangle)(G(\mathbf{x} + \mathbf{r}) - \langle G(\mathbf{x} + \mathbf{r}) \rangle) \rangle$ is the covariance function and $\rho(\mathbf{x}, \mathbf{r}) \rightarrow \rho(r)$, $r = |\mathbf{x} - \mathbf{y}|$, $\mathbf{y} = \mathbf{x} + \mathbf{r}$. For homogeneous random scalar fields in homogeneous and isotropic turbulence, the covariance function is only dependent on the distance r . Explicit representations of general homogeneous and isotropic random fields in terms of orthonormalized spherical harmonics and random measures on Borel sets in R^n can be found in Yadrenko [5]. Such fields can be constructed as the sum of a large number of plane, cylindrical or spherical waves with uniformly distributed random phase. The characteristic functional for homogeneous scalar Gaussian fields is according to (9.87) then

$$\theta_G[G] = \exp\left\{-\frac{1}{2}(KG, G) + i(\langle G \rangle, G)\right\}$$

The correlation operator K for homogeneous scalar fields in homogeneous and isotropic turbulence can be represented as (Wilczek and Meneveau [6])

$$(KG, G) = \int_{R^3} d\mathbf{x} \int_{R^3} d\mathbf{x}' G(\mathbf{x}) C(\mathbf{x}, \mathbf{x}') G(\mathbf{x}') \quad (13.9)$$

where $\mathbf{x}' = \mathbf{x} + \mathbf{r}$. The covariance function is reduced to $C(\mathbf{x}, \mathbf{x} + \mathbf{r}) = \sigma^2 \rho(r)$ and the correlation operator K emerges as

$$(KG, G) = \sigma^2 \int_{R^3} d\mathbf{x} G(\mathbf{x}) \int_{R^3} d\mathbf{r} \rho(\sqrt{\mathbf{r} \cdot \mathbf{r}}) G(\mathbf{x} + \mathbf{r}) \quad (13.10)$$

valid for Gaussian scalar fields in homogeneous and isotropic turbulence.

Summary

The probabilistic interpretation of the first condition (13.6) using $F(\mathcal{X}(\eta; \mathbf{x}, t)) = \mu\{\Phi(\mathbf{x}, t) < \mathcal{X}(\eta; \mathbf{x}, t)\}$ and $F_G(\eta) = \mu_G\{G(\hat{\mathbf{x}}) < \eta\}$ is then

$$\mu_G\{G(\hat{\mathbf{x}}) < \eta\} = \mu\{\mathcal{X}^{-1}(\Phi(\mathbf{x}, t)) < \eta\}$$

where \mathcal{X}^{-1} is the inverse mapping of \mathbf{X} , or

$$\mu_G\{\hat{G}(\mathbf{x}, t) < \varphi\} = \mu\{\Phi(\mathbf{x}, t) < \varphi\}$$

where $\hat{G}(\mathbf{x}, t) \equiv \mathcal{X}(G(\hat{\mathbf{x}}); t)$ is the image of a Gaussian reference field, or

$$\boxed{\mu_G\{G(\hat{\mathbf{x}}) < \eta\} = \mu\{\Phi(\mathbf{x}, t) < \mathcal{X}(\eta; \mathbf{x}, t)\}} \quad (13.11)$$

which can be regarded as the implicit mapping equation. The explicit version of the mapping pde is derived in the next section. The mapping \mathcal{X} thus constructed is local in the sense that any change of the Gaussian argument field $G(\hat{\mathbf{x}})$ at any location $\hat{\mathbf{x}} \neq \mathbf{Y}(\mathbf{x}, t)$ has no influence on the mapping at \mathbf{x} .

There are three fields involved in the present version of the mapping method:

- (1) The turbulent scalar field $\Phi(\mathbf{x}, t)$.
- (2) The Gaussian argument/reference field $G(\hat{\mathbf{x}})$.
- (3) The (local) image field $\hat{\Phi}(\mathbf{x}, t) \equiv \mathcal{X}(G(\hat{\mathbf{x}}); t)$, where $\hat{\mathbf{x}} = \mathbf{Y}(\mathbf{x}, t)$, yet to be determined, holds.

The image field $\hat{\Phi}(\mathbf{x}, t)$ is called surrogate field (the terminology was introduced by Pope [1]). Note that the Gaussian reference field $G(\hat{\mathbf{x}})$ is by definition non-intermittent as discussed in Sect. 16.2.

The complete mapping of domain of definition and scalar space is then

$$\begin{pmatrix} \mathcal{X}(\eta; t) \\ \mathbf{Y}^{-1}(t, \hat{\mathbf{x}}) \end{pmatrix} : \mathcal{R}_G \times \hat{\mathcal{D}} \rightarrow \mathcal{R}_\Phi \times \mathcal{D}$$

where $\hat{\mathcal{D}} = \mathbb{R}^3$. All that remains is to derive the equation for the mapping \mathcal{X} and its solution in the next section.

13.1.2 Mapping Equation for a Single Scalar

The mapping \mathcal{X} relates single-point statistics to Gaussian statistics; hence, no scale information can be computed by this particular version of the mapping method for homogeneous turbulence. The mapping $\mathbf{Y} : \mathcal{D} \rightarrow \hat{\mathcal{D}}$ needs to be constructed to relate the location \mathbf{x} in the flow domain \mathcal{D} to $\hat{\mathbf{x}}$ in the argument/test field domain $\hat{\mathcal{D}}$.

The mapping equation is derived from the first condition (C1) (13.6) by differentiating with respect to time. It follows that

$$\frac{\partial F}{\partial t} + \frac{\partial \mathcal{X}}{\partial t} \frac{\partial F}{\partial \varphi} = 0 \quad (13.12)$$

must hold, since the reference distribution function $F_G(\eta)$ in (13.6) is time independent. Comparison with (13.3) and (13.4) leads to

$$\frac{\partial \mathcal{X}}{\partial t} = Q(\varphi) + \frac{1}{Pe} \langle \Delta \Phi | \Phi(\mathbf{x}, t) = \varphi \rangle \quad (13.13)$$

where Pe denotes the Peclet (product of Reynolds and Prandtl or Schmidt number) number.

The closure model is now constructed in two steps:

(i) The conditional expectation of the turbulent field is equal to the conditional expectation of the image of the Gaussian reference or surrogate field

$$\langle \Delta \Phi | \Phi(\mathbf{x}, t) = \varphi \rangle \tilde{=} \langle \Delta \hat{\Phi} | \hat{\Phi}(\mathbf{x}, t) = \varphi \rangle \quad (13.14)$$

The most important property of this closure assumption for the mapping equation is the fact that the Gaussian reference measure allows explicit calculation of the conditional expectations in terms of the mapping and correlations of the Gaussian reference/surrogate field. The derivatives of the image field can be expressed in terms of the reference field using implicit differentiation as follows:

$$\frac{\partial \hat{\Phi}}{\partial x_\alpha} = \frac{\partial}{\partial x_\alpha} \mathcal{X}(G(\mathbf{Y}(\mathbf{x}, t), t), \text{ and } \frac{\partial \hat{\Phi}}{\partial x_\alpha} = \frac{\partial \mathcal{X}}{\partial \varphi} \frac{\partial G}{\partial \hat{x}_\beta} \frac{\partial Y_\beta}{\partial x_\alpha} \quad (13.15)$$

holds.

(ii) The so far undetermined relation between the location \mathbf{x} in the physical domain \mathcal{D} and $\hat{\mathbf{x}}$ in the reference space R^3 must be set up. A geometric mapping denoted by $\mathbf{Y} : \mathcal{D} \rightarrow \hat{\mathcal{D}} = R^3$, qualitatively sketched in Fig. 13.2, must be constructed to complete the closure model. For homogeneous turbulence, it is constructed as a stretching transformation uniform in physical space (as suggested by Pope [1]), hence

$$\frac{\partial Y_\beta}{\partial x_\alpha} = \delta_{\alpha\beta} m(t) \quad (13.16)$$

where m is time dependent,

$$m(t) = m_0 + m_1 \sqrt{t}, \quad m_0, m_1 > 0 \quad (13.17)$$

The assumption (13.17) for the geometric domain mapping $Y(t, \mathbf{x})$ implies that \mathcal{X} has an asymptotic state determined by $\mathcal{X}'' - \eta \mathcal{X}' = 0$, Eq. (13.23). The

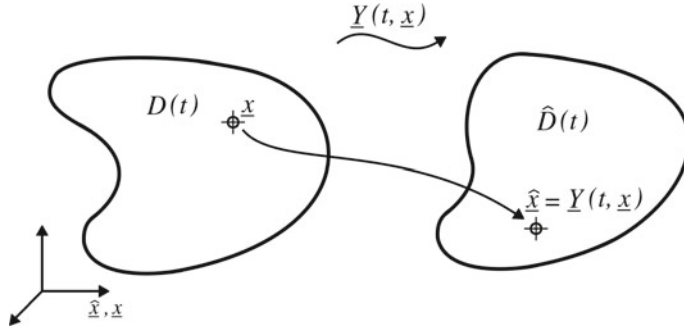


Fig. 13.2 Bijective mapping $\mathbf{Y}(t, \mathbf{x}) : \mathcal{D} \rightarrow \hat{\mathcal{D}}$ of the physical domain of definition \mathcal{D} onto the reference domain of definition $\hat{\mathcal{D}} = \mathbb{R}^3$ to complete the closure in the spatial description, Eq. (13.16) in Sect. 13.1

non-homogeneous case for flow domains \mathcal{D} with boundary $\partial\mathcal{D}$ is significantly more complicated, since the expression for $\mathbf{Y}(t)$ should be dependent on location $\mathbf{x} \in \mathcal{D}$ also. It is unlikely that a non-singular geometric mapping $\mathbf{Y} : \mathcal{D} \rightarrow \hat{\mathcal{D}}$ would suffice, and further research on this aspect of mapping methods is warranted. So far, there is no a priori justification for $\mathbf{Y}(t, \mathbf{x})$, it is determined by computer optimization.

Denoting the derivatives of the mapping with $\mathcal{X}' \equiv \frac{\partial \mathcal{X}}{\partial \varphi}$, $\dot{\mathcal{X}} \equiv \frac{\partial \mathcal{X}}{\partial t}$, hence

$$\frac{\partial \hat{\Phi}}{\partial x_\alpha} = \mathcal{X}' \frac{\partial G}{\partial \hat{x}_\beta} \frac{\partial Y_\beta}{\partial x_\alpha} \quad (13.18)$$

and for the Laplacian

$$\frac{\partial^2 \hat{\Phi}}{\partial x_\alpha \partial x_\alpha} = m^2 \left(\mathcal{X}'' \frac{\partial G}{\partial \hat{x}_\alpha} \frac{\partial G}{\partial \hat{x}_\alpha} + \mathcal{X}' \frac{\partial^2 G}{\partial \hat{x}_\alpha \partial \hat{x}_\alpha} \right) \quad (13.19)$$

The conditional expectation of the Laplacian can be established explicitly in terms of the mapping \mathcal{X} and correlations of the Gaussian reference field if and only if the derivatives of the mapping are completely specified by the condition $\Phi(\mathbf{x}) = \varphi$. This implies that the mapping must be local, i.e. the variation of the reference field at locations $\hat{\mathbf{x}}' \neq \hat{\mathbf{x}}$ has no influence on $\mathcal{X}(G(\hat{\mathbf{x}}), t)$. It follows then from $G(\hat{\mathbf{x}}) = \eta$ being the unique inverse image of $\hat{\Phi}(\mathbf{x}, t) = \varphi$ that

$$\langle \frac{\partial^2 \hat{\Phi}}{\partial x_\alpha \partial x_\alpha} | \hat{\Phi}(\mathbf{x}) = \varphi \rangle = m^2 \left(\mathcal{X}'' \langle \frac{\partial G}{\partial \hat{x}_\alpha} \frac{\partial G}{\partial \hat{x}_\alpha} | G(\hat{\mathbf{x}}) = \eta \rangle + \mathcal{X}' \langle \frac{\partial^2 G}{\partial \hat{x}_\alpha \partial \hat{x}_\alpha} | G(\hat{\mathbf{x}}) = \eta \rangle \right) \quad (13.20)$$

holds. The correlations of the Gaussian reference measure can be evaluated as follows (Pope [1]):

$$\langle \frac{\partial G}{\partial \hat{x}_\alpha} \frac{\partial G}{\partial \hat{x}_\alpha} | G(\hat{\mathbf{x}}) = \eta \rangle = \langle \frac{\partial G}{\partial \hat{x}_\alpha} \frac{\partial G}{\partial \hat{x}_\alpha} \rangle \quad (13.21)$$

and

$$\langle \frac{\partial^2 G}{\partial \hat{x}_\alpha \partial \hat{x}_\alpha} | G(\hat{\mathbf{x}}) = \eta \rangle = -\eta \langle \frac{\partial G}{\partial \hat{x}_\alpha} \frac{\partial G}{\partial \hat{x}_\alpha} \rangle \langle G^2 \rangle \quad (13.22)$$

The variance $\langle G^2 \rangle$ of the reference measure can be set to unity without restricting the generality of the result. This completes the closure of the mapping equation, and the resulting equation determining the mapping is thus given by

$$\frac{\partial \mathcal{X}}{\partial t} = Q(\eta) + \frac{1}{Pe} m(t)^2 \langle \frac{\partial G}{\partial \hat{x}_\alpha} \frac{\partial G}{\partial \hat{x}_\alpha} \rangle (\mathcal{X}'' - \eta \mathcal{X}') \quad (13.23)$$

valid for a single scalar in homogeneous turbulence. Remarkably, this is a linear, second-order pde of parabolic type. There is a source term Q , a drift term and a diffusive, i.e. a second derivative, term with respect to the scalar space present in the pde (13.23) for the mapping $\mathcal{X}(\varphi; \mathbf{x}, t)$. The drift is due to molecular diffusion $-\frac{m(t)^2}{Pe} \langle \frac{\partial G}{\partial \hat{x}_\alpha} \frac{\partial G}{\partial \hat{x}_\alpha} \rangle \eta \mathcal{X}'$; it is proportional to η , hence spreads the mapping away from the origin. The diffusive term has positive diffusivity, hence represents the main advantage of the present method, as it is the stable version of the diffusive term in contrast to the Pdf equation, where the coefficient of the second derivative is negative definite, hence always numerically unstable.

The initial and boundary conditions for the mapping pde follow from the required properties of the mapping. The mapping $\mathcal{X}(\eta)$ is defined on the real axis $\eta \in \mathcal{R}_G = \mathbb{R}^1$ with $\lim_{\eta \rightarrow -\infty} \mathcal{X}(\eta) = 0$ and $\lim_{\eta \rightarrow \infty} \mathcal{X}(\eta) = 1$; hence, $\mathcal{X}(\eta)$ is not square integrable, but the Jacobian (13.24)

$$J(\eta) \equiv \frac{d\mathcal{X}}{d\eta} \quad (13.24)$$

is, $J(\eta) \in L^2_{\mathbb{R}^1}$. The pde for the Jacobian follows from (13.23) by differentiation

$$\frac{\partial J}{\partial t} = \frac{\partial Q}{\partial \eta}(\eta) + m(t)^2 \frac{1}{Pe} \langle \frac{\partial G}{\partial \hat{x}_\alpha} \frac{\partial G}{\partial \hat{x}_\alpha} \rangle \left(\frac{\partial^2 J}{\partial \eta^2} - \eta \frac{\partial J}{\partial \eta} - J \right) \quad (13.25)$$

The boundary conditions are replaced by $J(\eta) \in L^2_{\mathbb{R}^1}$. The initial condition is specified by choosing $J_0(\eta)$

$$J(\eta; \mathbf{x}, 0) = J_0(\eta) \quad (13.26)$$

consistent with the mapping requirements (C1) and (C2) and the boundary conditions. The initial Pdf $f(\varphi; \mathbf{x}, 0)$ is usually specified, and the initial Jacobian J_0 of the mapping is then implicitly determined by

$$J_0(\eta) = \frac{f_G(\eta)}{f\left(\int_{-\infty}^{\eta} d\eta' J_0(\eta'); \mathbf{x}, 0\right)}$$

requiring iterative solution. It is easy to check that the integral $\int_{-\infty}^{\infty} d\eta J(t, \eta)$ remains unity for all time, since $J, Q \in L^2_{R^1}$.

An example is provided below to illustrate the construction of the initial condition and the solution of the mapping pde. Once the IVP for the Jacobian pde has been solved, the mapping is obtained by integration

$$\mathcal{X}(\eta; \mathbf{x}, t) = \int_{-\infty}^{\eta} d\eta' J(\eta'; \mathbf{x}, t) \quad (13.27)$$

and the Pdf can be computed without solving the Pdf equation (11.54) according to (14.19)

$$f(\mathcal{X}(\eta; \mathbf{x}, t); \mathbf{x}, t) = \frac{f_G(\eta)}{|J(\eta; \mathbf{x}, t)|} \quad (13.28)$$

valid for $|J(\eta; t)| > 0$, where $f_G(\eta)$ is the standard Gaussian Pdf with zero mean and unit variance and $\varphi = \mathcal{X}(\eta; t) : \varphi \in \mathcal{R}_\Phi$, $\eta = \mathcal{X}^{-1}(\varphi; t) : -\infty < \eta < \infty$. If for the time $t = 0$ the mapping is discontinuous, such as a combination of step functions, the Jacobian is not a classical function, but a sum of Dirac pseudo-functions and the division in (13.28) is not defined. Cdf and Pdf must then be computed directly without recourse to the mapping.

The pde for the Jacobian associated with the mapping for a single scalar is linear, but the higher dimensional case becomes very complicated. Hence, alternative methods become attractive, such as lifting, i.e. representing the solution as linear combination of a specified mapping $\mathcal{X}_L(\eta, t) \notin L^2_{R^1}$ that satisfies the asymptotic conditions at $\eta = \pm\infty$ and an unknown solution $\mathcal{X}(\eta, t) \in L^2_{R^1}$. This opens the possibility to represent the unknown solution in terms of an ONS basis, such as the Hermite function system, in $L^2_{R^1}$. The application of a Hermite basis for the solution of the pde for the Jacobian as alternative to the solution of the mapping pde is illustrated in Problem (13.3) with solution in Appendix F. Furthermore, the case of no source in the pdes for the Jacobian and the mapping can be solved analytically with the aid of separation of variables as shown in the next section.

The mapping pde (13.23) result was first obtained by Chen et al. [2] and generalized by Pope [1] to several variables using the fact that the N -variate Pdf can be represented as the product of N conditional Pdfs.

13.1.3 Solution of the Mapping pde for a Single Scalar

The IVP for the 1-d mapping pde (13.25), formulated in terms of the Jacobian $J(t, \eta) \in L^2_{R^1}$, can be solved analytically, if $Q(r, \eta) = 0$ and $m(t)$ is at most a function of time, the mapping can be recovered from (13.26) by integration. Let $J(0, \eta) \in L^2_{R^1}$ be specified as smooth function of η , then separation of variables

$$J(t, \eta) = A(t)B(\eta)$$

is applicable leading to

$$\frac{1}{m(t)^2 A} \frac{dA}{dt} = \frac{\epsilon_0}{B} \left(\frac{d^2 B}{d\eta^2} - \eta \frac{dB}{d\eta} - B \right)$$

where

$$\epsilon_0 \equiv \frac{1}{Pe} \left\langle \frac{\partial G}{\partial \hat{x}_\alpha} \frac{\partial G}{\partial \hat{x}_\alpha} \right\rangle$$

Since the left side is only a function of time and the right side only a function of η , both sides must be equal to a constant. Hence,

$$\frac{1}{m(t)^2 A} \frac{dA}{dt} = -\lambda^2$$

represents decay and

$$\frac{\epsilon_0}{B} \left(\frac{d^2 B}{d\eta^2} - \eta \frac{dB}{d\eta} - B \right) = -\lambda^2$$

with λ to be determined. The ode for $A(t)$ is solved by

$$A(t) = A(0) \exp \left[-\lambda^2 \int_0^t dt' m(t')^2 \right]$$

The initial value $A(0)$ needs to be reconsidered; once the eigenproblem for the homogeneous ode governing $B(\eta)$ has been solved. The ode for $B(\eta)$ has the standard form

$$\frac{d^2 B}{d\eta^2} - \eta \frac{dB}{d\eta} + nB = 0$$

where $n = \frac{\lambda^2}{\epsilon_0} - 1 = 0, 1, 2, \dots$, recognized as equation for the Hermite polynomials $B(\eta) = H_n(\eta)$, (4.30) (physicists version, details in [7] Sect. 18.3) as eigenfunctions with positive eigenvalues

$$\lambda_n^2 = \epsilon_0(n + 1), n = 0, 1, 2, \dots$$

The standard ode for the Hermite polynomials is conveniently recast for the Hermite functions (4.29)

$$\Psi_n(\eta) = (2^n n! \sqrt{\pi})^{-\frac{1}{2}} \exp\left(-\frac{\eta^2}{2}\right) H_n(\eta) \in L^2_{R^1}$$

which are orthonormal, since

$$(\Psi_n, \Psi_m) \equiv \int_{-\infty}^{\infty} d\eta \Psi_n(\eta) \Psi_m(\eta) = \delta_{n,m}$$

Hence, a non-trivial solution exists only for discrete values of $\lambda_n, n = 0, 1, 2, \dots$ and

$$A_n(t) = A_n(0) \exp[-(n+1)\epsilon_0 \int_0^t dt' m(t')^2]$$

where the $A_n(0)$ are the coordinates/expansion coefficients of the initial Jacobian $J(0, \eta)$ w.r.t. the Hermite ONS basis $\mathcal{B}_H \equiv \{\Psi_n(x), 0 \leq n \leq \infty\}$ according to

$$J(0, \eta) = \sum_{n=0}^{\infty} A_n(0) \Psi_n(\eta)$$

where

$$A_n(0) = (J(0, \eta), \Psi_n(\eta))$$

are the standard scalar products of $J(0, \eta)$ with the ONS basis functions $\Psi_n(\eta) \in \mathcal{B}_H$ without weight function. The solution of the pde (13.25) for the Jacobian $J(t, \eta)$ is then

$$J(t, \eta) = \sum_{n=0}^{\infty} A_n(0) \exp[-\lambda_n^2 \int_0^t dt' m(t')^2] \Psi_n(\eta) \quad (13.29)$$

where the eigenvalues are

$$\lambda_n^2 = \epsilon_0(n+1) > 0, \quad n = 0, 1, 2, \dots \quad (13.30)$$

The series is convergent for all time, since the initial series is convergent and the exponential factor in (13.29) is bounded by unity. The solution indicates that the Hermite function modes $\Psi_n(\eta)$ are damped with a rate increasing with n . Thus, the zeroth (Hermite function) mode (4.29) $\Psi_0 = \sqrt{\pi}^{-\frac{1}{2}} \exp\left(-\frac{\eta^2}{2}\right)$ will become dominant as time progresses and the Jacobian will approach a Gaussian shape, but there does not exist a non-zero asymptotic state for the model expression (13.17) as all modes decay eventually. A different model for $m(t)$ could be constructed, such that

$$\int_0^\infty dt' m(t')^2 < \infty$$

is finite; hence, an asymptotic state would possibly exist. However, such a model would be as arbitrary as (13.17) and its usefulness must be determined by comparison with DNS or experiments. The solution for the present example was obtained for $Q(\eta) = 0$; hence, there is no mechanism to maintain the turbulent flow and it decays as a consequence.

Numerical example for the CCK method

The essential properties of the Pdf equation (11.54) are illustrated with the aid of a simple example. The source $Q(\eta)$ in (11.54) is set to zero for convenience, and the Pdf solution is computed indirectly by solving the mapping pde (13.23) and then computing the Pdf according to (13.28). The reference measure μ_G is Gaussian explicitly given in terms of the Pdf

$$f_G(\eta) = \frac{1}{\sqrt{2\pi}} \exp\left(-\frac{1}{2}\eta^2\right)$$

with zero mean and unit variance. The initial values for the Jacobian of the mapping $\mathcal{X}(\eta)$ are determined by (13.28)

$$J_0(\eta) = \frac{f_G(\eta)}{f(\mathcal{X}_0(\eta); \mathbf{x}, 0)} \quad (13.31)$$

by specifying the initial Pdf $f(\mathcal{X}_0(\eta); \mathbf{x}, 0)$ constituting a nonlinear ode for $\mathcal{X}_0(\eta)$ as shown in Sect. 13.1.4. The relation (13.31) allows an alternative way to construct the initial values for $\mathcal{X}(\eta; 0)$ and the Pdf $f(\varphi; 0)$ by specifying the mapping first and then computing the initial Pdf. This is done for the purpose of illustration and the initial mapping \mathcal{X}_0 is constructed in terms of elementary functions. The initial condition for the present example is chosen as wildly different from a Gaussian to show the flexibility of the CCK method. It is set up in the form

$$\mathcal{X}_0(\eta, \eta_k, \alpha_k, w_k, k = 1, \dots, N) = \sum_{k=1}^N w_k \mathcal{G}(\alpha_k(\eta - \eta_k))$$

with $k_k \geq 0$, $\sum_{k=1}^N w_k = 1$ and

$$\mathcal{G}(x) \equiv \frac{1}{2}[1 + \tanh(x)] \quad (13.32)$$

The parameters for the present example are $N = 1$, weight $w = 1.0$, $\eta = -0.05$, $\alpha = 1.2$. The domain of definition R^1 for the mapping was truncated to $[-L, L]$

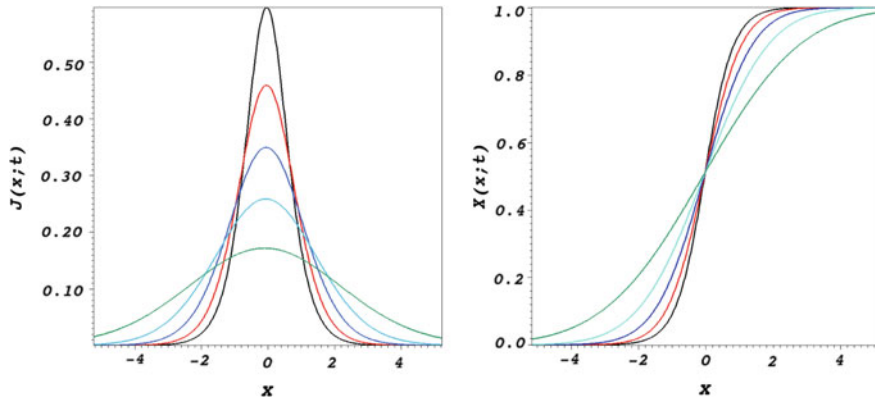


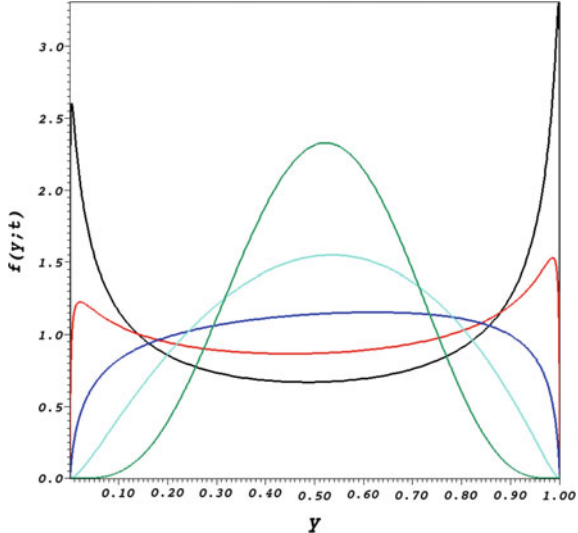
Fig. 13.3 Numerical solution of the mapping equation (13.23) for increasing times $t = 0.08$ (black), $t = 0.56$ (red), $t = 0.88$ (blue), $t = 1.2$ (light blue), $t = 1.6$ (green) for the Jacobian $J(y, t)$ (left graph) and the mapping $X(y, t)$ (right graph) in homogeneous turbulence. The image domain of $X(\eta; t)$ is $\mathcal{R}_\Phi = [0, 1]$

($L = 20$). The pure initial value problem for (13.23) is thus approximated by an IBVP with Dirichlet boundary conditions $X(-L, t) = 0$, $X(L, t) = 1$ (bounds of \mathcal{R}_Φ) by this truncation of the infinite domain of definition R^1 to the finite interval $[-L, L]$. The linear mapping pde (13.23) was solved using a standard finite-difference method fourth-order accurate in scalar space and a fourth-order Runge–Kutta time integrator. Analytic grid stretching was applied to the scalar axis to crowd the grid points near the origin. The result for the Pdf $f(\varphi; t)$ ($x = \varphi$) and $y = \eta$ in the graphs) is shown in Fig. 13.4 for the times $t = 0.08$ (black), $t = 0.56$ (red), $t = 0.88$ (blue), $t = 1.2$ (light blue), 1.6 (green); the association of times to line colour is the same in all graphs. The numerical result for the mapping $X(\eta, t)$ in the right graph of Fig. 13.3 indicates that reduction of the Pdf width is achieved by flattening the mapping, thus modifying the Jacobian $J(\eta, t)$ in Eq. (13.28) for the Pdf, and the Jacobian is spreading in η direction as seen in the left graph of the figure. The associated change of the Pdf with time is then shown in Fig. 13.4.

13.1.4 Initial Values for Mapping $X(\eta; 0)$

The solution of the mapping pde (13.23) requires the initial value $X(\eta; 0)$. There are two ways to determine the initial values, either the direct method by explicitly constructing it and then computing the initial Pdf $f(\varphi; 0)$ via (13.33) or solving iteratively equation (13.31) for $X(\eta; 0)$. The inverse Fourier transform generates the initial characteristic function $\theta(\zeta; 0) = \mathcal{F}^{-1}(f)$. This was done for the present example. The results show that the characteristic function for the example in Fig. 13.6 oscillates with slowly decaying amplitude as function of the wavenumber k

Fig. 13.4 Pdf $f(x; t)$ computed via (13.28) using the solution of the mapping Eq. (13.23) for increasing times from $t = 0.08$ (black line) to $t = 1.6$ (green line) in homogeneous turbulence, colour coding as in Fig. 13.3. The black line at $t = 0.08$ is close to the initial Pdf



(black lines in the lower graphs of Fig. 13.6) due to the rapid change of the gradient near the endpoints of $\varphi = 0, 1$. These oscillations are damped as time evolves, since the gradients at the endpoints decrease and Pdf approaches a Gaussian-type shape. However, the asymptotic Pdf is not Gaussian since the scalar space is the unit interval and not R^1 .

An alternative procedure is to construct the initial Pdf $f(\varphi; 0)$, $\varphi \in \mathcal{S}$ and determine the initial mapping by solving the IVP for the ode (13.31) numerically

$$\frac{\partial \mathcal{X}_0}{\partial \eta}(\eta) = \frac{f_G(\eta)}{f(\mathcal{X}_0(\eta); 0)} \quad (13.33)$$

for $\mathcal{X}_0(\eta)$ with the boundary condition $\mathcal{X}(-L; 0) = 0$, $L \gg 1$. The condition $\mathcal{X}(\infty; 0) = 1$ cannot be enforced as boundary condition, but it is satisfied in the weak sense according to the Bochner–Minlos theorem. An example for an initial Pdf is set up as a combination of beta functions ([7], Sect. 5.12)

$$f(\varphi; 0) = \sum_{i=1}^N w_i \frac{\Gamma(\alpha_i + \beta_i)}{\Gamma(\alpha_i)\Gamma(\beta_i)} \varphi^{\alpha_i-1} (1-\varphi)^{\beta_i-1}$$

$\varphi \in \mathcal{R}_\Phi$, $w_i \geq 0$, $\sum_{i=1}^N w_i = 1$. The solution $\mathcal{X}_0(\eta)$ of (13.33) and the Pdf $f(\varphi; 0)$ are shown in Fig. 13.5. The numerical solution ($N = 2$, $\alpha_1 = 3$, $\alpha_2 = 11$, $\beta_1 = 12$, $\beta_2 = 3$) of the IVP for the ode (13.33) employs a fourth-order Runge–Kutta–Williamson integration method with dynamic step size control.

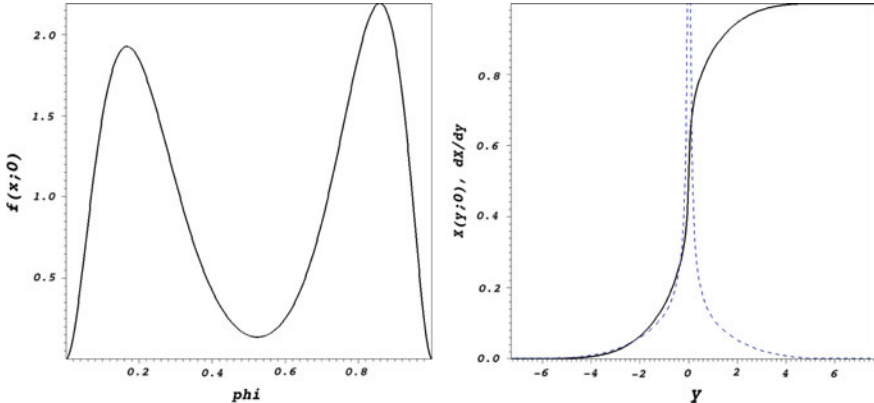


Fig. 13.5 Initial mapping $\mathcal{X}(\eta; 0)$ (right graph, $y = \eta$, the dashed line is the initial Jacobian J) computed numerically as solution of the ode (13.33) with the beta function Pdfs $f(\mathcal{X}(\eta; 0); 0)$ (left graph, $\text{phi} = \varphi = \mathcal{X}(\eta; 0)$) with $N = 2$ specified as input. The exponents of the beta function are $\alpha = (3, 11)$ and $\beta = (12, 3)$ and weights $w_1 = 0.5$, $w_2 = 1 - w_1$

Extended mapping method

The first variant of the mapping method transformed exclusively the scalar space. There is no a priori reason to exclude the time axis from consideration and this is done in the present section. A general transformation of the domain of definition of the Pdf equation (13.1) is considered extending the method just derived. The domain of definition for the extension is thus the space $\mathcal{R}_2 \equiv [0, T] \times \mathcal{R}_\Phi$, which is the image space of the extended mapping

$$\mathcal{X}(\tau, \eta) : [0, T] \times \mathcal{R}_G \rightarrow [0, T] \times \mathcal{R}_\Phi, \quad \mathcal{X}(\tau, \eta) \equiv \begin{pmatrix} \mathcal{X}_t(\tau, \eta) \\ \mathcal{X}_\Phi(\tau, \eta) \end{pmatrix} = \begin{pmatrix} t \\ \varphi \end{pmatrix} \quad (13.34)$$

and where $T > 0$ denotes the time interval and \mathcal{R}_Φ is the range of the values of Φ . The mapping is then two-dimensional and written as

$$t = \mathcal{X}_t(\tau, \eta), \quad \varphi = \mathcal{X}_\Phi(\tau, \eta) \quad (13.35)$$

The mapping must possess a unique inverse $\mathcal{X}^{-1}(t, \varphi) = [\mathcal{X}_t^{-1}(t, \varphi), \mathcal{X}_\Phi^{-1}(t, \varphi)]$ satisfying the same smoothness conditions as $\mathcal{X}(\tau, \eta)$

$$\tau = \mathcal{X}_t^{-1}(t, \varphi), \quad \eta = \mathcal{X}_\Phi^{-1}(t, \varphi) \quad (13.36)$$

with a positive Jacobian J defined by

$$J(\tau, \eta) \equiv \det \begin{pmatrix} \frac{\partial \mathcal{X}_t}{\partial \tau} & \frac{\partial \mathcal{X}_t}{\partial \eta} \\ \frac{\partial \mathcal{X}_\Phi}{\partial \tau} & \frac{\partial \mathcal{X}_\Phi}{\partial \eta} \end{pmatrix} = \frac{\partial \mathcal{X}_t}{\partial \tau} \frac{\partial \mathcal{X}_\Phi}{\partial \eta} - \frac{\partial \mathcal{X}_t}{\partial \eta} \frac{\partial \mathcal{X}_\Phi}{\partial \tau} \quad (13.37)$$

The mapping equations are established in two steps: First, the Pdf equation in the reference domain is set up and then the mapping condition that this Pdf is the image of the standard Gaussian is introduced. The function f^T defined by

$$f^T(\tau, \eta) \equiv f(\mathcal{X}_\Phi(\tau, \eta), \mathcal{X}_t(\tau, \eta)) \quad (13.38)$$

is the Pdf in the reference variables, but it is not Pdf with respect to η , since it is not necessarily normalized. The transport equation for f^T requires the transformation of the derivatives in Eq. (13.2). They are easily obtained with the aid of implicit differentiation

$$\frac{\partial}{\partial t} = \frac{\partial \mathcal{X}_t^{-1}}{\partial t} \frac{\partial}{\partial \tau} + \frac{\partial \mathcal{X}_\Phi^{-1}}{\partial t} \frac{\partial}{\partial \eta}, \quad \frac{\partial}{\partial \varphi} = \frac{\partial \mathcal{X}_t^{-1}}{\partial \varphi} \frac{\partial}{\partial \tau} + \frac{\partial \mathcal{X}_\Phi^{-1}}{\partial \varphi} \frac{\partial}{\partial \eta} \quad (13.39)$$

follow. The inverse transformation can be expressed in terms of the mapping itself (see Courant [8], vol.II, Chaps. 3 and 4) and

$$\frac{\partial}{\partial t} = \frac{1}{J} \left(\frac{\partial \mathcal{X}_t}{\partial \tau} \frac{\partial}{\partial \eta} - \frac{\partial \mathcal{X}_t}{\partial \eta} \frac{\partial}{\partial \tau} \right), \quad \frac{\partial}{\partial \varphi} = \frac{1}{J} \left(-\frac{\partial \mathcal{X}_\Phi}{\partial \tau} \frac{\partial}{\partial \eta} + \frac{\partial \mathcal{X}_\Phi}{\partial \varphi} \frac{\partial}{\partial \tau} \right) \quad (13.40)$$

where J denotes the Jacobian defined by (13.37). Substituting the derivatives in (13.2), the Pdf equation defined in the space \mathcal{D} spanned by τ and η emerges now in the form

$$\frac{\partial \mathcal{X}_t}{\partial \tau} \frac{\partial f^T}{\partial \eta} - \frac{\partial \mathcal{X}_t}{\partial \eta} \frac{\partial f^T}{\partial \tau} + \left\{ \frac{\partial \mathcal{X}_\Phi}{\partial \eta} \frac{\partial}{\partial \tau} - \frac{\partial \mathcal{X}_\Phi}{\partial \tau} \frac{\partial}{\partial \eta} \right\} (F_\varphi^T f^T) = 0 \quad (13.41)$$

where the flux in \mathcal{D} is defined by

$$F_\varphi^T(\tau, \eta) \equiv F_\varphi(\mathcal{X}_\Phi(\tau, \eta), \mathcal{X}_t(\tau, \eta)) \quad (13.42)$$

The extended mapping $\mathcal{X} = [\mathcal{X}_\Phi, \mathcal{X}_t]^T$ is now in part fixed by the requirement that the Pdf with respect to the reference variables is Gaussian

$$\frac{\partial \mathcal{X}_\Phi}{\partial \eta} f^T(\tau, \eta) = f_G(\eta), \quad \text{or} \quad f(\varphi, t) = \frac{f_G(\eta)}{\frac{\partial \mathcal{X}_\Phi}{\partial \eta}} \quad (13.43)$$

where $\varphi = \mathcal{X}_\Phi(\tau, \eta)$ holds and (13.38) was applied. The derivatives of f^T can be expressed in terms of f_G and we obtain

$$\frac{\partial f^T}{\partial \eta} = -\frac{f_G}{\left(\frac{\partial \mathcal{X}_\Phi}{\partial \eta}\right)^2} \left[\eta \frac{\partial \mathcal{X}_\Phi}{\partial \eta} + \frac{\partial^2 \mathcal{X}_\Phi}{\partial \eta^2} \right], \quad \text{and} \quad \frac{\partial f^T}{\partial \tau} = -\frac{f_G}{\left(\frac{\partial \mathcal{X}_\Phi}{\partial \eta}\right)^2} \frac{\partial^2 \mathcal{X}_\Phi}{\partial \eta \partial \tau} \quad (13.44)$$

The mapping equation is the result of the obvious fact that the Gaussian cancels out of the Pdf equation. The mapping equation is, therefore, established in the form

$$\left(-\eta \frac{\partial \mathcal{X}_\Phi}{\partial \eta} - \frac{\partial^2 \mathcal{X}_\Phi}{\partial \eta^2} + \frac{\partial \mathcal{X}_\Phi}{\partial \eta} \frac{\partial}{\partial \eta}\right) \left(\frac{\partial \mathcal{X}_\Phi}{\partial \tau} - F_\varphi^T \frac{\partial \mathcal{X}_t}{\partial \tau} \right) + \frac{\partial \mathcal{X}_\Phi}{\partial \eta} \frac{\partial}{\partial \tau} \left(F_\varphi^T \frac{\partial \mathcal{X}_t}{\partial \eta} \right) - F_\varphi^T \frac{\partial \mathcal{X}_t}{\partial \eta} \frac{\partial^2 \mathcal{X}_\Phi}{\partial \eta \partial \tau} = 0 \quad (13.45)$$

For known F_φ^T , this is a formidable nonlinear, second-order pde for the components \mathcal{X}_t and \mathcal{X}_Φ of the extended mapping.

Example

A special case is now considered by introducing the Ansatz

$$\frac{\partial \mathcal{X}_\Phi}{\partial \tau} = F_\varphi^T \frac{\partial \mathcal{X}_t}{\partial \tau} \quad (13.46)$$

providing a second equation for \mathcal{X}_t and \mathcal{X}_Φ . It has the beneficial effect to get rid of the first term group on the left side of (13.45). It follows then from the Pdf equation (13.45) that

$$\frac{\partial}{\partial \tau} \left(F_\varphi^T \frac{\partial \mathcal{X}_t}{\partial \eta} \right) = F_\varphi^T \frac{\partial \mathcal{X}_t}{\partial \eta} \frac{\partial^2 \mathcal{X}_\Phi}{\partial \eta \partial \tau} \quad (13.47)$$

must also be satisfied. There are now two distinct possibilities for this to happen:

(i) The temporal map is restricted to $\mathcal{X}_t(\eta, \tau) = \mathcal{X}_t(\tau)$, which then implies that $\partial \mathcal{X}_t / \partial \eta = 0$ and the second mapping condition (13.47) is trivially satisfied. Hence, the condition that the reference measure is Gaussian fails to determine the scale factor $\partial \mathcal{X}_t / \partial \tau$. The term $\mathcal{X}_t(\tau)$ is then an unknown parameter that can be used for the purpose of closure.

or

(ii) The dependence of \mathcal{X}_t on η is retained. The second mapping condition (13.47) can be combined with the Ansatz (13.46) to separate the equations. Integrating (13.46) and differentiating w.r.t. η leads to

$$\frac{\partial \mathcal{X}_\Phi}{\partial \eta}(\tau, \eta) = \frac{\partial}{\partial \eta} \left\{ \mathcal{X}_\Phi(0, \eta) \int_0^\tau d\tau' F_\varphi^T \frac{\partial \mathcal{X}_t}{\partial \tau'} \right\}$$

and (13.47) emerges now as a single equation for \mathcal{X}_t

$$\frac{\partial}{\partial \tau} \left(F_\varphi^T \frac{\partial \mathcal{X}_t}{\partial \eta} \right) = \frac{F_\varphi^T \frac{\partial \mathcal{X}_t}{\partial \eta} \frac{\partial}{\partial \eta} (F_\varphi^T \frac{\partial \mathcal{X}_t}{\partial \eta})}{\frac{\partial}{\partial \eta} \left\{ \mathcal{X}_\Phi(0, \eta) \int_0^\tau d\tau' F_\varphi^T \frac{\partial \mathcal{X}_t}{\partial \tau'} \right\}}$$

This pde must be solved for $\mathcal{X}_t(\tau, \eta)$. The second component \mathcal{X}_Φ follows then from the Ansatz according to

$$\mathcal{X}_\Phi(\tau, \eta) = \mathcal{X}_\Phi(0, \eta) \int_0^\tau d\tau' F_\varphi^T \frac{\partial \mathcal{X}_t}{\partial \tau'}$$

The complete mapping is now computable, once appropriate initial and boundary conditions are set up for \mathcal{X}_t and \mathcal{X}_Φ . This concludes the example.

13.2 Mapping Method for the Characteristic Function

The mapping method for characteristic functions is developed first for the simplest possible case of a single, passive scalar Φ with values in the scalar space $\mathcal{R}_\Phi = (-\infty, \infty)$ in homogeneous turbulence, where the velocity correlation drops out due to homogeneity. The starting point for the development of such a mapping for characteristic functions is the Eq. (11.54) governing the Pdf $f(\varphi; \mathbf{x}, t)$ for the values φ of a single scalar $\Phi(\mathbf{x}, t)$ transported by a turbulent flow field. This equation contains additional unknowns in the present form, namely, the conditional expectations $\langle v_\alpha | \Phi(\mathbf{x}, t) = \varphi \rangle$ of velocity and the scalar dissipation rate $\langle \epsilon_\Phi | \mathcal{C}_1 \rangle$ defined by (11.53).

The characteristic function $\theta(k; t)$ for homogeneous turbulence corresponding to the 1-d scalar Pdf $f(\varphi; t)$ is defined as the Fourier transform (see Sect. 15.1 for details)

$$\begin{aligned} \theta(k; t) &= \mathcal{F}^{-1}(f) \equiv \int_S d\varphi f(\varphi; t) \exp(i\varphi k), \quad f(\eta; t) = \mathcal{F}(\theta) \\ &\equiv \frac{1}{2\pi} \int_{-\infty}^{\infty} dk \theta(k; t) \exp(-i\varphi k) \end{aligned} \quad (13.48)$$

for $k \in R^1$, where the integration is over the scalar space $\mathcal{R}_\Phi = (-\infty, \infty)$. De Moivre's formula allows to split $\theta(k; t)$ into real, symmetric and imaginary, anti-symmetric parts

$$\theta(k; t) = Re(\theta)(k; t) + i Im(\theta)(k; t)$$

where real and imaginary parts are

$$Re(\theta)(k; t) = \int_S d\varphi f(\varphi; t) \cos(\varphi k), \quad Im(\theta)(k; t) = \int_S d\varphi f(\varphi; t) \sin(\varphi k)$$

hence $k \in R^+$, where $R^+ \equiv [0, \infty)$.

The characteristic function $\theta(k; t)$ as image of the Gaussian Pdf f_G

In the context of the CCK approach, the Pdf $f(\eta; t)$ of the scalar Φ in a turbulent flow field is regarded as the image of a Gaussian via the mapping $\varphi = \mathcal{X}(\eta, t) : (-\infty, \infty) \rightarrow \mathcal{R}_\Phi$; hence, the integral in (13.48) can be transformed accordingly

$$\theta(k; t) = \int_{-\infty}^{\infty} d\eta J(\eta, t) f(\mathcal{X}(\eta, t), t) \exp(ik\mathcal{X}(\eta, t))$$

where the Jacobian is $J(\eta, t) = \frac{\partial \mathcal{X}}{\partial \eta}(\eta, t) > 0$ due to the monotonicity of $\mathcal{X}(\eta)$. It follows from the properties of the mapping $\mathcal{X}(\eta, t)$ that $J(\eta) f(\varphi) = f_G(\eta)$ holds according to (13.28), thus

$$\theta(k; t) = \int_{-\infty}^{\infty} d\eta f_G(\eta) \exp(ik\mathcal{X}(\eta, t)) \quad (13.49)$$

transforms the reference Pdf $f_G(\eta)$ to the characteristic function $\theta(k; t)$. It is noteworthy that all information on the characteristic function $\theta(k; t)$ is contained in the mapping $\mathcal{X}(\eta; t)$. As time evolves, the mapping reflects the changes of the characteristic function.

Example

The relation (13.49) for the characteristic function and the associated mapping $\mathcal{X}(\eta; t)$ and Pdf $f(\varphi; t)$ is illustrated in a simple example in Fig. 13.6. The scalar space is defined as $\mathcal{R}_\Phi = [0, 1]$ and the source is set $Q = 0$ for simplicity. The closure model suggested in Sect. 13.1.2 is retained without change

$$m(t) = \sqrt{t}, \quad \epsilon_0 \equiv \frac{1}{Pe} \left(\frac{\partial G}{\partial \hat{x}_\alpha} \frac{\partial G}{\partial \hat{x}_\alpha} \right) = 1$$

where $m(t)$ is the time scale. The initial mapping \mathcal{X} is a combination of inverse hyperbolic functions

$$\mathcal{X}(\varphi; 0) = \sum_{i=1}^3 w_i \operatorname{arcsinh}[A_i(\eta - sh_i)]$$

with weights $w_1 = 0.25$, $w_2 = 0.35$, $1 - w_1 - w_2$ and numerical coefficients $A_1 = 4.8$, $A_2 = 4.2$, $A_3 = 2.0$, $sh_1 = -0.15$, $sh_2 = 0.18$, $sh_3 = 0.0$. The initial Jacobian $J(\eta; 0)$ is computed using (13.24) and the non-Gaussian initial Pdf follows then from (13.49) as image of the reference Gaussian. The solution $\mathcal{X}(\eta; t)$ allows immediate computation (13.49) of the characteristic function, whose real and imaginary parts are presented in the lower graphs of Fig. 13.6.

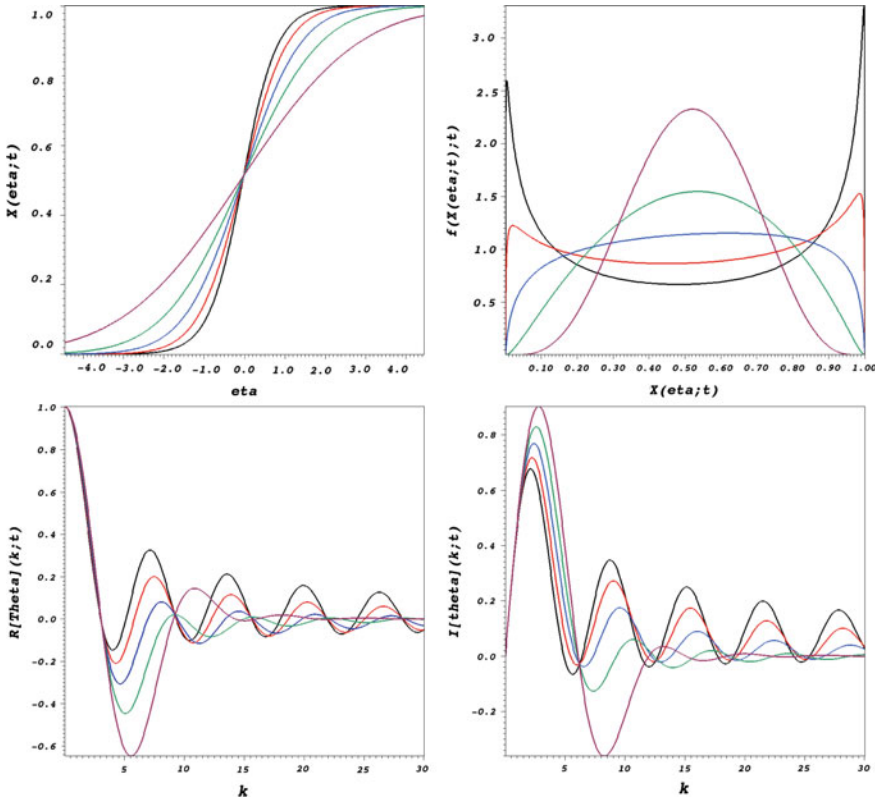


Fig. 13.6 Mapping $X(\varphi; t)$ (upper left graph), Pdf $f(X(\eta; t); t)$ (upper right graph), the real part of the characteristic function $\theta(\varphi; 0)$ (lower left graph) and the imaginary part (lower right graph) at time $t = 1.6$. The times shown in the upper two graphs are indicated by colour: $t = 0.08$ (black), $t = 0.56$ (red), $t = 0.88$ (blue), $t = 1.2$ (green), $t = 1.6$ (magenta)

The characteristic function as image of the Gaussian characteristic function θ_G

The characteristic function $\theta(k; t)$ can be expressed in terms of the standard Gaussian function and the associated mapping can be defined and its pde determined. The characteristic function $\theta_G(k; m, \sigma)$ of a Gaussian random variable is known

$$\theta_G(k; m, \sigma) = \exp[-imk - \frac{1}{2}(\sigma k)^2] \quad (13.50)$$

where m denotes the mean value and $\sigma^2 = \langle(\varphi - m)^2\rangle$ the variance. If it is introduced to (13.49), it becomes clear that the characteristic function θ can be regarded as the image of the Gaussian reference function θ_G according to

$$\theta[\theta_G](k; t) = \frac{1}{2\pi} \int_{-\infty}^{\infty} d\eta \int_{-\infty}^{\infty} dk' \theta_G(k'; m, \sigma) \exp\{i(k\mathcal{X}(\eta) - k'\eta)\} \quad (13.51)$$

For this definition to make sense, the conditions of the Bochner–Minlos theorem (Sect. 8.1) need to be checked to insure that $\theta[\theta_G](k, t)$ is indeed characteristic function. Setting $k = 0$

$$\theta[\theta_G](0; t) = \frac{1}{2\pi} \int_{-\infty}^{\infty} d\eta \int_{-\infty}^{\infty} dk' \theta_G(k'; m, \sigma) \exp(-ik'\eta)$$

and using (13.48) for the inner integral, the result

$$\theta[\theta](0; t) = \int_{-\infty}^{\infty} d\eta f_G(\eta; m, \sigma) = 1$$

is obtained, satisfying the first condition of the theorem. The second condition $|\theta| \leq 1$ is easily verified

$$|\theta[\theta_G](k; t)| \leq \int_{-\infty}^{\infty} d\eta \left| \frac{1}{2\pi} \int_{-\infty}^{\infty} dk' \theta_G(k'; m, \sigma) \exp(-k'\eta) \right|$$

since $|\exp(ik\mathcal{X}(\eta; t))| \leq 1$, and using (13.48) for the inner integral

$$|\theta[\theta_G](k; t)| \leq 1$$

is obtained. The third and fourth conditions in the Bochner–Minlos theorem follow easily from the properties of $\mathcal{X}(\eta; t)$ and the image $\theta[\theta_G](k, t)$ of $\theta_G(k; m, \sigma)$ is indeed characteristic function.

The definition (13.51) is the starting point for the derivation of the pde for $\theta[\theta](k; t)$

$$\frac{\partial \theta[\theta_G]}{\partial t}(k; t) = \frac{ik}{2\pi} \int_{-\infty}^{\infty} d\eta \int_{-\infty}^{\infty} dk' \theta_G(k'; m, \sigma) \frac{\partial \mathcal{X}}{\partial t}(\eta; t) \exp\{i(k\mathcal{X}(\eta; t) - k'\eta)\} \quad (13.52)$$

in terms of the dynamics of the mapping $\mathcal{X}(\eta; t)$.

The relation (13.51) shows that the image characteristic function $\theta[\theta_G](k; t)$ can be generalized to the non-local image in k -space of the reference characteristic function $\theta_{ref}(k')$. Specifically, θ maps a stationary characteristic function $\theta_{ref}(k')$ (reference function) onto a time-dependent characteristic function $\theta(k; t)$. The Gaussian reference function is explicitly given by (13.50), hence

$$\theta[\theta_{ref}] \equiv \int_{-\infty}^{\infty} dk' Y(k, k'; t) \theta_{ref}(k') = \int_{-\infty}^{\infty} dk' Y(k, k'; t) \exp\left(-\frac{1}{2}k'^2\right) \quad (13.53)$$

with complex, time-dependent kernel function $Y(k, k'; t)$

$$Y(k, k'; t) \equiv \frac{1}{2\pi} \int_{-\infty}^{\infty} d\eta \exp\{i(k\mathcal{X}(\eta, t) - k'\eta)\} \quad (13.54)$$

The kernel $Y(k, k'; t)$ is not a classical function, but a generalized function or distribution. For instance, setting $\mathcal{X}(\eta; t) = \eta$ implies

$$Y(k, k'; t) = \frac{1}{2\pi} \int_{-\infty}^{\infty} d\eta \exp\{i\eta(k - k')\} = \delta(k - k')$$

which is recognized as one of the representations (13.63) of the Dirac function generating the identity map for the characteristic function $\theta[\theta_G](k) = \theta_G(k)$.

13.2.1 Transport pde for the Image $\theta[\theta_G]$

It is straightforward to derive the transport pde for the image $\theta[\theta_G]$ of the Gaussian characteristic function $\theta_G(k)$ from its definition (13.53) and the pde for the mapping $\mathcal{X}(\eta; t)$ (13.23)

$$\frac{\partial \mathcal{X}}{\partial t}(\eta; t) = Q(\eta) + m^2(t)\epsilon_0\left(\frac{\partial^2 \mathcal{X}}{\partial \eta^2} - \eta \frac{\partial \mathcal{X}}{\partial \eta}\right)$$

The time rate of change of θ is then determined by $\frac{\partial \mathcal{X}}{\partial t}$

$$\frac{\partial \theta}{\partial t}[\theta_G] = \frac{ik}{2\pi} \int_{-\infty}^{\infty} d\eta \int_{-\infty}^{\infty} dk' \theta_G(k') \frac{\partial \mathcal{X}}{\partial t}(\eta; t) \exp[i(k\mathcal{X}(\eta; t) - k'\eta)] = R_1 + D_1 + D_2 \quad (13.55)$$

The terms R_1 , D_1 and D_2 generated by (13.23) are now evaluated in turn.

Source term R_1

The source $Q(\eta; t) \in L^2_{R^1}$ has the Fourier transform $\hat{Q}(k; t)$, hence

$$Q(\eta; t) = \frac{1}{2\pi} \int_{-\infty}^{\infty} dk \hat{Q}(k; t) \exp(-ik\eta)$$

can be introduced into R_1

$$R_1 = \frac{ik}{(2\pi)^2} \int_{-\infty}^{\infty} dk' \theta_G(k') \int_{-\infty}^{\infty} d\eta \int_{-\infty}^{\infty} dk'' \hat{Q}(k''; t) \exp[i(k\mathcal{X}(\eta; t) - (k' + k'')\eta)]$$

A few elementary steps lead to the convolution term

$$R_1 = \frac{ik}{2\pi} \int_{-\infty}^{\infty} dk' \theta_G(k') \int_{-\infty}^{\infty} dk'' Y(k, k''; t) \hat{Q}(k'' - k'; t) = \frac{ik}{2\pi} \int_{-\infty}^{\infty} dk' \theta_G(k') Y * \hat{Q}(k, k') \quad (13.56)$$

The terms generated by molecular diffusion require more effort. A semi-implicit representation can be obtained with the aid of the Jacobian $J(\eta; t)$ and its Fourier transform

$$\hat{J}(k; t) = \mathcal{F}^{-1}[J(\eta; t)] = \int_{\mathcal{R}_{\Phi}} d\varphi J(\varphi; t) \exp(i\varphi k) \quad (13.57)$$

The pde for the image characteristic function $\theta[\theta_G]$ contains two molecular diffusion terms D_1 and D_2 to be evaluated.

First molecular diffusion term D_1

The first diffusion term is defined by

$$D_1 \equiv m^2(t) \epsilon \frac{ik}{2\pi} \int_{-\infty}^{\infty} dk' \theta_G(k') I_2(k, k', \mathcal{X}), \quad I_2(k, k', \mathcal{X}) \equiv \int_{-\infty}^{\infty} d\eta \frac{\partial^2 \mathcal{X}}{\partial \eta^2} \exp[i(k\mathcal{X}(\eta; t) - k'\eta)]$$

appearing in the equation for $\theta[\theta_G]$ according to (13.52). The integral I_2 is reformulated using the Jacobian J

$$I_2 = \int_{-\infty}^{\infty} d\eta \frac{\partial J}{\partial \eta} \exp[i(k\mathcal{X}(\eta; t) - k'\eta)]$$

and its Fourier transform \hat{J}

$$I_2 = -\frac{i}{2\pi} \int_{-\infty}^{\infty} dk'' k'' \hat{J}(k'') \int_{-\infty}^{\infty} d\eta \exp[i(k\mathcal{X}(\eta; t) - (k' + k'')\eta)]$$

leading to

$$I_2 = -i \int_{-\infty}^{\infty} dk'' (k'' - k') \hat{J}(k'' - k') Y(k, k''; t)$$

and finally to

$$D_1 = \frac{k}{2\pi} m^2(t) \epsilon_0 \int_{-\infty}^{\infty} dk' \theta_G(k') \int_{-\infty}^{\infty} dk'' (k'' - k') \hat{J}(k'' - k') Y(k, k''; t) \quad (13.58)$$

This concludes the evaluation of the first molecular diffusion term.

Second molecular diffusion term

The second and last diffusion term is defined by

$$D_2 \equiv m^2(t) \epsilon_0 \frac{ik}{2\pi} \int_{-\infty}^{\infty} dk' \theta_G(k') I_3(k, k', \mathcal{X}), \quad I_3(k, k', \mathcal{X}) \equiv \int_{-\infty}^{\infty} d\eta \frac{\partial \mathcal{X}}{\partial \eta} \exp[i(k\mathcal{X}(\eta; t) - k'\eta)]$$

appearing in the equation for $\theta[\theta_G]$ according to (13.52). The integral I_3 is evaluated similarly to I_2 using the Fourier-transformed Jacobian and observing

$$i \frac{\partial Y}{\partial \hat{k}} = \int_{-\infty}^{\infty} d\eta \eta \exp[i(k\mathcal{X}(\eta; t) - k'\eta)]$$

leading to

$$I_3 = i \int_{-\infty}^{\infty} dk'' \hat{J}(k'' - k) \frac{\partial Y}{\partial k''}(k, k''; t)$$

and finally to

$$D_2 = -m^2(t) \epsilon_0 \frac{k}{2\pi} \int_{-\infty}^{\infty} dk' \theta_G(k') \int_{-\infty}^{\infty} dk'' \hat{J}(k'' - k') \frac{Y}{\partial k''}(k, k''; t) \quad (13.59)$$

This concludes the evaluation of the second molecular diffusion term.

IVP for the transport equation for $\theta[\theta_G]$

The transport pde for the image $\theta[\theta_G]$ of the Gaussian characteristic function $\theta_G(k)$ emerges then in the form

$$\begin{aligned} \frac{\partial}{\partial t} \theta[\theta_G] &= \frac{ik}{2\pi} \int_{-\infty}^{\infty} dk' \theta_G(k') \int_{-\infty}^{\infty} dk'' Y(k, k''; t) \hat{Q}(k'' - k') \\ &+ m(t)^2 \epsilon_0 \frac{k}{2\pi} \int_{-\infty}^{\infty} dk' \theta_G(k') \int_{-\infty}^{\infty} dk'' \hat{J}(k'' - k') \left[(k'' - k') Y(k, k''; t) - \frac{\partial Y}{\partial k''}(k, k'') \right] \end{aligned} \quad (13.60)$$

where hatted variables indicate Fourier transform and $\epsilon_0 \equiv \frac{1}{ScRe} \langle \nabla \Psi \cdot \nabla \Psi \rangle > 0$ is a constant. This equation is linear with respect to the distribution Y for specified $\hat{J}(k; t)$. The initial condition for $\theta[\theta_G]$ follows from the initial mapping $\mathcal{X}(\eta; 0)$ according to (13.53) and (13.54). The initial mapping $\mathcal{X}(\eta; 0)$ is computed by solving the ode (13.33)

$$\frac{\partial \mathcal{X}}{\partial \eta}(\eta; 0) = \frac{f_G(\eta)}{f(\mathcal{X}(\eta; 0); 0)}$$

for specified initial Pdf $f(\varphi; 0)$ as presented in Sect. 13.1.4. The initial Jacobian is then given by definition (13.24) and Fourier transformed according to (13.57), thus completing the setup of the initial condition.

The usefulness of (13.60) depends essentially of the way the asymptotic limit is approached. It follows from the definition of Y (13.54) that the Gaussian characteristic function is approached, if the mapping $\mathcal{X}(\eta; t) \rightarrow \eta$ and thus the generalized function $Y(k, k'; t) \rightarrow \delta(k - k')$. The mapping $\theta[\theta_G]$ approaches then the Gaussian characteristic function $\theta_G(\theta)$ according to (13.53).

Alternative mapping

The limit property can be modified by redefining the mapping and the kernel function. A simple, local modification of the definition of the mapping $Z : R^2 \rightarrow C$ (C denotes the complex plane)

$$Z(k, k', \eta; t) \equiv \frac{1}{2\pi} \exp[i(k\mathcal{X}(\eta; t) - k'\eta)] \quad (13.61)$$

which is a standard function. Its integral with respect to the wavenumber k produces the Dirac pseudo-function, since

$$\int_{-\infty}^{\infty} dk Z(k, k', \eta; t) = \frac{1}{2\pi} \int_{-\infty}^{\infty} dk \exp[i(k\mathcal{X}(\eta; t) - k'\eta)] = \frac{1}{\sqrt{2\pi}} \exp(-ik'\eta) \delta(\mathcal{X}(\eta; t)) \quad (13.62)$$

due to the representation

$$\delta(x - a) = \frac{1}{\sqrt{2\pi}} \int_{-\infty}^{\infty} dk \exp[ik(x - a)] \quad (13.63)$$

of the Dirac pseudo-function.

The characteristic function can be recovered from

$$\theta(k; t) = \int_{-\infty}^{\infty} dk' \theta_G(k') \int_{-\infty}^{\infty} d\eta Z(k, k', \eta; t) \quad (13.64)$$

It leads to the limit

$$Z(k, k', \eta; t) \rightarrow \frac{1}{2\pi} \exp[i\eta(k - k')] \text{ as } t \rightarrow \infty \quad (13.65)$$

since $\mathcal{X}(\eta; t) \rightarrow \eta$ and thus $\theta[\theta_G] \rightarrow \theta_G$. The corresponding transport equation follows immediately from

$$\frac{\partial Z}{\partial t} = ikZ(k, k', \eta; t) \frac{\partial \mathcal{X}}{\partial t}(\eta; t)$$

and (13.23) and emerges in the form

$$\boxed{\frac{\partial Z}{\partial t}(k, k', \eta; t) = ikQ(\eta)Z + m^2\epsilon_0 \left[\frac{\partial^2 Z}{\partial \eta^2} - \frac{1}{Z} \left(\frac{\partial Z}{\partial \eta} \right)^2 - \eta \frac{\partial Z}{\partial \eta} - ik'\eta Z \right]} \quad (13.66)$$

It is worth noting that the diffusive term has a positive coefficient, but a nonlinear term is present in contrast to the pde (13.23) for $\mathcal{X}(\eta; t)$. The initial condition for Z follows from the initial mapping $\mathcal{X}(\eta; 0)$ according to (13.53) and (13.54). The initial mapping $\mathcal{X}(\eta; 0)$ is computed, either by solving the ode (13.33) for a specified initial Pdf $f(\varphi; 0)$ as presented in Sect. 13.1.4, or by specifying the initial mapping $\mathcal{X}(\eta; 0)$ as done in the example below; the initial value $Z(k, k', \eta; 0)$ is in either case computed using the definition (13.61). The solution of the pde (13.66) for $Z(k, k', \eta; t)$ is not trivial because of the presence of a singular term. There are many possibilities for reformulation of the mapping method for characteristic functions to obtain a non-singular pde. This is a future project.

Example for the mapping $Z(k, k', \eta; t)$

An example for the complex mapping $Z(k, k', \eta; t)$, generated by the solution $\mathcal{X}(\eta; t)$ of the mapping pde (13.23) via (13.61), is constructed to evaluate its properties. The mapping $Z(k, k', \eta, ; t) : R^3 \rightarrow C^2$ (C^2 denotes the complex plane) follows from $\mathcal{X}(\eta, ; t) : R^1 \rightarrow \mathcal{R}_\Phi = [0, 1]$ according to its definition (13.61). The initial mapping \mathcal{X} is a combination of hyperbolic functions defined by (13.32)

$$\mathcal{X}(\varphi; 0) = \sum_{i=1}^N w_i \mathcal{G}[A_i(\eta - sh_i)]$$

($N = 1$, weight $w_1 = 1.0$, coefficients $A_1 = 1.2$, $sh_1 = -0.05$). The Jacobian J is computed using (13.24) and the non-Gaussian initial Pdf follows from (12.3) as image of the reference Gaussian. The solution of the mapping pde (13.23) and the associated Jacobian are shown in Fig. 13.7. The mapping $Z(k, k', \eta, ; t) : R^3 \rightarrow C^2$ (C^2 denotes the complex plane) follows from $\mathcal{X}(\eta, ; t) : R^1 \rightarrow \mathcal{R}_\Phi = [0, 1]$ according to its definition (13.61).

First, the characteristic function, being the Fourier transform of the Pdf shown in the left graph of Fig. 13.8, is considered. It reflects the development of the Pdf $f(\varphi; t)$ (where $\varphi = \mathcal{X}(\eta; t)$) with time. The oscillation at $k > 0$ is damped as time

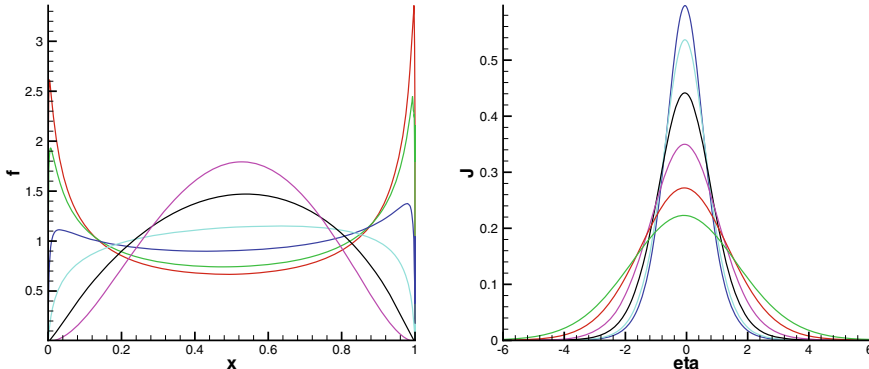


Fig. 13.7 The Pdf $f(\mathcal{X}(\eta; t); t)$ (left graph) and the Jacobian $J(\eta; t)$ (right graph) generated by the solution of the mapping pde (13.61) for $t = 0.067$ (red/green), $t = 0.405$ (green/blue), $t = 0.74$ (dark blue/red), $t = 1.07$ (blue/dark blue), $t = 1.35$ (black)

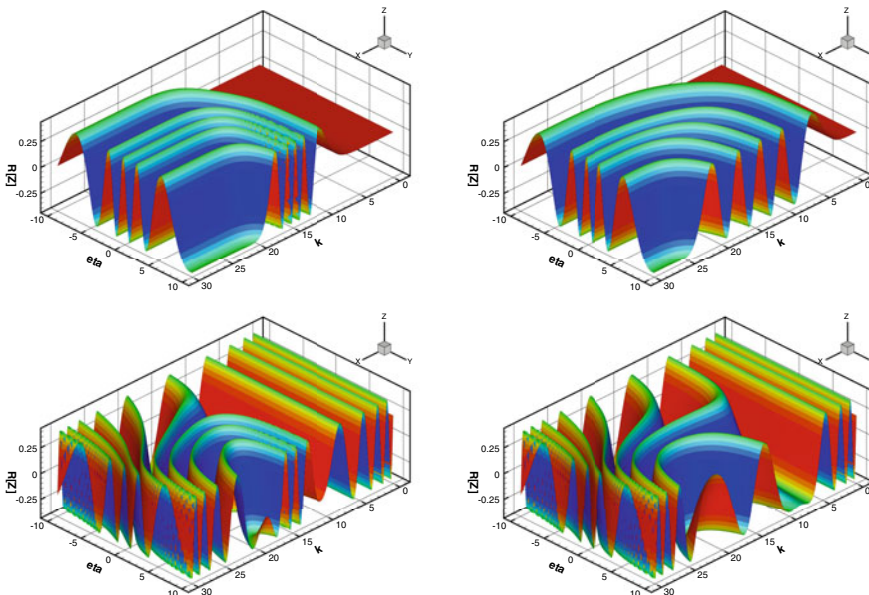


Fig. 13.8 Real part of the complex mapping function $Z(k, k', \eta; t)$ depicted as function of the wavenumber variable k and the coordinate η for $k' = 0$ in the upper graphs and for $k' = 3.2$ in the lower graphs. The left graphs are the initial state and the right graphs at the later time $t = 1.35$

increases corresponding to the decrease of the variation of the Pdf at the boundary points $\varphi = 0, 1$ of the range \mathcal{R}_Φ as can be seen in Fig. 13.6. Considering now the complex mapping $Z(k, k', \eta; t)$ presented as real and imaginary parts in Fig. 13.8 and 13.9 as function of the wavenumber variable k and the scalar range variable η at times $t = 0.067$ and $t = 1.35$ for two values of k' . The change of the mapping

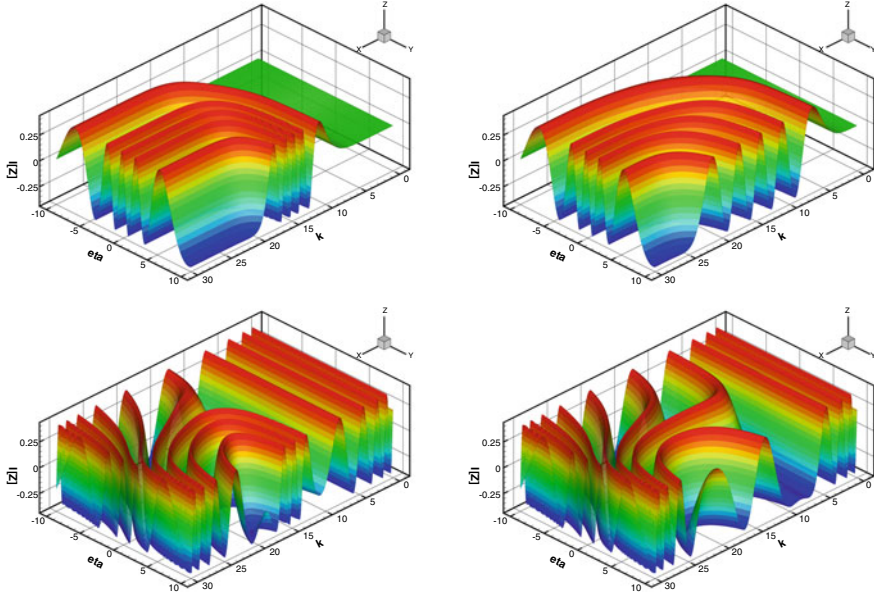


Fig. 13.9 Imaginary part of the complex mapping function $Z(k, k', \eta; t)$ depicted as colour-coded scalar field on the surface of the real part in Fig. 13.8 as function of the wavenumber k and the coordinate η for $k' = 0$ in the upper graphs and for $k' = 3.2$ in the lower graphs. The left graphs are the initial state and the right graphs at time $t = 1.35$

function $Z(k, k', \eta; t)$ is significant during the time interval $0, 1.35$ of the numerical simulation and concentrated near $\eta = 0$, where the mapping $\mathcal{X}(\eta; t)$ varies rapidly from zero to unity. The interpretation of the complex mapping function $Z(k, k', \eta; t)$ in the figure is helped by comparison with the linear map $\mathcal{X}(\eta; t) = A\eta + B$, which contains the identity map for $A = 1, B = 0$. The complex map Z emerges then according to (13.61) as

$$Z(k, k', \eta; t) = \frac{1}{2\pi} \exp(ikB) \{ \cos[\eta(kA - k')] + i \sin[\eta(kA - k')] \}$$

The linear map would be simply cosinus and sinus waves for the real and imaginary parts of Z . The actual map $\mathcal{X}(\eta; t)$ produces rapid distortion near $\eta = 0$ and the k -wavenumber range that increases with k' . These distortions spread in k and η directions as time increases as can be seen by comparing the right and left graphs.

13.3 Problems for this Chapter

Problem 13.1 Compute the analytic solution of the IVP for the mapping pde (13.23) for a single conserved ($Q(\eta) = 0$) scalar. The scalar space is the unit interval $\mathcal{R}_\Phi = [0, 1]$, and the initial condition is

$$\mathcal{X}(\eta; 0) = \sum_{k=1}^N w_k H(\eta - \eta_k), \quad w_k \geq 0, \quad \sum_{k=1}^N w_k = 1$$

where $H(\eta - \eta_k)$ denotes the unit step function located at η_k .

13.1.1: Rescale the time variable t to transform the mapping pde to the form

$$\left(\frac{\partial}{\partial \tau} + \eta \frac{\partial}{\partial \eta} - \frac{\partial^2}{\partial \eta^2} \right) \mathcal{X}(\eta, \tau) = 0$$

13.1.2: Transform the scalar variable using $\tilde{\eta} \equiv \eta \exp(-\tau)$ to obtain a new pde for \mathcal{X} .

13.1.3: Solve the new pde for \mathcal{X} . The Green's function approach is recommended, see Duffy [9], Sect. 4.1 for details.

13.1.4: Plot the solution $\mathcal{X}(\eta; t)$ for several times in $[0, 0.3]$.

Problem 13.2 Compute and plot the Jacobian $J(\eta; t)$ and the Pdf $f(\varphi; t)$ for $t > 0$ using the mapping $\mathcal{X}(\eta; t)$ of the previous problem 13.1.

Problem 13.3 Hermite spectral method

Solve the IVP of the pde for the Jacobian $J(t, \eta)$ (13.25) assuming no source for $\eta \in \mathbb{R}^1$ and the representation of J

$$J(t, \eta) = \sum_{n=0}^{\infty} A_n(t) \Psi_n(\eta)$$

w.r.t. the ONS basis $\mathcal{B} = \{\Psi_n(\eta) \in L^2_{\mathbb{R}^1}, n = 0, 1, 2, \dots, \infty\}$ formed by the Hermite functions $\Psi_n(\eta)$ as defined by (4.29). Use the modified model expression

$$m(t) = (m_0 + m_1 \sqrt{t}) \exp(-T_s t), \quad m_0 = 10^{-4}, \quad m_1 = 0.75, \quad T_s = 0.01$$

to guarantee the existence of an asymptotic state.

13.3.1: Derive the system odes for the coefficients $A_n(t)$ using the ONS property

$$(\Psi_n, \Psi_m) \equiv \int_{-\infty}^{\infty} d\eta \Psi_n(\eta) \Psi_m(\eta) = \delta_{m,n}$$

of the Hermite functions.

13.3.2: Show that

$$\int_{-\infty}^{\infty} d\eta J(t, \eta)$$

is an invariant of the pde (13.25).

13.3.3: Prove the derivative relation (4.31) for the Hermite functions and show that the entries to the matrix

$$C_{m,n} \equiv \int_{-\infty}^{\infty} d\eta \frac{d\Psi_n}{d\eta} \left(\frac{d\Psi_m}{d\eta} + \eta \Psi_m \right)$$

can be evaluated analytically.

13.3.4: Set up an initial condition for the Jacobian $J(0, \eta)$ by first setting up the initial mapping $X(0, \eta)$ as linear combination of tanh functions

$$X(0, \eta) = \sum_{k=1}^N w_k H_k(\eta), \quad H_k(\eta) \equiv \frac{1}{2}[1 + \tanh(A_k(\eta - s_k))]$$

and then compute the initial Jacobian by differentiation, choose $N = 3$. Compute the associated coefficients $A_n(0) = (J(0, \eta), \Psi_n(\eta))$ using the derivative relation (4.31).

13.3.5: Solve the odes for the $A_n(t)$ numerically for a time interval $[0, 2]$. An accurate solver such as the fourth-order Runge–Kutta integrator is recommended. Plot the results for the Jacobian, the mapping and the Pdf.

References

1. Pope, S.B.: Mapping closures for turbulent mixing and reaction. *Theoret. Computat. Fluid Dyn.* **2**, 255–270 (1991)
2. Chen, H., Chen, S., Kraichnan, R.H.: Probability distribution of a stochastically advected scalar field. *Phys. Rev. Lett.* **62**, 2657 (1989)
3. Pope, S.B.: *Turbulent Flows*. Cambridge University Press, Cambridge, U.K. (2001)
4. Adler, R.J., Taylor, J.E.: *Random Fields and Geometry*. Springer, New York (2007)
5. Yadrenko, M.I.: *Spectral Theory of Random Fields*. Optimization Software Inc., Publication Division, New York (1983)

6. Wilczek, M., Meneveau, C.: Pressure Hessian and viscous contributions to velocity gradient statistics based on Gaussian random fields. *JFM* **756**, 191–225 (2014)
7. Olver, F.W., Lozier, D.W., Boisvert, R.F., Clark, C.W.: *NIST Handbook of Mathematical Functions*. Cambridge University Press, U.K. (2010)
8. Courant, R.: *Differential & Integral Calculus. vol. II*, Blackie & Sons Ltd, London (1962)
9. Duffy, D.G.: *Green's Functions with Applications*. Chapman & Hall/CRC, Boca Raton, Florida (2001)

Chapter 14

$\mathcal{M}_1(N)$: Mappings for Velocity–Scalar and Position–Scalar Pdfs



The extension of mapping methods to velocity–scalar (spatial description) and position–scalar (material description) Pdfs requires some preparations. First, a useful property of the Pdf equation is derived and its consequences for mapping methods are considered. The Pdf equation is regarded as a first-order pde and a slight modification of the characteristic theory of this class of equations (see Courant and Hilbert [1], vol. II (1962), Chap. II) leads to the basic result. Furthermore, it will be shown that it is not necessary to resort to the Cdf equation (as done by Pope [2]) for the development of mapping methods.

The section is organized as follows. First, the mapping equation applicable to velocity–scalar Pdfs in the spatial description is established. Then particular multi-point mapping methods in the spatial and the material description are formulated. A mapping method for two-point Pdfs is then considered as an important special case of the multidimensional Pdf formalisms providing spatial scale information. Finally, a useful reduction property of multivariable Pdfs determined by mappings is proved.

14.1 Single-Point Mapping Equation for Homogeneous Turbulence

Incompressible fluids and passive scalars are assumed in the present section, the extension to compressible fluid mixtures is possible, but significantly more complicated thus clouding the development of the mapping approach. The spatial description is chosen for the present considerations. Let velocity $v_\alpha(t, \mathbf{x})$ and M scalar fields $\Phi_i(t, \mathbf{x})$, $i = 1, \dots, M$ be defined in a flow domain $\mathcal{D} \subset \mathbb{R}^3$ with nearly everywhere smooth boundary $\partial\mathcal{D}$. The set of all velocity and scalar fields

$$\Omega \equiv \{\mathbf{v}(\mathbf{x}), \Psi(\mathbf{x}), \mathbf{x} \in \mathcal{D}\}$$

is the phase space. The set of values velocity and the set of scalars can assume at any point in the flow field is denoted by $\Omega_{loc} \equiv \Omega_v \times \Omega_M$, where $\Omega_v = \mathbb{R}^3$ and $\Omega_M \subset \mathbb{R}^M$, the latter may be unbounded or compact, but must be convex. It may possess an intricate geometric structure as examples from turbulent combustion show [2–4]. The Navier–Stokes equations govern the evolution of the velocity field and it is assumed that the Leray version for incompressible fluids with a Green’s function is available, see Eqs. (26.131)–(26.133) in Sect. 26.9

$$\frac{\partial v_r}{\partial t} = -T_r - \frac{\partial}{\partial r} \left[\mathcal{P}_h(r, \theta, \zeta) \frac{1}{Re} \frac{\partial^2 v_r}{\partial r^2} (\mathbf{x} \in \partial\mathcal{D}) + \mathcal{P}_G(r, \theta, \zeta) R(\mathbf{x}), \mathbf{x} \in \mathcal{D} \right] + \frac{1}{Re} F_r$$

$$\frac{\partial v_\theta}{\partial t} = -T_\theta - \frac{1}{r} \frac{\partial}{\partial \theta} \left[\mathcal{P}_h(r, \theta, \zeta) \frac{1}{Re} \frac{\partial^2 v_r}{\partial r^2} (\mathbf{x} \in \partial\mathcal{D}) + \mathcal{P}_G(r, \theta, \zeta) R(\mathbf{x}), \mathbf{x} \in \mathcal{D} \right] + \frac{1}{Re} F_\theta$$

$$\frac{\partial v_z}{\partial t} = -T_z - \frac{\partial P_0}{\partial z} - \frac{\partial}{\partial z} \left[\mathcal{P}_h(r, \theta, \zeta) \frac{1}{Re} \frac{\partial^2 v_r}{\partial r^2} (\mathbf{x} \in \partial\mathcal{D}) + \mathcal{P}_G(r, \theta, \zeta) R(\mathbf{x}), \mathbf{x} \in \mathcal{D} \right] + \frac{1}{Re} F_z$$

where T_i denotes the convective and F_i ($i = r, \theta, z$) the viscous terms defined in Sect. 26.9. The pressure gradient components $\nabla(\mathcal{P}_h + \mathcal{P}_G)$ (harmonic plus Green’s function contributions) are expressed in terms of a Green’s function as surface and volume integrals as the example of periodic pipe flow, Eqs. (26.76) and (26.128) in Chap. 26, shows.

The Leray version of the Navier–Stokes pdes emerges thus as a set of three integro-differential equations for three velocity components written in generic form as

$$\frac{\partial v_\alpha}{\partial t} = R_\alpha[\mathbf{v}; t, \mathbf{x}], \quad \alpha = r, \theta, z \quad (14.1)$$

where the brackets indicate non-local dependence. The Green’s function method is available for compact domains bounded by orientable surfaces; hence, the generic form (14.1) of the Navier–Stokes pdes is valid for the wide class of flows considered in the present section.

The scalar fields are governed by the generic pdes (12.20)

$$\frac{\partial \Phi_i}{\partial t} = R_i(\Phi(t, \mathbf{x}), t, \mathbf{x}) \quad (14.2)$$

for $i = 1, \dots, M$. It is clear that the equations governing velocity and scalars have a common form and complete system of equations can be written in generic form as

$$\frac{\partial \Phi_i}{\partial t} = R_i[\Phi_1(t, \mathbf{x}), \dots, \Phi_N(t, \mathbf{x}); t, \mathbf{x}], \quad \text{for } i = 1 \dots, N \quad (14.3)$$

where $N = M + 3$ and $\Phi_i = v_i$ for $i = 1, 2, 3$ are the velocity components and the brackets indicate functional dependency.

The mapping approach to the treatment of turbulent flows is presented with Pdf equations as starting point. The emphasis is on mappings and the equations determining them, modelling aspects are a separate issue and will not be covered in the present section. Now suppose the velocity–scalar Pdf

$$f_N(\varphi_1, \dots, \varphi_N, t) \prod_{i=1}^N d\varphi_i = \mu_N \{ \varphi_i \leq \Phi_i \leq \varphi_i + d\varphi_i, i = 1(1)N \}$$

depends on $N = M + 3$ probabilistic variables, i.e. f_N integrates to unity with respect to $\varphi_1, \dots, \varphi_N$, the dependence on time and location is not probabilistic and called parametric. The transport equation for f_N in homogeneous turbulence is formally given by (details in Chap. 11)

$$\frac{\partial f_N}{\partial t} + \sum_{i=1}^N \frac{\partial}{\partial \varphi_i} [\langle R_i | \Phi_1 = \varphi_1, \dots, \varphi_N \rangle f_N] = 0 \quad (14.4)$$

where the fluxes R_i are subject to the condition that random variables Φ_i assume the values φ_i for $i = 1(1)N$ in Ω_{loc} . However, the particular structure of the conditional expectations $\langle R_i | \dots \rangle$ is not important at the present section, only continuous differentiability is assumed. Subsequent sections are devoted to the analysis of the fluxes.

Consider a local mapping of R^N onto Ω_{loc} , $\mathcal{X} : R^N \rightarrow \Omega_{loc}$,

$$\varphi_i = \mathcal{X}_i(\eta_1, \dots, \eta_N, t), \quad i = 1(1)N, \quad \eta \in R^N, \quad \varphi \in \Omega_{loc} \quad (14.5)$$

such that the Jacobian J defined by (23.130)

$$J \equiv \det \left(\frac{\partial \mathcal{X}_i}{\partial \eta_j} \right) > 0$$

remains positive. Let $f_G(\eta_1, \dots, \eta_N)$ be N -variate Gaussian and let

$$f_N^*(\mathcal{X}_1(\eta_1, \dots, \eta_N, t), \dots, \mathcal{X}_N(\eta_1, \dots, \eta_N, t), t) = \frac{f_G(\eta_1, \dots, \eta_N)}{J(\eta_1, \dots, \eta_N, t)} \quad (14.6)$$

be the Pdf defined by f_G and the Jacobian J . It is easy to check that $f_N^* \geq 0$ and that $f_N^*()$ integrates to unity. Finally, it will be shown that the image f_N^* satisfies the transport equation

$$\left(\frac{\partial f_N^*}{\partial t} \right)_{\underline{\varphi}} + \sum_{i=1}^N \frac{\partial}{\partial \varphi_i} \left(\frac{\partial \mathcal{X}_i}{\partial t} f_N^* \right) = 0 \quad (14.7)$$

where $\varphi_i = \mathcal{X}_i(\eta_1, \dots, \eta_N, t) \in \Omega_{loc}$.

Proof 1 The time rate of change of f_N^* for η fixed, follows at once from implicit differentiation

$$\left(\frac{\partial f_N^*}{\partial t} \right)_\eta = \left(\frac{\partial f_N^*}{\partial t} \right)_\varphi + \sum_{i=1}^N \left(\frac{\partial f_N^*}{\partial \varphi_i} \right)_t \left(\frac{\partial \mathcal{X}_i}{\partial t} \right)_\eta$$

where $\varphi_i = \mathcal{X}_i(\eta_1, \dots, \eta_N, t)$ was used. Differentiation of the right-hand side of (14.6) leads to

$$\frac{\partial}{\partial t} \left(\frac{f_G}{J} \right)_\eta = -\frac{f_G}{J^2} \left(\frac{\partial J}{\partial t} \right)_\eta$$

Using (14.6)

$$\frac{\partial}{\partial t} \left(\frac{f_G}{J} \right)_\eta = -f_N^* \left(\frac{1}{J} \frac{\partial J}{\partial t} \right)_\eta$$

follows. The time rate of change of the Jacobian is given as a sum of determinants by

$$\frac{\partial J}{\partial t} = \sum_{k=1}^N \begin{vmatrix} \frac{\partial \mathcal{X}_1}{\partial \eta_1} & \dots & \frac{\partial \dot{\mathcal{X}}_k}{\partial \eta_1} & \dots & \frac{\partial \mathcal{X}_N}{\partial \eta_1} \\ \cdot & & \cdot & & \cdot \\ \cdot & & \cdot & & \cdot \\ \frac{\partial \mathcal{X}_1}{\partial \eta_N} & \dots & \frac{\partial \dot{\mathcal{X}}_k}{\partial \eta_N} & \dots & \frac{\partial \mathcal{X}_N}{\partial \eta_N} \end{vmatrix}$$

where the notation

$$\dot{\mathcal{X}}_i \equiv \left(\frac{\partial \mathcal{X}_i}{\partial t} \right)_\eta$$

is introduced for the time derivative. Consider now a differentiable function $F(\mathcal{X}_1, \dots, \mathcal{X}_N)$, where the arguments are functions $\mathcal{X}_i(\eta_1, \dots, \eta_N, t)$ and differentiate

$$\frac{\partial F}{\partial \eta_i} = \sum_{k=1}^N \frac{\partial F}{\partial \mathcal{X}_k} \frac{\partial \mathcal{X}_k}{\partial \eta_i}$$

Cramer's rule leads to an expression for the derivatives with respect to the \mathcal{X}_i

$$J \frac{\partial F}{\partial \mathcal{X}_i} = \begin{vmatrix} \frac{\partial \mathcal{X}_1}{\partial \eta_1} & \dots & \frac{\partial F}{\partial \eta_1} & \dots & \frac{\partial \mathcal{X}_N}{\partial \eta_1} \\ \cdot & & \cdot & & \cdot \\ \cdot & & \cdot & & \cdot \\ \frac{\partial \mathcal{X}_1}{\partial \eta_N} & \dots & \frac{\partial F}{\partial \eta_N} & \dots & \frac{\partial \mathcal{X}_N}{\partial \eta_N} \end{vmatrix}$$

where the derivatives of F appear in the i th column. Setting $F \equiv \dot{\mathcal{X}}_i$ and summing over $i = 1(1)N$ produces

$$J \sum_{i=1}^N \frac{\partial \dot{\mathcal{X}}_i}{\partial \mathcal{X}_i} = \sum_{k=1}^N \begin{vmatrix} \frac{\partial \mathcal{X}_1}{\partial \eta_1} & \dots & \frac{\partial \mathcal{X}_{k-1}}{\partial \eta_1} & \frac{\partial \dot{\mathcal{X}}_k}{\partial \eta_1} & \frac{\partial \mathcal{X}_{k+1}}{\partial \eta_1} & \dots & \frac{\partial \mathcal{X}_N}{\partial \eta_1} \\ \vdots & & \vdots & & \vdots & & \vdots \\ \frac{\partial \mathcal{X}_1}{\partial \eta_N} & \dots & \frac{\partial \mathcal{X}_{k-1}}{\partial \eta_N} & \frac{\partial \dot{\mathcal{X}}_k}{\partial \eta_N} & \frac{\partial \mathcal{X}_{k+1}}{\partial \eta_N} & \dots & \frac{\partial \mathcal{X}_N}{\partial \eta_N} \end{vmatrix}$$

which is identical with the time rate of change of the Jacobian. It follows that

$$\left(\frac{1}{J} \frac{\partial J}{\partial t} \right)_{\underline{\eta}} = \sum_{i=1}^N \frac{\partial \dot{\mathcal{X}}_i}{\partial \mathcal{X}_i}$$

holds, which in fact Euler's theorem, [5] Chap. 2. Combining the results for the left- and the right-hand sides and using

$$\varphi_i = \mathcal{X}_i(\eta_1, \dots, \eta_N, t)$$

leads to the conclusion that f_N^* , as defined by (14.6), satisfies

$$\left(\frac{\partial f_N^*}{\partial t} \right)_{\underline{\varphi}} + \sum_{i=1}^N \frac{\partial f_N^*}{\partial \varphi_i} \dot{\mathcal{X}}_i + \sum_{i=1}^N f_N^* \frac{\partial \dot{\mathcal{X}}_i}{\partial \varphi_i} = 0$$

or

$$\left(\frac{\partial f_N^*}{\partial t} \right)_{\underline{\varphi}} + \sum_{i=1}^N \frac{\partial}{\partial \varphi_i} \left(\frac{\partial \mathcal{X}_i}{\partial t} f_N^* \right) = 0$$

as claimed.

Note that the particular properties of the Gaussian reference measure did not enter the proof, only its time independence was used. It follows that any other time-independent reference measures such as the measure with beta function density suitable for bounded scalars could serve the same purpose. Comparison of (14.7) with (14.4) shows that this result allows the set up of the mapping equations for any number of variables. It follows that $f_N = f_N^*$ holds, if

$$\frac{\partial \mathcal{X}_i}{\partial t} = \langle R_i | \Phi_1 = \varphi_1, \dots \rangle, \quad i = 1(1)N \quad (14.8)$$

and the initial and boundary conditions for (14.4) and (14.7) are the same.

The relations (14.7) are the central result for mapping methods. It is instructive to compare (14.7) with the dynamic equations for the scalars $\Phi_i(\underline{x}, t)$. The scalars are instantaneously governed by

$$\frac{\partial \Phi_i}{\partial t}(t, \mathbf{x}) = R_i(\Phi_1(i\mathbf{x}, t), \dots, \Phi_N(\mathbf{x}, t, \mathbf{x})) \quad (14.9)$$

for $i = 1(1)N$ and the right-hand sides R_i obviously do not depend on the parameters $\varphi_1, \dots, \varphi_N$. The dynamic equations for non-homogeneous flows may be taken at different points in the flow field and the location vectors \mathbf{x} are then labelled accordingly. The mapping Eq. (14.7) contain the conditional expectation of the same right-hand sides R_i , but the expectations depend on the conditioning parameters $\varphi_1, \dots, \varphi_N$ defined as the values of the $\Phi_i(t, \mathbf{x}^{(i)})$ at locations $\mathbf{x}^{(i)}$.

14.1.1 Time-Dependent Reference Measures

A time-dependent reference measure could add flexibility to the mapping method by, for instance, have the mean value of the reference measure follow the evolution of the mean value of the turbulence field. For this reason, time-dependent reference measures are briefly discussed. The generalization of (14.6) to time-dependent reference measures

$$f_N^*(\mathcal{X}_1(\eta_1, \dots, \eta_N, t), \dots, \mathcal{X}_N(\eta_1, \dots, \eta_N, t), t) = \frac{f_G(\eta_1, \dots, \eta_N, t)}{J(\eta_1, \dots, \eta_N, t)} \quad (14.10)$$

leads to a generalized equation for f_N^* . The dependence of the reference measure on time is established for the case of a non-degenerate N -variate Gaussian given by

$$f_N^*(\eta_1, \dots, \eta_N; t) = \{(2\pi)^N \det(M_{ij})\}^{-\frac{1}{2}} \exp\left\{-\frac{1}{2} \sum_{i=1}^N \sum_{j=1}^N (\eta_i - \mu_i(t)) M_{ij}^{-1} (\eta_j - \mu_j(t))\right\} \quad (14.11)$$

in terms of the time dependence of its mean value vector $\bar{(\cdot)}(t)$ and covariance matrix $M_{ij}(t)$. The equation for the Pdf defined by (14.10) can be shown to be

$$\left(\frac{\partial f_N^*}{\partial t} \right)_\varphi + \sum_{i=1}^N \frac{\partial}{\partial \varphi_i} \left(\frac{\partial \mathcal{X}_i}{\partial t} f_N^* \right) = f_N^* \frac{\partial \log(f_G)}{\partial t} \quad (14.12)$$

The derivative for the logarithm of the reference density f_G can be established if the particular form of f_G is known. It follows for the Gaussian that

$$\frac{\partial \log(f_G)}{\partial t} = \sum_{i=1}^N \frac{\partial \log(f_G)}{\partial \mu_i} \frac{\partial \mu_i}{\partial t} + \sum_{i=1}^N \sum_{j=1}^N \frac{\partial \log(f_G)}{\partial M_{ij}^{-1}} \frac{\partial M_{ij}^{-1}}{\partial t} \quad (14.13)$$

holds. It follows from the Pdf equation (14.4) that a time-dependent reference measure is inappropriate, if the right-hand side of the Pdf equation is zero.

The properties of the flux Eq. (14.7) depend essentially on the formulation of the basic laws. Their particular structure will be analysed in the following sections

for the spatial and material descriptions. The case of two-point Pdfs in the spatial description will then receive special attention to illustrate the properties of mapping methods that are able to produce scale information.

14.2 Multipoint Mapping Method in the Spatial Description

The independent variables in the spatial description ([5], Chap. 2, [6]) are the observer position \mathbf{x} and time t . The evaluation of the conditional expectations in (14.4) requires now the knowledge of the particular properties of the generic fluxes R_i as defined by (14.3). The variables/fields used in the context of multipoint mappings in the spatial description are listed below.

Symbols	Interpretation
t	Time
$\mathbf{x}^{(i)}, i = 1(1)K$	Locations in flow domain \mathcal{D}
$\mathbf{y}^{(i)}, i = 1(1)K$	Locations in R^3
$v_\alpha(t, \mathbf{x}), \Phi_j(t, \mathbf{x}), j = 1(1)M$	Turbulent vector and scalar fields
$v_\alpha(t, \mathbf{x}^{(i)}), \Phi_j(t, \mathbf{x}^{(i)}), j = 1(1)M, i = 1(1)K$	Values of turbulent vector and scalar fields at K multipoints
$\Phi_j^{(i)} \equiv \Phi_j(t, \mathbf{x}^{(i)}), j = 1(1)N, N = M + 3, i = 1(1)K$	Generic notation of values of turbulent fields at K multipoints
$\Omega = \{\mathbf{v}(t, \mathbf{x}), \Psi_j(t, \mathbf{x}), j = 1(1)N\}$	Spatial phase space
$R_j^{(i)}, j = 1(1)N, i = 1(1)K$	Generic notation of right sides
$L_j^{(i)}, N_j^{(i)}, j = 1(1)N, i = 1(1)K$	Local and non-local parts of $R_j^{(i)}$
$G_j(\mathbf{y}), j = 1(1)M$	Gaussian reference fields
$G_j^{(i)} \equiv G_j(\mathbf{y}^{(i)}), j = 1(1)M, i = 1(1)K$	Values at K multipoints in R^3
$\hat{\Phi}_j^{(i)} \equiv \mathcal{X}_j^{(i)}(G_j(t, \mathbf{y}^{(i)})), j = 1(1)N, i = 1(1)K$	Values of the images of the Gaussian reference field

To set up a multipoint structure, $1 \leq K < \infty$ discrete points $\mathbf{x}^{(i)} \in \mathcal{D}$, $1 \leq i \leq K$ are selected and at each point N generic variables are specified. The random variables $\Phi_j^{(i)}$ are regarded as the values of stochastic fields at one or more than one or even all points $\mathbf{x}^{(i)}$ in the flow field D . Furthermore, the fluxes and the components of the mapping are denoted analogously by $R_j^{(i)}$, $\mathcal{X}_j^{(i)}$ as listed above.

The fluxes $R_j^{(i)}$ can be split into a linear/local and nonlinear/integral contributions according to the transport equations (26.131)–(26.133)

$$R_j^{(i)} = L_j^{(i)}(\Phi_l^{(i)}, \frac{\partial \Phi_k^{(i)}}{\partial x_\alpha^{(i)}}, \dots) + N_j^{(i)}(\Phi_k, \frac{\partial \Phi_k}{\partial x_\alpha}, \dots), \quad 1 \leq j \leq N^{(i)}, \quad 1 \leq i \leq K \quad (14.14)$$

where the lack of a superscript in the integral contribution indicates that it depends on any location in the flow field. It should be noted that the presence of spatial derivatives in the $R_j^{(i)}$ required the extension to stochastic fields. Examples for the local and integral contributions can be found by inspection of the basic laws (2.6) to (2.7). It is easy to see that the linear part

$$L_j^{(i)} = \begin{cases} \frac{1}{Re} \frac{\partial^2 \Phi_j^{(i)}}{\partial x_\alpha^{(i)} \partial x_\alpha^{(i)}} & \text{for } 1 \leq j \leq 3 \\ \frac{1}{Pe} \frac{\partial^2 \Phi_j^{(i)}}{\partial x_\alpha^{(i)} \partial x_\alpha^{(i)}} & \text{for } 3 < j \end{cases} \quad (14.15)$$

is local, where $Pe = Re \ Sch$ (composition scalars) or $Pe \equiv Re \ Pr$ (energy) denotes the Peclet number, and

$$N_j^{(i)} = -T_j + \begin{cases} \frac{\partial}{\partial x_\alpha^{(i)}} (I_3 + I_2) & \text{for } 1 \leq j \leq 3 \\ 0 & \text{for } 3 < j \end{cases} \quad (14.16)$$

is integral and, therefore, non-local/functional since

$$I_3(\mathbf{x}) \equiv \int_{\mathcal{D}} d\nu(\mathbf{x}') G(\mathbf{x}, \mathbf{x}') \frac{\partial^2}{\partial x_\alpha' \partial x_\beta'} (v_\alpha v_\beta)(t, \mathbf{x}') \quad (14.17)$$

is a volume integral and

$$I_2(\mathbf{x}) \equiv \int_{\partial\mathcal{D}} dA_\alpha(\mathbf{x}') h_\alpha(\mathbf{x}') G(\mathbf{x}, \mathbf{x}') \quad (14.18)$$

is a surface integral involving non-homogeneous Neumann boundary vector h_α defined by (9.20)

$$h_\alpha(\mathbf{x}') = \frac{1}{Re} \frac{\partial^2 v_\alpha}{\partial x'_\beta \partial x'_\beta} + \frac{1}{Fr} g_\alpha - \frac{\partial P_0}{\partial x_\alpha} - \frac{\partial v_\alpha^b}{\partial t} - v_\beta^b \frac{\partial v_\alpha^b}{\partial x'_\beta}, \quad \mathbf{x} \in \partial\mathcal{D} \quad (14.19)$$

where \mathbf{v}^b is the velocity at the boundary $\partial\mathcal{D}$, P_0 is the base pressure introduced in Sect. 9.2.1, whose gradient is constant for the pipe flow and assumed known, and g_α is the external volume force. Both integrals contain the Green's function $G(\mathbf{x}, \mathbf{x}')$, see Chap. 26, Duffy [7] for details.

The Gaussian random variables representing the arguments of the mapping are also regarded as the values of Gaussian reference fields at K locations $\mathbf{y}^{(i)}, i = 1(1)K$ in the domain of definition R^3 of the fields $G_j, j = 1(1)N$. The argument fields $G_j(\mathbf{y})$ are homogeneous Gaussian fields with time-independent statistical properties.

The interpretation of the random variables $\Phi_j^{(i)}$ and $G_j^{(i)}$ as stochastic fields at K points in the respective domains of definition implies that there must be relations of

these K points $\mathbf{y}^{(i)}$ in R^3 for the Gaussian argument fields to the corresponding K points $\mathbf{x}^{(i)}$ in the flow domain \mathcal{D} for the turbulent field values $\Phi_j^{(i)}$, the identity map being the trivial example. These spatial mappings $\mathbf{Y}^{(i)} : \mathcal{D} \rightarrow R^3$ are denoted by

$$\mathbf{y}^{(i)} = \mathbf{Y}^{(i)}(t, \mathbf{x}^{(i)}), \quad i = 1(1)K \quad (14.20)$$

They are time-dependent and were defined as pure stretching (13.16) in the case of single-point Pdfs. The $\mathbf{Y}^{(i)}$, $i = 1(1)K$ are a closure tool and not determined at this point. The subsequent development will show that the $\mathbf{Y}^{(i)}$ may be constructed as function of the mapping \mathcal{X} .

The fundamental requirement of mapping methods is

the conditional expectations of the turbulent fields $\Phi_j^{(i)}$ at the multipoints $\mathbf{x}^{(i)} \in \mathcal{D}$ are equal to the expectations of the images of the Gaussian reference fields $\mathcal{X}_j^{(i)}(G_j^{(i)})$, called surrogate fields, at the multipoints $\mathbf{y}^{(i)} \in R^3$ for $i = 1(1)K$ and $j = 1(1)N$.

The fluxes taken at the image fields with $\hat{R}_j^{(i)}$ are denoted by

$$\begin{aligned} \hat{R}_j^{(i)} &= R_j^{(i)}(t, \mathcal{X}(G_l^{(p)}), l = 1(1)N, p = 1(1)K) \\ &= L_j^{(i)}(\mathcal{X}(G_l^{(p)}), \frac{\partial}{\partial x_\alpha^{(i)}}(\mathcal{X}G_l^{(p)}), l = 1(1)N, p = 1(1)K) + \\ &\quad \hat{N}_j^{(i)}(\mathcal{X}(G_l^{(p)}), \frac{\partial}{\partial x_\alpha^{(i)}}(\mathcal{X}G_l^{(p)}), l = 1(1)N, p = 1(1)K) \end{aligned} \quad (14.21)$$

and

$$\hat{\Phi}_j^{(i)} = \mathcal{X}_j^{(i)}(G_1^{(p)}(\mathbf{y}^{(p)}(t, \mathbf{x}^{(p)}))), l = 1(1)N, p = 1(1)K \quad (14.22)$$

for $j = 1(1)N$, $i = 1(1)K$. The mapping closure can be written in the form

$$\langle R_j^{(i)} | \Phi_1^{(1)} = \varphi_1^{(1)}, \dots \rangle = \langle \hat{R}_j^{(i)} | \Psi_1^{(1)} = \eta_1^{(1)}, \dots \rangle, \quad 1 \leq i \leq K, 1 \leq j \leq N^{(i)} \quad (14.23)$$

where the fact that the mapping has a positive Jacobian was used to express the conditions on the image variables in terms of the argument variables. The equations

$$\frac{\partial \mathcal{X}_j^{(i)}}{\partial t}(\eta_1^{(1)}, \dots, \eta_K^{(N^{(i)})}, \mathbf{x}^{(1)}, \dots, \mathbf{x}^{(K)}, t) = \langle \hat{R}_j^{(i)} | \Psi_1^{(1)} = \eta_1^{(1)}, \dots, \Psi_K^{(i)} \rangle \quad (14.24)$$

for $j = 1(1)N^{(i)}$ and $i = 1(1)K$ (with appropriate change of notation compared to (14.7)) are called flux equations. Introducing the representation (14.14) for the fluxes leads to

$$\frac{\partial X_j^{(i)}}{\partial t} = \langle \hat{L}_j^{(i)} | \Psi_1^{(1)} = \eta_1^{(1)}, \dots \rangle + \langle \hat{N}_j^{(i)} | \Psi_1^{(1)} = \eta_1^{(1)}, \dots \rangle \quad (14.25)$$

for $j = 1(1)N^{(i)}$, $i = 1(1)K$. The presence of non-local contributions $N_j^{(i)}$ needs attention, because they contain the values of the turbulent fields at locations $\mathbf{y} \neq \mathbf{x}(i)$ for all $i = 1(1)N$, where they are not image of a Gaussian argument field, since the mapping (being local, i.e. only defined for the $\mathbf{x}^{(i)}$, $i = 1(1)N$) is not defined. Extending the mapping to non-local (or functional) character does not make sense, since no tractable mapping equation would emerge. The only avenue open on the level of N -point Pdfs is the construction of an additional closure for the non-local terms (such a closure was outlined by Chen et al. [8]). This aspect of mapping methods will not be pursued in the present chapter.

The Pdf f_N^* defined by (14.6) is not solution of the Pdf transport equation (14.7) for $N > 1$ or non-homogeneous turbulence, if the mapping $X_j^{(i)}$ is only applied to the probabilistic variables $\Phi_j^{(i)}$. This is a consequence of the fact that the locations $\mathbf{x}^{(i)}$ in the spatial description are parameters and not probabilistic variables, since they are arbitrarily chosen and there is no transport equation governing them. However, it is clear from the structure of the convective term in (14.7) that the notion of the mapping can be extended to include $\mathbf{Z} : [R^3]^N \rightarrow [D]^N$, which is determined by

$$\frac{\partial Z_j^{(i)}}{\partial t} = X_j^{(i)}(\eta_1^{(1)}, \dots, \eta_K^{(N^{(i)})}, \mathbf{x}^{(1)}, \dots, t, \mathbf{x}^{(K)}) \quad (14.26)$$

for $j = 1, 2, 3$ and $i = 1(1)K$, where the subscripts of $X_j^{(i)}$ are arranged such that $j = 1, 2, 3$ correspond to the velocity vector. The closure is completed by requiring that \mathbf{Z} is the inverse map of \mathbf{Y} introduced in (5.7)

$$Z_j^{(i)} = \left(Y_j^{(i)} \right)^{-1}, \quad j = 1(1)N^{(i)}, \quad i = 1(1)K \quad (14.27)$$

It is clear that $\mathbf{Y} : [D]^N \rightarrow [R^3]^N$ has a unique inverse is a basic requirement. Hence, the mapping \mathbf{Y} for the domains of definition is in general a function of the same set of independent variables as the mapping \mathbf{X} of the range of values.

14.3 Multipoint Mapping Method in the Material Description

The independent variables in the material description ([5], Chap. 2, [6]) are the label \mathbf{X} identifying a material point and time τ . The choice for the label variable is usually the position at the reference time zero, the (Lagrangian) position $\Phi_\alpha(\tau, \mathbf{X}) : \mathcal{D}(0) \leftrightarrow \mathcal{D}(\tau)$ is a dependent variable determined by the Navier–Stokes equations. However, if the velocity is known in the spatial description $v_\alpha(t, \mathbf{x})$, it can be computed by solving the kinematic pathline odes

$$\frac{\partial}{\partial \tau} \Phi_\alpha(\tau, \mathbf{X}) = v_\alpha(\tau, \Phi(\tau, \mathbf{X})), \quad \alpha = 1, 2, 3 \quad (14.28)$$

with initial condition $\Phi_\alpha(0, \mathbf{X}) = X_\alpha$, $\alpha = 1, 2, 3$. The Lagrangean position field $\Phi_\alpha(\tau, \mathbf{X})$ is the key to the transformation of the spatial and material descriptions [5, 6]. The material description is conveniently formulated using the notation summarized in the table below.

Symbols	Interpretation
τ	Time
$\mathbf{X}^{(i)}, i = 1(1)K$	Labels (locations) in label space $\mathcal{D}(0)$
$\mathbf{y}^{(i)}, i = 1(1)K$	Locations in R^3
$\Phi_\alpha(\tau, \mathbf{X}), \Psi_j(\tau, \mathbf{X}), j = 1(1)M$	Turbulent position and scalar fields
$\Phi_\alpha(\tau, \mathbf{X}^{(i)}), \Phi_j(\tau, \mathbf{X}^{(i)}), j = 1(1)M, i = 1(1)K$	Values of turbulent vector and scalar fields at multi-labels
$\Psi_j^{(i)} \equiv \Psi_j(\tau, \mathbf{X}^{(i)}), j = 1(1)N, N = M + 3, i = 1(1)K$	Generic notation of values of turbulent fields at multi-labels
$\Omega^L = \{\Phi(\tau, \mathbf{X}), \Psi(\tau, \mathbf{X})\}$	material phase space
$\Omega_2 = \{\Phi(\tau, \mathbf{X}^{(i)}), i = 1, 2\} = R^3 \times R^3$	Six-dimensional material phase space, Sect. 14.4
$R_j^{(i)}, j = 1(1)N, i = 1(1)K$	Generic notation of right sides
$L_j^{(i)}, N_j^{(i)}, j = 1(1)N, i = 1(1)K$	Local and non-local parts of $R_j^{(i)}$
$G_j(\mathbf{y}), j = 1(1)M$	Gaussian reference fields
$G_j^{(i)} \equiv G_j(\mathbf{y}^{(i)}), j = 1(1)M, i = 1(1)K$	Values at K multipoints in R^3
$\hat{\Phi}_j^{(i)} \equiv \mathcal{X}_j^{(i)}(G_j(t, \mathbf{y}^{(i)})), j = 1(1)N, i = 1(1)K$	Values of the images of the

The basic laws in the material description have been derived in Sect. 2.5.2, they are given by mass balance (2.85)

$$\frac{1}{6} \epsilon_{\alpha\beta\gamma} \epsilon_{\delta\eta\omega} F_{\alpha\delta} F_{\beta\eta} F_{\gamma\omega} = 1$$

stating that the Jacobian $J(\tau, \mathbf{X}) = \det(\frac{\partial \Phi_\beta}{\partial X_\alpha}) = \frac{1}{6} \epsilon_{\alpha\beta\gamma} \epsilon_{\delta\eta\omega} F_{\alpha\delta} F_{\beta\eta} F_{\gamma\omega}$, the left side of the equation above, is unity, and momentum balance (2.86) as

$$\frac{\partial^2 \Phi_{\alpha}^{(i)}}{\partial \tau^2} = R_{\alpha}^{(i)} \quad (14.29)$$

where the superscript (i) denotes a particular label. The right-hand sides are

$$R_{\alpha}^{(i)} \equiv -\frac{1}{2R} \epsilon_{\alpha\beta\gamma} \epsilon_{\delta\eta\omega} F_{\beta\eta} F_{\gamma\omega} \frac{\partial P}{\partial X_{\delta}} + \frac{1}{2Re} \epsilon_{\theta\beta\gamma} \epsilon_{\delta\eta\omega} F_{\zeta\eta} F_{\phi\omega} \frac{\partial}{\partial X_{\delta}} \left(F_{\zeta\beta} F_{\phi\gamma} \frac{\partial^2 \Phi_{\alpha}}{\partial X_{\theta} \partial \tau} \right) + \frac{1}{Fr} G_{\alpha} \quad (14.30)$$

taken at label $\mathbf{X}^{(i)}$. The deformation gradient $F_{\alpha\beta}$ is defined by (2.82). The pressure can be expressed in terms of the velocity field as for the spatial description with the aid of a Green's function and velocity. Since the Green's function approach for the Poisson pde does not involve time derivatives, the result for the spatial description carries over to the material description using the transformation rules (Sect. 2.5) and transforming the volume and surface integrals. Adapting (14.17)

$$I_3(\mathbf{X}) \equiv \int_{\mathcal{D}(0)} d\nu(0, \mathbf{X}') J(\mathbf{X}) G(\Phi(\tau, \mathbf{X}), \Phi(\tau, \mathbf{X}')) \frac{\partial^2}{\partial x'_{\alpha} \partial x'_{\beta}} (v_{\alpha} v_{\beta})(\mathbf{X}')$$

in mixed formulation, where the second derivatives can be transformed to the material description resulting in lengthy expressions. The surface integral (14.18) is transformed using the relation $dA_{\alpha}(\tau, \mathbf{X}) = F_{\beta\alpha}^{-1} J dA_{\beta}(0, \mathbf{X})$ for the surface differentials in the material description ([5], Chap. 2.12)

$$I_2(\tau, \mathbf{X}) \equiv \int_{\partial\mathcal{D}(0)} dA_{\alpha}(0, \mathbf{X}') F_{\beta\alpha}^{-1}(\tau, \mathbf{X}') J(\tau, \mathbf{X}') h_{\alpha}(\Phi(\tau, \mathbf{X}')) G(\Phi(\tau, \mathbf{X}), \Phi(\tau, \mathbf{X}'))$$

are obtained using the Jacobian J to transform the integrals. The pressure in the material description is thus represented as a sum of a volume integral and a surface integral

$$P[\frac{\partial \Phi}{\partial \tau}(.); \tau, \mathbf{X}] = I_3[\frac{\partial \Phi}{\partial \tau}(.); \tau, \mathbf{X}] + I_2[\frac{\partial \Phi}{\partial \tau}(.); \tau, \mathbf{X}]$$

as in the spatial description.

A single passive scalar field $\Psi(\tau, \mathbf{X})$ is considered, the extension to a multitude of scalars as in the previous section is straightforward. The material version of the scalar pde is

$$\frac{\partial \Psi}{\partial \tau} = Q(\Psi) + \frac{1}{2Pe} \epsilon_{\theta\beta\gamma} \epsilon_{\delta\eta\omega} F_{\zeta\eta} F_{\phi\omega} \frac{\partial}{\partial X_{\delta}} \left(F_{\zeta\beta} F_{\phi\gamma} \frac{\partial \Psi}{\partial X_{\theta}} \right) \quad (14.31)$$

where the left side is the time rate of change of the scalar following a material point and $Q(\Psi)$ denotes a local source term and the last term is the Laplacian in the material description representing diffusion of the scalar $\Psi(\tau, \mathbf{X})$. Details for the transformation of dependent variables and derivatives can be found in [5] Chap. 2. The set of dependent variables consists now of position $\Phi(\tau, \mathbf{X}) \in \mathcal{D}(\tau)$ and scalar $\Psi(\tau, \mathbf{X})$

for $\mathbf{X} \in \mathcal{D}(0)$, the Lagrangean phase space is then $\Omega^L \equiv \{\Phi(\tau, \mathbf{X}), \Psi(\tau, \mathbf{X}), \mathbf{X} \in \mathcal{D}(0), \tau \geq 0\}$.

The mapping equations developed in Sect. 14.3 can be applied with minor modifications. The components of the local mapping (13.5)

$$\mathcal{X}_j^{(i)}(g_j^{(p)}, p = 1(1)K, l = 1(1)4, \tau), i = 1(1)K, j = 1(1)4 : [R^3 \times R^1]^K \rightarrow \{\Phi^{(i)}, \Psi^{(i)}, i = 1(1)K\} \quad (14.32)$$

($\mathcal{X}_j^{(i)}$ should not be confused with the label variable \mathbf{X}) are ordered such that $\mathcal{X}_j^{(i)}$ corresponds to Lagrangean position for $j = 1, 2, 3$ and to the scalar for $j = 4$, the superscript indicates the material points $\mathbf{X}^{(i)}$ selected in the label space (initial flow domain) $\mathcal{D}(0)$. The Gaussian random variables $g_j^{(i)}$ as the arguments of the mapping $\mathcal{X}_j^{(i)}$ are defined as the values of a Gaussian vector and a scalar field, $g_j^{(i)} \equiv G_j(\mathbf{y}^{(i)}), j = 1(1)3, g_j^{(i)} = G_4(\mathbf{y}^{(i)}), j = 4$ at locations $\mathbf{y}^{(i)} \in R^3$ for $i = 1(1)K$. These locations are computed as follows. The condition of a positive Jacobian $J(\tau, \mathbf{X})$ for the mapping $\mathcal{X}_j^{(i)}$ implies that there exists a unique inverse $(\mathcal{X}_j^{(i)})^{-1}$, which is for $j = 1, 2, 3$ the Gaussian distributed reference field at the $\mathbf{y}^{(i)} \in R^3$

$$G_j(\mathbf{y}^{(i)}) = \{\mathcal{X}_j^{(i)}\}^{-1}(\mathbf{X}^{(1)}, \dots, \mathbf{X}^{(N)}) \quad (14.33)$$

for $j = 1, 2, 3$. The locations $\mathbf{y}^{(i)} \in R^3$ are then set by the initial condition for the mapping

$$y_j^{(i)} = \{\mathcal{X}_j^{(i)}\}^{-1}(\mathbf{X}^{(1)}, \dots, \mathbf{X}^{(N)}, 0), \quad j = 1, 2, 3 \quad (14.34)$$

since $\Phi_j^{(i)} = X_j^{(i)}$ at $\tau = 0$. The locations $\mathbf{y}^{(i)}$ are thus set up and independent of time.

The flow domain $\mathcal{D}(\tau)$ is assumed materially invariant and thus a function of time, the general case of open and partially open domains (with entrance and exit sections) requires sophisticated modifications in the material description, see Pileckas [9], Constantin [10]. $\mathcal{D}(\tau)$ represents the range of the dependent variable position $\Phi(\tau, \mathbf{X})$, whereas $\mathcal{D}(0)$ is the domain of definition of the dependent variables Φ and Ψ .

The random variables $\Phi(\tau, \mathbf{X})$ for fixed time τ and label \mathbf{X} appearing in the Pdf equation (14.4) are interpreted as the values of stochastic fields at one or more than one labels $\mathbf{X}^{(i)} \in \mathcal{D}(0), i = 1(1)K$. A set of four variables $\Psi_j(\tau, \mathbf{X}^{(i)}), j = 1(1)4$ denoting position $\Phi_\alpha, \alpha = 1, 2, 3$ and scalar Ψ at the selected labels $\mathbf{X}^{(i)}, i = 1(1)K \in \mathcal{D}(0)$ is the set of $4K$ probabilistic variables in the Lagrangean Pdf $f_{4K}^L(\eta_1^{(1)}, \dots, \eta_4^{(K)}; \mathbf{X}^{(1)}, \dots, \mathbf{X}^{(K)}, \tau)$.

The right sides determining the evolution of $\Psi_j(\tau, \mathbf{X}^{(i)})$ according to (2.85), (2.86) and (14.31) are denoted by $R_j^{(i)}$ as before. They can be split into a linear/local and integral/functional contributions

$$\frac{\partial^2 \Psi_j^{(i)}}{\partial \tau^2} = R_j^{(i)} : R_j^{(i)} = L_j^{(i)}(\Psi_l^{(i)}, \frac{\partial \Psi_k^{(i)}}{\partial X_\alpha^{(i)}}, \dots) + N_j^{(i)}[\Psi_k, \frac{\partial \Psi_k}{\partial X_\alpha}, \dots], \quad \text{for } j = 1(1)3 \quad (14.35)$$

$$\frac{\partial \Psi_j^{(i)}}{\partial \tau} = R_j^{(i)} : R_j^{(i)} = L_j^{(i)}(\Psi_l^{(i)}, \frac{\partial \Psi_k^{(i)}}{\partial X_\alpha^{(i)}}, \dots) + N_j^{(i)}(\Psi_k^{(i)}, \frac{\partial \Psi_k^{(i)}}{\partial X_\alpha}, \dots), \text{ for } j = 4 \quad (14.36)$$

where the differentiation is with respect to the initial position/label \mathbf{X} , the lack of a superscript in the integral contribution indicates that it depends on any location \mathbf{X} in the label field $\mathcal{D}(0)$.

The fundamental requirement of mapping methods is the condition that the expectations of the turbulent fields $\Phi_j^{(i)} = \Psi_j(\tau, \mathbf{X}^{(i)})$ are equal to the expectations of the surrogate fields

$$\hat{\Psi}_j^{(i)} = \mathcal{X}_j^{(i)}(G_l(\mathbf{y}^{(p)}, p = 1(1)K, l = 1(1)4) \quad (14.37)$$

i.e. images of the Gaussian argument fields $G_j(\mathbf{y}^{(i)})$ and its derivatives at the locations $\mathbf{y}^{(i)}$ defined by (14.34) for $i = 1(1)K$, $j = 1(1)4$. If the $R_j^{(i)}$, taken at the image (surrogate) fields, are denoted by $\hat{R}_j^{(i)}$

$$\hat{R}_j^{(i)} = R_j^{(i)}[\mathcal{X}_l^{(p)}(G_m(\mathbf{y}^{(q)}, m = 1(1)4, q = 1(1)K), l = 1(1)4, p = 1(1)K), \tau] \quad (14.38)$$

for $i = 1(1)K$, $j = 1(1)4$, the mapping method can be formulated implicitly as

$$\langle R_j^{(i)} | \Phi_l^{(p)} = \varphi_l^{(p)}, l = 1(1)4, p = 1(1)K \rangle = \langle \hat{R}_j^{(i)} | \Psi_l^{(p)} = \eta_l^{(p)}, l = 1(1)4, p = 1(1)K \rangle \quad (14.39)$$

for $j = 1(1)4$, $i = 1(1)K$, where (14.5) relates the arguments φ and η . The fact that the mapping has a positive Jacobian was used to express the conditions on the image variables in terms of the argument variables. Introducing the representation (14.35) for the $R_j^{(i)}$ leads to the implicit mapping equations

$$\frac{\partial^2 \mathcal{X}_j^{(i)}}{\partial \tau^2} = \langle \hat{L}_j^{(i)} | \Psi_l^{(p)} = \eta_l^{(p)}, l = 1(1)N, p = 1(1)K \rangle + \langle \hat{N}_j^{(i)} | \Psi_l^{(p)} = \eta_l^{(p)}, l = 1(1)3, p = 1(1)K \rangle \quad (14.40)$$

for $j = 1, 2, 3$ and

$$\frac{\partial \mathcal{X}_j^{(i)}}{\partial \tau} = \langle \hat{L}_j^{(i)} | \Psi_l^{(p)} = \eta_l^{(p)}, l = 1(1)N, p = 1(1)K \rangle + \langle \hat{N}_j^{(i)} | \Psi_l^{(p)} = \eta_l^{(p)}, l = 4, p = 1(1)K \rangle \quad (14.41)$$

for $j = 4$. The non-local contributions $N_j^{(i)}$ present the same difficulty as in the spatial description, since they contain the values of the turbulent fields at labels $\mathbf{X} \neq \mathbf{X}^{(i)}$ for all $i = 1(1)N$.

Summary

All argument fields $G_j^{(i)}(\mathbf{y})$ are stationary and homogeneous Gaussian fields taken at the discrete locations $\mathbf{y}^{(i)} \in R^3$, $i = 1(1)K$. The deterministic conditions (14.33) and (14.34) at time $\tau = 0$ are enforced as initial conditions for the mapping $\mathcal{X}_j^{(i)}$, which approaches appropriate constants for $\tau \rightarrow \infty$, thus producing marginal Dirac Pdfs for position. There is no need to introduce time-dependent reference measures.

14.4 Mapping Method for Two-Point Pdfs in the Material Description

The mapping methods in the material description developed in Sect. 14.3 is outlined for a special case of particular importance. The Pdf for positions taken at two labels $\mathbf{X}^{(i)}$, $i = 1, 2$ in homogeneous turbulence is considered. The equation for the material, two-point position Pdf

$$f_2^L(\mathbf{q}^{(1)}, \mathbf{q}^{(2)}; \tau, \mathbf{X}^{(1)}, \mathbf{X}^{(2)}) = \langle \hat{f}_2^L \rangle$$

where \hat{f}_2^L is the coarse-grained Pdf

$$\hat{f}_2^L = \prod_{i=1}^2 \prod_{\alpha=1}^3 \delta(\Phi_\alpha(\tau, \mathbf{X}^{(i)}) - q_\alpha^{(i)})$$

follows from the same procedure as in the spatial description (the equation for the single label position Pdf is derived as solution to Problem 12.2). The result is, using the definition (14.30) for the right-hand side of momentum balance,

$$\frac{\partial^2 f_2^L}{\partial \tau^2} + \sum_{i=1}^2 \frac{\partial}{\partial q_\alpha^{(i)}} [\langle R_\alpha^{(i)} | \mathcal{V}_2 \rangle f_2^L] - \sum_{i=1}^2 \sum_{j=1}^2 \frac{\partial^2}{\partial q_\alpha^{(i)} \partial q_\beta^{(j)}} [\langle \frac{\partial \Phi_\alpha^{(i)}}{\partial \tau} \frac{\partial \Phi_\beta^{(j)}}{\partial \tau} | \mathcal{V}_2 \rangle f_2^L] = 0 \quad (14.42)$$

where the conditions are abbreviated by

$$\mathcal{V}_2 \equiv \{\Phi(\tau, \mathbf{X}^{(i)}) = \mathbf{q}^{(i)}, i = 1, 2\}$$

The IVP for this pde requires an initial condition, the Dirichlet variant is

$$f_2^L(\mathbf{q}^{(1)}, \mathbf{q}^{(2)}; 0, \mathbf{X}^{(1)}, \mathbf{X}^{(2)}) = f_0(\mathbf{q}^{(1)}, \mathbf{q}^{(2)}; \mathbf{X}^{(1)}, \mathbf{X}^{(2)})$$

which includes the set up of the labels, i.e. the initial positions, $\mathbf{X}^{(i)}$, $i = 1, 2$. The pde for the Lagrangean position Pdf (14.42) is of hyperbolic type in contrast to its parabolic spatial counterpart (11.50) in the previous section. It contains conditional expectations that cannot be computed using f_2^L alone. The set of all values $\Omega_2 \equiv \{\Phi(\tau, \mathbf{X}^{(i)}), i = 1, 2\} \subset R^3 \times R^3$ of the mapping $\mathcal{X}_j^{(i)} : \Omega_2 \rightarrow \Omega_2$ is the phase space for the two Lagrangean position variables.

The mapping equations developed in Sect. 14.3 can be specialized to the two-label position case. The components of the local mapping (13.5)

$$\mathcal{X}_j^{(i)}(g_l^{(p)}, p = 1, 2, l = 1(1)3, \tau), i = 1, 2, j = 1(1)3 : R^3 \times R^3 \rightarrow \{\Phi^{(i)}, i = 1, 2\} \quad (14.43)$$

are the Lagrangean position components for $j = 1, 2, 3$, the superscript indicates the material points $\mathbf{X}^{(i)}$, $i = 1, 2 \in \mathcal{D}(0)$. The Gaussian random variables $g_j^{(i)}$, as the arguments of the mapping $\mathcal{X}_j^{(i)}$, are defined as the values of a Gaussian vector $g_j^{(i)} = G_j(\mathbf{y}^{(i)})$, $j = 1(1)3$ at locations $\mathbf{y}^{(i)} \in R^3$ for $i = 1, 2$. These locations are computed as before: The Jacobian $J(\tau, \mathbf{X}) > 0$ implies $(\mathcal{X}_j^{(i)})^{-1}$, which is the Gaussian distributed reference field at the $\mathbf{y}^{(i)} \in R^3$ (14.33) $G_j(\mathbf{y}^{(i)}) = \{\mathcal{X}_j^{(i)}\}^{-1}(\mathbf{X}^{(i)}, \mathbf{X}^{(2)})$, $j = 1, 2, 3$. The locations $\mathbf{y}^{(i)} \in R^3$ are then set by the initial condition for the mapping (14.34) $y_j^{(i)} = \{\mathcal{X}_j^{(i)}\}^{-1}(\mathbf{X}^{(1)}, \mathbf{X}^{(2)}, 0)$, $j = 1, 2, 3$ since $\Phi_j^{(i)} = X_j^{(i)}$ at $\tau = 0$. The locations $\mathbf{y}^{(i)}$ are thus set up and independent of time. The flow domain $\mathcal{D}(\tau)$ represents the range of the dependent variable position $\Phi(\tau, \mathbf{X})$, for $\tau = 0$ it is the domain of definition of the dependent vector Φ .

The positions $\Phi(\tau, \mathbf{X}^{(i)})$ for fixed time τ and label $\mathbf{X}^{(i)}$, $i = 1, 2$ appearing in the Pdf equation (14.4) are interpreted as the values of stochastic fields at the indicated labels. The set of two times three variables $\Phi_j(\tau, \mathbf{X}^{(i)})$, $j = 1(1)3$ at the selected labels $\mathbf{X}^{(i)}$, $i = 1, 2 \in \mathcal{D}(0)$ is the set of 6 probabilistic variables in the Pdf $f_2^L(\eta_1^{(1)}, \dots, \eta_3^{(2)}; \mathbf{X}^{(1)}, \mathbf{X}^{(2)}, \tau)$.

The right sides determining the evolution of the positions $\Phi_j(\tau, \mathbf{X}^{(i)})$ according to (2.85), (2.86) are denoted by $R_j^{(i)}$, equation (14.30). They can be split into a linear/local and integral/functional contributions as before

$$R_j^{(i)} = L_j^{(i)}(\Phi_l^{(i)}, \frac{\partial \Phi_k^{(i)}}{\partial X_\alpha^{(i)}}, \dots) + N_j^{(i)}[\Phi_k, \frac{\partial \Phi_k}{\partial X_\alpha}, \dots] \quad (14.44)$$

for $j = 1, (1), 3$, $i = 1, 2$, where the differentiation is with respect to the initial position (label) \mathbf{X} , the lack of a superscript in the integral contribution indicates that it depends on any location \mathbf{X} in the label field $\mathcal{D}(0)$.

The requirement of mapping methods is the condition that the expectations of the turbulent fields $\Phi_j^{(i)} = \Phi_j(\tau, \mathbf{X}^{(i)})$, $i = 1, 2$ are equal to the expectations of the surrogate fields

$$\hat{\Phi}_j^{(i)} = \mathcal{X}_j^{(i)}(G_l(\mathbf{y}^{(p)}), p = 1, 2, l = 1(1)3) \quad (14.45)$$

i.e. images of the Gaussian argument fields $G_j(\mathbf{y}^{(i)})$ and its derivatives at the locations $\mathbf{y}^{(i)}$ defined by (14.34) for $i = 1, 2$, $j = 1(1)3$. If the fluxes computed for the image (surrogate) fields are denoted by $\hat{R}_j^{(i)}$

$$\hat{R}_j^{(i)} = R_j^{(i)}[\mathcal{X}_l^{(p)}(G_m(\mathbf{y}^{(q)}), m = 1(1)3, q = 1, 2), l = 1(1)3, p = 1, 2, \tau] \quad (14.46)$$

for $i = 1, 2$, $j = 1(1)3$, the mapping method can be formulated by time differentiation

$$\frac{\partial^2 \mathcal{X}_j^{(i)}}{\partial \tau^2} = \langle \hat{L}_j^{(i)} | \Psi_l^{(p)} = \eta_l^{(p)}, l = 1(1)3, p = 1, 2 \rangle + \langle \hat{N}_j^{(i)} | \Psi_l^{(p)} = \eta_l^{(p)}, l = 1(1)3, p = 1, 2 \rangle \quad (14.47)$$

for $j = 1, 2, 3$. The non-local contributions $N_j^{(i)}$ present the same difficulty as in the spatial description, since they contain the values of the turbulent fields at labels $\mathbf{X} \neq \mathbf{X}^{(i)}$ for all $i = 1(1)N$.

14.5 A Pdf Reduction Property for Multidimensional Mappings

The closure problem for mappings can be viewed as the construction of a global map corresponding to the local map which is to be determined as the solution of the mapping equation. The relation of the global map to the local map needs clarification since they act on the same class of reference and turbulence fields. If the global map is known we can calculate the statistics at any number of points as the image of Gaussian statistics. Hence, we can calculate the statistics at a single point which implies that there exists a relation between the mapping for a single variable and the mapping for many variables containing the single point. This relation can be obtained as follows. Pdfs possess a well-known reduction property given by

$$f_1(\varphi_N) = \int_{-\infty}^{\infty} d\varphi_1 \cdots \int_{-\infty}^{\infty} d\varphi_{N-1} f_N(\varphi_1, \dots, \varphi_N) \quad (14.48)$$

which must be retained if the Pdfs are transformed Gaussians. Let the local mapping be $\mathcal{X} : R^1 \rightarrow \Omega$, where Ω denotes the range of the scalar defined at a single point in the flow field $D(t)$, and the global (N-dimensional) mapping $\mathcal{X} : R^N \rightarrow \Omega^N$, then are the one-dimensional Pdf

$$f(y) = \frac{f_G(\eta)}{\frac{\partial \mathcal{X}}{\partial \eta}} \quad (14.49)$$

and the N-dimensional Pdf given by

$$f_N(y_1, \dots, y_N) = \frac{f_G(\eta_1, \dots, \eta_N)}{\det\left(\frac{\partial \mathcal{X}_i}{\partial \eta_j}\right)} \quad (14.50)$$

respectively, where $y = \mathcal{X}(\eta)$ and $\mathbf{y} = \mathcal{X}(\eta_1, \dots, \eta_N)$ hold. Application to the reduction property for Pdfs leads to

$$\frac{f_G(\eta)}{\frac{\partial \mathcal{X}}{\partial \eta}} = \int_{-\infty}^{\infty} d\varphi_1 \cdots \int_{-\infty}^{\infty} d\varphi_{N-1} \det\left(\frac{\partial \mathcal{X}_i}{\partial \eta_j}\right)_{N-1} \frac{f_G(\eta_1, \dots, \eta_N)}{\det\left(\frac{\partial \mathcal{X}_i}{\partial \eta_j}\right)_N} \quad (14.51)$$

where the subscripts on the Jacobian matrices indicate the rank. Since the Gaussian reference measure is the product of N one-dimensional measures, it follows that

$$\frac{\partial \mathcal{X}^{-1}}{\partial \eta} = \int_{-\infty}^{\infty} d\varphi_1 \cdots \int_{-\infty}^{\infty} d\varphi_{N-1} \frac{\det\left(\frac{\partial \mathcal{X}_i}{\partial \eta_j}\right)_{N-1}}{\det\left(\frac{\partial \mathcal{X}_i}{\partial \eta_j}\right)_N} \prod_{i=1}^{N-1} f_G(\eta_i) \quad (14.52)$$

holds. Denoting by $dG_i \equiv d\eta_i f_G(\eta_i)$ the differential of the standard Gaussian measure (zero mean and unit variance) we get

$$\left(\frac{\partial \mathcal{X}}{\partial \eta}\right)^{-1} = \int_{-\infty}^{\infty} dG_1 \cdots \int_{-\infty}^{\infty} dG_{N-1} \frac{\det\left(\frac{\partial \mathcal{X}_i}{\partial \eta_j}\right)_{N-1}}{\det\left(\frac{\partial \mathcal{X}_i}{\partial \eta_j}\right)_N} \quad (14.53)$$

as reduction property for mappings. It is worth noting that this relation can be extended to infinitely many variables since the Gaussian has a well-defined limit. It is easy to show that the reduction property appears in the form (note that $\eta \equiv \eta_N$)

$$\left(\frac{\partial \mathcal{X}}{\partial \eta}\right)^{-1} = \int_{-\infty}^{\infty} dG(\eta_1) \cdots \int_{-\infty}^{\infty} dG(\eta_{N-1}) \left(\frac{\partial}{\partial \eta_N} \mathcal{X}_N(\eta_1, \dots, \eta_N)\right)^{-1} \quad (14.54)$$

if the Jacobian matrices are triangular. This particular form of the reduction property expresses the one-dimensional map for the N th variable η_N in terms of the global or N -dimensional map for all variables η_1, \dots, η_N . It depends obviously on the Gaussian reference measure.

14.6 Summary

The original idea of mapping methods was aimed at producing a closure for the term representing the molecular transport effects in the Pdf equation and to enforce a particular asymptotic form of the solution. This idea can be extended significantly to a general approach to the formulation of the equations governing turbulence. In particular, the transport pdes obtained above as generalization of the CCK mapping method indicate that there is considerable freedom in setting up a mapping procedure. Its usefulness depends on two aspects:

- (i) The approach and form of the asymptotic state; and
- (ii) The number of independent variables.

The latter property becomes critical, if a large number of probabilistic variables are contemplated, for instance, multipoint and/or multi-time constructs in the Cdf/Pdf

equations. The mapping approach can be applied to the characteristic function, as the characteristic function for the reference Gaussian is explicitly known. The mapping of the reference Pdf to the characteristic function of the turbulent scalar field and the mapping of the reference characteristic function onto the function for the turbulent field were established resulting in complex mapping functions. The mapping function in the former case turns out to be a distribution.

References

1. Courant, R.: Differential & Integral Calculus. vol. II, Blackie & Sons Ltd, London (1962)
2. Pope, S.B.: Mapping closures for turbulent mixing and reaction. *Theoret. Computat. Fluid Dyn.* **2**, 255–270 (1991)
3. Pope, S.B.: Turbulent Flows. Cambridge University Press, Cambridge, U.K. (2001)
4. Poinsot, T., Veynante, D.: Theoretical and Numerical Combustion. R.T. Edwards, Philadelphia, PA (2001)
5. Kollmann, W.: Fluid Mechanics in Spatial and Material Description. University Readers, San Diego (2011)
6. Wu, J.-Z., Ma, H.-Y., Zhou, M.-D.: Vorticity and Vortex Dynamics. Springer, Berlin (2006)
7. Duffy, D.G.: Green's Functions with Applications. Chapman & Hall/CRC, Boca Raton, Florida (2001)
8. Chen, H., Chen, S., Kraichnan, R.H.: Probability distribution of a stochastically advected scalar field. *Phys. Rev. Lett.* **62**, 2657 (1989)
9. Pileckas, K.: Navier-Stokes system in domains with cylindrical outlets to infinity. In: Friedlander, S., Serre, D. (eds.) *Handbook of Mathematical Fluid Dynamics*, vol. 4, North Holland, pp. 447–647 (2007)
10. Constantin, P.: Lagrangian-Eulerian methods for uniqueness in hydrodynamic systems. *SIAM J. Math. Anal.* **49**, 1041–1047 (2015)

Chapter 15

Integral Transforms and Spectra



Integral transforms with respect to time and/or space yield scale information. The main transform tool to be discussed in the present section is Fourier transform between physical and spectral space. There is a variety of integral transforms available [1], the most recent development being the wavelet transform, see Daubechies [2], Meneveau [3] for the Navier–Stokes pdes in wavelet representation, Schneider and Vasilyev [4] for a survey on the application to fluid mechanics.

15.1 Fourier Transform (FT)

Vector and scalar fields in $L^2_{R^3}$ can be transformed according to (see, for instance, Gelfand and Vilenkin [5] for further details)

$$\hat{f}(\mathbf{k}) = \mathcal{F}f(\mathbf{x}), \quad f(\mathbf{x}) = \mathcal{F}^{-1}\hat{f}(\mathbf{k}) \quad (15.1)$$

where the Fourier transform operator pair is defined by

$$\mathcal{F}(\mathbf{k}) \equiv \frac{1}{(2\pi)^3} \int_{R^3} d\nu \exp(-i\mathbf{x} \cdot \mathbf{k}), \quad \mathcal{F}^{-1}(\mathbf{x}) \equiv \int_{R^3} d\mathbf{k} \exp(i\mathbf{x} \cdot \mathbf{k}). \quad (15.2)$$

The argument of the exponential must be dimensionless. If dimensional variable are used, the dimension of \mathbf{k} must be the inverse of the dimension of \mathbf{x} and the volume integrals must be divided by a scale factor in scalar products. However, the present development uses exclusively dimensionless variables.

There are several ways to write the Fourier transform depending where the factor $1/2\pi$ appears, using the Fourier kernel $\exp(2\pi i \mathbf{x} \cdot \mathbf{k})$ produces the symmetric version, i.e. no factor, but has the disadvantage that differentiation reintroduces the factor 2π . Hence, asymmetric versions (15.2) are frequently used, the particular form is

indicated in the individual sections. The product of two fields appears then in the form $f()g() = \mathcal{F}^{-1}\hat{f} * \hat{g}$, where

$$\hat{f} * \hat{g}(\mathbf{k}) = \int_{\mathbb{R}^3} d\mathbf{k}' \hat{f}(\mathbf{k}') \hat{g}(\mathbf{k} - \mathbf{k}') \quad (15.3)$$

defines convolution. If the independent variable \mathbf{x} has the dimension length L , then the wavenumber vector must have the dimension $1/L$ to insure that the argument of the Fourier kernel $\exp(i\mathbf{x} \cdot \mathbf{k})$ is dimensionless. Likewise, the argument field $f(\mathbf{x}) \in L^2_{\mathbb{R}^3}$, but $\hat{f}(\mathbf{k}) \in C^2_{\mathbb{R}^3}$ (space of square-integrable, complex-valued functions).

Fourier transform for $\mathcal{D} = [0, 2\pi]^3$

The space of square integrable functions $L^2_{[0, 2\pi]^3}$ has a Schauder ONS basis

$$\mathbf{z}(\mathbf{x}, \mathbf{k}) = \frac{1}{(2\pi)^3} \exp(-i\mathbf{x} \cdot \mathbf{k}) \quad (15.4)$$

where $\exp(-i\mathbf{x} \cdot \mathbf{k})$ is called Fourier kernel, Schauder bases are defined in Chap. 4.

15.2 Fourier Transformed Navier–Stokes Equations

An important tool for the investigation of homogeneous turbulence is Fourier transformation as discussed in Sect. 15.1. The velocity and pressure fields are decomposed into component motions (or modes) defined in the whole flow field of different length scales by

$$\hat{\mathbf{v}}_\alpha(\mathbf{k}, t) = \mathcal{F}v_\alpha(\mathbf{x}, t) = \frac{1}{(2\pi)^3} \int_{\mathcal{D}} d\nu v_\alpha(\mathbf{x}, t) \exp(-ik_\beta x_\beta) \quad (15.5)$$

$$\hat{p}(\mathbf{k}, t) = \mathcal{F}p(\mathbf{x}, t) = \frac{1}{(2\pi)^3} \int_{\mathcal{D}} d\nu p(\mathbf{x}, t) \exp(-ik_\beta x_\beta) \quad (15.6)$$

where \mathbf{k} denotes the wavenumber vector and the integration is carried out over the whole flow field \mathcal{D} . There is a problem with Fourier transform for homogenous turbulence since the velocity and pressure fluctuations do not vanish as $|\mathbf{x}|$ goes to infinity. Fourier transformation requires square-integrable argument functions and it follows that the integral, strictly speaking, is not well defined for homogeneous turbulence. This can be repaired using the Fourier–Stieltjes integral, for instance (see Batchelor [6]) or we can simply say that the integral is a generalized function and then proceed handling the transformation accordingly. The velocity in physical

space is a real function of its arguments and it follows that the Fourier transform must satisfy

$$\hat{v}_\alpha(\mathbf{k}, t) = \hat{v}_\alpha^*(-\mathbf{k}, t) \quad (15.7)$$

where the asterisk denotes the complex conjugate quantity. The inverse transformation leads to

$$v_\alpha(\mathbf{x}, t) = \mathcal{F}^{-1}\hat{v}_\alpha(\mathbf{k}) = \int_{-\infty}^{\infty} d\mathbf{k} \hat{v}_\alpha(\mathbf{k}, t) \exp(ik_\beta x_\beta) \quad (15.8)$$

This powerful tool will be applied to the Navier–Stokes system to elucidate the role of convection, pressure gradient and viscous diffusion.

Transformed mass balance

Application of Fourier transformation to the mass balance leads to the simple geometrical statement that

$$k_\alpha \hat{v}_\alpha(t, \mathbf{k}) = 0 \quad (15.9)$$

wavenumber and complex velocity amplitude are orthogonal.

Transformed momentum balance

The pressure equation can be deduced from the momentum balance by taking the divergence of the momentum balance which leads to

$$\Delta p = -\frac{\partial v_\alpha}{\partial x_\beta} \frac{\partial v_\beta}{\partial x_\alpha} \quad (15.10)$$

Fourier transformation produces the factor $-k^2$ for the Laplacian where

$$k^2 = k_1^2 + k_2^2 + k_3^2 \quad (15.11)$$

and an integral contribution for the nonlinear right-hand side

$$\hat{p}(\mathbf{k}, t) = - \int d\mathbf{k}' \frac{k'_\alpha k'_\beta}{k^2} \hat{v}_\alpha(\mathbf{k} - \mathbf{k}', t) \hat{v}_\beta(\mathbf{k}', t) \quad (15.12)$$

where mass balance was applied to $(k_\beta - k'_\beta) \hat{v}_\beta(\mathbf{k}', t) = k_\beta \hat{v}_\beta(\mathbf{k}', t)$. This result allows elimination of the pressure from the transformed momentum balance. For this purpose, the various terms in the momentum balance will be expressed in terms of their Fourier amplitudes. The unsteady term is given by (note that a single integral is written instead of three for convenience)

$$\frac{\partial v_\alpha}{\partial t} = \int d\mathbf{k} \frac{\partial}{\partial t} \hat{v}_\alpha(\mathbf{k}, t) \exp(i\mathbf{k} \cdot \mathbf{x}) \quad (15.13)$$

the viscous term by

$$\frac{1}{Re} \Delta v_\alpha = -\frac{1}{Re} \int d\mathbf{k} k^2 \hat{v}_\alpha(\mathbf{k}, t) \exp(i\mathbf{k} \cdot \mathbf{x}) \quad (15.14)$$

and the convective term by

$$v_\beta \frac{\partial v_\alpha}{\partial x_\beta} = i \int d\mathbf{k}'' \hat{v}_\beta(\mathbf{k}'') \exp(i\mathbf{k}'' \cdot \mathbf{x}) \int d\mathbf{k}' k'_\beta \hat{v}_\alpha(\mathbf{k}') \exp(i\mathbf{k}' \cdot \mathbf{x}) \quad (15.15)$$

which can be recast using $\mathbf{k} = \mathbf{k}' + \mathbf{k}''$ as

$$v_\beta \frac{\partial v_\alpha}{\partial x_\beta} = i \int d\mathbf{k} \exp(i\mathbf{k} \cdot \mathbf{x}) \int d\mathbf{k}' k'_\beta \hat{v}_\alpha(\mathbf{k}') \hat{v}_\beta(\mathbf{k} - \mathbf{k}') \quad (15.16)$$

The pressure gradient follows from (15.12) and the backward transform as

$$-\frac{\partial p}{\partial x_\alpha} = i \int d\mathbf{k} \exp(i\mathbf{k} \cdot \mathbf{x}) \int d\mathbf{k}' \frac{k_\alpha k'_\beta k_\gamma}{k^2} \hat{v}_\gamma(\mathbf{k}') \hat{v}_\beta(\mathbf{k} - \mathbf{k}') \quad (15.17)$$

The momentum balance follows now as an integral that must be zero for a class of argument functions, which in turn implies that the integrand must be zero

$$\left(\frac{\partial}{\partial t} + \frac{1}{Re} k^2 \right) \hat{v}_\alpha(\mathbf{k}) = -i \int d\mathbf{k}' k'_\beta \hat{v}_\beta(\mathbf{k} - \mathbf{k}') \left\{ \hat{v}_\alpha(\mathbf{k}') - \frac{k_\alpha k_\gamma}{k^2} \hat{v}_\gamma(\mathbf{k}') \right\} \quad (15.18)$$

The integral on the right-hand side contains the operator (23.33)

$$m_{\alpha\beta}(\mathbf{k}) \equiv \delta_{\alpha\beta} - \frac{k_\alpha k_\beta}{k^2} \quad (15.19)$$

which deserves closer scrutiny. Consider an arbitrary vector $w_\alpha(\mathbf{k})$ and apply this operator to it with a new vector as result

$$w_\alpha^*(\mathbf{k}) = m_{\alpha\beta} w_\beta(\mathbf{k}) \quad (15.20)$$

Checking its relation to the wavenumber vector \mathbf{k} leads to

$$k_\alpha w_\alpha^*(\mathbf{k}) = k_\alpha \left(\delta_{\alpha\beta} - \frac{k_\alpha k_\beta}{k^2} \right) w_\beta$$

which is obviously zero. It follows that $m_{\alpha\beta}$ projects an arbitrary vector \mathbf{w} on its solenoidal (or zero divergence) part \mathbf{w}^* . For this reason, $m_{\alpha\beta}$ is recognized as projection operator. The transformed momentum balance emerges in concise form as

$$\left(\frac{\partial}{\partial t} + \frac{1}{Re} k^2 \right) \hat{v}_\alpha(\mathbf{k}) = -im_{\alpha\gamma} \int d\mathbf{k}' k'_\beta \hat{v}_\beta(\mathbf{k} - \mathbf{k}') \hat{v}_\gamma(\mathbf{k}') \quad (15.21)$$

using this operator. The integral appearing in it shows the nature of the mode interaction occurring in the flow field. It should be noted that three wavenumbers are involved in this interaction: \mathbf{k} , \mathbf{k}' and $\mathbf{k} - \mathbf{k}'$. The remarkable property of these three vectors is the fact that they form a closed triangle for incompressible fluids. The interaction of the amplitudes $\hat{v}(\mathbf{k})$, $\hat{v}(\mathbf{k}')$ and $\hat{v}(\mathbf{k} - \mathbf{k}')$ is for this reason called *triad interaction*.

The integral in the transformed momentum balance can be rearranged by noting that it can be rewritten, using

$$k'_\beta \hat{v}_\beta(\mathbf{k} - \mathbf{k}') = (k'_\beta - k_\beta) \hat{v}_\beta(\mathbf{k} - \mathbf{k}') + k_\beta \hat{v}_\beta(\mathbf{k} - \mathbf{k}') \quad (15.22)$$

where the first term is zero due to mass balance (15.9), as the final version of the momentum balance

$$\boxed{\left(\frac{\partial}{\partial t} + \frac{1}{Re} k^2 \right) \hat{v}_\alpha(\mathbf{k}) = -ik_\beta m_{\alpha\gamma} \hat{v}_\beta * \hat{v}_\gamma(\mathbf{k})} \quad (15.23)$$

However, this equation represents the full Navier–Stokes system reduced to three odes in Fourier space, since mass balance is satisfied for all time if it is satisfied initially. The convolution appearing on the right side is defined by

$$\hat{v}_\beta * \hat{v}_\gamma(\mathbf{k}) \equiv \int d\mathbf{k}' \hat{v}_\beta(\mathbf{k} - \mathbf{k}') \hat{v}_\gamma(\mathbf{k}') \quad (15.24)$$

It can be interpreted as the essence of mode interaction. This can be seen as follows: Let the flow be given at a time instance by a single mode

$$\hat{v}_\alpha = a_\alpha \delta(\mathbf{k} - \mathbf{k}^o) + a_\alpha^* \delta(-\mathbf{k} - \mathbf{k}^o) \quad (15.25)$$

with $\mathbf{k}^o \neq 0$, the asterisk denotes complex conjugate. Then is the outcome of the convolution integral for the single mode according to its definition given by

$$\hat{v}_\alpha * \hat{v}_\gamma(\mathbf{k}) = a_\alpha a_\gamma \int d\mathbf{k} \delta(\mathbf{k}' - \mathbf{k}^o) \delta(\mathbf{k} - \mathbf{k}^o - \mathbf{k}') \quad (15.26)$$

which emerges as

$$\hat{v}_\alpha * \hat{v}_\gamma(\mathbf{k}) = a_\alpha a_\gamma \delta(\mathbf{k} - 2\mathbf{k}^o) + (a_\alpha a_\gamma^* + a_\alpha^* a_\gamma) \delta(\mathbf{k}) + a_\alpha^* a_\gamma^* \delta(\mathbf{k} + 2\mathbf{k}^o) \quad (15.27)$$

It follows that the convolution term produces non-zero amplitude values at wavenumbers $-2\mathbf{k}^o$ and $2\mathbf{k}^o$, i.e. twice the input wavenumber \mathbf{k}^o . The effect is, therefore, propagation to higher and lower wavenumbers. The right-hand side of the trans-

formed momentum balance produces non-zero amplitudes at wavenumber vectors of increasing length while preserving the orthogonality to the wavenumber vector. This transport of momentum to higher wavenumbers is counteracted by the viscous term which is apparently damping this growth. However, since the damping rate is proportional to the wavenumber squared, it follows that the damping will take effect only at the high wavenumber end of the range of amplitudes.

The particular form of mass balance (15.9) in wavenumber space as the condition, that the complex velocity amplitude is orthogonal the wavenumber vector, can be exploited to construct decompositions of the velocity field such that only two components are non-zero. Consider a non-zero wavenumber vector \mathbf{k} and an arbitrary unit vector not parallel to \mathbf{k} and construct the reference frame $(\mathbf{e}_i, \mathbf{e}_j, \mathbf{e}_k)$ in Fourier space

$$\mathbf{e}_i(\mathbf{k}) = \frac{\mathbf{k} \times \alpha}{\|\mathbf{k} \times \alpha\|}, \quad \mathbf{e}_j(\mathbf{k}) = \frac{\mathbf{k} \times \mathbf{i}}{k}, \quad \mathbf{e}_k = \frac{\mathbf{k}}{k} \quad (15.28)$$

Mass balance (15.9) implies that velocity has only two non-zero components in the directions \mathbf{e}_i and \mathbf{e}_j . This decomposition was introduced by Craya [7], it found application to the simulation of homogeneous turbulence. Another type of representation called complex helical wave decomposition was introduced by M. Lesieur based on eigenfunctions of the curl operator (Sect. 2.3.1), see [8] Sect. 4.5 for definition and further details.

Helicity density is defined as

$$h(\mathbf{x}) \equiv \mathbf{v} \cdot \mathbf{!} = \mathbf{v} \cdot \nabla \times \mathbf{v}, \quad (15.29)$$

and helicity by

$$\mathcal{H} \equiv \int_{\mathcal{D}} d\nu(\mathbf{x}) h(\mathbf{x}) \quad (15.30)$$

Helicity is an integral invariant for the flow of incompressible, inviscid fluids, see the solution of Problem 20.1 in Chap. 28.

References

1. Duffy, D.G.: Transform Methods for Solving Partial Differential Equations, 2nd edn. Chapman & Hall/CRC, Boca Raton, Florida (2004)
2. Daubechies, I.: Orthogonal bases of compactly supported wavelets. Commun. Pure Appl. Math. **41**, 909–996 (1988)
3. Meneveau, C.: Analysis of turbulence in the orthonormal wavelet representation. JFM **232**, 469–520 (1991)
4. Schneider, K., Vasilyev, O.V.: Wavelet methods in computational fluid dynamics. Annual Rev. Fluid Mech. **42**, 473–503 (2010)

5. Gelfand, I.M., Vilenkin, N.Y.: Generalized Functions, vol. 4. Academic Press, New York (1964)
6. Batchelor, G.K.: The Theory of Homogeneous Turbulence. Cambridge University Press (1967)
7. Craya, A.: Contribution à l'analyse de la turbulence associée à des vitesses moyennes. P.S.T. Ministere de l'Air, 345 (1958)
8. Lesieur, M.: Turbulence Fluids. Martinus Nijhoff Publishers, Dordrecht (1987)

Chapter 16

Intermittency



The term intermittency is applied to two distinct types of phenomena, externally and internally intermittent flows, [1] Chap. 7.2, Benzi and Biferale [2], Frisch [3], Chap. 8. Townsend [4] and Corrsin [5] observed in experiments on turbulent wakes and jets that turbulence away from the centre of the flow appeared as a random sequence of active bursts and quiescent intervals. Therefore, the flow field contains continuously changing subsets that are turbulent and subsets that are approximately non-turbulent (weakly turbulent), separated by an interface. This phenomenon is called external intermittency.

The second type of intermittency is associated with the temporal/spatial build-up of fine scale structures of turbulent flows. This type of internal intermittency is defined as deviation from strictly Gaussian stochastic field properties (see Adler and Taylor [6] for a detailed account of Gaussian fields), which are by definition perfectly random, hence non-intermittent.

The notion of (external) intermittency is also applicable to the transition from laminar to turbulent flow. Pomeau and Manneville [7] treat this transition with the tools of dynamical systems and show that three types of phenomena emerge as candidates for transition:

- Saddle-node bifurcation;
- Hopf bifurcation;
- Period-doubling bifurcation.

Barkley presents in [8] a detailed treatment of transitional, intermittent pipe flow utilizing dynamical models. Detailed information on the dynamical systems aspect can be found in Wiggins, [9], Chap. 20 and Kusnetsov [10].

16.1 External Intermittency

Experiments [5] provided the evidence that turbulent flows issuing into a quiescent environment form a well-defined, fluctuating boundary separating turbulent and non-turbulent zones. The mathematical description of this phenomenon can be based on a

scalar field $e(t, \mathbf{x})$ and a threshold value e_0 , whose local value allows discrimination between turbulent and non-turbulent states [11]. The discrimination is enabled by a finite set \mathcal{A} of non-contradictory statements formulated with the aid of the scalar field e . However, the working definition of turbulence in Sect. 3.1 cannot be verified in a single, local measurement of field variables, since it requires test of stochasticity and spectral extent. Hence, the scalar field (such as enstrophy, invariants of the rate of strain field, dissipation rate, etc.) is tested locally and the states of the flow are termed turbulent or non-turbulent in slight misuse of terminology. For instance, the condition may be

$$\mathcal{A} = \{e(t, \mathbf{x}) \geq e_0\}$$

with the scalar field being enstrophy $e \equiv |\nabla \times \mathbf{v}|$ and $0 < e_0 \ll ||e||$ being a threshold value inspired by experimental observations. The discrimination between states $e(t, \mathbf{x}) > e_0$ and $e(t, \mathbf{x}) < e_0$ is obviously strictly local for this example, i.e. involves only quantities at the time t and the observer position \mathbf{x} and the threshold e_0 . The scalar field $e(t, \mathbf{x})$ can be viewed as mapping $e : \mathcal{D} \rightarrow \mathbb{R}^1$, the preimage or fibre of an argument $y \in \mathbb{R}^1$ is a level surface $\mathbf{x}(y, e_0) = e^{-1}(y)$, if $e(t, \mathbf{x})$ is at least continuous.

The characteristic (distinct from the characteristic function/al (9.1) as Fourier transform of probability measures) or indicator function of subsets (zones) satisfying the conditions \mathcal{A} is defined by

$$\mathbf{1}_{\mathcal{A}}(t, \mathbf{x}) \equiv \begin{cases} 1 & \text{for } \mathcal{A} \text{ satisfied at time } t \text{ and location } \mathbf{x} \\ 0 & \text{otherwise} \end{cases} \quad (16.1)$$

The condition \mathcal{A} can be classified with respect to time and location as local or non-local, only the local case will be pursued in the following. The expectation of the indicator function measures, for fixed observer position \mathbf{x} , the average time the fluid satisfies the condition \mathcal{A}

$$\gamma(t, \mathbf{x}) = \langle \mathbf{1}_{\mathcal{A}} \rangle(t, \mathbf{x}) \quad (16.2)$$

It is called external intermittency factor, which is bounded by definition $0 \leq \gamma(t, \mathbf{x}) \leq 1$.

The example $\mathcal{A} \equiv \{e(t, \mathbf{x}) \geq e_0\}$ allows geometric interpretation assuming $e(t, \mathbf{x})$ being at least twice continuously differentiable. The level surface

$$S(t, \mathbf{x}, e_0) \equiv e(t, \mathbf{x}) - e_0 \quad (16.3)$$

is now the argument of the characteristic function $\mathbf{1}_{\mathcal{A}}(S)$. It is not materially invariant, but moves with velocity $\mathbf{v}^s(t, \mathbf{x}, e_0)$ different from the fluid velocity \mathbf{v} . It moves relative to the fluid in its normal direction with speed V

$$n_\alpha V = v_\alpha - v_\alpha^s \quad (16.4)$$

The derivatives of the characteristic function follow easily [11]

$$\frac{\partial \mathbf{1}_{\mathcal{A}}}{\partial t} = -v_{\alpha}^s n_{\alpha} |\nabla e| \delta(e(t, \mathbf{x}) - e_0), \quad \frac{\partial \mathbf{1}_{\mathcal{A}}}{\partial x_{\alpha}} = n_{\alpha} |\nabla e| \delta(e(t, \mathbf{x}) - e_0) \quad (16.5)$$

It follows at once from the derivatives that

$$\frac{\partial \mathbf{1}_{\mathcal{A}}}{\partial t} + v_{\alpha}^s \frac{\partial \mathbf{1}_{\mathcal{A}}}{\partial x_{\alpha}} = 0$$

holds. Furthermore, it is convenient to introduce conditional expectations for the set up of the dynamic equation for the intermittency factor. The turbulent zone expectation is then

$$\hat{\Phi} \equiv \frac{\langle \mathbf{1}_{\mathcal{A}} \Phi \rangle}{\gamma} \quad (16.6)$$

Multiplication with the characteristic function $\mathbf{1}_{\mathcal{A}}$ zeros out the non-turbulent part of the argument field Φ and the expectation of this product is then the product of the conditional expectation $\langle \mathbf{1}_{\mathcal{A}} \Phi \rangle = \langle \Phi | \mathcal{A} \text{ is satisfied} \rangle$ and the intermittency factor γ . The non-turbulent zone expectation is analogously defined by

$$\tilde{\Phi} \equiv \frac{\langle (1 - \mathbf{1}_{\mathcal{A}}) \Phi \rangle}{1 - \gamma} \quad (16.7)$$

It is now easy to derive the transport pde governing the dynamics of the intermittency factor [11]

$$\frac{\partial \gamma}{\partial t} + \langle \mathbf{v} \rangle \cdot \nabla \gamma = \nabla \cdot \mathbf{F} + S_{\gamma} \quad (16.8)$$

where the diffusive flux emerges in the form

$$\mathbf{F}(t, \mathbf{x}, e_0) = -\gamma(1 - \gamma)(\hat{\mathbf{v}} - \tilde{\mathbf{v}}) \quad (16.9)$$

and the source term as

$$S_{\gamma}(t, \mathbf{x}, e_0) = \langle V |\nabla e| \delta(e(t, \mathbf{x}) - e_0) \rangle \quad (16.10)$$

The form of the diffusive flux \mathbf{F} of γ (16.9) is determined by the relative motion of turbulent and non-turbulent zones and vanishes at the upper and lower bounds of the intermittency factor. The source term S_{γ} (16.10) represents the rate at which the volume of the turbulent zone grows at the expense of the non-turbulent zone. It can be expressed in terms of the divergence of the diffusive flux plus the source of the discriminating scalar e , details can be found in the solution to Problem 16.1 in and [11].

16.2 Internal Intermittency

Internal intermittency can be defined either structurally or statistically [1, 12]. The two definitions agree globally, but not locally.

Structural definition of internal intermittency

Let $e(t, \mathbf{x}, Re)$ be a non-negative scalar field (enstrophy, dissipation rate) determined by solutions of the Navier–Stokes pdes (hence a function of the Reynolds number) with mean value $\langle e \rangle$ and let $\mathcal{V}(t, e_i, 0 \leq e_i \leq ||e||)$ be the volume of the subset $\{\mathbf{x} : e(t, \mathbf{x}) > e_i\}$, then is the scalar (internally) intermittent iff

$$\lim_{Re \rightarrow \infty} \frac{\mathcal{V}(t, e_0)}{\mathcal{V}(t, 0)} = 0 \quad (16.11)$$

holds for $0 \leq e_0 \ll \langle e \rangle$. This definition implies that $e(t, \mathbf{x})$ becomes increasingly spiky, i.e. intermittent, as $Re \rightarrow \infty$. It is, unfortunately, at present not yet accessible to experiment or analytical theory.

Statistical definition of internal intermittency

A variable/field with zero mean is (internally) intermittent iff it has a Pdf different from a Gaussian with flatness factor larger than three. An internally intermittent Pdf has tails larger than a Gaussian and is larger than a Gaussian near the origin. Hence, very large and very small fluctuations are more likely than for a Gaussian process. The intermittency factor is now defined as the flatness factor

$$\gamma(e') \equiv \frac{\langle e'^4 \rangle}{\langle e'^2 \rangle^2} \quad (16.12)$$

where $e' \equiv e - \langle e \rangle$ denotes the fluctuation of the scalar e . The flatness factor, as well as various other correlations, is a measure for the deviation from Gaussianity. Experiments in homogeneous turbulence show that the flatness factor increases with the order of spatial derivative. Kuo and Corrsin [13] interpret this property as decrease in the partial volume, where enstrophy, dissipation rate, etc., are above the threshold, hence are not space filling and, therefore, intermittent. Sreenivasan [14] evaluated several measures for the characterization of internal intermittency by comparison with experimental data.

16.2.1 The Intermittency Generating Function of Wilczek et al. [15]

An interesting and useful idea was proposed by Wilczek et al. [15] for steady turbulence. Consider the velocity difference along a pathline

$$\Delta \mathbf{V}(\tau, \Delta\tau, \mathbf{X}) \equiv \mathbf{V}(\tau + \Delta\tau, \mathbf{X}) - \mathbf{V}(\tau, \mathbf{X}) \quad (16.13)$$

in the Lagrangean description (τ is time and \mathbf{X} the label of a material point) with non-degenerate covariance matrix

$$\Sigma_{\alpha\beta} \equiv \langle (\Delta V_\alpha - \langle \Delta V_\alpha \rangle)(\Delta V_\beta - \langle \Delta V_\beta \rangle) \rangle \quad (16.14)$$

in Cartesian coordinates, where the angular brackets denote the expectation operator, which is independent of time for steady turbulence. It is convenient to define normalized velocity differences by

$$W_\alpha \equiv \frac{\Delta V_\alpha}{\sqrt{\Sigma_{(\alpha\alpha)}}} \quad (16.15)$$

(repeated subscripts in parenthesis means no summation). The fine-grained Pdf (details in Chap. 11) of the normalized velocity difference is then defined by

$$\hat{f} \equiv \delta(\mathbf{W} - \mathbf{w}) \quad (16.16)$$

where \mathbf{w} denotes the sample space vector (see Chap. 11 for details). The Pdf of \mathbf{W} follows then

$$f(\mathbf{w}; \tau, \Delta\tau, \mathbf{X}) = \langle \delta(\mathbf{W} - \mathbf{w}) \rangle \quad (16.17)$$

as expectation of the fine-grained Pdf. The intermittency generating vector function emerges, if the time rate of change of the Pdf is derived

$$\frac{\partial}{\partial \tau} f(\mathbf{w}; \tau, \Delta\tau, \mathbf{X}) = -\frac{\partial}{\partial w_\alpha} [\varphi_\alpha(\mathbf{w}; \tau, \Delta\tau, \mathbf{X}) f(\mathbf{w}; \tau, \Delta\tau, \mathbf{X})] \quad (16.18)$$

where Cartesian coordinates were used and

$$\varphi_\alpha(\mathbf{w}; \tau, \Delta\tau, \mathbf{X}) = \frac{1}{\sqrt{\Sigma_{(\alpha\alpha)}}} \langle \Delta A_\alpha | \mathbf{W} = \mathbf{w} \rangle - w_\alpha (\langle \Delta A_{(\alpha)} W_{(\alpha)} \rangle - \langle \Delta A_{(\alpha)} \rangle \langle W_{(\alpha)} \rangle) \quad (16.19)$$

is called intermittency generating vector function. The Lagrangean acceleration is by definition

$$\mathbf{A}(\tau, \mathbf{X}) = \frac{\partial \mathbf{V}}{\partial \tau}(\tau, \mathbf{X})$$

and $\langle \mathbf{A} | B \rangle$ denotes the conditional expectation of \mathbf{A} subject to the event B . The role of the intermittency generating function $\varphi_\alpha(\mathbf{w}; \tau, \Delta\tau, \mathbf{X})$ can be deduced from Eq. (16.18). Turbulent flows steady in the mean must satisfy

$$\frac{\partial}{\partial w_\alpha} [\varphi_\alpha(\mathbf{w}; \tau, \Delta\tau, \mathbf{X}) f(\mathbf{w}; \tau, \Delta\tau, \mathbf{X})] = 0$$

There are two possibilities for this to happen: Either the intermittency generating vector vanishes,

(1) $\varphi_\alpha(\mathbf{w}; \tau, \Delta\tau, \mathbf{X}) = 0$. This implies that no restriction on the variation of the Pdf f with \mathbf{w} results, hence self-similar $f(\mathbf{w})$ is possible. Or the product

(2) $\varphi_\alpha(\mathbf{w}; \tau, \Delta\tau, \mathbf{X}) f(\mathbf{w}; \tau, \Delta\tau, \mathbf{X})$ is independent of \mathbf{w} . Clearly, this case does not allow self-similar variation of the Pdf as function of \mathbf{w} . This is the case of internal or Lagrangean intermittency. The intermittency generating vector φ_α (16.19) is controlled by the conditional expectation of the Lagrangean acceleration subject to the condition $\frac{\Delta\mathbf{v}}{\sigma} = \mathbf{w}$. This conditional moment is accessible to experiment and DNS [15, 16].

16.3 Problems for this Chapter

Problem 16.1 Consider the discriminating scalar $\Phi(t, \mathbf{x}) \geq 0$ governed by

$$\frac{\partial \Phi}{\partial t} + v_\alpha \frac{\partial \Phi}{\partial x_\alpha} = \frac{\partial}{\partial x_\alpha} \frac{1}{ScRe} \frac{\partial \Phi}{\partial x_\alpha} + Q(\Phi)$$

where Sc is the Schmidt number associated with the molecular diffusivity and $Q(t, \mathbf{x}, \Phi)$ the source term. Determine the source term (16.10) of the external intermittency factor $\gamma(t, \mathbf{x})$ (16.2) for $\mathcal{A} = \Phi(t, \mathbf{x}) - e_0$ as function of the discriminating scalar field $\Phi(t, \mathbf{x})$.

Problem 16.2 Compute the intermittency generating vector (16.19)

$$\varphi_\alpha(\mathbf{w}; \tau, \Delta\tau, \mathbf{X}) = \frac{1}{\sqrt{\Sigma_{(\alpha\alpha)}}} \langle \Delta A_\alpha | \mathbf{W} = \mathbf{w} \rangle - w_\alpha (\langle \Delta A_{(\alpha)} W_{(\alpha)} \rangle - \langle \Delta A_{(\alpha)} \rangle \langle W_{(\alpha)} \rangle)$$

for non-degenerate Gaussian statistics.

References

1. Tsinober, A.: An Informal Conceptual Introduction to Turbulence, 2nd edn. Springer, Dordrecht (2009)
2. Benzi, R., Biferale, L.: Intermittency in turbulence. In: Oberlack, M., Busse, F.H. (eds.) Theories of Turbulence. Springer, Wien (2002)
3. Frisch, U.: Turbulence: The Legacy of A.N. Kolmogorov. Cambridge University Press (1995)
4. Townsend, A.A.: Local isotropy in the turbulent wake of a cylinder. Austr. J. Sci. Res. **1**, 161–174 (1948)
5. Kennedy, D.A., Corrsin, S.: Spectral flatness factor and intermittency in turbulence and in non-linear noise. JFM **10**, 366–370 (1961)
6. Adler, R.J., Taylor, J.E.: Random Fields and Geometry. Springer, New York (2007)

7. Pomeau, Y., Manneville, P.: Intermittent transition to turbulence in dissipative dynamical systems. *Comm. Math. Phys.* **74**, 189–197 (1980)
8. Barkley, D.: Theoretical perspective on the route to turbulence in a pipe. *JFM* **803**, P1–1 (2016)
9. Wiggins, S.: *Introduction to Applied Nonlinear Dynamical Systems and Chaos*. Springer, New York (2003)
10. Kusnetsov, Y.A.: *Elements of Applied Bifurcation Theory*. Springer, New York (2004)
11. Byggstøyl, S., Kollmann, W.: Stress transport in the rotational and irrotational zones of turbulent shear flows. *Phys. Fluids* **29**, 1423–1429 (1986)
12. Moffatt, H.K.: Topological approach to problems of vortex dynamics and turbulence. *Prog. Astronaut. Aeronaut.* **112**, 141–152 (1988)
13. Kuo, A.Y.-S., Corrsin, S.: Experiments on internal intermittency and fine-structure distribution functions in fully turbulent fluid. *JFM* **50**, 285–319 (1971)
14. Sreenivasan, K.R.: On the fine-scale intermittency of turbulence. *JFM* **151**, 81–103 (1985)
15. Wilczek, M., Xu, H., Ouellette, N.T., Friedrich, R., Bodenschatz, E.: Generation of Lagrangian intermittency in turbulence by a self-similar mechanism. *New J. Phys.* **15**, 055015 (2013)
16. Mordant, N., Crawford, A.M., Bodenschatz, E.: The 3D structure of the Lagrangean acceleration in turbulent flows. *Phys. Rev. Lett.* **93**, 214501 (2004)

Chapter 17

Equilibrium Theory of Kolmogorov and Onsager



Homogeneous turbulence cannot be in equilibrium since the kinetic energy $\mathcal{K}(t)$ (kinetic energy is usually denoted by k , but the notation is changed to avoid confusion with the wavenumber) of turbulence can be shown to satisfy in this case

$$\frac{\partial \mathcal{K}}{\partial t} = -\frac{1}{Re} \left\langle \frac{\partial v_\alpha}{\partial x_\beta} \frac{\partial v_\alpha}{\partial x_\beta} \right\rangle \leq 0 \quad (17.1)$$

which does not contain any production term and the right-hand side is negative definite (the transport equation for the kinetic energy will be derived later). The statistical properties of homogeneous turbulent flow will evolve in time unless maintained by an appropriate (statistically homogeneous) external force field. However, this development can show approximate self-similarity or self-preservation in certain ranges of wavenumbers. If this is the case the term quasi-equilibrium is applied.

17.1 Energy Cascade

Turbulence is created by external excitation (forcing) of random motion or by the growth of small disturbances due to the inherent instability of shear flows, where the shearing rate is maintained by the boundary conditions. Homogeneous turbulence is produced by the former mechanism, whereas inhomogeneous turbulence is nearly always created by the latter phenomenon. Fluctuations are first excited at a length scale (a length that is typical for the mechanism that generates the motion) l_0 . These fluctuations at non-zero wavenumber interact according to the momentum balance (15.23) to create fluctuations at smaller length scales $l < l_0$, which is equivalent to higher wavenumbers $k > k_0$ (note that $l = \frac{2\pi}{k}$ holds). Thus a process of successive refinement is generated until the length scale of the fluctuations becomes small enough (or the associated wavenumbers become large enough) such that viscous damping becomes important. As viscous damping at $l_d = \frac{2\pi}{k_d}$ becomes the dominant effect, kinetic energy is transferred to internal energy and the fluctuations die out.

The precise mechanism responsible for the transfer of energy through the spectrum is not known. In fact, it is not clear whether this energy transfer process is local or non-local in wavenumber space. The concept of local and non-local transfer is rather vague: If the wavenumbers involved are different in length by less than a factor of two the transfer is called local, otherwise non-local. The analysis of experimental results (spectra, etc.) by Vassilicos [5] and references therein showed that the energy transfer was maximal for wavenumbers different by about an order of magnitude, hence would be non-local. On the other hand, Kolmogorov's notion of the energy cascade is based on the local transfer of energy from one wavenumber band to the neighbouring band and not to wavenumbers different by an order of magnitude or more.

Domaradzki and Rogallo [1] tried to shed some light on this question using direct simulations of homogeneous turbulence. Their analysis is based on (15.9) and (15.23), which can be rewritten, once more, as

$$(\frac{\partial}{\partial t} + \frac{1}{Re} k^2) \hat{v}_\alpha(\mathbf{k}) = -\frac{i}{2} P_{\alpha\beta\gamma} \int d\mathbf{k}' \hat{v}_\beta(\mathbf{k} - \mathbf{k}') \hat{v}_\gamma(\mathbf{k}') \quad (17.2)$$

where the operator $P_{\alpha\beta\gamma}$ includes differentiation according to

$$P_{\alpha\beta\gamma} \equiv k_\gamma (\delta_{\alpha\beta} - \frac{k_\alpha k_\beta}{k^2}) + k_\beta (\delta_{\alpha\gamma} - \frac{k_\alpha k_\gamma}{k^2}) \quad (17.3)$$

The transfer function appears in the momentum balance if it is written in terms of the energy amplitude

$$\frac{1}{2} |\hat{\mathbf{v}}(\mathbf{k})|^2 = \frac{1}{2} \hat{v}_\alpha(\mathbf{k}) \hat{v}_\alpha^*(\mathbf{k}) \quad (17.4)$$

where the asterisk indicates complex conjugate. It follows at once from (17.2) that the amplitude is governed by

$$\frac{\partial}{\partial t} \frac{1}{2} |\hat{\mathbf{v}}(\mathbf{k})|^2 = -2\nu k^2 \frac{1}{2} |\hat{\mathbf{v}}(\mathbf{k})|^2 + T(\mathbf{k}) \quad (17.5)$$

where the transfer function is defined by

$$T(\mathbf{k}) \equiv \frac{1}{2} \Im \left(\hat{v}_\alpha^* P_{\alpha\beta\gamma} \int d\mathbf{k}' \hat{v}_\beta(\mathbf{k} - \mathbf{k}') v_\gamma(\mathbf{k}') \right) \quad (17.6)$$

(\Im denotes the imaginary part of a complex number). The energy amplitude $E(k, t)$ and the transfer function $T(k, t)$ are now averaged geometrically over spherical shells of radius $k \equiv |\mathbf{k}|$ to eliminate directional dependencies in Fourier space according to

$$\int_{\partial\mathcal{D}} d\sigma f(\mathbf{k}) = \int ds \int dt f(\mathbf{k}) \left| \frac{\partial \mathbf{k}}{\partial s} \times \frac{\partial \mathbf{k}}{\partial t} \right| \quad (17.7)$$

where the surface is parameterized by s, t as $\mathbf{k}(s, t) \in \partial\mathcal{D} : 0 \leq s \leq 1, 0 \leq t \leq 1$. Specifically, the integral over the surface of a sphere in Fourier space results in the surface differential

$$d\sigma = k^2 \sin(\varphi) d\varphi d\theta$$

where k denotes the radius of the sphere and $0 \leq \theta \leq 2\pi$ and $0 \leq \varphi \leq \pi$ are the spherical coordinates. The surface integral leads to

$$E(k) = 4\pi k^2 \langle \frac{1}{2} |\mathbf{v}(\mathbf{k})|^2 \rangle \quad (17.8)$$

and

$$T(k) = 4\pi k^2 \langle T(\mathbf{k}) \rangle \quad (17.9)$$

explaining the factor k^2 . These expressions will be rederived below once the Fourier transform of two-point correlations and the associated spectrum are introduced and statistical averaging over the realizations of the flow field is carried out.

The spectrum obtained by Domaradski and Rogallo (1990) in one of the first DNS of homogeneous turbulence is shown in Fig. 17.1 for a turbulent Reynolds number based on the kinetic energy of turbulence and the Taylor scale of a low value $Re = 13.6$, the Taylor scale is defined by (19.22). The spectrum in the figure is normalized with $2\lambda(t)\mathcal{K}$ and the wavenumber with $\sqrt{2}\lambda(t)$, where $\lambda(t)$ is the time-dependent Taylor length scale.

The solid line is an analytic interpolant for the spectrum

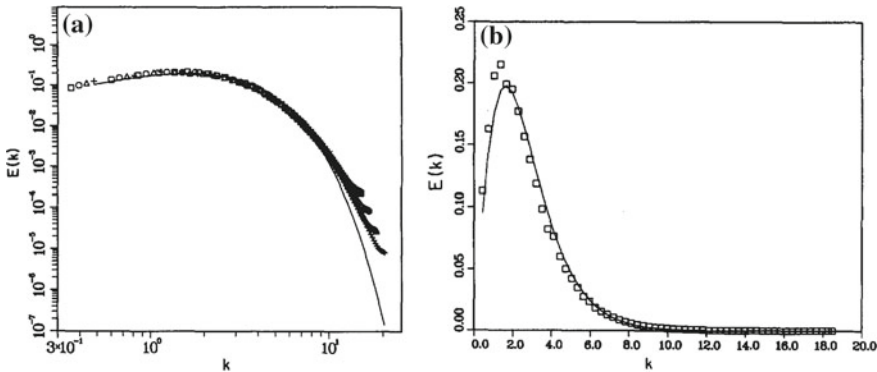
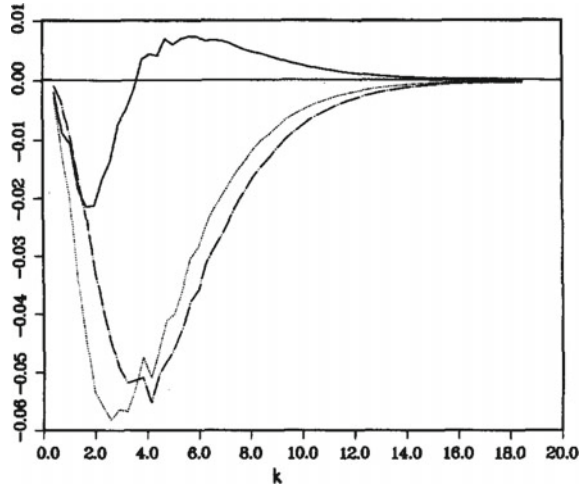


Fig. 17.1 Energy spectrum (logarithmic scale left, linear scale right graph) as function of the dimensionless wavenumber k according to Domaradski and Rogallo [1] at low Reynolds numbers ($R_\lambda = 13.6$ based on the Taylor scale) for isotropic and homogeneous turbulence. The full line is the Ling and Huang model spectrum (17.10) [4], the symbols are the DNS results at four different times normalized by $2\lambda(t)\langle u^2 \rangle$, and $\lambda(t)$ is the time-dependent Taylor length scale

Fig. 17.2 DNS computed spectral transfer function $T(k)$ (17.6) (solid line), the energy dissipation rate $-2\nu k^2 E(k)$ (broken line) and $\partial E/\partial t$ (dotted line) according to Domaradski and Rogallo [1]



$$E(k) = \frac{1}{3\sqrt{2}}k(1+k)\exp(-k) \quad (17.10)$$

suggested by Ling and Huang [4]. The corresponding transfer function and dissipation rate for the spectrum in Fig. 17.2 show that the transfer function is negative for small wavenumbers (large scales) and positive for large wavenumbers (small scales). Further analysis of the transfer functions for particular wavenumber bands lead Domaradski and Rogallo to the conclusion that the energy transfer for their simulation of low Reynolds number homogeneous turbulence is essentially local, but the interaction of wavenumber triads happens at disparate scales and is, therefore, mostly non-local. The latter means that energy is exchanged between disparate wavenumbers but the net energy transfer is small compared to the energy transferred locally.

17.2 Basic Assumptions of Kolmogorov–Onsager Theory

Kolmogorov assumes that the rate of dissipation of kinetic energy contained in the fluctuations, defined by

$$\epsilon \equiv \frac{1}{Re} \left\langle \frac{\partial v'_\alpha}{\partial x_\beta} \frac{\partial v'_\alpha}{\partial x_\beta} \right\rangle \quad (17.11)$$

approaches a bounded, non-zero and well-defined limit as the Reynolds number goes to infinity. This limit value

$$\epsilon_\infty = \lim_{Re \rightarrow \infty} \frac{1}{Re} \left\langle \frac{\partial v'_\alpha}{\partial x_\beta} \frac{\partial v'_\alpha}{\partial x_\beta} \right\rangle \quad (17.12)$$

could in general be zero, infinity or it could be indefinite. Recall that there are three ways to let Re go to infinity: Either the velocity scale or the length scale go to infinity or the viscosity goes to zero. The last possibility is the most intriguing one, since it implies that there is dissipation in inviscid flow. If the solution of the inviscid Navier–Stokes (Euler equations) is smooth (at least once continuously differentiable), it follows that the rate of dissipation for this flow must be zero. However, it is possible that singularities appear in the solution of the Euler equations and then we recognize the definition of the dissipation rate as given above as the product of a factor that approaches zero with a factor that goes to infinity and the result may well be finite. This depends on how the limit of infinite Reynolds numbers is approached and Kolmogorov simply makes the assumption that this indeed the case. His assumption can be restated by saying that the dissipation rate becomes independent of the Reynolds number if the Reynolds number is large enough.

Hypothesis of local isotropy

Fluctuations in spatial domains with linear dimension much smaller than the length scale l_0 (typical for the range where the energy is fed into the flow) are approximately statistically homogeneous and isotropic in space and stationary in time provided the Reynolds number is large enough.

Note that this hypothesis does not imply that the flow has to homogeneous or isotropic on a global scale. It refers to a range of scales smaller than the energy receiving range or, equivalently, to a range of wavenumbers larger than the energy receiving wavenumber k_0 . The notion of local isotropy can be interpreted in wavenumber space as follows: Energy is supplied to the turbulent fluctuations at a wavenumber $k_0 = \frac{2\pi}{l_0}$. The cascade mechanism (whatever that may be, we do not have a very clear idea how the cascade is realized in a turbulent flow) generated by the convective and pressure gradient interaction of different wavenumbers transports energy to successively higher wavenumbers until at $k \geq k_d$ the energy is dissipated. At high wavenumbers $k \gg k_0$ and sufficiently high Reynolds numbers the pressure gradient fluctuations diminish all directional bias inherited from the energy supply mechanism or the boundary conditions, thus producing locally isotropic small scale motion. The convective term is largely responsible for the transport of energy to higher wavenumbers.

Hypothesis of universal equilibrium

The fluctuations at wavenumbers $k \gg k_0$, which are locally isotropic and are not directly excited by external forces but receive their energy via the cascade mechanism, are in an equilibrium state governed by a similarity law depending on only a few *external* parameters. The Reynolds number must be sufficiently large.

This hypothesis can be better understood if the notion of the spectrum is introduced. For this purpose, we define first the spectral tensor

$$\Phi_{\alpha\beta}(\mathbf{x}, \mathbf{k}, t) \equiv \frac{1}{(2\pi)^3} \int d\nu R_{\alpha\beta}(\mathbf{x}, \mathbf{r}, t) \exp(-i\mathbf{k} \cdot \mathbf{r}) \quad (17.13)$$

as Fourier transform of the two-point correlation

$$R_{\alpha\beta}(\mathbf{x}, \mathbf{r}, t) \equiv \langle v'_\alpha(\mathbf{x}, t) v'_\beta(\mathbf{x} + \mathbf{r}, t) \rangle \quad (17.14)$$

where \mathbf{r} denotes the distance vector between the two points. The spectral tensor $\Phi_{\alpha\beta}$ is now integrated over spheres $K_k(0)$ of radius $k = |\mathbf{k}|$ to eliminate directional dependence. We obtain

$$\Psi_{\alpha\beta}(\mathbf{x}, k, t) = \int_{K_k(0)} dA \Phi_{\alpha\beta}(\mathbf{x}, \mathbf{k}, t) \quad (17.15)$$

where the surface differential for a sphere is given by $dA = k^2 \sin(\theta) d\varphi d\theta$. The energy spectrum is then defined by

$$E(\mathbf{x}, k, t) \equiv \frac{1}{2} \Psi_{\alpha\alpha}(\mathbf{x}, k, t) \quad (17.16)$$

The energy spectrum is in elementary fashion related to kinetic energy of turbulence and the rate of dissipation. It follows from (17.16) that

$$\mathcal{K}(\mathbf{x}, t) = \int_0^\infty dk E(\mathbf{x}, k, t) \quad (17.17)$$

must holds. The relation to the dissipation rate can be established, if it is recast as

$$\epsilon = \frac{1}{Re} \lim_{\mathbf{r} \rightarrow 0} \left\langle \frac{\partial v'_\alpha}{\partial y_\beta} \frac{\partial v'_\alpha}{\partial x_\beta} \right\rangle \quad (17.18)$$

where $\mathbf{y} = \mathbf{x} + \mathbf{r}$. Then is apparently

$$\epsilon = \frac{1}{Re} \lim_{\mathbf{r} \rightarrow 0} \frac{\partial^2}{\partial y_\beta \partial x_\beta} R_{\alpha\alpha} \quad (17.19)$$

and all that needs to be done is to transform the coordinates

$$\mathbf{r} = \mathbf{y} - \mathbf{x} \quad (17.20)$$

$$\mathbf{z} = \frac{1}{2}(\mathbf{y} + \mathbf{x}) \quad (17.21)$$

Using

$$\frac{\partial^2}{\partial y_\beta \partial x_\beta} = \frac{1}{4} \frac{\partial^2}{\partial z_\beta \partial z_\beta} - \frac{\partial^2}{\partial r_\beta \partial r_\beta} \quad (17.22)$$

we get

$$\epsilon = \frac{1}{Re} \lim_{\mathbf{r} \rightarrow 0} \left(\frac{1}{4} \frac{\partial^2}{\partial z_\beta \partial z_\beta} R_{\alpha\alpha} - \frac{\partial^2}{\partial r_\beta \partial r_\beta} R_{\alpha\alpha} \right) \quad (17.23)$$

It follows for homogeneous turbulence (which is invariant under translations) that

$$\epsilon = - \frac{1}{Re} \lim_{\mathbf{r} \rightarrow 0} \frac{\partial^2}{\partial r_\beta \partial r_\beta} R_{\alpha\alpha} \quad (17.24)$$

holds which can be expressed in terms of the spectrum using (II.37) and we get finally

$$\epsilon = \frac{1}{Re} \int dk k^2 E(\mathbf{x}, k, t) \quad (17.25)$$

as the desired relation between dissipation rate and the spectrum for homogeneous turbulence. Figure 17.3 shows qualitatively the energy and the dissipation rate spectra for high Reynolds number turbulence. Locally isotropic turbulence at high Reynolds numbers and at high wavenumbers $k \gg k_0$ has energy and dissipation rate spectra that depend on three parameters only: The wavenumber k , the mean dissipation rate ϵ and the viscosity ν or the Reynolds number Re . Note that here we used implicitly the basic assumption of Kolmogorov that the dissipation rate has a non-zero limit as $Re \rightarrow \infty$. If this limit was zero or did not exist, it could not be one of the parameters. The dissipation rate ϵ can be viewed as the amount of energy supplied to the high wavenumber range, if approximate equilibrium prevails. The viscosity/Reynolds number governs the removal of kinetic energy from the high wavenumber range. The hypothesis of local similarity applies to the energy spectrum in this range and we can apply dimensional analysis (see Meinsma [3] for a thorough

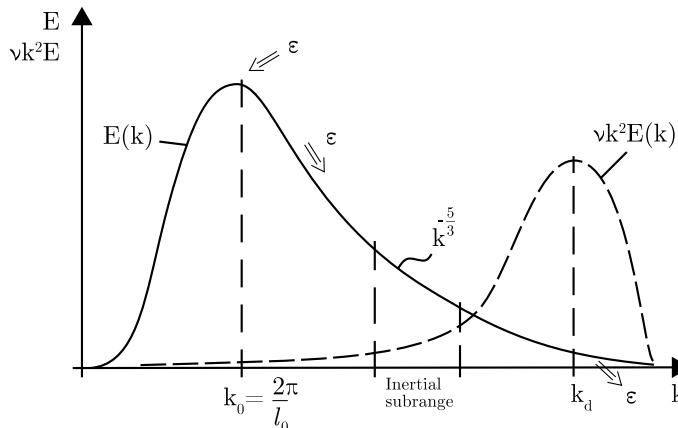


Fig. 17.3 Energy and dissipation rate spectra for homogeneous and isotropic turbulence

discussion of dimensional and scaling analysis) to establish the functional form of the spectrum

$$E(k) = \epsilon^{\frac{1}{4}} \nu^{\frac{5}{4}} E_c\left(\frac{k}{k_d}\right) \quad (17.26)$$

where the wavenumber must satisfy $k \gg k_0$ and E_c denotes a dimensionless function of the dimensionless argument $\frac{k}{k_d}$. The wavenumber k_d characterizes the dissipative range and is defined by

$$k_d = \frac{\epsilon^{\frac{1}{4}}}{\nu^{\frac{3}{4}}} \quad (17.27)$$

The dimensionless spectrum E_c is approximately universal if the high wavenumber range is locally isotropic and self-similar. This holds irrespective of the large scale (small wavenumber) motion which may be non-homogeneous and anisotropic.

Hypothesis of inviscid similarity (inertial subrange)

For sufficiently high Reynolds numbers a wavenumber range $k_0 \ll k \ll k_d$ exists where the spectrum is independent of the viscosity/Reynolds number. Dimensional analysis leads then to

$$E(k) = C \epsilon^{\frac{2}{3}} k^{-\frac{5}{3}} \quad (17.28)$$

valid for $k_0 \ll k \ll k_d$, where C denotes an unknown numerical constant. This is a celebrated result (Kolmogorov's five-thirds law) and it is in good agreement with existing experimental evidence.

17.3 Remarks

The spectrum in the inertial subrange was derived using the following assumptions for the high wavenumber range:

- (1) The dissipation rate ϵ is independent of the Reynolds number.
- (2) The fluctuations are locally isotropic.
- (3) Local similarity.
- (4) Inviscid similarity.

If any of those assumptions is violated the spectrum will deviate from Kolmogorov's five-thirds law. Furthermore, we note that ϵ is an expectation and not the fluctuating dissipation rate. There is no reason why the average dissipation rate and not the correlations of the fluctuating value should appear in the expressions for the spectrum. A refinement of the Kolmogorov form for the spectrum in the inertial subrange is given by (see Lesieur [2])

$$E(k) = C' \bar{\epsilon}^{\frac{2}{3}} k^{-\frac{5}{3}} (Lk)^{-\frac{4}{9}} \quad (17.29)$$

where μ is the logarithmic dispersion of $\nu \frac{\partial v'_\alpha}{\partial x_\beta} \frac{\partial v'_\alpha}{\partial x_\beta}$, $\bar{\epsilon}$ its spatial mean over a region of characteristic length L . The experimental value for the correction to the five-thirds law μ is between 0.4 and 0.5 making it too small to be detected reliably in the experiments.

A second point is the intermittent character of the spatial regions with significant dissipation, which is not taken into account in Kolmogorov's theory. If this intermittent character would invalidate Kolmogorov's hypotheses, it could not be argued that the microstructure of turbulence is determined by an average of the instantaneous dissipation rate over a spatial region of the same micro-region, because the energy is supplied from regions of larger scale.

References

1. Domaradski, J.A., Rogallo, R.S.: Local energy transfer and nonlocal interactions in homogenous, isotropic turbulence. *Phys. Fluids A* **2**, 413 (1990)
2. Lesieur, M.: *Turbulence in Fluids*. Martinus Nijhoff Publishers, Dordrecht (1987)
3. Meinsma, G.: Dimensional and scaling analysis. *SIAM Rev.* **61**, 159–184 (2019)
4. Ling, S.C., Huang, T.T.: *Phys. Fluids* **13**, 2912 (1970)
5. Vassilicos, J.C.: Dissipation in turbulent flows. *Ann. Rev. Fluid Mech.* **47**, 95–114 (2015)

Chapter 18

Homogeneous Turbulence



Turbulence with statistical properties invariant with respect to translation is called homogeneous. Homogeneity allows significant simplification of the statistical equations governing the dynamics. The special case of homogeneous and isotropic turbulence is considered first.

18.1 Homogeneous and Isotropic Turbulence

Homogeneous turbulence satisfying reflective symmetry is called isotropic, homogeneous turbulence. The statistical properties of a turbulent flow are determined by the n -point Pdf of velocity and the turbulence is isotropic and homogeneous if this pdf is independent of arbitrary rigid body rotations and reflections of the vector configurations (Batchelor [1]). This implies for the statistical moments of velocity products at n points that these moments depend only on the lengths and angles between the vector arguments. It follows then that the general form of isotropic tensors of second and third order involving two points \mathbf{x}^1 and \mathbf{x}^2 is given by

$$\langle v_\alpha(\mathbf{x}^1)v_\beta(\mathbf{x}^2) \rangle = Ar_\alpha r_\beta + B\delta_{\alpha\beta} \quad (18.1)$$

and

$$\langle v_\alpha(\mathbf{x}^1)v_\beta(\mathbf{x}^1)v_\gamma(\mathbf{x}^2) \rangle = Ar_\alpha r_\beta r_\gamma + Br_\alpha \delta_{\beta\gamma} + Cr_\beta \delta_{\alpha\gamma} + Dr_\gamma \delta_{\alpha\beta} \quad (18.2)$$

where the $r_\alpha^i = x_\alpha^{i+1} - x_\alpha^i$ for $i = 1, \dots, n - 1$ describe the configuration of n points $\{\mathbf{x}^i\}$. The mean velocity can be set to zero without restriction of generality, hence denote the velocity components without the prime fluctuations. The coefficients A, B, C, D are even functions of the distance r between the two points and the invariants of the tensors they represent. Tensors of order higher than three can be found in Batchelor [1], the second- and third-order tensors are sufficient for the present purpose.

The two-point correlation $R_{\alpha\beta}(\mathbf{r}) = \langle v_\alpha(\mathbf{x})v_\beta(\mathbf{x} + \mathbf{r}) \rangle$ is for isotropic, homogeneous turbulence written as

$$R_{\alpha\beta} = u^2 \left(\frac{f - g}{r^2} r_\alpha r_\beta + g \delta_{\alpha\beta} \right) \quad (18.3)$$

where

$$u^2 = \frac{1}{3} \langle v_\alpha(\mathbf{x})v_\alpha(\mathbf{x}) \rangle \quad (18.4)$$

measures the intensity of the velocity fluctuations, and the longitudinal correlation function

$$f(r) = \frac{1}{u_p^2} \langle v_p(\mathbf{x})v_p(\mathbf{x} + \mathbf{r}) \rangle \quad (18.5)$$

where $u_p^2 = \langle v_p^2(\mathbf{x}) \rangle$ and v_p is parallel to \mathbf{r} , and the transversal correlation function

$$g(r) = \frac{1}{u_n^2} \langle v_n(\mathbf{x})v_n(\mathbf{x} + \mathbf{r}) \rangle \quad (18.6)$$

where $u_n^2 = \langle v_n^2(\mathbf{x}) \rangle$ and v_n is normal to \mathbf{r} . Mass balance implies

$$g = f + \frac{1}{2} r \frac{df}{dr} \quad (18.7)$$

hence only a single scalar function $f(r)$ suffices to describe the spatial character of the two-point correlation function for isotropic turbulence.

The two-point correlation tensor

$$S_{\alpha\beta\gamma}(\mathbf{r}) = \langle v_\alpha(\mathbf{x})v_\beta(\mathbf{x})v_\gamma(\mathbf{x} + \mathbf{r}) \rangle$$

can be represented for isotropic, homogenous turbulence as

$$S_{\alpha\beta\gamma} = u^3 \left[\frac{K - rK'}{2r^3} r_\alpha r_\beta r_\gamma + \frac{2K + rK'}{4r} (r_\alpha \delta_{\beta\gamma} + r_\beta \delta_{\alpha\gamma}) - \frac{K}{2r} r_\gamma g \delta_{\alpha\beta} \right] \quad (18.8)$$

where the longitudinal triple correlation function is defined by

$$u^3 K(r) = \langle v_p^2(\mathbf{x})v_p(\mathbf{x} + \mathbf{r}) \rangle \quad (18.9)$$

It is a negative function of r and grows like r^3 for small r .

Mass and momentum balance can be used to establish the dynamical equation for the two-point correlations. The result is the von Karman–Howarth equation

$$\frac{\partial}{\partial t}(u^2(t)f(r, t)) = u^3 \left(\frac{\partial}{\partial r} + \frac{4}{r} \right) K(r, t) + 2\nu u^2 \left(\frac{\partial^2}{\partial r^2} + \frac{4}{r} \frac{\partial}{\partial r} \right) f(r, t) \quad (18.10)$$

This pde is not closed since it contains three unknown functions $u(t)$, $f(r, t)$ and $K(r, t)$.

18.2 Problems for this Chapter

Problem 18.1 Consider stationary and locally isotropic turbulence at high Re-number. A simple model for the energy spectrum can be constructed by defining a sequence of wavenumbers k_n , such that

$$k_{n+1} = 2k_n$$

Let the energy contained in the interval $[k_n, k_{n+1}]$ be $E(k)$ and the amount of energy transported during the time $\tau(E, k)$ from k_n to k_{n+1} be $\epsilon(k)$. Then compute

18.1.1 $\epsilon(k)$ as function of the spectrum $E(k)$, the wavenumber k and the time interval $\tau(E, k)$.

18.1.2 Determine the spectrally local time scale $\tau(E, k)$ in the inertial subrange of the spectrum using dimensional analysis.

18.1.3 Assuming that the amount of energy fed into the inertial subrange is equal to the amount removed from it, compute the form of the energy spectrum $E(k)$.

Reference

1. Batchelor, G.K.: The Theory of Homogeneous Turbulence. Cambridge University Press (1967)

Chapter 19

Length and Time Scales



The first and most important order of magnitude estimate concerns the rate of dissipation ϵ . This estimate is based on the definition of an eddy or coherent structure and two assumptions.

Definition of an eddy/coherent structure

The notion of an eddy is used frequently by various authors without a rigorous definition. For instance, Jimenez [1] defines an eddy loosely as a statistical construct in contrast to structures that evolve dynamically by definition; the example of the Lorenz system [2] as coherent structure is used to define coherence in terms of a short time Lyapunov exponent.

A coherent structure is defined presently as a subset of the flow domain, that is *organized in space, recurrent and persistent in time*

Adrian and Marusic [3]. An eddy is regarded in [3] as member of the subclass of coherent structures, which are also rotational as in [4]; a formal definition of coherent structure and an eddy is given below.

Further examples for eddy definitions can easily be found. Homogeneous turbulence can be approximated by 3-periodic flow fields in a cube, Sect. 4.1, the phase space Ω is spanned by the Fourier basis vectors, Eq. (4.3). Eddies can be defined by suitably weighted basis vectors in selected wavenumber intervals to represent recognizable structures with physically relevant properties. This idea was suggested by Tennekes and Lumley [5] (Sect. 8.2), they define an eddy as a wave packet in Fourier space such that the Fourier transform into physical space emerges as a localized (compact) entity, which they define as an eddy.

Moin and Moser [6] and Berkooz, Holmes and Lumley [7] base the statistical eddy definition on P(proper) O(orthogonal) D(ecomposition) of the flow field. Let

$$R_{\alpha\beta}(t, \mathbf{r}, \mathbf{x}) = \langle v_\alpha(t, \mathbf{x} + \mathbf{r}) v_\beta(\mathbf{x}) \rangle$$

be the two-point velocity correlation, then apply the Karhunen–Loeve expansion

$$v_\alpha(t, \mathbf{x}) = \sum_{n=0}^{\infty} a_n(t) e_\alpha^n(\mathbf{x}),$$

which is a representation of a stochastic field $v_\alpha(t, \mathbf{x})$ as an infinite linear combination of orthonormalized eigenvector functions $e_\alpha^n(\mathbf{x})$ of the eigenproblem

$$\int_{\mathcal{D}} d\nu(\mathbf{x}') R_{\alpha\beta}(t, \mathbf{r}, \mathbf{x}) \bar{e}_\beta^n(\mathbf{x}') = \lambda e_\alpha^n(\mathbf{x}), \quad \mathbf{r} \equiv \mathbf{x} - \mathbf{x}'$$

where the overbar denotes complex conjugate (Papoulis [8], Lumley [9] Sect. 3.6). This requires the eigenanalysis of the two-point correlation $R_{\alpha\beta}$ generating eigenvalues and the associated ONS eigenfunction vectors $e_\alpha^n(\mathbf{x})$. The positive eigenvalues λ are the energy of the eigenvectors, which are defined by Moin and Moser as characteristic eddies. These ideas lead to the present eddy/coherent structure definition. The Merriam-Webster dictionary defines coherent as *systematic or logical connection or consistent*. In the present context of fluid mechanics the definition:

coherent \Leftrightarrow spatially connected and consistent with the laws of fluid mechanics will be used.

Let Ω be the (spatial) vector phase space for a particular type of turbulent flow, it is assumed to be at least a Banach or a Hilbert space with a selected ONS (Schauder) vector base $\mathcal{B} = \{\mathbf{f}_k, k = 0, 1, \dots, \infty\}$. Hence, a velocity field $\mathbf{v} \in \Omega$ is represented (25.153) (Sect. 25.19 of Appendix C, solenoidal vector basis (25.164)) in the spatial description by

$$\mathbf{v}(t, \mathbf{x}) = \sum_{k=0}^{\infty} a_k(t) \mathbf{f}_k(\mathbf{x})$$

A realization of a turbulent flow at time t is then a point in the phase space Ω .

Definition An (instantaneous) eddy is a rotational coherent structure, that is the flow generated by a subset of terms in a representation of the velocity field

$$\mathbf{v}^e(t, \mathbf{x}; R^e, \{a_k^e(t)\}) = \sum_{k \in R_e \subset R^+} a_k^e(t) \mathbf{f}_k(\mathbf{x})$$

w.r.t. an ONS basis \mathcal{B} spanning the phase space Ω , where the index subset $R_e \subset R^+$ and the coefficients $a_k^e(t)$ determine the eddy/coherent structure properties. The coefficients $a_k(t)$ are stochastic processes in turbulent flows. A (statistical) eddy/coherent structure is then the ensemble average (6.4) of instantaneous eddies/coherent structures.

Note that selecting a finite subset of modes from a basis implies that the result depends on the basis \mathcal{B} chosen. However, it is the index set R_e that depends on

the basis; different bases will generate different index sets for the same physical entity. The definition presented above is a mathematical framework, the physical information is contained in the particular properties of the Schauder basis and the range of values for the coefficients $a_k(t)$, $k \in R_e$. Constructing a basis as in the POD context or the periodic pipe flow (Sect. 25.19) of Appendix C, introduces physical information in the eddy definition, furthermore, it indicates that not all bases are created equal and an optimal basis could improve the representation by keeping the number of modes to a minimum.

Jimenez [1] distinction between eddy and coherent structure is not made in the present book, eddies are defined as coherent structures that evolve in time as solutions of the Navier–Stokes pdes. Several candidates for this type of eddies have been constructed as blobs (compact or space filling) of vorticity with simple shapes such as Townsend’s model eddy, where the velocity is constructed in a cylindrical coordinate system

$$\mathbf{v}(r, \theta, z) = \Omega r \exp\left(-2 \frac{\mathbf{x} \cdot \mathbf{x}}{z_c^2}\right) \mathbf{e}_\theta \in L^2_{R^3} \quad (19.1)$$

with \mathbf{e}_θ being the unit vector in the azimuthal direction and z_c denoting the eddy size (see Davidson [10], Sect. 6.4.1 and the solution for Problem (20.6) in Appendix F for details), vortex rings (Sect. 20.5.1), Hill’s vortex (Sect. 20.5.3) and hairpin vortices for wall-bounded flows (attached eddy hypothesis of Perry [11]).

Definition of a scale

The notion of size of a scalar, vector or tensor field can be made explicit in terms of a norm. Let $\Phi(\mathbf{x})$ be an element of the phase space Ω , which is a Banach or Hilbert space, and let $\|\cdot\|$ be a selected norm and $w(\mathbf{x})$ a weight function, then is a scale for Φ defined by

$$O(\Phi) \equiv \langle \|w(\mathbf{x})\Phi\| \rangle \quad (19.2)$$

The definition of a scale requires the choice of a norm and a weight function. Unless otherwise stated, the norm is the L^2 norm and the weight function is unity.

Scales for the independent variables length and time are determined by the scales (19.2) of fields, i.e. they are typical values of length and time for the subset of the flow field, where $\langle w(\mathbf{x})\Phi \rangle$ is dominant.

Two basic assumptions

The assumptions are formulated as follows:

(i) First, it is assumed that the net rate R of energy supply to small eddies from larger ones is given by

$$R \sim \frac{1}{\tau} \quad (19.3)$$

where τ is the time scale (eddy turn-over time) of the larger eddies (the term eddy is widely used as a vague form of flow structure by many authors, however, a tentative definition is given above in the present section).

The estimate of the eddy turn-over time τ can be provided if a characteristic velocity (velocity scale) u and a corresponding length scale l exist, which are typical for the large eddies. The time scale is then given by

$$\tau \simeq \frac{l}{u} \quad (19.4)$$

and it follows that

$$R \sim \frac{u}{l} \quad (19.5)$$

holds. The energy supplied per unit time is, therefore, given by

$$\frac{u^2}{\tau} = \frac{u^3}{l} \quad (19.6)$$

(ii) The second assumption is that the turbulent flow is in approximate statistical equilibrium \Leftrightarrow The rate of energy supplied at large scales l is approximately equal to the rate at which energy is removed by viscous action at small scales.

It follows then that the order of magnitude estimate of the dissipation rate is given by

$$O(\epsilon) = \frac{u^3}{l} \quad (19.7)$$

where l is the length scale of the fluctuations receiving the energy. A sketch showing the flow of energy through the spectrum is given in Fig. 19.1. The spectrum $E(k)$ shows that there exists a continuous range of length scales $\frac{2\pi}{k}$ with positive energy. We need for the purpose of estimation of various terms in the moment equations length and time scales that determine their order of magnitude. These scales will be characteristic for different ranges of the spectrum.

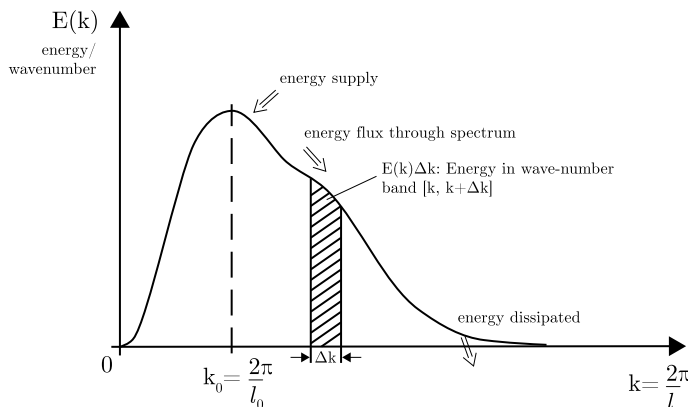


Fig. 19.1 Energy flow through the spectrum for homogeneous and isotropic turbulence

19.1 Dissipative Range of Scales (Kolmogorov Range)

The smallest scales (highest wavenumber range) are characterized by dissipation rate ϵ and viscosity ν and the corresponding scales are called dissipative or Kolmogorov scales:

$$\eta = \left(\frac{\nu^3}{\epsilon} \right)^{\frac{1}{4}} \text{ length} \quad (19.8)$$

$$v = (\nu \epsilon)^{\frac{1}{4}} \text{ velocity} \quad (19.9)$$

$$\tau = \left(\frac{\nu}{\epsilon} \right)^{\frac{1}{2}} \text{ time} \quad (19.10)$$

The Reynolds number for this range is then

$$Re_d = \frac{v\eta}{\nu} = 1 \quad (19.11)$$

19.2 Scale Relations

The estimate for the dissipation rate in terms of the large scales u and l allows the derivation of relations to the scales relevant for the dissipative range. The Kolmogorov length scale η can be regarded as estimate for the dissipation rate

$$\epsilon = \frac{\nu^3}{\eta^4} \quad (19.12)$$

which is on the other hand estimated by the large scales

$$\epsilon = \frac{u^3}{l} \quad (19.13)$$

which implies that

$$\frac{\eta}{l} = Re^{-\frac{3}{4}} \quad (19.14)$$

holds where the Reynolds number is defined by

$$Re \equiv \frac{ul}{\nu} \quad (19.15)$$

A similar relation can be found for the time scales. We denote by

$$T = \frac{l}{u} \quad (19.16)$$

the large time scale and it follows that the ratio of dissipative to large time scales is given by

$$\frac{\tau}{T} = \left(\frac{\nu}{\epsilon} \right)^{\frac{1}{2}} \frac{u}{l} \quad (19.17)$$

which emerges as

$$\frac{\tau}{T} = Re^{-\frac{1}{2}} \quad (19.18)$$

if the estimate for the dissipation rate is used. The ratio of the velocity scales follows at once

$$\frac{v}{u} = Re^{-\frac{1}{4}} \quad (19.19)$$

It follows that we have two ways of estimating the order of magnitude of the dissipation rate depending on the scales we wish to use. The large-scale estimate for approximate statistical equilibrium is given by

$$\epsilon = \frac{u^3}{l} \quad (19.20)$$

whereas the estimate in terms of the Kolmogorov scales is

$$\epsilon = \nu \frac{v^2}{\eta^2} \quad (19.21)$$

19.3 Taylor's Length Scale

A third intermediate length scale was suggested by G.I. Taylor. It is defined by

$$\epsilon = \nu \frac{u^2}{\lambda^2} \quad (19.22)$$

which implies the scale relations

$$\frac{\lambda}{l} = \frac{1}{Re^{\frac{1}{2}}} \quad (19.23)$$

$$\frac{\eta}{\lambda} = \frac{1}{Re^{\frac{1}{4}}} \quad (19.24)$$

Furthermore hold $\eta < \lambda < l$ and

$$\frac{v}{\eta} = \frac{u}{\lambda} \quad (19.25)$$

We note that the Taylor scale is a mixed scale in the sense that the dissipation rate is estimated using the large-scale u for the velocity and the parameter ν describing the smallest scales. The main application of the Taylor scale is to estimate spatial derivatives of first order according to

$$O\left(\frac{\partial v'_\alpha}{\partial x_\beta}\right) = \frac{u}{\lambda} \quad (19.26)$$

Some care has to be exercised in applying this estimate to correlations since derivatives outside the angular brackets scale with the large scales and not with the Taylor scale.

19.4 Macroscales

The macroscales or large scales can be derived from two-point correlations as follows:

$$L_\beta(\mathbf{x}, t) \equiv \int_0^\infty dr_\beta \frac{R_{\alpha\alpha}(\mathbf{x}, \mathbf{r}, t)}{R_{\alpha\alpha}(\mathbf{x}, 0, t)} \quad (19.27)$$

and similarly for the time scale

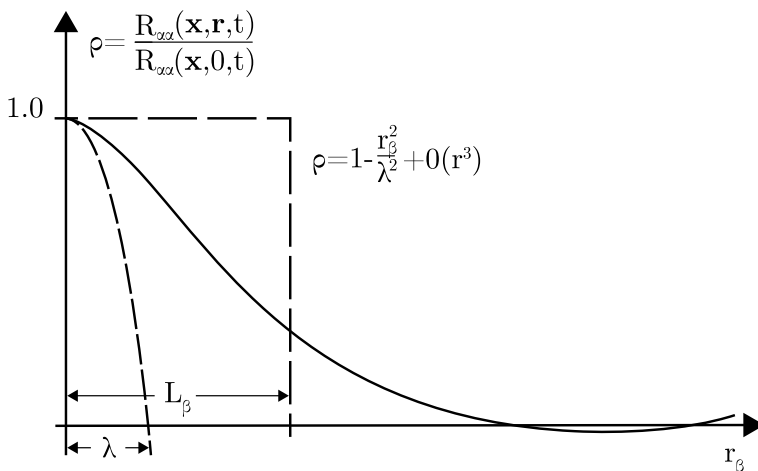


Fig. 19.2 Two-point correlation and definition of a macroscale

$$T(\mathbf{x}, t) \equiv \int_0^{\infty} d\tau \frac{\langle v'_{\alpha}(\mathbf{x}, t + \tau) v'_{\alpha}(\mathbf{x}, t) \rangle}{\langle v'_{\alpha}(\mathbf{x}, t) v'_{\alpha}(\mathbf{x}, t) \rangle} \quad (19.28)$$

The macro-length scale is closely related to the curvature of the two-point correlation at the origin as indicated in Fig.19.2.

References

1. Jimenez, J.: Coherent structures in wall-bounded turbulence. *JFM* **842**, P1-1-P1-100 (2018)
2. Lorenz, E.N.: Deterministic nonperiodic flow. *J. Atmos. Sci.* **20**, 130–141 (1963)
3. Adrian, R.J., Marusic, I.: Coherent structures in flow over hydraulic engineering surfaces. *J. Hydraulic Res.* **50**, 451–464 (2012)
4. Lozano-Durán, A., Jimenez, J.: Time-resolved evolution of coherent structures in turbulent channels: characterization of eddies and cascades. *JFM* **759**, 432–471 (2014)
5. Tennekes, H., Lumley, J.L.: *A First Course in Turbulence*. MIT Press, Cambridge MA (1972)
6. Moin, P., Moser, R.D.: Characteristic-eddy decomposition of turbulence in a channel. *JFM* **200**, 471–509 (1989)
7. Berkooz, G., Holmes, P., Lumley, J.L.: The proper orthogonal decomposition in the analysis of turbulent flows. *Ann. Rev. Fluid Mech.* **25**, 539–575 (1993)
8. Papoulis, A.: *Probability, Random Variables and Stochastic Processes*. McGraw-Hill (1965)
9. Lumley, J.L.: *Stochastic tools in Turbulence*. Academic Press (1970)
10. Davidson, P.A.: *Turbulence*. Oxford University Press, Oxford, U.K. (2004)
11. Perry, A.E., Marusic, I.: A wall-wake model for the turbulence structure of boundary layers. Part 1. Extension of the attached eddy hypothesis. *JFM* **298**, 361–388 (1998)

Chapter 20

The Structure of Turbulent Flows



Structural properties of turbulent flows have been the subject of experimental and theoretical research for a long time, see the proceedings of the IUTAM symposium in Cambridge U.K. 1989 [1] for the topological and geometric aspects of flow structures. Wray and Hunt [2] in these proceedings put forward a definition of structures and propose an algorithm for their classification. This will be discussed in detail in Sect. 20.2.

In particular, the structures in wall-bounded flows are relevant for the transport mass, momentum and energy, hence important for a variety of applications, see Tsinober [3] Chap. 7, Marusic [4], Adrian [5], Adrian and Marusic [6] (properties and organization of coherent structures, defined in Sect. 20.5) in wall turbulence at high Reynolds numbers and their statistical significance), Dallmann [7] (classification of near-wall structures), Surana et al. [8] (classification of separation structures near wall boundaries using Taylor series expansions and dynamical systems theory), Chong et al. [9] (topological properties of skin friction and surface vorticity in the wall boundary), Ganapathisubramani et al. [10] (effect of large scale motions on small scales in wall turbulence), Lawson and Dawson [11] and Wilczek et al. [12, 13] (velocity gradient dynamics and turbulent structure) and references therein.

One of the fundamental structures emerging in boundary layers is a coherent structure shaped like a hairpin, Chong et al. [9], Lozano-Durán and Jimenez [14], Shekar and Graham [15]. This structure has been shown to be responsible for the transport of mass and momentum from the wall into the active region of boundary layers (see Marusic [4] for an overview of recent research). The hairpin structures are recognized as level surfaces of enstrophy (3.16) or the swirling strength defined as the imaginary part of the complex eigenvalue of the deformation rate $\nabla \mathbf{v}$ (Yang and Pullin [16], also called velocity gradient tensor). Hairpin structures are also generated away from wall boundaries during intense interaction of vortex rings [17], resulting from bending and folding of vortex tubes.

The structures detected in homogeneous and isotropic turbulence by Leung et al. [18] with the aid of Minkowski functionals exhibit a variety of blob-like forms. There are four Minkowski functionals in 3-d space $V_i, i = 0, \dots, 3$ defined by

(Sahni et al. [18, 19], Griffiths et al. [20]) for a measurable subset $\mathcal{B} \in \mathbb{R}^3$ with bounding surface $\partial\mathcal{B}$

$$V_0 = V \text{ (Volume)}, \quad V_1 = S \text{ (Surface area)}, \quad V_2 = \frac{1}{3\pi} \int_{\partial\mathcal{B}} dA \frac{1}{2}(\kappa_1 + \kappa_2), \quad V_3 = \frac{1}{2\pi} \int_{\partial\mathcal{B}} dA \kappa_1 \kappa_2 \quad (20.1)$$

where κ_1, κ_2 denote the principal curvatures of the bounding surface $\partial\mathcal{B}$, hence $\frac{1}{2}(\kappa_1 + \kappa_2)$ is the mean and $\kappa_1 \kappa_2$ the Gaussian curvature, and V_3 is recognized as a topological invariant called the Euler characteristic ([21], Chap. 8) according to the Gauss–Bonnet theorem.

In turbulent shear flows away from wall boundaries, a different type of structure has emerged, which is thought to contribute to the transport of energy from large to small scales: The vortex reconnection [22–25] flow. Tube-like regions with significant levels of enstrophy close in antiparallel configuration reconnect and then separate, but bridge vortices remain with much smaller length scale. For sufficiently high Reynolds numbers the process possibly repeats itself on the bridge vortices, thus creating smaller and smaller elongated vortical structures.

20.1 Transforms

Integral transforms of flow fields are relevant for the interpretation of turbulent flows, see Chap. 15. The most important one is Fourier transform and its finite-dimensional version for the numerical simulation, spectral analysis and related matters such as time and length scales of turbulent flows.

20.2 Definition and Classification of Flow Structures

Subsets of flow fields carrying information relevant to the character of turbulence are called structures. They are classified as

- (i) spatial—determined by the flow field at a specified instant;
- (ii) material—structures bounded by materially invariant point sets thus evolving in time;
- (iii) general—structures moving relative to the fluid such as sets bounded by propagating surfaces.

20.3 Characteristic Scales

The notion of a structure relevant to the physical and chemical processes in a turbulent flow needs to be established. The first step is the definition of geometric characteristics of subsets of the flow field that possibly carry relevant physical and chemical

properties. The second step is the introduction of such physical and chemical properties. The scalar and vector fields are assumed to be at least three times continuously differentiable, i.e. no shock waves are present.

The fields are given in a domain $\mathcal{D} \subset R^3$ with boundary $\partial\mathcal{D}$. The flow is turbulent and it is assumed that a dissipative range of length scales exists characterized by the Kolmogorov scales η (19.8), v (19.9), τ (19.10)

$$\eta = \left(\frac{\nu^3}{\epsilon} \right)^{\frac{1}{4}} \text{length}, v = (\nu\epsilon)^{\frac{1}{4}} \text{velocity}, \tau = \left(\frac{\nu}{\epsilon} \right)^{\frac{1}{2}} \text{time}$$

The Reynolds number for this range is then

$$Re_d = \frac{v\eta}{\nu} = 1 \quad (20.2)$$

where ν is the kinematic viscosity, ϵ the statistical average of the dissipation rate. The coordinates are made dimensionless by division with η for the following analysis.

20.4 Spatial/Eulerian Structures

Spatial structures are defined as measurable (the notion of measure is a generalization of length, area, volume, etc., see, for instance, Bogachev, vol.1 [26], Chap. 1) subsets of the flow domain, fully specified by physical and chemical properties to be discussed below. The most important and elementary properties of the subsets are their measure m_C (Minkowski functional V_0 , (20.1)) and their dimension d_C , the Minkowski functionals V_1, V_2, V_3 do not exist for subsets with noninteger d_C . The usual definition of dimension as the number of base vectors (coordinates) to specify any vector is not sufficient for the present purpose and a more general point of view is taken. The notions of dimension due to Caratheodory and Hausdorff ([27], Sect. 2.10, [28], Sect. 1.1) introduced in Sect. 23.3 are applied as appropriate, since they allow noninteger values for the dimension.

20.4.1 Line-Type Structures

Subsets of the flow field $\mathcal{D} \subset R^3$ with Hausdorff dimension $d_H \leq 1$ are called **line type** structures. The vector fields defined on \mathcal{D} (velocity, vorticity, Lamb vector and related fields) generate vector lines (the vectors are tangential) according to

$$\frac{dx_\alpha}{ds} = v_\alpha(\mathbf{x}(s), t), \quad \alpha = 1, 2, 3 \quad (20.3)$$

with an arbitrary initial condition $\mathbf{x}(0) = \mathbf{x}_0 \in \mathcal{D}$, s denotes the arclength measured along the vector line. Time t is constant in the spatial description, hence is the system of odes with respect to arclength s always autonomous. Vector lines can be used as one of the tools to establish the characteristics of the underlying vector field by regarding arclength as analogous to time.

Consider a finite set of initial conditions \mathbf{x}^i , $i = 1, \dots, N$. The vector lines through this set can be analysed with the aid of algebraic topology (braids, knots and linking number [21], entanglement [29]) and dynamical systems theory [30–32]. Dynamical system theory provides the critical structures of the vector lines: critical points, limit cycles, invariant tori and invariant sets of dimension $d_H > 2$. Critical points and limit cycles are the main line-type structures. Wu et al. [33] proposed a vorticity dynamics theory of 3-d flow separation exploiting the relation of skin friction and vorticity on fixed wall boundaries. Serra and Haller [34] established recently a rigorous global variational theory of objective Eulerian coherent structures (ECS).

20.4.2 Surface-Type Structures

Subsets of the flow field $\mathcal{D} \subset \mathbb{R}^3$ with Hausdorff dimension $1 < d_H \leq 2$ are called **surface-type** structures. The vector fields relevant to the turbulent and combustion flows are velocity, vorticity, the Lamb vector and various flux vector fields. Combustion flows contain subsets of particular importance called reaction or flames zones. These reaction zones can be approximated by propagating surfaces [35] if the chemical reactions are sufficiently fast. This type of structure is called Lagrangean discussed in Sect. 20.5. The local structures containing flames zones are considered in the following as surface and volume type. Propagating surfaces in reacting and non-reacting turbulent flows may develop singularities in finite time [36] in contrast to materially invariant surfaces. In particular, cusp singularities are an identifying characteristic of propagating surfaces in the spatial description.

The physical interpretation of the vector field is irrelevant for the discussion of geometric properties. The vector tube is an important tool for the construction of surface-type structures. Vector tubes are defined as the set of vector lines that pass through a specified line \mathcal{S}_1 that is not a vector line. An example for such a surface is the tube formed by the vector lines passing through a circle or any other simple, closed line. The geometry of this surface depends principally on the underlying vector field: If the vector field is solenoidal (such as vorticity), the vector tube carries a constant flux, if the vector field is not solenoidal (such as velocity in combustion flows) this ceases to be true. This is a consequence of the first Helmholtz theorem ([37] Sect. 3.2.1) for solenoidal vector fields

$$\int_{\mathcal{S}_1} da \mathbf{n} \cdot \mathbf{v} = \int_{\mathcal{S}_2} da \mathbf{n} \cdot \mathbf{v} \quad (20.4)$$

where S_i , $i = 1, 2$ are two smooth cross sections of the tube with unit normal vector \mathbf{n} pointing outward. If the vector field is vorticity, the circulation of the tube is constant along it. If the vector field has non-zero divergence, then it follows from mass balance in the spatial description and the Gauss divergence theorem that

$$\int_{S_1} da \mathbf{n} \cdot \mathbf{v} = \int_{S_2} da \mathbf{n} \cdot \mathbf{v} + \int_{\mathcal{D}} d\nu \frac{\partial \rho}{\partial t} \quad (20.5)$$

holds, where \mathcal{D} denotes the vector tube bounded by the two cross sections and the sidewall formed by the vector lines. The relation (20.4) indicates what to expect in a turbulent environment. The vector tube through a starting circle will be deformed and stretched significantly as the tube is computed by solving (20.3). Hence, the starting circle will be stretched and distorted such that the vector flux through it remains constant. This implies that different parts of the cross-section of the tube must approach each other, thus limiting the computation if numerical self-intersection is to be avoided.

The case of surfaces defined as level surfaces of a non-negative and smooth scalar field $\Phi(t, \mathbf{x})$ defined on $\mathcal{D} \in R^3$

$$S_\Phi(t, \varphi) = \{\mathbf{x} : \Phi(t, \mathbf{x}) = \varphi\} \quad (20.6)$$

where $0 \leq \varphi < \infty$, offers the possibility to compute the area $A(t, \varphi)$ without determining the location of the surface. Specifically, a theorem of geometric measure theory (see Federer [38], Maz'ja [39], Chap. 1.2.3, p.37 for proof)

Theorem: Let $F(t, \mathbf{x})$ be a Borel-measurable non-negative function on an open domain $\mathcal{D} \in R^3$, let $\Phi(t, \mathbf{x}) \in C^\infty(\mathcal{D})$. Then

$$\int_{\mathcal{D}} d\nu(\mathbf{x}) F(\mathbf{x}) |\nabla \Phi(t, \mathbf{x})| = \int_0^\infty d\varphi \int_{S_\Phi(\varphi)} dA(\mathbf{x} F(\mathbf{x})) \quad (20.7)$$

holds. This theorem can be used with the aid of suitable integral transforms to express surface integrals in terms of volume integrals. Let the level surface be contained in a compact domain \mathcal{D} , hence does not intersect the boundary $\partial\mathcal{D}$. Let the Borel-measurable function be

$$F(\mathbf{x}) = f(\mathbf{x}) \delta(\Phi(\mathbf{x}) - \varphi) \quad (20.8)$$

where $f(\mathbf{x}) \in L^2(\mathcal{D})$. Then

$$\int_{\mathcal{D}} d\nu(\mathbf{x}) f(\mathbf{x}) \delta(\Phi(\mathbf{x}) - \varphi) |\nabla \Phi(t, \mathbf{x})| = \int_{S_\Phi(\varphi)} dA(\mathbf{x}) f(\mathbf{x}) \quad (20.9)$$

holds. Choosing $f(\mathbf{x}) = 1$ leads to the relation

$$A_\Phi(\varphi) = \int_{\mathcal{D}} d\nu(\mathbf{x}) \delta(\Phi(\mathbf{x}) - \varphi) |\nabla \Phi(t, \mathbf{x})| \quad (20.10)$$

between a volume integral and the surface area. The range of $0 \leq \Phi < \infty$ indicates that Laplace transformation

$$\tilde{A}_\Phi = \mathcal{L}(A_\Phi) \quad (20.11)$$

or, explicitly

$$\tilde{A}_\Phi(s) = \int_0^\infty d\varphi A_\Phi(\varphi) \exp(-s\varphi) \quad (20.12)$$

where the argument $s = \sigma + i\omega$ is complex, can be applied to remove the Dirac function. Application of the co-area formula (20.10) leads to

$$\tilde{A}_\Phi(s) = \int_{\mathcal{D}} d\nu(\mathbf{x}) |\nabla \Phi| \exp(-s\Phi(\mathbf{x})) \quad (20.13)$$

This is a powerful result as it allows the computation of the transformed surface area of level surfaces without determining the location of a single level surface. Furthermore, the computation of the integrals as function of s is much more efficient than direct methods based on discretization (such as triangulation with its well-known pitfalls) of the level surface.

The inverse Laplace transform provides the desired result for the surface area

$$A_\Phi(\varphi) = \mathcal{L}^{-1}(\tilde{A}_\Phi) \quad (20.14)$$

or, explicitly

$$A_\Phi(\varphi) = \frac{1}{2\pi i} \lim_{T \rightarrow \infty} \int_{u-iT}^{u+iT} \tilde{A}_\Phi(s) ds \exp(s\varphi) \quad (20.15)$$

where T is a real number such that the contour path of the integration is in the region of convergence of $\tilde{A}_\Phi(s)$. Further details can be found in [40].

20.4.3 Volume-Type Structures

Subsets of the flow field $\mathcal{D} \subset \mathbb{R}^3$ with Hausdorff dimension $2 < d_H \leq 3$ are called **volume type** structures. Volume-type structures may have dimensions less than three, hence may not fill the Euclidean space \mathbb{R}^3 , thus reflecting the intermittent properties

of the flow. The Minkowski functional V_0 is interpreted as the d_C measure of the structure, hence can be computed if the volume-type structure is measurable. The functionals V_1, \dots, V_3 may not exist for structures with fractal dimension. However, if the dimension of the volume type structure is three and the boundary is sufficiently smooth, then the Minkowski functionals V_1 to V_3 are computable and the latter is then the Euler number of the bounding surface.

20.5 Material/Lagrangean Structures

Lagrangean structures are defined as subsets of the flow domain, which maintain their identity as the flow evolves in time. The boundaries of such structures are distinguished by a temporally invariant property. The boundary may consist of the same material points (i.e. points that move with the fluid velocity at their location, the boundary is then called materially invariant) or the boundary points may move relative to the fluid (propagating boundary). The latter case is particularly important for turbulent combustion, where the bounding surface may be defined as a level surface embedded in the flame zone. The recognition and computation of Lagrangean structures can be based on their variational theory, see Farazmand and Haller [41]. The notion of coherent structures is made precise in the following definition (Wiggins [42], Waleffe [43], Chini [44]).

Lagrangean coherent structure (LCS)

A subset of a flow field is called coherent structure iff it is an invariant manifold generated by the solution of the IVP for the three pathline odes (2.81)

$$\frac{d\Phi}{d\tau} = \mathbf{v}(\tau, \Phi), \quad \Phi(0, \mathbf{X}) = \mathbf{X}(p), \quad p \in I$$

where τ is time and $\Phi(\tau, \mathbf{X})$ location in the flow field \mathcal{D} of a material point (material description) and $\mathbf{v}(t, \mathbf{x})$ is the velocity in the spatial description. The initial condition is defined as a set of material points in \mathcal{D} in terms of a Lagrangean multi-index p set I .

The definition provides the mathematical framework, but the physical relevance is determined by the initial set of material points $\mathbf{X}(p)$, $p \in I$ and the Eulerian velocity field $\mathbf{v}(t, \mathbf{x})$. For instance, the initial condition may enclose a region with high enstrophy levels, such as vortex rings, Townsend's model eddy, etc., discussed below.

Several solutions of the Euler and Navier–Stokes pdes are known, which contain compact patches of vorticity moving along straight or circular paths and exhibit the essential features of coherent structures in turbulent flows. Straight vortex columns combined with the assumption of periodicity along the column axis (helical wave decomposition and viscous simulation, Melander and Hussain [45]) and compact domains equivalent to tori are examples related to coherent structures. Two of the latter types of solutions are discussed in the next sections.

20.5.1 Vortex Rings

Vortex rings are defined as compact sets of material points with closed loop vorticity lines and with vorticity surfaces having the topological structure of a torus. If the fluid is inviscid and the vorticity is smooth, the vortex ring is a Lagrangean structure; for viscous fluids, the vorticity spreads into the surrounding fluid and material invariance is obviously lost. Vortex rings are observed with the aid of visualization techniques in many turbulent flows, see, for instance, Glezer and Coles for experimental results [46] and Bergdorf et al. [47] for DNS simulations. In particular, vortex rings are observed at the initial section of jets, wakes and enclosed flows such as the input valve flow in the cylinders of IC engines, the IUTAM Symposium [48] 2006 contains further results and references.

The geometry of vortex rings can be described by a set of elementary parameters. Assuming cylindrical coordinates centred at the ring and Fourier expansion with respect to the azimuthal coordinate, the parameters are defined for the zero mode data at a reference time. The ring centreline radius and its second moment are defined by the azimuthal vorticity ω_θ (Saffman [49], Archer et al. [50], Fukumoto and Moffatt [51])

$$R_0 = \frac{1}{\Gamma} \int dr dz r \omega_\theta(r, z), \quad R_2^2 = \frac{1}{\Gamma} \int dr dz r^2 \omega_\theta(r, z) \quad (20.16)$$

and thickness of the ring by

$$\delta_0 = \sqrt{R_2^2 - R_0^2} \quad (20.17)$$

The slenderness ratio ϵ is then

$$\epsilon = \frac{\delta_0}{R_0} \quad (20.18)$$

Rings with $\epsilon < 0.36$ are regarded as slender, Archer [50]. Vortex rings are generated experimentally by a temporally controlled movement of a piston in a circular pipe, hence are the properties of the piston and its movement available for the definition of parameters. Reynolds numbers for single vortex rings can be defined in several ways. Three definitions are commonly employed:

First, the standard definition of the Reynolds number (2.8) $Re \equiv \frac{UD}{\nu}$, where U is a nominal piston velocity and D a nominal piston diameter;

Second, the Reynolds number based on the initial circulation Γ_0 of a vortex ring

$$Re_\Gamma \equiv \frac{|\Gamma_0|}{\nu} \quad (20.19)$$

where ν is the kinematic viscosity;

Third, the initial propagation velocity V_0 of a ring can be approximated (20.21) and used as velocity scale. Together with the initial ring radius, it defines the Reynolds number

$$Re_V \equiv \frac{V_0 R_0}{\nu} \quad (20.20)$$

The propagation speed of slender rings can be estimated (Saffman [49]) by

$$V_0 = \frac{\Gamma_0}{4\pi R_0} \left[\ln\left(\frac{8R_0}{\delta_0}\right) + C \right] \quad (20.21)$$

where δ_0 is the effective core radius and the parameter C depends on the shape of the vorticity distribution, corrections are necessary for non-slender rings. Fukumoto and Moffatt [51] carried out an investigation of the asymptotic properties of a single vortex ring using matched asymptotic expansions. They establish a third-order theory for the translation velocity of the ring incorporating the slowing down effect due to the elliptical deformation of the vortex core.

The reference time t_0 based on U , D and the reference time using the initial circulation of a ring is defined by

$$t_0^* \equiv \frac{R_0^2}{\Gamma} \quad (20.22)$$

are can be applied for the presentation of results, time made dimensionless with t_0^* is usually denoted with an asterisk.

Two flows generated by the viscous interaction of vortex rings simulated numerically provide examples for Eulerian surface-type structures enclosing regions with high levels of enstrophy as defined in Sect. 20.4.2. They are briefly discussed in light of the numerical simulation results in [17, 52, 53] since interactions of this type of vortex structures are an important aspect of turbulent flows and accessible to accurate numerical simulation without excessive computational requirements due to the compactness of the domain of interest.

Vortex ring sequence

The case of two interacting vortex rings is considered first. The numerical simulation with a hybrid spectral–finite difference solver is run for the time interval $[0, 14]$ as reported in [52]. The boundary conditions are designed to generate a sequence of vortex rings emitted from a circular pipe by a piston movement.

Experimental evidence [54, 55] suggests that vortex rings can be grouped into laminar, wavy, turbulence producing and turbulent rings depending on the standard Reynolds number (2.8) $Re = U_0 D_0 / \nu$, where U_0 is the maximum velocity of the axial velocity at the entrance boundary and D_0 the diameter of the pipe used to generate vortex rings, the present Reynolds number being $Re = 2000$ is in the turbulent regime according to [55].

The motion of vortex filaments [56], straight and circular vortex tubes is subject to instabilities [57, 58], which appear as smaller, ring-like structures [59–61], if made visible with the aid of a colouring agent approximating streaklines. The present example illustrates the Eulerian flow structures that result from the viscous interaction of two co-rotating vortex rings with azimuthal (swirling) flow within

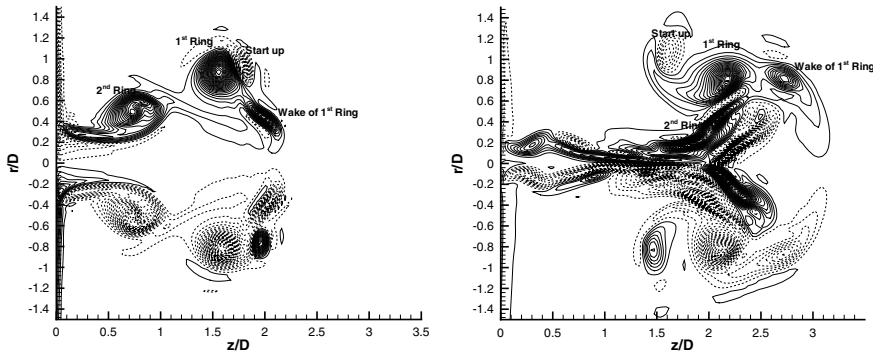


Fig. 20.1 Isolines of the azimuthal vorticity component $\tilde{\Omega}_\theta$ in the plane $\theta = 0$ at time $t = 6.007$ (left graph) and $t = 9.0$ (right graph). Full lines are positive and dashed lines negative values, equally spaced. Vorticity of the opposite sign generated by the start-up near the entrance has been entrained into both rings (labelled start-up) [52]

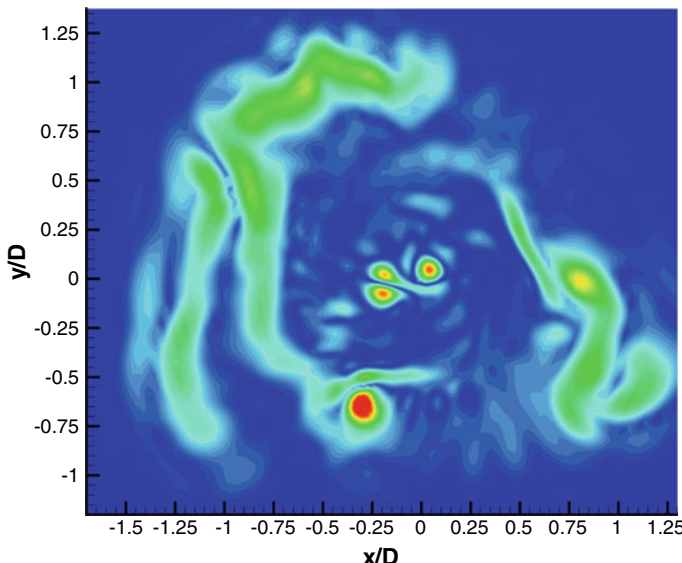


Fig. 20.2 Colour-coded distribution of enstrophy (red denotes high and blue low values) in the plane $z = 3.0$ at time $t = 14.0$ [52]. The plane cuts through four vortex tubes generated in the wake of the rings by the stretching effect of the rings

each ring in opposite direction plus the start-up vortex with opposite orientation of vorticity. A few snapshots of the progress of the interaction are shown in Fig. 20.1 as isolines of the vorticity component ω_θ in the plane $\theta = 0$ for two times with the initial structure indicated, Fig. 20.2 shows the distribution of enstrophy in the wake region and Fig. 20.3 illustrates the geometric properties of vector surfaces generated by integrating the vorticity field starting from closed lines (circles) in forward and backward directions, the starting circles are visible in the right graphs as the

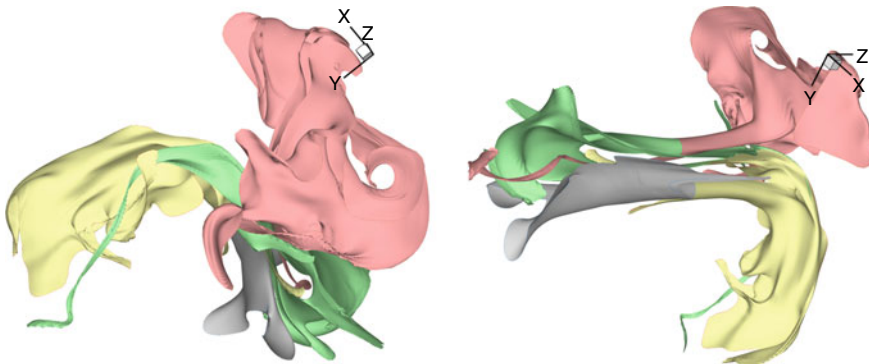


Fig. 20.3 Two views of two vector surfaces generated by vorticity by integrating vorticity starting from circles in forward (yellow/pink surfaces) and backward (grey/green surfaces) direction at time $t = 14.0$ for the simulation of two vortex rings [52]. The two disjoint circles serving as starting point for the forward and backward integration along the vorticity field are visible in the right graph as the bounding line separating differently coloured surfaces

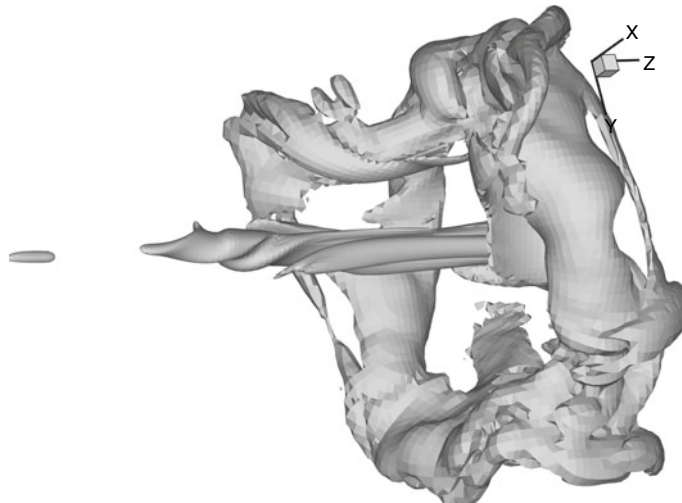


Fig. 20.4 Isosurface of enstrophy $|\omega| = 2.744$ (max $e = 11.629$) at time $t = 14.0$ (end of simulation). The positive z -axis is the direction of propagation of the vortex rings

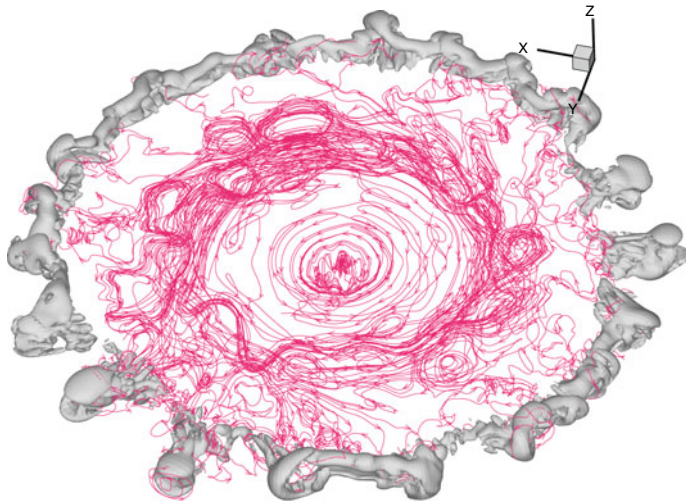


Fig. 20.5 Enstrophy level surface (red lines are vector lines for the vorticity in wake of the rings) after vortex ring collision for the Reynolds number $Re_\Gamma = 2701.82$ (20.19) at $t = 14.1$ [17]. The experimental result is in Fig. 28.12 Appendix F for comparison

boundary between colours. The end of the simulation at time $t = 14.0$ in Fig. 20.4 presents the enstrophy level surface for $e = 23.6\%$ of the maximum norm after the completion of the merger of the two vortex rings. The azimuthal velocity within the rings generates a wake with strong axial vorticity, while the two initial rings and the start-up vortex cannot be distinguished anymore (Fig. 20.5).

Vortex ring collision

The second example for Eulerian structures is provided by the numerical simulation of the vortex ring collision, documented experimentally by Nickels in his PhD thesis [62], see also the flow visualization from this thesis in fig.123 (solution of Problem 20.3 in Appendix F). The initial condition for the flow generated by the collision of two vortex rings is the superposition of two vortex rings with opposite sign of circulation such that they approach each other along their common axis to produce the desired interaction. Hence, the basic data of one of the initial rings are used as reference values: The ring centreline radius and its second moment are defined by (Saffman [49], Archer et al. [50]) (20.16)

$$R_0 = \frac{1}{\Gamma} \int dr dz r \omega_\theta(r, z), \quad R_2^2 = \frac{1}{\Gamma} \int dr dz r^2 \omega_\theta(r, z)$$

and thickness by (20.17) $\delta_0 = \sqrt{R_2^2 - R_0^2}$. The Reynolds numbers for single vortex rings can be defined in several ways. For the present example the definition (20.19)

$$Re_\Gamma \equiv \frac{|\Gamma_0|}{\nu}$$

is used (Nickels 123, Appendix F), where Γ_0 is the initial circulation (zeroth mode) of one of the rings and ν the kinematic viscosity. The level surfaces of enstrophy at the end of the simulation at $t = 14.1$ shows the individual structures as the experiment in Fig. 28.12 in the right graph.

20.5.2 Chaplygin–Lamb Dipole

The interaction of counterrotating vortex tubes has been observed in turbulent flows (see [23] for DNS results); hence, solutions of the Euler pdes with compact distribution of vorticity are of interest, which possess the essential features of vortex tubes. The example of vortex dipoles, as investigated by Lamb [63] and in detail by Chaplygin (see the paper by Meleshko and van Heijst [64], for references in the Russian literature) more than a century ago, falls in this category. The vorticity contained in the dipole does not spread to surrounding fluid if the viscosity is zero and the vortical domain is materially invariant; thus, it is a Lagrangean structure.

Let the flow domain be $\mathcal{D} = R^2$, let the fluid be incompressible and inviscid. The two-dimensional flow is generated by a straight, circular vortex tube with radius a moving with velocity v_0 normal to the vortex tube, hence adding the uniform velocity $-v_0$ leads to steady flow around a stationary cylinder. It is convenient to set up the problem in polar coordinates (r, θ) , with the origin at the centre of the cylinder. The flow outside the cylinder is then irrotational, hence a potential flow determined by the streamfunction

$$\Psi_\infty(r, \theta) = v_0(r - \frac{a^2}{r}) \sin \theta \quad (20.23)$$

generated by a doublet plus parallel flow and valid for $r > a$. The velocity components can be recovered by differentiation

$$v_r(r, \theta) = \frac{1}{r} \frac{\partial \Psi}{\partial \theta}, \quad v_\theta(r, \theta) = -\frac{\partial \Psi}{\partial r} \quad (20.24)$$

valid for Ψ_∞ outside the cylinder and for Ψ inside the cylinder. The flow is rotational for $r < a$, the pde for the streamfunction Ψ follows from the definition of the non-zero vorticity component $\omega = \omega_z$

$$\omega = \frac{1}{r} \frac{\partial}{\partial r} (r v_\theta) - \frac{1}{r} \frac{\partial v_r}{\partial \theta} \quad (20.25)$$

leading to

$$\frac{\partial^2 \Psi}{\partial r^2} + \frac{1}{r} \frac{\partial \Psi}{\partial r} + \frac{1}{r^2} \frac{\partial^2 \Psi}{\partial \theta^2} = -\omega \quad (20.26)$$

The complete specification of the IVP for the subdomain $r < a$ requires the pde for ω and the boundary conditions at $r = a$. The requirement that the velocity components inside and outside the cylinder are continuous leads to the boundary conditions

$$\Psi(a, \theta) = \Psi_\infty(a, \theta), \quad \frac{\partial \Psi}{\partial r}(a, \theta) = \frac{\partial \Psi_\infty}{\partial r}(a, \theta) \quad (20.27)$$

The nonlinear pde for ω is, however, not applied, but the vorticity ω is constructed explicitly as local function of Ψ . Two variants are considered, first the symmetric case

$$\omega(r, \theta) = n^2 \Psi(r, \theta) \quad (20.28)$$

and the asymmetric case

$$\omega(r, \theta) = n^2 (\Psi(r, \theta) - \lambda) \quad (20.29)$$

where λ is an arbitrary non-zero constant. The coefficient n is defined by

$$n \equiv \frac{b}{a} \quad (20.30)$$

where a is the radius of the cylinder and $b = 3.8317$ is determined such that the boundary conditions at $r = a$ are satisfied as shown in the solution for problem (20.2) in Appendix E. $J_1(r)$ denotes the ordinary Bessel function of the first kind.

The symmetric solution of the pde (20.26) for the streamfunction $\Psi(r, \theta)$ can be computed without difficulty, the details can be found as solution of problem 20.2 in Appendix E. The symmetric solution of the streamfunction pde (20.26) with vorticity specified by (20.28) emerges in the form

$$\Psi(r, \theta) = \frac{2v_0 a}{b J_1'(b)} J_1\left(\frac{br}{a}\right) \sin(\theta) \quad (20.31)$$

valid for $0 \leq r \leq a$, $J_1'(r)$ denotes the derivative of the Bessel function $J_1(r)$. The streamlines within the cylinder are plotted in Fig. 20.6 for $a = 1.0$, $v_0 = 1.0$. It is evident in the figure that the cylinder contains a pair of parallel and counterrotating vortices. It can be shown [64] that the induced velocity moves the cylinder in a straight pathline.

The asymmetric solution of the pde (20.26) with vorticity specified by (20.29) can be computed as in the symmetric case, the details can be found as solution of problem 20.3 in Appendix E. The asymmetric solution of the streamfunction pde (20.26) with vorticity specified by (20.29) emerges in the form

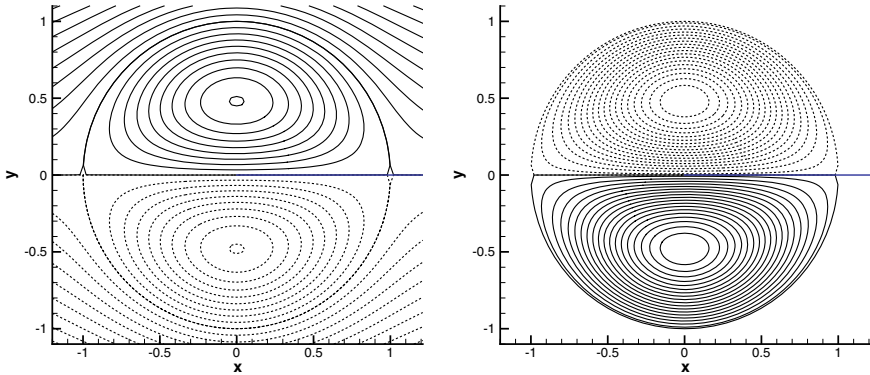


Fig. 20.6 Streamlines (left graph) given by (20.31) inside and (20.23) outside the cylinder and vorticity (right graph) in the cylinder $0 \leq r \leq a$ for $a = 1.0$, $v_0 = 1.0$ for the Chaplygin–Lamb dipole with $\lambda = 0$ (symmetric case), dashed lines indicate negative values

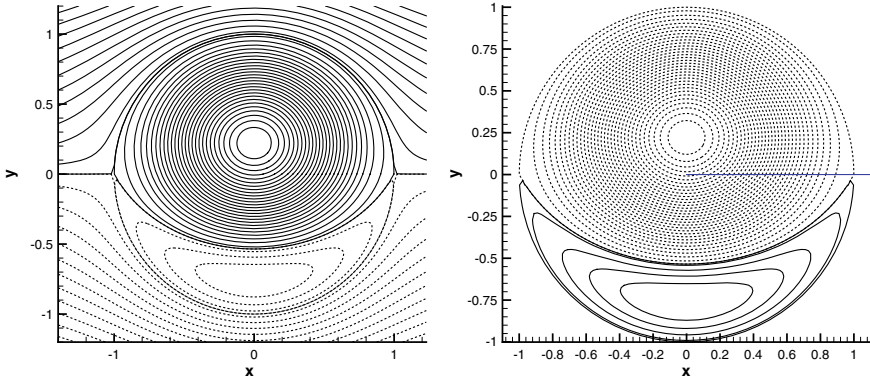


Fig. 20.7 Streamlines (left graph) given by (20.32) inside and (20.23) outside the cylinder and vorticity ω (right graph) in the cylinder $0 \leq r \leq a$ for the Chaplygin–Lamb dipole with $\frac{\lambda}{av_0} = 0.5$ (asymmetric case, the blue line is the positive x -axis through the origin)

$$\Psi(r, \theta) = \frac{2v_0a}{bJ_1'(b)} J_1\left(\frac{br}{a}\right) \sin(\theta) + \lambda \left[1 - \frac{J_0\left(\frac{br}{a}\right)}{J_1'(b)}\right] \quad (20.32)$$

valid for $0 \leq r \leq a$. The streamlines and the vorticity within the cylinder for $a = 1.0$, $v_0 = 1.0$ and $\frac{\lambda}{av_0} = 0.5$ are plotted in Fig. 20.7.

The structure of the dipole solution of the steady-state Euler pdes is similar to a pair of counterrotating vortex tubes. The relevance to turbulent flows depends on its stability properties in inviscid and slightly viscous environments and the possible connection with singularities.

The question of finite-time singularity (FTS) starting from smooth initial conditions for the Euler and Navier–Stokes equations is still unanswered despite

determined analytical and numerical efforts for several decades, Gibbon [65], Kerr [66, 67]. Shelley et al. [68] analysed the dynamics of a pair of straight, counterrotating vortex tubes by numerical means for Reynolds numbers in the range 1000–3500. Disturbances in axial direction destabilizes the tubes leading to vortex reconnection with reconnection time weakly increasing with Reynolds number. However, no temporal regime indicating the development towards FTS was observed. The reason for this is the structure of the initial conditions, which are not solutions of the steady-state Euler pdes and require thus adjustment in a viscous environment.

In contrast, the simulations of Orlandi et al. [25, 69] for the evolution of a pair of colliding dipoles, with Chaplygin–Lamb dipoles as initial condition, show that finite-time singularities may occur for the Euler pdes, but this problem cannot be resolved numerically as infinite resolution would be required. The interaction of vortex dipoles leads to strong distortion of the dipole cores and viscous interaction for finite Reynolds numbers. The interaction of a vortex dipole with a fixed wall simulated numerically by Kramer et al. [70] for the 2-d case shows strong interaction with the wall once the dipole is close enough by detachment and roll-up of the boundary layer and subsequent viscous rebound.

20.5.3 Hill's Vortex as Solution of the Bragg–Hawthorne pde

A steady, axisymmetric solution of the Euler equations for an incompressible fluid, called Hill's vortex, is derived. It is shown in [53], Sect. 5.6, that a single nonlinear pde for the streamfunction $d\Psi(r, z) = rv_z dr - rv_r dz$ in cylindrical coordinates r, θ, z with velocity $\mathbf{v} = (v_r, v_\theta, v_z)$ called Bragg–Hawthorne or Squire–Long pde

$$\frac{\partial^2 \Psi}{\partial z^2} + r \frac{\partial}{\partial r} \left(\frac{1}{r} \frac{\partial \Psi}{\partial r} \right) = r^2 \frac{dH}{d\Psi} - \frac{1}{2} \frac{dC^2}{d\Psi} \quad (20.33)$$

can be established and solutions can be constructed. It is remarkable that analytic solutions exist for this streamfunction pde, which is not based on symmetries eliminating the nonlinear convective terms. The right side in (20.33) contains the possibly nonlinear terms in form of the Bernoulli function $H(\Psi)$ and the circulation $C(\Psi)$. This nonlinear pde was first obtained by Bragg and Hawthorne [71] and found several important applications (see [37, 49, 72]).

The solution called Hill's vortex is obtained by specifying the flow domain as the sphere $\mathcal{D} = \{(r, z) : 0 \leq \sqrt{r^2 + z^2} \leq R\}$ and the boundary condition on $\partial\mathcal{D} = \{(r, z) : \sqrt{r^2 + z^2} = R\}$ as Dirichlet condition $\Psi = 0$. The Bernoulli function H and the circulation C for Hill's vortex are linear functions of the streamfunction Ψ set to

$$H = -A\Psi, \quad C = 0 \quad (20.34)$$

Note that the definitions for H and C amount to specifying the azimuthal vorticity according to

$$\frac{\partial^2 \Psi}{\partial z^2} + r \frac{\partial}{\partial r} \left(\frac{1}{r} \frac{\partial \Psi}{\partial r} \right) = -r \Omega_\theta \quad (20.35)$$

as $\Omega_\theta = r A$, $C = 0$ implies $v_\theta = 0$. The Bragg–Hawthorne pde (20.33) is then given by

$$\frac{\partial^2 \Psi}{\partial z^2} + r \frac{\partial}{\partial r} \left(\frac{1}{r} \frac{\partial \Psi}{\partial r} \right) = -r^2 A \quad (20.36)$$

with the Dirichlet boundary condition

$$\Psi(r, z) = 0, \text{ where } r^2 + z^2 = R^2 \quad (20.37)$$

A class of analytic solutions can be obtained with elementary transformations, but a simple Ansatz suffices for the particular case of Hill's vortex. Observing that the radial symmetry property of the solution is preserved by the left-hand side in (20.36) and that the right-hand side is symmetric, the Ansatz for the solution of the BVP is constructed in even powers with respect to the radial coordinate in the form

$$\Psi(r, z) = A(\alpha r^2 + \beta r^2 z^2 + \gamma r^4) \quad (20.38)$$

Substitution into the pde (20.36) leads to

$$\gamma = -\frac{1}{8}$$

and the boundary conditions produces the relation

$$\alpha + \beta R^2 - r^2(\beta + \frac{1}{8}) = 0$$

which determines α and β by requiring that the coefficients of powers of r are zero

$$\alpha = \frac{1}{8} R^2, \quad \beta = \alpha$$

and the solution emerges then in the form

$$\Psi(r, z) = \frac{1}{8} A r^2 R^2 \left[1 - \frac{(r^2 + z^2)}{R^2} \right] \quad (20.39)$$

valid for $r^2 + z^2 \leq R^2$. The solution outside the sphere can be determined by the requirement $H = C = 0$, hence potential flow. The streamfunction for the flow over a sphere is well known (see White [73], Sect. 8.8, for instance, note that it is in spherical coordinates)

$$\Psi(r, z) = -\frac{1}{2} U_\infty r^2 \left[1 - \left(\frac{R}{\sqrt{r^2 + z^2}} \right)^3 \right] \quad (20.40)$$

Matching the two streamfunctions on $\partial\mathcal{D}$, hence requiring that velocity is continuous across the boundary, determines A in terms of the velocity at infinity, $A = 6U_\infty/R^2$ and the sphere becomes streamsurface with $\Psi = 0$. The streamfunctions in the whole space (in cylindrical coordinates) are thus computed in the form

$$\Psi(r, z) = \begin{cases} \frac{3}{4} U_\infty r^2 \left[1 - \frac{(r^2 + z^2)}{R^2} \right] & \text{for } r^2 + z^2 \leq R^2 \\ -\frac{1}{2} U_\infty r^2 \left[1 - \left(\frac{R}{\sqrt{r^2 + z^2}} \right)^3 \right] & \text{for } r^2 + z^2 > R^2 \end{cases} \quad (20.41)$$

and the solution is complete with

$$v_z = \frac{1}{r} \frac{\partial \Psi}{\partial r} \text{ and } v_r = -\frac{1}{r} \frac{\partial \Psi}{\partial z} \quad (20.42)$$

and $v_\theta = 0$ since $C = 0$ was set at the outset, Eq. (20.34). The resulting streamlines in the meridional plane are shown in the left graph of Fig. 20.8 compared to potential flow inside the sphere (right graph). The potential flow inside the sphere is generated by a doublet plus parallel flow; hence, it is singular at the origin. The Hill vortex solution (20.41) is non-singular and has found applications in droplet/bubble flows. The 3-d streamlines inside the bubble are shown in Fig. 20.9.

It is shown in [53] that higher order explicit solutions can be obtained with the aid of transform techniques for

$$H(\Psi) = H_0 + \lambda\Psi \text{ and } C(\Psi) = \pm\alpha\Psi$$

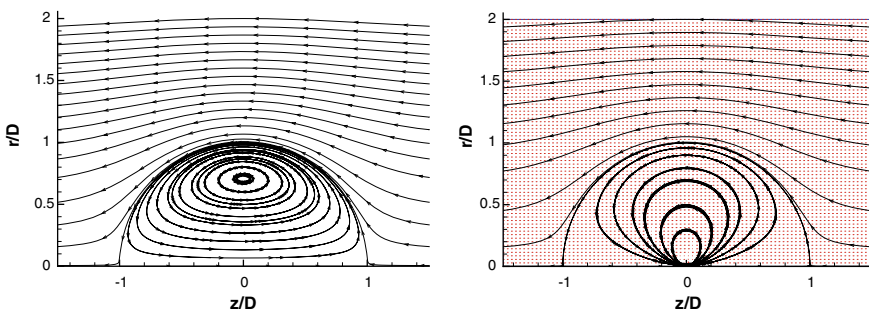


Fig. 20.8 Streamlines for Hill's vortex assuming potential flow outside the sphere \mathcal{D} (Eq. 20.41, left graph) and potential flow everywhere (right graph), the flow is the result of a doublet at the origin plus parallel flow from the right. Note that the flow outside the bubble is the same in both cases

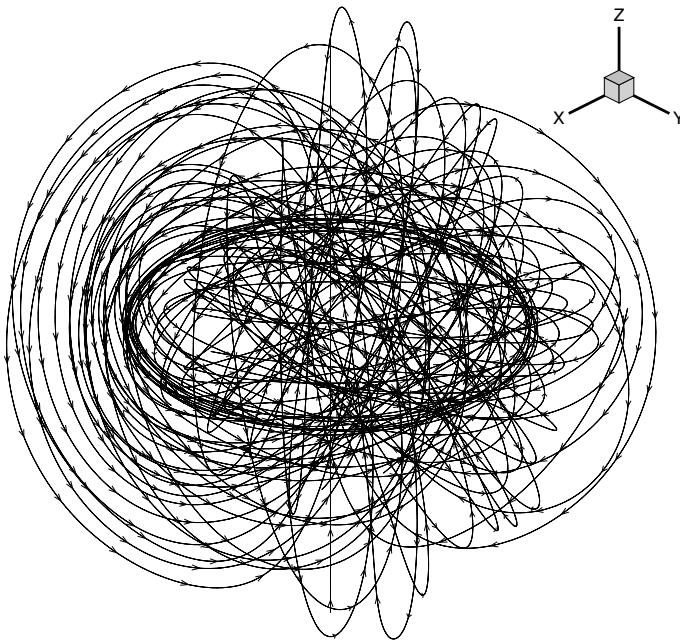


Fig. 20.9 Streamlines inside the Hill's vortex for $\alpha = 10$, $\lambda = 1$, $c = 0.2$. All lines are confined to the sphere with radius $R = 0.449470878$

with λ , α being constants, generating a nonlinear right side in the pde (20.33) for the streamfunction. For $\alpha \neq 0$ circulation in the bubble produces cellular flow that cannot be extended continuously to potential flow outside the bubble, which is close to but not exactly spherical.

20.6 Large-Scale Motion in Jupiter's Atmosphere

Colour enhanced images received on July, 15. 2018. from NASA's Juno spacecraft reveal very interesting structural information on Jupiter's highly turbulent atmosphere. Figures 20.10 and 20.11 show the northern hemisphere of Jupiter from a distance of 6,200–25,300 km. The atmosphere is about $h = 5 \cdot 10^3$ km thick according to the Galileo atmospheric probe, temperature drops in the lowest layer called troposphere (about 50 km thick) from about $T = 420$ K at the pressure $p = 10^7$ Pa to about $T = 140$ K and $p = 10^4$ Pa in the stratosphere. Above the stratosphere at about 320 km and $p = 10^{-1}$ Pa it starts to increase in the thermosphere and exosphere to about $T = 900$ K and $p = 10^{-4}$ Pa at the outer edge of the exosphere. Jupiter does not have a solid surface; hence, the isobaric surface of $p = 1$ bar is



Fig. 20.10 Swirling clouds in the dynamic North Temperate Belt of Jupiter taken by the NASA spacecraft Juno from 7000 km distance on October, 29. 2018. The white blobs are anticyclonic storms. It is noticeable that they contain more small-scale turbulence structures than the surrounding atmosphere

formally defined as surface of Jupiter. The composition of the atmosphere is about 90% H_2 plus roughly 10% Helium and some trace compounds.

The wind speeds in the violent storms were estimated by NASA scientists to be up to about $100 \frac{m}{s}$, a rough estimate for the Reynolds number based on thickness of the atmospheric layer and a typical value for the storm speed is $Re \approx 10^{11}$. The turbulent motion in Jupiter's atmosphere is dominated by three external force fields: planetary rotation, gravity and electromagnetic forces. The observations made possible by NASA's space probes show that the atmosphere has a banded structures with bands parallel to the equator containing violent large-scale motions within them dominated by vorticity called cyclonic and anticyclonic storms and shear regions between the bands. The largest anticyclonic structure is the great red spot in the southern hemisphere not visible in Figs. 20.10 and 20.11. This red spot is a rotating high-pressure storm that has been observed for more than three centuries; hence, its time scale is speculated to be of the order of several centuries.

There is a surprising similarity between the enstrophy in the wake region Fig. 20.2 of the interacting vortex rings at very low Reynolds number (of the order 10^3) and the storms visible as white islands on Jupiter, Fig. 20.11 at enormous Reynolds



Fig. 20.11 Swirling cloudscape in Jupiter's atmosphere taken by the NASA spacecraft Juno from 11,350 km distance on May, 23. 2018

numbers of the order 10^{11} . Regions with high values of enstrophy emerge in both flows as islands with elliptical cross sections indicating large-scale structures.

Comments: The enormous Reynolds number (of the order of 10^{11}) estimated for the planetary turbulence on Jupiter does not lead to homogenization of the turbulent flow as the most recent DNS results for homogeneous turbulence show. The large-scale structures are quite distinct and there are quite a number of them. It could be speculated that the non-random external forces generated by gravity and planetary rotation exert possibly an ordering influence on the turbulent flow field. However, there is not enough information available to prove or disprove the conjecture.

20.7 Problems for this Chapter

Problem 20.1 Determine the pde for helicity density $h(t, \mathbf{x}) \equiv \mathbf{v} \cdot \mathbf{!}$ for the flow of an incompressible Newtonian fluid. Define helicity \mathcal{H} by (15.30) and establish the equation for it.

Problem 20.2 Compute the solution Ψ of the pde (20.26) for the Chaplygin–Lamb dipole streamfunction

$$\frac{\partial^2 \Psi}{\partial r^2} + \frac{1}{r} \frac{\partial \Psi}{\partial r} + \frac{1}{r^2} \frac{\partial^2 \Psi}{\partial \theta^2} = -\omega$$

for $\omega(r, \theta) = n^2 \Psi(r, \theta)$ requiring continuity of velocity across the cylinder surface $r = a$. Plot streamlines and vorticity within the cylinder.

Problem 20.3 Compute the solution Ψ of the pde (20.26) for the Chaplygin–Lamb dipole streamfunction

$$\frac{\partial^2 \Psi}{\partial r^2} + \frac{1}{r} \frac{\partial \Psi}{\partial r} + \frac{1}{r^2} \frac{\partial^2 \Psi}{\partial \theta^2} = -\omega$$

for $\omega(r, \theta) = n^2(\Psi(r, \theta) - \lambda)$, where λ is an arbitrary constant, requiring continuity of velocity across the cylinder surface $r = a$. Plot streamlines and vorticity within the cylinder and the vorticity profiles for several values of λ along the vertical axis $\theta = \frac{\pi}{2}$.

Problem 20.4 Determine the material deformation gradient as measured by deformation gradient and deformation rate (velocity gradient) for the restricted Euler system. The restricted Euler flow is governed by (2.122) introduced in Sect. 2.7.

(4.1) Derive the pde for the deformation gradient $F_{\alpha\beta}$ in mixed formulation using the spatial deformation rate $A_{\alpha\beta}$.

(4.2) Derive the transport pde for the deformation rate $A_{\alpha\beta}$ in the spatial description.

(4.3) Establish the odes for the non-trivial invariants Q (2.114) and R (2.115).

Hint: Use the Cayley–Hamilton theorem

$$A_{\alpha\gamma} A_{\gamma\delta} A_{\delta\beta} + Q A_{\alpha\beta} + R \delta_{\alpha\beta} = 0$$

valid for traceless matrices $A_{\alpha\beta}$.

(4.4) Solve the odes for the invariants Q and R and plot the results in the $R - Q$ phase plane for $-8 \leq R, Q \leq 8$. Show that there appears a cusp singularity (defined as $x^2 - y^3 = 0$ for $x = y = 0$ in standard form) at the origin.

Problem 20.5 One of many Lagrangean line structures in turbulent flows is considered in elementary form. The example, called Shilnikov system, is constructed as simplified velocity field that contains several critical points. The solution of the autonomous Shilnikov system [74, 75] for the Lagrangean position field $\Phi_1(\mathbf{X}, \tau)$, $\Phi_2(\mathbf{X}, \tau)$, $\Phi_3(\mathbf{X}, \tau)$

$$\frac{d\Phi_1}{d\tau} = \Phi_1 \Phi_3 - w \Phi_2$$

$$\frac{d\Phi_2}{d\tau} = w\Phi_1 + \Phi_2\Phi_3$$

$$\frac{d\Phi_3}{d\tau} = P + \Phi_3 - \frac{1}{3}\Phi_3^3 - (\Phi_1^2 + \Phi_2^2)(1 + q\Phi_1 + e\Phi_3)$$

generates such a structure, where $\Phi_\alpha(\mathbf{X}, \tau)$ is the position (Cartesian coordinates) of a material point at time τ , which started at \mathbf{X} at time zero, and $w = 10$, $e = 0.5$, $q = 0.7$ are constants and $P > 0$ is the bifurcation parameter.

(5.1) Compute the critical points $\frac{d\Phi_\alpha}{d\tau} = 0$, $\alpha = 1, 2, 3$ for $P > 0$. Show that the critical points are on the \mathbf{e}_3 -axis and that the location of the critical points depends only on the bifurcation parameter P . Compute the value P_c of P separating the case of three real critical points from a single real critical point and two complex conjugate points.

(5.2) Choose two values for the bifurcation parameter $0 < P < P_c$, $P_c < P < \infty$ and plot the solutions.

Problem 20.6 Townsend's model eddy (19.1) is a localized blob of vorticity defined in $\mathcal{D} = \mathbb{R}^3$ (Davidson [76], Sect. 6.4.1, cylindrical coordinates) by $v_r = v_z = 0$ and

$$v_\theta = \Omega r \exp(-2 \frac{\mathbf{x} \cdot \mathbf{x}}{z_c^2})$$

where $z_c > 0$ denotes the eddy length scale and Ω is a measure for the angular speed. Assume solenoidal external force, $\nabla \cdot \mathbf{G} = \frac{1}{r} \frac{\partial}{\partial r} (r G_r) + \frac{1}{r} \frac{\partial G_\theta}{\partial \theta} + \frac{\partial G_z}{\partial z} = 0$.

(6.1) Compute vorticity in cylindrical coordinates.

(6.2) Split the right-hand side of the pressure pde

$$\Delta p(\mathbf{x}) = 2Q_A$$

where $Q_A \equiv -\frac{1}{2} \nabla \mathbf{v} : \nabla \mathbf{v}$, into $Q_A = Q_S + Q_W$. Strain rate and rotation rate tensors are defined by $\mathbf{s} = \frac{1}{2}(\mathbf{A} + \mathbf{A}^T)$ and $W = \frac{1}{2}(\mathbf{A} - \mathbf{A}^T)$ and $Q_S = -\rho \frac{1}{2} \text{trace}(\mathbf{s}^2)$, $Q_W = -\rho \frac{1}{2} \text{trace}(\mathbf{W}^2)$ [13]. Compute the solution of the Poisson pde for p and separate the contributions of Q_S and Q_W . Plot the radial profiles for the azimuthal velocity and enstrophy, the right hand sides $Q_A(r, 0)$, $Q_S(r, 0)$, $Q_W(r, 0)$ and the associated pressure.

References

1. Moffatt, H.K., Tsinober, A. (eds.): Topological Fluid Mechanics. IUTAM Symposium Cambridge, Cambridge University Press, Proc (1989)
2. Wray, A.A., Hunt, J.C.R.: Algorithms for classification of turbulent structures. In: Proceedings of the IUTAM Symposium, pp. 95–104. Cambridge U.K., Cambridge Univ. Press (1989)

3. Tsinober, A.: An Informal Conceptual Introduction to Turbulence, 2nd edn. Springer, Dordrecht (2009)
4. Marusic, I.: Unraveling turbulence near walls. *JFM* **630**, 1–4 (2009)
5. Adrian, R.J.: Hairpin vortex organization in wall turbulence. *Phys. Fluids* **19**(041301), 1–16 (2007)
6. Adrian, R.J., Marusic, I.: Coherent structures in flow over hydraulic engineering surfaces. *J. Hydraulic Res.* **50**, 451–464 (2012)
7. Dallmann, U.: Topological structures of three-dimensional flow separation. DVLR-AVA Bericht no. 221-82 A 07 (1983)
8. Surana, A., Grunberg, O., Haller, G.: Exact theory of three-dimensional flow separation. Part 1. Steady separation. *JFM* **564**, 57–103 (2006)
9. Chong, M.S., Monty, J.P., Chin, C., Marusic, I.: The topolgy of skin friction and surface vorticity fields in wall-bounded flows. *J. Turbul.* **13**, 1–10 (2012)
10. Ganapathisubramani, B., Hutchins, N., Monty, J.P., Chung, D., Marusic, I.: Amplitude and frequency modulation in wall turbulence. *JFM* **712**, 61–91 (2012)
11. Lawson, J.M., Dawson, J.R.: On velocity gradient dynamics and turbulent structure. *JFM* **780**, 60–98 (2015)
12. Wilczek, M., Meneveau, C.: Pressure Hessian and viscous contributions to velocity gradient statistics based on Gaussian random fields. *JFM* **756**, 191–225 (2014)
13. Vlaykov, D.G., Wilczek, M.: On the small-scale structure of turbulence and its impact on the pressure field. *JFM* **861**, 422–446 (2018)
14. Lozano-Durán, A., Jimenez, J.: Time-resolved evolution of coherent structures in turbulent channels: Characterization of eddies and cascades. *JFM* **759**, 432–471 (2014)
15. Shekar, A., Graham, M.D.: Exact coherent states with hairpin-like vortex structure in channel flow. *JFM* **849**, 76–89 (2018)
16. Yang, Y., Pullin, D.I.: Geometric study of Lagrangian and Eulerian structures in turbulent channel flow. *JFM* **674**, 67–92 (2011)
17. Kollmann, W., Prieto, M.I.: DNS of the collision of co-axial vortex rings. *Comput. Fluids* **73**, 47–64 (2013)
18. Leung, T., Swaminathan, N., Davidson, P.A.: Geometry and interaction of structures in homogeneous isotropic turbulence. *JFM* **710**, 453–481 (2012)
19. Sahni, V., Sathyaprakash, B., Shandarin, S.F.: Shapefinders: s new shape diagnostic for large-scale structures. *Astrophys. J.* **495**, L1–L4 (1998)
20. Griffiths, R.A.C., Chen, J.H., Kolla, H., Cant, R.S., Kollmann, W.: Three-dimensional topology of turbulent premixed flame interaction. *Proc. Combust. Inst.* **35**, 1341–1348 (2015)
21. Fulton, W.: Algebraic Topology. Springer, New York (1995)
22. Hussain, F., Duraisamy, K.: Mechanics of viscous vortex reconnection. *Phys. Fluids* **23**, 021701 (4) (2011)
23. Ni, Q., Hussain, F., Wang, J., Chen, S.: Analysis of Reynolds number scaling for viscous vortex reconnection. *Phys. Fluids* **24**, 105102 (12) (2012)
24. van Rees, W.M., Hussain, F., Koumoutsakos, P.: Vortex tube reconnection at $Re=10^4$. *Phys. Fluids* **24**, 075105 (2012)
25. Orlandi, P., Carnevale, G.F.: Nonlinear amplification of vorticity in inviscid interaction of orthogonal Lamb dipoles. *Phys. Fluids* **19**, 057106 (2007)
26. Bogachev, V.I.: Measure Theory, vol. 1. Springer, New York (2006)
27. Federer, H.: Geometric Measure Theory. Springer, Berlin (1969)
28. Pesin, Y.B.: Dimension Theory in Dynamical Systems, p. 60637. The University of Chicago Press, Chicago (1997)
29. Barenghi, C.F., Ricca, R.L., Samuels, D.C.: How tangled is a tangle ? *Physica D* **157**, 197–206 (2001)
30. Hasselblatt, B., Katok, A.: A First Course in Dynamics: With a Panaorama of Recent Developments. Cambridge University Press (2003)
31. Kusnetsov, Y.A.: Elements of Applied Bifurcation Theory. Springer, New York (2004)

32. Wiggins, S.: *Introduction to Applied Nonlinear Dynamical Systems and Chaos*. Springer, New York (2003)
33. Wu, J.-Z., Tramel, R.W., Zhu, F.L., Yin, X.Y.: A vorticity dynamics theory of three-dimensional flow separation. *Phys. Fluids* **12**, 1932–1954 (2000)
34. Serra, M., Haller, G.: Objective Eulerian coherent structures. *Chaos* **26**, 053110 (2016)
35. Candel, S.M., Poinsot, T.J.: Flame stretch and the balance equation for the flame area. *Combust. Sci. and Tech.* **70**, 1–15 (1990)
36. Girimaji, S.S., Pope, S.B.: Propagating surfaces in isotropic turbulence. *JFM* **234**, 247–277 (1992)
37. Wu, J.-Z., Ma, H.-Y., Zhou, M.-D.: *Vorticity and Vortex Dynamics*. Springer, Berlin (2006)
38. Federer, H.: Curvature measures. *Trans. Am. Math. Soc.* **93**, 418–491 (1959)
39. Maz'ja, V.G.: *Sobolev Spaces*. Springer, Berlin (1985)
40. Kollmann, W., Chen, J.H.: Dynamics of the flame surface area in turbulent non-premixed combustion. Twenty-fifth Symposium (Int.) on Combustion, The Combustion Institute, pp. 1091–1098 (1994)
41. Farazmand, M., Haller, G.: Computing Lagrangian coherent structures from their variational theory. *Chaos* **22**, 013128 (2012)
42. Wiggins, S.: Coherent structures and chaotic advection in three dimensions. *JFM* **654**, 1–4 (2010)
43. Waleffe, F.: Exact coherent structures in channel flow. *JFM* **435**, 93–102 (2001)
44. Chini, G.P.: Exact coherent structures at extreme Reynolds number. *JFM* **794**, 1–4 (2016)
45. Melander, M.V., Hussain, F.: Polarized vorticity dynamics on a vortex column. *Phys. Fluids A* **5**, 1992–2003 (1993)
46. Glezer, A., Coles, D.: An experimental study of a turbulent vortex ring. *JFM* **211**, 243 (1990)
47. Bergdorf, M., Koumoutsakos, P., Leonard, A.: Direct numerical simulation of vortex rings at $Re_\gamma = 7500$. *JFM* **581**, 495–505 (2007)
48. Borisov, V.I.: *Hamiltonian Dynamics, Vortex Structures, Turbulence*, vol. 6. Springer, Dordrecht, IUTAM book series (2008)
49. Saffman, P.G.: *Vortex Dynamics*. Cambridge University Press, Cambridge, U.K. (1992)
50. Archer, P.J., Thomas, T.G., Coleman, G.N.: Direct numerical simulation of vortex ring evolution from the laminar to the early turbulent regime. *JFM* **598**, 201–226 (2008)
51. Fukumoto, Y., Moffatt, H.K.: Motion and expansion of a viscous vortex ring: elliptical slowing down and diffusive expansion. In: Hunt, J.C.R., Vassilicos, J.C. (eds.) *Turbulence Structure and Vortex Dynamics*. Cambridge Univ. Press (2000)
52. Kollmann, W.: Simulation of vorticity dominated flows using a hybrid approach: i formulation. *Comput. Fluids* **36**, 1638–1647 (2007)
53. Kollmann, W.: *Fluid Mechanics in Spatial and Material Description*. University Readers, San Diego (2011)
54. Maxworthy, T.: The Structure and Stability of Vortex Rings. *JFM* **51**, 15–32 (1972)
55. Dziedzic, M., Leutheusser, H.J.: An experimental study of viscous vortex rings. *Exp. Fluids* **21**, 315–324 (1996)
56. Leonard, A.: On the motion of thin vortex tubes. *Comput. Fluid Dyn, Theor* (2009). in press
57. Dazin, A., Dupont, P., Stanislas, M.: Experimental characterisation of the instability of the vortex ring. Part I: Linear phase. *Exp. Fluids* **40**, 383–399 (2006)
58. Dazin, A., Dupont, P., Stanislas, M.: Experimental characterisation of the instability of the vortex ring. Part II: Non-linear phase. *Exp. Fluids* **41**, 401–419 (2006)
59. Leweke, T., Williamson, C.H.K.: Three-dimensional Instabilities of a Counterrotating Vortex Pair. In: Maurel, A., Petitjeans, P. (eds.) *LNP*, vol. 555, pp. 221–230. Springer (2000)
60. Faddy, J.M., Pullin, D.I.: Evolution of vortex structures in a model of the turbulent trailing vortex. In: Kida, S. (ed.) *IUTAM Symposium on Elementary Vortices and Coherent Structures*, pp. 259–264. Springer (2006)
61. Lim, T.T., Nickels, T.B.: *Vortex Rings. Fluid Vortices*, pp. 95–153. Kluwer Academic (1995)
62. Nickels, T.B.: *Turbulent Coflowing Jets and Vortex Ring Collisions*. University of Melbourne, Australia (1993). PhD thesis

63. Lamb, H.: *Hydrodynamics*. 3rd ed., Cambridge University Press (1906)
64. Meleshko, V.V., van Heijst, G.J.F.: On Chaplygin's investigations of two-dimensional vortex structures in an inviscid fluid. *JFM* **272**, 157–182 (1994)
65. Gibbon, J.D.: The three-dimensional Euler equations: where do we stand? *Physica D* **237**, 1894–1904 (2008)
66. Kerr, R.M.: The role of singularities in turbulence. In: Kida, S. (ed.) *Unstable and Turbulent Motion in Fluids*, World Scientific Publishing, Singapore
67. Kerr, R.M.: A new role for vorticity and singular dynamics in turbulence. In: Debnath, L. (ed.) *Nonlinear Instability Analysis*, vol. II, pp. 15–68. WIT Press, Southampton U.K. (2001)
68. Shelley, M.J., Meiron, D.I., Orszag, S.A.: Dynamical aspects of vortex reconnection in perturbed anti-parallel vortex tubes. *JFM* **246**, 613–652 (1993)
69. Orlandi, P., Pirozzoli, S., Carnevale, G.F.: Vortex events in Euler and Navier-Stokes simulations with smooth initial conditions. *JFM* **690**, 288–320 (2012)
70. Kramer, W., Clercx, H.J.H., van Heijst, G.J.F.: Vorticity dynamics of a dipole colliding with a no-slip wall. *Phys. Fluids* **19**, 126603 (2007)
71. Bragg, S.L., Hawthorne, W.R.: Some exact solutions of the flow through annular cascade discs. *J. Aero. Sci.* **17**, 243–249 (1950)
72. Derzhko, O., Grimshaw, R.: Solitary waves with recirculation zones in axisymmetric rotating flows. *J. Fluid Mech.* **464**, 217–250 (2002)
73. White, F.M.: *Fluid Mechanics*. McGraw Hill, 6th edn (2008)
74. Mullin, T., Juel, A., Peacock, T.: Sil'nikov chaos in fluid flows. In: Vassilicos, J.C., Hunt, J.C.R., Vassilicos, J.C. (eds.) *Intermittency in Turbulent Flows*, Cambridge University Press, Cambridge University Press (2001)
75. Shilnikov, L.P., Shilnikov, A.L., Turaev, D.V., Chua, L.O.: *Methods of qualitative theory in nonlinear dynamics*. vol. I, World Scientific, London (1998)
76. Davidson, P.A.: *Turbulence*. Oxford University Press, Oxford, U.K. (2004)

Chapter 21

Wall-Bounded Turbulent Flows



The statistical and structural properties of turbulence near fixed wall boundaries have been and still are the subject of intensive experimental and computational research efforts. The reviews of Marusic [1], Jimenez [2, 3], Wu and Moin [4] (DNS of smooth pipes), Chan et al. [5] (DNS of rough pipes) provide a detailed picture of the current state of knowledge. These research papers and reviews provide the information to identify the central aspects of theoretical, numerical and experimental research on wall-bounded, turbulent flows:

(i) Statistical properties of turbulent flow next to fixed wall boundaries. This includes statistical moments, two-point correlations and scale relations and internal intermittency (Sect. 16.2). The dependence of the friction factor on Reynolds number and the roughness parameter is central to theory and applications.

(ii) The structures dominating the turbulent flow next to fixed wall boundaries. This includes geometric and topological properties, definition of coherence, criteria for the recognition of coherent structures (see Sect. 20.5 for definition). Smits [6] presents evidence for four main types of organized structures in wall-bounded turbulent flows:

- (ii.1) Near-wall streaks;
- (ii.2) Horseshoe/Hairpin vortical structures;
- (ii.3) Large-scale motions (LSM);
- (ii.4) Very Large-scale motions or superstructures (VLSM).

(iii) The asymptotic state of turbulent flow in pipes, its existence and uniqueness. The fact that pipe flow is linearly stable for all Reynolds numbers raises the question of ergodicity of turbulent pipe flow.

(iv) The limit of infinite Reynolds number of turbulent flow in pipes. This includes the existence and regularity of an asymptotic state for this limit, the existence of a smooth wall boundary and the effects of wall roughness and the relation of Navier–Stokes solutions to solutions of the Euler equations.

The limit of the expectation of dissipation rate as $Re \rightarrow \infty$ should be well defined and positive according to the Kolmogorov–Onsager hypotheses, but there is no proof for this. Wall-bounded flows are constrained by the no-slip condition, and hence local Reynolds numbers formed with local turbulence parameters approach zero as the boundary is approached.

The present section is organized as follows. First, a brief introduction to statistical methods relevant to (i) is provided for the analysis of wall-bounded turbulent flows, an example for the engineering treatment of such flows is given in Appendix E, Chap. 27. Then turbulent flows through pipes as an example for wall-bounded flows with fundamental and practical importance are treated in detail and some DNS results are briefly discussed.

21.1 Statistical Description of Turbulent Flows

The property (TF.1), that turbulent flows are apparently random, indicates that statistical methods are applicable to their description. It is assumed that the turbulence measure exists, but very little is known about its structure. Furthermore, it is tacitly assumed that turbulence is ergodic, i.e. the phase space Ω does not consist of disjoint subsets, and hence time averages in the material description equal ensemble averages. Note that time averaging in the spatial description corresponds to time averaging in the material description over sets of labels (initial locations \mathbf{X}), i.e. material points that pass through the observer position \mathbf{x} at some later time, thus hiding a possible lack of ergodicity. Shebalin [7] shows that for ideal (inviscid) homogeneous turbulence helical (15.30) invariance allows the formation of disjoint subsets of phase space, hence non-ergodic properties. The discovery of quasi-Keplerian flows in astrophysics [8] and DNS of particular rotating flows [9] indicate the existence of flows stable at high Reynolds numbers initiated by finite disturbances, see also Tsinober [10] for a discussion of ergodicity in Eulerian and Lagrangean descriptions and experimental results. Ergodicity is an open question at the current level of knowledge.

Accepting the assumption of ergodicity for finite Reynolds numbers, statistical methods instead of probabilistic methods are applicable to the description of turbulent flows. Ensemble averaging is introduced formally by applying angular brackets defined by

$$\langle \Phi \rangle(\mathbf{x}, t) \equiv \lim_{N \rightarrow \infty} \frac{1}{N} \sum_{i=1}^N \Phi^{(i)}(\mathbf{x}, t) \quad (21.1)$$

where the superscript i denotes the sample number to the variables used for the description of the flows (density, velocity, pressure, etc.). The angular brackets are regarded as an operator acting on the argument contained between them. It can be shown without difficulty that the angular brackets commute with linear operations (addition, subtraction, differentiation, integration, etc.) and that non-random factors can be moved in and out of the brackets, but they do not commute with nonlinear operations (multiplication, division, etc.). In particular, it follows that (unfortunately)

$$\langle \Phi_\alpha \Phi_\beta \rangle \neq \langle \Phi_\alpha \rangle \langle \Phi_\beta \rangle \quad (21.2)$$

holds as genuine inequality. Reynolds suggested to split a random variable Φ into mean value $\langle \Phi \rangle$ and fluctuation Φ' according to

$$\Phi = \langle \Phi \rangle + \Phi' \quad (21.3)$$

Application of the angular brackets to this split leads to the elementary and useful results

$$\langle \langle \Phi \rangle \rangle = \langle \Phi \rangle, \quad \langle \Phi' \rangle = 0 \quad (21.4)$$

In particular, velocity and pressure are split

$$v_\alpha = \langle v_\alpha \rangle + v'_\alpha, \quad p = \langle p \rangle + p' \quad (21.5)$$

It is now possible to evaluate the expectation (i.e. application of the angular brackets) of a product: Split the variables

$$\langle \Phi_\alpha \Phi_\beta \rangle = \langle \langle \langle \Phi_\alpha \rangle + \Phi'_\alpha \rangle \langle \Phi_\beta \rangle + \Phi'_\beta \rangle \rangle$$

and use the fact that the brackets commute with linear operations

$$\langle \Phi_\alpha \Phi_\beta \rangle = \langle \langle \Phi_\alpha \rangle \langle \Phi_\beta \rangle \rangle + \langle \langle \Phi_\alpha \rangle \Phi'_\beta \rangle + \langle \Phi'_\alpha \langle \Phi_\beta \rangle \rangle + \langle \Phi'_\alpha \Phi'_\beta \rangle$$

Non-random factors can be moved out of the brackets showing that the second and third terms are zero. Hence, the relation

$$\langle \Phi_\alpha \Phi_\beta \rangle = \langle \Phi_\alpha \rangle \langle \Phi_\beta \rangle + \langle \Phi'_\alpha \Phi'_\beta \rangle \quad (21.6)$$

is obtained quantifying the inequality (21.2). The random variables Φ_α and Φ_β (for $\alpha \neq \beta$) satisfying

$$\langle \Phi'_\alpha \Phi'_\beta \rangle = 0 \quad (21.7)$$

are called uncorrelated. If the stronger condition holds that the variables Φ_α and Φ_β are statistically independent, then it can be shown that they are uncorrelated, but uncorrelated does not imply statistical independence unless the variables are jointly Gaussian.

The centred moments $\langle \varphi'_\alpha \varphi'_\beta \rangle$ are called correlations (if the fluctuations are vectors, as the notation suggests, they form the correlation tensor) and the diagonal ($\alpha = \beta$) elements are the variances and the off-diagonal ($\alpha \neq \beta$) elements are the covariances.

21.1.1 Moment Equations Derived from the Navier–Stokes pdes

The moments of order one and two are of particular interest to the prediction of turbulence in engineering problems. Hence, the equations for moments of order one and two will be derived by applying algebraic operations and the averaging operator to the Navier–Stokes equations for incompressible fluids. Mass balance is given by (2.6)

$$\frac{\partial v_\alpha}{\partial x_\alpha} = 0$$

and momentum balance by (2.7)

$$\frac{\partial v_\alpha}{\partial t} + v_\beta \frac{\partial v_\alpha}{\partial x_\beta} = -\frac{\partial p}{\partial x_\alpha} + \frac{1}{Re} \frac{\partial^2 v_\alpha}{\partial x_\beta \partial x_\beta} + \frac{1}{Fr} g_\alpha$$

where it was assumed that characteristic values for length L and velocity U exist defining the Reynolds number (2.8)

$$Re = \frac{UL}{\nu} \gg 1$$

and its value is sufficiently large to produce turbulent flow, and Fr denotes the Froude number defined by (22.2). The external volume force per unit mass g_α is assumed non-random, i.e. $g_\alpha = \langle g_\alpha \rangle$. Splitting the velocity in mass balance produces

$$\frac{\partial \langle v_\alpha \rangle}{\partial x_\alpha} + \frac{\partial v'_\alpha}{\partial x_\alpha} = 0$$

and averaging leads to

$$\frac{\partial \langle v_\alpha \rangle}{\partial x_\alpha} = 0 \quad (21.8)$$

since the angular brackets commute with the linear operations addition and differentiation. Subtraction of averaged and original form of mass balance shows that the fluctuations satisfy mass balance as well

$$\frac{\partial v'_\alpha}{\partial x_\alpha} = 0 \quad (21.9)$$

which is again a consequence of the linearity of the mass balance.

Splitting of the dependent variables and averaging the momentum balance lead to

$$\frac{\partial \langle v_\alpha \rangle}{\partial t} + \langle v_\beta \frac{\partial v_\alpha}{\partial x_\beta} \rangle = -\frac{\partial \langle p \rangle}{\partial x_\alpha} + \frac{1}{Re} \Delta \langle v_\alpha \rangle + \frac{1}{Fr} g_\alpha \quad (21.10)$$

The nonlinear convection term can be modified using mass balance

$$\langle v_\beta \frac{\partial v_\alpha}{\partial x_\beta} \rangle = \frac{\partial}{\partial x_\beta} \langle v_\alpha v_\beta \rangle \quad (21.11)$$

and it follows that for incompressible fluids it suffices to consider $\langle v_\alpha v_\beta \rangle$ only. The general rules for averaging lead to

$$\langle v_\alpha v_\beta \rangle = \langle v_\alpha \rangle \langle v_\beta \rangle + \langle v'_\alpha v'_\beta \rangle \quad (21.12)$$

and the averaged momentum equations appear as

$$\frac{\partial \langle v_\alpha \rangle}{\partial t} + \langle v_\beta \rangle \frac{\partial \langle v_\alpha \rangle}{\partial x_\beta} = -\frac{\partial \langle p \rangle}{\partial x_\alpha} - \frac{\partial}{\partial x_\beta} \langle v'_\alpha v'_\beta \rangle + \frac{1}{Re} \Delta \langle v_\alpha \rangle + \frac{1}{Fr} g_\alpha \quad (21.13)$$

Comparison of the averaged momentum balance to the original or instantaneous momentum balance shows that a new term appears, namely, $\langle v'_\alpha v'_\beta \rangle$. Its origin is obviously the nonlinear convective term in the instantaneous balance. Defining

$$\tau_{\alpha\beta}^t \equiv -\rho \langle v'_\alpha v'_\beta \rangle \quad (21.14)$$

it is clear that $\tau_{\alpha\beta}^t$ has the dimension of a stress and it is called Reynolds stress tensor. It is a symmetric positive definite tensor of rank two. The most important fact concerning the averaged Navier–Stokes system is the appearance of the new unknowns called Reynolds stress tensor. We recall that the instantaneous Navier–Stokes system is closed (determinate), i.e. the number of pdes is equal to the number of unknowns. This is no longer true for the averaged system: The number of equations is still four, whereas the number of unknowns is now ten (mean pressure, three mean velocity components plus the six Reynolds stress components). The averaged system is, therefore, termed non-closed or underdeterminate and additional equations must be found or constructed to close the system of moment equations. For this purpose, we need to establish the equations for the fluctuating momentum. Subtraction of (21.13) from the momentum balance (2.7) leads to

$$\frac{\partial v'_\alpha}{\partial t} + v'_\beta \frac{\partial v'_\alpha}{\partial x_\beta} + \langle v_\beta \rangle \frac{\partial v'_\alpha}{\partial x_\beta} + v'_\beta \frac{\partial \langle v_\alpha \rangle}{\partial x_\beta} - \frac{\partial}{\partial x_\beta} \langle v'_\alpha v'_\beta \rangle = -\frac{\partial p'}{\partial x_\alpha} + \frac{1}{Re} \frac{\partial^2 v'_\alpha}{\partial x_\beta \partial x_\beta} \quad (21.15)$$

Multiplication with the fluctuating velocity component v'_γ and adding the equation for v'_γ multiplied with v'_α and averaging generate the transport equation for the Reynolds stress tensor

$$\begin{aligned} \frac{\partial}{\partial t} \langle v'_\alpha v'_\gamma \rangle + \langle v'_\beta \rangle \frac{\partial}{\partial x_\beta} \langle v'_\alpha v'_\gamma \rangle &= -\langle v'_\alpha v'_\beta \rangle \frac{\partial \langle v_\gamma \rangle}{\partial x_\beta} - \langle v'_\beta v'_\gamma \rangle \frac{\partial \langle v_\alpha \rangle}{\partial x_\beta} + \langle p' \left(\frac{\partial v'_\alpha}{\partial x_\gamma} + \frac{\partial v'_\gamma}{\partial x_\alpha} \right) \rangle \\ &+ \frac{\partial}{\partial x_\beta} \left(\frac{1}{Re} \frac{\partial}{\partial x_\beta} \langle v'_\alpha v'_\gamma \rangle - \langle v'_\alpha v'_\beta v'_\gamma \rangle - \delta_{\beta\gamma} \langle p' v'_\alpha \rangle - \delta_{\alpha\beta} \langle p' v'_\gamma \rangle \right) - \frac{1}{Re} \langle \frac{\partial v'_\alpha}{\partial x_\beta} \frac{\partial v'_\gamma}{\partial x_\beta} \rangle \end{aligned} \quad (21.16)$$

The transport equation for the Reynolds stress tensor contains now a number of new unknown terms. The total diffusive flux is defined by

$$\mathcal{F}_{\alpha\gamma\beta} \equiv \frac{1}{Re} \frac{\partial}{\partial x_\beta} \langle v'_\alpha v'_\gamma \rangle - \langle v'_\alpha v'_\beta v'_\gamma \rangle - \delta_{\beta\gamma} \langle p' v'_\alpha \rangle - \delta_{\alpha\beta} \langle p' v'_\gamma \rangle \quad (21.17)$$

it contains two types of additional unknown correlations, namely, the triple correlations of velocity components and the velocity–pressure correlations. The correlation of the fluctuating pressure with the fluctuating rate of strain components constitutes another set of six new unknowns

$$\Phi_{\alpha\beta} \equiv \langle p' \left(\frac{\partial v'_\alpha}{\partial x_\beta} + \frac{\partial v'_\beta}{\partial x_\alpha} \right) \rangle \quad (21.18)$$

which is a symmetric tensor of rank two. The construction of a Green's function for the BVP of the pressure pde (9.19) (Appendix D) allows to express the fluctuating pressure as functional of the fluctuating velocity as shown in the next section. Thus, the pressure correlations are determined by two-point correlations of velocity as explicitly shown below for pipe flow.

Finally, the six components of the symmetric dissipation rate tensor

$$\epsilon_{\alpha\beta} \equiv \frac{1}{Re} \langle \frac{\partial v'_\alpha}{\partial x_\gamma} \frac{\partial v'_\beta}{\partial x_\gamma} \rangle \quad (21.19)$$

are also new unknowns. Their variation near fixed wall boundaries is decisive for the computation of wall-bounded shear flows, Pope [11], Durbin and Petterson Reif [12]. It is shown in the next section that the moment equations of order one and two have integro-differential character for incompressible fluids.

21.1.2 Moment Equations Derived from the Leray Version of the Navier–Stokes pdes

The equations for the second order, one point velocity variances $\langle v_r^2(\mathbf{x}) \rangle$, covariances $\langle v_r(\mathbf{x}) v_\theta(\mathbf{x}) \rangle$, etc. in cylindrical coordinates are considered strictly in velocity form with pressure eliminated with the aid of a formal solution of the Poisson pde for the pressure. The equations are given for the example of turbulent flow through a pipe

using the Green's function developed in detail in Chap. 26 instead of the general approach employing the abstract Leray–Stokes operator (Sect. 23.10). The moment equations follow from the Leray version of the momentum balances using standard manipulations as in Sect. 21.1.1. The radial momentum balance leads to

$$\begin{aligned} \frac{\partial \langle v_r^2 \rangle}{\partial t}(\mathbf{x}) + \langle v_r T_r \rangle - \frac{1}{Re} \langle v_r F_r \rangle = \\ -\langle v_r(\mathbf{x}) \frac{\partial}{\partial r} \mathcal{P}_h(r, \theta, \zeta | \frac{1}{Re} \frac{\partial^2 v_r}{\partial r'^2}(\mathbf{y} \in \partial\mathcal{D})) \rangle - \langle v_r(\mathbf{x}) \frac{\partial}{\partial r} \mathcal{P}_G(r, \theta, \zeta | R(\mathbf{y}), \mathbf{y} \in \mathcal{D}) \rangle \end{aligned} \quad (21.20)$$

and the azimuthal balance to

$$\begin{aligned} \frac{\partial \langle v_r v_\theta \rangle}{\partial t}(\mathbf{x}) + \langle v_r T_\theta \rangle - \frac{1}{Re} \langle v_r F_\theta \rangle = \\ -\langle v_r(\mathbf{x}) \frac{1}{r} \frac{\partial}{\partial \theta} \mathcal{P}_h(r, \theta, \zeta | \frac{1}{Re} \frac{\partial^2 v_r}{\partial r'^2}(\mathbf{y} \in \partial\mathcal{D})) \rangle - \langle v_r(\mathbf{x}) \frac{1}{r} \frac{\partial}{\partial \theta} \mathcal{P}_G(r, \theta, \zeta | R(\mathbf{y}), \mathbf{y} \in \mathcal{D}) \rangle \end{aligned} \quad (21.21)$$

and the axial balance to

$$\begin{aligned} \frac{\partial \langle v_r v_z \rangle}{\partial t}(\mathbf{x}) + \langle v_r T_z \rangle - \frac{1}{Re} \langle v_r F_z \rangle = -\langle v_r(\mathbf{x}) \frac{\partial P_0}{\partial z} \rangle \\ -\langle v_r(\mathbf{x}) \frac{\partial}{\partial z} \mathcal{P}_h(r, \theta, \zeta | \frac{1}{Re} \frac{\partial^2 v_r}{\partial r'^2}(\mathbf{y} \in \partial\mathcal{D})) \rangle - \langle v_r(\mathbf{x}) \frac{\partial}{\partial z} \mathcal{P}_G(r, \theta, \zeta | R(\mathbf{y}), \mathbf{y} \in \mathcal{D}) \rangle \end{aligned} \quad (21.22)$$

where $\mathbf{y} = (r', \theta', z') \in \mathcal{D}$. Similar equations can be derived without difficulty for other components of the Reynolds stress tensor. The expectations of convective and viscous terms are the same as in Eq. (21.16) for the Reynolds stress tensor. The interesting parts are correlations of a velocity component with the (disturbance) pressure gradient term (26.76), which is a surface integral, and (26.128), which is a volume integral, derived in Chap. 26 of Appendix D. The second-order moments $\langle v_r(\mathbf{x}) p_h[\mathbf{v}] \rangle$ and $\langle v_r(\mathbf{x}) p_G[\mathbf{v}] \rangle$ of the radial velocity component at \mathbf{x} with the harmonic part of the disturbance pressure and the Green's function part contain two-point correlations. They can be expressed as functionals of the velocity field

$$\begin{aligned} \langle v_r(\mathbf{x}) \mathcal{P}_h(r, \theta, \zeta | \frac{1}{Re} \frac{\partial^2 v_r}{\partial r'^2}(\mathbf{y} \in \partial\mathcal{D})) \rangle = \sum_{k=-\infty}^{\infty} \frac{r^k}{k} \mathcal{F}(k, 0 | \frac{1}{Re} \frac{\partial^2}{\partial r'^2} \langle v_r(\mathbf{x}) v_r(\mathbf{y} \in \partial\mathcal{D}) \rangle \exp(ik\theta)) \\ + \sum_{k=-\infty}^{\infty} \sum_{m=-\infty}^{\infty} \frac{2I_k(\beta r)}{\beta[I_{k-1}(\beta) + I_{k+1}(\beta)]} \mathcal{F}(k, m | \frac{1}{Re} \frac{\partial^2}{\partial r'^2} \langle v_r(\mathbf{x}) v_r(\mathbf{y} \in \partial\mathcal{D}) \rangle \exp[i(k\theta + m\zeta)]) \end{aligned}$$

the prime on the sums indicates that singular terms with $k = 0$ or $m = 0/\beta = 0$ in the denominator must be omitted, I_k , K_k denote modified Bessel function of first and second kind, and

$$\langle v_r(\mathbf{x}) \mathcal{P}_G(r, \theta, \zeta | R(\mathbf{y}), \mathbf{y} \in \mathcal{D}) \rangle = \mathcal{F}^{-1}(\theta, \zeta) \int_0^1 d\rho \rho \mathcal{F}(k, m | \langle v_r(\mathbf{x}) R(\mathbf{y} \in \mathcal{D}) \rangle G_{k,m}(\rho, r))$$

since Fourier transform and its inverse are linear operators. The expression $R(r, \theta, z)$ denotes the rhs (26.12) of the Poisson pde for the disturbance pressure $p(r, \theta, z) = p_h(r, \theta, z) + p_G(r, \theta, z)$ with basic pressure $P_0(z)$ being a linear, non-periodic function of z and the gradient a known, periodic constant. The modal 1-d Green's functions $G_{k,m}(\rho, r)$ (26.120) are adapted to the representation of disturbance pressure fields

$$p_G(r, \theta, z, t) = \sum_{k,n,m} \hat{p}^{k,n,m}(t) f_{k,n,m}(r, \theta, z)$$

with scalar modes $f_{k,n,m}(r, \theta, z)$ being elements of a Schauder basis \mathcal{B} spanning the separable Hilbert space for scalar fields p_G . Details can be found in Appendix D.

It was shown in Sect. 26.3 that the Neumann-type boundary conditions for the disturbance pressure is given by (26.17)

$$h(\mathbf{x}) = \frac{1}{Re} \left[\frac{\partial}{\partial r} \left(\frac{1}{r} \frac{\partial}{\partial r} (r v_r) \right) + \frac{1}{r^2} \frac{\partial^2 v_r}{\partial \theta^2} + \frac{\partial^2 v_r}{\partial z^2} - \frac{2}{r^2} \frac{\partial v_\theta}{\partial \theta} \right]$$

which is for the outer (and only) part of the boundary reduced to

$$h(\mathbf{x}) = \frac{1}{Re} \frac{\partial^2 v_r}{\partial r^2}$$

for $\mathbf{x} = (1, \theta, z) \in \partial\mathcal{D}$ due to the no-slip condition and mass balance. The Green's function for the pipe flow domain generates two contributions: a surface integral and a volume integral. It is worth noting that the former is absent in the case of $\mathcal{D} = \mathbb{R}^3$, since the domain does not have a boundary.

Hierarchy of the moment equations

It is clear that any attempt to terminate the system of moment equations for mean velocity and mean pressure by deriving higher moment equations failed as six new balance equations emerged for the Reynolds stress components, but contained 18 new triple velocity correlations, 3 new pressure–velocity correlations, 6 new pressure strain rate and 6 new dissipation rate terms. Hence, 33 additional unknowns appeared and closure becomes an elusive goal. Carrying the moment equations to higher order worsens the situation considerably and the conclusion is reached that there is no finite and closed system of moment equations. The system of moment equations is,

therefore, recognized as being countably infinite. It is called the *Hierarchy of moment equations* or Friedman–Keller system.

This hierarchy raises the fundamental question of solvability. Any method of truncating the infinite system of moment pdes is bound to fail, if the countably infinite system of moment pdes is not solvable. Vishik and Fursikov proved ([13], Chap. VI and next section below), that the system is solvable by showing, that the linear equation for the characteristic functional is solvable, which implies that the sequence of moments is in principle computable as Fréchet/Gateaux derivatives of the characteristic functional at the origin of the test function space \mathcal{N} .

Properties of the moment hierarchy

The solvability of the infinite chain of moment equations was proved by Vishik and Fursikov [13]. This solvability theorem needs some preparation. Denote the multipoint moments of the turbulence measure $\mu(t, \mathbf{v})$, $\mathbf{v} \in \Omega$ by

$$m_k(t, \mathbf{x}^1, \dots, \mathbf{x}^k, \alpha^1, \dots, \alpha^k, n_1, \dots, n_k) = \langle v_{\alpha^1}^{n_1}(\mathbf{x}^1), \dots, v_{\alpha^k}^{n_k}(\mathbf{x}^k) \rangle \equiv \int_{\Omega} d\mu(t, \mathbf{v}) v_{\alpha^1}^{n_1}(\mathbf{x}^1), \dots, v_{\alpha^k}^{n_k}(\mathbf{x}^k), \mathbf{x}^j \in \mathcal{D}, 1 \leq j \leq k \quad (21.23)$$

where $\mathcal{D} \in \mathbb{R}^3$ is the flow domain, Ω is the phase space (5.10) (Sect. 5.2), $(\Omega, \mathcal{A}, \mu)$ is the measure space of turbulence (Sect. 6.2). Note that $\langle \cdot \rangle$ denotes an operator representing the functional integral in (21.23). The Navier–Stokes pdes are written as abstract evolution pdes

$$\frac{d}{dt} \mathbf{v} + \mathbf{A}\mathbf{v} + \mathbf{B}(\mathbf{v}) = \mathbf{g}(t), \quad t \in [0, T], \quad T < \infty \quad (21.24)$$

valid for a finite time interval $[0, T]$, where \mathbf{A} is a self-adjoint positive definite operator and \mathbf{B} a bilinear, bounded operator and the right-hand side vector $\mathbf{g} \in L_{\infty}(0, T; \mathcal{H}^{-1})$, see [13], Chap. IV.1 for the technical details.

Moment solvability theorem, Vishik and Fursikov [13]

Let the initial moments satisfy

$$\int_{\Omega} d\mu(0, \mathbf{v}) \|\mathbf{v}(0, \mathbf{x})\|^k < \infty \quad (21.25)$$

then has the IVP for the infinite chain of moment equations

$$\frac{dm_k}{dt} = R_k, \quad k = 1, \dots, \infty \quad (21.26)$$

a solution satisfying

$$m_k(t) \in L_{\infty}(0, T; \mathcal{H}^0(k)) \cap L_1(0, T; V(2, k)) \quad (21.27)$$

and

$$\frac{dm_k}{dt} \in L_1(0, T; V(1, k)), \text{ for } 1 \leq k \leq \infty \quad (21.28)$$

Furthermore, there exists a spatial turbulence measure $\mu(t)$ satisfying initially the norm condition (21.25) such that the inequalities

$$\sup_{0 \leq t \leq T} \int_{\Omega} d\mu(t, \mathbf{v}) \|\mathbf{v}(t, \mathbf{x})\|^k \leq 2^{\frac{k}{2}} \int_{\Omega} d\mu(0, \mathbf{v}) \left(\|\mathbf{v}(T, \mathbf{x})\|^2 + \int_0^T d\tau \|\mathbf{g}(\tau, \mathbf{x})\|_{-1}^2 \right)^{\frac{k}{2}} \quad (21.29)$$

and

$$\int_0^T d\tau \left(\int_{\Omega} d\mu(\tau, \mathbf{v}) \|\mathbf{v}(\tau)\|_1^2 \|\mathbf{v}(\tau)\|^{k-2} \right) \leq 2^{\frac{k}{2}} \int_{\Omega} d\mu(0, \mathbf{v}) \left(\|\mathbf{v}(T)\|^2 + \int_0^T d\tau \|\mathbf{g}(\tau)\|_{-1}^2 \right)^{\frac{k}{2}} < \infty, \quad k \geq 2 \quad (21.30)$$

hold. The proof can be found in Vishik and Fursikov [13] 1988, Lemma 1.1 and Theorem 2.4 in Chap. VI.

The right-hand side vector R_k becomes increasingly complicated as $k \rightarrow \infty$, see, for instance, the single-point moment equations (21.13), (21.16) for $k = 1, 2$ above. The essential condition for this theorem to hold is that the initial turbulence measure $\mu(0)$ must have finite moments of all orders $0 < k \leq \infty$.

Closure of the moment equations

All the equations in the moment hierarchy are coupled, nonlinear, partial integro-differential equations. The complexity of the moment equations increases rapidly with the order of the moments and inspection of the second-order or Reynolds stress equations (21.16) shows that there is little incentive to go beyond this order. The exact computation of statistical moments seems to be impossible. However, there are two ways out of this difficulty.

(1) Direct approach: Terminate the number of moment pdes at a finite level and partition the unknowns into two groups, the resolved variables, for which the pdes are to be solved, and the additional unknowns termed non-closed variables. Additional information has to be provided (using dimensional analysis, order of magnitude estimates, norm estimates and embedding theorems from functional analysis, experiment, DNS, etc.) to obtain a closed system of equations. This is the domain of turbulence modelling, which has so far failed to acquire a rigorous basis as there is no systematic procedure to improve accuracy and to converge to a proper limit consistent with probability theory (see Chap. 27 for an example of a turbulence model and empirical results for the mean velocity). The minimal requirement for moderate success of closure models is the solvability of the system of moment equations discussed below.

(2) Indirect approach: It is possible to establish a single equation containing all the information contained in the infinite hierarchy of moment equations (due to Hopf, [14]), it can be regarded as a partial differential equation for a complex-valued

function of infinitely many variables, but this equation has functional character and the formulation of proper IBVPs and their solution has proved rather difficult. This particular issue is pursued further in Sect. 10.4 for steady, fully developed turbulent flows.

The functional equation has interesting properties, it is, for instance, linear and contains second Gateaux/Fr'echet (also called variational) derivatives associated with the nonlinear convective and pressure gradient terms appearing in the spatial version of the Navier–Stokes pdes. The statistical moments are the Fréchet–Gateaux derivatives of the characteristic functional at the origin of the argument/test function space \mathcal{N}_p , see Eq. (9.6) in Sect. 9.1. This functional equation and its variants are the subject of Chaps. 9 and 10, the latter section develops a systematic method for the solution of the steady-state pde for finite-dimensional projected characteristic functions θ_N defined by (25.14). It has the potential for a systematic solution of the moment problem. These matters are discussed in greater detail in the sections starting with Chap. 9.

21.2 Pipe Flow

The flow through straight, circular pipes has been the subject of research for more than 100 years, with Osborne Reynolds' famous 1883 investigation of transition and development of turbulence marking the beginning of the modern era. Experimental research for over a century has brought vast improvements in techniques, resolution and accuracy, Smits [15], Smits et al. [6]. In particular, the research of Smits and coworkers on turbulent pipe flow in a closed facility at elevated pressure (the Princeton superpipe, see the review [6] for references up to 2011) contributed enormously to the understanding of turbulence as the Reynolds number is increased. Some conjectures on the friction factor as the Reynolds number go to infinity and the structure of the near-wall turbulence is discussed in Chap. 22. Pipe flow is of fundamental interest for several reasons, specifically

(iii.1) Practical: Pipe flow is an essential part of myriad industrial devices operating at Reynolds numbers in the turbulent regime. The prediction of the friction factor and the mean pressure gradient connected to it is of prime importance as they determine, for instance, the consumption of energy for pumping oil through pipelines.

(iii.2) Numerical: DNS of turbulent pipe flow is an important tool to analyse turbulent flows, but it faces several serious challenges.

First, the choice of a coordinate system for \mathcal{D} , the choice of the description, i.e. the independent variables and the associated definition of the flow domain \mathcal{D} (compact or non-compact, Pileckas [16]) and the boundary conditions. Cylindrical coordinates create singular terms in the Navier–Stokes pdes that lead to pole or parity conditions for numerical methods to insure smoothness near the coordinate axis $r = 0$, see Sect. 25.7 for scalar and Sect. 25.12 in Appendix C for vector fields.

Second, the method of numerical approximations, discretization and treatment of the near-wall regions, [17–20]; time integration, [21].

Third, the solution methods for the resulting set of equations, check the CTR publications, Stanford, for recent developments.

(iii.3), (iv.1) Theoretical: The existence of an asymptotic state in Sect. 3.2, the limit of infinite Reynolds number in Chap. 22, the Kolmogorov–Onsager hypotheses in Sect. 22.2 and the development of singularities of the second kind, defined in theorem (3.15) in Chap. 3, ergodicity in Sect. 23.9, the effects of roughness, the flow structures dominating turbulent transport of mass, momentum and energy requires a definition of coherent, vortical structures, Eq. (21.33) and discussed in Chap. 20.

21.2.1 (iii.2) Numerical Aspects

Several DNS and LES simulations of fully developed turbulent flow through straight pipes have appeared recently, Ahn et al. [22] reporting simulation results for $Re_\tau = 180, 544, 934$, in particular, turbulence statistics, and evidence for the interactions between the near-wall and outer regions., Eggels et al. [23] reported detailed results in terms one- and two-point moments and spectra for a DNS (second-order accurate finite volume method) and compared the simulations with experiments, El Khoury et al. [24] presented accurate simulations using a spectral element solver for Re_τ up 1000, Fukagata and Kasagi [25], developed a highly energy-conservative second-order accurate finite difference method for the cylindrical coordinate system and verified its properties in pipe flow simulations, Wu et al. [4] 2008 reported simulation results for fully developed incompressible turbulent pipe flow at Reynolds number $Re_D = 44000$ and achieved good agreement with the Princeton superpipe experiments, and the simulation of Reynolds' experiment by Wu et al. [26]. All the simulations cited use periodicity in axial direction as the artificial boundary condition. This needs to be justified.

Domain considerations and boundary conditions

The boundary conditions for the periodic pipe flow are the no-slip condition for velocity and non-homogeneous Neumann conditions for the pressure at the pipe wall. The Neumann conditions for the Poisson pde determining the pressure (9.19) follow from the momentum balance in radial direction applied to the wall and the no-slip condition at the wall leading to (9.20) and (9.22). In axial direction, the artificial periodicity condition is imposed assuming that the length of the periodicity interval is much larger than integral length scale. This is more than convenient as the consideration of alternatives shows. The simulation of the whole range of flow character from laminar to transitional to fully turbulent would require a semi-infinite length of the pipe, where the entrance conditions provide the control of the simulation. Let the Reynolds number (2.8) be above the standard (industrial) critical value for turbulent flow $Re \approx 2300$ (Moody chart, White [27], Chap. 6), then would the simulation of the flow starting with laminar plus disturbances at the entrance that require hundreds of pipe diameters in length to resolve the instabilities and the transition to turbulence. The properties of disturbances are essential for pipe flow, since it can be shown that

pipe flow is linearly stable for all Reynolds numbers, [28]. It is clear that in the spatial description, the simulation of pipe flow with realistic entrance and exit conditions faces serious difficulties.

The situation is no better in the material description, where a materially invariant flow domain is fixed initially as a finite part of the pipe with invariant, finite volume. As time progresses, the flow domain moves with the fluid and is stretched as the central part of the material domain is flushed out of any finite and fixed part of the pipe, but part of the domain boundary remains at the wall, i.e. the initial location, and creating a turbulent boundary layer, while thinning out the core part of the domain due to material invariance. Asymptotically, the flow domain approaches an orientable set in R^3 with finite and invariant volume, but infinite area of the bounding surface. The materially invariant domain $\mathcal{D}(\tau)$ becomes non-compact as $\tau \rightarrow \infty$. Hence, it is equally useless for analytical investigation and as flow domain for numerical simulations. The evolution of a simple materially invariant flow domain $\mathcal{D}(\tau)$ is illustrated in Fig. 21.1. The flow is assumed fully developed, laminar (to enable analytic computations) and the velocity is then the Hagen–Poiseuille solution

$$\mathbf{v}(r, \theta, z) = \begin{pmatrix} 0 \\ 0 \\ U_0[1 - (2r)^2] \end{pmatrix} \quad (21.31)$$

The initial flow domain is set as the cylinder $\mathcal{D}(0) = \{(r, \theta, z) : 0 \leq r \leq 0.5, 0 \leq \theta \leq 2\pi, 0 \leq z \leq L\}$, the boundaries $\partial\mathcal{D}_0(\tau) = \{0 \leq r \leq 0.5, z = 0\}$ and $\partial\mathcal{D}_1(\tau) = \{0 \leq r \leq 0.5, z = L\}$ at $\tau = 0$ move with the fluid (material description, as defined in Sect. 2.5). The solution of the pathline odes (2.81) is then

$$\Phi(\tau, \mathbf{X}(p)) = \begin{pmatrix} X_r \\ X_\theta \\ U_0[1 - (2X_r)^2]\tau + X_z(p) \end{pmatrix}$$

($0 \leq X_z(p) = pL \leq L$, $0 \leq p \leq 1$ is a Lagrangean line parameter for the part of the boundary on the pipe wall), where L ($L = 1$ for Fig. 21.1) is the axial extent of the domain and the radial and azimuthal (material) coordinates $\Phi_\alpha(\tau, \mathbf{X}) = X_\alpha$, $\alpha = r, \theta$ are time independent for the Hagen–Poiseuille solution, which implies at once that the domain volume is also invariant. The domain boundaries are shown in Fig. 21.1 for three times $\tau = 0$ (black), $= 2$ (red), $= 20$ (blue). The domain is thinning with time indicating the asymptotic properties that the volume is constant, while the surface area of the boundary grows over all bounds. The bounding surface $\partial\mathcal{D}(\tau)$ for turbulent flow would undergo stretching and distortion. The boundary values for velocity or any other dependent variable would not be known making numerical solution methods inapplicable.

Periodicity in axial direction offers an alternative to this dilemma, but the price that has to be paid is its artificial character. For instance, turbulent puffs in a realistic pipe domain of finite length would be flushed out of the domain after sufficient time, whereas for periodic boundary conditions they would re-enter the domain.

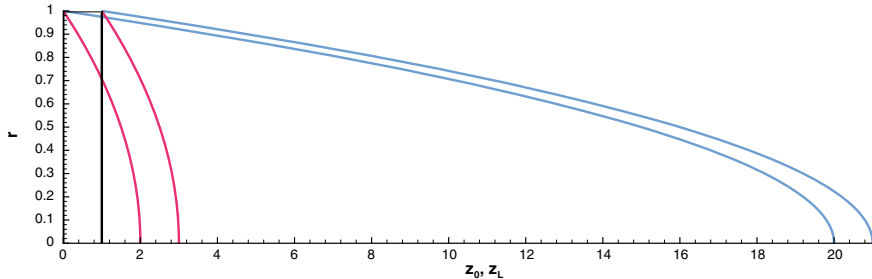


Fig. 21.1 Materially invariant, compact flow domain $\mathcal{D}(\tau)$ for the DNS simulation of pipe flow at times $\tau = 0$ (black, initial domain $\mathcal{D}(0) = \{0 \leq r \leq 0.5, 0 \leq \theta \leq 2\pi, 0 \leq z \leq L\}$), $\tau = 2$ (red), $\tau = 20$ (blue). The domain $\mathcal{D}(\tau)$ is constructed as materially invariant in laminar Hagen–Poiseuille flow (21.31) for ease of computation and for the sole purpose of illustration. The fluid is incompressible implying invariant volume, a property shared by laminar and turbulent flows

Furthermore, two-point correlations in axial direction would always be periodic in axial direction.

21.2.2 (iii.3), (iv.1) Theoretical Aspects

Transition from laminar to turbulent flow and the definition of a critical Reynolds number are radically different from other shear flows, Barkley [29].

Stability and transition

Linear stability theory proves that pipe flow is stable for all Reynolds numbers, [28]. The transition to turbulence is, therefore, subcritical, which is defined as transition due to finite disturbances without linear instability. Hence, linear stability analysis does not provide a critical Reynolds number and another approach to the computation of a critical Reynolds number has to be taken. Pipe flow instability proceeds from forming puffs (Darbyshire and Mullin [30] 1995) to weak and subsequently strong slugs to a percolation transition to fully developed turbulence with Prandtl friction law relation (Barkley [29], Fig. 36, Duguet et al. [31]). The stability behaviour of Couette flows changes from subcritical of plane Couette to supercritical for circular Taylor–Couette flows, see Faisst and Eckhardt [32] and Ostilla-Monico et al. [33] for an in-depth DNS analysis.

Critical Reynolds number

Turbulence occurs in pipes at small Reynolds numbers as localized patches called puffs. Puffs are generated artificially (by disturbing the laminar pipe flow, [30]), they are metastable for Reynolds numbers above a limit $Re \approx 1760$ and decay with a characteristic time scale $\tau_D(Re)$, which increases rapidly with the Reynolds number.

However, puffs may also split and generate new puffs as observed by Wygnanski et al. [34] 1975. The time scale $\tau_S(Re)$ associated with splitting decreases with Reynolds number. The critical Reynolds number Re_{cr} for pipe flow is defined indirectly as the number, where

$$\tau_D(Re_{cr}) = \tau_S(Re_{cr}) \quad (21.32)$$

holds. The numerical value for pipe flow of incompressible fluids is about $Re_{cr} = 2040$, (Avila et al. [35], Barkley [29]) based on experimental and DNS results. This value for the critical Reynolds number Re_{cr} is within the transitional range indicated in the Moody chart, see for instance White, [27].

21.2.3 Fully Developed Turbulent Flow Through Circular Pipes

The theoretical aspects of fully developed turbulent flow through straight, circular pipes are discussed with the aid of the Hopf fde, Sect. 9.2, and the solenoidal ONS basis constructed in Sect. 25.19 of Appendix C. The Hopf fde (established in Sect. 9.2.3 for non-random and random external forces) in cylindrical coordinates appropriate for the flow through circular pipes emerges as Eq. (10.7)

$$\begin{aligned} \frac{\partial \theta}{\partial t}[\mathbf{y}; t] = & -i[(y_r, \mathcal{F}_r)_c + (y_r, \mathcal{F}_r)_\nu + (y_\theta, \mathcal{F}_\theta)_c + (y_\theta, \mathcal{F}_\theta)_\nu + (y_z, \mathcal{F}_z)_c + (y_z, \mathcal{F}_z)_\nu] + \\ & i[(y_r, \Pi_r) + (y_\theta, \Pi_\theta) + (y_z, \Pi_z)] + \frac{i}{Fr}[(y_r, G_r \theta[\mathbf{y}]) + (y_\theta, G_\theta \theta[\mathbf{y}]) + (y_z, G_z \theta[\mathbf{y}])] - i(y_z, \frac{\partial P_0}{\partial z} \theta[\mathbf{y}]) \end{aligned}$$

where $\mathbf{y} \in \mathcal{N}_p$, derived in Sect. 10.4.1. The scalar products $(y_\alpha, \mathcal{F}_\alpha)_c$ for convection and $(y_\alpha, \mathcal{F}_\alpha)_\nu$ for the viscous terms are computed in the solution of Problem (10.2) in Appendix F. If the argument/test functions (Sect. 5.4) covers argument/test function spaces \mathcal{N} are solenoidal, the pressure gradient functional $[\Pi_r, \Pi_\theta, \Pi_z]^T$ can be eliminated by partial integration as shown in Sect. 9.2.5. Steady-state pipe flow allows the separation of a non-random base pressure gradient ∇P_0 that is constant and regarded as external control parameter. The Hopf fde is then

$$\begin{aligned} 0 = & -i[(y_r, \mathcal{F}_r)_c + (y_r, \mathcal{F}_r)_\nu + (y_\theta, \mathcal{F}_\theta)_c + (y_\theta, \mathcal{F}_\theta)_\nu + (y_z, \mathcal{F}_z)_c + (y_z, \mathcal{F}_z)_\nu] + \\ & + \frac{i}{Fr}[G_r(y_r, \theta[\mathbf{y}]) + G_\theta(y_\theta, \theta[\mathbf{y}])] + i(\frac{1}{Fr}G_z - \frac{\partial P_0}{\partial z})(y_z, \theta[\mathbf{y}]) \end{aligned}$$

for solenoidal ONS argument fields $\mathbf{y}(\mathbf{x}) \in \mathcal{N}_p$. The convective term in radial direction is given by (10.8) and the viscous contribution in the same direction by (10.9).

In light of the discussion on flow domains and boundary conditions, the spatial domain with the periodic boundary conditions in axial direction is chosen as

realistic option. However, this boundary condition is not physical, but essential for the construction of the solenoidal ONS basis (10.16) $\mathcal{B}_e = \{e_\alpha^{k,n,m}(r, \theta, z) = h_k(\theta) \chi_\alpha^{e,k,n,m}(r) h_m(z), \alpha = r, \theta, z\}$ for the test function space \mathcal{N}_p (Sect. 10.4.1). The solenoidal ONS vector modes $e_\alpha^{k,n,m}(r, \theta, z), \alpha = r, \theta, z$ are the product of Fourier modes (15.2) and the radial shape function vector $\chi_\alpha^{e,k,n,m}(r)$ defined in Eq. (25.164), Sect. 25.22.

The projected characteristic functional θ_N defined by (25.14) is for fully developed turbulent flow in a straight, circular pipe in statistical steady state governed by a linear pde (10.21) derived in Sect. 10.4.1

$$\sum_{k,n,m} \sum_{l,o,p} A_{k,n,m}^{l,o,p} \frac{\partial^2 \theta_N}{\partial y_{k,n,m} \partial y_{l,o,p}} = \frac{i}{Re} \sum_{k,n,m} B_{k,n,m} \frac{\partial \theta_N}{\partial y_{k,n,m}} + C \theta_N$$

with coefficients defined by (10.22), (10.23), (10.24). The projected characteristic functional θ_N is a standard function of a rapidly increasing number $M(N)$ (10.18) of independent variables. These independent variables $y_{k,n,m} \in R^{M(N)}$ are the coefficients of the representation

$$\mathbf{y}(\mathbf{x}) = \sum_{k,n,m} y_{k,n,m} \mathbf{e}^{k,n,m}(\mathbf{x})$$

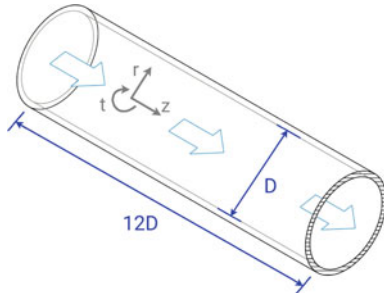
of an argument/test function $\mathbf{y}(\mathbf{x}) \in \mathcal{N}_p$ with $\mathbf{e}^{k,n,m}(\mathbf{x}) \in \mathcal{B}_e$ being the solenoidal ONS basis (10.16). The solenoidal basis vector fields $\mathbf{e}^{k,n,m}(\mathbf{x})$ satisfy the no-slip boundary condition and the parity conditions insuring smoothness at $r = 0$, and hence do the test/argument functions also satisfy these conditions. The approximation of the characteristic functional $\theta[\mathbf{y}(\mathbf{x})]$ by the projection $\theta_N(y_{k,n,m})$ is not at discrete points in the flow domain \mathcal{D} of argument / test functions $\mathbf{y}(\mathbf{x}) \in \mathcal{N}_p$ or discretized argument fields, but vector fields represented by the truncated expansions given above.

A solution method for the pde for θ_N has not yet been developed, but it could be a promising starting point for research into turbulent pipe flow and the numerical simulation of its statistical properties. An elementary example is presented in Appendix F, solution to Problem (10.4), to illustrate the computation of the coefficients.

21.3 DNS Examples

Examples for the numerical simulation of fully developed turbulent flows of a Newtonian fluid at Reynolds numbers currently accessible to direct simulations are presented. The examples are the flow of a compressible fluid at subsonic Mach numbers along flat plate boundary layers and the flow of an incompressible fluid through a straight pipe. The main purpose of the examples is to show the flow structures emerging in such flows near the wall (Fig. 21.2).

Fig. 21.2 Flow domain \mathcal{D} for the DNS simulation of turbulent pipe flow, the length of the pipe is $30D$. The Newtonian fluid is incompressible



The recognition of coherent structures has been the subject of debate for a long time; however, a useful and frequently applied criterion has been suggested by Wray and Hunt [36]. It is based on the invariant Q (21.33), i.e. a scalar field measuring for $Q > 0$ the prevalence of enstrophy over strain, which is regarded as indicator of coherent, vortical structures, [4, 37, 38]. Figure 21.3 shows a qualitative sketch of a hairpin structure (ii.2) in a wall-bounded shear layer according to Adrian and Marusic, [37]. This type of structure is common to the wall-bounded flows discussed below.

21.3.1 Turbulent Pipe Flow

The data were generated by F. Ries (EKT, TU Darmstadt, 2018) using a second-order accurate finite volume discretization technique of the pipe flow domain, the solution was computed in the pimpleFoam framework within openFOAM, and the results and the graphical illustrations were generously provided by F. Ries, EKT TU-Darmstadt, [39].

The geometry of the flow domain \mathcal{D} is shown in Fig. 21.2, the relevant Reynolds numbers are based on the wall shear velocity \tilde{u}_τ (27.15) and pipe radius \tilde{R} (tilde indicates dimensional quantity)

$$Re_{u_\tau} = \frac{\tilde{u}_\tau \tilde{R}}{\tilde{\nu}} = 180$$

and the bulk velocity \tilde{U} (volume flow rate divided by area of the pipe cross section) and pipe diameter $\tilde{D} = 2\tilde{R}$ according to (2.8)

$$Re = \frac{\tilde{U} \tilde{D}}{\tilde{\nu}} = 5500$$

The simulations apply the artificial periodic boundary condition in axial direction. The DNS results were obtained using finite disturbances to kick off the turbulence

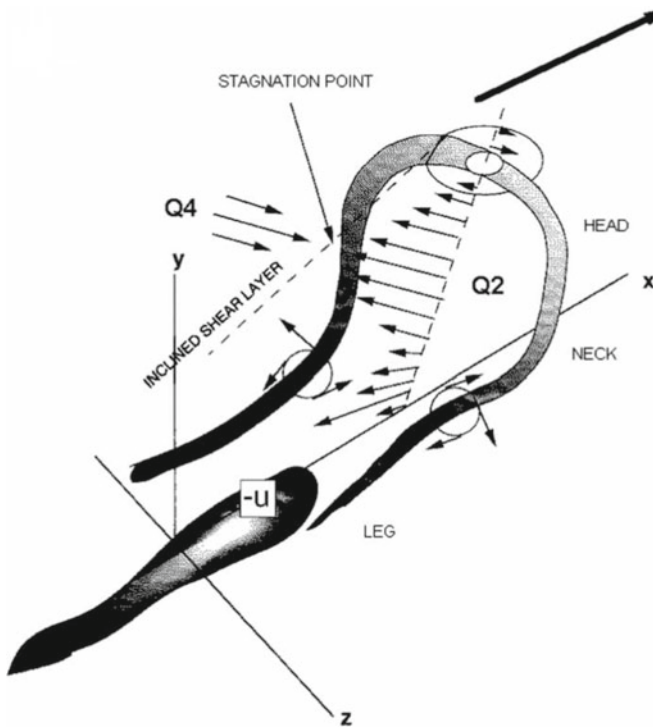


Fig. 21.3 Hairpin structure near a fixed wall boundary, Adrian and Marusic [37], reproduced with permission. The induced velocity moves fluid from the wall towards the centre of the pipe. See Fig. 21.9 for numerically computed hairpin structures

and the solver was run until approximate statistical equilibrium was reached. The Reynolds number is high enough ($Re > 1760$, Avila et al. [35]; Barkley [29]) that the puffs created by the external disturbance grow and split forming slugs and eventually coalesce to become fully developed turbulence, [39].

All structures determined by Smits [6] (ii.1) to (ii.4) are dominated by rotation, and hence is vorticity the relevant vector field together with the symmetric rate of strain tensor field. Chong et al. [40] proposed a classification scheme for 3-d flow fields based on the eigenanalysis of the rate of deformation tensor $A_{\alpha\beta} \equiv \frac{\partial v_\alpha}{\partial x_\beta}$, Eq. (2.113), where the eigenvalues λ and eigenvectors \mathbf{e} are the non-trivial solutions of

$$(A_{\alpha\beta} - \lambda \delta_{\alpha\beta}) \mathbf{e}_\beta = 0$$

The characteristic equation for incompressible fluids $\lambda^3 + Q\lambda + R = 0$ contains two invariants Q (the third invariant is the divergence of velocity, thus zero), defined by (21.33),

$$Q \equiv \frac{1}{2}(R_{\alpha\beta}R_{\alpha\beta} - s_{\alpha\beta}s_{\alpha\beta}) = \frac{1}{4}(e^2 - 2s_{\alpha\beta}s_{\alpha\beta}) \quad (21.33)$$

where $R_{\alpha\beta}$ (3.6) is the antisymmetric spin or rotation tensor and $e(\mathbf{x})$ is enstrophy, and the second invariant R is defined by

$$R \equiv -\det[\mathbf{A}] \quad (21.34)$$

Other vorticity measures have been suggested in the past, for instance, Truesdell, [41], Chap. V, defines a kinematical vorticity number \mathcal{W} by

$$\mathcal{W} \equiv \frac{e}{\sqrt{2s_{\alpha\beta}s_{\alpha\beta}}}$$

where $e(\mathbf{x})$ is enstrophy (3.16) and $s_{\alpha\beta}(\mathbf{x})$ the rate of strain (2.53). It could serve as alternative to (21.33), but has not yet found application (it is a ratio, hence possibly singular). More recently, Liu et al. [43] have suggested a similar vorticity measure Ω defined in Eq. (21.37) that has been successfully applied to the recognition of vortical structures. Enstrophy in pipe flow DNS is shown in Fig. 21.4 in the $r - z$ plane through the pipe axis for a subsection of length $3.5D$ of the full flow domain, length $12D$ (D is the pipe diameter). The colour bar indicates that the level of instantaneous enstrophy $e(\mathbf{x})$ is the highest at the pipe wall, where velocity is zero. This can be explained by inspection of the definition of vorticity in cylindrical coordinates (21.35)

$$\Omega \equiv \begin{pmatrix} \Omega_r \\ \Omega_\theta \\ \Omega_z \end{pmatrix} = \begin{pmatrix} \frac{1}{r} \frac{\partial v_z}{\partial \theta} - \frac{\partial v_\theta}{\partial z} \\ \frac{\partial v_r}{\partial z} - \frac{\partial v_z}{\partial r} \\ \frac{1}{r} \frac{\partial}{\partial r} (r v_\theta) - \frac{1}{r} \frac{\partial v_r}{\partial \theta} \end{pmatrix} \quad (21.35)$$

At the boundary $\partial\mathcal{D} = \{r = \frac{1}{2}, 0 \leq \theta \leq 2\pi, 0 \leq z \leq L\}$ with no-slip condition for velocity, vorticity emerges as non-zero vector parallel to the boundary

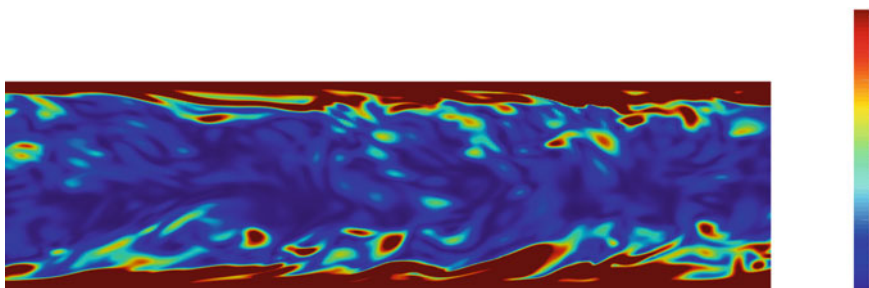


Fig. 21.4 Colour-coded enstrophy distribution in plane through the axis in the axial range of length $3.5D$ out of the total $L = 12D$. Data provided by F. Ries, TU-Darmstadt 2018

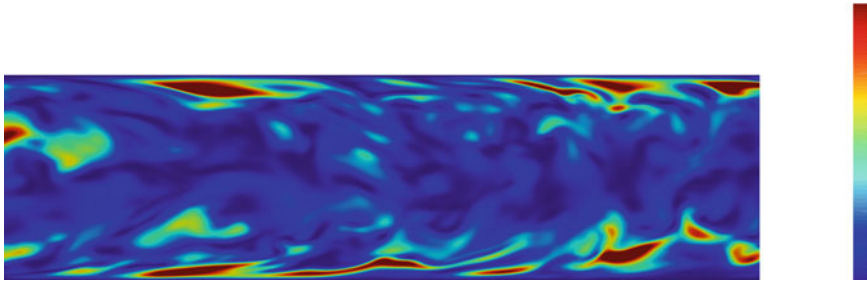


Fig. 21.5 Instantaneous kinetic energy in a plane through the coordinate axis $r = 0$ for the DNS simulation of turbulent pipe flow, data provided by F. Ries, TU-Darmstadt 2018

$$\boldsymbol{\Omega} = \begin{pmatrix} 0 \\ -\frac{\partial v_z}{\partial r} \\ \frac{\partial v_\theta}{\partial r} \end{pmatrix} \quad (21.36)$$

Two conclusions are immediate, the wall-normal component Ω_r is zero, but the wall parallel components Ω_θ and Ω_z are non-zero at a wall boundary with no-slip condition. Therefore, vorticity is parallel to wall boundaries but non-zero at the wall and enstrophy is non-zero at wall boundaries. Inspection of the near-wall layer reveals that the enstrophy distribution shows in the upper part the footprint of a (ii.1) near-wall streak and in the lower part several isolated relative maxima that can be interpreted as cuts through a (ii.2) structure, i.e. signatures of hairpin vortices. Comparison with the instantaneous kinetic energy of the fluctuating velocity in the same plane in Fig. 21.5 shows that the relative maxima of the kinetic energy are located near the heads of the hairpins. Kinetic energy shows relative maxima near the wall, but it is zero at the wall as required by the no-slip condition.

A closer look at the $Q(r, \theta, z)$ field is presented in Figs. 21.6 and 21.8. Figures 21.7 and 21.8 show the same level surface for the Q (21.33) field in the full domain in Fig. 21.6 (length $12D$) or the same small subset of the flow pipe domain (length $3.5D$) with another field colour coding the Q -level surfaces. The level surfaces of $Q(t, \mathbf{x})$ in Figs. 21.7 and 21.8 are shown in a small subset $0 \leq z \leq 1.5D$ for $0 \leq \theta \leq \pi$ with the core removed to improve the visibility of the near-wall structures. The level value of Q is positive, and therefore the vorticity within closed level surfaces is dominant compared to the rate of strain. Figure 21.7 shows the level surfaces of $Q(t, \mathbf{x})$ with the instantaneous axial velocity on the surfaces colour coded. The surfaces closest to the wall boundary are blue, i.e. slow compared to surface parts further away from the wall. In the centre of the two Figs. 21.7 and 21.8, a nascent hairpin-type structure is visible. The instantaneous axial velocity at the structure is moderately positive. The colour coding of the dynamic pressure in Fig. 21.8 indicates the middle of the range (yellow).

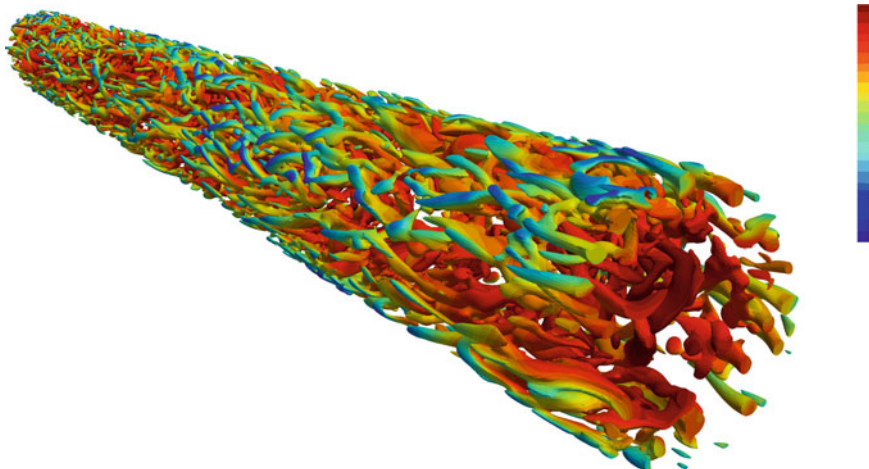


Fig. 21.6 Level surfaces of Q variable (21.33) colour coded with the axial velocity in DNS simulation of turbulent pipe flow domain of length $12D$, data provided by F. Ries, TU-Darmstadt 2018

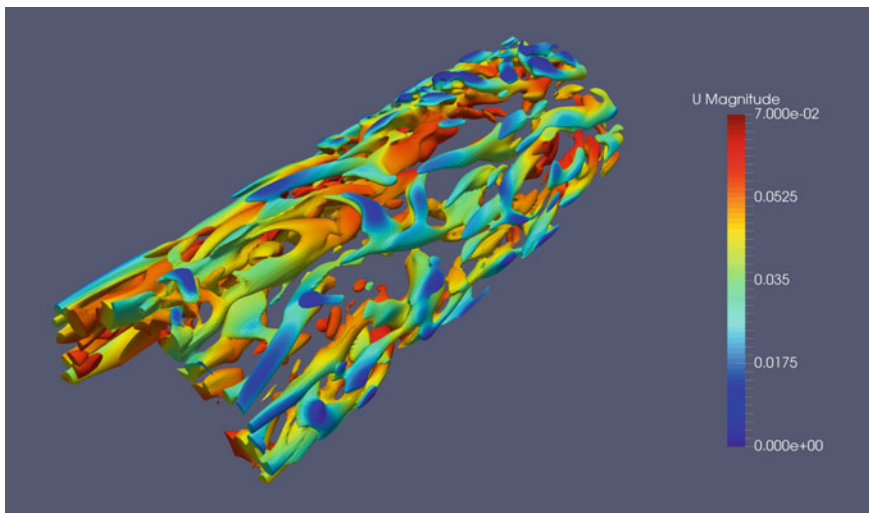


Fig. 21.7 Detail of the Q -surface in Fig. 21.6 with the axial velocity colour coded. A yellow coloured hairpin vortex is visible left of the centre of the figure. The main flow direction is from left to right

21.3.2 Compressible Boundary Layer Flows

Several DNS studies were using a sixth-order compact finite difference method plus spatial filtering combined with a third-order Runge–Kutta time integrator for the solution of the compressible Navier–Stokes pdes [42] of the formation and development

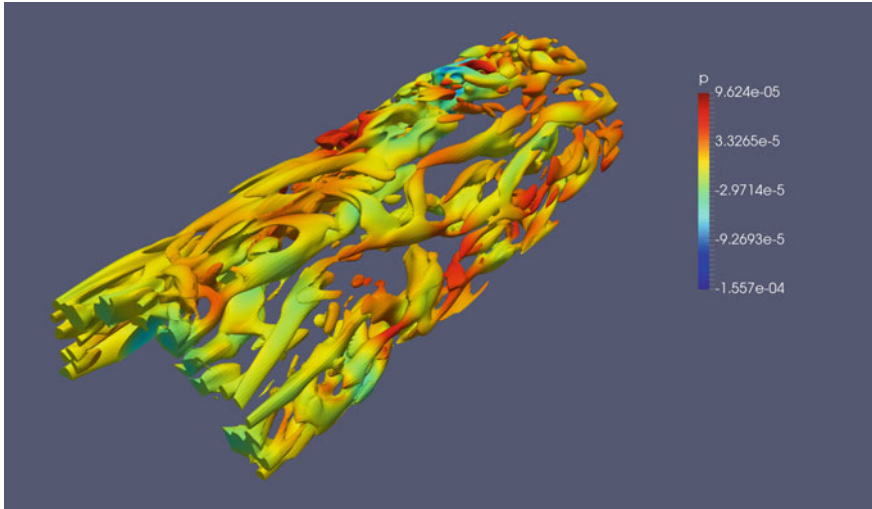


Fig. 21.8 Detail of the Q -surface in Fig. 21.6 with the dynamic pressure colour coded

of hairpin vortices in flat plate boundary layers by Wang et al. [43], Tian et al. [42] indicate that vortex rings may emerge in the later stage of the hairpin vortex development. The DNS simulations of the compressible Navier–Stokes pdes start at the entrance section with laminar flow plus Tollmien–Schlichting wave disturbances [44] to induce instability and transition. The Tollmien–Schlichting waves develop into Lambda vortex structures that subsequently form the hairpin structures. The identification of a vortical structure is based on the scalar Ω

$$\Omega(t, \mathbf{x}) \equiv \frac{||\mathbf{R}||_F^2}{||\mathbf{\omega}||_F^2 + ||\mathbf{R}||_F^2 + \epsilon} \quad (21.37)$$

where $\sigma_{\alpha\beta}$ is the rate of strain (2.53), $R_{\alpha\beta}$ is the spin tensor (3.6) containing the vorticity components (2.51) as entries, (ϵ is a small numerical safety value, $||\cdot||_F$ denotes the Frobenius matrix norm, [45]). A vortical structure is recognized in [42], if $|\Omega| > 0.5$. The structures at the late stage of transition are shown in Fig. 21.9 according to Tian et al. [42]. The vortex ring structures start as deformed lateral vortex tube termed lambda vortex as seen in Fig. 21.9 upstream of the hairpin vortices. It develops into the well-known hairpin that consists of two counterrotating vortex tubes approximately oriented in streamwise direction called legs, an open ring-like vortex head approximately laterally oriented and necks connecting legs and heads. The head and neck parts of the hairpin vortex may approach a ring structure under controlled conditions in DNS simulations [42].

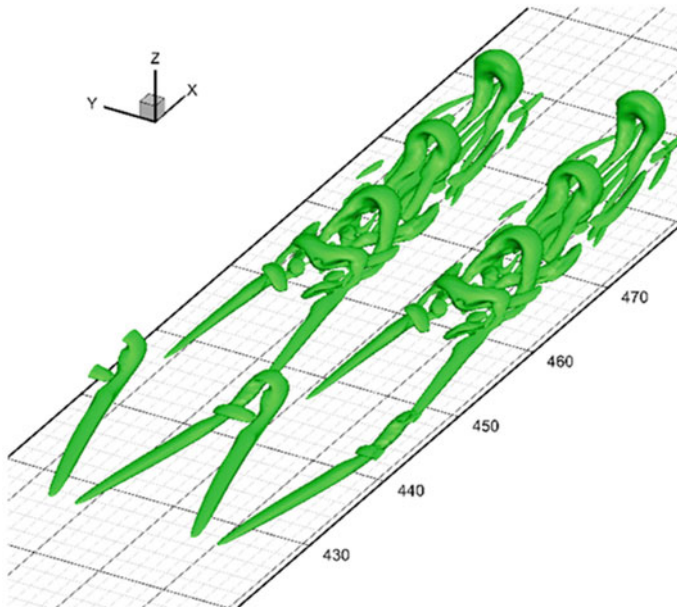


Fig. 21.9 Hairpin structure in the late stage of transition according to the DNS simulation of Tian et al. [42] observed in a compressible boundary layer. The structures are defined as level surfaces of $\Omega = 0.5$, (21.37). The lambda vortices upstream of the hairpins at lower left corner show the earlier stages of the development

21.4 Problems for this Chapter

Problem 21.1 Consider the fully developed, turbulent flow of an incompressible, Newtonian fluid through a plane channel between two plates at $x_2 = 0$ and $x_2 = h$. Use dimensionless variables based on the kinematic viscosity ν and the wall shear velocity u_τ (27.15).

1.1 Derive the averaged x-momentum balance for this flow.

1.2 Express the divergence of the Lamb vector (2.54) in terms of velocity, flexion (2.55) and enstrophy (3.16) and average the result.

1.3 Determine the Taylor series expansions for the fluctuation velocity, vorticity and flexion components close to the lower wall. Derive the expansion for the dimensionless divergence of the Lamb vector and its average close to the lower wall. Show that the divergence of the Lamb vector must be negative at the wall.

References

1. Marusic, I.: Unraveling turbulence near walls. *JFM* **630**, 1–4 (2009)
2. Jimenez, J.: Turbulent flows over rough walls. *Ann. Rev. Fluid Mech.* **36**, 173–196 (2004)
3. Jimenez, J.: Near-wall turbulence. *Phys. Fluids* **25**, 101302 (2013)
4. Wu, X., Moin, P.: A direct numerical simulation study of the mean velocity characteristics in turbulent pipe flow. *JFM* **608**, 81–112 (2008)
5. Chan, L., MacDonald, M., Chung, D., Hutchins, N., Ooi, A.: A systematic investigation of roughness height and wavelength in turbulent pipe flow in the transitionally rough regime. *JFM* **771**, 743–777 (2015)
6. Smits, A.J., McKeon, B.J., Marusic, I.: High-Reynolds number wall turbulence. *Annu. Rev. Fluid Mech.* **43**, 353–375 (2011)
7. Shebalin, J.V.: Phase space structure in ideal homogeneous turbulence. *Phys. Lett. A* **250**, 319–322 (1998)
8. Balbus, S.A.: When is high Reynolds number shear flow not turbulent? *JFM* **824**, 1–4 (2017)
9. Lopez, J.M., Avila, M.: Boundary-layer turbulence in experiments on quasi-Keplerian flows. *JFM* **817**, 21–34 (2017)
10. Tsinuber, A.: *An Informal Conceptual Introduction to Turbulence*, 2nd edn. Springer, Dordrecht (2009)
11. Pope, S.B.: *Turbulent Flows*. Cambridge University Press, Cambridge, U.K. (2001)
12. Durbin, P.A.: *Petterson Reif. Statistical Theory and Modeling for Turbulent Flows*. Wiley, B.A. (2011)
13. Vishik, M.J., Fursikov, A.V.: *Mathematical Problems of Statistical Hydromechanics*. Kluwer Academic Publication, Dordrecht (1988)
14. Hopf, E.: Statistical hydromechanics and functional calculus. *J. Rat. Mech. Anal.* **1**, 87–123 (1952)
15. Smits, A.J. (ed.): *IUTAM Symposium on Reynolds Number Scaling in Turbulent Flow*. Kluwer Academic Publishers, Dordrecht (2004)
16. Pileckas, K.: Navier-Stokes system in domains with cylindrical outlets to infinity. In: Friedlander, S., Serre, D. (eds.) *Handbook of Mathematical Fluid Dynamics*, vol. 4, pp. 447–647. North Holland (2007)
17. Boyd, J.P.: *Chebyshev and Fourier Spectral Methods*. Dover Publication Inc., Mineola, New York (2001)
18. Canuto, C., Hussaini, M.Y., Zang, T.A.: *Spectral Methods in Fluid Dynamics*. Springer, Berlin (1988)
19. Loulou, P., Moser, R.D., Mansour, N.N., Cantwell, B.J.: Direct Numerical Simulation of Incompressible Pipe Flow Using a B-spline Spectral Method, p. 110436. Memor, NASA Techn (1997)
20. Moser, R.D., Kim, J., Mansour, N.N.: DNS of turbulent channel flow. *Phys. Fluids* **11**, 943–945 (1999)
21. Williamson, J.H.: Low-storage Runge-Kutta schemes. *J. Comput. Phys.* **35**, 48–56 (1980)
22. Ahn, J.J., Lee, L., Sung, H.J.: Direct numerical simulations of fully developed turbulent pipe flows for $Re_\tau = 180, 544$ and 934 . *Int. J. Heat Fluid Flow* **44**, 222–228 (2013)
23. Eggels, J., Unger, F., Weiss, M., Westerweel, J., Adrian, R., Friedrich, R., Nieuwstadt, F.: Fully developed turbulent pipe flow: a comparison between direct numerical simulation and experiment. *JFM* **268**, 175–209 (1994)
24. El Khoury, G.K., Schlatter, P., Noorani, A., Fischer, P.F., Brethower, G., Johanson, A.V.: Direct numerical simulation of turbulent pipe flow at moderately high Reynolds numbers. *Flow Turbulence Combust.* **91**, 475–495 (2013)
25. Fukagata, K., Kasagi, N.: Highly energy-conservative finite-difference method for the cylindrical coordinate system. *J. Comput. Phys.* **181**, 478–498 (2002)
26. Wu, X., Moin, P., Adrian, R.J., Baltzer, J.R.: Osborne Reynolds pipe flow: Direct simulation from laminar through gradual transition to fully developed turbulence. *Proceedings of the National Academy of Sciences of the United States of America* **112**(26), 7920–7924 (2015)

27. White, F.M.: *Fluid Mechanics*. McGraw Hill, 6th edn (2008)
28. Schmid, P.J., Henningson, D.S.: *Stability and Transition in Shear Flows*. Springer (2001)
29. Barkley, D.: Theoretical perspective on the route to turbulence in a pipe. *JFM* **803**, P1–1 (2016)
30. Darbyshire, A., Mullin, T.: Transition to turbulence in constant-mass-flux pipe-flow. *JFM* **289**, 83–114 (1995)
31. Duguet, Y., Willis, A.P., Kerswell, R.R.: Slug genesis in cylindrical pipe flow. *JFM* **663**, 180–208 (2010)
32. Faisst, H., Eckhardt, B.: Transition from the Couette-Taylor system to the plane Couette system. *Phys. Rev. E* **61**, 7227–7230 (2000)
33. Ostillia-Monico, R., Verzicco, R., Grossmann, S., Lohse, D.: The near-wall region of highly turbulent Taylor-Couette flow. *JFM* **788**, 95–117 (2016)
34. Wygnanski, I., Sokolov, M., Friedman, D.: Transition in a pipe. Part 2. The equilibrium puff. *JFM* **68**, 283–304 (1975)
35. Avila, K., Moxey, D., de Lozar, A., Avila, M., Barkley, D., Hof, B.: The onset of turbulence in pipe flow. *Science* **333**(6039), 192–196 (2011)
36. Wray, A.A., Hunt, J.C.R.: Algorithms for Classification of Turbulent Structures. In: *Proceedings of the IUTAM Symposium*, pp. 95–104. Cambridge Univ. Press, Cambridge U.K. (1989)
37. Adrian, R.J., Marusic, I.: Coherent structures in flow over hydraulic engineering surfaces. *J. Hydraulic Res.* **50**, 451–464 (2012)
38. Serra, M., Haller, G.: Objective Eulerian coherent structures. *Chaos* **26**, 053110 (2016)
39. Ries, F., Nishad, K., Dressler, L., Janicka, J., Sadiki, A.: Evaluating large-eddy simulation results based on error analysis. *Theor. Comp. Fluid Dyn.* **32**, 733–752 (2018)
40. Chong, M.S., Perry, A.E., Cantwell, B.J.: A general classification of three-dimensional flow fields. *Phys. Fluids A* **2**, 765–777 (1990)
41. Truesdell, C.A.: *The Kinematics of Vorticity*. Indiana University Press, Bloomington, Indiana (1954)
42. Tian, S., Gao, Y., Lui, C., Yang, Y.: DNS study on large vortex ring formation in late flow transition. In: *2018 AIAA Aerospace Sciences Meeting*. Kissimmee, Florida (2018)
43. Wang, Y., Al-Dujaly, H., Tang, J., Liu, C.: DNS Study on hairpin vortex structure in turbulence. In: *53rd AIAA Aerospace Sciences Meeting*. Kissimmee, Florida (2015)
44. Schlichting, H.: *Boundary Layer Theory*. McGraw-Hill (1987)
45. Golub, G.H., Van Loan, C.F.: *Matrix Computations*. Johns Hopkins Studies in the Mathematical Sciences (1996)

Chapter 22

The Limit of Infinite Reynolds Number for Incompressible Fluids



The Reynolds number defined by (2.8) is the dimensionless parameter appearing in the momentum balance (2.7) of the Navier–Stokes equations that indicates the fundamental character of the flow of an incompressible fluid. The parameters determining this number are the length scale L , the velocity scale U and the kinematic viscosity $\tilde{\nu}$ as measure of resistance to shearing motion or the dynamic viscosity $\tilde{\mu} = \tilde{\rho}\tilde{\nu}$ plus density. This number can be computed, if the following condition is satisfied: Length and velocity scales characteristic for the flow can be identified. The definition of length and velocity scales is in general not unique and in some cases there is no obvious a priori choice for them. It follows from the definition of the Reynolds number that there are three physical processes (letting a dimensional physical variable approach a suitable limit value) that produce infinity for Re . First, the length scale L can go to infinity, second, the velocity scale U can go to infinity and third, the viscosity ν can go to zero. The first and second possibilities are unrealistic, since the universe is bounded and velocity cannot exceed the speed of light. Hence, only the third way $\nu \rightarrow 0$ will be considered.

The physical limit is based on the properties of either the dynamic viscosity as temperature approaches absolute zero or the kinematic viscosity as the pressure is increased. The former method is available for Helium only, which becomes a superfluid at temperatures below the λ -temperature $\tilde{T} = 2.17$ K at atmospheric pressure. However, it is subject to quantum-mechanical phenomena that do not have counterparts in classical fluid mechanics, and hence is not suitable as limit for Navier–Stokes turbulence. Compressing air to very high pressures to decrease the kinematic viscosity thus achieving high Reynolds numbers in pipe flows has been successfully applied by Smits and collaborators [1] and references therein. Physical conditions for this limit will be established and a physical limit will be discussed below in the context of Onsager’s conjecture [2], pursued further by Eyink [3].

The mathematical limit will be defined and analysed with the aid of dimensional arguments and the Navier–Stokes equations assumed valid as the viscosity approaches zero, viscosity being a non-negative, dimensional parameter in the context of Navier–Stokes theory. It is distinct from the physical limit, which depends at

a given temperature and pressure on the statistics of the elementary particles constituting the fluid and the solid material forming eventually present wall boundaries.

It is assumed that suitable length and velocity scales can be identified and the Reynolds number (2.8) is thus properly defined. The strong form of the dimensionless Navier–Stokes equations in the spatial description for an incompressible fluid in a simple, compact domain \mathcal{D} with boundary $\partial\mathcal{D}$ is then derived in Cartesian coordinates from mass balance (2.6) and momentum balance (2.7)

$$\frac{\partial v_\alpha}{\partial x_\alpha} = 0, \quad \frac{Dv_\alpha}{Dt} = -\frac{\partial P}{\partial x_\alpha} + \frac{1}{Re} \Delta v_\alpha + \frac{1}{Fr} g_\alpha \quad (22.1)$$

where D/Dt is the substantial time derivative, g_α denotes a dimensionless volume force field assumed known and

$$Fr \equiv \frac{\tilde{U}^2}{\tilde{\rho}\tilde{g}\tilde{L}} \quad (22.2)$$

defines the Froude number as the ratio of the inertial to external field forces (\tilde{g} is a characteristic value for the external force (per unit mass) field, for instance, the acceleration of gravity). Flows influenced by heat transfer generate the dimensionless factor called Grashof number Gr defined as the ratio of buoyant to viscous force. For pipes, the definition

$$Gr_D = \frac{\tilde{g}\tilde{\beta}(\tilde{T}_s - \tilde{T}_\infty)D^3}{\tilde{\nu}^2} \quad (22.3)$$

is adopted, where \tilde{g} is the acceleration of gravity, $\tilde{\beta}$ is the coefficient of thermal expansion, \tilde{T}_s and \tilde{T}_∞ are the surface and bulk temperature, \tilde{D} is the pipe diameter and $\tilde{\nu}$ is the kinematic viscosity. Density $\tilde{\rho}$ is assumed constant for the incompressible fluids considered and $\tilde{P} = \tilde{p}/\tilde{\rho}$ for convenience.

The equations are valid in the domain \mathcal{D} and the type of the equations for $0 < Re < \infty$ requires conditions for velocity on the complete boundary $\partial\mathcal{D}$. The boundary $\partial\mathcal{D}$ is closed, i.e. it does not have a boundary, and it may be the union of a finite number of disjoint surfaces $\partial\mathcal{D}_i$, $i = 1, \dots, N$. The conditions on the individual parts of the boundary need not be the same, the boundary may be a solid wall, and hence $v_\alpha = 0$ on and vorticity parallel to some $\partial\mathcal{D}_i$, or an inflow/outflow boundary with Dirichlet or Neumann conditions or a combination of them.

Several vector and tensor fields derived from velocity play an important role in the analysis of the limit $Re \rightarrow \infty$ and interpretation of the Navier–Stokes equations and their solutions. Vorticity and vector fields derived from it are discussed in Sect. 22.1 that are relevant for the kinematics and dynamics of turbulent flows and the limit of singular vorticity.

The development of singularities of the second kind requires a version of the Navier–Stokes pdes (Duchon and Robert [4]) different from the strong form (22.1) given above, since the velocity and stress fields may cease to be differentiable as $Re \rightarrow \infty$. Two versions are introduced for the investigation of this limit.

Singular vector fields: Weak solutions

Weak solutions of the Navier–Stokes pdes defined by (2.40) in Sect. 2.2 are one of the tools suitable for the analysis of the limit $Re \rightarrow \infty$. An integrable vector field $\mathbf{v}(t, \mathbf{x})$ is weak solution iff

$$\int_0^\infty dt \{ (v_\alpha, \frac{\partial u_\alpha}{\partial t}) + \frac{1}{Re} (v_\alpha, \Delta u_\alpha) + (v_\alpha, v_\beta \frac{\partial u_\alpha}{\partial x_\beta}) \} = -(v_\alpha^0, u_\alpha^0) \quad (22.4)$$

holds for all test vectors $\mathbf{u}(\mathbf{x}, t) \in C_\infty$, where $C_T \equiv \{\mathbf{u}(\mathbf{x}, t) \in C_{\mathcal{D} \times [0, T)}^\infty \cap L^2_{\mathcal{D} \times [0, T)}\}$, $\nabla \cdot \mathbf{u} = 0$, $\mathbf{u}(\mathbf{x}, t)$ has compact support} and the initial fields \mathbf{u}^0 are elements of C_0 . All derivatives have been rolled over to the test vectors by means of partial integration.

Singular vector fields: Filtered solutions

Scalar, vector and tensor fields can be coarse grained or filtered (the same operation as in LES methods, Sagaut [5], filtering is indicated by the overbar)

$$\bar{\mathbf{v}}_l(\mathbf{x}) \equiv \int_{\mathcal{D}} d\mathbf{r} G_l(\mathbf{r}) \mathbf{v}(\mathbf{x} + \mathbf{r}) \quad (22.5)$$

where the kernel/weight/filter function G_l is constructed in the form

$$G_l(\mathbf{r}) \equiv l^{-d} G\left(\frac{\mathbf{r}}{l}\right) \quad (22.6)$$

with the aid of a dimensionless shape function G , where $d = 3$ is the dimension of the flow domain and $l > 0$ is the filter scale. Coarse graining, defined as multiplication with the filter and integrating over the flow domain and denoted by the overbar, mass and momentum balances lead to (Eyink [3])

$$\nabla \cdot \bar{\mathbf{v}}_l = 0 \quad (22.7)$$

and

$$\frac{\partial}{\partial t} \bar{\mathbf{v}}_l + \nabla \cdot [\bar{\mathbf{v}}_l \bar{\mathbf{v}}_l + \bar{\boldsymbol{\theta}}_l] = -\nabla \bar{p}_l + \nu \Delta \bar{\mathbf{v}}_l \quad (22.8)$$

It produces the symmetric subgrid scale stress (sgs) tensor

$$\bar{\boldsymbol{\tau}}_l = \overline{(\mathbf{v} \otimes \mathbf{v})_l} - \bar{\mathbf{v}}_l \otimes \bar{\mathbf{v}}_l \quad (22.9)$$

Any effort for solving the filtered pdes requires additional information on the sgs stresses (see Sagaut [5]; Garnier et al. [6] for detailed development of LES methods).

22.1 A Bounded Vector Field Derived From Vorticity

A vector field is constructed that remains bounded for enstrophy (3.16) approaching infinity, thus allowing the analysis and presentation of the neighbourhood of singular vorticity structures. Vorticity defined by (2.51) in the spatial description

$$\omega_\alpha \equiv \epsilon_{\alpha\beta\gamma} \frac{\partial v_\gamma}{\partial x_\beta}$$

where $\epsilon_{\alpha\beta\gamma}$ denotes the Levi-Civita symbol, which is a measure for the amount of rotation around a material point in the flow field \mathcal{D} as discussed in Sect. 2.3. The dynamical equation for vorticity follows at once from (2.51) and the dimensionless Navier–Stokes equations (2.6), (2.7), it is given by (2.52) for compressible fluids and reduced to

$$\frac{D\omega_\alpha}{Dt} = \omega_\beta \frac{\partial v_\alpha}{\partial x_\beta} + \frac{1}{Re} \Delta \omega_\alpha \quad (22.10)$$

for incompressible fluids. The properties of (22.10) are discussed in Sect. 2.3 for the spatial description and the material counterpart of vorticity in Sect. 2.6. The literature on vorticity is vast, see Truesdell [7] (collection of kinematic results up to 1954), Saffman, [8] (dynamics, vortex rings), Majda and Bertozzi, [9] (singularities, weak solutions of Euler and Navier–Stokes equations, numerical aspects) and Wu et al. [10] (exhaustive treatment of kinematics and dynamics of vorticity) and references therein. If vorticity remains smooth as $Re \rightarrow \infty$, i.e. twice continuously differentiable, thus does not develop singularities, then is the vorticity pde (22.10) reduced to the condition (2.109) [11], that vorticity is frozen, for further details on frozen vector fields see [12] and Sect. 2.6.3.

Vorticity may become unbounded for solutions of the Euler and possibly the Navier–Stokes equations. Unfortunately, the question of the existence of singular solutions of the 3-d Euler and Navier–Stokes equations have not been settled so far, see Gibbon [13], Kerr [14, 15] for a detailed discussion of this issue and [16] for a recent conjecture based on numerical simulations. However, Kolmogorov (Chap. 17) and Onsager (Sect. 22.2) laid the foundation for the theory of turbulence based on the conjecture that a turbulent velocity field develops singularities of the second kind as the Reynolds number grows to infinity such that the expectation of the dissipation rate approaches a positive and well-defined limit value. This conjecture has indirect experimental and numerical support, and hence tools for the investigation of this conjecture are highly desirable.

A vector field \mathbf{b} can be constructed for this purpose that is locally the one-to-one image of vorticity, remains bounded as vorticity becomes singular and shares the critical points with vorticity,

$$b_\alpha \equiv \frac{\omega_\alpha}{(1 + \omega_\beta \omega_\beta)^{\frac{1}{2}}} \quad (22.11)$$

assuming that all variables are dimensionless. It is easy to check that the inverse relation is given by

$$\omega_\alpha = \frac{b_\alpha}{(1 - b_\beta b_\beta)^{\frac{1}{2}}} \quad (22.12)$$

If vorticity varies in the range $(-\infty, \infty)$, the derived vector field \mathbf{b} varies in $(-1, 1)$. The derived vector field is a local function of the vorticity field, and hence it is straightforward to establish the dynamic equations for it. The strong form of this pde can be given in mixed formulation involving both vector fields

$$\begin{aligned} \frac{Db_\alpha}{Dt} &= (\delta_{\alpha\beta} - b_\alpha b_\beta) b_\gamma \frac{\partial v_\beta}{\partial x_\gamma} + \frac{(\delta_{\alpha\beta} - b_\alpha b_\beta)}{Re} (\delta_{\beta\gamma} - \omega_\beta \omega_\gamma) \Delta b_\gamma \\ &- \frac{(\delta_{\alpha\beta} - b_\alpha b_\beta)}{(1 - b^2)^{\frac{1}{2}}} [\omega_\beta (\delta_{\gamma\delta} - \omega_\gamma \omega_\delta) + \omega_\gamma (\delta_{\beta\delta} - \omega_\beta \omega_\delta) + \omega_\delta (\delta_{\beta\gamma} - \omega_\beta \omega_\gamma)] \epsilon_{\gamma\delta} \end{aligned} \quad (22.13)$$

The dissipation rate tensor (21.19) of the derived vector field is denoted by

$$\epsilon_{\alpha\beta} \equiv \frac{1}{Re} \frac{\partial b_\alpha}{\partial x_\gamma} \frac{\partial b_\beta}{\partial x_\gamma}$$

The transformation to the derived vector pde is completed with the aid of (22.11)

$$\begin{aligned} \frac{Db_\alpha}{Dt} &= (\delta_{\alpha\beta} - b_\alpha b_\beta) b_\gamma \frac{\partial v_\beta}{\partial x_\gamma} + \frac{(\delta_{\alpha\beta} - b_\alpha b_\beta)}{(1 - b^2)Re} ((1 - b^2) \delta_{\beta\gamma} - b_\beta b_\gamma) \Delta b_\gamma \\ &- \frac{(\delta_{\alpha\beta} - b_\alpha b_\beta)}{(1 - b^2)^2} [b_\beta ((1 - b^2) \delta_{\gamma\delta} - b_\gamma b_\delta) + b_\gamma ((1 - b^2) \delta_{\beta\delta} - b_\beta b_\delta) + b_\delta ((1 - b^2) \delta_{\beta\gamma} - b_\beta b_\gamma)] \epsilon_{\gamma\delta} \end{aligned} \quad (22.14)$$

The invariant $b^2 = b_\gamma b_\gamma$ (length of \mathbf{b} squared) is governed by

$$\frac{Db^2}{Dt} = 2(1 - b^2) b_\beta b_\gamma \frac{\partial v_\beta}{\partial x_\gamma} + \frac{(1 - 2b^2)}{Re} \Delta b^2 - 2(1 - b^2) \epsilon_{\gamma\gamma} - 2 \frac{(2 - 5b^2)}{(1 - b^2)} b_\gamma b_\delta \epsilon_{\gamma\delta} \quad (22.15)$$

An example will now be constructed to gain understanding of the properties of the pde for $b_\alpha(t, \mathbf{x})$.

Assuming that the rate of stretch expression $(1 - b) \partial v_1 / \partial x_1 \rightarrow 0$ as $b \rightarrow 1$, the condition for the solution of (22.14) to be bounded as $b \rightarrow 1$, it is necessary that the viscous terms

$$\frac{1 - 2b^2}{Re} \Delta b^2 - 2(1 - b^2) \epsilon_{\gamma\gamma} - 2 \frac{(2 - 5b^2)}{(1 - b^2)} b_\gamma b_\delta \epsilon_{\gamma\delta} \rightarrow 0$$

as $b \rightarrow 1$. If this is the case,

$$(1 - 2b^2)\Delta b^2 = 2(1 - b^2)\frac{\partial b_\gamma}{\partial x_\beta}\frac{\partial b_\gamma}{\partial x_\beta} + \frac{1}{2}\frac{(2 - 5b^2)}{(1 - b^2)}\frac{\partial b^2}{\partial x_\beta}\frac{\partial b^2}{\partial x_\beta}$$

holds independent of the Reynolds number. It follows from this nonlinear second-order pde that the sign of the Laplacian is negative for $b^2 > 1/2$ but positive for $b^2 < 1/2$. The solution can be obtained by numerical methods.

Consider the case when $b \rightarrow 1$, then is the Laplacian of b negative semi-definite and the sum of the viscous terms could be zero even if $3b\epsilon_{11}/(1 - b)$ remains non-zero. If they exactly cancel and the deformation rate is non-singular at $b = 1$, the limit value (i.e. the singularity of vorticity) would move with the fluid at the given instant and location. In this case, the representation

$$\epsilon_{11} = (1 - b)\mathcal{F}(\mathbf{b}, \mathbf{x}, t)$$

where \mathcal{F} is a bounded unknown function would be possible in the neighbourhood of the vortical singularity. The stronger requirement that the second term vanishes as $b \rightarrow 1$ implies that the spatial variation of b is such that there are no singularities in its gradient as b approaches unity.

The limit of infinite Reynolds number poses an intriguing question for the viscous terms in (22.14): Does the limit

$$\lim_{Re \rightarrow \infty} \frac{1}{Re} \Delta b + \frac{\epsilon_{11}}{(1 - b)} \frac{3b}{(1 + b)} \quad (22.16)$$

exist? The answer depends on the local value of b . For points \mathbf{x} in the flow field where $b < 1$ holds in the limit and the solution remains smooth, the limit is zero. For points \mathbf{x} , where $\lim_{Re \rightarrow \infty} b = 1$, the limit for the viscous terms may be either zero or non-zero or may not exist at all. If it exists and is zero the inviscid (Eulerian) version of (22.13) is obtained

$$\frac{Db_\alpha}{Dt} = (\delta_{\alpha\gamma} - b_\alpha b_\gamma) b_\beta \frac{\partial v_\gamma}{\partial x_\beta} \quad (22.17)$$

If it exists and is non-zero and the \mathbf{b} field remains smooth, it must be less than one to be consistent with the boundedness of \mathbf{b} . If the derivatives of the \mathbf{b} -field become singular in the limit, cusp-type singularities would appear.

The first term on the right side of (22.13) represents vortex stretching. It is clear that it is damped as $b \rightarrow 1$ and vanishes in this limit, unless the deformation rate becomes singular.

22.2 The Kolmogorov–Onsager Conjecture

Kolmogorov [17] and Onsager [2] conjectured that the statistical average of the dissipation rate (1.5) approaches a well-defined, positive limit value as $Re \rightarrow \infty$. This is a consequence of the assumption of approximate equilibrium of energy supply

at large scales l with conversion of energy into internal energy at small scales leading to the remarkable estimate (19.7)

$$O(\epsilon) = \frac{u^3}{l}$$

independent of viscosity, where u is the velocity scale and l is the integral length scale. Specifically, the velocity scale $u^2 = \|\mathbf{v}\|_{L^2}^2$ is the rms velocity and

$$u^2 = \|\mathbf{v}\|_{L^2}^2 \equiv \frac{1}{T} \int_0^T dt \int_{\mathcal{D}} d\nu w(\mathbf{x}) |\mathbf{v}|^2 \quad (22.18)$$

is the L^2 -norm with $w(\mathbf{x}) \geq 0$ as weight function with dimension L^{-3} . The length scale l is defined as the integral scale (19.27) $l = |\mathbf{L}|$, where

$$L_\beta(\mathbf{x}) \equiv \int_0^\infty dr_\beta \frac{\langle v_\alpha(\mathbf{x}) v_\alpha(\mathbf{x} + \mathbf{r}) \rangle}{\langle v_\alpha(\mathbf{x}) v_\alpha(\mathbf{x}) \rangle}$$

denotes the integral length scales in the coordinate directions. It is now possible to define the dimensionless dissipation rate $D(\epsilon)$ by

$$D(\epsilon) \equiv \frac{l \langle \epsilon \rangle}{u^3} \quad (22.19)$$

Kolmogorov's assumption and Onsager's conjecture are now expressed as

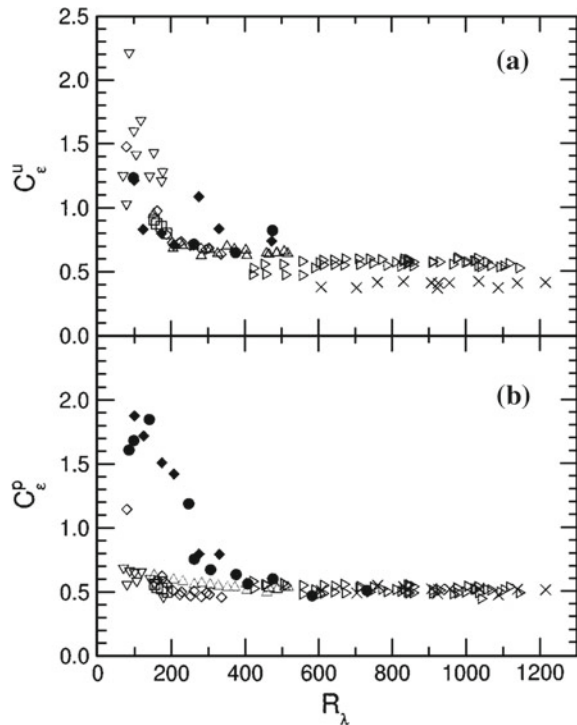
$$\lim_{Re \rightarrow \infty} D(\epsilon) = D_\infty > 0. \quad (22.20)$$

22.2.1 Experimental and Numerical Evidence

The dimensionless dissipation rate can be deduced from experiments and computed in DNS simulations for finite Reynolds numbers. The results are very instructive. The DNS results for homogeneous, isotropic turbulence reviewed by Sreenivasan [18] for Reynolds numbers $Re_\lambda \leq 218$ (Fig. 1, λ denotes the Taylor micro-scale, (19.22)) and Kaneda et al. [19] for $Re_\lambda \leq 1200$ (Fig. 3) show clearly the tendency to asymptote to a value $D_\infty \approx 0.5$. Pearson et al. [20] summarize the experimental results (Mydlarski and Wahrhaft [21, 22]; Gamard and George [23]) for homogeneous turbulence and a variety of shear flows for Reynolds numbers Re_λ up to 1200 reproduced in Fig. 22.1. The agreement with the numerical results for homogeneous turbulence is remarkable in Fig. 22.1, as

$$0.4 < D(\epsilon) \leq 0.7 \quad (22.21)$$

Fig. 22.1 Normalized dissipation rate (22.19) $D(\epsilon) = C_\epsilon^u$ (length scale l computed as the area under the autocorrelation function) and $D(\epsilon) = C_\epsilon^p$ (l determined from the spectrum) for a number of shear flows according to Pearson et al. [20]



holds for experimental and numerical data, the variation is mostly due to the different definitions of scales for different flows. The numerical and experimental results are evidence that turbulent flow fields develop singularities of the second kind (defined in theorem (3.15) in Chap. 3), such that the expectation of the dissipation rate asymptotes to a non-zero value for the Reynolds number approaching infinity. The structure and dynamics of these singularities are still unknown, see Eyink [3], Gibbon [13], Kerr [14, 15] for relevant analysis and numerical simulations.

22.2.2 Analysis

The conjecture (22.20) raises for $Re \rightarrow \infty$ the question of the regularity of the velocity fields and thus the validity of the strong (differential) form of the Navier–Stokes pdes, Onsager [2], Eyink [3]. The definition of the dissipation rate (1.5) implies that

$$\langle \frac{\partial v_\alpha}{\partial x_\beta} \frac{\partial v_\alpha}{\partial x_\beta} \rangle \rightarrow \infty$$

as $Re \rightarrow \infty$, while the kinetic energy remains bounded. Hence, the velocity field must develop singularities of the second kind, as defined for Theorem (3.15). Furthermore, the statistical expectation of $s_{\alpha\beta}s_{\alpha\beta}$ is in homogeneous turbulence equal to the expectation of enstrophy. Therefore, the analysis of the limit $Re \rightarrow \infty$ can as well be based on enstrophy.

The tool for the analysis is the notion of Hölder continuity with order $0 < \alpha < 1$ (it is called Lipschitz continuity for the standard case $\alpha = 1$)

$$|\tilde{\mathbf{v}}(\tilde{\mathbf{x}} + \tilde{\mathbf{r}}) - \tilde{\mathbf{v}}(\tilde{\mathbf{x}})| \leq \tilde{c}\tilde{r}^\alpha \quad (22.22)$$

(tilde denotes dimensional quantities), where α and the constant c are independent of $\tilde{\mathbf{x}}$, $\tilde{\mathbf{r}}$. The physical dimension of velocity is length L over time T , which implies that the constant \tilde{c} in (22.22) has the physical dimension

$$O(\tilde{c}) = \frac{L^{1-\alpha}}{T}$$

This is not acceptable but easily corrected by defining reference values for length \tilde{l}_0 and time $\tilde{\tau}_0$ (as required for the Reynolds number) and multiplying (22.22) with $\tilde{\tau}_0/\tilde{l}_0$ leading to

$$|\mathbf{v}(\mathbf{x} + \mathbf{r}) - \mathbf{v}(\mathbf{x})| \leq c'r^\alpha \quad (22.23)$$

where $\mathbf{v} \equiv \frac{\tilde{\mathbf{v}}\tilde{\tau}_0}{l_0}$ and $r \equiv \frac{\tilde{r}}{l_0}$ are dimensionless velocity and distance and the (new) constant $c' \equiv \frac{\tilde{c}l_0^{1-\alpha}}{\tilde{\tau}_0}$ is dimensionless, i.e. its value does not change with a change of units of measurement.

Coarse graining or filtering (22.5) is an operation defined as

$$\tilde{\mathbf{v}}_l(\tilde{\mathbf{x}}) \equiv \int_{\mathcal{D}} d\tilde{\mathbf{r}} \tilde{G}_l(\tilde{\mathbf{r}}) \tilde{\mathbf{v}}(\tilde{\mathbf{x}} + \tilde{\mathbf{r}})$$

where the kernel/filter function $\tilde{G}_l(\tilde{\mathbf{r}})$ is constructed as, for instance, given by (22.6), with $l > 0$ denoting the filter scale. The physical dimension of the kernel must be L^{-3} to insure that the filtered and unfiltered velocities have the same physical dimension.

Coarse graining mass and momentum balances lead to (Eyink, [3]) (22.7) and (22.8) produce the subgrid scale stress tensor (22.9) $\tilde{\mathbf{g}}_l = (\tilde{\mathbf{v}} \otimes \tilde{\mathbf{v}})_l - \tilde{\mathbf{v}}_l \otimes \tilde{\mathbf{v}}_l$. Consider now turbulent flows at $Re \gg 0$, then the viscous term in the coarse-grained momentum balance (22.8) for a filter scale l in the inertial range length scales can be estimated as (22.18)

$$||\tilde{\nu} \Delta \tilde{\mathbf{v}}_l|| \leq C \frac{\tilde{\nu}}{\tilde{l}^2} ||\tilde{\mathbf{v}}_l|| \quad (22.24)$$

where C is a positive, dimensionless constant and \tilde{l} is the filter scale. Note that the estimate holds for the coarse-grained velocity, but not for the instantaneous velocity,

which may not be differentiable. Hence, the viscous term in (22.8) can be neglected for $Re \gg 0$ and \tilde{l} in the inertial range leading to

$$\frac{\partial}{\partial \tilde{t}} \bar{\mathbf{v}}_l + \nabla \cdot (\bar{\mathbf{v}}_l \bar{\mathbf{v}}_l + \bar{\mathbf{g}}_l) = -\nabla \bar{p}_l \quad (22.25)$$

From this pde, the equation for the large-scale kinetic energy

$$\tilde{e}_l \equiv \frac{1}{2} \bar{\mathbf{v}}_l \cdot \bar{\mathbf{v}}_l \quad (22.26)$$

follows at once

$$\frac{\partial}{\partial \tilde{t}} \tilde{e}_l + \nabla \cdot \tilde{\mathbf{J}}_l = -\tilde{\Pi}_l \quad (22.27)$$

where the energy flux is defined by

$$\tilde{\mathbf{J}}_l \equiv (\tilde{e}_l + \bar{p}_l) \bar{\mathbf{v}}_l + \bar{\mathbf{v}}_l \cdot \bar{\mathbf{g}}_l \quad (22.28)$$

and the rate of deformation work term (Tennekes and Lumley, [24], also called the inertial dissipation rate) by

$$\tilde{\Pi}_l \equiv \nabla \bar{\mathbf{v}}_l : \bar{\mathbf{g}}_l \quad (22.29)$$

The rate of deformation term represents the transfer rate of energy from large to small scales, it has the dimension of the dissipation rate. Eyink [3] argues that the energy flux (22.28) and the deformation rate (22.29) depend only on the velocity difference $\delta \mathbf{v}(\mathbf{r}, \mathbf{x}) = \mathbf{v}(\mathbf{x} + \mathbf{r}) - \mathbf{v}(\mathbf{x})$, hence

$$\tilde{\Pi}_l(\delta \tilde{\mathbf{v}}) = -\nabla \delta \tilde{\mathbf{v}} : \tilde{\mathbf{g}}(\delta \tilde{\mathbf{v}}) \quad (22.30)$$

The order of magnitude of the rate of deformation work term (22.29) is then

$$O(\tilde{\Pi}_l) = \frac{|\delta \tilde{\mathbf{v}}(\tilde{l}, \tilde{\mathbf{x}})|^3}{\tilde{l}} \quad (22.31)$$

Following Onsager's assumption, that the velocity field is Hölder continuous (22.22) with exponent $0 < \alpha < 1$ (see Sect. 23.7 for definitions), the estimate (22.31) emerges as

$$O(\tilde{\Pi}_l) = \frac{\tilde{l}^{3\alpha-1}}{\tilde{\tau}_0^{3\alpha}} \quad (22.32)$$

The rate of deformation work $\tilde{\Pi}_l$ is for statistically steady state independent of the length scale \tilde{l} iff the Hölder exponent has the specific value $\alpha = \frac{1}{3}$.

This estimate has several important properties:

(i) The velocity is bounded according to (22.22) for all $0 < \alpha < 1$, but the rate of deformation work term may be singular. The singularity, if it exists, is of second order, see theorem (3.15) in Chap. 3.

(ii) If $\alpha > \frac{1}{3}$, then $\tilde{\Pi}_l \rightarrow 0$ as $l \rightarrow 0$ and the dissipation rate approaches zero as $Re \rightarrow \infty$. This was proved by Constantin et al. [25].

(iii) If $\alpha \leq \frac{1}{3}$, the velocity field is Hölder singular as $Re \rightarrow \infty$. The Onsager conjecture thus produced a testable property of dissipation rate for $Re \rightarrow \infty$.

22.2.3 Weierstrass Function

The Weierstrass function $W_\alpha(x)$ [26] is an example for Hölder continuous functions in 1-d for $0 < \alpha < 1$, and it is defined by

$$W_\alpha(x) \equiv \lim_{N \rightarrow \infty} \sum_{n=0}^N b^{-n\alpha} \cos(b^n \pi x) \quad (22.33)$$

where $b \geq 7$ is an odd integer and the constraint $ab > 1 + \frac{3\pi}{2}$ must be satisfied. The constraint implies that the derivative

$$\frac{dW_\alpha}{dx}(x) = -\pi \lim_{N \rightarrow \infty} \sum_{n=0}^N b^{n(1-\alpha)} \sin(b^n \pi x) \quad (22.34)$$

does not converge for any location x , since $0 < \alpha < 1$ and $b > 1$. The Hausdorff dimension of its graph is bounded from above by $D \leq 2 + \frac{\ln(a)}{\ln(b)}$, hence $1 \leq D \leq 2$ if $ab > 1$. The Hölder exponent is then

$$\alpha = -\frac{\ln(a)}{\ln(b)} \quad (22.35)$$

The Weierstrass function is, therefore, continuous, but nowhere differentiable for the values chosen for a and b . Figure 22.2 illustrates approximations (partial sums) of the Hölder continuous Weierstrass function (22.33) for two values of the Hölder exponent α . The lines in each graph show the function for the number of series terms N increasing from $N = 2$ to $N = 32$. Figure 22.3 shows the derived field (22.11) associated with the derivative of the Weierstrass function

$$b_W(x) \equiv \lim_{N \rightarrow \infty} \frac{\frac{dW}{dx}}{(1 + (\frac{dW}{dx})^2)^{\frac{1}{2}}} \quad (22.36)$$

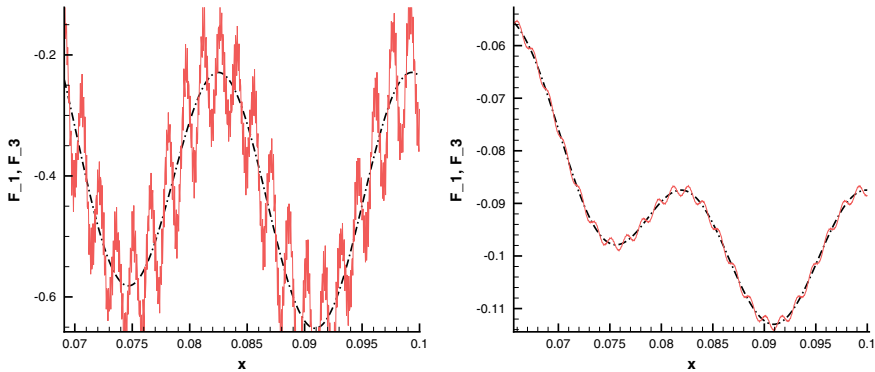


Fig. 22.2 Partial sums of the Weierstrass function $W(x)$ (22.33) for two Hölder exponents $\alpha = 1/3$ (left graph) and $\alpha = 0.95$ (right graph). The red line refers to $N = 32$ and the black dot-dashed line $N = 2$

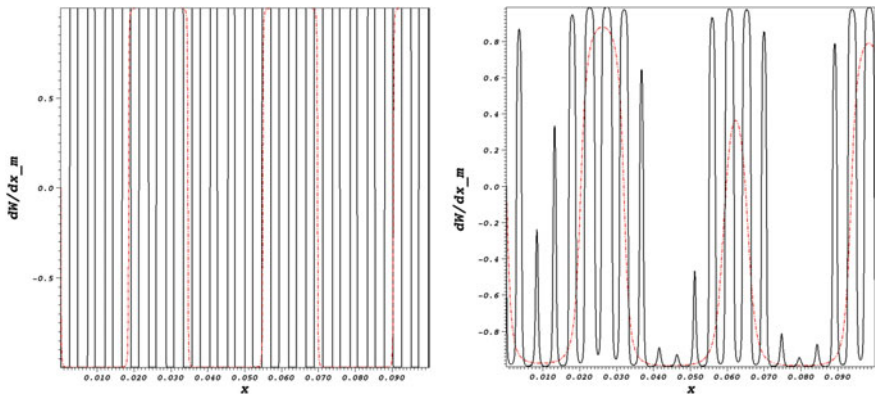


Fig. 22.3 Partial sums of the bounded field (22.11) defined by the derivative of the Weierstrass function (22.33) $b(x) = dW/dx / [1 + (dW/dx)^2]^{1/2}$ for two Hölder exponents $\alpha = 1/3$ (left graph) and $\alpha = 0.95$ (right graph). The black line refers to $N = 3$ and the red dot-dashed line $N = 2$. Note, that $-1 \leq b(x) \leq 1$ holds for the presentation of the singular derivative dW/dx

which plays the role of vorticity and where

$$\frac{dW_N}{dt}(x) \equiv -\pi \sum_{n=0}^N b^{n(1-\alpha)} \sin(b^n \pi x) \quad (22.37)$$

is the partial sum of the divergent derivative series (22.34). The evaluation of the partial sums of (22.36) in Fig. 22.3 is bounded but nowhere differentiable. Increasing the number N of series terms in dW_N/dx to compute $dW_N/dx / (1 + (dW_N/dx)^2)^{1/2}$ quickly fills the domain of the graph.

The idea of constructing smooth random functions as finite Fourier series that approach non-smooth functions as the wavelength approaches zero, such as the Weierstrass function and the Fourier–Wiener series,

$$f(x) = a_0 + \sqrt{2} \sum_{k=1}^m [a_k \cos\left(\frac{2\pi kx}{L}\right) + b_k \sin\left(\frac{2\pi kx}{L}\right)]$$

where L is the length of the periodicity interval and the coefficients a_k and b_k are independently Gaussian distributed, which has lead to useful tools for computational purposes, Filip et al. [27], for instance, in the Chebfun software package, [28]. They are an attractive alternative to designing random walks to generate random functions.

22.3 Duchon–Robert Distribution

It would be highly desirable to describe the emergence of singularities of the second kind in weak solutions of the Navier–Stokes pdes explicitly as term in the strong form of the mechanical energy equation. This has been proposed by Duchon and Robert [4], who constructed a term in the mechanical energy pde describing the lack of smoothness in the velocity field. They consider a cube with periodic boundary conditions as flow domain \mathcal{D} for mathematical convenience. The term is constructed with the aid of an infinitely differentiable, symmetric, positive mollifier, i.e. a scalar function $\varphi(\mathbf{x}) \geq 0$ with compact support in \mathcal{D} and finite integral scaling with $\epsilon > 0$ according to

$$\varphi_\epsilon(\mathbf{w}) = \frac{1}{\epsilon^3} \varphi\left(\frac{\mathbf{w}}{\epsilon}\right), \quad \lim_{\epsilon \rightarrow 0} \varphi_\epsilon(\mathbf{x}) = \delta(\mathbf{x}) \quad (22.38)$$

($\delta(\mathbf{x})$ is the Dirac pseudo-function). The limit $\epsilon \rightarrow 0$ of

$$D[\mathbf{v}] \equiv \lim_{\epsilon \rightarrow 0} D_\epsilon[\mathbf{v}] \quad (22.39)$$

defines a functional of \mathbf{v} independent of the φ , where

$$D_\epsilon[\mathbf{v}] = \frac{1}{4} \int_{\mathcal{D}_\varphi} d\mathbf{w} \nabla \varphi_\epsilon(\mathbf{w}) \cdot \Delta \mathbf{v} (\Delta \mathbf{v})^2 \quad (22.40)$$

and $\Delta(\mathbf{v}) \equiv \mathbf{v}(\mathbf{x} + \mathbf{w}) - \mathbf{v}(\mathbf{x})$ for \mathbf{x} and $\mathbf{x} + \mathbf{w}$ in the flow domain \mathcal{D} for a time interval $0 < T \leq \infty$. An example for the scalar $\varphi(\mathbf{w})$ defining the mollifier is given below.

Melander et al. [29] presented an explicit example for the scalar function $\varphi(\mathbf{i})$ in a different context. The tool for the design is the profile function ($r = \sqrt{\mathbf{i} \cdot \mathbf{i}}$)

$$e(r) \equiv \exp\left[-\frac{c}{r} \exp\left(\frac{1}{r-1}\right)\right] \in L^\infty_R, \quad 0 \leq r \leq 1$$

which has the unit interval $[0, 1]$ as compact support in R^1 for $c > 0$ ($e(0.5) = 0.5$ implies $c = 2.56085$). The scalar function is then defined as

$$\varphi(\mathbf{1}) \equiv \begin{cases} 1 & \text{for } r \leq r_i \\ 1 - \frac{e(r-r_i)}{r_o-r_i} & \text{for } r_i < r < r_o \\ 0 & \text{for } r_o \leq r \end{cases}$$

for $0 < r_i < r_o < 1$. The scalar $\varphi(r)$ is zero at $r = 1$ and in C^∞ , but does not have a Taylor series expansion, and hence is not analytic.

The mechanical energy equation for any weak solution of the Navier–Stokes pdes is easily derived from the Navier–Stokes pdes and modified by Duchon and Robert [4] as

$$\frac{\partial}{\partial t}\left(\frac{1}{2}\mathbf{v} \cdot \mathbf{v}\right) + \nabla \cdot (\mathbf{v}\left(\frac{1}{2}\mathbf{v} \cdot \mathbf{v} + p\right)) = \frac{1}{Re}\Delta\left(\frac{1}{2}\mathbf{v} \cdot \mathbf{v}\right) - \frac{1}{Re}\nabla\mathbf{v} : \nabla\mathbf{v} - D[\mathbf{v}] \quad (22.41)$$

The reduction of kinetic energy is thus due to two distinct reasons, viscous dissipation and the possible lack of smoothness of the velocity field. It is easy to show that $D[\mathbf{v}] = 0$ for smooth arguments \mathbf{v} , see the solution of Problem 22.3 in Appendix F.

22.4 The Physical Limit: Extrapolation of Smits' Formula for Pipe Flow

The results of the analysis obtained in the previous sections do not apply directly to turbulent shear flows bounded by fixed walls, since the local expectation of the dissipation rate does not approach a non-zero value as $Re \rightarrow \infty$ everywhere in the flow field. Hence, a near-wall layer has to be defined, such that the scaling relations hold for the core flow away from this layer, but not in it. It is proposed to define the near-wall layer by

$$\mathcal{D}_w \equiv \{\mathbf{x} \subset \mathcal{D} : D_\infty = 0\} \quad (22.42)$$

as the set of all points, where the asymptotic dissipation rate is zero. It is argued below using the available experimental evidence that the near-wall layer is not empty. The core layer is then the set of points $\mathcal{D} - \mathcal{D}_w$, where the Kolmogorov–Onsager conjecture $D_\infty > 0$ holds.

A vast amount of experimental evidence is available for pipe flow, check the IUTAM Proceedings [30] and references therein. The friction factor f is related to the wall stress by

$$f(Re, \frac{e}{d}) = \frac{8\tau_w}{\rho U^2} \quad (22.43)$$

where τ_w is the wall shear stress and U is the bulk velocity (mass flow divided by density and area), which can be represented by Prandtl's universal law of friction for smooth pipes (Schlichting [31]) based on Nikuradse's [32] 1933 experimental data

$$\frac{1}{\sqrt{f}} = 2 \log(Re\sqrt{f}) - 0.8 \quad (22.44)$$

where the Reynolds number is now defined by (U is the bulk velocity, d is the pipe diameter)

$$Re = \frac{Ud}{\nu} \quad (22.45)$$

and for rough pipes

$$\frac{1}{\sqrt{f}} = 2 \log\left(\frac{d}{e}\right) + 1.14 \quad (22.46)$$

where e is the average roughness height. Both correlations have been established by experiments in the range $5 \cdot 10^5 \leq Re \leq 3 \cdot 10^6$. The recent measurements of Smits and collaborators [33] in their compressed pipe extended the range of Reynolds numbers considerably. Zagarola and Smits propose [33] new friction factor correlations (recently updated in McKeon et al. [34])

$$\frac{1}{\sqrt{f}} = 1.884 \log(Re\sqrt{f}) - 0.331 \quad (22.47)$$

valid for $10^4 \leq Re \leq 3.5 \cdot 10^7$ and

$$\frac{1}{\sqrt{f}} = 1.869 \log(Re\sqrt{f}) - 0.241 - \frac{233}{(Re\sqrt{f})^{0.9}} \quad (22.48)$$

valid in the same Reynolds number range but also accounting for the near-wall velocity profile. Assuming validity of the experimental correlation (22.44) for smooth pipes to higher Reynolds numbers shows (Fig. 22.4) that the friction factor decays quickly with Reynolds number. It is easy to see that the limit value for f as $Re \rightarrow \infty$ is indeed zero. The first two experimental correlations can be written in the form

$$\frac{1 - \alpha\sqrt{f} \log(\sqrt{f})}{\sqrt{f}} = \alpha \log(Re) - \beta \quad (22.49)$$

(where $\alpha = 2, \beta = 0.8$ for (22.44) and $\alpha = 1.884, \beta = 0.331$ for (22.47)), which proves that $\lim_{Re \rightarrow \infty} f = 0$ since the right side approaches ∞ and the only limit value for f , that is consistent with it, is zero. A slight modification of this argument shows that the same holds for (22.48). Hence, it could be speculated that the limit $Re \rightarrow \infty$ of the friction factor for smooth pipes is zero. On the other hand, the correlation for rough pipes (22.46) is independent of the Reynolds number, hence clearly indicating

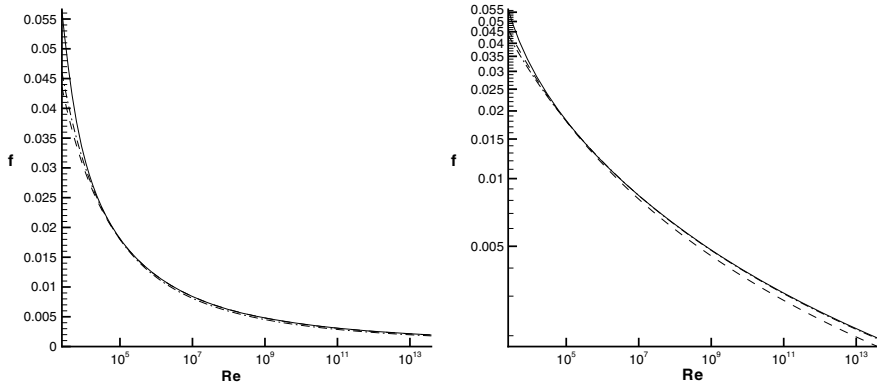


Fig. 22.4 Friction coefficient for smooth pipes as function of Reynolds number (semi-logarithmic scale left and logarithmic scale right figure) for the Prandtl correlation (22.44) (dot-dashed line), the Smits correlation (22.47) (dashed line) and the Smits correlation accounting for the near-wall velocity (22.48) (full line). The limit of f for $Re \rightarrow \infty$ is zero for all extrapolated experimental correlations

a non-zero limit, again assuming that the experimental correlation can be extended to the limit.

The limit of zero viscosity, hence the only acceptable limit of infinite Reynolds number as argued above, can be achieved to experimental accuracy for liquid Helium II (superfluid Helium) below the λ -temperature of about two Kelvin [35]. For temperatures close to absolute zero, liquid Helium consists essentially of the inviscid superfluid Helium. Turbulent flows of superfluid Helium II can be generated, for instance, by moving a grid through the fluid in a cylinder. The mechanism of shear generated vorticity is absent for the inviscid Helium II, but turbulence is created, which decays similar to classical fluid turbulence. Quantum-mechanical effects lead to the appearance of vortex filaments with diameter on the atomic scale. The line vortices with quantized circulation interact by spontaneously reconnecting, which is a Quantum-mechanical phenomenon. It is thought that the classical viscous dissipation is replaced by a dissipative process generating sound during the reconnection events (Vinen, [36]). The dynamics of superfluid Helium at zero temperature is described by the nonlinear Schroedinger equation for a weakly interacting Bose–Einstein condensate (see Vinen, [36] for details), which leads to modified Euler equations if the chemical potential of a boson and the strength of the repulsive interaction between bosons are specified. The modified Euler equations contain a quantum stress tensor, and hence they are not the limit of the classical Navier–Stokes equations for zero viscosity. It follows that Helium II does not behave like a classical viscous fluid in the limit of zero viscosity.

The extrapolation of experimental evidence raises several fundamental questions:

- (i) Does a limit $Re \rightarrow \infty$ exist for fluids that satisfy the classical Navier–Stokes as the limit of zero viscosity is approached? What is the relation of the solutions of the Navier–Stokes equations as $Re \rightarrow \infty$ to the Euler equations?

(ii) Is there such a thing as a smooth pipe for $Re \rightarrow \infty$ for the limit of zero viscosity?

(iii) If all pipes are rough for the limit, does a limit exist for rough pipes? If yes, how does it depend on roughness?

22.4.1 Existence of a Physical Limit

The physical realization of the zero viscosity limit can be achieved, if ν is a monotonically increasing function of the absolute temperature with zero as limit for $T = 0$. However, the only substance known to exhibit a liquid phase with zero viscosity is Helium, all other gases become solid as zero temperature is approached. But Helium II is not a suitable candidate for the zero viscosity limit of classical flows governed by the Navier–Stokes equations, since its motion is influenced by quantum-mechanical effects and turbulence decays via a different mechanism [36]. The alternative method of increasing the Reynolds number (2.8) is compression, which has been done successfully by Smits [33], in the superpipe experiments.

22.5 The Mathematical Limit

Navier–Stokes turbulence is described either by the phase space Ω of the Navier–Stokes equations (Sect. 5.2) and the turbulence measure μ or the the nuclear space \mathcal{N} of test functions and the characteristic functional $\theta[\mathbf{y}]$ governed by the Hopf equation (9.40) as derived in Sect. 9.2. The phase space Ω is the dual space \mathcal{N}' of the nuclear space \mathcal{N} of test functions. The limit $Re \rightarrow \infty$ can be applied in two distinct ways:

(i) The solution $\theta[\mathbf{y}; t, Re]$ of the Hopf equation (9.40) is subject to the limit operation $\theta[\mathbf{y}; t, \infty] = \lim_{Re \rightarrow \infty} \theta[\mathbf{y}; t, Re]$.

(ii) The Hopf equation (9.40) is subject to the limit operation.

The limit (ii) of infinite Reynolds number can be investigated for the Hopf equation and its domain of definition \mathcal{N} for the characteristic functional $\theta[\mathbf{y}(\mathbf{x}); t]$ by letting $\tilde{\nu} \rightarrow 0/ Re \rightarrow \infty$

$$\theta[\mathbf{y}(\mathbf{x}); t] = \langle \exp[i \int_{\mathcal{D}} d\mathbf{x} \mathbf{y}(\mathbf{x}) \cdot \mathbf{v}(\mathbf{x}, t)] \rangle \quad (22.50)$$

where $\mathbf{y}(\mathbf{x}) \in \mathcal{N}$ is the argument vector field and $\mathbf{x} \in \mathcal{D}$, t denote the parametric dependence on location and time. The angular brackets (21.1) denote the statistical expectation operator, and the probabilistic operator is defined by (6.4) in Sect. 9.2.

The derivation of the Hopf equation associated with the Euler equations is

$$\frac{\partial}{\partial t} \theta[\mathbf{y}; t] = \int_{\mathcal{D}} d\mathbf{x} y_\alpha(\mathbf{x}) \left\{ i \frac{\partial}{\partial x_\beta} \lim_{\mathbf{x}' \rightarrow \mathbf{x}} \frac{\delta^2 \theta}{\delta y_\beta(\mathbf{x}') \delta y_\alpha(\mathbf{x})} [\mathbf{y}; t] + i P_\alpha[\mathbf{y}; t, \mathbf{x}] + i \left(\frac{1}{Fr} g_\alpha(\mathbf{x}) - \frac{\partial P_0}{\partial x_\alpha} \right) \theta[\mathbf{y}; t] \right\} \quad (22.51)$$

where the contribution of the pressure gradient follows (9.25) and (9.26) in Sect. 9.2.3 by setting the viscous terms to zero, and the result is then

$$\begin{aligned} P_\alpha[\mathbf{y}; t, \mathbf{x}] &\equiv \int_{\mathcal{D}} d\nu(\tilde{\mathbf{x}}) \frac{\partial G}{\partial x_\alpha}(\mathbf{x}, \tilde{\mathbf{x}}) \frac{\partial^2}{\partial \tilde{x}_\gamma \partial \tilde{x}_\beta} \frac{\delta^2 \theta}{\delta y_\gamma \delta y_\beta} [\mathbf{y}; t, \tilde{\mathbf{x}}, \tilde{\mathbf{x}}] \\ &+ \int_{\partial\mathcal{D}} dA(\tilde{\mathbf{x}}) \frac{\partial G}{\partial x_\alpha}(\mathbf{x}, \tilde{\mathbf{x}}) n_\gamma(\tilde{\mathbf{x}}) \left\{ \frac{\partial}{\partial \tilde{x}_\beta} \frac{\delta^2 \theta}{\delta y_\beta \delta y_\gamma} [\mathbf{y}; t, \tilde{\mathbf{x}}, \tilde{\mathbf{x}}] + (g_\gamma - \frac{\partial v_\gamma^b}{\partial t}(t, \tilde{\mathbf{x}})) \theta[\mathbf{y}; t] \right\} \end{aligned} \quad (22.52)$$

The Green's function appears in the volume and surface integrals, the latter contain the time derivative of the boundary values for velocity $v_\gamma^b(t, \mathbf{x})$.

22.5.1 Hopffde for the Limit (ii) of Infinite Reynolds Number

The case of an inviscid fluid governed by the Euler equations is of particular interest since it is relevant to the limit of infinite Reynolds number of the Navier–Stokes pdes. The assumption

$$\lim_{Re \rightarrow \infty} (\hat{y}_\alpha(\mathbf{k}), \frac{k^2}{Re} \frac{\delta \theta}{\delta \hat{y}_\alpha(\mathbf{k})}) = 0, \quad \forall \hat{\mathbf{y}} \in \mathcal{N} \quad (22.53)$$

in an open neighbourhood $U \subset \mathcal{N}$ of the origin, which leads to the fde

$$\frac{\partial \theta}{\partial t} = (\hat{y}_\alpha(\mathbf{k}), k_\beta P_{\alpha\gamma} \int d\mathbf{k}' \frac{\delta^2 \theta}{\delta \hat{y}_\beta(\mathbf{k} - \mathbf{k}') \delta \hat{y}_\gamma(\mathbf{k}')}) \quad (22.54)$$

This is one of the possibilities for the inviscid fde for solutions of the Euler pdes that remain smooth enough as $Re \rightarrow \infty$, such that the assumption (22.53) holds. However, it is clear that the assumption (22.53) is inconsistent with the Kolmogorov hypotheses (see Chap. 17) resting on the assumption: The rate of dissipation of kinetic energy contained in the fluctuations is defined by

$$\langle \epsilon \rangle \equiv \frac{1}{Re} \langle \frac{\partial v'_\alpha}{\partial x_\beta} \frac{\partial v'_\alpha}{\partial x_\beta} \rangle \quad (22.55)$$

approaches a bounded, non-zero and well-defined limit $\langle \epsilon \rangle_\infty$ as $Re \rightarrow \infty$. To see the relation of the dissipation rate $\langle \epsilon \rangle$ to the assumption (22.53), $\langle \epsilon \rangle$ is expressed in terms of the characteristic functional.

The instantaneous dissipation rate $\epsilon(\mathbf{x})$ is the inverse Fourier transform of the spectral dissipation rate $\hat{\epsilon}(\mathbf{k})$

$$\epsilon(\mathbf{x}) = \frac{1}{(2\pi)^3} \int_{R^3} d\mathbf{k} \hat{\epsilon}(\mathbf{k}) \exp(i\mathbf{x} \cdot \mathbf{k}) = \mathcal{F}^{-1} \hat{\epsilon}(\mathbf{k}) \quad (22.56)$$

where the spectral dissipation rate is

$$\hat{\epsilon}(\mathbf{k}) = -\frac{1}{Re} \frac{1}{(2\pi)^3} \int_{R^3} d\mathbf{k}' k'_\beta (k_\beta - k'_\beta) \hat{v}_\alpha(\mathbf{k}') \hat{v}_\alpha(\mathbf{k} - \mathbf{k}') \quad (22.57)$$

The integral in (22.57) is recognized as convolution (15.3), hence is the spectral dissipation rate

$$\hat{\epsilon}(\mathbf{k}) = -\frac{1}{Re} (k_\beta \hat{v}_\alpha) * (k_\beta \hat{v}_\alpha) \quad (22.58)$$

the convolution of first derivatives. The second Fréchet derivative

$$\frac{\delta^2 \theta[\hat{\mathbf{y}}]}{\delta \hat{y}_\alpha(\mathbf{k}) \delta \hat{y}_\alpha(\mathbf{k} - \mathbf{k}')} = -\langle \hat{v}_\alpha(\mathbf{k}) \hat{v}_\alpha(\mathbf{k} - \mathbf{k}') \exp[i(\hat{\mathbf{y}}, \hat{\mathbf{v}})] \rangle \quad (22.59)$$

can be adapted to generate the desired relation of the spectral dissipation rate

$$\langle \hat{\epsilon}(\mathbf{k}) \exp[i(\hat{\mathbf{y}}, \hat{\mathbf{v}})] \rangle = \frac{1}{Re} \frac{1}{(2\pi)^3} \int_{R^3} d\mathbf{k}' k'_\beta (k_\beta - k'_\beta) \frac{\delta^2 \theta[\hat{\mathbf{y}}]}{\delta \hat{y}_\alpha(\mathbf{k}') \delta \hat{y}_\alpha(\mathbf{k} - \mathbf{k}')} \quad (22.60)$$

to the characteristic functional. The expectation of the spectral dissipation rate is then the right side expression at the origin $\hat{\mathbf{y}} = 0$

$$\langle \hat{\epsilon}(\mathbf{k}) \rangle = \frac{1}{Re} \frac{1}{(2\pi)^3} \int_{R^3} d\mathbf{k}' k'_\beta (k_\beta - k'_\beta) \frac{\delta^2 \theta[\hat{\mathbf{y}}]}{\delta \hat{y}_\alpha(\mathbf{k}') \delta \hat{y}_\alpha(\mathbf{k} - \mathbf{k}')} \Big|_{\hat{\mathbf{y}}=0} \quad (22.61)$$

of the test function space \mathcal{N} . Assumption (22.53) implies that the first Fréchet derivative is zero for all $\hat{\mathbf{y}} \in \mathcal{N}$ in an open neighbourhood U of the origin, hence is the second derivative zero in this neighbourhood. Hence, Assumption (22.53) implies that the dissipation rate is zero thus contradicting the Kolmogorov–Onsager conjecture. This rough outline of the Reynolds number limit deserves further analysis.

Summary

The expression (22.61) obtained for the spectral dissipation rate depends essentially on the second functional derivative of the characteristic functional at the origin of the test function space \mathcal{N} . The regularity properties of this second derivative depend, in turn, on the characteristic functional and the test function space. Assumption (22.53) put forward in Sect. 22.5.1 raises several fundamental questions: What are the smoothness properties of the solutions of the Euler pdes, which are generated as limit of the Navier–Stokes solutions as $Re \rightarrow \infty$? What is the structure of eventual singularities of the second kind in the solutions of the Euler pdes? These questions remain unresolved so far.

22.6 Problems for this Chapter

Problem 22.1 Consider a materially invariant admissible circuit \mathcal{C} , as defined in Sect. 2.6.3, embedded in a flow field \mathcal{D} . The incompressible fluid is in turbulent motion governed by the Navier–Stokes pdes. Assume that appropriate reference values exist and the Reynolds number $Re \gg 1$ is well defined.

22.1.1 establish the time rate of change of circulation Γ defined in the material description by

$$\Gamma(\mathcal{C}, \tau) = \int_{\mathcal{C}(\tau)} \mathbf{V}(\tau, \mathbf{X}(p)) \cdot d\Phi(\tau, \mathbf{X}(p)) \quad (22.62)$$

where the circuit \mathcal{C} at the reference time is specified by $\mathbf{X}(p)$ with $0 \leq p \leq 1$ being Lagrangean line parameter (Lagrangean line parameters are materially invariant), $\Phi(\tau, \mathbf{X})$ denotes the position of a material point at time τ that was at \mathbf{X} at the reference time. Velocity in the material description is by definition $\mathbf{V} = \frac{\partial \Phi}{\partial \tau}$.

22.1.2: Transform the result of (22.1.1) to the spatial description.

22.1.3: Compute the circulation using the Navier–Stokes pdes for $0 \ll Re < \infty$ and inviscid fluids.

22.1.4: Evaluate the limit $Re \rightarrow \infty$ under following assumptions:

(a) The vorticity field remains smooth ! $\in C_{\mathcal{D}}^1$.

(b) The vorticity field becomes Hölder continuous with exponent $\alpha \leq \frac{1}{3}$.

Problem 22.2 Orlandi and Carnevale [37] argue that the nonlinear amplification of vorticity in inviscid interaction is a candidate for the appearance of a finite-time singularity of the second kind starting from smooth initial data, check Eq. (3.15) in Chap. 3 for definition. The ode

$$\frac{\partial \Phi}{\partial t} = \Phi^2$$

with initial condition $\Phi(0) > 0$ is a simplified version of the vorticity pde. It has a finite-time singularity developing from positive initial data. Prove this.

Problem 22.3 Show that the Duchon–Robert smoothness term $D(\mathbf{v})$ in Sect. 22.3 is zero for the following class of velocity fields $\mathbf{v}(\mathbf{x}, t)$:

$$\int_{\mathcal{D}} d\mathbf{w} |\mathbf{v}(\mathbf{x} + \mathbf{w}, t) - \mathbf{v}(\mathbf{x}, t)|^3 \leq C(t) |\mathbf{w}| \sigma(|\mathbf{w}|)$$

where $\int_0^T dt C(t) < \infty$ and $\lim_{|\mathbf{w}| \rightarrow 0} \sigma(|\mathbf{w}|) = 0$.

References

1. Smits, A.J., McKeon, B.J., Marusic, I.: High-Reynolds number wall turbulence. *Annu. Rev. Fluid Mech.* **43**, 353–375 (2011)
2. Onsager, L.: Statistical hydrodynamics. *Nuovo Cimento* **6**(Suppl.), 279–287 (1949)
3. Eyink, G.L.: Dissipative anomalies in singular Euler flows. *Physica D* **237**, 1956–1968 (2008)
4. Duchon, J., Robert, R.: Inertial energy dissipation for weak solutions of incompressible Euler and Navier–Stokes equations. *Nonlinearity* **13**, 249–255 (2000)
5. Sagaut, P.: *Large Eddy Simulation for Incompressible Flows*. Springer, Berlin (1998)
6. Garnier, E., Adams, N., Sagaut, P.: *Large Eddy Simulation for Compressible Flows*. Springer, New York (2009)
7. Truesdell, C.A.: *The Kinematics of Vorticity*. Indiana University Press, Bloomington, Indiana (1954)
8. Saffman, P.G.: *Vortex Dynamics*. Cambridge University Press, Cambridge, U.K. (1992)
9. Majda, A.J., Bertozzi, A.L.: *Vorticity and Incompressible Flow*. Cambridge University Press, Cambridge, U.K. (2002)
10. Wu, J.-Z., Ma, H.-Y., Zhou, M.-D.: *Vorticity and Vortex Dynamics*. Springer, Berlin (2006)
11. Vladimirov, V.A., Moffatt, H.K.: On general transformations and variational principles for the magnetohydrodynamics of ideal fluids. Part 1. Fundamental principles. *JFM* **283**, 125–139 (2001)
12. Kollmann, W.: *Fluid Mechanics in Spatial and Material Description*. University Readers, San Diego (2011)
13. Gibbon, J.D.: The three-dimensional Euler equations: where do we stand? *Physica D* **237**, 1894–1904 (2008)
14. Kerr, R.M.: The role of singularities in turbulence. In: Kida, S. (ed.) *Unstable and Turbulent Motion in Fluids*, World Scientific Publishing, Singapore
15. Kerr, R.M.: A new role for vorticity and singular dynamics in turbulence. In: Debnath, L. (ed.) *Nonlinear Instability Analysis*, vol. II, pp. 15–68. WIT Press, Southampton U.K. (2001)
16. Orlandi, P., Pirozzoli, S., Carnevale, G.F.: Vortex events in Euler and Navier–Stokes simulations with smooth initial conditions. *JFM* **690**, 288–320 (2012)
17. Kolmogorov, A.N.: The local structure of turbulence in incompressible viscous fluid for very large Reynolds numbers. *Dokl. Akad. Nauk SSSR* **30**, 9–13 (1941)
18. Sreenivasan, K.R.: An update on the energy dissipation rate in isotropic turbulence. *Phys. Fluids* **10**, 528–529 (1998)
19. Kaneda, Y., Ishihara, T., Yokokawa, M., Uno, A.: Energy dissipation rate and energy spectrum in high resolution direct numerical simulations of turbulence in a box. *Phys. Fluids* **15**, L21 (2003)
20. Pearson, B.R., Krogstad, P.A., van de Water, W.: Measurements of the turbulent energy dissipation rate. *Phys. Fluids* **14**, 1288–1290 (2002)

21. Mydlarski, L., Wahrhaft, Z.: On the onset of high-Reynolds-number grid-generated wind tunnel turbulence. *JFM* **320**, 331 (1996)
22. Mydlarski, L., Wahrhaft, Z.: Passive scalar statistics in high-Peclet-number grid turbulence. *JFM* **358**, 135 (1998)
23. Gamard, S., George, W.K.: Reynolds number dependence of energy spectra in the overlap region of isotropic turbulence. *Flow Turbul. Comb.* **63**, 443 (1999)
24. Tennekes, H., Lumley, J.L.: *A First Course in Turbulence*. MIT Press, Cambridge MA (1972)
25. Constantin, P., Weinan, E., Titi, E.S.: Onsager's conjecture on the energy conservation for solutions of Euler's equation. *Commun. Math. Phys.* **165**, 207–209 (1994)
26. Falconer, K.: *The Geometry of Fractal Sets*. Oxford University Press (1984)
27. Filip, S., Javeed, A., Trefethen, L.N.: Smooth random functions, Random ODE's and Gaussian processes. *SIAM Rev.* **61**, 185–205 (2019)
28. Driscoll, T.A., Hale, N., Trefethen, L.N.: *Chebfun Guide*. Pafnuty Publications, Oxford (2014)
29. Melander, M.V., McWilliams, J.C., Zabusky, N.J.: Axisymmetrization and vorticity-gradient intensification of an isolated two-dimensional vortex through filamentation. *JFM* **178**, 137–159 (1987)
30. Smits, A.J. (ed.): *IUTAM Symposium on Reynolds Number Scaling in Turbulent Flow*. Kluwer Academic Publishers, Dordrecht (2004)
31. Schlichting, H.: *Boundary Layer Theory*. McGraw-Hill (1987)
32. Nikuradse, J.: Laws of flow in rough pipes. *NACA TM* **1292**, (1933)
33. Zagarola, M.V., Smits, A.J.: Mean-flow scaling of turbulent pipe flow. *JFM* **373**, 33–79 (1998)
34. McKeon, B.J., Swanson, C.J., Zagarola, M.V., Donnelly, R.J., Smits, A.J.: Friction factors for smooth pipe flow. *JFM* **511**, 41–44 (2004)
35. Donnelly, R.J.: Background on Superfluid Turbulence. In: Smits, A.J. (ed.) *IUTAM Symposium on Reynolds Number Scaling in Turbulent Flow*, pp. 92–100. Kluwer Academic Publishers, Dordrecht (2004)
36. Vinen, W.F.: Superfluid Turbulence: Experiments, Physical Principles, and Outstanding Problems. In: Smits, A.J. (ed.) *IUTAM Symposium on Reynolds Number Scaling in Turbulent Flow*, pp. 101–108. Kluwer Academic Publishers, Dordrecht (2004)
37. Orlandi, P., Carnevale, G.F.: Nonlinear amplification of vorticity in inviscid interaction of orthogonal Lamb dipoles. *Phys. Fluids* **19**, 057106 (2007)

Chapter 23

Appendix A: Mathematical Tools



The derivation and analysis of the basic equation describing turbulence generated by solutions of the Navier–Stokes equations require several mathematical tools collected and briefly discussed and relevant references are given in the present appendix.

23.1 Compactness

Let T be a topological space (Munkres [1] general topology, Hatcher [2] algebraic topology) and $\mathcal{G} = \{G_\alpha\}$ a collection of open subsets of T , a subset S of T is compact if every open covering \mathcal{G}

$$S \subseteq \bigcup_{\alpha} G_{\alpha} \quad (23.1)$$

of S has a finite subcovering $\{G_{\alpha 1}, \dots, G_{\alpha n}\}$.

23.2 Limits

Let $\{x_k, k = 1, \dots, \infty\}$ be a sequence of numbers, then is the limit inferior defined by

$$\liminf_{n \rightarrow \infty} x_n \equiv \lim_{n \rightarrow \infty} (\inf_{k \geq n} x_k) = \varliminf_{n \rightarrow \infty} x_n \quad (23.2)$$

where \inf denotes the infimum of the sequence, and the limit superior by

$$\limsup_{n \rightarrow \infty} x_n \equiv \lim_{n \rightarrow \infty} (\sup_{k \geq n} x_k) = \varlimsup_{n \rightarrow \infty} x_n \quad (23.3)$$

where \sup denotes the supremum of the sequence.

23.3 Caratheodory, Hausdorff and Box Dimensions

The dimension is an intrinsic property of a mathematical object independent of the space in which the object is embedded. Several definitions of dimension will be given for spaces relevant to the theory of turbulent fluid flow.

Euclidean space R^n : The notion of dimension is generalized from the usual topological dimension, which assumes only integer values, to deal with complex structures. There are several, closely related dimensions that serve this purpose. They can be regarded as indicator of complexity of the structures emerging in turbulent flows.

Caratheodory measure and dimension

The starting point is the construction of a measure (the size in a general sense) of a set X that leads to the dimension of the set. The Caratheodory structure for a set X is a collection \mathcal{F} of subsets of X with $\emptyset \in \mathcal{F}$ (Pesin, [3], Chap. 1) and three set functions $\zeta, \eta, \psi : \mathcal{F} \rightarrow [0, \infty)$ with the following properties. It is assumed that two of the three set functions η and ψ can be constructed, satisfying three conditions:

$$(A.1) \eta(\emptyset) = \psi(\emptyset) = 0 \text{ and } \eta(U), \psi(U) > 0 \forall U \neq \emptyset \in \mathcal{F};$$

(A.2) For any $\delta > 0, \epsilon > 0$ can be found such that $\eta(U) < \delta$ for all $U \in \mathcal{F}$ with $\psi(U) \leq \epsilon$;

(A.3) For any $\epsilon > 0$ there exists a finite or countable subcollection $\mathcal{G} \subset \mathcal{F}$ such that $X \subset \bigcup_{U \in \mathcal{G}} U$ and $\psi(\mathcal{G}) \equiv \sup\{\psi(U) : U \in \mathcal{G}\} \leq \epsilon$.

The set function ζ is a tool to extend the applicability of the C -structure. A collection of subsets \mathcal{F} and three set functions ζ and η, ψ satisfying (A.1), (A.2), (A.3) is called C -structure (Caratheodory dimension structure) $\tau = (\mathcal{F}, \zeta, \eta, \psi)$ on X . For a subset $Z \subset X$ and two numbers $\alpha \in R, \epsilon > 0$, the Caratheodory α -measure $m_C(Z, \alpha)$ is constructed using

$$M_C(Z, \alpha, \epsilon) \equiv \inf_{\mathcal{G}} \left\{ \sum_{U \in \mathcal{G}} \zeta(U) \eta(U)^\alpha \right\} \quad (23.4)$$

where the infimum is taken over all finite or countable subcollections \mathcal{G} covering Z . The Caratheodory α -measure is then defined as the limit $\epsilon \rightarrow 0$ of M_C

$$m_C(Z, \alpha) = \lim_{\epsilon \rightarrow 0} M_C(Z, \alpha, \epsilon) \quad (23.5)$$

for the C -structure on X . It has the properties

$$(C.1) m_C(\emptyset, \alpha) = 0 \text{ for } \alpha > 0;$$

$$(C.2) m_C(Z_1, \alpha) \leq m_C(Z_2, \alpha) \text{ for } Z_1 \subset Z_2 \subset X;$$

$$(C.3) m_C\left(\bigcup_{i \geq 0} Z_i, \alpha\right) \leq \sum_{i \geq 0} m_C(Z_i, \alpha) \text{ for } Z_i \subset X, i = 1, 2, \dots$$

This measure has a crucial property due to (C.2) that determines the dimension. Let the subset Z be fixed, then exists a critical value $-\infty \leq \alpha_c \leq \infty$ such that

$$m_C(Z, \alpha) = \infty \text{ for } \alpha < \alpha_c, \quad m_C(Z, \alpha) = 0 \text{ for } \alpha > \alpha_c \quad (23.6)$$

holds, the proof is elementary, see [3], Proposition 1.2. This critical value is called the Caratheodory dimension of the subset Z :

$$d_C(Z) \equiv \alpha_c = \inf\{\alpha : m_C(Z, \alpha) = 0\} = \sup\{\alpha : m_C(Z, \alpha) = \infty\} \quad (23.7)$$

It has the following properties:

- (D.1) $d_C(\emptyset) \leq 0$;
- (D.2) $d_C(Z_1) \leq d_C(Z_2)$ for $Z_1 \subset Z_2 \subset X$;
- (D.3) $d_C(\bigcup_{i \geq 0} Z_i) = \sup_{i \geq 0} d_C(Z_i)$ where $Z_i \subset X$ for $i = 1, 2, \dots$

Hausdorff measure and dimension

The Hausdorff dimension is obtained as special case of the Caratheodory dimension by making the following choices: The set X is the Euclidean space R^m endowed with a metric $\rho(x, y)$, the collection of subsets \mathcal{F} is defined as the collection of all open subsets of R^m and the set functions are defined as $\zeta(U) = 1$, $\eta(U) = \psi(U) = \text{diam}(U)$ for all $U \in \mathcal{F}$, where the diameter of an open subset is defined by $\text{diam}(U) \equiv \sup_{x, y \in U} \rho(x, y)$. The Hausdorff α -measure of $Z \subset R^m$ for $\alpha \geq 0$ is then defined by

$$m_H(Z, \alpha) = \liminf_{\epsilon \rightarrow 0} \inf_{\mathcal{G}} \left\{ \sum_{U \in \mathcal{G}} (\text{diam}U)^\alpha \right\} \quad (23.8)$$

and the Hausdorff dimension is

$$d_H(Z) = \inf\{\alpha : m_H(Z, \alpha) = 0\} = \sup\{\alpha : m_H(Z, \alpha) = \infty\} \quad (23.9)$$

The Hausdorff dimension has the following properties (Pesin [3], Chap. 2):

- (H.1) $d_H(\emptyset) \leq 0$ and $d_H(Z) \geq 0$ for any $Z \subset R^m$;
- (H.2) $d_H(Z_1) \leq d_H(Z_2)$ for $Z_1 \subset Z_2 \subset R^m$;
- (H.3) $d_H(\bigcup_{i \geq 0} Z_i) = \sup_{i \geq 0} d_H(Z_i)$ where $Z_i \subset R^m$ for $i = 1, 2, \dots$;
- (H.4) If Z is a finite or countable set, the $d_H(Z) = 0$.

Box dimensions

Choosing on R^m the same C -structure as for the Hausdorff measure, the upper and lower box dimensions \bar{d}_B , \underline{d}_B can be defined with the finite or countable coverings \mathcal{G} generated by open sets of diameter ϵ as

$$\begin{aligned} \bar{d}_B(Z) &= \inf\{\alpha : \bar{r}_B(Z, \alpha) = 0\} = \sup\{\alpha : \bar{r}_B(Z, \alpha) = \infty\} \\ \underline{d}_B(Z) &= \inf\{\alpha : \underline{r}_B(Z, \alpha) = 0\} = \sup\{\alpha : \underline{r}_B(Z, \alpha) = \infty\} \end{aligned} \quad (23.10)$$

where

$$\bar{r}_B(Z, \alpha) = \overline{\liminf}_{\epsilon \rightarrow 0} \inf_{\mathcal{G}} \left\{ \sum_{U \in \mathcal{G}} \epsilon^\alpha \right\}, \quad \underline{r}_B(Z, \alpha) = \underline{\liminf}_{\epsilon \rightarrow 0} \inf_{\mathcal{G}} \left\{ \sum_{U \in \mathcal{G}} \epsilon^\alpha \right\} \quad (23.11)$$

where $\overline{\lim}$ and varliminf are defined by (23.3) and (23.2). Theorem 2.2 in Sect. 1.2 of [3] implies an equivalent definition of the upper and lower box dimensions

$$\overline{d}_B(Z) = \overline{\lim}_{\epsilon \rightarrow 0} \frac{\log N(Z, \epsilon)}{\log \frac{1}{\epsilon}}, \quad \underline{d}_B(Z) = \lim_{\epsilon \rightarrow 0} \frac{\log N(Z, \epsilon)}{\log \frac{1}{\epsilon}} \quad (23.12)$$

where $N(Z, \epsilon)$ is the least number of balls with radius ϵ to cover subset Z .

23.4 Chaos

A dynamical system is chaotic iff (Ruelle, [4], Wiggins [5] Chap. 30)

- (i) The system is sensitive to initial conditions,
- (ii) It is topologically mixing,
- (iii) It has dense periodic orbits.

are satisfied. Topological mixing is defined for continuous maps $T_t : \Omega \rightarrow \Omega$ of a topological space Ω onto itself as the property that there exists an integer $N > 0$ such that for two open sets $A, B \subset \Omega$ $T_{nt}(A) \cap B \neq \emptyset$ for $n > N$ applications of the map T_t . The periodic solutions (orbits) of the system are dense in phase space Ω if every point is approached arbitrarily close by the solutions. Lorenz (1963) [6] summarized (i) as ‘When the present determines the future, but the approximate present does not approximately determine the future’.

Note that chaotic systems do not necessarily possess a mechanism for spreading energy over the whole range of scales/modes. Turbulence has such a mechanism, in the spatial description recognized as the nonlinear convective term, hence the property chaotic is not sufficient to define turbulence, as has been argued in Sect. 3.1.

23.5 Levi-Civita Symbol

The Levi-Civita symbol $\epsilon_{\alpha\beta\gamma}$ is defined by

$$\epsilon_{\alpha\beta\gamma} \equiv \begin{cases} 1 & \text{for } (\alpha\beta\gamma) = (1, 2, 3), (2, 3, 1), (3, 1, 2) \\ -1 & \text{for } (\alpha\beta\gamma) = (1, 3, 2), (3, 2, 1), (2, 1, 3) \\ 0 & \text{otherwise} \end{cases} \quad (23.13)$$

The Levi-Civita symbol is a pseudotensor, because under an orthogonal transformation of Jacobian determinant $J = -1$ (i.e. a rotation composed with a reflection),

it acquires a minus sign. It is antisymmetric, i.e. $\epsilon_{\alpha\beta\gamma} = -\epsilon_{\beta\alpha,\gamma}$, $\epsilon_{\alpha\beta\gamma} = -\epsilon_{\alpha\gamma,\beta}$, $\epsilon_{\alpha\beta\gamma} = -\epsilon_{\gamma\beta,\alpha}$. The Levi-Civita symbol is applied to the computation of determinants, vector products and related expressions.

23.6 Multi-index Notation

Consider a smooth, M -dimensional vector function $\mathbf{F}(\mathbf{x}, \mathbf{y}, \dots)$ with derivatives up to order p , where $\mathbf{x} \in R^n$ is the independent variable/vector and $\mathbf{y}(\mathbf{x}) \in R^M$ the dependent variables. Partial derivatives are denoted compactly using multi-indices $\alpha = (\alpha_1, \alpha_2, \dots, \alpha_n)$ defined as follows:

$$\partial^\alpha \equiv \frac{\partial^{|\alpha|}}{\partial^{\alpha_1} x_1 \partial^{\alpha_2} x_2 \cdots \partial^{\alpha_n} x_n} = \prod_{k=1}^n \partial_k^{\alpha_k} \quad (23.14)$$

where

$$\partial_k^{\alpha_k} = \frac{\partial^{\alpha_k}}{\partial x_k^{\alpha_k}} \quad (23.15)$$

The set of n -dimensional arrays α of non-negative and finite integers is denoted by N_0^n and

$$|\alpha| \equiv \sum_{k=1}^n \alpha_k, \quad \alpha \in N_0^n \quad (23.16)$$

The partial derivatives of order k are collected in finite sets denoted by $\mathbf{y}^{(k)}$, $k = 1, \dots, n$ as used in Sect. 2.1.3 for the Lie group analysis. For instance, the set $\mathbf{y}^{(1)}$ contains all partial first derivatives $\frac{\partial y_m}{\partial x_k}$, $m = 1, \dots, M$, $k = 1, \dots, n$.

Elementary properties of multi-indices

For multi-indices $\alpha, \beta \in N_0^n$ and $\mathbf{x} = (x_1, x_2, \dots, x_n) \in R^n$ many operations can be defined for multi-indices analogous to single indices:

Componentwise sum and difference $\alpha \pm \beta = (\alpha_1 \pm \beta_1, \alpha_2 \pm \beta_2, \dots, \alpha_n \pm \beta_n)$, partial order $\alpha \leq \beta \iff \alpha_k \leq \beta_k \forall k \in \{1, 2, \dots, n\}$, the factorial of a multi-index $\alpha \in N_0^n$ is $\alpha! = \alpha_1! \cdot \alpha_2! \cdots \alpha_n!$, the binomial coefficients are for multi-indices

$$\binom{\alpha}{\beta} = \binom{\alpha_1}{\beta_1} \binom{\alpha_2}{\beta_2} \cdots \binom{\alpha_n}{\beta_n} = \frac{\alpha!}{\beta! (\alpha - \beta)!}$$

the multi-nominal coefficients are defined by

$$\binom{k}{\alpha} = \frac{k!}{\alpha_1! \alpha_2! \cdots \alpha_n!} = \frac{k!}{\alpha!}$$

and $k = |\alpha|$, $\alpha \in N_0^n$. The power of the vector \mathbf{x} to the multi-index α is defined by

$$\mathbf{x}^\alpha = \prod_{k=1}^n x_k^{\alpha_k}$$

The multi-index notation allows the extension of many formulae from elementary calculus to the corresponding multi-variable case. In all the following, $\mathbf{x}, \mathbf{y}, \mathbf{h} \in R^n$, $\alpha, \nu \in N_0^n$ and $f, g, a_\alpha : R^n \rightarrow R$.

Multi-nomial theorem

$$\left(\sum_{i=1}^n x_i \right)^k = \sum_{|\alpha|=k} \binom{k}{\alpha} \mathbf{x}^\alpha$$

Multi-binomial theorem

$$(\mathbf{x} + \mathbf{y})^\alpha = \sum_{\nu \leq \alpha} \binom{\alpha}{\nu} \mathbf{x}^\nu \mathbf{y}^{\alpha-\nu}$$

where $(\mathbf{x} + \mathbf{y})^\alpha = \prod_{k=1}^n (x_k + y_k)^{\alpha_k}$.

The Leibniz formula for smooth scalar functions $f(\mathbf{x})$ and $g(\mathbf{x})$ is

$$\partial^\alpha (fg) = \sum_{\nu \leq \alpha} \binom{\alpha}{\nu} \partial^\nu f \partial^{\alpha-\nu} g$$

The Taylor series for an analytic function f in n variables is then

$$f(\mathbf{x} + \mathbf{h}) = \sum_{\alpha \in N_0^n} \frac{1}{\alpha!} \partial^\alpha f(\mathbf{x}) \mathbf{h}^\alpha$$

Integration by parts for smooth functions with compact support in a bounded domain $\mathcal{D} \subset R^n$

$$\int_{\mathcal{D}} v(\partial^\alpha u) d\nu = (-1)^{|\alpha|} \int_{\mathcal{D}} (\partial^\alpha v) u d\nu$$

holds. This formula is used for the definition of distributions and weak derivatives, if the test scalar or vector fields $v(\mathbf{x}) \in C^\infty(\mathcal{D})$.

23.7 Function Spaces

A variety of function spaces is required for the presentation of the material. The definitions and relevant references are collected in the present section. Consider a compact flow domain denoted by $\mathcal{D}(t) \subset R^3$ with boundary $\partial\mathcal{D}(t)$. The boundary is assumed to be orientable and sufficiently smooth such that a normal vector exists nearly everywhere. The surface area for the boundary $\partial\mathcal{D}$ must satisfy

$$0 < \int_{\partial\mathcal{D}} dA < \infty$$

and the volume of the flow domain is thus bounded and non-zero. $\mathcal{D}(t)$ is called the domain of definition or flow domain for the turbulence fields.

The development of mapping methods in Chap. 12 requires properties of scalar and vector Gaussian fields. The domain of definition is $\mathcal{D} = R^3$ for Gaussian reference fields and their range is $\hat{\mathcal{D}} = R^1$ for scalar and $\hat{\mathcal{D}} = R^3$ for vector fields. Cartesian coordinate systems are set up in both domains and denoted by $\mathbf{x} \in \mathcal{D}(t)$ and $\hat{\mathbf{x}} \in \hat{\mathcal{D}}$, respectively.

Banach and Hilbert spaces

Various functions of scalar, vector and tensor character will be defined on \mathcal{D} and called turbulence fields. Functions defined on $\hat{\mathcal{D}}$ will be called reference or argument fields. Various sets of fields will be considered and they will be embedded in various function spaces. The most important Banach and Hilbert spaces will be discussed briefly (see Adams [7], Kreyszig [8], Werner [9] for fundamental theory and further details). A class of Banach spaces is given by

$$L^p(\mathcal{D}) \equiv \{\Phi(\mathbf{x}) | \Phi : \mathcal{D} \rightarrow R^1, \Phi \text{ measurable}, \int_{\mathcal{D}} d\nu |\Phi(\mathbf{x})|^p < \infty\} \quad (23.17)$$

with norm

$$\|\Phi\|_p = \|\Phi\|_{L^p(\mathcal{D})} \equiv \left\{ \int_{\mathcal{D}} d\nu |\Phi(\mathbf{x})|^p \right\}^{\frac{1}{p}} \quad (23.18)$$

which is a Hilbert space for $p = 2$ with scalar product

$$(\Phi, \Psi) \equiv \int_{\mathcal{D}} d\nu \Phi(\mathbf{x}) \cdot \Psi(\mathbf{x}) \quad (23.19)$$

A Hilbert space H possesses an orthonormal basis, all bases have the same cardinality. The cardinality of a basis is defined as dimension of a Hilbert space. Hence, the dimension of a Hilbert space is either finite or \aleph_0 representing countably infinite (cardinality of the integers) dimension.

Sobolev spaces

A different class of function spaces can be constructed by requiring weak differentiability up to a certain order. These spaces are called Sobolev spaces and are defined by

$$W^{m,p}(\mathcal{D}) \equiv \{\Phi(\mathbf{x}) | \partial^\alpha \Phi \in L^p, |\alpha| \leq m\} \quad (23.20)$$

where α is a multi-index and ∂^α is defined by (23.14), $|\alpha|$ denotes the multi-index sum (23.16) with $\alpha_k \geq 0$ and integer. The Sobolev norm is defined by

$$\|\Phi\|_{m,p,\mathcal{D}} \equiv \begin{cases} \left(\sum_{|\alpha| \leq m} \|\partial^\alpha \Phi\|_{L^p(\mathcal{D})}^p \right)^{\frac{1}{p}} & \text{for } 1 \leq p < \infty \\ \max_{|\alpha| \leq m} \|\partial^\alpha \Phi\|_{L^\infty(\mathcal{D})} & \text{for } p = \infty \end{cases} \quad (23.21)$$

where the subscript $L^p(\mathcal{D})$ indicates the L^p norm (23.18). Note that the definition (23.21) must employ dimensionless quantities to be dimensionally consistent. For $p = 2$, a Hilbert space is obtained with scalar product

$$(\Phi, \Psi)_{m,\mathcal{D}} \equiv \sum_{|\alpha| \leq m} \int_{\mathcal{D}} d\nu \partial^\alpha \Phi \partial^\alpha \Psi \quad (23.22)$$

The general properties of these spaces can be found in the literature on functional analysis [7–9].

Dual space

Consider a normed space X over a field K (either the real line R^1 or the complex plane C), then is the space $B(X, K)$ called the dual space of X and is denoted X' . The elements in X' are bounded linear functionals defined on X . The norm of a linear functional $f \in X'$ is given by

$$\|f\| = \sup_{x \leq 1} |f(x)| \quad (23.23)$$

The dual space X' is, therefore, a Banach space. For example, the linear operator $f : C^0([a, b]) \rightarrow R^1$ defined by

$$f(x) \equiv \int_a^b ds K(s) x(s)$$

for $x \in C^0([a, b])$, where the kernel $K(s)$ belongs to $C^0([a, b])$, is in $C'([a, b])$ with norm $\|f\| = \int_a^b ds |K(s)|$.

Function spaces for the Navier–Stokes pdes

Several function spaces are used in the review of the theoretical analysis of the Navier–Stokes pdes for the motion of an incompressible fluid in Sect. 2.2. All variables are assumed dimensionless and the Reynolds (2.8) number is thus properly defined. The space $C^k(\mathcal{D})$ of all vector fields $\mathbf{v}(\mathbf{x})$ defined in the (flow) domain \mathcal{D} with continuous derivatives ∂^α (23.14) up to order $|\alpha| \leq k$ for all $\alpha \in N_0^k$ is the space $C_\sigma^k(\mathcal{D})$ for $k \geq 1$ defined by

$$C_\sigma^k(\mathcal{D}) \equiv \{\mathbf{v} \in C^k(\mathcal{D}) : \nabla \cdot \mathbf{v} = 0\}$$

where subscript σ indicates the zero divergence condition, the space of smooth function is then $C^\infty(\mathcal{D}) = \bigcap_{k=0}^{\infty} C^k(\mathcal{D})$. The space of functions with compact support is $C_0^k(\mathcal{D}) = \{\mathbf{v} \in C^k(\mathcal{D}) : \text{supp}(\mathbf{v}) \text{ is compact} \subset \mathcal{D}\}$ indicated by the subscript 0. Further information on function spaces can be found in the vast literature on functional analysis, for instance, Adams [7], Werner [9], von Wahl [10], Sohr [11], Vishik and Fursikov [12], Temam [13], Suhubi [14], Rudin [15].

$L_{loc}^s([0, T); L^q(\mathbf{D})^n)$:

Consider the Banach space $L^s(\mathcal{D})$, $1 \leq s < \infty$, of square-integrable vector fields defined on the domain \mathcal{D} subset of \mathbb{R}^n , $n \geq 2$, with norm (23.18), for $s = 2$ it is a Hilbert space with scalar product (23.19). A vector field $\mathbf{v}(\mathbf{x})$ is element of $L_{loc}^q(\mathcal{D})$, if $\mathbf{v} \in L^q(\mathcal{B})$ for each open ball $\mathcal{B} \subset \mathcal{D}$; furthermore, $L^q \subset L_{loc}^q$ and $L^q = L_{loc}^q$ if \mathcal{D} is compact, i.e. contains all accumulation points. The notation $L_{loc}^s([0, T); L^q(\mathcal{D})^n)$, $1 \leq s < \infty$, indicates then that vector fields $\mathbf{v}(t, \mathbf{x})$ are elements of $L_{loc}^s([0, T))$ as function of t for fixed $\mathbf{x} \in \mathcal{D}$ and elements of $L_{loc}^s(\mathcal{D})^n$ as function of x_α for $\alpha = 1, \dots, n$ and fixed time t . The norm of the Banach space $L_{loc}^s([0, T); L^q(\mathbf{D})^n)$ is then defined by (Sohr [11], Chap. I.2.4)

$$\|\mathbf{v}\|_{q,s,T} \equiv \left(\int_0^T dt \|\mathbf{v}\|_q^s(t) \right)^{\frac{1}{s}} \quad (23.24)$$

with $1 \leq q, s \leq \infty$ and (23.18). For $q = 2$, it is a Hilbert space with scalar product (23.19).

$L_{loc}^2([0, T); L^2(\mathbf{D})^n)$:

This definition is $L_{loc}^s([0, T); L^q(\mathbf{D})^n)$ adapted to matrix functions $F_{\alpha\beta}(\mathbf{x}) : \mathcal{D} \rightarrow \mathbb{R}^{n^2}$, $\alpha, \beta = 1, \dots, n$. The matrix fields are used in the setup of external force fields according to $f_\alpha(t, \mathbf{x}) = f_\alpha^0(t, \mathbf{x}) + \frac{\partial F_{\alpha\beta}}{\partial x_\beta}(t, \mathbf{x})$.

$L_{loc}^\infty([0, T); L_\sigma^2(\mathbf{D})^n)$:

The space $L_\sigma^2(\mathcal{D})^n$ is defined as the closure of $C_{0,\sigma}^\infty(\mathcal{D})$ with respect to the norm (23.18). Closure means that the limits of all sequences in $C_{0,\sigma}^\infty$ convergent with respect to this norm are elements of $L_\sigma^2(\mathcal{D})^n$.

$L_{loc}^2([0, T); W_{0,\sigma}^{1,2}(\mathbf{D}))$:

The Sobolev space $W_{0,\sigma}^{1,2}(\mathcal{D})$ is defined as the closure of $C_{0,\sigma}^\infty(\mathcal{D})$ with respect to the Sobolev norm (23.18). Closure means that the limits of all sequences in $C_{0,\sigma}^\infty$ convergent with respect to this norm are elements of $W_{0,\sigma}^{1,2}(\mathcal{D})$.

Nuclear spaces

Topological vector spaces that can be taken as domain of definition of characteristic functionals must satisfy additional properties. They are explained in Sect. 5.4.

Hölder spaces

Hölder spaces consisting of functions satisfying a Hölder condition are basic in areas of functional analysis relevant to solving partial differential equations, and in the analysis of dynamical systems. Hölder continuity plays an important role in the

theory of homogeneous turbulence at high Reynolds numbers, see Chap. 17. The Hölder space $C^{k,\alpha}(\mathcal{D})$, where \mathcal{D} is an open subset of some Euclidean space and $k \geq 0$ an integer, consists of those functions on \mathcal{D} having continuous derivatives up to order k and such that the k^{th} partial derivatives are Hölder continuous with exponent α , where $0 < \alpha \leq 1$. This is a locally convex topological vector space. If the Hölder coefficient

$$|f|_{C^{0,\alpha}} = \sup_{x \neq y \in \mathcal{D}} \frac{|f(x) - f(y)|}{|x - y|^\alpha} \quad (23.25)$$

is finite, then the function $f(x)$ is said to be (uniformly) Hölder continuous with exponent α in \mathcal{D} . In this case, the Hölder coefficient serves as a seminorm. If the Hölder coefficient is merely bounded on compact subsets of \mathcal{D} , then the function f is said to be locally Hölder continuous with exponent α in \mathcal{D} .

23.8 Schauder Bases

Let Ω denote a Banach space over the field F of real or complex numbers, a Schauder basis is a sequence $\{f_n(\mathbf{x}) \in \Omega, n = 0, 1, \dots, \infty\}$ of elements of the Banach space Ω such that for every element $v \in \Omega$ there exists a unique sequence $\{a_n \in F, n = 0, 1, \dots, \infty\}$ of scalars, so that

$$v(\mathbf{x}) = \sum_{n=0}^{\infty} a_n f_n(\mathbf{x})$$

holds, where the convergence is understood with respect to the norm topology,

$$\lim_{n \rightarrow \infty} \left\| v - \sum_{k=0}^n a_k f_k \right\|_{\Omega} = 0$$

A Schauder basis must be ordered since the series may not converge unconditionally.

23.9 Ergodicity

Let $(\Omega, \mathcal{A}, \mu)$ be a probability space and $T : \Omega \rightarrow \Omega$ be a measure-preserving mapping (such as the Lagrangean position field for the motion of incompressible fluids), then is the mapping T ergodic with respect to the measure μ (or the measure is ergodic with respect to the mapping) if

$$\forall A \in \mathcal{A} : T^{-1}(A) = A \rightarrow \mu(a) = 0 \text{ or } \mu(A) = 1 \quad (23.26)$$

holds. This is one of several equivalent definitions, see [16] for further details.

Trace class operators

Let H be a separable Hilbert space of scalar fields $u(\mathbf{x})$ over the domain $\mathcal{D} \subset R^3$ with scalar product $(\cdot, \cdot)_H$ and with ONS basis $\{f_k(\mathbf{x}), k = 1, \dots, \infty\}$, let $A : H \rightarrow Y$ mapping H into the Hilbert space Y , then is A trace class iff

$$\text{trace}|A| = \sum_{k=1}^{\infty} ((A^* A)^{\frac{1}{2}} f_k, f_k)_H < \infty \quad (23.27)$$

The trace of A

$$\text{trace} A = \sum_{k=1}^{\infty} (A f_k, f_k)_H \quad (23.28)$$

is then absolutely convergent and independent of the basis.

Pseudo-differential operators

Consider a linear differential operator with constant coefficients,

$$P(D) := \sum_{\alpha} a_{\alpha} \partial^{\alpha}$$

which acts on smooth functions u with compact support in R^n . This operator can be written as a composition of a Fourier transform, a simple multiplication by the polynomial function called the symbol

$$\sigma_P(\xi) = \sum_{\alpha} a_{\alpha} \xi^{\alpha} \quad (23.29)$$

and an inverse Fourier transform, in the form

$$P(D)u(x) = \frac{1}{(2\pi)^n} \int_{\mathbb{R}^n} \int_{\mathbb{R}^n} e^{i(x-y)\xi} \sigma_P(\xi) u(y) dy d\xi \quad (23.30)$$

where $\alpha = (\alpha_1, \dots, \alpha_n)$ is a multi-index defined as modification of (23.14) by

$$\partial^{\alpha} \equiv \prod_{k=1}^n (-i \partial_k)^{\alpha_k} \quad (23.31)$$

suitable for Fourier transform. Equation (23.30) can be derived using Fourier transform, noting that the Fourier transform of a smooth function $u(\mathbf{x})$, compactly supported in R^n , is

$$\hat{u}(\xi) := \int e^{-iy\xi} u(\mathbf{y}) dy$$

and Fourier's inversion formula gives

$$u(\mathbf{x}) = \frac{1}{(2\pi)^n} \int e^{ix\xi} \hat{u}(\xi) d\xi$$

By applying $P(D)$ to this representation of u and using

$$P(D) e^{i(x-y)\xi} = e^{i(x-y)\xi} \sigma_P(\xi)$$

Equation (23.30) follows.

23.10 Leray–Stokes Operator

The Leray–Stokes operator is composed of the Laplacian and a projection operator called Leray projection. Hence, the Leray projection operator \mathbb{P}_σ needs to be defined first. It projects a vector field $\mathbf{v}(\mathbf{x}) \in H^2$ onto a solenoidal vector field $\mathbb{P}_\sigma \mathbf{v} \in H^2(\mathcal{D}) \cap V$, where $V \equiv \{\mathbf{v}(\mathbf{x}) \in H^2 : \nabla \cdot \mathbf{v} = 0\}$. The Leray projection operator can be defined either using pseudo-differential operators or the Helmholtz decomposition, both definitions are briefly discussed.

Pseudo-differential operator definition

The Leray projection in the former approach is defined as follows. For vector fields \mathbf{v} ($n \geq 2$), the Leray projection \mathbb{P}_σ is defined by

$$\mathbb{P}_\sigma(\mathbf{v}) = \mathbf{v} - \nabla \Delta^{-1}(\nabla \cdot \mathbf{v}) \quad (23.32)$$

This definition must be understood in the sense of pseudo-differential operators (Sect. 23.9): its matrix-valued Fourier multiplier $\sigma_{kj}(\mathbf{k})$ or symbol of a pseudo-differential operator established in Sect. 15.2 Eq. (15.19), is given by

$$\sigma_{kj}(\mathbf{k}) = \delta_{kj} - \frac{k_k k_j}{|\mathbf{k}|^2}, \quad 1 \leq k, j \leq n \quad (23.33)$$

where δ_{kj} is the Kronecker delta. Formally, it means that for all $\mathbf{v} \in \mathcal{S}(\mathbb{R}^n)^n$, i.e. elements of the Schwartz space $\mathcal{S}(\mathbb{R}^n)$, the Leray projection is given by

$$\mathbb{P}_\sigma(\mathbf{v})_k(x) = \frac{1}{(2\pi)^{n/2}} \int_{\mathbb{R}^n} \left(\delta_{kj} - \frac{k_k k_j}{|\mathbf{k}|^2} \right) \hat{v}_j(\mathbf{k}) e^{i\mathbf{k} \cdot \mathbf{x}} d\mathbf{k}, \quad 1 \leq k \leq n \quad (23.34)$$

The Fourier-transformed vector field $\hat{\mathbf{v}}(\mathbf{k})$ is defined by (15.2) as

$$\hat{f}(\mathbf{k}) \equiv \mathcal{F}f(\mathbf{x}) = \frac{1}{(2\pi)^3} \int_{\mathbb{R}^3} d\nu \exp(-i\mathbf{x} \cdot \mathbf{k}) f(\mathbf{x})$$

with \mathbf{k} denoting the wavenumber vector. Note that Schwartz space \mathcal{S} is defined as the space of rapidly decreasing functions on \mathbb{R}^n

$$\mathcal{S}(R^n) = \{f \in C^\infty(R^n) : \|f\|_{\alpha,\beta} < \infty \quad \forall \alpha, \beta \in \mathbb{Z}_+^n\} \quad (23.35)$$

where α, β are multi-indices, $C^\infty(R^n)$ is the set of smooth functions from R^n to C , and $\|f\|_{\alpha,\beta} = \sup_{\mathbf{x} \in R^n} |\mathbf{x}|^\alpha \partial^\beta f(\mathbf{x})$. A rapidly decreasing function is essentially a function $f(\mathbf{x})$ such that $f(\mathbf{x}), \partial f(\mathbf{x}), \partial^2 f(\mathbf{x}), \dots$ all exist everywhere on R^n and go to zero as $|\mathbf{x}| \rightarrow \infty$ faster than any inverse power of $|\mathbf{x}|$, hence $\mathcal{S}(R^n) \subset C^\infty(R^n)$.

Helmholtz decomposition definition

The latter approach is based on the Helmholtz decomposition. One can show that a given vector field \mathbf{v} can be decomposed as $\mathbf{v} = \nabla q + \mathbf{u}$, with $\nabla \cdot \mathbf{u} = 0$. Different to the usual Helmholtz decomposition, the Helmholtz–Leray decomposition of \mathbf{v} is unique (up to an additive constant for q). Then we can define $\mathbb{P}(\mathbf{v})$ as $\mathbb{P}(\mathbf{v}) = \mathbf{u}$.

Properties of the Leray projection

The Leray projection has the following useful properties:

The Leray projection is a projection: $\mathbb{P}_\sigma[\mathbb{P}_\sigma(\mathbf{u})] = \mathbb{P}_\sigma(\mathbf{u})$ for all $\mathbf{u} \in \mathcal{S}(R^n)^n$.

The Leray projection is a divergence-free operator: $\nabla \cdot [\mathbb{P}_\sigma(\mathbf{u})] = 0$ for all $\mathbf{u} \in \mathcal{S}(R^n)^n$.

The Leray projection is the identity for solenoidal vector fields: $\mathbb{P}_\sigma(\mathbf{u}) = \mathbf{u}$ for all $\mathbf{u} \in \mathcal{S}(R^n)^n$ such that $\nabla \cdot \mathbf{u} = 0$.

The Leray projection vanishes for the gradient fields: $\mathbb{P}_\sigma(\nabla\phi) = 0$ for all $\phi \in \mathcal{S}(R^n)$.

Definition of the Stokes operator A

The Stokes operator A is an unbounded and linear operator defined by

$$A := -\mathbb{P}_\sigma \Delta \quad (23.36)$$

where $\Delta \equiv \nabla^2$ is the Laplacian. Since A is unbounded, we must also give its domain of definition, which is defined as $\mathcal{D}(A) = H^2 \cap V$, where $V = \{\mathbf{u} \in (H_0^1(\mathcal{D}))^n \mid \mathbf{u} = 0\}$. Here, \mathcal{D} is a bounded open set in \mathbb{R}^n (usually $n = 2, 3$), $H^2(\mathcal{D})$ and $H_0^1(\mathcal{D})$ are the standard Sobolev spaces and the divergence of \mathbf{u} is taken in the distribution sense.

For a given domain \mathcal{D} , which is open, bounded and has C^2 boundary, the Stokes operator A is a self-adjoint positive definite operator with respect to the L^2 inner product. It has an ONS basis of eigenfunctions $w_k, k = 1, \dots, \infty$ corresponding to eigenvalues $\lambda_k |_{k=1}^\infty$, which satisfy $0 < \lambda_1 < \lambda_2 \leq \lambda_3 \dots \leq \lambda_k \leq \dots$ and $\lambda_k \rightarrow \infty$ as $k \rightarrow \infty$. The smallest eigenvalue is unique and positive, and hence these properties allow the definition of powers of the Stokes operator. Let $\alpha > 0$ be a real number, the power A^α is then defined by

$$\mathbf{u} \in \mathcal{D}(A) : A^\alpha \mathbf{u} = \sum_{k=1}^{\infty} \lambda_k^\alpha u_k \mathbf{w}_k \quad (23.37)$$

where the coefficients are $u_k := (\mathbf{u}, \mathbf{w}_k)$ and (\cdot, \cdot) is the $L^2(\mathcal{D})$ inner product.

The inverse A^{-1} of the Stokes operator is a bounded, compact, self-adjoint operator in the space $H := \{\mathbf{u} \in (L^2(\mathcal{D}))^n \mid \operatorname{div} \mathbf{u} = 0 \text{ and } \gamma(\mathbf{u}) = 0\}$. Furthermore, the inverse operator $A^{-1} : H \rightarrow V$ is injective.

23.11 n -Sphere and n -Ball

The definition of the Lèvy-Laplacian (9.83) involves a limit of the surface area of the n -sphere as the dimension $n \rightarrow \infty$. This limit is ambiguous since the surface area of any sphere with finite radius approaches zero for $n \rightarrow \infty$. Hence, the geometric and topological properties of the n -sphere and n -ball are essential for the proper evaluation and interpretation of this limit. The notions of sphere and ball in n -dimensional Euclidean and more general linear vector spaces are defined and then their topological and geometric properties are discussed.

n -sphere and n -ball in Euclidean spaces

Consider the n -dimensional Euclidean space with Cartesian coordinates. The n -dimensional ball with radius ρ is defined as the set

$$\mathcal{B}_n(\rho) \equiv \{\mathbf{x} : \sum_{i=1}^n x_i^2 \leq \rho^2\} \quad (23.38)$$

The volume $V_n(\rho)$ of the n -ball $\mathcal{B}_n(\rho)$ with radius ρ and centred at the origin in Euclidean space R^n is the n -dimensional Riemann integral

$$V_n(\rho) = \int_{\mathcal{B}_n(\rho)} dx_1 \cdots dx_n \quad (23.39)$$

The surface of this ball is the $n - 1$ -dimensional manifold defined by

$$\mathcal{S}_n(\rho) \equiv \{\mathbf{x} : \sum_{i=1}^n x_i^2 = \rho^2\} \quad (23.40)$$

embedded in R^n . The surface area of this manifold is

$$A_n(\rho) = \int_{\mathcal{S}_n(\rho)} d\sigma \quad (23.41)$$

where $d\sigma$ denotes the $n - 1$ -dimensional surface differential. It will be constructed below for hypersurfaces defined implicitly.

n -sphere and n -ball in linear vector spaces

The n -sphere $S_n(\rho)$ and n -ball $B_n(\rho)$ of radius ρ can be defined more generally in normed vector spaces by

$$\mathcal{S}_n(\rho) \equiv \{x \in V : \|x\| = \rho\} \quad (23.42)$$

and

$$\mathcal{B}_n(\rho) \equiv \{x \in V : \|x\| \leq \rho\} \quad (23.43)$$

The shape of the unit sphere depends crucially on the norm used to define it, Eqs. (23.43) and (23.42). This is illustrated in the right graph of Fig. 23.3 for 2-d and Fig. 23.4 for 3-d. The L_p norms

$$\|\mathbf{x}\| = \left(\sum_{i=1}^n |x_i|^p \right)^{\frac{1}{p}} \quad (23.44)$$

are used to plot the unit spheres. The right graph in Fig. 23.3 shows the shapes of S_2 for $p = 0.5, \dots, 9.0$ as indicated in the figure. The shape of S_3 embedded in R^3 is illustrated in Fig. 23.4 for $p = 0.5$ in the left and for $p = 3.0$ in the right graph. It is evident that for $p \neq 2$ corner points and ridges may occur. The n -balls enclosed by the n -spheres are convex for $p \geq 1$, but not for $p < 1$.

23.12 Differentiation of Functionals and Measures

Mappings of a function space X into a function space Y and of a function space X into a finite-dimensional Euclidean space R^n are considered that are smooth enough to allow the definition of differentials and derivatives. In particular, derivatives of functionals $X \rightarrow R^1$ are discussed as preparation for the derivation of the Hopf functional differential equation and its variants in Sect. 9.2. Furthermore, mappings and differentiation of measures are addressed to lay the groundwork for the discussion of variants of the Hopf equation.

Gateaux differential and derivatives

Consider the real locally convex vector spaces $X = \{u(\mathbf{x}) : \mathbf{x} \in \mathcal{D} \subset R^3\}$ (\mathcal{D} denotes the flow domain with boundary $\partial\mathcal{D}$) and Y and the linear topological vector space \mathcal{T} of operators $F \in \mathcal{T} : X \rightarrow Y$, let $F \in \mathcal{T}$ have the domain of definition $\mathcal{D}(F)$ open subset of X .

First derivative

If the limit (Dalecky and Fomin, [17] Chap. IV, Suhubi [14])

$$\delta F[u(\cdot)](w) = \lim_{\epsilon \rightarrow 0} \frac{1}{\epsilon} \{F[u + \epsilon w] - F[u]\} \quad (23.45)$$

exists for $u \in \mathcal{D}$ and $u + \epsilon w \in \mathcal{D}$ for some interval containing $\epsilon = 0$, then is $\delta F[u](w)$ called the Gateaux differential of the operator F at the vector u in the direction w . If the limit exists for every $w \in \mathcal{D}$, the functional F is called Gateaux differentiable at $u \in \mathcal{D}$. Specifically, the Gateaux derivative in Hilbert spaces X can be deduced from the representation

$$\delta F[u](w) = (w, \frac{\delta F}{\delta u}) \quad (23.46)$$

of the Gateaux differential. This expression is justified by the Riesz–Markov–Kakutani representation theorem [15], which states that for any positive linear functional mapping a locally compact Hausdorff space $\hat{H}(\hat{D})$ into R^1 : $\hat{\Phi} \in \hat{H} \rightarrow \lim_{\epsilon \rightarrow 0} \frac{\partial}{\partial \epsilon} \Lambda[\hat{\Phi} + \epsilon h] \in R^1$, and there exists a unique regular Borel measure μ on \hat{D} , such that

$$\lim_{\epsilon \rightarrow 0} \frac{\partial}{\partial \epsilon} \Lambda[\hat{\Phi} + \epsilon h] = \int_{\hat{D}} \frac{\delta \Lambda}{\delta \hat{\Phi}(\hat{\mathbf{x}})} h(\hat{\mathbf{x}}) d\mu(\hat{\mathbf{x}})$$

holds for all continuous functionals $\Lambda[\hat{\Phi}(\cdot)]$.

For the example of turbulent flows, the characteristic functionals are of fundamental importance with the domain of definition being the nuclear space of argument/test functions $X = \mathcal{N}$ and the image space being the complex plane C^1 .

Consider now vector Hilbert spaces X and Y with countably infinite, ordered Schauder bases, let $\mathcal{B} = \{f^k(\mathbf{x}), k = 1, \dots, \infty\}$ be an countably infinite ordered and orthonormalized (ONS) basis spanning X , hence the representation

$$u(\mathbf{x}) = \sum_{k=1}^{\infty} f^k(\mathbf{x}) c_k \quad (23.47)$$

can be constructed, where $c_k = (f^k, u)$ and likewise for w . Since $u(\mathbf{x}) = \sum_{k=1}^{\infty} c_k f^k(\mathbf{x})$, it follows that

$$u(\mathbf{x}) = \lim_{n \rightarrow \infty} \sum_{k=1}^n c_k f^k(\mathbf{x})$$

holds. An operator $F[u(\cdot)] : X \rightarrow Y$ (note that $F[u(\cdot)]$ is called a functional, if $Y = R^1$ or the complex plane C^2) is then defined for arguments $u_n(\mathbf{x}) \equiv \sum_{k=1}^n c_k f^k(\mathbf{x})$ since $u_n \in X$. This operator applied to u_n generates for $Y = R^1$ a standard function of n independent variables

$$f_n(c_1, \dots, c_n) \equiv F\left[\sum_{k=1}^n c_k f^k(\mathbf{x})\right], \quad (c_1, \dots, c_n) \in R^n \quad (23.48)$$

inheriting the regularity properties of F . The first Gateaux derivative for arguments $u_n(\mathbf{x}) = \sum_{k=1}^n f^k(\mathbf{x}) c_k$ and directions $w_n(\mathbf{x}) = \sum_{k=1}^n f^k(\mathbf{x}) d_k$, $d_k \equiv (f^k, w)$ is according to (23.45)

$$\begin{aligned}\delta F[u_n(.)](w) &= \lim_{\epsilon \rightarrow 0} \frac{1}{\epsilon} \{F[u_n + \epsilon w_n] - F[u_n]\} = \\ &\lim_{\epsilon \rightarrow 0} \frac{1}{\epsilon} \{f_n(c_1 + \epsilon d_1, \dots, c_n + \epsilon d_n) - f_n(c_1, \dots, c_n)\}\end{aligned}$$

The regularity of f_n (23.48) allows a Taylor series expansion leading to

$$\delta F[u_n(.)](w_n) = \sum_{k=1}^n d_k \frac{\partial f_n}{\partial c_k}(c_1, \dots, c_n) = \int_{\mathcal{D}} d\nu w(\mathbf{x}) \sum_{k=1}^n f^k(\mathbf{x}) \frac{\partial f_n}{\partial c_k}(c_1, \dots, c_n) \quad (23.49)$$

The first Gateaux derivative is then according to (23.46), hence

$$\frac{\delta F}{\delta u}[u; \mathbf{x}] = \lim_{n \rightarrow \infty} \sum_{k=1}^n f^k(\mathbf{x}) \frac{\partial f_n}{\partial c_k}(c_1, \dots, c_n)$$

(23.50)

where $\mathbf{x} \in \mathcal{D}$, $c_k = (u, f^k)$ and $f_n(c_1, \dots, c_n)$ is defined by (23.48), is the desired result for the first derivative assuming convergence of the limit. Two examples for the computation of the first Gateaux derivative are presented below.

Second derivative

The second Gateaux differential is for sufficiently differentiable functionals $F \in \mathcal{T} : X \rightarrow Y$ defined by

$$\delta^2 F[u(.)](v, w) = \lim_{\epsilon \rightarrow 0} \frac{1}{\epsilon} \{\delta F[u(.) + \epsilon v(.)](w) - \delta F[u(.)](w)\} \quad (23.51)$$

where $\delta F[u(.)](w)$ in turn is given by (23.45), hence

$$\delta^2 F[u(.)](v, w) = \lim_{\epsilon \rightarrow 0} \frac{1}{\epsilon^2} \{F[u(.) + \epsilon w(.) + \epsilon v(.)] - F[u(.) + \epsilon w(.)] - F[u(.) + \epsilon v(.)] + F[u(.)]\} \quad (23.52)$$

holds in an open neighbourhood of $u(\mathbf{x}) \in X$ containing $\epsilon w(\mathbf{x})$ and $\epsilon v(\mathbf{x})$ for all $\epsilon < 1$ and for all $\mathbf{x} \in \mathcal{D}$. The second Gateaux derivative in Hilbert spaces X can be deduced from the representation

$$\delta^2 F[u](v, w) = (w(\mathbf{x}), (v(\mathbf{x}'), \frac{\delta^2 F}{\delta u(\mathbf{x}) \delta u(\mathbf{x}')})) \quad (23.53)$$

of the second-order Gateaux differential.

Consider now the vector Hilbert spaces X and Y with countably infinite ordered Schauder bases introduced above, let $\mathcal{B} = \{f^k(\mathbf{x}), k = 1, \dots, \infty\}$ be an ordered, countably infinite ONS base spanning X , hence the representation $u(\mathbf{x}) = \sum_{k=1}^{\infty} f^k(\mathbf{x}) c_k$ can be constructed as for the first derivative above, where $c_k = (f^k, u)$ and likewise $d_k = (f^k, w)$ for $w(\mathbf{x})$ and $e_k = (f^k, v)$ for $v(\mathbf{x})$. The representation of $u(\mathbf{x})$ with

respect to the basis implies that the second Gateaux differential emerges as

$$\begin{aligned}\delta^2 F[u(.)](v, w) &= \lim_{\epsilon \rightarrow 0} \frac{1}{\epsilon^2} \lim_{n \rightarrow \infty} \{ f_n(c_1 + \epsilon(d_1 + e_1), \dots, c_n + \epsilon(d_n + e_n)) \\ &\quad - f_n(c_1 + \epsilon d_1, \dots, c_n + \epsilon d_n) - f_n(c_1 + \epsilon e_1, \dots, c_n + \epsilon e_n) + f_n(c_1, \dots, c_n)\}\end{aligned}$$

The regularity of f_n (23.48) allows Taylor series expansions leading to

$$\delta^2 F[u(.)](v, w) = \lim_{n \rightarrow \infty} \sum_{k=1}^n \sum_{m=1}^n d_k e_m \frac{\partial^2 f_n}{\partial c_k \partial c_m}(c_1, \dots, c_n)$$

The second Gateaux derivative is, therefore, contained in

$$\delta^2 F[u(.)](v, w) = \lim_{n \rightarrow \infty} \int_{\mathcal{D}} d\nu(\mathbf{x}) v(\mathbf{x}) \int_{\mathcal{D}} d\nu(\mathbf{x}') w(\mathbf{x}') \sum_{k=1}^n \sum_{m=1}^n f^k(\mathbf{x}) f^m(\mathbf{x}') \frac{\partial^2 f_n}{\partial c_k \partial c_m}(c_1, \dots, c_n)$$

according to (23.53), hence

$$\frac{\delta^2 F}{\delta u(\mathbf{x}) \delta u(\mathbf{x}')}[u(.)] = \lim_{n \rightarrow \infty} \sum_{k=1}^n \sum_{m=1}^n f^k(\mathbf{x}) f^m(\mathbf{x}') \frac{\partial^2 f_n}{\partial c_k \partial c_m}(c_1, \dots, c_n)$$

(23.54)

holds for X being Hilbert space with basis \mathcal{B} , where $\mathbf{x}, \mathbf{x}' \in \mathcal{D}$, $c_k = (u, f^k)$ and $f_n(c_1, \dots, c_n)$ is defined by (23.48), is the desired expression for the second derivative assuming convergence of the limit.

Example: First Gateaux derivative of a linear functional

The case of a linear operator T allows straightforward computation of the Gateaux differential, first without recourse to a basis and then with respect to an ONS basis. It follows from (23.45) that

$$\delta T[u](w) = \lim_{\epsilon \rightarrow 0} \frac{1}{\epsilon} \{ T[u] + \epsilon T[w] - T[u] \} \quad (23.55)$$

holds using the linearity of T and thus

$$\delta T[u](w) = T[w] \quad (23.56)$$

is the desired differential. It shows that the Gateaux differential of a linear operator is also a linear operator. The Gateaux derivative (23.46) can be deduced from the representation (23.45) of the Gateaux differential. If the linear operator is represented by

$$T[u] = \int_{x=a}^b dx K(x) u(x)$$

the Gateaux derivative emerges then in the form

$$\frac{\delta T}{\delta u}[u(.); x] = K(x)$$

independent of $u(.)$ as ordinary function of location $x \in \mathcal{D}$.

The second Gateaux derivative is easily computed for a linear functional by

$$\delta^2 T[u](v, w) = \lim_{\epsilon \rightarrow 0} \frac{1}{\epsilon} \{ \delta T[u + \epsilon v](w) - \delta T[u](w) \} \quad (23.57)$$

but (23.56) holds, hence $\delta T[u + \epsilon v](w) = T[w]$ and

$$\delta^2 T[u](v, w) = 0 \quad (23.58)$$

is obtained.

Consider now an ONS basis $\mathcal{B} \equiv \{f^k(x), k = 1, \dots, \infty\}$ in the Hilbert space X of functions $u(x)$ defined on the interval $\mathcal{D} \equiv [a, b] \subset R^1$ and the linear operators T represented by

$$T(u) = \int_a^b dx K(x)u(x), \quad K(x) = \sum_{k=1}^{\infty} f^k(x)K^k, \quad K^k = (f^k, K) \quad (23.59)$$

with respect to the ONS basis. The Gateaux differential is then according to (23.46)

$$\delta T[u](w) = \sum_{k=1}^{\infty} K^k w^k = \int_a^b dx w(x) \sum_{k=1}^{\infty} (f^k, K) f^k(x) \quad (23.60)$$

The Gateaux derivative is thus given by

$$\frac{\delta T}{\delta u}[u(.); x] = \sum_{k=1}^{\infty} (f^k, K) f^k(x) \quad (23.61)$$

It is in fact independent of u and the direction w due to the linearity of T .

The representation (23.48) for the linear functional as limit $n \rightarrow \infty$ is easily evaluated for the linear functional

$$f_n(c_1, \dots, c_n) = \int_a^b dx K(x) \sum_{k=1}^n c_k f^k(x) = \sum_{k=1}^n c_k (f^k, K)$$

hence

$$\frac{\partial f_n}{\partial c_k} = (f^k, K)$$

and the first Gateaux derivative is then according to (23.50)

$$\frac{\delta F}{\delta u}[u; \mathbf{x}] = \lim_{n \rightarrow \infty} \sum_{k=1}^n (f^k, K) f^k(\mathbf{x}) = \sum_{k=1}^{\infty} (f^k, K) f^k(\mathbf{x})$$

in agreement with the previous result (23.61).

Example: Nonlinear functional defined on a Sobolev space

The functional $F[u] : W_p^m(a, b) \rightarrow \mathbb{R}^1$ (Suhubi [14], Chap. 9.2), where $W_p^m(a, b)$, $a < b$ denotes the Sobolev space of m times differentiable functions $u(x)$ defined on the interval $\mathcal{D} = [a, b] \subset \mathbb{R}^1$ with the norm (2.42) (see Sect. 23.7 and Adams [7] for details on Sobolev spaces)

$$\|u\| = \left(\sum_{0 \leq \alpha \leq m} \int_a^b dx \left| \frac{d^\alpha u}{dx^\alpha} \right|^p \right)^{\frac{1}{p}}$$

provides an instructive example for the connection of Gateaux derivatives to partial derivatives of functions of a finite number of independent variables. The functional $F[u]$ is explicitly given by

$$F[u] = \int_a^b dx f(u, u', \dots, u^{(m)}) \quad (23.62)$$

where the prime denotes the standard derivative with respect to location $x \in \mathcal{D}$. The function $f(u, u', \dots, u^{(m)})$ is assumed to be differentiable with respect to its arguments. The Gateaux derivative of F in the direction $w(x) \in W_p^m(a, b)$ is easily computed

$$\delta F[u](w) = \int_a^b dx \left[\frac{\partial f}{\partial u} w + \frac{\partial f}{\partial u'} w' + \dots + \frac{\partial f}{\partial u^{(m)}} w^{(m)} \right] \quad (23.63)$$

If $w^{(n)}(x) = 0$ on the boundary $\partial\mathcal{D} = a, b$ for $1 \leq n \leq m$ partial integration can be used

$$\int_a^b dx \frac{\partial f}{\partial u^{(n)}} w^{(n)} = (-1)^n \int_a^b dx \frac{d^n}{dx^n} \left(\frac{\partial f}{\partial u^{(n)}} \right) w(x) \quad (23.64)$$

leading to the result

$$\delta F[u](w) = \int_a^b dx \frac{\delta F[u]}{\delta u(x)} w(x) \quad (23.65)$$

where

$$\frac{\delta F[u]}{\delta u(x)} = \frac{\partial f}{\partial u} - \frac{d}{dx} \left(\frac{\partial f}{\partial u'} \right) \cdots + (-1)^m \frac{d^m}{dx^m} \left(\frac{\partial f}{\partial u^{(m)}} \right) \quad (23.66)$$

is the Euler or variational derivative of F .

The finite-dimensional analogue of this result, where $F[u] \rightarrow f(u_1, \dots, u_m) : R^m \rightarrow R^1$ is a function of m variables, follows at once

$$\delta f[u](w) = \sum_{i=1}^m \frac{\partial f}{\partial u_i} w_i \quad (23.67)$$

The arguments u and w are now vectors in R^m equipped, for instance, with a Cartesian coordinate system. Choosing the unit vector e_i , $1 \leq i \leq m$ produces

$$\delta f[u](e_i) = \frac{\partial f}{\partial u_i} e_i \text{ hence } \frac{\delta f[u]}{\delta u(x)} = \frac{\partial f}{\partial u_i}(x) \quad (23.68)$$

the partial derivative in direction e_i .

Fréchet differential and derivative

Let X, Y be Banach spaces and U an open subset of X , let $f : U \rightarrow Y$ be a function mapping U into Y . The function f is Fréchet differentiable at $x \in U$, if there exists a bounded linear operator $A_x : V \rightarrow Y$, such that

$$\lim_{h \rightarrow 0} \frac{1}{\|h\|_X} \|f(x + h) - f(x) - A_x(h)\|_Y = 0 \quad (23.69)$$

exists for all sequences of non-zero elements $\{h_n\}$ in X , which converge to the zero vector as $n \rightarrow \infty$. If A_x exists, it is denoted by $\delta f(x) = A_x$ and called Fréchet differential.

The Gateaux differential is more general, as it can be defined for locally convex spaces than the Fréchet differential, which is defined on Banach and Hibert spaces. If both Gateaux and Fréchet differentials exist, they agree, but there are functionals, which are Gateaux but not Fréchet differentiable, since the Gateaux differential is not necessarily linear.

Example: Fréchet differential for finite-dimensional Euclidian spaces

The example of finite-dimensional Euclidian spaces $X = R^n$ and $Y = R^m$, m, n positive integers, and a function $f(x) \in C^1 : U \rightarrow R^m$ with U an open subset of X having all partial derivatives being continuous at a point $x \in U$ provides the relation to the Fréchet differential. Noting that $x \in U$ is a n -vector and $f(x) \in Y$ and m -vector, the definition (23.69) of the Fréchet differential implies

$$\lim_{\mathbf{h} \rightarrow 0} \frac{1}{\|\mathbf{h}\|_X} \|\mathbf{f}(\mathbf{x} + \mathbf{h}) - \mathbf{f}(\mathbf{x}) - \mathbf{A}_x(\mathbf{h})\|_Y = 0 \quad (23.70)$$

Introducing a canonical basis in R^n with $\{\mathbf{e}_\alpha\}$ orthonormal unit vectors $\mathbf{x} = (\mathbf{x}, \mathbf{e}_\alpha)\mathbf{e}_\alpha$ and letting $\mathbf{h} = h_\alpha \mathbf{e}_\alpha$, $h_\alpha = (\mathbf{h}, \mathbf{e}_\alpha)$ for $\alpha = 1, \dots, n$ using the Einstein summation convention for Greek subscripts, it follows

$$f_\alpha(\mathbf{x} + \mathbf{h}) - f_\alpha(\mathbf{x}) = f_\alpha(\mathbf{x}) + h_\beta \frac{\partial f_\alpha}{\partial x_\beta}(\mathbf{x}) - f_\alpha(\mathbf{x}), \quad 1 \leq \beta \leq n, \quad 1 \leq \alpha \leq m \quad (23.71)$$

and thus

$$(\delta f)_\alpha(\mathbf{h}) = h_\beta J_{\alpha\beta}(\mathbf{x}) \quad (23.72)$$

emerges as the Fréchet differential. It is a linear function of the increment \mathbf{h} and the Jacobian

$$J_{\alpha\beta}(\mathbf{x}) \equiv \frac{\partial f_\alpha}{\partial x_\beta}(\mathbf{x}) \quad (23.73)$$

It is seen that for functions $f(\mathbf{x}) \in C^1$ the Fréchet differential exists and is continuous. The converse does not hold: A function may be Fréchet differentiable, but have no continuous partial derivatives.

Variational derivatives of functionals

Let X be a manifold of functions $y(\mathbf{x})$, which are defined in the domain $\mathcal{D} \subset R^3$, and let the image space be the real line $Y = R^1$, let $F : X \rightarrow R^1$ be a differentiable functional, then is the first variational derivative defined by

$$\begin{aligned} \langle \frac{\delta F[y(\mathbf{x})]}{\delta y(x)}, h(\mathbf{x}) \rangle &\equiv \int_{\mathcal{D}} d\nu(\mathbf{x}') \frac{\delta F[y(\mathbf{x})]}{\delta y(\mathbf{x}')} h(\mathbf{x}') \\ &= \lim_{\epsilon \rightarrow 0} \frac{1}{\epsilon} \{F[y(\mathbf{x}) + \epsilon h(\mathbf{x})] - F[y(\mathbf{x})]\} = \frac{d}{d\epsilon} F[y + \epsilon h]|_{\epsilon=0} \end{aligned} \quad (23.74)$$

where $h(\mathbf{x})$ is in an appropriate space of test functions, i.e. $h \in X$. If the manifold is subset of a Banach space, the variational derivative is the Fréchet derivative, if it is a locally convex topological space it is the Gateaux derivative.

The integral containing the variational derivative in (23.74) can be removed by choosing the Dirac pseudo-function $h(\mathbf{x}') = \delta(\mathbf{x}' - \mathbf{x})$ as test function. However, the Dirac pseudo-function is in general not in X , and hence it has to be represented as limit

$$\frac{\delta F[y(\mathbf{x})]}{\delta y(x)} = \lim_{n \rightarrow \infty} \int_{\mathcal{D}} d\nu(\mathbf{x}') \frac{\delta F[y(\mathbf{x})]}{\delta y(\mathbf{x}')} \delta_n(\mathbf{x}' - \mathbf{x}) \quad (23.75)$$

of functions $\delta_n(\mathbf{x}' - \mathbf{x}) \in X$ for (23.74) to make sense.

Normal and regular forms of the second differentials

The essential properties of the second variational derivative are discussed since they emerge as central part of the Hopf equation in Sect. 9.2. Consider a twice differentiable functional $F(u)$ with second Gateaux derivatives

$$\frac{\delta^2 F(u)}{\delta u(\mathbf{x})^2}$$

and

$$\frac{\delta^2 F(u)}{\delta u(\mathbf{x})\delta u(\mathbf{x}')}$$

being continuous functions of \mathbf{x}, \mathbf{x}' , let $h(\mathbf{x}) \in L_2(\mathcal{D})$, then is the second Gateaux differential called

normal form iff

$$\delta^2 F[u] = \int_{\mathcal{D}} d\nu(\mathbf{x}) \frac{\delta^2 F(u)}{\delta u(\mathbf{x})^2} h(\mathbf{x})^2 + \int_{\mathcal{D}} d\nu(\mathbf{x}) \int_{\mathcal{D}} d\nu(\mathbf{x}') \frac{\delta^2 F(u)}{\delta u(\mathbf{x})\delta u(\mathbf{x}')} h(\mathbf{x})h(\mathbf{x}') \quad (23.76)$$

The second differential is called

regular form iff

$$\delta^2 F[u] = \int_{\mathcal{D}} d\nu(\mathbf{x}) \int_{\mathcal{D}} d\nu(\mathbf{x}') \frac{\delta^2 F(u)}{\delta u(\mathbf{x})\delta u(\mathbf{x}')} h(\mathbf{x})h(\mathbf{x}') \quad (23.77)$$

These definitions are relevant for the analysis of the Lévy-Laplacian [18]. Functionals with second differential in regular form automatically satisfy the Lévy-Laplacian.

Functional Taylor series

Let X be a Hilbert space of functions $y(\mathbf{x})$ defined in \mathcal{D} , let $f(y)$ be twice strongly differentiable in an open neighbourhood U of $y(\mathbf{x})$, then is the Taylor series for $y(\mathbf{x}) + h(\mathbf{x}) \in U$ given by

$$f(y + h) = f(y) + \left(\frac{\delta f}{\delta y(\mathbf{x})}, h(\mathbf{x}) \right) + \frac{1}{2} \left(\left(\frac{\delta^2 f}{\delta y(\mathbf{x})\delta y(\mathbf{x}')}, h(\mathbf{x}), h(\mathbf{x}') \right) + r(y, h) \right) \quad (23.78)$$

where $r(y, h)$ denotes the remainder.

Differentiation of measures

The Radon–Nikodym theorem is a result in measure theory [19, 20], which states that, given a measurable space (X, Σ) , if a σ -finite measure ν on (X, Σ) is absolutely continuous with respect to a σ -finite measure μ on (X, Σ) , then there is a measurable function $f : X \rightarrow [0, \infty)$, such that for any measurable subset $A \subset X$,

$$\nu(A) = \int_A d\nu(x) = \int_A f(x) d\mu(x) \quad (23.79)$$

The function f is called the Radon–Nikodym derivative and denoted by

$$f(x) = \frac{d\nu}{d\mu} \quad (23.80)$$

The derivatives of a measure can be defined (see Dalecky and Fomin [17], Chap. IV sect.2) as follows. Consider a linear space (X, \mathcal{U}) , where X denotes the set of functions defined on the domain \mathcal{D} and \mathcal{U} is a σ -algebra of subsets of X . The σ -algebra \mathcal{U} is invariant under shift by an element of a linear topological subspace $\mathcal{K} \subset X$. Consider the linear space \mathcal{M} of measures defined on (X, \mathcal{U}) with values in the linear topological space Y . For example, if $Y = [0, 1]$, then the measures in \mathcal{M} are probability measures.

Integration over particular, compact subsets in finite-dimensional spaces

The mean value of a functional $F[y]$ defined in a Hilbert space H is defined as the limit

$$\mathcal{M}_{(y_0, \rho)} F[y] = \lim_{n \rightarrow \infty} M_n F[y] \quad (23.81)$$

This definition requires the construction of a basis $\mathcal{B} = \{f_k(x)\}_1^n$ in the Hilbert space H . The functional $F[y]$ is then projected onto the n -dimensional subspace according to [18]

$$f(c_1, \dots, c_n) = F\left[\sum_{k=1}^n c_k f_k(x)\right] \quad (23.82)$$

Here the expansion coefficients c_k are given by $c_k = (y, f_k)$, $y(x) \in H$ with respect to the basis \mathcal{B} . The n -dimensional mean is then defined by

$$M_n F[y] = \frac{1}{\mathcal{A}_n} \int_{\sum_{k=1}^n (c_k - c_{0k})^2 = \rho^2} f(c_1, \dots, c_n) d\sigma_n \quad (23.83)$$

where \mathcal{A}_n denotes the surface area of the n -dimensional sphere centred at the origin in the Euclidean space R_n . The limit $n \rightarrow \infty$ must be considered in detail to insure that the definition of the mean makes sense. For this purpose, integration over finite-dimensional domains is discussed in the present section. The principal examples are the volume and the surface area of a sphere. It is helpful that the geometry of the sphere in n -dimensional Euclidean space allows the construction of a spherical system of coordinates. This is established first. Then several methods for the computation of the volume of the n -ball in the Euclidean space R^n for integer $n > 0$ are available (see the proof of H. Weyl's theorem in Gray [21], Appendix A). Two methods are presented in Sects. 23.12.1 and 23.12.1 and then conclusions are drawn from results and examples are discussed.

The standard methods of Riemann/Lebesgue integration apply to domains with finite dimension, but do not extend to infinite-dimensional domains. This will be

examined for the particular domain relevant to the definition of the Lévy-Laplacian defined as n -ball with finite radius $0 < r < \infty$. Several methods for the computation of integrals over generalized spherical domains are presented. First the approach (Smirnov [22], Wang [23], Folland [24]) based on a recursive relation between volumes of unit balls in dimensions $1 \leq n < \infty$ is applied to the computation of the volume. The second method (Courant [25], Guzman [26]) for the computation of the surface area and more general integrals over implicitly defined hypersurfaces is then discussed in detail. It uses a suitable function of the radius for the computation of the volume and surface area in n dimensions. The dimension n is assumed positive and integer in both methods. The volume and surface area of a ball are the main integrals considered. But first a brief discussion of the Lebesgue integral is given for use in various sections.

23.12.1 Lebesgue Integral

The Riemann/Darboux integral is well known, and hence only the Lebesgue integral is briefly discussed, (there exists an enormous amount of literature on the Lebesgue integral, see, for instance, Taylor [27], Lerner [28], Chap. 2.4). Consider the measure space $(\Omega, \mathcal{A}, \mu)$, let Ω be finite dimensional and let $f(x) : \Omega \rightarrow (-\infty, \infty)$ be a measurable function, i.e. the sets $S_t \equiv \{x | f(x) > t\}$ are in \mathcal{A} for all t (Borel sets for all t), let

$$\mathbf{1}_S(x) \equiv \begin{cases} 1 & \text{for } x \in S_t \\ 0 & \text{otherwise} \end{cases} \quad (23.84)$$

be the indicator function of S_t , then is the Lebesgue integral over the indicator function defined as

$$\int \mathbf{1}_S(x) \mu(dx) = \mu(S_t) \quad (23.85)$$

the measure of the set S_t . Simple functions are linear combinations of indicator functions $f(x) = \sum_k f_k \mathbf{1}_k(x)$, the integral over a measurable set $B \in \mathcal{A}$ is thus

$$\int_B f(x) \mu(dx) = \sum_k a_k \mu(S_k \cap B) \quad (23.86)$$

Consider now a measurable, non-negative function $f(x)$, then is the Lebesgue integral defined by

$$\int_B f(x) \mu(dx) = \sup \left\{ \sum_k a_k \mu(S_k \cap B) : 0 \leq \sum_k a_k S_k(x) \leq f(x), x \in B \right\} \quad (23.87)$$

The extension to signed functions is easily achieved by $f(x) = f^+(x) - f^-(x)$, $f^+(x) = \max(f(x), 0)$ $f^-(x) = \max(-f(x), 0)$. A measurable function is Lebesgue integrable if

$$\int_B |f(x)|\mu(dx) < \infty \quad (23.88)$$

holds. The values of the Lebesgue and Riemann integrals agree if both exist, there are functions that are Lebesgue integrable but not Riemann/Darboux and vice versa.

Recursive method for volume integrals

The volume $V_n(\rho)$ of the ball $\mathcal{B}_n(\rho)$ (23.39) is computed by setting up a recursive relation and then solving it. The simple rescaling transformation $x_i = \rho \rho_i$ implies $V_n(\rho) = C_n \rho^n$ thus shows that only the ball with unit radius $C_n \equiv V_n(1)$ needs to be computed, where C_n denotes the volume of the n -dimensional unit ball

$$C_n = \int_{\mathcal{B}_n(1)} dx_1 \dots dx_n \quad (23.89)$$

Consider now the plane $x_1 = \text{constant}$ intersecting the ball $\mathcal{B}_n(1)$ assuming $|x_1| < 1$, then is the intersection the $n - 1$ -dimensional ball with radius $\sqrt{1 - x_1^2}$ and volume $V_{n-1} = C_{n-1}(1 - x_1^2)^{\frac{1}{2}(n-1)}$. The volume of $\mathcal{B}_n(\rho)$ can be recovered by integration over all $-1 < x_1 < 1$ intersecting \mathcal{B}_n , hence

$$C_n = 2C_{n-1} \int_0^1 dx_1 (1 - x_1^2)^{\frac{1}{2}(n-1)} \quad (23.90)$$

The volume C_n of the unit ball is now computed in two steps: First, the integral over x_1 is determined and second, the result is applied to C_{n-1} producing a recursive relation that can be solved. The integral

$$I_n = \int_0^1 dx_1 (1 - x_1^2)^{\frac{1}{2}(n-1)} \quad (23.91)$$

can be transformed to a trigonometric integral using $x_1 = \cos(\phi)$, $dx_1 = \sin(\phi)d\phi$, hence

$$I_n = \int_0^{\frac{\pi}{2}} d\phi \sin^n(\phi) = \begin{cases} \frac{\pi}{2} \frac{1.3.5\dots(n-1)}{2.4.6\dots n} & \text{for } n \text{ even} \\ \frac{2.4.6\dots(n-1)}{1.3.5\dots n} & \text{for } n \text{ odd} \end{cases}$$

This result can be represented conveniently with the aid of the Γ -function ([29], Chap. 6, [30]). Using the relations $2.4.6\dots(n-1) = 2^{\frac{1}{2}(n-1)} \Gamma(\frac{1}{2}(n+1))$ for n

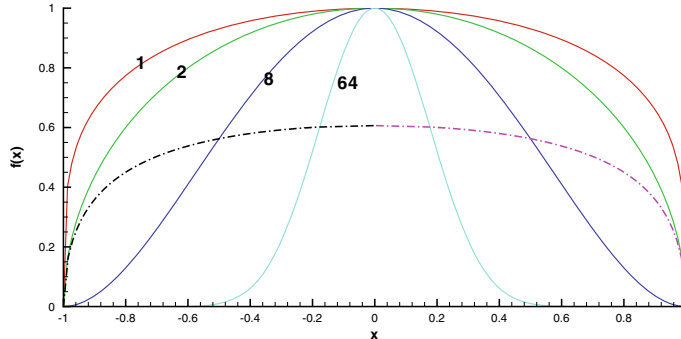


Fig. 23.1 Integrand of (23.90) leading to the recursive relation (23.93) for several values of the dimension n , which is indicated on the lines. The dimension $n = 2$ produces a circle (green line), all other dimensions result in non-circular graphs. The dot-dashed lines indicate the locations of diagonal points $(1/\sqrt{n}, \dots, 1/\sqrt{n})$, $(-1/\sqrt{n}, \dots, -1/\sqrt{n})$ as function of dimension n , the limit $n \rightarrow \infty$ is $x = 0$ and $f(x) = e^{-0.5}$. The limit $n \rightarrow \infty$ of the integrand is zero except unity at $x = 0$; therefore, the integral is zero for the limit

odd and $2.4.6\dots n = 2^{\frac{n}{2}} \Gamma(\frac{n}{2} + 1)$ for n even, and $\Gamma(\frac{n}{2} + 1) = \frac{1}{2^n} \sqrt{\pi} \cdot 1.3.5\dots(2n - 1)$ (Abramovic and Stegun, [29], Chap. 6) produce after some algebra the desired result for the integral (23.91)

$$I_n = \frac{1}{2} \sqrt{\pi} \frac{\Gamma(\frac{1}{2}(n + 1))}{\Gamma(\frac{1}{2}n + 1)} \quad (23.92)$$

valid for $n > 0$ even and odd (Fig. 23.1).

The recursive relation for the volume of the unit ball follows from (23.90) and (23.92)

$$C_n = 2I_n C_{n-1} \rightarrow C_n = C_{n-1} \sqrt{\pi} \frac{\Gamma(\frac{1}{2}(n + 1))}{\Gamma(\frac{1}{2}n + 1)}$$

holds for $n > 0$. Substituting the same relation once more for C_{n-1}

$$C_{n-1} = \sqrt{\pi} \frac{\Gamma(\frac{1}{2}n)}{\Gamma(\frac{1}{2}(n + 1))} C_{n-2} \rightarrow C_n = \frac{2\pi}{n} C_{n-2} \quad (23.93)$$

The solution of the recursive relation (23.93) can be computed if two initial values are specified. This is the case since $C_2 = \pi$ (area of the unit circle) and $C_3 = \frac{4\pi}{3}$ (volume of the unit ball) are known. For $n = 2k$, even repeated application of (23.93) produces

$$C_n = \left(\frac{2\pi}{n}\right) \left(\frac{2\pi}{n-2}\right) \cdots \left(\frac{2\pi}{4}\right) C_2 \rightarrow C_n = \frac{2^{\frac{n}{2}} \pi^{\frac{n}{2}}}{n(n-2) \cdots 4 \cdot 2}$$

Similarly, for $n = 2k + 1$ odd it follows that

$$C_n = \frac{2^{\frac{1}{2}(n+1)} \pi^{\frac{1}{2}(n-1)}}{n(n-2)(n-4) \cdots 3.1}$$

holds. These results can be combined using $1.3.5\ldots(n-2).n = \frac{n}{\sqrt{\pi}} 2^{\frac{1}{2}(n-1)} \Gamma(\frac{n}{2})$ and $2.4.6\ldots(n-2).n = 2^{\frac{n}{2}} \Gamma(\frac{n}{2} + 1)$ leading to the desired result

$$C_n = V_n(1) = \frac{\pi^{\frac{1}{2}n}}{\Gamma(\frac{1}{2}n + 1)} \quad (23.94)$$

valid for $n > 0$. The volume of the n -dimensional ball $\mathcal{B}_n(\rho)$ is then

$$V_n(\rho) = \frac{\pi^{\frac{1}{2}n} \rho^n}{\Gamma(\frac{1}{2}n + 1)}$$

(23.95)

the product of the volume of the unit ball times the n th power of the radius.

Level set method for surface integrals

A surface of dimension $0 < k \leq n$ embedded in R^n is a C^1 mapping $\mathbf{g} : \mathcal{D} \subset R^k \rightarrow R^n$, where \mathcal{D} is a closed, connected, measurable subset of R^k called domain of definition. The integral over this surface of an integrable function $f(\mathbf{x})$, $\mathbf{x} \in R^n$ is then (Guzman, [26], Chap. 5)

$$I_A[f(\mathbf{x})] = \int_A f(\mathbf{g}(\mathbf{t})) \sqrt{\det \left(\sum_{m=1}^n \frac{\partial g_m}{\partial t_i} \frac{\partial g_m}{\partial t_j} \right)} \prod_{l=1}^k dt_l \quad (23.96)$$

where $\mathbf{x} = \mathbf{g}(\mathbf{t})$, $\mathbf{t} \in \mathcal{D} \subset R^k$. Consider a C^1 scalar field $\Phi(x_1, \dots, x_n)$ mapping R^n onto the range $\mathcal{R}_\Phi \subset R^1$ of the scalar field, a level surface (or fiber or preimage of a point in \mathcal{R}_Φ) is defined the set of all points in R^n satisfying

$$\Phi(x_1, \dots, x_n) = \rho, \quad \rho \in \mathcal{R}_\Phi \quad (23.97)$$

The set of all preimage points for a given $\rho \in \mathcal{R}_\Phi$ is $B(\rho) = \{(x_1, \dots, x_n) : \Phi(x_1, \dots, x_n) = \rho\} \subset R^n$. This set $B(\rho)$ is not necessarily bounded or connected, and hence conditions are imposed on the scalar field $\Phi(x_1, \dots, x_n)$ such that the surfaces defined by (23.97) are compact without boundary for a suitable range of values in \mathcal{R} and they can be represented as the union of a finite number of disjoint patches, where (23.97) can be solved uniquely for one of the coordinates, say $x_n(x_1, \dots, x_{n-1}, \rho)$. The surface integral (23.96) is the sum of the integrals over all patches. It remains to construct the mapping $\mathbf{g} : R^{n-1} \rightarrow R^n$ generated by the scalar field (23.97) and to determine the surface differential.

Surface differential

Consider a patch and a point \mathbf{x}^0 on it, where $\Phi(\mathbf{x}^0) = \rho$ and an open neighbourhood $U(\mathbf{x}^0)$ exists with $x_n = f(x_1, \dots, x_{n-1}, \rho)$ being the unique, differentiable and non-

zero solution of (23.97) in U . The mapping \mathbf{g} is then explicitly constructed as

$$g_i = t_i, \text{ for } t_i = x_i, 1 \leq i \leq n-1, g_n = f(t_1, \dots, t_{n-1}, \rho) \quad (23.98)$$

where $\mathbf{t} \in R^{n-1}$. The gradient of $g_i(\mathbf{t}) : U(\mathbf{x}^0) \subset R^{n-1} \rightarrow R^n$ is computed using

$$\frac{\partial \Phi}{\partial x_i} + \frac{\partial \Phi}{\partial x_n} \frac{\partial x_n}{\partial x_i} = 0, \quad 1 \leq i < n$$

for $x_n = f(x_1, \dots, x_{n-1}, \rho)$ leading to

$$\frac{\partial g_i}{\partial t_j} = \begin{cases} 0 & \text{for } i < n, i \neq j \\ 1 & \text{for } i < n, i = j \\ \frac{\partial f}{\partial t_j} & \text{for } j = n-1 \end{cases}$$

for $1 \leq i \leq n, 1 \leq j < n$ and

$$\frac{\partial f}{\partial t_j} = -\frac{\frac{\partial \Phi}{\partial x_j}}{\frac{\partial \Phi}{\partial x_n}} \quad (23.99)$$

The surface differential $d\sigma$ is then according to (23.96)

$$d\sigma = \sqrt{\det \left(\sum_{m=1}^n \frac{\partial g_m}{\partial t_i} \frac{\partial g_m}{\partial t_j} \right)} \prod_{l=1}^{n-1} dt_l \quad (23.100)$$

The final step is the computation of the determinant

$$D_n \equiv \left| \sum_{m=1}^n \frac{\partial g_m}{\partial t_i} \frac{\partial g_m}{\partial t_j} \right|$$

where the symmetric matrix has the structure

$$\sum_{m=1}^n \frac{\partial g_m}{\partial t_i} \frac{\partial g_m}{\partial t_j} = \begin{pmatrix} 1 + \left(\frac{\partial f}{\partial t_1} \right)^2 & \frac{\partial f}{\partial t_1} \frac{\partial f}{\partial t_2} & \dots & \frac{\partial f}{\partial t_1} \frac{\partial f}{\partial t_{n-1}} \\ \frac{\partial f}{\partial t_2} \frac{\partial f}{\partial t_1} & 1 + \left(\frac{\partial f}{\partial t_2} \right)^2 & \dots & \frac{\partial f}{\partial t_2} \frac{\partial f}{\partial t_{n-1}} \\ \vdots & \vdots & \ddots & \vdots \\ \frac{\partial f}{\partial t_{n-1}} \frac{\partial f}{\partial t_1} & \frac{\partial f}{\partial t_{n-1}} \frac{\partial f}{\partial t_2} & \dots & 1 + \left(\frac{\partial f}{\partial t_{n-1}} \right)^2 \end{pmatrix}$$

Developing the determinant D along the first row shows that it can be broken up into the sum of two determinants $D = D_0 + D_1$ where

$$D_0 = \begin{vmatrix} 1 & 0 & \cdots & 0 \\ \frac{\partial f}{\partial t_2} \frac{\partial f}{\partial t_1} & 1 + \left(\frac{\partial f}{\partial t_2}\right)^2 & \cdots & \frac{\partial f}{\partial t_2} \frac{\partial f}{\partial t_{n-1}} \\ \cdot & \cdot & \cdots & \cdot \\ \cdot & \cdot & \cdots & \cdot \\ \frac{\partial f}{\partial t_{n-1}} \frac{\partial f}{\partial t_1} & \frac{\partial f}{\partial t_{n-1}} \frac{\partial f}{\partial t_2} & \cdots & 1 + \left(\frac{\partial f}{\partial t_{n-1}}\right)^2 \end{vmatrix}$$

and

$$D_1 = \begin{vmatrix} \left(\frac{\partial f}{\partial t_1}\right)^2 & \frac{\partial f}{\partial t_1} \frac{\partial f}{\partial t_2} & \cdots & \frac{\partial f}{\partial t_1} \frac{\partial f}{\partial t_{n-1}} \\ \frac{\partial f}{\partial t_2} \frac{\partial f}{\partial t_1} & 1 + \left(\frac{\partial f}{\partial t_2}\right)^2 & \cdots & \frac{\partial f}{\partial t_2} \frac{\partial f}{\partial t_{n-1}} \\ \cdot & \cdot & \cdots & \cdot \\ \cdot & \cdot & \cdots & \cdot \\ \frac{\partial f}{\partial t_{n-1}} \frac{\partial f}{\partial t_1} & \frac{\partial f}{\partial t_{n-1}} \frac{\partial f}{\partial t_2} & \cdots & 1 + \left(\frac{\partial f}{\partial t_{n-1}}\right)^2 \end{vmatrix}$$

Consider the second determinant, it can be reduced to

$$D_1 = \frac{\partial f}{\partial t_1} \begin{vmatrix} \frac{\partial f}{\partial t_1} & \frac{\partial f}{\partial t_2} & \cdots & \frac{\partial f}{\partial t_{n-1}} \\ \frac{\partial f}{\partial t_2} \frac{\partial f}{\partial t_1} & 1 + \left(\frac{\partial f}{\partial t_2}\right)^2 & \cdots & \frac{\partial f}{\partial t_2} \frac{\partial f}{\partial t_{n-1}} \\ \cdot & \cdot & \cdots & \cdot \\ \cdot & \cdot & \cdots & \cdot \\ \frac{\partial f}{\partial t_{n-1}} \frac{\partial f}{\partial t_1} & \frac{\partial f}{\partial t_{n-1}} \frac{\partial f}{\partial t_2} & \cdots & 1 + \left(\frac{\partial f}{\partial t_{n-1}}\right)^2 \end{vmatrix}$$

and subtracting the first row multiplied with $\frac{\partial f}{\partial t_2}$ from the second row and continuing this procedure down to the last row produces

$$D_1 = \frac{\partial f}{\partial t_1} \begin{vmatrix} \frac{\partial f}{\partial t_1} \frac{\partial f}{\partial t_2} & \cdots & \frac{\partial f}{\partial t_{n-1}} \\ 0 & 1 & \cdots & 0 \\ \cdot & \cdot & \cdots & \cdot \\ \cdot & \cdot & \cdots & \cdot \\ 0 & 0 & \cdots & 1 \end{vmatrix}$$

Hence

$$D = D_0 + \left(\frac{\partial f}{\partial t_1}\right)^2$$

follows. This step can be repeated by expanding D_0 along the first row and splitting

$$D = \begin{vmatrix} 1 & 0 & \cdots & 0 \\ \frac{\partial f}{\partial t_3} \frac{\partial f}{\partial t_2} & 1 + \left(\frac{\partial f}{\partial t_3}\right)^2 & \cdots & \frac{\partial f}{\partial t_3} \frac{\partial f}{\partial t_{n-1}} \\ \cdot & \cdot & \cdots & \cdot \\ \cdot & \cdot & \cdots & \cdot \\ \frac{\partial f}{\partial t_{n-1}} \frac{\partial f}{\partial t_2} & \frac{\partial f}{\partial t_{n-1}} \frac{\partial f}{\partial t_3} & \cdots & 1 + \left(\frac{\partial f}{\partial t_{n-1}}\right)^2 \end{vmatrix} + \left(\frac{\partial f}{\partial t_1}\right)^2 + \left(\frac{\partial f}{\partial t_2}\right)^2$$

down to the last determinant $D_0 = 1 + \left(\frac{\partial f}{\partial t_{n-1}}\right)^2$ of a 1×1 matrix. Hence

$$D = 1 + \sum_{j=1}^{n-1} \left(\frac{\partial f}{\partial t_j} \right)^2$$

is obtained and the surface differential (23.100) emerges in the form

$$d\sigma = \sqrt{1 + \sum_{j=1}^{n-1} \left(\frac{\partial f}{\partial t_j} \right)^2} \prod_{l=1}^{n-1} dt_l \quad (23.101)$$

where $\mathbf{t} \in \mathcal{D} \subset R^k$. It can be expressed in terms of the scalar field using (23.98) and (23.99)

$$d\sigma = \sqrt{1 + \sum_{j=1}^{n-1} \left(\frac{\partial \Phi}{\partial x_j} \right)^2} \prod_{l=1}^{n-1} dx_l$$

or

$$d\sigma = \frac{||\nabla \Phi||}{||\mathbf{e}_n \cdot \nabla \Phi||} \prod_{j=1}^{n-1} dx_j \quad (23.102)$$

where $||\nabla \Phi|| = (\nabla \Phi \cdot \nabla \Phi)^{\frac{1}{2}}$ denotes the L^2 -norm of the scalar gradient and \mathbf{e}_n denotes the unit vector normal to the level surface.

Surface integral: n -Sphere with radius ρ

A sphere with radius ρ is generated as level surface of the scalar field

$$\Phi(x_1, x_2, \dots, x_n) \equiv \sum_{i=1}^n x_i^2 = \rho^2 \quad (23.103)$$

by (23.40) $\mathcal{S}_n(r) = \{\mathbf{x} : \Phi(\mathbf{x}) = \rho^2\}$ with two patches for $x_n = \pm \rho$. The surface area $A_n(\rho)$ of a ball in R^n is computed with the aid of a suitably chosen function $f(x_1, \dots, x_n)$ integrated over a $(n-1)$ -dimensional surface patch

$$I_n(\rho) = \int_{\mathcal{S}_n(\rho)} f(x_1, \dots, x_n) d\sigma \quad (23.104)$$

which is specified by (23.97). The coordinate $x_n(x_1, \dots, x_n, \rho)$ in this patch is a solution of (23.97) and the integral over the complete level surface is the sum of the integrals over all patches. The surface differential (23.102) shows that this integral is

$$I_n(\rho) = \int_{\mathcal{S}_n(\rho)} f(x_1, \dots, x_n) \frac{1}{\left| \frac{\partial \Phi}{\partial x_n} \right|} \left[\sum_{i=1}^n \left(\frac{\partial \Phi}{\partial x_i} \right)^2 \right]^{\frac{1}{2}} dx_1 \cdots dx_{n-1} \quad (23.105)$$

The function $f(x_1, \dots, x_n)$ is now specified for the computation of the surface area of a ball as $f(x_1, \dots, x_n) = f(r)$, $r^2 = \sum_{i=1}^n x_i^2$ in the ball $\mathcal{B}_n(\rho)$ and $\Phi(\mathbf{x}) = r^2$ for $0 \leq r \leq \rho$. The idea is to start with the volume integral

$$V_n(f) = \int_{\mathcal{B}_n(\rho)} f(r) \prod_{j=1}^n dx_j \quad (23.106)$$

and to express it as iterated integral over the level surface and the integral over the normal direction. The surface differential (23.102) can be introduced to write the volume integral $V_n(f)$

$$V_n(f) = \int_{\mathcal{B}_n(\rho)} \frac{f(r)}{\left| \frac{\partial \Phi}{\partial x_n} \right|} \left[\sum_{i=1}^n \left(\frac{\partial \Phi}{\partial x_i} \right)^2 \right]^{\frac{1}{2}} \prod_{j=1}^n dx_j \quad (23.107)$$

as iterated integral. Since for $\Phi(x_1, x_2, \dots, x_n) = \sum_{i=1}^n x_i^2 = r^2$, $0 \leq r \leq \rho$ $\frac{\partial \Phi}{\partial x_j} = 2x_j$ thus $\|\nabla \Phi\| = 2r$ and $2rdr = \frac{\partial \Phi}{\partial x_n} dx_n$

$$I_n(f) = \int_0^\rho dr f(r) \int_{\mathcal{S}_n(\rho)} d\sigma \quad (23.108)$$

The integration over the surface is by definition the $(n-1)$ -dimensional area of $\mathcal{S}(\rho)$ denoted by $A_n(\rho)$ and the volume integral emerges in the form

$$I_n(f) = \int_0^\rho dr f(r) A_n(r) \quad (23.109)$$

The surface area is a homogeneous function of the radius ρ , hence $A_n(\rho) = A_n(1)\rho^{n-1}$, where $A_n(1)$ is the surface area of the unit n -ball, and the volume integral is now given by

$$I_n(f) = A_n(1) \int_0^\rho dr f(r) r^{n-1} \quad (23.110)$$

This result is the key for the computation of the surface area $A_n(1)$. The following choice for $\rho = \infty$ and

$$f(r) = \exp(-r^2) = \exp\left(-\sum_{i=1}^n x_i^2\right) \quad (23.111)$$

produces

$$I_n(f) = A_n(1) \int_0^\infty dr \exp(-r^2) r^{n-1}, \quad I_n(f) = \left[\int_{-\infty}^\infty dr \exp(-r^2) \right]^n \quad (23.112)$$

These integrals are known, [30]

$$\int_{-\infty}^\infty dr \exp(-x^2) = \sqrt{\pi}, \quad \int_0^\infty dr \exp(-r^2) r^{n-1} = \frac{1}{2} \Gamma\left(\frac{n}{2}\right) \quad (23.113)$$

where $\Gamma(x)$ is the Gamma function. The surface area of the unit ball is then

$$A_n(1) = \frac{2\pi^{\frac{n}{2}}}{\Gamma\left(\frac{n}{2}\right)} \quad (23.114)$$

and

$$A_n(\rho) = \frac{2\pi^{\frac{n}{2}} \rho^{n-1}}{\Gamma\left(\frac{n}{2}\right)} \quad (23.115)$$

is the surface area of a n -dimensional sphere of radius ρ . Putting $f(r) = 1$ in (23.109) and using the result (23.115) just obtained lead to

$$I_n(f) = \frac{2\pi^{\frac{n}{2}}}{\Gamma\left(\frac{n}{2}\right)} \int_0^\rho dr r^{n-1} \quad (23.116)$$

which emerges as the volume of the n -dimensional ball in the form

$$V_n(\rho) = \frac{2\pi^{\frac{n}{2}} \rho^n}{n \Gamma\left(\frac{n}{2}\right)} = \frac{\pi^{\frac{n}{2}} \rho^n}{\Gamma\left(\frac{n}{2} + 1\right)} = \frac{\mathcal{A}_n}{n} \quad (23.117)$$

which agrees with the result obtained with the recursive method in Sect. 23.12.1.

The method of Wang and Folland

Wang [23] developed a method to compute the volume of a family of compact subsets of R^n topologically equivalent to the unit ball called generalized balls based on ideas of Folland [24]. Specifically, the compact domains considered are defined by

$$B_{p_1, \dots, p_n} \equiv \{(x_1, \dots, x_n) : \sum_{j=1}^n |x_j|^{p_j} \leq 1\} \quad (23.118)$$

where $p_j > 0, \forall j = 1, \dots, n$. Wang [23] proves the following theorem.

Theorem: The volume V of the unit ball B_{p_1, \dots, p_n} for $p_1 > 0, \dots, p_n > 0$ embedded in R^n is given by

$$V(B_{p_1, \dots, p_n}) = 2^n \frac{\prod_{j=1}^n \Gamma(1 + \frac{1}{p_j})}{\Gamma(1 + \sum_{j=1}^n \frac{1}{p_j})} \quad (23.119)$$

Proof: The volume V is defined as integral

$$V(B_{p_1, \dots, p_n}) = \int_{B_{p_1, \dots, p_n}} d\mathbf{x} \quad (1)$$

embedded in R^n and using Cartesian coordinates. Since $p_j > 0, \forall j$ the coordinate transformation

$$x_j = y_j^{\frac{2}{p_j}}, \quad 1 \leq j \leq n$$

can be applied. The transformed domain is then the standard ball in R^n

$$\mathcal{B}_n = \{(y_1, \dots, y_n) : y_1^2 + \dots + y_n^2 \leq 1\}$$

The Jacobian determinant $J = \det(\partial x_j / \partial y_k)$ is easily computed

$$J = \frac{2^n}{\prod_{j=1}^n p_j} \prod_{j=1}^n y_j^{\frac{2}{p_j} - 1}$$

and the volume in the transformed coordinates follows in the form

$$V(B_{p_1, \dots, p_n}) = \int_{B_{p_1, \dots, p_n}} d\mathbf{x} = \frac{2^n}{\prod_{j=1}^n p_j} \int_{\mathcal{B}_n} d\mathbf{y} \prod_{j=1}^n |y_j|^{\frac{2}{p_j} - 1} \quad (2)$$

It remains to compute the integral

$$I_n(\alpha_1, \dots, \alpha_n) \equiv \int_{\mathcal{B}_n} d\mathbf{y} \prod_{j=1}^n |y_j|^{\alpha_j}, \quad I_1(\alpha_n) = \int_{B_1} dy_n |y_n|^{\alpha_n}, \quad B_1 = \{y_n : y_n^2 \leq 1\} \quad (3)$$

over the standard ball with unit radius, where $\alpha_j \equiv \frac{2}{p_j} - 1 > -1$ abbreviates the exponents. The integration in I_n is organized by starting with y_1

$$I_n = \int_{-1}^1 |y_1|^{\alpha_1} \int_{y_2^2 + \dots + y_n^2 \leq 1 - y_1^2} \prod_{j=2}^n |y_j|^{\alpha_j} dy_j dy_1$$

and rescaling $y_j \equiv rz_j$, $j = 2, \dots, n$ with $r = \sqrt{1 - y_1^2}$, hence

$$I_n = \int_{-1}^1 |y_1|^{\alpha_1} r^{n-1 + \sum_{j=2}^n \alpha_j} \int_{z_2^2 + \dots + z_n^2 \leq 1} \prod_{j=2}^n |z_j|^{\alpha_j} dz_j dy_1$$

or

$$I_n = 2 \int_0^1 y_1^{\alpha_1} (1 - y_1^2)^{\frac{1}{2}(n-1) + \frac{1}{2} \sum_{j=2}^n \alpha_j} dy_1 \int_{z_2^2 + \dots + z_n^2 \leq 1} \prod_{j=2}^n |z_j|^{\alpha_j} dz_j$$

leading to the recursive relation

$$I_n(\alpha_1, \dots, \alpha_n) = 2 \int_0^1 y_1^{\alpha_1} (1 - y_1^2)^{\frac{1}{2}(n-1) + \frac{1}{2} \sum_{j=2}^n \alpha_j} dy_1 I_{n-1}(\alpha_2, \dots, \alpha_n)$$

The integral over y_1 can be expressed in terms of the Γ function once the transformation $z_1 \equiv y_1^2$ is applied

$$I_n(\alpha_1, \dots, \alpha_n) = \int_0^1 z_1^{\frac{1}{2}(\alpha_1 - 1)} (1 - z_1)^{\frac{1}{2}(n-1) + \frac{1}{2} \sum_{j=2}^n \alpha_j} dz_1 I_{n-1}(\alpha_2, \dots, \alpha_n)$$

The Γ -function satisfies the relation

$$\int_0^1 x^{n-1} (1 - x)^{m-1} = \frac{\Gamma(n)\Gamma(m)}{\Gamma(n+m)}$$

Hence, the final form of the recursive relation

$$I_n(\alpha_1, \dots, \alpha_n) = \frac{\Gamma(\frac{1}{2}(\alpha_1 + 1)) \Gamma(\frac{1}{2}(n + 1 + \sum_{j=2}^n \alpha_j))}{\Gamma(\frac{1}{2}(2 + n + \sum_{j=1}^n \alpha_j))} I_{n-1}(\alpha_2, \dots, \alpha_n)$$

valid for $1 \leq j \leq n$ is obtained. Denoting the coefficient of the recursive relation by

$$F_n(\alpha_1, \dots, \alpha_n) = \frac{\Gamma(\frac{1}{2}(\alpha_1 + 1))\Gamma(\frac{1}{2}(n + 1 + \sum_{j=2}^n \alpha_j))}{\Gamma(\frac{1}{2}(2 + n + \sum_{j=1}^n \alpha_j))}$$

the relation emerges as

$$I_n(\alpha_1, \dots, \alpha_n) = F_n(\alpha_1, \dots, \alpha_n)I_{n-1}(\alpha_2, \dots, \alpha_n)$$

Repeated application of it

$$I_n(\alpha_1, \dots, \alpha_n) = F_n(\alpha_1, \dots, \alpha_n)F_{n-1}(\alpha_2, \dots, \alpha_n)I_{n-2}(\alpha_3, \dots, \alpha_n)$$

etc. leads to

$$I_n(\alpha_1, \dots, \alpha_n) = F_n(\alpha_1, \dots, \alpha_n)F_{n-1}(\alpha_2, \dots, \alpha_n) \cdots F_2(\alpha_{n-1}, \alpha_n)I_1(\alpha_n) \quad (4)$$

The 1-d integral on the right side is given by (3), the evaluation is elementary

$$I_1(\alpha_n) = \int_{-1}^1 dy_n |y_n|^{\alpha_n} = 2 \int_0^1 dy_n y_n^{\alpha_n} = \frac{2}{\alpha_n + 1}$$

The product of the coefficients allows cancellation of a factor

$$F_n(\alpha_1, \dots, \alpha_n)F_{n-1}(\alpha_2, \dots, \alpha_n) \cdots F_2(\alpha_{n-1}, \alpha_n) = \frac{\prod_{j=1}^{n-1} \Gamma(\frac{1}{2}(1 + \alpha_j))\Gamma(\frac{1}{2}(1 + \alpha_n) + 1)}{\Gamma(\frac{1}{2}(2 + n + \sum_{j=1}^n \alpha_j))} \quad (5)$$

The last term in the numerator is evaluated as

$$\Gamma(\frac{1}{2}(1 + \alpha_n) + 1) = \frac{1}{2}(1 + \alpha_n)\Gamma(\frac{1}{2}(1 + \alpha_n)) \quad (6)$$

canceling the integral $I_1(\alpha_n)$. Substituting (5) and (6) in (4)

$$I_n(\alpha_1, \dots, \alpha_n) = \frac{\prod_{j=1}^n \Gamma(\frac{1}{2}(1 + \alpha_j))}{\Gamma(\frac{1}{2}(2 + n + \sum_{j=1}^n \alpha_j))}$$

concludes the computation of I_n . The volume is thus according to (2)

$$V(B_{p_1, \dots, p_n}) = \frac{2^n}{\prod_{j=1}^n p_j} I_n(\alpha_1, \dots, \alpha_n)$$

and, using the definition $\alpha_j = \frac{2}{p_j} - 1$, the result

$$V(B_{p_1, \dots, p_n}) = \frac{2^n}{\prod_{j=1}^n p_j} \frac{\prod_{j=1}^n \Gamma(\frac{1}{p_j})}{\Gamma(1 + \sum_{j=1}^n \frac{1}{p_j})} = 2^n \frac{\prod_{j=1}^n \Gamma(\frac{1}{p_j} + 1)}{\Gamma(1 + \sum_{j=1}^n \frac{1}{p_j})}$$

is obtained. This concludes the proof.

An orthant or hyperoctant $O(B_{p_1, \dots, p_n})$ [31] is the analogue in R^n of a quadrant in the plane or an octant in three dimensions. A closed orthant in R^n is a subset defined by constraining each Cartesian coordinate to be non-negative or non-positive. Such a subset is defined by a system of inequalities: $\epsilon_1 x_1 \geq 0, \epsilon_2 x_2 \geq 0, \dots, \epsilon_n x_n \geq 0$, where each ϵ_i is either +1 or -1. It follows that the generalized ball in R^n has 2^n orthants with the same volume

$$V(O(B_{p_1, \dots, p_n})) = \frac{\prod_{j=1}^n \Gamma(\frac{1}{p_j} + 1)}{\Gamma(1 + \sum_{j=1}^n \frac{1}{p_j})}$$

since the volume $V(B_{p_1, \dots, p_n})$ (23.118) depends only on $|x_j|$.

Integration is a linear operation, and hence it applies to finite unions and intersections of generalized balls shifted to arbitrary locations in R^n . Hence, the family of generalized balls can be extended to form a finite algebra of subsets of R^n with respect to integration.

23.13 Examples

Courant's method allows the computation of volume and surface area of compact, non-spherical subsets of R^n that are smooth images of balls. The case of an n -dimensional ellipsoid is considered first. The level surfaces are then defined by

$$\Phi(x_1, x_2, \dots, x_n) = \sum_{i=1}^n \left(\frac{x_i}{a_i}\right)^2 \tag{23.120}$$

being constant, where $a_i > 0$ for all i is assumed. The ellipsoid is then

$$A_n(\rho) \equiv \{\mathbf{x} : \Phi(x_1, \dots, x_n) \leq \rho^2\} \quad (23.121)$$

and its surface is the set

$$\mathcal{S}_n(\rho) \equiv \{\mathbf{x} : \Phi(x_1, \dots, x_n) = \rho^2\} \quad (23.122)$$

The Riemann integral

$$V_n(\rho) = \int_{\mathcal{S}_n(\rho)} \cdots \int dx_1 \cdots dx_n \quad (23.123)$$

can be transformed according to $\rho_i = \frac{x_i}{a_i}$ and leads to

$$\int_{\mathcal{S}_n(\rho)} \cdots \int dx_1 \cdots dx_n = \prod_{i=1}^n a_i \int_{\mathcal{S}_n(\rho)} \cdots \int d\rho_1 \cdots d\rho_n \quad (23.124)$$

The integral on the right side is the volume of the n -ball, hence

$$V_n(\rho) = \frac{\pi^{\frac{n}{2}} \rho^n}{\Gamma(\frac{n}{2} + 1)} \prod_{i=1}^n a_i \quad (23.125)$$

where ρ can be set to unity without restricting generality, hence

$$V_n(1) = \frac{\pi^{\frac{n}{2}}}{\Gamma(\frac{n}{2} + 1)} \prod_{i=1}^n a_i \quad (23.126)$$

is the volume of the n -dimensional ellipsoid $\mathcal{S}_n(1)$.

23.14 Problems for Sect. 23.14

Problem 23.12.1: *Compute the volume*

$$V_n^p(\rho) = \int_{\|\mathbf{x}\|_p < \rho} d\mathbf{x}$$

of the ball $B_n(\rho) \equiv \{x \in R^n : \|x\|_p \leq \rho\}$ with radius $\rho = 1$ (unit ball) in R^n for the L^p norm (23.18)

$$\|\mathbf{x}\|_p \equiv \left(\sum_{j=1}^n |\mathbf{x}|^p \right)^{\frac{1}{p}}$$

for $p = 1$, where \mathbf{x} is a n -dimensional vector.

Problem 23.12.2: Compute the volume

$$V_n^p(\rho) = \int_{\|\mathbf{x}\|_p < \rho} d\mathbf{x}$$

of the ball $B_n(\rho) \equiv \{x \in R^n : \|x\|_p \leq \rho\}$ with radius $\rho = 1$ (unit ball) in R^n for the L^p norm (23.18)

$$\|\mathbf{x}\|_p \equiv \left(\sum_{j=1}^n |\mathbf{x}|^p \right)^{\frac{1}{p}}$$

for $1 < p < \infty$. Plot the volume $V_n^p(1)$ as function of n and p .

Problem 23.12.3: Compute the volume of the generalized balls (23.118) for $n = 3$ and $\mathbf{p} = (0.2, 0.5, 2)^T$ and $\mathbf{p} = (0.2, 1.5, 2)^T$. Plot the balls and the volume $V(0.2, p_2, 2)$ as function of $0.1 \leq p_2 \leq 10$.

23.15 Spherical Coordinates in R^n

Blumenson [32], Miller [33], Yeh [34], Chap. 26.11 have shown that spherical coordinates can be defined in R^n for dimensions $n \geq 2$, but the coordinates are not unique. Their particular definition has proved useful and will be applied to the computation of special integrals in the following sections. Let $\{x_1, x_2, \dots, x_n\}$ be the Cartesian coordinates of a vector of length r , then are the spherical coordinates $\{r, \phi_1, \phi_2, \dots, \phi_{n-2}, \phi_{n-1}\}$, where $0 \leq \rho < \infty$, $0 \leq \phi_k \leq \pi$, $k = 1, \dots, n-2$, $0 \leq \phi_{n-1} \leq 2\pi$, and transform to the Cartesian coordinates for $n > 2$ according to

$$\begin{aligned} x_1 &= r \cos(\phi_1), \quad x_j = r \cos \phi_j \prod_{k=1}^{j-1} \sin \phi_k, \quad 2 \leq j \leq n-2 \\ x_{n-1} &= r \cos \phi_{n-1} \prod_{k=1}^{n-2} \sin \phi_k \\ x_n &= r \sin \phi_{n-1} \prod_{k=1}^{n-2} \sin \phi_k \end{aligned} \tag{23.127}$$

and for $n = 2$

$$x_1 = r \cos \phi_{n-1}, \quad x_2 = r \sin \phi_{n-1} \tag{23.128}$$

The Jacobian J of the transformation from Cartesian to

$$J(r, \phi_1, \dots, \phi_{n-2}) = \left| \frac{\partial(x_1, x_2, \dots, x_n)}{\partial(r, \phi_1, \dots, \phi_{n-1})} \right| \tag{23.129}$$

spherical coordinates can be constructed explicitly [33]

$$J(r, \phi_1, \dots, \phi_{n-2}) = \begin{cases} r & \text{for } n = 2 \\ r^{n-1} \prod_{k=1}^{n-2} \sin^{n-1-k} \phi_k & \text{for } n > 2 \end{cases} \quad (23.130)$$

by induction. The volume differential is then

$$dV_n = J(r, \phi_1, \dots, \phi_{n-2}) dr \prod_{k=1}^{n-1} d\phi_k = r^{n-1} dr d\phi_{n-1} \begin{cases} 1 & \text{for } n = 2 \\ \prod_{k=1}^{n-2} \sin^{n-1-k} \phi_k d\phi_k & \text{for } n > 2 \end{cases} \quad (23.131)$$

and the volume of the n -ball can be recovered by integration

$$V_n(\rho) = \begin{cases} \int_0^\rho dr r^{n-1} \int_0^{2\pi} d\phi_{n-1} & \text{for } n = 2 \\ \int_0^\rho dr r^{n-1} \int_0^\pi d\phi_1 \cdots \int_0^\pi d\phi_{n-2} \int_0^{2\pi} d\phi_{n-1} \prod_{k=1}^{n-2} \sin^{n-1-k} \phi_k & \text{for } n > 2 \end{cases} \quad (23.132)$$

or

$$V_n(\rho) = 2\pi \frac{\rho^n}{n} \begin{cases} 1 & \text{for } n \leq 2 \\ \prod_{k=1}^{n-2} \int_0^\pi d\phi_k \sin^{n-1-k} \phi_k & \text{for } n > 2 \end{cases} \quad (23.133)$$

Orthogonality of the unit vectors in the spherical coordinate system implies that the volume differential is the product of the radial differential dr times the surface differential $d\sigma_n$, hence

$$d\sigma_n(\rho) = \rho^{n-1} d\phi_{n-1} \begin{cases} 1 & \text{for } n = 2 \\ \prod_{k=1}^{n-2} \sin^{n-1-k} \phi_k d\phi_k & \text{for } n > 2 \end{cases} \quad (23.134)$$

and the surface differential of the unit sphere is then

$$d\sigma_n(1) = d\phi_{n-1} \begin{cases} 1 & \text{for } n = 2 \\ \prod_{k=1}^{n-2} \sin^{n-1-k} \phi_k d\phi_k & \text{for } n > 2 \end{cases} \quad (23.135)$$

The surface area of the unit sphere can be recovered by integration

$$\mathcal{A}_n(1) = 2\pi \begin{cases} 1 & \text{for } n = 2 \\ \prod_{k=1}^{n-2} \int_0^\pi d\phi_k \sin^{n-1-k} \phi_k & \text{for } n > 2 \end{cases} \quad (23.136)$$

and for arbitrary radius the result

$$\mathcal{A}_n(\rho) = \rho^{n-1} \mathcal{A}_n(1) \quad (23.137)$$

is obtained for the surface area of a sphere. The volume of the n -ball is then given by

$$V_n(\rho) = \frac{\rho}{n} \mathcal{A}_n(\rho) \quad (23.138)$$

Note that the subscript n in the surface area \mathcal{A}_n refers to the dimension of the embedding space R^n , the sphere is a manifold of dimension $n - 1$.

The integration for the surface area can be carried out with the aid of elementary integrals involving trigonometric functions

$$\int_0^\pi d\phi_k \sin^{n-1-k} \phi_k = \sqrt{\pi} \frac{\Gamma(\frac{1}{2}(n-k))}{\Gamma(\frac{1}{2}(n-k+1))} \quad (23.139)$$

valid for $n \geq 2$ and $1 \leq k \leq n - 2$. The surface area can be checked with the general result (23.115), computation shows that

$$M_n \equiv \prod_{k=1}^{n-2} \int_0^\pi d\phi_k \sin^{n-1-k} \phi_k = \frac{\pi^{\frac{n}{2}-1}}{\Gamma(\frac{n}{2})} \quad (23.140)$$

holds for $n > 2$. For instance, $n = 3$ leads to $M_3 = 2$ by integration, which agrees with the formula (23.140) using $\Gamma(\frac{3}{2}) = \frac{1}{2}\pi^{\frac{1}{2}}$.

23.16 Applications of Spherical Coordinates

Integrals over the n -ball, centred at the origin, and its surface can be set up in spherical coordinates. Three examples are considered for later application to the evaluation of the Lèvy-Laplacian and an example for averaging over an infinite-dimensional sphere.

23.16.1 Integrand x_k

The integral defined in Cartesian coordinates by

$$I_n^1(\rho) \equiv \int_{S_n(\rho)} d\sigma x_k \quad (23.141)$$

for $1 \leq k \leq n$ is transformed to spherical coordinates. Without restricting generality it can be assumed that $k = 1$, hence $x_1 = r \cos \phi_1$ and using (23.134)

$$I_n^1(\rho) = \rho^n \begin{cases} \int_0^{2\pi} \cos(\phi_1) d\phi_{n-1} & \text{for } n = 2 \\ 2\pi \int_0^\pi d\phi_1 \cos(\phi_1) \sin^{n-2}(\phi_1) \int_0^\pi d\phi_2 \cdots \int_0^\pi d\phi_{n-2} \prod_{k=2}^{n-2} \sin^{n-1-k} \phi_k & \text{for } n > 2 \end{cases} \quad (23.142)$$

follows. Since

$$\int \cos(\phi_1) d\phi_1 = \sin(\phi_1), \quad \int d\phi_1 \cos(\phi_1) \sin^{n-2}(\phi_1) = \frac{1}{n-1} \sin^{n-1}(\phi_1) \quad (23.143)$$

hold, the conclusion

$$I_n^1(\rho) = 0 \quad (23.144)$$

is reached.

23.16.2 Integrand x_k^2

The integral defined in Cartesian coordinates by

$$I_n^2(\rho) \equiv \int_{S_n(\rho)} d\sigma x_k^2 \quad (23.145)$$

for $1 \leq k \leq n$ is transformed to spherical coordinates. Without restricting generality it can be assumed that $k = 1$, hence $x_1 = r \cos \phi_1$ and using (23.134)

$$I_n^2(\rho) = \rho^{n+1} \begin{cases} \int_0^{2\pi} \cos^2(\phi_1) d\phi_{n-1} & \text{for } n = 2 \\ 2\pi \int_0^\pi d\phi_1 \cos^2(\phi_1) \sin(\phi_1) & \text{for } n = 3 \\ 2\pi \int_0^\pi d\phi_1 \cos^2(\phi_1) \sin^{n-2}(\phi_1) \int_0^\pi d\phi_2 \cdots \int_0^\pi d\phi_{n-2} \prod_{k=2}^{n-2} \sin^{n-1-k} \phi_k & \text{for } n > 3 \end{cases} \quad (23.146)$$

follows. The integrals over ϕ_1 are given by

$$\int \cos^2(\phi_1) d\phi_1 = \frac{1}{2} \phi_1 + \frac{1}{4} \sin(2\phi_1),$$

$$\int d\phi_1 \cos^2(\phi_1) \sin^{n-2}(\phi_1) = \int d\phi_1 \sin^{n-2}(\phi_1) - \int d\phi_1 \sin^n(\phi_1) \quad (23.147)$$

and using (23.139)

$$\int_0^\pi d\phi_1 \cos^2(\phi_1) \sin^{n-2}(\phi_1) = \begin{cases} \frac{\pi}{2} & \text{for } n = 2 \\ \sqrt{\pi} \frac{\Gamma(\frac{1}{2}(n-1))}{n\Gamma(\frac{n}{2})} & \text{for } n > 2 \end{cases} \quad (23.148)$$

leading to the intermediate result

$$I_n^2(\rho) = \rho^{n+1} \begin{cases} \pi & \text{for } n = 2 \\ \frac{4\pi}{3} & \text{for } n = 3 \\ 2\pi\sqrt{\pi} \frac{\Gamma(\frac{1}{2}(n-1))}{n\Gamma(\frac{n}{2})} J_n & \text{for } n > 3 \end{cases} \quad (23.149)$$

It remains to compute the integrals over $\phi_2 \dots, \phi_{n-2}$ abbreviated by

$$J_n \equiv \int_0^\pi d\phi_2 \dots \int_0^\pi d\phi_{n-2} \prod_{k=2}^{n-2} \sin^{n-1-k} \phi_k \quad (23.150)$$

for $n > 3$. Inspection of (23.140) shows that

$$J_n = M_{n-1} = \frac{\pi^{\frac{n-3}{2}}}{\Gamma(\frac{n-1}{2})} \quad (23.151)$$

holds and the final result for $n \geq 2$ is thus given by

$$I_n^2(\rho) = \rho^{n+1} \frac{2\pi^{\frac{n}{2}}}{n\Gamma(\frac{n}{2})} \quad (23.152)$$

It is evident that $I_n^2(\rho)$ has the dimension of an $(n+1)$ -volume. Furthermore, it can be related to the n -volume of the ball (23.95) with radius ρ and $1 \leq k \leq n$

$$I_n^2(\rho) = \int \dots \int_{S_n(\rho)} d\sigma x_k^2 = \rho V_n(\rho) \quad (23.153)$$

This integral is independent of k due to the symmetries of the n -sphere. It is crucial for the evaluation of the Lévy-Laplacian.

23.16.3 Integrand $x_k x_l$ for $k \neq l$

For the present example, the assumption $n > 2$ must be made for the surface integral to make sense. The integral defined in Cartesian coordinates by

$$I_n^{1,2}(\rho) \equiv \int_{S_n(\rho)} d\sigma x_k x_l \quad (23.154)$$

for $n > 2$ and $1 \leq k, l \leq n$ and $k \neq l$ is transformed to spherical coordinates. Without restricting generality it can be assumed that $k = 1, l = 2$, hence $x_1 = r \cos \phi_1, x_2 = r \sin(\phi_1) \cos(\phi_2)$ according to (23.127) and using (23.134)

$$I_n^{1,2}(\rho) = \rho^{n+1} \begin{cases} \int_0^\pi d\phi_1 \sin^2(\phi_1) \int_0^{2\pi} d\phi_2 \cos(\phi_2) & \text{for } n = 3 \\ 2\pi K_n \int_0^\pi d\phi_1 \sin^{n-1}(\phi_1) \cos(\phi_1) \int_0^\pi d\phi_2 \sin^{n-3}(\phi_2) \cos(\phi_2) & \text{for } n > 4 \end{cases} \quad (23.155)$$

follows, where

$$K_n \equiv \prod_{k=3}^{n-2} \int_0^\pi d\phi_k \sin^{n-1-k} \phi_k \quad (23.156)$$

The integrals over ϕ_1 are given by

$$\int d\phi_1 \sin^{n-1} \phi_1 \cos \phi_1 = \frac{1}{n} \sin^n \phi_1, \quad \int d\phi_2 \sin^{n-3} \phi_2 \cos \phi_2 = \frac{1}{n-2} \sin^{n-2} \phi_2 \quad (23.157)$$

and

$$K_n = M_{n-2} = \frac{\pi^{\frac{n}{2}-2}}{\Gamma(\frac{n}{2}-1)} \quad (23.158)$$

The result is thus

$$I_n^{1,2}(\rho) = 0 \quad (23.159)$$

23.16.4 Surface Average of an Analytic Function Over the n -Sphere

The definition of the Lévy-Laplacian (9.83) rests on the ratio of surface integrals to surface area of spheres in R^n . This form of surface average is illustrated with an example that allows easy passage of the dimension n to infinity. Consider an analytic function $f(x_1)$ bounded in R^n with Taylor series in Cartesian coordinates

$$f(x_1) = f(0) + x_1 \frac{\partial f}{\partial x_1}(0) + \frac{1}{2!} x_1^2 \frac{\partial^2 f}{\partial x_1^2}(0) + \frac{1}{k!} x_1^k \frac{\partial^k f}{\partial x_1^k}(0) + \dots \quad (23.160)$$

absolutely convergent in an open neighbourhood of the origin containing the unit sphere. The surface average is defined as the surface integral divided by the area

$$I_n(f; \rho) \equiv \frac{1}{A_n(\rho)} \int_{S_n(\rho)} d\sigma_n f(x_1) \quad (23.161)$$

for spheres with radius $\rho \leq 1$, where $A_n(\rho)$ is the surface area of the n -ball (23.115) and $d\sigma_n$ denotes the surface differential (23.134) in R^n , the dimension is assumed to be $n > 2$. The limit of the surface average for the dimension $n \rightarrow \infty$ is zero over zero, hence indeterminate, thus opening the door to a non-zero and finite ratio in this limit.

The Taylor series can be substituted for $f(x_1)$ leading to

$$I_n(f; \rho) = f(0) + \sum_{k=1}^{\infty} \frac{1}{k!} \frac{\partial^k f}{\partial x_1^k}(0) \frac{1}{A_n(\rho)} \int_{S_n(\rho)} d\sigma_n x_1^k \quad (23.162)$$

The ratio of the integral and the area is bounded

$$\frac{1}{A_n(\rho)} \left| \int_{S_n(\rho)} d\sigma_n x_1^k \right| \leq \frac{1}{A_n(\rho)} \int_{S_n(\rho)} d\sigma_n |x_1^k| \leq 1 \quad (23.163)$$

since $|x_1^k| \leq 1$ and the integrated series is, therefore, absolutely convergent. Transformation to spherical coordinates according to Sects. 23.15 (23.127) and (23.134) produces

$$I_n(f; \rho) = f(0) + \sum_{k=1}^{\infty} \frac{\rho^k}{k!} \frac{\partial^k f}{\partial x_1^k}(0) c_k^n \quad (23.164)$$

with coefficients defined by

$$\begin{aligned} c_k^n &\equiv \frac{\rho^{n-1}}{A_n(\rho)} \int_0^{\pi} d\phi_1 \cdots \int_0^{\pi} d\phi_{n-2} \int_0^{2\pi} d\phi_{n-1} \cos^k(\phi_1) \prod_{p=1}^{n-2} \sin^{n-1-p}(\phi_p) \\ &= \frac{\Gamma(\frac{n}{2})}{\pi^{\frac{n}{2}-1}} \begin{cases} \int_0^{\pi} d\phi_1 \cos(x_1)^k \sin(\phi_1) & \text{for } n = 3 \\ \int_0^{\pi} d\phi_1 \cos(x_1)^k \sin^{n-2}(\phi_1) \int_0^{\pi} d\phi_2 \cdots \int_0^{\pi} d\phi_{n-2} \prod_{p=2}^{n-2} \sin^{n-1-p}(\phi_p) & \text{for } n > 3 \end{cases} \quad (23.165) \end{aligned}$$

where the product of integrals is recognized as (23.140)

$$M_{n-1} = \int_0^{\pi} d\phi_2 \cdots \int_0^{\pi} d\phi_{n-2} \prod_{p=2}^{n-2} \sin^{n-1-p}(\phi_p) = \frac{\pi^{\frac{1}{2}(n-1)-1}}{\Gamma(\frac{1}{2}(n-1))} \quad (23.166)$$

by shifting the index p . The coefficients are then ($n \geq 3$)

$$c_k^n = \frac{1}{\sqrt{\pi}} \frac{\Gamma(\frac{n}{2})}{\Gamma(\frac{1}{2}(n-1))} \begin{cases} \int_0^\pi d\phi_1 \cos(x_1)^k \sin^{n-2}(\phi_1) & \text{for } k \text{ even} \\ 0 & \text{for } k \text{ odd} \end{cases} \quad (23.167)$$

The coefficients c_k^n are zero for k odd as the substitution $x = \sin(\phi_1)$, $dx = \cos(\phi_1) d\phi_1$ and $\cos^2(\phi_1) = 1 - \sin^2(\phi_1)$ imply, hence

$$I_n(f; \rho) = f(0) + \sum_{k=1}^{\infty} \frac{\rho^{2k}}{(2k)!} \frac{\partial^{2k} f}{\partial x_1^{2k}}(0) c_{2k}^n \quad (23.168)$$

and

$$c_{2k}^n = \frac{1}{\sqrt{\pi}} \frac{\Gamma(\frac{n}{2})}{\Gamma(\frac{1}{2}(n-1))} \int_0^\pi d\phi_1 \cos^{2k}(\phi_1) \sin^{n-2}(\phi_1) \quad (23.169)$$

It remains to evaluate the coefficients c_{2k}^n with the aid of elementary trigonometric integrals. The case $n = 3$ is easily computed (use $\Gamma(\frac{3}{2}) = \frac{\sqrt{\pi}}{2}$)

$$c_{2k}^3 = \frac{2\Gamma(\frac{3}{2})}{(2k+1)\pi^{\frac{1}{2}}} = \frac{1}{2k+1} \quad (23.170)$$

and the resulting series for the surface average follows then

$$I_3(f; \rho) = f(0) + \sum_{k=1}^{\infty} \frac{\rho^{2k}}{(2k+1)(2k)!} \frac{\partial^{2k} f}{\partial x_1^{2k}}(0) \quad (23.171)$$

The case $n > 3$ needs more work. The recursive relation

$$\int dx \sin^n(x) \cos^m(x) = \frac{1}{n+m} \sin^{n+1}(x) \cos^{m-1}(x) + \frac{m-1}{n+m} \int dx \sin^n(x) \cos^{m-2}(x) \quad (23.172)$$

can be applied leading to

$$\int_0^\pi d\phi_1 \cos^{2k}(\phi_1) \sin^{n-2}(\phi_1) = \prod_{p=1}^k \frac{2k-2p+1}{2k-2p+n} \int_0^\pi d\phi_1 \sin^{n-2}(\phi_1) \quad (23.173)$$

and together with (23.139) produces the desired result

$$\int_0^\pi d\phi_1 \cos^{2k}(\phi_1) \sin^{n-2}(\phi_1) = \sqrt{\pi} \frac{\Gamma(\frac{1}{2}(n-1))}{\Gamma(\frac{1}{2}n)} \prod_{p=1}^k \frac{2k-2p+1}{2k-2p+n} \quad (23.174)$$

The coefficients (23.169) emerge thus in the form

$$c_{2k}^n = \prod_{p=1}^k \frac{2k-2p+1}{2k-2p+n} \quad (23.175)$$

and the series for the surface average is then

$$I_n(f; \rho) = f(0) + \sum_{k=1}^{\infty} \frac{\rho^{2k}}{(2k)!} \frac{\partial^{2k} f}{\partial x_1^{2k}}(0) \prod_{p=1}^k \frac{2k-2p+1}{2k-2p+n} \quad (23.176)$$

in surprisingly simple form suitable for the limit $n \rightarrow \infty$.

The previous result (23.153) in Sect. 23.16.2 for the integrand x_k^2 is a special case of Eq. (23.176) derived above. It can be recovered by truncating the Taylor series (23.160) to a single term

$$f(x_1) = \frac{1}{2!} x_1^2 \frac{\partial^2 f}{\partial x_1^2}(0), \quad \frac{1}{2!} \frac{\partial^2 f}{\partial x_1^2}(0) = 1$$

and with the surface area (23.115)

$$\begin{aligned} \mathcal{A}_n I_n(f; \rho) &= \mathcal{A}_n \sum_{k=1}^1 \frac{\rho^{2k}}{(2k)!} \frac{\partial^{2k} f}{\partial x_1^{2k}}(0) \prod_{p=1}^k \frac{2k-2p+1}{2k-2p+n} \\ &= \frac{2\pi^{\frac{n}{2}} \rho^{n-1}}{\Gamma(\frac{n}{2})} \left(\rho^{2k} \prod_{p=1}^k \frac{2k-2p+1}{2k-2p+n} \right)_{k=1} = \frac{2\pi^{\frac{n}{2}} \rho^{n+1}}{n \Gamma(\frac{n}{2})} \end{aligned}$$

is obtained in agreement with (23.153).

It follows from the general result (23.176) that the limit of infinite dimensions for the geometric surface average can be computed

$$\lim_{n \rightarrow \infty} \frac{1}{\mathcal{A}_n(\rho)} \int_{S_n(\rho)} d\sigma_n f(x_1) = f(0) \quad (23.177)$$

which holds for any radius $\rho < \infty$. It was shown in Sect. 23.17.1 that the origin $r = 0$ is on the surface of the sphere in the limit $n \rightarrow \infty$, and hence shares the geometric surface average (23.177) the property $I_\infty(f; \rho) : f(x_1) \rightarrow f(0)$, mapping the argument function $f(x_1)$ to a pure number $f(0)$, with the Dirac pseudo-function. Hence, the geometric average $I_\infty(f; \rho)$ is a linear functional defined on the space of analytic functions $f(x_1)$, $x_1 \in R^1$. This concludes the examples for the surface integrals over the n -sphere.

Comment: The result obtained in the present section illustrates the fact that the limit $n \rightarrow \infty$ of an integral with bounded integrands is zero, whereas dividing the integral by the volume of the domain to compute the geometric average and then passing to the limit of infinite dimension is not necessarily zero.

23.17 Integration in Infinite-Dimensional Spaces

Functional integration has a long history, Skorohod 1974 ([35], integration in Hilbert spaces), Egorov et al. 1993 ([36], approximate evaluation of functional integrals), deWitt-Morette et al. 1997 ([37], Simon 2004 [38], Cartier and DeWitt-Morette 2006 [39], functional integrals in quantum mechanics), but it still poses fundamental difficulties. This is due to several reasons, the main being the fact, that the standard Riemann/Lebesgue approach to integration fails to produce anything useful as the dimension goes to infinity. The Hilbert cube and the infinite-dimensional ball (23.38) and its boundary the Hilbert sphere (23.40) play an important role as analytic examples for this failure.

23.17.1 Properties of n -Sphere and n -Ball as $n \rightarrow \infty$

The n -spheres and n -ball are compact sets for normed vector spaces with finite dimension n . However, this and many other properties do not hold for the limit $n = \infty$, see [40] for detailed discussion and proofs. The fact that the unit ball is not compact even for infinite-dimensional Euclidian space can be proved easily by observing that an orthogonal, Cartesian coordinate system can be set up and thus a sequence of points on the sphere can be constructed $\{(x_1, x_2, \dots)_i, i = 1, \dots, \infty : (\dots, x_{i-1} = 0, x_i = 1, x_{i+1} = 0, \dots)\}$ that does not contain a convergent subsequence, the details of the proof can be found in Robinson [41], proposition 1.25 on page 38.

Another surprising and counter-intuitive fact is that for $n \rightarrow \infty$ the origin is located on the sphere, since the point $(x_1, \dots, x_n) = (1/\sqrt{n}, \dots, 1/\sqrt{n})$ has the distance $\rho = \sum_{i=1}^n 1/n = 1$ to the origin for finite n , passing to the limit $n \rightarrow \infty$ shows that the origin is in fact a limit point on the sphere S_∞ . Since sequences with positive and negative coordinates can be constructed, infinitely many such limit points exist as $n \rightarrow \infty$. For instance, the sequence of points on $S_n(1)$

$$(x_1, \dots, x_n) = (a_1/\sqrt{n}, \dots, a_n/\sqrt{n}), n = 1, \dots, \infty$$

with coefficients constructed, such that

$$\rho^2 = \sum_{i=1}^n a_i^2/n = 1$$

holds, is on $S_n(1)$ for all n and the limit point is on $S_\infty(1)$. The coefficients a_i can be regarded as divergent series with partial sums satisfying

$$\sum_{i=1}^n a_i^2 = n$$

On the other hand are all finite-dimensional unit spheres $S_n(1)$ subsets of $S_\infty(1)$ since they consist of points $(x_1, \dots, x_n, 0, \dots)$ with $r = 1$. These properties can be formulated rigorously, see the main theorem in Benyamin and Sternfeld [40].

The standard Riemann integral of a standard integrable function defined on a domain in the Euclidian space R^1 requires the discretization of the domain into measurable subdomains and the integral is then approximated by a sum. Each contribution to this sum is the product of the measure of the subdomain times a value of the integrand in it. A limit procedure must be devised such that the approximating sums converge as the measure of the subdomains goes to zero and the integrand must be well enough behaved so that the limit of the sum, the integral, is independent of the location in the subdomains where the value of the integrand is specified. This method can be generalized to $1 < n < \infty$ dimensions, but fails for $n = \infty$ since the measure of subdomains is zero (as shown for the sphere in Sect. 23.17.2 below) no matter how the discretization of an infinite-dimensional space is attempted. Hence, integration in infinite-dimensional spaces poses a fundamental problem since the standard Riemann and Lebesgue measures/integrals do not generalize to infinite-dimensional spaces [42].

It can be proved that on a infinite-dimensional and separable Banach space Ω only trivial, locally finite (every point has a neighbourhood of finite measure) and translation invariant, i.e. $\mu(\mathbf{x} + B) = \mu(B)$, $\forall B \in \mathcal{B}$, $\forall \mathbf{x} \in \Omega$, Borel measures exist [43]. Trivial means that the measure of every measurable subset of the Banach space is zero. Conversely, every translation-invariant measure, that is not identically zero, is infinite for every open subset.

To gain a better understanding of integration in infinite-dimensional spaces, the Riemann/ Lebesgue integration of simple functions over simple domains in finite-dimensional $N < \infty$ Euclidean space has been considered in Sect. 23.12 and then the limit $N \rightarrow \infty$ was evaluated explicitly in Sect. 23.17.2 for the surface area and the volume of spheres/balls. As consequence of these results, alternative ways of constructing measures and integrals in infinite-dimensional spaces are developed in the present section. First, the limit $n \rightarrow \infty$ for volume and surface area of the n -ball are computed to illustrate the paradoxical results for Riemann/Lebesgue integration in infinite-dimensional spaces. Then an important example for an alternative approach to integration in function spaces is presented by specifying the Gaussian measure , which can be given explicitly in terms of the characteristic functional.

23.17.2 *Limit $n \rightarrow \infty$ of Lebesgue/Riemann Surface Area and Volume*

The results for surface and volume integrals are applied to the investigation of the limit as the dimension approaches infinity. The volume of the unit sphere $V_n(1)$ given by (23.94) is considered first. Stirling's asymptotic formula [29, 30] for the Gamma function

$$\Gamma(x+1) = \sqrt{2\pi}x^{x+\frac{1}{2}} \exp(-x + \frac{\theta}{12x}) \quad (23.178)$$

valid for $x > 0$ and where $0 < \theta < 1$ holds is applied to determine the limit $n \rightarrow \infty$. It follows then that the volume of the unit sphere is for $n > 1$

$$V_n(1) = \frac{\pi^{\frac{n}{2}} \exp(\frac{n}{2} - \frac{\theta}{6n})}{\sqrt{2\pi}(\frac{n}{2})^{\frac{1}{2}(n+1)}} \quad (23.179)$$

The variation of $V_n(1)$ for $n \rightarrow \infty$ is determined by

$$X_n = \frac{\pi^{\frac{n}{2}} \exp(\frac{n}{2})}{(\frac{n}{2})^{\frac{1}{2}(n+1)}}, \quad V_n(1) = \frac{\exp(-\frac{\theta}{6n})}{\sqrt{2\pi}} X_n \quad (23.180)$$

which can be rewritten in the form

$$X_n = \frac{1}{\sqrt{e\pi}} \left(\frac{2e\pi}{n} \right)^{\frac{1}{2}(n+1)} \quad (23.181)$$

The limit of X_n as $n \rightarrow \infty$ is zero and the conclusion

$$\lim_{n \rightarrow \infty} V_n(1) = 0 \quad (23.182)$$

is reached. For spheres with radius $\rho \neq 1$ and finite, the result is the same since

$$\rho^n X_n = \frac{1}{\sqrt{e\pi\rho^2}} \left(\frac{2e\pi\rho^2}{n} \right)^{\frac{1}{2}(n+1)} \quad (23.183)$$

also goes to zero as $n \rightarrow \infty$. If the limit of $\rho^n X_n$ is required to be finite, say unity, then it is seen that the radius of the sphere must increase with dimension according to

$$\rho = \frac{1}{\sqrt{e\pi}} \left(\frac{n}{2} \right)^{\frac{1}{2}(1+\frac{1}{n})} \quad (23.184)$$

hence roughly with the square root of the dimension.

The limit for the surface area of the n -sphere can be easily determined if the ratio of surface area to volume of the unit sphere is computed. It follows at once from (23.114) and (23.94)

$$\frac{\mathcal{A}_n(1)}{V_n(1)} = \frac{2\pi^{\frac{n}{2}}}{\Gamma(\frac{n}{2})} \frac{\Gamma(\frac{n}{2} + 1)}{\pi^{\frac{n}{2}}} \quad (23.185)$$

which is thus given by $\frac{\mathcal{A}_n(1)}{V_n(1)} = n$. Hence is the area limit $\lim_{n \rightarrow \infty} \mathcal{A}_n(1)$ determined by

$$nX_n = 2\sqrt{e\pi} \left(\frac{2e\pi}{n} \right)^{\frac{1}{2}(n-1)} \quad (23.186)$$

and its limit value is zero as for the volume. Hence,

$$\lim_{n \rightarrow \infty} \mathcal{A}_n(1) = 0 \quad (23.187)$$

is the result. It does not change for spheres with positive radius $\rho \neq 1$ since

$$n\rho^{n-1}X_n = 2\sqrt{e\pi} \left(\frac{2\rho^2 e\pi}{n} \right)^{\frac{1}{2}(n-1)} \quad (23.188)$$

approaches zero for $n \rightarrow \infty$.

The conclusion is that both surface area and volume of the unit sphere approach zero as the dimension goes to infinity. This result is now compared to the volume of the n -cube with sidelength 2ρ . The volume $C_n(\rho)$ is obviously given by

$$C_n(\rho) = 2^n \rho^n \quad (23.189)$$

and the limit as $n \rightarrow \infty$ is thus

$$\lim_{n \rightarrow \infty} C_n(\rho) = \begin{cases} \infty & \text{for } \rho > 1 \\ 1 & \text{for } \rho = 1/2 \\ 0 & \text{for } \rho < 1 \end{cases} \quad (23.190)$$

This seems to contradict the limit for the sphere, which is zero for any radius $\rho \geq 0$. However, a sphere is the subset of the n -cube with sidelenth 2ρ and contains the n -cube with sidelength $L_n < 2\rho$. Therefore, the n -volume of the sphere $V_n(\rho)$ is bounded by the volumes $C_n(\rho)$ and $C_n(L_n)$ of the n -cubes. It remains to determine the sidelength L_n of the n -cube inside the n -sphere with radius ρ . It is easy to show by induction, that the diagonal D_n of the n -cube inside the n -sphere with radius D_n has the sidelength L_n given by

$$L_n = \frac{2}{\sqrt{n}} D_n \quad (23.191)$$

The cube is contained in the sphere if $D_n = \rho$ and the sidelength is thus

$$L_n(\rho) = \frac{2}{\sqrt{n}} \rho \quad (23.192)$$

The volume of the n -sphere is therefore bounded according to

$$\frac{2^n}{n^{\frac{n}{2}}} \rho^n < V_n(\rho) < 2^n \rho^n \quad (23.193)$$

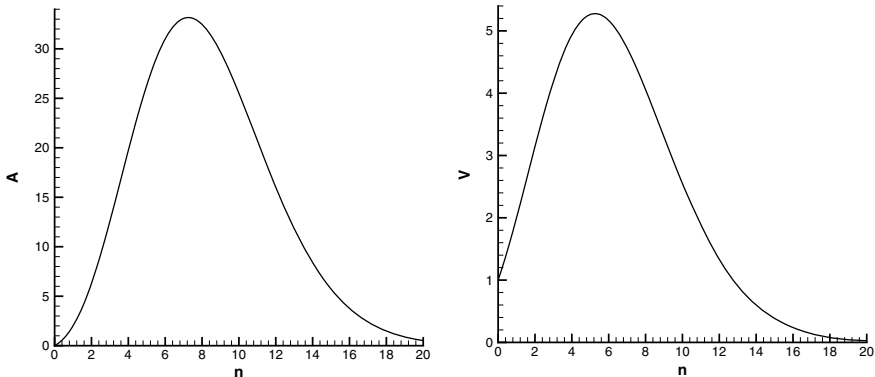


Fig. 23.2 Surface area $A(1)$ (left graph) and volume $V(1)$ of the n -ball as function of dimension n in linear scale

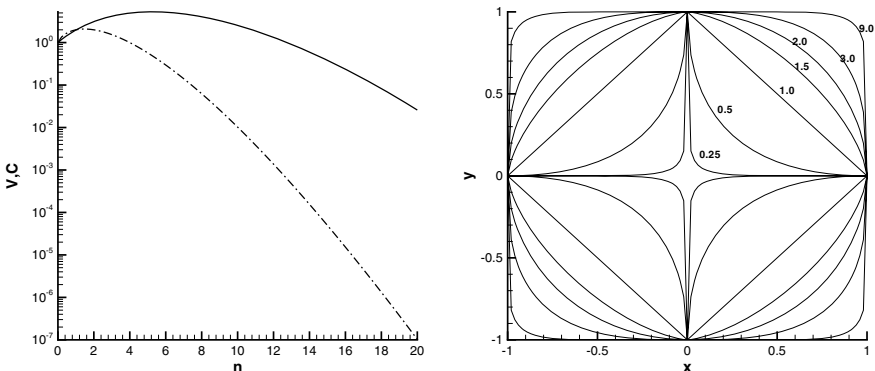


Fig. 23.3 Volume of the n -sphere $V_n(1)$ (full line) and the volume of the n -cube $C_n(\frac{2}{\sqrt{n}})$ with sidelength $\frac{2}{\sqrt{n}}$ (dot-dashed line) as function of the dimension n in logarithmic scale (left graph) and the shape of 2-d spheres for various L_p norms (values of p are indicated on curves) in the right graph. The 2-d balls for $p < 1$ are not convex

Dividing by ρ^n produces

$$\frac{2^n}{n^{\frac{n}{2}}} < V_n(1) < 2^n \quad (23.194)$$

Stirling's asymptotic formula for the Γ -function can be applied to evaluate $V_n(1)$ and the result is shown in the left graph of Fig. 23.3. It confirms that the included n -cube approaches zero volume no matter what the radius of the n -sphere is since the sidelength decreases rapidly with dimension according to (23.192). Hence, the inequality (23.194) becomes trivial as $n \rightarrow \infty$ (Fig. 23.2).

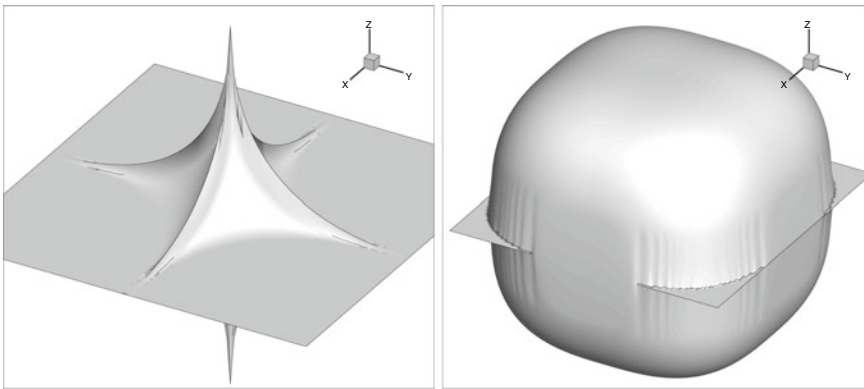


Fig. 23.4 Shape of the unit sphere in R^3 for L_p -norms with $p = 0.5$ (left graph) and $p = 3.0$ (right graph). The balls for $p < 1$ are not convex

This paradoxical situation can be traced to the use of the Riemann/Lebesgue measure for integration which is known to be unsuitable for the limit $n \rightarrow \infty$. This will be discussed in detail below.

23.18 Gaussian Measures

The paradoxical properties of the Riemann/Lebesgue measure in the limit of $n \rightarrow \infty$ can be avoided, if it is replaced by another measure such as a Gaussian measure μ_G . Gaussian measures possess a characteristic functional θ given by (see [18], Chap. 1.3, and [44]) $\theta(y) = \exp\{-\frac{1}{2}(Ky, y)_H + (a, y)_H\}$, where $y(x) \in H$ is the argument field defined over the domain \mathcal{D} and taken from a Hilbert space H , K is a positive operator of trace class in H called correlation operator of the measure μ_G and $a(x) \in H$ is the mean field. The scalar product in H is denoted by $(., .)_H$. An operator K is positive if it is self-adjoint and $(Ky, y)_H \geq 0$ holds for all $y \in H$, it is trace class if H is separable (i.e. every orthonormal system in H is countable) and if $\sum_{j=1}^{\infty} |(K\varphi_j, \psi_j)| < \infty$ holds for arbitrary, complete, orthonormal systems $\{\varphi_j\}, \{\psi_j\}$ in H . In the following, the mean vector is set to zero, i.e. the Gaussian measure is centred.

Consider an orthogonal projection operator P projecting H onto a finite-dimensional subspace H_N where N is its dimension. The measure μ_P is then also Gaussian with correlation operator $K_P = P K P$ and the density of μ_N with respect to the Lebesgue measure in R^N is given by

$$\rho(x) = \frac{1}{\sqrt{(2\pi)^N \det K_P}} \exp\left\{-\frac{1}{2}(K_P^{-1}x, x)_{R^N}\right\} \quad (23.195)$$

for $x \in H_N$ where $(., .)_{R^N}$ is the scalar product in R^N . Let $\{\varphi_k(x)\}_0^\infty$ be a canonical basis in H , then an orthogonal projection operator can be defined by

$$P_N y = \sum_{k=1}^N y_k \varphi_k, \quad y_k = (y, \varphi_k)_H \quad (23.196)$$

and the integration of any functional $F(y)$ admitting an approximation by a sequence of cylinder functions $F_N(y) = F(P_N y)$ is then reduced to a finite-dimensional integral. The projected Gaussian measure emerges then in the form

$$\mu_P(dy) = \prod_{k=1}^N \frac{\lambda_k}{\sqrt{2\pi}} \exp\left(-\frac{1}{2}\lambda_k^2 y_k^2\right) dy_k \quad (23.197)$$

The canonical basis in H is the orthogonal basis consisting of the eigenvectors of the operator $T = K^{-\frac{1}{2}}$ normalized in H . Then holds $T\varphi_k = \lambda_k \varphi_k$ with λ_k denoting the eigenvalues. The functional integral with respect to a Gaussian measure appears in the present case as

$$\int_H F_P(y) \mu(dy) = \lim_{N \rightarrow \infty} (2\pi)^{-\frac{N}{2}} \int_{R^N} F_N(y_1, \dots, y_N) \prod_{k=1}^N \lambda_k \exp\left(-\frac{1}{2}\lambda_k^2 y_k^2\right) dy_k \quad (23.198)$$

Examples for the computation of Gaussian integrals are given below.

23.18.1 Example: Lebesgue/Riemann and Gaussian Volumes of an n -Ball for $n > 2$

The Gaussian measure of a ball with radius ρ in R^N is computed with the aid of spherical coordinates (23.127) and compared to the result for the Riemann/Lebesgue measure. The volume of a ball in N -dimensional space for Lebesgue and Gaussian measures can be computed without difficulty. The standard Riemann/Lebesgue volume of the ball with radius ρ is the integral

$$I_N^L(\rho) = \int_{B_N(\rho)} \mu_L(d\mathbf{x}) \quad (23.199)$$

where

$$\mu_L(d\mathbf{x}) = \prod_{k=1}^N dx_k \quad (23.200)$$

is the Riemann/Lebesgue N -volume differential. The integral is now transformed to spherical coordinates according to (23.127) using the Jacobian J given by (23.130)

$$I_N^L(\rho) = \int_0^\rho dr \int_0^\pi d\phi_1 \cdots \int_0^\pi d\phi_{N-2} \int_0^{2\pi} d\phi_{N-1} r^{N-1} \prod_{k=1}^{N-2} \sin^{N-1-k} \phi_k \quad (23.201)$$

It can be partially evaluated

$$I_N^L(\rho) = \frac{\rho^N}{N} \int_0^\pi d\phi_1 \cdots \int_0^\pi d\phi_{N-2} \int_0^{2\pi} d\phi_{N-1} \prod_{k=1}^{N-2} \sin^{N-1-k} \phi_k \quad (23.202)$$

which is useful for the computation of the Gaussian volume below. The result is known (23.117) (derived in Sects. 23.12.1 and 23.12.1)

$$I_N^L(\rho) = \frac{2\pi^{\frac{N}{2}} \rho^N}{N \Gamma(\frac{N}{2})} = \frac{\pi^{\frac{N}{2}} \rho^N}{\Gamma(\frac{N}{2} + 1)}$$

It follows then that

$$\int_0^\pi d\phi_1 \cdots \int_0^\pi d\phi_{N-2} \int_0^{2\pi} d\phi_{N-1} \prod_{k=1}^{N-2} \sin^{N-1-k} \phi_k = \frac{2\pi^{\frac{N}{2}}}{\Gamma(\frac{N}{2})} \quad (23.203)$$

holds. The Gaussian volume is defined by

$$I_N^G(\rho) = \int_{B_N(\rho)} \mu_G(d\mathbf{x}) \quad (23.204)$$

where the Gaussian volume differential is for $\lambda_k = 1, k = 1, \dots, N$ according to (23.197)

$$\mu_G(d\mathbf{x}) = (2\pi)^{-\frac{N}{2}} \prod_{k=1}^N \exp\left(-\frac{1}{2}x_k^2\right) dx_1 \cdots dx_N$$

in Cartesian coordinates. Transformation to spherical coordinates leads to

$$I_N^G(\rho) = (2\pi)^{-\frac{N}{2}} \int_0^\rho dr r^{N-1} \exp\left(-\frac{1}{2}r^2\right) \int_0^\pi d\phi_1 \cdots \int_0^\pi d\phi_{N-2} \int_0^{2\pi} d\phi_{N-1} \prod_{k=1}^{N-2} \sin^{N-1-k} \phi_k \quad (23.205)$$

defines the Gaussian N -volume differential in spherical coordinates by

$$\mu_G(d\mathbf{x}) = (2\pi)^{-\frac{N}{2}} dr r^{N-1} \exp\left(-\frac{1}{2}r^2\right) \prod_{k=1}^{N-1} d\Phi_k$$

where $0 \leq \Phi_k \leq \pi$, $k = 1, \dots, N-2$, $0 \leq \Phi_{N-1} \leq 2\pi$. Using (23.203) leads to the desired result for the Gaussian volume of the N -ball (normalizing the radial integration variable $\zeta = r/\rho$)

$$I_N^G(\rho) = \begin{cases} \frac{\rho^2}{\sqrt{\pi}}(1 - \exp(-\frac{1}{2}\rho^2\zeta^2)) \text{ for } N = 2 \\ \frac{\rho^N}{2^{\frac{N}{2}-1}\Gamma(\frac{N}{2})} \int_0^1 d\zeta \zeta^{N-1} \exp\left(-\frac{\rho^2}{2}\zeta^2\right) \text{ for } N > 2 \end{cases} \quad (23.206)$$

or as ratio of Gaussian to standard volumes

$$\frac{I_N^G(\rho)}{I_N^L(\rho)} = \frac{N}{(2\pi)^{\frac{N}{2}}} \int_0^1 d\zeta \zeta^{N-1} \exp\left(-\frac{\rho^2}{2}\zeta^2\right) \quad (23.207)$$

It is easy to prove that the Gaussian volume is smaller than the standard volume, $I_N^G(\rho) < I_N^L(\rho)$, as illustrated in Fig. 23.6. The dependence of the volume on dimension N and radius ρ in Fig. 23.5 indicates that for any dimension there is a radius such that the volume gets arbitrarily close to unity (the computation was done numerically using a second-order accurate integration method in double precision, since the integral cannot be evaluated in closed form except for $N = 2$), the Gaus-

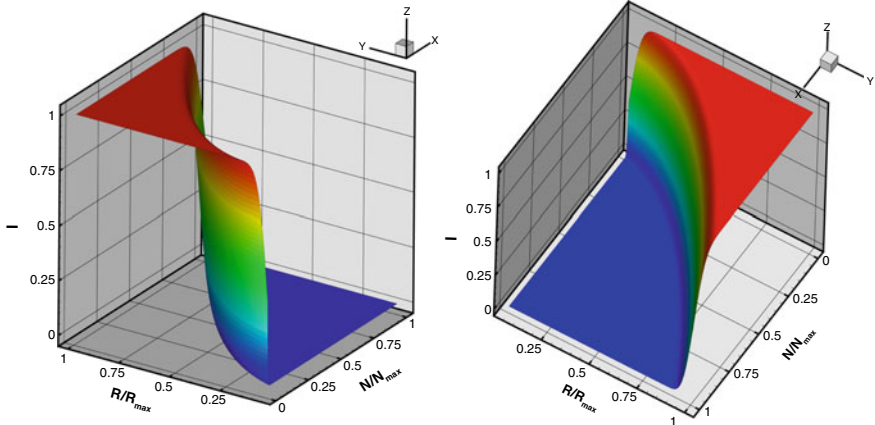


Fig. 23.5 Two views of the Gaussian volume $I_N^G(\rho)$ of N -balls as function of the normalized dimension $N/\max N$ ($\max N = 400$) and the normalized radius $\rho/\max \rho$ ($\max \rho = 20$). Colour coding of $I_N^G(\rho)$: red corresponds to unity, blue to zero. Note that for finite dimension N exists a radius $R(N)$, such that the Gaussian volume is close to unity for given accuracy. The radius $R(N)$ varies asymptotically as $R(N) \approx N^{\frac{1}{2}}$ (Eq. (23.184)) as evident in the graphs

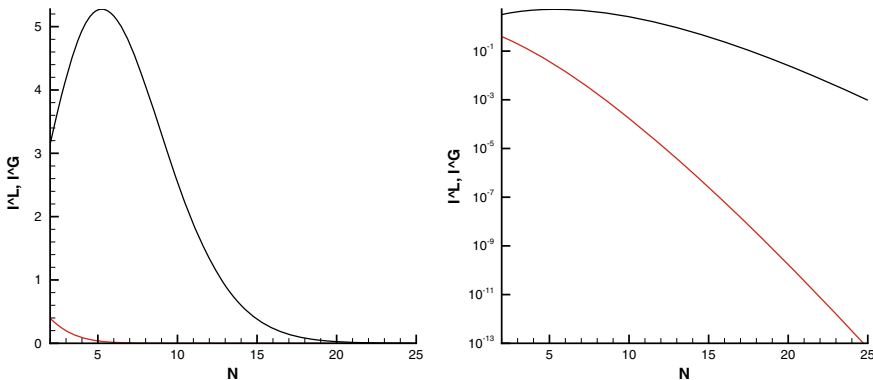
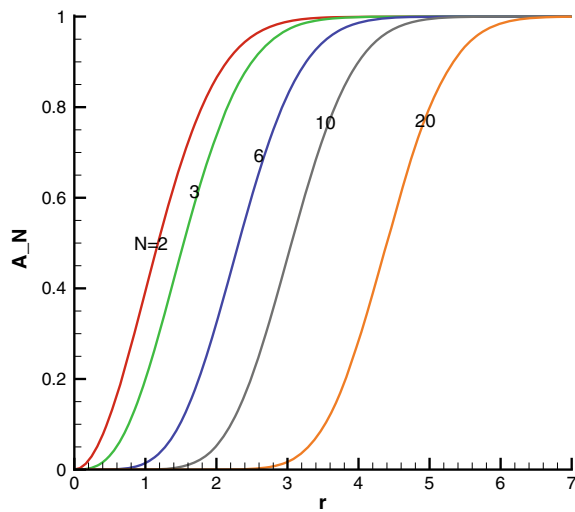


Fig. 23.6 The volume of the unit ball as function of dimension measured with the aid of Riemann / Lebesgue integration (black line) and Gaussian integration (red line) shown in linear scale (left graph) and log-scale (right graph)

Fig. 23.7 Gaussian volumes of a N -ball as function of the radius, dimensions N as indicated on the lines



sian volume of N -balls approaches zero as $N \rightarrow \infty$ for fixed, finite radius ρ , but approaches unity as both the radius $\rho \rightarrow \infty$ and the dimension $N \rightarrow \infty$. This is consistent with the fact that the Gaussian probability measure exists on R^∞ and the Gaussian integral over the infinite-dimensional Euclidean space R^∞ must be unity. A few profiles of the volume as function of the radius ρ of the ball are shown in Fig. 23.7 for $N = 2, 3, 6, 10, 20$.

The comparison of Riemann/Lebesgue and Gaussian integrals for the unit ball in Fig. 23.6 for finite dimension shows that the Riemann/Lebesgue integral possesses a maximum, whereas the Gaussian integral monotonically decreases with increasing dimension.

23.18.2 Gaussian Measure on the Space of Infinite Sequences

Let H be a separable Hilbert space, then is H isometric to the Hilbert space of infinite sequences l^2 . Recall that two metric spaces X and Y are isometric, if there exists a bijective map $f : X \rightarrow Y$ between them, such that $d_Y(f(x), f(y)) = d_X(x, y)$ for all $x, y \in X$ (d_X, d_Y denote the metrics in X and Y). The phase space of a turbulent flow is a separable Hilbert space, and hence it is instructive to construct measures on spaces of infinite sequences, the Gaussian measure being chosen as example. Consider the set l of infinite sequences $\{x_k, k = 1, \dots, \infty, |x_k| < \infty\}$ of real numbers. The Gaussian measure is given (see Klauder, [42], Chap. 3) by

$$\mu(d\mathbf{x}) = \lim_{N \rightarrow \infty} \prod_{k=1}^N \sqrt{\frac{b}{2\pi}} \exp\left(-\frac{b}{2}x_k^2\right) dx_k \quad (23.208)$$

where $\mathbf{x} \in l$. The space of infinite sequences l will be extended to a well-defined space containing the support of the Gaussian measure. This will be done in three steps following Klauder, [42], Chap. 3.

Convergent sequences have zero measure

The space l^2 of quadratically convergent sequences seems to be a candidate for the domain of definition Ω of the Gaussian measure. However, this is unfortunately not the case, in fact, it will be shown that the space of quadratically convergent sequences is a subset $l^2 \equiv \{\mathbf{x} \in l : \sum_{k=1}^{\infty} x_k^2 < \infty\} \subset \Omega$ with zero measure and $l^2 \neq \Omega$. This can be seen as follows.

Assume $\Omega = l^2$, let $c > 0$ be real number, then is $\exp\left(-\frac{c}{2} \sum_{k=1}^{\infty} x_k^2\right) < \infty$ well defined for $|c| < \infty$ and the Gaussian measure of this exponential (denoted by angular brackets) is

$$f(c) \equiv \langle \exp\left(-\frac{c}{2} \sum_{k=1}^{\infty} x_k^2\right) \rangle = \int_{\Omega} \mu(d\mathbf{x}) \exp\left(-\frac{c}{2} \sum_{k=1}^{\infty} x_k^2\right)$$

which is by definition of the Gaussian measure (23.208)

$$\langle \exp\left(-\frac{c}{2} \sum_{k=1}^{\infty} x_k^2\right) \rangle = \lim_{N \rightarrow \infty} \prod_{k=1}^N \sqrt{\frac{b_k}{2\pi}} \int_{-\infty}^{\infty} dx_k \exp\left[-\frac{1}{2}(b_k + c)x_k^2\right]$$

where

$$\sqrt{\frac{b_k}{2\pi}} \int_{-\infty}^{\infty} dx_k \exp\left[-\frac{1}{2}(b_k + c)x_k^2\right] = \sqrt{\frac{b_k}{b_k + c}} \leq \sqrt{\frac{b}{b + c}}$$

Hence

$$0 \leq \langle \exp(-\frac{c}{2} \sum_{k=1}^{\infty} x_k^2) \rangle < \lim_{N \rightarrow \infty} \left(\frac{b}{b+c} \right)^{\frac{N}{2}} = 0$$

for $c > 0$. From this result, it follows that for $c \geq 0$

$$\lim_{c \rightarrow 0} \langle \exp(-\frac{c}{2} \sum_{k=1}^{\infty} x_k^2) \rangle = 0 \quad (23.209)$$

holds for all $\mathbf{x} \in l^2$. Likewise, it is evident that the limit $c \rightarrow 0$ does not commute with the $\langle \cdot \rangle$ operation

$$\langle \lim_{c \rightarrow 0} \exp(-\frac{c}{2} \sum_{k=1}^{\infty} x_k^2) \rangle = 1$$

and for $c < 0$, $b_k + c > 0$ for all k

$$\lim_{c \rightarrow 0} \langle \exp(-\frac{c}{2} \sum_{k=1}^{\infty} x_k^2) \rangle = \infty$$

hold. Hence, the function $f(c)$

$$f(c) = \begin{cases} 0 & \text{for } c > 0 \\ 1 & \text{for } c = 0 \\ \infty & \text{for } c < 0 \end{cases}$$

is discontinuous and monotonically decreasing and it must be concluded that $l^2 \neq \Omega$ and l^2 is a subspace of Ω of Gaussian measure zero.

Extending the support of the measure

Restricting the support space Ω to l^2 does not produce anything useful, since

$$\mu(\{\mathbf{x} : \sum_{k=1}^{\infty} x_k^2 < \infty\}) = 0 \quad (23.210)$$

holds for all $\mathbf{x} \in l^2$, i.e. $\mu(l^2) = 0$, according to the previous Sect. 23.18.2. Hence, the support space Ω must be bigger than l^2 and contain sequences with unbounded l^2 -norm $\|\mathbf{x}\|^2 = \sum_{k=1}^{\infty} x_k^2 = \infty$. Hence, let $\sum_{k=1}^{\infty} x_k^2 = \infty$, then construct a sequence $\lambda_k > 0, k = 1, \dots, \infty$ such that $\sum_{k=1}^{\infty} \lambda_k < \infty$, the reason for this construction will become clear at the end of this section. Choose $\mathbf{x} \in \Omega : \sum_{k=1}^{\infty} x_k^2 = \infty$ such that

$$\sum_{k=1}^{\infty} \lambda_k x_k^2 < \infty \quad (23.211)$$

holds, then is

$$\langle \sum_{k=1}^{\infty} \lambda_k x_k^2 \rangle = \int_{\Omega} \mu(d\mathbf{x}) \sum_{k=1}^{\infty} \lambda_k x_k^2 = \sum_{k=1}^{\infty} \lambda_k \int_{\Omega} \mu(d\mathbf{x}) x_k^2$$

well defined. The integral on the right side can be evaluated according to (23.208)

$$\int_{\Omega} \mu(d\mathbf{x}) x_k^2 = \lim_{N \rightarrow \infty} \prod_{n=1}^N \sqrt{\frac{b_k}{2\pi}} \int_{-\infty}^{\infty} dx_n x_n^2 \exp\left(-\frac{b_k}{2} x_n^2\right) = \sqrt{\frac{b_k}{2\pi}} \int_{-\infty}^{\infty} dx_k x_k^2 \exp\left(-\frac{b_k}{2} x_k^2\right)$$

thus

$$\int_{\Omega} \mu(d\mathbf{x}) x_k^2 = \frac{1}{b_k}$$

and

$$\langle \sum_{k=1}^{\infty} \lambda_k x_k^2 \rangle = \sum_{k=1}^{\infty} \frac{\lambda_k}{b_k} < \infty \quad (23.212)$$

The extended domain Ω is thus defined as

$$\Omega = \{\mathbf{x} : \sum_{k=1}^{\infty} \lambda_k x_k^2 < \infty \ \forall \{\lambda_k\}_0^{\infty} : \lambda_k \geq 0, \sum_{k=1}^{\infty} \frac{\lambda_k}{b_k} < \infty\} \quad (23.213)$$

It remains to verify that $\mu(\Omega) = 1$ holds. Consider

$$\langle \exp\left(-\frac{c}{2} \sum_{k=1}^{\infty} \lambda_k x_k^2\right) \rangle = \int_{\Omega} \mu(d\mathbf{x}) \exp\left(-\frac{c}{2} \sum_{k=1}^{\infty} \lambda_k x_k^2\right)$$

for $c > 0$ and $\sum_{k=1}^{\infty} \lambda_k < \infty$, which is by definition (23.208)

$$\langle \exp\left(-\frac{c}{2} \sum_{k=1}^{\infty} x_k^2\right) \rangle = \lim_{N \rightarrow \infty} \prod_{k=1}^N \sqrt{\frac{b_k}{2\pi}} \int_{-\infty}^{\infty} dx_k \exp\left[-\frac{1}{2}(b_k + c\lambda_k)x_k^2\right]$$

where

$$\sqrt{\frac{b_k}{2\pi}} \int_{-\infty}^{\infty} dx_k \exp\left[-\frac{1}{2}(b_k + c\lambda_k)x_k^2\right] = \sqrt{\frac{b_k}{b_k + c\lambda_k}}$$

Thus

$$\lim_{N \rightarrow \infty} \prod_{k=1}^N \sqrt{\frac{b_k}{2\pi}} \int_{-\infty}^{\infty} dx_k \exp[-\frac{1}{2}(b_k + c\lambda_k)x_k^2] = \lim_{N \rightarrow \infty} \prod_{k=1}^N \sqrt{\frac{1}{1 + \frac{c}{b_k}\lambda_k}}$$

The infinite product $\prod_{k=1}^{\infty} (1 + \frac{c}{b_k}\lambda_k)$ is convergent if the infinite series $\sum_{k=1}^{\infty} \frac{c}{b_k}\lambda_k$ is convergent, which is precisely the condition for the sequence $\{\lambda_k\}$ (23.213). Hence,

$$\langle \exp(-\frac{c}{2} \sum_{k=1}^{\infty} \lambda_k x_k^2) \rangle = \frac{1}{\sqrt{\prod_{k=1}^{\infty} (1 + \frac{c}{b_k}\lambda_k)}} \quad (23.214)$$

follows and letting $c \rightarrow 0$ leads to $\mu(\Omega) = 1$ independent of the sequence $b_k, k = 1, \dots, \infty$. Note that the subspace of quadratically convergent sequences has measure zero in the extended domain Ω (23.213). It is not known whether this also holds for the turbulence measure.

23.18.3 Characteristic Functional

The characteristic functional $\theta(\mathbf{t})$ for \mathbf{t} in a space of infinite sequences \mathcal{N} (test function space to be specified below) is defined as Fourier transform of the measure μ by

$$\theta(\mathbf{t}) = \langle \exp(i \sum_{k=1}^{\infty} t_k x_k) \rangle \quad (23.215)$$

Choose the space $\mathcal{N} = l^1 = \{\mathbf{t} : \sum_{k=1}^{\infty} |t_k| < \infty\}$, then is the argument of the exponent $\sum_{k=1}^{\infty} t_k x_k$ well defined, since with the aid of Hölder's inequality (Kreyszig, [8])

$$\begin{aligned} \left| \sum_{k=1}^{\infty} t_k x_k \right| &\leq \sum_{k=1}^{\infty} |t_k| |x_k| = \sum_{k=1}^{\infty} |t_k|^{\frac{1}{2}} |t_k|^{\frac{1}{2}} |x_k| \\ &\leq \left(\sum_{k=1}^{\infty} |t_k| \right)^{\frac{1}{2}} \left(\sum_{k=1}^{\infty} |t_k| |x_k|^2 \right)^{\frac{1}{2}} < \infty \end{aligned}$$

holds according to step (2) above: $|t_k| \equiv \lambda_k > 0 : \sum_{k=1}^{\infty} \lambda_k < \infty$ and $\sum_{k=1}^{\infty} \lambda_k x_k^2 < \infty$. The characteristic functional is thus computed as follows:

$$\int_{\Omega} \mu(d\mathbf{x}) \exp(i \sum_{k=1}^{\infty} t_k x_k) = \lim_{N \rightarrow \infty} \prod_{k=1}^N \sqrt{\frac{b_k}{2\pi}} \int_{-\infty}^{\infty} dx_k \exp[i t_k x_k - \frac{b_k}{2} x_k^2]$$

Noting the relation, $i t_k x_k - \frac{b_k}{2} x_k^2 = -\frac{b_k}{2} (x_k - \frac{i}{b_k} t_k)^2 - \frac{1}{2b_k} t_k^2$, it follows

$$\theta(\mathbf{t}) \equiv$$

$$\int_{\Omega} \mu(d\mathbf{x}) \exp(i \sum_{k=1}^{\infty} t_k x_k) = \lim_{N \rightarrow \infty} \exp\left(-\frac{1}{2b_k} \sum_{k=1}^N t_k^2\right) \prod_{k=1}^N \sqrt{\frac{b_k}{2\pi}} \int_{-\infty}^{\infty} dx_k \exp\left[-\frac{b_k}{2} (x_k - \frac{i}{b_k} t_k)^2\right]$$

and finally

$$\theta(\mathbf{t}) = \exp\left(-\frac{1}{2b_k} \sum_{k=1}^{\infty} t_k^2\right) \quad (23.216)$$

is obtained as characteristic functional of the Gaussian measure defined on the support space (23.213) and the space of argument sequences (test function space) $\mathcal{N} = \{\mathbf{t} : \sum_{k=1}^{\infty} |t_k| < \infty\}$.

Comments

- (1) The countably infinite-dimensional support space (23.213) for Gaussian measures constructed in the previous section has the remarkable feature that the subspace $l^2 \subset \Omega$ of elements with finite norm $\|\mathbf{x}\|^2 = \sum_{k=1}^{\infty} x_k^2$ has the Gaussian measure zero in Ω , while the Gaussian measure of the support space is $\mu(\Omega) = 1$.
- (2) The space of arguments \mathcal{N} for the characteristic functional (23.216) associated with the Gaussian measure μ is the space of absolutely convergent sequences $\mathcal{N} = l^1 = \{\mathbf{t} : \sum_{k=1}^{\infty} |t_k| < \infty\}$ depending on the Gaussian measure via the sequence $\{b_k, k = 1, \dots, \infty\}$.
- (3) In general, the space of arguments for the characteristic functional θ must be a nuclear space \mathcal{N} , see Gelfand and Vilenkin [45] for the definition and properties of nuclear spaces.
- (4) The support/phase space Ω of the measure μ and the space \mathcal{N} of arguments/test functions for the characteristic functional θ are different for the limit $N \rightarrow \infty$. The dual \mathcal{N}' of the nuclear space \mathcal{N} of test functions contains the phase space Ω . The dual \mathcal{N}' is the space of generalized vector functions defined in the flow domain \mathcal{D} (the dual \mathcal{N}' is defined as the vector space of all continuous linear functionals defined on \mathcal{N} , [15] Chap. 3.1).

23.19 Lagrangean and Eulerian Statistics

Statistical information can be given in the material/Lagrangean or spatial/Eulerian description raising the question how to transform this information from one description to the other, a problem addressed by Lumley more than 50 years ago in his PhD thesis [46]. Since then the notion of internal intermittency (Sect. 16.2) has been rigorously defined leading to the investigation of the Pdfs of spatial and material variables and their relation, see Homann et al. [47], Kamps et al. [48] and references therein.

To formulate this situation, consider the flow of an incompressible fluid completely specified in the Eulerian description by the velocity field $\mathbf{v}(\mathbf{x}, t)$, as function of the

observer position \mathbf{x} and time t , and its Lagrangean counterpart $\mathbf{V}(\mathbf{X}, \tau)$, as function of the label \mathbf{X} (initial position) and time τ . The Eulerian and Lagrangean velocities agree iff $\mathbf{x} = \Phi(\mathbf{X}, \tau)$ and $t = \tau$, where Φ is the Lagrangean position field being the solution of the path integral version

$$\Phi(\mathbf{X}, \tau) = \mathbf{X} + \int_0^\tau d\tau' \mathbf{v}(\Phi(\mathbf{X}, \tau'), \tau')$$

of the IVP for the pathline odes

$$\frac{d\Phi}{d\tau} = \mathbf{v}(\Phi(\mathbf{X}, \tau), \tau), \quad \Phi(\mathbf{X}, 0) = \mathbf{X}$$

see Sect. 2.5 and [49, 50] for further details. Existence and uniqueness of the solution of the IVP follow from the continuity of $\mathbf{v}(\Phi(\mathbf{X}, \tau), \tau)$ and the first derivatives $\frac{\partial \mathbf{v}}{\partial \Phi}(\Phi(\mathbf{X}, \tau), \tau)$ and the Picard–Lindelöf theorem, Hartmann [51], hence are existence and uniqueness assured, if the velocity field is at least twice continuously differentiable.

The Eulerian velocity field in a turbulent flow is a stochastic field, where $\mathbf{v}(\mathbf{x}, t)$ is element of the phase space Ω_E equipped with the σ -algebra \mathcal{A}_E of Borel events and the probability measure μ_E . For instance, the mean velocity is then

$$\langle \mathbf{v} \rangle(\mathbf{x}, t) = \int_{\Omega_E} \mathbf{v} d\mu_E(\mathbf{v})$$

where the integral is, unfortunately, a functional integral impossible to evaluate except for a few particular measures such as the Gaussian (see Sect. 23.17 in Appendix A for details). However, not everything is lost, since it is not necessary to evaluate, but only to transform the integral.

The assumption that the velocity field is at least continuously differentiable for $Re < \infty$ is considered first. The solution of the IVP of the pathline odes generates then a bijective mapping $\varphi : \Omega_E \rightarrow \Omega_L$ on the functional level

$$\Phi(\mathbf{X}, \tau) = \varphi[\mathbf{v}; \mathbf{X}, \tau] \quad (23.217)$$

(functional dependence on the velocity field \mathbf{v} , parametric dependence on label \mathbf{X} and time τ separated by the semicolon) associating a Lagrangean position field with an Eulerian velocity field. This mapping has a unique inverse

$$\mathbf{v}(\mathbf{x}, t) = \varphi^{-1}[\Phi; \mathbf{x}, t] \quad (23.218)$$

Thus, the statistics of the position fields can be determined by transformation of the Eulerian velocity field. For instance, the mean position field is now

$$\langle \Phi \rangle(\mathbf{X}, \tau) = \int_{\Omega_L} \varphi^{-1}[\Phi] \frac{d\mu_E(\mathbf{v})}{d\mu_L(\Phi)} d\mu_L(\Phi) \quad (23.219)$$

This result is valid iff the probability measures are continuous with respect to each other, which is true as long as the Lagrangean position field is the bijective image of the Eulerian velocity field according to (23.217).

Now consider the general case that the velocity field fails to remain continuously differentiable as $Re \rightarrow \infty$. The transformation of the Eulerian velocity to the Lagrangean position and vice versa is given by $\varphi[\mathbf{v}]$ and its inverse $\varphi^{-1}[\Phi]$. There is evidence that the velocity field is not differentiable as $Re \rightarrow \infty$, but only Hölder continuous (22.22) $|\mathbf{v}(\mathbf{x} + \mathbf{r}) - \mathbf{v}(\mathbf{x})| \leq cr^\alpha$ with exponent $0 < \alpha \leq \frac{1}{3}$ ($r = |\mathbf{r}|$, c is a positive constant), see Onsager [52] and the discussion in Eyink [53], Tsinober [54] Chap. 6 and Sect. 22.2.2.

The general considerations lead to functional mappings to transform Eulerian to Lagrangean variables lacking explicit representation and involving functional integrals for the computation of statistical quantities. Lumley [46] suggested for this reason an approach starting with finite amounts of information to avoid functional integrals. The single-point statistics of the Eulerian velocity are specified by the Pdf $f_E(\mathbf{u}; \mathbf{x}, t)$, which is a single time Pdf, whereas the single-point statistics of the Lagrangean velocity are given by $f_L(\mathbf{w}; \mathbf{X}, \tau)$, which, in fact, is a two-time Pdf since the label \mathbf{X} is position at time zero and the Pdf depends also on the current time $0 \leq \tau$.

The Lagrangean position field as mapping of the Navier–Stokes pdes in the spatial description to the equations in the material description has for turbulent flows stochastic properties, hence can be regarded as an example for a stochastic mapping.

23.20 Problems for Sects. 23.17 to 23.20

Problem (23.19.1): *The Lebesgue integrals $I_N(f)$ over the ball $\mathcal{B}(r)$ of radius $0 < r < \infty \in \mathbb{R}^N$ for $N > 2$*

$$I_N(f) \equiv \int_{\mathcal{B}_N} d\mu_N f(\rho), \quad d\mu_N = \prod_{k=1}^N dx_k$$

vanish as $N \rightarrow \infty$ for bounded integrands $f(\rho)$.

(23.9.1.1) *Construct a modified measure differential $d\mu_R$*

$$d\mu_R(\mathbf{x}) \equiv \frac{d\mu_N}{N(\mathbf{x})}$$

for the computation of the geometric average in the form

$$\bar{I}_N(f; r) = \int_{\mathcal{B}_N(r)} d\mu_R f(\mathbf{x})$$

such that the limit $N \rightarrow \infty$ is non-zero. It is recommended to use spherical coordinates, see Sect. 23.15 for definitions. Hint: Try the surface area as stretching factor.

References

1. Munkres, J.R.: Topology, 2nd edn. Prentice Hall, Upper Saddle River, New Jersey (2015)
2. Hatcher, A.: Algebraic Topology. Cambridge University Press, Cambridge U.K (2002)
3. Pesin, Y.B.: Dimension Theory in Dynamical Systems, p. 60637. The University of Chicago Press, Chicago (1997)
4. Ruelle, D.: Elements of Differentiable Dynamics and Bifurcation Theory. Academic Press (1989)
5. Wiggins, S.: Introduction to Applied Nonlinear Dynamical Systems and Chaos. Springer, New York (2003)
6. Lorenz, E.N.: Deterministic nonperiodic flow. *J. Atmos. Sci.* **20**, 130–141 (1963)
7. Adams, R.A.: Sobolev Spaces. Academic Press, New York (1975)
8. Kreyszig, E.: Introductory Functional Analysis with Applications. J. Wiley, New York (1989)
9. Werner, D.: Funktionalanalysis, 6th edn. Springer, New York (2007)
10. Von Wahl, W.: The Equations of Navier-Stokes and Abstract Parabolic Equations. Vieweg, Braunschweig (1985)
11. Sohr, H.S.: The Navier-Stokes Equations. Springer, Basel (2001)
12. Vishik, M.J., Fursikov, A.V.: Mathematical Problems of Statistical Hydromechanics. Kluwer Academic Publication, Dordrecht (1988)
13. Temam, R.: Infinite Dimensional Dynamical Systems in Mechanics and Physics. Springer, New York (1988)
14. Suhubi, E.: Functional Analysis. Kluwer Academic Publication, Dordrecht (2000)
15. Rudin, W.: Functional Analysis, 2nd edn. McGraw-Hill Education (Asia), Singapore (2005)
16. Walters, P.: An Introduction to Ergodic Theory. Springer (1982)
17. Dalecky, YuL, Fomin, S.V.: Measures and Differential Equations in Infinite-Dimensional Space. Kluwer Academic Publ, Dordrecht (1991)
18. Feller, M.N.: The Lévy-Laplacian. Cambridge University Press (2005)
19. Conway, J.: A course in Functional Analysis. Springer, New York (1990)
20. Bogachev, V.I.: Measure Theory, vol. 1. Springer, New York (2006)
21. Gray, A.: Tubes. Addison-Wesley Publication, Comp (1990)
22. Smirnov, V.I.: A Course of Higher Mathematics, vol. II, Pergamon Press, Oxford (1964)
23. Wang, X.: Volumes of generalized unit balls. *Math. Mag.* **78**, 390–395 (2005)
24. Folland, G.B.: How to integrate a polynomial over a sphere. *Am. Math. Month.* **108**, 446–448 (2001)
25. Courant, R.: Differential & Integral Calculus, vol. II, Blackie & Sons Ltd, London (1962)
26. Guzman, A.: Derivatives and Integrals of Multivariable Functions. Birkhäuser Boston (2003)
27. Taylor, M.E.: Measure Theory and Integration. AMS Graduate Studies in Math., vol. 76 (2006)
28. Lerner, N.: A Course on Integration Theory. Birkhäuser/Springer Basel (2014)
29. Abramowitz, M., Stegun, I.A.: Handbook of Mathematical Functions. Dover, New York (1972)
30. Olver, F.W., Lozier, D.W., Boisvert, R.F., Clark, C.W.: NIST Handbook of Mathematical Functions. Cambridge University Press, U.K. (2010)
31. Roman, S.: Advanced Linear Algebra. Graduate Texts in Mathematics, Springer, Berlin (2005)
32. Blumenson, L.E.: A derivation of n-dimensional spherical coordinates. *Am. Math. Month.* **67**, 63–66 (1960)

33. Miller, K.S.: *Multidimensional Gaussian Distributions*. Wiley, New York (1963)
34. Yeh, J.: *Real Analysis*, 2nd edn. World Scientific, New Jersey (2006)
35. Skorohod, A.V.: *Integration in Hilbert Space*. Springer, New York (1974)
36. Egorov, A.D., Sobolevsky, P.I., Yanovich, L.A.: *Functional Integrals: Approximate Evaluation and Applications*. Kluwer Academic Publication, Dordrecht (1993)
37. DeWitt-Morette, C., Cartier, P., Folacci, A.: *Functional Integration*. Plenum Press, New York and London (1997)
38. Simon, B.: *Functional Integration and Quantum Physics*. AMS Chelsea Publication, Providence, Rhode Island (2004)
39. Cartier, P., DeWitt-Morette, C.: *Functional Integration: Action and Symmetries*. Cambridge University Press, Cambridge U.K (2006)
40. Benyamin, Y., Sternfeld, Y.: Spheres in infinite-dimensional normed spaces are Lipschitz contractible. *Proc. Amer. Math. Soc.* **88**, 439–445 (1983)
41. Robinson, J.C.: *Infinite-Dimensional Dynamical Systems*. Cambridge Texts (2001)
42. Klauder, J.R.: *A Modern Approach to Functional Integration*. Birkhaeuser/Springer, New York (2010)
43. Hunt, B.R., Sauer, T., Yorke, J.A.: Prevalence: a translation-invariant almost every on infinite-dimensional spaces. *Bull. Amer. Math. Soc.* **27**, 217–238 (1992)
44. Bogachev, V.I.: Gaussian Measures, p. 62. American Mathematical Society, Mathematical surveys and monographs vol (1998)
45. Gelfand, I.M., Vilenkin, N.Y.: *Generalized Functions*, vol. 4. Academic Press, New York (1964)
46. Lumley, J.L.: The Mathematical Nature of the Problem of Relating Lagrangian and Eulerian Statistical Functions in Turbulence. *Mécanique de la Turbulence*, CNRS no. 108, Marseille, France (1962)
47. Homann, H., Kamps, O., Friedrich, R., Grauer, R.: Bridging from Eulerian to Lagrangian statistics in 3D hydro- and magnetohydrodynamic turbulent flow. *New J. Phys.* **11**, 073020 (2009)
48. Kamps, O., Friedrich, R., Grauer, R.: Exact relation between Eulerian and Lagrangean velocity increment statistics. *Phys. Rev. E* **79**, 066301 (2009)
49. Wu, J.-Z., Ma, H.-Y., Zhou, M.-D.: *Vorticity and Vortex Dynamics*. Springer, Berlin (2006)
50. Kollmann, W.: *Fluid Mechanics in Spatial and Material Description*. University Readers, San Diego (2011)
51. Hartmann, P.: *Ordinary Differential Equations*. SIAM, Philadelphia (2002)
52. Onsager, L.: Statistical hydrodynamics. *Nuovo Cimento* **6**(Suppl.), 279–287 (1949)
53. Eyink, G.L.: Dissipative anomalies in singular Euler flows. *Physica D* **237**, 1956–1968 (2008)
54. Tsinober, A.: *An Informal Conceptual Introduction to Turbulence*, 2nd edn. Springer, Dordrecht (2009)

Chapter 24

Appendix B: Example for a Measure on a Ball in Hilbert Space



The functional integrals, which are the limits of Riemann/Lebesgue integrals as $n \rightarrow \infty$, are zero for bounded functionals; hence, it is instructive to design examples of unbounded functionals that integrate to non-zero values. Vishik and Fursikov [1], Chap. II.3, provided such an example for the integral over a ball in Hilbert space.

Measures defined on the ball $K_\rho(\Omega) = \{\mathbf{v}(\mathbf{x}) = \sum_{i=1}^{\infty} v_i \mathbf{e}^i(\mathbf{x}) : \sum_{i=1}^{\infty} v_i^2 < \rho^2\}$ with radius ρ centered at the origin of the Hilbert space Ω can be constructed using the following steps:

Define a sequence of real numbers $\{r_j, j = 1, \dots, \infty\}$ satisfying

$$\sum_{j=1}^{\infty} r_j^2 \leq \rho^2 \quad (24.1)$$

and non-negative functions $p_j(y)$, $y \in [-r_j, r_j]$, $j = 1, \dots, \infty$ such that

$$\int_{-r_j}^{r_j} dy p_j(y) = 1 \quad (24.2)$$

holds. For instance, the $p_j(y)$ can be set to

$$p_j(y) = \begin{cases} \frac{1}{r_j} & \text{for } y \in [-r_j, r_j] \\ 0 & \text{otherwise} \end{cases} \quad (24.3)$$

A finite-dimensional measure is then constructed as Riemann integral

$$\mu_m(\omega) = \int_{\omega} \prod_{j=1}^m p_j(v_j) dv_j, \forall \omega \in \mathcal{A}(\Omega_m) \quad (24.4)$$

where $\mathbf{v}(\mathbf{x}) = \sum_{j=1}^m v_j \mathbf{e}^j(\mathbf{x}) \in \Omega_m$, $\mathbf{x} \in \mathcal{D}$ with respect to the ONS basis $\{\mathbf{e}^1, \dots, \mathbf{e}^m\}$ of Ω_m . To check whether this sequence of finite-dimensional measures μ_m defines a probability measure on the Borel σ -algebra \mathcal{A} , the condition (6.24) must hold for a non-negative exponent γ . The norm in the Hilbert space Ω is given by

$$\|\mathbf{v}\|^2 = \sum_{i,j=1}^{\infty} v_i v_j (\mathbf{e}^i, \mathbf{e}^j) \quad (24.5)$$

Since $\{\mathbf{e}^j\}$, $j = 1, \dots, \infty$ is ONS basis of Ω , it follows that

$$\|\mathbf{v}\|^2 = \sum_{j=1}^{\infty} v_j^2 \quad (24.6)$$

holds. The restricted norm is then

$$\|\mathbf{v}\|_{(m)}^2 = \sum_{j=1}^m v_j^2 \quad (24.7)$$

The integral in the condition (6.24) for $\gamma > 0$ emerges in the form

$$\int_{\Omega_m} \|\mathbf{v}\|_{(m)}^{\gamma} \mu_m(d\mathbf{v}) = \int_{\Omega_m} \left(\sum_{j=1}^m v_j^2 \right)^{\frac{\gamma}{2}} \prod_{j=1}^m p_j(v_j) dv_j \quad (24.8)$$

Choose $\gamma = 2$, then

$$\int_{\Omega_m} \|\mathbf{v}\|_{(m)}^2 \mu_m(d\mathbf{v}) = \sum_{j=1}^m \int_{\Omega_m} v_j^2 \prod_{j=1}^m p_j(v_j) dv_j \quad (24.9)$$

is obtained, which can be evaluated using the definition of $p_j(v_j)$

$$\int_{\Omega_m} v_j^2 \prod_{j=1}^m p_j(v_j) dv_j = \prod_{j=1}^m \int_{-r_j}^{r_j} v_j^2 p_j(v_j) dv_j \quad (24.10)$$

and

$$\int_{-r_j}^{r_j} \left(\frac{v_j}{r_j} \right)^2 p_j(v_j) dv_j < 1 \quad (24.11)$$

due to (24.2). It follows that

$$\sup_m \int_{\Omega_m} \|\mathbf{v}\|_{(m)}^\gamma \mu_m(d\mathbf{v}) = \sum_{j=1}^m r_j^2 \int_{-r_j}^{r_j} \left(\frac{v_j}{r_j}\right)^2 p_j(v_j) dv_j < \sum_{j=1}^m r_j^2 < \rho^2 \quad (24.12)$$

holds for $\gamma = 2$, hence is (6.24) satisfied and the sequence $\{\mu_m, m = 1, \dots, \infty\}$ defines a σ -additive measure μ on the Borel σ -algebra $\mathcal{A}(\Omega)$. It remains to show that this measure is concentrated on the ball $K_\rho(\Omega)$ in Hilbert space Ω . The ball K_ρ is the intersection of all cylinder sets $K_\rho^m(\Omega) \oplus \Omega_m^\perp$, which form an ordered sequence $K_\rho^n(\Omega) \oplus \Omega_n^\perp \subset K_\rho^m(\Omega) \oplus \Omega_m^\perp$ for $m < n$, hence

$$\int_{K_\rho(\Omega)} \mu(d\mathbf{v}) = \lim_{m \rightarrow \infty} \int_{K_\rho^m(\Omega) \oplus \Omega_m^\perp} \mu(d\mathbf{v}) \quad (24.13)$$

where

$$\int_{K_\rho^m(\Omega) \oplus \Omega_m^\perp} \mu(d\mathbf{v}) = \int_{K_\rho^m(\Omega)} \prod_{j=1}^m p_j(v_j) dv_j = \prod_{j=1}^m \int_{-r_j}^{r_j} p_j(v_j) dv_j = 1 \quad (24.14)$$

It follows that the measure is indeed concentrated on the ball $K_\rho(\Omega)$.

Reference

1. Vishik, M.J., Fursikov, A.V.: Mathematical Problems of Statistical Hydromechanics. Kluwer Academic Publication, Dordrecht (1988)

Chapter 25

Appendix C: Scalar and Vector Bases for Periodic Pipe Flow



Bases are constructed for separable Hilbert spaces relevant for the solutions of the Navier–Stokes pdes. In addition, analytic test functions are constructed for the purpose of evaluating representations of scalar and vector fields with respect to bases defined over a compact domain \mathcal{D} , the straight cylinder being an explicit example. Scalar and vector basis functions for the phase space Ω (realizations of a turbulent flow) and the test function space \mathcal{N}_p (argument functions of the characteristic functional) plus analytic functions, for the purpose of testing numerically the convergence properties of the bases, are constructed using cylindrical coordinates suitable for the periodic flow through straight pipes with circular cross section. The numerical test functions are designed observing the parity conditions at the coordinate axis $r = 0$, essential for the smooth representations of scalar and vector fields with respect to bases defined in cylindrical coordinates. The basis for the Hilbert space \mathcal{N}_p for doubly periodic scalar fields satisfying homogeneous Dirichlet conditions at the outer boundary is considered first. The construction of the basis is reviewed, and an example for a family of numerical test functions (not to be mistaken as the arguments of Fourier transform also called test functions) is given that allows the construction of arbitrarily intricate analytic test functions by linear combination.

The second part is the construction of a vector base over the same domain \mathcal{D} for doubly periodic vector fields. Two cases are considered, the general case allowing arbitrary values for the divergence of the vector fields, and the solenoidal case for fields with zero divergence. The construction of basis functions is conveniently done in the complex plane, and the scalar and vector fields are then the backward 2-d Fourier transform with respect to the azimuthal and axial directions of the complex basis vectors.

Flow domain \mathcal{D}

The domain of definition (or flow domain) $\mathcal{D} \subset \mathbb{R}^3$ is a straight cylinder with circular cross section defined by

$$\mathcal{D} \equiv \{(r, \theta, z) : 1 \leq r \leq 1, 0 \leq \theta \leq 2\pi, 0 \leq z \leq 2\pi L\} \quad (25.1)$$

where cylindrical coordinates r (radius), θ (azimuthal angle) and z (axial coordinate) are defined with origin at the centre of the left boundary, and the axial extent of the cylindrical domain is assumed to be $L \gg 1$ and integer. This domain \mathcal{D} is fixed in the spatial description, and it is open, i.e. fluid is entering and leaving it. The scalar and vector fields (denoted by $y(\mathbf{x})$ and $\mathbf{y}(\mathbf{x})$) defined on this domain are doubly periodic with respect to the azimuthal θ and axial z -directions. It follows that the domain \mathcal{D} has only one closed boundary $\partial\mathcal{D} = \{(r, \theta, z) : r = 1\}$, the outer cylinder surface. The coordinate axis $r = 0$ is not boundary, since any point $(0, \theta, z)$, $\theta \in [0, 2\pi]$, $z \in (0, 2\pi L)$ is an inner point, but scalar and vector fields must satisfy certain restrictions (called parity conditions) on the axis to guarantee smoothness.

25.1 Modified Jacobi Polynomials $\mathcal{P}_n^{a,b}(r)$

The non-periodic radial coordinate direction requires a family of orthonormal modes that is sufficiently flexible to accommodate parity and boundary conditions. The Jacobi polynomials are chosen for this purpose as suggested by Leonard and Wray [1]. The radial modes are then designed with the aid of the classical Jacobi polynomials $P_n^{a,b}(x)$ (see Abramowitz and Stegun [2], Chap. 22 and Olver et al. [3], Chap. 18) defined on the interval $[-1, 1]$

$$P_n^{a,b}(x) = \sum_{m=0}^n \binom{n+a}{m} \binom{n+b}{n-m} \left(\frac{x-1}{2}\right)^{n-m} \left(\frac{x+1}{2}\right)^m \quad (25.2)$$

with weight function

$$w^{a,b}(x) = (1-x)^a (1+x)^b \quad (25.3)$$

and orthogonality relation

$$\int_{-1}^1 dx w^{a,b}(x) P_n^{a,b}(x) P_l^{a,b}(x) = \delta_{n,l} \frac{2^{a+b+1} \Gamma(n+a+1) \Gamma(n+b+1)}{(2n+a+b+1) \Gamma(n+1) \Gamma(n+a+b+1)} \quad (25.4)$$

The Jacobi parameters are restricted to $a > -1$, $b > -1$. Figure 25.1 shows the normalized (left graph) and the modified (right graph) Jacobi polynomials defined below for $a = 1.25$, $b = 0.75$ and $n = 0, 1, 2, 3, 20$; compare the left graph with Fig. 18.4.2 in the NIST handbook [3] Sect. 18.4.

The Jacobi polynomials (25.2) are defined on the interval $[-1, 1]$, hence require transformation to $[0, 1]$ and further modifications to accommodate parity conditions, symmetry properties and boundary conditions. They are transformed to the unit interval according to

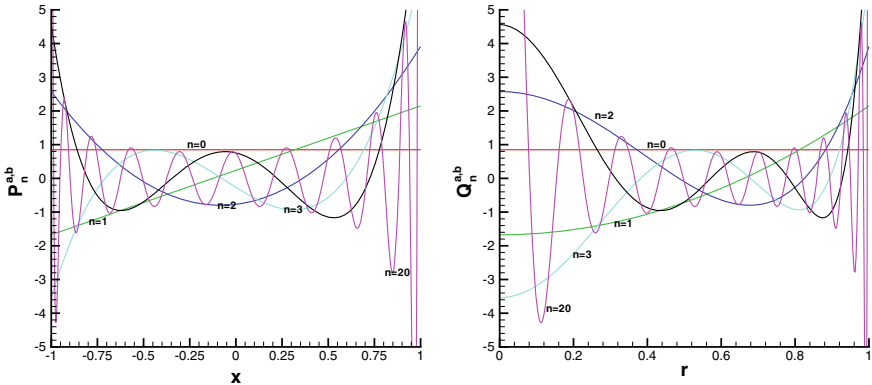


Fig. 25.1 Normalized standard Jacobi polynomials $P_n^{a,b}(x)$ (25.2) (left graph), $x \in [-1, 1]$ and normalized, modified polynomials $\mathcal{P}_n^{a,b}(r)$ (25.6), $r \in [0, 1]$ (right graph) for Jacobi parameters $a = 1.25$, $b = 0.75$ and $n = 0, 1, 2, 3, 20$ as indicated in the graphs. The basis functions are constructed by modifying the symmetric polynomials $\mathcal{P}_n^{a,b}(r)$ to satisfy divergence, parity and boundary conditions, see Figs. 25.2 to 25.5 in Sect. 25.5 of Appendix C and 25.12

$$x(r) = 2r^2 - 1, \quad r \in [0, 1], \quad r(x) = \sqrt{\frac{1}{2}(x+1)}, \quad x \in [-1, 1] \quad (25.5)$$

to the normalized radial domain $[0, 1]$. The modified and normalized Jacobi polynomials $\mathcal{P}_n^{a,b}(r)$ are then defined by $\mathcal{P}_n^{a,b}(r) \equiv N_n^{a,b} P_n^{a,b}(x(r))$ with weight function $w^{a,b}(r)$, thus

$$\boxed{\mathcal{P}_n^{a,b}(r) = N_n^{a,b} \sum_{m=0}^n \binom{n+a}{m} \binom{n+b}{n-m} (r^2 - 1)^{n-m} r^{2m}, \quad w^{a,b}(r) = 2(1-r^2)^a r^{2b+1}} \quad (25.6)$$

with $a > -1$, $b > -1$ and $r \in [0, 1]$. The weight function $w^{a,b}(r)$ is the product of the transformed weight function (25.3) times the Jacobian $\frac{dx}{dr} \equiv J = 4r$. The normalization factor is then given by

$$N_n^{a,b} = \left[\frac{(2n+a+b+1)\Gamma(n+1)\Gamma(n+a+b+1)}{\Gamma(n+a+1)\Gamma(n+b+1)} \right]^{\frac{1}{2}} \quad (25.7)$$

where Γ denotes the Gamma function ($\Gamma(n+1) = n!$ for $n \geq 0$ and integer [3], Chap. 5). Two special values are noted for later use

$$N_n^{2,b} = \left[(2n+b+3) \prod_{m=1}^2 \frac{n+b+m}{n+m} \right]^{\frac{1}{2}}, \quad N_n^{4,b} = \left[(2n+b+5) \prod_{m=1}^4 \frac{n+b+m}{n+m} \right]^{\frac{1}{2}} \quad (25.8)$$

The particular choice of the domain mapping (25.5) allows control of the symmetry with respect to the radial direction, which is one of the requirements of the parity conditions discussed in the next section. The Jacobi parameters a, b are chosen in the following sections according to fluid properties, parity and boundary conditions. The first parameter is a positive integer and the second $b(k)$ is in general a function of the azimuthal wavenumber k ; it is set in subsequent sections once the parity conditions are established.

25.2 Orthonormalization of the Modified Polynomials

$$\mathcal{P}_n^{a,b}(r)$$

It is easy to show that the $\mathcal{P}_n^{a,b}(\mathbf{x})$ satisfy in \mathcal{D} the orthonormality relation

$$(\mathcal{P}_n^{a,b}, \mathcal{P}_m^{a,b}) \equiv \int_0^1 dr w^{a,b}(r) \mathcal{P}_n^{a,b}(r) \mathcal{P}_m^{a,b}(r) = \delta_{mn} \quad (25.9)$$

if the modified weight function given in (25.10), generated by the weight function for the original Jacobi polynomials (25.3) ([3], Chap. 18) and the coordinate transformation (25.5),

$$w^{a,b}(r) = 2(1 - r^2)^a r^{2b+1} \quad (25.10)$$

is used in the scalar product (23.22).

25.3 Test Function Space \mathcal{N}_p : Scalar Fields

The construction of a Schauder basis in the test function spaces \mathcal{N}_p (for scalar and vector cases) for the example of the pipe flow periodic in axial direction is the vehicle for the explanation of the method. The scalar fields $y(r, \theta, z)$ defined on \mathcal{D} periodic with respect to the azimuthal and axial directions serve as arguments for the characteristic functional and are elements of the separable Hilbert space $\mathcal{N}_p = \{y(r, \theta, z) : y(1, \theta, z) = 0, 0 \leq z \leq L, y \in C_D^\infty \cap L_D^2\}$ (called test function space, the subscript p indicates periodic flow in axial direction) with scalar product

$$(y, s) \equiv \int_{\mathcal{D}} d\nu w(r) y(r, \theta, z) s^*(r, \theta, z) \quad (25.11)$$

$y(\mathbf{x}), s(\mathbf{x}) \in \mathcal{N}_p$ and weight function $w(r) \geq 0$ (the asterisk denotes complex conjugate) that depends on the particular system of basis functions to be determined below. The norm is defined by $\|y\| = \sqrt{(y, y)}$. A separable Hilbert space possesses countably infinite (equivalent) bases; hence, there is considerable freedom for the con-

struction of a base. Let $\mathcal{B} = \{f_{a,b}^{k,n,m}(r, \theta, z), n = 0, \dots, \infty, k = -\infty, \dots, \infty, m = -\infty, \dots, \infty\}$ be an orthonormal basis spanning \mathcal{N}_p , then is an element $y(r, \theta, z)$ represented by

$$y(r, \theta, z) = \sum_{k,n,m} y_{k,n,m} f_{a,b}^{k,n,m}(r, \theta, z) : \{y_{k,n,m}\} \in l^2 \rightarrow y(r, \theta, z) \in \mathcal{N}_p \quad (25.12)$$

mapping an infinite sequence to a function in \mathcal{N}_p . The scalar product defining the coordinates/expansion coefficients $y_{k,n,m}$ is the inverse map

$$y_{k,n,m} = (y, f_{a,b}^{k,n,m}) : y(r, \theta, z) \in \mathcal{N}_p \rightarrow \{y_{k,n,m}\} \in l^2 \quad (25.13)$$

The representation (25.12) of the scalar fields w.r.t. the basis

$$\mathcal{B} = \{f_{a,b}^{k,n,m}(r, \theta, z) = \mathcal{F}_k(\theta) \chi_n^{k,a,b}(r) \mathcal{F}_m(z)\}$$

to be made explicit in subsequent sections, in the scalar product (25.11), leads to

$$(y, s) =$$

$$\sum_{k=-\infty}^{\infty} \sum_{m=-\infty}^{\infty} \sum_{n=0}^{\infty} \sum_{n'=0}^{\infty} y_{k,n,m} s_{k,n',m}^* \int_0^1 dr w^{a,b}(r) \chi_n^{k,a,b}(r) \chi_{n'}^{k,a,b,*}(r), \quad w^{a,b}(r) = 2(1-r^2)^a r^{2b+1}$$

due to the orthonormality of the azimuthal and axial modes $\mathcal{F}_k(\theta)$ and $\mathcal{F}_m(z)$ defined in the next section. Allowance is made for the radial mode/shape functions $\chi_n^k(r)$ to be non-orthogonal and complex valued as discussed in the sections of vector bases, the Jacobi parameters $a, b(k)$ and the weight functions $w^{a,b(k)}(r)$ will also be set in the later sections to satisfy parity and boundary conditions.

25.4 Projected Functionals

The projection of a functional $\theta[y]$, $y \in \mathcal{N}_p$ onto the finite-dimensional Euclidean space spanned by the coordinates / coefficients $y_{k,n,m}$ of the basis functions in

$$\mathcal{B}_{N_\theta, N_r, N_z} \equiv \{f_{a,b}^{k,n,m}(r, \theta, z) : k = -\frac{1}{2}N_\theta, \dots, \frac{1}{2}N_\theta, n = 0, \dots, N_r, m = -\frac{1}{2}N_z, \dots, \frac{1}{2}N_z - 1\},$$

$$\lim_{N_\theta, N_r, N_z \rightarrow \infty} \mathcal{B}_{N_\theta, N_r, N_z} = \mathcal{B}, \text{ is then}$$

$$\theta_N(y_{-\frac{1}{2}N_\theta, 0, -\frac{1}{2}N_z}, \dots, y_{\frac{1}{2}N_\theta-1, N_r, \frac{1}{2}N_z-1}) \equiv \theta\left[\sum_{k=-\frac{1}{2}N_\theta, n=0, m=-\frac{1}{2}N_z}^{\frac{1}{2}N_\theta-1, N_r, \frac{1}{2}N_z-1} y_{k,n,m} f_{a,b}^{k,n,m}(\mathbf{x})\right] \quad (25.14)$$

where θ_N is a standard function of $N_\theta(N_r + 1)N_z$ variables $y_{k,n,m}$ ($N \equiv \max((N_r + 1), N_\theta, N_z)$ for graphic presentation purposes). The arguments of the functional are cylinder functions, see Dalecky and Fomin [4], Chap. 2 for general definition. If the scalar field $y(r, \theta, z)$ is real-valued, the FFT consistent storage (defined by Rogallo, 1981, [5], for the numerical solution of the Navier–Stokes pdes) is applied: $k = 0, \dots, \frac{1}{2}N, m = 0, \dots, N, n = 0, \dots, N_r, N$ a power of 2, to allow use of FFT software; hence, storage requirements are significantly reduced.

Comments

The projection defined in (25.14) is the characteristic functional $\theta[\mathbf{y}(\cdot); t]$ restricted to a linear subspace of \mathcal{N}_p consisting of arguments with a finite number of terms in the representation (25.73), hence, a standard function of a finite number of coefficients of basis elements. An argument $y^{k,n,m}$ with a finite number of terms generates a solenoidal vector field according to (25.73), thus defining it for every point in the flow field without additional assumptions. This projection is different from the projection resulting from choosing a finite number of points in the flow field \mathcal{D} and constructing pdes for the Pdfs and Cdfs (governing the statistical properties of the scalar and/or vector fields at the chosen points in the flow field) with the aid of the Dirac pseudo-function. Choosing N points $\mathbf{x}^{(i)} \in \mathcal{D}, i = 1, \dots, N$, the N -point Cdf (and the Pdf and characteristic function derived from it) is the expectation of the coarse-grained Cdf

$$\hat{F}_{4N} \equiv \Pi_{i=1}^N H(\varphi_i - \Phi(\mathbf{x}^{(i)}, t)) H(\mathbf{v}^{(i)} - \mathbf{v}(\mathbf{x}^{(i)}, t))$$

and thus a function of the variables $\mathbf{v}^{(i)}$. These variables cannot be extended to 3-d vector fields without additional assumptions. The effect of this projection is a pde containing additional unknown correlations, thus creating a closure problem.

25.5 Bases for the Test Function Space \mathcal{N}_p

The elements $y(\mathbf{x})$ of the test function space \mathcal{N}_p over the flow domain \mathcal{D} equipped with a cylindrical coordinate system $O(r, \theta, z)$ are subject to kinematic conditions at the axis $r = 0$ to insure smoothness and uniqueness. These kinematic (called parity conditions) constraints link the radial variation to the azimuthal wavenumber k and can be established with the aid of discrete Fourier transformation of scalar and vector fields $y(r, \theta, z) \in \mathcal{N}_p$ with respect to the normalized, azimuthal, discrete Fourier modes/kernels. Fourier transformation is defined by

$$\hat{f}(\mathbf{k}) = \mathcal{F}f(\mathbf{x}), \quad f(\mathbf{x}) = \mathcal{F}^{-1}\hat{f}(\mathbf{k}) \quad (25.15)$$

where the Fourier transform operator pair is defined by (15.2). The transformed variables are identified by hats, and θ denotes the angular coordinate. The argument of the exponential must be dimensionless. Hence, if variables with physical dimension are employed, the dimension of the wavenumber vector \mathbf{k} must be the inverse of the dimension of \mathbf{x} . It is convenient to define the Fourier modes slightly different from the transformation kernel

$$h_k(\theta) \equiv \frac{1}{\sqrt{2\pi}} \exp(ik\theta) \quad (25.16)$$

satisfying orthonormality

$$(h_k, h_l) \equiv \int_0^{2\pi} d\theta h_k(\theta) h_l^*(\theta) = \delta_{k,l} \quad (25.17)$$

where the asterisk indicates complex conjugate. The complex conjugate of the kernel is the inverse kernel

$$h_\theta^{-1}(k) \equiv \frac{1}{\sqrt{2\pi}} \exp(-ik\theta) = h_k^*(\theta) \quad (25.18)$$

The first step in constructing the system of basis modes is to establish the parity conditions.

25.6 Discrete Fourier Transform w.r.t. the Angular Coordinate

The representation of an argument field $y(\mathbf{x}) \in \mathcal{N}_p$ appears then in the form

$$y(r, \theta, z, t) = \sum_{k=-\infty}^{\infty} \hat{y}^k(r, z, t) h_k(\theta) \quad (25.19)$$

using the complex version of the trigonometric functions (25.16). The complex-valued Fourier coefficients $\hat{y}^k(r, z, t)$ are defined by

$$\hat{y}^k(r, z, t) = \int_0^{2\pi} d\theta y(r, \theta, z, t) h_k^*(\theta) \quad (25.20)$$

for $k = 0, \pm 1, \pm 2, \dots$. The fact that scalar field $y(r, \theta, z)$ is real implies that

$$\hat{y}^{-k}(r, z, t) = \hat{y}^{*,k}(r, z, t) \quad (25.21)$$

holds. Hence, the expansion (25.19) can be reformulated as

$$y(r, \theta, z, t) = y^0 h_0 + \sum_{k=1}^{\infty} [\hat{y}^k(r, z, t) h_k(\theta) + \hat{y}^{*,k}(r, z, t) h_k^*(\theta)] \quad (25.22)$$

where y^0 and $h_0 = 1/\sqrt{2\pi}$ are real. If the complex-valued coefficients \hat{y}^k are split into real and imaginary parts

$$\hat{y}^k = y_r^k + i y_i^k \quad (25.23)$$

the expansion emerges in the real form

$$y(r, \theta, z, t) = \frac{1}{\sqrt{2\pi}} y^0(r, z, t) + \sqrt{\frac{2}{\pi}} \sum_{k=1}^{\infty} [y_r^k(r, z, t) \cos(k\theta) - y_i^k(r, z, t) \sin(k\theta)] \quad (25.24)$$

where the axisymmetric mode $y^0 = \hat{y}^0$ is strictly real. It is clear that the complex-valued coefficients \hat{y}^k in (25.19) need to be computed only for $k \geq 0$ since the coefficients for $k < 0$ follow from (25.21).

The kinematic (or parity) conditions can now be formulated for the complex-valued Fourier amplitudes $\hat{y}^k(r, z)$, and details can be found in [6, 7]. Time dependence will not be indicated in the following sections.

25.7 Scalar Parity Conditions for Azimuthal Wavenumbers $k \geq 0$

Elementary analysis using Fourier series and Taylor series expansions at $r = 0$ leads to restrictions for the Fourier amplitudes/modes $\hat{y}^k(r, z)$ of a scalar field $y(r, \theta, z)$. They must satisfy the growth law

$$O(\hat{y}^k) = r^k, \quad k \geq 0 \quad (25.25)$$

at the coordinate axis $r = 0$ and the radial symmetry condition

$$\hat{y}^k(r, z) = \begin{cases} k \text{ even:} & \text{symmetric with respect to } r \\ k \text{ odd:} & \text{antisymmetric with respect to } r \end{cases} \quad (25.26)$$

Violation of these conditions leads to non-uniqueness and/or singularity at the axis $r = 0$. It will be shown in a later section that the axial velocity component is subject to the same parity conditions as scalar fields.

25.7.1 Design Requirements for the Scalar Basis Functions

The construction of the complex-valued scalar expansion modes must be done in such a way that the

(S1) the condition at the boundary $\partial\mathcal{D}$ is satisfied;

$$y(r, \theta, z) = 0 \text{ for } (r, \theta, z) \in \partial\mathcal{D} \quad (25.27)$$

(S2) the parity conditions (25.25) and (25.26) with respect to the azimuthal wavenumber k are satisfied.

25.7.2 Construction of Scalar Basis Functions

The scalar basis functions are conveniently constructed in Fourier space, since the parity conditions are formulated in this space; once they are set up inverse Fourier transformation generates the basis functions in physical space. A family of scalar expansion functions to serve as basis in the argument/test function space \mathcal{N}_p is constructed assuming periodicity in axial direction, the azimuthal direction is automatically periodic for smooth fields. The complex-valued azimuthal Fourier coefficients $\hat{y}^k(r, z)$ defined in Eq. (25.19) are expanded in radial direction in terms of a real-valued, orthonormalized, polynomial system $\{q_{k,n}^{a,b(k)}(r), n = 0, 1, 2, \dots\}$ with weight function $w^{a,b(k)}(r)$ (25.10)

$$\hat{y}^k(r, z) = \sum_{n=0}^{\infty} \hat{y}_{n,k}(z) q_{k,n}^{a,b(k)}(r) \quad (25.28)$$

where the complex-valued expansion coefficients in (25.28) are denoted by $\hat{y}_{n,k}(z)$ with n denoting the radial expansion index and k the azimuthal wavenumber. The expansion for negative wavenumbers k is defined by $q_{-k,n}^{a,b(k)} = q_{k,n}^{*,a,b(k)}$.

Periodicity in axial direction allows the expansion in Fourier series with respect to z . The complex coefficients $\hat{y}_{n,k}(z)$ are thus

$$\hat{y}^k(r, z) = \sum_{n=0}^{\infty} \sum_{m=-\infty}^{\infty} \hat{y}_{k,n,m} q_{k,n}^{a,b(k)}(r) h_m(z) \quad (25.29)$$

where the axial Fourier modes are defined as for the azimuthal direction (25.16) by

$$h_m(z) \equiv \frac{1}{\sqrt{2\pi}} \exp(imz) \quad (25.30)$$

and $z \in [0, 2\pi]$.

A scalar field $y(r, \theta, z) \in \mathcal{N}_p$ is thus represented by

$$y(r, \theta, z) = \sum_{k=-\infty}^{\infty} \sum_{m=-\infty}^{\infty} \sum_{n=0}^{\infty} \hat{y}_{k,n,m} f_{a,b(k)}^{k,n,m}(r, \theta, z) \quad (25.31)$$

with respect to the orthonormalized basis $\mathcal{B}_p \equiv \{f_{a,b(k)}^{k,n,m}(r, \theta, z) : n \in [0, \infty], k \in (-\infty, \infty), m \in (-\infty, \infty)\}$

$$f_{a,b}^{k,n,m}(r, \theta, z) \equiv h_k(\theta) q_{k,n}^{a,b}(r) h_m(z) = \frac{1}{\sqrt{2\pi}} \exp(ik\theta) q_{k,n}^{a,b}(r) \frac{1}{\sqrt{2\pi}} \exp(imz) \quad (25.32)$$

The polynomial system and the associated weight function for the radial modes $q_n^{a,b,k}(r)$ are set up in Sect. 25.8. The evaluation of a scalar field specified in the basis $f_{a,b}^{k,n,m}(r, \theta, z)$ according to (25.31) must take into account the dependence of the radial modes on the azimuthal wavenumber k ; hence,

$$y(r, \theta, z) = \sum_{k=-\infty}^{\infty} \frac{1}{\sqrt{2\pi}} \exp(ik\theta) \sum_{m=-\infty}^{\infty} \frac{1}{\sqrt{2\pi}} \exp(imz) \sum_{n=0}^{\infty} \hat{y}_{k,n,m} q_{k,n}^{a,b(k)}(r) \quad (25.33)$$

the summation over the radial index n for given wavenumbers k and m must be done first.

The condition (25.21) insuring that the scalar field $y(r, \theta, z)$ is real emerges in the form

$$\sum_{m=-\infty}^{\infty} h_m(z) \sum_{n=0}^{\infty} \hat{y}_{n,-k,m} q_{-k,n}^{a,b}(r) = \sum_{m=-\infty}^{\infty} h_m^*(z) \sum_{n=0}^{\infty} \hat{y}_{k,n,m}^* q_{k,n}^{a,b}(r)$$

where

$$\hat{y}_{n,-k,m} h_{-m}(z) = \hat{y}_{k,n,m}^* h_m^*(z) \quad (25.34)$$

holds, since the conjugate of a product is the product of the conjugates and $q_{-k,n}^{a,b}(r) = q_{k,n}^{a,b}(r)$ and real.

25.8 Radial Modes for Homogeneous Dirichlet Conditions

The modified and normalized Jacobi polynomials $\mathcal{P}_n^{a,b}(r)$ (25.6) adapted to the radial range $[0, 1]$ are the essential tool for the design of the radial modes. They are symmetric with respect to zero in $[0, 1]$; hence, further modification is required to satisfy the parity condition (S2) and the homogeneous Dirichlet condition at the outer boundary $\partial\mathcal{D}$. This can be done by choosing a suitable value for the Jacobi parameter a and

defining the Jacobi parameter $b(k)$ as function of the azimuthal wavenumber k . It is desirable to preserve orthonormality, hence is the ONS relation (25.9)

$$\int_0^1 dr w^{a,b}(r) \mathcal{P}_n^{a,b}(r) \mathcal{P}_m^{a,b}(r) = \delta_{mn}$$

with weight function (25.10) $w^{a,b}(r) = 2(1-r^2)^a r^{2b+1}$ the starting point for the construction of basis functions. Rearrangement of the integrand

$$\int_0^1 dr \omega^{a,\gamma}(r) [r^{b(k)}(1-r^2)^\gamma \mathcal{P}_n^{a,b(k)}(r)] [r^{b(k)}(1-r^2)^\gamma \mathcal{P}_m^{a,b(k)}(r)] = \delta_{mn}$$

with weight function $\omega^{a,\gamma}(r) = 2r(1-r^2)^{a-2\gamma}$ indicates the generic form of the modes. A third parameter γ has been introduced to control the variation of the modes near the boundary without violating the ONS property. The generic shape function is now defined as

$$q_{k,n}^{a,b(k),\gamma}(r) = r^{b(k)}(1-r^2)^\gamma \mathcal{P}_n^{a,b(k)}(r), \quad b(k) \geq 0 \quad (25.35)$$

with an additional parameter $\gamma \geq 0$ and the generic weight function

$$\omega^{a,\gamma}(r) = 2r(1-r^2)^{a-2\gamma} \quad (25.36)$$

Clearly, the Jacobian parameters a, b and the new parameter γ have important roles to play:

(J1) a controls the properties of the weight function, if $a < 2\gamma$ $\omega^{a,\gamma}(r)$ is singular at the boundary;

(J2) $b(k)$ controls the parity conditions (S1) and (S2);

(J3) γ controls the variation near the boundary, $\gamma = 1$ implies zero value and $\gamma = 2$ zero value and zero first radial derivative at $r = 1$.

The values $\gamma = 1 \rightarrow a = 2$ and $b(k) = k$ create the shape function

$$q_n^k(r) \equiv q_{k,n}^{a,b(k),\gamma}(r) = r^{b(k)}(1-r^2)^\gamma \mathcal{P}_n^{a,b(k)}(r), \quad b(k) \geq 0 \quad (25.37)$$

with weight function

$$\omega(r) = 2r \quad (25.38)$$

for scalar field representation consistent with growth and symmetry required by parity conditions. Note that the variation of $q_{k,n}^{a,b(k)}(r)$ near the boundary is linear w.r.t. $\epsilon \equiv 1 - r$, since $1 - r^2 = (1 - r)(1 + r)$. The orthonormality of the $q_{k,n}^{a,b(k)}(r)$ follows from the observation

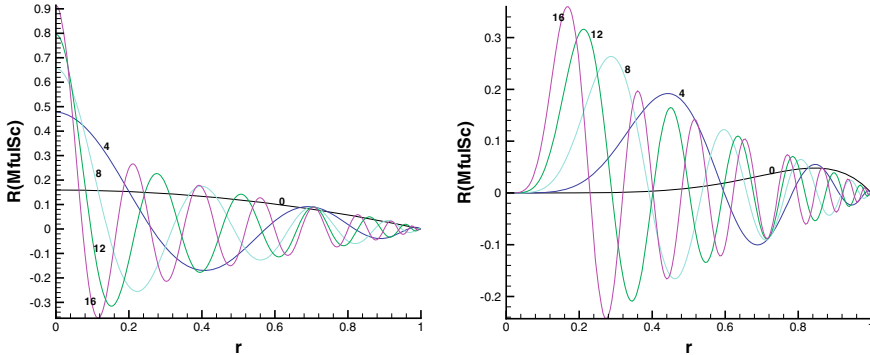


Fig. 25.2 Radial shape functions $q_{k,n}^{a,b(k)}(r)$ (25.37) for the scalar modes and Jacobi parameters $a = 2, b(k) = k$ are illustrated for several radial mode indices. The shape functions for two azimuthal wavenumbers are shown, $k = 0$ in the left graph and $k = 5$ in the right graph. Both design requirements (S1) and (S2) are satisfied and the derivative at the outer boundary is non-zero. The radial mode indices n are indicated by the numbers in the graphs

$$\begin{aligned} \omega^a(r) q_{k,n}^{a,b(k)}(r) q_{k,l}^{a,b(k)}(r) &= 2r(1-r^2)^{a-2} r^{2b(k)} (1-r^2)^2 \mathcal{P}_n^{a,b(k)} \mathcal{P}_l^{a,b(k)} = \\ &2(1-r^2)^a r^{2b(k)+1} \mathcal{P}_n^{a,b(k)} \mathcal{P}_l^{a,b(k)} = w^{a,k}(r) \mathcal{P}_n^{a,b(k)}(r) \mathcal{P}_l^{a,b(k)}(r) \end{aligned} \quad (25.39)$$

and (25.9), (25.10). Figure 25.2 shows the radial shape functions $q_{k,n}^{a,b}(r)$ (25.37) constructed with the transformed, normalized Jacobi polynomials defined in $[0, 1]$ for scalar fields and the Jacobi parameters $a = 2, b(k) = k$. The azimuthal wavenumbers are $k = 0$ (left graph) and $k = 5$ (right graph) and the radial indices $n = 0, 4, 8, 12$ as indicated in the graphs. The radial modes for $k = 0$ are symmetric with respect to $r = 0$ and non-zero at the coordinate axis $r = 0$, and the modes for $k > 0$ are zero at the axis and either symmetric or antisymmetric according to the parity condition (25.26).

For comparison, Fig. 25.3 shows the radial shape functions for the radial velocity component v_r constructed with the transformed, normalized Jacobi polynomials $s_n^k(r)$ (25.106) for the Jacobi parameters $a = 2, b(k) = |k - 1|$. The azimuthal wavenumbers in the plot are $k = 1$ (left graph) and $k = 6$ (right graph) and the radial indices $n = 0, 2, 4, 6, 8, 12$ as indicated. The radial modes for $k = 1$ (and all odd k) are symmetric with respect to r and non-zero at the coordinate axis $r = 0$ to compare with the scalar shape functions for $k = 0$ sharing the symmetry properties. The modes for $|k - 1| \neq 0$ (and all even k) are zero at the axis and antisymmetric according to the parity condition (25.26). The scalar shape functions for $a = 2, b(k) = k$ and radial velocity functions for $a = 2, b(k) = |k - 1|$ are for the same values of $b(k)$ different since $s_{k,n}^{a,b(k)} = (1-r^2)q_{k,n}^{a,b(k)}$.

The normalized scalar basis function (25.32) is now denoted by

$$f^{k,n,m}(r, \theta, z) = h_k(\theta) q_n^k(r) h_m(z)$$

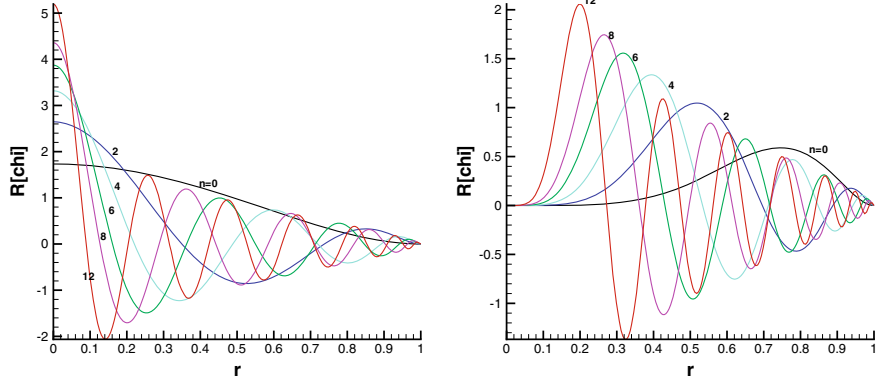


Fig. 25.3 Radial shape functions $s_{k,n}^{a,b(k)}(r) = (1-r^2)q_{k,n}^{a,b(k)}(r)$ (25.106) for the radial vector component modes for the Jacobi parameters $a = 2$, $b(k) = |k - 1|$. The azimuthal wavenumber $k = 1$ (left graph) and $k = 6$ (right graph) for comparison with Fig. 25.2. The divergence of the vector modes is non-zero. Note that the derivative at the outer boundary is zero. The radial mode indices n are indicated by numbers

They satisfy the requirements (S1), (S2) and the condition on the outer boundary for scalar fields. The orthonormality of the $f^{k,n,m}(r, \theta, z)$ follows from the relation (25.9) for the $\mathcal{P}_n^{a,k}(r)$ and (25.39)

$$\int_0^1 dr \omega(r) q_n^k(r) q_m^k(r) = \delta_{mn}$$

with the weight function $\omega(r)$ (25.37). Hence,

$$(f^{k,n,m}, f^{*,n',k',m'}) = \delta_{k,k'} \delta_{m,m'} \delta_{n,n'} \quad (25.40)$$

holds, where the asterisk denotes complex conjugate. This concludes the construction of an orthonormalized base in phase $\Omega_{\mathcal{D}}$ and test function spaces \mathcal{N}_p for scalar fields.

25.9 Representation of Scalar Fields

The complete expansion for scalar fields such as the argument/test field $y(\mathbf{x})$, satisfying the homogeneous Dirichlet condition on the outer boundary $\partial\mathcal{D}$ in Jacobi–Fourier form (Jacobi–Fourier space is defined in Sect. 25.21.1), is then

$$y(\mathbf{x}) = \sum_{k,n,m} \hat{y}_{k,n,m} f^{k,n,m}(r, \theta, z) = \lim_{N_r, N_{\theta}, N_z \rightarrow \infty} y^{N_r, N_{\theta}, N_z}(r, \theta, z) \quad (25.41)$$

where the finite-dimensional projections are defined by

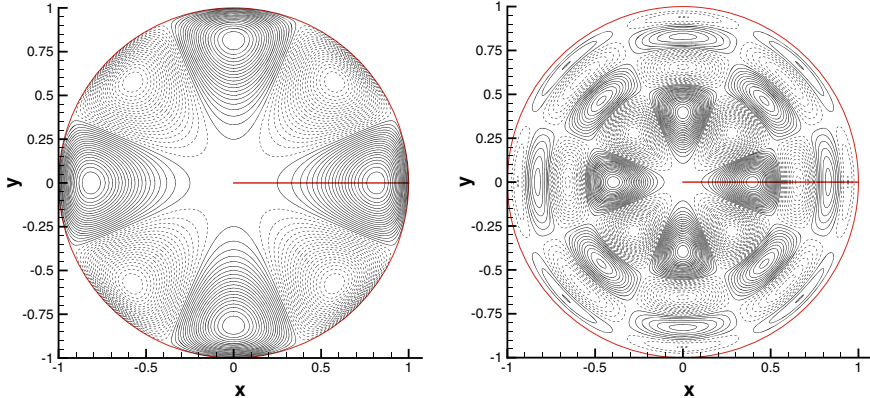


Fig. 25.4 Cross section $z = 0$ of the real part of the basis modes $f^{k,n,m}(r, \theta, z)$ in Jacobi–Fourier form for the radial index $n = 0$ (modified Jacobi polynomial) and the azimuthal wavenumber $k = 4$ (Fourier polynomial, left graph) and $n = 2, k = 4$ (right graph), the axial wavenumber is $m = 0$. The red circle indicates the boundary of the flow domain \mathcal{D}

$$y^{N_r, N_\theta, N_z}(r, \theta, z) \equiv \sum_{n=1}^{N_r} \sum_{k=-\frac{N_\theta}{2}}^{\frac{N_\theta}{2}-1} \sum_{m=-\frac{N_z}{2}}^{\frac{N_z}{2}-1} \hat{y}_{k,n,m} h_k(\theta) q_n^k(r) h_m(z) \quad (25.42)$$

with respect to the scalar, orthonormal basis $\{f^{k,n,m}(r, \theta, z)\}$ constructed in the previous section, Eq. (25.32). The expansion in physical space is obtained by backward 2-d Fourier transform with respect to the azimuthal and axial directions.

The coefficients $\hat{y}_{k,n,m}$ must satisfy the relation (25.34) to insure that the test field is real-valued. Examples for the scalar basis functions are shown in Fig. 25.4 as isolines at the axial section $z = 0$. The radial index is $n = 0$ and the azimuthal wavenumber $k = 4$ in the left graph and $n = 2, k = 4$ in the right graph. The real part of the scalar mode $f^{k,n,m}(r, \theta, z)$ for $n = 2, k = 4$ and $m = 2$ is illustrated in Fig. 25.5 as colour-coded level surfaces. The value of this mode at the coordinate axis $r = 0$ is zero according to the parity condition (25.25). The scalar product (y, s) of two scalar fields $y(r, \theta, z), s(r, \theta, z)$ in \mathcal{N}_p emerges as

$$(y, s) = \sum_{k=-\infty}^{\infty} \sum_{n=0}^{\infty} \sum_{m=-\infty}^{\infty} y_{k,n,m} s_{k,n,m}^* \quad (25.43)$$

since the scalar modes are orthonormalized.

Analytic test fields for homogeneous Dirichlet boundary values

The analytic fields for the test of the representation (25.41) are constructed with the aid of the exponential function, and the outer boundary is at $r = 1$ (dimensionless), see the scales chosen for the Reynolds number defined by (2.8). The general

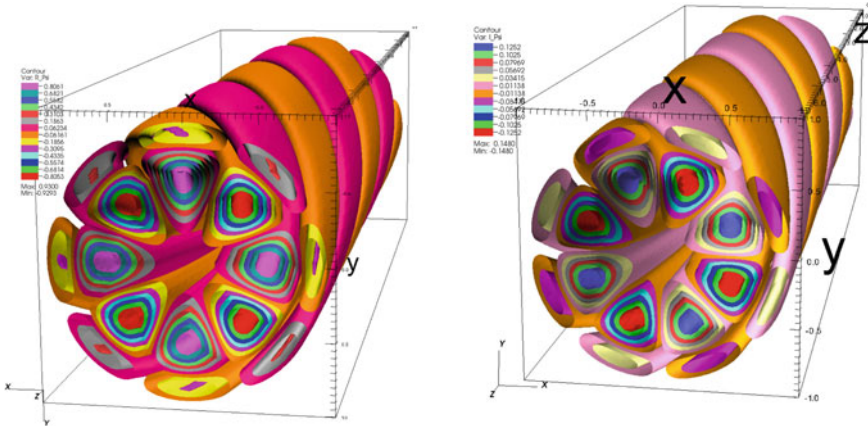


Fig. 25.5 Colour-coded level surfaces of the real (left graph) and imaginary (right graph) part of the scalar mode $f^{k,n,m}(r, \theta, z)$ in Jacobi–Fourier form for the radial index $n = 2$, azimuthal wavenumber $k = 4$, axial wavenumber $m = 2$

expression for the test field is set by

$$\mathcal{F}(r, \theta, z) = (1 - r^2)\hat{\mathcal{F}}(r, \theta, z) \quad (25.44)$$

where $\hat{\mathcal{F}}(r, \theta, z)$ is smooth, i.e. bounded and differentiable in \mathcal{D} . The function $\hat{\mathcal{F}}$ is composed as product

$$\hat{\mathcal{F}}(r, \theta, z) = \mathcal{G}(x(r, \theta), y(r, \theta))\mathcal{H}(z) \quad (25.45)$$

where $x(r, \theta)$, $y(r, \theta)$ are the Cartesian coordinates in a cross section $z = \text{constant}$ related to the cylindrical coordinates by $x(r, \theta) = r \cos(\theta)$, $y(r, \theta) = r \sin(\theta)$. The building block for the first example is specified in the form

$$\mathcal{G}(r, \theta) = \exp\left\{-\frac{1}{2\sigma^2}[(x - x_0)^2 + (y - y_0)^2]\right\} \quad (25.46)$$

by choosing the three parameters $\sigma > 0$, x_0 , y_0 , and

$$\mathcal{H}(z) = \cos(2\pi m \frac{z}{L}) \quad (25.47)$$

Alternatively, the axial profile can be lifted and

$$\mathcal{G}_L(r, \theta) = \exp\left\{-\frac{1}{2\sigma^2}[(x - x_0)^2 + (y - y_0)^2]\right\} - \exp\left[-\frac{1}{2\sigma^2}(x_0^2 + y_0^2)\right] \quad (25.48)$$

hence

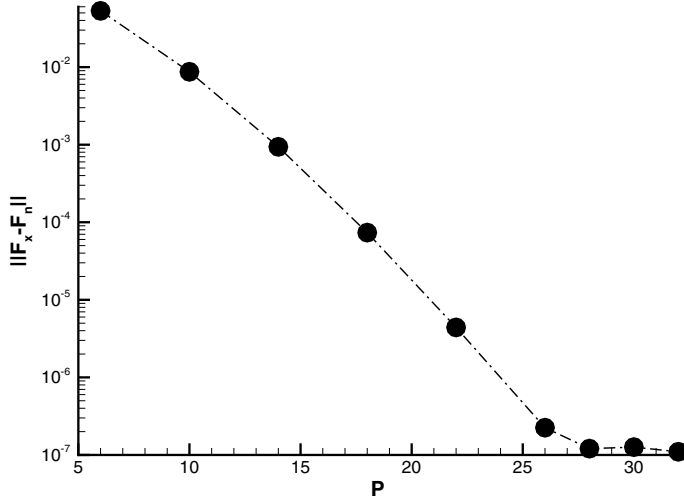


Fig. 25.6 Maximum norm of the difference between test function $F_x \equiv y(r, \theta, z)$ with $\mathcal{H}(z) = \cos(m_0 z)$ (25.51) (single term $A_{1,1,1} = 1$) and the finite-dimensional projection $F_n \equiv y^{N_r, N_\theta, N_z}$ (25.41) of its representation in the base $\{f^{k,n,m}(r, \theta, z)\}$ (25.32) as function of $P = N \equiv \max(N_r, N_\theta, N_z)$, a scalar mode $f^{2,4,2}(r, \theta, z)$ is presented in Fig. 25.5 in terms of colour-coded level surfaces

$$\mathcal{G}(r, \theta) = \mathcal{G}_L(r, \theta) + \exp\left[-\frac{1}{2\sigma^2}(x_0^2 + y_0^2)\right] \quad (25.49)$$

and

$$\mathcal{F}(r, \theta, z) = (1 - r^2)\{\mathcal{G}_L(r, \theta)\mathcal{H}(z) + \exp\left[-\frac{1}{2\sigma^2}(x_0^2 + y_0^2)\right]\}\mathcal{H}(z) \quad (25.50)$$

is obtained. Clearly, finite linear combinations can be constructed by indexing the parameters, $\sigma_{i,j} > 0$, $x_0 \leftarrow x_i$, $y_0 \leftarrow y_j$ and axial wavenumbers m_k . The numerical test function without lifting is then

$$\mathcal{F}(r, \theta, z) = (1 - r^2) \sum_i \sum_j \sum_k A_{ijk} \exp\left\{-\frac{1}{2\sigma_{ij}^2}[(x - x_i)^2 + (y - y_j)^2]\right\} \mathcal{H}_k(z) \quad (25.51)$$

and with lifting

$$\begin{aligned} \mathcal{F}(r, \theta, z) = & (1 - r^2) \sum_i \sum_j \sum_k A_{ijk} \left[\exp\left\{-\frac{1}{2\sigma_{ij}^2}[(x - x_i)^2 + (y - y_j)^2]\right\} - \exp\left\{-\frac{1}{2\sigma_{ij}^2}(x_i^2 + y_j^2)\right\} \right] \mathcal{H}_k(z) \\ & + (1 - r^2) \sum_i \sum_j \sum_k A_{ijk} \exp\left\{-\frac{1}{2\sigma_{ij}^2}(x_i^2 + y_j^2)\right\} \mathcal{H}_k(z) \end{aligned} \quad (25.52)$$

The real and finite coefficients A_{ijk} can be freely chosen. The properties of the base (25.32) can be illustrated by computing the coefficients (coordinates) of the numerical test function (25.51) for $\mathcal{H}(z) = \cos(m_0 z)$ and the parameters $r_0 = 0.6$, $\theta_0 = 3\pi/4$, $\sigma = 0.3$, $m_0 = 2$ as function of $N = N_r = N_\theta = N_z$. The maximum norm of the error $y(\mathbf{x}) - y^{N_r, N_\theta, N_z}(\mathbf{x})$ in Fig. 25.6 indicates exponential convergence. This concludes the construction and accuracy verification of the scalar basis spanning the Hilbert space \mathcal{N}_p .

25.10 Function Spaces: Vector Fields

The vector fields $\mathbf{v}(r, \theta, z)$ and $\mathbf{y}(r, \theta, z)$ defined in the flow domain \mathcal{D} are elements of separable Hilbert vector spaces $\mathcal{V}_{\mathcal{D}} = \{v_\alpha(r, \theta, z), \alpha = r, \theta, z : v_\alpha(1, \theta, z) = 0, 0 \leq z \leq L, v_\alpha \in C_{\mathcal{D}}^\infty \cap L_{\mathcal{D}}^2\}$ and $\mathcal{N}_{\mathcal{D}}$ defined as the dual of $\mathcal{V}_{\mathcal{D}}$ (the subscript p indicates pipe flow periodic in axial direction). It should be noted that all coordinates and scalar and vector fields are dimensionless, and the vector fields in $\mathcal{V}_{\mathcal{D}}$ and their dual satisfy homogenous Dirichlet boundary conditions. Hence, the same basis can be used in both phase and test vector spaces. Furthermore, all vector fields are real, but it is convenient to apply Fourier transformation in the periodic directions for the straightforward application of the parity conditions.

The scalar product is for complex-valued vector fields $v_\alpha, w_\alpha \in \mathcal{V}_{\mathcal{D}}$ defined by

$$(\mathbf{v}, \mathbf{w}) \equiv \int_{\mathcal{D}} w(r)v_\alpha(r, \theta, z)w_\alpha^*(r, \theta, z)drd\theta dz \quad (25.53)$$

where $w(r) \geq 0$ is a weight function to be determined below, the asterisk indicates complex conjugate and repeated Greek subscripts imply as usual summation.

25.11 Bases in Phase \mathcal{V}_p and the Test Function \mathcal{N}_p Spaces

The elements of the function spaces \mathcal{N}_p and \mathcal{V}_p , the domain of definition \mathcal{D} equipped with a cylindrical coordinate system, are subject to kinematic conditions at the axis $r = 0$ to insure smoothness and uniqueness as for scalar fields in the previous section. These kinematic conditions link the radial variation of the vector components to the azimuthal wavenumber k and can be established with the aid of discrete Fourier transformation of a vector field $v_\alpha(r, \theta, z) \in \mathcal{V}_p$ with respect to the azimuthal and axial coordinates. The normalized, complex-valued, azimuthal Fourier modes (25.16)

$$v_\alpha(r, \theta, z, t) = \sum_{k=-\infty}^{\infty} \hat{v}_\alpha^k(r, z, t)h_k(\theta) \quad (25.54)$$

satisfy orthogonality (25.17) ($\alpha = r, \theta, z$) using the complex version of the trigonometric functions (25.16). The complex-valued coefficients $\hat{v}_\alpha^k(r, z, t)$ are then defined by

$$\hat{v}_\alpha^k(r, z, t) = \int_0^{2\pi} d\theta v_\alpha(r, \theta, z, t) h_k^*(\theta) \quad (25.55)$$

for the azimuthal wavenumbers $k = 0, \pm 1, \pm 2, \dots$. The fact that $v_\alpha(r, \theta, z)$ is real implies that

$$\hat{v}_\alpha^{-k}(r, z, t) = \hat{v}_\alpha^{*,k}(r, z, t) \quad (25.56)$$

must hold. Hence, the expansion (25.54) can be reformulated as

$$v_\alpha(r, \theta, z, t) = \hat{v}_\alpha^0 h_0 + \sum_{k=1}^{\infty} [\hat{v}_\alpha^k(r, z, t) h_k(\theta) + \hat{v}_\alpha^{*,k}(r, z, t) h_{*,k}(\theta)] \quad (25.57)$$

where the axisymmetric mode $v_\alpha^0 = \hat{v}_\alpha^0$ is strictly real. If the complex-valued coefficients \hat{v}_α^k are split into real and imaginary parts

$$\hat{v}_\alpha^k = v_{\alpha,r}^k + i v_{\alpha,i}^k, \quad k \neq 0 \quad (25.58)$$

and $\hat{v}_\alpha^0 = v_{\alpha,r}^0$, the expansion emerges in strictly real form as

$$v_\alpha(r, \theta, z, t) = \frac{1}{\sqrt{2\pi}} v_{\alpha,r}^0(r, z, t) + \sqrt{\frac{2}{\pi}} \sum_{k=1}^{\infty} [v_{\alpha,r}^k(r, z, t) \cos(k\theta) - v_{\alpha,i}^k(r, z, t) \sin(k\theta)] \quad (25.59)$$

The complex-valued coefficients \hat{v}_α^k in (25.54) need to be computed only for $k \geq 0$ since the coefficients for $k < 0$ follow from (25.56). The kinematic (or parity) conditions can now be formulated for the complex-valued vector Fourier amplitudes $\hat{v}_\alpha^k(r, z)$ [6, 7].

25.12 Vector Parity Conditions for Azimuthal Wavenumbers $k \geq 0$

Smooth vector fields $\hat{v}_\alpha^k(r, z, t)$ must satisfy the kinematic condition in physical space

$$\lim_{r \rightarrow 0} \frac{1}{r} \left(\frac{\partial v_\theta}{\partial \theta} + v_r \right) = O(1), \quad \lim_{r \rightarrow 0} \frac{1}{r} \left(\frac{\partial v_r}{\partial \theta} - v_\theta \right) = O(1) \quad (25.60)$$

to guarantee non-singular variation near $r = 0$. The full set of properties of the vector modes $\hat{v}_r^{n,k}(r)$, $\hat{v}_\theta^{n,k}(r)$, $\hat{v}_z^{n,k}(r)$ can be established without difficulty [7]. They are given by

$$\hat{v}_r^{n,k}(0) + ik\hat{v}_\theta^{n,k}(0) = 0 \quad (25.61)$$

which is non-trivial only for $k = 1$, the symmetry conditions

$$\hat{v}_\alpha^{n,k}(r) = \begin{cases} k \text{ even:} & \text{antisymmetric with respect to } r \\ k \text{ odd:} & \text{symmetric with respect to } r \end{cases} \quad (25.62)$$

for $\alpha = r, \theta$ and

$$\hat{v}_z^{n,k}(r) = \begin{cases} k \text{ even:} & \text{symmetric with respect to } r \\ k \text{ odd:} & \text{antisymmetric with respect to } r \end{cases} \quad (25.63)$$

for the axial component. The growth laws

$$O(\hat{v}_r^{n,k}(r)) = O(\hat{v}_\theta^{n,k}(r)) = r^{|k-1|} \quad (25.64)$$

must hold near $r = 0$. The growth rate for the axial vector component $\hat{v}_z^{n,k}(r)$ is the same as for a scalar field

$$O(\hat{v}_z^{n,k}) = r^k \quad (25.65)$$

Violation of the parity conditions leads to singularity or non-uniqueness at the coordinate axis $r = 0$. There is only one (symmetric) mode for each vector component that is non-zero at the coordinate axis $r = 0$: Wavenumber $k = 1$ for the radial and azimuthal components and wavenumber $k = 0$ for the axial component. The conditions (25.62) and (25.63) imply that all modes non-zero at the axis must be symmetric with respect to the radial coordinate. Higher order tensors fields satisfy more intricate parity conditions with components possessing non-zero values at the axis for more than one wavenumber.

25.13 Design Requirements for the Vector Basis Functions

The construction of the complex-valued vector expansion modes must be done in such a way that the requirements

(V1) the zero divergence condition (25.66) for vector modes;

$$\mathbf{v} \in \mathcal{V}_D : \nabla \cdot \mathbf{v}(r, \theta, z) = 0 \Rightarrow \frac{1}{r} \frac{d}{dr}(r\hat{v}_r^k) + \frac{ik}{r}\hat{v}_\theta^k + im\hat{v}_z^k = 0 \quad \forall k, m \quad (25.66)$$

(V2) the homogeneous Dirichlet condition at the boundary $\partial\mathcal{D}$;

$$\hat{v}_\alpha^k(1, z, t) = 0, \quad \alpha = r, \theta, z \quad (25.67)$$

(V3) the parity conditions with respect to the azimuthal wavenumber k stated in Sect. 25.12;

(V4) the axis condition (25.68) for the azimuthal vector mode $k = 1$;

$$\hat{v}_r^k(0, z, t) + ik\hat{v}_\theta^k(0, z, t) = 0 \quad (25.68)$$

are satisfied for general (i.e. non-zero divergence) or solenoidal vector fields in \mathcal{V}_D . The zero divergence condition (V1) is optional and two cases are considered:

(i) general vector basis that allows arbitrary values for the divergence applicable to compressible fluids and

(ii) solenoidal vector basis with zero divergence for incompressible fluids.

25.14 Representation of a Vector Field

A family of vector expansion functions is constructed assuming periodicity in axial direction, while the azimuthal direction is automatically periodic for smooth fields. Leonard and Wray [1] proposed for the stability analysis of pipe flow and the expansion for velocity and vorticity in the complex form

$$v_\alpha(t, \mathbf{x}) = \sum_{n,k} \hat{v}_\alpha^{n,k}(r, z, t) h_k(\theta) = \sum_{k,n,m} \hat{v}_{k,n,m}(t) f_\alpha^{k,n,m}(r, \theta, z) \quad (25.69)$$

($\alpha = r, \theta, z$), where the complex-valued expansion coefficients are denoted by $\hat{v}_{k,n,m}(t)$ with n being the radial mode index, k the azimuthal and m the axial wavenumber. The complex vector expansion functions $f_\alpha^{k,n,m}(r, \theta, z)$ and the real vectors $F_\alpha^n(r, \theta, z)$ are then defined analogous to the scalar modes in Sect. 25.7.2, the latter being the backward Fourier transform with respect to the azimuthal and axial directions

$$f_\alpha^{k,n,m}(r, \theta, z) \equiv h_k(\theta) \chi_\alpha^{k,n,m}(r) h_m(z)$$

$$F_\alpha^n(r, \theta, z) = \mathcal{F}^{-1} \left\{ \sum_{k=-\infty}^{\infty} \sum_{m=-\infty}^{\infty} f_\alpha^{k,n,m}(r, \theta, z) \right\} \quad (25.70)$$

with $h_k(\theta)$ is defined by (25.16) and $h_m(z)$ by (25.30) analogously in Eq. (25.33) and the radial vector modes (called radial shape functions) $\chi_\alpha^{k,n,m}(r)$ to be constructed below.

The number of radial modes is N_r , and the azimuthal and axial wavenumber ranges are $k \in [-\frac{N_\theta}{2}, \frac{N_\theta}{2} - 1]$ and $m \in [-\frac{N_z}{2}, \frac{N_z}{2} - 1]$, respectively, for finite-dimensional projections and $N_\theta = N_z = \infty$ for complete bases in separable Hilbert spaces, hence are the coefficients of the azimuthal terms in (25.69)

$$\hat{v}_\alpha^{n,k}(r, z, t) = \sum_m \hat{v}_{k,n,m}(t) \chi_\alpha^{k,n,m}(r) h_m(z) \quad (25.71)$$

and the representation of an element of \mathcal{V}_D with respect to the vector basis $\hat{\mathcal{B}}_p = \{f_\alpha^{k,n,m}(r, \theta, z)\}$ (25.69) is then

$$v_\alpha(t, \mathbf{x}) = \sum_{k,n,m} \hat{v}_{k,n,m}(t) f_\alpha^{k,n,m}(r, \theta, z) \quad (25.72)$$

The coefficients $\hat{v}^{k,n,m}(t)$ can be regarded as coordinates in the infinite-dimensional space spanned by the vector basis $\hat{\mathcal{B}}_p$. The finite-dimensional projections are defined by

$$v_\alpha^{N_r, N_\theta, N_z}(r, \theta, z, t) \equiv \sum_{n=1}^{N_r} \sum_{k=-\frac{N_\theta}{2}}^{\frac{N_\theta}{2}-1} \sum_{m=-\frac{N_z}{2}}^{\frac{N_z}{2}-1} \hat{v}_{k,n,m}(t) f_\alpha^{k,n,m}(r, \theta, z) \quad (25.73)$$

for $\alpha = r, \theta, z$ without enforcing the reality conditions (25.56), where the weight function is $\omega(r) = 2r$, required for the computation of the complex-valued coefficients.

The design of the radial vector modes in the next section follows closely the scalar case. The expression for the scalar product of two vector fields \mathbf{v}, \mathbf{s} is for ONS base analogous to the scalar field case (25.43) and given by

$$(y, s) = \sum_{k=-\infty}^{\infty} \sum_{n=0}^{\infty} \sum_{m=-\infty}^{\infty} \hat{y}_{k,n,m} \hat{s}_{k,n,m}^*, \quad \omega(r) = 2r \quad (25.74)$$

Note that the summation over the components is implied in the definition of the coefficients $\hat{v}^{k,n,m}(t)$ multiplying the vector modes.

Comments:

The representation (25.73) w.r.t. an ONS basis $\mathcal{B}_p = \{f_\alpha^{k,n,m}(r, \theta, z), k = -\infty, \infty, 1 \leq n < \infty, -\infty < m < \infty\}$ is a finite-dimensional projection of an expansion w.r.t. the 3-d (real-valued) vector modes $F_\alpha^n(r, \theta, z)$

$$v_\alpha(r, \theta, z) \equiv \sum_{n=1}^{\infty} a_n(t) F_\alpha^n(r, \theta, z)$$

with real-valued coefficients $a_n(t)$. The divergence of the velocity field

$$\nabla \cdot \mathbf{v} = \sum_{n=1}^{\infty} a_n(t) \nabla \cdot \mathbf{F}^n$$

is noted for the construction of solenoidal basis vectors in subsequent sections, and it is for cylindrical coordinates in the flow domain \mathcal{D} given by

$$\nabla \cdot \mathbf{F}^n = \frac{1}{r} \frac{\partial}{\partial r} (r F_r^n) + \frac{1}{r} \frac{\partial F_\theta^n}{\partial \theta} + \frac{\partial F_z^n}{\partial z}$$

The particular structure of the flow domain \mathcal{D} and the assumption of periodicity in axial direction can be exploited to represent the real basis vectors $F_\alpha^p(r, \theta, z)$ as 3-d, complex-valued, vector modes $f_\alpha^{k,n,m}$

$$F_\alpha^n(r, \theta, z) = \sum_{m=-\infty}^{\infty} \sum_{k=-\infty}^{\infty} f_\alpha^{k,n,m}(r, \theta, z), \quad \alpha = r, \theta, z$$

with divergence

$$\nabla \cdot \mathbf{f}^{k,n,m} = \frac{1}{r} \frac{\partial}{\partial r} (r f_r^{k,n,m}) + \frac{ik}{r} f_\theta^{k,n,m} + im f_z^{k,n,m}$$

The representation of vector fields emerges then in the form

$$v_\alpha(r, \theta, z) = \sum_{n=1}^{\infty} \sum_{m=-\infty}^{\infty} \sum_{k=-\infty}^{\infty} \hat{v}_{k,n,m}(t) f_\alpha^{k,n,m}(r, \theta, z)$$

where the complex-valued modes are defined by (25.70) for $\alpha = r, \theta, z$ as product of three complex-valued individual modes. The basis vectors are set up in their complex form in the next section.

25.15 Construction of the Vector Modes for Homogeneous Dirichlet Conditions

The building blocks $\chi_\alpha^{n,k}(r)$, $\alpha = r, \theta, z$ in the radial direction of the vector modes, are the transformed Jacobi polynomials $\mathcal{P}_n^{a,b(k)}(r)$ (25.6); as suggested by Leonard and Wray [1] in a slightly different form to accommodate the outer boundary condition for a solenoidal basis, the difference to the scalar modes is the Jacobi parameter $b(k) = |k - 1|$ as a result of the parity requirement (25.64) for the radial and azimuthal vector components, and the axial component varies like a scalar field. The radial and azimuthal factors of the vector modes are constructed with the aid of two shape function sets $q_{k,n}^{a,b(k)}(r)$ and $s_{k,n}^{a,b(k)}(r)$ with suitable values of the Jacobi parameter a and $b(k)$. In both cases, the growth rates near the coordinate axis $r = 0$ and the symmetry properties are determined by the azimuthal wavenumber via the factor $r^{b(k)}$ according to the parity conditions. The complete vector modes emerge as a product of Jacobi and Fourier functions.

The construction is guided by the ONS condition (25.9)

$$2 \int_0^1 dr (1-r^2)^a r^{2b(k)+1} \mathcal{P}_n^{a,b(k)}(r) \mathcal{P}_m^{a,b(k)}(r) = \delta_{mn}$$

Simple rearrangement of the integrand leads to

$$\int_0^1 dr \omega^{a,\gamma}(r) [r^{b(k)} (1-r^2)^\gamma \mathcal{P}_n^{a,b(k)}(r)] [r^{b(k)} (1-r^2)^\gamma \mathcal{P}_m^{a,b(k)}(r)] = \delta_{mn}$$

with weight function $\omega^{a,\gamma}(r) = 2r(1-r^2)^{a-2\gamma}$. This form of the ONS condition allows the construction of the radial and azimuthal shape functions. The generic shape function of the form

$$\chi_n^{b(k),\gamma}(r) \equiv r^{b(k)} (1-r^2)^\gamma \mathcal{P}_n^{a,b(k)}(r) \quad (25.75)$$

satisfies the design conditions (V2) and $b(k) = |k-1|$ satisfies the parity condition (V3) for radial and azimuthal and $b(k) = k$ for the scalar/axial component, and conditions (V1) and (V4) link components to be verified once all vector components have been designed.

25.16 Radial Shape Function

The radial shape functions are considered for compressible and incompressible fluids. For the compressible case, no additional constraint is necessary and the choice $\gamma = 1$, $a = 2\gamma = 2$, $b(k) = |k-1|$ defines

$$q_{k,n}^{a,b(k)}(r) = \chi_n^{|k-1|,1} = r^{|k-1|} (1-r^2) \mathcal{P}_n^{2,|k-1|}(r) \quad (25.76)$$

with weight function

$$\omega(r) \equiv \omega^{2\gamma,\gamma}(r) = 2r \quad (25.77)$$

For the incompressible case an additional constraint emerges. The radial direction is for the present flow domain normal to the boundary and mass balance implies that the normal derivative of the radial modes must also be zero. It is clear then that the choice $\gamma = 2$, $a = 2\gamma = 4$, $b(k) = |k-1|$ defines

$$s_{k,n}^{a,b(k)} = \chi_n^{|k-1|,2} = r^{|k-1|} (1-r^2)^2 \mathcal{P}_n^{4,|k-1|}(r) \quad (25.78)$$

with weight function

$$\omega(r) = \omega^{2\gamma,\gamma}(r) = 2r \quad (25.79)$$

It is easy to check that $ds_{k,n}^{a,b(k)}/dr(1) = 0$ holds.

Azimuthal shape function

The choice $\gamma = 1, a = 2\gamma = 2, b(k) = |k - 1|$ defines the azimuthal shape function

$$q_{k,n}^{a,b(k)} \equiv \chi_n^{|k-1|,1} = r^{|k-1|}(1-r^2)\mathcal{P}_n^{2,|k-1|}(r) \quad (25.80)$$

with the same weight function $\omega(r)$

$$\omega(r) = \omega^{2\gamma,\gamma}(r) = 2r \quad (25.81)$$

as the radial case for compressible fluids.

Axial shape function

The axial component behaves like a scalar; hence, the choice $\gamma = 1, a = 2\gamma = 2, b(k) = k$ defines the axial shape function already defined by (25.37) for the scalar case

$$q_n^k(r) \equiv \chi_n^{k,1} = r^k(1-r^2)\mathcal{P}_n^{2,k}(r)$$

with the same weight function $\omega(r)$

$$\omega(r) = \omega^{2\gamma,\gamma}(r) = 2r \quad (25.82)$$

as the radial and azimuthal cases. By design, the weight function $\omega(r)$ is the same for all three vector components.

Derivatives of the shape functions

The vector operations' divergence and curl require radial derivatives of the radial shape functions. The essential part of the radial derivative is the derivative of the modified Jacobi polynomials (25.6). The first derivative for $k \geq 0$ follows from the derivative relation for the Jacobi polynomials ([3], Chap. 18.9) and equations (25.6), (25.5) for $a \geq 0, b(k) \geq 0$

$$\frac{d\mathcal{P}_n^{a,b(k)}}{dr}(r) = N_n^{a,b(k)} \frac{dP_n^{a,b(k)}}{dx} \frac{dx}{dr}, \quad \frac{dP_n^{a,b(k)}}{dx} = \frac{1}{2}(n+a+b(k)+1)P_{n-1}^{a+1,b(k)+1}(x) \quad (25.83)$$

hence,

$$\frac{d\mathcal{P}_n^{a,b(k)}}{dr}(r) = 2r(n+a+b(k)+1)N_n^{a,b(k)}P_{n-1}^{a+1,b(k)+1}(x(r)) \quad (25.84)$$

or

$$\begin{aligned} \frac{d\mathcal{P}_n^{a,b(k)}}{dr}(r) &= \\ 2r(n+a+b(k)+1) &\left(\frac{(2n+a+b(k)+1)\Gamma(n+1)\Gamma(n+a+b(k)+1)}{\Gamma(n+a+1)\Gamma(n+b(k)+1)} \right)^{\frac{1}{2}} \mathcal{P}_{n-1}^{a+1,b(k)+1}(x(r)) \end{aligned} \quad (25.85)$$

is obtained with the aid of (25.83). The second radial derivative is easily obtained using (25.85)

$$\begin{aligned} \frac{d^2 \mathcal{P}_n^{a,b(k)}}{dr^2}(r) &= N_n^{a,b(k)} \left[\frac{d \mathcal{P}_n^{a,b(k)}}{dx} \frac{d^2 x}{dr^2} + \frac{d^2 \mathcal{P}_n^{a,b(k)}}{dx^2} \left(\frac{dx}{dr} \right)^2 \right] \\ &= 2(n+a+b(k)+1) \left(\frac{(2n+a+b(k)+1)\Gamma(n+1)\Gamma(n+a+b(k)+1)}{\Gamma(n+a+1)\Gamma(n+b(k)+1)} \right)^{\frac{1}{2}} \mathcal{P}_{n-1}^{a+1,b(k)+1}(r) \\ &\quad + 2r(n+a+b(k)+1) \left(\frac{(2n+a+b(k)+1)\Gamma(n+1)\Gamma(n+a+b(k)+1)}{\Gamma(n+a+1)\Gamma(n+b(k)+1)} \right)^{\frac{1}{2}} \frac{d \mathcal{P}_{n-1}^{a+1,b(k)+1}}{dr}(r) \end{aligned} \quad (25.86)$$

It finds application in computing the radial derivative of the curl of the vector potential. The derivatives of the shape functions are now easy to compute.

Derivatives of the radial shape functions

For compressible fluids ($a = 2, b(k) = |k - 1|$) follows from (25.76)

$$\frac{dq_{k,n}^{a,b(k)}}{dr}(r) = \begin{cases} -2r\mathcal{P}_n^{a,b(k)}(r) + (1-r^2)\frac{d\mathcal{P}_n^{a,b(k)}}{dr}(r) & \text{for } b(k) = 0 \\ [b(k)r^{b(k)-1}(1-r^2) - 2r^{b(k)+1}]\mathcal{P}_n^{a,b(k)}(r) + r^{b(k)}(1-r^2)\frac{d\mathcal{P}_n^{a,b(k)}}{dr}(r) & \text{for } b(k) > 0 \end{cases} \quad (25.87)$$

The derivative for compressible fluids is non-zero at the outer boundary $r = 1$, since

$$\frac{dq_{k,n}^{a,b(k)}}{dr}(1) = -2N_n^{a,b(k)} \frac{\Gamma(n+a+1)}{\Gamma(n+1)\Gamma(a)}$$

hold according to (25.6) and (25.7).

For incompressible fluids ($a = 4, b(k) = |k - 1|$), the first derivative follows from the mode definition (25.78)

$$\begin{aligned} \frac{ds_{k,n}^{a,b(k)}}{dr}(r) &= \\ (1-r^2) \begin{cases} -4r\mathcal{P}_n^{a,b(k)}(r) + (1-r^2)\frac{d\mathcal{P}_n^{a,b(k)}}{dr}(r) & \text{for } b(k) = 0 \\ [b(k)r^{b(k)-1}(1-r^2) - 4r^{b(k)+1}]\mathcal{P}_n^{a,b(k)}(r) + r^{b(k)}(1-r^2)\frac{d\mathcal{P}_n^{a,b(k)}}{dr}(r) & \text{for } b(k) > 0 \end{cases} \end{aligned} \quad (25.88)$$

Derivatives of the azimuthal shape functions

The derivative of the azimuthal shape function ($a = 2, b(k) = |k - 1|$) follows from (25.80). The result is the same as for the radial shape function for compressible fluids, hence

$$\frac{dq_{k,n}^{a,b(k)}}{dr}(r) = \begin{cases} -2r\mathcal{P}_n^{a,b(k)}(r) + (1-r^2)\frac{d\mathcal{P}_n^{a,b(k)}}{dr}(r) & \text{for } b(k) = 0 \\ [b(k)r^{b(k)-1}(1-r^2) - 2r^{b(k)+1}]\mathcal{P}_n^{a,b(k)}(r) + r^{b(k)}(1-r^2)\frac{d\mathcal{P}_n^{a,b(k)}}{dr}(r) & \text{for } b(k) > 0 \end{cases} \quad (25.89)$$

Derivatives of the axial shape functions

The derivative of the axial shape function ($a = 2, b(k) = k$) follows from (25.80).

$$\frac{dq_{k,n}^{a,b(k)}}{dr}(r) = \begin{cases} -2r\mathcal{P}_n^{a,b(k)}(r) + (1-r^2)\frac{d\mathcal{P}_n^{a,b(k)}}{dr}(r) & \text{for } b(k) = 0 \\ [b(k)r^{b(k)-1}(1-r^2) - 2r^{b(k)+1}]\mathcal{P}_n^{a,b(k)}(r) + r^{b(k)}(1-r^2)\frac{d\mathcal{P}_n^{a,b(k)}}{dr}(r) & \text{for } b(k) > 0 \end{cases} \quad (25.90)$$

The expressions for higher derivatives become increasingly complicated, but they can be computed without difficulty using the properties of the Jacobi polynomials [3], in particular, recursive derivative relations.

25.17 (i) Construction of a General Vector Basis

The Jacobi parameter $a = 2$ is assumed throughout this section, and it will be dropped from the notation up to the section on solenoidal vector bases, $q_n^{b(k)}(r) \equiv q_{k,n}^{2,b(k)}(r) = r^{|k|}(1-r^2)\mathcal{P}_n^{2,|k|}(r)$ (25.80). The construction of the basis for the general case is straightforward since the condition (V1) (zero divergence) is not included in the design requirements. The complex-valued radial shape vector is then defined using (25.80) as

$$\chi_r^{n,k}(r) = q_n^{2,|k-1|}(r) \quad (25.91)$$

$$\chi_\theta^{n,k}(r) = iq_n^{2,|k-1|}(r) \quad (25.92)$$

$$\chi_z^{n,k}(r) = q_n^{2,k}(r) \quad (25.93)$$

The complete, complex-valued vector basis functions $f_\alpha^{k,n,m}$ are constructed with the aid of the parity conditions and the kinematic condition (25.68)

$$f_\alpha^{k,n,m}(r, \theta, z) = h_k(\theta)\chi_\alpha^{n,k}(r)h_m(z), \quad \alpha = r, \theta, z \quad (25.94)$$

It is easy to check that the parity and kinematic axis conditions (V2) to (V4) are satisfied. Orthonormality follows from (25.53)

$$(\mathbf{f}^{k,n,m}, \mathbf{f}^{n',k',m'}) = (f_r^{k,n,m}, f_r^{n',k',m'}) + (f_\theta^{k,n,m}, f_\theta^{n',k',m'}) + (f_z^{k,n,m}, f_z^{n',k',m'}) \quad (25.95)$$

where the individual terms are orthonormal, for instance,

$$(f_\theta^{k,n,m}, f_\theta^{n',k',m'}) = \int_0^{2\pi} d\theta h_k(\theta)h_{k'}^*(\theta) \int_0^1 dr \omega(r) \chi_\theta^{n,k}(r) \chi_\theta^{*,n',k'}(r) \int_0^{2\pi} dz h_m(z) h_{m'}^*(z)$$

with weight function $\omega(r)$ given by (25.38), hence

$$(f_\theta^{k,n,m}, f_\theta^{n',k',m'}) = \delta_{k,k'} \int_0^1 dr \omega(r) \chi_\theta^{n,k}(r) \chi_\theta^{*,n',k}(r) \delta_{m,m'}$$

according to (25.17) and

$$(f_\theta^{k,n,m}, f_\theta^{n',k',m'}) = 2\delta_{k,k'} \int_0^1 dr r^{2|k-1|+1} \mathcal{P}_n^{0,|k-1|}(r) \mathcal{P}_{n'}^{0,|k-1|}(r) \delta_{m,m'} = \frac{1}{3} \delta_{k,k'} \delta_{n,n'} \delta_{m,m'} \quad (25.96)$$

according to the orthonormality relation (25.9) for the $\mathcal{P}_n^{a,b}(r)$ with $a = 2$ and $b = |k - 1|$. Orthonormality for the first and third terms in (25.95) follows analogously. Hence,

$$(\mathbf{f}^{k,n,m}, \mathbf{f}^{n',k',m'}) = 3\delta_{k,k'} \delta_{n,n'} \delta_{m,m'} \quad (25.97)$$

holds. The factor three can be removed by rescaling the weight function, if desired.

25.18 Divergence of the Basis

The divergence of the basis vectors f_r , f_θ , f_z follows at once from equations (25.66) and (25.88)

$$\nabla \cdot \mathbf{f}^{k,n,m}(r, \theta, z) = \frac{1}{r} \frac{d}{dr} (r f_r^{k,n,m}) + \frac{ik}{r} f_\theta^{k,n,m} + im f_z^{k,n,m}$$

The evaluation of the derivative of $P_n^{a,b}(x)$ (the Jacobi parameters are $a = 2$, $b(k) = |k|$) is according to [3], Chap. 18.9 (iii) the Jacobi polynomial with shifted parameters (25.83)

$$\frac{dP_n^{0,b(k)}}{dx}(x(r)) = \begin{cases} 0 & \text{for } n = 0 \\ \frac{1}{2}(n + b(k) + 1) P_{n-1}^{1,b(k)+1}(x) & \text{for } n > 0 \end{cases} \quad (25.98)$$

where $b(k) \geq 0$ and $x(r)$ is given by (25.5) and using implicit differentiation applied to the shifted Jacobi polynomial $\mathcal{P}_n^{0,b(k)}(r) = N_n^{0,b(k)} P_n^{0,b(k)}(x(r))$ (25.6)

$$\frac{d\mathcal{P}_n^{0,b(k)}}{dr} = 4N_n^{0,b(k)} r \frac{dP_n^{0,b(k)}}{dx} \quad (25.99)$$

hence

$$\nabla \cdot \mathbf{f}^{k,n,m} = h_k(\theta) \left\{ \frac{1}{r} \left[[(1+k)r^k(1-r^2) - 2r^{k+2}] \mathcal{P}_n^{0,k} + r^{k+1}(1-r^2) \frac{d\mathcal{P}_n^{0,k}}{dr} \right. \right. \\ \left. \left. + ik\chi_\theta^{k,n} \right] + im\chi_z^{k,n} \right\} h_m(z) \quad (25.100)$$

for $k \geq 0$, where the derivative follows from (25.99) and (25.98), is obtained.

25.18.1 Numerical Test Functions: Non-zero Divergence

Vector test fields are constructed as the sum of the basic flow plus disturbances for homogeneous Dirichlet boundary conditions. The vector fields are set up in Cartesian coordinates and then transformed to cylindrical coordinates (25.104) to insure satisfaction of the parity conditions summarized in Sect. 25.12. The test field expressions for the Cartesian components are given by

$$\mathcal{F}_\alpha(r, \theta, z) = (1 - r^2) \hat{\mathcal{F}}_\alpha(r, \theta, z) \quad (25.101)$$

where $\alpha = 1, 2, 3$ and the reduced vector $\hat{\mathcal{F}}_\alpha(r, \theta, z)$ is smooth, i.e. bounded and differentiable in \mathcal{D} . Let $\omega_n \in [0, 1]$ be the n th sample of a random number ω chosen with uniform probability in the unit interval, then are the following parameters set up for the design of the test vector field:

$$r_0^n = 0.9\omega_n, \quad \theta_0^n = 2\pi\omega_n, \quad z_0^n = 2\pi\omega_n \\ \sigma_n = 0.05 + 0.45\omega_n, \quad m_0^n = \frac{1}{2}(\alpha + n - 1), \quad A_\alpha^n = 2(\omega_n(\alpha) - \frac{1}{2})$$

The random number ω is sampled anew for each Cartesian vector component α , hence $\omega_n(\alpha)$. The Cartesian vector components are denoted by $\hat{\mathcal{F}}_\alpha^n$ keeping in mind that the Cartesian components are chosen independently by resampling $\omega \in [0, 1]$. They are thus constructed in the form

$$\hat{\mathcal{F}}_\alpha^n(r, \theta, z) = \exp\left\{-\frac{1}{2\sigma_n^2}[(r \cos(\theta) - r_0^n \cos(\theta_0^n))^2 + (r \sin(\theta) - r_0^n \sin(\theta_0^n))^2 + \cos^2(m_0^n(z - z_0^n))]\right\} \quad (25.102)$$

The coordinate transformation is given for convenience

$$x_1(r, \theta) = r \cos(\theta), \quad x_2(r, \theta) = r \sin(\theta), \quad x_3 = z \\ r(x_1, x_2) = \sqrt{x_1^2 + x_2^2}, \quad \theta(x_1, x_2) = \arctan\left(\frac{x_2}{x_1}\right), \quad z = x_3 \quad (25.103)$$

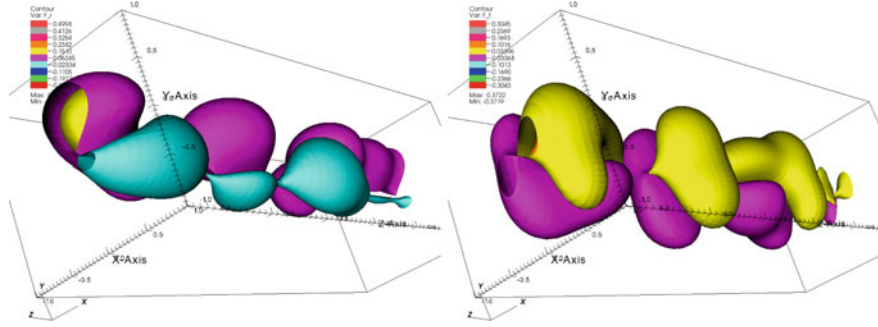


Fig. 25.7 Colour-coded level surfaces of the 3-d radial (left graph) and azimuthal (right graph) numerical test vector components (disturbances). They satisfy the parity conditions (25.25) for all azimuthal wavenumbers k

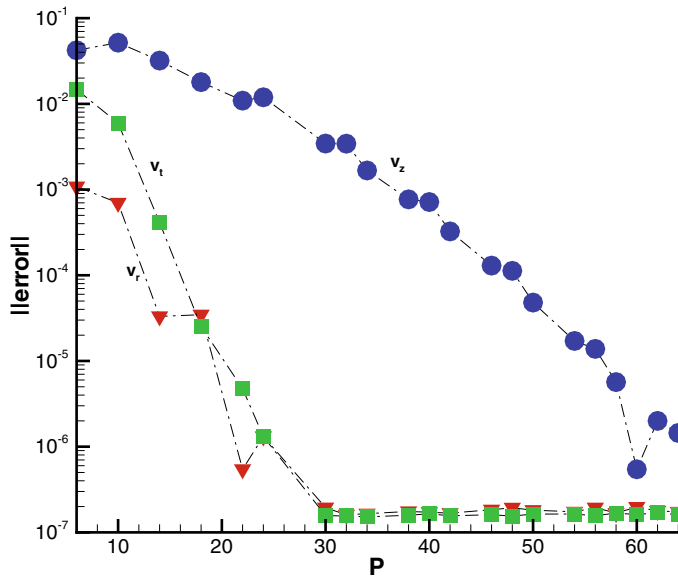


Fig. 25.8 Maximum norm of the difference between the test vector components v_r, v_θ, v_z in cylindrical coordinates (25.105) (shown in Fig. 25.7 as colour-coded level surfaces for the radial and azimuthal components) and the finite-dimensional projections v_r^P, v_θ^P, v_z^P (25.41) of its representation in the vector base $\{f_\alpha^{k,n,m}(r, \theta, z)\}, \alpha = r, \theta, z$ (25.94) as function of $P \equiv \max(N_r, N_\theta, N_z)$ (v_r - red triangles, v_θ - green squares, v_z - blue circles)

together with the vector component transformation

$$\begin{aligned}
 v_r &= v_1 \cos(\theta) + v_2 \sin(\theta), & v_\theta &= -v_1 \sin(\theta) + v_2 \cos(\theta), & v_z &= v_3 \\
 v_1 &= v_r \cos(\theta) - v_\theta \sin(\theta), & v_2 &= v_r \sin(\theta) + v_\theta \cos(\theta), & v_3 &= v_z
 \end{aligned} \tag{25.104}$$

The test vector field is then composed of the basic flow $(1 - r^2)\delta_{\alpha,3}$ plus disturbance contributions

$$\mathcal{F}_\alpha(r, \theta, z) = (1 - r^2) \sum_n A_\alpha^n \hat{\mathcal{F}}_\alpha^n(r, \theta, z) + (1 - r^2)\delta_{\alpha,3} \quad (25.105)$$

where the sum contains a finite number of terms. An example for the vector field consisting of two terms ($n = 1, 2$) is shown in Fig. 25.7 for the radial and azimuthal disturbance components according to (25.104). The properties of the base (25.94) can be illustrated by computing the coefficients (coordinates) of the test vector field (25.105) for the parameters specified above as function of the projection cut off $P = N_r = N_\theta = N_z$. The maximum norms of the errors $|v_\alpha - v_\alpha^{N_r, N_\theta, N_z}|$, $\alpha = r, \theta, z$ in Fig. 25.8 indicate exponential convergence for all components. The slower convergence of the axial component (blue circles) is due to length scales (for instance, randomly chosen σ_n) smaller than for the other components. The properties of the test vector field are illustrated in Fig. 25.7 as three-dimensional level surfaces. The 3-d plots show the isosurfaces of the radial velocity component in the left graph and the azimuthal component in the right graph. The parameter $\sigma_n \in [0.05, 0.5]$ controls the width of the individual Gaussian terms in (25.105); hence, the spatial range of scales can be set as desired for testing.

25.19 (ii) Construction of a Solenoidal Vector Basis

There are several ways to construct a solenoidal basis for a linear vector space. One way is to exploit the fact that the vector elements of the space are periodic w.r.t. one or two spatial directions, which allows the zero divergence condition to determine the third vector component given the other two. Another method is to construct a basis for a vector potential \mathcal{A} first (similar to the previous section), and then compute the curl of \mathcal{A} and modify it to satisfy parity and boundary conditions and orthogonalize it using the (numerically stabilized) Gram–Schmidt procedure (see, for instance, Kreyszig [8], Chap. 3.4, Golub and Van Loan [9]) to obtain a solenoidal ONS. The Gram–Schmidt method orthonormalizes a given basis in a sequence of linear combinations of basis vectors (not vector components), hence preserves the zero divergence property of the given solenoidal basis. Both methods will be developed with the former approach discussed first.

25.20 Solenoidal Vector Basis for Doubly Periodic Flow Fields, First Method

Solenoidal vector bases are constructed for the phase and test function spaces suitable for flows of an incompressible fluid assuming doubly periodic variation in space. The expansion functions $f_\alpha^{k,n,m}(r, \theta, z)$ for compressible flows

$$f_{\alpha}^{k,n,m}(r, \theta, z) \equiv h_k(\theta) \chi_{\alpha}^{k,n,m}(r) h_m(z)$$

Equation (25.70), $\alpha = r, \theta, z$ set up in the previous section are orthonormal, but fail to satisfy the divergence condition (V1). The radial mode $\chi_r^{k,n,m}(r)$ is expected to depend in the solenoidal case also on the axial wavenumber m due to the zero divergence condition (25.66), which links all three vector components for the solenoidal expansion function to be established below. The first radial derivative results in a shift of the radial mode index according to (25.83) and is non-zero at the outer boundary. However, mass balance for incompressible fluids demands that the radial derivative of v_r is also zero at the boundary. This can be achieved in the generic shape function (25.35) by choosing $\gamma = 2$ and thus $a = 2\gamma = 4$ leading to the modification of the Jacobi polynomials (25.6) in the form (Wray [1])

$$s_{k,n}^{a,b(k)}(r) = r^{b(k)}(1 - r^2)^2 \mathcal{P}_n^{a,b(k)}(r) \quad (25.106)$$

with weight function

$$\omega(r) = 2r \quad (25.107)$$

due to (25.36) and orthonormality relation

$$\int_0^1 dr \omega(r) s_{k,n}^{4,b(k)}(r) s_{k,m}^{4,b(k)}(r) = \delta_{m,n} \quad (25.108)$$

It is evident that the choice $a = 4$ for the Jacobi parameter insures that the weight function is the same for the $q_{k,n}^{2,b(k)}(r)$ and the $s_{k,n}^{4,b(k)}(r)$. The expansion functions are thus set up in the form (25.70) for the three cases covering all relevant wavenumber combinations. Both versions $q_{k,n}^{a,b(k)}(r)$ (25.80) with $a = 2$ and $s_{k,n}^{a,b(k)}(r)$ (25.106) with $a = 4$ of modified Jacobi polynomials with the common weight function (25.79) will find application in the construction of the complex-valued radial modes $\chi_{\alpha}^{k,n,m}(r)$ below.

25.20.1 Modes $k = m = 0$

The modes are reduced to

$$f_{\alpha}^{k,n,m}(r, \theta, z) = \frac{1}{2\pi} \delta_{k,0} \chi_{\alpha}^{0,n,0}(r) \delta_{m,0} \quad (25.109)$$

for $k = m = 0$. The divergence condition (V1) determines the radial shape function as it emerges in the form

$$\frac{1}{r} \frac{d}{dr} (r \chi_{\alpha}^{0,n,0}) = 0$$

hence $r\chi_r^{n,0,0}(r) = \text{const.}$ is the general solution. The only non-zero solution would be $\chi_r^{n,0,0} = \text{const.}/r$, thus singular at $r = 0$. Hence,

$$\chi_r^{0,n,0} = 0, \quad k = m = 0$$

is the only radial shape function consistent with the outer boundary condition and insuring smoothness at the coordinate axis $r = 0$. The complex-valued radial shape functions and the associated weight functions (25.79) for the azimuthal and axial components are now determined by the parity and outer boundary conditions. The result is

$$\chi_r^{0,n,0}(r) = 0 \quad (25.110)$$

$$\chi_\theta^{0,n,0}(r) = q_{k,n}^{a,|k-1|}(r) = r(1-r^2)\mathcal{P}_n^{2,1}(r) \quad (25.111)$$

$$\chi_z^{0,n,0}(r) = q_{k,n}^{a,k}(r) = (1-r^2)\mathcal{P}_n^{2,0}(r) \quad (25.112)$$

with $\mathcal{P}_n^{a,b(k)}(r)$ according to (25.6) representing azimuthal and axial motion for $k = m = 0$ independent of θ and z . The design requirements (V1) to (V4) in Sect. 25.12 are clearly satisfied. The mode $\chi_z^{0,0,0} = 1 - r^2$ is proportional to the laminar and steady solution of the Navier–Stokes pdes (Schlichting [10], for instance, derives the constant, which is proportional to the axial pressure gradient) for an incompressible fluid. The radial mode $\chi_r^{k,n,m}$ is for $k = m = 0$ zero (25.112) and, obviously, cannot be orthonormalized; hence, it is not part of the basis and the radial term $\chi_r^{0,n,0}$ drops out of representation of an element of \mathcal{V}_p in (25.73).

25.20.2 Modes $k > 0, m = 0$

For $m = 0, k > 0$ the modes are reduced to

$$f_\alpha^{k,n,m}(r, \theta, z) = \frac{1}{\sqrt{2\pi}} h_k(\theta) \chi_\alpha^{k,n,0}(r) \delta_{m,0} \quad (25.113)$$

where the complex-valued radial shape functions and the weight functions are constructed using $s_n^{a,b(k)}(r)$ and $q_n^{a,b(k)}(r)$

$$\chi_r^{k,n,0}(r) = s_{k,n}^{4,|k-1|}(r) \quad (25.114)$$

$$\chi_\theta^{k,n,0}(r) = \frac{i}{k} \frac{d}{dr} (r s_{k,n}^{4,|k-1|}) \quad (25.115)$$

$$\chi_z^{k,n,0}(r) = q_{k,n}^{2,k}(r) \quad (25.116)$$

with the common weight function (25.79). It is clear that the divergence condition (V1)

$$\frac{1}{r} \frac{d}{dr} (r \hat{v}_r^k) + \frac{ik}{r} \hat{v}_\theta^k = 0 \quad (25.117)$$

is satisfied. The smoothness condition (V4) at the coordinate axis $r = 0$ can be checked easily

$$\hat{v}_r^k(0, z, t) + ik \hat{v}_\theta^k(0, z, t) = s_{k,n}^{4,|k-1|}(r) + ik \frac{i}{k} \frac{d}{dr} (r s_{k,n}^{4,|k-1|})$$

and thus

$$\hat{v}_r^k(0, z, t) + ik \hat{v}_\theta^k(0, z, t) = -r \frac{d}{dr} (s_{k,n}^{4,|k-1|})$$

which is zero at $r = 0$ for all azimuthal wavenumbers k as required. The boundary condition (V2) for the radial and azimuthal components follows from

$$\frac{ds_{k,n}^{4,k}}{dr}(r) = (1 - r^2) \begin{cases} -4r \mathcal{P}_n^{4,0}(r) + (1 - r^2) \frac{d\mathcal{P}_n^{4,0}}{dr}(r) & \text{for } k=0 \\ [|k|r^{|k|-1}(1 - r^2) - 4r^{|k|+1}] \mathcal{P}_n^{4,|k|}(r) + r^{|k|}(1 - r^2) \frac{d\mathcal{P}_n^{4,|k|}}{dr}(r) & \text{for } |k|>0 \end{cases} \quad (25.118)$$

by inspection. The parity conditions (V3) are explicitly built into the shape functions (25.116), hence satisfy $\chi_r^{k,n,0}$ and $\chi_z^{k,n,0}$ (V2) and (V3). The azimuthal component satisfies the parity condition (V3) since it is homogeneous with respect to r , as can be seen from

$$\chi_\theta^{k,n,0}(r) = \frac{i}{k} \frac{d}{dr} (r s_{k,n}^{4,|k-1|}) = \frac{i}{k} s_{k,n}^{4,|k-1|} + \frac{i}{k} r \frac{d}{dr} (s_{k,n}^{4,|k-1|})$$

The first term on the right-hand side satisfies the parity conditions, and the second term has the dependence on r reduced by differentiation, which is then restored by the factor r in the divergence. Thus (V2) and (V3) are satisfied for the azimuthal shape function involving a radial derivative. The outer boundary condition is also satisfied by $\chi_\theta^{k,n,0}$ due to the 2-d divergence (25.117). The radial and axial components satisfy orthonormality, but the azimuthal does not; hence, a method to restore it must be applied for the wavenumber range $k > 0, m = 0$.

25.20.3 Axial Modes $m \neq 0$

For $m \neq 0$ and all $k \geq 0$, the modes are fully three-dimensional (25.70)

$$f_\alpha^{k,n,m}(r, \theta, z) = h_k(\theta) \chi_\alpha^{k,n,m}(r) h_m(z) \quad (25.119)$$

where the complex-valued radial shape functions are

$$\chi_r^{k,n,m}(r) = s_{k,n}^{4,|k-1|}(r) \quad (25.120)$$

$$\chi_\theta^{k,n,m}(r) = iq_{k,n}^{2,|k-1|}(r) \frac{\mathcal{P}_n^{4,|k-1|}(0)}{\mathcal{P}_n^{2,|k-1|}(0)} \quad (25.121)$$

$$\chi_z^{k,n,m}(r) = \frac{i}{m} \left[\frac{d\chi_r^{k,n,m}}{dr} + \frac{1}{r} (\chi_r^{k,n,m} + ik\chi_\theta^{k,n,m}) \right] \quad (25.122)$$

Note that the axial component is then given in terms of $s_{k,n}^{4,|k-1|}$ and $q_{k,n}^{2,|k-1|}$ by

$$\chi_z^{k,n,m}(r) = \frac{i}{m} \left[\frac{ds_{k,n}^{4,|k-1|}}{dr} + \frac{1}{r} (s_{k,n}^{4,|k-1|} - kq_{k,n}^{2,|k-1|}(r) \frac{\mathcal{P}_n^{4,|k-1|}(0)}{\mathcal{P}_n^{2,|k-1|}(0)}) \right] \quad (25.123)$$

The zero divergence condition (V1) Eq. (25.66) is according to the mode structure (25.70)

$$\frac{1}{r} \frac{d}{dr} (r\chi_r^{k,n,m}) + \frac{ik}{r} \chi_\theta^{k,n,m} + im\chi_z^{k,n,m} = 0 \quad (25.124)$$

It is easily verified that

$$\begin{aligned} & \frac{1}{r} \frac{d}{dr} (r\chi_r^{k,n,m}) + \frac{ik}{r} \chi_\theta^{k,n,m} + im\chi_z^{k,n,m} = \\ & \frac{1}{r} \frac{d}{dr} (rs_{k,n}^{4,|k-1|}) - \frac{k}{r} q_{k,n}^{2,|k-1|} \frac{\mathcal{P}_n^{4,|k-1|}(0)}{\mathcal{P}_n^{2,|k-1|}(0)} + im \frac{i}{m} \left[\frac{ds_{k,n}^{4,|k-1|}}{dr} + \frac{1}{r} (s_{k,n}^{4,|k-1|} - kq_{k,n}^{2,|k-1|}(r) \frac{\mathcal{P}_n^{4,|k-1|}(0)}{\mathcal{P}_n^{2,|k-1|}(0)}) \right] = 0 \end{aligned} \quad (25.125)$$

holds for $m > 0$, and the cases $k = m = 0$ and $k > 0, m = 0$ follow likewise; all modes are thus solenoidal. The kinematic condition (V4) Eq. (25.68) for the azimuthal wavenumber $k = 1$ at the coordinate axis $r = 0$

$$\chi_r^{n,1,m}(0) + i\chi_\theta^{n,1,m}(0) = s_{k,n}^{4,0}(0) - q_{k,n}^{2,0}(0) \frac{\mathcal{P}_n^{4,0}(0)}{\mathcal{P}_n^{2,0}(0)} = 0 \quad (25.126)$$

is satisfied since $s_{k,n}^{4,0}(0) = q_{k,n}^{2,0}(0) \frac{\mathcal{P}_n^{4,0}(0)}{\mathcal{P}_n^{2,0}(0)}$ holds according to (25.80) and (25.78). This implies that the axial mode (25.123) remains bounded as $r \rightarrow 0$. The boundary condition (V2) holds for all components. The parity conditions (V3) are explicitly built into the shape functions (25.123), and it is easy to check that they are satisfied. The weight function is given by (25.79) for all cases. The radial shape functions (real or imaginary part as appropriate) for all components are shown in Fig. 25.9 for $k = 0$ and Fig. 25.10 for $k = 5$, and the axial wavenumber is $m = 2$ for both graphs. It is evident from these figures that the radial, wall-normal component satisfies the zero divergence condition at the outer boundary, which implies that the derivative normal to the wall must be zero.

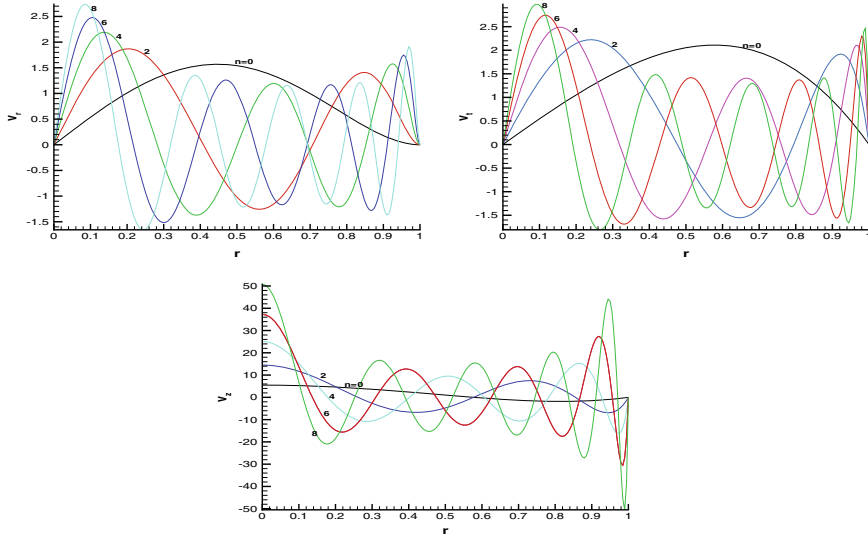


Fig. 25.9 Radial shape functions for the vector components modes $\chi_{\alpha}^{k,n,m}(r)$, $\alpha = r, \theta, z$ in Jacobi-Fourier form (radial modes: real part in upper left, azimuthal modes: imaginary part in upper right, axial modes: imaginary part in lower graph) set up in Sect. 25.19 of Appendix C for the axial wavenumber $m = 2$ and the azimuthal wavenumber $k = 0$. The divergence of all vector modes is zero, but the modes are not orthonormalized. The radial mode indices n are indicated by numbers

25.20.4 Radial Derivative

The derivative appearing in the axial coefficient can be expressed in terms of the radial modes with shifted parameters as shown in Sect. 25.16 equation (25.88)

$$\begin{aligned} \frac{d}{dr} q_{k,n}^{0,|k-1|} &= 2(n + |k - 1| + 1)r^{|k-1|+1}(1 - r^2)\mathcal{P}_{n-1}^{1,|k-1|+1}(r) \\ &+ [|k - 1|r^{|k-1|-1} - (2 + |k - 1|)r^{|k-1|+1}]\mathcal{P}_n^{0,|k-1|}(r) \end{aligned} \quad (25.127)$$

valid for $n > 0$ and

$$\frac{d}{dr} q_{k,0}^{0,|k-1|} = [|k - 1|r^{|k-1|-1} - (2 + |k - 1|)r^{|k-1|+1}]\mathcal{P}_0^{0,|k-1|}(r) \quad (25.128)$$

for $n = 0$. The growth laws near the axis $r = 0$ are also satisfied as can be checked using the Taylor series for $q_{k,n}^{0,k}(r)$

$$q_{k,n}^{0,k}(r) = \frac{1}{k!} \frac{d^k}{dr^k} q_{k,n}^{0,k}(0)r^k + O(r^{k+2})$$

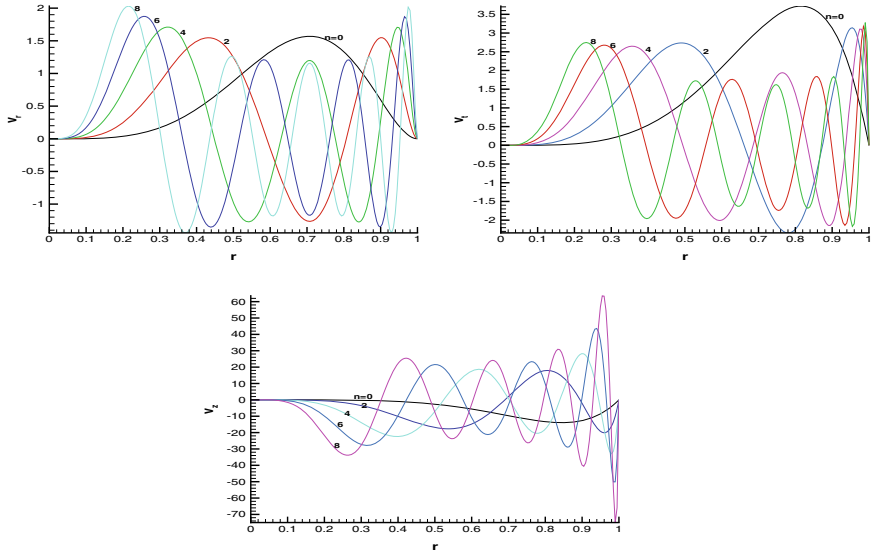


Fig. 25.10 Radial shape functions for the vector components modes $\chi_{\alpha}^{k,n,m}(r)$, $\alpha = r, \theta, z$ in Jacobi–Fourier form (radial modes: real part in upper left, azimuthal modes: imaginary part in upper right, axial modes: imaginary part in lower graph) set up in Sect. 25.19 of Appendix C for the axial wavenumber $m = 2$ and the azimuthal wavenumber $k = 5$. The divergence of all vector modes is zero, but the modes are not orthonormalized. The radial mode indices n are indicated by numbers

This concludes the construction of a solenoidal basis for \mathcal{V}_D . The only step remaining is to check orthogonality, and any modification to insure orthogonality must not destroy the zero divergence property.

25.20.5 Incomplete Orthonormality of the Solenoidal Vector Components

The components of the solenoidal base vectors (25.70) are orthonormalized with respect to the azimuthal and axial directions, but not necessarily in radial direction.

$$(\mathbf{f}^{k,n,m}, \mathbf{f}^{n',k',m'}) = (f_r^{k,n,m}, f_r^{n',k',m'}) + (f_{\theta}^{k,n,m}, f_{\theta}^{n',k',m'}) + (f_z^{k,n,m}, f_z^{n',k',m'}) \quad (25.129)$$

The three components of the basis vectors are now considered in detail.

Orthonormality of the radial component $f_r^{k,n,m}(r, \theta, z)$

The radial component of the vector base is according to the previous section given by

$$f_r^{k,n,m}(r, \theta, z) = \begin{cases} 0 & \text{for } k = m = 0 \\ \frac{1}{\sqrt{2\pi}} h_k(\theta) \delta_{m,0} s_{k,n}^{2,k-1}(r) & \text{for } k > 0, m = 0 \\ h_k(\theta) h_m(z) s_{k,n}^{2,k-1}(r) & \text{for } m \neq 0 \end{cases} \quad (25.130)$$

The contribution to the scalar product (25.129) is, therefore,

$$(f_r^{k,n,m}, f_r^{n',k',m'}) = \delta_{k,k'} \delta_{m,m'} \int_0^1 dr \omega(r) \chi_r^{k,n,m}(r) \chi_r^{*,n',k,m}(r)$$

where the shape functions are defined by (25.112), (25.116), (25.123) and the weight function by (25.38). The radial component drops out of the representation (25.73) for $k = m = 0$; hence, only the cases $m = 0$, $k > 0$ and $m \neq 0$, $k \geq 0$ need to be considered. The radial shape function is for both cases up to a constant proportional to $s_{k,n}^{k-1}(r)$ and

$$\int_0^1 dr \omega(r) \chi_r^{k,n,m}(r) \chi_r^{*,n',k,m}(r) = \delta_{n,n'}$$

follows by inspection of (25.116) and (25.123) excluding $k = m = 0$. Therefore, the radial vector component satisfies orthonormality.

Incomplete orthonormality of the azimuthal component $f_\theta^{k,n,m}(r, \theta, z)$

The azimuthal component of the vector base is according to the previous section given by

$$f_\theta^{k,n,m}(r, \theta, z) = \begin{cases} \frac{1}{2\pi} \delta_{k,0} \delta_{m,0} q_{k,n}^{0,1}(r) & \text{for } k = m = 0 \\ \frac{1}{\sqrt{2\pi}} h_k(\theta) \delta_{m,0} \frac{i}{k} \frac{d}{dr} (r s_{k,n}^{2,k-1}) & \text{for } k > 0, m = 0 \\ h_k(\theta) h_m(z) i q_{k,n}^{0,k-1}(r) \frac{\mathcal{P}_n^{2,k-1}(0)}{\mathcal{P}_n^{0,k-1}(0)} & \text{for } m \neq 0 \end{cases} \quad (25.131)$$

The contribution to the scalar product to be evaluated is then

$$(f_\theta^{k,n,m}, f_\theta^{n',k',m'}) = \delta_{k,k'} \delta_{m,m'} \int_0^1 dr \omega(r) \chi_\theta^{k,n,m}(r) \chi_\theta^{*,n',k,m}(r)$$

where $q_{k,n}^{a,b(k)}(r)$ is given by (25.80) and the weight function $\omega(r)$ by (25.38). The orthonormality relation (25.9) implies

$$(f_\theta^{k,n,m}, f_\theta^{n',k',m'}) = \delta_{k,k'} \delta_{m,m'} \begin{cases} \delta_{n,n'} & \text{for } k = m = 0 \\ \frac{1}{k^2} \int_0^1 dr \omega(r) \frac{d}{dr} (r s_{k,n}^{2,k-1}) \frac{d}{dr} (r s_{k,n'}^{2,k-1}) & \text{for } k > 0, m = 0 \\ \delta_{n,n'} \left[\frac{\mathcal{P}_n^{2,k-1}(0)}{\mathcal{P}_n^{0,k-1}(0)} \right]^2 & \text{for } m \neq 0 \end{cases} \quad (25.132)$$

It is clear that the azimuthal components are not orthogonal with respect to the radial direction.

Incomplete orthonormality of the axial component $f_z^{k,n,m}(r, \theta, z)$

The axial component of the vector base is according to the previous section given by

$$f_z^{k,n,m}(r, \theta, z) = \begin{cases} \frac{1}{2\pi} \delta_{k,0} \delta_{m,0} q_{k,n}^{0,0}(r) & \text{for } k = m = 0 \\ \frac{1}{\sqrt{2\pi}} h_k(\theta) \delta_{m,0} q_{k,n}^{0,k}(r) & \text{for } k > 0, m = 0 \\ h_k(\theta) h_m(z) \frac{i}{m} \left[\frac{ds_{k,n}^{2,k-1}}{dr} + \frac{1}{r} (s_{k,n}^{2,k-1} - k q_{k,n}^{0,k-1}(r) \frac{\mathcal{P}_n^{2,k-1}(0)}{\mathcal{P}_n^{0,k-1}(0)}) \right] & \text{for } m \neq 0 \end{cases} \quad (25.133)$$

The contribution to the scalar product is given by

$$(f_z^{k,n,m}, f_z^{n',k',m'}) = \delta_{k,k'} \delta_{m,m'} \int_0^1 dr \omega(r) \chi_z^{k,n,m}(r) \chi_z^{*,n',k,m}(r)$$

where $q_{k,n}^{a,b(k)}(r)$ is given by (25.80) and the weight function by (25.38). The orthonormality relation (25.9) implies

$$(f_z^{k,n,m}, f_z^{n',k',m'}) = \delta_{k,k'} \delta_{m,m'} \begin{cases} \delta_{n,n'} & \text{for } k=m=0 \\ \delta_{n,n'} & \text{for } k>0, m=0 \\ \frac{1}{m^2} F_z^{n,n',k} & \text{for } m \neq 0 \end{cases} \quad (25.134)$$

where

$$F_z^{n,n',k} \equiv \int_0^1 dr \omega(r) \left[\frac{ds_{k,n}^{2,k-1}}{dr} + \frac{1}{r} (s_{k,n}^{2,k-1} - k q_{k,n}^{0,k-1} \frac{\mathcal{P}_n^{2,k-1}(0)}{\mathcal{P}_n^{0,k-1}(0)}) \right] \left[\frac{ds_{k,n'}^{2,k-1}}{dr} + \frac{1}{r} (s_{k,n'}^{2,k-1} - k q_{k,n'}^{0,k-1} \frac{\mathcal{P}_{n'}^{2,k-1}(0)}{\mathcal{P}_{n'}^{0,k-1}(0)}) \right] \quad (25.135)$$

It is clear that the axial components are not orthogonal with respect to the radial direction. The orthonormalization of the individual vector components is not convenient for the solenoidal basis.

25.20.5.1 Computation of the Expansion Coefficients for Incomplete Orthogonality

The partial orthogonality of the vector modes implies that the coordinates (expansion coefficients) $\hat{v}^{k,n,m}(t)$ for any finite-dimensional projection (25.73) are determined by a system of linear equations. Consider a solenoidal vector field $v_\alpha(r, \theta, z)$ in the finite-dimensional linear vector space spanned by $\{f_\alpha^{k,n,m}(r, \theta, z), 1 \leq n \leq N_r, -\frac{N_\theta}{2} \leq k \leq \frac{N_\theta}{2} - 1, -\frac{N_z}{2} \leq m \leq \frac{N_z}{2} - 1\}$. Multiplication of this vector field with the weight

function (25.79) and the complex conjugate of a mode p, k, m and integration over the flow domain leads to the linear system

$$\sum_{n=1}^{N_r} \mathcal{A}_\alpha^{n,p,k,m} \hat{v}_\alpha^{k,n,m} = \mathcal{R}_\alpha^{p,k,m} \quad (25.136)$$

where

$$\mathcal{A}_\alpha^{n,p,k,m} = \int_0^1 dr \omega(r) \chi_\alpha^{*,p,k,m}(r) \chi_\alpha^{k,n,m}(r) \quad (25.137)$$

and

$$\mathcal{R}_\alpha^{p,k,m} = \int_0^{2\pi} d\theta h_{*,k}(\theta) \int_0^1 dr \omega(r) \chi_\alpha^{*,p,k,m}(r) \int_0^{2\pi} dz h_m^*(z) v_\alpha(r, \theta, z) \quad (25.138)$$

(no sum over α). The evaluation of partial orthogonality in the previous section shows that the radial vector component is in fact orthonormal; hence, $\mathcal{A}_r^{n,p,k,m} = \delta_{n,p}$ holds and the coefficients $\hat{v}_r^{k,n,m}$ can be computed as $N_r \rightarrow \infty$.

The situation is different for the azimuthal and axial components. For the azimuthal component follows from (25.132)

$$\mathcal{A}_\theta^{n,p,k,m} = \begin{cases} \delta_{n,p} & \text{for } k = m = 0 \\ \frac{1}{k^2} \int_0^1 dr \omega(r) \frac{d}{dr} (r s_{k,n}^{2,k-1}) \frac{d}{dr} (r s_{k,p}^{2,k-1}) & \text{for } k > 0, m = 0 \\ \delta_{n,p} \left[\frac{\mathcal{P}_{0,k-1}^{2,k-1}(0)}{\mathcal{P}_n^{0,k-1}(0)} \right]^2 & \text{for } m \neq 0 \end{cases} \quad (25.139)$$

requiring solution of the linear system (25.136). Likewise follows from (25.134) for the axial component

$$\mathcal{A}_z^{n,p,k,m} = \begin{cases} \delta_{n,p} & \text{for } m = 0 \\ \frac{1}{m^2} F_z^{n,p,k} & \text{for } m \neq 0 \end{cases} \quad (25.140)$$

where $F_z^{n,p,k}$ is a complicated integral defined by (25.135).

Limit $N_r \rightarrow \infty$

The question arises whether the finite-dimensional matrices $\mathcal{A}_\alpha^{n,p,k,m}$ define an invertible linear operator as $N_r \rightarrow \infty$, hence allows the computation of the coordinates with respect to the basis $\mathcal{B} = \{f_\alpha^{k,n,m}(r, \theta, z), n = 1, \dots, \infty\}$ for $\alpha = \theta, z$ and all wavenumbers k, m .

Consider the azimuthal component (25.139), where the cases $m = 0, k > 0$ and $m \neq 0$ need to be analyzed. The necessary condition for solvability is that the coefficient matrix $\mathcal{A}(N_r)$ is non-singular as $N_r \rightarrow \infty$. If this condition does not hold, the linear operator determining to coordinates (expansion coefficients) in the Hilbert space \mathcal{N}_s of solenoidal vector fields cannot be inverted for $N_r \rightarrow \infty$.

Consider the case $m \neq 0$: The matrix \mathcal{A} is is its determinant the product of the diagonal entries

$$\det(\mathcal{A}) = \prod_{n=1}^{N_r} \left[\frac{\mathcal{P}_n^{2,k-1}(0)}{\mathcal{P}_n^{0,k-1}(0)} \right]^2$$

which can be evaluated according to (25.6)

$$\det(\mathcal{A}) = \prod_{n=1}^{N_r} \frac{(2n+k+2)(n+k+1)(n+k)}{(2n+k)(n+1)(n+2)}$$

The product exists for the limit $N_r \rightarrow \infty$ iff the series

$$\sum_{n=1}^{\infty} B_n^k < \infty$$

is convergent, where the terms B_n^k are defined by

$$B_n^k = \frac{(2n+k+2)(n+k+1)(n+k)}{(2n+k)(n+1)(n+2)} - 1$$

The example $k = 1$ shows that

$$B_n^1 = \frac{2}{2n+1}$$

and the series is equivalent to the absolute values of the harmonic series, thus divergent. The obvious consequence is that the determinant as infinite product is divergent. The conclusion is reached that the solenoidal basis developed in the present section is applicable to finite-dimensional spaces, but not to the limit of infinite-dimensional Hilbert spaces unless an orthonormalization procedure is applied.

25.21 Solenoidal Vector Basis for Doubly Periodic Flow Fields, Second Method

Solenoidal vector test fields are constructed as the sum of the basic flow plus disturbances for homogeneous Dirichlet boundary conditions. The vector fields with zero divergence are conveniently set up in Cartesian coordinates as the curl of an arbitrary vector field as described in Sect. 25.18.1 and then transformed to cylindrical

coordinates (25.104) to insure satisfaction of the parity conditions summarized in Sect. 25.12.

The test field expressions for the Cartesian components of a vector field with arbitrary divergence are given in Sect. 25.18.1 in the form

$$A_\alpha(r, \theta, z) = (1 - r^2) \hat{A}_\alpha(r, \theta, z)$$

where $\alpha = 1, 2, 3$ is the Cartesian vector index. The solenoidal test field is then constructed as curl, which appears in Cartesian coordinates as

$$\Omega_\alpha = \epsilon_{\alpha\beta\gamma} \frac{\partial A_\gamma}{\partial x_\beta} \quad (25.141)$$

where $\epsilon_{\alpha\beta\gamma}$ denotes the Levi-Civita symbol, and in cylindrical coordinates as

$$\Omega = \begin{pmatrix} \frac{1}{r} \frac{\partial A_z}{\partial \theta} - \frac{\partial A_\theta}{\partial z} \\ \frac{1}{r} \frac{\partial A_r}{\partial z} - \frac{\partial A_z}{\partial r} \\ \frac{1}{r} \frac{\partial}{\partial r} (r A_\theta) - \frac{1}{r} \frac{\partial A_r}{\partial \theta} \end{pmatrix} \quad (25.142)$$

The curl in other coordinate systems can be derived by transformation of the Cartesian case (Panton [11], Appendix C).

Alternatively, the curl of an arbitrary vector field (A_r, A_θ, A_z) , regarded as vector potential, can be computed directly in cylindrical coordinates. For the present case of doubly periodic flows, the curl of the vector field modes \mathbf{A} is then according to (25.142)

$$\Omega_r^{n,k,m} = \frac{ik}{r} A_z - im A_\theta \quad (25.143)$$

$$\Omega_\theta^{n,k,m} = im A_r - \frac{\partial A_z}{\partial r} \quad (25.144)$$

$$\Omega_z^{n,k,m} = \frac{1}{r} \frac{\partial}{\partial r} (r A_\theta) - \frac{ik}{r} A_r \quad (25.145)$$

thus producing a solenoidal test vector field $(\Omega_r, \Omega_\theta, \Omega_z)$. An example for a mode computed as curl of a velocity (left graph) and a vector potential (right graph) mode for $n = 2, k = 3, m = 5$ is shown in Fig. 25.11 at $\theta = z = 0.0$. If the velocity mode $v(r, \theta, z)$ constructed in Sect. 25.17 in Appendix C, equations (25.94) in Appendix C with radial shape functions (25.93) is used as vector potential (left graph), the curl field does not satisfy the boundary condition for all components; in fact, the boundary values are $\text{curl}_r(1) = 0.0$, $\text{curl}_\theta(1) = 70.99296$, $\text{curl}_z(1) = -56.921$ consistent for the curl of a velocity field; note that the $\nabla \times \mathbf{v}$ vector is non-zero at and parallel to the boundary. It is clear that a modified vector potential must be constructed to satisfy the no-slip condition for all components of $\nabla \times \mathbf{A}$. This is done in Eq. (25.146); the resulting curl is shown in the right graph. Thus, the desired solenoidal velocity modes have been set up as curl of a suitable vector potential $\mathbf{A}(r, \theta, z)$.

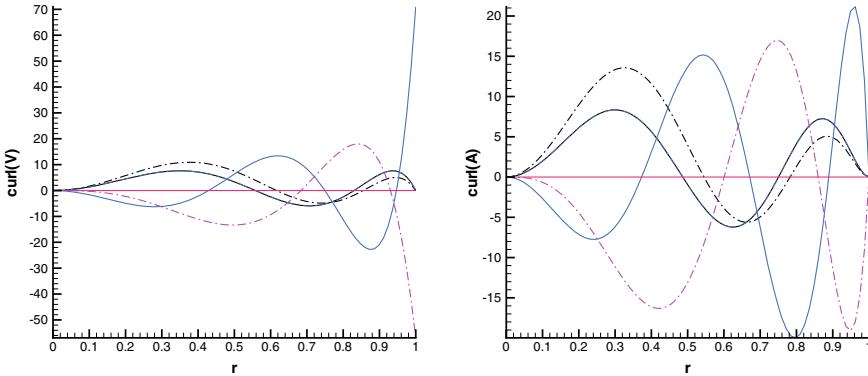


Fig. 25.11 Curl of a complex velocity mode $\mathbf{f}^{k,n,m}$ (25.70) in Jacobi–Fourier form (left graph) compared to the curl of a vector potential mode $\mathbf{A}^{k,n,m}$ (25.148) based on the shape function (25.146) (right graph) for $n = 2$, $k = 3$, $m = 5$ as function of r for $\theta = z = 0.0$. Real parts are the full lines and dash-dotted lines are the imaginary parts; colours signify the components: black—radial, blue—azimuthal and red—axial. The radial component of the curl of the velocity mode in the left graph is zero at the boundary $r = 1$, since the vector mode $\mathbf{f}^{k,n,m}$ is zero at the boundary. The curl Ω of the vector potential mode $\mathbf{A}^{k,n,m}$ in the right graph satisfies the boundary condition for all components

25.21.1 Jacobi–Fourier Space

Periodicity in one or more spatial directions can be exploited by Fourier transformation. The present flow domain has two periodic directions (azimuthal and axial), and thus allows setting up complex-valued basis vector fields as products of radial shape functions (modified Jacobi polynomials) and Fourier kernels. This makes the formulation and enforcement of parity conditions easy, and details are given in Appendix B. The set of complex-valued basis vectors is called Jacobi–Fourier space. The basis vector fields in physical space are then the inverse (2-d in the present case) Fourier transforms of the complex-valued basis fields in Jacobi–Fourier space. Jacobi–Fourier space is assumed a Banach or Hilbert space over the field of complex or real numbers; the particular function space should be clear from the context, and they are discussed in Sect. 5.4.

25.21.2 Modified Vector Potential Set Up in Jacobi–Fourier Form

It is straightforward to construct a vector potential \mathbf{A} that generates a curl field satisfying the homogenous boundary condition for all three components. The general considerations in Sect. 25.8 lead to the generic radial shape function (25.35), which is selected with the parameter values $\gamma = 2$, $a = 2\gamma = 4$, and the second Jacobi

parameter $b(k)$ is used to control the parity conditions. The weight function is then the same as for the velocity field $\omega(r) = 2r$, and the radial shape function for the modified vector potential emerges as

$$s_{A,n}^k(r) = r^{b(k)}(1-r^2)^2 \mathcal{P}_n^{4,b(k)}(r) \quad (25.146)$$

and for $\chi_z^k(r)/r$

$$\chi_z^k(r)/r \equiv r_{A,n}^k(r) = r^{b(k)-1}(1-r^2)^2 \mathcal{P}_n^{4,b(k)}(r) \quad (25.147)$$

and its radial derivative valid for $k > 0$, with weight function $\omega_A(r) = 2r$. The vector potential mode

$$A_\alpha^{k,n,m}(r, \theta, z) = h_k(\theta) \chi_\alpha^{A,n,k}(r) h_m(z), \quad \alpha = r, \theta, z \quad (25.148)$$

is built with shape functions

$$\chi_r^{A,n,k}(r) = s_{A,n}^{|k-1|}(r) \quad (25.149)$$

$$\chi_\theta^{A,n,k}(r) = i s_{A,n}^{|k-1|}(r) \quad (25.150)$$

$$\chi_z^{A,n,k}(r) = s_{A,n}^k(r) \quad (25.151)$$

The complete, complex-valued vector basis functions $A_\alpha^{k,n,m}$ satisfy the parity conditions and the kinematic condition (25.68). The vector potential modes are also orthonormalized as the construction in Sect. 25.15 shows.

Either way, this approach insures zero divergence but does not preserve orthogonality. Hence, an orthonormalization procedure, such as the numerically stabilized Gram–Schmidt method, has to be employed to produce a solenoidal and orthogonal base to be considered later in Sect. 25.22. The representation of a solenoidal velocity field is based on the curl modes (25.143) to (25.145). The result is the expansion

$$v_\alpha(r, \theta, z) = \sum_{k,n,m} \hat{v}_{k,n,m} \mathcal{G}_\alpha^{k,n,m}(r, \theta, z), \quad \alpha = r, \theta, z \quad (25.152)$$

of the velocity field with respect to the basis

$$\mathcal{B}_A = \{\mathcal{G}_\alpha^{k,n,m}(r, \theta, z) = \text{curl}[h_k(\theta) \chi_\alpha^{A,n,k}(r) h_m(z)]\} \quad (25.153)$$

The basis vectors are composed of three factors according to

$$\mathcal{G}_\alpha^{k,n,m} \equiv \text{curl}[h_k(\theta) \chi_\alpha^{A,n,k}(r) h_m(z)] = h_k(\theta) \Omega_\alpha^{n,k,m}(r) h_m(z) \quad (25.154)$$

Substituting (25.143) to (25.145)

$$\mathcal{G}_\alpha^{k,n,m} = h_k(\theta) \chi_\alpha^{G,n,k,m}(r) h_m(z) \quad (25.155)$$

with radial shape functions generated by the curl of the modified vector potential \mathbf{A}

$$\chi_r^{G,n,k,m}(r) = \begin{cases} -im\chi_\theta^{A,n,k} & k = 0 \\ ikr_A^k - im\chi_\theta^{A,n,k} & k > 0 \end{cases} \quad (25.156)$$

$$\chi_\theta^{G,n,k,m}(r) = im\chi_r^{A,n,k} - \frac{d\chi_z^{A,n,k}}{dr} \quad (25.157)$$

$$\chi_z^{G,n,k,m}(r) = \begin{cases} 2\frac{d}{dr}\chi_\theta^{A,n,k} - ik\frac{d}{dr}\chi_r^{A,n,k} & r = 0 \\ \frac{d}{dr}\chi_\theta^{A,n,k} + \frac{1}{r}(\chi_\theta^{A,n,k} - ik\chi_r^{A,n,k}) & r > 0 \end{cases} \quad (25.158)$$

completes the construction of the Schauder basis. The radial and azimuthal components are non-singular at $r = 0$, whereas the axial component is also non-singular due to the parity condition (25.61). This is a preliminary result as the basis vectors $\mathcal{G}_\alpha^{k,n,m}$ are not yet orthonormalized. This is done in the next section.

25.22 Gram–Schmidt Orthonormalization

The solenoidal basis \mathcal{B}_A (25.153) defined as the curl of the modified vector potential (25.143), (25.144), (25.145) is not orthonormal w.r.t. to the scalar product (25.53)

$$(\mathbf{u}, \mathbf{v}) = \int_{\mathcal{D}} d\nu \omega(r) \mathbf{u}(r, \theta, z) \mathbf{v}^*(r, \theta, z)$$

The weight function $\omega(r)$ is given by (25.38) for the flow domain \mathcal{D} defined in (25.1) Chap. 25. The basis vectors are defined by (25.154) $\mathcal{G}_\alpha^{k,n,m}(r, \theta, z) = h_k(\theta) \Omega_\alpha^{n,k,m}(r) h_m(z)$, $\alpha = r, \theta, z$. Orthonormality requires that the scalar product satisfies the ONS condition

$$(\mathcal{G}^{k,n,m}, \mathcal{G}^{n',k',m'}) = (\mathcal{G}_r^{k,n,m}, \mathcal{G}_r^{n',k',m'}) + (\mathcal{G}_\theta^{k,n,m}, \mathcal{G}_\theta^{n',k',m'}) + (\mathcal{G}_z^{k,n,m}, \mathcal{G}_z^{n',k',m'}) = \delta_{k,k'} \delta_{n,n'} \delta_{m,m'}$$

It was shown in the previous section that this is not true and needs to be corrected. Integration with respect to the angular and axial directions leads to

$$(\mathcal{G}^{k,n,m}, \mathcal{G}^{n',k',m'}) = \delta_{k,k'} \delta_{m,m'} \int_0^1 dr \omega(r) \Omega^{k,n,m}(r) \cdot \Omega^{n',k',m'}(r) \quad (25.159)$$

with the common weight function (25.77) $\omega(r) = 2r$. The radial shape functions form a complex-valued vector

$$\Omega^{k,n,m}(r) = [\Omega_r^{k,n,m}(r), \Omega_\theta^{k,n,m}(r), \Omega_z^{k,n,m}(r)]^T \quad (25.160)$$

with components defined in Sect. 25.19 of Appendix C for all relevant azimuthal and axial wavenumbers. This vector field needs to be orthonormalized. The original Gram–Schmidt procedure generating the orthogonal sequence of vectors $\mathbf{u}^{k,n,m}(r)$ is designed as follows:

$$\begin{aligned} \mathbf{u}^0(k, m, r) &= \Omega^{k,0,m}(r) \\ \mathbf{u}^1(k, m, r) &= \Omega^{k,1,m}(r) - \frac{(\mathbf{u}^0(k, m, r), \Omega^{k,1,m})}{\|\mathbf{u}^0(k, m, r)\|^2} \mathbf{u}^0(k, m, r) \\ \mathbf{u}^2(k, m, r) &= \Omega^{k,2,m}(r) - \frac{(\mathbf{u}^0(k, m, r), \Omega^{k,2,m})}{\|\mathbf{u}^0(k, m, r)\|^2} \mathbf{u}^0(k, m, r) - \frac{(\mathbf{u}^1(k, m, r), \Omega^{k,2,m})}{\|\mathbf{u}^1(k, m, r)\|^2} \mathbf{u}^1(k, m, r) \\ &\quad \dots \\ &\quad \dots \\ \mathbf{u}^n(k, m, r) &= \Omega^{k,n,m}(r) - \sum_{j=0}^{n-1} \frac{(\mathbf{u}^j(k, m, r), \Omega^{k,n,m})}{\|\mathbf{u}^j(k, m, r)\|^2} \mathbf{u}^j(k, m, r) \end{aligned}$$

This procedure computes a sequence of orthogonal vectors $\mathbf{u}^n(k, m, r)$ that can be normalized

$$\begin{aligned} \mathbf{e}^{k,n,m}(r, \theta, z) &= h_k(\theta) \chi_\alpha^{e,k,n,m} h_m(z) \\ \chi_\alpha^{e,k,n,m} &\equiv \frac{\mathbf{u}^n(k, m, r)}{\|\mathbf{u}^n(k, m, r)\|} \end{aligned} \quad (25.161)$$

to create the ONS basis

$$\mathcal{B}_e = \{e_\alpha^{e,k,n,m}(r, \theta, z), \alpha = r, \theta, z\} \quad (25.162)$$

The Hilbert spaces \mathcal{N}_p and \mathcal{N}_s containing the test vectors $\mathbf{y}(\mathbf{x})$, $\mathbf{x} \in \mathcal{D}$, serving as arguments for the characteristic functional $\Theta[\mathbf{y}(\cdot); t]$, are spanned by the ONS bases for \mathcal{N}_p

$$\mathcal{B} = \{f_\alpha^{k,n,m}(r, \theta, z) = h_k(\theta) \chi_\alpha^{k,n,m}(r) h_m(z), \alpha = r, \theta, z\}, \nabla \cdot \mathbf{f}^{k,n,m} \neq 0$$

with basis functions defined in Eq. (25.70) allowing non-zero dilatation, and the solenoidal basis

$$\mathcal{B}_e = \{e_\alpha^{k,n,m}(r, \theta, z) = h_k(\theta) \chi_\alpha^{e,k,n,m}(r) h_m(z), \alpha = r, \theta, z\}, \nabla \cdot \mathbf{e}^{k,n,m} = 0$$

with basis functions (25.162) defined above, spanning the subspace $\mathcal{N}_s \subset \mathcal{N}_p$ of the Hilbert vector space \mathcal{N}_p . The radial shape functions $\chi_\alpha^{e,n,k,m}(r)$ for the ONS unit vector functions $e_\alpha^{n,k,m}(r, \theta, z)$ are represented in Jacobi–Fourier form as series in terms of the shape functions $\chi_{alpha}^{A,n,k}(r)$ of the vector potential A_α

$$\chi_\alpha^{e,k,n,m}(r) = \sum_{n'=0}^n C_{n'}^{n,k,m} \chi_\alpha^{A,n',k}(r), \quad \alpha = r, \theta, z \quad (25.163)$$

The coefficient array $C_{n'}^{n,k,m}$ requires the evaluation of various scalar products, which are done using Gauss–Lobatto quadrature in double precision. The computation of this coefficient array $C_{n'}^{n,k,m}$, $0 \leq n' \leq n$ is for this reason quite time-consuming. However, the representation defined above has the advantage that derivatives of the ONS vectors $e_\alpha^{n,k,m}(r, \theta, z)$ can be expressed in terms of derivatives of the vector potential A_α , which in turn are combinations of Fourier and modified Jacobi polynomials allowing analytic evaluation without recourse to numerical approximations such as finite-difference methods.

An example for the radial shape functions making up the solenoidal Gram–Schmidt ONS modes $e_\alpha^{k,n,m}(r, \theta, z) \in \mathcal{B}_e$ according to (25.162) is presented in Figs. 25.12, 25.14, specifically for the radial shape functions $\chi_\alpha^{e,k,n,m}(r)$ for the radial indices $n = 0, 2, 4, 8, 16$ as indicated in the graphs and the azimuthal and axial wavenumbers $k = 6, m = 2$. The solenoidal ONS modes are the result of the stabilized Gram–Schmidt procedure plus normalization applied to the solenoidal, but non-ONS modes (25.148) with shape vectors $\chi_\alpha^{A,n,k}(r)$ computed as the curl of the vector potential $\mathbf{A}(r, \theta, z)$ with radial shape functions (25.151) as outlined in Sect. 25.21.2.

The shape functions (25.161) in \mathcal{B}_e (25.162) are complex valued; Fig. 25.12 shows the real parts in the left and the imaginary parts in the right column with the radial component in the first, the azimuthal in the second and the axial component in the third row. The radial shape functions of the input basis vectors (25.151) for the Gram–Schmidt procedure are shown in Fig. 25.13 for the same azimuthal and axial wavenumbers.

The modes for the preliminary non-ONS basis are constructed as curl of a vector potential \mathcal{A} ; hence, they are linearly independent, solenoidal and satisfy the parity conditions (Sect. 25.12), but they are not orthonormalized. The Gram–Schmidt procedure constructs, for fixed azimuthal wavenumber k , which insures that pole and boundary conditions remain valid, and axial wavenumber m , linear combinations of the input vector modes, hence maintains the zero divergence property. The radial modes for different wavenumbers k and m are not and need not be orthogonal as orthonormality is insured by the Fourier factor of the modes. Several figures, (25.15) to (25.20), illustrate the geometrical properties in Jacobi–Fourier form and physical space of the ONS velocity modes. Figures 25.14 and 25.15 show the radial shape function $\chi_r^{e,k,n,m}(r)$ as function of the radial coordinate r (x-axis in the figure) and the azimuthal wavenumber k (y-axis) for the radial mode indices $n = 0$ and $n = 16$ (the modes are discrete functions of the wavenumber k , but are shown as continuous

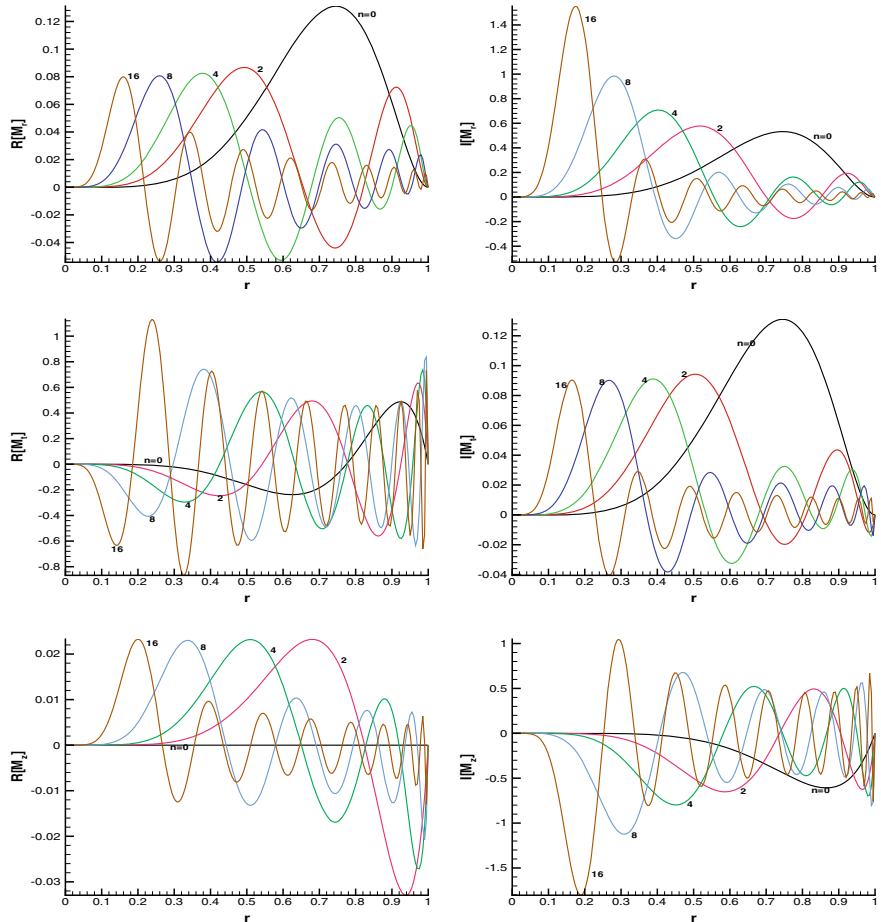


Fig. 25.12 Solenoidal, ONS, radial shape functions $\chi_{\alpha}^{e,k,n,m}(r)$ in Jacobi–Fourier form resulting from the Gram–Schmidt orthonormalization of the curl of the vector potential with radial shape functions $\chi_{\alpha}^{A,n,k}(r)$, $\alpha = r, \theta, z$, Eq. (25.148). The radial mode indices are $n = 0, 2, 4, 8, 16$ as indicated on the lines, the azimuthal wavenumber $k = 6$ and the axial wavenumber $m = 2$ are fixed. The real parts are in the left and the imaginary parts in the right column. The shape functions for the radial component are in the first, the shape functions for the azimuthal component in the second and the third row contains the functions for the axial component

surfaces for the sake of presentation). The variation of the shape function is consistent with the top graphs in Fig. 25.12, and the dependence of the wavenumber k is determined by the parity condition (25.64), which requires $O(\chi_{\alpha}^{e,k,n,m}) = r^{|k-1|}$ near $r = 0$ for the radial and azimuthal components, hence pushes the shape function away from the coordinate axis $r = 0$ with increasing k .

The radial shape functions $\chi_{\alpha}^{e,n,k,m}(r)$ for the ONS unit vector functions $e_{\alpha}^{n,k,m}(r, \theta, z)$ are represented as series w.r.t. n' in terms of the shape functions $\chi_{\alpha}^{A,n',k,m}(r)$ of the

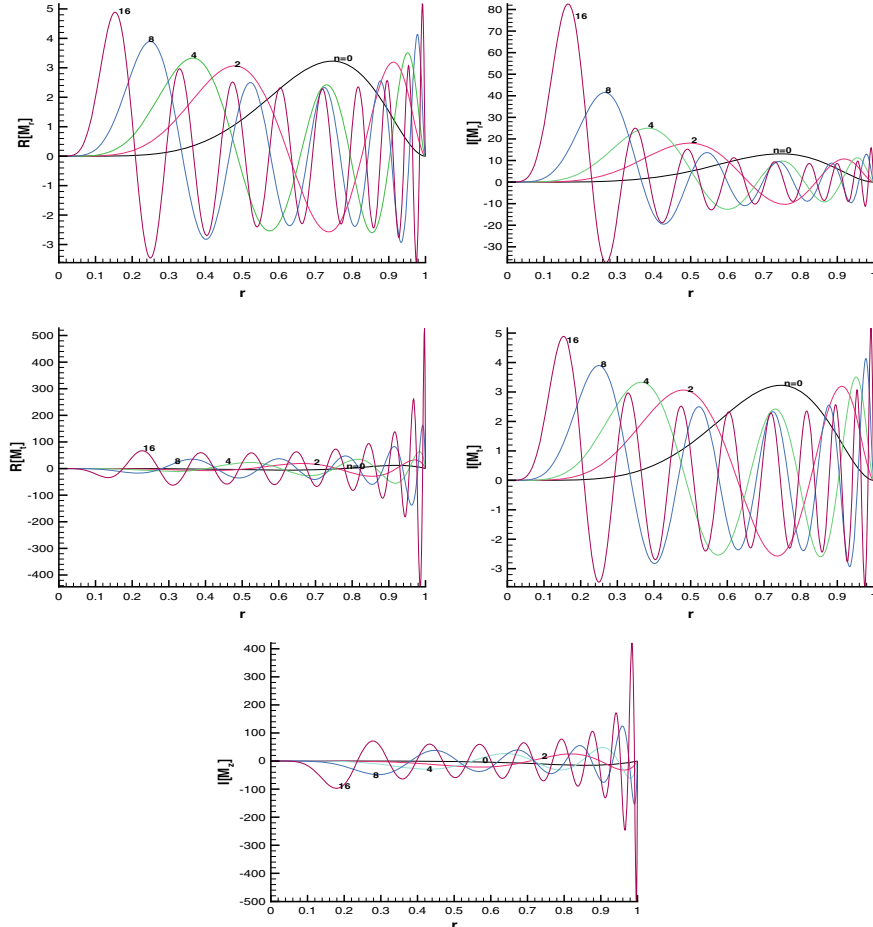


Fig. 25.13 Solenoidal, non-ONS, radial shape functions $\chi_{\alpha}^{G,k,nm}(r)$ (25.158) for the vector component modes constructed as curl of the vector potential \mathbf{A} for comparison with the ONS modes in Fig. 25.12. The radial mode indices are $n = 0, 2, 4, 8, 16$ as indicated on the lines, the azimuthal wavenumber $k = 6$ and the axial wavenumber $m = 2$ are fixed. The real parts are in the left and the imaginary parts in the right column except for the axial component in the third row, which has only the imaginary part non-zero. The shape functions for the radial component are in the first, the shape functions for the azimuthal component in the second and the third row contains the functions for the axial component

curl of the vector potential A_{α} according to (25.163). The representation (25.163) defined above has the advantage that derivatives of the ONS vectors $e_{\alpha}^{n,k,m}(r, \theta, z)$ can be expressed in terms of derivatives of the vector potential A_{α} , which in turn are combinations of Fourier and modified Jacobi polynomials, allowing analytic evaluation without recourse to numerical methods.

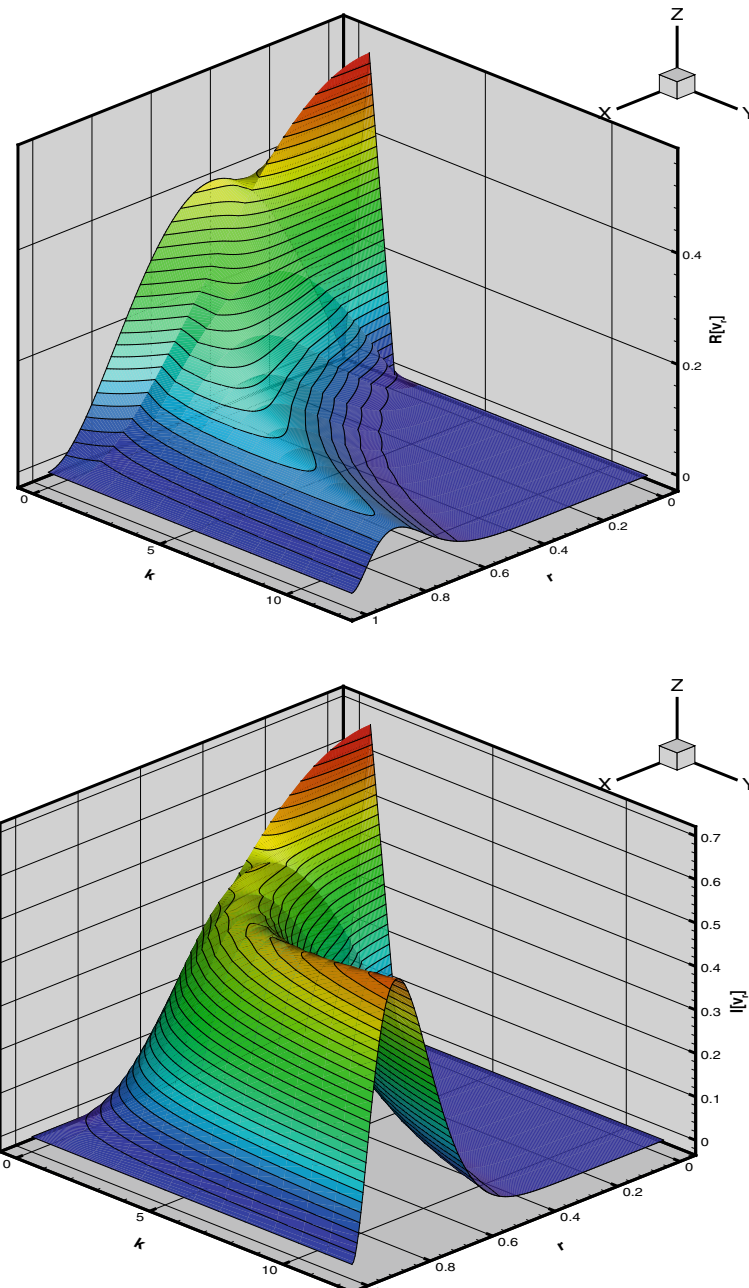


Fig. 25.14 Radial shape functions $\chi_r^{e,k,n,m}(r)$ according to (25.161) for a solenoidal, radial ONS mode $\mathbf{e}^{n,k,m}(r, \theta, z)$ (real part: upper graph, imaginary part: lower graph) for the radial index $n = 0$ after Gram–Schmidt orthonormalization as function of r (x-axis) and the azimuthal wavenumber k (y-axis) at the axial wavenumber $m = 2$

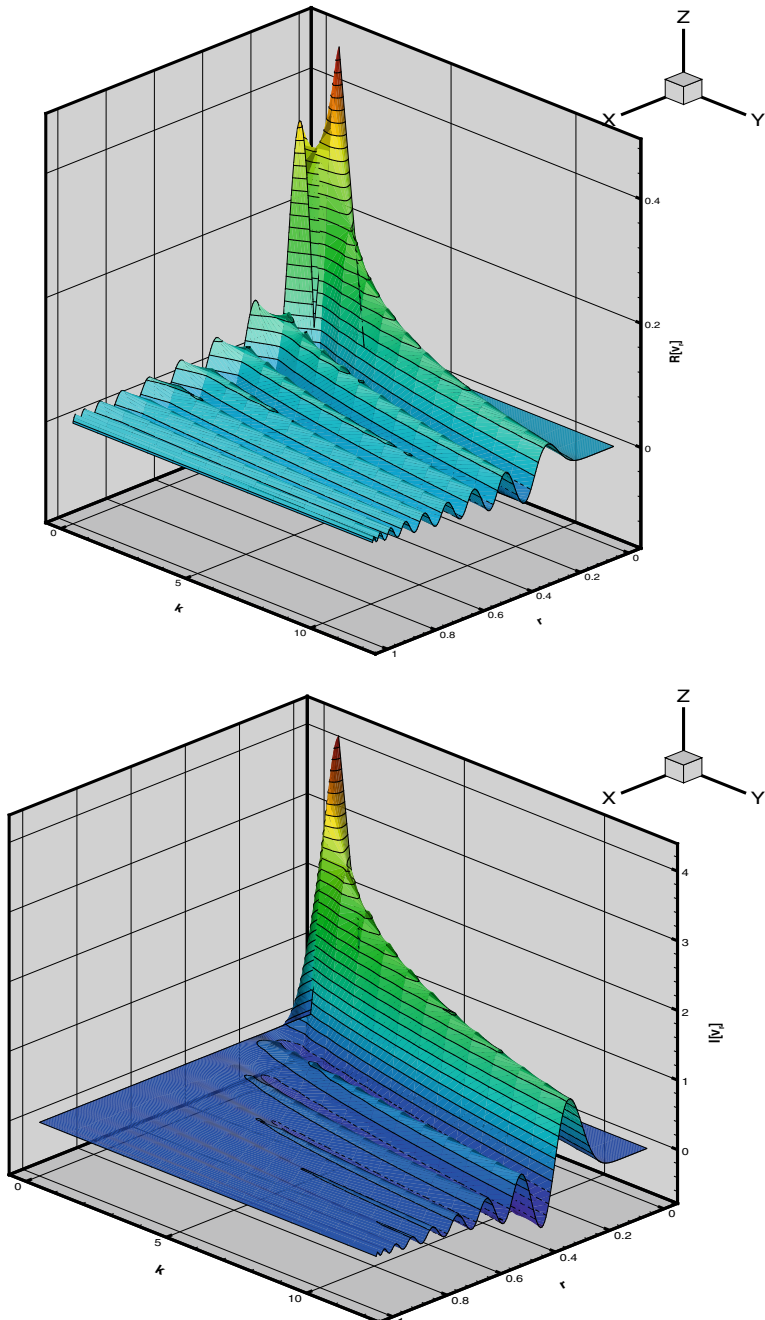


Fig. 25.15 Radial shape functions $\chi_r^{e,k,n,m}(r)$ according to (25.161) for a solenoidal, radial ONS mode $\mathbf{e}^{n,k,m}(r, \theta, z)$ (real part: upper graph, imaginary part: lower graph) for the radial index $n = 16$ after Gram–Schmidt orthonormalization as function of r (x -axis) and the azimuthal wavenumber k (y -axis) at the axial wavenumber $m = 2$. The basis functions are orthogonal and divergence free to machine accuracy

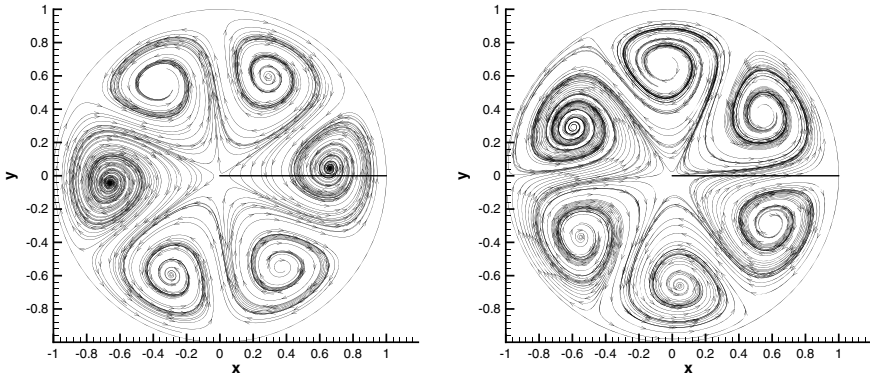


Fig. 25.16 Vector lines of the complex-valued, Gram–Schmidt orthonormalized and solenoidal ONS vector mode $\mathbf{e}^{n,k,m}(r, \theta, z)$ (25.163) (constructed in Jacobi–Fourier form) in the cross section $0 \leq r \leq 1$, $0 \leq \theta \leq 2\pi$ at $z = 0$ for the radial index $n = 0$, the azimuthal wavenumber $k = 3$, axial wavenumber $m = 1$. Shown are the vector lines for real part of the ONS mode $\mathbf{e}^{n,k,m}(r, \theta, z)$ in the left graph and the imaginary part in the right graph

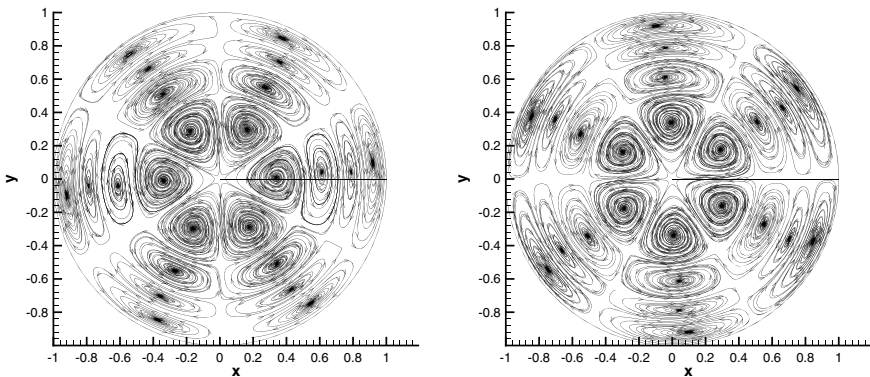


Fig. 25.17 Vector lines of the complex-valued, Gram–Schmidt orthonormalized and solenoidal ONS vector mode $\mathbf{e}^{n,k,m}(r, \theta, z)$ (25.163) (constructed in Jacobi–Fourier form) in the cross section $0 \leq r \leq 1$, $0 \leq \theta \leq 2\pi$ at $z = 0$ for the radial index $n = 3$, the azimuthal wavenumber $k = 3$, axial wavenumber $m = 1$. Shown are the vector lines for real part of the ONS mode $\mathbf{e}^{n,k,m}(r, \theta, z)$ in the left and the imaginary part in the right graph

Streamlines of a complex-valued vector mode $\mathbf{e}^{n,k,m}(r, \theta, z)$ in a cross section $z = \text{constant}$ provide some insight into the flow structure of a particular mode. Two examples of vector lines generated by real and imaginary parts of the complex-valued solenoidal ONS modes in Jacobi–Fourier form are shown in Figs. 25.16 and 25.17. They clearly satisfy homogeneous Dirichlet conditions on $\partial\mathcal{D}$ and the pole conditions, and are orthonormalized. The vector lines generated by the projection into a $z = \text{constant}$ plane of real and imaginary parts of the complex-valued ONS vector modes $\mathbf{e}^{n,k,m}(r, \theta, z)$ in the cross section at $z = 0$ are plotted for the radial mode

indices $n = 0, 3$. The modes exhibit a number of critical points as the motion has cellular structure that increases with the value of the radial mode index n . However, the flow cells are not isolated as the vector lines connecting different cells indicate. The composition of the orthogonalized modes is given according to (25.163) in the table below for the radial index $n = 3$, the azimuthal wavenumber $k = 3$ and the axial wavenumber $m = 1$, with norm $\|\mathbf{e}^{n,k,m}\| = 0.897718350792$ after the Gram–Schmidt procedure

$0 \leq n' \leq n$	$real[C_{n'}(n, k, m)]$	$imag[C_{n'}(n, k, m)]$
0	-0.122308821731	$9.080497084216E - 003$
1	$-8.48949402708E - 002$	$1.551174757215E - 002$
2	0.438463433914	$2.441227024005E - 002$
3	1.0	0.0

The ONS basis modes (25.163) in Jacobi–Fourier form are simply the Gram–Schmidt modes divided by their norm $\|\mathbf{e}^{n,k,m}\|$.

An element $\mathbf{y}(\mathbf{x})$ of the argument space \mathcal{N}_p (the construction of a basis for the phase space Ω is analogous) is represented thus in complex Jacobi–Fourier space by

$$y_\alpha(r, \theta, z) = \sum_{n=0}^{\infty} \sum_{k=0}^{\infty} \sum_{m=0}^{\infty} \hat{y}_{n,k,m} e_\alpha^{n,k,m}(r, \theta, z) \quad (25.164)$$

for $\alpha = r, \theta, z$, $\mathbf{e}^{n,k,m}(r, \theta, z) \in \mathcal{B}_e$ and coefficients $\hat{y}_{n,k,m} = (e_\alpha^{n,k,m}, y_\alpha)$. The representation in physical space is then achieved by the inverse Fourier transform w.r.t. azimuthal and axial wavenumbers k, m

$$y_\alpha(r, \theta, z) = \sum_{n=0}^{\infty} \mathcal{F}^{-1} \left[\sum_{k=0}^{\infty} \sum_{m=0}^{\infty} \hat{y}_{n,k,m} e_\alpha^{n,k,m}(r, \theta, z) \right] \quad (25.165)$$

for $\alpha = r, \theta, z$. The representation (25.165) can be recast as expansion w.r.t. the radial mode index n

$$y_\alpha(r, \theta, z) = \sum_{n=0}^{\infty} Y_n E_\alpha^n(r, \theta, z) \quad (25.166)$$

where E_α^n denotes the compound expansion function in physical space and

$$Y_n = \max_{k,m} |\hat{y}_{n,k,m}| \quad (25.167)$$

are the coefficients of the compound expansion functions in terms of the complex-valued coefficients $\hat{y}_{n,k,m}$ of the complex ONS modes $e_\alpha^{n,k,m}(r, \theta, z)$ constructed to satisfy the zero divergence, boundary and parity conditions. Fourier transform is a linear operation, hence

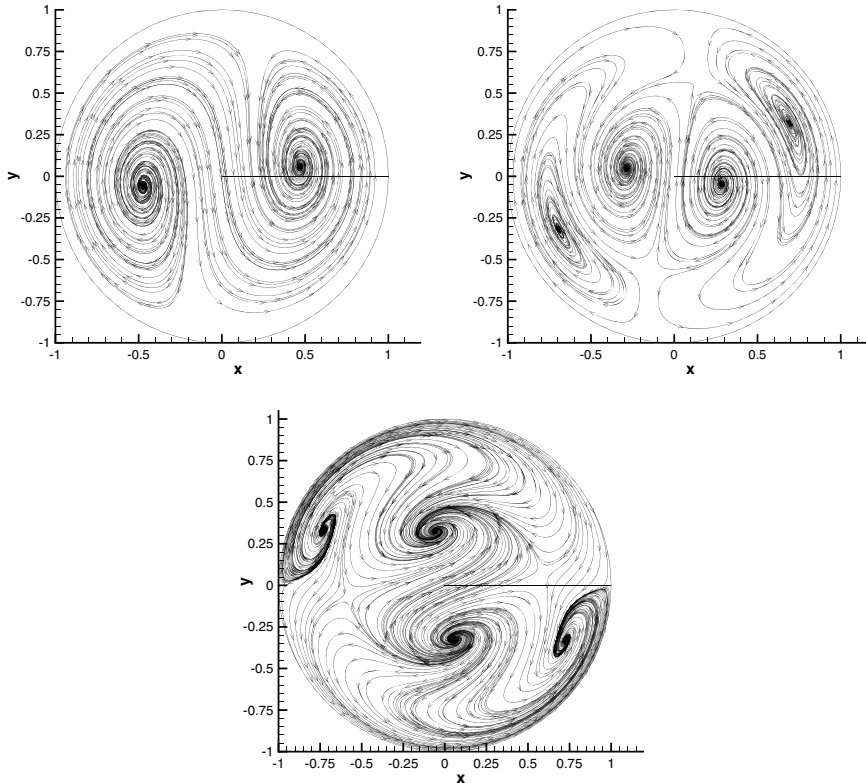


Fig. 25.18 Streamlines of the real-valued, Gram–Schmidt orthonormalized and solenoidal ONS vector mode $\mathbf{e}^{n,k,m}(r, \theta, z)$ (25.163) in Jacobi–Fourier form transformed back to physical space using FFT are depicted in the cross section $0 \leq r \leq 1$, $0 \leq \theta \leq 2\pi$ at $z = 0$ and for the radial index $n = 0$, the azimuthal wavenumber $k = 1$, axial wavenumber $m = 1$ in the upper left graph, for $n = 1, k = 1, m = 1$ in the upper right graph and for $n = 1, k = 1, m = 3$ in the lower graph

$$E_\alpha^n(r, \theta, z) \equiv \mathcal{F}^{-1} \left[\sum_{k=0}^{\infty} \sum_{m=0}^{\infty} \frac{\hat{y}_{n,k,m}}{Y_n} e_\alpha^{n,k,m}(r, \theta, z) \right] \quad (25.168)$$

are the solenoidal, compound, 3-d expansion functions in physical space represented as linear functionals of the complex-valued basis functions $\mathbf{e}^{n,k,m}(r, \theta, z)$. The complex-valued expansion modes $\mathbf{e}^{n,k,m}(r, \theta, z)$ satisfy the parity conditions, and thus the modes for the azimuthal wavenumber $k = 1$ are the only ones non-zero at the coordinate axis $r = 0$, but the compound 3-d expansion functions E_α^n are linear combinations of complex modes and are non-zero at the axis if any coefficients $\hat{y}_{n,1,m}$ are non-zero.

Examples for the transformation of the complex modes in Figs. 25.16 and 25.17 to physical space using FFT are shown in Figs. 25.18, 25.20 for cross sections at $z = 0$ and 25.19 for the plane $\theta = 0$. The streamlines generated by the velocity modes pro-

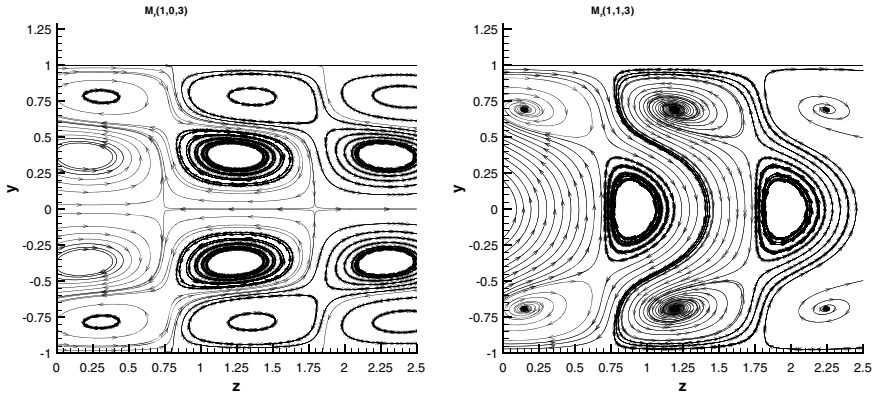
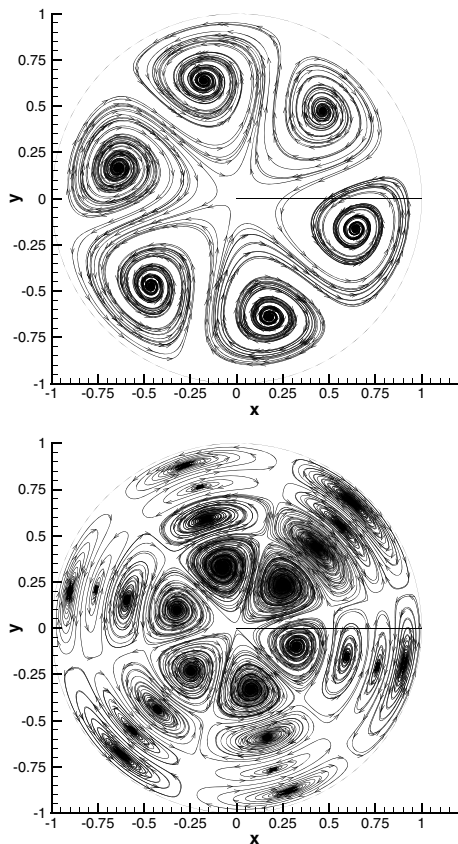


Fig. 25.19 Streamlines of the real-valued, Gram–Schmidt orthonormalized and solenoidal ONS vector mode $\mathbf{e}^{n,k,m}(r, \theta, z)$ (25.163) in Jacobi–Fourier form transformed back to physical space using FFT are depicted in the plane $0 \leq r \leq 1$, $0 \leq z \leq 2.5$ at $\theta = 0$ and for the radial index $n = 1$, the azimuthal wavenumber $k = 0$ (left graph) and $k = 1$ (right graph), the axial wavenumber $m = 3$

Fig. 25.20 Streamlines of the real-valued, Gram–Schmidt orthonormalized and solenoidal ONS vector mode $\mathbf{e}^{n,k,m}(r, \theta, z)$ (25.163) constructed in Jacobi–Fourier form and transformed back to physical space using FFT in the cross section $0 \leq r \leq 1$, $0 \leq \theta \leq 2\pi$ at $z = 0$ for the radial index $n = 0$, the azimuthal wavenumber $k = 3$, axial wavenumber $m = 1$ corresponding to Fig. 25.16. The lower graph shows the vector lines for $n = 3$ in physical space corresponding to Fig. 25.17



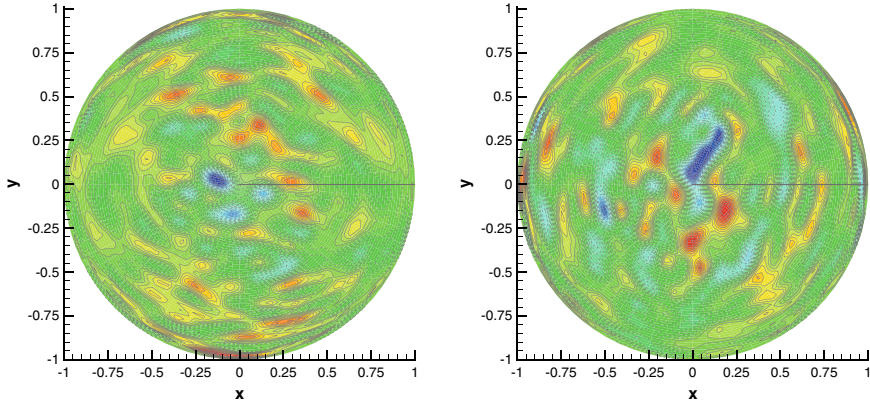


Fig. 25.21 Contour colours/lines of the Cartesian components y_x (left graph) and y_y (right graph) for the test field (25.169) in the cross section $z = 0.087664$ and $N = 16$ modes w.r.t. the solenoidal ONS basis \mathcal{B}_e for the periodic pipe flow example

jected onto the plane $z = \text{constant}$ possess a number of critical points due to motion in z -direction, since the 2-d divergence is not zero. The lines also indicate that the individual structures are connected. The streamlines for the azimuthal wavenumber $k = 1$ are special, since they allow non-zero radial and azimuthal velocities at the coordinate axis $r = 0$, Fig. 25.18 according to the parity conditions (Sect. 25.12). The axial mode component $e_z^{n,k,m}(r, \theta, z)$ is non-zero at the axis $r = 0$ for the azimuthal wavenumber $k = 0$ only, and all higher modes must be zero at the axis. The streamlines in the plane $\theta = 0$ in Fig. 25.19 indicate that for the azimuthal wavenumber $k = 0$ no streamlines cross the axis $r = 0$, whereas motion across the axis occurs for $k = 1$ according to the parity conditions.

The individual vortical structures are clearly connected as the streamlines indicate. The streamlines verify that the vector modes satisfy the boundary conditions, the parity conditions insuring smooth variation of all three components near the origin $r = 0$ and zero divergence, which is satisfied to machine accuracy according to computational checks. The appearance of sinks and sources in Fig. 25.20, which are not possible in solenoidal vector fields, is due to the velocity component normal to the plane of the projected flow.

The properties of the particular basis \mathcal{B}_e (25.162) developed above are illustrated in Fig. 25.21 with an example constructed as random combinations of $N = N_r = N_\theta = N_z$ basis elements,

$$y_\alpha(r, \theta, z) = \sum_{n=0}^{N_r} \sum_{k=0}^{N_\theta} \sum_{m=0}^{N_z} \frac{\hat{A}_{n,k,m}}{n + k + 2m + 1} e_\alpha^{n,k,m}(r, \theta, z) \quad (25.169)$$

where $\alpha = r, \theta, z$, $\mathbf{e}^{n,k,m}(r, \theta, z) \in \mathcal{B}_e$ and the coefficients $\hat{A}_{N_r, N_\theta, N_z}$ are arbitrarily chosen in $[-1, 1]$ with uniform probability.

The plot indicates the power of expansions w.r.t. to a suitable basis and shows that the test field $\mathbf{y}(r, \theta, z)$ satisfies the boundary and parity (smooth variation near $r = 0$) conditions and the constraint $\nabla \cdot \mathbf{y} = 0$. The example field \mathbf{y} does not satisfy the momentum balances, but using the expansion w.r.t. ONS basis fields $\mathbf{e}^{n,k,m}(r, \theta, z)$ would convert the Navier–Stokes pdes into a system of odes, since boundary, parity and zero divergence conditions are satisfied by the basis vectors and, therefore, by any linear combination with coefficients independent of location.

References

1. Leonard, A., Wray, A.: A new numerical method for the simulation of three-dimensional flow in a pipe. Lecture Notes in Physics, vol. 170, (E. Krause, ed.), Springer, p. 335 (1982)
2. Abramowitz, M., Stegun, I.A.: Handbook of Mathematical Functions. Dover, New York (1972)
3. Olver, F.W., Lozier, D.W., Boisvert, R.F., Clark, C.W.: NIST Handbook of Mathematical Functions. Cambridge University Press, U.K. (2010)
4. Dalecky, YuL, Fomin, S.V.: Measures and Differential Equations in Infinite-Dimensional Space. Kluwer Academic Publ, Dordrecht (1991)
5. Rogallo, R.S.: Numerical Experiments in Homogeneous Turbulence (1981). NASA-TM-81315
6. Boyd, J.P.: Chebyshev and Fourier Spectral Methods. Dover Publ. Inc., Mineola, New York (2001)
7. Kollmann, W.: Simulation of vorticity dominated flows using a hybrid approach: I formulation. *Comput. Fluids* **36**, 1638–1647 (2007)
8. Kreyszig, E.: Introductory Functional Analysis with Applications. Wiley, New York (1989)
9. Golub, G.H., Van Loan, C.F.: Matrix Computations. Johns Hopkins Studies in the Mathematical Sciences (1996)
10. Schlichting, H.: Boundary Layer Theory. McGraw-Hill (1987)
11. Panton, R.L.: Incompressible Flow. Wiley, New York, 2nd ed (1996)

Chapter 26

Appendix D: Green's Function for Periodic Pipe Flow



The Navier–Stokes equations governing the flow of a single incompressible fluid contain the pressure gradient as the local effect of the surface force per unit area. It is straightforward to derive the Poisson pde for the pressure and the associated boundary conditions. The Green's function is one of the methods to solve the Poisson pde for the pressure and thus eliminate the pressure from the Navier–Stokes equations. This method is worked out in detail for an important case with simple boundary. The purpose of this section is to construct a representation of the pressure P as sum of three contributions:

- (1) The base pressure $P_0(z)$ independent of the velocity field and varying only in one coordinate direction;
- (2) The (complementary or harmonic) pressure p_h governed by Laplace's pde enforcing non-homogeneous boundary conditions dependent on the viscous stress acting on the boundary;
- (3) The (Green's function) pressure p_G governed by Poisson's pde with solution expressed with the aid of Green's function reflecting the source terms as explained in Sect. 26.5. This is done for a particular compact domain of interest for the investigation of turbulent flows through pipes.

26.1 Domain of Definition

The domain of definition (or flow domain) $\mathcal{D} \subset R^3$ is assumed compact with orientable and nearly everywhere smooth boundary $\partial\mathcal{D}$. For the pipe flow example, it is a straight cylinder with circular cross section defined by

$$\mathcal{D} \equiv \{(r, \theta, z) : 1 \leq r \leq 1, 0 \leq \theta \leq 2\pi, 0 \leq z \leq 2\pi L\} \quad (26.1)$$

where cylindrical coordinates r (radius), θ (azimuthal angle), and z (axial coordinate) are defined with origin at the centre of the left boundary, and the axial extent of

the cylindrical domain $2\pi L \gg 1$ is assumed to be an integer multiple L of 2π . All variables are made dimensionless using the pipe radius \tilde{R} and the volume flow rate \tilde{Q} as reference quantities (tilde indicates dimensional variables). The Reynolds number is then defined slightly different from (2.8) by

$$Re \equiv \frac{\tilde{Q}}{\pi \tilde{R} \tilde{\nu}} \quad (26.2)$$

where $\tilde{\nu}$ denotes the kinematic viscosity, and the dimensionless velocity and pressure emerge for pipe flow in the form

$$v_\alpha = \frac{\tilde{v}_\alpha \pi \tilde{R}^2}{\tilde{Q}}, \quad p = \frac{\tilde{p} \pi^2 \tilde{R}^4}{\tilde{Q}^2} \quad (26.3)$$

where the pressure for incompressible fluids is actually the ratio of pressure and the constant density.

The domain \mathcal{D} is fixed in the spatial description and it is open, i.e. fluid is entering and leaving it. The scalar field total pressure, defined on this domain and denoted by $P(t, \mathbf{x})$, is represented as sum of the basic pressure $P_0(z) = \frac{dP_0}{dz} z$, linear and non-periodic with respect to the axial coordinate z , plus disturbances $p(t, \mathbf{x})$ doubly periodic with respect to θ and z .

$$P(t, \mathbf{x}) = P_0(z) + p(t, \mathbf{x}) \quad (26.4)$$

The disturbance pressure $p(t, \mathbf{x})$ in turn is the sum of two contributions, the solution called complementary or harmonic pressure $p_h(t, r, \theta, z)$ of the (homogeneous) Laplace pde satisfying the non-homogeneous boundary conditions and the Green's function pressure $p_G(t, r, \theta, z)$ as solution of the (non-homogeneous) Poisson pde with homogeneous boundary conditions.

The gradient of the basic pressure dP_0/dz is assumed constant and known for the particular example of pipe flow. The velocity, the gradients of complementary and Green's function pressures are then periodic with respect to the axial direction and Fourier expansions can be applied.

It follows then for the example of pipe flow that the domain \mathcal{D} has only one boundary $\partial\mathcal{D} = \{(r, \theta, z) : r = 1\}$, the outer cylinder surface. The boundary $\partial\mathcal{D}$ is closed since the domain and its boundary are periodic in axial direction; hence, it is topologically equivalent to a torus. The coordinate axis $r = 0$ is not boundary as it consists of inner points. Fourier analysis with respect to θ shows that the complex-valued scalar modes $\tilde{p}(r, k, z)$ are subject to parity conditions dependent on the azimuthal wavenumber k to insure boundedness and smooth variation near the axis [1, 2]. These parity conditions serve as second boundary condition at the coordinate axis $r = 0$ for the radial modes of the solution governed by the linear Sturm-Liouville ode discussed in Sect. 26.4.

26.2 Function Spaces: Scalar Fields

The scalar disturbance field $p(r, \theta, z)$ (time dependence is not indicated in the following) defined on \mathcal{D} periodic with respect to the azimuthal and axial directions are elements of the separable Hilbert space $\Omega_{\mathcal{D}}$

$$\Omega_{\mathcal{D}} = \{p(r, \theta, z) : \mathbf{n} \cdot \nabla p(1, \theta, z) = h(\theta, z), 0 \leq \theta \leq 2\pi, 0 \leq z \leq 2\pi L, \\ p \in C_{\mathcal{D}}^\infty \cap L_{\mathcal{D}}^2, h \in C_{\partial\mathcal{D}}^\infty \cap L_{\partial\mathcal{D}}^2\} \quad (26.5)$$

where \mathbf{n} denotes the unit normal pointing outward, $C_{\mathcal{D}}^\infty$ is the space of infinitely often continuously differentiable scalar fields and $L_{\mathcal{D}}^2$ is the space of square-integrable function defined on $\mathcal{D}/\partial\mathcal{D}$.

The scalar product is defined by

$$(f, g) \equiv \int_{\mathcal{D}} d\nu w(r) f(r, \theta, z) g^*(r, \theta, z) \quad (26.6)$$

where the volume differential is $d\nu = r dr d\theta dz$, the asterisk denotes complex conjugate with weight function $w(r) \geq 0$ that depends on the particular system of basis functions chosen for the representation of scalar fields. The norm is defined by

$$\|f\| = \sqrt{(f, f)} \quad (26.7)$$

A separable Hilbert space possesses countably infinite (equivalent) bases; hence, there is considerable freedom for the construction of a base. Let $\{f^{k,n,m}(r, \theta, z)\}$, $n = 0, \dots, \infty$, $k = 0, \dots, \infty$, $m = 0, \dots, \infty$ be an orthonormal basis in $\Omega_{\mathcal{D}}$ (set up with the aid of orthogonal polynomials, [3, 4]), then is an element $y(r, \theta, z) \in \Omega$ represented by

$$y(r, \theta, z) = \sum_{n,k,m=0}^{\infty} y^{k,n,m} f^{k,n,m}(r, \theta, z) \quad (26.8)$$

with coordinates/expansion coefficients

$$y^{k,n,m} = (y, f^{k,n,m}) \quad (26.9)$$

Scalar and vector bases for the flow through circular, straight pipes are constructed in Appendix C, Chap. 25.

The investigation of turbulent flows is based on the characteristic functionals to be discussed in later sections; they are the limits of cylinder functionals constructed on finite-dimensional subspaces, Sect. 6.3. The relation between the characteristic functional and cylinder functionals is provided by projection operators. The projec-

tion of a functional $\theta[y]$, $y \in \Omega_{\mathcal{D}}$ onto the finite-dimensional subspace spanned by $\{f_{k,n,m} : n = 0, \dots, N_r, k = 0, N_{\theta}, m = 0, N_z\}$ is a cylinder functional defined by

$$\theta_N(y_0^{0,0}, \dots, y_{N_r, N_{\theta}, N_z}) \equiv \theta\left[\sum_{k,n,m=0}^{N_r, N_{\theta}, N_z} y^{k,n,m} f_{k,n,m}\right] \quad (26.10)$$

where θ_N is a standard function of $N_r N_{\theta} N_z$ variables $y^{k,n,m}$, $N \equiv \max(N_r, N_{\theta}, N_z)$ is used for plotting. The parameters N_{θ} and N_z can be adapted to FFT numerical routines.

26.3 Poisson pde for the Disturbance Pressure

The Navier–Stokes pdes for incompressible fluids contain time derivatives in three out of the four equations. Leray (see Majda and Bertozzi [5] Chap. 1.8, they discuss the case $\mathcal{D} = R^3$) devised a method to eliminate the pressure and reduce the Navier–Stokes equations to a system of three evolution equations for the velocity components that maintains the zero divergence property for all time if it was zero initially. These evolution equations are nonlinear integro-differential pdes, since the pressure gradient is expressed as an integral over the flow domain and the boundaries. This approach will be developed in the following for the domain \mathcal{D} being compact, and the resulting pdes are called Leray version of the Navier–Stokes system. Cylindrical coordinates are used suitable for the example of pipe flow.

The starting point for the derivation of the Leray form is the pde for the pressure, which follows from mass and momentum balances as Poisson pde

$$-\Delta P = R(\mathbf{x}) \quad (26.11)$$

with right-hand side defined for cylindrical coordinates by

$$R(r, \theta, z) \equiv \left(\frac{\partial v_r}{\partial r}\right)^2 + \frac{1}{r^2} \left(\frac{\partial v_{\theta}}{\partial \theta} + v_r\right)^2 + \left(\frac{\partial v_z}{\partial z}\right)^2 + \frac{2}{r} \frac{\partial v_{\theta}}{\partial r} \left(\frac{\partial v_r}{\partial \theta} - v_{\theta}\right) + 2 \frac{\partial v_r}{\partial z} \frac{\partial v_z}{\partial r} + \frac{2}{r} \frac{\partial v_z}{\partial \theta} \frac{\partial v_{\theta}}{\partial z} \quad (26.12)$$

The parity conditions for scalar fields imply that all terms in Eq. (26.12) are bounded as $r \rightarrow 0$. The Laplacian for cylindrical coordinates is given by [2]

$$\Delta \equiv \frac{1}{r} \frac{\partial}{\partial r} \left(r \frac{\partial}{\partial r}\right) + \frac{1}{r^2} \frac{\partial^2}{\partial \theta^2} + \frac{\partial^2}{\partial z^2} \quad (26.13)$$

The pde for the pressure disturbance is linear in p , but the right-hand side is quadratically nonlinear with respect to velocity. The aim of the derivation is a representation of the solution $p(r, \theta, z)$ containing the right-hand side $R(r, \theta, z)$ explicitly. This

allows then the reduction of the Navier–Stokes system to a set of three equations called the Leray formulation.

The Poisson pde (26.11) for the pipe flow example contains the disturbance pressure only

$$-\Delta p = R(r, \theta, z) \quad (26.14)$$

since $\Delta P_0 = 0$ holds.

Boundary conditions for the Poisson pde

The boundary conditions for velocity considered in the following are the no-slip conditions $\mathbf{v} = 0$; other conditions can be dealt with analogously. The solution of (26.11) for the disturbance pressure is determined by Neumann conditions at the outer boundary

$$\mathbf{n} \cdot \nabla P = h(\mathbf{x}) \quad (26.15)$$

as consequence of the no-slip condition for velocity, where $\mathbf{x} \in \partial\mathcal{D}$ and \mathbf{n} denotes the outward unit normal vector.

The base pressure P_0 for the pipe flow example is a function of the axial coordinate z only, hence does not enter the momentum balance normal to the boundary. Thus

$$\mathbf{n} \cdot \nabla p = h(r, \theta, z) \quad (26.16)$$

and the boundary condition for the fixed wall $\partial\mathcal{D} = \{(r, \theta, z) : r = 1\}$ can be set up explicitly with the aid of the radial momentum balance leading to

$$h(\mathbf{x}) = \frac{1}{Re} \left[\frac{\partial}{\partial r} \left(\frac{1}{r} \frac{\partial}{\partial r} (r v_r) \right) + \frac{1}{r^2} \frac{\partial^2 v_r}{\partial \theta^2} + \frac{\partial^2 v_r}{\partial z^2} - \frac{2}{r^2} \frac{\partial v_\theta}{\partial \theta} \right] \quad (26.17)$$

where the unit normal is $(n_r, n_\theta, n_z) = (1, 0, 0)$ and $Re > 0$ denotes the Reynolds number. Application of fixed wall boundary conditions $\mathbf{v} = 0$ and mass balance on $\partial\mathcal{D}$ implies that derivatives with respect to directions parallel to the boundary must be zero, hence

$$h(\mathbf{x}) = \frac{1}{Re} \frac{\partial^2 v_r}{\partial r^2} \quad (26.18)$$

is obtained for the gradient component of the disturbance pressure normal to the outer boundary.

26.4 Fourier Transform of the Poisson pde

Velocity \mathbf{v} and the scalar field p are assumed three times continuously differentiable. This implies that vector and scalar field are periodic with respect to the angular coordinate θ . Periodicity with respect to the axial direction is an additional assumption.

tion determining the class of flows to be analysed for the example of flows through straight pipes. Periodicity with respect to θ and z will be assumed in the following, thus allowing the application of 2-d Fast Fourier transform (FFT). Smooth fields periodic with respect to θ and ζ admit the discrete Fourier transform (Canuto et al. [6]) denoted by

$$\varphi(r, \theta, \zeta) = \mathcal{F}_N^{-1}(\theta, \zeta | \hat{\varphi}(r, k, m)), \quad \hat{\varphi}(r, k, m) = \mathcal{F}_N(k, m | \varphi(r, \theta, \zeta)) \quad (26.19)$$

where $\theta_k = 2\pi k/N$ and $\zeta_m = 2\pi m/N$ are the discrete collocation points, for $\theta \neq \theta_k$, $\zeta \neq \zeta_m$ the transform interpolates the values of φ . The explicit forms are given by

$$\mathcal{F}_N(k, m | \varphi(r, \theta, \zeta)) \equiv \frac{1}{N^2} \sum_{k=0}^{N-1} \sum_{m=0}^{N-1} \varphi(r, \theta_k, \zeta_m) \exp(-i(k\theta_k + m\zeta_m)) \quad (26.20)$$

where $k = -N/2, \dots, N/2 - 1$, $m = -N/2, \dots, N/2 - 1$ and

$$\mathcal{F}_N^{-1}(\theta, \zeta | \hat{\varphi}(r, k, m)) \equiv \sum_{k=-N/2}^{N/2-1} \sum_{m=-N/2}^{N/2} \hat{\varphi}(r, k, m) \exp(i(k\theta_k + m\zeta_m)) \quad (26.21)$$

where $k = 0, \dots, N - 1$, $m = 0, \dots, N - 1$. The discrete Fourier transform becomes for $N \rightarrow \infty$ the standard transform denoted by \mathcal{F} and its inverse by \mathcal{F}^{-1} . The numerical application of the discrete Fourier transforms can be done efficiently with widely available FFT software.

The transformation of the Poisson pde (26.14) for the disturbance pressure $p(r, \theta, z)$ is considered first, and then the Neumann boundary values for it (26.18) are transformed. Variables in Fourier space are denoted with a hat.

Transformation of the Poisson pde

It is convenient to rescale the axial coordinate z according to

$$\zeta \equiv \frac{z}{L}, \quad \beta \equiv \frac{|m|}{L} \quad (26.22)$$

where $\zeta \in [0, 2\pi]$ and the Poisson pde (26.11) is then

$$-\left[\frac{1}{r} \frac{\partial}{\partial r} \left(r \frac{\partial}{\partial r} \right) + \frac{1}{r^2} \frac{\partial^2}{\partial \theta^2} + \frac{1}{L^2} \frac{\partial^2}{\partial \zeta^2} \right] p(r, \theta, \zeta) = R(r, \theta, \zeta) \quad (26.23)$$

The disturbance pressure p is then transformed according to (26.20)

$$p(r, \theta, \zeta) = \mathcal{F}_N^{-1}(\theta, \zeta | \hat{p}(r, k, m)) \quad (26.24)$$

with coefficients emerging as integrals (26.21)

$$\hat{p}(r, k, m) = \mathcal{F}_N(k, m | p(r, \theta, \zeta)) \quad (26.25)$$

Fourier transform of the Poisson pde (26.23) with respect to the angular and axial coordinates θ, ζ leads to a system of odes

$$-\frac{1}{r} \left[\frac{d}{dr} \left(r \frac{d\hat{p}_{k,m}}{dr} \right) - \left(\frac{k^2}{r} + \beta^2 r \right) \hat{p}_{k,m} \right] \hat{p}_{k,m} = \hat{R}_{k,m}(r) \quad (26.26)$$

for the azimuthal and axial wavenumbers $0 \leq k < \infty$ and $-\infty < m < \infty$, where \hat{R} denotes the Fourier-transformed right-hand side

$$R(r, \theta, \zeta) = \mathcal{F}_N^{-1}(\theta, \zeta | \hat{R}(r, k, m)) \quad (26.27)$$

with coefficients emerging as integrals

$$\hat{R}(r, k, m) = \mathcal{F}_N(k, m | R(r, \theta, \zeta)) \quad (26.28)$$

according to the inverse Fourier transformation (26.20), (26.21). The boundary conditions for the Sturm–Liouville odes (26.26) depend on the azimuthal wavenumber k , and they are established in Sect. 26.6.

Relation to the Sturm–Liouville ode

The system of odes (26.26) contains the Sturm–Liouville operator \mathcal{L} (Hartmann [7], Chap. XI.4, Duffy [8], Sect. 2.3), which is defined by

$$\mathcal{L} \equiv \frac{1}{w(r)} \left[\frac{d}{dr} p(r) \frac{d}{dr} - q(r) \right] \quad (26.29)$$

where $w(r) > 0$, $p(r) > 0$ in $[0, 1]$, $w(r), p(r), q(r)$ are at least continuous. The Sturm–Liouville ode on the unit interval is then

$$-\mathcal{L}\hat{p}(r, k, m) = f(r) \quad (26.30)$$

The ode (26.26) for the radial coefficients $\hat{p}(r, k, m)$ is now recognized as Sturm–Liouville ode, if the coefficients are identified as

$$w(r) = r > 0, \quad p(r) = r > 0, \quad \text{for } r \in (0, 1), \quad q(r) = \frac{k^2}{r} + r\beta^2 \quad (26.31)$$

The odes are singular since the coefficient $q(r)$ is singular at $r = 0$. Two cases for the right-hand side function are considered in the following: The regular function $f(r)$ given by a smooth velocity field according to (26.12) for the complementary pressure field and the Dirac pseudo-function for the computation of the Green's function. The former case is discussed first, the Green's function pressure p_G is determined in Sect. 26.7.

The right-hand side term for the determination of the Green's function is the Dirac pseudo-function

$$f(r, \rho) = \frac{1}{r} \delta(r - \rho) \quad (26.32)$$

which results in the odes for the Green's functions $G_{k,m}(r)$

$$-\frac{1}{r} \left[\frac{d}{dr} \left(r \frac{d}{dr} \right) - \left(\frac{k^2}{r} + \beta^2 r \right) \right] G_{k,m} = \frac{1}{r} \delta(r - \rho) \quad (26.33)$$

The coefficient $1/r$ of the Dirac function is due to the cylindrical coordinate system. It is convenient for the solution of (26.29) to multiply the ode with $w(r) = r$ and to define a modified Sturm–Liouville operator $\hat{\mathcal{L}}$

$$\hat{\mathcal{L}} \equiv w(r) \mathcal{L} = \frac{d}{dr} p(r) \frac{d}{dr} - q(r), \quad \hat{f}(r, \rho) \equiv w(r) f(r, \rho) \quad (26.34)$$

and

$$-\hat{\mathcal{L}} G_{k,m}(r, \rho) = \delta(r - \rho), \quad -\hat{\mathcal{L}} \hat{p}(r, k, m) = r \hat{f}(r) \quad (26.35)$$

Integration of the ode (26.33) with respect to the radial coordinate yields important regularity properties of the Green's function, obtained in Sect. 26.7.

Transformation of boundary values

The assumption of periodicity with respect to the axial direction has several useful implications. First, the periodicity in axial direction implies that the domain boundary $\partial\mathcal{D}$ is compact, since the flow domain is topologically equivalent to a torus. This opens the door for the application of the Gauss divergence theorem. Second, the disturbance pressure and its radial derivative can be expanded in 2-d Fourier series. Hence,

$$h(\theta, \zeta) = \mathcal{F}_N^{-1}(\theta, \zeta | \hat{h}(k, m)) \quad (26.36)$$

or explicitly

$$h(\theta, \zeta) = \sum_{k=-N/2}^{N/2-1} \sum_{m=-N/2}^{N/2} \hat{h}(k, m) \exp(i(k\theta_k + m\zeta_m)) \quad (26.37)$$

holds, where $\theta, \zeta \in [0, 2\pi]$, in complex form with complex-valued coefficients $\hat{h}_{k,m}$,

$$\hat{h}(k, m) = \mathcal{F}_N(\theta, \zeta | \frac{1}{Re} \frac{\partial^2 v_r}{\partial r^2}(1, \theta, \zeta)) \quad (26.38)$$

or explicitly

$$\hat{h}(k, m) = \frac{1}{4\pi^2 Re} \int_0^{2\pi} d\theta \int_{z=0}^{2\pi L} dz \frac{\partial^2 v_r}{\partial r^2}(1, \theta, \zeta) \exp[-i(k\theta + m\zeta)] \quad (26.39)$$

where $v_r(r, \theta, \zeta)$ is the radial velocity component (26.18). Equation (26.36) is in real form given by

$$h(\theta, \zeta) = \sum_{k=0}^{\infty} \sum_{m=0}^{\infty} \epsilon_k \epsilon_m [a_{k,m} \cos(k\theta) \cos(m\zeta) + b_{k,m} \sin(k\theta) \cos(m\zeta) + c_{k,m} \cos(k\theta) \sin(m\zeta) + d_{k,m} \sin(k\theta) \sin(m\zeta)] \quad (26.40)$$

where the Fourier coefficients are given by

$$\begin{aligned} a_{k,m} &= \frac{1}{\pi^2 Re} \int_{-\pi}^{\pi} d\theta \int_0^{2\pi L} d\zeta \cos(k\theta) \cos(m\zeta) \frac{\partial^2 v_r}{\partial r^2}(1, \theta, \zeta) \\ b_{k,m} &= \frac{1}{\pi^2 Re} \int_{-\pi}^{\pi} d\theta \int_0^{2\pi L} d\zeta \sin(k\theta) \cos(m\zeta) \frac{\partial^2 v_r}{\partial r^2}(1, \theta, \zeta) \\ c_{k,m} &= \frac{1}{\pi^2 Re} \int_{-\pi}^{\pi} d\theta \int_0^{2\pi L} d\zeta \cos(k\theta) \sin(m\zeta) \frac{\partial^2 v_r}{\partial r^2}(1, \theta, \zeta) \\ d_{k,m} &= \frac{1}{\pi^2 Re} \int_{-\pi}^{\pi} d\theta \int_0^{2\pi L} d\zeta \sin(k\theta) \sin(m\zeta) \frac{\partial^2 v_r}{\partial r^2}(1, \theta, \zeta) \end{aligned} \quad (26.41)$$

and the numerical coefficients by

$$\epsilon_k \equiv \begin{cases} 1 & \text{for } k = 0 \\ 2 & \text{for } k > 0 \end{cases}, \quad \epsilon_m \equiv \begin{cases} 1 & \text{for } m = 0 \\ 2 & \text{for } m > 0 \end{cases} \quad (26.42)$$

for convenience. The radial velocity component v_r is assumed known and at least three times continuously differentiable, the Reynolds number Re is a positive constant. The conditions at the outer boundary are of Neumann type, but the conditions on the coordinate axis $r = 0$ require the parity conditions set up in the next section. Once this is done, the complete BVP can be assembled.

26.4.1 Parity Conditions for the Modal Form of Scalar Fields

The cylindrical coordinate system for pipe flows implies periodicity of continuous scalar and vector fields with respect to the angular coordinate θ . Hence, Fourier transform can be applied and scalar fields are then represented as series

$$p(r, \theta, \zeta) = \sum_{k=0}^{\infty} \hat{p}(r, k, \zeta) \exp(ik\theta) \quad (26.43)$$

where $\hat{p}(r, k, \zeta)$ are the azimuthal Fourier or scalar modes. For real fields it follows that $\hat{p}(r, -k, \zeta) = \hat{p}^*(r, k, \zeta)$ holds (the asterisk denotes complex conjugate); hence, only the modes for $k \geq 0$ need to be computed. The scalar modes $\hat{p}(r, k, \zeta)$ are subject to kinematic conditions (called parity or pole conditions, [1, 2]) at the coordinate axis $r = 0$ that depend on the azimuthal wavenumber k . The parity conditions can be summarized for the scalar modes $\hat{p}(r, k, \zeta)$ as follows ([2], Sect. 3.1):

$$\lim_{r \rightarrow 0} \hat{p}(r, k, \zeta) = O(r^k),$$

$$\hat{p}(r, k, \zeta) = \begin{cases} k = 2m, m = 0, 1, \dots & \text{symmetry w.r.t } r \\ k = 2m + 1, m = 0, 1, \dots & \text{antisymmetry w.r.t. } r \end{cases} \quad (26.44)$$

The values of the scalar modes at $r = 0$ are then

$$\frac{\partial \hat{p}}{\partial r}(0, k, \zeta) = 0, \text{ for } k = 0 \quad (26.45)$$

and

$$\hat{p}(0, k, \zeta) = 0, \text{ for } k > 0 \quad (26.46)$$

The mode for the wavenumber $k = 0$ requires an additional condition such as

$$\int_0^1 dr \hat{p}(r, 0, \zeta) = 0 \quad (26.47)$$

to obtain uniqueness. The formulation of the Navier–Stokes pdes in cylindrical coordinates and Fourier transformation with respect to the azimuthal coordinate θ produces a system of pdes for the complex-valued vector and scalar modes that do not contain the zeroth pressure mode $\hat{P}(r, 0, \zeta)$; hence, the additional condition (26.47) is not required for the Navier–Stokes pdes. All scalar modes $k > 0$ must satisfy homogeneous Dirichlet conditions at the coordinate axis $r = 0$ due to parity (26.46), hence insuring uniqueness.

26.5 Representation of the Pressure

The solution of the BVP for the Poisson pde (26.23) with the non-homogeneous boundary values (26.18) can be represented as a linear combination of two linear BVPs:

- (1) The complementary or harmonic solution p_h of the Laplace pde with non-homogeneous boundary conditions;

$$-\Delta p_h = 0, \quad \mathbf{n} \cdot \nabla p_h = h(\mathbf{x}) \quad (26.48)$$

An example will be given relevant to the Poisson pde for the disturbance pressure.

- (2) The solution p_G of the (non-homogeneous) Poisson pde with homogeneous boundary conditions.

$$-\Delta p_G = R(r, \theta, \zeta), \quad \mathbf{n} \cdot \nabla p_G = 0 \quad (26.49)$$

The solution of this BVP can be expressed in terms of a Green's function. This will be shown in the next section.

Linearity of the Laplace pde and the boundary conditions allows the solution to be represented as linear combination of p_h and p_G . The total pressure P is, therefore, given by

$$P(r, \theta, \zeta) = P_0(\zeta) + p_h(r, \theta, \zeta) + p_G(r, \theta, \zeta) \quad (26.50)$$

where $P_0(\zeta)$ is a known linear function of ζ , p_h is the solution of (26.48) and p_G is the solution of (26.49). The harmonic and Green's function pressures are now constructed for the pipe flow example.

26.6 Solution of the BVP for the Complementary Pressure p_h

The solution of the BVP (26.48) for $p_h(r, \theta, \zeta)$ can be accomplished with the aid of Fourier transformation leading to the BVP of a linear second-order ode, which can be solved analytically. The pressure p_h can be represented as Fourier series with respect to the azimuthal and axial coordinates

$$p_h(r, \theta, \zeta) = \mathcal{F}_N^{-1}(\theta, \zeta | \hat{p}_h(r, k, m)) \quad (26.51)$$

where the coefficients $\hat{p}_h(r, k, m)$ are complex valued. Application of the 2-d Fourier transform to the Laplace pde leads to the Sturm–Liouville ode as shown in Sect. 26.4, Eq. (26.26). The homogeneous form of this ode for $\hat{p}(r, k, m)$

$$\frac{1}{r} \frac{d}{dr} \left(r \frac{d\hat{p}}{dr} \right) - \left(\frac{k^2}{r^2} + \beta^2 \right) \hat{p} = 0 \quad (26.52)$$

is closely related to the modified Bessel ode [4]

$$x^2 \frac{d^2 y}{dx^2} + x \frac{dy}{dx} - (x^2 + k^2) y = 0 \quad (26.53)$$

for $y(x)$, $x \in [0, \infty)$. It has a regular singularity at $x = 0$ and an irregular singularity at $x = \infty$.

The boundary conditions at the coordinate axis are determined by the requirement that the solution is bounded at $r = 0$, which can be made explicit for the Fourier amplitudes as parity condition (26.45), (26.46)

$$\begin{aligned} \frac{\partial}{\partial r} \hat{p}_h(0, k, m) &= 0, \quad \text{for } k = 0 \\ \hat{p}_h(0, k, m) &= 0, \quad \text{for } k \neq 0 \end{aligned} \quad (26.54)$$

The conditions at the outer boundary are non-homogeneous Neumann conditions (26.37).

$$\frac{\partial}{\partial r} \hat{p}_h(1, k, m) = \hat{h}(k, m), \quad \text{for all } k \quad (26.55)$$

It is evident that the complex Fourier modes for $k = 0$ are the solution of a pure, non-homogeneous Neumann boundary value problem, whereas for $k \neq 0$ mixed, non-homogeneous Dirichlet–Neumann problem must be solved.

Computation of the complementary pressure p_h

The solution for the complementary (or harmonic) part of the pressure is constructed in several steps and an example relevant to the pipe flow is discussed later in Sect. 26.6. The axial wavenumbers $m = 0$ and $m \neq 0$ are considered separately, since the resulting odes have different properties.

Axial wavenumber $m = 0$ and non-homogeneous boundary values

Setting the axial wavenumber m to zero, $\hat{p}_h = \hat{p}_h(r, k, 0)$, produces the homogeneous Sturm–Liouville ode

$$\frac{1}{r} \left[\frac{d}{dr} \left(r \frac{d \hat{p}_h}{dr} \right) - \frac{k^2}{r} \hat{p}_h \right] = 0 \quad (26.56)$$

with pure Neumann boundary conditions for $k = 0$

$$\frac{\partial \hat{p}_h}{\partial r}(0, 0, 0) = 0, \quad \frac{\partial \hat{p}_h}{\partial r}(1, 0, 0) = \hat{h}(0, 0) \quad (26.57)$$

and mixed Dirichlet–Neumann conditions

$$\hat{p}_h(0, k, 0) = 0, \quad \frac{\partial \hat{p}_h}{\partial r}(1, k, 0) = \hat{h}(k, 0) \quad (26.58)$$

for $k > 0$. The ode is homogeneous, hence has the general solution $\hat{p}_h(r, k, 0) = Ar^\alpha$ with characteristic equation $\alpha(\alpha - 1) + \alpha = k^2$, hence $\alpha = \pm k$. The solution must

be bounded for $r = 0$, hence $\hat{p}_h(r, k, 0) = Ar^k$. The constant A follows from the second boundary condition at $r = 1$ and the desired result is thus

$$\hat{p}_h(r, k, 0) = \frac{\hat{h}(k, 0)}{k} r^k \quad (26.59)$$

valid for $k > 0$. For $k = 0$, no solution exists that satisfies both boundary conditions and the mode $\hat{p}_h(r, 0, 0)$ must be excluded. It should be noted that $k = m = 0$ corresponds to harmonic pressure modes independent of the azimuthal and axial coordinates, hence are part of $P_0(\zeta)$ (Fig. 26.2).

Axial wavenumbers $m \neq 0$ and non-homogeneous boundary values

This example is a modification of the previous one, and the coefficients of the SL operator (26.29) are the same as before, except $|m| > 0$ is assumed. The SL ode is now given by

$$\frac{1}{r} \frac{d}{dr} \left(r \frac{d\hat{p}_h}{dr} \right) - \left(\frac{k^2}{r^2} + \beta^2 \right) \hat{p}_h = 0 \quad (26.60)$$

with pure Neumann boundary conditions for $k = 0$

$$\frac{\partial \hat{p}_h}{\partial r}(0, 0, m) = 0, \quad \frac{\partial \hat{p}_h}{\partial r}(1, 0, m) = \hat{h}(0, m) \quad (26.61)$$

and mixed Dirichlet–Neumann conditions

$$\hat{p}_h(0, k, m) = 0, \quad \frac{\partial \hat{p}_h}{\partial r}(1, k, m) = \hat{h}(k, m) \quad (26.62)$$

for $k > 0$ as in the previous section. The ode for $m \neq 0$ can be recast as the modified Bessel ode (26.53) for $y(x, k, m)$, $x \in [0, \infty)$. Simple rescaling of the radial coordinate r using β defined by (26.22)

$$x \equiv \beta r, \quad x \in [0, \beta] \quad (26.63)$$

leads to

$$\left[x^2 \frac{d^2}{dx^2} + x \frac{d}{dx} - (x^2 + k^2) \right] y(x, k, m) = 0 \quad (26.64)$$

where

$$y(x, k, m) = \hat{p}_h\left(\frac{x}{\beta}, k, m\right) \quad (26.65)$$

The range of the rescaled variable x is $[0, \beta]$ and the boundary condition is rescaled accordingly

$$\frac{dy}{dx}(x, k, m) = \frac{1}{\beta} \frac{d\hat{p}_h}{dr}(r, k, m), \quad \rightarrow \quad \frac{dy}{dx}(\beta, k, m) = \frac{1}{\beta} \hat{h}(k, m) \quad (26.66)$$

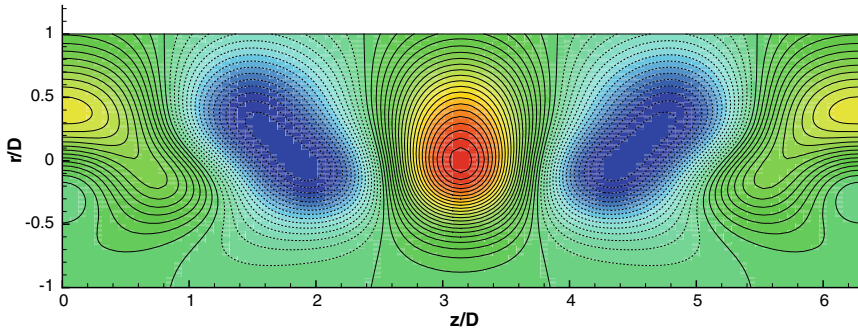


Fig. 26.1 Cross section at $\theta = \pi/2$ of the test field $f(r, \theta, \zeta)$ for the harmonic pressure $p_h(r, \theta, \zeta)$, negative values of r are defined as radial coordinates for $\theta + \pi$. The test field provides the Neumann boundary values shown in Fig. 26.3

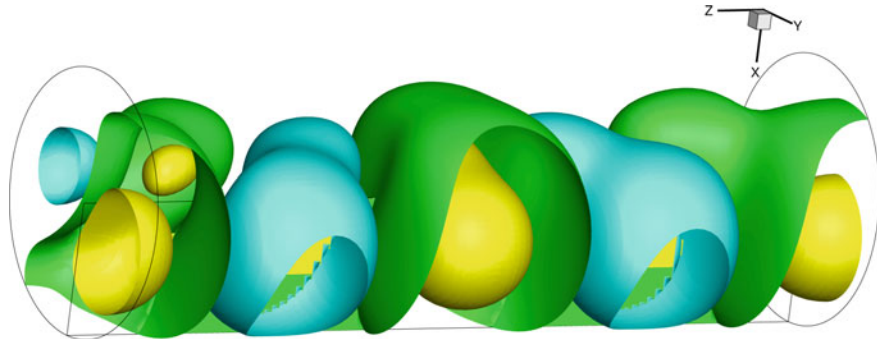


Fig. 26.2 Level surfaces of the test field for the level values: $f = 1.1191$ yellow, $f = 0.0707$ green, $f = -0.61305$ blue

The modified Bessel ode (26.53) has two linearly independent solutions $I_k(x)$ and $K_k(x)$ called modified Bessel functions of the first and second kind, respectively, their properties can be found in the literature [3, 4]. The general solution is then a linear combination of modified Bessel functions

$$y(x, k, m) = A I_k(x) + B K_k(x) \quad (26.67)$$

The modified Bessel function of the second kind $K_k(x)$ is singular at the origin, hence $B = 0$. The boundary condition requires the first derivative of Bessel functions [4]

$$\frac{d I_k}{dx} = \begin{cases} \frac{1}{2}(I_{k-1} + I_{k+1}) & \text{for } k > 0 \\ I_1 & \text{for } k = 0 \end{cases} \quad (26.68)$$

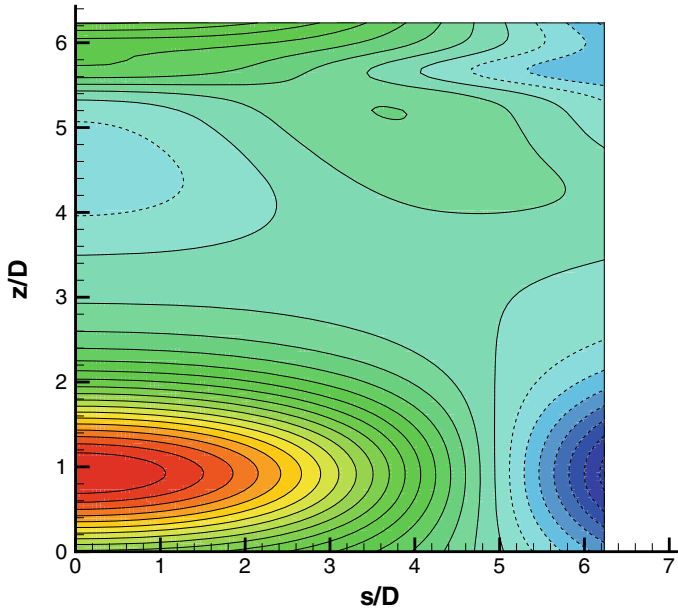


Fig. 26.3 Doubly periodic Neumann boundary values $dph/dr(\theta, \zeta)$ at the boundary $\partial\mathcal{D} = \{(r, \theta, \zeta) : r = 1\}$ provided by the test field f for the harmonic pressure p_h . The azimuthal variable is denoted by $s \equiv r\theta$, $0 \leq s \leq 2\pi$ for $r = 1$

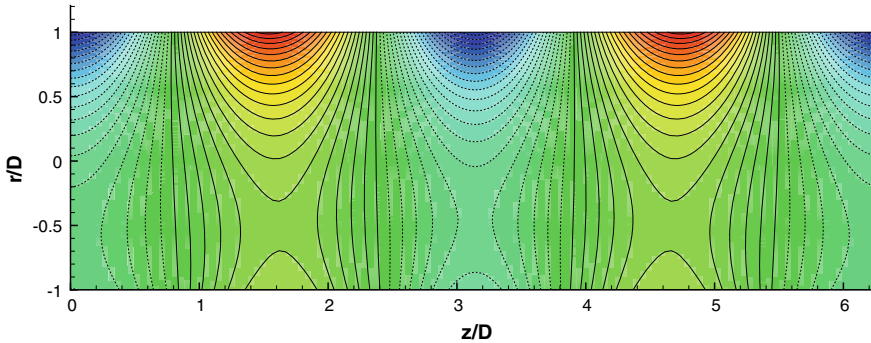


Fig. 26.4 Axial–radial section at $\theta = \pi/2$ of the solution p_h (26.72) of the BVP for the Laplacian pde with non-homogeneous boundary conditions in Fig. 26.3 for the complementary pressure p_h . Compare p_h with the test field f in Fig. 26.1

The integration constant A is determined by the Neumann condition at the outer boundary leading for $k = 0$ to the solution

$$y(x, 0, m) = \frac{I_0(x)\hat{h}(0, m)}{\beta I_1(\beta)} \quad (26.69)$$

and transforming back to the original variables

$$\hat{p}_h(r, 0, m) = \frac{I_0(\beta r) \hat{h}(0, m)}{\beta I_1(\beta)} \quad (26.70)$$

as solution for the azimuthal wavenumber $k = 0$ and axial wavenumbers $m > 0$. The solution for $k > 0$ follows similarly

$$\hat{p}_h(r, k, m) = \frac{2I_k(\beta r) \hat{h}(k, m)}{\beta [I_{k-1}(\beta) + I_{k+1}(\beta)]} \quad (26.71)$$

concluding the computation of the Fourier coefficients for this example. The complete solution for the complementary or harmonic part of the pressure is then

$$p_h(r, \theta, \zeta) = \sum_{k=-\infty}^{\infty} \sum_{m=-\infty}^{\infty} \frac{\hat{h}(k, 0)}{k} r^k \exp(ik\theta) + \sum_{k=-\infty}^{\infty} \sum_{m=-\infty}^{\infty} \frac{2I_k(\beta r) \hat{h}(k, m)}{\beta [I_{k-1}(\beta) + I_{k+1}(\beta)]} \exp[i(k\theta + m\zeta)]$$

(26.72)

where $r \in [0, 1]$, $\theta \in [0, 2\pi]$, $\zeta \in [0, 2\pi]$, $\beta = |m|/L$ and the prime on sum symbols indicates that terms with $k = 0$ or $m = 0/\beta = 0$ in the denominator must be omitted. The solution (26.72) is evidently linked to the velocity field via the Fourier coefficients $\hat{h}(k, m)$ of the viscous term (26.37)

$$\hat{h}(k, m) \mid \frac{1}{Re} \frac{\partial^2 v_r}{\partial r^2} (\mathbf{x} \in \partial\mathcal{D}) = \frac{1}{4\pi^2 Re} \int_0^{2\pi} d\theta \int_{z=0}^{2\pi L} dz \frac{\partial^2 v_r}{\partial r^2} (1, \theta, z) \exp[-i(k\theta + m\zeta)] \quad (26.73)$$

at the wall boundary. This result expresses the complementary pressure as linear functional of the wall stress generated by the flow (denoted by $\hat{h}(k, m) \mid \frac{1}{Re} \frac{\partial^2 v_r}{\partial r^2}$), and the terms to the left of the vertical bar are the local arguments, whereas the terms to the right indicate the functional dependence. Furthermore, the Fourier transform

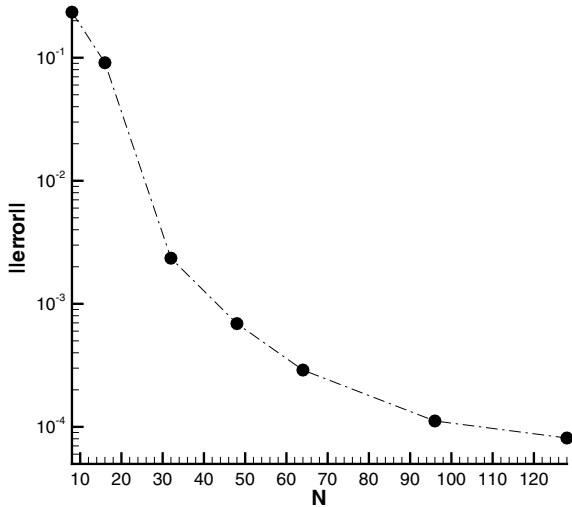
$$\hat{h}(k, m) \mid \frac{1}{Re} \frac{\partial^2 v_r}{\partial r^2} (\mathbf{x} \in \mathcal{D}) = \mathcal{F}(k, m) \mid \frac{1}{Re} \frac{\partial^2 v_r}{\partial r^2} (\mathbf{x} \in \partial\mathcal{D}) \quad (26.74)$$

acts as linear operator on the wall stress and the harmonic pressure is recognized as linear functional \mathcal{P}_h of the wall stress

$$p_h(r, \theta, \zeta) = \mathcal{P}_h(r, \theta, \zeta) \mid \frac{1}{Re} \frac{\partial^2 v_r}{\partial r^2} (\mathbf{x} \in \partial\mathcal{D})$$

where the explicit form of the functional is

Fig. 26.5 Maximum error of the complementary pressure gradient on the outer boundary as function of the number of Fourier modes N for an analytic test field



$$\begin{aligned}
 \mathcal{P}_h(r, \theta, \zeta | \frac{1}{Re} \frac{\partial^2 v_r}{\partial r^2} (\mathbf{x} \in \partial\mathcal{D})) &\equiv \sum_{k=-\infty}^{\infty} \frac{r^k}{k} \mathcal{F}(k, 0 | \frac{1}{Re} \frac{\partial^2 v_r}{\partial r^2} (\mathbf{x} \in \partial\mathcal{D})) \exp(ik\theta) \\
 &+ \sum_{k=-\infty}^{\infty} \sum_{m=-\infty}^{\infty} \frac{2I_k(\beta r)}{\beta[I_{k-1}(\beta) + I_{k+1}(\beta)]} \mathcal{F}(k, m | \frac{1}{Re} \frac{\partial^2 v_r}{\partial r^2} (\mathbf{x} \in \partial\mathcal{D})) \exp[i(k\theta + m\zeta)]
 \end{aligned} \tag{26.76}$$

with $\beta(m) = |m|/L$ according to (26.22). The notation $\mathcal{P}_h(r, \theta, \zeta | \frac{1}{Re} \frac{\partial^2 v_r}{\partial r^2} (\mathbf{x} \in \partial\mathcal{D}))$ indicates functional dependence of p_h on the wall stress on the domain boundary $\partial\mathcal{D}$ for the particular case $\partial\mathcal{D} = \{(r, \theta, \zeta) : r = 1\}$.

The correctness of the solution (26.72) is checked by computing the radial derivative of the solution numerically on a uniformly spaced grid. The infinite bounds for the Fourier series in (26.72) are replaced by N and evaluated using FFT and a third-order accurate finite-difference expression. The result is compared with the analytically specified Neumann boundary values, computed as derivative of the test pressure field (26.77), as function of the number of grid points N in the azimuthal direction.

The maximum norm of the error for the pipe flow example as function of the number of Fourier modes N is plotted in Fig. 26.5. The error decreases rapidly up to $N \approx 30$ and then the error due to the numerical computation of the radial derivative becomes dominant.

Analytic example

An example for the computation of the harmonic pressure field is shown in Fig. 26.1 constructed with the aid of elementary functions.

$$p(r, \theta, z) = \sum_{i=1}^N \sum_{j=1}^M \frac{A_{i,j}}{\sqrt{2\pi}\sigma_i} \exp\left\{-\frac{1}{2\sigma_i^2} [(r \cos \theta - r_i^0 \cos \theta_i^0)^2 + (r \sin \theta - r_i^0 \sin \theta_i^0)^2]\right\} \cos(k_{i,j} z) \quad (26.77)$$

where $r \in [0, 1]$, $\theta \in [0, 2\pi]$, $z \in [0, 2\pi L]$ and with coefficients $A_{i,j}$, axial wavenumbers $k_{i,j}$ and parameters σ_i , r_i^0 , θ_i^0 chosen randomly within realizable bounds, the number of terms in the sums are set to $M = 5$ and $N = 2$. The analytic expression for the test field (26.77) allows easy computation of the Neumann boundary values $\partial p_h / \partial r$ shown in Fig. 26.3.

A section $\theta = \pi/2$ of the solution (26.72) is presented in Fig. 26.4. Comparison of the $r - z$ section for p_h with the test field (26.77) in Fig. 26.1 shows significant differences, since the complementary solution p_h depends on the Neumann boundary values (26.17) and is independent of the right-hand side of the Poisson pde (26.23).

26.7 Green's Theorem and its Application

Consider two arbitrary, differentiable scalar fields $\Phi(\mathbf{x})$ and $\Psi(\mathbf{x})$ defined in \mathcal{D} with boundary $\partial\mathcal{D}$, then the identity

$$\int_{\mathcal{D}} d\nu (\Phi \Delta \Psi - \Psi \Delta \Phi) = \int_{\partial\mathcal{D}} dA \mathbf{n} \cdot (\Phi \nabla \Psi - \Psi \nabla \Phi) \quad (26.78)$$

holds called Green's theorem, where \mathbf{n} is the unit normal vector pointing outward. Green's theorem follows from the vector identity

$$\nabla \cdot (\Phi \nabla \Psi) = \nabla \Phi \cdot \nabla \Psi + \Phi \Delta \Psi \quad (26.79)$$

and the Gauss divergence theorem.

Regularity conditions for the modal Green's function $G_{k,m}(r, \rho)$

The properties of the modal Green's function $G_{k,m}(r, \rho)$ for the azimuthal and axial wavenumbers k and m on $r = \rho$ are evaluated with the aid of the Sturm–Liouville ode (26.33)

$$-\frac{1}{r} \left[\frac{d}{dr} \left(r \frac{d}{dr} \right) - \left(\frac{k^2}{r} + \beta^2 r \right) \right] G_{k,m} = \frac{1}{r} \delta(r - \rho)$$

Integration of this ode over the interval $r \in [\rho - \epsilon, \rho + \epsilon]$ with $0 < \epsilon \ll 1$ leads to

$$\frac{dG_{k,m}^+}{dr} - \frac{dG_{k,m}^-}{dr} = -\frac{1}{\rho} \text{ or } \frac{dG_{k,m}^+}{dx} - \frac{dG_{k,m}^-}{dx} = -\frac{1}{\beta\rho} \quad (26.80)$$

for the jump height, where $x = \beta r$ and

$$\frac{dG_{k,m}^+}{dr} = \lim_{\epsilon \rightarrow 0} \frac{dG_{k,m}}{dr}(\rho + \epsilon, \rho), \quad \frac{dG_{k,m}^-}{dr} = \lim_{\epsilon \rightarrow 0} \frac{dG_{k,m}}{dr}(\rho - \epsilon, \rho) \quad (26.81)$$

Further integration shows that the Green's function $G_{k,m}(r, \rho)$ is continuous at $r = \rho > 0$.

$$G_{k,m}^+(\rho, \rho) = G_{k,m}^-(\rho, \rho) \quad (26.82)$$

These two regularity conditions (26.80) and (26.82) allow the construction of the solution for the domains $0 \leq r < \rho < 1$ and $\rho < r \leq 1$. It is convenient to establish the solution for $m = 0$ and $m > 0$ separately.

1-d Green's functions for the radial Fourier modes

Fourier transform of the Poisson pde leads to a system of Sturm–Liouville odes for the radial direction equation (26.26) and the associated modal Greens' functions (26.33)

$$-\frac{1}{r} \frac{d}{dr} \left(r \frac{dG_{k,m}}{dr} \right) + \left(\frac{k^2}{r^2} + \beta^2 \right) G_{k,m} = \frac{1}{r} \delta(r - \rho)$$

for the azimuthal and axial wavenumbers $0 < k < \infty, -\infty < m < \infty$. The homogeneous boundary conditions for $G_{k,m}(r, \rho)$ are according to Sect. 26.5 dependent on the azimuthal and axial wavenumbers k and m

$$\begin{aligned} \frac{\partial G_{0,m}}{\partial r}(0, \rho) &= 0, \quad \text{for } k = 0 \\ G_{k,m}(0, \rho) &= 0, \quad \text{for } k \neq 0 \end{aligned} \quad (26.83)$$

The conditions at the outer boundary are homogeneous Neumann conditions (26.37).

$$\frac{dG_{k,m}}{dr}(1, \rho) = 0, \quad \text{for all } k \quad (26.84)$$

The Green's functions are computed for two cases, $m = 0$ and $m \neq 0$, separately since the odes have different solutions.

Axial wavenumber $m = 0$

The Sturm–Liouville odes are for $m = 0$ and $r \neq \rho$ reduced to homogeneous Euler odes

$$r^2 \frac{d^2 G_{k,0}}{dr^2} + r \frac{dG_{k,0}}{dr} - k^2 G_{k,0} = 0 \quad (26.85)$$

with homogeneous boundary conditions

$$G_{k,0}(0, \rho) = 0, \quad \frac{dG_{k,0}}{dr}(1, \rho) = 0 \quad (26.86)$$

The solution is a power of r using the Ansatz $G_{k,0}(r, \rho) = Ar^\alpha$. The ode generates the algebraic relation $\alpha = \pm k$ and the general solution

$$G_{k,0}(r, \rho) = A(\rho)r^k + B(\rho)r^{-k} \quad (26.87)$$

is obtained.

Subdomain $r \in [0, \rho]$

The general solution (26.87) must satisfy the boundary condition at $r = 0$, hence $B(\rho) = 0$ and

$$G_{k,0}(r, \rho) = A(\rho)r^k \quad (26.88)$$

for $r \in [0, \rho]$ is obtained. The remaining coefficient $A(\rho)$ is determined by the conditions at $r = \rho$.

Subdomain $r \in (\rho, 1]$

The general solution (26.87) is now written as

$$G_{k,0}(r, \rho) = C(\rho)r^k + D(\rho)r^{-k} \quad (26.89)$$

The boundary condition at $r = 1$ requires the first derivative

$$\frac{G_{k,0}}{dr}(r, \rho) = kC(\rho)r^{k-1} - kD(\rho)r^{-k-1} \quad (26.90)$$

The boundary condition at $r = 1$ leads to $C(\rho) = D(\rho)$ and

$$G_{k,0}(r, \rho) = C(\rho)(r^k + r^{-k}) \quad (26.91)$$

The remaining coefficients $A(\rho)$ and $C(\rho)$ are determined by the regularity conditions at $r = \rho$.

Continuity at $r = \rho$

Continuity at $r = \rho$ leads to

$$A(\rho)\rho^k = C(\rho)\rho^k\left(1 + \frac{1}{\rho^{2k}}\right) \quad (26.92)$$

hence

$$A(\rho) = C(\rho)\left(1 + \frac{1}{\rho^{2k}}\right) \quad (26.93)$$

can be applied to eliminate $A(\rho)$.

Jump condition at $r = \rho$

The jump condition (26.80)

$$\frac{dG_{k,m}}{dr}(r^+, \rho) - \frac{dG_{k,m}}{dr}(r^-, \rho) = -\frac{1}{\rho}$$

leads to

$$C(\rho) = \frac{1}{2k} \rho^k \quad (26.94)$$

completing the computation of the coefficients A, B, C, D .

Green's function for $m = 0, k > 0$

The Green's function emerges from the relations established in the previous sections in the form

$$G_{k,0}(r, \rho) = \frac{1}{2k} \begin{cases} r^k \rho^k (1 + \frac{1}{\rho^{2k}}) & \text{for } 0 \leq r < \rho \\ r^k \rho^k (1 + \frac{1}{r^{2k}}) & \text{for } \rho \leq r < 1 \end{cases} \quad (26.95)$$

valid for $m = 0$ and $k > 0$.

Green's function for $m = 0, k = 0$

The ode (26.33) is for $k = 0$ and $m = 0$ reduced to

$$-\frac{d}{dr}(r \frac{dG_{0,0}}{dr}) = \delta(r - \rho) \quad (26.96)$$

with solution in the subdomains $[0, \rho)$ and $(\rho, 1]$

$$G_{0,0}(r, \rho) = \begin{cases} A(\rho) \ln r + B(\rho) & \text{for } 0 \leq r < \rho \\ C(\rho) \ln r + D(\rho) & \text{for } \rho < r \leq 1 \end{cases} \quad (26.97)$$

The homogeneous Neumann boundary conditions imply $A = C = 0$, hence

$$G_{0,0}(r, \rho) = \begin{cases} B(\rho) & \text{for } 0 \leq r < \rho \\ D(\rho) & \text{for } \rho < r \leq 1 \end{cases} \quad (26.98)$$

Continuity at $r = \rho$ (26.82) requires $B(\rho) = D(\rho)$, but the solution is inconsistent with the jump condition (26.81). This leads to the conclusion that mode $k = 0, m = 0$ cannot be part of the disturbance pressure field. The mode $k = 0, m = 0$ corresponds to a pressure disturbance independent of the radial and axial coordinates, hence is not a disturbance, but included in P_0 .

Axial wavenumbers $m \neq 0$

The Sturm–Liouville odes are closely related to Bessel's odes for $m \neq 0$. This can be seen if the rescaling (26.22)

$$x \equiv \beta r \leftrightarrow r = \frac{x}{\beta} \quad (26.99)$$

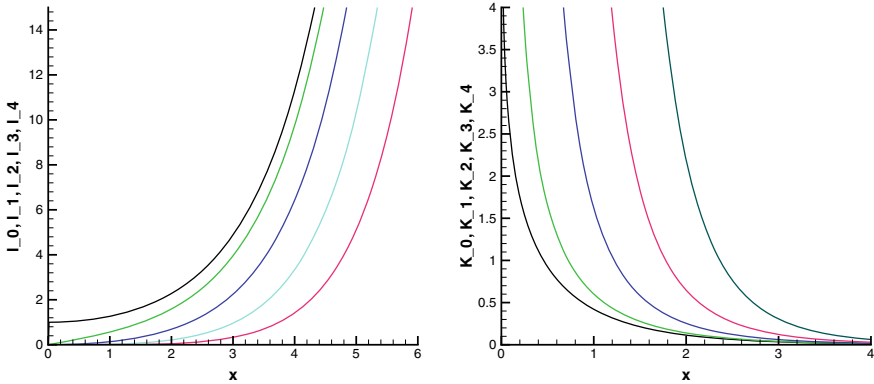


Fig. 26.6 Modified Bessel functions of the first kind $I_k(x)$ (left graph) and the second kind $K_k(x)$ (right graph) for the azimuthal wavenumbers $k = 0, \dots, 4$

is applied, where $\beta \equiv \frac{|m|}{L}$. For $r \neq \rho$, the ode for the Green's function emerges as the modified Bessel ode (26.53)

$$x^2 \frac{d^2 G_{k,m}}{dx^2} + x \frac{dG_{k,m}}{dx} - (k^2 + x^2) G_{k,m} = 0 \quad (26.100)$$

where $x \in [0, \beta]$. The modified Bessel ode (26.53) has two linearly independent solutions $I_k(x)$ and $K_k(x)$ called modified Bessel functions of the first and second kind, respectively, their properties can be found in the literature [3, 4], the first five modified Bessel functions are shown in Fig. 26.6. The first derivatives of the modified Bessel functions [4] are noted for later use.

$$\frac{dI_k}{dx} = \begin{cases} I_1(x) & \text{for } k = 0 \\ \frac{1}{2}[I_{k-1}(x) + I_{k+1}(x)] & \text{for } k \neq 0 \end{cases} \quad (26.101)$$

$$\frac{dK_k}{dx} = \begin{cases} -K_1(x) & \text{for } k = 0 \\ -\frac{1}{2}[K_{k-1}(x) + K_{k+1}(x)] & \text{for } k \neq 0 \end{cases} \quad (26.102)$$

The Green's function is now computed for the two subdomains of $[0, \beta]$.

Subdomain $r \in [0, \rho] \leftrightarrow x \in [0, \beta\rho]$

The Green's function is a linear combination of modified Bessel functions

$$G_{k,m}(x, \rho) = A(\rho)I_k(x) + B(\rho)K_k(x) \quad (26.103)$$

The boundary condition at $r = 0$ requires boundedness, hence $B = 0$ and the Green's function is reduced to

$$G_{k,m}(x, \rho) = A(\rho)I_k(x) \quad (26.104)$$

Subdomain $r \in (\rho, 1] \Leftrightarrow x \in (\beta\rho, \beta]$

The Green's function is a linear combination of modified Bessel functions

$$G_{k,m}(x, \rho) = C(\rho)I_k(x) + D(\rho)K_k(x) \quad (26.105)$$

The boundary condition at $r = 1 \Leftrightarrow x = \beta\rho$ requires the first derivative of $G_{k,m}(\beta, \rho)$ to vanish, thus

$$C(\rho) \frac{dI_k}{dx}(\beta) + D(\rho) \frac{dK_k}{dx}(\beta) = 0 \quad (26.106)$$

is obtained. This relation allows the elimination of $D(\rho)$

$$D(\rho) = \gamma C(\rho) \quad (26.107)$$

where the coefficient is defined as

$$\gamma(\beta, k) \equiv -\frac{\frac{dI_k}{dx}(\beta)}{\frac{dK_k}{dx}(\beta)} \quad (26.108)$$

The Green's function is then in the present subdomain

$$G_{k,m}(x, \rho) = C(\rho)[I_k(x) + \gamma K_k(x)] \quad (26.109)$$

Continuity at $r = \rho \Leftrightarrow x = \beta\rho$

Continuity at $x = \beta\rho$ leads to

$$A(\rho)I_k(\beta\rho) = C(\rho)[I_k(\beta\rho) + \gamma K_k(\beta\rho)] \quad (26.110)$$

Eliminating $A(\rho)$ using

$$A(\rho) = C(\rho) \frac{I_k(\beta\rho) + \gamma K_k(\beta\rho)}{I_k(\beta\rho)} \quad (26.111)$$

produces the Green's function

$$G_{k,m}(x, \rho) = C(\rho) \begin{cases} \frac{I_k(\beta\rho) + \gamma K_k(\beta\rho)}{I_k(\beta\rho)} I_k(x) & \text{for } 0 \leq x < \beta\rho \\ I_k(x) + \gamma K_k(x) & \text{for } \beta\rho \leq x < \beta \end{cases} \quad (26.112)$$

according to the derivative relations (26.101) and (26.102). The coefficient $C(\rho)$ is finally determined by the jump condition (26.80).

Jump condition at $r = \rho \leftrightarrow x = \beta\rho$

The jump condition (26.80)

$$\frac{dG_{k,m}}{dx}(x^+, \rho) - \frac{dG_{k,m}}{dx}(x^-, \rho) = -\frac{1}{\beta\rho} \quad (26.113)$$

where

$$\frac{dG_{k,m}}{dx}(x^+, \rho) = \frac{1}{2}C(\rho)[I_{k-1}(\beta\rho) + I_{k+1}(\beta\rho) - \gamma[K_{k-1}(\beta\rho) + K_{k+1}(\beta\rho)]] \quad (26.114)$$

$$\frac{dG_{k,m}}{dx}(x^-, \rho) = \frac{1}{2}C(\rho)[I_{k-1}(\beta\rho) + I_{k+1}(\beta\rho)] \frac{I_k(\beta\rho) + \gamma K_k(\beta\rho)}{I_k(\beta\rho)} \quad (26.115)$$

combined with relation (26.112) leads to the desired coefficient

$$C(\rho) = \frac{1}{\beta\gamma\rho\delta} I_k(\beta\rho) \quad (26.116)$$

where $\delta(\beta, \rho, k)$ is defined by

$$\delta(\beta, \rho, k) \equiv \begin{cases} I_0(\beta\rho)K_1(\beta\rho) + K_0(\beta\rho)I_1(\beta\rho) & \text{for } k = 0 \\ \frac{1}{2}\{I_k(\beta\rho)[K_{k-1}(\beta\rho) + K_{k+1}(\beta\rho)] + K_k(\beta\rho)[I_{k-1}(\beta\rho) + I_{k+1}(\beta\rho)]\} & \text{for } k > 0 \end{cases} \quad (26.117)$$

valid for all k and $m \neq 0$.

Green's function for $m \neq 0$

The Green's function emerges from the relations established in the previous sections in the form

$$G_{k,m}(r, \rho) = \frac{1}{\beta\gamma\rho\delta} \begin{cases} I_k(\beta r)[I_k(\beta\rho) + \gamma K_k(\beta\rho)] & \text{for } 0 \leq r < \rho \\ I_k(\beta\rho)[I_k(\beta r) + \gamma K_k(\beta r)] & \text{for } \rho \leq r < 1 \end{cases} \quad (26.118)$$

valid for all k and $m \neq 0$. The factor $1/\rho$ cancels with the ρ in the integral determining the Green's function pressure in Sect. 26.7 Eq. (26.126). Thus it is convenient for the computation of the Green's function pressure to modify Green's function

$$G_{k,m}^\rho(r, \rho) = \rho G_{k,m}(r, \rho) \quad (26.119)$$

for the wavenumber range $|m| > 0$ to take advantage of this cancellation.

Complete Green's function

The results from the previous sections can be summarized

$$G_{k,m}(r, \rho) = \begin{cases} \frac{1}{2k} r^k \rho^k (1 + \frac{1}{\rho^{2k}}) & \text{for } m = 0, k > 0 \text{ and } 0 \leq r < \rho \\ \frac{1}{2k} r^k \rho^k (1 + \frac{1}{r^{2k}}) & \text{for } m = 0, k > 0 \text{ and } \rho \leq r < 1 \\ \frac{1}{\beta\gamma\rho^\delta} I_k(\beta r) [I_k(\beta\rho) + \gamma K_k(\beta\rho)] & \text{for } m \neq 0 \text{ and } 0 \leq r < \rho \\ \frac{1}{\beta\gamma\rho^\delta} I_k(\beta r) [I_k(\beta r) + \gamma K_k(\beta r)] & \text{for } m \neq 0 \text{ and } \rho \leq r < 1 \end{cases} \quad (26.120)$$

where I_k , K_k denote the modified Bessel function of first and second kind. Equation (26.120) represents the desired Green's function that is valid for both subdomains and all azimuthal and axial wavenumbers. Note that for the wavenumber combination $k = 0, m = 0$ no Green's exists consistent with the boundary and jump conditions, see discussion of Eq. (26.96).

The coefficients β , γ , δ are defined by Eqs. (26.22), (26.108), (26.117). The symmetry properties of the Green's function are evident in Eq. (26.120): $G_{k,m}(r, \rho)$ is symmetric for $m = 0$ and $k > 0$, but for $m \neq 0$ the symmetry holds for the product $\rho\delta(\beta, \rho, k)G_{k,m}(r, \rho)$, since the boundary conditions at $r = 0$ (Dirichlet) and $r = 1$ (Neumann) are of different types as a consequence of the parity conditions (Sect. 26.4.1).

Green's function pressure p_G

The final expression for Green's function pressure p_G follows from Green's theorem adapted to the Sturm–Liouville odes (26.33), (26.30). It is convenient to use the modified Sturm–Liouville operator (26.34) to set up the odes for the Green's function and the pressure modes

$$-\hat{\mathcal{L}}G_{k,m}(r, \rho) = \delta(r - \rho), \quad -\hat{\mathcal{L}}\hat{p}(r, k, m) = r\hat{R}(r, k, m) \quad (26.121)$$

with right-hand side defined by (26.12) in physical space and its Fourier transform $\hat{R}(r, k, m)$ (26.28). Combining the odes

$$G_{k,m}\hat{\mathcal{L}}\hat{p} - \hat{p}\hat{\mathcal{L}}G_{k,m} = G_{k,m}(r, \rho)r\hat{R}(r, k, m) - \hat{p}(r, k, m)\delta(r - \rho) \quad (26.122)$$

and integrating

$$\int_0^1 dr [G_{k,m}\hat{\mathcal{L}}\hat{p} - \hat{p}\hat{\mathcal{L}}G_{k,m}] = \int_0^1 dr G_{k,m}(r, \rho)r\hat{R}(r, k, m) - \hat{p}(\rho, k, m) \quad (26.123)$$

The integral on the left-hand side can be evaluated and leads to

$$\int_0^1 dr [G_{k,m}\hat{\mathcal{L}}\hat{p} - \hat{p}\hat{\mathcal{L}}G_{k,m}] = r \left(\hat{p} \frac{G_{k,m}}{dr} - G_{k,m} \frac{d\hat{p}}{dr} \right)_0^1 \quad (26.124)$$

The pressure modes \hat{p} and the Green's function $G_{k,m}$ satisfy the same homogeneous boundary conditions, hence

$$\int_0^1 dr [G_{k,m} \hat{\mathcal{L}} \hat{p} - \hat{p} \hat{\mathcal{L}} G_{k,m}] = 0 \quad (26.125)$$

and the modal form of the Green's function pressure for specified azimuthal and axial wavenumbers k, m is thus given by

$$\hat{p}_G(k, m, r) = \int_0^1 d\rho \rho \hat{R}(\rho, k, m) G_{k,m}(\rho, r) \quad (26.126)$$

where $\hat{R}(\rho, k, m) = \mathcal{F}(k, m|R(\mathbf{x}), \mathbf{x} \in \mathcal{D})$ denotes the right-hand side of the Sturm–Liouville ode (26.29). Fourier transformation back to physical space (26.21) leads to

$$p_G(r, \theta, \zeta) = \mathcal{P}_G(\theta, \zeta|R(\mathbf{x}), \mathbf{x} \in \mathcal{D}) \quad (26.127)$$

where the linear functional is defined by

$$\mathcal{P}_G(r, \theta, \zeta|R(\mathbf{x}), \mathbf{x} \in \mathcal{D}) \equiv \mathcal{F}^{-1}(\theta, \zeta | \int_0^1 d\rho \rho \mathcal{F}(k, m|R(\mathbf{x}), \mathbf{x} \in \mathcal{D}) G_{k,m}(\rho, r)) \quad (26.128)$$

This relation determines the non-local dependence of the Green's function pressure p_G on the scalar field $R(r, \theta, \zeta)$ that is a combination of products of derivatives of the velocity field according to (26.12).

Example for the modal 1-d Green's function

The Green's function obtained in the previous section is illustrated in Figs. 26.7 and 26.8.

The boundary conditions for the selected azimuthal wavenumbers $k > 0$ are the mixed homogeneous Dirichlet/Neumann conditions given by (26.54), (26.55). They are clearly satisfied as the radial profiles of $G_{k,m}(r, \rho)$ in Fig. 26.8.

The results for an analytic test function

$$f(r) = \frac{r^k}{\sqrt{1+r^{2k}}} \sum_{n=1}^{N_r} A_n \cos(2\pi n r) \quad (26.129)$$

where $k = 3$, $N_r = 4$ and the coefficients A_n are chosen randomly in $[0, 1]$, are shown in Fig. 26.9 to Fig. 26.12. The integration in (26.126) for the Green's function pressure p_G was done numerically using the trapezoidal rule. The left graph contains the right-hand side function $R(r) = -\mathcal{L}f(r)$ and the right the numerically computed solution

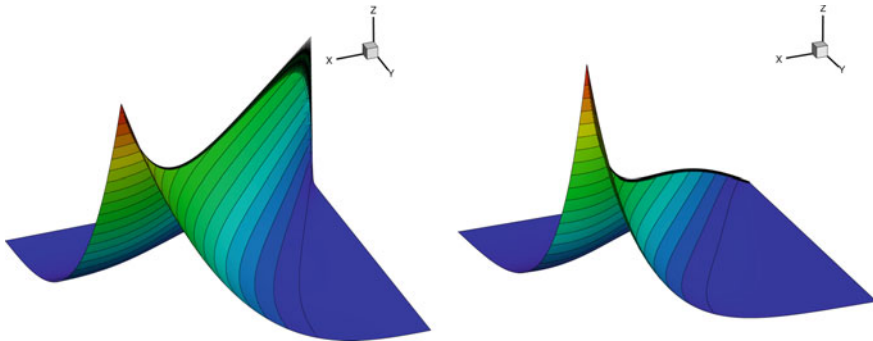


Fig. 26.7 Normalized modal 1-d Green's functions $G_{k,m}(r, \rho) / ||G_{k,m}||$ (26.120) as function of the radial location r (x -axis) and the jump location ρ (y -axis) for $k = 3, m = 0$ (left graph, $||G_{k,m}|| = 0.333333$) and $G_{k,m}^\rho(r, \rho) / ||G_{k,m}||$ for $k = 3, m = 4$ (right graph, $||G_{k,m}|| = 0.212878$)

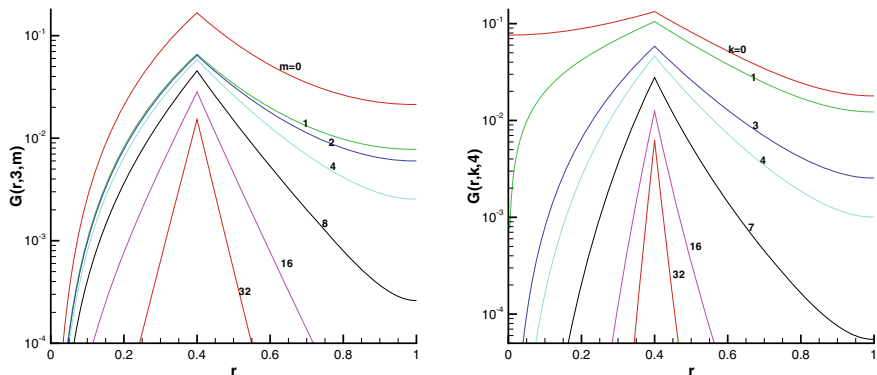


Fig. 26.8 Radial profiles of the modal 1-d Green's functions $G_{k,m}(r, \rho)$ (26.120) at $\rho = 0.4$ for $m = 4$ and several k (right graph) and $k = 3$ and several m (left graph). Note that the modes $G_{0,m}(r, \rho)$ satisfy the homogeneous Neumann condition at $r = 0$, due to the parity condition (26.45), as seen as the top red line in the right graph

consisting of the complementary (26.72) and Green's function pressure (26.126). Figure 26.10 shows the error as difference between test function and the numerically computed solution, and the maximum norm of the error is $||\text{error}(r, \rho)|| = 3.713e - 04$ for $N = 128$ Fourier modes for azimuthal and axial directions.

Example for the linear functionals for the harmonic and the Green's function pressure

The linear functional (26.76) determining the complementary or harmonic pressure p_h and the linear functional (26.128) fixing the Green's function pressure p_G are illustrated with the aid of a test pressure field (26.77).

The 2-d plots in the plane $\theta = 0(r > 0)/\theta = \pi(r < 0)$ in Fig. 26.11 exhibit the effect of the Neumann boundary condition imposed on the pipe wall $r = 1$ in the

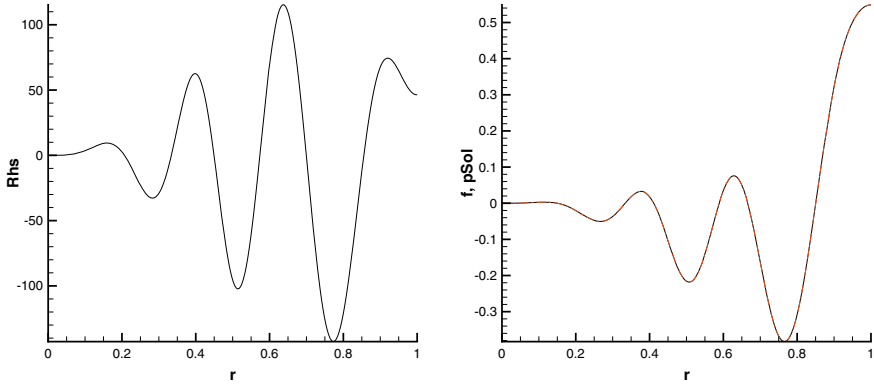
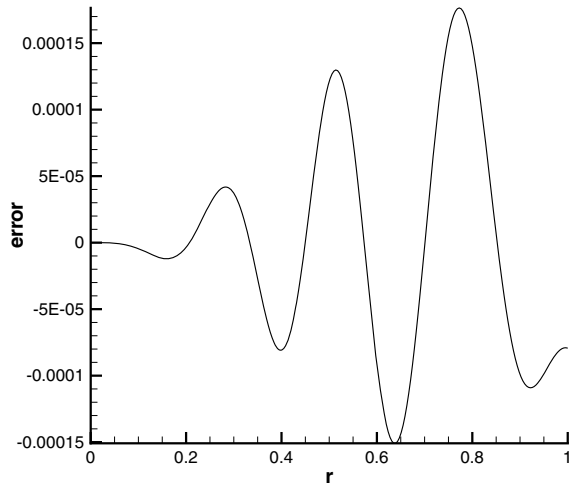


Fig. 26.9 Test example for $m = 4$ and $k = 3$: Right-hand side function $R(r) = -\mathcal{L}f(r)$ with Sturm–Liouville operator defined by (26.29) (left graph). Test function $f(r)$ (26.129) (black line) and the disturbance pressure $p_h + p_G$ (26.72), (26.127) (red, dash-dotted line) are shown in the right graph

Fig. 26.10 Test example for $m = 4$ and $k = 3$: Difference between test function $f(r)$ and numerically computed disturbance pressure $p = p_h + p_G$ (26.72). The maximum norm of the error is $\|error(r, \rho)\| = 3.713e - 04$



upper graph and the effect of the right-hand side $R(r, \theta, \zeta)$ (26.12) in the lower graph. The linear functional (26.76) generates the harmonic pressure determined by the Neumann boundary conditions on the pipe wall and the kinematic parity conditions in Sect. 26.4.1 on the coordinate axis $r = 0$. The harmonic pressure assumes its maximum on the outer boundary and decays according to a power law or modified Bessel functions as seen in the upper graph. The linear functional (26.128) on the other hand is dominated by the right-hand side $R(r, \theta, \zeta) = -\mathcal{L}f$, which is evident in the right graph of Fig. 26.11.

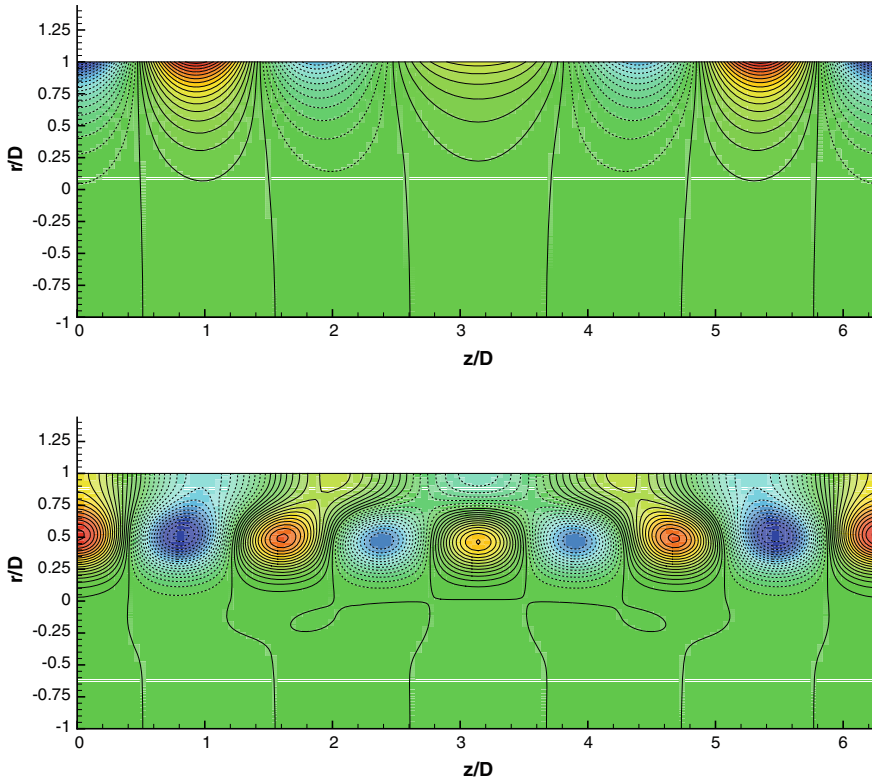


Fig. 26.11 Test function results in the plane $\theta = 0(r > 0)/\pi(r < 0)$ for the application of the linear functional (26.76) for the harmonic pressure (upper graph) and the linear functional (26.128) for the Green's function pressure (lower graph). The disturbance pressure p is the sum of harmonic p_h and Green's function pressure p_G , the difference between p and the test function is the absolute error

Two radial profiles of the results at $\theta = 0.0$, $z/L = 1.346$ (left graph) and $\theta = 0.0$, $z/L = 2.244$ (right graph) are shown in Fig. 26.12. The test function $f(r, \theta, \zeta)$ and the disturbance pressure $p(r, \theta, \zeta) = p_h(r, \theta, \zeta) + p_G(r, \theta, \zeta)$ are in close agreement with maximum norm of the error $e \equiv |f - p_G|$ computed as $\|e\| = 8.25e - 04$ for $N_\theta = N_\zeta = 128$ Fourier modes. The profiles of the Green's function pressure (blue line), the disturbance pressure (red dot-dashed line) and the harmonic pressure (green line) show that the Green's function pressure satisfies the zero gradient condition at the pipe wall, whereas the harmonic pressure assumes the correct gradient condition at $r = 1$.

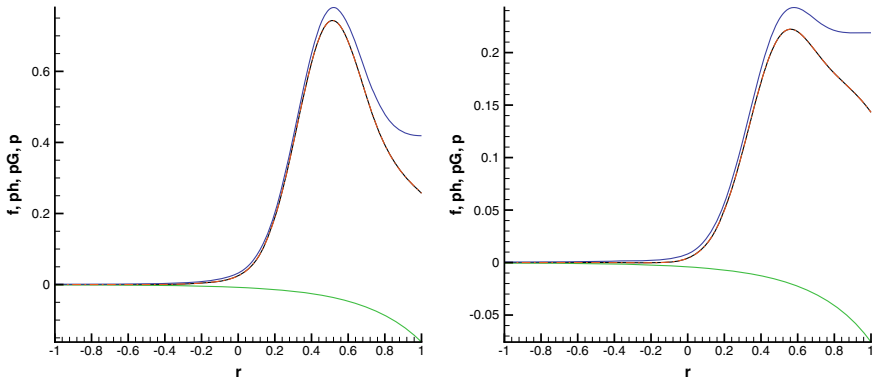


Fig. 26.12 Radial profiles at $\theta = 0.0$, $z/L = 1.346$ (left graph) and $\theta = 0.0$, $z/L = 2.244$ (right graph). The test function $f(r, \theta, \zeta)$ is the black, the disturbance pressure $p(r, \theta, \zeta) = p_h(r, \theta, \zeta) + p_G(r, \theta, \zeta)$ the red dash-dotted, the Green's function pressure $p_G(r, \theta, \zeta)$ the blue and the harmonic pressure $p_h(r, \theta, \zeta)$ the green line. The maximum norm of the error $e(r, \theta, \zeta) \equiv |f(r, \theta, \zeta) - p(r, \theta, \zeta)|$ is $\|e\| = 8.25e-04$, the difference between test function and computed disturbance pressure is not discernible

26.8 Solution of the Poisson pde for the Disturbance Pressure

It follows from the previous sections that the solution of the Poisson pde (26.11) for the pressure $P(r, \theta, \zeta)$ is a linear functional of the right-hand side $R(r, \theta, \zeta)$ (26.12) and the viscous stress on the boundary. The representation (26.50) of the pressure can be given explicitly using (26.76) and (26.128) for flow though straight pipes with periodicity in axial direction

$$P(r, \theta, \zeta) = P_0(\zeta) + \mathcal{P}_h(r, \theta, \zeta) \frac{1}{Re} \frac{\partial^2 v_r}{\partial r^2} (\mathbf{x} \in \partial\mathcal{D}) + \mathcal{P}_G(r, \theta, \zeta) R(\mathbf{x}), \mathbf{x} \in \mathcal{D} \quad (26.130)$$

as a consequence of Green's theorem (26.78) applied to the Sturm–Liouville boundary value problem. The linear functionals (26.76) and (26.128) are a combination of 2-d Fourier operators and radial Green's functions. The performance of this version of the pressure computation has not yet been evaluated.

Summary

The Green's function approach was applied to the flow of a Newtonian fluid with constant density through straight pipes with circular cross section. It was assumed that the flow is periodic in axial direction with periodicity interval $L \geq 1$ a multiple of 2π . This assumption allowed the 2-d fast Fourier Transform (with respect to azimuthal and axial directions) of the velocity and disturbance pressure fields. The pressure for the periodic pipe flow was shown to be a sum of three contributions (26.50): (1) The basic pressure $P_0(z)$, which is a linear function of the axial coordinate, hence

its axial derivative is constant; (2) The harmonic disturbance pressure p_h being a linear functional (26.76) of the Neumann boundary values of the pressure, it has the structure of a surface integral over $\partial\mathcal{D}$; (3) The Green's function pressure p_G being a linear functional (26.128) of the right-hand side R of the Poisson pde for the pressure, it has the structure of a volume integral over \mathcal{D} .

The Green's function for the radial direction is the solution of a Sturm–Liouville boundary value problem. This problem requires the parity conditions for scalar fields in cylindrical coordinates for complete setup and solution leading to explicit expressions for the harmonic pressure and the Green's function. The analytic results were verified numerically with analytical test fields.

26.9 Leray Version of the Navier–Stokes pdes

The representation of the pressure solution using Green's functions (26.130) can be applied to the Navier–Stokes pdes in the cylindrical domain \mathcal{D} defined by (26.1) for incompressible, Newtonian fluids using cylindrical coordinates. The particular (non-homogeneous Neumann) boundary values for the pressure gradient follow from the momentum balance normal to the boundary $\mathbf{n} \cdot \nabla P = h$ (26.17)

$$h(\mathbf{x}) = \frac{1}{Re} \left[\frac{\partial}{\partial r} \left(\frac{1}{r} \frac{\partial}{\partial r} (r v_r) \right) + \frac{1}{r^2} \frac{\partial^2 v_r}{\partial \theta^2} + \frac{\partial^2 v_r}{\partial z^2} - \frac{2}{r^2} \frac{\partial v_\theta}{\partial \theta} \right]$$

where n_α denotes the outward pointing unit normal vector. This expression is for fixed wall boundaries reduced to (26.18)

$$h(\mathbf{x}) = \frac{1}{Re} \frac{\partial^2 v_r}{\partial r^2}$$

The solution of (26.11) is then represented in terms of the Green's function $G(\mathbf{x}, \mathbf{y})$ in the form given by Eq. (26.130). It is now evident that the pressure gradient in the momentum balances can be expressed in terms of velocity and its boundary values, and the momentum balances emerge as integro-differential equations. Mass balance enters this system only as condition for the initial velocity field, $\nabla \cdot \mathbf{v}(0, \mathbf{x}) = 0$. The Leray version of the radial momentum balance is then given by

$$\frac{\partial v_r}{\partial t} = -T_r - \frac{\partial}{\partial r} \mathcal{P}_h(r, \theta, \zeta | \frac{1}{Re} \frac{\partial^2 v_r}{\partial r^2} (\mathbf{x} \in \partial\mathcal{D})) - \frac{\partial}{\partial r} \mathcal{P}_G(r, \theta, \zeta | R(\mathbf{x}), \mathbf{x} \in \mathcal{D}) + \frac{1}{Re} F_r$$

(26.131)

and the azimuthal balance by

$$\boxed{\frac{\partial v_\theta}{\partial t} = -T_\theta - \frac{1}{r} \frac{\partial}{\partial \theta} \mathcal{P}_h(r, \theta, \zeta) \frac{1}{Re} \frac{\partial^2 v_r}{\partial r^2} (\mathbf{x} \in \partial \mathcal{D}) - \frac{1}{r} \frac{\partial}{\partial \theta} \mathcal{P}_G(r, \theta, \zeta | R(\mathbf{x}), \mathbf{x} \in \mathcal{D}) + \frac{1}{Re} F_\theta} \quad (26.132)$$

and the axial balance by

$$\boxed{\frac{\partial v_z}{\partial t} = -T_z - \frac{\partial P_0}{\partial z} - \frac{\partial}{\partial z} \mathcal{P}_h(r, \theta, \zeta) \frac{1}{Re} \frac{\partial^2 v_r}{\partial r^2} (\mathbf{x} \in \partial \mathcal{D}) - \frac{\partial}{\partial z} \mathcal{P}_G(r, \theta, \zeta | R(\mathbf{x}), \mathbf{x} \in \mathcal{D}) + \frac{1}{Re} F_z} \quad (26.133)$$

The basic pressure gradient $-\partial P_0 / \partial z > 0$ and constant for the pipe flow case; it is determined by the mass flow rate through the pipe and acts as a uniform, external force. The linear functionals \mathcal{P}_h and \mathcal{P}_G are defined by (26.76) and (26.128). The convective terms T_i ($i = r, \theta, z$) are defined by

$$T_r = v_r \frac{\partial v_r}{\partial r} + v_z \frac{\partial v_r}{\partial z} + \frac{v_\theta}{r} \left(\frac{\partial v_r}{\partial \theta} - v_\theta \right) \quad (26.134)$$

$$T_\theta = v_r \frac{\partial v_\theta}{\partial r} + v_z \frac{\partial v_\theta}{\partial z} + \frac{v_\theta}{r} \left(\frac{\partial v_\theta}{\partial \theta} + v_r \right) \quad (26.135)$$

$$T_z = v_r \frac{\partial v_z}{\partial r} + \frac{v_\theta}{r} \frac{\partial v_z}{\partial \theta} + v_z \frac{\partial v_z}{\partial z} \quad (26.136)$$

and the viscous terms F_i for Newtonian fluids by

$$F_r = \frac{\partial}{\partial r} \left(\frac{1}{r} \frac{\partial}{\partial r} (r v_r) \right) + \frac{1}{r^2} \frac{\partial^2 v_r}{\partial \theta^2} + \frac{\partial^2 v_r}{\partial z^2} - \frac{2}{r^2} \frac{\partial v_\theta}{\partial \theta} \quad (26.137)$$

$$F_\theta = \frac{\partial}{\partial r} \left(\frac{1}{r} \frac{\partial}{\partial r} (r v_\theta) \right) + \frac{1}{r^2} \frac{\partial^2 v_\theta}{\partial \theta^2} + \frac{\partial^2 v_\theta}{\partial z^2} + \frac{2}{r^2} \frac{\partial v_r}{\partial \theta} \quad (26.138)$$

$$F_z = \frac{1}{r} \frac{\partial}{\partial r} \left(r \frac{\partial v_z}{\partial r} \right) + \frac{1}{r^2} \frac{\partial^2 v_z}{\partial \theta^2} + \frac{\partial^2 v_z}{\partial z^2} \quad (26.139)$$

The right-hand side $R(r, \theta, \zeta)$ is given in Eq. (26.12) for the pipe flow example. The axial component of the gradient of the basic pressure P_0 is constant according to the assumptions stated for pipe flow in the beginning of Appendix D. It is clear that the number of pdes is reduced by one as mass balance, i.e. the Poisson pde for the pressure, is eliminated. It is straightforward to prove with the aid of the energy method that the divergence of velocity remains zero if it was zero initially; the details of the proof can be found in Majda and Bertozzi [5] Sect. 1.8. This version, consisting of three equations (26.131) and (26.132) and (26.133), of the Navier–Stokes pdes is called Leray pdes; it finds application in the theoretical analysis of existence and

regularity of the solutions of the Navier–Stokes equations. Further development of the theory can be found in Constantin and Foias [9], Constantin [10].

Summary

The formal solution of the Poisson pde for the pressure using the Green’s function method allows the reduction of the number of equations in the Navier–Stokes system from four to three. The resulting nonlinear equations are for incompressible fluids of integro-differential type that makes them very difficult to study and solve.

References

1. Boyd, J.P.: Chebyshev and Fourier Spectral Methods. Dover Publ. Inc., Mineola, New York (2001)
2. Kollmann, W.: Simulation of vorticity dominated flows using a hybrid approach: i formulation. *Comput. Fluids* **36**, 1638–1647 (2007)
3. Abramowitz, M., Stegun, I.A.: Handbook of Mathematical Functions. Dover, New York (1972)
4. Olver, F.W., Lozier, D.W., Boisvert, R.F., Clark, C.W.: NIST Handbook of Mathematical Functions. Cambridge University Press, U.K. (2010)
5. Majda, A.J., Bertozzi, A.L.: Vorticity and Incompressible Flow. Cambridge University Press, Cambridge, U.K. (2002)
6. Canuto, C., Hussaini, M.Y., Zang, T.A.: Spectral Methods in Fluid Dynamics. Springer, Berlin (1988)
7. Hartmann, P.: Ordinary Differential Equations. SIAM, Philadelphia (2002)
8. Duffy, D.G.: Green’s Functions with Applications. Chapman & Hall/CRC, Boca Raton, Florida (2001)
9. Constantin, P., Foias, C.: Navier–Stokes Equations. University of Chicago Press (1988)
10. Constantin, P.: Euler equations, navier–stokes equations and turbulence. In: Mathematical Foundation of Turbulent Viscous Flows. Lecture Notes in Mathematics, vol. 1871, pp. 1–43 (2006)

Chapter 27

Appendix E: Semi-empirical Treatment of Simple Wall-Bounded Flows



Engineering models for turbulent flows are sets of finite numbers of equations (usually of differential type) to mimic the properties of selected classes of turbulent flows. They cannot claim rigorosity, since they apply unsupported guesses together with experimental information, dimensional analysis and mathematical properties to express the additional unknown terms (called closure models) as functions of the system variables. The results of model computations and an enormous number of experimental data have been condensed by T. B. Nickels in a finite set of analytical formulae that do not require the solution of differential equations, for the complete mean velocity with positive and negative pressure gradients, discussed in Sect. 27.1.2.

One of the earliest closure models is due to Prandtl, and it has retained its usefulness, since it deals with wall-bounded turbulent flows relevant to myriad applications. It is briefly considered to illustrate a method of generating closure models for engineering applications. Sophisticated closure strategies including the pdes for Reynolds stresses are discussed in Pope [1], Davidson [2], Jakirlic [3], Poinsot and Veynante [4], Durbin and Petterson Reif [5] and ample references therein.

27.1 Exact Moment pdes for Fully Developed Turbulent Channel Flow

The fully developed turbulent flow between two parallel flat plates is considered, neglecting the influence of the lateral sidewalls. The mean velocity profile is developed using closure assumptions and experimental information and compared to DNS results.

For comparison with accurate numerical simulations without closure models, the mean velocity $\langle u \rangle(y)$ and the mean pressure difference $\langle p \rangle(x, y) - p_w(x)$ are shown in Figs. 27.1 and 27.2 based on the DNS data of Moser et al. [6], Lee and Moser [7] (at higher Reynolds numbers than [6]).

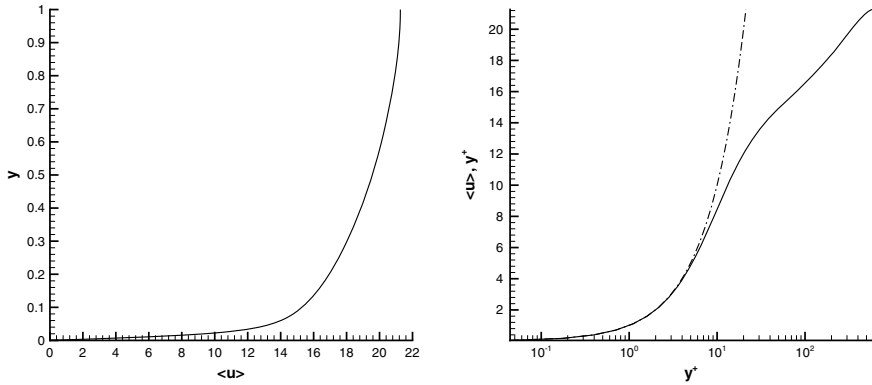


Fig. 27.1 Mean velocity $\langle u \rangle (2y/h)$, $0 \leq y \leq h/2$ in linear (left graph) and semi-logarithmic scale (right graph) as function of y^+ for turbulent channel flow according to the DNS simulation data of Moser et al. [6]. The Reynolds number based on the wall shear velocity u^* (27.15) and the channel half-width δ is $Re_\tau = 590$. The right graph shows the mean velocity in semi-logarithmic scale and the exact solution $u^+ = y^+$ valid in the viscous sublayer as dot-dashed line

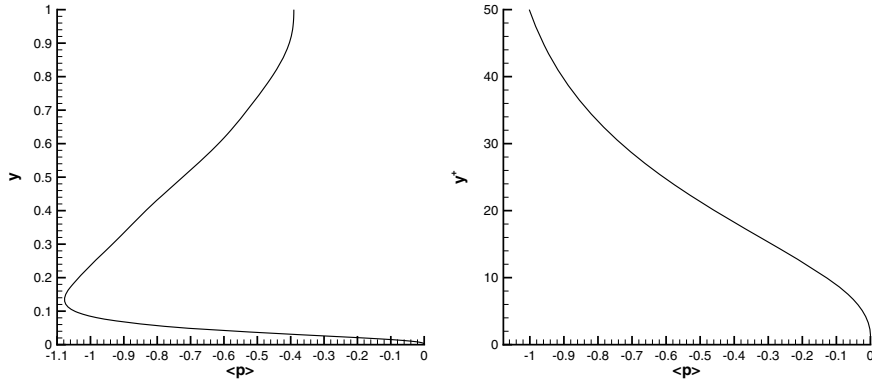


Fig. 27.2 Mean pressure $\langle p \rangle(x, 2y/h) - p_w(x)$ (left graph, where p_w is the mean wall pressure) and near-wall variation (right graph) as function of y^+ for turbulent channel flow according to the DNS simulation data of Moser et al. [6]. The Reynolds number based on the wall shear velocity u^* (27.15) and the channel half-width δ is $Re_\tau = 590$

Nickels [8] developed an interpolation formula for the mean velocity for a class of simple, wall-bounded turbulent shear flows such as boundary layers and channel flow that represents accurately the DNS results discussed in Sect. 27.1.2.

Fully developed means that all statistical one-point moments except the mean pressure are independent of the x -coordinate along the channel. The turbulent flow is plane in the mean, i.e. all mean values and one-point correlations are independent of the lateral coordinate z , and it is steady in the mean, i.e. all mean values and one-time correlations are time independent. The latter condition implies that the mean pressure gradient along the channel must be maintained by an external source (pump);

otherwise, the flow would decay. This external source provides the energy input that balances in the mean the loss of mechanical energy due to viscous dissipation. The averaged Navier–Stokes equations (21.8) and (21.13) are for steady (in the mean) plane flows reduced to

$$\frac{\partial \langle u \rangle}{\partial x} + \frac{\partial \langle v \rangle}{\partial y} = 0 \quad (27.1)$$

and

$$\langle u \rangle \frac{\partial \langle u \rangle}{\partial x} + \langle v \rangle \frac{\partial \langle u \rangle}{\partial y} = -\frac{1}{\rho} \frac{\partial \langle p \rangle}{\partial x} + \frac{\partial}{\partial x} [\nu \frac{\partial \langle u \rangle}{\partial x} - \langle u'^2 \rangle] + \frac{\partial}{\partial y} [\nu \frac{\partial \langle u \rangle}{\partial y} - \langle u' v' \rangle] \quad (27.2)$$

$$\langle u \rangle \frac{\partial \langle v \rangle}{\partial x} + \langle v \rangle \frac{\partial \langle v \rangle}{\partial y} = -\frac{1}{\rho} \frac{\partial \langle p \rangle}{\partial y} + \frac{\partial}{\partial x} [\nu \frac{\partial \langle v \rangle}{\partial x} - \langle u' v' \rangle] + \frac{\partial}{\partial y} [\nu \frac{\partial \langle v \rangle}{\partial y} - \langle v'^2 \rangle] \quad (27.3)$$

The boundary conditions are given by no-slip at the walls

$$\langle u \rangle(x, 0) = \langle v \rangle(x, 0) = \langle u \rangle(x, H) = \langle v \rangle(x, H) = 0 \quad (27.4)$$

$$\langle u'^2 \rangle(x, 0) = \langle u' v' \rangle(x, 0) = \langle v'^2 \rangle(x, 0) = 0$$

$$\langle u'^2 \rangle(x, H) = \langle u' v' \rangle(x, H) = \langle v'^2 \rangle(x, H) = 0$$

The assumption of fully developed turbulent flow implies that mean velocity and stress profiles are self-similar, i.e. $\langle u \rangle(y)$, $\langle v \rangle(y)$ and $\langle v'_\alpha v'_\beta \rangle(y)$ hold. However, the mean pressure depends $\langle p \rangle(x, y)$ in a particular way on x and y as will be shown below as a consequence of the averaged momentum balances.

The averaged mass balance implies then that

$$\frac{\partial \langle v \rangle}{\partial y} = 0$$

holds and the boundary conditions imply

$$\langle v \rangle = 0 \quad (27.5)$$

which is the first part of the solution, obtained without recourse to a closure assumption.

The averaged momentum balances emerge thus in the form

$$0 = -\frac{1}{\rho} \frac{\partial \langle p \rangle}{\partial x} + \frac{\partial}{\partial y} [\nu \frac{\partial \langle u \rangle}{\partial y} - \langle u' v' \rangle] \quad (27.6)$$

$$0 = -\frac{1}{\rho} \frac{\partial \langle p \rangle}{\partial y} - \frac{\partial}{\partial y} \langle v'^2 \rangle \quad (27.7)$$

They constitute the remaining system to be solved and it is clear that we have only two equations for four unknowns: $\langle u \rangle(y)$, $\langle p \rangle(x, y)$, $\langle u'v' \rangle(y)$, $\langle v'^2 \rangle(y)$.

The mean pressure field is considered next. Integrating the y -momentum balance from the wall into the flow field leads to

$$\frac{1}{\rho} \langle p \rangle(x, y) = -\langle v'^2 \rangle(y) + C(x) \quad (27.8)$$

where $C(x)$ is an arbitrary function of x . Setting y to zero and using the boundary condition for the Reynolds stress component shows that

$$C(x) = \frac{1}{\rho} \langle p \rangle(x, 0) \quad (27.9)$$

holds and, denoting the wall pressure by $P_0(x) \equiv \langle p \rangle(x, 0)$, we find that the pressure is given by

$$\langle p \rangle(x, y) = P_0(x) - \rho \langle v'^2 \rangle(y) \quad (27.10)$$

This is the solution for the mean pressure, but it is not explicit, since it contains two unknowns, the mean pressure $\langle p \rangle(x, y)$ and the normal stress component $\langle v'^2 \rangle(y)$. It is important to recognize that for turbulent flows, unlike laminar flows, the mean pressure is not uniform across the channel/pipe and boundary layers but varies with the Reynolds stress component $\langle v'^2 \rangle(y)$ as the DNS simulation of Moser et al. [6] clearly shows for channel flow in Figs. 27.1 and 27.2. The Reynolds normal stress profiles $\langle u^2 \rangle(y)$ (full line), $\langle v^2 \rangle$ (dot-dashed line) and $\langle w^2 \rangle$ (dashed line) obtained by DNS are shown in Fig. 27.3 with near variation as function of y^+ in the right graph. The shear stress component together with the total shear stress (dot-dashed line) is presented in Fig. 27.4 (left graph), and near-wall details are shown in the right graph. Note that the total shear stress (27.20) derived below is a rare analytic result deduced from the geometric symmetries of the averaged flow field and the condition that the turbulent flow is fully developed.

However, it is sufficient for the present purpose to differentiate (27.10) with respect to x

$$\frac{\partial \langle p \rangle}{\partial x} = \frac{\partial P_0}{\partial x} \quad (27.11)$$

It becomes clear then that the pressure gradient in the x -momentum balance can be replaced by the wall pressure gradient $\partial P_0 / \partial x$. Since the wall pressure is not part of the solution, but easily accessible to measurement, it is assumed known in the following. The wall pressure must be maintained by external means to keep the turbulent flow at a steady state in the mean.

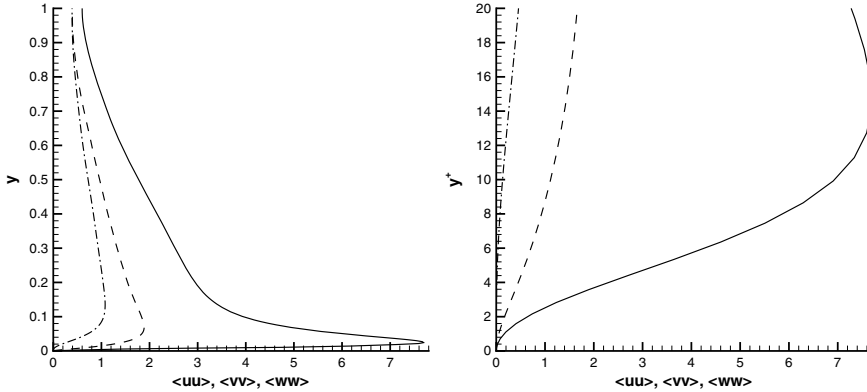


Fig. 27.3 Normal stress component profiles, $\langle u^2 \rangle (2y/h)$ (full line), $\langle v^2 \rangle (2y/h)$ (dot-dashed line), $\langle w^2 \rangle (2y/h)$ (dashed line), for turbulent channel flow according to the DNS data of Moser et al. [6]. The Reynolds number based on the wall shear velocity u^* (27.15) and the channel half-width δ is $Re_\tau = 590$. The right graph shows the near-wall variation as function of y^+

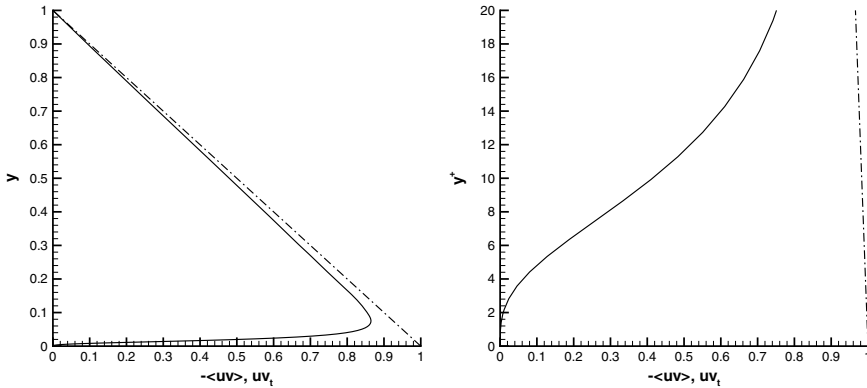


Fig. 27.4 The Reynolds shear stress $-(uv)(x, 2y/h)$ and the total shear stress $-(uv) + \frac{1}{Re} \frac{\partial \langle U \rangle}{\partial y}$ (dot-dashed line) for turbulent channel flow according to the DNS data of Moser et al. [6] for $Re_\tau = 590$. The right graph shows the near-wall variation as function of y^+

Integrated x -momentum balance

The x -momentum balance is now given by

$$0 = -\frac{1}{\rho} \frac{\partial P_0}{\partial x} + \frac{\partial}{\partial y} \left[\nu \frac{\partial \langle u \rangle}{\partial y} - \langle u' v' \rangle \right] \quad (27.12)$$

containing only two unknown terms, the mean velocity and the Reynolds shear stress. Inspecting equation (27.12), it becomes apparent that it contains the pressure gradient term, which is at most a function of x but not y , and the viscous and turbulent stress terms, which are for fully developed turbulent flows a function of y but not x . It

follows that the pressure gradient and the stress term must be constants to satisfy the condition of fully developed flow. Integrating the momentum balance (27.12) from the wall into the flow field, the relation

$$C = -\frac{y}{\rho} \frac{\partial P_0}{\partial x} + \nu \frac{\partial \langle u \rangle}{\partial y} - \langle u' v' \rangle \quad (27.13)$$

is obtained. The integration constant C follows from the boundary condition at the lower wall $y = 0$: $\langle u' v' \rangle(0) = 0$. Defining the wall shear stress τ_0 by

$$\tau_0 = \mu \frac{\partial \langle u \rangle}{\partial y}(0) \quad (27.14)$$

and the wall shear velocity u^* by

$$u^* = \sqrt{\frac{\tau_0}{\rho}} \quad (27.15)$$

the integration constant

$$C = \frac{\tau_0}{\rho} = u^{*2} \quad (27.16)$$

emerges. The integrated momentum balance is then

$$\nu \frac{\partial \langle u \rangle}{\partial y} - \langle u' v' \rangle = \frac{\tau_0}{\rho} + \frac{y}{\rho} \frac{\partial P_0}{\partial x} \quad (27.17)$$

The condition of a fully developed channel flow leads to the relation between the wall shear stress and the pressure gradient. The mean velocity profile must be symmetric with respect to the center of the channel, hence are the laminar and the turbulent shear stress components zero at $y = h/2$ and

$$0 = \frac{\tau_0}{\rho} + \frac{h}{2\rho} \frac{\partial P_0}{\partial x}$$

or

$$\frac{1}{\rho} \frac{\partial P_0}{\partial x} = -\frac{2}{h} \frac{\tau_0}{\rho} = -\frac{2}{h} u^{*2} \quad (27.18)$$

follows. The integrated momentum balance appears finally as

$$\nu \frac{\partial \langle u \rangle}{\partial y} - \langle u' v' \rangle = u^{*2} \left(1 - \frac{2y}{h}\right) \quad (27.19)$$

This equation can be regarded as exact solution for the total shear stress $\tau_t \equiv \nu \frac{\partial \langle u \rangle}{\partial y} - \langle u'v' \rangle$

$$\tau_t = u^{*2} \left(1 - \frac{2y}{h}\right) \quad (27.20)$$

hence a linear profile. This exact result is clearly reflected in the DNS result in Fig. 27.3 (right graph) showing the turbulent part of the total shear stress being nearly linear except close to the wall boundary. Equation (27.19) cannot be solved for the mean velocity or the turbulent shear stress without a closure model, since it contains those two unknowns: The mean velocity $\langle u \rangle(y)$ and the Reynolds shear stress component $\langle u'v' \rangle(y)$.

Dimensionless forms

The integrated momentum balance (27.19) can be made dimensionless in several ways. A Reynolds number is defined by

$$Re \equiv \frac{u^*h}{\nu} \quad (27.21)$$

using the wall property u^* and the global (or outer) property h and define the dimensionless velocities by

$$u^+ \equiv \frac{\langle u \rangle}{u^*}, \quad u \equiv \frac{u'}{u^*}, \quad v \equiv \frac{v'}{u^*} \quad (27.22)$$

and the dimensionless wall distance by

$$\eta \equiv \frac{y}{h} \quad (27.23)$$

The integrated momentum balance (27.19) is made dimensionless using these mixed scales

$$\frac{1}{Re} \frac{du^+}{d\eta} - \langle uv \rangle = 1 - 2\eta \quad (27.24)$$

It is useful for the analysis of the centre part of the channel away from the wall boundaries. A second version of the dimensionless momentum balance is obtained if the wall distance is made dimensionless using wall variables only

$$y^+ \equiv y \frac{u^*}{\nu} \quad (27.25)$$

leading to

$$\frac{du^+}{dy^+} - \langle uv \rangle = 1 - \frac{2}{Re} y^+ \quad (27.26)$$

This version is useful for the analysis of the near-wall region of the flow.

27.1.1 The Closure Problem

It is not yet feasible to produce direct (non-iterative) numerical solution schemes for infinite systems of pdes or functional differential equations. It follows that there are two ways to approach this difficult problem: Either a rigorous method is found to identify the modes relevant to a turbulent flow in the hope that this number is finite and, therefore, in principle accessible to numerical solution methods, or a procedure has to be devised to truncate this infinite system of moment equations at a finite level using experimental, DNS information and theoretical arguments. The construction of such a truncation cannot be done rigorously and this constitutes a serious difficulty usually called the closure problem. We should keep in mind that for many applications the knowledge of mean velocity and mean pressure is sufficient to answer questions arising in industrial design and development. Hence, we will attempt to close the system of moment equations at a low level (first- and second-order moments) using empirical expressions for additional unknowns appearing in the moment equations.

Significant effort has been directed during the last 50 years to the development of sophisticated closure models for wall-bounded turbulent flows (Pope [1], Chap. 11, Durbin and Petterson Reif [5], Davidson [2], Chap. 4) to construct solvable systems of equations for mean fields and second-order moments. Results from DNS simulations of turbulence near fixed walls, analytic tools and experimental data have been applied successfully to improve turbulence closures for first- and second-order moments. For instance, Jakirlic and Hanjalic [3] apply DNS results to develop a closure model for the pdes governing the dissipation rate tensor and/or its trace, which are very difficult to measure, Pearson et al. [9] and which have been recognized as the weakest link in many closure models.

Turbulence model based on the idea of mixing length

The absence of a rigorous theory of turbulent flows leads to attempts at predicting the properties of turbulent flows for industrial applications. Unfortunately, no systematic method of approximation has been found so far, apart from DNS, which is not accessible for applications at high Reynolds numbers and flow domains with geometrically complex boundaries. Hence, a set of tools called closure models based on experimental and elementary mathematical properties have been developed to interpolate between verified flow cases. They cannot be systematically refined, hence have not yet reached the level of approximation with rigorous error estimates, but serve as a mere guide for the designer.

Closure models for the first-order moment equations for the mean velocity $\langle v_\alpha \rangle$ and the mean pressure $\langle p \rangle$ obtained in the previous section (21.8), (21.13) are based on assumptions that express the additional unknowns, the Reynolds stresses $\langle v'_\alpha v'_\beta \rangle$, in terms of the mean velocity. In general, this assumption appears as

$$\tau_{\alpha\beta}^t = \mathcal{F}_{\alpha\beta}(\nabla \langle \mathbf{v} \rangle, \dots) \quad (27.27)$$

where $\nabla \langle \mathbf{v} \rangle$ denotes the mean deformation rate and the dots indicate the dependence on higher derivatives and transport coefficients. The mixing length model of Prandtl is one of these models and it will be discussed in detail.

The closure models of Boussinesq and Prandtl

Prandtl based his closure model on the idea suggested first by Boussinesq to define a turbulent viscosity analogous to the material property viscosity. The Reynolds stresses are thus modelled by

$$-\rho \langle v'_\alpha v'_\beta \rangle = \mu_t \left(\frac{\partial \langle v_\alpha \rangle}{\partial x_\beta} + \frac{\partial \langle v_\beta \rangle}{\partial x_\alpha} \right) - \frac{2}{3} \rho \delta_{\alpha\beta} k \quad (27.28)$$

where $\mu_t(\mathbf{x}, t)$ is the turbulent viscosity, which is a flow property depending on location and time in contrast to μ , which is the material property called dynamic viscosity (which is essentially a function of temperature), and k denotes the kinetic energy of turbulence defined by

$$k(\mathbf{x}, t) \equiv \frac{1}{2} \langle v'_\alpha v'_\alpha \rangle = \frac{1}{2} (\langle u'^2 \rangle + \langle v'^2 \rangle + \langle w'^2 \rangle) \quad (27.29)$$

(we will frequently use the notation $u = v_1$, $v = v_2$, $w = v_3$ for Cartesian components). Prandtl constructed the turbulent viscosity as the product of a velocity scale v^* and a length scale l and density ρ (which is constant for incompressible flows)

$$\mu_t = \rho v^* l \quad (27.30)$$

This construction is analogous to the expression for the laminar viscosity in statistical mechanics, where

$$\mu = \rho V \lambda \quad (27.31)$$

where $V = \sqrt{\langle v'_\alpha v'_\alpha \rangle}$ is the molecular velocity scale (v'_α denotes here the velocity of particles) and λ is the mean free path length. We interpret the scales in turbulent flows as follows.

v^* is a measure for the intensity of the velocity fluctuations and l is the distance over which the changes of the mean velocity are of order unity. For the construction of velocity and length scales in turbulent flows, a restriction is introduced: We consider only turbulent flows with strong mean shear. Examples for this type of flow are boundary layers, jets, wakes and mixing layers. Let the $x_1 = x$ -direction be the main flow direction and the $x_2 = y$ -direction, where the flow changes rapidly and $x_3 = z$ the lateral direction, where the flow does not change appreciably, and then we can construct the velocity scale according to Prandtl as

$$v^* = l \left| \frac{\partial \langle u \rangle}{\partial y} \right| \quad (27.32)$$

and the turbulent viscosity is thus

$$\mu_t = \rho l^2 \left| \frac{\partial \langle u \rangle}{\partial y} \right| \quad (27.33)$$

The length scale $l(\mathbf{x}, t)$ for this restricted class of flows is called Prandtl mixing length. There is no general way to construct this length unless one or more pdes for turbulence quantities are added to the system of averaged Navier–Stokes equations. However, there are special cases where the length scale has been established. We consider wall-bounded flows such as the boundary layer, pipe and channel flows. For this type of flows, the mixing length is essentially a function of the wall distance; for the fully turbulent high shear region in channels, it is given by

$$l = \kappa y \quad (27.34)$$

where y is the normal distance from the wall and $\kappa = 0.41$ is the von Karman constant that has been determined by comparison with experimental data. It must be modified very close to the wall and in the center of the channel, where the shear stress ceases to be dominant as it approaches zero.

Application of the mixing length model

The mean velocity in the turbulent channel flow can be determined if we apply a closure model to express the Reynolds shear stress $\langle u'v' \rangle$ in terms of the mean velocity. We apply the mixing length model (27.28), (27.33), (27.34) for this purpose and obtain for the Reynolds shear stress (dividing by the constant density)

$$-\langle u'v' \rangle = \nu_t \frac{\partial \langle u \rangle}{\partial y} \quad (27.35)$$

and

$$\nu_t = l^2 \left| \frac{\partial \langle u \rangle}{\partial y} \right| \quad (27.36)$$

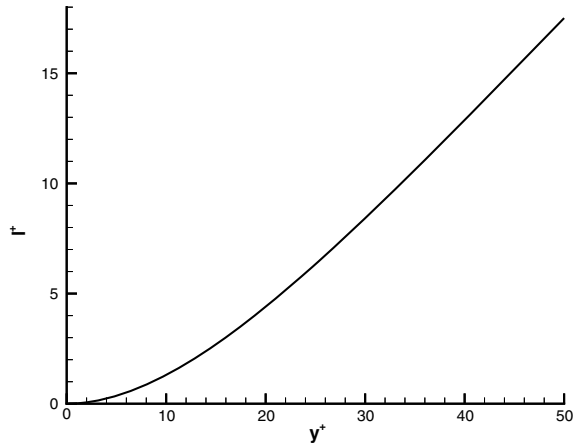
and the mixing length $l(y)$ is only a function of the wall distance y . We recall that this model is applicable to the regions of turbulent flows where the mean shear is strong; hence, we restrict it to the near-wall layer of the channel flow. Furthermore, it should be noted that (27.28) requires in general the kinetic energy of turbulence $k(\mathbf{x}, t)$, which is not known, but the mixing length model for the Reynolds shear stress component does not require it since $\delta_{12} = 0$.

The mixing length model in dimensionless form appropriate for the near-wall layer is then given by

$$-\langle uv \rangle = l^{+2} \left| \frac{du^+}{dy^+} \right| \left| \frac{du^+}{dy^+} \right| \quad (27.37)$$

and the integrated momentum balance (27.26) emerges as

Fig. 27.5 Mixing length in the near-wall layer of a fully developed turbulent channel flow with the van Driest wall correction



$$\frac{du^+}{dy^+} + l^{+2} \left(\frac{du^+}{dy^+} \right)^2 = 1 - \frac{2}{Re} y^+ \quad (27.38)$$

appropriate for the lower half of the channel describing the lower wall (the second term on the left side is negative in the upper half of the channel). The mixing length model is complete once we specify the the mixing length $l^+(y^+)$ and the ode with the boundary condition $u^+(0) = 0$ can then be solved analytically. The ode is a quadratic polynomial for du^+/dy^+ with the roots given by

$$\frac{du^+}{dy^+} = -\frac{1}{2l^{+2}} \left[-1 \pm \sqrt{1 + 4l^{+2}(1 - \frac{2y^+}{Re})} \right]$$

Since u^+ must be non-negative, the positive root is the realizable one and we recast the solution as

$$\frac{du^+}{dy^+} = \frac{2(1 - \frac{2y^+}{Re})}{1 + \sqrt{1 + 4l^{+2}(1 - \frac{2y^+}{Re})}}$$

Integration produces the desired result

$$u^+(y^+) = 2 \int_0^{y^+} dy \frac{(1 - \frac{2y}{Re})}{1 + \sqrt{1 + 4l^{+2}(y)(1 - \frac{2y}{Re})}} \quad (27.39)$$

It remains to specify the mixing length as function of the distance from the wall.

The suggestion of Prandtl (27.34) $l^+ = \kappa y^+$ is valid in the turbulent part of the near-wall layer, where the turbulent shear stress dominates, but it is not valid very close to the wall, where the turbulent shear stress is less important than the laminar

shear stress. Hence, an empirical correction of the mixing length must be introduced to account for the variation of the turbulent shear stress very close to the wall. This correction was suggested by Van Driest and the mixing length in the near wall is then given by

$$l^+(y^+) = \kappa y^+ [1 - \exp(-\frac{y^+}{A^+})] \quad (27.40)$$

where $A^+ = 26$ (Van Driest damping factor) was determined by comparison with measurements. The variation of the mixing length with wall distance is shown in Fig. 27.5, and it is clear that it approaches the Prandtl model with increasing wall distance. The momentum balance is now a closed ode for the single unknown $u^+(y^+)$

$$\frac{du^+}{dy^+} + \kappa^2 y^{+2} [1 - \exp(-\frac{y^+}{A^+})]^2 \left(\frac{du^+}{dy^+} \right)^2 = 1 - \frac{2}{Re} y^+ \quad (27.41)$$

with the boundary condition

$$u^+(0) = 0 \quad (27.42)$$

It has the analytic solution (27.39) which appears now in the form

$$u^+(y^+) = 2 \int_0^{y^+} dy \frac{(1 - \frac{2y}{Re})}{1 + \sqrt{1 + 4\kappa^2 y^2 (1 - \frac{2y}{Re}) [1 - \exp(-\frac{y}{A^+})]^2}} \quad (27.43)$$

This profile of the mean velocity in the near-wall layer of fully developed turbulent channel flow is shown in Fig. 27.6. The profile is quite different from the laminar one; it is much fuller and thus less susceptible to separation under the influence of positive pressure gradients.

Two special cases are now considered, where the wall distance satisfies

$$y^+ \ll \frac{1}{2} Re \quad (27.44)$$

The first case is the viscous sublayer: Restricting the wall distance further to values close to the wall, such that

$$|\langle uv \rangle| \ll \left| \frac{du^+}{dy^+} \right| \quad (27.45)$$

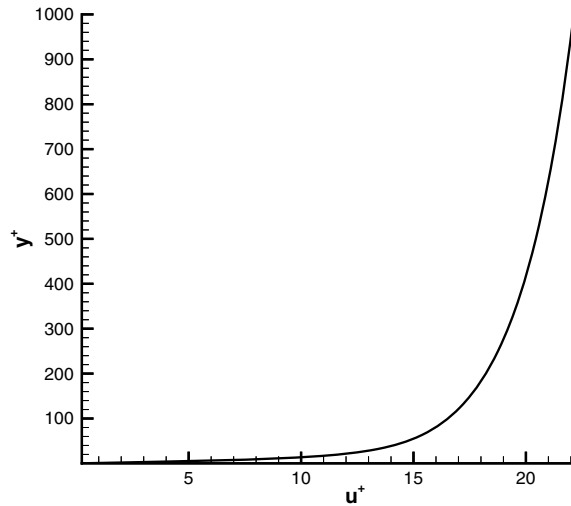
holds, simplifies the integrated momentum balance (27.26) to

$$\frac{du^+}{dy^+} = 1 \quad (27.46)$$

which has the solution

$$u^+ = y^+ \quad (27.47)$$

Fig. 27.6 Mean velocity in the near-wall layer of a fully developed turbulent channel flow ($Re = 10,000$) according to the mixing length model with the van Driest wall correction (27.43) in linear scale



This famous result, called the **law of the wall**, shows that the mean velocity in the viscous sublayer of the inner layer of the channel flow varies linearly with wall distance. The second case is the fully turbulent part of the inner layer (it can be regarded as the outer part of the inner layer) where

$$\left| \frac{du^+}{dy^+} \right| \ll |\langle uv \rangle| \quad (27.48)$$

holds, and hence the laminar shear stress is negligible compared to the turbulent stress. The mixing length (27.34) is now applicable, because we are outside the viscous sublayer, and the integrated momentum balance (27.41) is reduced to

$$\kappa^2 y^{+2} \left(\frac{du^+}{dy^+} \right)^2 = 1 \quad (27.49)$$

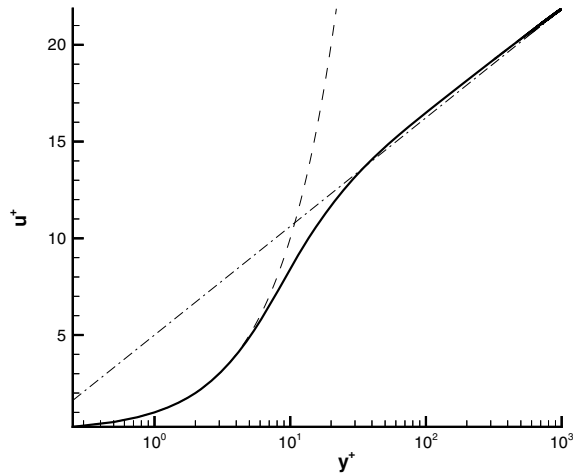
which has the solution

$$u^+ = \frac{1}{\kappa} \log(y^+) + B \quad (27.50)$$

where the constant $B = 5.0$ is again determined by comparison with experiments (it is in fact a weak function of Re). This is called the logarithmic profile valid in the log layer, which is the outer part of the near-wall layer. The near-wall layer is thus composed of three layers: The viscous sublayer, an intermediate layer and the log layer. The general form of the mean velocity profile is given by the integral solution (27.43), which contains all three layers. The results

for the near-wall layer with the two special cases are shown in Fig. 27.7, where the viscous sublayer profile (27.47) is the dashed line and the logarithmic profile (27.50)

Fig. 27.7 Mean velocity in the near-wall layer of a fully developed turbulent channel flow ($Re = 10,000$) according to the mixing length model with the van Driest wall correction (27.43) in semi-logarithmic scale. The dashed line is the law of the wall (27.47) and the dot-dashed line is the logarithmic profile (27.50)



as dot-dashed line. The viscous sublayer extends from $y^+ = 0$ to about $y^+ = 5$, the intermediate layer from $y^+ = 5$ to about $y^+ = 30$ and the log layer from $y^+ = 30$ to an upper limit that depends on the Reynolds number. The mean velocity in the inner part of the channel flow (outside the near-wall layer) is governed by a profile deviating from the near-wall function (27.43) called the law of the wake. The mixing length associated with this part of the flow is essentially constant. Details can be found in the literature, for instance, Cebeci and Bradshaw [10], Schlichting [11].

27.1.2 Empirical Mean Velocity Profiles: The Nickels Interpolant

The turbulent flow near-wall boundaries is of enormous importance for myriad applications; hence, numerous experimental and numerical research works have been carried out to determine the elementary properties of turbulent flows with wall boundaries. The empirical theories based on experiments, closure assumptions and numerical simulations provide the mean velocity profiles in flows with mean pressure gradient.

Wosnik, Castillo and George [12] constructed a refined theory for the mean velocity and skin friction in fully developed turbulent pipe and channel flows. The analysis is based on scaling relations developed from dimensional arguments and physical insight. They show that the mean velocity for pipe and channel flows requires the meso-layer as part of the near-wall layer.

Nickels [13] developed a composite velocity profile expression valid for boundary layers, channel and pipe flows that covers the complete layer for a significant range of pressure gradients. It consists of approximations for the three layers that are

consistent with the boundary conditions and the asymptotic properties (free stream conditions or symmetry axis).

The sublayer

The functional form chosen for the sublayer is according to Nickels [13]

$$u^+ = y_c^+ \left\{ 1 - \left[1 + 2 \frac{y^+}{y_c^+} + \frac{1}{2} (3 - p_x^+ y_c^+) \left(\frac{y^+}{y_c^+} \right)^2 - \frac{3}{2} p_x^+ y_c^+ \left(\frac{y^+}{y_c^+} \right)^3 \right] \exp \left(- \frac{3 y^+}{y_c^+} \right) \right\} \quad (27.51)$$

satisfying the boundary condition $u^+(0) = 0$ and asymptotically approaches a constant as $y^+ \rightarrow \infty$, y_c^+ is a parameter that measures the thickness of the sublayer. The pressure gradient parameter is defined by

$$p_x^+ \equiv \frac{\nu}{\rho U_\tau^3} \frac{dp}{dx} \quad (27.52)$$

where ν is the kinematic viscosity and $U_\tau = \sqrt{\frac{\tau_w}{\rho}}$ is the wall shear velocity.

The logarithmic region

The logarithmic region of a boundary layer is the outer part of the inner layer where viscosity is negligible. Nickels constructs the profile in this region such that it satisfies the boundary condition without interfering with the correct growth in the sublayer and asymptotes to a constant as $y^+ \rightarrow \infty$. The result is given by

$$u^+ = \frac{1}{6\kappa} \ln \left[\frac{1 + (0.6 \frac{y^+}{y_c^+})^6}{1 + \eta^6} \right] \quad (27.53)$$

where $\eta = \frac{y}{\delta}$ and κ is the von Karman constant. The von Karman constant in fact varies with the pressure gradient, hence

$$\frac{\kappa}{\kappa_0} = \frac{1}{\sqrt{1 + p_x^+ y_c^+}} \quad (27.54)$$

where $\kappa_0 = 0.39$.

The wake region

The wake region (or outer part of the boundary layer) is approximated by

$$w(\eta) = b \left[1 - \exp \left(- \frac{5(\eta^4 + \eta^8)}{1 + 5\eta^3} \right) \right] \quad (27.55)$$

where b is a measure of the wake strength (equivalent to Coles' wake parameter, [14]).

The composite profile

The sum of the profiles for the three regions of a boundary layer emerges according to Nickels [13] in the form

$$u^+(y^+) = y_c^+ \left\{ 1 - \left[1 + 2 \frac{y^+}{y_c^+} + \frac{1}{2} (3 - p_x^+ y_c^+) \left(\frac{y^+}{y_c^+} \right)^2 - \frac{3}{2} p_x^+ y_c^+ \left(\frac{y^+}{y_c^+} \right)^3 \right] \exp\left(-\frac{3y^+}{y_c^+}\right) \right\} \\ + \frac{1}{6\kappa_0} \sqrt{1 + p_x^+ y_c^+} \ln\left(\frac{1 + (0.6 \frac{y^+}{y_c^+})^6}{1 + \eta^6}\right) + b \left[1 - \exp\left(-\frac{5(\eta^4 + \eta^8)}{1 + 5\eta^3}\right) \right] \quad (27.56)$$

The von Karman constant is $\kappa_0 = 0.39$ and the sublayer parameter y_c^+ can be computed as the smallest positive root of

$$p_x^+ y_c^{+3} + y_c^{+2} - R_c^2 = 0 \quad (27.57)$$

once the pressure gradient parameter p_x^+ is known. The Reynolds number $R_c = 12$ has a universal value, for justification see Nickels [13]. Equation (27.56) is valid with very good accuracy for the range of pressure gradients $-0.02 \leq p_x^+ \leq 0.06$. Note that strong pressure gradients lead to values $|p_x^+| > 0.005$. The final expression (27.56) for the mean velocity profile depends on three parameters: (i) The boundary layer thickness δ , (ii) The pressure gradient parameter p_x^+ and (iii) The wake parameter b . The Reynolds number is not set a priori but is determined iteratively by setting two parameters, for instance, δ and p_x^+ and iterating the wake parameter b until a specified Reynolds number is reached.

The example of a flat plate boundary layer with zero pressure gradient is characterized by $p_x^+ = 0$, hence is y_c according to (27.57) $y_c = R_c = 12$ and the velocity profile is determined by the thickness $\delta(x)$ and the wake parameter b

$$u^+(y^+) = y_c^+ \left\{ 1 - \left[1 + 2 \frac{y^+}{y_c^+} + \frac{3}{2} \left(\frac{y^+}{y_c^+} \right)^2 \right] \exp\left(-\frac{3y^+}{y_c^+}\right) \right\} \\ + \frac{1}{6\kappa_0} \ln\left(\frac{1 + (0.6 \frac{y^+}{y_c^+})^6}{1 + \eta^6}\right) + b \left[1 - \exp\left(-\frac{5(\eta^4 + \eta^8)}{1 + 5\eta^3}\right) \right] \quad (27.58)$$

The wake parameter b can be computed using experimental results as shown by Coles [14]. It requires the knowledge of boundary layer thickness δ , the displacement thickness δ^* and the wall shear velocity u^* leading to

$$b \approx \frac{\delta^*}{\delta} \frac{u_\infty}{u^*} - \frac{1}{\kappa} \quad (27.59)$$

Two examples for the Nickels method are shown in Fig. 27.8.

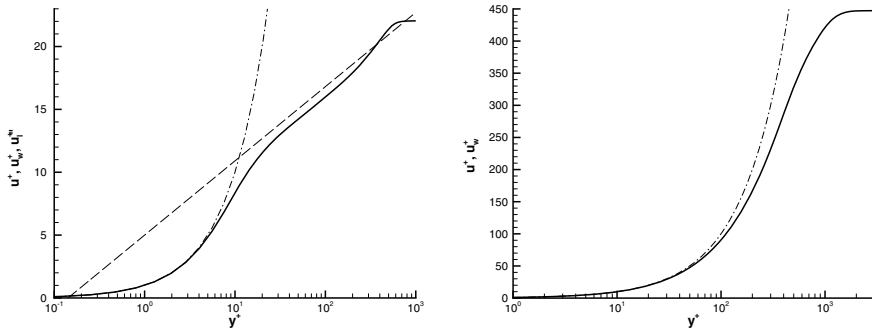


Fig. 27.8 Mean velocity for a fully developed turbulent boundary layer according to the Nickels correlation (27.56) in semi-logarithmic scale. The pressure gradient parameter is for the left/right graph $p_x = 0.002/ - 0.002$ and the wake parameter $b = 2.0$ is the same for both graphs ($\nu = 10^{-5} \text{ m}^2/\text{s}$, $\delta = 0.05 \text{ m}$, $u^* = 0.1 \text{ m/s}$ in both graphs). The dot-dashed line is the law of the wall (27.47), and the dashed line is the logarithmic profile (27.50)

Modifications for channel and pipe flows

Channel and pipe flows require a modification of the definition for η according to

$$\eta \equiv \frac{y}{R}, \quad \eta \equiv \frac{y}{h}$$

where R is the pipe radius and h the half-width of the channel. The logarithmic profile is modified to

$$u^+ = \frac{1}{6\kappa} \ln \left[\frac{1 + (0.6 \frac{y^+}{y_c})^6}{1 + \eta^6 + \eta^{12}} \right] \quad (27.60)$$

where the only change is in the denominator of the argument of the logarithm, and the wake profile to

$$w(\eta) = b \left[1 - \exp \left(-\frac{5(\eta^4 + \eta^8)}{1 + 5\eta^3 + 10.5\eta^8} \right) \right] \quad (27.61)$$

where the change is in the denominator of the argument of the exponential function. There is no discernible difference between pipe and channel flows.

References

1. Pope, S.B.: *Turbulent Flows*. Cambridge University Press, Cambridge, U.K. (2001)
2. Davidson, P.A.: *Turbulence*. Oxford University Press, Oxford, U.K. (2004)
3. Jakirlic, S., Hanjalic, K., Tropea, C.: Modeling rotating and swirling turbulent flows: a perpetual challenge. *AIAA J.* **40**, 1984–1996 (2002)

4. Poinsot, T., Veynante, D.: *Theoretical and Numerical Combustion*. R.T. Edwards, Philadelphia, PA (2001)
5. Durbin, P.A., Petterson Reif, B.A.: *Statistical Theory and Modeling for Turbulent Flows*. Wiley (2011)
6. Moser, R.D., Kim, J., Mansour, N.N.: DNS of turbulent channel flow. *Phys. Fluids* **11**, 943–945 (1999)
7. Lee, M., Moser, R.D.: Direct numerical simulation of turbulent channel flow up to $Re_\tau = 5200$. *JFM* **774**, 395–415 (2015)
8. Nickels, T.B.: *Turbulent Coflowing Jets and Vortex Ring Collisions*. University of Melbourne, Australia. Ph.D. thesis (1993)
9. Pearson, B.R., Krogstad, P.A., van de Water, W.: Measurements of the turbulent energy dissipation rate. *Phys. Fluids* **14**, 1288–1290 (2002)
10. Cebeci, T., Bradshaw, P.: *Momentum Transfer in Boundary Layers*. Hemisphere Publisher Corp, Washington (1977)
11. Schlichting, H.: *Boundary Layer Theory*. McGraw-Hill (1987)
12. Wosnik, M., Castillo, L., George, W.K.: A theory for turbulent pipe and channel flow. *JFM* **421**, 115–145 (2000)
13. Nickels, T.B.: Inner scaling for wall-bounded flows subject to large pressure gradients. *JFM* **521**, 217–239 (2004)
14. Coles, D.E.: The law of the wake in the turbulent boundary layer. *JFM* **1**, 191–226 (1956)

Chapter 28

Appendix F: Solutions to Problems



The solutions to the problems set at the end of each chapter are presented here. In some of the solutions, literature references are provided and additional material has been added to aid the interpretation of the results. The notational conventions introduced in Chap. 1 are used throughout, the summation convention applies to Greek subscripts, and lower case symbols indicate the spatial (Eulerian) and upper case symbols the material (Lagrangean) description. Vector and tensor variables are identified by boldface symbols. The Cartesian coordinates are denoted by x_α , v_α $\alpha = 1, 2, 3$, etc. or x, y, z, u, v, w , etc. interchangeably.

Solutions to problems in Chap. 2: Navier–Stokes equations.

Problem (2.1): Derive the dimensional vorticity pde (2.62) for a single, compressible Newtonian fluid using Cartesian coordinates.

Solution:

Mass balance (2.1)

$$\frac{D\rho}{Dt} + \rho \frac{\partial v_\alpha}{\partial x_\alpha} = 0$$

and momentum balance (2.2) divided by density

$$\frac{\partial v_\gamma}{\partial t} + v_\delta \frac{\partial v_\gamma}{\partial x_\delta} = -\frac{1}{\rho} \frac{\partial p}{\partial x_\gamma} + \frac{1}{\rho} \frac{\partial \tau_{\gamma\delta}}{\partial x_\delta} + g_\gamma$$

lead to

$$\frac{\partial \omega_\alpha}{\partial t} + v_\delta \frac{\partial \omega_\alpha}{\partial x_\delta} + \epsilon_{\alpha\beta\gamma} \frac{\partial v_\delta}{\partial x_\beta} \frac{\partial v_\gamma}{\partial x_\delta} = \frac{1}{\rho^2} \frac{\partial \rho}{\partial x_\beta} \frac{\partial p}{\partial x_\alpha} - \frac{1}{\rho} \epsilon_{\alpha\beta\gamma} \frac{\partial^2 p}{\partial x_\beta \partial x_\gamma} + \epsilon_{\alpha\beta\gamma} \frac{\partial}{\partial x_\beta} \left(\frac{1}{\rho} \frac{\partial \tau_{\gamma\delta}}{\partial x_\delta} \right) + \epsilon_{\alpha\beta\gamma} \frac{\partial g_\beta}{\partial x_\gamma}$$

by applying the curl $\epsilon_{\alpha\beta\gamma} \frac{\partial(\cdot)_\gamma}{\partial x_\beta}$ to the momentum balance. Note that the antisymmetry of the Levi-Civita symbol implies

$$\frac{1}{\rho} \epsilon_{\alpha\beta\gamma} \frac{\partial^2 p}{\partial x_\beta \partial x_\gamma} = 0$$

It remains to evaluate the term $\epsilon_{\alpha\beta\gamma} \frac{\partial v_\delta}{\partial x_\beta} \frac{\partial v_\gamma}{\partial x_\delta}$ using the relations (2.52) and (2.53)

$$\frac{\partial v_\delta}{\partial x_\beta} = s_{\beta\delta} - \frac{1}{2} \epsilon_{\delta\beta\eta} \omega_\eta, \quad \epsilon_{\alpha\beta\gamma} \epsilon_{\alpha\delta\eta} = \delta_{\beta\delta} \delta_{\gamma\eta} - \delta_{\beta\eta} \delta_{\gamma\delta}$$

The result is

$$\epsilon_{\alpha\beta\gamma} \frac{\partial v_\delta}{\partial x_\beta} \frac{\partial v_\gamma}{\partial x_\delta} = \omega_\alpha s_{\beta\beta} - \omega_\beta s_{\alpha\beta}$$

Noting that $s_{\beta\beta} = \frac{\partial v_\beta}{\partial x_\beta}$, mass balance can be used

$$\epsilon_{\alpha\beta\gamma} \frac{\partial v_\delta}{\partial x_\beta} \frac{\partial v_\gamma}{\partial x_\delta} = -\omega_\alpha \frac{1}{\rho} \frac{D\rho}{Dt} - \omega_\beta \frac{\partial v_\alpha}{\partial x_\beta}$$

and

$$\frac{D\omega_\alpha}{Dt} - \omega_\alpha \frac{1}{\rho} \frac{D\rho}{Dt} = \omega_\beta s_{\alpha\beta} + \frac{1}{\rho^2} \frac{\partial \rho}{\partial x_\beta} \frac{\partial p}{\partial x_\alpha} + \epsilon_{\alpha\beta\gamma} \frac{\partial}{\partial x_\beta} \left(\frac{1}{\rho} \frac{\partial \tau_{\gamma\delta}}{\partial x_\delta} \right) + \epsilon_{\alpha\beta\gamma} \frac{\partial g_\beta}{\partial x_\gamma}$$

The terms on the left side can be combined,

$$\frac{D\omega_\alpha}{Dt} = \rho \frac{D}{Dt} \left(\frac{\omega_\alpha}{\rho} \right) + \omega_\alpha \frac{1}{\rho} \frac{D\rho}{Dt}$$

and the final result

$$\rho \frac{D}{Dt} \left(\frac{\omega_\alpha}{\rho} \right) = \omega_\beta s_{\alpha\beta} + \frac{1}{\rho^2} \frac{\partial \rho}{\partial x_\beta} \frac{\partial p}{\partial x_\alpha} + \epsilon_{\alpha\beta\gamma} \frac{\partial}{\partial x_\beta} \left(\frac{1}{\rho} \frac{\partial \tau_{\gamma\delta}}{\partial x_\delta} \right) + \epsilon_{\alpha\beta\gamma} \frac{\partial g_\beta}{\partial x_\gamma}$$

is obtained. Note that the external force has no effect on the vorticity dynamics if it is the gradient of a potential.

Comments:

Bennett [1] and Wu et al. [2], Chap. 4, contain further material on vorticity dynamics.

Problem (2.2): Verify that (2.69)

$$\frac{\Omega_\alpha(\tau, \mathbf{X})}{R(\tau, \mathbf{X})} = \frac{\Omega_\beta(0, \mathbf{X})}{R(0, \mathbf{X})} \frac{\partial \Phi_\alpha}{\partial X_\beta}(\tau, \mathbf{X})$$

is the solution of the vorticity pde (2.65)

$$\frac{D}{Dt} \left(\frac{\omega_\alpha}{\rho} \right) = \frac{\omega_\beta}{\rho} s_{\alpha\beta}$$

for inviscid and barotropic fluids.

Solution:

Differentiation of the solution in the material description leads to

$$\frac{\partial}{\partial \tau} \left(\frac{\Omega_\alpha(\tau, \mathbf{X})}{R(\tau, \mathbf{X})} \right) = \frac{\Omega_\beta(0, \mathbf{X})}{R(0, \mathbf{X})} \frac{\partial V_\alpha}{\partial X_\beta}(\tau, \mathbf{X})$$

The rules for the transformation from material to spatial description

$$t = \tau, \mathbf{x} = \Phi(\tau, \mathbf{X}), V_\alpha(\tau, \mathbf{X}) = v_\alpha(t, \mathbf{x})$$

results in

$$\frac{\partial V_\alpha}{\partial X_\beta} = \frac{\partial}{\partial X_\beta} v_\alpha(\tau, \Phi(\tau, \mathbf{X}))$$

and implicit differentiation produces

$$\frac{\partial v_\alpha}{\partial X_\beta} = \frac{\partial v_\alpha}{\partial x_\gamma} \frac{\partial \Phi_\gamma}{\partial X_\beta}$$

Hence

$$\frac{\partial}{\partial \tau} \left(\frac{\Omega_\alpha(\tau, \mathbf{X})}{R(\tau, \mathbf{X})} \right) = \frac{\Omega_\beta(0, \mathbf{X})}{R(0, \mathbf{X})} \frac{\partial \Phi_\gamma}{\partial X_\beta} \frac{\partial v_\alpha}{\partial x_\gamma}$$

Applying the solution once more

$$\frac{\Omega_\beta(0, \mathbf{X})}{R(0, \mathbf{X})} \frac{\partial \Phi_\gamma}{\partial X_\beta} = \frac{\Omega_\gamma(\tau, \mathbf{X})}{R(\tau, \mathbf{X})}$$

finally, after transformation to the spatial description, produces

$$\frac{D}{Dt} \left(\frac{\omega_\alpha}{\rho} \right) = \frac{\omega_\beta}{\rho} s_{\alpha\beta}$$

as claimed.

Comments:

This solution was discovered by Cauchy, see the historical comments in Truesdell [3]. Note that Eq. (2.65) can be transformed to the material description according to $t = \tau$ and $\mathbf{x} = \Phi(\tau, \mathbf{X})$, \mathbf{X} is the position of a material point at time zero [4], leading to an IVP for the system of three odes

$$\frac{dY_\alpha}{d\tau} = S_{\alpha\beta} Y_\beta, \quad Y_\alpha(0, \mathbf{X}) = Y_\alpha^0(\mathbf{X}), \quad \alpha, \beta = 1, 2, 3$$

where $Y_\alpha^0(\mathbf{X})$ denotes the initial vector of

$$Y_\alpha(\tau, \mathbf{X}) \equiv \frac{\omega_\alpha(\tau, \Phi(\tau, \mathbf{X}))}{\rho(\tau, \Phi(\tau, \mathbf{X}))}$$

and the symmetric rate of strain tensor in the material description emerges as

$$S_{\alpha\beta}(\tau, \mathbf{X}) \equiv s_{\alpha\beta}(\tau, \Phi(\tau, \mathbf{X}))$$

(upper case letters denotes material, lower case spatial description). If the rate of strain tensor $s_{\alpha\beta}(t, \mathbf{x})$ and the Lagrangean position field $\Phi(\tau, \mathbf{X})$ are known, the system of odes for Y_α is linear with variable coefficients. The rate of strain tensor is symmetric, hence are the time-dependent eigenvalues real and the trace is zero due to mass balance. However, the solution of the IVP for this system is non-trivial, since the rate of strain $S_{\alpha\beta}(\tau, \mathbf{X})$ may be a very complicated function of time τ for turbulent flows via the position field $\Phi(\tau, \mathbf{X})$.

Problem (2.3): Consider the flow of an inviscid, incompressible fluid with vorticity non-zero in a compact subdomain \mathcal{D}_Ω governed by the Euler pdes in $\mathcal{D} = \mathbb{R}^3$, let the vorticity be specified initially as a smooth vector field $\Omega_\alpha(0, \mathbf{X}) \in L^2_{\mathcal{D}}$, and then establish the equation for the Lagrangean position field $\Phi_\alpha(\tau, \mathbf{X})$ in terms of vorticity $\Omega_\alpha(0, \mathbf{X})$ at the reference time.

Solution:

Incompressible fluid implies that density $\rho(t, \mathbf{x})$ is constant. The solution of the vorticity equation for inviscid and barotropic flows is known (see Eq. (2.69) in Sect. 2.3.2)

$$\frac{\Omega_\alpha(\tau, \mathbf{X})}{R(\tau, \mathbf{X})} = \frac{\Omega_\beta(0, \mathbf{X})}{R(0, \mathbf{X})} \frac{\partial \Phi_\alpha}{\partial X_\beta}(\tau, \mathbf{X}) \quad (28.0.1)$$

where the material description is used and density $R(\tau, \mathbf{X}) = \rho(t, \mathbf{x})$ is constant. The Biot–Savart law holds for incompressible flows in the form (see Eq. (2.56) in Sect. 2.3) using the spatial description

$$v_\alpha(t, \mathbf{x}) = -\frac{1}{4\pi} \int_{\mathcal{D}} d\nu(\mathbf{y}) \epsilon_{\alpha\beta\gamma} \frac{(x_\beta - y_\beta)\omega_\gamma}{|\mathbf{x} - \mathbf{y}|^3} + \frac{\partial H}{\partial x_\alpha} \quad (28.0.2)$$

where $H(\mathbf{x})$ denotes a scalar potential. The flow domain in the present example is $\mathcal{D} = \mathbb{R}^3$, hence $H = 0$. Transformation of the Biot–Savart law to the material description using Sect. 2.5 leads to

$$\frac{\partial \Phi_\alpha}{\partial \tau}(\tau, \mathbf{X}) = -\frac{1}{4\pi} \int_{\mathbb{R}^3} d\nu(\mathbf{y}) \epsilon_{\alpha\beta\gamma} \frac{(\Phi_\beta(\tau, \mathbf{X}) - y_\beta)}{|\Phi(\tau, \mathbf{X}) - \mathbf{y}|^3} \Omega_\gamma(\tau, \Phi^*(t, \mathbf{y}))$$

where $\Phi^*(t, \mathbf{y})$ is the inverse map (initial position of a material point that is at \mathbf{y} at time $t = \tau$) of $\Phi(\tau, \mathbf{X})$. Since the position field $\Phi(\tau, \mathbf{X})$ is a diffeomorphism of the flow domain $\mathcal{D} = \mathbb{R}^3$ (see Sect. 2.5 in chapter Kinematics [4]), it follows that the integration can be carried out over the domain at reference time zero using

$$d\nu(\mathbf{y}) = d\nu(\mathbf{Y}) J(\tau, \mathbf{Y})$$

where J is the Jacobian determinant. Furthermore, for incompressible flows $J = 1$ (see mass balance in the material description, Eq. (2.87) in Sect. 2.5.3) and

$$\frac{\partial \Phi_\alpha}{\partial \tau}(\tau, \mathbf{X}) = -\frac{1}{4\pi} \int_{\mathbb{R}^3} d\nu(\mathbf{Y}) \epsilon_{\alpha\beta\gamma} \frac{(\Phi_\beta(\tau, \mathbf{X}) - \Phi_\beta(\tau, \mathbf{Y}))}{|\Phi(\tau, \mathbf{X}) - \Phi(\tau, \mathbf{Y})|^3} \Omega_\gamma(\tau, \mathbf{Y})$$

is obtained. Substitution of (2.69) leads to the desired result

$$\frac{\partial \Phi_\alpha}{\partial \tau}(\tau, \mathbf{X}) = -\frac{1}{4\pi} \int_{\mathbb{R}^3} d\nu(\mathbf{Y}) \epsilon_{\alpha\beta\gamma} \frac{(\Phi_\beta(\tau, \mathbf{X}) - \Phi_\beta(\tau, \mathbf{Y}))}{|\Phi(\tau, \mathbf{X}) - \Phi(\tau, \mathbf{Y})|^3} \Omega_\delta(0, \mathbf{Y}) \frac{\partial \Phi_\gamma}{\partial Y_\delta}(\tau, \mathbf{Y})$$

with initial condition $\Phi(0, \mathbf{X}) = \mathbf{X}$. This is the integro-differential equation replacing the Euler pdes for incompressible, inviscid fluids driven by a smooth distribution of vorticity. Once this equation has been solved, velocity and acceleration follow by differentiation.

Comments:

For further details, consult Chap. 2, Sect. 2.5, in the book [5] by Majda and Bertozzi. An alternative result is Weber’s equation (28.3) expressing the velocity in the material description in terms of the inverse deformation gradient, the velocity at the reference time and a pathline integral over a scalar field, see the solution to Problem 2.6.

Problem (2.4): Consider the flow of an incompressible, Newtonian fluid. Define the Lamb vector by (2.54) $\mathbf{L} \equiv \boldsymbol{\omega} \times \mathbf{v}$, where $\boldsymbol{\omega} \equiv \nabla \times \mathbf{v}$ denotes the vorticity vector.

(2.4.1) Show that the convective acceleration is the sum of the Lamb vector and the gradient of a scalar field.

(2.4.2) Compute the Lamb vector, the flexion vector (2.55) $\mathbf{f} \equiv \nabla \times \boldsymbol{\omega}$ and the divergence of the Lamb vector for an unidirectional parallel flow

$$v_\alpha = U(x_2, t)\delta_{\alpha,1}$$

in Cartesian coordinates.

(2.4.3) Establish the transport pde for the Lamb vector and its divergence.

Solution:

The convective acceleration is in the spatial description given by $\mathbf{v} \cdot \nabla \mathbf{v}$, the solenoidal flexion vector is defined by $\mathbf{f} \equiv \nabla \times \boldsymbol{\omega}$ (Truesdell [3] Chap. IV 44), and it will be used below.

(2.4.1) The convective acceleration can be recast using the vector relation

$$\frac{\partial v_\alpha}{\partial x_\beta} = \frac{\partial v_\beta}{\partial x_\alpha} - \epsilon_{\alpha\beta\gamma}\omega_\gamma$$

in Cartesian coordinates. Hence,

$$v_\beta \frac{\partial v_\alpha}{\partial x_\beta} = v_\beta \frac{\partial v_\beta}{\partial x_\alpha} - \epsilon_{\alpha\beta\gamma} v_\beta \omega_\gamma$$

holds. The first term is recognized as

$$v_\beta \frac{\partial v_\alpha}{\partial x_\beta} = \frac{\partial}{\partial x_\alpha} \left(\frac{1}{2} v_\beta v_\beta \right)$$

and the second as the Lamb vector

$$\epsilon_{\alpha\beta\gamma} v_\beta \omega_\gamma = -L_\alpha$$

Hence,

$$v_\beta \frac{\partial v_\alpha}{\partial x_\beta} = \frac{\partial}{\partial x_\alpha} \left(\frac{1}{2} v_\beta v_\beta \right) + L_\alpha$$

with the kinetic energy as scalar field, is obtained.

(2.4.2) Vorticity for plane and parallel flow is orthogonal to the plane of the flow, hence

$$\omega_\alpha = -\delta_{\alpha,3} \frac{dU}{dx_2}$$

and enstrophy is thus $e = (\frac{dU}{dx_2})^2$. The Lamb vector is then

$$L_\alpha = -\delta_{\alpha,3} U \frac{dU}{dx_2}$$

and its divergence is

$$\nabla \cdot \mathbf{L} = -e - U \frac{d^2 U}{dx_2^2}$$

It is clear that $\nabla \cdot \mathbf{L}$ may be positive, if $\frac{d^2 U}{dx_2^2} < 0$ and the last term on the right side dominates, or negative if the second derivative term is small compared to enstrophy on the right side.

The flexion vector $\mathbf{f} = \nabla \times \omega$ has only one non-zero component

$$f_1 = -\frac{d^2 U}{dx_2^2}$$

The divergence of the Lamb vector contains, therefore, the product $\mathbf{v} \cdot \mathbf{f}$ and enstrophy $e \nabla \cdot \mathbf{L} = -e + \mathbf{v} \cdot \mathbf{f}$. This relation holds generally [6], not only for parallel shear flows.

(2.4.3) The transport pdes for the Lamb vector and its divergence follow from mass and momentum balances. Cross vector multiplication of momentum (2.2) and vorticity balance (2.63) leads to

$$\frac{DL_\alpha}{Dt} = \epsilon_{\alpha\beta\gamma} v_\gamma \omega_\delta \frac{\partial v_\beta}{\partial x_\delta} - \epsilon_{\alpha\beta\gamma} \omega_\beta \frac{\partial p}{\partial x_\gamma} + \frac{1}{Re} \Delta L_\alpha$$

Taking the divergence of this pde produces the desired pde for the divergence of the Lamb vector $\mathcal{D} \equiv \nabla \cdot \mathbf{L}$

$$\frac{D\mathcal{D}}{Dt} = -\frac{\partial v_\delta}{\partial x_\alpha} \frac{\partial L_\alpha}{\partial x_\delta} + \epsilon_{\alpha\beta\gamma} \frac{\partial}{\partial x_\alpha} (v_\gamma \omega_\delta \frac{\partial v_\beta}{\partial x_\delta}) - \epsilon_{\alpha\beta\gamma} \frac{\partial}{\partial x_\alpha} (\omega_\beta \frac{\partial p}{\partial x_\gamma}) + \frac{1}{Re} \Delta \mathcal{D}$$

Equivalent versions of this pde can be found in Hamman et al. [6].

References:

Truesdell [3] and Hamman et al. [6] are relevant references, the latter contains a detailed analysis of the divergence of the Lamb vector in laminar and turbulent flows.

Problem (2.5): Determine the symmetries of the heat pde

$$\frac{\partial T}{\partial t} - \frac{\partial^2 T}{\partial x^2} = 0$$

defined on $\mathcal{D} = [0, \infty] \times R^1$.

(2.5.1) Change the notation to $x \rightarrow x_1$, $t \rightarrow x_2$, $T \rightarrow y_1$ and determine the prolonged operator $X^{(2)}$ and the condition for symmetry transformations.

(2.5.2) Compute the total derivatives determining the infinitesimals appearing in the condition for symmetry transformations.

(2.5.3) Establish the equations for the infinitesimals.

(2.5.5) Solve the equations for the infinitesimals.

(2.5.6) Choose a set of values for the parameters and compute the global transformation.

Solution:

(2.5.1) Changing the notation to $x \rightarrow x_1$, $t \rightarrow x_2$, $T \rightarrow y_1$ to be consistent with Sect. 2.1.3, leads to the heat pde in the form

$$\frac{\partial y_1}{\partial x_2} - \frac{\partial^2 y_1}{\partial x_1^2} = 0, \text{ or } y_{1,2}(x_1, x_2, y_1) - y_{1,11}(x_1, x_2, y_1) = 0, \text{ or } F(y_{1,2}, y_{1,11}) = 0$$

with $F(y_{1,2}, y_{1,11}) \equiv \frac{\partial y_1}{\partial x_2} - \frac{\partial^2 y_1}{\partial x_1^2}$. The prolonged generator (2.34) is thus reduced to

$$X^{(2)} = \zeta_{1,2} \frac{\partial}{\partial y_{1,2}} + \zeta_{1,11} \frac{\partial}{\partial y_{1,11}}$$

The conditions (2.35) determining the symmetry transformation emerge as

$$X^{(2)}(y_{1,2} - y_{1,11}) = 0, \text{ on } y_{1,2} - y_{1,11} = 0$$

The next step is to apply $X^{(2)}$ to $y_{1,2} - y_{1,11}$

$$\zeta_{1,2} - \zeta_{1,11} = 0, \text{ on } y_{1,2} - y_{1,11} = 0 \tag{1}$$

(2.5.2) To carry out the differentiations, the recursive relation (2.31) and the definition of the total first derivative (2.21) are applied. They are reduced to

$$\frac{\mathcal{D}}{\mathcal{D}x_i} = \frac{\partial}{\partial x_i} + y_{k,i} \frac{\partial}{\partial y_k}$$

if applied to $\boldsymbol{\eta}(\mathbf{x}, \mathbf{y})$, $\boldsymbol{\xi}(\mathbf{x}, \mathbf{y})$

$$\begin{aligned} \zeta_{1;1} &= \frac{\mathcal{D}\eta_1}{\mathcal{D}x_1} - y_{1,1} \frac{\mathcal{D}\xi_1}{\mathcal{D}x_1} - y_{1,2} \frac{\mathcal{D}\xi_2}{\mathcal{D}x_1} \\ &= \frac{\partial\eta_1}{\partial x_1} + y_{1,1} \frac{\partial\eta_1}{\partial y_1} - y_{1,1} \left(\frac{\partial\xi_1}{\partial x_1} + y_{1,1} \frac{\partial\xi_1}{\partial y_1} \right) - y_{1,2} \left(\frac{\partial\xi_2}{\partial x_1} + y_{1,1} \frac{\partial\xi_2}{\partial y_1} \right) \end{aligned} \quad (2)$$

and likewise

$$\begin{aligned} \zeta_{1;2} &= \frac{\mathcal{D}\eta_1}{\mathcal{D}x_2} - y_{1,1} \frac{\mathcal{D}\xi_1}{\mathcal{D}x_2} - y_{1,2} \frac{\mathcal{D}\xi_2}{\mathcal{D}x_2} \\ &= \frac{\partial\eta_1}{\partial x_2} + y_{1,2} \frac{\partial\eta_1}{\partial y_1} - y_{1,1} \left(\frac{\partial\xi_1}{\partial x_2} + y_{1,2} \frac{\partial\xi_1}{\partial y_1} \right) - y_{1,2} \left(\frac{\partial\xi_2}{\partial x_2} + y_{1,2} \frac{\partial\xi_2}{\partial y_1} \right) \end{aligned} \quad (3)$$

Finally, using the recursive relation (2.32) for $s = 2$ and the total first derivative applied to $\zeta_{i;k}(x_1, x_2, y_1, y_{1,1}, y_{1,2})$

$$\frac{\mathcal{D}}{\mathcal{D}x_i} = \frac{\partial}{\partial x_i} + y_{k,i} \frac{\partial}{\partial y_k} + y_{k,ij} \frac{\partial}{\partial y_{k,j}}$$

hence

$$\begin{aligned} \zeta_{1;11} &= \frac{\mathcal{D}\zeta_{1;1}}{\mathcal{D}x_1} - y_{1,11} \frac{\mathcal{D}\xi_1}{\mathcal{D}x_1} - y_{1,12} \frac{\mathcal{D}\xi_2}{\mathcal{D}x_1} \\ &= \frac{\partial\zeta_{1;1}}{\partial x_1} + y_{1,1} \frac{\partial\zeta_{1;1}}{\partial y_1} + y_{1,11} \frac{\partial\zeta_{1;1}}{\partial y_{1,1}} + y_{1,12} \frac{\partial\zeta_{1;1}}{\partial y_{1,2}} - y_{1,11} \left[\frac{\partial\xi_1}{\partial x_1} + y_{1,1} \frac{\partial\xi_1}{\partial y_1} \right] - y_{1,12} \left[\frac{\partial\xi_2}{\partial x_1} + y_{1,1} \frac{\partial\xi_2}{\partial y_1} \right] \end{aligned}$$

is obtained. The $\zeta_{1;1}$ can be eliminated with the aid of (2) leading to

$$\begin{aligned} \zeta_{1;11} &= \frac{\partial^2\eta_1}{\partial x_1^2} + y_{1,1} \frac{\partial^2\eta_1}{\partial x_1 \partial y_1} - y_{1,1} \left(\frac{\partial^2\xi_1}{\partial x_1^2} + y_{1,1} \frac{\partial^2\xi_1}{\partial x_1 \partial y_1} \right) - y_{1,2} \left(\frac{\partial^2\xi_2}{\partial x_1^2} + y_{1,1} \frac{\partial^2\xi_2}{\partial x_1 \partial y_1} \right) \\ &\quad + y_{1,1} \left[\frac{\partial^2\eta_1}{\partial x_1 \partial y_1} + y_{1,1} \frac{\partial^2\eta_1}{\partial y_1^2} - y_{1,1} \left(\frac{\partial^2\xi_1}{\partial x_1 \partial y_1} + y_{1,1} \frac{\partial^2\xi_1}{\partial y_1^2} \right) - y_{1,2} \left(\frac{\partial^2\xi_2}{\partial x_1 \partial y_1} + y_{1,1} \frac{\partial^2\xi_2}{\partial y_1^2} \right) \right] \\ &\quad + y_{1,11} \left[\frac{\partial\eta_1}{\partial y_1} - \frac{\partial\xi_1}{\partial x_1} - 2y_{1,1} \frac{\partial\xi_1}{\partial y_1} - y_{1,2} \frac{\partial\xi_2}{\partial y_1} \right] - y_{1,12} \left[\frac{\partial\xi_2}{\partial x_1} + y_{1,1} \frac{\partial\xi_2}{\partial y_1} \right] \\ &\quad - y_{1,11} \left[\frac{\partial\xi_1}{\partial x_1} + y_{1,1} \frac{\partial\xi_1}{\partial y_1} \right] - y_{1,12} \left[\frac{\partial\xi_2}{\partial x_1} + y_{1,1} \frac{\partial\xi_2}{\partial y_1} \right] \end{aligned} \quad (4)$$

The infinitesimals $\zeta_{1;2}$ using (3) and $\zeta_{1;11}$ using (4) are now substituted in (1) and, noting that $y_{1,11} = y_{1,2}$ holds according to (1), the following result

$$\begin{aligned} & \frac{\partial \eta_1}{\partial x_2} - \frac{\partial^2 \eta_1}{\partial x_1^2} + y_{1,2} \frac{\partial \eta_1}{\partial y_1} - y_{1,1} \left(\frac{\partial \xi_1}{\partial x_2} + y_{1,2} \frac{\partial \xi_1}{\partial y_1} \right) - y_{1,2} \left(\frac{\partial \xi_2}{\partial x_2} + y_{1,2} \frac{\partial \xi_2}{\partial y_1} \right) \\ & - y_{1,1} \frac{\partial^2 \eta_1}{\partial x_1 \partial y_1} + y_{1,1} \left(\frac{\partial^2 \xi_1}{\partial x_1^2} + y_{1,1} \frac{\partial^2 \xi_1}{\partial x_1 \partial y_1} \right) + y_{1,2} \left(\frac{\partial^2 \xi_2}{\partial x_1^2} + y_{1,1} \frac{\partial^2 \xi_2}{\partial x_1 \partial y_1} \right) \\ & - y_{1,1} \left[\frac{\partial^2 \eta_1}{\partial x_1 \partial y_1} + y_{1,1} \frac{\partial^2 \eta_1}{\partial y_1^2} - y_{1,1} \left(\frac{\partial^2 \xi_1}{\partial x_1 \partial y_1} + y_{1,1} \frac{\partial^2 \xi_1}{\partial y_1^2} \right) - y_{1,2} \left(\frac{\partial^2 \xi_2}{\partial x_1 \partial y_1} + y_{1,1} \frac{\partial^2 \xi_2}{\partial y_1^2} \right) \right] \\ & - y_{1,2} \left[\frac{\partial \eta_1}{\partial y_1} - \frac{\partial \xi_1}{\partial x_1} - 2y_{1,1} \frac{\partial \xi_1}{\partial y_1} - y_{1,2} \frac{\partial \xi_2}{\partial y_1} \right] + y_{1,12} \left[\frac{\partial \xi_2}{\partial x_1} + y_{1,1} \frac{\partial \xi_2}{\partial y_1} \right] \\ & + y_{1,2} \left[\frac{\partial \xi_1}{\partial x_1} + y_{1,1} \frac{\partial \xi_1}{\partial y_1} \right] + y_{1,12} \left[\frac{\partial \xi_2}{\partial x_1} + y_{1,1} \frac{\partial \xi_2}{\partial y_1} \right] = 0 \end{aligned}$$

is obtained. Rearranging the terms

$$\begin{aligned} & \frac{\partial \eta_1}{\partial x_2} - \frac{\partial^2 \eta_1}{\partial x_1^2} + y_{1,1} \left[-\frac{\partial \xi_1}{\partial x_2} + \frac{\partial^2 \xi_1}{\partial x_1^2} - 2 \frac{\partial^2 \eta_1}{\partial x_1 \partial y_1} \right] + y_{1,2} \left[2 \frac{\partial \xi_1}{\partial x_1} - \frac{\partial \xi_2}{\partial x_2} + \frac{\partial^2 \xi_2}{\partial x_1^2} \right] \\ & + y_{1,1}^2 \left[2 \frac{\partial^2 \xi_1}{\partial x_1 \partial y_1} - \frac{\partial^2 \eta_1}{\partial y_1^2} \right] + y_{1,1} y_{1,2} \left[3 \frac{\partial \xi_1}{\partial y_1} + 2 \frac{\partial^2 \xi_2}{\partial x_1 \partial y_1} \right] + y_{1,2}^2 \frac{\partial \xi_2}{\partial y_1} \\ & + y_{1,1}^2 y_{1,2} \frac{\partial^2 \xi_2}{\partial y_1^2} + y_{1,1}^3 \frac{\partial^2 \xi_1}{\partial y_1^2} + 2y_{1,12} \frac{\partial \xi_2}{\partial x_1} + 2y_{1,1} y_{1,12} \frac{\partial \xi_2}{\partial y_1} = 0 \end{aligned}$$

produces the explicit form of the conditions (2.35) determining the transformations.

(2.5.3) Noting that the infinitesimals are only functions of the parameters x_1, x_2, y_1 , the equation has to hold for arbitrary values $y_{1,1}, y_{1,2}, \dots$, therefore, the coefficients of $y_{1,1}, y_{1,2}, y_{1,1}^2, y_{1,1} y_{1,2}, y_{1,1}^3, y_{1,1}^2 y_{1,2}, y_{1,12}, y_{1,12} y_{1,1}$ must be zero. It is advantageous to start with the coefficients of $y_{1,12}$ and $y_{1,12} y_{1,1}$, hence $\frac{\partial \xi_2}{\partial x_1} = 0, \frac{\partial \xi_2}{\partial y_1} = 0$ must hold. The coefficient of $y_{1,1} y_{1,2}$ leads to $\frac{\partial \xi_1}{\partial y_1} = 0$. Continuing these manipulations produces the final system of equations

$$\frac{\partial \xi_1}{\partial y_1} = 0, \tag{T.1}$$

$$\frac{\partial \xi_2}{\partial x_1} = 0, \tag{T.2}$$

$$\frac{\partial \xi_2}{\partial y_1} = 0, \tag{T.3}$$

$$\frac{\partial^2 \eta_1}{\partial y_1^2} = 0, \quad (T.4)$$

$$2 \frac{\partial \xi_1}{\partial x_1} - \frac{\partial \xi_2}{\partial x_2} = 0, \quad (T.5)$$

$$-\frac{\partial \xi_1}{\partial x_2} + \frac{\partial^2 \xi_1}{\partial x_1^2} = 0 \quad (T.6)$$

$$-2 \frac{\partial^2 \eta_1}{\partial x_1 \partial y_1} = 0, \frac{\partial \eta_1}{\partial x_2} - \frac{\partial^2 \eta_1}{\partial x_1^2} = 0 \quad (T.7)$$

The first four Eqs. (T.1) to (T.4) can be integrated

$$\xi_1 = \xi_1(x_1, x_2), \quad \xi_2 = \xi_2(x_2), \quad \eta_1(x_1, x_2, y_1) = f_0(x_1, x_2) + f_1(x_1, x_2)y_1$$

Integration of (T.5) using (T.2) and (T.3) yields

$$\xi_1(x_1, x_2) = \frac{1}{2} \frac{d \xi_2}{d x_2} x_1 + g(x_2)$$

Furthermore, noting that $\frac{\partial^2 \xi_1}{\partial x_1^2} = 0$ according to $\xi_2(x_2)$ and (T.5), (T.6) appears with these results as

$$f_1(x_1, x_2) = -\frac{1}{8} \frac{d^2 \xi_2}{d x_2^2} x_1^2 - \frac{1}{2} \frac{d g}{d x_2} x_1 + h(x_2)$$

Collecting the results and substituting η_1 in (T.7) leads to

$$y_1 \left[-\frac{1}{8} \frac{d^3 \xi_2}{d x_2^3} x_1^2 - \frac{1}{2} \frac{d^2 g}{d x_2^2} x_1 + \frac{d h}{d x_2} + \frac{1}{4} \frac{d^2 \xi_2}{d x_2^2} \right] + \frac{\partial f_0}{\partial x_2} - \frac{\partial^2 f_0}{\partial x_1^2} = 0$$

(2.5.5) This equation must hold for arbitrary x_1, x_2, y_1 , hence

$$-\frac{1}{8} \frac{d^3 \xi_2(x_2)}{d x_2^3} x_1^2 - \frac{1}{2} \frac{d^2 g(x_2)}{d x_2^2} x_1 + \frac{d h(x_2)}{d x_2} + \frac{1}{4} \frac{d^2 \xi_2(x_2)}{d x_2^2} = 0 \quad (5)$$

and

$$\frac{\partial f_0}{\partial x_2}(x_1, x_2) - \frac{\partial^2 f_0}{\partial x_1^2}(x_1, x_2) = 0 \quad (6)$$

follow. Equation (5) must hold for arbitrary x_1 , thus the coefficients of x_1 must be zero. Hence, $\xi_2(x_2)$ must be a second-order polynomial

$$\frac{d^3\xi_2(x_2)}{dx_2^3} = 0, \rightarrow \xi_2(x_2) = c_0 + c_1x_2 + c_2x_2^2$$

$$\frac{d^2g(x_2)}{dx_2^2} = 0 \rightarrow g(x_2) = b_0 + b_1x_2$$

$$\xi_1(x_1, x_2) = \frac{1}{2} \frac{d\xi_2(x_2)}{dx_2} x_1 + g(x_2), \rightarrow \xi_1(x_1, x_2) = b_0 + \frac{1}{2}c_1x_1 + b_1x_2 + c_2x_1x_2$$

$$\frac{dh(x_2)}{dx_2} + \frac{1}{4} \frac{d^2\xi_2}{dx_2^2} = 0 \rightarrow h(x_2) = a_0 - \frac{1}{2}c_2x_2$$

Finally, $\eta_1(x_1, x_2, y_1) = f_1(x_1, x_2) + f_2(x_1, x_2)y_1$ and the relation for $f_1(x_1, x_2)$ above lead to

$$\eta_1(x_1, x_2, y_1) = \left[a_0 - \frac{1}{2}c_2 \left(x_2 + \frac{1}{2}x_1^2 \right) - \frac{1}{2}b_1x_1 \right] y_1 + f_0(x_1, x_2)$$

with $f_0(x_1, x_2)$ being the solution of

$$\frac{\partial f_0}{\partial x_2} - \frac{\partial^2 f_0}{\partial x_1^2} = 0 \quad (7)$$

The final result for the infinitesimals is thus

$$\xi_1(x_1, x_2) = b_0 + \frac{1}{2}c_1x_1 + b_1x_2 + c_2x_1x_2 \quad (8)$$

$$\xi_2(x_2) = c_0 + c_1x_2 + c_2x_2^2 \quad (9)$$

$$\eta_1(x_1, x_2, y_1) = \left[a_0 - \frac{1}{2}c_2 \left(x_2 + \frac{1}{2}x_1^2 \right) - \frac{1}{2}b_1x_1 \right] y_1 + f_0(x_1, x_2) \quad (10)$$

containing six arbitrary parameters $c_0, c_1, c_2, a_0, b_0, b_1$ and the solution $f_0(x_1, x_2)$ of the pde (7), which is identical to the heat pde in the problem statement. The global transformations follows from Lie's first theorem (2.28) as IVP

$$\frac{dx_1^*}{d\epsilon} = \xi_1(x_1^*, x_2^*), \frac{dx_2^*}{d\epsilon} = \xi_2(x_2^*), \frac{dy_1^*}{d\epsilon} = \eta_1(x_1^*, x_2^*, y_1^*)$$

with initial conditions $\mathbf{x}^*(0) = \mathbf{x}, \mathbf{y}^*(0) = \mathbf{y}$, specifically

$$\frac{dx_1^*}{d\epsilon} = b_0 + \frac{1}{2}c_1x_1^* + b_1x_2^* + c_2x_1^*x_2^*, x_1^*(0) = x_1 \quad (11)$$

$$\frac{dx_2^*}{d\epsilon} = c_0 + c_1x_2^* + c_2x_2^{*2}, x_2^*(0) = x_2 \quad (12)$$

$$\frac{dy_1^*}{d\epsilon} = \left[a_0 - \frac{1}{2}c_2 \left(x_2^* + \frac{1}{2}x_1^{*2} \right) - \frac{1}{2}b_1x_1^* \right] y_1^* + f_0(x_1^*, x_2^*), y_1^*(0) = y_1 \quad (13)$$

(2.5.6) The solution of this system of odes for the parameters $c_0 = 0$, $c_1 = 0$, $c_2 = 1$, $a_0 = 0$, $b_0 = 0$, $b_1 = 0$ and the solution $f_0 = 0$ of (7) is straightforward.

$$\frac{dx_1^*}{d\epsilon} = x_1^* x_2^*, \quad x_1^*(0) = x_1 \quad (14)$$

$$\frac{dx_2^*}{d\epsilon} = x_2^{*2}, \quad x_2^*(0) = x_2 \quad (15)$$

$$\frac{dy_1^*}{d\epsilon} = -\frac{1}{2} \left(x_2^* + \frac{1}{2} x_1^{*2} \right) y_1^*, \quad y_1^*(0) = y_1 \quad (16)$$

The solution of Eq. (15) emerges as

$$x_2^*(x_2, \epsilon) = \frac{x_2}{1 - \epsilon x_2}$$

and Eq. (14) leads to

$$x_1^*(x_1, x_2, \epsilon) = \frac{x_1}{1 - \epsilon x_2}$$

and finally Eq. (16) to

$$\frac{dy_1^*}{d\epsilon} = -\frac{1}{2} \left[\frac{x_2}{1 - \epsilon x_2} + \frac{1}{2} \frac{x_1^2}{(1 - \epsilon x_2)^2} \right] y_1^*$$

with solution

$$y_1^*(x_1, x_2, y_1, \epsilon) = \frac{y_1}{\sqrt{1 - \epsilon x_2}} \exp \left[-\frac{1}{4} \frac{\epsilon x_1^2}{(1 - \epsilon x_2)} \right]$$

The global solutions for other choices for the parameter values can be found in [7].

The prolongation operator $X^{(p)}$ can be in general represented as sum of irreducible operators, which are elements of a linear vector space. Any linear combination of the irreducible operators generates an invariant transformation of the differential system $\mathbf{F} = 0$. For the present example, these elements are Oberlack [7]

$$X_1 = \frac{\partial}{\partial x_1}$$

$$X_2 = \frac{\partial}{\partial x_2}$$

$$X_3 = y_1 \frac{\partial}{\partial y_1}$$

$$X_4 = x_1 \frac{\partial}{\partial x_1} + 2x_2 \frac{\partial}{\partial x_2}$$

$$X_5 = x_1 x_2 \frac{\partial}{\partial x_1} + x_2^2 \frac{\partial}{\partial x_2} - \frac{1}{2} \left(\frac{1}{2} x_1^2 + x_2 \right) y_1 \frac{\partial}{\partial y_1}$$

$$X_6 = x_2 \frac{\partial}{\partial x_1} - \frac{1}{2} x_1 y_1 \frac{\partial}{\partial y_1}$$

sorted according to the parameters $c_0, c_1, c_2, a_0, b_0, b_1$.

Comments:

The heat pde is a popular example to illustrate the Lie group machinery, see Oberlack et al. [7, 8]. Other examples include the nonlinear Burgers pde (see Definition (1.2) and solution in Chap. 1), [9].

Problem (2.6): Integrate the Euler pdes (2.9)

$$\begin{aligned} \frac{\partial v_\alpha}{\partial x_\alpha} &= 0 \\ \frac{\partial v_\alpha}{\partial t} + v_\beta \frac{\partial v_\alpha}{\partial x_\beta} &= - \frac{\partial p}{\partial x_\alpha} \end{aligned}$$

governing the motion of an incompressible, inviscid fluid, along a pathline (Weber's equation).

- (2.6.1) Write the Euler pdes in mixed spatial/material description.
- (2.6.2) Transform to strictly material form.
- (2.6.3) Reformulate the momentum balance using (2.94) such that integration along a pathline starting at \mathbf{X} becomes possible.

Solution:

The integration along a pathline requires some preparation. The material description should be used, since quantities for fixed label \mathbf{X} (defined as the position at the reference time zero) vary along pathlines as time τ evolves.

- (2.6.1) The substantial derivative in the spatial description (2.3) is the time derivative in the material description, hence

$$\frac{\partial v_\alpha}{\partial x_\alpha} = 0, \quad \frac{\partial V_\alpha}{\partial \tau} = - \frac{\partial p}{\partial x_\alpha}$$

are the Euler pdes in mixed description.

- (2.6.2) The velocity in the material description is $V_\alpha(\tau, \mathbf{X}) = \frac{\partial \Phi_\alpha}{\partial \tau}(\tau, \mathbf{X})$ iff $\mathbf{x} = \Phi(\tau, \mathbf{X})$, $t = \tau$, the spatial gradient transforms then according to (2.94)

$$\frac{\partial}{\partial x_\alpha} = F_{\beta\alpha}^{-1} \frac{\partial}{\partial X_\beta}$$

where $F_{\alpha\beta} = \frac{\partial\Phi_\beta}{\partial X_\alpha}$ (2.82) is the material deformation gradient. The material version of the Euler pdes is then

$$J = 1, \frac{\partial^2\Phi_\alpha}{\partial\tau^2} = -F_{\beta\alpha}^{-1} \frac{\partial P}{\partial X_\beta}, F_{\alpha\beta} = \frac{\partial\Phi_\beta}{\partial X_\alpha}$$

where $P(\tau, \mathbf{X}) = p(t(\tau), \mathbf{x}(\tau, \mathbf{X}))$ is the pressure in the material description and the Jacobian $J(\tau, \mathbf{X})$ is the determinant of the deformation gradient $F_{\alpha\beta}$. Multiplication with the deformation gradient leads to the momentum balance

$$F_{\alpha\beta} \frac{\partial^2\Phi_\alpha}{\partial\tau^2} = -\frac{\partial P}{\partial X_\beta}$$

suitable for pathline integration.

(2.6.3) Pulling a time derivative out of the left side produces

$$\frac{\partial}{\partial\tau} \left(\frac{\partial\Phi_\alpha}{\partial X_\beta} \frac{\partial\Phi_\alpha}{\partial\tau} \right) - \frac{\partial\Phi_\alpha}{\partial\tau} \frac{\partial^2\Phi_\alpha}{\partial\tau\partial X_\beta} = -\frac{\partial P}{\partial X_\beta}$$

and observing

$$\frac{\partial\Phi_\alpha}{\partial\tau} \frac{\partial}{\partial X_\beta} \left(\frac{\partial\Phi_\alpha}{\partial\tau} \right) = \frac{1}{2} \frac{\partial}{\partial X_\beta} \left(\frac{\partial\Phi_\alpha}{\partial\tau} \frac{\partial\Phi_\alpha}{\partial\tau} \right)$$

leads to

$$\frac{\partial}{\partial\tau} \left(\frac{\partial\Phi_\alpha}{\partial X_\beta} \frac{\partial\Phi_\alpha}{\partial\tau} \right) = -\frac{\partial}{\partial X_\beta} \left(P - \frac{1}{2} \frac{\partial\Phi_\alpha}{\partial\tau} \frac{\partial\Phi_\alpha}{\partial\tau} \right)$$

This version of the momentum balance can be integrated along the pathline identified by the initial position/label \mathbf{X}

$$\left(\frac{\partial\Phi_\alpha}{\partial X_\beta} \frac{\partial\Phi_\alpha}{\partial\tau} \right)(\tau, \mathbf{X}) - \left(\frac{\partial\Phi_\alpha}{\partial X_\beta} \frac{\partial\Phi_\alpha}{\partial\tau} \right)(0, \mathbf{X}) = - \int_0^\tau d\tau' \frac{\partial}{\partial X_\beta} \left(P - \frac{1}{2} \frac{\partial\Phi_\alpha}{\partial\tau} \frac{\partial\Phi_\alpha}{\partial\tau} \right)$$

or

$$(F_{\alpha\beta} V_\alpha)(\tau, \mathbf{X}) - V_\beta(0, \mathbf{X}) = -\frac{\partial}{\partial X_\beta} \int_0^\tau d\tau' [P(\mathbf{V}; \tau', \mathbf{X}) - \frac{1}{2} |\mathbf{V}|^2(\tau', \mathbf{X})]$$

since $F_{\alpha\beta}(0, \mathbf{X}) = \delta_{\alpha,\beta}$ holds. Multiplication with the inverse deformation gradient $F_{\beta\gamma}^{-1}$ results in the desired relation

$$V_\gamma(\tau, \mathbf{X}) = F_{\beta\gamma}^{-1}(\tau, \mathbf{X}) \left\{ V_\beta(0, \mathbf{X}) - \frac{\partial}{\partial X_\beta} \int_0^\tau d\tau' [P(\mathbf{V}; \tau', \mathbf{X}) - \frac{1}{2} |\mathbf{V}|^2(\tau', \mathbf{X})] \right\} \quad (28.3)$$

expressing the velocity in the material description in terms of the inverse deformation gradient, velocity at the reference time and a pathline integral over the scalar field $P(\mathbf{V}; \tau', \mathbf{X}) - \frac{1}{2} |\mathbf{V}|^2(\tau', \mathbf{X})$.

Comments:

This result was discovered by Weber in 1868 (hence called Weber's formula), the derivation presented above is due to Constantin [10]. The Weber formula is equivalent to the conservation of circulation as Constantin proves in [10]. It is a first integral of the momentum balances for the flow of inviscid and incompressible fluids. Recalling the definition of velocity and the deformation gradient in the material description, an alternative version for the equation governing the Lagrangean position field with specified pressure as IVP for a nonlinear first-order pde

$$\frac{\partial \Phi_\gamma}{\partial \tau}(\tau, \mathbf{X}) = \left(\frac{\partial \Phi_\beta}{\partial X_\gamma} \right)^{-1}(\tau, \mathbf{X}) \left\{ V_\beta(0, \mathbf{X}) - \frac{\partial}{\partial X_\beta} \int_0^\tau d\tau' \left[P\left(\frac{\partial \Phi}{\partial \tau}; \tau', \mathbf{X}\right) - \frac{1}{2} \frac{\partial \Phi_\alpha}{\partial \tau} \frac{\partial \Phi_\alpha}{\partial \tau}(\tau', \mathbf{X}) \right] \right\}$$

with $\Phi_\alpha(0, \mathbf{X}) = X_\alpha$ as initial condition is obtained. Mass balance implies that the pressure is a complicated functional $P(\frac{\partial \Phi}{\partial \tau}; \tau', \mathbf{X})$ of the position field via the solution of the Poisson pde for the (spatial) pressure. If the vorticity is specified initially on a compact subdomain, the Euler pdes emerge in a different integral form as the solution to Problem (2.3) illustrates.

Solutions to problems in Chap. 3: Basic properties of turbulent flows

Problem (3.1): Derive the pde for the dimensionless mean kinetic energy $k \equiv \frac{1}{2} \langle v'_\alpha v'_\alpha \rangle$ assuming a viscous, incompressible Newtonian fluid. Identify production, viscous destruction and the turbulent flux terms.

Solution:

Representing velocity and pressure as $v_\alpha = \langle v_\alpha \rangle + v'_\alpha$, $p = \langle p \rangle + p'$ in the Navier-Stokes pdes leads to the pde for the fluctuating velocity

$$\frac{\partial v'_\alpha}{\partial t} + v'_\beta \frac{\partial v'_\alpha}{\partial x_\beta} + \langle v_\beta \rangle \frac{\partial v'_\alpha}{\partial x_\beta} + v'_\beta \frac{\partial \langle v_\alpha \rangle}{\partial x_\beta} - \frac{\partial}{\partial x_\beta} \langle v'_\alpha v'_\beta \rangle = -\frac{\partial p'}{\partial x_\alpha} + \frac{1}{Re} \Delta v'_\alpha$$

Multiplication with v'_α and averaging produces the desired pde for k

$$\frac{\partial k}{\partial t} + \langle v_\beta \rangle \frac{\partial k}{\partial x_\beta} + \frac{\partial T_\beta}{\partial x_\beta} = P - \epsilon$$

where the fact that the fluctuating velocity is solenoidal was used several times. The production term is defined by

$$P \equiv -\langle v'_\alpha v'_\beta \rangle \frac{\partial \langle v_\alpha \rangle}{\partial x_\beta}$$

It is positive, hence produces kinetic energy, in high shear regions of turbulent flows, but it is not positive definite as the example of asymmetric channel flow shows. The viscous destruction term, called dissipation rate, is defined by

$$\epsilon \equiv \frac{1}{Re} \langle \frac{\partial v'_\alpha}{\partial x_\beta} \frac{\partial v'_\alpha}{\partial x_\beta} \rangle$$

It is a sum of squares, hence always non-negative. The turbulent flux consists of three contributions

$$T_\alpha = \frac{1}{2} \langle v'_\alpha v'_\alpha v'_\beta \rangle + \langle v'_\alpha p' \rangle - \frac{1}{Re} \frac{\partial k}{\partial x_\alpha}$$

namely, the triple velocity correlation, the (non-local) pressure–velocity correlation and the viscous flux of kinetic energy.

References:

The pde for the kinetic energy of turbulence is the basis of a variety of moment closures, see Pope [11] for detailed information on the flux T_α of kinetic energy and the dissipation rate ϵ and further references.

Problem (3.2): Derive the pde for the dimensionless mean enstrophy $\langle e^2 \rangle$ defined by (3.16) in homogeneous turbulence with zero mean flow for an incompressible Newtonian fluid with constant viscosity $\hat{\nu} > 0$.

Solution:

Homogeneity means translational invariance, hence

$$\frac{\partial}{\partial x_\alpha} \langle \dots \rangle = 0$$

holds for all single-point expectations and zero mean implies $v_\alpha = v'_\alpha$. Momentum balance (2.2) for an incompressible Newtonian fluid with constant viscosity possessing relevant length and velocity scales leads then to the pde

$$\frac{\partial v'_\alpha}{\partial t} = -v'_\beta \frac{\partial v'_\alpha}{\partial x_\beta} - \frac{\partial p'}{\partial x_\alpha} + \frac{1}{Re} \Delta v'_\alpha$$

where $p \leftarrow p/\rho$ and the Reynolds number is given by (2.8). Application of the curl $\epsilon_{\alpha\beta\gamma} \frac{\partial}{\partial x_\beta}$ to the momentum balance produces

$$\frac{\partial \omega'_\alpha}{\partial t} = -\epsilon_{\alpha\beta\gamma} \frac{\partial}{\partial x_\beta} (v'_\delta \frac{\partial v'_\alpha}{\partial x_\delta}) + \frac{1}{Re} \Delta \omega'_\alpha$$

The relation of the fluctuating deformation rate to the rate of strain $s_{\alpha\beta}$ and vorticity

$$\frac{\partial v'_\alpha}{\partial x_\beta} = s'_{\alpha\beta} - \frac{1}{2} \epsilon_{\alpha\beta\gamma} \omega'_\gamma, \quad \frac{\partial v'_\alpha}{\partial x_\beta} - \frac{\partial v'_\beta}{\partial x_\alpha} = -\epsilon_{\alpha\beta\gamma} \omega'_\gamma$$

and $\epsilon_{\alpha\beta\gamma} \epsilon_{\gamma\delta\eta} = \delta_{\alpha\delta} \delta_{\beta\eta} - \delta_{\alpha\eta} \delta_{\beta\delta}$ lead after a few, simple manipulations to

$$\frac{\partial \omega'_\alpha}{\partial t} = -v'_\beta \frac{\partial \omega'_\alpha}{\partial x_\beta} + \omega'_\beta \frac{\partial v'_\alpha}{\partial x_\beta} + \frac{1}{Re} \Delta \omega'_\alpha$$

The pde for enstrophy $e^2 = \omega'_\alpha \omega'_\alpha$ follows then

$$\frac{\partial e^2}{\partial t} = -v'_\beta \frac{\partial e^2}{\partial x_\beta} + 2\omega'_\alpha \omega'_\beta s'_{\alpha\beta} + \frac{1}{Re} \Delta e^2 - \frac{2}{Re} \frac{\partial \omega'_\alpha}{\partial x_\beta} \frac{\partial \omega'_\alpha}{\partial x_\beta}$$

in a few steps. Averaging and applying the assumption of homogeneity leads finally to the desired result

$$\frac{\partial \langle e^2 \rangle}{\partial t} = 2 \langle \omega'_\alpha \omega'_\beta s'_{\alpha\beta} \rangle - \frac{2}{Re} \langle \frac{\partial \omega'_\alpha}{\partial x_\beta} \frac{\partial \omega'_\alpha}{\partial x_\beta} \rangle$$

The dynamics of the mean enstrophy is determined by the balance between the vortex stretching term $2 \langle \omega'_\alpha \omega'_\beta s'_{\alpha\beta} \rangle$ and the viscous destruction term $\frac{2}{Re} \langle \frac{\partial \omega'_\alpha}{\partial x_\beta} \frac{\partial \omega'_\alpha}{\partial x_\beta} \rangle > 0$.

References:

Enstrophy plays an important role in wall-bounded turbulent flows, see Tsinober [12] for analysis and discussion of experimental results.

Problem (3.3): Consider the pde for the mean enstrophy for homogeneous turbulence obtained in the previous problem.

(3.3.1) Solve the pde assuming that the vortex stretching term has the form

$$\langle \omega_\alpha \omega_\beta \frac{\partial v_\alpha}{\partial x_\beta} \rangle \approx A e^{\frac{3}{2}}$$

where $A > 0$ is a constant and the initial value $e(0) > 0$ is known.

(3.3.2) Determine the pde for $\langle e^2 \rangle$ for 2-d ($v_3 = 0$) homogeneous turbulent flow. Solve the pde for the cases

$$\nu \left\langle \frac{\partial \omega_\alpha}{\partial x_\beta} \frac{\partial \omega_\alpha}{\partial x_\beta} \right\rangle \approx 0$$

and

$$\nu \left\langle \frac{\partial \omega_\alpha}{\partial x_\beta} \frac{\partial \omega_\alpha}{\partial x_\beta} \right\rangle \approx B \frac{\langle e^2 \rangle}{\tau}$$

where $B > 0$ and $\tau > 0$ are constants and the initial value $\langle e^2 \rangle(0)$ is known.

Solution:

The enstrophy pde for homogeneous turbulence from the previous problem is

$$\frac{\partial \langle e^2 \rangle}{\partial t} = 2 \langle \omega'_\alpha \omega'_\beta \delta'_{\alpha\beta} \rangle - \frac{2}{Re} \left\langle \frac{\partial \omega'_\alpha}{\partial x_\beta} \frac{\partial \omega'_\alpha}{\partial x_\beta} \right\rangle$$

This pde is indeterminate as it contains three unknown correlations; hence, simple expressions are constructed for two of them to illustrate the possible effect of these correlations on the evolution of enstrophy. The initial value $\langle e^2 \rangle(0) > 0$ is given in each case.

(3.3.1) For inviscid fluids and 3-d turbulence the expression

$$\langle \omega_\alpha \omega_\beta \frac{\partial v_\alpha}{\partial x_\beta} \rangle \approx A e^{\frac{3}{2}}$$

is suggested. The pde is then given by

$$\frac{\partial \langle e^2 \rangle}{\partial t} = A \langle e^2 \rangle^{\frac{3}{2}}$$

The solution of the IVP follows from integration

$$\int \frac{d \langle e^2 \rangle}{\langle e^2 \rangle^{\frac{3}{2}}} = At + c$$

Hence

$$\langle e^2 \rangle(t) = \frac{\langle e^2 \rangle(0)}{\left(1 - \frac{1}{2} A \sqrt{\langle e^2 \rangle(0) t}\right)^2}$$

The solution blows up for $t \rightarrow \frac{2}{A \sqrt{\langle e^2 \rangle(0)}}$.

(3.3.2) Consider 2-d turbulence, i.e. $v'_3 = 0$, then is $i \omega'_\alpha = \delta_{\alpha,3} \omega'(x_1, x_2, t)$ and $\langle e^2 \rangle = \langle \omega'^2 \rangle$. It follows, that

$$2\omega'_\alpha \omega'_\beta s'_{\alpha\beta} = 0$$

holds for purely geometric reasons; hence, there is no vortex stretching. The pde for enstrophy in 2-d turbulence emerges in the form

$$\frac{\partial \langle e^2 \rangle}{\partial t} = -\frac{2}{Re} \langle \frac{\partial \omega'}{\partial x_\beta} \frac{\partial \omega'}{\partial x_\beta} \rangle$$

Two expressions for the viscous destruction are considered.

(a) Inviscid fluids and $\omega' \in C^1 \cap L_2$, then

$$\frac{\partial \langle e^2 \rangle}{\partial t} = 0$$

with solution

$$\langle e^2 \rangle(t) = \langle e^2 \rangle(0)$$

Enstrophy is, therefore, invariant.

(b) For viscous fluids the expression

$$\frac{2}{Re} \langle \frac{\partial \omega'_\alpha}{\partial x_\beta} \frac{\partial \omega'_\alpha}{\partial x_\beta} \rangle \approx B \frac{\langle e^2 \rangle(t)}{\tau}$$

is suggested, where $B, \tau > 0$ are constants. The solution of the IVP is then

$$\langle e^2 \rangle(t) = \langle e^2 \rangle(0) \exp\left(-\frac{Bt}{\tau}\right)$$

Thus enstrophy decays in 2-d turbulence for the present expression for the viscous correlation. The exact form of the viscous correlation is unknown and it is not a local function, but a functional of the velocity field and its curl.

Problem (3.4): Consider the Euler equations, i.e. the Navier–Stokes pdes (2.6) and (2.7) for an inviscid, incompressible fluid

$$\frac{Dv_\alpha}{Dt} = -\frac{\partial p}{\partial x_\alpha}, \quad \frac{\partial v_\alpha}{\partial x_\alpha} = 0$$

(3.4.1) Derive the vorticity transport equation from the Euler equations. Show that it can be written in terms of the rate of strain tensor

$$s_{\alpha\beta} \equiv \frac{1}{2} \left(\frac{\partial v_\alpha}{\partial x_\beta} + \frac{\partial v_\beta}{\partial x_\alpha} \right)$$

The vector field called vortex stretching term is defined as

$$s_\alpha \equiv \omega_\beta \frac{\partial v_\alpha}{\partial x_\beta}$$

Express it in terms of the rate of strain tensor $s_{\alpha\beta}$.

(3.4.2) Derive the transport equation for enstrophy (3.16). Define the vorticity stretch factor $\alpha(t, \mathbf{x})$ by

$$\alpha(t, \mathbf{x}) \equiv \frac{\omega_\alpha s_{\alpha\beta} \omega_\beta}{e^2}$$

and express the right side of the enstrophy pde in terms of α .

(3.4.3) Let the vorticity stretch factor $\alpha(t, \mathbf{x})$ be a given scalar field, then transform the enstrophy equation to the material description and solve it for the initial condition $e(0, \mathbf{X}) = e_0(\mathbf{X})$, where $\mathbf{X} \in \mathcal{D}(0) = \mathbb{R}^3$.

(3.4.4) Derive the transport equation for the stretch vector field $\sigma_\alpha \equiv \omega_\beta \frac{\partial v_\alpha}{\partial x_\beta}$ (Ohkitani's equation). Introduce the pressure Hessian (2.117)

$$P_{\alpha\beta} \equiv \frac{\partial^2 p}{\partial x_\alpha \partial x_\beta}$$

into the transport pde.

(3.4.5) Show that the second substantial time derivative of vorticity is proportional to the pressure Hessian.

(3.4.6) Define the vector field $\delta_\alpha(t, \mathbf{x}) \equiv \epsilon_{\alpha\beta\gamma} \omega_\beta s_{\gamma\delta} \omega_\delta$ and derive its transport pde. Show that the right-hand side is proportional to the pressure Hessian.

(3.4.7) Redefine the stretch vector field

$$\chi_\alpha(t, \mathbf{x}) \equiv \frac{1}{e^2} \epsilon_{\alpha\beta\gamma} \omega_\beta s_{\gamma\delta} \omega_\delta$$

where

$$\alpha(t, \mathbf{x}) = \frac{1}{e^2} \omega_\alpha s_{\alpha\beta} \omega_\beta$$

is the vorticity stretch factor defined in (2), and the analogous fields replacing the rate of strain with the pressure Hessian

$$\chi_\alpha^p(t, \mathbf{x}) \equiv \frac{1}{e^2} \epsilon_{\alpha\beta\gamma} \omega_\beta P_{\gamma\delta} \omega_\delta, \quad \alpha^p(t, \mathbf{x}) \equiv \frac{1}{e^2} \omega_\alpha P_{\alpha\beta} \omega_\beta$$

Derive the transport equations for the stretch factor α and the stretch vector χ_α .

Solution:

(3.4.1) Applications of the curl to the momentum balance produce the vorticity pde

$$\frac{D\omega_\alpha}{Dt} = \sigma_\alpha \quad (1)$$

where the stretching vector is defined by $\sigma_\alpha \equiv \omega_\beta s_{\alpha\beta}$ and the rate of strain by $s_{\alpha\beta} \equiv \frac{1}{2}(\frac{\partial v_\alpha}{\partial x_\beta} + \frac{\partial v_\beta}{\partial x_\alpha})$.

(3.4.2) The pde for enstrophy squared e^2 follows at once

$$\frac{De^2}{Dt} = 2\omega_\alpha \omega_\beta s_{\alpha\beta}$$

which is recast in the form

$$\frac{De}{Dt} = \alpha(\mathbf{x}, t)e \quad (2)$$

containing the local stretch factor

$$\alpha(\mathbf{x}, t) \equiv \frac{1}{e^2} \omega_\alpha s_{\alpha\beta} \omega_\beta$$

(3.4.3) Let $\alpha(\mathbf{x}, t)$ be known, then the pde (2) can be transformed to an IVP in the material description according to $\Phi(\mathbf{X}, \tau) = \mathbf{x}, \tau = t$

$$\frac{\partial e}{\partial \tau} = \alpha(\mathbf{X}, \tau)e(\mathbf{X}, \tau), \quad e(\mathbf{X}, 0) = e_0(\mathbf{X})$$

with initial values e_0 specified for all positions \mathbf{X} at the reference time $\tau = 0$. The solution of this IVP is straightforward

$$e(\mathbf{X}, \tau) = e_0(\mathbf{X}) \exp\left[\int_0^\tau d\tau' \alpha(\mathbf{X}, \tau')\right]$$

Note that the integral is along the pathline of the material point that started at \mathbf{X} .

(3.4.4) The pde for the stretching vector $\sigma_\alpha = \omega_\beta \frac{\partial v_\alpha}{\partial x_\beta}$ (called Ohkitani's equation) follows from

$$\frac{D\sigma_\alpha}{Dt} = \frac{\partial v_\alpha}{\partial x_\beta} \frac{D\omega_\beta}{Dt} + \omega_\beta \frac{D}{Dt}(\frac{\partial v_\alpha}{\partial x_\beta})$$

Using the relation

$$\frac{D}{Dt}(\frac{\partial v_\alpha}{\partial x_\beta}) = \frac{\partial}{\partial x_\beta}(\frac{Dv_\alpha}{Dt}) - \frac{\partial v_\gamma}{\partial x_\beta} \frac{\partial v_\alpha}{\partial x_\gamma}$$

the pde for σ_α

$$\frac{D\sigma_\alpha}{Dt} = \frac{\partial v_\alpha}{\partial x_\beta} \frac{D\omega_\beta}{Dt} - \sigma_\gamma \frac{\partial v_\alpha}{\partial x_\gamma} + \omega_\beta \frac{\partial}{\partial x_\beta} \left(\frac{Dv_\alpha}{Dt} \right)$$

follows. The vorticity pde (1) and the differentiated momentum balance

$$\frac{\partial}{\partial x_\beta} \left(\frac{Dv_\alpha}{Dt} \right) = -P_{\alpha\beta}$$

where $P_{\alpha\beta}$ denotes the pressure Hessian (2.117)

$$P_{\alpha\beta} = \frac{\partial^2 p}{\partial x_\alpha \partial x_\beta}$$

lead to the desired pde

$$\frac{D\sigma_\alpha}{Dt} = -\omega_\beta P_{\alpha\beta} \quad (3)$$

for the stretch vector σ_α .

(3.4.5) The pde for the stretch vector has an interesting consequence following from the vorticity pde (1) by substantial differentiation

$$\frac{D}{Dt} \left(\frac{D\omega_\alpha}{Dt} \right) = \frac{D}{Dt} (\omega_\beta s_{\alpha\beta}) = \frac{D\sigma_\alpha}{Dt}$$

and the definition of the stretch vector

$$\frac{D^2\omega_\alpha}{Dt^2} = -\omega_\beta P_{\alpha\beta}$$

(3.4.6) The vector field $\omega \times \mathbf{e}$ or in Cartesian coordinates $\delta_\alpha = \epsilon_{\alpha\beta\gamma} \omega_\beta \omega_\delta s_{\gamma\delta}$ is governed by a pde that follows from the vorticity pde (1) and the pde (3) for stretch vector

$$\frac{D\delta_\alpha}{Dt} = -\epsilon_{\alpha\beta\gamma} \omega_\beta \omega_\delta P_{\gamma\delta}$$

The evolution of δ_α is clearly dominated by the pressure Hessian. (3.4.7) Define $\chi \equiv \frac{1}{e^2} \delta_\alpha = \frac{1}{e^2} \epsilon_{\alpha\beta\gamma} \omega_\beta \omega_\delta s_{\gamma\delta}$, recall the vorticity stretch factor $\alpha(\mathbf{x}, t) = \frac{1}{e^2} \omega_\alpha s_{\alpha\beta} \omega_\beta$ from (2) and define the stretch fields proportional to the pressure Hessian

$$\chi_\alpha^P \equiv \frac{1}{e^2} \epsilon_{\alpha\beta\gamma} \omega_\beta P_{\gamma\delta} \omega_\delta, \quad \alpha^P \equiv \frac{1}{e^2} \omega_\alpha P_{\alpha\beta} \omega_\beta$$

The pde for the vorticity stretch field follows from

$$\frac{D\alpha}{Dt} = -\frac{2}{e^3} \frac{De}{Dt} + \frac{1}{e^2} \frac{D}{Dt} (\omega_\alpha s_{\alpha\beta} \omega_\beta)$$

The first term on the right can be evaluated as follows:

$$\frac{2}{e^3} \frac{De}{Dt} = \frac{2}{e} \alpha \frac{De}{Dt} = 2\alpha^2$$

since $\frac{De}{Dt} = \alpha e$. The second term is

$$\frac{1}{e^2} \frac{D}{Dt} (\omega_\alpha s_{\alpha\beta} \omega_\beta) = \frac{1}{e^2} \frac{D}{Dt} (\omega_\alpha \sigma_\alpha) = \frac{1}{e^2} \sigma_\alpha \frac{D\omega_\alpha}{Dt} + \frac{1}{e^2} \omega_\alpha \frac{D\sigma_\alpha}{Dt}$$

and using (1) $\frac{D\omega_\alpha}{Dt} = \sigma_\alpha$ and (3) $\frac{D\sigma_\alpha}{Dt} = -\omega_\beta P_{\alpha\beta}$ the result

$$\frac{1}{e^2} \frac{D}{Dt} (\omega_\alpha s_{\alpha\beta} \omega_\beta) = \frac{1}{e^2} \sigma_\alpha \sigma_\alpha - \alpha^P$$

is obtained. The pde for α is thus

$$\frac{D\alpha}{Dt} = -2\alpha^2 + \frac{1}{e^2} \sigma_\alpha \sigma_\alpha - \alpha^P$$

An alternative version follows from $\chi_\alpha \chi_\alpha = \frac{1}{e^4} \epsilon_{\alpha\beta\gamma} \epsilon_{\alpha\eta\zeta} \omega_\beta \omega_\eta s_{\gamma\delta} s_{\zeta\chi} \omega_\delta \omega_\chi$ using $\epsilon_{\alpha\beta\gamma} \epsilon_{\alpha\eta\zeta} = \delta_{\beta\eta} \delta_{\gamma\zeta} - \delta_{\beta\zeta} \delta_{\gamma\eta}$, hence

$$\chi_\alpha \chi_\alpha = \frac{1}{e^2} \omega_\delta s_{\gamma\delta} s_{\gamma\chi} \omega_\chi - \frac{1}{e^4} \omega_\beta \omega_\gamma s_{\gamma\delta} s_{\beta\chi} \omega_\delta \omega_\chi$$

or

$$\chi_\alpha \chi_\alpha = \frac{1}{e^2} \sigma_\alpha \sigma_\alpha - \alpha^2$$

The alternative version is thus given by

$$\frac{D\alpha}{Dt} = -2\alpha^2 + \chi_\alpha \chi_\alpha - \alpha^P$$

Finally, the pde for the stretch vector χ_α follows from

$$\frac{D\chi_\alpha}{Dt} = \frac{D}{Dt} \left(\frac{1}{e^2} \epsilon_{\alpha\beta\gamma} \omega_\beta s_{\gamma\delta} \omega_\delta \right)$$

Using similar steps as before the result

$$\frac{D\chi_\alpha}{Dt} = -2\alpha \chi_\alpha - \chi_\alpha^P$$

is obtained. The odes containing substantial time derivatives can be integrated in the material description, if the right-hand side is known. The integrals are then along pathlines for specified initial position \mathbf{X} .

References:

The material for this problem was taken from Chap. 2 of the article by Gibbon et al. in [13], which contains more details and further material on Euler singularities. The authors of this paper make a serious effort to present the pdes in a clear, concise form to aid the interpretation. This is achieved using variables in mixed spatial/material description, placing the transformation (2.80) and the substantial derivative at the centre for the interpretation of the equations.

The paper by Wilczek and Meneveau [14] analyses the pressure Hessian in detail based on Gaussian random velocity fields. The role of the pressure Hessian in preventing finite-time singularity induced by the local self-amplification is evaluated for Gaussian random fields. The Gaussian field analysis contributes to the understanding of the extent and role of non-Gaussianity (internal intermittency) observed in DNS simulations.

Solutions to problems in Chap. 4: Flow domains and bases

Problem (4.1): The Jacobi orthogonal polynomials $P_n^{\alpha,\beta}(x)$, which are the solutions of the ode

$$(1-x^2) \frac{d^2 P_n^{\alpha,\beta}}{dx^2} + [\beta - \alpha - (\alpha + \beta + 2)x] \frac{d P_n^{\alpha,\beta}}{dx} + n(n + \alpha + \beta + 1) P_n^{\alpha,\beta} = 0$$

are related to the Sturm–Liouville ode, which in turn appears in the construction of basis functions and the evaluation of certain functional integrals. Hence, clarify this relation by determining the eigenvalues and eigenfunctions of the Sturm–Liouville operator (6.35)

$$\mathcal{L} \equiv \frac{1}{w(x)} \left[\frac{d}{dx} \left(p(x) \frac{d}{dx} \right) - q(x) \right]$$

defined on the interval $[-1, 1]$ for $p(x) = (1-x)^{\alpha+1}(1+x)^{\beta+1}$, $q(x) = 0$ and weight function $w(x) = (1-x)^\alpha(1+x)^\beta$. Assume $\alpha, \beta > -1$.

(4.1.1) Show that the Sturm–Liouville operator is self-adjoint, i.e. $(\mathcal{L}u, v) = (u, \mathcal{L}v)$ holds with respect to the scalar product

$$(u, v) \equiv \int_{-1}^1 dx w(x) u(x) v(x)$$

for $u(x), v(x) \in C^2_{[-1,1]}$.

(4.1.2) Verify that the Jacobi polynomials are eigenfunctions of the Sturm–Liouville operator for the specified coefficients.

(4.1.3) Expand the test function $f(x) = \sin(\pi kx)$ for $k = 1$ and $k = 16$ in terms of the Jacobi basis $\{P_n^{\alpha, \beta}, n = 0, 1, 2, \dots\}$ for $\alpha = \beta = 0$ fixed. Compute and plot the error

$$e(N) \equiv |f(x) - \sum_{i=0}^N c_i P_i^{\alpha, \beta}|$$

as function of N and the test function $f(x)$ together with partial sums of the expansion.

Solution:

(4.1.1): Let $u(x), v(x) \in C^2_{[-1, 1]}$, then is the Sturm–Liouville operator with the specified coefficients given by

$$\mathcal{L}_{\alpha, \beta} = \frac{1}{(1-x)^\alpha (1+x)^\beta} \frac{d}{dx} \left[(1-x)^{\alpha+1} (1+x)^{\beta+1} \frac{d}{dx} \right]$$

and the scalar product is

$$(\mathcal{L}_{\alpha, \beta} u, v) = \int_{-1}^1 dx \frac{d}{dx} \left[(1-x)^{\alpha+1} (1+x)^{\beta+1} \frac{du}{dx} \right] v(x)$$

It can be evaluated using partial integration, hence

$$(\mathcal{L}_{\alpha, \beta} u, v) = (1-x)^{\alpha+1} (1+x)^{\beta+1} \frac{du}{dx} v(x) \Big|_{x=\pm 1} - \int_{-1}^1 dx \frac{dv}{dx} \left[(1-x)^{\alpha+1} (1+x)^{\beta+1} \frac{du}{dx} \right]$$

The boundary terms vanish since $\alpha > -1, \beta > -1$ and

$$(\mathcal{L}_{\alpha, \beta} u, v) = - \int_{-1}^1 dx \frac{dv}{dx} \left[(1-x)^{\alpha+1} (1+x)^{\beta+1} \frac{du}{dx} \right]$$

follows. Using partial integration once more

$$(\mathcal{L}_{\alpha, \beta} u, v) = \int_{-1}^1 dx u(x) \frac{d}{dx} \left\{ [(1-x)^{\alpha+1} (1+x)^{\beta+1}] \frac{dv}{dx} \right\}$$

is obtained. The differential part of the integrand is recognized as the Sturm–Liouville operator

$$\frac{d}{dx} \left\{ [(1-x)^{\alpha+1}(1+x)^{\beta+1}] \frac{dv}{dx} \right\} = w(x) \mathcal{L}_{\alpha, \beta} v(x)$$

and

$$(\mathcal{L}_{\alpha, \beta} u, v) = (u, \mathcal{L}_{\alpha, \beta} v)$$

follows as claimed.

(4.1.2): The eigenproblem for the Sturm–Liouville operator is the system of non-zero solutions $\Phi(x)$ of $-\mathcal{L}\Phi = \lambda\Phi$ with eigenvalues λ (the negative sign insures non-negative eigenvalues). Expanding the Sturm–Liouville operator leads to

$$\mathcal{L}_{\alpha, \beta} \Phi + \lambda \Phi = (1-x)^2 \frac{d^2 \Phi}{dx^2} + \frac{d\Phi}{dx} \frac{d}{dx} \left[(1-x)^{\alpha+1}(1+x)^{\beta+1} \right] + \lambda \Phi$$

and

$$\mathcal{L}_{\alpha, \beta} \Phi + \lambda \Phi = (1-x)^2 \frac{d^2 \Phi}{dx^2} + [\beta - \alpha - (\alpha + \beta + 2)x] \frac{d\Phi}{dx} + \lambda \Phi$$

Comparison to the ode defining the Jacobi polynomials shows that $\Phi(x) = P_n^{\alpha, \beta}(x)$ with eigenvalue $\lambda = n(n + \alpha + \beta + 1)$ holds.

(4.1.3): The test function $f(x) = \sin(\pi kx)$ is expanded in terms of the basis $\{P_n^{\alpha, \beta}(x), n = 0, 1, 2, \dots\}$ with weight $w(x) = (1-x)^\alpha(1+x)^\beta$

$$f(x) = \lim_{N \rightarrow \infty} \sum_{n=0}^N c_n P_n^{\alpha, \beta}$$

Orthogonality of the basis functions $P_n^{\alpha, \beta}(x)$ allows easy computation of the coefficients c_n

$$c_n = \frac{1}{||P_n^{\alpha, \beta}||^2} \int_{-1}^1 dx w(x) P_n^{\alpha, \beta}(x) f(x), n = 0, 1, 2, \dots$$

where

$$||P_n^{\alpha, \beta}||^2 = \int_{-1}^1 dx w(x) (P_n^{\alpha, \beta})^2(x) = \frac{2^{\alpha+\beta+1} \Gamma(n + \alpha + 1) \Gamma(n + \beta + 1)}{(2n + \alpha + \beta + 1) \Gamma(n + 1) \Gamma(n + \alpha + \beta + 1)}$$

according to [15], Chap. 18. The maximum norm of the error $e(P)$ for the Jacobi parameters $\alpha = \beta = 0$ and weight function $w(x) = (1-x)(1+x)$ is shown in Fig. 28.1 for the wavenumbers $k = 1$ (left graph) and $k = 16$ (right graph) in

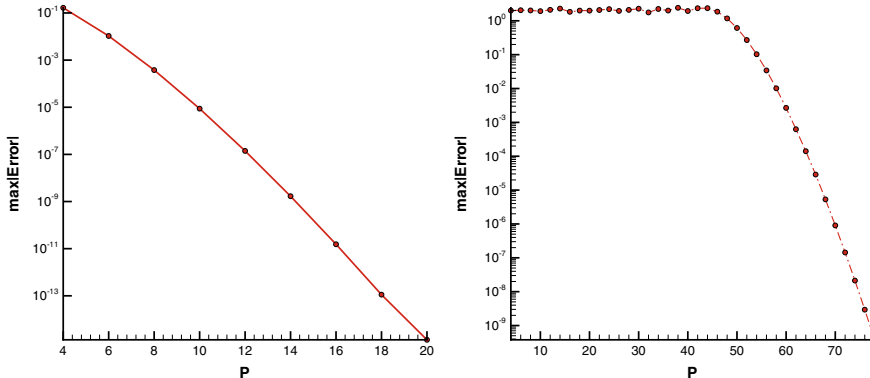


Fig. 28.1 Maximum norm of the error $e(P)$ in representing the test function $f(x) = \sin(k\pi x)$ on $[-1, 1]$ for $k = 1$ (left graph) and $k = 16$ (right graph), P denotes the number of terms in the partial sums for the expansion with the Jacobi parameters $\alpha = \beta = 0$

semi-logarithmic coordinate scale. The rate of convergence is typical for spectral methods. The number of modes for representation to machine accuracy is $P = 20$ for $k = 1$ and $P = 80$ for $k = 16$. The properties of the partial sum $f_{b24}(x) = \sum_{n=0}^P c_n P_n^{\alpha, \beta}(x)$ as approximation of the oscillatory test function are illustrated in Fig. 28.2, for $P = 24$ the error is of order unity, whereas for $P \geq 80$ convergence is limited by the round-off error.

Comments: The properties of orthogonal polynomials such as the Jacobi polynomials can be found in references [15, 16]. An early numerical application of (modified) Jacobi polynomials to pipe flows is given by Leonard and Wray [17] in 1982. The modifications are necessary for the transformation to the radial domain $[0, 1]$ and to satisfy the parity conditions ([18, 19]) to insure smoothness and uniqueness at the axis $r = 0$ and boundary conditions.

Problem (4.2): The Hermite functions (Sect. 4.3.3) are a basis for the space $\Omega = C_{R^1}^\infty \cap L^2_{R^1}$ of functions defined on the unbounded domain R^1 . Determine the coordinates c_i with respect to the basis $\{\Psi_n(x) : n = 0, 1, \dots, \infty\}$ of the test function

$$f(x) = \frac{\cos(kx)}{\sqrt{2\pi\sigma^2}} \exp\left(-\frac{1}{2\sigma^2}(x - x_0)^2\right)$$

for $k = 4$, $x_0 = 0.0$ and $\sigma = 0.5$ as defined in Eq. (4.33) of Sect. 4.3.3. Compute the maximum norm of the error

$$e(N) \equiv |f(x) - \sum_{i=0}^N c_i \Psi_i^x|$$

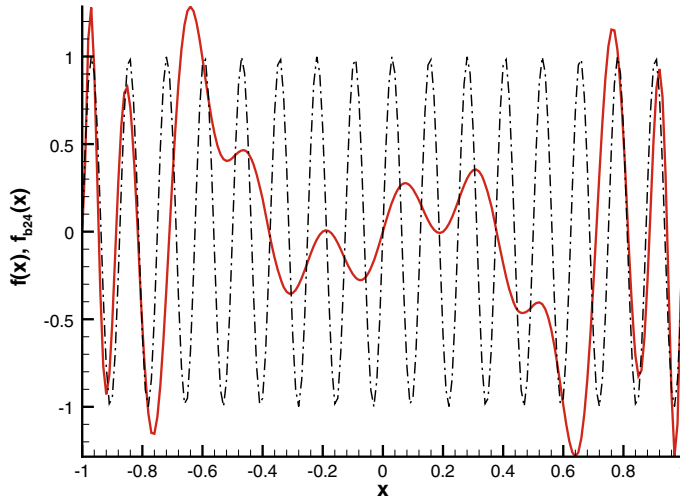


Fig. 28.2 Test function $f(x) = \sin(k\pi x)$ (black dot-dashed line) and partial sum $f_{b24}(x) = \sum_{n=0}^P c_n P_n^{\alpha, \beta}(x)$ ($P = 24$, full red line) for $k = 16$ on $[-1, 1]$. The error for $P = 24$ is of order unity, for $P \geq 80$ it is reduced to machine accuracy as the right graph in Fig. 28.1 indicates

as function of N . Plot the coefficients c_i , the error $e(N)$ and the test function compared to the approximation for $N = 20$ terms.

Solution:

The representation $f(x) = \sum_{j=0}^{\infty} c_j \Psi_j(x)$ (4.33) is determined by the coordinates (4.34)

$$c_j = (f, \Psi_j), j = 0, 1, 2, \dots, \infty$$

The scalar products (f, Ψ_j) are computed numerically using a second-order accurate method. The results are shown in the left graph of Fig. 28.3. The associated error (maximum norm) in the right graph verifies the spectral convergence rate. The quality of the representation (4.33) for $N = 20$ terms is illustrated in Fig. 28.4. The number of terms $N = 20$ is clearly insufficient to represent the test function with acceptable accuracy, but increasing the N to 90 or more leads to satisfactory representation approaching machine accuracy.

Comments: The properties of orthogonal polynomials such as the Hermite polynomials and Hermite functions can be found in [15, 16]. Note that there are two

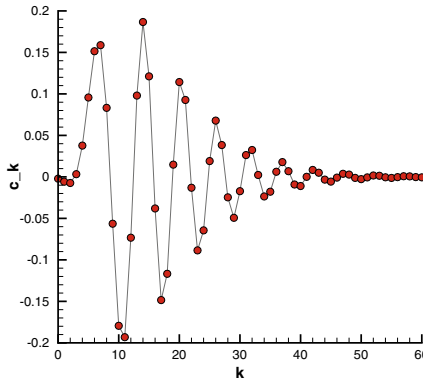
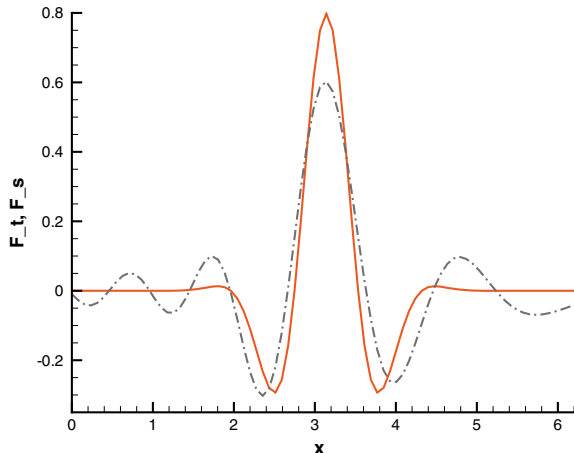


Fig. 28.3 Coordinates of the test function $f(x)$ (red symbols, left graph) with respect to the Hermite function basis and the maximum norm of the error $e(N)$ (right graph) in representing the test function $f(x) = \frac{\cos(kx)}{\sqrt{2\pi\sigma^2}} \exp(-\frac{1}{2\sigma^2}(x - x_0)^2)$ with $k = 4$, $x_0 = 0$, $\sigma = 0.5$ on $R^1 = [-\infty, \infty]$, N denotes the number of terms in the partial sums for the expansion (4.33)

Fig. 28.4 Test function $f(x) \in C_{R^1}^\infty \cap L_{R^1}^2$ (red line) and the approximation

$$f_N(x) = \sum_{i=0}^N c_i \Psi_i^x \text{ for}$$

$N = 20$ terms (black dot-dashed line) using the Hermite function basis. The difference between test function and approximation is not discernible for $N > 80$ as the right graph in Fig. 28.3 indicates



slightly different definitions of Hermite polynomials, and the present example uses the physicist's version (4.30)

$$H_n(x) = (-1)^n \exp(x^2) \frac{d^n}{dx^n} \exp(-x^2)$$

valid for $n = 0, 1, \dots, \infty$.

Problem (4.3): Solve the BVPs for the Poisson pdes

$$\epsilon_{\delta\eta\alpha} \frac{\partial\omega_\alpha}{\partial x_\eta} = \frac{\partial^2 v_\eta}{\partial x_\delta \partial x_\eta} - \frac{\partial^2 v_\delta}{\partial x_\eta \partial x_\eta}$$

or in symbolic notation

$$\nabla \times \boldsymbol{\omega} = \nabla(\nabla \cdot \mathbf{v}) - \Delta \mathbf{v}$$

for the disturbance velocity for a doubly periodic flow in a cubic domain \mathcal{D} in Cartesian coordinates. The domain is defined by

$$\mathcal{D} \equiv \{(x_1, x_2, x_3) : 0 \leq x_1 \leq 2\pi L_1, -L_2 \leq x_2 \leq L_2, -\pi L_3 \leq x_3 \leq \pi L_3\}$$

with x_1 and x_3 as periodic directions. Velocity is the sum of the disturbance field $\mathbf{v}(\mathbf{x})$ periodic with respect to x_1 and x_3 and a basic/mean field

$$V_\alpha(x_1, x_2, x_3) = \delta_{\alpha,1} V_1(x_2) + v_\alpha(x_1, x_2, x_3)$$

The basic field $V_1(x_2)$ is assumed known, for instance, constructed analytically using the Gaussian error function. Assume an incompressible fluid.

(4.3.1) Fourier transform the Poisson pde to set up the BVP for the odes governing the complex-valued Fourier modes $\hat{v}_\alpha^{k,m}(x_2, t)$, where k and m are the wavenumbers corresponding to x_1 and x_3 .

(4.3.2) Solve the BVP for the Fourier modes.

Solution:

The solution relies of FFT to reduce it to a set of BVPs for linear second-order odes. The Poisson pdes for an incompressible fluid are reduced to

$$-\Delta \mathbf{v} = \nabla \times \boldsymbol{\omega}$$

plus Dirichlet boundary conditions.

(4.3.1): The disturbance velocity \mathbf{v} is assumed three times continuously differentiable. This implies that vector fields are periodic with respect to the Cartesian coordinates x_1 and x_3 , thus allowing the application of 2-d fast Fourier transform (FFT), Boyd [18]. Smooth fields periodic with respect to x_1 and x_3 admit the discrete Fourier transform (Canuto et al. [20] 1988) denoted by

$$\varphi(x_1, x_2, x_3) = \mathcal{F}_N^{-1}(x_1, x_3 | \hat{\varphi}(k, x_2, m)), \quad \hat{\varphi}(k, x_2, m) = \mathcal{F}_N(k, m | \varphi(x_1, x_2, x_3))$$

where $x_{1,k} = 2\pi k/N$ and $x_{3,m} = 2\pi m/N$ are the discrete collocation points, for $x_1 \neq x_{1,k}$, $x_3 \neq x_{3,m}$ the transform interpolates the values of φ between the discrete collocation points. The explicit forms are given by

$$\mathcal{F}_N(k, m | \varphi(x_1, x_2, x_3)) \equiv \frac{1}{N^2} \sum_{k=0}^{N-1} \sum_{m=0}^{N-1} \varphi(x_{1,k}, x_2, x_{3,m}) \exp(-i(kx_{1,k} + mx_{3,m}))$$

where $k = -N/2, \dots, N/2 - 1$, $m = -N/2, \dots, N/2 - 1$ and the inverse transform by

$$\mathcal{F}_N^{-1}(x_1, x_3 | \hat{\varphi}(k, x_2, m)) \equiv \sum_{k=-N/2}^{N/2-1} \sum_{m=-N/2}^{N/2} \hat{\varphi}(k, x_2, m) \exp(i(kx_{1,k} + mx_{3,m}))$$

where $k = 0, \dots, N - 1$, $m = 0, \dots, N - 1$. The discrete Fourier transform becomes for $N \rightarrow \infty$ the standard transform denoted by \mathcal{F} and its inverse by \mathcal{F}^{-1} . The numerical application of the discrete Fourier transforms can be done efficiently with widely available FFT software.

The transformation of the Poisson pdes for the disturbance velocity components $v_\alpha(\mathbf{x})$ is established first, and then the Dirichlet/ Neumann boundary values for it are transformed (variables in Fourier space are denoted with hat). It is convenient to rescale the coordinates x_1 and x_3 according to (26.22) $\zeta_i \equiv \frac{x_i}{L_i}$, $i = 1, 3$, $\beta_1 \equiv \frac{|k|}{L_1}$, $\beta_3 \equiv \frac{|m|}{L_3}$ where $\zeta_i \in [0, 2\pi]$ and the Poisson pdes are then (26.23)

$$-\left[\frac{1}{L_1^2} \frac{\partial^2}{\partial \zeta_1^2} + \frac{\partial^2}{\partial x_2^2} + \frac{1}{L_3^2} \frac{\partial^2}{\partial \zeta_3^2} \right] v_\alpha(\zeta_1, x_2, \zeta_3) = R_\alpha(\zeta_1, x_2, \zeta_3)$$

for $\alpha = 1, 2, 3$, where the right-hand side is abbreviated by

$$R_\alpha(\zeta_1, x_2, \zeta_3) \equiv \epsilon_{\alpha\beta\gamma} \frac{\partial \omega_\gamma}{\partial x_\beta}(\zeta_1, x_2, \zeta_3)$$

The disturbance velocity components v_α are then transformed according to (26.20)

$$v_\alpha(\zeta_1, x_2, \zeta_3) = \mathcal{F}_N^{-1}(\zeta_1, \zeta_3 | \hat{v}_\alpha(k, x_2, m))$$

with coefficients (called modes) emerging as integrals (26.21)

$$\hat{v}_\alpha(k, x_2, m) = \mathcal{F}_N(k, m | v_\alpha(\zeta_1, x_2, \zeta_3))$$

also denoted by $\hat{v}_\alpha^{k,m}(x_2)$, $\hat{R}_\alpha^{k,m}(x_2)$. Fourier transform of the Poisson pde (26.23) with respect to x_1 and x_3 leads to a system of linear, second-order odes (called modal odes) (26.26)

$$-\left(\frac{d^2}{dx_2^2} - \beta^2 \right) \hat{v}_\alpha^{k,m}(x_2) = \hat{R}_\alpha^{k,m}(x_2)$$

valid in the interval $x_2 \in [-L_2, L_2]$ and depending on the longitudinal and lateral wavenumbers $0 \leq k < \infty$ and $-\infty < m < \infty$, where $\beta^2 \equiv \beta_1^2 + \beta_2^2$ and $\hat{R}_\alpha^{k,m}(x_2)$ denotes the Fourier-transformed right-hand side (26.27)

$$R_\alpha(\zeta_1, x_2, \zeta_3) = \mathcal{F}_N^{-1}(\zeta_1, \zeta_3 | \hat{R}_\alpha^{k,m}(x_2)), \quad \hat{R}_\alpha^{k,m}(x_2) = \mathcal{F}_N(k, m | R_\alpha(\zeta_1, x_2, \zeta_3))$$

according to the Fourier transformation (26.20), (26.21).

The boundary conditions for the ode (26.26) are either of Dirichlet or Neumann type and may depend on the wavenumbers k and m . The Fourier-transformed disturbance velocities vanish on the boundaries; hence, homogeneous Dirichlet conditions $\hat{v}_\alpha^{k,m}(x_2) = 0$ for $x_2 = \pm L_2$ are prescribed.

(4.3.2): The complex modes $\hat{v}_\alpha^{k,m}(x_2)$ are determined by the BVP (26.26) with homogeneous boundary conditions. Simplifying the notation

$$x \leftarrow x_2, \quad L \leftarrow L_2, \quad y(x) \leftarrow \hat{v}_\alpha^{k,m}(x_2), \quad R(x) \leftarrow \hat{R}_\alpha^{k,m}(x_2)$$

the typical BVP emerges in the form

$$y'' - \beta^2 y = -R, \quad y(\pm L) = 0$$

The solution of this BVP for the linear ode with constant coefficients has the form

$$y(x) = c_1 y_1(x) + c_2 y_2(x) + y_p(x)$$

where y_1 and y_2 are two linearly independent solutions of the homogeneous ode

$$y'' - \beta^2 y = 0$$

and $y_p(x)$ is a particular solution on the non-homogeneous ode $y'' - \beta^2 y = -R$.

Solution of the homogeneous ode

The (complementary) solution of the homogeneous ode $y'' - \beta^2 y = 0$ is straightforward. It has exponential form

$$y(x) = c \exp(\lambda x)$$

hence $\lambda^2 = \beta^2$ and thus $y_1 = \exp(\beta x)$, $y_2 = \exp(-\beta x)$, and

$$y_c(x) = c_1 \exp(\beta x) + c_2 \exp(-\beta x)$$

follows as general (complementary) solution of the homogenous ode.

Solution of the non-homogeneous ode

The particular solution of the non-homogeneous ode $y'' - \beta^2 y = -R$ is computed with the aid of variation of the parameters $u_1(x) \leftarrow c_1$ and $u_2(x) \leftarrow c_2$. The particular solution is thus written as

$$y_p(x) = u_1(x)y_1(x) + u_2(x)y_2(x)$$

The first derivative is

$$y'_p(x) = u'_1(x)y_1(x) + u'_2(x)y_2(x) + u_1(x)y'_1(x) + u_2(x)y'_2(x)$$

At this point the condition

$$u'_1(x)y_1(x) + u'_2(x)y_2(x) = 0$$

is introduced, and it is one of the equations determining the unknowns $u_1(x)$ and $u_2(x)$. Hence,

$$y'_p(x) = u_1(x)y'_1(x) + u_2(x)y'_2(x)$$

is now differentiated

$$y''_p(x) = u'_1(x)y'_1(x) + u'_2(x)y'_2(x) + u_1(x)y''_1(x) + u_2(x)y''_2(x)$$

Using the odes $y'' - \beta^2 y = 0$ and $y'' - \beta^2 y = -R$ generates the second equation

$$u'_1 y'_1 + u'_2 y'_2 = -R$$

for the computation of u_1 and u_2 .

The final result for $u_1(-L) = u_2(-L) = 0$ is the general solution

$$y(x) = c_1 \exp(\beta x) + c_2 \exp(-\beta x)$$

$$- \frac{1}{2\beta} \int_{-L}^x dx' R(x') \exp[-\beta(x' - x)] + \frac{1}{2\beta} \int_{-L}^x dx' R(x') \exp[-\beta(x - x')]$$

or

$$y(x) = c_1 \exp(\beta x) + c_2 \exp(-\beta x) + \frac{1}{\beta} \int_{-L}^x dx' R(x') \sinh[\beta(x' - x)]$$

completing the solution procedure. The constants c_1 and c_2 are determined by the boundary conditions. Returning to the original notation produces the general solution of the BVP

$$\hat{v}_\alpha^{k,m}(x_2) = c_1 \exp(\beta x_2) + c_2 \exp(-\beta x_2) + \frac{1}{\beta} \int_{-L_2}^{x_2} dx'_2 \hat{R}_\alpha^{k,m}(x'_2) \sinh[\beta(x'_2 - x_2)] \quad (28.4)$$

for the complex-valued Cartesian vector modes, $\alpha = 1, 2, 3$ and $\beta^2 = \beta_1^2 + \beta_3^2 = (\frac{k}{L_1})^2 + (\frac{m}{L_3})^2$.

It remains to compute the constants c_1 and c_2 . Application of the homogeneous Dirichlet conditions $\hat{v}_\alpha^{k,m}(\pm L_2) = 0$ leads to the final result in Fourier space

$$\begin{aligned}\hat{v}_\alpha^{k,m}(x_2) = & -\frac{\exp(\beta(x_2 - L_2))}{2\beta \sinh(2\beta L_2)} \int_{-L_2}^{L_2} dx'_2 \hat{R}_\alpha^{k,m}(x'_2) \sinh[\beta(x'_2 - x_2)] \\ & + \frac{\exp(-\beta(x_2 + L_2))}{2\beta \exp(2\beta L_2) \sinh(2\beta L_2)} \int_{-L_2}^{L_2} dx'_2 \hat{R}_\alpha^{k,m}(x'_2) \sinh[\beta(x'_2 - x_2)] \\ & + \frac{1}{\beta} \int_{-L_2}^{x_2} dx'_2 \hat{R}_\alpha^{k,m}(x'_2) \sinh[\beta(x'_2 - x_2)]\end{aligned}\quad (28.5)$$

Inverse Fourier transformation (FFT) restores the disturbance velocity in physical space

$$v_\alpha(x_1, x_2, x_3) = \mathcal{F}_N^{-1}(x_1, x_3 | \hat{v}_\alpha^{k,m}(x_2)), \quad \alpha = 1, 2, 3 \quad (28.6)$$

completing the task. The solution of the homogeneous BVP for the Poisson pde governing the disturbance velocity is thus reduced to quadratures and 2-d Fourier transforms.

Comments: This example shows that the Cartesian case (plane shear layer) is much simpler than the axisymmetric case (periodic pipe flow, see Sect. 9.2.2 using Green's functions for the pressure). Both cases show the advantage of the Fourier basis for the solution of linear BVPs.

Problem (4.4): Let $\Omega = \{\mathbf{v}(\mathbf{x}) \in L^2_{\mathcal{D}} \cap C^2_{\mathcal{D}}\}$ be the phase space for the compact flow domain $\mathcal{D} \subset \mathbb{R}^3$ with n. e. smooth boundary $\partial\mathcal{D}$, Ω is then Hilbert space w.r.t.

$$\|\mathbf{v}\|^2 = (\mathbf{v} \cdot \mathbf{v})$$

and scalar product

$$(\mathbf{v}, \mathbf{w}) \equiv \int_{\mathcal{D}} d\nu v_\alpha(\mathbf{x}) w_\alpha(\mathbf{x})$$

(Cartesian coordinates), let $F[\mathbf{v}] : \Omega \rightarrow \mathbb{R}^1$ be a linear functional defined by

$$F[\mathbf{v}] \equiv \int_{\mathcal{D}} d\nu K_\alpha(\mathbf{x}) v_\alpha(\mathbf{x})$$

for $K_\alpha(\mathbf{x}) \in \Omega$.

(4.4.1): Compute the first Gateaux derivative of the functional $F[\mathbf{v}]$ w.r.t. $\mathbf{v}(\mathbf{x})$.

(4.4.2): Compute the first Gateaux derivative of (4.4.1) w.r.t. the ONS vector basis $\mathcal{B} \equiv \{\mathbf{f}^k(\mathbf{x}), k = 1, \dots, \infty\}$.

(4.4.3): Compute the second Gateaux derivative w.r.t. $\mathbf{v}(\mathbf{x})$.

Hint: Consult Sect. 23.12.

Solution:

The Gateaux derivative (23.46) is defined in Sect. 23.12, hence is the Gateaux differential

$$\delta F[\mathbf{v}(\cdot)] = \lim_{\epsilon \rightarrow 0} \frac{1}{\epsilon} \{F[\mathbf{v} + \epsilon \mathbf{h}] - F[\mathbf{v}]\}, \quad \mathbf{h} \in \Omega$$

containing the first Gateaux derivative

$$\delta F[\mathbf{v}(\cdot)] = \int_{\mathcal{D}} d\nu h_{\alpha} \frac{\delta F}{\delta v_{\alpha}(\mathbf{x})}$$

Consider now the Hilbert space Ω equipped with an ONS vector basis $\mathcal{B} \equiv \{\mathbf{f}^n(\mathbf{x}), n = 1, \dots, \infty\}$, then is

$$f_n((\mathbf{v}, \mathbf{f}^1), \dots, (\mathbf{v}, \mathbf{f}^n)) \equiv F\left[\sum_{k=1}^n (\mathbf{v}, \mathbf{f}^k) \mathbf{f}^k(\mathbf{x})\right]$$

a projection of the functional F onto the space of regular functions $C_{R^n}^2$ defined in R^n (note that the variation of $\mathbf{v}(\mathbf{x})$ in Ω implies variation of the coefficients $(\mathbf{v}, \mathbf{f}^k)$ without change of the basis vectors). The first Gateaux differential for argument fields $\mathbf{v}(\mathbf{x}) = \sum_{k=1}^n (\mathbf{v}, \mathbf{f}^k) \mathbf{f}^k(\mathbf{x})$ is then

$$\delta F[\mathbf{v}(\cdot)] = \lim_{\epsilon \rightarrow 0} \frac{1}{\epsilon} \{F\left[\sum_{k=1}^n c_k \mathbf{f}^k(\mathbf{x}) + \epsilon \sum_{k=1}^n d_k \mathbf{f}^k(\mathbf{x})\right] - F\left[\sum_{k=1}^n c_k \mathbf{f}^k(\mathbf{x})\right]\}$$

where the sequences $c_k, d_k, k = 1, \dots, n$ define the finite-dimensional argument fields \mathbf{v} and \mathbf{h} . Hence,

$$\delta F[\mathbf{v}(\cdot)] = \lim_{\epsilon \rightarrow 0} \frac{1}{\epsilon} \{f_n(c_1 + \epsilon d_1, \dots, c_n + \epsilon d_n) - f_n(c_1, \dots, c_n)\}$$

where $f(c_1, \dots, c_n)$ inherits the smoothness properties of the functional $F\left[\sum_{k=1}^n c_k \mathbf{f}^k(\mathbf{x})\right]$ since $c_k = (\mathbf{v}, \mathbf{f}^k)$, etc. Taylor series expansion leads to

$$\delta F[\mathbf{v}(\cdot)] = \lim_{\epsilon \rightarrow 0} \frac{1}{\epsilon} \{ f_n(c_1, \dots, c_n) + \epsilon \sum_{k=1}^n d_k \frac{\partial f_n}{\partial c_k} + r_n - f_n(c_1, \dots, c_n) \}$$

Since $O(r_n) = \epsilon^3$ it follows that the first Gateaux differential is given by

$$\delta F[\mathbf{v}(\cdot)] = (h, \sum_{k=1}^n \frac{\partial f_n}{\partial c_k} \mathbf{f}^k), \quad \forall \mathbf{v}(\mathbf{x}) = \sum_{k=1}^n c_k \mathbf{f}^k(\mathbf{x})$$

and the first Gateaux derivative is according to (23.46)

$$\frac{\delta F}{\delta v_\alpha} [\mathbf{v}(\cdot); \mathbf{x}] = \sum_{k=1}^n \frac{\partial f_n}{\partial c_k} f_\alpha^k(\mathbf{x}), \quad \text{where } f_n((\mathbf{v}, \mathbf{f}^1), \dots, (\mathbf{v}, \mathbf{f}^n)) \equiv F[\sum_{k=1}^n (\mathbf{v}, \mathbf{f}^k) \mathbf{f}^k(\mathbf{x})]$$

Letting $n \rightarrow \infty$ produces the final result

$$\frac{\delta F}{\delta v_\alpha} [\mathbf{v}(\cdot); \mathbf{x}] = \sum_{k=1}^{\infty} \frac{\partial f_n}{\partial c_k} f_\alpha^k(\mathbf{x})$$

where $f_n((\mathbf{v}, \mathbf{f}^1), \dots, (\mathbf{v}, \mathbf{f}^\infty)) \equiv F[\sum_{k=1}^{\infty} (\mathbf{v}, \mathbf{f}^k) \mathbf{f}^k(\mathbf{x})]$, $c_k = (\mathbf{v}, \mathbf{f}^k)$. Note that the derivative is a functional of $\mathbf{v}(\cdot)$ and a function of location $\mathbf{x} \in \mathcal{D}$.

(4.4.1): The functional F is linear, thus $F[\mathbf{v} + \epsilon \mathbf{h}] = F[\mathbf{v}] + \epsilon F[\mathbf{h}]$ holds, implying

$$\delta F[\mathbf{v}(\cdot)] = \int_{\mathcal{D}} d\nu K_\alpha(\mathbf{x}) h_\alpha(\mathbf{x})$$

and

$$\frac{\delta F}{\delta v_\alpha(\mathbf{x})} = K_\alpha(\mathbf{x})$$

emerges as desired result.

(4.4.2): Let $\mathcal{B} \equiv \{\mathbf{f}^k(\mathbf{x}), k = 1, \dots, \infty\}$ be the ONS vector basis for Ω introduced above, then

$$v_\alpha(\mathbf{x}) = \sum_{k=1}^{\infty} (\mathbf{v}, \mathbf{f}^k) f_\alpha^k(\mathbf{x}), \quad \forall \mathbf{v} \in \Omega, \quad K_\alpha(\mathbf{x}) = \sum_{k=1}^{\infty} (\mathbf{K}, \mathbf{f}^k) f_\alpha^k(\mathbf{x}), \quad \mathbf{K} \in \Omega$$

and

$$F[\mathbf{v}(\cdot)] = \sum_{k=1}^{\infty} (\mathbf{K}, \mathbf{f}^k) (\mathbf{v}, \mathbf{f}^k)$$

hold. The first Gateaux differential is then

$$\delta F[\mathbf{v}(\cdot)] = \int_{\mathcal{D}} d\nu h_\alpha(\mathbf{x}) \sum_{k=1}^{\infty} (\mathbf{K}, \mathbf{f}^k) f_\alpha^k(\mathbf{x})$$

hence

$$\frac{\delta F}{\delta v_\alpha}[\mathbf{v}(\cdot); \mathbf{x}] = \sum_{k=1}^{\infty} (\mathbf{K}, \mathbf{f}^k) f_\alpha^k(\mathbf{x})$$

emerges as the first Gateaux derivative.

(4.4.3): The second Gateaux derivative is computed in analog fashion to the first derivative. Thus, the second Gateaux differential is then

$$\delta^2 F[\mathbf{v}(\cdot); \mathbf{x}] = \lim_{\epsilon \rightarrow 0} \frac{1}{\epsilon} \{ \delta F[\mathbf{v}(\cdot) + \epsilon \mathbf{h}(\cdot); \mathbf{x}] - \delta F[\mathbf{v}(\cdot); \mathbf{x}] \}$$

However, the first Gateaux derivative is independent of the vector argument field $\mathbf{v}(\mathbf{x})$ for linear functionals, hence

$$\delta^2 F[\mathbf{v}(\cdot); \mathbf{x}] = 0$$

and the second Gateaux derivative of a linear functional is, therefore, zero.

Comments: The first Gateaux derivative of a linear functional turns out to be independent of the vector argument field $\mathbf{v}(\mathbf{x})$ and is merely a standard function of location $\mathbf{x} \in \mathcal{D} \subset \mathbb{R}^3$, thus possessing standard derivatives with respect to location $\mathbf{x} \in \mathcal{D}$. All Gateaux/Fréchet derivatives of order two or higher are zero, see Sect. 23.12 for further details.

Solutions to problems in Chap. 6: Probability measure for incompressible turbulence.

Problem 6.1: Compute the Wiener integral of the functional

$$F[f(x)] = \exp\{\lambda \int_0^1 dy w(y) f^2(y)\}$$

directly (without using the Cameron–Martin theorems), where λ is a real number and $w(x) > 0$, $x \in [0, 1]$, over the space C_0 of continuous functions $f(x)$, $x \in [0, 1]$ with respect to the Wiener measure.

(6.1.1) Use the definition of the Wiener integral and the relation (6.43)

$$\int_{-\infty}^{\infty} \cdots \int_{-\infty}^{\infty} dx_1 \cdots dx_N \exp\left(-\sum_{i=1}^N \sum_{j=1}^N a_{i,j} x_i x_j\right) = \pi^{\frac{N}{2}} [\det(a_{i,j})]^{-\frac{1}{2}}$$

valid for positive definite matrices $a_{i,j}$ to derive a recursive relation for the determinant of $a_{i,j}$. Establish the ode and the boundary conditions for $N \rightarrow \infty$.

(6.1.2) Solve the ode for $w(x) = 1$, compute the value of the functional integral and plot it as function of λ .

Solution:

This problem illustrates the relation of certain Wiener integrals to the Sturm-Liouville ode. Let the domain $[0, 1]$ be discretized in equally spaced intervals of length $\Delta x = \frac{1}{N}$, $N > 1$. The functional $F[f(x)]$ becomes then a standard function of N variables

$$F(f_1, \dots, f_N) = \exp\left[\lambda \Delta x \sum_{j=1}^N w_j f_j^2\right]$$

where $w_j \equiv w(j\Delta x)$, $f_j \equiv f(j\Delta x)$.

(6.1.1) The definition (6.31) of the Wiener integral implies

$$\int_C \exp\left\{\lambda \int_0^x dx w(x) f^2(x)\right\} d\mu_w(f) = \lim_{N \rightarrow \infty} \frac{1}{(\pi \Delta x)^{\frac{N}{2}}} \int_{-\infty}^{\infty} \cdots \int_{-\infty}^{\infty} dy_1 \cdots dy_N \exp\left[\sum_{j=1}^N \lambda(\Delta x)^2 w_j \frac{y_j^2}{\Delta x} - \frac{y_1^2}{\Delta x} - \sum_{j=1}^{N-1} \frac{(y_{j+1} - y_j)^2}{\Delta x}\right]$$

requiring the limit of determinants. The transformation $z_j = y_j / (\Delta x)^{\frac{1}{2}}$ leads to

$$\int_C \exp\left\{\lambda \int_0^x dx w(x) f^2(x)\right\} d\mu_w(f) = \lim_{N \rightarrow \infty} \frac{1}{\pi^{\frac{N}{2}}} \int_{-\infty}^{\infty} \cdots \int_{-\infty}^{\infty} dz_1 \cdots dz_N \exp\left[-\left[\sum_{j=1}^N -\lambda(\Delta x)^2 w_j z_j^2 + (z_{j+1} - z_j)^2\right]\right]$$

The terms in the exponent can be rearranged such that the coefficient matrix $a_{i,j}$ defined by

$$\sum_{i=1}^N \sum_{j=1}^N z_i a_{i,j} z_j = z_1^2 + \sum_{i=1}^{N-1} (z_{i+1} - z_i)^2 - \sum_{i=1}^N \lambda(\Delta x)^2 w_i z_i^2$$

can be determined. The sum on the right-hand side is

$$\begin{aligned} z_1^2 + \sum_{i=1}^{N-1} (z_{i+1} - z_i)^2 - \sum_{i=1}^N \lambda(\Delta x)^2 w_i z_i^2 = \\ z_1^2 (1 - \lambda(\Delta x)^2 w_1) + (z_2 - z_1)^2 - \lambda(\Delta x)^2 w_2 z_2^2 + (z_3 - z_2)^2 - \lambda(\Delta x)^2 w_3 z_3^2 + \dots \\ + (z_N - z_{N-1})^2 - \lambda(\Delta x)^2 w_{N-1} z_{N-1}^2 - \lambda(\Delta x)^2 w_N z_N^2 \end{aligned}$$

Simple rearrangement leads to

$$\begin{aligned} z_1^2 + \sum_{i=1}^{N-1} (z_{i+1} - z_i)^2 - \sum_{i=1}^N \lambda(\Delta x)^2 w_i z_i^2 = \\ z_1^2 (2 - \lambda(\Delta x)^2 w_1) - z_1 z_2 + z_2^2 (2 - \lambda(\Delta x)^2 w_2) - z_1 z_2 - z_2 z_3 + z_3^2 (2 - \lambda(\Delta x)^2 w_3) - z_2 z_3 - z_3 z_4 + \dots \\ + z_{N-1}^2 (2 - \lambda(\Delta x)^2 w_{N-1}) - z_{N-1} z_N + z_N^2 (1 - \lambda(\Delta x)^2 w_N) - z_{N-1} z_N \end{aligned}$$

The coefficient matrix $a_{i,j}$ is apparently tridiagonal and can be read off the previous expression

$$a_{i,j} = \begin{pmatrix} 2 - \lambda(\Delta x)^2 w_1 & -1 & 0 & \cdots & 0 & 0 \\ -1 & 2 - \lambda(\Delta x)^2 w_2 & -1 & \cdots & 0 & 0 \\ 0 & -1 & 2 - \lambda(\Delta x)^2 w_3 & \cdots & 0 & 0 \\ \cdots & \cdots & \cdots & \cdots & \cdots & \cdots \\ \cdots & \cdots & \cdots & \cdots & \cdots & \cdots \\ 0 & 0 & 0 & \cdots & 2 - \lambda(\Delta x)^2 w_{N-1} & -1 \\ 0 & 0 & 0 & \cdots & -1 & 1 - \lambda(\Delta x)^2 w_N \end{pmatrix}$$

The Wiener integral emerges thus in the form

$$\int_C \exp\{\lambda \int_0^1 dx w(x) f^2(x)\} d\mu_w(f) = \lim_{N \rightarrow \infty} [\det(a_{i,j})]^{-\frac{1}{2}}$$

according to the hint (6.43) given in the text. Its value can be computed if the limit of the determinants can be determined. The computation of the determinant $|a_{i,j}|$ proceeds by expansion with respect to the elements in the first row. The first step in this expansion is then

$$\begin{aligned}
& \det(a_{i,j}) = \\
& (2 - \lambda(\Delta x)^2 w_1) \det \begin{pmatrix} 2 - \lambda(\Delta x)^2 w_2 & -1 & \cdots & 0 & 0 \\ -1 & 2 - \lambda(\Delta x)^2 w_3 & \cdots & 0 & 0 \\ \cdots & \cdots & \cdots & \cdots & \cdots \\ \cdots & \cdots & \cdots & \cdots & \cdots \\ 0 & 0 & \cdots & 2 - \lambda(\Delta x)^2 w_{N-1} & -1 \\ 0 & 0 & \cdots & -1 & 1 - \lambda(\Delta x)^2 w_N \end{pmatrix} \\
& + \det \begin{pmatrix} -1 & -1 & \cdots & 0 & 0 & 0 \\ 0 & 2 - \lambda(\Delta x)^2 w_3 & \cdots & 0 & 0 & 0 \\ \cdots & \cdots & \cdots & \cdots & \cdots & \cdots \\ \cdots & \cdots & \cdots & \cdots & \cdots & \cdots \\ 0 & 0 & \cdots & 2 - \lambda(\Delta x)^2 w_{N-1} & -1 & 0 \\ 0 & 0 & \cdots & -1 & 1 - \lambda(\Delta x)^2 w_N & 0 \end{pmatrix}
\end{aligned}$$

The second term on the right-hand side developed with respect to the first row

$$\begin{aligned}
& \det \begin{pmatrix} -1 & -1 & \cdots & 0 & 0 & 0 \\ 0 & 2 - \lambda(\Delta x)^2 w_3 & \cdots & 0 & 0 & 0 \\ \cdots & \cdots & \cdots & \cdots & \cdots & \cdots \\ \cdots & \cdots & \cdots & \cdots & \cdots & \cdots \\ 0 & 0 & \cdots & 2 - \lambda(\Delta x)^2 w_{N-1} & -1 & 0 \\ 0 & 0 & \cdots & -1 & 1 - \lambda(\Delta x)^2 w_N & 0 \end{pmatrix} \\
& = - \det \begin{pmatrix} 2 - \lambda(\Delta x)^2 w_3 & \cdots & 0 & 0 \\ \cdots & \cdots & \cdots & \cdots \\ \cdots & \cdots & \cdots & \cdots \\ 0 & \cdots & 2 - \lambda(\Delta x)^2 w_{N-1} & -1 \\ 0 & \cdots & -1 & 1 - \lambda(\Delta x)^2 w_N \end{pmatrix}
\end{aligned}$$

having the same structure as the determinant of the minor in the first term. Denoting the determinant of the $(N - k + 1)$ -dimensional principal minor of $a_{i,j}$ located in the lower right corner by D_k^N , $1 \leq k \leq N - 2$ with $k - 1$ rows/columns removed from $a_{i,j}$ in the upper left corner, the relation

$$D_1^N = [2 - \lambda(\Delta x)^2 w_k] D_2^N - D_3^N$$

emerges. Observe that $\det(a_{i,j}) = D_1^N$ holds. This process can be repeated and the recurrence relation

$$D_k^N = [2 - \lambda(\Delta x)^2 w_k] D_{k+1}^N - D_{k+2}^N$$

is obtained for $1 \leq k \leq N - 2$. The determinant of the one-dimensional minor $k = N$ is

$$D_N^N = 1 - \lambda(\Delta x)^2 w_N$$

and the two-dimensional minor $k = N - 1$

$$D_{N-1}^N = (2 - \lambda(\Delta x)^2 w_{N-1})(1 - \lambda(\Delta x)^2 w_N) - 1$$

or

$$D_{N-1}^N = 1 - \lambda(\Delta x)^2(w_{N-1} + 2w_N) + \lambda^2(\Delta x)^4 w_{N-1} w_N$$

according to the matrix $a_{i,j}$ given above. Writing $D_k^N = D^N(k\Delta x)$, the recurrence relation appears as

$$\frac{1}{\Delta x^2}[D^N(k\Delta x) - 2D^N((k+1)\Delta x) + D^N((k+2)\Delta x)] = -\lambda w(k\Delta x)D^N((k+1)\Delta x)x \quad (\text{E.1})$$

for $1 \leq k \leq N - 2$. The relation for $k = N - 1$ can be rearranged using the relation for $k = N$

$$\begin{aligned} \frac{1}{\Delta x}[D^N(N\Delta x) - D^N((N-1)\Delta x)] &= \\ \lambda\Delta x[w(N\Delta x) + w((N-1)\Delta x)] - \lambda^2(\Delta x)^3 w((N-1)\Delta x)w(N\Delta x) \end{aligned} \quad (\text{E.2})$$

and then the relation for $k = N$ emerges in the form

$$D_N(N\Delta x) = 1 - \lambda(\Delta x)^2 w(N\Delta x) \quad (\text{E.3})$$

It follows that $D^N(k\Delta x)$ is the solution of the finite difference equation (E.1) with boundary conditions (E.2) and (E.3). Passing to the limits $N \rightarrow \infty/\Delta x \rightarrow 0$, such that $\lim_{N \rightarrow \infty} N\Delta x = 1$, produces $D(x) = \lim_{N \rightarrow \infty} D^N(k\Delta x)$ and the ode

$$\frac{d^2 D}{dx^2} + \lambda w(x)D(x) = 0 \quad (\text{E.4})$$

with two boundary conditions at $x = 1$

$$D(1) = 0 \quad (\text{E.5})$$

$$\frac{dD}{dx}(1) = 0 \quad (\text{E.6})$$

The Wiener integral is, therefore, given by

$$\int_C \exp\{\lambda \int_0^1 dx w(x) f^2(x)\} d\mu_w(f) = \lim_{N \rightarrow \infty} [D^N(\Delta x)]^{-\frac{1}{2}} = [D(0)]^{-\frac{1}{2}}$$

where $\lim_{N \rightarrow \infty} D^N(\Delta x) = D(0)$ holds. This result is valid if the quadratic form $a_{i,j}$ in (6.43) is positive definite for all $N > 1$.

(6.1.2): Set $w(x) = 1$, then is the ode (E.4) linear with constant coefficients

$$\frac{d^2D}{dx^2} + \lambda D(x) = 0 \quad (\text{E.7})$$

subject to the boundary conditions (E.5) and (E.6). This linear second-order ode for the determinant of an infinite-dimensional matrix is a special version of the Sturm–Liouville ode (6.35) encountered in a different context. The general solution of (E.7) is

$$D(x) = c_1 \sin(\sqrt{\lambda}x) + c_2 \cos(\sqrt{\lambda}x)$$

Boundary condition (E.5) provides the relation

$$D(1) = 1 \rightarrow c_1 \sin(\sqrt{\lambda}) + c_2 \cos(\sqrt{\lambda}) = 1$$

and condition (E.6) a second relation

$$\frac{dD}{dx}(1) = 0 \rightarrow c_1 \sqrt{\lambda} \cos(\sqrt{\lambda}) - c_2 \sqrt{\lambda} \sin(\sqrt{\lambda}) = 0$$

The coefficients emerge as $c_1 = \sin(\sqrt{\lambda})$ and $c_2 = \cos(\sqrt{\lambda})$ and the solution is

$$D(x) = \sin(\sqrt{\lambda}) \sin(\sqrt{\lambda}x) + \cos(\sqrt{\lambda}) \cos(\sqrt{\lambda}x)$$

which can be rearranged using the trigonometric relation

$$\cos(a - b) = \cos(a) \cos(b) + \sin(a) \sin(b)$$

leading to

$$D(x) = \cos(\sqrt{\lambda}(1 - x))$$

This is an important result in its own right as it represents the value of the determinant $D(0)$ of an infinite matrix $a_{i,j}$. The value of the functional integral is thus given by

$$\int_C \exp\{\lambda \int_0^1 dx w(x) f^2(x)\} d\mu_w(f) = \frac{1}{\sqrt{\cos(\sqrt{\lambda})}}$$

completing the solution. The value of λ is clearly restricted by $0 \leq \lambda < \frac{\pi^2}{4}$. The result is plotted in Fig. 28.5 in semi-logarithmic scale. The value of the Wiener integral becomes singular as $\lambda \rightarrow \frac{\pi^2}{4}$.

Comments: This solution shows how the relation between functional integral and ordinary differential equations arises as presented by Gelfand and Yaglom [21]. Further references are Cameron and Martin [22], Montroll [23], Cameron and Martin who obtained this result by means of a linear transformation of C_0 in [24].

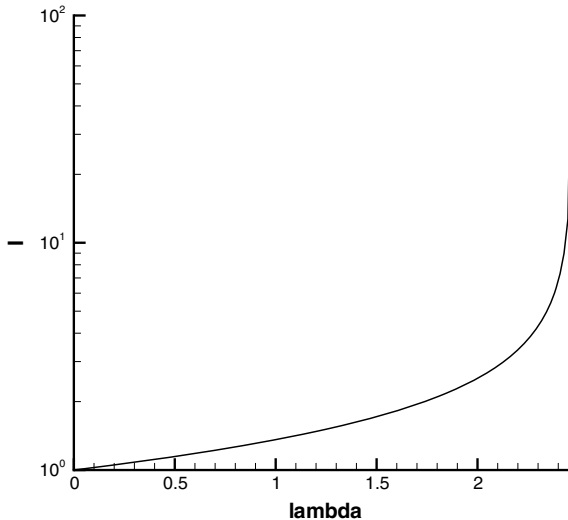


Fig. 28.5 Semi-logarithmic plot of the functional integral with respect to the Wiener measure $I \equiv \int_C \exp\{\lambda \int_0^1 dx w(x) f^2(x)\} d\mu_w(f)$ for $w(x) = 1$ as function of λ , $0 \leq \lambda < \pi^2/4$

Problem 6.2: Compute the Wiener integral (6.39) for $p(x) = 1$, $q(x) = 0$ and $w(x) = (x + \alpha)^{-2}$, where $0 < \alpha < \infty$ is assumed. Plot the solution of the associated Sturm–Liouville ode for several values of λ and the functional integral as function of λ for several values of α .

Solution:

The Sturm–Liouville ode (6.36) emerges for the specified coefficients as

$$\frac{d^2 f}{dx^2} + \frac{\lambda}{(x + \alpha)^2} f(x) = 0$$

This ode is homogeneous with respect to $x + \alpha$, hence has solutions in the form

$$f_\lambda(x) = (x + \alpha)^\beta$$

The characteristic equation is $\beta^2 - \beta + \lambda = 0$ with roots

$$\beta_{1,2} = \frac{1}{2} \pm \sqrt{1 - 4\lambda}$$

which are real for $\lambda \leq \lambda_0$, $\lambda_0 \equiv \frac{1}{4}$. For convenience $\lambda = \frac{1}{4} - \nu^2$, hence $\nu \geq 0$ for $\lambda \leq \lambda_0$, thus

$$\beta_{1,2} = \frac{1}{2} \pm \nu$$

and two linearly independent solutions are given by

$$f_\lambda(x) = \begin{cases} (x + \alpha)^{\frac{1}{2} + \nu} \\ (x + \alpha)^{\frac{1}{2} - \nu} \end{cases}$$

The general solution of the Sturm–Liouville ode is then

$$f_\lambda(x) = A(x + \alpha)^{\frac{1}{2} + \nu} + B(x + \alpha)^{\frac{1}{2} - \nu}$$

The boundary condition $\frac{df_\lambda}{dx}(1) = 0$ generates a single-parameter family of solutions

$$f_\lambda(x) = A(x + \alpha)^{\frac{1}{2} + \nu} \left[1 - \left(\frac{1+2\nu}{1-2\nu} \right) \left(\frac{1+\alpha}{x+\alpha} \right)^{2\nu} \right] \quad (\text{E.8})$$

with

$$f_\lambda(0) = A\alpha^{\frac{1}{2} + \nu} \left[1 - \left(\frac{1+2\nu}{1-2\nu} \right) \left(\frac{1+\alpha}{\alpha} \right)^{2\nu} \right]$$

as value at $x = 0$, and the value

$$f_\lambda(1) = A(1 + \alpha)^{\frac{1}{2} + \nu} \left[1 - \left(\frac{1+2\nu}{1-2\nu} \right) \right]$$

at $x = 1$. Theorem 1 (6.39) in Sect. 6.3.4 states that the Wiener integral is then

$$\int_C \exp\left(\lambda \int_0^1 dx w(x) f^2(x)\right) d\mu_w(f) = 2 \left\{ \frac{\nu \alpha^{\nu - \frac{1}{2}} (1+\alpha)^{\nu + \frac{1}{2}}}{(2\nu-1)\alpha^{2\nu} + (2\nu+1)(1+\alpha)^{2\nu}} \right\}^{\frac{1}{2}} \quad (\text{E.9})$$

where $\nu = \sqrt{\frac{1}{4} - \lambda}$ for $\lambda < \lambda_0$, the constant A drops out of this expression.

Figure 28.6 shows four solutions (E.8) of the Sturm–Liouville ode for $\nu = 0.01$ ($\lambda = 0.2499$, green line) to $\nu = 0.17702$ ($\lambda = 0.21866$, blue line). It is evident that the solutions have no zero crossings within $[0, 1]$ and the value at $x = 0$ is non-zero and approaches zero as $\lambda \rightarrow \lambda_0$. As ν approaches the limit value zero ($\lambda \rightarrow \lambda_0 = \frac{1}{4}$), the solution (E.8) of the ode approaches zero.

Figure 28.7 shows the value of the Wiener integral (E.9) as function of λ for several values of α . The functional integral $\lambda = \lambda_0$ is indeterminate for $\lambda \rightarrow \lambda_0$, since the numerator and denominator in (6.39) approach zero. Evaluating the value of $I(\alpha, \lambda)$ for $\lambda \rightarrow \lambda_0 = \frac{1}{4}$ yields

$$I(\alpha, \lambda_0) = \frac{\left(\frac{1+\alpha}{\alpha}\right)^{\frac{1}{4}}}{\left(1 + \frac{1}{2}\alpha\right)^{\frac{1}{2}}}$$

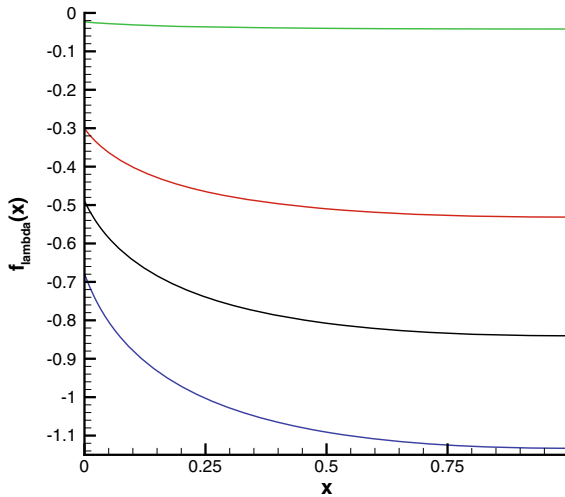


Fig. 28.6 Solutions of the Sturm–Liouville ode determining the functional integral for $\nu = 0.01$ ($\lambda = 0.2499$, green line), $\nu = 0.10253$ ($\lambda = 0.23948$, red line), $\nu = 0.14465$ ($\lambda = 0.22907$, black line) and $\nu = 0.17702$ ($\lambda = 0.21866$, blue line). Note that $f_\lambda(0) \neq 0$ holds for $\lambda < \lambda_0$

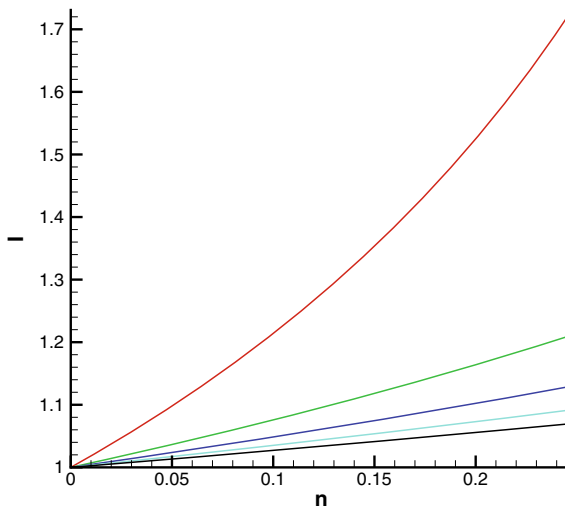


Fig. 28.7 The functional Wiener integral $I(\alpha, \lambda) = \int_C \exp\left(\lambda \int_0^1 dx w(x) f^2(x)\right) d\mu_w(f)$ as function of $\lambda < \frac{1}{4}$ for several, equally spaced values of α , starting with $\alpha = 0.01$ (red line) and down to $\alpha = 0.91$ (black line)

For $\lambda > \lambda_0$, the parameter ν becomes complex, thus making the functional integral complex. The Wiener integral $I(\alpha, \lambda_0)$ is singular for the limit $\alpha \rightarrow 0$ and zero for $\alpha \rightarrow \infty$.

Solutions to problems in Chap. 7: Functional differential equations

Problem 7.1: Consider the space of continuous functions $C = \{f(x), x \in \mathcal{D}\}$, where $\mathcal{D} = [0, 1]$. Solve the IVP for the functional differential equation

$$\frac{\delta F[f]}{\delta f(x)} = b(x)f(x)^n F[f]$$

where $n > 0$ is integer, for the functional $F[f] : C \rightarrow \mathbb{R}^1$.

Solution:

The properties of the exponential function $f(x) = e^{g(x)} : df/dx = f dg/dx$ indicate that the solution of the fde has the form

$$F[f] = \exp\left\{\frac{1}{n+1} \int_{\mathcal{D}} dx b(x) f^{n+1}(x)\right\}$$

It is straightforward to check this using the Definition (9.11) of the Gateaux functional differential $DF[f](h)$ containing the functional derivative according to (23.65)

$$DF[f](h) = \int_{\mathcal{D}} dx \frac{\delta F[f]}{\delta f(x)} h(x)$$

The differential can be computed according to

$$DF[f](h) = \lim_{\epsilon \rightarrow 0} \frac{d}{d\epsilon} F[f(x) + \epsilon h(x)]$$

hence

$$DF[f](h) = \lim_{\epsilon \rightarrow 0} \frac{d}{d\epsilon} \exp\left\{\frac{1}{n+1} \int_{\mathcal{D}} dx b(x) [f(x) + \epsilon h(x)]^{n+1}\right\}$$

The derivative and the limit of the integral can be computed with the aid of the binomial theorem leading to

$$\lim_{\epsilon \rightarrow 0} \frac{d}{d\epsilon} \exp\left\{\frac{1}{n+1} \int_{\mathcal{D}} dx b(x) [f(x) + \epsilon h(x)]^{n+1}\right\} = \int_{\mathcal{D}} dx b(x) f^n(x) F[f] h(x)$$

and thus

$$\frac{\delta F[f]}{\delta f(x)} = b(x)f(x)^n F[f]$$

as claimed. The functional

$$F[f] = \exp\left\{\frac{1}{n+1} \int_{\mathcal{D}} dx b(x) f^{n+1}(x)\right\}$$

is indeed the solution of the fde.

Reference: This problem was posed by Klauder, [25], Chap. 3.

Problem 7.2: Consider the space of twice continuously differentiable functions $C^2 = \{f(x), x \in \mathcal{D}\}$, where $\mathcal{D} = [0, 1]$. Solve the functional differential equation

$$\frac{\delta F[f]}{\delta f(x)} = \left[-\frac{d^2 f}{dx^2} + cf(x) + gf^3(x)\right]F[f]$$

where c, g are constants, for the functional $F[f] : C \rightarrow \mathbb{R}^1$.

Solution: The properties of the exponential function $f(x) = e^{g(x)} : df/dx = f dg/dx$ can be applied as in the previous problem. They indicate that the solution of the fde has the general form

$$F[f] = \exp\left\{\int_{\mathcal{D}} dx A(x) K[f(x)]\right\}$$

where K is a local function of $f(x)$ to be determined. As for the previous problem, the definition (9.11) of the Gateaux functional differential $DF[f](h)$ provides the tool to compute the functional derivative according to (23.65)

$$DF[f](h) = \int_{\mathcal{D}} dx \frac{\delta F[f]}{\delta f(x)} h(x)$$

hence

$$DF[f](h) = \lim_{\epsilon \rightarrow 0} \frac{d}{d\epsilon} F[f(x) + \epsilon h(x)]$$

holds. The present case requires a restriction of the space of test functions $h(x)$: $h(x) = 0$ for $x \in \partial\mathcal{D}$.

For the determination of $K(f(x))$, it is useful to consider first the simpler fde

$$\frac{\delta F[f]}{\delta f(x)} = \left\{-\frac{d^2 f}{dx^2}(x)\right\}F[f] \quad (1)$$

The result of the previous problem suggests the ansatz

$$F[f] = \exp\left\{\int_{\mathcal{D}} dx \left(\frac{df}{dx}\right)^n\right\}$$

with $n > 1$ and integer. The derivative and the limit of the integral can be computed leading to the derivative relation

$$\lim_{\epsilon \rightarrow 0} \frac{d}{d\epsilon} \exp\left\{\int_{\mathcal{D}} dx \left[\frac{df}{dx} + \epsilon \frac{dh}{dx}\right]^n\right\} = n \int_{\mathcal{D}} dx \left(\frac{df}{dx}\right)^{n-1} F[f] \frac{dh}{dx}$$

To put the integral into the proper form for the functional derivative, the product rule for standard differentiation can be applied

$$\frac{d}{dx} \left[\left(\frac{df}{dx}\right)^{n-1} h \right] = \frac{dh}{dx} \left(\frac{df}{dx}\right)^{n-1} + (n-1)h \left(\frac{df}{dx}\right)^{n-2} \frac{d^2 f}{dx^2}$$

Integration over \mathcal{D} and using $h(x) = 0, x \in \partial\mathcal{D}$ produces

$$\int_{\mathcal{D}} dx \left(\frac{df}{dx}\right)^{n-1} F[f] \frac{dh}{dx} = -(n-1) \int_{\mathcal{D}} dx \left(\frac{df}{dx}\right)^{n-2} \frac{d^2 f}{dx^2} F[f] h(x)$$

and substituting this result into the derivative relation

$$\lim_{\epsilon \rightarrow 0} \frac{d}{d\epsilon} \exp\left\{\int_{\mathcal{D}} dx \left[\frac{df}{dx} + \epsilon \frac{dh}{dx}\right]^n\right\} = -n(n-1) \int_{\mathcal{D}} dx \left(\frac{df}{dx}\right)^{n-2} \frac{d^2 f}{dx^2} F[f] h(x)$$

the Gateaux derivative

$$\frac{\delta F[f]}{\delta f(x)} = -n(n-1) \left(\frac{df}{dx}\right)^{n-2} \frac{d^2 f}{dx^2} F[f]$$

is obtained. The solution of the simpler fde (1) is now arrived at

$$F[f] = \exp\left\{\frac{1}{2} \int_{\mathcal{D}} dx \left(\frac{df}{dx}\right)^2\right\}$$

by choosing $n = 2$. Combining this result with the solution of the previous problem

$$\frac{\delta F[f]}{\delta f(x)} = b(x) f(x)^n F[f]$$

produces the desired solution for $A(x) = 1$ and

$$K[f(x)] = \frac{1}{2} \left(\frac{df}{dx} \right)^2 + \frac{c}{2} f^2(x) + \frac{g}{4} f^4(x)$$

The explicit form of the solution is thus

$$F[f] = \exp \left\{ \int_{\mathcal{D}} dx \left[\frac{1}{2} \left(\frac{df}{dx} \right)^2 + \frac{c}{2} f^2(x) + \frac{g}{4} f^4(x) \right] \right\}$$

where c and g are constants.

Reference: This problem was posed by Klauder, [25], Chap. 3.

Solutions to problems for Chap. 9: Exact equations for characteristic functionals

Problem (9.1): Solve the pure IVP for the Burgers pde (1.2) with initial condition $u(0, x) = u_0(x) \in L^2_{\mathcal{D}} \cap C_{\mathcal{D}}^\infty$, $\mathcal{D} = (-\infty, \infty)$, using the Hopf–Cole transformation (1.3) as indicated in Chap. 1.

Solution: The dimensionless solution $u(t, x)$, defined in $[0, T] \times (-\infty, \infty)$, of the Burgers pde

$$\frac{\partial u}{\partial t} + u \frac{\partial u}{\partial x} = \frac{1}{2Re} \frac{\partial^2 u}{\partial x^2}$$

with initial condition $u(0, x) = u_0(x) \in L^2_{(-\infty, \infty)}$ can be constructed by transformation. The Hopf–Cole transformation

$$\Psi(x, t) = \exp(Re \int_x^\infty dx' u(x', t))$$

can be rearranged

$$\log \Psi = Re \int_x^\infty dx' u(t, x')$$

and inverted

$$u(t, x) = - \frac{1}{Re \Psi} \frac{\partial \Psi}{\partial x}$$

Differentiation produces

$$\frac{\partial u}{\partial x} = \frac{1}{Re \Psi^2} \left(\frac{\partial \Psi}{\partial x} \right)^2 - \frac{1}{Re \Psi} \frac{\partial^2 \Psi}{\partial x^2}$$

Now integrate the pde

$$\int_x^\infty dx' \left[\frac{\partial u}{\partial t} + \frac{1}{2} \frac{\partial u^2}{\partial x'} - \frac{1}{2Re} \frac{\partial^2 u}{\partial x'^2} \right] = 0$$

hence

$$\frac{\partial}{\partial t} \int_x^\infty dx' u(t, x') - \frac{1}{2} u^2(t, x) + \frac{1}{2Re} \frac{\partial u}{\partial x}(t, x) = 0$$

holds. Substitution of u and its derivative leads to

$$\frac{\partial}{\partial t} \left(\frac{1}{Re} \log(\Psi) \right) - \frac{1}{2Re^2} \frac{1}{\Psi^2} \left(\frac{\partial \Psi}{\partial x} \right)^2 + \frac{1}{2Re^2} \left[\frac{1}{\Psi^2} \left(\frac{\partial \Psi}{\partial x} \right)^2 - \frac{1}{\Psi} \frac{\partial^2 \Psi}{\partial x^2} \right] = 0$$

which can be simplified to the linear parabolic pde

$$\frac{\partial \Psi}{\partial t} = \frac{1}{2Re} \frac{\partial^2 \Psi}{\partial x^2}$$

The initial value for Ψ transforms to

$$\Psi(0, x) = \exp \left[Re \int_x^\infty dx' u_0(x') \right]$$

The solution of the IVP for the linear heat pde is well known

$$\Psi(t, x) = \sqrt{\frac{Re}{2\pi t}} \int_{-\infty}^\infty dx' \Psi(0, x') \exp \left[-Re \frac{(x - x')^2}{2t} \right]$$

Transforming back to $u(t, x)$ using $u(t, x) = -\frac{1}{Re\Psi} \frac{\partial \Psi}{\partial x}$ and

$$\frac{\partial \Psi}{\partial x} = -\frac{Re^{\frac{3}{2}}}{\sqrt{2\pi t}} \int_{-\infty}^\infty dx' \frac{(x - x')}{t} \Psi(0, x') \exp \left[-Re \frac{(x - x')^2}{2t} \right]$$

leads to the desired result

$$u(t, x) = \frac{\int_{-\infty}^\infty dx' \frac{(x - x')}{t} \exp \left\{ Re \left[\int_{x'}^\infty dx'' u_0(x'') - \frac{(x - x')^2}{2t} \right] \right\}}{\int_{-\infty}^\infty dx' \exp \left\{ Re \left[\int_{x'}^\infty dx'' u_0(x'') - \frac{(x - x')^2}{2t} \right] \right\}}$$

Reference: There is a vast literature on the Burgers pde and the Hopf–Cole transformation, and extensions include random external force fields and further generalizations, see Woyczyński [26] and references therein.

Problem (9.2): Derive the Hopf fde for the characteristic functional $\theta[y; t]$ for the pure IVP of the Burgers pde (1.2). Use the result obtained in Problem (9.1) to establish the solution operator and its inverse.

Solution: The IVP for the Burgers pde

$$\frac{\partial u}{\partial t} + u \frac{\partial u}{\partial x} = \frac{1}{2Re} \frac{\partial^2 u}{\partial x^2}$$

with initial condition $u(0, x) = u_0(x)$ element of the phase space $\Omega = L^2_{R^1} \cap C^\infty_{R^1}$ for $tRe < \infty$. The solution operator T_t generates a bijective mapping; hence, (6.3) holds. Thus

$$\frac{\partial}{\partial t} \int_{\Omega} \mu_0(du(0, x)) \exp[i(y, u)] = -i(y, \int_{\Omega} \mu_0(du(0, x)) \exp[i(y, u)] [\frac{1}{2} \frac{\partial}{\partial x} (u^2) - \frac{1}{2Re} \frac{\partial^2 u}{\partial x^2}])$$

allows moving the time derivative inside the integral over the phase space. The Gateaux derivative (9.14) can be evaluated

$$\frac{\delta \theta}{\delta y(x)}[y; t] = i \int_{\Omega} d\mu(t, u) u(t, x) \exp[i(y, u)]$$

and likewise the second derivative

$$\frac{\delta^2 \theta}{\delta y(x) \delta y(x)}[y; t] = - \int_{\Omega} d\mu(t, u) u^2(t, x) \exp[i(y, u)]$$

Hence, the fde

$$\frac{\partial \theta}{\partial t} = \frac{1}{2}(y, [i \frac{\partial}{\partial x} \frac{\delta^2 \theta}{\delta y(x) \delta y(x)} + \frac{1}{Re} \frac{\partial^2}{\partial x^2} \frac{\delta \theta}{\delta y(x)}])$$

is obtained.

The solution operator T_t follows from the previous problem

$$T_t = - \frac{\int_{-\infty}^{\infty} d\zeta \zeta \exp[tRe(\int_0^{\infty} d\zeta' \cdot - \frac{1}{2} \zeta^2)]}{\int_{-\infty}^{\infty} d\zeta \exp[tRe(\int_0^{\infty} d\zeta' \cdot - \frac{1}{2} \zeta^2)]}$$

valid for $tRe < \infty$, where the transformations $\zeta \equiv \frac{x'-x}{t}$ and $\zeta' \equiv \frac{x''-x'}{t}$ were used for the inner and outer integrals. The inverse operator T_{-t} is then

$$T_{-t} = \frac{\int_{-\infty}^{\infty} d\zeta \zeta \exp[tRe(\int_{-\infty}^0 d\zeta' + \frac{1}{2}\zeta^2)]}{\int_{-\infty}^{\infty} d\zeta \exp[tRe(\int_{-\infty}^0 d\zeta' + \frac{1}{2}\zeta^2)]}$$

where the transformed variables of the inner and outer integrals are now $\zeta \equiv -\frac{x'-x}{t}$ and $\zeta' \equiv -\frac{x''-x'}{t}$. The numerical evaluation of the inverse operator is non-trivial, since it is the explicit solution of the Burgers pde with negative diffusivity.

Reference: Janocha et al. [9] contain a detailed analysis of the transformation groups of the fde obtained above for the pure IVP of the Burgers pde.

Problem (9.3): Solve the Hopf fde for the Burgers pde using the solution operator established in Problem (9.2). The initial condition is the characteristic functional $\theta[y; 0]$ for Gaussian stochastic fields with zero mean.

(9.3.1): Specify the initial condition for Gaussian random fields in terms of the covariance function $R(x, x') \equiv \langle u(0, x)u(0, x') \rangle$ and zero mean. Assume that the covariance function is delta-correlated $R(x, x') = \sigma_0^2 \delta(x - x')$, $\sigma_0 > 0$.

(9.3.2): Construct a basis in L_D^2 using Hermite functions (physicists version) $\Psi_n(x)$ (4.29) as defined in ([15], Chap. 18).

(9.3.3): Adapt the initial condition to the Hermite basis.

(9.3.4): Adapt the fde obtained in Problem (9.2) to the basis constructed in section (9.3.2).

(9.3.5): Solve the fde (9.2) using the relation (6.3) for the measure μ at times zero and $t > 0$ assuming that the solution operator generates a bijective map of l^2 , isomorphic to L_D^2 , onto itself.

Solution: The parabolic fde for the characteristic functional $\theta[y; t]$ obtained in the previous Problem (9.2)

$$\frac{\partial \theta}{\partial t} = \frac{1}{2} \left(y, \left[i \frac{\partial}{\partial x} \frac{\delta^2 \theta}{\delta y(x) \delta y(x)} + \frac{1}{Re} \frac{\partial^2}{\partial x^2} \frac{\delta \theta}{\delta y(x)} \right] \right) \quad (1)$$

with initial condition $\theta[y; 0] = \theta_0[y]$ can be solved for a limited time interval. For the definition of the characteristic functional at time $t = 0$, consider the Hilbert space $\mathcal{H} = L_2(\mathcal{D})$ of square-integrable functions $y(x)$ defined on $\mathcal{D} = (-\infty, \infty)$ with scalar product $(y, w) = \int_{-\infty}^{\infty} dx y(x) w^*(x)$ and norm (22.18)

$$\|y\|^2 = (y, y^*) = \int_{-\infty}^{\infty} dx y(x) y^*(x)$$

where the asterisk denotes complex conjugate.

(9.3.1): The Gaussian characteristic functional is explicitly given by (9.87)

$$\theta_G[y] = \exp\left\{-\frac{1}{2}(Ky, y) + i(a, y)\right\}$$

where $y(x)$ is the scalar argument function defined over the domain \mathcal{D} and taken from the Hilbert space \mathcal{H} with scalar product $(., .)$, K is a positive operator of trace class (An operator A defined on a separable Hilbert space with basis $e_n(\mathbf{x})$, $n \in [1, \infty)$ is positive iff $(Ay, y) \geq 0$, $\forall y \in \mathcal{H}$, it is a trace class or nuclear operator, if it is compact and the trace in \mathcal{H} (9.88) $\text{tr}(A) \equiv \sum_k (Ae_k, e_k) < \infty$ exists and is absolutely convergent, i.e. $\text{tr}(|A|) \equiv \sum_k ((A^*A)^{\frac{1}{2}}e_k, e_k) < \infty$, where A^* is the adjoint operator (9.69) independent of the basis.) in \mathcal{H} called correlation operator of the Gaussian measure μ_G and $a(x) \in \mathcal{H}$ is the mean field. For the present case of a Gaussian measure with zero mean the correlation operator K

$$K(x) = \int_{-\infty}^{\infty} dx' R(x, x').$$

is specified in terms of the covariance function $R(x, x') \equiv \langle u(0, x)u(0, x') \rangle$ of the initial data of the Burgers pde. Hence,

$$(Ky, y) = \int_{-\infty}^{\infty} dx \int_{-\infty}^{\infty} dx' y(x') R(x, x') y^*(x)$$

is the argument in the initial characteristic functional (9.87) emerging in the form

$$\theta_G[y; 0] = \exp\left\{-\frac{1}{2} \int_{-\infty}^{\infty} dx \int_{-\infty}^{\infty} dx' y(x') R(x, x') y^*(x)\right\}$$

The specification of $R(x, x')$ is important for the construction of a basis in \mathcal{H} and the functional integration with respect to the initial measure $\mu(0, u)$. It is set by

$$R(x, x') = \sigma_0^2 \delta(x - x') \rightarrow \theta_G[y; 0] = \exp\left\{-\frac{1}{2} \sigma_0^2 \|y\|^2\right\} \quad (1)$$

in order to control the strength $\sigma_0 \in L^2_{\mathcal{D}}$ of the initial Pdf.

(9.3.2): The solution operator for the IVP of the Burgers pde

$$T_t = -\frac{\int_{-\infty}^{\infty} d\zeta \zeta \exp[t \text{Re}(\int_0^{\infty} d\zeta' \cdot - \frac{1}{2}\zeta^2)]}{\int_{-\infty}^{\infty} d\zeta \exp[t \text{Re}(\int_0^{\infty} d\zeta' \cdot - \frac{1}{2}\zeta^2)]}$$

was obtained in Problem (9.2)), where $\zeta \equiv \frac{x'-x}{t}$ and $\zeta' \equiv \frac{x''-x'}{t}$. The solution operator furnishes then a bijective mapping of Ω onto itself; hence, (6.3)

$$\mu(t, B) = \mu_0(T_{-t}B), B \in \mathcal{A}$$

is applicable as long as T_t is defined and uniquely invertible

$$\theta[y; t] = \int_{\Omega} d\mu(t, u) \exp[i(y, u)] = \int_{\Omega} d\mu(0, u) \exp[i(y, T_t(u))]$$

Substituting the solution operator leads to

$$\theta[y; t] = \int_{\Omega} d\mu(0, u) \exp[i(y, -\frac{\int_{-\infty}^{\infty} d\zeta \zeta \exp[t \operatorname{Re}(\int_0^{\infty} d\zeta' u(\zeta') - \frac{1}{2}\zeta^2)]}{\int_{-\infty}^{\infty} d\zeta \exp[t \operatorname{Re}(\int_0^{\infty} d\zeta' u(\zeta') - \frac{1}{2}\zeta^2)]})]$$

The functional integral with respect to the initial measure $\mu(0, u)$ requires some preparation.

The space of initial scalar fields $y(x)$, $x \in (-\infty, \infty)$ is the Hilbert space $\mathcal{H} = L^2_{\mathcal{D}}$. It has a an orthonormal basis defined by the set of Hermite functions ([15], Chap.18) (4.29)

$$\Psi_n(x) = (2^n n! \sqrt{\pi})^{-\frac{1}{2}} \exp(-\frac{x^2}{2}) H_n(x)$$

for $n = 0, 1, \dots, \infty$, where $H_n(x)$ denotes the n th-order Hermite polynomial (4.30)

$$H_n(x) = (-1)^n \exp(x^2) \frac{d^n}{dx^n} \exp(-x^2)$$

as defined in Sect. 4.3.3, and several Hermite functions $\Psi_n(x)$ are shown in Fig. 4.6 for $n = 0, 1, 2, 7, 30$. An element $y(x) \in \mathcal{H}$ is thus represented by a convergent series $y(x) = \sum_{j=0}^{\infty} y_j \Psi_j(x)$ with inverse relation $y_j = (y, \Psi_j)$, $j = 0, 1, 2, \dots, \infty$ with $\{y_0, y_1, \dots, y_{\infty}\}$.

(9.3.3): The covariance function $R(x, x') \in L^2_{\mathcal{D}} \times L^2_{\mathcal{D}}$ specified in Eq. (1) defining the Gaussian initial condition can be expanded in the Hermite basis (28.15) $\{\Psi_n(x), 0 \leq n \leq \infty\}$ as limit $R(x, x') = \lim_{n \rightarrow \infty} R^n(x, x')$, where

$$R^n(x, x') = \sum_{i=0}^n \sum_{j=0}^n \Psi_i(x) R_{i,j}^n \Psi_j(x')$$

The quadratic coefficient matrix

$$R_{i,j}^n = ((R(x, x'), \Psi_i(x)), \Psi_j(x'))$$

is symmetric, since $R(x, x')$ depends on $|x - x'|$ only according to the problem statement. Hence, $R_{i,j}^n$ has $n + 1$ real and distinct eigenvalues and $n + 1$ linearly independent eigenvectors. The eigenvectors form an orthogonal matrix \mathbf{T} such that $\Lambda_{i,j} = T_{i,k}^T R_{k,m}^n T_{m,j}$ and $\Lambda_{i,j} = \delta_{i,j} \lambda_{(i)}$ (no sum over indices in parenthesis, \mathbf{T}^T is the transpose of \mathbf{T}) is a diagonal matrix with the eigenvalues as diagonal entries. The representation of $R^n(x, x')$ is now linearly transformed to the eigenvector basis in \mathbb{R}^{n+1}

$$R^n(x, x') = \sum_{i=0}^n \sum_{j=0}^n \Psi_i(x) T_{i,k} \Lambda_{k,m} T_{m,j}^T \Psi_j(x')$$

The special case of delta-correlated $R(x, x')$ leads to the correlation operator $K(x) = \sigma_0^2$ as multiplication.

(9.3.4): The Hermite basis $\{\Psi_n(x), 0 \leq n \leq \infty\}$ constructed for the Hilbert space \mathcal{H} implies that a functional $\theta[y(\cdot)] : \mathcal{H} \rightarrow \mathbb{R}^1$ emerges as function of infinitely many variables $\hat{\theta}[y_0, y_1, \dots, y_\infty; t]$ due to the representation $y(x) = \sum_{j=0}^\infty y_j \Psi_j(x)$. The first Gateaux differential is then according to (23.46) $DT(u)(w) = (w, \frac{\delta T}{\delta u})$

$$D\theta[y(\cdot)](h) = \sum_{j=0}^\infty h_j \frac{\partial \hat{\theta}}{\partial y_j}(y_0, y_1, \dots, y_\infty; x)$$

It follows that $\frac{\delta \theta}{\delta y(x)}$ in the Hopf fde is replaced by $\frac{\partial \hat{\theta}}{\partial y_j}$ by virtue of the ONS basis. Likewise, the second Gateaux derivative $\frac{\delta^2 \theta}{\delta y(x) \delta y(x)}$ is replaced by $\frac{\partial^2 \hat{\theta}}{\partial y_j \partial y_k}$. The Hopf fde (1) for the characteristic functional $\theta[y_0, y_1, \dots, y_\infty; t]$ emerges in terms of the Hermite basis as

$$\frac{\partial \hat{\theta}}{\partial t} = \frac{1}{2} \sum_{j=0}^\infty y_j [i \frac{\partial^3 \hat{\theta}}{\partial x \partial^2 y_j} + \frac{1}{Re} \frac{\partial^3 \hat{\theta}}{\partial x^2 \partial y_j}] \quad (2)$$

an equation for the characteristic function $\hat{\theta}[y_0, y_1, \dots, y_\infty]$.

(9.3.5): The correlation operator for the initial condition emerges in l^2 as

$$(Ky, y) = \int_{-\infty}^{\infty} dx y(x) \int_{-\infty}^{\infty} dx' R(x, x') y(x') = \sum_{k=0}^{\infty} \sum_{j=0}^{\infty} y_k R_{k,j} y_j$$

where

$$R_{k,j} \equiv \int_{-\infty}^{\infty} dx \Psi_k(x) \int_{-\infty}^{\infty} dx' R(x, x') \Psi_j(x') \}$$

The initial characteristic functional is then

$$\hat{\theta}_G[\mathbf{y}; 0] = \exp\left\{-\frac{1}{2} \sum_{k=0}^{\infty} \sum_{j=0}^{\infty} y_k R_{k,j} y_j\right\}, \quad \mathbf{y} \in l^2$$

Consider the projection of the correlation operator onto R^n and

$$\hat{\theta}_n[\mathbf{y}; 0] = \exp\left\{-\frac{1}{2} \sum_{k=0}^n \sum_{j=0}^n y_k R_{k,j} y_j\right\}$$

Furthermore, assume that the matrix $R_{k,j}$ is non-singular, then exists the Pdf f_n associated with $\hat{\theta}_n$ via Fourier transform as multivariate Gaussian

$$f_n(\mathbf{x}, 0) = \frac{1}{\sqrt{(2\pi)^n \det(R_{k,j})}} \exp\left\{-\frac{1}{2} \mathbf{x}_k R_{k,j}^{-1} \mathbf{x}_j\right\}$$

The correlation operator is a positive trace class operator, hence has the projection onto R^n positive eigenvalues $\sigma_j^2 > 0$, $0 \leq j \leq n$ and $R_{k,j}$ is, therefore, invertible. Furthermore, the eigenvectors form a linear transformation matrix $T_{i,j}$ transforming $R_{k,j}$ to diagonal form

$$T_{i,k}^{-1} R_{k,j} T_{j,m} = \begin{pmatrix} \sigma_0^2 & 0 & \cdots & 0 \\ 0 & \sigma_1^2 & \cdots & 0 \\ \vdots & \vdots & \ddots & \vdots \\ 0 & 0 & \cdots & \sigma_{n-1}^2 \end{pmatrix}$$

The special case of a delta-correlated $R(x, x') = \sigma_0^2 \delta(x - x')$ is straightforward, since the coefficient matrix is diagonal $R_{i,j}^n = \sigma_0^2 \delta_{i,j}$ and $T_{i,j}$ is the unit matrix, hence

$$T_{i,k}^{-1} R_{k,j} T_{j,m} = \sigma_0^2 \delta_{i,m}$$

The measure differential for the functional integral over l^2 at the reference time zero is then

$$d\mu(0, \mathbf{y}) = \lim_{n \rightarrow \infty} \prod_{j=0}^n \frac{1}{\sigma_0 \sqrt{2\pi}} \exp\left(-\frac{1}{2} \frac{y_j^2}{\sigma_0^2}\right) dy_j$$

and the solution of the fde (1) emerges as

$$\hat{\theta}[\mathbf{y}; t] = \lim_{n \rightarrow \infty} \int_{R^n} \prod_{j=0}^n \frac{1}{\sigma_0 \sqrt{2\pi}} \exp\left(-\frac{1}{2} \frac{y_j^2}{\sigma_0^2}\right) dy_j$$

$$\exp\left\{ -i \sum_{k=0}^n \int_{\mathcal{D}} dx \Psi_k(x) \frac{\int_{-\infty}^{\infty} d\zeta \zeta \exp[t \operatorname{Re}(\sum_{m=0}^n y_m \int_0^{\infty} d\zeta' \Psi_m(\zeta') - \frac{1}{2} \zeta^2)]}{\int_{-\infty}^{\infty} d\zeta \exp[t \operatorname{Re}(\sum_{p=0}^n y_p \int_0^{\infty} d\zeta' \Psi_p(\zeta') - \frac{1}{2} \zeta^2)]} \right\}$$

where $\{\Psi_j(\mathbf{x}), j = 0, \dots, \infty\}$ is the Hermite function basis, and a few functions are shown in Fig. 4.6. The argument $y(x) = \sum_{j=0}^{\infty} y_j \Psi_j(x)$ is represented as series with respect to the Hermite basis $\{\Psi_n(x), 0 \leq n \leq \infty\}$ constructed above. The Reynolds number Re

$$Re \equiv \frac{\rho_0 U D}{\mu}$$

where U is the velocity, D is the length scale and $\frac{\mu}{\rho_0}$ is a dimensional parameter analogous to the kinematic viscosity in the Navier–Stokes pdes. The Reynolds number is a positive parameter in the Burgers pde, and all variables are thus dimensionless as they should be for analysis and interpretation.

Comments: The present example is based on the explicit analytic solution operator T_t , which is not available for the IBVP of the Navier–Stokes pdes for Reynolds numbers in the turbulent range. Note that the Gaussian measure differential $d\mu(0, \mathbf{y})$, (23.208), in contrast to the Lebesgue measure differential

$$d\mu_L(0, \mathbf{y}) = \lim_{n \rightarrow \infty} \prod_{j=0}^n dy_j$$

in Euclidian space, produces a non-trivial result for the functional integral, as has been shown in Sect. 23.18.2. The quantitative evaluation of this type of result is not a trivial matter, see Egorov et al. [27] for numerical methods and relations to stochastic processes and Shen and Wray, [28] for steady-state solutions.

Problem (9.4): Consider an analytic functional $R[y]$ defined on the phase space of scalar fields $\Omega = \{y(\mathbf{x}) \in L^2_{R^3}\}, \mathbf{x} \in R^3$ and Gaussian stochastic fields $f_i(\mathbf{x})$ with zero mean and positive definite correlation tensor defined by

$$K_{i,j}(\mathbf{x}, \mathbf{x}') \equiv \langle f_i(\mathbf{x}) f_j(\mathbf{x}') \rangle$$

Prove the relation

$$\langle f_i(\mathbf{x}) R[f] \rangle = \int_{R^3} d\nu K_{i,j}(\mathbf{x}, \mathbf{x}') \langle \frac{\delta R}{\delta f_j}[f; \mathbf{x}'] \rangle$$

for homogeneous and isotropic Gaussian fields.

Solution: The functional $R[f]$ is analytic, hence possesses a functional Taylor series

$$R[f] = R[0] + \sum_{n=1}^{\infty} \frac{1}{n!} \int d\nu(\mathbf{x}_1) \cdots \int d\nu(\mathbf{x}_n) f_{i_1}(\mathbf{x}_1) \cdots f_{i_n}(\mathbf{x}_n) R_{i_1, \dots, i_n}^n(\mathbf{x}_1, \dots, \mathbf{x}_n)$$

where

$$R_{i_1, \dots, i_n}^n(\mathbf{x}_1, \dots, \mathbf{x}_n) \equiv \left(\frac{\delta^n R[f]}{\delta f_{i_1}(\mathbf{x}_1) \cdots \delta f_{i_n}(\mathbf{x}_n)} \right)_{\mathbf{f}=0}$$

Multiplication with $f_j(\mathbf{x})$ and averaging with respect to the Gaussian measure produces

$$\langle f_j(\mathbf{x}) R[f] \rangle = \sum_{n=1}^{\infty} \frac{1}{n!} \int d\nu(\mathbf{x}_1) \cdots \int d\nu(\mathbf{x}_n) \langle f_j(\mathbf{x}) f_{i_1}(\mathbf{x}_1) \cdots f_{i_n}(\mathbf{x}_n) \rangle R_{i_1, \dots, i_n}^n(\mathbf{x}_1, \dots, \mathbf{x}_n)$$

The evaluation of the statistical moment $\langle f_j(\mathbf{x}) f_{i_1}(\mathbf{x}_1) \cdots f_{i_n}(\mathbf{x}_n) \rangle$ for joint Gaussian distributions with zero mean and $n > 2$ is the sum over all permutations of $n+1$ indices $\{j, i_1, \dots, i_n\}$ in groups of two $\{j, i_1\}, \dots, \{i_l, i_m\}$, etc. disregarding order for $n+1$ even, for $n+1$ odd the moment is zero. This sum contains precisely n terms $\{j, i_p\}$, $p = 1, \dots, n$, hence

$$\langle f_j(\mathbf{x}) f_{i_1}(\mathbf{x}_1) \cdots f_{i_n}(\mathbf{x}_n) \rangle = \sum_{p=1}^n K_{j, i_p}(\mathbf{x}, \mathbf{x}_p) \langle f_{i_1}(\mathbf{x}_1) i \cdots f_{i_{p-1}}(\mathbf{x}_{p-1}) \cdots f_{i_{p+1}}(\mathbf{x}_{p+1}) \cdots f_{i_n}(\mathbf{x}_n) \rangle$$

and

$$\begin{aligned} \langle f_j(\mathbf{x}) R[f] \rangle &= \sum_{n=1}^{\infty} \frac{1}{n!} \int d\nu(\mathbf{x}_1) \cdots \int d\nu(\mathbf{x}_n) \\ &\sum_{p=1}^n K_{j, i_p}(\mathbf{x}, \mathbf{x}_p) \langle f_{i_1}(\mathbf{x}_1) \cdots f_{i_{p-1}}(\mathbf{x}_{p-1}) \cdots f_{i_{p+1}}(\mathbf{x}_{p+1}) \cdots f_{i_n}(\mathbf{x}_n) \rangle R_{i_1, \dots, i_n}^n(\mathbf{x}_1, \dots, \mathbf{x}_n) \end{aligned}$$

Further simplification is possible, if the Gaussian measure is homogeneous and isotropic making $R_{i_1, \dots, i_n}^n(\mathbf{x}_1, \dots, \mathbf{x}_n)$ and the moments $\langle f_j(\mathbf{x}) f_{i_1}(\mathbf{x}_1) \cdots f_{i_n}(\mathbf{x}_n) \rangle$ symmetric. Then

$$\sum_{p=1}^n K_{j,i_p}(\mathbf{x}, \mathbf{x}_p) \langle f_{i_1}(\mathbf{x}_1) \cdots f_{i_{p-1}}(\mathbf{x}_{p-1}) \cdots f_{i_{p+1}}(\mathbf{x}_{p+1}) \cdots f_{i_n}(\mathbf{x}_n) \rangle R_{i_1, \dots, i_n}^n(\mathbf{x}_1, \dots, \mathbf{x}_n) = \\ n K_{j,i_1}(\mathbf{x}, \mathbf{x}_1) \langle f_{i_2}(\mathbf{x}_2) \cdots f_{i_n}(\mathbf{x}_n) \rangle R_{i_1, i_2, \dots, i_n}^n(\mathbf{x}_1, \mathbf{x}_2, \dots, \mathbf{x}_n)$$

follows and

$$\langle f_j(\mathbf{x}) R[f] \rangle = \int d\nu(\mathbf{x}_1) K_{j,i_1}(\mathbf{x}, \mathbf{x}_1) \\ \sum_{n=1}^{\infty} \frac{1}{(n-1)!} \int d\nu(\mathbf{x}_2) \cdots \int d\nu(\mathbf{x}_n) \langle f_{i_2}(\mathbf{x}_2) \cdots f_{i_n}(\mathbf{x}_n) \rangle R_{i_1, i_2, \dots, i_n}^n(\mathbf{x}_1, \mathbf{x}_2, \dots, \mathbf{x}_n) \quad (1)$$

is obtained. Consider now the Gateaux derivative of the functional Taylor series using again the symmetry of the integrand

$$\frac{\delta R[f]}{\delta f_{i_1}(\mathbf{x}_1)} = \sum_{n=1}^{\infty} \frac{1}{(n-1)!} \int d\nu(\mathbf{x}_2) \cdots \int d\nu(\mathbf{x}_n) f_{i_2}(\mathbf{x}_2) \cdots f_{i_n}(\mathbf{x}_n) R_{i_1, i_2, \dots, i_n}^n(\mathbf{x}_1, \mathbf{x}_2, \dots, \mathbf{x}_n) \quad (2)$$

Substituting (2) in Eq. (1) leads to

$$\langle f_j(\mathbf{x}) R[f] \rangle = \int d\nu(\mathbf{x}_1) K_{j,i_1}(\mathbf{x}, \mathbf{x}_1) \langle \frac{\delta R[f]}{\delta f_{i_1}(\mathbf{x}_1)} \rangle$$

completing the proof.

Reference: Novikov [29, 30] discusses the Hopf fde in the spatial description with a stochastic Gaussian, homogeneous and isotropic external force. The material relevant to the present Problem is contained in Chap. 2. of the paper.

Solutions to Problems for Chap. 10

Problem (10.1): Solve the fde for the characteristic functional $\theta[\mathbf{y}(\cdot); t]$

$$\frac{\partial}{\partial t} \theta[\mathbf{y}; t] = i \int_{\mathcal{D}} d\mathbf{x} \mathbf{y}_\alpha(\mathbf{x}) \left(\frac{1}{Fr} g_\alpha(\mathbf{x}) - \frac{\partial P_0}{\partial x_\alpha} \right) \theta[\mathbf{y}; t]$$

governed by the truncated Hopf fde (9.40) driven solely by a constant external force

$$F_\alpha \equiv \frac{1}{Fr} g_\alpha - \frac{\partial P_0}{\partial x_\alpha}$$

The initial functional is the Gaussian

$$\theta_G[\mathbf{y}; t] = \exp\left\{-\frac{1}{2}(\mathbf{K} \cdot \mathbf{y}, \mathbf{y}) + i(\mathbf{a}, \mathbf{y})\right\}$$

with correlation operator \mathbf{K} and zero mean $\mathbf{a} = 0$.

(10.1.1): Solve the IVP for the ode governing $\theta[\mathbf{y}]$ with Gaussian initial condition.

(10.1.2): Show that the characteristic functional remains Gaussian and evaluate the effect of the external force on it.

Solution: The fde for the constant external force is a linear, first-order ode

$$\frac{d}{dt}\theta[\mathbf{y}; t] = iA\theta[\mathbf{y}; t]$$

where $A[\mathbf{y}] \equiv F_\alpha \int_{\mathcal{D}} d\mathbf{x} y_\alpha(\mathbf{x})$.

(10.1.1): The ode can be solved using the Ansatz

$$\theta[\mathbf{y}; t] = C \exp(\lambda t)$$

with complex C . The solution is straightforward

$$\theta[\mathbf{y}; t] = \theta_G[\mathbf{y}] \exp\{iA[\mathbf{y}]t\}$$

(10.1.2): Substituting the explicit Gaussian leads to

$$\theta[\mathbf{y}; t] = \exp\left\{-\frac{1}{2}(\mathbf{K} \cdot \mathbf{y}, \mathbf{y}) + iA[\mathbf{y}]t\right\}$$

It shows that the effect of a constant external force is to modify the mean.

Comments: The effect of a constant external force vector on the characteristic functional is to modify the mean vector for a Gaussian initial condition linearly in time. The generalization to non-random, external force fields $g_\alpha(\mathbf{x})$ requires minor modifications, i.e. $A[\mathbf{y}, \mathbf{g}] \equiv \int_{\mathcal{D}} d\mathbf{x} y_\alpha(\mathbf{x}) g_\alpha(\mathbf{x})$. The solution of the truncated Hopf fde is then

$$\theta[\mathbf{y}; t] = \exp\left\{-\frac{1}{2}(\mathbf{K} \cdot \mathbf{y}, \mathbf{y}) + i(\mathbf{g}, \mathbf{y})t\right\}$$

with mean vector $\mathbf{g}(\mathbf{x})t$ growing linearly with time.

Problem (10.2): Transform the Hopf fde (9.40) to cylindrical coordinates in \mathcal{D} . The explicit form of the pressure gradient term as functional of the velocity is not required. Hint: Consult Sect. 9.2.

Solution: The Navier–Stokes pdes for an incompressible fluid set in cylindrical coordinates defined in the domain of definition \mathcal{D} (4.4) for the periodic pipe flow are given by mass balance

$$\frac{1}{r} \frac{\partial}{\partial r} (r v_r) + \frac{1}{r} \frac{\partial v_\theta}{\partial \theta} + \frac{\partial v_z}{\partial z} = 0$$

and momentum balances (see Appendix C of Panton [31])

$$\frac{\partial v_r}{\partial t} + T_r(\mathbf{v}) = -\frac{1}{\rho} \frac{\partial p}{\partial r} + \frac{1}{Re} \left[\frac{\partial}{\partial r} \left(\frac{1}{r} \frac{\partial}{\partial r} (r v_r) \right) + \frac{1}{r^2} \frac{\partial^2 v_r}{\partial \theta^2} + \frac{\partial^2 v_r}{\partial z^2} - \frac{2}{r^2} \frac{\partial v_\theta}{\partial \theta} \right] + \frac{1}{Fr} G_r \quad (28.7)$$

for the radial direction,

$$\frac{\partial v_\theta}{\partial t} + T_\theta(\mathbf{v}) = -\frac{1}{r \rho} \frac{\partial p}{\partial \theta} + \frac{1}{Re} \left[\frac{\partial}{\partial r} \left(\frac{1}{r} \frac{\partial}{\partial r} (r v_\theta) \right) + \frac{1}{r^2} \frac{\partial^2 v_\theta}{\partial \theta^2} + \frac{\partial^2 v_\theta}{\partial z^2} + \frac{2}{r^2} \frac{\partial v_r}{\partial \theta} \right] + \frac{1}{Fr} G_\theta \quad (28.8)$$

for the azimuthal direction and

$$\frac{\partial v_z}{\partial t} + T_z(\mathbf{v}) = -\frac{1}{\rho} \frac{\partial p}{\partial z} + \frac{1}{Re} \left[\frac{1}{r} \frac{\partial}{\partial r} (r \frac{\partial v_z}{\partial r}) + \frac{1}{r^2} \frac{\partial^2 v_z}{\partial \theta^2} + \frac{\partial^2 v_z}{\partial z^2} \right] + \frac{1}{Fr} G_z - \frac{\partial P_0}{\partial z} \quad (28.9)$$

for the axial direction, where G_r , G_θ , G_z are the components of a dimensionless external force per unit mass with Fr denoting the Froude number (22.2). The axial momentum balance contains the only non-zero component of the externally imposed basic pressure gradient, which is a negative constant. The convective terms are defined by

$$T_r(\mathbf{v}) = \frac{\partial(v_r^2)}{\partial r} + \frac{\partial(v_r v_z)}{\partial z} + \frac{1}{r} \frac{\partial(v_r v_\theta)}{\partial \theta} + \frac{1}{r} (v_r^2 - v_\theta^2) \quad (28.10)$$

$$T_\theta(\mathbf{v}) = \frac{\partial(v_\theta v_r)}{\partial r} + \frac{\partial(v_\theta v_z)}{\partial z} + \frac{1}{r} \frac{\partial(v_\theta^2)}{\partial \theta} + \frac{2}{r} v_\theta v_r \quad (28.11)$$

$$T_z(\mathbf{v}) = \frac{\partial(v_z v_r)}{\partial r} + \frac{\partial(v_z^2)}{\partial z} + \frac{1}{r} \frac{\partial(v_z v_\theta)}{\partial \theta} + \frac{1}{r} v_z v_r \quad (28.12)$$

The scalar product is

$$(\mathbf{y}, \mathbf{v}) = \int_{\mathcal{D}} dr d\theta dz r [y_r v_r + y_\theta v_\theta + y_z v_z]$$

for cylindrical coordinates in \mathcal{D} and the preliminary form (9.10) of the Hopf fde emerges as

$$\frac{\partial \theta}{\partial t} [\mathbf{y}; t] = -i [(y_r, \mathcal{F}_r) + (y_\theta, \mathcal{F}_\theta) + (y_z, \mathcal{F}_z)]$$

where

$$\begin{aligned} \mathcal{F}_r = \int_{\Omega} \mu(d\mathbf{v}(t, \mathbf{x})) \exp[i(\mathbf{y}, \mathbf{v}(t, \mathbf{x}))] & \left\{ \frac{\partial}{\partial r} (v_r^2) + \frac{\partial}{\partial z} (v_r v_z) + \frac{1}{r} \frac{\partial}{\partial \theta} (v_r v_\theta) + \frac{1}{r} (v_r^2 - v_\theta^2) \right. \\ & \left. + \frac{1}{\rho} \frac{\partial p}{\partial r} - \frac{1}{Re} \left[\frac{\partial}{\partial r} \left(\frac{1}{r} \frac{\partial}{\partial r} (r v_r) \right) + \frac{1}{r^2} \frac{\partial^2 v_r}{\partial \theta^2} + \frac{\partial^2 v_r}{\partial z^2} - \frac{2}{r^2} \frac{\partial v_\theta}{\partial \theta} \right] - \frac{1}{Fr} G_r \right\} \end{aligned}$$

and

$$\mathcal{F}_\theta = \int_{\Omega} \mu(d\mathbf{v}(t, \mathbf{x})) \exp[i(\mathbf{y}, \mathbf{v}(t, \mathbf{x}))] \left\{ \frac{\partial}{\partial r} (v_\theta v_r) + \frac{\partial}{\partial z} (v_\theta v_z) + \frac{1}{r} \frac{\partial}{\partial \theta} (v_\theta^2) + \frac{2}{r} v_\theta v_r + \frac{1}{r \rho} \frac{\partial p}{\partial \theta} \right. \\ \left. - \frac{1}{Re} \left[\frac{\partial}{\partial r} \left(\frac{1}{r} \frac{\partial}{\partial r} (r v_\theta) \right) + \frac{1}{r^2} \frac{\partial^2 v_\theta}{\partial \theta^2} + \frac{\partial^2 v_\theta}{\partial z^2} + \frac{2}{r^2} \frac{\partial v_r}{\partial \theta} \right] - \frac{1}{Fr} G_\theta \right\}$$

and

$$\mathcal{F}_z = \int_{\Omega} \mu(d\mathbf{v}(t, \mathbf{x})) \exp[i(\mathbf{y}, \mathbf{v}(t, \mathbf{x}))] \left\{ \frac{\partial}{\partial r} (v_z v_r) + \frac{\partial}{\partial z} (v_z^2) + \frac{1}{r} \frac{\partial}{\partial \theta} (v_z v_\theta) + \frac{1}{r} v_z v_r + \frac{1}{\rho} \frac{\partial p}{\partial z} \right. \\ \left. - \frac{1}{Re} \left[\frac{1}{r} \frac{\partial}{\partial r} (r \frac{\partial v_z}{\partial r}) + \frac{1}{r^2} \frac{\partial^2 v_z}{\partial \theta^2} + \frac{\partial^2 v_z}{\partial z^2} \right] - \frac{1}{Fr} G_z - \frac{\partial P_0}{\partial z} \right\}$$

The convective terms in \mathcal{F}_r can be expressed in terms of Gateaux derivatives of the characteristic functional according to (9.6) in Sect. 9.2. They contain second Fréchet/Gateaux derivatives, which are understood as the limit $\mathbf{x} \rightarrow \mathbf{x}'$

$$\frac{\delta^2 \theta}{\delta y_\alpha \delta y_\beta} [\mathbf{y}; t, \mathbf{x}] = \lim_{\mathbf{x}' \rightarrow \mathbf{x}} \frac{\delta^2 \theta}{\delta y_\alpha(\mathbf{x}') \delta y_\beta(\mathbf{x})}$$

for $\alpha, \beta = r, \theta, z$ assuming that the limit exists. The radial component of the convective terms is then

$$-i(y_\alpha, \int_{\Omega} \mu(d\mathbf{v}) \exp[i(\mathbf{y}, \mathbf{v})] \frac{\partial}{\partial r} (v_r v_\alpha)) = i(y_\alpha, \frac{\partial}{\partial r} \frac{\delta^2 \theta}{\delta y_r \delta y_\alpha} [\mathbf{y}; t, \mathbf{x}])$$

analogous to (9.16). This can be carried out for all terms in \mathcal{F}_α , $\alpha = r, \theta, z$ leading to three contributions.

(i) Radial contribution \mathcal{F}_r

$$-i(y_r, \mathcal{F}_r)_c = i \left\{ (y_r, \frac{\partial}{\partial r} \frac{\delta^2 \theta}{\delta y_r^2} [\mathbf{y}; t, \mathbf{x}]) + (y_r, \frac{\partial}{\partial z} \frac{\delta^2 \theta}{\delta y_r \delta y_z} [\mathbf{y}; t, \mathbf{x}]) \right. \\ \left. + (y_r, \frac{1}{r} \frac{\partial}{\partial \theta} \frac{\delta^2 \theta}{\delta y_r \delta y_\theta} [\mathbf{y}; t, \mathbf{x}]) + (y_r, \frac{1}{r} (\{\frac{\delta^2 \theta}{\delta y_r^2} [\mathbf{y}; t, \mathbf{x}] - \frac{\delta^2 \theta}{\delta y_\theta^2} [\mathbf{y}; t, \mathbf{x}]\})) \right\}$$

for the convective terms. Likewise, the viscous terms generate first Gateaux derivatives

$$-i(y_r, \mathcal{F}_r)_\nu = \frac{1}{Re} \left\{ (y_r, \frac{\partial}{\partial r} (\frac{1}{r} \frac{\partial}{\partial r} (r \frac{\delta\theta}{\delta y_r(\mathbf{x})})) + (y_r, \frac{1}{r^2} \frac{\partial^2}{\partial \theta^2} \frac{\delta\theta}{\delta y_r(\mathbf{x})}) \right. \\ \left. + (y_r, \frac{\partial^2}{\partial z^2} \frac{\delta\theta}{\delta y_r(\mathbf{x})}) - (y_r, \frac{2}{r^2} \frac{\partial}{\partial \theta} \frac{\delta\theta}{\delta y_\theta(\mathbf{x})}) \right\}$$

The disturbance pressure gradient generates non-local contributions according to the structure of the Green's function as shown in Sect. 9.2.1. The explicit form in terms of velocity is not required for the steady-state solution and it is left in its implicit form (9.26), Sect. 9.2.1.

$$-i(y_r, \int_{\Omega} \mu(d\mathbf{v}(t, \mathbf{x})) \exp[i(\mathbf{y}, \mathbf{v}(t, \mathbf{x}))] \frac{1}{\rho} \frac{\partial p}{\partial r}) = i(y_r, \Pi_r[\mathbf{y}, \mathbf{G}; \mathbf{x}, t])$$

The external force leads to

$$-i(y_r, \int_{\Omega} \mu(d\mathbf{v}(t, \mathbf{x})) \exp[i(\mathbf{y}, \mathbf{v}(t, \mathbf{x}))] \frac{1}{Fr} G_r) = i \frac{1}{Fr} (y_r, G_r \theta[\mathbf{y}; t])$$

The same steps are required for the azimuthal and axial components. The contributions to the azimuthal component emerge in the analogous form.

(ii) Azimuthal contribution \mathcal{F}_θ

$$-i(y_\theta, \mathcal{F}_\theta)_c = i \left\{ (y_\theta, \frac{\partial}{\partial r} \frac{\delta^2 \theta}{\delta y_\theta \delta y_r} [\mathbf{y}; t, \mathbf{x}]) + (y_\theta, \frac{\partial}{\partial z} \frac{\delta^2 \theta}{\delta y_\theta \delta y_z} [\mathbf{y}; t, \mathbf{x}]) \right. \\ \left. + (y_\theta, \frac{1}{r} \frac{\partial}{\partial \theta} \frac{\delta^2 \theta}{\delta y_\theta^2} [\mathbf{y}; t, \mathbf{x}]) + (y_\theta, \frac{2}{r} \frac{\delta^2 \theta}{\delta y_\theta \delta y_r} [\mathbf{y}; t, \mathbf{x}]) \right\}$$

and for the viscous terms

$$-i(y_\theta, \mathcal{F}_r)_\nu = \frac{1}{Re} \left\{ (y_\theta, \frac{\partial}{\partial r} (\frac{1}{r} \frac{\partial}{\partial r} (r \frac{\delta\theta}{\delta y_\theta(\mathbf{x})})) + (y_\theta, \frac{1}{r^2} \frac{\partial^2}{\partial \theta^2} \frac{\delta\theta}{\delta y_\theta(\mathbf{x})}) \right. \\ \left. + (y_\theta, \frac{\partial^2}{\partial z^2} \frac{\delta\theta}{\delta y_\theta(\mathbf{x})}) + (y_\theta, \frac{2}{r^2} \frac{\partial}{\partial \theta} \frac{\delta\theta}{\delta y_r(\mathbf{x})}) \right\}$$

The pressure gradient is

$$-i(y_\theta, \int_{\Omega} \mu(d\mathbf{v}(t, \mathbf{x})) \exp[i(\mathbf{y}, \mathbf{v}(t, \mathbf{x}))] \frac{1}{\rho r} \frac{\partial p}{\partial \theta}) = i(y_\theta, \Pi_\theta[\mathbf{y}, \mathbf{G}; \mathbf{x}, t])$$

and the external force leads to

$$-i(y_\theta, \int_{\Omega} \mu(d\mathbf{v}(t, \mathbf{x})) \exp[i(\mathbf{y}, \mathbf{v}(t, \mathbf{x}))] \frac{1}{Fr} G_\theta) = i \frac{1}{Fr} (y_\theta, G_\theta \theta[\mathbf{y}; t])$$

(iii) Axial contribution \mathcal{F}_z

The convective part of the axial component is given by

$$\begin{aligned} -i(y_z, \mathcal{F}_z)_c &= i \left\{ (y_z, \frac{\partial}{\partial r} \frac{\delta^2 \theta}{\delta y_z \delta y_r} [\mathbf{y}; t, \mathbf{x}]) + (y_z, \frac{\partial}{\partial z} \frac{\delta^2 \theta}{\delta y_z^2} [\mathbf{y}; t]) \right. \\ &\quad \left. + (y_z, \frac{1}{r} \frac{\partial}{\partial \theta} \frac{\delta^2 \theta}{\delta y_z \delta y_\theta} [\mathbf{y}; t, \mathbf{x}]) + (y_z, \frac{1}{r} (\{\frac{\delta^2 \theta}{\delta y_z \delta y_r} [\mathbf{y}; t, \mathbf{x}]\})) \right\} \end{aligned}$$

and the viscous terms are

$$-i(y_z, \mathcal{F}_z)_\nu = \frac{1}{Re} \left\{ (y_z, \frac{1}{r} \frac{\partial}{\partial r} (r \frac{\partial}{\partial r} \frac{\delta \theta}{\delta y_z(\mathbf{x})})) + (y_z, \frac{1}{r^2} \frac{\partial^2}{\partial \theta^2} \frac{\delta \theta}{\delta y_z(\mathbf{x})}) + (y_z, \frac{\partial^2}{\partial z^2} \frac{\delta \theta}{\delta y_z(\mathbf{x})}) \delta y_\theta(\mathbf{x})) \right\}$$

The pressure gradient generates non-local contributions according to the structure of the Green's function as shown in Sect. 9.2.1. The explicit form in terms of velocity is not required for the steady-state solution and it is left in its implicit form (9.26), Sect. 9.2.1.

$$-i(y_z, \int_{\Omega} \mu(d\mathbf{v}(t, \mathbf{x})) \exp[i(\mathbf{y}, \mathbf{v}(t, \mathbf{x}))] \frac{1}{\rho} \frac{\partial p}{\partial z}) = i(y_z, \Pi_z[\mathbf{y}, \mathbf{G}; \mathbf{x}, t])$$

The external force and the axial component of the basic pressure gradient lead to

$$-i(y_z, \int_{\Omega} \mu(d\mathbf{v}(t, \mathbf{x})) \exp[i(\mathbf{y}, \mathbf{v}(t, \mathbf{x}))] (\frac{1}{Fr} G_z + \frac{\partial P_0}{\partial z})) = i(y_z, (\frac{1}{Fr} G_z + \frac{\partial P_0}{\partial z}) \theta[\mathbf{y}; t])$$

Summary

Collecting the terms for convection, viscous effects, pressure gradient and external forces, the Hopf fde for cylindrical coordinates in the flow domain \mathcal{D} appears in the implicit form

$$\begin{aligned} \frac{\partial \theta}{\partial t} [\mathbf{y}; t] &= -i[(y_r, \mathcal{F}_r)_c + (y_r, \mathcal{F}_r)_\nu + (y_\theta, \mathcal{F}_\theta)_c + (y_\theta, \mathcal{F}_\theta)_\nu + (y_z, \mathcal{F}_z)_c + (y_z, \mathcal{F}_z)_\nu] \\ &\quad + i[(y_r, \Pi_r) + (y_\theta, \Pi_\theta) + (y_z, \Pi_z)] + \frac{i}{Fr} [(y_r, G_r \theta[\mathbf{y}]) + (y_\theta, G_\theta \theta[\mathbf{y}]) \\ &\quad + (y_z, G_z \theta[\mathbf{y}])] - i(y_z, \frac{\partial P_0}{\partial z} \theta[\mathbf{y}]) \end{aligned}$$

Explicit representation of the disturbance pressure gradient functional Π_α (9.26) in terms of velocity requires the construction of a Green's function, and an example is provided in Sect. 9.2.2. The external force field \mathbf{G} is assumed constant in \mathcal{D} (gravity as prime example), and the extension to stochastic forces is discussed in Sect. 9.2.2.

The sum of the explicit convection terms is given by

$$\begin{aligned}
 -i(y_\alpha, \mathcal{F}_\alpha)_c &= i \left\{ (y_r, \frac{\partial}{\partial r} \frac{\delta^2 \theta}{\delta y_r^2} [\mathbf{y}; t, \mathbf{x}]) + (y_r, \frac{\partial}{\partial z} \frac{\delta^2 \theta}{\delta y_r \delta y_z} [\mathbf{y}; t, \mathbf{x}]) \right. \\
 &\quad + (y_r, \frac{1}{r} \frac{\partial}{\partial \theta} \frac{\delta^2 \theta}{\delta y_r \delta y_\theta} [\mathbf{y}; t, \mathbf{x}]) + (y_r, \frac{1}{r} \{ \frac{\delta^2 \theta}{\delta y_r \delta y_r} [\mathbf{y}; t, \mathbf{x}] - \frac{\delta^2 \theta}{\delta y_\theta \delta y_\theta} [\mathbf{y}; t, \mathbf{x}] \}) \\
 &\quad + (y_\theta, \frac{\partial}{\partial r} \frac{\delta^2 \theta}{\delta y_\theta \delta y_r} [\mathbf{y}; t, \mathbf{x}]) + (y_\theta, \frac{\partial}{\partial z} \frac{\delta^2 \theta}{\delta y_\theta \delta y_z} [\mathbf{y}; t, \mathbf{x}]) + (y_\theta, \frac{1}{r} \frac{\partial}{\partial \theta} \frac{\delta^2 \theta}{\delta y_\theta^2} [\mathbf{y}; t, \mathbf{x}]) \\
 &\quad + (y_\theta, \frac{2}{r} \frac{\delta^2 \theta}{\delta y_\theta \delta y_r} [\mathbf{y}; t, \mathbf{x}]) + (y_z, \frac{\partial}{\partial r} \frac{\delta^2 \theta}{\delta y_z \delta y_r} [\mathbf{y}; t, \mathbf{x}]) + (y_z, \frac{\partial}{\partial z} \frac{\delta^2 \theta}{\delta y_z^2} [\mathbf{y}; t, \mathbf{x}]) \\
 &\quad \left. + (y_z, \frac{1}{r} \{ \frac{\partial}{\partial \theta} \frac{\delta^2 \theta}{\delta y_z \delta y_\theta} [\mathbf{y}; t, \mathbf{x}] + \frac{\delta^2 \theta}{\delta y_z \delta y_r} [\mathbf{y}; t, \mathbf{x}] \}) \right\}
 \end{aligned}$$

much more complicated than in the Cartesian case in Chap. 10.

The sum of the explicit viscous terms is a collection of first derivative terms

$$\begin{aligned}
 -i(y_\alpha, \mathcal{F}_\alpha)_\nu &= \frac{1}{Re} \left\{ (y_r, \frac{\partial}{\partial r} (\frac{1}{r} \frac{\partial}{\partial r} (r \frac{\delta \theta}{\delta y_r(\mathbf{x})})) + (y_r, \frac{1}{r^2} \frac{\partial^2}{\partial \theta^2} \frac{\delta \theta}{\delta y_r(\mathbf{x})}) \right. \\
 &\quad + (y_r, \frac{\partial^2}{\partial z^2} \frac{\delta \theta}{\delta y_r(\mathbf{x})}) - (y_r, \frac{2}{r^2} \frac{\partial}{\partial \theta} \frac{\delta \theta}{\delta y_\theta(\mathbf{x})}) + (y_\theta, \frac{\partial}{\partial r} (\frac{1}{r} \frac{\partial}{\partial r} (r \frac{\delta \theta}{\delta y_\theta(\mathbf{x})})) \\
 &\quad + (y_\theta, \frac{1}{r^2} \frac{\partial^2}{\partial \theta^2} \frac{\delta \theta}{\delta y_\theta(\mathbf{x})}) + (y_\theta, \frac{\partial^2}{\partial z^2} \frac{\delta \theta}{\delta y_\theta(\mathbf{x})}) + (y_\theta, \frac{2}{r^2} \frac{\partial}{\partial \theta} \frac{\delta \theta}{\delta y_r(\mathbf{x})}) \\
 &\quad + (y_z, \frac{1}{r} \frac{\partial}{\partial r} (r \frac{\partial}{\partial r} \frac{\delta \theta}{\delta y_z(\mathbf{x})})) + (y_z, \frac{1}{r^2} \frac{\partial^2}{\partial \theta^2} \frac{\delta \theta}{\delta y_z(\mathbf{x})}) + (y_z, \frac{\partial^2}{\partial z^2} \frac{\delta \theta}{\delta y_z(\mathbf{x})}) \delta y_\theta(\mathbf{x})) \left. \right\}
 \end{aligned}$$

The parity conditions in Sect. 25.12 and partial integration allow reformulation of singular terms. For instance, the convective term

$$\begin{aligned}
 (y_r, \frac{1}{r} \frac{\partial}{\partial \theta} \frac{\delta^2 \theta}{\delta y_r \delta y_\theta} [\mathbf{y}; t, \mathbf{x}]) &= 2 \int_0^{2\pi} d\theta \int_0^1 dr \int_0^{2\pi} dz y_r(\theta, r, z) \frac{\partial}{\partial \theta} \frac{\delta^2 \theta}{\delta y_r \delta y_\theta} [\mathbf{y}; t, \mathbf{x}] \\
 &= -2 \int_0^{2\pi} d\theta \int_0^1 dr \int_0^{2\pi} dz \frac{\partial y_r}{\partial \theta} \frac{\delta^2 \theta}{\delta y_r \delta y_\theta} [\mathbf{y}; t, \mathbf{x}]
 \end{aligned}$$

contains ultimately a bounded integrand since $w(r)/r = 2$. Another example is the viscous term

$$(y_r, \frac{\partial}{\partial r}(\frac{1}{r} \frac{\partial}{\partial r}(r \frac{\delta\theta}{\delta y_r(\mathbf{x})})) = -2 \int_0^{2\pi} d\theta \int_0^1 dr \int_0^{2\pi} dz \frac{\partial y_r}{\partial r}(\theta, r, z) \frac{\partial}{\partial r}(r \frac{\delta\theta}{\delta y_r}[\mathbf{y}; t, \mathbf{x}])$$

where $\mathbf{x} = [\theta, r, z]^{-1}$ denotes location in \mathcal{D} . These examples illustrate a mechanism for spreading the solution $\theta_N(\mathbf{y})$ to a wider range of arguments

$$\mathbf{y} = \sum_{k,n,m} y_{k,n,m} \mathbf{e}^{k,n,m}(\mathbf{x})$$

since several integrals with triple products or without the weight function $w(r) = 2r$ do not have the proper form for the application of the orthogonality relations. This concludes the solution.

Problem (10.3): Apply the conditions of steady-state and solenoidal vector fields \mathbf{y} to the Hopf fde for cylindrical coordinates in the flow domain \mathcal{D} obtained in the previous Problem (10.2).

(10.3.1) Specialize the result to constant \mathbf{G} and $\frac{\partial P_0}{\partial z}$.

(10.3.2) Show that the scalar product of two modes in \mathcal{B}_e is reduced to an integral w.r.t. the radial coordinate.

Hint: Consult Sect. 9.2.

Solution: Steady state implies

$$\frac{\partial \theta}{\partial t}[\mathbf{y}; t] = 0$$

and solenoidal arguments \mathbf{y}

$$i[(y_r, \Pi_r) + (y_\theta, \Pi_\theta) + (y_z, \Pi_z)] = 0$$

according to Sect. 10.1. The steady-state version of the Hopf fde for cylindrical coordinates in \mathcal{D} is thus the orthogonality condition

$$\begin{aligned} & -i[(y_r, \mathcal{F}_r)_c + (y_r, \mathcal{F}_r)_\nu + (y_\theta, \mathcal{F}_\theta)_c + (y_\theta, \mathcal{F}_\theta)_\nu + (y_z, \mathcal{F}_z)_c + (y_z, \mathcal{F}_z)_\nu] \\ & + \frac{i}{Fr} [(y_r, G_r \theta[\mathbf{y}]) + (y_\theta, G_\theta \theta[\mathbf{y}]) + (y_z, G_z \theta[\mathbf{y}])] + i(y_z, \frac{\partial P_0}{\partial z} \theta[\mathbf{y}]) = 0 \end{aligned}$$

(10.3.1) Assuming \mathcal{G} and $\frac{\partial P_0}{\partial z}$ being non-zero constants, the result simplifies to

$$-i[(y_r, \mathcal{F}_r)_c + (y_r, \mathcal{F}_r)_\nu + (y_\theta, \mathcal{F}_\theta)_c + (y_\theta, \mathcal{F}_\theta)_\nu + (y_z, \mathcal{F}_z)_c + (y_z, \mathcal{F}_z)_\nu] \\ + \frac{i}{Fr} [G_r(y_r, \theta[\mathbf{y}]) + G_\theta(y_\theta, \theta[\mathbf{y}])] + i(\frac{\partial P_0}{\partial z} + \frac{1}{Fr} G_z)(y_z, \theta[\mathbf{y}]) = 0$$

valid for $\mathbf{y} \in \mathcal{N}$.

(10.3.2) Let $\mathbf{e}^{k,n,m}(r, \theta, z)$ and $\mathbf{e}^{o,p,q}(r, \theta, z)$ be two modes in \mathcal{B}_e , and then is the scalar product according to (9.2)

$$(\mathbf{e}^{k,n,m}, \mathbf{e}^{o,p,q}) = \int_0^1 dr \int_0^{2\pi} d\theta \int_0^{2\pi} dz w(r) h_k(\theta) \chi_\alpha^{e,k,n,m}(r) h_m(z) h_o(\theta) \chi_\alpha^{e,o,p,q}(r) h_q(z)$$

where the measure differential is $d\nu = d\mathbf{x}w(\mathbf{x}) = 2rdrd\theta dz$ with weight function $w(\mathbf{x}) = 2r$ (25.38). The integrations over θ and z lead to the conditions $k = o$ and $m = q$; hence,

$$(\mathbf{e}^{k,n,m}, \mathbf{e}^{o,p,q}) = \int_0^1 dr w(r) \chi_\alpha^{e,k,n,m}(r) \chi_\alpha^{e,k,p,m}(r)$$

is a single integral as claimed. If the radial modes are orthonormal, the result is $(\mathbf{e}^{k,n,m}, \mathbf{e}^{o,p,q}) = \delta_{k,o} \delta_{n,p} \delta_{m,q}$.

Problem (10.4): Consider the flow through a straight, circular pipe periodic in axial direction. A solenoidal ONS basis \mathcal{B}_e was constructed in Sect. 25.21 spanning the test function space \mathcal{N} for the characteristic functional $\theta[\mathbf{y}; t]$, $\mathbf{y} \in \mathcal{N}$. Solve the BVP for the projected characteristic functional $\theta_N(y_{0,0,0}, \dots, y_{\frac{1}{2}N,N,N})$ introduced in Sect. 10.4 w.r.t. the basis \mathcal{B}_e .

(10.4.1) Apply the pde (10.21) to the single mode $N = 0$, set up the boundary condition and solve it for $y \geq 0$.

(10.4.2) Compute the coefficients $a_{k,n,m}^{l,o,q,r,s,t}$ in $A_{k,n,m}^{r,s,t} = \sum_{l,o,q} y_{l,o,q} a_{k,n,m}^{l,o,q,r,s,t}$ and $C_z^{0,n,0}$ in $C(y_{0,n,0}) = \frac{\partial P_0}{\partial z} \sum_{n=0}^N C_z^{0,n,0} y_{0,n,0}$ the pde (10.21) for several modes, say $N = 2$ and plot the results.

Hint: Consult Chap. 25 in Appendix C.

Solution:

The solenoidal vector basis \mathcal{B}_e (10.16) for test/argument vector fields $\mathbf{y}(\mathbf{x})$ in the domain of the periodic pipe flow has been constructed in Sect. 25.21 of Appendix C as product of three $1-d$ modes

$$\mathcal{B}_e = \{e_\alpha^{k,n,m}(r, \theta, z) = h_k(\theta) \chi_\alpha^{e,k,n,m}(r) h_m(z), \alpha = r, \theta, z\}$$

where $h_k(\theta)$ and $h_m(z)$ are the azimuthal and axial Fourier modes (25.16), (25.30) and $\chi_{\alpha}^{e,k,n,m}(r)$ is the radial mode/shape function (25.164).

Coefficient $A_{k,n,m}^{r,s,t}$:

The coefficient $A_{k,n,m}^{r,s,t}$ is expanded in three term groups

$$A_{k,n,m}^{r,s,t} = \sum_{l,o,p} y_{l,o,p} a_{k,n,m}^{l,o,p,r,s,t}$$

where

$$a_{k,n,m}^{l,o,p,r,s,t} \equiv R_{k,n,m}^{l,o,p,r,s,t} + i l T_{k,n,m}^{l,o,p,r,s,t} + i p Z_{k,n,m}^{l,o,p,r,s,t} \quad (1)$$

according to (10.22). The term groups are defined by

$$R_{k,n,m}^{l,o,p,r,s,t} \equiv \left(\frac{\partial}{\partial r} e_{\alpha}^{l,o,p}, e_{\alpha}^{k,n,m} e_r^{r,s,t} \right), \quad T_{k,n,m}^{l,o,p,r,s,t} \equiv \left(\frac{1}{r} e_{\alpha}^{l,o,p}, e_{\alpha}^{k,n,m} e_r^{r,s,t} \right), \quad Z_{k,n,m}^{l,o,p,r,s,t} \equiv \left(e_{\alpha}^{l,o,p}, e_{\alpha}^{k,n,m} e_r^{r,s,t} \right)$$

with implied summation $\alpha = r, \theta, z$. The lengthy computation of the term groups is straightforward, starting with $R_{k,n,m}^{l,o,p,r,s,t}$ and observing (15.2) (overbars denote complex conjugate)

$$\begin{aligned} \left(\frac{\partial}{\partial r} e_r^{l,o,p}, e_r^{k,n,m} e_r^{r,s,t} \right) &= \int_0^1 dr w(r) \int_0^{2\pi} d\theta \int_0^{2\pi} dz \frac{1}{2\pi} \exp[i(l\theta + pz)] \frac{d}{dr} \chi_r^{e,l,o,p} \\ &\quad \overline{\exp[i(k\theta + mz)] \chi_r^{e,k,n,m} \exp[i(r\theta + tz)] \chi_r^{e,r,s,t}} \end{aligned}$$

The result is

$$\begin{aligned} R_{k,n,m}^{l,o,p,r,s,t} &= \left(\frac{\partial}{\partial r} e_{\alpha}^{l,o,p}, e_{\alpha}^{k,n,m} e_r^{r,s,t} \right) = \delta_{l,k+r} \delta_{p,m+t} \int_0^1 dr w(r) \left[\frac{d}{dr} \chi_r^{e,l,o,p} \overline{\chi_r^{e,k,n,m}} \overline{\chi_r^{e,r,s,t}} \right. \\ &\quad \left. + \frac{d}{dr} \chi_{\theta}^{e,l,o,p} \overline{\chi_{\theta}^{e,k,n,m}} \overline{\chi_r^{e,r,s,t}} + \frac{d}{dr} \chi_z^{e,l,o,p} \overline{\chi_z^{e,k,n,m}} \overline{\chi_r^{e,r,s,t}} \right] \end{aligned}$$

and

$$\begin{aligned} T_{k,n,m}^{l,o,p,r,s,t} &= \left(\frac{1}{r} e_{\alpha}^{l,o,p}, e_{\alpha}^{k,n,m} e_{\theta}^{r,s,t} \right) = \delta_{l,k+r} \delta_{p,m+t} \int_0^1 dr \frac{w(r)}{r} \left[\chi_r^{e,l,o,p} \overline{\chi_r^{e,k,n,m}} \overline{\chi_{\theta}^{e,r,s,t}} \right. \\ &\quad \left. + \chi_{\theta}^{e,l,o,p} \overline{\chi_{\theta}^{e,k,n,m}} \overline{\chi_r^{e,r,s,t}} + \chi_z^{e,l,o,p} \overline{\chi_z^{e,k,n,m}} \overline{\chi_{\theta}^{e,r,s,t}} \right] \end{aligned}$$

and

$$Z_{k,n,m}^{l,o,p,r,s,t} = (e_{\alpha}^{l,o,p}, e_{\alpha}^{k,n,m} e_z^{r,s,t}) = \delta_{l,k+r} \delta_{p,m+t} \int_0^1 dr w(r) [\chi_r^{e,l,o,p} \overline{\chi_r^{e,k,n,m}} \overline{\chi_z^{e,r,s,t}} \\ + \chi_{\theta}^{e,l,o,p} \overline{\chi_{\theta}^{e,k,n,m}} \overline{\chi_z^{e,r,s,t}} + \chi_z^{e,l,o,p} \overline{\chi_z^{e,k,n,m}} \overline{\chi_z^{e,r,s,t}}]$$

This completes the computation of the term groups constituting $A_{k,n,m}^{r,s,t}$.

Coefficient $B_{k,n,m}$:

According to (10.23) the coefficient $B_{k,n,m}$ is expanded

$$B_{k,n,m} = \sum_{r,s,t} y_{r,s,t} b_{k,n,m}^{r,s,t}$$

w.r.t. the solenoidal basis \mathcal{B}_e (10.16), where

$$b_{k,n,m}^{r,s,t} = \left(\frac{\partial e_{\alpha}^{e,r,s,t}}{\partial r}, \frac{\partial e_{\alpha}^{e,k,n,m}}{\partial r} \right) + \left(\frac{1}{r} \frac{\partial e_{\alpha}^{e,r,s,t}}{\partial \theta}, \frac{1}{r} \frac{\partial e_{\alpha}^{e,k,n,m}}{\partial \theta} \right) + \left(\frac{\partial e_{\alpha}^{e,r,s,t}}{\partial z}, \frac{\partial e_{\alpha}^{e,k,n,m}}{\partial z} \right)$$

The contributions to $b_{k,n,m}$ are now computed in turn. The radial derivative term is then

$$\left(\frac{\partial e_{\alpha}^{e,r,s,t}}{\partial r}, \frac{\partial e_{\alpha}^{e,k,n,m}}{\partial r} \right) = \delta_{r,k} \delta_{t,m} \int_0^1 dr w(r) \frac{d \chi_{\alpha}^{e,r,s,t}}{dr} \overline{\frac{d \chi_{\alpha}^{e,k,n,m}}{dr}}$$

and the azimuthal derivative term is

$$\left(\frac{1}{r} \frac{\partial e_{\alpha}^{e,r,s,t}}{\partial \theta}, \frac{1}{r} \frac{\partial e_{\alpha}^{e,k,n,m}}{\partial \theta} \right) = -k^2 \delta_{r,k} \delta_{t,m} \int_0^1 dr w(r) \frac{1}{r^2} \chi_{\alpha}^{e,r,s,t} \overline{\chi_{\alpha}^{e,k,n,m}}$$

and the axial derivative term is

$$\left(\frac{\partial e_{\alpha}^{e,r,s,t}}{\partial z}, \frac{\partial e_{\alpha}^{e,k,n,m}}{\partial z} \right) = -m^2 \delta_{r,k} \delta_{s,n} \delta_{t,m}$$

where the overbar denotes complex conjugate. The coefficient $B_{k,n,m}$ emerges then in the form

$$B_{k,n,m} = \sum_{r,s,t} y_{r,s,t} \left\{ \int_0^1 dr w(r) \frac{d \chi_{\alpha}^{e,k,s,m}}{dr} \overline{\frac{d \chi_{\alpha}^{e,k,n,m}}{dr}} - k^2 \int_0^1 dr w(r) \frac{1}{r^2} \chi_{\alpha}^{e,k,s,m} \overline{\chi_{\alpha}^{e,k,n,m}} - m^2 \delta_{s,n} \right\} \quad (2)$$

The integrals are computed using Gauss–Lobatto quadrature.

Coefficient C :

According to (10.24) it is proportional to the basic pressure gradient

$$C(y_{0,0,0}, \dots, y_{\frac{1}{2}N,N,N}) \equiv \sum_{k,n,m} y_{k,n,m} (e_{\alpha}^{k,n,m}, \nabla_{\alpha}^c P_0)$$

The sum has non-zero terms only for wavenumbers $r = k$ and $t = m$, hence

$$C(y_{0,0,0}, \dots, y_{\frac{1}{2}N,N,N}) = \frac{\partial P_0}{\partial x_{\alpha}} \sum_{n,k,m} C_{\alpha}^{k,n,m} y_{n,k,m}, \quad \alpha = r, \theta, z$$

as derived in Sect. 10.4.1). It appears in this section as

$$C(y_{0,n,0}) = \frac{\partial P_0}{\partial z} \sum_{n=0}^N C_z^{0,n,0} y_{0,n,0} \quad (3)$$

for the present example of the periodic pipe flow with the basic pressure gradient in axial direction. Two cases for N are now considered in detail.

(10.4.1) Solution for a single mode, $N = 0$. The element $\mathbf{e}^{k,n,m}(r, \theta, z)$ with shape functions $\chi_{\alpha}^{e,k,n,m}(r)$, $\alpha = r, \theta, z$ for $n = 0, k = 0, m = 0$ is the single mode selected for the evaluation of the coefficients in Eq. (10.21). The radial profiles of the shape functions $\chi_{\alpha}^{e,0,0,0}(r)$ are shown in Fig. 28.8. The figure indicates that for the selected mode $k = 0$ the radial component is identically zero, and the azimuthal is real and the axial is imaginary (recall that the shape function $\chi_{\alpha}^{e,k,n,m}(r)$ is multiplied with the complex Fourier mode $h_k(\theta)h_m(z)$ to complete the mode). The figure contains also the shape functions for wavenumbers $k = 1$ and $k = 2$ to indicate the effect of the vector parity conditions. The radial and azimuthal shape functions are zero at the coordinate axis $r = 0$ for $k = 0, 2$ (upper left and lower graphs), but non-zero for $k = 1$ (upper right graph) to allow flow across the coordinate axis $r = 0$. The non-zero axis values for $k = 1$ must be such that $\chi_r^{e,1,0,0}(0) + i\chi_{\theta}^{e,1,0,0}(0) = 0$ holds according to the parity condition (25.61). Furthermore, Fig. 28.9 shows the radial profiles $\chi_{\alpha}^{e,k,0,0}(r)$ for all azimuthal wavenumbers $k \in [0, P/2]$ ($P = N = 72$ approximation, FFT consistent storage). The effect of the parity conditions (25.64) $O(\chi_r^{e,k,0,0}(r)) = O(\chi_{\theta}^{e,k,0,0}(r)) = r^{|k-1|}$ and $O(\chi_z^{e,k,0,0}(r)) = r^k$ near $r = 0$ is evident as the shape functions are pushed towards $r = 1$ with increasing wavenumber k . It is useful to notice that the selected mode ($k=0, n=0, m=0$) has a complex shape function vector $\chi_{\alpha}^{e,0,0,0}(r)$, but the components are either imaginary (for $\chi_r^{e,k,n,m}$ and $\chi_z^{e,k,n,m}$) or real (for $\chi_{\theta}^{e,k,n,m}$ as evident in Fig. 28.8).

The coefficients of (10.21), defined by (10.22), (10.23), (10.24) and expanded above in Eqs. (1), (2), (3), emerge for $N = 0$ as scalars

$$A_{0,0,0}^{0,0,0} = y_{0,0,0} R_{0,0,0}^{0,0,0,0,0,0}$$

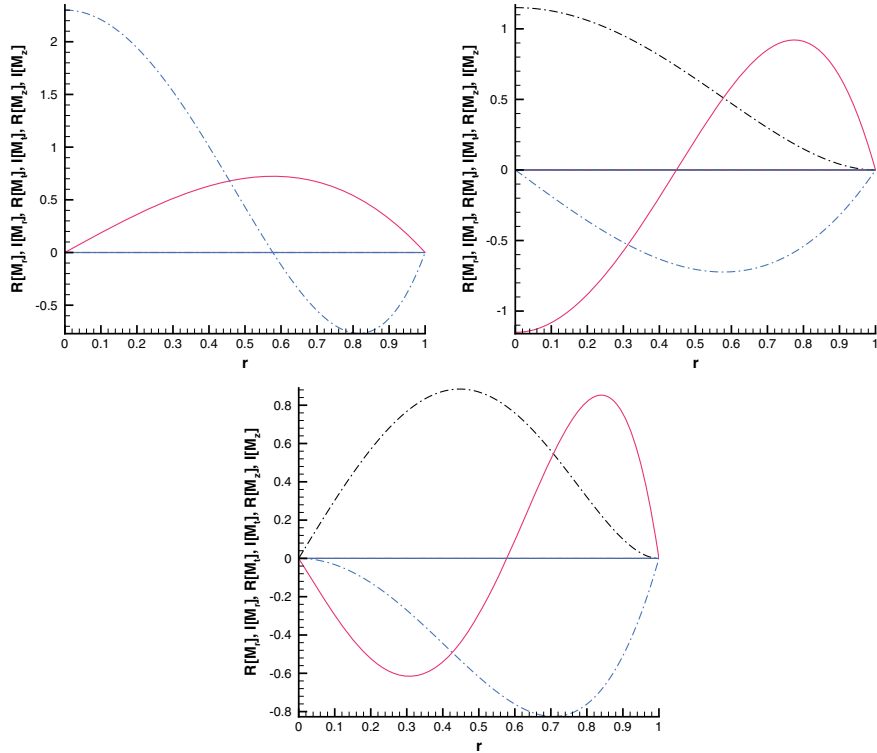


Fig. 28.8 Shape functions $\chi_{\alpha}^{e,k,0,0}(r)$ for the radial mode index $n = 0$, the axial wavenumber $m = 0$ and the azimuthal wavenumbers $k = 0, 1, 2$. The components are indicated by $\alpha = r$ (black), $\alpha = \theta$ (red) and $\alpha = z$ (blue), real parts are full and imaginary parts are dot-dashed lines. The upper left graph is for the azimuthal wavenumber $k = 0$ (the selected mode), the upper right for $k = 1$ and the lower graph for $k = 2$ illustrating the parity conditions, Sect. 25.12, Appendix C, which require for $k = 1$ that the axial values satisfy $\chi_r^{e,1,0,0}(0) + i\chi_{\theta}^{e,1,0,0}(0) = 0$ as the upper right graph verifies

with $R_{0,0,0}^{0,0,0,0,0,0} = (\frac{\partial}{\partial r}e_{\alpha}^{0,0,0}, e_{\alpha}^{0,0,0}e_r^{0,0,0})$ and

$$\begin{aligned} \left(\frac{\partial}{\partial r}e_{\alpha}^{0,0,0}, e_{\alpha}^{0,0,0}e_r^{0,0,0} \right) &= \int_0^1 dr w(r) \left[\frac{d}{dr} \chi_r^{e,0,0,0} \overline{\chi_r^{e,0,0,0}} \right. \\ &\quad \left. + \frac{d}{dr} \chi_{\theta}^{e,0,0,0} \overline{\chi_{\theta}^{e,0,0,0}} + \frac{d}{dr} \chi_z^{e,0,0,0} \overline{\chi_z^{e,0,0,0}} \right] \end{aligned}$$

where the integrals are evaluated numerically using Gauss–Lobatto quadrature. Figure 28.8 shows that the radial shape function $\chi_r^{e,0,0,0}$ for $n = k = m = 0$ is zero, hence, $R_{0,0,0}^{0,0,0,0,0,0} = 0$. However, the azimuthal and axial shape functions are non-zero; hence, the scalar products obtained above are reduced to

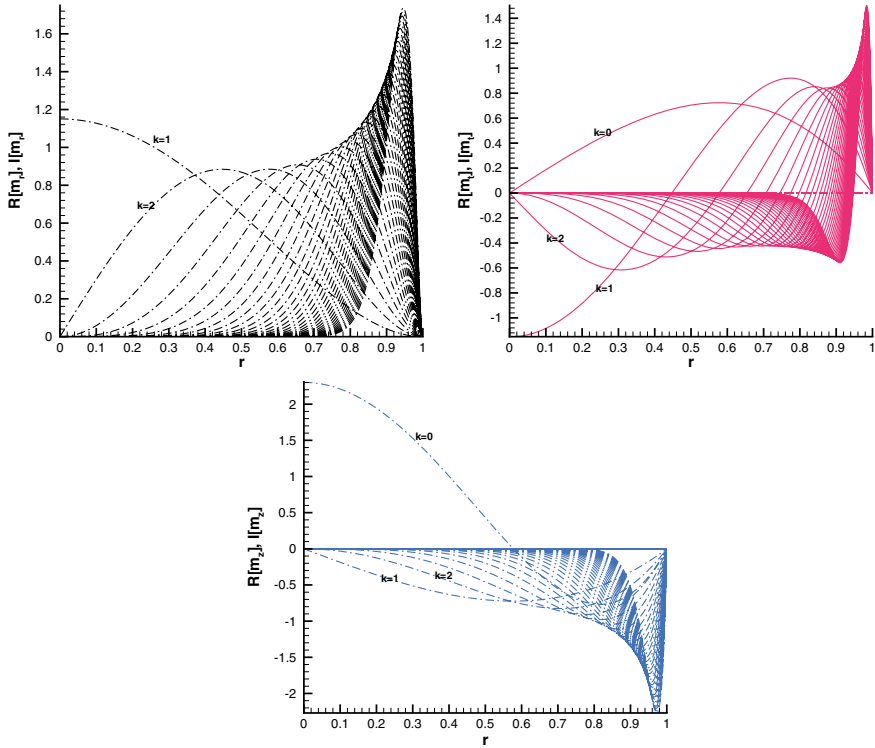


Fig. 28.9 Shape functions $\chi_{\alpha}^{e,k,0,0}(r)$ for the axial wavenumber $m = 0$ and all azimuthal wavenumbers k for a given level of projection ($N = P = 72$). The components are indicated by $\alpha = r$ (imaginary part, black, the shape function $\chi_r^{e,0,0,0}$ is zero), $\alpha = \theta$ (real part, red) and $\alpha = z$ (imaginary part, blue). The upper left graph is for the radial component, the upper right for azimuthal and the lower graph for the axial component. Wavenumbers $k = 0, 1, 2$ are indicated, the higher wavenumbers are increasingly crowded to the outer boundary $r = 1$

$$T_{0,0,0}^{0,0,0,0,0,0} = \left(\frac{1}{r} e_{\alpha}^{0,0,0}, e_{\alpha}^{0,0,0} e_{\theta}^{0,0,0} \right) = \int_0^1 dr w(r) \frac{1}{r} [\chi_{\theta}^{e,0,0,0} \overline{\chi_{\theta}^{e,0,0,0}} \chi_{\theta}^{e,0,0,0} + \chi_z^{e,0,0,0} \overline{\chi_z^{e,0,0,0}} \chi_z^{e,0,0,0}]$$

and

$$Z_{0,0,0}^{0,0,0,0,0,0} = (e_{\alpha}^{0,0,0}, e_{\alpha}^{0,0,0} e_z^{0,0,0}) = \int_0^1 dr w(r) [\chi_{\theta}^{e,0,0,0} \overline{\chi_{\theta}^{e,0,0,0}} \chi_z^{e,0,0,0} + \chi_z^{e,0,0,0} \overline{\chi_z^{e,0,0,0}} \chi_z^{e,0,0,0}]$$

They are, however, multiplied by the wavenumbers and the coefficient is thus

$$A_{0,0,0}^{0,0,0} = 0$$

The coefficient $B_{0,0,0}$ obtained above (2) is reduced to $B_{0,0,0} \equiv b_{0,0,0}^{0,0,0} y_{0,0,0}$ where

$$b_{0,0,0}^{0,0,0} = \int_0^1 dr w(r) \left\{ \frac{d\chi_\theta^{e,0,0,0}}{dr} \overline{\frac{d\chi_\theta^{e,0,0,0}}{dr}} + \frac{d\chi_z^{e,0,0,0}}{dr} \overline{\frac{d\chi_z^{e,0,0,0}}{dr}} \right\}$$

for the same reasons.

The final coefficient C is according to (3) reduced to a single term

$$C(y_{0,0,0}) = \frac{\partial P_0}{\partial z} C_z^{0,0,0} y_{0,0,0}$$

where $C_z^{0,0,0} = (e_z^{0,0,0}, h)$, $h(r, \theta, z) = 1$ and

$$C_z^{0,0,0} = \int_0^1 dr w(r) \chi_z^{e,0,0,0}$$

which is non-zero. The result is a linear, first-order ode

$$\frac{1}{Re} b_{0,0,0} \frac{d\theta_0}{dy_{0,0,0}} + \frac{\partial P_0}{\partial z} C_z^{0,0,0} \theta_0 = 0$$

for $\theta_0(y_{0,0,0})$ with constant coefficients for the domain $y_{0,0,0} \in [0, \infty)$. The boundary condition $\theta_1(0) = 1$ is provided by the Bochner–Minlos Theorem (10.25). The solution

$$\theta_0(y_{0,0,0}) = \exp\left(-Re \frac{\partial P_0}{\partial z} \frac{C_z^{0,0,0}}{b_{0,0,0}^{0,0,0}} y_{0,0,0}\right) \quad (28.13)$$

is an exponential function valid for $y_{0,0,0} \geq 0$. The numerical values for the present basis (10.16) are $C_z^{0,0,0} = -0.5100085$ (the basic pressure gradient is also negative, hence $C_z^{0,0,0} \frac{\partial P_0}{\partial z} \geq 0$) and $b_{0,0,0}^{0,0,0} = \left\| \frac{d\chi^{e,0,0,0}}{dr} \right\|^2 = 39.8090639$, obtained using Gauss–Lobatto quadrature. The argument of the exponential is a real number, hence is $\theta_0(y_{0,0,0})$ a decaying exponential and the first two conditions of the Bochner–Minlos theorem (Sect. 8.1) are met for $y_{0,0,0} \geq 0$.

(10.4.2) Solution for several modes, $N = 2$.

The general expressions for the coefficients A , B and C have been established above. The procedure for the setup of the pde for $N > 0$ is the same as for $N = 0$ in the previous section. The complex-valued coefficient matrix $A_{k,n,m}^{r,s,t}$ is then after some lengthy computations

$$A_{k,n,m}^{r,s,t} = \sum_{l=0}^{N/2} \sum_{o=0}^N \sum_{q=0}^N y_{l,o,q} a_{k,n,m}^{l,o,q,r,s,t}$$

where

$$\begin{aligned}
 a_{k,n,m}^{l,o,q,r,s,t} &\equiv \delta_{l,k+r} \delta_{q,m+t} \int_0^1 dr w(r) \\
 &\left\{ \frac{d}{dr} \chi_r^{e,l,o,q} \overline{\chi_r^{e,k,n,m}} \overline{\chi_r^{e,r,s,t}} + \frac{d}{dr} \chi_\theta^{e,l,o,q} \overline{\chi_\theta^{e,k,n,m}} \overline{\chi_r^{e,r,s,t}} + \frac{d}{dr} \chi_z^{e,l,o,q} \overline{\chi_z^{e,k,n,m}} \overline{\chi_r^{e,r,s,t}} \right. \\
 &+ \frac{il}{r} \left[\chi_r^{e,l,o,q} \overline{\chi_r^{e,k,n,m}} \overline{\chi_\theta^{e,r,s,t}} + \chi_\theta^{e,l,o,q} \overline{\chi_\theta^{e,k,n,m}} \overline{\chi_\theta^{e,r,s,t}} + \chi_z^{e,l,o,q} \overline{\chi_z^{e,k,n,m}} \overline{\chi_\theta^{e,r,s,t}} \right] \\
 &\left. + iq \left[\chi_r^{e,l,o,q} \overline{\chi_r^{e,k,n,m}} \overline{\chi_z^{e,r,s,t}} + \chi_\theta^{e,l,o,q} \overline{\chi_\theta^{e,k,n,m}} \overline{\chi_z^{e,r,s,t}} + \chi_z^{e,l,o,q} \overline{\chi_z^{e,k,n,m}} \overline{\chi_z^{e,r,s,t}} \right] \right\}
 \end{aligned}$$

where the integral is evaluated numerically for $N = 2$, and the weight function is given in Eq. (25.38) as $w(r) = 2r$. This completes the computation of the term groups constituting the complex-valued matrix $A_{k,n,m}^{r,s,t}$.

The computation of $B_{k,n,m}$ proceeds along the same lines according to Eq. (2) and leading to

$$B_{k,n,m} = \sum_{r=0}^{N/2} \sum_{s=0}^N \sum_{t=0}^N y_{r,s,t} b_{k,n,m}^{r,s,t}$$

where

$$b_{k,n,m}^{r,s,t} = \int_0^1 dr w(r) \left\{ \frac{d\chi_\alpha^{e,k,s,m}}{dr} \overline{\frac{d\chi_\alpha^{e,k,n,m}}{dr}} - \frac{k^2}{r^2} \chi_\alpha^{e,k,s,m} \overline{\chi_\alpha^{e,k,n,m}} \right\} - m^2 \delta_{s,n}$$

to be evaluated for $N > 0$.

Finally, the coefficient C is according to Eq. (3)

$$C(y_{k,n,m}) = \delta_{k,0} \delta_{m,0} \frac{\partial P_0}{\partial z} \sum_{n=0}^N (e_z^{0,n,0}, h) y_{0,n,0}$$

where $C_z^{0,n,0} = (e_z^{0,n,0}, h)$ in (3) and $h(r) = 1$. The term $C_z^{0,n,0}$ is shown as function of the radial mode index n in the main text (Fig. 10.1 in Sect. 10.4.1).

The pde for the projected characteristic function θ_N has been established in Eq. (10.21) in Sect. 10.4.1, and it emerges in the form

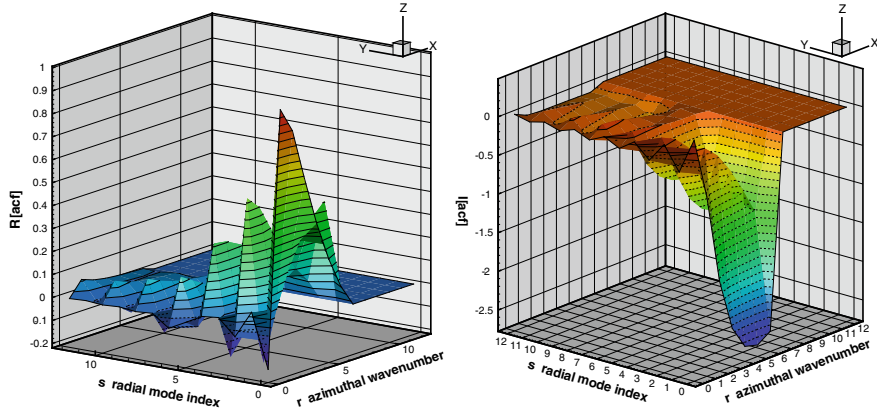


Fig. 28.10 Coefficient $a_{k,n,m}^{l,o,q,r,s,t}$ as function of r (azimuthal wavenumber) and s (radial mode index) for $o = 2, t = 1, k = 1, n = 2, m = 1$ in the pde (10.21), real part in the left and imaginary part in the right graph. The truncation level is $N = 12$

$$i \sum_{k,n,m} \sum_{l,o,q} \sum_{r,s,t} a_{k,n,m}^{l,o,q,r,s,t} y_{l,o,q} \frac{\partial^2 \theta_N}{\partial y_{k,n,m} \partial y_{l,o,q}} + \frac{1}{Re} \sum_{k,n,m} \sum_{r,s,t} b_{k,n,m}^{r,s,t} y_{r,s,t} \frac{\partial \theta_N}{\partial y_{k,n,m}} \\ -i \frac{\partial P_0}{\partial z} \sum_{n=0}^N C_z^{0,n,0} y_{0,n,0} \theta_N = 0$$

plus the boundary condition $\theta_N(y_{k,n,m}) = 1$ at the origin $y_{k,n,m} = 0, \forall k, n, m$.

The results for coefficient A , written in the form

$$A_{k,n,m}^{r,s,t} = \sum_{l,o,q} y_{l,o,q} a_{k,n,m}^{l,o,q,r,s,t}$$

as linear function of the independent variables $y_{l,o,q}$ ($0 \leq k, l, r \leq N/2$ are azimuthal wavenumbers, $0 \leq n, o, s \leq N$ radial mode indices and $0 \leq m, q, t \leq N$ axial wavenumbers), are shown in terms of $a_{k,n,m}^{l,o,q,r,s,t}$ in Fig. 28.10 as function of s, t for $o = 2, r = 2, k = 1, n = 2, m = 2$ and the truncation $N = 12$. The coefficient $a_{k,n,m}^{l,o,q,r,s,t}$ of the second derivative is only weakly dependent on the axial wavenumber t in Fig. 28.10 due to the effect of the curl acting on the modified vector potential $\mathbf{A}(r, \theta, z)$ according to Eq. (25.160) (Fig. 28.11).

Comments: The results for $N = 0$ in Problem (10.4.1) lead to the expected exponential solution for the projected characteristic function $\theta_N(y_{0,0,0})$. Figure 28.9 shows that for azimuthal wavenumbers $k > 0$ the radial shape functions $\chi_r^{e,k,0,0}(r)$ are not zero and the axial component $\chi_z^{k,0,0}(r)$ does not integrate to zero; hence, stochastic solutions are possible and the basic pressure gradient can be expected to have a

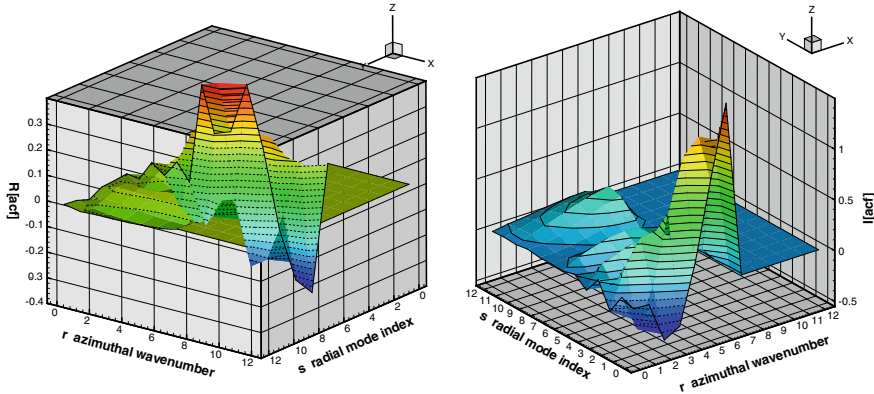


Fig. 28.11 Coefficient $a_{k,n,m}^{l,o,q,r,s,t}$ as function of r (azimuthal wavenumber) and s (radial mode index) for $o = 2, t = 1, k = 3, n = 5, m = 1$ in the pde (10.21), real part in the left and imaginary part in the right graph. The truncation level is $N = 12$

significant influence on the solution. Note that the finite-dimensional approximation of the characteristic functional is defined by (25.14)

$$\theta_N(y_{k,n,m}) \equiv \theta \left[\sum_{k=0}^{N/2} \sum_{n=0}^N \sum_{m=0}^N y_{k,n,m} \mathbf{e}^{k,n,m}(\mathbf{x}) \right]$$

with the argument field

$$\mathbf{y}(r, \theta, z) = \sum_{k=0}^{N/2} \sum_{n=0}^N \sum_{m=0}^N y_{k,n,m} \mathbf{e}^{k,n,m}(r, \theta, z)$$

being element of the subspace of \mathcal{N} spanned by finite-dimensional sets of coefficients. For the present example in section (10.4.1) $N = P = 0$ $\theta_1(y_{0,0,0})$ is a function of a single coefficient $y_{0,0,0}$ and the characteristic functional depends on a single vector field $\mathbf{y}(r, \theta, z) = y_{0,0,0} \mathbf{e}^{0,0,0}(r, \theta, z)$, where $\mathbf{e}^{0,0,0}(r, \theta, z)$ is element of the solenoidal ONS basis \mathcal{B}_e with radial shape functions shown in the upper left graph in Fig. 28.8.

The case $N > 0$ leads to a linear, second-order pde (10.21) with rapidly growing number $M(N)$ (10.18) of independent variables (for instance, $M(2) = 50$); however, not all coefficients $A_{k,n,m}^{l,o,q,r,s,t}$, $B_{k,n,m}$, $C_z^{k,n,m}$ are non-zero as the expressions derived at the beginning of the solution indicate. The preliminary discussion of the pde for the projected characteristic functional shows that further research is required on the mathematical properties of this pde and efficient numerical means to compute the solution.

Solutions to problems for Chap. 11: Transport equations for finite-dimensional characteristic functions, Pdfs and Cdfs

Problem (11.1) A random variable $Y(t)$ defined on R^1 is specified by the Pdf

$$f_Y(t) = \frac{1}{2} \exp(-|t|)$$

Compute the characteristic function $\theta(\zeta)$ and all statistical moments using θ .

Solution: The characteristic function $\theta(\zeta)$ is defined by (28.14)

$$\theta_1(\mathbf{y}^1; t) = \int_{\Omega^1} d\mu^1(t, \mathbf{v}^1) \exp[iy_\alpha^1 v_\alpha(t, \mathbf{x}^1)] \quad (28.14)$$

which is simply denoted by $\theta(\zeta)$

$$\theta(\zeta) = \int_{-\infty}^{\infty} dt f_Y(t) \exp(i\zeta t)$$

hence

$$\theta(\zeta) = \frac{1}{2} \int_{-\infty}^{\infty} dt \exp(i\zeta t - |t|)$$

or

$$\theta(\zeta) = \frac{1}{2} \int_{-\infty}^0 dt \exp(i\zeta t + t) + \frac{1}{2} \int_0^{\infty} dt \exp(i\zeta t - t)$$

The integrals are elementary and

$$\theta(\zeta) = \frac{1}{1 + \zeta^2}$$

is obtained.

The statistical moments follow by differentiation at the origin

$$i^n \langle Y^n \rangle = \frac{d^n \theta}{d\zeta^n}(\zeta = 0)$$

They appear as coefficients of the Taylor series centred at the origin

$$\theta(\zeta) = \sum_{n=0}^{\infty} \frac{\zeta^n}{n!} \frac{d^n \theta}{d\zeta^n}(0)$$

It is convenient to expand the characteristic function

$$\theta(\zeta) = \sum_{n=0}^{\infty} (-1)^n \zeta^{2n}$$

convergent for $|\zeta| < 1$. Comparison of the series results in

$$\frac{d^n \theta}{d\zeta^n}(0) = \begin{cases} (-1)^{\frac{n}{2}} n! & \text{for } n \text{ even} \\ 0 & \text{for } n \text{ odd} \end{cases}$$

and thus the moments for $n \geq 0$

$$\langle Y^n \rangle = \begin{cases} n! & \text{for } n \text{ even} \\ 0 & \text{for } n \text{ odd} \end{cases}$$

follow, where $(-1)^{\frac{n}{2}} = i^n$ was used.

Reference: Lukacs' book [32] contains a detailed analysis of characteristic functions.

Problem 11.2: Consider the random variable $\epsilon > 0$ such that

$$\Phi = \ln\left(\frac{\epsilon}{\epsilon_0}\right)$$

is Gaussian with mean $\langle \Phi \rangle$ and variance $0 < \sigma^2 < \infty$, $0 < \epsilon_0 < \infty$ is a reference value.

(11.2.1) Compute the Pdf $f(\epsilon)$ of ϵ .

(11.2.2) Determine the moments $\langle \epsilon^n \rangle$ for $n > 0$ and integer as function of $\langle \Phi \rangle$, σ and n .

(11.2.3) Set $\epsilon_0 = \langle \epsilon \rangle$ and compute the ratio $\frac{\langle \epsilon^n \rangle}{\langle \epsilon \rangle^n}$.

(11.2.4) Let

$$\frac{\langle \epsilon^2 \rangle}{\langle \epsilon \rangle^2} = A \left(\frac{L}{r}\right)^\mu$$

where A, L, μ are positive constants, $r > 0$ is a parameter. Establish the dependence of $\langle \epsilon^n \rangle / \langle \epsilon \rangle^n$ on $A, L/r, \mu$ and n .

Solution: The log-normal random variable ϵ is related to the Gaussian variable $\Phi : (0, \infty) \rightarrow (-\infty, \infty)$ via

$$\Phi = \ln\left(\frac{\epsilon}{\epsilon_0}\right)$$

The Pdf of the Gaussian variable Φ is

$$f(\Phi) = \frac{1}{\sigma \sqrt{2\pi}} \exp\left[-\frac{1}{2\sigma^2}(\Phi - \langle \Phi \rangle)^2\right]$$

(11.2.1) The Pdf of ϵ follows from the relation $\Phi = \ln(\frac{\epsilon}{\epsilon_0})$, which is a one-to-one mapping of $(0, \infty)$ onto $(-\infty, \infty)$, and the given Gaussian Pdf for Φ . The Cdf of ϵ is by definition

$$F(\epsilon) = \int_{\epsilon_0 e^{\Phi} \leq \epsilon} d\Phi f(\Phi)$$

and the Pdf is thus

$$f(\epsilon) = \frac{d}{d\epsilon} \int_{\epsilon_0 e^{\Phi} \leq \epsilon} d\Phi f(\Phi) = \frac{d}{d\epsilon} \int_{-\infty}^{\ln \frac{\epsilon}{\epsilon_0}} d\Phi f(\Phi)$$

The integral can be computed

$$\frac{d}{d\epsilon} \int_{-\infty}^{\ln \frac{\epsilon}{\epsilon_0}} d\Phi \exp\left[-\frac{1}{2\sigma^2}(\Phi - \langle \Phi \rangle)^2\right] = \frac{1}{\epsilon} \exp\left[-\frac{1}{2\sigma^2}(\ln(\frac{\epsilon}{\epsilon_0}) - \langle \Phi \rangle)^2\right]$$

The Pdf of the log-normal variable ϵ is thus

$$f(\epsilon) = \frac{1}{\sigma\sqrt{2\pi}} \frac{1}{\epsilon} \exp\left[-\frac{1}{2\sigma^2}(\ln(\frac{\epsilon}{\epsilon_0}) - \langle \Phi \rangle)^2\right]$$

(11.2.2) The statistical moments of ϵ are defined by

$$\langle \epsilon^n \rangle = \int_0^{\infty} d\epsilon f(\epsilon)$$

Transformation to the Gaussian variable Φ using $d\Phi = d\epsilon/\epsilon$ and the explicit form of the Pdf leads to

$$\langle \epsilon^n \rangle = \frac{\epsilon_0^n}{\sigma\sqrt{2\pi}} \int_{-\infty}^{\infty} d\Phi \exp[n\Phi - \frac{1}{2\sigma^2}(\Phi - \langle \Phi \rangle)^2]$$

Rearranging the argument of the exponential

$$n\Phi - \frac{1}{2\sigma^2}(\Phi - \langle \Phi \rangle)^2 = \frac{1}{2\sigma^2}(\Phi - n\sigma - \langle \Phi \rangle)^2 + \frac{1}{2}(n^2\sigma^2 + 2n\langle \Phi \rangle)$$

leads to

$$\langle \epsilon^n \rangle = \epsilon_0^n \exp\left[\frac{1}{2}(n^2\sigma^2 + 2n\langle \Phi \rangle)\right] \frac{1}{\sigma\sqrt{2\pi}} \int_{-\infty}^{\infty} d\Phi \exp\left[-\frac{1}{2\sigma^2}(\Phi - n\sigma - \langle \Phi \rangle)^2\right]$$

Since

$$\frac{1}{\sigma\sqrt{2\pi}} \int_{-\infty}^{\infty} d\Phi \exp\left[-\frac{1}{2\sigma^2}(\Phi - n\sigma - \langle \Phi \rangle)^2\right] = 1$$

the desired result

$$\langle \epsilon^n \rangle = \epsilon_0^n \exp\left[\frac{1}{2}(n^2\sigma^2 + 2n\langle \Phi \rangle)\right]$$

follows.

(11.2.3) Set $\epsilon_0 = \langle \epsilon \rangle$, then the result in the previous section produces for $n = 1$

$$\langle \epsilon \rangle = \langle \epsilon \rangle \exp\left[\frac{1}{2}(\sigma^2 + 2\langle \Phi \rangle)\right]$$

hence $\sigma^2 + 2\langle \Phi \rangle = 0$ or

$$\langle \Phi \rangle = -\frac{1}{2}\sigma^2$$

and finally

$$\frac{\langle \epsilon^n \rangle}{\langle \epsilon \rangle^n} = \exp\left[\frac{n}{2}(n-1)\sigma^2\right]$$

emerges according to the result of part 2.

(11.2.4) Combining

$$\frac{\langle \epsilon^2 \rangle}{\langle \epsilon \rangle^2} = A\left(\frac{L}{r}\right)^\mu$$

and

$$\frac{\langle \epsilon^2 \rangle}{\langle \epsilon \rangle^2} = \exp(\sigma^2)$$

and applying the logarithm leads to

$$\sigma^2 = \ln A + \mu \ln\left(\frac{L}{r}\right)$$

The result of part 3 of the present problem implies then

$$\frac{\langle \epsilon^n \rangle}{\langle \epsilon \rangle^n} = A^{\frac{n(n-1)}{2}} \left(\frac{L}{r}\right)^{\frac{\mu}{2}n(n-1)}$$

This holds for ϵ being log-normal.

Comments: Variables with log-normal statistics play an important role for the analysis of dissipation rate, see Chap. 6. in Pope [11], Davidson [33] Sect. 6.5.2 and Sect. 6.5.3, Tsinober [12]. Models for inertial range intermittency have been developed to explain the deviations from the predictions of Kolmogorov's 1941 original hypotheses, and the model of Kolmogorov and Obukhov (1962) [34] is based on log-normal distributions.

Problem 11.3: Consider the dynamics of a passive scalar $0 \leq \Phi(t, \mathbf{x}) \leq 1$ in a turbulent flow. Specialize the transport pde (11.52) for the Pdf $f_N(\varphi_1, \dots, \varphi_N)$ of N scalars to the Pdf $f(\varphi)$ for a single scalar Φ and show that the diffusive term in scalar space has negative diffusivity. You may assume that the scalar sources depend locally on the scalars only $Q(\varphi(1), \dots, \varphi^{(N)})$ and not on velocity. The following model expression for the diffusive term in scalar space (R.L. Curl [35]) is suggested

$$-\frac{\partial^2}{\partial \varphi^2} \langle \Gamma \nabla \Phi \cdot \nabla \Phi \delta(\Phi(t, \mathbf{x}) - \varphi) \rangle \approx \frac{c}{\tau} \left[4 \int_0^\varphi d\varphi' f(\varphi + \varphi') f(\varphi - \varphi') - f(\varphi) \right]$$

to mimic the effect of the diffusive term, where the time scale $\tau > 0$ is independent of Φ and c is a positive constant. Show that this expression

(11.3.1) leaves normalization and mean unchanged;

(11.3.2) reduces the variance.

Solution: The Pdf Eq. (11.52) for the velocity–scalar Pdf

$$f_N(\mathbf{A}E_1, \dots, \mathbf{A}E_N, \varphi_1, \dots, \varphi_N; \mathbf{x}^{(1)}, \dots, \mathbf{x}^{(N)}, t)$$

at N points $\mathbf{x}^{(i)}$ and time t

$$\begin{aligned} \frac{\partial f_N}{\partial t} + \frac{\partial}{\partial x_\beta} (v_\beta f_N) - \frac{\partial}{\partial x_\beta} \left(\mu \frac{\partial f_N}{\partial x_\beta} \right) - \frac{\partial}{\partial v_\alpha} \left(\langle \frac{\partial p}{\partial x_\alpha} | \mathcal{V}_N \rangle f_N \right) + g_\alpha \frac{\partial f_N}{\partial v_\alpha} + \sum_{i=1}^n \frac{\partial}{\partial \varphi_i} [Q_i(\varphi_1, \dots, \varphi_n) f_N] \\ + \frac{\partial^2}{\partial v_\alpha \partial v_\gamma} (\langle \epsilon_{\alpha\gamma} | \mathcal{V}_N \rangle f_N) + \sum_{i=1}^n \frac{\partial^2}{\partial v_\alpha \partial \varphi_i} (\langle \epsilon_{\alpha i} | \mathcal{V}_N \rangle f_N) + \sum_{i=1}^n \sum_{j=1}^n \frac{\partial^2}{\partial \varphi_i \partial \varphi_j} (\langle \epsilon_{ij} | \mathcal{V}_N \rangle f_N) = 0 \end{aligned}$$

where the conditioning event is

$$\mathcal{V}_N \equiv \{ \mathbf{v}(\mathbf{x}^{(1)}, t) = \mathbf{A}E^{(1)}, \dots, \mathbf{v}(\mathbf{x}^{(N)}, t) = \mathbf{A}E^{(N)}, \Phi(\mathbf{x}^{(1)}, t) = \varphi_1, \dots, \Phi(\mathbf{x}^{(N)}, t) = \varphi_N \}$$

and the dissipation rates are defined by (11.53) and can be reduced to the pde for the Pdf $f(\varphi)$ of a single scalar ($\varphi = \varphi_1$) by integration over all other probabilistic variables $\mathbf{A}E_1, \dots, \mathbf{A}E_N, \varphi_2, \dots, \varphi_N$

$$\frac{\partial f}{\partial t} + \langle v_\alpha | \mathcal{C}_1 \rangle \frac{\partial f}{\partial x_\alpha} + \frac{\partial}{\partial \varphi} [\mathcal{Q}(\varphi) f] = \frac{\partial}{\partial x_\alpha} (\Gamma \frac{\partial f}{\partial x_\alpha}) - \frac{\partial^2}{\partial \varphi^2} (\langle \epsilon_\Phi | \mathcal{C}_1 \rangle f)$$

where $\mathcal{Q}(\varphi) = \int_0^1 d\varphi^{(2)} \cdots \int_0^1 d\varphi^{(N)} \mathcal{Q}(\varphi, \varphi^{(2)}, \dots, \varphi^{(N)})$.

The effect of the model expression on statistical moments requires the evaluation of integrals

$$I_n \equiv \int_0^1 d\varphi \varphi^n \int_0^\varphi d\varphi' f(\varphi + \varphi') f(\varphi - \varphi')$$

for $n \geq 0$ and integer. These integrals can be evaluated analytically in a few steps. First, the linear transformation $\hat{\varphi} \equiv \varphi - \varphi'$ for the inner integral is applied

$$I_n = \int_0^1 d\varphi \varphi^n \int_0^\varphi d\hat{\varphi} f(\hat{\varphi}) f(2\varphi - \hat{\varphi})$$

The integral can be split as follows:

$$I_n = \int_0^1 d\varphi \varphi^n \int_0^1 d\hat{\varphi} f(\hat{\varphi}) f(2\varphi - \hat{\varphi}) - \int_0^1 d\varphi \varphi^n \int_\varphi^1 d\hat{\varphi} f(\hat{\varphi}) f(2\varphi - \hat{\varphi})$$

The second integral on the left side

$$\hat{I}_n \equiv \int_0^1 d\varphi \varphi^n \int_\varphi^1 d\hat{\varphi} f(\hat{\varphi}) f(2\varphi - \hat{\varphi})$$

is now transformed using $\varphi^* \equiv 2\varphi - \hat{\varphi}$ leading to

$$\hat{I}_n = \int_0^1 d\varphi \varphi^n \int_{2\varphi-1}^\varphi d\varphi^* f(2\varphi - \varphi^*) f(\varphi^*)$$

The lower bound $2\varphi - 1$ of the inner integral can be simplified if the following properties are observed: For $0 \leq \varphi \leq \frac{1}{2}$ the lower bound is $2\varphi - 1 < 0$ and can be set to zero, since $f(\varphi^*) = 0$ in this range. For $\frac{1}{2} \leq \varphi \leq 1$ φ^* is in the range $0 \leq \varphi^* \leq 2\varphi - 1$, hence $-\varphi^* \geq 1 - 2\varphi$ or $2\varphi - \varphi^* \geq 1$, which also implies $f(2\varphi - \varphi^*) = 0$. The conclusion is reached that the lower bound is zero and the integral is

$$\hat{I}_n = \int_0^1 d\varphi \varphi^n \int_0^\varphi d\varphi^* f(\varphi^*) f(2\varphi - \varphi^*)$$

and thus $\hat{I}_n = I_n$ holds. It follows that I_n is now

$$I_n = \frac{1}{2} \int_0^1 d\varphi \varphi^n \int_0^1 d\varphi' f(\varphi + \varphi') f(\varphi - \varphi')$$

The sequence of integrations can be interchanged

$$I_n = \frac{1}{2} \int_0^1 d\varphi' f(\varphi') \int_0^1 d\varphi \varphi^n f(2\varphi - \varphi')$$

and transformed once more using $\hat{\varphi} = 2\varphi - \varphi'$ or $\varphi = \frac{1}{2}(\hat{\varphi} + \varphi')$, hence

$$I_n = \frac{1}{2^{n+2}} \int_0^1 d\varphi' f(\varphi') \int_0^1 d\hat{\varphi} (\hat{\varphi} + \varphi')^n f(\hat{\varphi})$$

where the integration bounds of the inner integral are $\varphi = 0 \rightarrow \hat{\varphi} = -\varphi' \rightarrow \hat{\varphi} = 0$ and likewise $\varphi = 1 \rightarrow \hat{\varphi} = 2 - \varphi' \rightarrow \hat{\varphi} = 1$ are applied. The integral can be evaluated with the aid of the binomial theorem resulting in

$$I_n = \frac{1}{2^{n+2}} \sum_{j=0}^n \binom{n}{j} \langle \Phi^j \rangle \langle \Phi^{n-j} \rangle$$

This result allows the computation of the effect of the model expression on moment of any order.

(11.3.1) Normalization $n = 0$: $I_0 = \frac{1}{4}$ and

$$\frac{c}{\tau} [4 \int_0^1 d\varphi \int_0^\varphi d\varphi' f(\varphi + \varphi') f(\varphi - \varphi') - 1] = \frac{c}{\tau} [4I_0 - 1] = 0$$

Normalization remains unchanged.

Mean value $n = 1$: $I_1 = \frac{1}{4} \langle \Phi \rangle$ and thus

$$\frac{c}{\tau} [4 \int_0^1 d\varphi \varphi \int_0^\varphi d\varphi' f(\varphi + \varphi') f(\varphi - \varphi') - \langle \Phi \rangle] = \frac{c}{\tau} [4I_1 - \langle \Phi \rangle] = 0$$

The mean value remains unchanged.

(11.3.2) The time rate of change of the variance $n = 2$: $(\varphi - \langle \Phi \rangle)^2 = \varphi^2 - 2\varphi\langle \Phi \rangle + \langle \Phi \rangle^2$ and $I_2 = \frac{1}{8}[\langle \Phi^2 \rangle + \langle \Phi \rangle^2]$, emerges as

$$\begin{aligned} \frac{c}{\tau} \left[4 \int_0^\varphi d\varphi (\varphi^2 - 2\varphi\langle \Phi \rangle + \langle \Phi \rangle^2) \int_0^\varphi d\varphi' f(\varphi + \varphi') f(\varphi - \varphi') - \langle (\Phi - \langle \Phi \rangle)^2 \rangle \right] = \\ \frac{c}{\tau} [4(I_2 - 2I_1\langle \Phi \rangle + I_0\langle \Phi \rangle^2) - \langle (\Phi - \langle \Phi \rangle)^2 \rangle] \end{aligned}$$

and

$$\frac{c}{\tau} \left[4 \left(\frac{1}{8}[\langle \Phi^2 \rangle + \langle \Phi \rangle^2] - \frac{1}{2}\langle \Phi \rangle^2 + \frac{1}{4}\langle \Phi \rangle^2 \right) - \langle (\Phi - \langle \Phi \rangle)^2 \rangle \right] = -\frac{c}{2\tau} \langle (\Phi - \langle \Phi \rangle)^2 \rangle < 0$$

Hence, the variance is indeed reduced with time.

Comments: The model expression shows the qualitatively correct behaviour for the first three moments, but it does not approach the proper asymptotic Pdf for decaying turbulence. It is seen from this example that a process that reduces the variance of a Pdf should have integral and not differential form to be numerically stable. There is an alternative way for treating the diffusion in scalar space using mappings due to Chen et al. [36], see Chap. 12 for details.

Problem 11.4: Compute the Gateaux derivative with respect to $v_\alpha(\mathbf{x}, t)$ of the pressure represented in terms of the Green's function as shown in Sect. 11.1 for non-homogeneous Neumann conditions for the pressure and homogeneous Dirichlet boundary conditions for the momentum balances. Specialize the Gateaux derivative to harmonic directions.

Solution: The pressure is represented (as established in Sect. 11.1, Eq. (11.13) incorporating the Neumann boundary condition (9.22) by means of the divergence theorem) by

$$\begin{aligned} p[\mathbf{v}(., t), \frac{\partial \mathbf{v}}{\partial t}; \mathbf{x}] = \int_{\mathcal{D}} d\nu(\mathbf{y}) \left\{ G(\mathbf{x}, \mathbf{y}) \frac{\partial^2}{\partial y_\beta \partial y_\gamma} (v_\beta v_\gamma) \right. \\ \left. + \frac{\partial}{\partial y_\beta} \left[G(\mathbf{x}, \mathbf{y}) \left(\frac{1}{Re} \frac{\partial^2 v_\beta}{\partial y_\gamma \partial y_\gamma} - \frac{\partial v_\beta}{\partial t} - v_\gamma \frac{\partial v_\beta}{\partial y_\gamma} \right) \right] \right\} \end{aligned}$$

explicitly showing the dependence on velocity. The velocities $\mathbf{v}(\mathbf{x}, t)$ and $\mathbf{w}(\mathbf{x})$ are elements of the phase space Ω (convex, linear, normed vector space) and satisfy the momentum boundary conditions. The Gateaux derivative is according to Sect. 23.12 contained in the Gateaux differential (23.45)

$$Dp(\mathbf{v})(\mathbf{w}) = \lim_{\epsilon \rightarrow 0} \frac{1}{\epsilon} [p(\mathbf{v} + \epsilon \mathbf{w}) - p(\mathbf{v})]$$

according to (23.46)

$$Dp(\mathbf{v})(\mathbf{w}) = (w_\alpha, \frac{\delta p}{\delta v_\alpha})$$

Partial integration for the first term T_1 results in

$$\begin{aligned} T_1 &\equiv \int_{\mathcal{D}} d\nu(\mathbf{y}) G(\mathbf{x}, \mathbf{y}) \frac{\partial^2}{\partial y_\beta \partial y_\gamma} [(v_\beta + \epsilon w_\beta)(v_\gamma + \epsilon w_\gamma) - v_\beta v_\gamma] \\ &= 2\epsilon \int_{\partial\mathcal{D}} dA(\mathbf{y}) n_\beta [G v_\gamma \frac{\partial w_\beta}{\partial y_\gamma} - \frac{\partial G}{\partial y_\gamma} v_\beta w_\gamma] \\ &\quad + 2\epsilon \int_{\mathcal{D}} d\nu(\mathbf{y}) \frac{\partial^2 G}{\partial y_\beta \partial y_\gamma} v_\gamma w_\beta + O(\epsilon^2) \end{aligned}$$

The boundary values for velocity $\mathbf{v}(\mathbf{x}, t) = 0, \mathbf{x} \in \partial\mathcal{D}$ imply

$$T_1 = 2\epsilon \int_{\mathcal{D}} d\nu(\mathbf{y}) \frac{\partial^2 G}{\partial y_\beta \partial y_\gamma} v_\gamma w_\beta + O(\epsilon^2)$$

For non-homogeneous boundary values for velocity, a surface contribution would appear. The second group of terms T_2 in the representation of the pressure leads to

$$\begin{aligned} T_2 &\equiv \int_{\mathcal{D}} d\nu(\mathbf{y}) \frac{\partial}{\partial y_\beta} \left[G(\mathbf{x}, \mathbf{y}) \left(\frac{1}{Re} \frac{\partial^2}{\partial y_\gamma \partial y_\gamma} (v_\gamma + \epsilon w_\gamma) - \frac{\partial}{\partial t} (v_\beta + \epsilon w_\beta) - (v_\gamma + \epsilon w_\gamma) \frac{\partial}{\partial y_\gamma} (v_\beta + \epsilon w_\beta) \right) \right] \\ &\quad - \int_{\mathcal{D}} d\nu(\mathbf{y}) \frac{\partial}{\partial y_\beta} \left[G(\mathbf{x}, \mathbf{y}) \left(\frac{1}{Re} \frac{\partial^2 v_\beta}{\partial y_\gamma \partial y_\gamma} - \frac{\partial v_\beta}{\partial t} - v_\gamma \frac{\partial v_\beta}{\partial y_\gamma} \right) \right] = \\ &\epsilon \int_{\mathcal{D}} d\nu(\mathbf{y}) \frac{\partial G}{\partial y_\beta} \frac{\partial}{\partial y_\gamma} \left(\frac{1}{Re} \frac{\partial w_\beta}{\partial y_\gamma} - w_\gamma v_\beta - w_\beta v_\gamma \right) - 2\epsilon \int_{\mathcal{D}} d\nu(\mathbf{y}) G(\mathbf{x}, \mathbf{y}) \frac{\partial w_\gamma}{\partial y_\beta} \frac{\partial v_\beta}{\partial y_\gamma} + O(\epsilon^2) \end{aligned}$$

Partial integration and elementary manipulations produce the intermediary result

$$\begin{aligned} T_2 &= \epsilon \int_{\partial\mathcal{D}} dA(\mathbf{y}) n_\gamma \frac{\partial G}{\partial y_\beta} \left(\frac{1}{Re} \frac{\partial w_\beta}{\partial y_\gamma} - w_\gamma v_\beta - w_\beta v_\gamma \right) - 2\epsilon \int_{\partial\mathcal{D}} dA(\mathbf{y}) n_\beta G \frac{\partial v_\beta}{\partial y_\gamma} w_\gamma \\ &\quad - \epsilon \int_{\mathcal{D}} d\nu(\mathbf{y}) \frac{\partial^2 G}{\partial y_\beta \partial y_\gamma} \left(\frac{1}{Re} \frac{\partial w_\beta}{\partial y_\gamma} - w_\gamma v_\beta - w_\beta v_\gamma \right) + 2\epsilon \int_{\mathcal{D}} d\nu(\mathbf{y}) \frac{\partial G}{\partial y_\beta} \frac{\partial v_\beta}{\partial y_\gamma} w_\gamma \end{aligned}$$

The homogeneous Dirichlet conditions for the momentum balance lead to

$$T_2 = \epsilon \int_{\partial\mathcal{D}} dA(\mathbf{y}) n_\gamma \frac{\partial G}{\partial y_\beta} \frac{1}{Re} \frac{\partial w_\beta}{\partial y_\gamma} - \epsilon \int_{\mathcal{D}} d\nu(\mathbf{y}) \frac{\partial^2 G}{\partial y_\beta \partial y_\gamma} \left(\frac{1}{Re} \frac{\partial w_\beta}{\partial y_\gamma} - w_\gamma v_\beta - w_\beta v_\gamma \right) + 2\epsilon \int_{\mathcal{D}} d\nu(\mathbf{y}) \frac{\partial G}{\partial y_\beta} \frac{\partial v_\beta}{\partial y_\gamma} w_\gamma$$

It remains to deal with the viscous terms, which appear as consequence of the Neumann boundary values for the pressure. Applying the divergence theorem again to the first term results in

$$T_2 = \epsilon \int_{\mathcal{D}} d\nu(\mathbf{y}) \frac{\partial G}{\partial y_\beta} \frac{1}{Re} \Delta w_\beta + 2\epsilon \int_{\mathcal{D}} d\nu(\mathbf{y}) \frac{\partial}{\partial y_\gamma} \left(\frac{\partial G}{\partial y_\beta} v_\beta \right) w_\gamma$$

Adding T_1 and T_2 leads to

$$T_1 + T_2 = 2\epsilon \int_{\mathcal{D}} d\nu(\mathbf{y}) \left[\frac{\partial^2 G}{\partial y_\beta \partial y_\gamma} v_\beta + \frac{\partial}{\partial y_\gamma} \left(\frac{\partial G}{\partial y_\beta} v_\beta \right) \right] w_\gamma + \epsilon \int_{\mathcal{D}} d\nu(\mathbf{y}) \frac{\partial G}{\partial y_\beta} \frac{1}{Re} \Delta w_\beta + O(\epsilon^2)$$

Specializing this result to harmonic test functions, i.e. $\Delta \mathbf{w} = 0$, yields the Gateaux derivative

$$\frac{\delta p[\mathbf{v}(., t); \mathbf{x}]}{\delta v_\alpha(\mathbf{y})} = \frac{\partial^2 G(\mathbf{x}, \mathbf{y})}{\partial y_\beta \partial y_\alpha} v_\beta(\mathbf{y}, t) + \frac{\partial}{\partial y_\alpha} \left(\frac{\partial G(\mathbf{x}, \mathbf{y})}{\partial y_\beta} v_\beta(\mathbf{y}, t) \right)$$

valid for homogeneous Dirichlet conditions for the momentum balances, Neumann conditions for Poisson pde for the pressure and harmonic test functions.

Comments: The Gateaux derivative for the compact domain with boundary $\partial\mathcal{D}$ and pure Neumann conditions emerges with an additional term compared to the unbounded domain $\mathcal{D} = \mathbb{R}^3$ in Sect. 11.1.

Problem (11.5): Consider the turbulent flow of an incompressible Newtonian fluid in a compact domain \mathcal{D} and the special case of homogeneous, isotropic turbulence in $\mathcal{D} = \mathbb{R}^3$. The dynamics of the velocity gradient tensor (2.113)

$$A_{\alpha\beta}(t, \mathbf{x}) \equiv \frac{\partial v_\alpha}{\partial x_\beta}$$

in the spatial description are to be analysed. The pde for $A_{\alpha\beta}$ has been derived in Sect. 2.7, Eq. (2.116)

$$\frac{\partial A_{\alpha\beta}}{\partial t} + v_\gamma \frac{\partial A_{\alpha\beta}}{\partial x_\gamma} = -A_{\alpha\gamma} A_{\gamma\beta} - P_{\alpha\beta} + \frac{1}{Re} \frac{\partial^2 A_{\alpha\beta}}{\partial x_\gamma \partial x_\gamma}$$

where external forces are absent. It contains the pressure Hessian (2.117)

$$P_{\alpha\beta} \equiv \frac{\partial^2 p}{\partial x_\alpha \partial x_\beta}$$

Carry out the following steps:

(11.5.1) Decompose the pressure Hessian into a traceless (deviatoric) and a non-zero trace (dilatational) contribution in terms of the velocity gradient tensor and compute the traceless part with the aid of a Green's function for a compact domain with Neumann boundary conditions for the pressure and the domain $\mathcal{D} = R^3$.

Hint: Consult Appendix D, Chap. 26, for the construction of Green's functions.

(11.5.2) Decompose the velocity gradient tensor into a symmetric $S_{\alpha\beta}$ and anti-symmetric part $W_{\alpha\beta}$. Derive the transport pdes for both.

(11.5.3) Establish the pde for the Pdf $f(\mathbf{a}; \mathbf{x}, t)$ for the values $a_{\alpha\beta}$ of the velocity gradient tensor $A_{\alpha\beta}$ at a single-point $\mathbf{x} \in \mathcal{D} = R^3$ for homogeneous, isotropic turbulence using the approach of Chap. 11.

Solution (11.4.1): The pressure Hessian is decomposed into a dilatational and a deviatoric contribution according to

$$H_{\alpha\beta} = \frac{1}{3} \text{tr}(\mathbf{H}) \delta_{\alpha\beta} + B_{\alpha\beta}$$

The deviatoric part is traceless, i.e. $\text{tr}(\mathbf{B}) = 0$, as the application of the trace to the decomposition shows. The Poisson pde for the pressure (9.19) follows from mass and momentum balances; hence,

$$\Delta p = -\text{tr}(A_{\alpha\beta} A_{\beta\gamma}) = -\text{tr}(\mathbf{A}^2) \quad (1)$$

with Neumann boundary conditions (9.22)

$$n_\alpha \frac{\partial p}{\partial x_\alpha} = h(\mathbf{v}), \quad h(\mathbf{v}) = n_\alpha \left[\frac{1}{Re} \frac{\partial^2 v_\alpha}{\partial x'_\beta \partial x'_\beta} - \frac{\partial v_\alpha}{\partial t} - v_\beta \frac{\partial v_\alpha}{\partial x'_\beta} \right]$$

where n_α denotes the unit normal vector pointing outward on $\partial\mathcal{D}$. The Poisson pde for the pressure can be solved using the concept of Green's function $G(\mathbf{x}, \mathbf{x}')$, which is the solution of

$$-\Delta_{\mathbf{x}} G(\mathbf{x}, \mathbf{x}') = \delta(\mathbf{x} - \mathbf{x}'), \quad n_\alpha(\mathbf{x}') \frac{\partial G}{\partial x_\alpha}(\mathbf{x}, \mathbf{x}') = 0, \quad \mathbf{x}' \in \partial\mathcal{D}, \quad \mathbf{x} \in \mathcal{D}$$

in the domain $\mathcal{D} \subset R^3$ with boundary $\partial\mathcal{D}$, thus allowing computation of the deviatoric part by simply differentiating the solution

$$p(t, \mathbf{x}) = \int_{\mathcal{D}} d\nu(\mathbf{x}') G(\mathbf{x}, \mathbf{x}') \text{tr}(\mathbf{A}^2)(\mathbf{x}') - \int_{\partial\mathcal{D}} dA(\mathbf{x}') G(\mathbf{x}, \mathbf{x}') h(\mathbf{x}')$$

It is clear that the differentiation applies to the Green's function only. The special case $\mathcal{D} = \mathbb{R}^3$ is well known

$$G(\mathbf{x}, \mathbf{x}') = -\frac{1}{4\pi} \frac{1}{|\mathbf{x} - \mathbf{x}'|}$$

valid for $\mathcal{D} = \mathbb{R}^3$ as there is no boundary and thus no boundary integral. The result is then for the Hessian of the pressure in homogeneous and isotropic turbulence

$$B_{\alpha\beta}(\mathbf{x}, t) = -\frac{1}{4\pi} \int_{\mathbb{R}^3} d\nu(\mathbf{x}') \left[\frac{\delta_{\alpha\beta}}{|\mathbf{x} - \mathbf{x}'|^3} - 3 \frac{(x_\alpha - x'_\alpha)(x_\beta - x'_\beta)}{|\mathbf{x} - \mathbf{x}'|^5} \right] \text{tr}(\mathbf{A}^2(\mathbf{x}', t)) \quad (2)$$

The decomposition of the pressure Hessian $H_{\alpha\beta}$ consists thus of a local, dilatational term and a deviatoric, non-local term $B_{\alpha\beta}$

$$H_{\alpha\beta} = -\frac{1}{3} \text{tr}(\mathbf{A}^2) \delta_{\alpha\beta} + B_{\alpha\beta} \quad (3)$$

due to (1). The integral in the latter (2) must be considered a principal value expression.

(11.5.2): The elementary decomposition of the pressure Hessian into a symmetric

$$S_{\alpha\beta} \equiv \frac{1}{2} (A_{\alpha\beta} + A_{\beta\alpha})$$

and an antisymmetric part results in

$$W_{\alpha\beta} \equiv \frac{1}{2} (A_{\alpha\beta} - A_{\beta\alpha}), \quad A_{\alpha\beta} = S_{\alpha\beta} + W_{\alpha\beta}$$

Vorticity is defined by (2.51), and hence $\omega_\alpha = -2\epsilon_{\alpha\beta\gamma} W_{\beta\gamma}$, $2W_{\beta\gamma} = -\epsilon_{\alpha\beta\gamma}\omega_\alpha$, leads to transport pdes for symmetric and antisymmetric parts easily obtained from mass and momentum balances. The resulting pdes are for the symmetric part using (2.116)

$$\frac{S_{\alpha\beta}}{\partial t} + v_\gamma \frac{\partial S_{\alpha\beta}}{\partial x_\gamma} = \frac{1}{2} \left[-A_{\alpha\gamma} A_{\gamma\beta} - P_{\alpha\beta} + \frac{1}{Re} \frac{\partial^2 A_{\alpha\beta}}{\partial x_\gamma \partial x_\gamma} - A_{\beta\gamma} A_{\gamma\alpha} - P_{\beta\alpha} + \frac{1}{Re} \frac{\partial^2 A_{\beta\alpha}}{\partial x_\gamma \partial x_\gamma} \right]$$

and using the symmetry of the Hessian and its decomposition

$$\frac{S_{\alpha\beta}}{\partial t} + v_\gamma \frac{\partial S_{\alpha\beta}}{\partial x_\gamma} = -\frac{1}{2} (A_{\alpha\gamma} A_{\gamma\beta} + A_{\beta\gamma} A_{\gamma\alpha}) + \frac{1}{3} \text{tr}(\mathbf{A}^2) \delta_{\alpha\beta} - B_{\alpha\beta} + \frac{1}{Re} \frac{\partial^2 S_{\beta\alpha}}{\partial x_\gamma \partial x_\gamma}$$

Furthermore, using $tr(\mathbf{A}^2) = tr(\mathbf{S}^2) + tr(\mathbf{W}^2)$ and $\omega_\alpha = -2\epsilon_{\alpha\beta\gamma}W_{\beta\gamma}$ and $2W_{\beta\gamma} = -\epsilon_{\alpha\beta\gamma}\omega_\alpha$

$$\frac{\partial S_{\alpha\beta}}{\partial t} + v_\gamma \frac{\partial S_{\alpha\beta}}{\partial x_\gamma} = -\frac{1}{2}[S_{\alpha\gamma}S_{\gamma\beta} - \frac{1}{3}tr(\mathbf{S}^2)\delta_{\alpha\beta}] - \frac{1}{4}[\omega_\alpha\omega_\beta - \frac{1}{3}tr(\boldsymbol{\omega}^2)\delta_{\alpha\beta}] - B_{\alpha\beta} + \frac{1}{Re} \frac{\partial^2 S_{\beta\alpha}}{\partial x_\gamma \partial x_\gamma}$$

follows. The pde for the antisymmetric part is the vorticity pde (2.63) in Sect. 2.3.2,

$$\frac{\partial \omega_\alpha}{\partial t} + v_\beta \frac{\partial \omega_\alpha}{\partial x_\beta} = S_{\alpha\beta}\omega_\beta + \frac{1}{Re} \Delta \omega_\alpha$$

The pde for the symmetric part $S_{\alpha\beta}$ is non-local due to the presence of $B_{\alpha\beta}$, whereas the pde for $W_{\alpha\beta}$ in terms of vorticity is strictly local.

(11.5.3) The derivation of the pde for the Pdf $f(\mathbf{a}; \mathbf{x}, t)$ is based on the coarse-grained, N -point velocity–velocity gradient Cdf \hat{F} defined by (11.3)

$$\hat{F}_{dN} \equiv \prod_{i=1}^N H(\mathbf{A}^{(i)} - \mathbf{v}(\mathbf{x}^{(i)}, t)) H(\mathbf{a}^{(i)} - \mathbf{A}(\mathbf{x}^{(i)}, t))$$

in Chap. 11, where $d = 12$ is the number of sample space values at a point and $H(\mathbf{x} - \mathbf{x}_0)$ denotes the Heaviside step function (11.4), $N = 1$ for single-point Cdf/Pdfs. The Cdf is then $F_{dN}(\mathbf{A}^{(1)}, \dots, \mathbf{A}^{(N)}, \mathbf{a}^{(1)}, \dots, \mathbf{a}^{(N)}) = \langle \hat{F}_{dN} \rangle$ (the angular brackets denote ensemble averaging) and the Pdf follows then (11.48)

$$f_{dN} = \frac{\partial^{dN} F_{dN}}{\partial v_1^{(1)} \cdots \partial a_{3,3}^{(N)}}$$

as discussed in Chap. 11. Implicit differentiation leads to (see (11.6), (11.7))

$$\frac{\partial \hat{F}_d}{\partial t} = -\frac{\partial v_\alpha}{\partial t}(\mathbf{x}, t) \frac{\partial \hat{F}_d}{\partial v_\alpha} - \frac{\partial A_{\alpha\beta}}{\partial t}(\mathbf{x}, t) \frac{\partial \hat{F}_d}{\partial a_{\alpha\beta}}$$

and

$$\frac{\partial \hat{F}_d}{\partial x_\alpha} = -\frac{\partial v_\beta}{\partial x_\alpha}(\mathbf{x}, t) \frac{\partial \hat{F}_d}{\partial v_\beta} - \frac{\partial A_{\beta\gamma}}{\partial x_\alpha}(\mathbf{x}, t) \frac{\partial \hat{F}_d}{\partial a_{\beta\gamma}}$$

The time derivative provides the link to the Navier–Stokes and the velocity gradient pdes, hence (2.7) and (2.116)

$$\begin{aligned} \frac{\partial \hat{F}_d}{\partial t} &= -(-v_\beta \frac{\partial v_\alpha}{\partial x_\beta} - \frac{\partial p}{\partial x_\alpha} + \frac{1}{Re} \frac{\partial^2 v_\alpha}{\partial x_\beta \partial x_\beta}) \frac{\partial \hat{F}_d}{\partial v_\alpha} \\ &\quad - (-v_\gamma \frac{\partial A_{\alpha\beta}}{\partial x_\gamma} - A_{\alpha\gamma}A_{\gamma\beta} - P_{\alpha\beta} + \frac{1}{Re} \frac{\partial^2 A_{\alpha\beta}}{\partial x_\gamma \partial x_\gamma}) \frac{\partial \hat{F}_d}{\partial a_{\alpha\beta}} \end{aligned}$$

The convective group of terms can be evaluated explicitly

$$v_\gamma \left[\frac{\partial v_\alpha}{\partial x_\gamma} \frac{\partial \hat{F}_d}{\partial v_\alpha} + \frac{\partial A_{\alpha\beta}}{\partial x_\gamma} \frac{\partial \hat{F}_d}{\partial a_{\alpha\beta}} \right] = -v_\gamma \frac{\partial \hat{F}_d}{\partial x_\gamma}$$

and decomposing the pressure and the pressure Hessian the preliminary version of the pde for the coarse-grained Cdf

$$\begin{aligned} \frac{\partial \hat{F}_d}{\partial t} + v_\gamma \frac{\partial \hat{F}_d}{\partial x_\gamma} &= - \left[- \int_{\mathcal{D}} d\nu(\mathbf{x}') \frac{\partial G}{\partial x_\alpha}(\mathbf{x}, \mathbf{x}') \text{tr}(\mathbf{A}^2)(\mathbf{x}') + \int_{\partial\mathcal{D}} dA(\mathbf{x}') \frac{\partial G}{\partial x_\alpha}(\mathbf{x}, \mathbf{x}') h(\mathbf{x}') \right. \\ &\quad \left. + \frac{1}{Re} \frac{\partial^2 v_\alpha}{\partial x_\beta \partial x_\beta} \frac{\partial \hat{F}_d}{\partial v_\alpha} \right] - \left[-A_{\alpha\gamma} A_{\gamma\beta} + \frac{1}{3} \text{tr}(\mathbf{A}^2) \delta_{\alpha\beta} - B_{\alpha\beta} + \frac{1}{Re} \frac{\partial^2 A_{\alpha\beta}}{\partial x_\gamma \partial x_\gamma} \right] \frac{\partial \hat{F}_d}{\partial a_{\alpha\beta}} \end{aligned}$$

follows. Differentiation with respect to the sample space variables and averaging generates the preliminary version of the Pdf equation

$$\begin{aligned} \frac{\partial f_d}{\partial t} + v_\alpha \frac{\partial f_d}{\partial x_\alpha} &= - \left\langle \left[- \int_{\mathcal{D}} d\nu(\mathbf{x}') \frac{\partial G}{\partial x_\alpha}(\mathbf{x}, \mathbf{x}') \text{tr}(\mathbf{A}^2)(\mathbf{x}') + \int_{\partial\mathcal{D}} dA(\mathbf{x}') \frac{\partial G}{\partial x_\alpha}(\mathbf{x}, \mathbf{x}') h(\mathbf{x}') \right. \right. \\ &\quad \left. \left. + \frac{1}{Re} \frac{\partial^2 v_\alpha}{\partial x_\beta \partial x_\beta} \frac{\partial \hat{f}_d}{\partial v_\alpha} \right] \right\rangle - \left\langle \left[-A_{\alpha\gamma} A_{\gamma\beta} + \frac{1}{3} \text{tr}(\mathbf{A}^2) \delta_{\alpha\beta} - B_{\alpha\beta} + \frac{1}{Re} \frac{\partial^2 A_{\alpha\beta}}{\partial x_\gamma \partial x_\gamma} \right] \frac{\partial \hat{f}_d}{\partial a_{\alpha\beta}} \right\rangle \end{aligned}$$

The terms on the right-hand side can be reformulated as conditional expectations, where the conditioning expression is abbreviated by (11.18)

$$\mathcal{V}_d(\mathbf{x}) \equiv \{v_\alpha(\mathbf{x}, t) = v_\alpha, A_{\alpha\beta}(\mathbf{x}, t) = a_{\alpha\beta}, \alpha, \beta = 1, 2, 3\}$$

for convenience. Observe that the coefficients of the derivatives of \hat{f} are independent of the sample space variables $\mathbf{A}\mathbf{E}$, $a_{\alpha\beta}$, and averaging is a linear operation; hence, the right-hand side can be evaluated term by term

$$\left\langle \int_{\mathcal{D}} d\nu(\mathbf{x}') \frac{\partial G}{\partial x_\alpha}(\mathbf{x}, \mathbf{x}') \text{tr}(\mathbf{A}^2)(\mathbf{x}') \frac{\partial \hat{f}_d}{\partial v_\alpha} \right\rangle = \frac{\partial}{\partial v_\alpha} \int_{\mathcal{D}} d\nu(\mathbf{x}') \frac{\partial G}{\partial x_\alpha}(\mathbf{x}, \mathbf{x}') \langle \text{tr}(\mathbf{A}^2)(\mathbf{x}') \hat{f}_d \rangle$$

The coarse-grained Pdf \hat{f}_d is a product of Dirac pseudo-functions according to (11.49); hence,

$$\langle \text{tr}(\mathbf{A}^2)(\mathbf{x}') \hat{f}_d \rangle = \langle \text{tr}(\mathbf{A}^2)(\mathbf{x}') \prod_{\alpha=1}^3 \delta(v_\alpha - v_\alpha(\mathbf{x}, t)) \prod_{\alpha=1, \beta=1}^3 \delta(a_{\alpha\beta} - A_{\alpha\beta}(\mathbf{x}, t)) \rangle$$

is a two-point correlation. It can be recast as to product of a conditional expectation and the Pdf

$$\langle \text{tr}(\mathbf{A}^2)(\mathbf{x}') \hat{f}_d \rangle = \langle \text{tr}(\mathbf{A}^2)(\mathbf{x}') | \mathcal{V}_d(\mathbf{x}) \rangle f_d(\mathbf{A}\mathbf{E}, \mathbf{a}; \mathbf{x}, t)$$

and thus

$$\begin{aligned} \left\langle \int_{\mathcal{D}} d\nu(\mathbf{x}') \frac{\partial G}{\partial x_\alpha}(\mathbf{x}, \mathbf{x}') \text{tr}(\mathbf{A}^2)(\mathbf{x}') \frac{\partial \hat{f}_d}{\partial v_\alpha} \right\rangle = \\ \int_{\mathcal{D}} d\nu(\mathbf{x}') \frac{\partial G}{\partial x_\alpha}(\mathbf{x}, \mathbf{x}') \frac{\partial}{\partial v_\alpha} \left\{ \langle \text{tr}(\mathbf{A}^2)(\mathbf{x}') | \mathcal{V}_d(\mathbf{x}) \rangle f_d(\mathbf{v}, \mathbf{a}; \mathbf{x}, t) \right\} \end{aligned}$$

is obtained. Note that the conditional expectations are functions of the sample space variables. All other terms can be handled in the same way leading to

$$\begin{aligned} \frac{\partial f_d}{\partial t} + v_\gamma \frac{\partial f_d}{\partial x_\gamma} = \int_{\mathcal{D}} d\nu(\mathbf{x}') \frac{\partial G}{\partial x_\alpha}(\mathbf{x}, \mathbf{x}') \frac{\partial}{\partial v_\alpha} \left\{ \langle \text{tr}(\mathbf{A}^2)(\mathbf{x}') | \mathcal{V}_d(\mathbf{x}) \rangle f_d(\mathbf{v}, \mathbf{a}; \mathbf{x}, t) \right\} \\ - \int_{\partial\mathcal{D}} dA(\mathbf{x}') \frac{\partial G}{\partial x_\alpha}(\mathbf{x}, \mathbf{x}') \frac{\partial}{\partial v_\alpha} \left\{ \langle h(\mathbf{x}') | \mathcal{V}_d(\mathbf{x}) \rangle f_d(\mathbf{v}, \mathbf{a}; \mathbf{x}, t) \right\} \\ - \frac{1}{Re} \frac{\partial}{\partial v_\alpha} \left\{ \langle \frac{\partial^2 v_\alpha}{\partial x_\beta \partial x_\beta} | \mathcal{V}_d(\mathbf{x}) \rangle f_d(\mathbf{v}, \mathbf{a}; \mathbf{x}, t) \right\} - \frac{1}{Re} \frac{\partial}{\partial a_{\alpha\beta}} \left\{ \langle \frac{\partial^2 A_{\alpha\beta}}{\partial x_\gamma \partial x_\gamma} | \mathcal{V}_d(\mathbf{x}) \rangle f_d(\mathbf{v}, \mathbf{a}; \mathbf{x}, t) \right\} \\ - \frac{\partial}{\partial a_{\alpha\beta}} \left\{ [-a_{\alpha\gamma} a_{\gamma\beta} + \frac{1}{3} \text{tr}(\mathbf{a}^2) \delta_{\alpha\beta} - \langle B_{\alpha\beta} | \mathcal{V}_d(\mathbf{x}) \rangle] f_d(\mathbf{v}, \mathbf{a}; \mathbf{x}, t) \right\} \end{aligned}$$

Several variants of the pde for the Pdf f_d can be established, for instance, Wilczek and Meneveau [14] derive an equivalent formulation using two-point correlations. The Pdf equation for $\mathcal{D} = R^3$ and homogeneous, isotropic turbulence reduces to

$$\begin{aligned} \frac{\partial f_d}{\partial t} = \int_{\mathcal{D}} d\nu(\mathbf{x}') \frac{\partial G}{\partial x_\alpha}(\mathbf{x}, \mathbf{x}') \frac{\partial}{\partial v_\alpha} \left\{ \langle \text{tr}(\mathbf{A}^2)(\mathbf{x}') | \mathcal{V}_d(\mathbf{x}) \rangle f_d(\mathbf{v}, \mathbf{a}; \mathbf{x}, t) \right\} \\ - \frac{1}{Re} \frac{\partial}{\partial v_\alpha} \left\{ \langle \frac{\partial^2 v_\alpha}{\partial x_\beta \partial x_\beta} | \mathcal{V}_d(\mathbf{x}) \rangle f_d(\mathbf{v}, \mathbf{a}; \mathbf{x}, t) \right\} - \frac{1}{Re} \frac{\partial}{\partial a_{\alpha\beta}} \left\{ \langle \frac{\partial^2 A_{\alpha\beta}}{\partial x_\gamma \partial x_\gamma} | \mathcal{V}_d(\mathbf{x}) \rangle f_d(\mathbf{v}, \mathbf{a}; \mathbf{x}, t) \right\} \\ - \frac{\partial}{\partial a_{\alpha\beta}} \left\{ [-a_{\alpha\gamma} a_{\gamma\beta} + \frac{1}{3} \text{tr}(\mathbf{a}^2) \delta_{\alpha\beta} - \langle B_{\alpha\beta} | \mathcal{V}_d(\mathbf{x}) \rangle] f_d(\mathbf{v}, \mathbf{a}; \mathbf{x}, t) \right\} \end{aligned}$$

where

$$\frac{\partial G}{\partial x_\alpha}(\mathbf{x}, \mathbf{x}') = \frac{1}{4\pi} \frac{(x_\alpha - x'_\alpha)}{|\mathbf{x} - \mathbf{x}'|^3}$$

holds and the integral must be treated as principal value. The equation for the Pdf has integro-differential character in both cases.

Comments: The material for this problem was taken from the paper by Wilczek and Meneveau [14], and slightly modified to adapt to the present notation. The case of compact domains with Neumann boundary conditions for the pressure is considerably more complicated than the case $\mathcal{D} = R^3$, and an example is provided in Chap. 26.

Solutions to problems for Chap. 12: Properties and construction of Mappings

Problem 12.1: The initial value problem (IVP) for the ode

$$\frac{dY}{dt} = -CY^2$$

with C being a positive constant and initial condition $Y(0) = Y_0$ generates an injective mapping $Y(t) : R^1 \rightarrow R^1$.

(12.1.1) Compute the solution of the IVP.

(12.1.2) Let the initial value $Y_0 \geq 0$ be a random variable with Pdf $f_Y(y; 0)$, determine the Pdf of $Y(t)$ for $t \geq 0$.

(12.1.3) Determine the asymptotic Pdf $f_Y(y; \infty)$.

Solution: The solution of the IVP for an equation or a system of equations generates a diffeomorphism

$$Y(t) = T_t Y(0)$$

mapping the interval of initial values \mathcal{D}_0 onto the interval \mathcal{D}_t at a later time, if the inverse solution operator T_t^{-1} is unique and has the same smoothness properties as T_t . If the initial value is a random variable, the solution at later times is a random variable with Pdf that follows from the general relation for measures (6.3)

$$\mu(t, B) = \mu_0(T_{-t}B), \quad B \in \mathcal{A}$$

for events B in the σ -algebra \mathcal{A} , which is the σ -algebra of the Lebesgue measure on R^1 . The Pdf at time $t \geq 0$ is then related to the Pdf of the initial values according to (12.3)

$$f_Y(y; t) = f_Y(y; 0) \left| \frac{dT_t^{-1}(y)}{dy} \right|$$

where $y = T_t(y_0)$ and $y_0 = T_t^{-1}(y)$.

(12.1.1) The solution of the IVP is elementary, and the result is

$$Y(t) = \frac{Y(0)}{1 + CY(0)t}$$

The solution operator is thus

$$T_t(y_0) = \frac{y_0}{1 + Cty_0} \quad \text{for } 0 \leq y_0 \leq \infty$$

mapping $\mathcal{D}_0 = [0, \infty)$ onto $\mathcal{D}_t = [0, \frac{1}{Ct}) \subset \mathcal{D}_0$, and the mapping is thus contracting. It is evident that for negative arguments the solution blows up in finite time; hence, the initial values are restricted to $Y(0) \geq 0$. The inverse is thus

$$T_t^{-1}(y) = \frac{y}{1 - Cty}, y \in \mathcal{D}_t = [0, \frac{1}{Ct})$$

and the derivative

$$\frac{dT_t^{-1}(y)}{dy} = \frac{1}{(1 - Cty)^2}, y \in \mathcal{D}_t$$

(12.1.2) Let $f_Y(y_0; 0)$, $0 \leq y_0 \leq \infty$ be the Pdf of the initial values, and then is the Pdf at a later time

$$f_Y(y; t) = \begin{cases} \frac{f_Y(\frac{y}{1-Cty}; 0)}{(1-Cty)^2} & \text{for } y \in \mathcal{D}_t \\ 0 & \text{otherwise} \end{cases}$$

(12.1.3) The asymptotic Pdf $\lim_{t \rightarrow \infty} f_Y(y; t)$ follows from the fact that

$$\int_0^\infty dy f_Y(y; t) = 1$$

holds for all time and $\lim_{t \rightarrow \infty} \mathcal{D}_t = [0]$ is a single point and

$$\lim_{t \rightarrow \infty} f_Y(y; t) = 0 \text{ for } y \neq 0$$

hence,

$$\lim_{t \rightarrow \infty} f_Y(y; t) = \delta(y)$$

is the asymptotic Pdf.

Comments: The mapping generated by the solution of the IVP does not preserve the form of the Pdf due to its nonlinearity. This can be seen, for example, for an initially log-normal Pdf

$$f_Y(y; 0) = \frac{1}{\sigma\sqrt{2\pi}} \exp\left[-\frac{1}{2\sigma^2}(\ln(y) - \langle y \rangle)^2 - \ln(y)\right]$$

which emerges for $t > 0$ in the form

$$f_Y(y; t) = \frac{1}{(1 - Cty)^2} \frac{1}{\sigma\sqrt{2\pi}} \exp\left\{-\frac{1}{2\sigma^2} \left[\ln\left(\frac{y}{1 - Cty}\right) - \langle y \rangle \right]^2 - \ln\left(\frac{y}{1 - Cty}\right)\right\}$$

Obviously, $\langle y \rangle$ is not mean value and σ is not variance for $t > 0$. Figure 28.12 shows the initial log-normal Pdf as dash-dotted line and the image Pdfs at two times $t = 0.1, 0.2$ as full line for $C = 1.0$, initial mean value $\langle y \rangle = 0.1$ and variance $\sigma = 0.5$. The mapping is contractive since $\mathcal{D}_t = [0, \frac{1}{Ct})$, and the asymptotic image

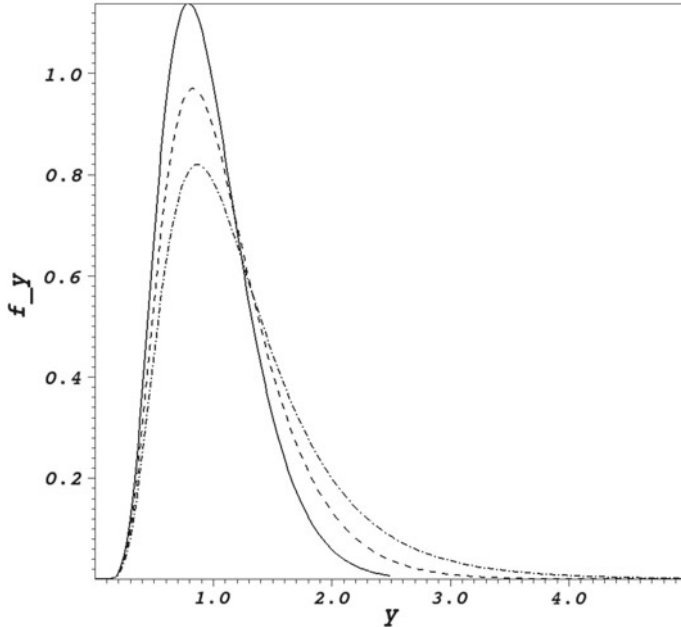


Fig. 28.12 Pdf mapped by the solution of the ode: $t = 0$ dash-dotted line (log-normal Pdf), image Pdf at $t = 0.1$ as dashed line and image Pdf at $t = 0.2$ as full line for $C = 1.0$, initial mean value $\langle y \rangle = 0.1$ and variance $\sigma = 0.5$. Obviously, the ode generates a reduction of variance with zero as asymptotic limit

domain is the single-point $\{0\}$. The Pdfs look similar, but the analytic expression for $f_Y(y; t)$ shows that they are not log-normal for $t > 0$.

Problem 12.2: Derive the single label Pdf equation for position $\Phi_\alpha(\tau, \mathbf{X})$ in the material description. Use the coarse-grained Pdf

$$\hat{f} \equiv \prod_{\alpha=1}^3 \delta(\Phi_\alpha(\tau, \mathbf{X}) - q_\alpha)$$

and the Navier–Stokes pdes (2.85), (2.86) in the material description to follow the procedure in Chap. 11.

Solution: The averaged coarse-grained Pdf generates the desired Pdf

$$f(\mathbf{q}; \tau, \mathbf{X}) = \langle \prod_{\alpha=1}^3 \delta(\Phi_\alpha(\tau, \mathbf{X}) - q_\alpha) \rangle$$

Differentiation w.r.t. time produces

$$\frac{\partial \hat{f}}{\partial \tau} + \frac{\partial \Phi_\alpha}{\partial \tau} \frac{\partial \hat{f}}{\partial q_\alpha} = 0$$

Momentum balance (2.86) contains a second derivative w.r.t. time, and hence

$$\frac{\partial^2 \hat{f}}{\partial \tau^2} + \frac{\partial^2 \Phi_\alpha}{\partial \tau^2} \frac{\partial \hat{f}}{\partial q_\alpha} - \frac{\partial \Phi_\alpha}{\partial \tau} \frac{\partial \Phi_\beta}{\partial \tau} \frac{\partial^2 \hat{f}}{\partial q_\alpha \partial q_\beta} = 0$$

is needed. Averaging produces the preliminary version for the Pdf equation

$$\frac{\partial^2 f}{\partial \tau^2} + \frac{\partial}{\partial q_\alpha} \langle \frac{\partial^2 \Phi_\alpha}{\partial \tau^2} \hat{f} \rangle - \frac{\partial^2}{\partial q_\alpha \partial q_\beta} \langle \frac{\partial \Phi_\alpha}{\partial \tau} \frac{\partial \Phi_\beta}{\partial \tau} \hat{f} \rangle = 0$$

The Navier–Stokes pdes (2.85), (2.86) allow substitution of the second time derivative of the position

$$\begin{aligned} & \frac{\partial^2 f}{\partial \tau^2} - \frac{1}{2} \epsilon_{\alpha\beta\gamma} \epsilon_{\delta\eta\omega} \frac{\partial}{\partial q_\alpha} \langle F_{\beta\eta} F_{\gamma\omega} \frac{\partial P}{\partial X_\delta} \rangle \\ & + \frac{1}{2Re} \epsilon_{\theta\beta\gamma} \epsilon_{\delta\eta\omega} \frac{\partial}{\partial q_\alpha} \langle F_{\zeta\eta} F_{\phi\omega} \frac{\partial}{\partial X_\delta} (F_{\zeta\beta} F_{\phi\gamma} \frac{\partial^2 \Phi_\alpha}{\partial X_\theta \partial \tau}) \rangle - \frac{\partial^2}{\partial q_\alpha \partial q_\beta} \langle \frac{\partial \Phi_\alpha}{\partial \tau} \frac{\partial \Phi_\beta}{\partial \tau} \hat{f} \rangle + \frac{1}{Fr} G_\alpha \frac{\partial f}{\partial q_\alpha} = 0 \end{aligned}$$

The final form of the equation is written in terms of conditional expectations

$$\begin{aligned} & \frac{\partial^2 f}{\partial \tau^2} - \frac{1}{2} \epsilon_{\alpha\beta\gamma} \epsilon_{\delta\eta\omega} \frac{\partial}{\partial q_\alpha} \left(\langle F_{\beta\eta} F_{\gamma\omega} \frac{\partial P}{\partial X_\delta} | \Phi = \mathbf{q} \rangle f \right) \\ & + \frac{1}{2Re} \epsilon_{\theta\beta\gamma} \epsilon_{\delta\eta\omega} \frac{\partial}{\partial q_\alpha} \left(\langle F_{\zeta\eta} F_{\phi\omega} \frac{\partial}{\partial X_\delta} (F_{\zeta\beta} F_{\phi\gamma} \frac{\partial^2 \Phi_\alpha}{\partial X_\theta \partial \tau}) | \Phi = \mathbf{q} \rangle f \right) \\ & - \frac{\partial^2}{\partial q_\alpha \partial q_\beta} \left(\langle \frac{\partial \Phi_\alpha}{\partial \tau} \frac{\partial \Phi_\beta}{\partial \tau} | \Phi = \mathbf{q} \rangle f \right) + \frac{1}{Fr} G_\alpha \frac{\partial f}{\partial q_\alpha} = 0 \end{aligned}$$

This is the equation for the position Pdf $f(\mathbf{q}; \tau, \mathbf{X})$ at a single label \mathbf{X} in the material description. It is a hyperbolic pde containing unknown conditional correlations. The probabilistic vector argument \mathbf{q} of the Pdf has the role of location as it is a possible value of the Lagrangean position field at time τ and the material point identified by the label \mathbf{X} .

Solutions to problems for Chap. 13:

Problem 13.1: Compute the analytic solution of the IVP for the mapping pde (13.23) for a single conserved ($Q(\eta) = 0$) scalar. The scalar space is the unit interval $\mathcal{R}_\Phi = [0, 1]$, and the initial condition is

$$X(\eta; 0) = \sum_{k=1}^N w_k H(\eta - \eta_k), \quad w_k \geq 0, \quad \sum_{k=1}^N w_k = 1$$

where $H(\eta - \eta_k)$ denotes the unit step function located at η_k .

(13.1.1): Rescale the time variable t to transform the mapping pde to the form

$$\left(\frac{\partial}{\partial \tau} + \eta \frac{\partial}{\partial \eta} - \frac{\partial^2}{\partial \eta^2} \right) X(\eta, \tau) = 0$$

(13.1.2): Transform the scalar variable using $\hat{\eta} \equiv \eta \exp(-\tau)$ to obtain a new pde for X .

(13.1.3): Solve the new pde for X . The Green's function approach is recommended, see Duffy [37], Sect. 4.1 for details.

(13.1.4): Plot the solution $X(\eta; t)$ for several times in $[0, 0.3]$.

Solution: The mapping pde (13.23) for a conserved scalar is reduced to

$$\frac{\partial X}{\partial t} = m(t)^2 \epsilon_0 (X'' - \eta X')$$

where $X(\eta; t) : R^1 \rightarrow [0, 1]$ and

$$\epsilon_0 \equiv \frac{1}{ScRe} \left\langle \frac{\partial \Psi}{\partial \zeta_\alpha} \frac{\partial \Psi}{\partial \zeta_\alpha} \right\rangle$$

is the dissipation rate of the Gaussian reference field $\Psi(\mathbf{i})$, hence a positive constant.

(13.1.1): The rescaling is a transformation $\tau \equiv g(t)$, and hence $d\tau = \frac{dg}{dt} dt$ and $\frac{dg}{dt}$ can be set to

$$\frac{dg}{dt} = m^2(t) \epsilon_0, \quad g(t) = \epsilon_0 \int_0^t dt' m(t')^2$$

leading to the desired pde

$$\left(\frac{\partial}{\partial \tau} + \eta \frac{\partial}{\partial \eta} - \frac{\partial^2}{\partial \eta^2} \right) X(\eta, \tau) = 0$$

(13.1.2): The transformation $\hat{\tau} = \tau$ and $\hat{\eta} = \eta \exp(-\tau)$ implies

$$\frac{\partial}{\partial \tau} = \frac{\partial}{\partial \hat{\tau}} - \eta \exp(-\tau) \frac{\partial}{\partial \hat{\eta}}, \quad \frac{\partial}{\partial \eta} = \exp(-\hat{\tau}) \frac{\partial}{\partial \hat{\eta}}, \quad \frac{\partial^2}{\partial \eta^2} = \exp(-2\hat{\tau}) \frac{\partial^2}{\partial \hat{\eta}^2}$$

The mapping pde emerges then in the form

$$\frac{\partial X}{\partial \hat{\tau}} = \exp(-2\hat{\tau}) \frac{\partial^2 X}{\partial \hat{\eta}^2}$$

as diffusion pde with time-dependent diffusivity. This diffusivity can be incorporated in the time variable

$$\hat{t} \equiv g(\hat{\tau}), \quad \frac{\partial}{\partial \hat{\tau}} = \frac{\partial}{\partial \hat{t}} \frac{dg}{d\hat{\tau}}$$

by setting

$$\frac{dg}{d\hat{\tau}} = \exp(-2\hat{\tau}), \quad g(\hat{\tau}) = \frac{1}{2}[1 - \exp(-2\hat{\tau})]$$

The final result for the mapping pde is

$$\frac{\partial X}{\partial \hat{t}} = \frac{\partial^2 X}{\partial \hat{\eta}^2}$$

the standard diffusion pde. The initial condition remains the same

$$X(\eta; 0) = \sum_{k=1}^N w_k H(\eta - \eta_k), \quad w_k \geq 0, \quad \sum_{k=1}^N w_k = 1$$

since $\hat{\eta} = \eta$ at time $t = \tau = \hat{\tau} = 0$.

(13.1.3): The solution $X(\eta; t)$ of the IVP for the mapping pde defined on $\hat{\eta} \in R^1$ is well known; it can, for instance, be expressed in terms of the Green's function (Duffy [37], Sect. 4.1)

$$G(\hat{\eta}; \hat{t} | \hat{\eta}_0, \hat{t}_0) = \frac{H(\hat{t} - \hat{t}_0)}{\sqrt{4\pi(\hat{t} - \hat{t}_0)}} \exp\left[-\frac{(\hat{\eta} - \hat{\eta}_0)^2}{4(\hat{t} - \hat{t}_0)}\right]$$

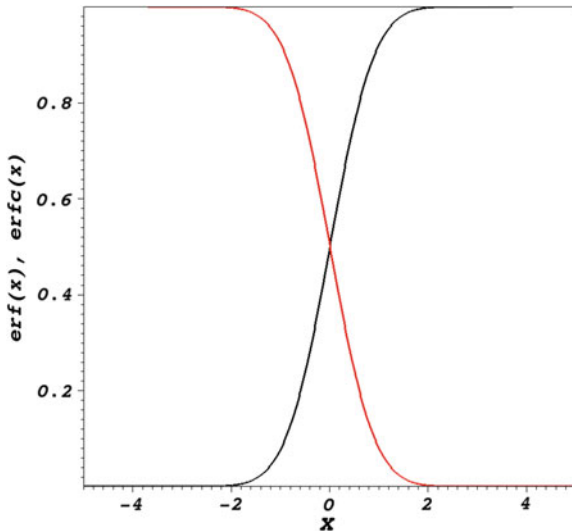
as

$$X(\hat{\eta}; \hat{t}) = \int_{-\infty}^{\infty} X(\hat{\eta}; \hat{t}_0) G(\hat{\eta}; \hat{t} | \hat{\eta}_0; \hat{t}_0) d\hat{\eta}_0$$

for $\hat{t} \geq \hat{t}_0$. For the present example $\hat{\eta} = \eta \exp(-\tau)$ and $\hat{t}(t) = \frac{1}{2}[1 - \exp(-2\epsilon_0 \int_0^t dt' m^2(t'))]$, $\hat{t}_0 = 0$, $0 \leq \hat{t} \leq \frac{1}{2}$ for $0 \leq t \leq \infty$, $\hat{\eta}_0 = \eta_0$, hence

$$X(\eta; t) = \int_{-\infty}^{\infty} X(\eta_0; \hat{t}_0) G(\eta \exp[-\hat{t}(t)]; \hat{t}(t) | \eta_0; 0) d\eta_0$$

Fig. 28.13 Gaussian error function (black line) and its complement (red line)



where the Green's function emerges as

$$G(\eta; t|\eta_0; 0) = \frac{H(\hat{t}(t))}{\sqrt{4\pi\hat{t}(t)}} \exp\left\{-\frac{[\eta \exp(-\hat{t}(t)) - \eta_0]^2}{4\hat{t}(t)}\right\}$$

The particular choice $m(t) = \sqrt{t}$ simplifies the expression for $\hat{t}(t)$ to $\hat{t}(t) = \frac{1}{2}[1 - \exp(-\epsilon_0 t^2)] = \frac{1}{2}A$ with the abbreviation $A(\epsilon_0, t) \equiv 1 - \exp(-\epsilon_0 t^2)$. The Green's function is then

$$G(\eta; t|\eta_0; 0) = \frac{1}{\sqrt{2\pi A}} \exp(-B^2)$$

valid for $t \geq 0$, where the abbreviation

$$B(\eta, \eta_0, t) \equiv \frac{1}{\sqrt{2A(t)}} [\eta_0 - \eta \exp(-\frac{1}{2}A(t))]$$

was introduced to simplify the equations. Noting that $A(t) \geq 0$ for $t \geq 0$, $H(\frac{1}{2}A)$ can be replaced by unity.

The solution of the IVP for the mapping pde is then

$$X(\eta; t) = \frac{1}{\sqrt{2\pi A}} \int_{-\infty}^{\infty} X(\eta_0; 0) \exp(-B^2) d\eta_0$$

and specifically for the given initial condition it emerges in the form

$$X(\eta; t) = \frac{1}{\sqrt{2\pi A}} \sum_{k=0}^N w_k \int_{\eta_k}^{\infty} \exp(-B^2) d\eta_0$$

This result can be expressed in terms of the error function

$$\text{erf}(x) = \frac{1}{\sqrt{\pi}} \int_{-\infty}^x dt \exp(-t^2) = \frac{2}{\sqrt{\pi}} \int_0^x dt \exp(-t^2)$$

or the complementary error function

$$\text{erfc}(x) = 1 - \text{erf}(x)$$

(Fig. 28.13) by transforming the individual integrals using

$$\begin{aligned} \zeta &= B(\eta_0, \eta, t), \quad d\eta_0 = \sqrt{2A} d\zeta \\ \eta_0 = \eta_k \rightarrow \zeta_k &= \frac{1}{\sqrt{2A}} [\eta_k - \eta \exp(-\frac{1}{2} A)] \end{aligned}$$

The mapping is then given by

$$X(\eta; t) = \begin{cases} \sum_{k=1}^N w_k H(\eta - \eta_k) & \text{for } t = 0 \\ \sum_{k=0}^N w_k \text{erfc} \left\{ \frac{1}{\sqrt{2A(t)}} [\eta_k - \eta \exp(-\frac{1}{2} A(t))] \right\} & \text{for } t > 0 \end{cases}$$

(13.1.4): The solution $X(\eta; t)$ is plotted in Fig. 28.14 for $N = 2$, $w_1 = w_2 = 0.4$ at times $t = 0.01, 0.1, 0.2, 0.3$. Note that the Green's function is valid on R^1 , hence the spreading of $X(\eta; t)$ into $\eta < 0$ and $\eta > 1$. The solution for a reference Pdf defined in a compact domain of definition such as the unit interval requires a different Green's function, see Duffy [37] for details.

Reference: Pope (1991) [38] derived the analytic solution of the mapping pde (13.23).

Problem 13.2: Compute and plot the Jacobian $J(\eta; t)$ and the Pdf $f(\varphi; t)$ for $t > 0$ using the mapping $X(\eta; t)$ of the previous problem (13.1).

Solution: The Jacobian J is for the present 1-d example

$$X(\eta; t) = \frac{1}{\sqrt{2\pi A(t)}} \sum_{k=0}^N w_k \int_{\eta_k}^{\infty} \exp[-B^2(\eta, \eta_0, t)] d\eta_0$$

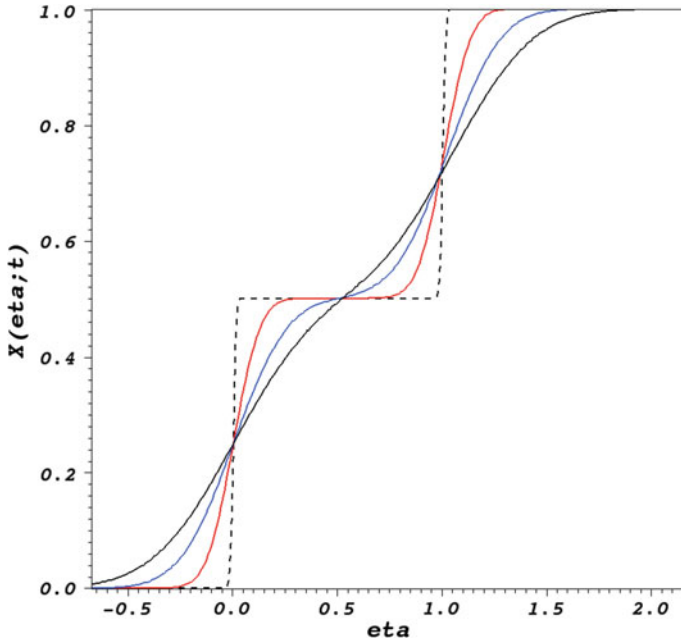


Fig. 28.14 Solution $X(\eta; t)$ of the mapping pde (13.23) for $t = 0.01$ (dashed line, close the initial condition), $t = 0.01$ (blue line), $t = 0.2$ (red line) and $t = 0.3$ (black line)

where $B(\eta, \eta_0, t) = \frac{1}{\sqrt{2A(t)}}[\eta_0 - \eta \exp(-\frac{1}{2}A(t))]$, simply the first derivative of the mapping

$$J(\eta; t) = \frac{\partial X}{\partial \eta}(\eta; t)$$

Implicit differentiation leads to

$$J(\eta; t) = \frac{\exp(-\frac{1}{2}A)}{A^{\frac{3}{2}}\sqrt{2\pi}} \sum_{k=1}^N w_k \left[J_1^k(\eta_k) - \eta \exp(-\frac{1}{2}A) J_0^k(\eta_k) \right]$$

where the abbreviations

$$J_0^k(\eta_k) \equiv \int_{\eta_k}^{\infty} d\eta_0 \exp(-B^2), \quad J_1^k(\eta_k) \equiv \int_{\eta_k}^{\infty} d\eta_0 \eta_0 \exp(-B^2)$$

and $A(\epsilon_0, t) \equiv 1 - \exp(-\epsilon_0 t^2)$ as in the previous problem were introduced to unclutter the result. The integrals in J_0^k and J_1^k can be evaluated resulting in

$$J_0^k(\eta_k) = \sqrt{2\pi A} \operatorname{erfc}\left[\frac{1}{\sqrt{2A}}(\eta_k - \eta \exp(-\frac{1}{2}A))\right]$$

and

$$J_1^k(\eta_k) = A \exp\left[-\frac{1}{2A}(\eta_k - \eta \exp(-\frac{1}{2}A))^2\right] + \eta \exp(-\frac{1}{2}A) J_0^k(\eta_k)$$

Substituting these results in the expression for the Jacobian leads to

$$J(\eta; t) = \frac{\exp(-\frac{1}{2}A)}{A^{\frac{3}{2}} \sqrt{2\pi}} \sum_{k=1}^N w_k \exp\left[-\frac{1}{2A}(\eta_k - \eta \exp(-\frac{1}{2}A))^2\right]$$

Note that this expression for the Jacobian is valid for $t > 0$ as shown in Chap. 13 (the absolute signs can be omitted since the mapping is monotonically increasing), for $t = 0$ the derivative of the mapping and the Cdf does not exist in the usual sense and Dirac functions at η_k appear in the Jacobian. These can be computed by differentiation of the initial mapping

$$X(\eta; 0) = \sum_{k=1}^N w_k H(\eta - \eta_k)$$

(Fig. 28.14 contains the mapping $X(\eta; t)$ at time $t = 0.01$ close to the initial condition as dashed line), where $H(\eta)$ denotes the unit step function, leading to

$$J(\eta; 0) = \sum_{k=1}^N w_k \delta(\eta - \eta_k)$$

The relation (13.28) for the Pdf

$$f(X(\eta; 0); 0) \sum_{k=1}^N w_k \delta(\eta - \eta_k) = f_G(\eta)$$

cannot be solved for $f(\varphi; 0)$, $\varphi = X(\eta; 0)$. Hence, the Pdf $f(\varphi; t)$ is computed for $t > 0$ according to (13.28), $\varphi = X(\eta; t)$ to avoid the initial singularity

$$f(X(\eta; t); t) = \frac{A^{\frac{3}{2}} \exp[-\frac{1}{2}(\eta^2 - A)]}{\sum_{k=1}^N w_k \exp\left[-\frac{1}{2A}(\eta_k - \eta \exp(-\frac{1}{2}A))^2\right]}$$

It shown in Fig. 28.16 for the indicated times (Fig. 28.15).

Reference: Pope (1991) [38] presents results for different initial conditions.

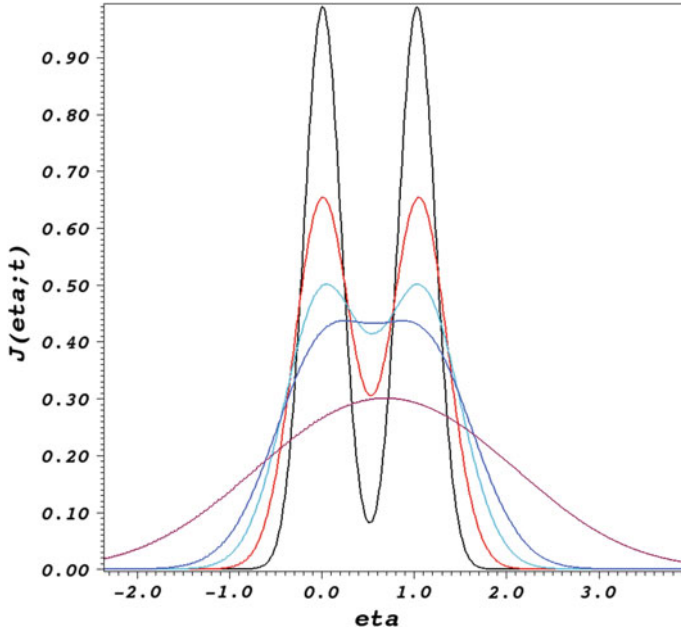


Fig. 28.15 Jacobian $J(\eta; t)$ of the mapping pde (13.23) for $t = 0.2$ (black line), $t = 0.3$ (red line), $t = 0.4$ (light blue line), $t = 0.5$ (blue line) and $t = 1.0$ (magenta line). The initial condition consists of two Dirac pseudo-functions at $\eta = 0$ and $\eta = 1$

Problem 13.3: Hermite spectral method

Solve the IVP of the pde for the Jacobian $J(t, \eta)$ (13.25) assuming no source for $\eta \in R^1$ and the representation of J

$$J(t, \eta) = \sum_{n=0}^{\infty} A_n(t) \Psi_n(\eta)$$

w.r.t. the ONS basis $\mathcal{B} = \{\Psi_n(\eta) \in L^2_{R^1}, n = 0, 1, 2, \dots, \infty\}$ formed by the Hermite functions $\Psi_n(\eta)$ as defined by (4.29). Use the modified model expression

$$m(t) = (m_0 + m_1 \sqrt{t}) \exp(-T_s t), \quad m_0 = 10^{-4}, \quad m_1 = 0.75, \quad T_s = 0.01$$

to guarantee the existence of an asymptotic state.

(13.3.1): Derive the system odes for the coefficients $A_n(t)$ using the ONS property

$$(\Psi_n, \Psi_m) \equiv \int_{-\infty}^{\infty} d\eta \Psi_n(\eta) \Psi_m(\eta) = \delta_{m,n}, \quad \Psi_n, \Psi_m \in \mathcal{B}$$

of the Hermite functions.

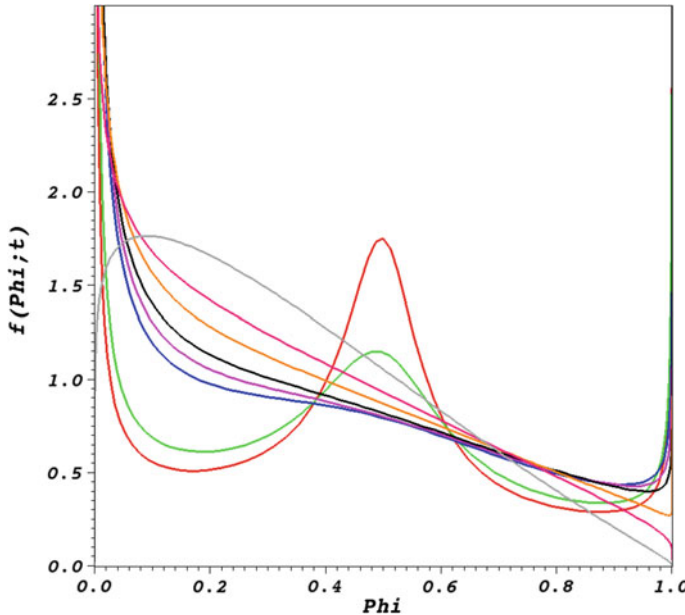


Fig. 28.16 The Pdf $f(\varphi; t)$ of the mapping pde (13.23) for $t = 0.2$ (red), $t = 0.3$ (green), $t = 0.4$ (blue), $t = 0.5$ (pink), $t = 0.6$ (black), $t = 0.7$ (brown), $t = 0.8$ (red) and $t = 1.0$ (grey). The initial Pdf consists of two Dirac pseudo-functions at $\varphi = 0$ and $\varphi = 1$

(13.3.2): Show that

$$\int_{-\infty}^{\infty} d\eta J(t, \eta)$$

is an invariant of the pde (13.25).

(13.3.3): Prove the derivative relation (4.31) for the Hermite functions and show that the entries to the matrix

$$C_{m,n} \equiv \int_{-\infty}^{\infty} d\eta \frac{d\Psi_n}{d\eta} \left(\frac{d\Psi_m}{d\eta} + \eta \Psi_m \right)$$

can be evaluated analytically.

(13.3.4): Set up an initial condition for the Jacobian $J(0, \eta)$ by first setting up the initial mapping $X(0, \eta)$ as linear combination of tanh functions

$$X(0, \eta) = \sum_{k=1}^N w_k H_k(\eta), \quad H_k(\eta) \equiv \frac{1}{2} [1 + \tanh(A_k(\eta - s_k))]$$

and then compute the initial Jacobian by differentiation, choose $N = 3$. Compute the associated coefficients $A_n(0) = (J(0, \eta), \Psi_n(\eta))$ using the derivative relation (4.31).

(13.3.5): Solve the odes for the $A_n(t)$ numerically for a time interval $[0, 2]$. An accurate solver such as the fourth-order Runge–Kutta integrator is recommended. Plot the results for the Jacobian, the mapping and the Pdf.

Solution: The pde for the Jacobian (13.25) with zero source can be restated as

$$\frac{\partial J}{\partial t} = m(t)^2 \epsilon_0 \frac{\partial}{\partial \eta} \left(\frac{\partial J}{\partial \eta} - \eta J \right) \quad (1)$$

where

$$\epsilon_0 \equiv \frac{1}{Pe} \left\langle \frac{\partial G}{\partial \hat{x}_\alpha} \frac{\partial G}{\partial \hat{x}_\alpha} \right\rangle$$

is a positive factor.

(13.3.1): The solution $J(t, \eta)$ is square integrable; hence, it can be represented by

$$J(t, \eta) = \sum_{n=0}^{\infty} A_n(t) \Psi_n(\eta), \quad \Psi_n \in \mathcal{B}, \forall n \quad (2)$$

The equations for the coefficients A_n are obtained by multiplying (1) with Ψ_m , integrating over R^1 , using partial integration to move the outer derivative to Ψ_m

$$\frac{dA_m}{dt} = -\epsilon_0 \sum_{n=0}^{\infty} A_n \left[\left(\frac{d\Psi_m}{d\eta}, \frac{d\Psi_n}{d\eta} \right) - \left(\frac{d\Psi_m}{d\eta}, \eta \Psi_n \right) \right]$$

and partial integration for the second term on the right side resulting in the system

$$\frac{dA_m}{dt} + \epsilon_0 \sum_{n=0}^{\infty} A_n C_{m,n} = -\epsilon_0 A_m$$

where

$$C_{m,n} \equiv \int_{-\infty}^{\infty} d\eta \frac{d\Psi_n}{d\eta} \left(\frac{d\Psi_m}{d\eta} + \eta \Psi_m \right)$$

(13.3.2): Integration of the pde (1) over R^1 leads to $\frac{d}{dt} \int_{-\infty}^{\infty} d\eta J(t, \eta) = 0$ since all integrands are in $L^2_{R^1}$. This proves that the integral is an invariant of the pde for the Jacobian.

(13.3.3): The relation for the first derivative of the Hermite functions follows from the relation (18.9.25)

$$\frac{d}{d\eta} \left(\exp(-\eta^2) H_n(\eta) \right) = -\exp(-\eta^2) H_{n+1}(\eta) \quad (3)$$

in [15], Sect. 18.9 for the Hermite polynomials $H_n(\eta)$ and the definition (4.29)

$$\Psi_n(\eta) = (2^n n! \sqrt{\pi})^{-\frac{1}{2}} \exp(-\frac{\eta^2}{2}) H_n(\eta)$$

of the Hermite functions. Rewriting (3) as

$$\frac{d}{d\eta} \left(\exp(-\frac{1}{2}\eta^2) \Psi_n(\eta) \right) = -\exp(-\frac{1}{2}\eta^2) \Psi_{n+1}(\eta) \sqrt{\frac{2^{n+1}(n+1)!\sqrt{\pi}}{2^n n! \sqrt{\pi}}}$$

and differentiating the product leads to

$$\frac{d\Psi_n}{d\eta} = \eta\Psi_n - \sqrt{2(n+1)}\Psi_{n+1}$$

Combined with the recursive relation (4.32)

$$\eta\Psi_n(\eta) = \begin{cases} \sqrt{\frac{1}{2}(n+1)}\Psi_{n+1}(\eta) + \sqrt{\frac{1}{2}n}\Psi_{n-1}(\eta) & \text{for } n > 0 \\ \sqrt{\frac{1}{2}(n+1)}\Psi_{n+1}(\eta) & \text{for } n = 0 \end{cases}$$

the final version of the first derivative expression (4.31)

$$\frac{d\Psi_n}{d\eta} = \begin{cases} -\sqrt{\frac{1}{2}(n+1)}\Psi_{n+1}(\eta) + \sqrt{\frac{1}{2}n}\Psi_{n-1}(\eta) & \text{for } n > 0 \\ -\sqrt{\frac{1}{2}(n+1)}\Psi_{n+1}(\eta) & \text{for } n = 0 \end{cases}$$

is obtained. These relations allow computation of first derivatives to machine accuracy. Observing

$$\frac{d\Psi_n}{d\eta} + \eta\Psi_n = \begin{cases} \sqrt{\frac{1}{2}n}\Psi_{n-1}(\eta) & \text{for } n > 0 \\ 0 & \text{for } n = 0 \end{cases}$$

and using the derivative relation, the entries to the matrix $C_{m,n}$ can be computed

$$C_{m,n} = \begin{cases} 0 & \text{for } m = 0 \\ -\sqrt{(n+1)m}(\Psi_{n+1}, \Psi_{m-1}) & \text{for } n = 0, m > 0 \\ -\sqrt{(n+1)m}(\Psi_{n+1}, \Psi_{m-1}) + \sqrt{nm}(\Psi_{n-1}, \Psi_{m-1}) & \text{for } n > 0, m > 0 \end{cases}$$

The Hermite functions are orthonormalized allowing the analytic evaluation of the scalar products

$$\sum_{n=0}^{\infty} A_n C_{m,n} = \begin{cases} 0 & \text{for } m = 0 \\ A_1 & \text{for } m = 1 \\ -\sqrt{(m-1)m} A_{m-2} + m A_m & \text{for } m > 1 \end{cases}$$

The system of odes for the coefficients $A_n(t)$ is thus reduced to

$$\frac{dA_m}{dt} = \begin{cases} -\epsilon A_m & \text{for } m = 0 \\ -\epsilon(m+1)A_m & \text{for } m = 1 \\ -\epsilon[(m+1)A_m - \sqrt{m(m-1)}A_{m-2}] & \text{for } m > 1 \end{cases} \quad (4)$$

with initial values $A_m(0)$ set up in the next section.

(13.3.4): The initial condition for the Jacobian is constructed using analytic expressions, first setting up the initial mapping

$$X(0, \eta) = \sum_{k=1}^N w_k H_k(\eta), \quad H_k(\eta) \equiv \frac{1}{2}[1 + \tanh(A_k(\eta - s_k))]$$

with $N = 3$, $A_k = [1.8, 1.5, 1.285714]^T$, $s_k = [-0.5, 0.6, 0]^T$, $w_k = [0.32051, 0.3333, 0.346153]^T$ and then computing the initial Jacobian

$$J(0, \eta) = \sum_{k=1}^N w_k G_k(\eta), \quad G_k(\eta) \equiv \frac{A_k}{2[\cosh(A_k(\eta - s_k))]} = \frac{dH_k}{d\eta}$$

as derivative of the initial mapping; both steps can be done analytically.

(13.3.5): The system of odes (4) obtained in the previous section is solved numerically for the Jacobian $J(t, \eta)$ using a fourth-order accurate Runge–Kutta time integrator for a system of $N = 400$ Hermite modes to represent the Jacobian and $M = 600$ grid points in η direction for the numerical integration. At each time step, the current mapping $X(t, \eta)$ is computed numerically as integral of the Jacobian using a second-order accurate method. The results are shown in Figs. 28.17 and 28.18. The Jacobian $J(t, \eta)$ in the left graph of Fig. 28.17 shows spreading and the mapping $X(t, \eta)$ a significant amount of flattening as time evolves. The associated Pdf $f(t, \varphi)$, $\varphi = X(t, \eta)$, $\varphi \in [0, 1]$, $\eta \in \mathbb{R}^1$ in Fig. 28.18 reduces its width without affecting the mean value for the time interval $[0, 2.5]$ shown. The definition (13.28) of the Pdf $f(X(t, \eta))$ indicates that the Pdf would be Gaussian; if the Jacobian was a constant, the shape of the Jacobian deviating from a linear function in the example generates the non-Gaussian Pdfs. The perfect Gaussian cannot be reached for the bounded image domain $\varphi = X(\eta, t) \in [0, 1]$ as a mapping of the unit interval onto \mathbb{R}^1 is necessarily nonlinear, but the Pdf becomes increasingly closer to a Gaussian

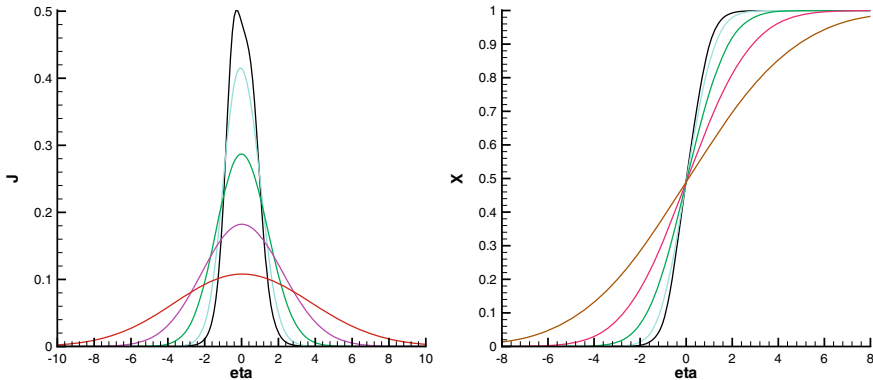


Fig. 28.17 Jacobian $J(t, \eta)$ (left graph) at $t = 0$ (black line), $t = 0.5767$ (light blue line), $t = 1.0573$ (green line), $t = 1.538$ (red line), $t = 2.0186$ (brown line) and the associated mapping $X(t, \eta)$ (right graph) at the same times. The solutions were obtained with $nBasis = 400$ Hermite function modes

for decreasing variance and the Jacobian closer to a constant in the centre of the unit interval. The Gaussian would be obtained according to (13.28); if the range of the image variable φ was R^1 instead of $[0, 1]$, the mapping $X(\eta; t)$ was a linear function of η and the Jacobian $J(\eta, t) = \frac{dX}{d\eta}$ as its slope a positive constant.

The temporal variation of the Hermite basis coefficients / coordinates $A_m(t)$

$$J(t, \eta) = \sum_{m=0}^{\infty} A_m(t) \Psi_m(\eta) \text{ w.r.t. the Hermite basis}$$

$$\mathcal{B} \equiv \{\Psi_n(\eta), n = 0, 1, 2, \dots, \eta \in R^1\} \quad (28.15)$$

in the phase space Ω can be gleaned from the lower graph in Fig. 28.18. The coefficients spread to higher modes (w.r.t. the mode index n) as time evolves, indicating the limit $t \rightarrow \infty$ as nearly uniform distribution appropriate for the Dirac pseudo-function, which represents the Pdf for zero fluctuations. Recall that the Fourier transform of the Dirac pseudo-function is a constant; for the Hermite basis, it approaches a constant as $n \rightarrow \infty$. This effect limits the time interval for the numerical solution of the linear system of odes (4) as spectral backscatter develops ultimately destroying the numerical solution. Furthermore, this approach is not suitable for multivariable Pdfs since the relation of the Jacobian to the mapping (14.50) becomes intricate and nonlinear.

Comments:

The evolution of the coordinates / coefficients w.r.t. the Hermite function basis indicates that asymptotically a nearly uniform distribution is established, hence, a solution that is close to the Dirac pseudo-function. The Dirac pseudo-function can be

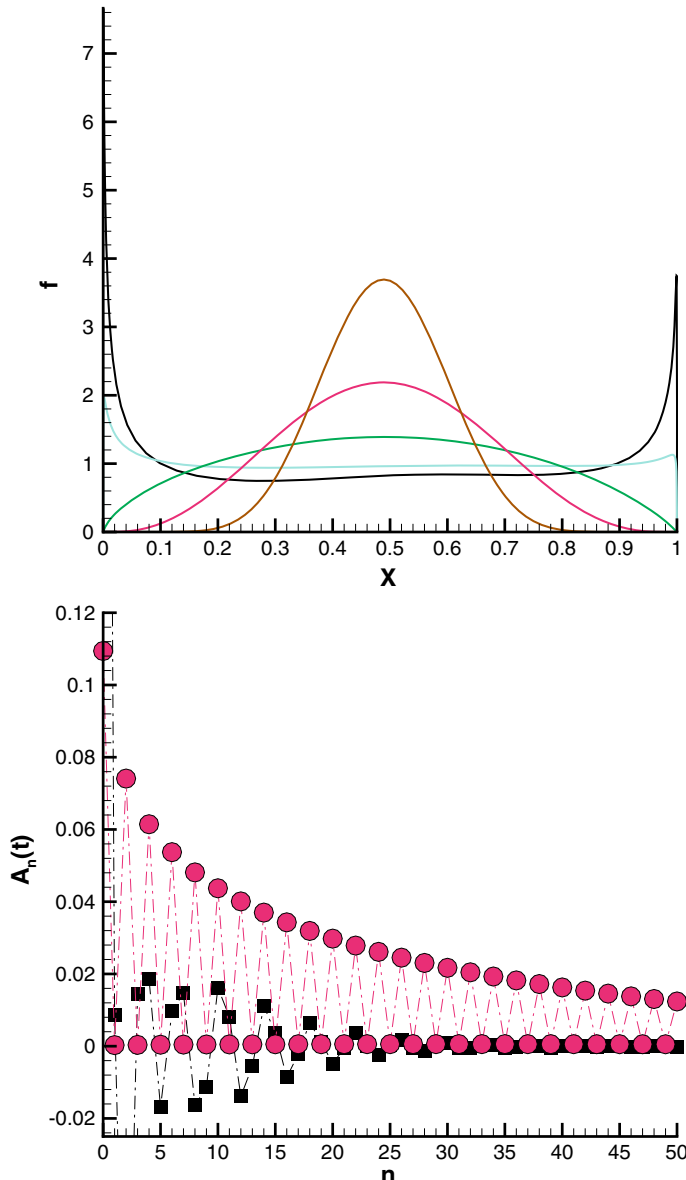


Fig. 28.18 Pdf $f(t, \varphi)$, $\varphi = X(t, \eta)$ (upper graph) at $t = 0$ (black line), $t = 0.5767$ (light blue line), $t = 1.0573$ (green line), $t = 1.538$ (red line), $t = 2.0186$ (brown line) and coefficients $A_n(t)$ (2) of the Hermite basis functions, computed as solutions to the system of Eq. (4), for the Jacobian $J(\eta; t)$ shown in the left graph of Fig. 28.17 as function of the radial mode index n for $t = 0$ (black squares, the values for $n = 0$, $A_0(0) = 0.599341$ and $n = 2$, $A_2(0) = -0.114256$ are outside the graph) and $t = 2.5$ (red circles). The numerical solutions were obtained with the spectral range $n(\text{Basis}) = 400$ Hermite function modes

represented in the Hermite basis, for instance, let $\delta(\eta - \eta_0)$ with $\eta_0 = 0$ be formally expanded

$$\delta(\eta) = \sum_{n=0}^{\infty} (\delta, \Psi_n) \Psi_n(\eta)$$

then are the coefficients $(\delta, \Psi_n) = \Psi_n(0)$ and

$$\delta(\eta) = \sum_{n=0}^{\infty} \Psi_n(0) \Psi_n(\eta)$$

The coefficients can be evaluated according to (4.29) $\Psi_n(0) = (2^n n! \sqrt{\pi})^{-\frac{1}{2}} H_n(0)$ in terms of the values $H_n(0)$ of the Hermite polynomials at $\eta = 0$. The explicit expression for the polynomials ([15], Sect. 18.5)

$$H_n(\eta) = \begin{cases} n! \sum_{m=0}^{\frac{n}{2}} \frac{(-1)^{\frac{n}{2}-m}}{(2m)! (\frac{n}{2}-m)!} (2\eta)^{2m} & \text{for } n \text{ even} \\ n! \sum_{m=0}^{\frac{n-1}{2}} \frac{(-1)^{\frac{n-1}{2}-m}}{(2m+1)! (\frac{n-1}{2}-m)!} (2\eta)^{2m+1} & \text{for } n \text{ odd} \end{cases}$$

leads to

$$H_n(0) = \begin{cases} \frac{n! (-1)^{\frac{n}{2}}}{(\frac{n}{2})!} & \text{for } n \text{ even} \\ 0 & \text{for } n \text{ odd} \end{cases}$$

and

$$\Psi_n(0) = (2^n n! \sqrt{\pi})^{-\frac{1}{2}} \begin{cases} \frac{n! (-1)^{\frac{n}{2}}}{(\frac{n}{2})!} & \text{for } n \text{ even} \\ 0 & \text{for } n \text{ odd} \end{cases}$$

or

$$\Psi_{2m}(0) = (-1)^m \frac{\sqrt{(2m)!}}{m! 2^m \sqrt{\pi}}, \quad m = 0, 1, 2, \dots$$

The formal representation

$$\delta(\eta) = \frac{1}{\sqrt{\pi}} \sum_{m=0}^{\infty} (-1)^m \frac{\sqrt{(2m)!}}{m! 2^m} \Psi_{2m}(\eta)$$

of the Dirac pseudo-function in the Hermite function basis is thus obtained. It is an alternating series for specified argument $-\infty < \eta < \infty$; it would be convergent according to the Leibniz criterium if the terms approach zero as $n \rightarrow \infty$. However, the ratio $|\Psi_{2m+2}(0)| / |\Psi_{2m}(0)|$ of the coefficients can be shown to approach unity similar to the Fourier-transformed (15.2) Dirac function

$$\mathcal{F}[\delta(\eta - \eta_0)] = \frac{1}{2\pi} \int_{-\infty}^{\infty} d\eta \delta(\eta - \eta_0) \exp(-2\pi i k \eta) = \frac{1}{2\pi} \exp(-2\pi i k \eta_0)$$

which is a positive constant for $\eta_0 = 0$ and wavenumber $k \neq 0$; for $\eta_0 \neq 0$, a complex exponential appears.

The Hermite expansion / representation w.r.t. the basis (28.15) has the spectral convergence property but lacks a fast transform method such as FFT for the Fourier basis.

Solutions to problems for Chap. 16: Intermittency

Problem 16.1: Consider the discriminating scalar $\Phi(t, \mathbf{x}) \geq 0$ governed by

$$\frac{\partial \Phi}{\partial t} + v_\alpha \frac{\partial \Phi}{\partial x_\alpha} = \frac{\partial}{\partial x_\alpha} \Gamma \frac{\partial \Phi}{\partial x_\alpha} + Q(\Phi)$$

where Γ is the molecular diffusivity and $Q(t, \mathbf{x})$ the source term. Determine the source term (16.10) of the external intermittency factor $\gamma(t, \mathbf{x})$ (16.2) for $\mathcal{A} = \Phi(t, \mathbf{x}) - e_0$ as function of the discriminating scalar field $\Phi(t, \mathbf{x})$.

Solution: Since Φ is discriminating scalar, the surface, where $S \equiv \Phi(t, \mathbf{x}) - e_0$ holds, moves relative to the fluid with velocity \mathbf{v}^s . The characteristic function (16.1)

$$\mathbf{1}_{\mathcal{A}}(t, \mathbf{x}) = \begin{cases} 1 & \text{for } S(t, \mathbf{x}) = 0 \\ 0 & \text{otherwise} \end{cases}$$

possesses generalized derivatives (16.5); hence, they can be combined

$$\frac{\partial \mathbf{1}_{\mathcal{A}}}{\partial t} + v_\alpha \frac{\partial \mathbf{1}_{\mathcal{A}}}{\partial x_\alpha} = V |\nabla \Phi| \delta(S)$$

The characteristic function $\mathbf{1}_{\mathcal{A}}$ is a unit step function of S ; hence, implicit differentiation can be applied leading to

$$\frac{\partial \mathbf{1}_{\mathcal{A}}}{\partial t} = \frac{d \mathbf{1}_{\mathcal{A}}}{dS} \frac{\partial \Phi}{\partial t}$$

and

$$\frac{\partial \mathbf{1}_{\mathcal{A}}}{\partial x_\alpha} = \frac{d \mathbf{1}_{\mathcal{A}}}{dS} \frac{\partial \Phi}{\partial x_\alpha}$$

Hence

$$\frac{\partial \mathbf{1}_{\mathcal{A}}}{\partial t} + v_\alpha \frac{\partial \mathbf{1}_{\mathcal{A}}}{\partial x_\alpha} = \left(\frac{\partial \Phi}{\partial t} + v_\alpha \frac{\partial \Phi}{\partial x_\alpha} \right) \delta(S)$$

holds. The substantial derivative of the discriminating scalar can be expressed in terms of the right side of Φ , producing the desired result

$$S_\gamma = \langle \left[\frac{\partial}{\partial x_\alpha} \Gamma \frac{\partial \Phi}{\partial x_\alpha} + Q \right] \delta(S) \rangle$$

after averaging.

Comments: The source term indicates that the intermittency factor moves relative to the mean velocity field according to its pde (16.8).

Problem 16.2: Compute the intermittency generating vector (16.19)

$$\varphi_\alpha(\mathbf{w}; \tau, \Delta\tau, \mathbf{X}) = \frac{1}{\sqrt{\Sigma_{(\alpha\alpha)}}} \langle \Delta A_\alpha | \mathbf{W} = \mathbf{w} \rangle - w_\alpha (\langle \Delta A_{(\alpha)} W_{(\alpha)} \rangle - \langle \Delta A_{(\alpha)} \rangle \langle W_{(\alpha)} \rangle)$$

for non-degenerate Gaussian statistics.

Solution: The generating vector (16.19) contains two statistical moments of acceleration $\langle \Delta A_\alpha | \mathbf{W} = \mathbf{w} \rangle$ and $\langle \Delta A_{(\alpha)} V_{(\alpha)} \rangle$. Assuming that the associated random vector

$$\mathbf{x} \equiv \{W_1, \dots, W_3, \Delta A_1, \dots, \Delta A_3\}$$

is Gaussian implies that their Pdf is given by

$$f(\mathbf{x}) = \frac{1}{\sqrt{(2\pi)^n \det(\Sigma)}} \exp\left(-\frac{1}{2} (x_\alpha - \langle x_\alpha \rangle) \Sigma_{\alpha\beta}^{-1} (x_\beta - \langle x_\beta \rangle)\right)$$

where $n = 6$ and

$$\Sigma_{\alpha\beta} = \langle (x_\alpha - \langle x_\alpha \rangle)(x_\beta - \langle x_\beta \rangle) \rangle$$

denotes the covariance matrix. The Gaussian measure is assumed non-degenerate, i.e. $\det(\Sigma) > 0$. The random vector can be partitioned $\mathbf{x} = \{\mathbf{x}^1, \mathbf{x}^2\}$ with subvectors $\mathbf{x}^1 \equiv \{W_1, \dots, W_3\}$, $\mathbf{x}^2 \equiv \{\Delta A_1, \dots, \Delta A_3\}$ and the covariance matrix is then partitioned accordingly

$$\Sigma = \begin{pmatrix} \Sigma^{11} & \Sigma^{12} \\ \Sigma^{21} & \Sigma^{22} \end{pmatrix}$$

containing quadratic submatrices with dimension $\frac{n}{2} = 3$. The unconditional moment follows then at once

$$\langle \Delta A_\beta W_\beta \rangle = \Sigma_{\beta\beta}^{12} + \langle \Delta A_\beta \rangle \langle W_\beta \rangle$$

where the implied summation range is $1 \leq \beta \leq \frac{n}{2}$. The conditional moment $\langle \Delta A_\alpha | \mathbf{W} = \mathbf{w} \rangle$ is a linear function of the conditioning parameter w_α according to [39]

$$\langle \Delta A_\alpha | \mathbf{W} = \mathbf{w} \rangle = \langle \Delta A_\alpha \rangle + \Sigma_{\alpha\beta}^{21} (\Sigma^{11})_{\beta\gamma}^{-1} (w_\gamma - \langle W_\gamma \rangle)$$

Finally, the intermittency generating vector field $\varphi_\alpha(\mathbf{w})$ emerges in the form

$$\frac{1}{\sqrt{\Sigma_{(\alpha\alpha)}}} \langle \Delta A_\alpha | \mathbf{W} = \mathbf{w} \rangle - w_\alpha (\langle \Delta A_{(\alpha)} W_{(\alpha)} \rangle - \langle \Delta A_{(\alpha)} \rangle \langle W_{(\alpha)} \rangle) =$$

$$\frac{1}{\sqrt{\Sigma_{(\alpha\alpha)}}} [\langle \Delta A_\alpha \rangle + \Sigma_{\alpha\beta}^{21} (\Sigma^{11})_{\beta\gamma}^{-1} (w_\gamma - \langle W_\gamma \rangle)] - w_\alpha (\Sigma_{(\alpha\alpha)}^{12} + \langle \Delta A_{(\alpha)} \rangle \langle W_{(\alpha)} \rangle - \langle \Delta A_{(\alpha)} \rangle \langle W_{(\alpha)} \rangle)$$

as function of unconditioned moments and the conditioning parameter \mathbf{w} . It is computable if mean and covariances are specified (subscripts in parenthesis indicate exclusion from the summation convention).

Reference: Wilczek et al. [40] considered the case of homogeneous and isotropic turbulence, which leads to a non-negative scalar field $v = \sqrt{\mathbf{v} \cdot \mathbf{v}}$, since velocity is statistically independent of direction.

Solutions to problems in Chap. 18: Homogeneous turbulence

Problem 18.1: Consider stationary and locally isotropic turbulence at high Re-number. A simple model for the energy spectrum can be constructed by defining a sequence of wavenumbers k_n , such that

$$k_{n+1} = 2k_n$$

Let the energy contained in the interval $[k_n, k_{n+1}]$ be $E(k)$ and the amount of energy transported during the time $\tau(E, k)$ from k_n to k_{n+1} be $\epsilon(k)$. Then compute

(18.1.1) $\epsilon(k)$ as function of the spectrum $E(k)$, the wavenumber k and the time interval $\tau(E, k)$.

(18.1.2) Determine the spectrally local time scale $\tau(E, k)$ in the inertial subrange of the spectrum using dimensional analysis.

(18.1.3) Assuming that the amount of energy fed into the inertial subrange is equal to the amount removed from it, compute the form of the energy spectrum $E(k)$.

Solution: (18.1.1) The wavenumber cascade formed by doubling an initial wavenumber $k_0 > 0$ $\{2^n k_0, k = 0, 1, 2, \dots\}$ with energies per unit wavenumber $\{E(k_0), E(2k_0), \dots, E(2^n k_0), \dots\}$ is maintained by the flux $\epsilon(k)$ transporting energy from k_n to k_{n+1} , hence

$$\epsilon(k) = \frac{\Delta k E(k)}{\tau(E, k)}$$

Since $\Delta k = k$ according to the design of the cascade

$$\epsilon(k) = \frac{k E(k)}{\tau(E, k)}$$

follows.

(18.1.2) Dimensional analysis (time $=T$, length $=L$) using $\{\tau\} = T$ leads to

$$\tau(E, k) = ck^\alpha E^\beta \rightarrow T = L^{-\alpha} \left(\frac{L^3}{T^2}\right)^\beta$$

hence

$$\tau(R, k) = c(k^3 E)^{-\frac{1}{2}}$$

where $c > 0$ is an undetermined constant.

(18.1.3) The amount of energy entering $\epsilon(k_n)$ and leaving $\epsilon(k_{n+1})$ a cascade interval per unit time being equal implies that

$$\frac{d}{dk} \left(\frac{kE(k)}{\tau(E, k)} \right) = 0$$

must hold in the inertial subrange. Using the result from (2) leads to

$$\frac{d}{dk} \left(k^{\frac{5}{2}} E^{\frac{3}{2}}(k) \right) = 0$$

Working out the differentiation results in

$$\frac{dE}{dk} + \frac{5}{3} \frac{E}{k} = 0$$

with solution

$$E(k) = ck^{-\frac{5}{3}}$$

The condition of stationary and locally isotropic turbulence requires an external force field. The design of such a force field is a non-trivial matter, see [41, 42] and references therein.

Solutions to problems in Chap. 20: The structure of turbulent flows

Problem 20.1: Determine the pde for helicity density $h(t, \mathbf{x}) \equiv \mathbf{v} \cdot \boldsymbol{\omega}$ for the flow of an incompressible Newtonian fluid. Define helicity \mathcal{H} by (15.30) and establish the equation for it.

Solution: The pde for helicity (15.29) follows from

$$\frac{\partial h}{\partial t} = \omega_\alpha \frac{\partial v_\alpha}{\partial t} + v_\alpha \frac{\partial \omega_\alpha}{\partial t}$$

and the balances for momentum (2.7)

$$\frac{\partial v_\alpha}{\partial t} = -v_\beta \frac{\partial v_\alpha}{\partial x_\beta} - \frac{\partial p}{\partial x_\alpha} + \frac{1}{Re} \frac{\partial^2 v_{\alpha\beta}}{\partial x_\beta \partial x_\beta} + g_\alpha$$

and vorticity (2.63)

$$\frac{\partial \omega_\alpha}{\partial t} = -v_\beta \frac{\partial \omega_\alpha}{\partial x_\beta} + \omega_\beta \frac{\partial v_\alpha}{\partial x_\beta} + \frac{1}{Re} \frac{\partial^2 \omega_\alpha}{\partial x_\beta \partial x_\beta}$$

The result is the pde

$$\frac{\partial h}{\partial t} = -v_\alpha \frac{\partial h}{\partial x_\alpha} + \frac{\partial T_\alpha}{\partial x_\alpha} + \omega_\alpha g_\alpha - \frac{2}{Re} \frac{\partial \omega_\alpha}{\partial x_\beta} \frac{\partial v_\alpha}{\partial x_\beta}$$

where the non-convective flux is given by

$$T_\alpha = \frac{1}{2} \omega_\alpha v_\beta v_\beta - \omega_\alpha p + \frac{1}{Re} \frac{\partial h}{\partial x_\alpha}$$

Helicity \mathcal{H} is the volume integral of helicity density, and hence

$$\frac{d\mathcal{H}}{dt} = - \int_{\partial\mathcal{D}} dA(\mathbf{x}) n_\alpha v_\alpha h + \int_{\partial\mathcal{D}} dA(\mathbf{x}) n_\alpha T_\alpha + \int_{\mathcal{D}} d\nu(\mathbf{x}) \omega_\alpha g_\alpha - \frac{2}{Re} \int_{\mathcal{D}} d\nu(\mathbf{x}) \frac{\partial \omega_\alpha}{\partial x_\beta} \frac{\partial v_\alpha}{\partial x_\beta}$$

holds, where the Gauss divergence theorem was used.

Comments: If velocity is parallel to the domain boundary $\partial\mathcal{D}$, the first term on the right side vanishes. Furthermore, if the external force is zero, the dynamics of helicity are determined by the net flux through the boundary and the dissipative integral

$$\frac{d\mathcal{H}}{dt} = \int_{\partial\mathcal{D}} dA(\mathbf{x}) n_\alpha T_\alpha - \frac{2}{Re} \int_{\mathcal{D}} d\nu(\mathbf{x}) \frac{\partial \omega_\alpha}{\partial x_\beta} \frac{\partial v_\alpha}{\partial x_\beta}$$

Letting $\nu \rightarrow 0/Re \rightarrow \infty$ and assuming that $\int_{\mathcal{D}} d\nu(\mathbf{x}) \frac{\partial \omega_\alpha}{\partial x_\beta} \frac{\partial v_\alpha}{\partial x_\beta}$ remains bounded lead to

$$\frac{d\mathcal{H}}{dt} = \int_{\partial\mathcal{D}} dA(\mathbf{x}) n_\alpha \omega_\alpha \left(\frac{1}{2} v_\beta v_\beta - p \right)$$

which contains the net flux of helicity through the boundary but no sinks or sources. If vorticity is parallel to the boundary (as for fixed walls), it follows that $d\mathcal{H}/dt = 0$, i.e. helicity is an inviscid invariant. Note that the boundedness assumption for $\int_{\mathcal{D}} d\nu(\mathbf{x}) \frac{\partial \omega_\alpha}{\partial x_\beta} \frac{\partial v_\alpha}{\partial x_\beta}$ is inconsistent with Kolmogorov's hypothesis that the statistical expectation of the dissipation rate has a non-zero and bounded limit value.

Problem 20.2: Compute the solution Ψ of the pde (20.26) for the Chaplygin–Lamb dipole streamfunction

$$\frac{\partial^2 \Psi}{\partial r^2} + \frac{1}{r} \frac{\partial \Psi}{\partial r} + \frac{1}{r^2} \frac{\partial^2 \Psi}{\partial \theta^2} = -\omega$$

for $\omega(r, \theta) = n^2 \Psi(r, \theta)$ requiring continuity of velocity across the cylinder surface $r = a$. Plot streamlines and vorticity within the cylinder.

Solution: The solution of the linear and homogeneous pde (20.26) for the streamfunction Ψ within the cylinder $0 \leq r \leq a$ follows from the separation of variables

$$\Psi(r, \theta) = Z(r)T(\theta)$$

Hence, $Z(r)$ is governed by

$$r^2 \frac{d^2 Z}{dr^2} + r \frac{dZ}{dr} + (n^2 r^2 - C)Z = 0$$

and $T(\theta)$ by

$$\frac{d^2 T}{d\theta^2} + CT = 0$$

The boundary conditions on $r = a$ (20.27) lead to ($\eta = nr$ and $n = \frac{b}{a}$ Eq. (20.30))

$$\Psi(r, \theta) = \alpha J_1\left(\frac{br}{a}\right) \sin(\theta)$$

and

$$\frac{\partial \Psi}{\partial r}(a, \theta) = 2v_0 \sin(\theta)$$

The latter condition implies that $C = 1$ and $T(\theta) = \sin(\theta)$ hold. The radial component $Z(\eta)$, $\eta \equiv nr$, is then governed by

$$\eta^2 \frac{d^2 Z}{d\eta^2} + \eta \frac{dZ}{d\eta} + (\eta^2 - 1)Z = 0$$

This is the standard form of the homogeneous Bessel ode with solutions [15] Eq. (10.2.1). The solution is thus linear combination of Bessel functions of the first and second kind

$$Z(\eta) = \alpha J_1(\eta) + \beta Y_1(\eta)$$

where $0 \leq \eta \leq na$. The solution must be bounded, hence $\beta = 0$. The remaining constants b and α are determined by the boundary conditions at $r = a$. The velocity component v_r must be zero on $r = a$ and continuous across $r = a$, hence $\Psi(a, \theta) =$

0. A non-trivial solution is obtained, if the parameter b is set to a value where $J_1(b) = 0$, hence $b = 3.8317$ is the smallest positive root of J_1 . The value of α is determined by the condition that the azimuthal velocity component v_r is continuous across $r = a$; hence,

$$n \frac{dZ}{d\eta}(b) = 2v_0$$

and

$$\alpha = \frac{2v_0 a}{b \frac{dJ_1}{d\eta}(b)}$$

where $\frac{dJ_1}{d\eta}(b) = -J_0(b)$. The solution is finally given by

$$\Psi(r, \theta) = -\frac{2v_0 a}{b J_0(b)} J_1\left(\frac{br}{a}\right) \sin(\theta)$$

The streamfunction is plotted in Fig. 20.6.

Reference: Most of the material for this problem was taken from the paper by Meleshko and van Heijst [43], Chap. 3, p. 167.

Problem 20.3: Compute the solution Ψ of the pde (20.26) for the Chaplygin–Lamb dipole streamfunction

$$\frac{\partial^2 \Psi}{\partial r^2} + \frac{1}{r} \frac{\partial \Psi}{\partial r} + \frac{1}{r^2} \frac{\partial^2 \Psi}{\partial \theta^2} = -\omega$$

for $\omega(r, \theta) = n^2(\Psi(r, \theta) - \lambda)$, where λ is an arbitrary constant, requiring continuity of velocity across the cylinder surface $r = a$. Plot streamlines and vorticity within the cylinder and the vorticity profiles for several values of λ along the vertical axis $x = 0$.

Solution: The solution of the linear and homogeneous pde (20.26) for the streamfunction Ψ within the cylinder $0 \leq r \leq a$ proceeds analogously to the previous problem (12.2). The linear pde for the streamfunction emerges in the form

$$\frac{\partial^2 \Psi}{\partial r^2} + \frac{1}{r} \frac{\partial \Psi}{\partial r} + \frac{1}{r^2} \frac{\partial^2 \Psi}{\partial \theta^2} = -n^2(\Psi(r, \theta) - \lambda)$$

It is clear that the streamfunction $\Psi(r, \theta)$ can be represented as sum

$$\Psi(r, \theta) = \Psi^{(1)}(r, \theta) + \Psi^{(2)}(r)$$

where

$$\frac{\partial^2 \Psi^{(1)}}{\partial r^2} + \frac{1}{r} \frac{\partial \Psi^{(1)}}{\partial r} + \frac{1}{r^2} \frac{\partial^2 \Psi^{(1)}}{\partial \theta^2} = -n^2 \Psi^{(1)}(r, \theta)$$

and

$$\frac{d^2\Psi^{(2)}}{dr^2} + \frac{1}{r} \frac{d\Psi^{(2)}}{dr} = -n^2(\Psi^{(2)}(r) - \lambda)$$

are the appropriate equations. The boundary conditions for $\Psi^{(1)}(r, \theta)$ are the same as for $\Psi(r, \theta)$ in the previous problem, and the solution is, therefore, known. The boundary conditions for $\Psi^{(2)}(r)$ are thus

$$\Psi^{(2)}(a) = 0, \quad \frac{d\Psi^{(2)}}{dr}(a) = 0$$

and the sum $\Psi^{(1)} + \Psi^{(2)}$ satisfies then the pde and the boundary conditions.

It remains to compute the solution $\Psi^{(2)}(r)$. Defining the shifted streamfunction

$$\zeta(r) \equiv \Psi^{(2)}(r) - \lambda$$

the pde

$$r^2 \frac{d^2\zeta}{dr^2} + r \frac{d\zeta}{dr} + n^2 r^2 \zeta = 0$$

is obtained for it with boundary conditions

$$\zeta(a) = -\lambda, \quad \frac{d\zeta}{dr}(a) = 0$$

Transforming the independent coordinate $\eta \equiv nr$ leads then to

$$\eta^2 \frac{d^2\zeta}{d\eta^2} + \eta \frac{d\zeta}{d\eta} + \eta^2 \zeta = 0$$

with (bounded) solution

$$\zeta(\eta) = \alpha J_0(\eta)$$

The integration constant α is fixed by the boundary condition $\zeta(na) = -\lambda$. Thus

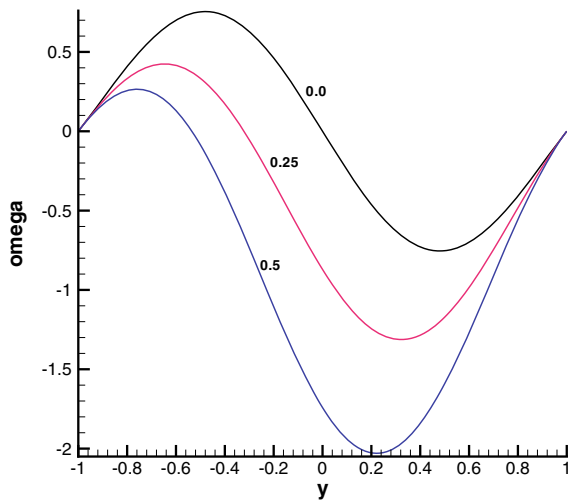
$$\zeta(\eta) = -\lambda \frac{J_0(\eta)}{J_0(b)}$$

or

$$\Psi^{(2)}(r) = \lambda \left[1 - \frac{J_0(\frac{br}{a})}{J_0(b)} \right]$$

follows from it. It remains to check that the second boundary condition is also satisfied. Hence,

Fig. 28.19 Vorticity profiles at $x = 0$ for three values of λ as indicated on the lines



$$\frac{d\zeta}{dr}(a) = 0 \rightarrow \frac{d\zeta}{d\eta} = 0 \rightarrow \frac{d\zeta}{d\eta}(b) = \lambda \frac{J_1(b)}{J_0(b)} = 0$$

since $J_1(b) = 0$, where the relation $dJ_0/d\eta = -J_1$ ([15], Sect. 10.6) was applied.

The complete solution is then given by

$$\Psi(r, \theta) = -\frac{2v_0a}{bJ_0(b)} J_1\left(\frac{br}{a}\right) \sin(\theta) + \lambda \left[1 - \frac{J_0\left(\frac{br}{a}\right)}{J_0(b)} \right]$$

using the result of problem (12.2). Vorticity $\omega(r, \theta)$ follows as

$$\omega(r, \theta) = \frac{2v_0a}{bJ_0(b)} J_1\left(\frac{br}{a}\right) \sin(\theta) - \lambda \left[1 - \frac{J_0\left(\frac{br}{a}\right)}{J_0(b)} \right]$$

The profiles along the vertical axis $x = 0$ of $\omega(r, \theta)$ are plotted in Fig. 28.19 for three values of $\lambda = 0.0, 0.25, 0.5$. Symmetry with respect to the horizontal axis $y = 0$ is evidently lost for $\lambda \neq 0$. Streamlines and vorticity are shown in Fig. 20.7. It is evident that the dipole consists of two vortex tubes of unequal strength with the weaker tube wrapping around the stronger one. Further details can be found in the reference below.

Reference: The paper by Meleshko and van Heijst [43], in particular, Chap. 3, p. 168, is the main source for this problem. The Chaplygin–Lamb dipole is the initial flow structure in jets with centre body such as the flow through valves in IC engines. Counter-rotating vortex tubes are highly susceptible to instability and break up into smaller structures, see, for instance, the experimental results of Nickels [44] and the numerical simulations of Shelley et al. [45]. The completion of the breakup of colliding vortex rings is illustrated in Fig. 28.20 as obtained by Nickels [44].

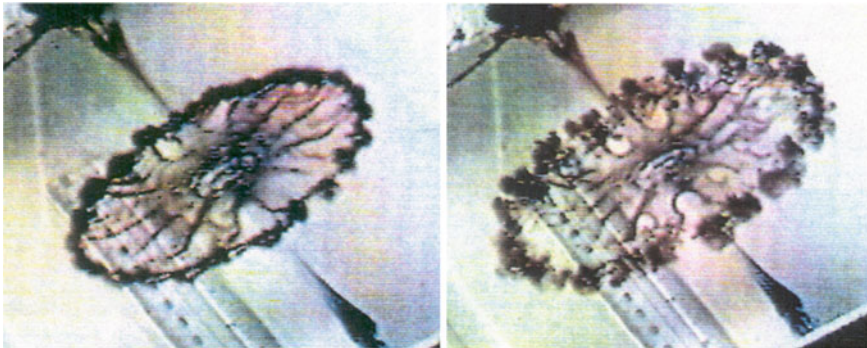


Fig. 28.20 Visualization of the Nickels vortex ring collision experiment ([46], reproduced with permission) for the initial Reynolds number $Re = 1000$. Vortex reconnection is in progress leading to a larger number of small rings compared to $Re = 1000$ in the left graph. The trailing vortex sheet, indicated by the spokes inside the ring in the left graph, undergoes a different instability forming radial tubes. Vortex reconnection is completed in the right graph and the small rings have suffered considerable distortion. The trailing vortex sheet is barely recognizable

Problem (20.4): Determine the material deformation gradient as measured by deformation gradient and deformation rate (velocity gradient) for the restricted Euler system. The restricted Euler flow is governed by (2.122) introduced in Sect. 2.7.

- (4.1) Derive the pde for the deformation gradient $F_{\alpha\beta}$ in mixed formulation using the spatial deformation rate $A_{\alpha\beta}$.
- (4.2) Derive the transport pde for the deformation rate $A_{\alpha\beta}$ in the spatial description.
- (4.3) Establish the odes for the non-trivial invariants Q (2.114) and R (2.115).

Hint: Use the Cayley–Hamilton theorem

$$A_{\alpha\gamma} A_{\gamma\delta} A_{\delta\beta} + Q A_{\alpha\beta} + R \delta_{\alpha\beta} = 0$$

valid for traceless matrices $A_{\alpha\beta}$.

- (4.4) Solve the odes for the invariants Q and R and plot the results in the $R - Q$ phase plane for $-8 \leq R, Q \leq 8$. Show that there appears a cusp singularity (defined as $x^2 - y^3 = 0$ for $x = y = 0$ in standard form) at the origin.

Solution: The deformation gradient is defined by (2.82)

$$F_{\alpha\beta}(\tau, \mathbf{X}) \equiv \frac{\partial \Phi_\alpha}{\partial X_\beta}(\tau, \mathbf{X})$$

in the material description, where $\Phi = (\tau, \mathbf{X})$ denotes the Lagrangean position field, and the deformation rate by

$$A_{\alpha\beta}(t, \mathbf{x}) \equiv \frac{\partial v_\alpha}{\partial x_\beta}(t, \mathbf{x})$$

in the spatial description.

(4.1) Differentiate the deformation gradient in the material description

$$\frac{\partial F_{\alpha\beta}}{\partial \tau} = \frac{\partial V_\alpha}{\partial X_\beta}$$

and transform $V_\alpha(\tau, \mathbf{X}) = v_\alpha(t, \mathbf{x})$ iff $\tau = t$ and $\mathbf{x} = \Phi(\tau, \mathbf{X})$

$$\frac{\partial F_{\alpha\beta}}{\partial \tau} = \frac{\partial}{\partial X_\beta} v_\alpha(t, \Phi(\tau, \mathbf{X}))$$

Implicit differentiation leads to

$$\frac{\partial}{\partial X_\beta} v_\alpha(t, \Phi(\tau, \mathbf{X})) = \frac{\partial v_\alpha}{\partial x_\gamma} \frac{\partial \Phi_\gamma}{\partial X_\beta}$$

and thus to

$$\frac{\partial F_{\alpha\beta}}{\partial \tau} = A_{\alpha\gamma} F_{\gamma\beta}$$

with initial condition $F_{\alpha\beta}(0, \mathbf{X}) = \delta_{\alpha\beta}$. This equation is in mixed formulation since $A_{\alpha\beta}$ is in spatial and $F_{\alpha\beta}$ in material description.

(4.2) Differentiation of the deformation rate in the spatial description produces

$$\frac{\partial A_{\alpha\beta}}{\partial t} = \frac{\partial}{\partial x_\beta} \frac{\partial v_\alpha}{\partial t}$$

Differentiation of the momentum balance

$$\frac{\partial v_\alpha}{\partial t} = -v_\gamma \frac{\partial v_\alpha}{\partial x_\gamma} - \frac{\partial P}{\partial x_\alpha} + \frac{1}{Re} \Delta v_\alpha$$

leads to

$$\frac{D A_{\alpha\beta}}{Dt} = -A_{\beta\gamma} A_{\alpha\gamma} - \frac{\partial^2 P}{\partial x_\alpha \partial x_\beta} + \frac{1}{Re} \Delta A_{\alpha\beta}$$

containing the pressure Hessian $\frac{\partial^2 P}{\partial x_\alpha \partial x_\beta}$. The deformation rate $A_{\alpha\beta}$ in restricted Euler system, explained in Sect. 2.7, is governed by (2.122)

$$\frac{d A_{\alpha\beta}}{d\tau} = -(A_{\alpha\gamma} A_{\gamma\beta} - \frac{1}{3} \delta_{\alpha\beta} A_{\gamma\delta} A_{\delta\gamma})$$

where $A_{\alpha\beta}(\tau, \mathbf{X})$ is the spatial deformation rate transformed to the material description (see Sect. 2.5).

(4.3) Use the definition (2.114) of the invariant $Q = -\frac{1}{2}A_{\alpha\beta}A_{\beta\alpha}$ to differentiate

$$\frac{dQ}{d\tau} = -\frac{1}{2}\left(\frac{dA_{\alpha\beta}}{d\tau}A_{\beta\alpha} + A_{\alpha\beta}\frac{dA_{\beta\alpha}}{d\tau}\right)$$

and substituting the time derivatives using the restricted Euler equation leads to

$$\frac{dQ}{d\tau} = \frac{1}{2}\left((A_{\alpha\gamma}A_{\gamma\beta} - \frac{1}{3}\delta_{\alpha\beta}A_{\gamma\delta}A_{\delta\gamma})A_{\beta\alpha} + A_{\alpha\beta}(A_{\beta\gamma}A_{\gamma\alpha} - \frac{1}{3}\delta_{\alpha\beta}A_{\gamma\delta}A_{\delta\gamma})\right)$$

and due to $A_{\alpha\alpha} = 0$

$$\frac{dQ}{d\tau} = \frac{1}{2}(A_{\alpha\gamma}A_{\gamma\beta}A_{\beta\alpha} + A_{\alpha\beta}A_{\beta\gamma}A_{\gamma\alpha})$$

Using the definition (2.115) of R , the final result

$$\frac{dQ}{d\tau} = -3R$$

is obtained.

The ode for R is derived similarly using (2.115) to differentiate

$$\frac{dR}{d\tau} = -\frac{1}{3}\left(\frac{dA_{\alpha\beta}}{d\tau}A_{\beta\gamma}A_{\gamma\alpha} + A_{\alpha\beta}\frac{dA_{\beta\gamma}}{d\tau}A_{\gamma\alpha} + A_{\alpha\beta}A_{\beta\gamma}\frac{dA_{\gamma\alpha}}{d\tau}\right)$$

and substituting using the restricted Euler system

$$\begin{aligned} \frac{dR}{d\tau} = & \frac{1}{3}\left((A_{\alpha\gamma}A_{\gamma\beta} - \frac{1}{3}\delta_{\alpha\beta}A_{\gamma\delta}A_{\delta\gamma})A_{\beta\eta}A_{\eta\alpha}\right. \\ & \left.+ A_{\alpha\beta}(A_{\beta\delta}A_{\delta\gamma} - \frac{1}{3}\delta_{\beta\gamma}A_{\delta\eta}A_{\eta\delta})A_{\gamma\alpha} + A_{\alpha\beta}A_{\beta\gamma}(A_{\gamma\eta}A_{\eta\alpha} - \frac{1}{3}\delta_{\gamma\alpha}A_{\eta\delta}A_{\delta\eta})\right) \end{aligned}$$

and using (2.114) and suitable renaming of subscripts the ode

$$\frac{dR}{d\tau} = A_{\alpha\gamma}A_{\gamma\beta}A_{\beta\eta}A_{\eta\alpha} - \frac{4}{3}Q^2$$

emerges. The quadruple product can be simplified with the aid of the Cayley–Hamilton theorem $A_{\alpha\gamma}A_{\gamma\delta}A_{\delta\beta} + QA_{\alpha\beta} + R\delta_{\alpha\beta} = 0$ to deal with the quadruple product

$$A_{\alpha\gamma}A_{\gamma\beta}A_{\beta\eta}A_{\eta\alpha} = -(QA_{\alpha\eta} + R\delta_{\alpha\eta})A_{\eta\alpha}$$

It is reduced to

$$A_{\alpha\gamma}A_{\gamma\beta}A_{\beta\eta}A_{\eta\alpha} = 2Q^2$$

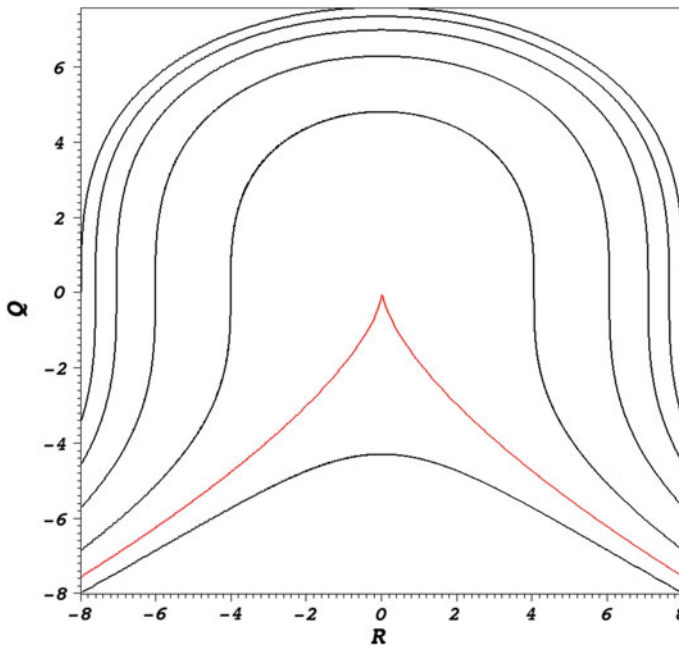


Fig. 28.21 Intrinsic vector lines in the $Q - R$ invariant plane, the line for $c = 0$ with the cusp singularity at the origin is shown in red. Note that the standard form of the cusp singularity $x^2 = y^3$ is obtained for $x = \frac{R}{2}$ and $y = -\frac{Q}{3}$

since $A_{\alpha\alpha} = 0$. The final result is thus

$$\frac{dR}{d\tau} = \frac{2}{3}Q^2$$

(4.4) The system $\frac{dQ}{d\tau} = -3R$, $\frac{dR}{d\tau} = \frac{2}{3}Q^2$ can be recast as

$$Q^2 dQ + \frac{9}{2} R dR = 0$$

by eliminating $d\tau$. This differential form can be integrated leading to

$$Q^3 + \frac{27}{4}R^2 = c$$

with c as arbitrary constant. The vector lines in the $Q - R$ phase plane are shown in Fig. 28.21 for various values of the integration constant c . The cusp singularity appears for $c = 0$ and rescaling $x = \sqrt{27}R$, $y = -9Q$ produces the standard form of a cusp singularity $x^2 - y^3 = 0$. The vector line containing this singularity is shown as red line in Fig. 28.21.

Comments: The odes for the two invariants Q and R were first obtained by Vieillefosse [47, 48]. Cantwell [49] investigated the homogeneous case and showed that certain geometrical features of finescale motions observed in DNS simulations are reproduced by the solution of the restricted Euler system. Recent extensions of the restricted Euler system and extensive comparisons with DNS results are reviewed by Meneveau [50].

Problem 20.5: One of many Lagrangean line structures in turbulent flows is considered in elementary form. The example, called Shilnikov system, is constructed as simplified velocity field that contains several critical points. The solution of the autonomous Shilnikov system [51, 52] for the Lagrangean position field $\Phi_1(\mathbf{X}, \tau), \Phi_2(\mathbf{X}, \tau), \Phi_3(\mathbf{X}, \tau)$

$$\begin{aligned}\frac{d\Phi_1}{d\tau} &= \Phi_1\Phi_3 - w\Phi_2 \\ \frac{d\Phi_2}{d\tau} &= w\Phi_1 + \Phi_2\Phi_3 \\ \frac{d\Phi_3}{d\tau} &= P + \Phi_3 - \frac{1}{3}\Phi_3^3 - (\Phi_1^2 + \Phi_2^2)(1 + q\Phi_1 + e\Phi_3)\end{aligned}$$

generates such a structure, where $\Phi_\alpha(\mathbf{X}, \tau)$ is the position (Cartesian coordinates) of a material point at time τ that started at \mathbf{X} at time zero, and $w = 10$, $e = 0.5$, $q = 0.7$ are constants and $P > 0$ is the bifurcation parameter.

(5.1) Compute the critical points $\frac{d\Phi_\alpha}{d\tau} = 0, \alpha = 1, 2, 3$ for $P > 0$. Show that the critical points are on the \mathbf{e}_3 -axis and that the location of the critical points depends only on the bifurcation parameter P . Compute the value P_c of P separating the case of three real critical points from a single real critical point and two complex conjugate points.

(5.2) Choose two values for the bifurcation parameter $0 < P < P_c, P_c < P < \infty$ and plot the solutions.

Solution:

(5.1) Critical points are defined by $\frac{d\Phi_\alpha}{d\tau} = 0, \alpha = 1, 2, 3$, hence

$$\Phi_1\Phi_3 - w\Phi_2 = 0 \quad (1)$$

$$w\Phi_1 + \Phi_2\Phi_3 = 0 \quad (2)$$

$$P + \Phi_3 - \frac{1}{3}\Phi_3^3 - (\Phi_1^2 + \Phi_2^2)(1 + q\Phi_1 + e\Phi_3) = 0 \quad (3)$$

determines the critical points. Multiplying (1) with Φ_2 and (2) with Φ_1 and subtracting produces

$$w(\Phi_1^2 + \Phi_2^2) = 0,$$

thus $\Phi_1 = \Phi_2 = 0$ follows since $w \neq 0$. Therefore, all critical points must be on the \mathbf{e}_3 -axis. Equation (3) is thus reduced to $P + \Phi_3 - \frac{1}{3}\Phi_3^3 = 0$ or

$$\Phi_3^3 - 3\Phi_3 - 3P = 0 \quad (4)$$

showing that the critical values only depend upon the bifurcation parameter P . Putting this polynomial into standard form

$$\Phi_3^3 + 3\hat{p}\Phi_3 + 2\hat{q} = 0, \quad \hat{p} = -1, \quad \hat{q} = -\frac{3}{2}P$$

helps in the root computation, see Rektorys [53], Sect. 1.20. The discriminant $D \equiv -\hat{p}^3 - \hat{q}^2$ is then

$$D = 1 - \frac{9}{4}P^2$$

and the critical value of P is $P_c = \pm\frac{2}{3}$, only $P = \frac{2}{3}$ needs to be considered. Two cases need to be analysed:

Case $0 < P < P_c$: The discriminant D is positive; hence, there are three real roots of Eq. (4). The roots can be given explicitly using for convenience the parameter $r \equiv \sqrt{|\hat{p}|}$ for $\hat{q} > 0$ and $r \equiv -\sqrt{|\hat{p}|}$ for $\hat{q} < 0$, the latter is true, hence $r = -1$. The three real roots of (4) are then

$$\Phi_3^{(1)} = -2r \cos\left[\frac{1}{3} \arccos\left(\frac{3}{2}P\right)\right],$$

$$\Phi_3^{(2)} = 2r \cos\left[\frac{\pi}{3} - \frac{1}{3} \arccos\left(\frac{3}{2}P\right)\right],$$

$$\Phi_3^{(3)} = 2r \cos\left[\frac{\pi}{3} + \frac{1}{3} \arccos\left(\frac{3}{2}P\right)\right]$$

The roots for $P = 0.5 < P_c$ are $\Phi_3^{(1)} = 1.94224179$, $\Phi_3^{(2)} = -1.3843671$, $\Phi_3^{(3)} = -0.55787468$.

Case $P_c < P < \infty$: The discriminant D is negative; hence, there are one real and two complex conjugate roots of (4). The sole real root is then

$$\Phi_3^{(1)} = -2r \cosh\left[\frac{1}{3} \operatorname{arccosh}\left(\frac{3}{2}P\right)\right]$$

and the complex conjugate roots are given by

$$\Phi_3^{(2)} = r \cosh\left[\frac{1}{3} \arccos\left(\frac{3}{2}P\right)\right] + ir\sqrt{3} \sinh\left(\frac{3}{2}P\right),$$

$$\Phi_3^{(3)} = r \cosh\left[\frac{1}{3} \arccos\left(\frac{3}{2}P\right)\right] - ir\sqrt{3} \sinh\left(\frac{3}{2}P\right)$$

The numerical values for $P = 0.8 > P_c$ are specified as

$$\begin{aligned}\Phi_3^{(1)} &= 2.04319191, \\ \Phi_3^{(2)} &= (-1.02159595, -0.361904144), \\ \Phi_3^{(3)} &= (-1.02159595, 0.361904144).\end{aligned}$$

(12.5.2) The Shilnikov system is solved numerically using the fourth-order Runge–Kutta method. Two solutions are presented: $P = 0.5 < P_c$ and $P_c < P = 0.8$. The initial position of the material point for $P = 0.5 < P_c$ is close to the vertical axis inside the bubble

$$X_1 = -0.05, \quad X_2 = 0.07, \quad X_3 = 0.0$$

and for $P = 0.8 > P_c$ it is outside the bubble

$$X_1 = -0.0006, \quad X_2 = 0.0004, \quad X_3 = -2.043192.$$

The solution for $P = 0.5 < P_c$ is shown in Fig. 28.22 with close-ups near the critical points. Time histories are presented in Fig. 28.23. The pathlines form a bubble between the critical points $\Phi_3^{(1)} = 1.94224179$, $\Phi_3^{(2)} = -1.3843671$.

The solution for $P_c < P = 0.8$ is shown in Fig. 28.24 and time histories of $\Phi(\mathbf{X}, \tau)$ in Fig. 28.25. The detail of the time history $\Phi_3(\tau)$ in the right graph of 28.25 verifies that the sudden change observed (red line) in the left graph is sufficiently resolved. The time histories show that the material point undergoes oscillations as it moves around the bubble in a regular pattern with quiet zones between them. These zones are associated with the motion of the material point through the centre of the bubble towards the opposite critical point; this is seen in the right upper and lower graphs in Figs. 28.22 and 28.24. It can be shown that the critical points possess a stable and an unstable manifold and are connected by a heteroclinic orbit/pathline. This holds for both sets of critical values of the bifurcation parameter P .

Comments: The Shilnikov system in the present example generates the formation of a bubble as the figures indicate, where the pathline of a material point circles around the bubble until it gets close to the unstable manifold of one of two critical points, then moving along the axis of the bubble to the other critical point and the motion is repeated. Low-dimensional dynamics leading to Shilnikov chaos have been observed experimentally in the Taylor–Couette flow and flows of liquid metals with applied magnetic fields and liquid crystal convection, see Mullin et al. [51] for more details.

There is an enormous amount of material on dynamical systems available, see, for instance, Shilnikov et al. [52], Wiggins [54], Kusnetsov [55], Barkley [56], and references therein. Applications to fluid mechanics require the construction of a vector field approximating the flow phenomenon of interest, for instance, the formation of a recirculation zone can be investigated with the aid of dynamical system theory, [57] (the velocity field is numerically computed as solution of the Navier–Stokes pdes and interpolated locally taking into account mass balance and the parity conditions for cylindrical coordinates). Barkley [56] constructs dynamical models for the analysis of turbulent boundary layers. Haller et al. [58] constructed power series approximations

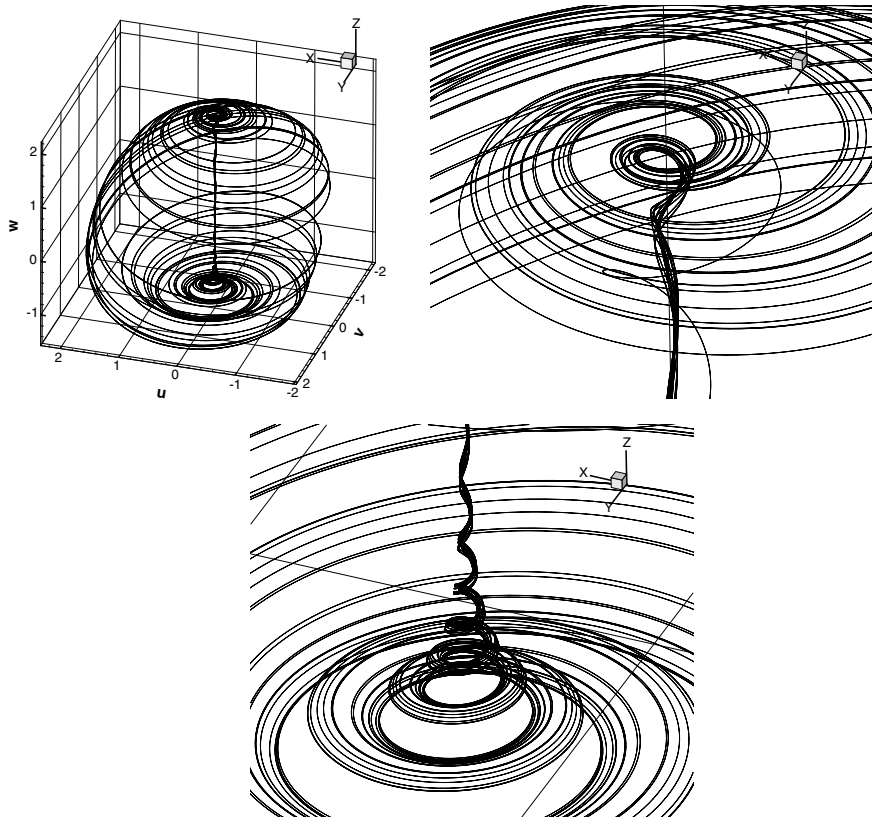


Fig. 28.22 Pathline for the Shilnikov system with $P = 0.5 < P_c$ and details near the critical points in the upper right and lower graphs

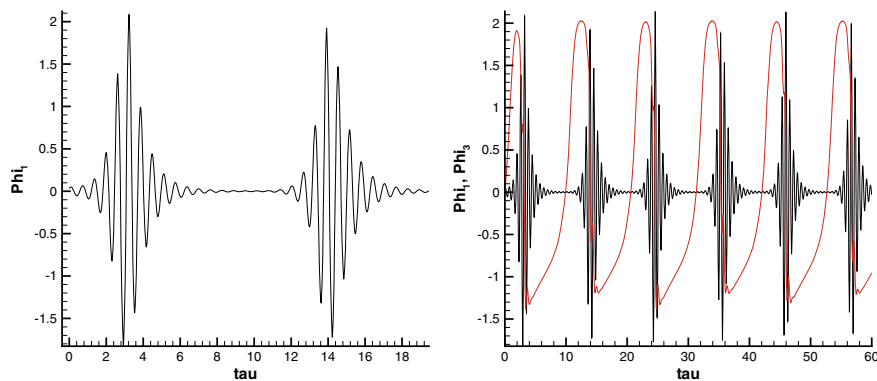


Fig. 28.23 Time histories for the material coordinates $\Phi_1(\tau)$ (left graph) and $\Phi_1(\tau)$ and $\Phi_3(\tau)$ (red line) for $P = 0.5 < P_c$ for the Shilnikov system

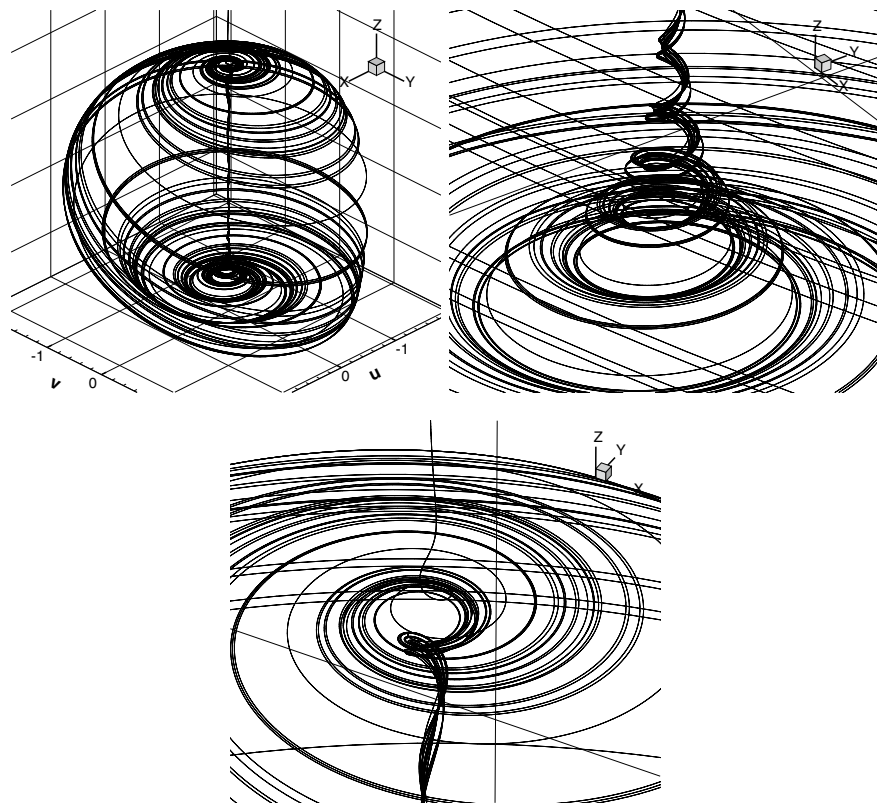


Fig. 28.24 Pathline for the Shilnikov system and $P = 0.8 < P_c$ and details near the critical points in the upper right and lower graphs

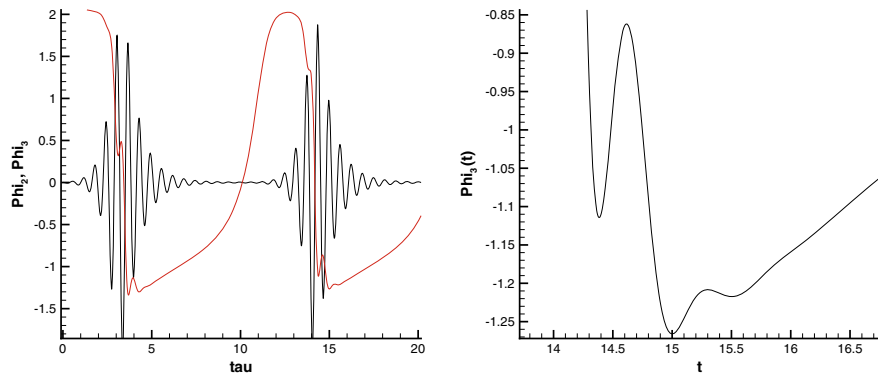


Fig. 28.25 Time history of the material coordinates $\Phi_1(\tau)$ and $\Phi_3(\tau)$ (red line) for the Shilnikov system with $P = 0.8 > P_c$. The time history of $\Phi_2(\tau)$ is similar to Φ_1 but out of phase

of steady flows near fixed-wall boundaries to analyse near-wall structures using dynamical system ideas. The emergence and destruction of critical points is relevant for the dynamics of turbulent flows as they can be classified [59] to gain an overview of possible line structures, in particular, pathlines near heteroclinic and homoclinic orbits/pathlines. The transition from laminar to turbulent flow is one of the successful applications.

Problem (12.6): Townsend's model eddy (19.1) is a localized blob of vorticity defined in $\mathcal{D} = R^3$ (Davidson [33], Sect. 6.4.1, cylindrical coordinates) by $v_r = v_z = 0$ and

$$v_\theta = \Omega r \exp\left(-2 \frac{\mathbf{x} \cdot \mathbf{x}}{z_c^2}\right)$$

where $z_c > 0$ denotes the eddy length scale and Ω is a measure for the angular speed. Assume solenoidal external force, $\nabla \cdot \mathbf{G} = \frac{1}{r} \frac{\partial}{\partial r} (r G_r) + \frac{1}{r} \frac{\partial G_\theta}{\partial \theta} + \frac{\partial G_z}{\partial z} = 0$.

(6.1) Compute vorticity in cylindrical coordinates.

(6.2) Split the right-hand side of the pressure pde

$$\Delta p(\mathbf{x}) = 2Q_A$$

where $Q_A \equiv -\frac{1}{2} \nabla \mathbf{v} : \nabla \mathbf{v}$, into $Q_A = Q_S + Q_W$. Strain rate and rotation rate tensors are defined by $\mathbf{s} = \frac{1}{2}(\mathbf{A} + \mathbf{A}^T)$ and $\mathbf{W} = \frac{1}{2}(\mathbf{A} - \mathbf{A}^T)$ and $Q_S = -\rho \frac{1}{2} \text{tr}(\mathbf{s}^2)$, $Q_W = -\rho \frac{1}{2} \text{tr}(\mathbf{W}^2)$, [60]. Compute the solution of the Poisson pde for p and separate the contributions of Q_S and Q_W . Plot the radial profiles for the azimuthal velocity and enstrophy, the right-hand sides $Q_A(r, 0)$, $Q_S(r, 0)$, $Q_W(r, 0)$ and the associated pressure.

Solution: Townsend's model eddy is defined by the velocity field

$$\mathbf{v}(r, \theta, z) = \Omega r \exp\left(-2 \frac{\mathbf{x} \cdot \mathbf{x}}{z_c^2}\right) \mathbf{e}_\theta \in L^2_{R^3}$$

in cylindrical coordinates, where $\mathbf{x} \cdot \mathbf{x} = r^2 + z^2$ ($\Omega = 1.0$, $z_c = 0.5$ for the plots). The pressure field induced by it is determined by the Poisson pde

$$\Delta p(\mathbf{x}) = 2Q_A(\mathbf{x}), \mathbf{x} \in \mathcal{D}$$

which emerges in cylindrical coordinates as (Appendix in [57])

$$\begin{aligned} \frac{1}{r} \frac{\partial}{\partial r} (r \frac{\partial p}{\partial r}) + \frac{1}{r^2} \frac{\partial^2 p}{\partial \theta^2} + \frac{\partial^2 p}{\partial z^2} &= \rho \left[\frac{1}{r} \frac{\partial}{\partial r} (r G_r) + \frac{1}{r} \frac{\partial G_\theta}{\partial \theta} + \frac{\partial G_z}{\partial z} \right] \\ -\rho \left[\left(\frac{\partial v_r}{\partial r} \right)^2 + \frac{1}{r^2} \left(\frac{\partial v_\theta}{\partial \theta} + v_r \right)^2 + \left(\frac{\partial v_z}{\partial z} \right)^2 + \frac{2}{r} \frac{\partial v_\theta}{\partial r} \left(\frac{\partial v_r}{\partial \theta} - v_\theta \right) + 2 \frac{\partial v_r}{\partial z} \frac{\partial v_z}{\partial r} + \frac{2}{r} \frac{\partial v_z}{\partial \theta} \frac{\partial v_\theta}{\partial z} \right] \end{aligned}$$

and for solenoidal external force

$$Q_A = -\frac{\rho}{2} \left[\left(\frac{\partial v_r}{\partial r} \right)^2 + \frac{1}{r^2} \left(\frac{\partial v_\theta}{\partial \theta} + v_r \right)^2 + \left(\frac{\partial v_z}{\partial z} \right)^2 + \frac{2}{r} \frac{\partial v_\theta}{\partial r} \left(\frac{\partial v_r}{\partial \theta} - v_\theta \right) + 2 \frac{\partial v_r}{\partial z} \frac{\partial v_z}{\partial r} + \frac{2}{r} \frac{\partial v_z}{\partial \theta} \frac{\partial v_\theta}{\partial z} \right]$$

follows. For $\mathcal{D} = R^3$ the solution is

$$p(\mathbf{x}) = -\frac{1}{4\pi} \int_{\mathcal{D}} d\nu' \frac{2Q_A(\mathbf{x}')}{|\mathbf{x} - \mathbf{x}'|}$$

using the standard Green's function for R^3 .

(6.1) The vorticity in cylindrical coordinates is given by

$$\boldsymbol{\Omega}(r, \theta, z) = \begin{pmatrix} \frac{1}{r} \frac{\partial v_z}{\partial \theta} - \frac{\partial v_\theta}{\partial z} \\ \frac{\partial v_r}{\partial z} - \frac{\partial v_z}{\partial r} \\ s \frac{1}{r} \frac{\partial}{\partial r} (r v_\theta) - \frac{1}{r} \frac{\partial v_r}{\partial \theta} \end{pmatrix}$$

The components are for the Townsend model eddy reduced to

$$\boldsymbol{\Omega}(r, \theta, z) = 2 \frac{v_\theta}{r} \begin{pmatrix} -\frac{2rz}{z_c^2} \\ 0 \\ 1 - \frac{2r^2}{z_c^2} \end{pmatrix}$$

with the associated enstrophy

$$e(r, z) = \frac{1}{2} \sqrt{\boldsymbol{\Omega} \cdot \boldsymbol{\Omega}} = \frac{v_\theta}{r} \sqrt{1 - \frac{4r^2}{z_c^2} + \frac{4r^2}{z_c^4} (r^2 + z^2)}$$

The right-hand side terms of the pressure pde are then

$$Q_A = -\frac{\rho}{2} \left[\frac{1}{r^2} \left(\frac{\partial v_\theta}{\partial \theta} \right)^2 - \frac{2}{r} v_\theta \frac{\partial v_\theta}{\partial r} \right]$$

The azimuthal velocity is explicitly given, hence

$$\frac{\partial v_\theta}{\partial \theta} = 0$$

and

$$\frac{\partial v_\theta}{\partial r} = \frac{v_\theta}{r} \left(1 - \frac{4r^2}{z_c^2} \right)$$

resulting in

$$Q_A(r, z) = \rho \left(\frac{v_\theta}{r} \right)^2 \left(1 - \frac{4r^2}{z_c^2} \right) = \rho \Omega^2 \exp \left[-\frac{4}{z_c^2} (r^2 + z^2) \right] \left(1 - \frac{4r^2}{z_c^2} \right)$$

which is bounded for $r \rightarrow 0$, since $\frac{v_\theta}{r} = \Omega \exp \left[-\frac{2}{z_c^2} (r^2 + z^2) \right]$, thus

$$Q_A(0, z) = \rho \Omega^2 \exp \left(-\frac{4z^2}{z_c^2} \right)$$

is the variation on the coordinate axis $r = 0$. The components of the rate of strain tensor in cylindrical coordinate (Panton [31], Appendix B) are

$$\mathbf{s} = \begin{pmatrix} \frac{\partial v_r}{\partial r} & \frac{1}{2} \left(\frac{1}{r} \frac{\partial v_r}{\partial \theta} + \frac{\partial v_\theta}{\partial r} - \frac{v_\theta}{r} \right) & \frac{1}{2} \left(\frac{\partial v_r}{\partial z} + \frac{\partial v_z}{\partial r} \right) \\ \text{sym.} & \frac{1}{r} \frac{\partial v_\theta}{\partial \theta} + \frac{v_r}{r} & \frac{1}{2} \left(\frac{1}{r} \frac{\partial v_z}{\partial \theta} + \frac{\partial v_\theta}{\partial z} \right) \\ \text{sym.} & \text{sym.} & \frac{\partial v_z}{\partial z} \end{pmatrix}$$

It is reduced to

$$\mathbf{s} = \begin{pmatrix} 0 & \frac{1}{2} \left(\frac{\partial v_\theta}{\partial r} - \frac{v_\theta}{r} \right) & 0 \\ \text{sym.} & 0 & \frac{1}{2} \frac{\partial v_\theta}{\partial z} \\ \text{sym.} & \text{sym.} & 0 \end{pmatrix} = -2 \frac{v_\theta}{r} \begin{pmatrix} 0 & \frac{r^2}{z_c^2} & 0 \\ \frac{r^2}{z_c^2} & 0 & \frac{r z}{z_c^2} \\ 0 & \frac{r z}{z_c^2} & 0 \end{pmatrix}$$

for the Townsend model eddy. The product \mathbf{s}^2 is easily computed

$$\mathbf{s}^2 = 4 \left(\frac{v_\theta}{r} \right)^2 \begin{pmatrix} \frac{r^4}{z_c^4} & 0 & \frac{r^3 z}{z_c^4} \\ 0 & \frac{r^2(r^2+z^2)}{z_c^4} & 0 \\ \frac{r^3 z}{z_c^4} & 0 & \frac{r^2 z^2}{z_c^4} \end{pmatrix}$$

and the right-hand side of the Poisson pde for the pressure due to the strain rate is then ([60])

$$Q_S = -\rho \frac{1}{2} \text{tr}(\mathbf{s}^2) = -4 \rho \left(\frac{v_\theta}{r} \right)^2 \frac{r^2(r^2+z^2)}{z_c^4}$$

obviously negative semi-definite as claimed in [60]. The right-hand side for the rotation tensor follows at once from

$$Q_W = Q_A - Q_S = \rho \left(\frac{v_\theta}{r} \right)^2 \left[1 - \frac{4r^2}{z_c^2} + \frac{4r^2(r^2+z^2)}{z_c^4} \right]$$

which is positive semi-definite since $-\text{tr}(\mathbf{W}^2) = 2|\boldsymbol{\Omega}|^2 \geq 0$. The contributions of the rate of strain \mathbf{s} and the rate of rotation \mathbf{W} to the pressure field $p = p_s + p_W$ are computed by numerical integration according to

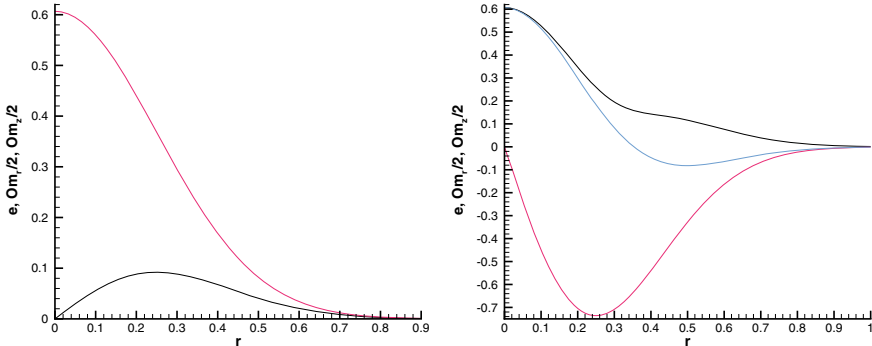


Fig. 28.26 Azimuthal velocity profile (v_θ black, $\frac{v_\theta}{r}$ red line, left graph) and enstrophy $r_z = \frac{1}{2}\sqrt{\Omega_r^2 + \Omega_z^2}$ (black line) and the vorticity components $\frac{1}{2}\Omega_r(r, z)$ (red), $\frac{1}{2}\Omega_z(r, z)$ (blue) for the Townsend model eddy in the right graph. All profiles are at $z = 0.25$

$$p_s(\mathbf{x}) = -\frac{1}{4\pi} \int_{\mathcal{D}} d\nu' \frac{2Q_s(\mathbf{x}')}{|\mathbf{x} - \mathbf{x}'|}$$

since the Green's function is known. Figure 28.26 shows the azimuthal velocity $v_\theta(r, z)$, the $v_\theta/r(r, z)$ profiles in the left and the enstrophy together with the vorticity components $\Omega_r(r, 0)$ (red), $\Omega_z(r, 0)$ (blue) at $z = 0.5d_0$ in the right graph for the Townsend model eddy. The effects of the right-hand side vectors $Q_A(r, 0)$ (black line), $Q_S(r, 0)$ (red line) and $Q_W(r, 0)$ (blue line in the left graph) on the pressure are presented in the right graph (p_A black, p_S red and p_W blue line) of Fig. 28.27. The resulting pressures due to the rate of deformation Q_A , the rate of strain Q_S and vorticity Q_W are shown in Fig. 28.27.

Comments: Townsend's model eddy represents a blob of swirling fluid with characteristic length scale z_c . An ensemble of such eddies randomly distributed in space has the longitudinal correlation function

$$f(r) = \exp\left(-\frac{r^2}{z_c^2}\right)$$

according to Townsend [61]. Further information on the model eddy can be found in Davidson's book [33], Sect. 6.4.1.

Vlaykov and Wilczek [60] investigated the impact of small-scale structures on the pressure field and used the Townsend model eddy to illustrate the pressure variations near it and to draw conclusions from the distributions of $Q[A]$, $Q[S]$ and $Q[W]$ in DNS of homogeneous turbulence how they affect the instantaneous pressure. They computed the two-point correlations of Q_A , Q_S and Q_W and found that the Q_A -correlation, in contrast to the rate of strain and rotation terms, is of the order of the

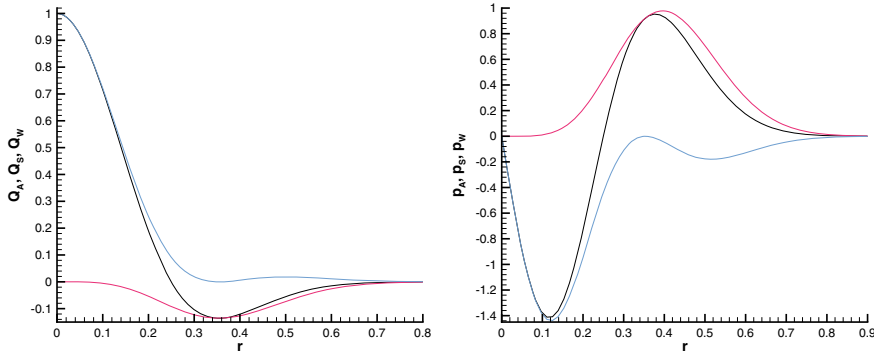


Fig. 28.27 Profiles of the rhs vectors $Q_A(r, 0)$ due to the rate of deformation in black, $Q_S(r, 0)$ due to the rate of strain in red and $p_W(r, 0)$ due to vorticity in blue (left graph) and the pressure profiles $p[Q_A](r, 0)$ black, $p[Q_S](r, 0)$ red and $p[Q_W](r, 0)$ blue line (right graph) for the Townsend model eddy. All profiles are at $z = 0$

Kolmogorov microscale and approximately independent of the Reynolds number. The main conclusion reached by Vlaykov and Wilczek as result of statistical evaluation of DNS data for homogeneous turbulence is that the pressure in regions with intense velocity gradient fluctuations is determined more locally than in other regions.

Solutions to problems in Chap. 21: Wall-bounded turbulent flows

Problem 21.1: Consider the fully developed, turbulent flow of an incompressible, Newtonian fluid through a plane channel between two plates at $x_2 = 0$ and $x_2 = h$. Use dimensionless variables based on the kinematic viscosity ν and the wall shear velocity u^* (27.15).

(21.1.1) Derive the averaged x-momentum balance for this flow.

(21.1.2) Express the divergence of the Lamb vector in terms of velocity, flexion (2.55) and enstrophy (3.16) and average the result.

(21.1.3) Determine the Taylor series expansions for the fluctuation velocity, vorticity and flexion components close to the lower wall. Derive the expansion for the dimensionless divergence of the Lamb vector and its average close to the lower wall. Show that the divergence of the Lamb vector must be negative at the wall.

Solution: The split of variables into mean and fluctuation is developed in Sect. 21.1 of Chap. 21. Variables are made dimensionless in the near-wall region using the kinematic viscosity ν and the wall shear velocity $u^{*2} = \frac{\tau_0}{\rho}$ (27.15), specifically

$$t^+ \equiv t \frac{u^{*2}}{\nu}, \quad y^+ \equiv y \frac{u^*}{\nu}, \quad u^+ \equiv \frac{\langle u \rangle}{u^*}, \quad u'' \equiv \frac{u'}{u^*}$$

doubly primed variables u'' are fluctuations of the dimensionless mean variables u^+ . The Reynolds number is defined by $Re \equiv \frac{u^* h}{\nu}$.

(21.1.1) The averaged mass (27.1)

$$\frac{\partial \langle u \rangle}{\partial x} + \frac{\partial \langle v \rangle}{\partial y} = 0$$

and momentum (27.6), (27.7) balances

$$0 = -\frac{\partial \langle p \rangle}{\partial x} + \frac{\partial}{\partial y} [\nu \frac{\partial \langle u \rangle}{\partial y} - \langle u' v' \rangle], \quad 0 = -\frac{\partial \langle p \rangle}{\partial y} - \frac{\partial}{\partial y} \langle v'^2 \rangle$$

(p is actually p/ρ) are taken from Sect. 27.1. Fully turbulent flow parallel to two plates implies that $\langle u \rangle$ is only a function of y and $\langle v \rangle = 0$. Hence, the averaged mass balance is satisfied. It is shown in Sect. 27.1 that the mean pressure is the sum of the mean wall pressure $p_w(x^+)$ and the lateral normal stress $\langle v'^2 \rangle(y^+)$ (27.10) and longitudinal averaged momentum balance emerges in integrated form (27.17)

$$\nu \frac{\partial \langle u \rangle}{\partial y} - \langle u' v' \rangle = u^{*2} \left(1 - \frac{2y}{h}\right)$$

or as dimensionless version

$$\frac{du^+}{dy^+} - \langle u'' v'' \rangle = 1 - \frac{2}{Re} y^+$$

(21.1.2) The divergence of the Lamb vector $\nabla \cdot \mathbf{L}$

$$\frac{\partial L_\alpha}{\partial x_\alpha} = \epsilon_{\alpha\beta\gamma} \frac{\partial \omega_\beta}{\partial x_\alpha} v_\gamma + \epsilon_{\alpha\beta\gamma} \omega_\beta \frac{\partial v_\gamma}{\partial x_\alpha}$$

can be recast in terms of flexion (2.55) and enstrophy (3.16)

$$\frac{\partial L_\alpha}{\partial x_\alpha} = v_\gamma f_\gamma - \omega_\beta \omega_\beta$$

or in symbolic notation

$$\nabla \cdot \mathbf{L} = \mathbf{v} \cdot \mathbf{f} - \boldsymbol{\omega} \cdot \boldsymbol{\omega}$$

Averaging leads to the divergence of the mean Lamb vector

$$\frac{\partial \langle L_\alpha \rangle}{\partial x_\alpha} = \langle v_\gamma \rangle \langle f_\gamma \rangle - \langle \omega_\beta \rangle \langle \omega_\beta \rangle + \langle v'_\gamma f'_\gamma \rangle - \langle \omega'_\beta \omega'_\beta \rangle$$

(21.1.3) Taylor series expansion of the fluctuating velocity (u'', v'', w'') with respect to the wall-normal direction y^+ in Cartesian coordinates (x^+, y^+, z^+) with x^+ being the mean flow direction leads to

$$u''(x^+, y^+, z^+, t^+) = a_1 y^+ + a_2 y^{+2} + a_3 y^{+3} + O(y^{+4})$$

$$v''(x^+, y^+, z^+, t^+) = b_2 y^{+2} + b_3 y^{+3} + O(y^{+4})$$

$$w''(x^+, y^+, z^+, t^+) = c_1 y^+ + c_2 y^{+2} + c_3 y^{+3} + O(y^{+4})$$

as a consequence of mass balance, where the coefficients are defined by

$$a_j(x^+, z^+, t^+) \equiv \frac{1}{j!} \frac{\partial^j u''}{\partial y^{+j}}(0), \quad b_j(x^+, z^+, t^+) \equiv \frac{1}{j!} \frac{\partial^j v''}{\partial y^{+j}}(0), \quad c_j(x^+, z^+, t^+) \equiv \frac{1}{j!} \frac{\partial^j w''}{\partial y^{+j}}(0)$$

The expansions for vorticity $\omega_j'' = \omega_j' \frac{\nu}{u^{*2}}$ and flexion $f_j'' = f_j' \frac{\nu^2}{u^{*3}}$ follow likewise

$$\omega_x''(x^+, y^+, z^+, t^+) = a_0^\omega + a_1^\omega y^+ + a_2^\omega y^{+2} + a_3^\omega y^{+3} + O(y^{+4})$$

$$\omega_y''(x^+, y^+, z^+, t^+) = b_1^\omega y^+ + b_2^\omega y^{+2} + b_3^\omega y^{+3} + O(y^{+4})$$

$$\omega_z''(x^+, y^+, z^+, t^+) = c_0^\omega + c_1^\omega y^+ + c_2^\omega y^{+2} + c_3^\omega y^{+3} + O(y^{+4})$$

where

$$a_j^\omega(x^+, z^+, t^+) \equiv \frac{1}{j!} \frac{\partial^j \omega_x''}{\partial y^{+j}}(0), \quad b_j^\omega(x^+, z^+, t^+) \equiv \frac{1}{j!} \frac{\partial^j \omega_y''}{\partial y^{+j}}(0), \quad c_j^\omega(x^+, z^+, t^+) \equiv \frac{1}{j!} \frac{\partial^j \omega_z''}{\partial y^{+j}}(0)$$

and

$$f_x''(x^+, y^+, z^+, t^+) = a_0^f + a_1^f y^+ + a_2^f y^{+2} + a_3^f y^{+3} + O(y^{+4})$$

$$f_y''(x^+, y^+, z^+, t^+) = b_0^f + b_1^f y^+ + b_2^f y^{+2} + b_3^f y^{+3} + O(y^{+4})$$

$$f_z''(x^+, y^+, z^+, t^+) = c_0^f + c_1^f y^+ + c_2^f y^{+2} + c_3^f y^{+3} + O(y^{+4})$$

where

$$a_j^f(x^+, z^+, t^+) \equiv \frac{1}{j!} \frac{\partial^j f_x''}{\partial y^{+j}}(0), \quad b_j^f(x^+, z^+, t^+) \equiv \frac{1}{j!} \frac{\partial^j f_y''}{\partial y^{+j}}(0), \quad c_j^f(x^+, z^+, t^+) \equiv \frac{1}{j!} \frac{\partial^j f_z''}{\partial y^{+j}}(0)$$

The no-slip condition on the wall boundary implies that the vorticity component normal to it vanishes $\omega_y = \omega_y^+ = \omega_y'' = 0$. The flexion vector at the wall boundary is reduced to

$$f_\alpha = \begin{pmatrix} \frac{\partial \omega_3}{\partial x_2} \\ \frac{\partial \omega_1}{\partial x_3} - \frac{\partial \omega_3}{\partial x_1} \\ -\frac{\partial \omega_1}{\partial x_2} \end{pmatrix}$$

The divergence of the Lamb vector is strictly negative at the wall

$$\frac{\partial L_\alpha}{\partial x_\alpha} = -\omega_\beta \omega_\beta, \quad \frac{\partial \langle L_\alpha \rangle}{\partial x_\alpha} = -\langle \omega_\beta \rangle \langle \omega_\beta \rangle - \langle \omega_\beta \omega_\beta \rangle$$

since $\omega_\beta \omega_\beta \geq 0$.

The multiplication of the Taylor series for velocity and flexion vector fluctuations and averaging produces the series

$$\begin{aligned} \langle v_\gamma'' f_\gamma'' \rangle &= \langle a_1 a_0^f + c_1 c_0^f \rangle y^+ + \langle a_1 a_1^f + a_2 a_0^f + b_2 b_0^f + c_1 c_1^f + c_2 c_0^f \rangle y^{+2} \\ &+ \langle a_1 a_2^f + a_2 a_1^f + a_3 a_0^f + b_2 b_1^f + b_3 b_0^f + c_1 c_2^f + c_2 c_1^f + c_3 c_0^f \rangle y^{+3} + O(y^{+4}) \end{aligned}$$

Hence, the correlation is zero at the wall and grows with the slope

$$\frac{\partial}{\partial y^+} \langle v_\gamma'' f_\gamma'' \rangle(0) = \langle a_1 a_0^f + c_1 c_0^f \rangle$$

The same operations applied to the fluctuating enstrophy lead to

$$\begin{aligned} \langle \omega_\gamma'' \omega_\gamma'' \rangle &= \langle a_0^{\omega 2} + c_0^{\omega 2} \rangle + 2 \langle a_0^\omega a_1^\omega + c_0^\omega c_1^\omega \rangle y^+ + \langle a_1^{\omega 2} + 2a_0^\omega a_2^\omega + b_1^{\omega 2} + c_1^{\omega 2} + 2c_0^\omega c_2^\omega \rangle y^{+2} \\ &+ 2 \langle a_0^\omega a_3^\omega + a_1^\omega a_2^\omega + b_1^\omega b_2^\omega + c_0^\omega c_3^\omega + c_1^\omega c_2^\omega \rangle y^{+3} + O(y^{+4}) \end{aligned}$$

The value at the wall is thus non-zero $\langle \omega_\gamma'' \omega_\gamma'' \rangle(0) = \langle a_0^{\omega 2} + c_0^{\omega 2} \rangle$ with slope

$$\frac{\partial}{\partial y^+} \langle \omega_\gamma'' \omega_\gamma'' \rangle(0) = 2 \langle a_0^\omega a_1^\omega + c_0^\omega c_1^\omega \rangle$$

which may be positive or negative.

Solutions to problems in Chap. 22: The limit of infinite Reynolds number for incompressible fluids.

Problem (22.1): Consider a materially invariant admissible circuit \mathcal{C} , as defined in Sect. 2.6.3, embedded in a flow field \mathcal{D} . The incompressible fluid is in turbulent motion governed by the Navier–Stokes pdes. Assume that appropriate reference values exist and the Reynolds number $Re \gg 1$ is well defined.

(22.1.1) Establish the time rate of change of circulation Γ , defined in the material description by

$$\Gamma(\mathcal{C}, \tau) = \int_{\mathcal{C}(\tau)} \mathbf{V}(\tau, \mathbf{X}(p)) \cdot d\Phi(\tau, \mathbf{X}(p))$$

where the circuit \mathcal{C} at the reference time is specified by $\mathbf{X}(p)$ with $0 \leq p \leq 1$ being Lagrangean line parameter (Lagrangean line parameters are materially invariant), $\Phi(\tau, \mathbf{X})$ denotes the position of a material point at time τ that was at \mathbf{X} at the reference time. Velocity in the material description is by definition $\mathbf{V} = \frac{\partial \Phi}{\partial \tau}$.

(22.1.2): Transform the result of (22.1.1) to the spatial description.

(22.1.3): Compute the circulation using the Navier–Stokes pdes for $0 \ll Re < \infty$ and inviscid fluids.

(22.1.4): Evaluate the limit $Re \rightarrow \infty$ under following assumptions:

(a) The vorticity field remains smooth $\omega \in C_D^1$.

(b) The vorticity field becomes Hölder continuous with exponent $\alpha \leq \frac{1}{3}$.

Solution: 22.1:

The time rate of change of Γ

$$\frac{d}{d\tau} \Gamma(\mathcal{C}, \tau) = \frac{d}{d\tau} \int_{\mathcal{C}(\tau)} \mathbf{V}(\tau, \mathbf{X}(p)) \cdot d\Phi(\tau, \mathbf{X}(p))$$

can be evaluated by transforming the integral to the reference time zero using $dx_\alpha(p, t) = F_{\alpha\beta}(\mathbf{X}(p), \tau) dX_\beta(p)$ ([4], Sect. 2.10). Hence, for the vector field velocity $V_\alpha(\tau, \mathbf{X})$ in Cartesian coordinates

$$\frac{d}{d\tau} \Gamma(\mathcal{C}, \tau) = \frac{d}{d\tau} \int_{\mathcal{C}(0)} V_\alpha(\tau, \mathbf{X}(p)) F_{\alpha\beta}(\tau, \mathbf{X}(p)) dX_\beta(p)$$

is obtained, where $F_{\alpha\beta} = \frac{\partial \Phi_\alpha}{\partial X_\beta}$ is the Lagrangean deformation gradient tensor (2.82). The time derivative commutes with integration, hence

$$\frac{d}{d\tau} \Gamma(\mathcal{C}, \tau) = \int_{\mathcal{C}(0)} \left[\frac{\partial V_\alpha}{\partial \tau}(\tau, \mathbf{X}(p)) F_{\alpha\beta}(\tau, \mathbf{X}(p)) + V_\alpha(\tau, \mathbf{X}(p)) \frac{\partial F_{\alpha\beta}}{\partial \tau}(\tau, \mathbf{X}(p)) \right] dX_\beta(p)$$

follows. Using (2.82) and implicit differentiation to get

$$\frac{\partial F_{\alpha\beta}}{\partial \tau}(\mathbf{X}, \tau) = \frac{\partial V_\alpha}{\partial X_\beta}(\mathbf{X}, \tau) = \frac{\partial v_\alpha}{\partial X_\beta}(t, \Phi(\tau, \mathbf{X})) = \frac{\partial v_\alpha}{\partial x_\gamma}(t, \mathbf{x}) \frac{\partial \Phi_\gamma}{\partial X_\beta}(\tau, \mathbf{X})$$

hence

$$\frac{d}{d\tau} \Gamma(\mathcal{C}, \tau) = \int_{\mathcal{C}(\tau)} \left[\frac{\partial V_\gamma}{\partial \tau}(\tau, \mathbf{X}(p)) + V_\alpha(\tau, \mathbf{X}(p)) \frac{\partial v_\alpha}{\partial x_\gamma}(t, \mathbf{x}) \right] dx_\gamma(t, \mathbf{x}(p))$$

in mixed formulation (note the transformation rule $\mathbf{v}(t, \mathbf{x}) = \mathbf{V}(\tau, \mathbf{X})$ for $\mathbf{x} = \Phi(\tau, \mathbf{X})$, $t = \tau$). The pure material description follows from the transformation rules and (25.128) as

$$\frac{d}{d\tau} \Gamma(\mathcal{C}, \tau) = \int_{\mathcal{C}(\tau)} \left[\frac{\partial V_\gamma}{\partial \tau}(\tau, \mathbf{X}(p)) + \frac{1}{2F} \epsilon_{\gamma\beta\xi} \epsilon_{\delta\eta\omega} V_\alpha(\tau, \mathbf{X}(p)) F_{\beta\eta} F_{\xi\omega} \frac{\partial V_\alpha}{\partial X_\delta}(\tau, \mathbf{X}(p)) \right] d\Phi_\gamma(\tau, \mathbf{X}(p)) \quad (28.16)$$

where $F = \det(\mathbf{F})$ is the Jacobian, which is unity for incompressible fluids.

(22.1.2): Transform the result of (22.1.1) to the spatial description.

The equation

$$\frac{d}{d\tau} \Gamma(\mathcal{C}, \tau) = \int_{\mathcal{C}(\tau)} \left[\frac{\partial V_\gamma}{\partial \tau}(\tau, \mathbf{X}(p)) + V_\alpha(\tau, \mathbf{X}(p)) \frac{\partial v_\alpha}{\partial x_\gamma}(t, \mathbf{x}) \right] dx_\gamma(t, \mathbf{x}(p))$$

was obtained in the previous step; hence, the pure spatial version of (28.16) is as follows:

$$\frac{d}{dt} \Gamma(\mathcal{C}, t) = \int_{\mathcal{C}(t)} \left[\frac{Dv_\gamma}{Dt}(t, \mathbf{x}(p)) + v_\alpha(t, \mathbf{x}(p)) \frac{\partial v_\alpha}{\partial x_\gamma}(t, \mathbf{x}(p)) \right] dx_\gamma(t, \mathbf{x}(p)) \quad (28.17)$$

using $\frac{\partial V_\gamma}{\partial \tau} = \frac{Dv_\gamma}{Dt}$, where $\mathbf{x}(p)$ is the parametric form of the circuit $\mathcal{C}(t)$ at time t .

(22.1.3): Compute the circulation using the Navier–Stokes pdes for $0 \ll Re < \infty$ and inviscid fluids.

The time rate of change of circulation according to the previous section is (28.17)

$$\frac{d\Gamma}{dt}(\mathcal{C}, t) = \int_{\mathcal{C}(t)} \left[\frac{Dv_\gamma}{Dt}(t, \mathbf{x}(p)) + v_\alpha(t, \mathbf{x}(p)) \frac{\partial v_\alpha}{\partial x_\gamma}(t, \mathbf{x}(p)) \right] dx_\gamma(t, \mathbf{x}(p))$$

The second term can be evaluated noting that

$$\int_{\mathcal{C}(t)} v_\alpha(t, \mathbf{x}(p)) \frac{\partial v_\alpha}{\partial x_\gamma}(t, \mathbf{x}(p)) dx_\gamma(t, \mathbf{x}(p)) = \frac{1}{2} \int_{\mathcal{C}(t)} \frac{\partial}{\partial x_\gamma}(v_\alpha v_\alpha)(t, \mathbf{x}(p)) dx_\gamma(t, \mathbf{x}(p)) = 0$$

holds, since the differential on the right side is exact; hence,

$$\frac{d\Gamma}{dt}(\mathcal{C}, t) = \int_{\mathcal{C}(t)} \frac{Dv_\alpha}{Dt}(t, \mathbf{x}(p)) dx_\alpha(t, \mathbf{x}(p))$$

is the desired kinematic result in the spatial description and

$$\frac{d\Gamma}{d\tau}(\mathcal{C}, \tau) = \int_{\mathcal{C}(\tau)} \frac{\partial V_\gamma}{\partial \tau}(\tau, \mathbf{X}(p)) d\Phi_\gamma(\tau, \mathbf{X}(p)) \quad (28.18)$$

in the material description. The time rate of change of circulation is determined by the line integral of acceleration. It follows that the circulation is independent of time if acceleration can be represented as the gradient of a scalar potential.

Inviscid fluids: The momentum balance (2.2) is reduced to

$$\frac{Dv_\alpha}{Dt} = -\frac{\partial}{\partial x_\alpha}(p + \Phi)$$

where the acceleration of gravity $g_\alpha = -\frac{\partial \Phi}{\partial x_\alpha}$ is the gradient of a potential Φ . Acceleration is, therefore, the gradient of the scalar field $p + \Phi$ and it follows that

$$\frac{d\Gamma}{dt}(\mathcal{C}, t) = 0$$

holds.

Viscous fluids: The momentum balance (2.2) is recast in terms of vorticity

$$\frac{Dv_\alpha}{Dt} = -\frac{\partial}{\partial x_\alpha}(p + \Phi) - \frac{1}{Re}\epsilon_{\alpha\beta\gamma}\frac{\partial\omega_\gamma}{\partial x_\beta}$$

Hence,

$$\frac{d\Gamma}{dt}(\mathcal{C}, t) = -\frac{1}{Re}\epsilon_{\alpha\beta\gamma}\int_{\mathcal{C}(t)}\frac{\partial\omega_\gamma}{\partial x_\beta}(t, \mathbf{x}(p))dx_\alpha(t, \mathbf{x}(p))$$

is non-zero for viscous fluids. Note that the gradient of a scalar field such as $p + \Phi$ integrates to zero for a closed path $\mathcal{C}(t)$.

(22.1.4): Evaluate the limit $Re \rightarrow \infty$ under the following assumptions:

(a) The vorticity field remains smooth $\omega \in C_D^1$.

If vorticity remains smooth as $Re \rightarrow \infty$, the integral over the circuit remains bounded and

$$\lim_{Re \rightarrow \infty} \frac{d\Gamma}{dt}(\mathcal{C}, t) = 0$$

holds. Vorticity becomes a frozen vector field and enstrophy an inviscid invariant.

(b) The vorticity field becomes Hölder continuous with exponent $\alpha \leq \frac{1}{3}$.

The derivative of vorticity becomes singular as $Re \rightarrow \infty$ and it follows that

$$\lim_{Re \rightarrow \infty} \frac{1}{Re} \frac{d\Gamma}{dt}(\mathcal{C}, t)$$

is indeterminate. This has serious implications, since the limit $Re \rightarrow \infty$ is singular and the Kelvin theorem does not hold in this limit, see Tsinober [12] Chap. 6 and Sect. 22.2.2.

Problem 22.2: Orlandi and Carnevale [62] argue that the nonlinear amplification of vorticity in inviscid interaction is a candidate for the appearance of a finite-time

singularity of the second kind starting from smooth initial data, check Eq. (3.15) in Chap. 3 for definition. The ode

$$\frac{\partial \Phi}{\partial t} = \Phi^2$$

with initial condition $\Phi(0) > 0$ is a simplified version of the vorticity pde. It has a finite-time singularity developing from positive initial data. Prove this.

Solution:

The solution of the ode is straightforward using separation of variables

$$\frac{d\Phi}{\Phi^2} = dt$$

hence

$$-\Phi^{-1} = t + c$$

The initial condition leads to $c = -\Phi^{-1}(0)$ and finally to

$$\Phi(t) = -\frac{1}{t - \Phi^{-1}(0)} \text{ or } \Phi(t) = \frac{\Phi(0)}{1 - t\Phi(0)}$$

It is evident that this solution becomes singular for $\Phi(0) > 0$ at time $t^* = \frac{1}{\Phi(0)}$. The larger the initial value, the sooner the singularity appears.

Comments: The vorticity pde (2.63) for incompressible and inviscid fluids is

$$\frac{D\omega_\alpha}{Dt} = s_{\alpha\beta}\omega_\beta$$

hence

$$\frac{De^2}{Dt} = 2\omega_\alpha s_{\alpha\beta}\omega_\beta$$

where $s_{\alpha\beta}$ is the rate of strain tensor (2.53) and $e^2 \equiv \omega_\alpha\omega_\alpha$ enstrophy squared (3.16). If the coordinate system is rotated at time t to the eigendirections of the (symmetric) rate of strain tensor and if vorticity is aligned with the eigendirection with a positive eigenvalue proportional to vorticity, then the ode of the problem is valid for the time interval this assumption holds. Hence, this situation is a candidate for a finite-time singularity. However, even for the Euler equations exists a phenomenon called depletion of nonlinearity (Frisch [63], Sect. 7.8) counteracting the formation of a singularity.

Problem 22.3: Show that the Duchon–Robert smoothness term $D(\mathbf{v})$ in Sect. 22.3 is zero for the following class of velocity fields: $\mathbf{v}(\mathbf{x}, t)$

$$\int_{\mathcal{D}} d\mathbf{w} |\mathbf{v}(\mathbf{x} + \mathbf{w}, t) - \mathbf{v}(\mathbf{x}, t)|^3 \leq C(t) |\mathbf{w}| \sigma(|\mathbf{w}|)$$

where $\int_0^T dt C(t) < \infty$ and $\lim_{|\mathbf{w}| \rightarrow 0} \sigma(|\mathbf{w}|) = 0$.

Solution:

The smoothness term (22.40) with mollifier (22.38) added to the weak form of the energy pde (22.41) is

$$D_\epsilon[\mathbf{v}] = \frac{1}{4} \int_{\mathcal{D}_\varphi} d\mathbf{w} \nabla \varphi_\epsilon(\mathbf{w}) \cdot \Delta \mathbf{v} (\Delta \mathbf{v})^2, \quad \Delta(\mathbf{v}) \equiv \mathbf{v}(\mathbf{x} + \mathbf{w}) - \mathbf{v}(\mathbf{x})$$

hence

$$|D_\epsilon[\mathbf{v}]| \leq \int_{\mathcal{D}} d\mathbf{w} |\nabla \varphi_\epsilon(\mathbf{w})| |\Delta \mathbf{v}|^3$$

Integration over the space–time domain $\mathcal{D} \times [0, T]$ leads to

$$\int_0^T dt \int_{\mathcal{D}} d\mathbf{x} |D_\epsilon[\mathbf{v}]| \leq \int_0^T dt \int_{\mathcal{D}} d\mathbf{x} \int_{\mathcal{D}} d\mathbf{w} |\nabla \varphi_\epsilon(\mathbf{w})| |\Delta \mathbf{v}|^3$$

and using the properties of the velocity field and (22.38) $\varphi_\epsilon = \frac{1}{\epsilon^3} \varphi(\frac{\mathbf{w}}{\epsilon})$

$$\int_0^T dt \int_{\mathcal{D}} d\mathbf{x} |D_\epsilon[\mathbf{v}]| \leq \int_0^T dt C(t) \int_{\mathcal{D}} d\mathbf{w} \frac{1}{\epsilon^4} |\nabla \varphi(\frac{\mathbf{w}}{\epsilon})| |\mathbf{w}| \sigma(|\mathbf{w}|)$$

Setting $\mathbf{w} = \epsilon \mathbf{z}$ leads to $d\mathbf{w} = \epsilon^3 d\mathbf{z}$ and

$$\int_0^T dt \int_{\mathcal{D}} d\mathbf{x} |D_\epsilon[\mathbf{v}]| \leq \int_0^T dt C(t) \int_{\mathcal{D}} d\mathbf{z} |\nabla \varphi(\mathbf{z})| |\mathbf{z}| \sigma(\epsilon |\mathbf{z}|)$$

and letting $\epsilon \rightarrow 0$ results in

$$\lim_{\epsilon \rightarrow 0} \int_0^T dt \int_{\mathcal{D}} d\mathbf{x} |D_\epsilon[\mathbf{v}]| = 0$$

since $\int_0^T dt C(t) < \infty$ and $\sigma(\epsilon \mathbf{z}) \rightarrow 0$ as $\epsilon \rightarrow 0$.

Reference: The solution was taken from the paper ([64], proposition 3) by Duchon and Robert.

Solutions to problems in Sect. 23.12: Integration in finite-dimensional spaces.

Problem 23.12.1: Compute the volume

$$V_n(\rho) = \int_{\|\mathbf{x}\| < \rho} d\mathbf{x}$$

of the ball $B_n(\rho) \equiv \{x \in R^n : \|x\| \leq \rho\}$ with radius $\rho = 1$ (unit ball) in R^n for the L^2 norm in Cartesian coordinates

$$\|\mathbf{x}\| \equiv \left(\sum_{j=1}^n |x_j|^2 \right)^{\frac{1}{2}}$$

where \mathbf{x} is a n -dimensional vector.

Solution: Consider the product space $R_{\mathbf{x}}^n \otimes R_t^+$ with the product measure $\mu_n \otimes \mu_1$ and define the integral

$$I \equiv \iint_{(\mathbf{x}, \rho) \in R_{\mathbf{x}}^n \otimes R_\rho^+, \|\mathbf{x}\| < \rho} \rho \exp(-\rho^2) d\rho d\mathbf{x}$$

This integral can be recast with the aid of the characteristic function

$$\mathbf{1}_{(\mathbf{x}, \rho) \in R_{\mathbf{x}}^n \otimes R_\rho^+, \|\mathbf{x}\| < \rho}(\mathbf{x}, \rho) = \begin{cases} 1 & \text{if } \mathbf{x} \in R_{\mathbf{x}}^n \text{ and } \|\mathbf{x}\| < \rho \\ 0 & \text{otherwise} \end{cases}$$

hence

$$V_n(\rho) = \int_{R_{\mathbf{x}}^n} \mathbf{1}_{(\mathbf{x}, \rho) \in R_{\mathbf{x}}^n \otimes R_\rho^+, \|\mathbf{x}\| < \rho}(\mathbf{x}, \rho) d\mathbf{x}$$

and

$$I = \int_{R_{\mathbf{x}}^n} \int_0^\infty \mathbf{1}_{(\mathbf{x}, \rho) \in R_{\mathbf{x}}^n \otimes R_\rho^+, \|\mathbf{x}\| < \rho}(\mathbf{x}, \rho) \rho \exp(-\rho^2) d\rho d\mathbf{x}$$

This integral can be computed in two ways. Notice that

$$I = \int_0^\infty d\rho V_n^p(\rho) \rho \exp(-\rho^2)$$

holds, if the integration over $B^n(\rho)$ is carried out first. Rescaling the spatial variable \mathbf{x} according to $y_\alpha \equiv \frac{x_\alpha}{\rho}$, $\alpha = 1, \dots, n$, hence $d\mathbf{x} = dy \rho^n$ and

$$I = V_n^p(1) \int_0^\infty d\rho \rho^{1+n} \exp(-\rho^2)$$

The second factor on the right side is recognized as the Gamma function ([15], Chap. 5) defined by

$$\Gamma(z) = \int_0^\infty dt t^{z-1} \exp(-t), \quad t = \rho^2, \quad \Gamma(z) = 2 \int_0^\infty d\rho \rho^{2z-1} \exp(-\rho^2)$$

hence

$$\int_0^\infty d\rho \rho^{1+n} \exp(-\rho^2) = \frac{1}{2} \Gamma\left(\frac{n}{2} + 1\right)$$

and finally

$$I = V_n^p(1) \frac{1}{2} \Gamma\left(\frac{n}{2} + 1\right) \quad (\text{E.10})$$

Furthermore, the integration can be done directly

$$I = \int_0^\infty \int_{R_x^n} \mathbf{1}_{(\mathbf{x}, \rho) \in R_x^n \otimes R_\rho^+, ||\mathbf{x}|| < \rho}(\mathbf{x}, \rho) \rho \exp(-\rho^2) d\mathbf{x} d\rho = \int_{R^n} \left(\int_{||\mathbf{x}||}^\infty \rho \exp(-\rho^2) d\rho \right) d\mathbf{x}$$

hence

$$I = \frac{1}{2} \int_{R^n} \exp(-||\mathbf{x}||^2) d\mathbf{x}$$

and

$$I = \frac{1}{2} \pi^{\frac{n}{2}}$$

Combining the result with (E.11) leads to the desired expression

$$V_n(1) = \frac{\pi^{\frac{n}{2}}}{\Gamma(\frac{n}{2} + 1)}$$

in agreement with Eq. (23.94).

Reference: See Lerner [65] Sect. 4.5 page 211 for the proof and Wang [66], Folland [67] in Sect. 23.12.1 for the extension to generalized balls, and also Problem 23.12.3.

Problem 23.12.2: Compute the volume

$$V_n^p(\rho) = \int_{\|\mathbf{x}\|_p < \rho} d\mathbf{x}$$

of the ball $B_n(\rho) \equiv \{\mathbf{x} \in R^n : \|\mathbf{x}\|_p \leq \rho\}$ with radius $\rho = 1$ (unit ball) in R^n for the L^p norm (23.18)

$$\|\mathbf{x}\|_p \equiv \left(\sum_{j=1}^n |\mathbf{x}|^p \right)^{\frac{1}{p}}$$

for $1 < p < \infty$. Plot the volume $V_n^p(1)$ as function of n and p .

Solution: Consider the product space $R_x^n \otimes R_t^+$ with the product measure $\mu_n \otimes \mu_1$ and define the integral

$$I \equiv \iint_{(\mathbf{x}, \rho) \in R_x^n \otimes R_\rho^+, \|\mathbf{x}\|_p < \rho} \rho^{p-1} \exp(-\rho^p) d\rho d\mathbf{x}$$

Figure 23.4 illustrates the shape of spheres in L^p spaces for the dimension $n = 3$ and two L^p norms for $p = 0.5, p = 3.0$. This integral can be recast with the aid of the characteristic function

$$\mathbf{1}_{(\mathbf{x}, \rho) \in R_x^n \otimes R_\rho^+, \|\mathbf{x}\|_p < \rho}(\mathbf{x}, \rho) = \begin{cases} 1 & \text{if } \mathbf{x} \in R_x^n \text{ and } \|\mathbf{x}\|_p < \rho \\ 0 & \text{otherwise} \end{cases}$$

hence

$$V_n^p(\rho) = \int_{R_x^n} \mathbf{1}_{(\mathbf{x}, \rho) \in R_x^n \otimes R_\rho^+, \|\mathbf{x}\|_p < \rho}(\mathbf{x}, \rho) d\mathbf{x}$$

and

$$I = \int_{R_x^n} \int_0^\infty \mathbf{1}_{(\mathbf{x}, \rho) \in R_x^n \otimes R_\rho^+, \|\mathbf{x}\|_p < \rho}(\mathbf{x}, \rho) \rho^{p-1} \exp(-\rho^p) d\rho d\mathbf{x}$$

This integral can be computed in two ways. Notice that

$$I = \int_0^\infty d\rho V_n^p(\rho) \rho^{p-1} \exp(-\rho^p)$$

holds, if the integration over $B^n(\rho)$ is carried out first. Rescaling the spatial variable \mathbf{x} according to $y_\alpha \equiv \frac{x_\alpha}{\rho}$, $\alpha = 1, \dots, n$, hence $d\mathbf{x} = dy \rho^n$ and

$$I = V_n^p(1) \int_0^\infty d\rho \rho^{p+n-1} \exp(-\rho^p)$$

The second factor on the right side is recognized as the Gamma function ([15], Chap. 5) defined by

$$\Gamma(z) = \int_0^\infty dt t^{z-1} \exp(-t), \quad t = \rho^2, \quad \Gamma(z) = 2 \int_0^\infty d\rho \rho^{2z-1} \exp(-\rho^2)$$

hence

$$\int_0^\infty d\rho \rho^{p+n-1} \exp(-\rho^p) = \frac{1}{p} \Gamma\left(\frac{n}{p} + 1\right)$$

and finally

$$I = V_n^p(1) \frac{1}{p} \Gamma\left(\frac{n}{p} + 1\right) \quad (\text{E.11})$$

Furthermore, the integration can be done directly

$$I = \int_0^\infty \int_{R_{\mathbf{x}}^n} \mathbf{1}_{(\mathbf{x}, \rho) \in R_{\mathbf{x}}^n \otimes R_\rho^+}(\mathbf{x}, \rho) \rho^{p-1} \exp(-\rho^p) d\mathbf{x} d\rho = \int_{R^n} \left(\int_{||\mathbf{x}||}^\infty \rho^{p-1} \exp(-\rho^p) d\rho \right) d\mathbf{x}$$

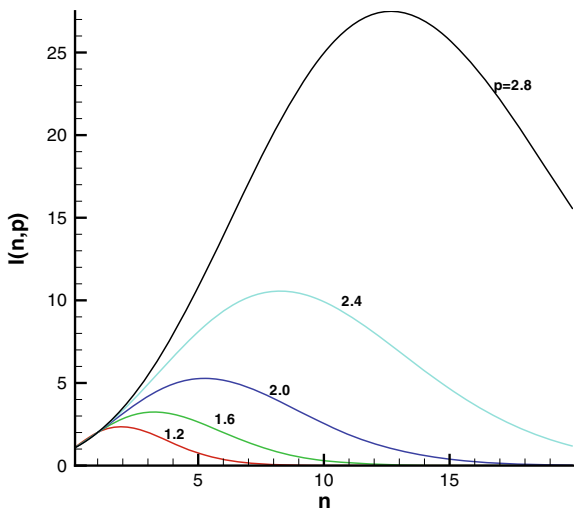
hence

$$I = \frac{1}{p} \int_{R^n} \exp(-||\mathbf{x}||^p) d\mathbf{x} = \frac{1}{p} \left(\int_{R^1} \exp(-|\rho|^p) d\rho \right)^n$$

and

$$I = \frac{2^n}{p^{n+1}} \Gamma\left(\frac{1}{p}\right)^n$$

Fig. 28.28 Volume integral $V_n^p(1)$ of the unit ball as function of dimension n for several values of p (23.18) as indicated



Combining the result with Eq. (E.10) leads to the desired expression

$$V_n^p(1) = \left(\frac{2}{p}\right)^n \frac{\Gamma(\frac{1}{p})^n}{\Gamma(\frac{n}{p} + 1)}$$

Fig. 28.28 shows the volume of the unit ball as function of the dimension n for $p = 2.8$ to 1.2 starting on top with the black line for $p = 2.8$. The dependence of the volume as function of dimension has the typical bell-shaped curve with maximum that shifts to higher dimension for increasing p . This is consistent with the shape of the ball that approaches a cube with increasing p as Fig. 23.4 illustrates. This is clearly evident in Fig. 28.29 where $V_n^p(1)$ is plotted as function of the dimension n and the exponent p . The variation with respect to the exponent p for given dimension n is not monotonic (Fig. 28.30).

Reference: Lerner [65] Sect. 4.5 page 212 and Wang [66], Folland [67] in Sect. 23.12.1.

Problem (23.12.3): Compute the volume of the generalized balls (23.118) for $n = 3$ and $\mathbf{p} = (0.2, 0.5, 2)^T$ and $\mathbf{p} = (0.2, 1.5, 2)^T$. Plot the balls and the volume $V(0.2, p_2, 2)$ as function of $0.1 \leq p_2 \leq 10$.

Solution: The volume of generalized balls is according to Wang's theorem given by Eq. (23.118)

$$V(B_{p_1, \dots, p_n}) = 2^n \frac{\prod_{j=1}^n \Gamma(1 + \frac{1}{p_j})}{\Gamma(1 + \sum_{j=1}^n \frac{1}{p_j})}$$

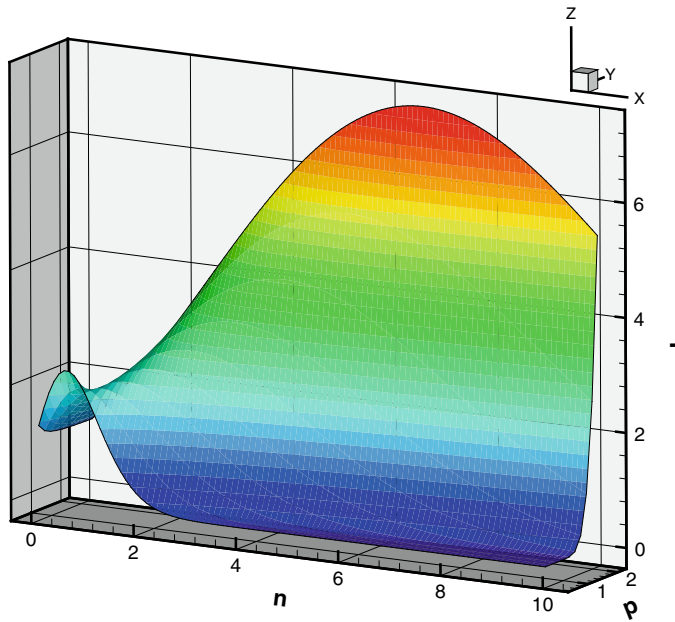


Fig. 28.29 Volume integral $V_n^p(1)$ of the unit ball in R^n as function of dimension n and the norm exponent p (23.18)

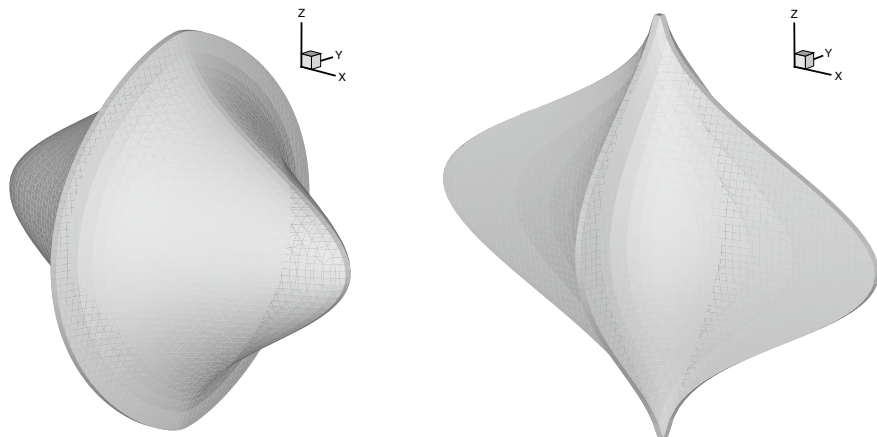
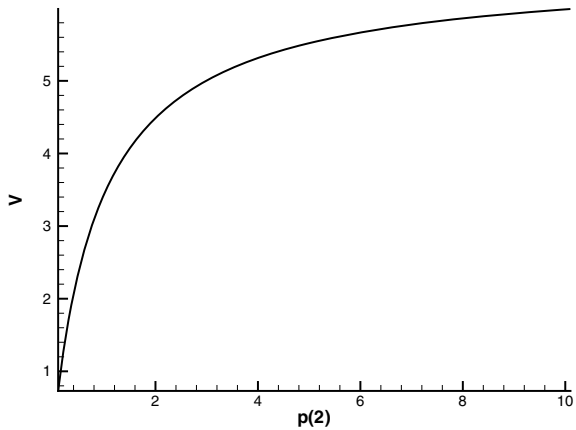


Fig. 28.30 Generalized balls (23.118) for $p_1 = 0.2, p_2 = 1.5, p_3 = 2$ (left graph) and $p_1 = 0.2, p_2 = 0.5, p_3 = 2$ (right graph)

Fig. 28.31 Volume of generalized balls (23.118) $V(0.2, p_2, 2)$ as function of p_2



where $n = 3$ for the present problem. The volumes are then $V(2, 0.5, 2.5) = 2.37408733$ and $V(0.2, 0.5, 2) = 0.121241763$. The variation of the volume $V(0, 2, p(2), 2)$ as function of $p(2)$ is shown in Fig. 28.31. The profile of the volume indicates the approach to a positive and finite asymptotic value for $p(2) \rightarrow \infty$.

The generalized balls $B_{p_1, \dots, p_n} \equiv \{(x_1, \dots, x_n) : \sum_{j=1}^n |x_j|^{p_j} \leq 1\}$ are dominated by p_2 increasing with $p_j, j \neq 2$ kept constant, generating a spindly structure in the x_2 -direction.

Comments: The generalized balls are not convex, if one of the exponents $p_j < 1$, but they are convex if $p_j \geq 1 \forall j$. The volume obtained above agrees, of course, with the result for balls in L^p spaces computed in Problem (23.12.2)

$$V_n^p(1) = \left(\frac{2}{p}\right)^n \frac{\Gamma(\frac{1}{p})^n}{\Gamma(\frac{n}{p} + 1)} = 2^n \frac{\Gamma(1 + \frac{1}{p})^n}{\Gamma(\frac{n}{p} + 1)},$$

by setting the exponents $p_j = p, \forall j$. Balls in Euclidean space R^n play an important role in the evaluation of integrals over compact sets with orientable boundary and the Lévy-Laplacian, which is one of several Laplacians defined in infinite-dimensional spaces.

Problem (23.19.1): The Lebesgue integrals $I_N(f)$ over the ball $\mathcal{B}(r)$ of radius $0 < r < \infty \in R^N$ for $N > 2$

$$I_N(f) \equiv \int_{\mathcal{B}_N} d\mu_N f(\rho), \quad d\mu_N = \prod_{k=1}^N dx_k$$

vanish as $N \rightarrow \infty$ for bounded integrands $f(\rho)$.

(23.19.1.1) Construct a modified measure differential $d\mu_R$

$$d\mu_R(\mathbf{x}) \equiv \frac{d\mu_N}{N(\mathbf{x})}$$

for the computation of the geometric average in the form

$$\bar{I}_N(f; r) = \int_{\mathcal{B}_N(r)} d\mu_R f(\mathbf{x})$$

such that the limit $N \rightarrow \infty$ is non-zero. It is recommended to use spherical coordinates, see Sect. 23.15 for definitions.

Solution: The Lebesgue measure differential in R^N equipped with spherical coordinates (Sect. 23.15) is given by

$$d\mu_N = \rho^{N-1} d\rho \prod_{k=1}^{N-2} \sin^{N-1-k}(\Phi_k) d\Phi_k d\Phi_{N-1}$$

for $0 \leq \rho \leq r$ and $0 \leq \Phi_k \leq \pi$, $1 \leq k \leq N-2$, $0 \leq \Phi_{N-1} \leq 2\pi$. The modified measure differential is constructed in the form

$$d\mu_R = \frac{d\mu_N}{N(r, \Phi_1, \dots, \Phi_{N-1})}$$

The first attempt to construct the denominator is

$$N(r) = rA(r) = \frac{2\pi^{\frac{N}{2}} r^N}{\Gamma(\frac{N}{2})}$$

only a function of the ball radius r , where $A(r)$ is the area of the sphere (23.115). The geometric average of a function $f(\rho, \Phi_1, \dots, \Phi_{N-1})$

$$\bar{I}_N(f) = \frac{\Gamma(\frac{N}{2})}{2\pi^{\frac{N}{2}}} \int_0^1 d\zeta \zeta^{N-1} \int_0^\pi d\Phi_1, \dots, \int_0^\pi d\Phi_{N-2} \prod_{k=1}^{N-2} \sin^{N-1-k}(\Phi_k) \int_0^{2\pi} d\Phi_{N-1} f(r\zeta, \Phi_1, \dots, \Phi_{N-1})$$

where $\zeta \equiv \frac{\rho}{r}$. The integration can be carried out for $f(r\zeta)$ with the aid of (23.140) resulting in

$$\bar{I}_N(f) = \int_0^1 d\zeta \zeta^{N-1} f(r\zeta)$$

The $N \rightarrow \infty$ can be evaluated and, unfortunately, the result

$$\lim_{N \rightarrow \infty} \int_0^1 d\zeta \zeta^{N-1} f(r\zeta) = 0$$

is obtained for bounded $f(r)$.

This result indicates how to construct a modified measure differential with a bounded and non-zero result. The new choice

$$N(\rho) \equiv A(\rho) = \frac{2\pi^{\frac{N}{2}} \rho^{N-1}}{\Gamma(\frac{N}{2})}$$

for the denominator is the surface area of a sphere with the current radius ρ . The geometric average for an integrable function $f(\rho)$ over a ball of radius r is then

$$\bar{I}_N(f) = \int_0^r d\rho f(\rho) \frac{\rho^{N-1}}{N(\rho)} \int_0^\pi d\Phi_1 \cdots \int_0^\pi d\Phi_{N-2} \prod_{k=1}^{N-2} \sin^{N-1-k}(\Phi_k) \int_0^{2\pi} d\Phi_{N-1}$$

Using (check Sects. 23.12.1 and 23.11 for derivation)

$$\frac{1}{N(\rho)} \prod_{k=1}^{N-2} \int_0^\pi d\Phi_k \sin^{N-1-k}(\Phi_k) = \frac{1}{2\pi \rho^{N-1}}$$

it can be evaluated without difficulty and

$$\lim_{N \rightarrow \infty} \bar{I}_N(f) = \int_0^r d\rho f(\rho)$$

is obtained, which has the desired properties.

Comments: The example verifies that a simple stretching transformation of the Lebesgue measure differential in spherical coordinates, using the surface area of the sphere with the local radius ρ , generates a geometric average that carries over to the limit $\rightarrow \infty$ leading to a bounded and non-zero integral over R^∞ . Specifically, it was shown in Sect. 23.17.2 that the volume of a ball with radius ρ remains positive for the limit $n \rightarrow \infty$, if the radius increases with the square root of the dimension according to Eq. (23.184).

References

1. Bennett, A.: *Lagrangian Fluid Dynamics*. Cambridge University Press, Cambridge, U.K. (2006)
2. Wu, J.-Z., Ma, H.-Y., Zhou, M.-D.: *Vorticity and Vortex Dynamics*. Springer, Berlin (2006)
3. Truesdell, C.A.: *The Kinematics of Vorticity*. Indiana University Press, Bloomington, Indiana (1954)
4. Kollmann, W.: *Fluid Mechanics in Spatial and Material Description*. University Readers, San Diego (2011)
5. Majda, A.J., Bertozzi, A.L.: *Vorticity and Incompressible Flow*. Cambridge University Press, Cambridge, U.K. (2002)
6. Hamman, C.W., Klewicki, J.C., Kirby, R.M.: On the Lamb vector divergence in Navier-Stokes flows. *JFM* **610**, 261–284 (2008)
7. Oberlack, M.: *Symmetrie, Invarianz und Selbstähnlichkeit in der Turbulenz*. Shaker, Aachen, Germany (2000)
8. Oberlack, M., Waclawczyk, M., Rosteck, A., Avsarkisov, V.: Symmetries and their importance for statistical turbulence theory. *Bull. J. SME* **2**, 1–72 (2015)
9. Janocha, D.D., Waclawczyk, M., Oberlack, M.: Lie symmetry analysis of the Hopf functional-differential equation. *Symmetry* **7**, 1536–1566 (2015)
10. Constantin, P.: Euler equations, Navier-Stokes equations and turbulence. In: *Mathematical Foundation of Turbulent Viscous Flows*. Lecture Notes in Mathematics, vol. 1871, pp. 1–43 (2006)
11. Pope, S.B.: *Turbulent Flows*. Cambridge University Press, Cambridge, U.K. (2001)
12. Tsinuber, A.: *An Informal Conceptual Introduction to Turbulence*, 2nd edn. Springer, Dordrecht (2009)
13. Gibbon, J.D., Galanti, B., Kerr, R.M.: Stretching and compression of vorticity in the 3D Euler equations. In: Hunt, J.C.R., Vassilicos, J.C. (eds.) *Turbulence Structure and Vortex Dynamics*, Cambridge University Press (2000)
14. Wilczek, M., Meneveau, C.: Pressure Hessian and viscous contributions to velocity gradient statistics based on Gaussian random fields. *JFM* **756**, 191–225 (2014)
15. Olver, F.W., Lozier, D.W., Boisvert, R.F., Clark, C.W.: *NIST Handbook of Mathematical Functions*. Cambridge University Press, U.K. (2010)
16. Abramowitz, M., Stegun, I.A.: *Handbook of Mathematical Functions*. Dover, New York (1972)
17. Leonard, A., Wray, A.: A new numerical method for the simulation of three-dimensional flow in a pipe. In: Krause E. (ed.) *Lecture Notes in Physics* **170**. Springer, p. 335 (1982)
18. Boyd, J.P.: *Chebyshev and Fourier Spectral Methods*. Dover Publ. Inc., Mineola, New York (2001)
19. Kollmann, W.: Simulation of vorticity dominated flows using a hybrid approach: I formulation. *Comput. Fluids* **36**, 1638–1647 (2007)
20. Canuto, C., Hussaini, M.Y., Zang, T.A.: *Spectral Methods in Fluid Dynamics*. Springer, Berlin (1988)
21. Gelfand, I.M., Yaglom, A.M.: Integration in functional spaces and its application in quantum physics. *J. Math. Physics* **1**, 48–69 (1960)
22. Cameron, R.H., Martin, W.T.: Evaluation of various Wiener integrals by use of certain Sturm-Liouville differential equations. *Bull. Am. Math. Soc.* **51**, 73–90 (1945)
23. Montroll, E.W.: Markoff chains, Wiener integrals and quantum theory. *Comm. Pure Appl. Math.* **5**, 415–453 (1952)
24. Cameron, R.H., Martin, W.T.: Transformations of Wiener integrals under a general class of linear transformations. *Trans. Am. Math. Soc.* **58**, 184–219 (1945)
25. Klauder, J.R.: *A Modern approach to Functional Integration*. Birkhaeuser/Springer, New York (2010)
26. Woyczyński, W.A.: *Burgers-KPZ Turbulence: Goettingen Lectures*. Lecture Notes in Math, vol. 1700. Springer, Berlin (1999)
27. Egorov, A.D., Sobolevsky, P.I., Yanovich, L.A.: *Functional Integrals: Approximate Evaluation and Applications*. Kluwer Academic Publication, Dordrecht (1993)

28. Shen, H.H., Wray, A.A.: Stationary turbulent closure via the Hopf functional equation. *J. Stat. Phys.* **65**, 33–52 (1991)
29. Novikov, E.A.: Random-force method in turbulence theory. *Sov. Phys. JETP* **17**, 1449–1454 (1963)
30. Novikov, E.A.: Functionals and the random-force method in turbulence theory. *Sov. Phys. JETP* **20**, 1290–1294 (1965)
31. Panton, R.L.: *Incompressible Flow*, 2nd edn. Wiley, New York (1996)
32. Lukacs, E.: *Characteristic Functions*. Hafner Publication, New York (1970)
33. Davidson, P.A.: *Turbulence*. Oxford University Press, Oxford, U.K. (2004)
34. Kolmogorov, A.N.: A refinement of previous hypotheses concerning the local structure of turbulence in a viscous, incompressible fluid at high Reynolds number. *JFM* **13**, 82–85 (1962)
35. Curl, R.L.: Dispersed phase mixing: part i. theory and effects in simple reactors. *AIChE J.* **9**, 175–181 (1963)
36. Chen, H., Chen, S., Kraichnan, R.H.: Probability distribution of a stochastically advected scalar field. *Phys. Rev. Lett.* **62**, 2657 (1989)
37. Duffy, D.G.: *Green's Functions with Applications*. Chapman & Hall/CRC, Boca Raton, Florida (2001)
38. Pope, S.B.: Mapping closures for turbulent mixing and reaction. *Theoret. Computat. Fluid Dyn.* **2**, 255–270 (1991)
39. Miller, K.S.: *Multidimensional Gaussian Distributions*. Wiley, New York (1963)
40. Wilczek, M., Xu, H., Ouellette, N.T., Friedrich, R., Bodenschatz, E.: Generation of Lagrangian intermittency in turbulence by a self-similar mechanism. *New J. Phys.* **15**, 055015 (2013)
41. Sagaut, P., Cambron, C.: *Homogeneous Turbulence Dynamics*. Cambridge University Press, New York (2008)
42. Kuksin, S., Shirikyan, A.: *Mathematics of Two-dimensional turbulence*, Cambridge Tracts in Mathematics, vol. 194. Cambridge University Press, U.K. (2012)
43. Meleshko, V.V., van Heijst, G.J.F.: On Chaplygin's investigations of two-dimensional vortex structures in an inviscid fluid. *JFM* **272**, 157–182 (1994)
44. Nickels, T.B.: *Turbulent Coflowing Jets and Vortex Ring Collisions*. University of Melbourne, Australia (1993). PhD thesis
45. Shelley, M.J., Meiron, D.I., Orszag, S.A.: Dynamical aspects of vortex reconnection in perturbed anti-parallel vortex tubes. *JFM* **246**, 613–652 (1993)
46. Nickels, T.B.: Inner scaling for wall-bounded flows subject to large pressure gradients. *JFM* **521**, 217–239 (2004)
47. Vieillefosse, P.: Local interaction between vorticity and shear in a perfect incompressible fluid. *J. Phys. France* **43**, 837–842 (1982)
48. Vieillefosse, P.: Internal motion of a small element of fluid in an inviscid flow. *Physica A* **125**, 150–162 (1984)
49. Cantwell, B.J.: Exact solution of a restricted Euler equation for the velocity gradient tensor. *Phys. Fluids A* **4**, 782–793 (1992)
50. Meneveau, C.: Lagrangian dynamics and models of the velocity gradient tensor in turbulent flows. *Annua. Rev. Fluid Mech.* **43**, 219–245 (2011)
51. Mullin, T., Juel, A., Peacock, T.: Sil'nikov Chaos in Fluid Flows. In: Vassilicos, J.C. (ed.) *Intermittency in Turbulent Flows*, Cambridge University Press. J.C.R. Hunt and J.C. Vassilicos, eds., Cambridge University Press (2001)
52. Shilnikov, L.P., Shilnikov, A.L., Turaev, D.V. Chua, L.O.: *Methods of Qualitative Theory in Nonlinear Dynamics*. vol.I, World Scientific, London (1998)
53. Rektorys, K. (ed.): *Survey of Applicable Mathematics*. MIT Press, Cambridge Mass (1969)
54. Wiggins, S.: *Introduction to Applied Nonlinear Dynamical Systems and Chaos*. Springer, New York (2003)
55. Kusnetsov, Y.A.: *Elements of Applied Bifurcation Theory*. Springer, New York (2004)
56. Barkley, D.: Theoretical perspective on the route to turbulence in a pipe. *JFM* **803**, P1–1 (2016)
57. Kollmann, W., Prieto, M.I.: DNS of the collision of co-axial vortex rings. *Comput. Fluids* **73**, 47–64 (2013)

58. Surana, A., Grunberg, O., Haller, G.: Exact theory of three-dimensional flow separation. Part 1. Steady separation. *JFM* **564**, 57–103 (2006)
59. Chong, M.S., Perry, A.E., Cantwell, B.J.: A general classification of three-dimensional flow fields. *Phys. Fluids A* **2**, 765–777 (1990)
60. Vlaykov, D.G., Wilczek, M.: On the small-scale structure of turbulence and its impact on the pressure field. *JFM* **861**, 422–446 (2018)
61. Townsend, A.A.: The Structure of Turbulent Shear Flow. Cambridge University Press (1956)
62. Orlandi, P., Carnevale, G.F.: Nonlinear amplification of vorticity in inviscid interaction of orthogonal Lamb dipoles. *Phys. Fluids* **19**, 057106 (2007)
63. Frisch, U.: Turbulence: The Legacy of A.N. Kolmogorov. Cambridge University Press (1995)
64. Duchon, J., Robert, R.: Inertial energy dissipation for weak solutions of incompressible Euler and Navier-Stokes equations. *Nonlinearity* **13**, 249–255 (2000)
65. Lerner, N.: A Course on Integration Theory. Birkh/"auser/Springer Basel (2014)
66. Wang, X.: Volumes of Generalized Unit Balls. *Math. Mag.* **78**, 390–395 (2005)
67. Folland, G.B.: How to integrate a polynomial over a sphere. *Am. Math. Mont.* **108**, 446–448 (2001)

Bibliography

1. Arnold, V.I., Goryonov, V.V., Lyashko, O.V., Vasil'ev, V.A.: *Singularity Theory I*. Springer, Berlin (1988)
2. Arnold, V.I. (ed.): *Dynamical Systems VIII: Singularity Theory II*, Encyclopaedia of Math. Sci. vol. 39, Springer, Berlin (1993)
3. Arnold, V.I., Khesin, B.A.: *Topological Methods in Hydrodynamics*. Springer, New York (1998)
4. De Silva, C., Marusic, I., Woodcock, J., Meneveau, C.: Scaling of second and higher-order structure functions in turbulent boundary layers. *JFM* **769**, 654–686 (2015)
5. Doering, C.R., Gibbon, J.D.: *Applied Analysis of the Navier-Stokes Equations*. Cambridge University Press (1995)
6. Donsker, M.D., Lions, J.L.: Fréchet-Volterra Variational equations, boundary value problems and function space integrals. *Acta Mathematica* , 147–228 (1962)
7. Feng, G., O'Brien, E.E.: A mapping closure for multi-species Fickian diffusion. *Phys. Fluids A* **3**, 956–959 (1991)
8. Foias, C., Manley, O., Rosa, R., Temam, R.: *Navier-Stokes Equations and Turbulence*, Encyclopedia of Mathematics and its Applications 83. Cambridge University Press, Cambridge U.K (2001)
9. Friedlander, S., Serre, D. (eds.): *Handbook of Mathematical Fluid Dynamics*, vol. 2. Elsevier, Amsterdam (2003)
10. Gerolymos, G.A., Vallet, I.: The dissipation tensor ϵ_{ij} in wall turbulence. *JFM* **807**, 386–418 (2016)
11. Monin, A.S.: On the Lagrangian equations of the hydrodynamics of an incompressible viscous fluid. *PMM* **26**, 320–327 (1962)
12. Sakai, T., Redekopp, L.G.: An application of one-sided Jacobi polynomials for spectral modeling of vector fields in polar coordinates. *J. Comput. Phys.* **228**, 7069–7085 (2009)
13. Sato, H.: Characteristic Functional of a Probability Measure absolutely continuous with respect to a Gaussian Radon Measure. Office of Naval Research Report (1984). N00014-81-K-0373
14. Shnirelman, A.: Weak solutions of incompressible euler equations. In: Friedlander, S., Serre, D. (eds.) *Handbook of Mathematical Fluid Dynamics*, Vol. 2. North-Holland, pp. 87–116 (2003)
15. Surhone, L.M., Timpson, M.T., Marseken, S.F.: *N-Sphere*. Betascript Publishing (2009)
16. Testa, F.J., Rosen, G.: Theory for incompressible fluid turbulence. *J. Frankl. Inst.* **297**, 127–133 (1974)
17. Townsend, A.A.: Equilibrium layers and wall turbulence. *JFM* **11**, 97–120 (1961)

18. Uglanov, A.V.: *Integration on Infinite-Dimensional Surfaces and its Applications*, Mathematics and its Applications, vol. 496. Kluwer Academic Publication, Dordrecht (2000)
19. Woodcock, J.D., Marusic, I.: The statistical behaviour of attached eddies. *Phys. Fluids* **27**, 015104 (2015)
20. Yang, X., Marusic, I., Meneveau, C.: Moment generating functions and scaling laws in the inertial layer of turbulent wall-bounded flows. *JFM* **791** (2016)

Index

Symbols

R^+ , 235
 R^3 , 7, 9, 18, 34, 74, 94, 207, 257, 311
 R^n , 35, 413, 414
 n -ball, 120, 394, 395, 428, 434
 n -sphere, 394, 395, 423, 424, 427, 428, 430, 431

A

Abbreviation, 10, 50, 197
Acceleration, 696
Acoustic, 60
Adjoint, 154, 612
 operator, 115, 147
Algebra, 106, 107, 407
 finite, 107
 σ , 104–108, 404, 448
Amplification, 50
Analysis, 1
Ansatz, 323
Argument
 field, 164, 207, 209
Assumption, 33
Asymptotic, 2, 4, 8, 32, 42, 63, 66, 67
Attractor, 64, 66, 67, 69, 102
 dimension, 66
 strange, 94
Axiom, 22

B

Balance, 18, 20, 42
 energy, 21
 compressible material, 43
 compressible spatial, 21
 mass, 65

compressible material, 42
compressible spatial, 18
incompressible material, 41
incompressible spatial, 19
momentum, 65
 compressible material, 43
 compressible spatial, 18
 incompressible material, 42, 259
 incompressible spatial, 19
Ball, 7, 120, 394, 447, 449
 generalized, 413
Barotropic, 36, 50, 561, 562
Base, 390
 B-spline, 84
 countably infinite, 454, 509
Basin, 93
Basis, 404
 Schauder, 73, 74, 76, 77, 151, 270, 454
 solenoidal, 78
 vector fields, 476
 solenoidal, 480

Bernoulli
 function, 39, 60, 61
 relation, 60
 theorem, 38
Bessel
 function, 132, 340
 first kind, 320
 modified, 520
 ode, 517, 519

Bifurcation
 Hopf, 277
 period-doubling, 277
 saddle-node, 277
Bijective, 213, 438
Bilinear, 341
Biot–Savart, 34, 562

- Boltzmann, 1
- Borel
- algebra, 108, 125
 - event, 443
 - set, 102
- Boundary layer, 61, 80, 82, 307, 549, 556
- Boundary Value Problem (BVP), 129, 181, 515, 516
- Boundary values
- Dirichlet, 28, 59, 76, 137, 181
 - Neumann, 59, 181, 511, 537
 - Robin, 181
- Bounded, 341
- Boussinesq, 549
- Bragg–Hawthorne, 322
- B-spline, 83, 84
- Bubble, 684
- Burgers
- pde, 3, 160, 610, 611
- Burgers, J.M., 3, 160, 608
- Burst
- active, 277
- C**
- Cantwell, B.J., 20, 22, 26
- Cardinality, 10, 105, 205, 387
- Cascade, 77, 285
- Cauchy, A.L., 43, 562
- Cayley–Hamilton theorem, 328, 678
- Chain, 341
- Chain rule, 24
- Chaos, 66, 146, 384
- Chaotic, 2, 3, 55
- Chaplygin–Lamb dipole, 319, 322
- Chebyshev polynomial, 83
- Chen, Chen and Kraichnan (CCK), 203, 204, 228
- Chong, M.S., 307
- Circuit, 48
- admissible, 47
- Circulation, 311, 374, 378, 694, 696
- Classification, 65, 83, 94, 307, 308
- Closure, 30, 95
- assumption, 6, 103
 - mapping equation, 205, 257
 - model, 8, 222, 541
 - problem, 6, 265
- Codomain, 209
- Coefficient
- Hölder, 390
- Coherent, 299, 300
- Coles, D.E., 556
- Collocation, 512, 589
- Compact, 28–30, 34, 74, 75, 83, 94, 96, 120, 142, 154, 428, 612
- Complete, 20, 21, 29, 31, 73, 74, 109
- Complex, 76, 124, 271
- conjugate, 124, 271, 273, 286, 463, 467, 489, 509
 - helical wave, 274
- Complexity, 63, 342
- Compressible, 6, 17, 18, 21, 34, 35, 42, 47, 60, 61
- inviscid, 36
- Continua, 1
- Continuity, 206, 328, 367, 443
- Hölder, 389, 390
- Continuum
- hypothesis, 1, 2
- Convective, 538
- Convergence, 30, 73, 312, 467, 480
- absolute, 57
 - conditional, 57
 - weak, 58
- Convergent, 227
- Convex, 395, 432
- Coordinates
- Cartesian, 414
 - cylindrical, 131, 452, 507
 - spherical
 - in R^n , 419
- Correlation, 7, 102, 154, 223, 224, 292, 373
- operator, 147, 612
 - tensor, 161
 - two-point, 290, 296
- Corrsin, S., 64, 277, 280
- Couette, 39
- Countable, 433
- Countably, 341
- Counter rotation, 677
- Covariance, 220
- Covering, 381
- Craya, A., 274
- Crocce, 60, 61
- Crocce–Vazsonyi, 60, 61
- Cumulative distribution function (Cdf), 6, 101, 196
- Curl, 34, 35, 58
- Cusp singularity, 310, 328, 364
- D**
- Damköhler number, 22
- Decomposition, 274
- Helmholtz, 392

- Definition of turbulence, 64
Deformation
 rate, 33
Degree of freedom, 67
Dense, 57
Density, 19, 47
Dependence
 sensitive, 56
Depletion of nonlinearity, 698
Derivative
 partial, 400
 substantial, 50, 70, 360
 variational, 401, 402
 weak, 180
Description, 1
 material, 2, 40
 spatial, 2, 17, 18, 131, 452, 508
Determinant, 41, 45, 79, 110, 112, 208, 252, 563, 597, 598
Diagonal, 615
Diffeomorphism, 40, 208, 209, 563, 651
Dilatation, 61, 76
Dimension, 149, 150, 382
 Caratheodory, 382
 fractal, 59
 Hausdorff, 63
 integer, 1
 physical, 11, 269, 457
Dirac
 Pdf, 262
 pseudo function, 179, 197, 242, 371, 402, 427, 513
Direct Numerical Simulation (DNS), 5, 55, 83, 88, 102, 217, 282, 314, 319, 343, 365, 541, 542, 544, 545, 547, 548, 583
Discrete, 1
Discrimination, 278
Disjoint, 104, 185, 334, 360, 408
Dissipation, 280, 288, 289
 function, 21
 rate, 4, 59, 68, 280, 288, 290, 291, 372
 conditional, 198
Dissipative, 59
Distribution
 Duchon–Robert, 20, 371
Disturbance, 322
Divergence, 18, 29, 34
Domain, 74, 208, 404
 compact, 183, 645
 flow, 451, 507
 of definition, 11, 153, 219, 231, 256, 261, 264, 375, 387, 389, 395, 451, 507
 space–time, 29
Dopazo, C., 5
Dual space, 73
Duchon–Robert, 29
Dynamical system, 56
- E**
Eddy, 299, 301
Eigendirection, 698
Eigenfunction, 111
Eigenproblem, 35, 110, 300
 curl, 35
 Laplacian, 35
Eigenvalue, 35, 110, 111, 307, 350, 698
Eigenvector, 35, 39, 350, 434, 615
Elliptic fde, 115
Energy, 18, 42, 59
 internal, 60
 Pdf, 371
 specific, 43
 internal, 43
 kinetic, 43
 potential, 43
Enstrophy, 4, 62, 69, 278, 280, 317, 318, 355, 362, 367, 565, 576, 698
Enthalpy, 2, 21
 total, 61
Entropy, 2
Equation
 characteristic, 350
Ergodic, 334
Ergodicity, 66, 67, 94, 334, 390
Ess sup, 95
Euclidean
 space, 401
Euler, 20
Euler number, 308, 313
Existence, 9, 28, 29
 of singularity, 4
Expectation
 conditional, 189
- F**
Factor
 scale, 233
Fast Fourier Transform (FFT), 456
Feigenbaum M., 67
Fibre, 278
Field, 6, 8, 10
 argument
 Gaussian, 221
 Lagrangian position, 17, 40

- random
 - Gaussian, 204, 220
- reference
 - Gaussian, 222
- scalar, 452, 508
 - periodic, 454, 509
- vector
 - periodic, 90, 589
- Finite Time Singularity (FTS), 321, 322
- Flexion, 34, 51, 355
 - vector, 564
- Flow
 - Beltrami, 61
 - domain, 6, 11, 28, 40, 42, 58, 60, 67, 73–75, 80, 82, 84, 85, 94, 131, 140, 180
 - laminar, 55
 - map, 40
 - parallel, 564
 - plane, 34
 - potential, 319
 - rate, 19, 75
 - turbulent, 55
 - wall-bounded, 307
- Fluid
 - compressible, 44
 - ideal, 47, 55
 - incompressible, 9, 19, 64
 - Newtonian, 55, 59, 101
- Flux, 47
 - conditional, 196
 - diffusive, 187
 - divergence, 197
 - heat, 44
 - pressure, 194
 - source, 192
 - vector, 185
 - viscous, 191
- Folland, G.B., 149, 405, 413
- Force
 - external, 4
 - non-random, 125
 - random, 126
 - gravitational, 132
- Forcing
 - stochastic, 31
- Fourier, 8, 206
 - amplitude, 76, 458
 - vector, 468
 - coefficient, 515
 - kernel, 269
 - series, 458
 - space, 75
- transform, 8, 74, 119, 204, 206, 207, 234, 241, 456, 467, 511
 - discrete, 512, 589
- Fourier–Stieltjes
 - integral, 270
- Fourier transform (FT), 269
- Fox, R.O., 6, 179
- Fractal, 1, 10
- Fréchet
 - derivative, 182, 212
 - differentiable, 401
 - differential, 401, 402
- Friction, 307
 - factor, 75, 372
 - Darcy, 173
- Friedman–Keller, 341
- Frisch, U., 22, 277
- Froude number, 360
- Froude, W., 19, 36, 60
- Frozen, 48, 49, 362
- Frozen field operator, 48
- Frozen vector field, 47, 48
- Function, 405, 412
 - Bernoulli, 38
 - characteristic, 8, 119
 - cylinder, 150
 - Gamma, 77, 193, 406, 413, 415
 - Green, 181
 - probability, 208
- Functional, 150, 203, 207
 - characteristic, 4, 8, 12, 104, 119, 121, 123, 509
 - Gaussian, 153, 208, 612
 - space–time, 119, 141
 - spatial, 119
 - cylinder, 509
 - equation, 104
 - linear, 522, 532, 536
 - Minkowski, 307
 - pde, 115
- Functional differential equation (fde), 148
 - Lévy–Poisson, 116
- G
- Galerkin, 84
- Gateaux
 - derivative, 11, 103, 126, 399, 400
 - differentiable, 123
 - differential, 11, 126, 395, 398
- Gauss–Bonnet theorem, 308
- Gaussian, 8, 102, 108, 277
 - multivariate, 615

- Gauss, K.F., 43
- Geometry, 349
- Gradient
- deformation, 37, 40–43, 48
- Green
- function, 20, 128, 130, 131, 142, 376, 507
- Group, 22
- Lie, 20
- H**
- Hagen–Poiseuille, 345
- Haller, G., 310, 313, 684
- Harmonic
- solution, 129
- Heat, 63, 609
- equation, 3
- Heaviside, 180
- Helical, 334
- Helicity, 274
- density, 274
- Helmholtz, H., 36, 38, 392, 393
- Hermite
- function, 85, 160, 611, 613
 - polynomial, 85, 613
 - spectral method, 245, 661
- Hessian, 173
- functional, 120, 127, 145, 148, 172
 - pressure, 49, 50, 70, 71, 201, 579, 581, 583, 646, 647, 679
 - variational, 175
- Hierarchy
- LMN, 6, 179, 197
 - moment equations, 341, 342
- Hilbert space, 404, 428
- Hilbert vector space, 467
- Hill's vortex, 301, 322–324
- Hinze, J.O., 64
- Hölder exponent, 4, 369
- Homeomorphism, 125
- Hopf
- equation, 8, 104, 375, 395
 - fde, 124, 210
- Hopf–Cole, 3
- transformation, 160, 608
- Hopf, E., 9, 30, 119, 123, 125, 137–140
- Hull, 49
- Hyperoctant, 417
- Hypothesis, 68
- I**
- IC engine, 677
- Ideal gas, 21
- Image
- field, 209, 211, 222
- Incomplete, 42
- Incompressible, 6, 59
- Infinite, 7, 8, 57, 59, 79, 104–108, 110
- countably, 104, 208
 - sequence, 73
- Infinite limit
- Reynolds number, 359
- Initial-Boundary Value Problem (IBVP), 20, 33, 66, 93, 102, 187, 225, 320
- Initial Value Problem (IVP), 3, 4, 140, 160, 187, 215, 443, 562, 577, 580, 608
- Injective, 393
- Instability, 285, 677
- Integral
- functional, 109, 613
 - Wiener, 112
- Integration, 404, 428
- partial, 400
- Integro-differential equation, 142, 510, 537, 563
- Integro-differential pde, 8
- Interaction, 315
- Interface, 277
- Intermittency, 59, 277, 293
- external, 277
 - internal, 280
- Invariance, 41, 187, 334, 575
- material, 314
- Invariant, 49, 66, 139, 274, 278, 291, 295, 350
- inviscid, 673
 - topological, 308
- Inverse, 10, 23
- Invertible, 4, 25, 41, 102, 163, 489, 613, 615
- Inviscid, 62
- Irrotational, 58, 61
- Isotropic, 220
- Isotropy
- local, 68
- J**
- Jacobian, 40, 41, 402
- Jet, 80, 85, 549
- K**
- Karhunen–Loeve, 300
- Kepler, J., 67, 94
- Kernel, 115, 212, 238, 241, 270, 361, 388, 457
- Fourier, 270

Klauder, J.R., 57, 103, 121

Knudsen

number, 1

Kolmogorov

extension theorem, 106

scale, 68

Kolmogorov, A.N., 9, 68, 119, 285, 364

Kraichnan, 206

Kraichnan, R.H., 3, 8

Limit, 75, 344

Linear, 2–4

Lipschitz

continuity, 41, 367

Logarithm

natural, 57

Loop

closed, 314

Lumley, J.L., 8, 140, 442, 444

Lundgren, T.S., 6, 179, 197

L

L^2 , 207

Lagrange, J.-L., 10

Lamb

surface, 39

vector, 34, 37, 51, 61, 309, 310

Lamb–Gromeka, 38

Lamb vector

divergence, 39, 693

Laminar, 20, 66, 94, 315

Laminar flow, 2

Laplace, 59, 508, 517

operator, 131

transform, 312

Laplacian, 35, 49

cylindrical coordinates, 510

generalized, 116, 120

Lévy, 116

Large Eddy Simulation (LES), 361

compressible, 6

embedded RANS, 6

Lebesgue

integral, 405

Lebesgue, H.L., 111, 404, 406, 428, 429

integral, 405

measure, 95, 196

Length, 49, 65, 67

Leray, 29, 132, 510

axial momentum balance, 339, 538

azimuthal momentum balance, 339, 538

equation, 142

Navier–Stokes, 537, 538

radial momentum balance, 537

LES-RANS, 6

Lesieur, M., 274

Levi-Civita, 34, 42, 46, 362, 491

Lévy-Laplacian, 150, 394

Lewis–Kraichnan, 119, 141, 142

equation, 5, 8, 123, 141–143

Lie group, 23

Lie, S., 20, 22

Lifting, 225

M

Mach

number, 22, 56

Magneto-hydromechanics, 47

Mandelbrot, 59

Manifold, 98, 394, 402, 421, 684

invariant, 313

Mapping, 203, 204, 207, 241

bijective, 163, 205, 206, 443, 610, 613

injective, 205

linear, 205

local, 208

surjective, 205

Mapping approach, 8

Marusic, I., 307, 333

Mass, 208

flow rate, 538

fraction, 2

Master equation, 1

Materially invariant, 43

Material point, 40

Matrix

infinite-dimensional, 110

positive definite, 112

Mean free path, 1

Measure, 1, 42, 203

cylindrical, 105

derivative, 404

Gaussian, 9, 109, 203, 204, 209, 266,

429, 433

differential, 103

reference, 253, 266

Hausdorff, 63

probability, 203, 404

reference, 224

space, 341

turbulence, 4, 9

Wiener, 108, 109

zero, 1

Metric, 108

Millennium, 9

- Minkowski, 307
- Mixed boundary conditions, 519
- Mixing, 217
 - layer, 80, 85, 549
 - length, 548, 550, 551
 - model, 549
 - topological, 56
- Mode
 - radial
 - vector, 472
- Moin, P., 5
- Mollifier, 371, 699
- Moment, 8
 - hierarchy, 341
 - multipoint, 341
 - statistical, 6, 7, 124
- Momentum, 208
 - balance, 35
- Moser, R., 5, 541
- Multidimensional, 206
- Multi-index, 23, 116
- N**
- Navier Stokes
 - equations, 17, 20, 33, 55, 63, 67, 94, 209, 375
 - Fourier transformed, 270
 - incompressible
 - dimensionless, 360
 - material description, 41
- Newtonian fluid, 538
- Nickels, T.B., 554, 556
- Noncompact, 32, 75, 80, 82, 85, 96
- Non-integrability, 20
- Non-intermittent, 277
- Nonlinear, 2, 3
- Nonlinearity, 20, 101
- Non-locality, 20
- Norm, 400, 454, 509
 - L_p , 395, 432
 - Sobolev, 30, 387, 389
- Notation, 10
- Nuclear, 154, 375, 442, 612
- Nuclear space, 396
- Null space, 115, 147
- O**
- Oberlack, M., 26, 27
- Objective, 310
- Observer position, 18
- Onsager, L., 4, 68, 285, 364
- Operation
 - binary, 22
- Operator, 147
 - correlation, 153
 - expectation, 12, 103
 - Fourier, 10
 - linear, 399, 401
 - nuclear, 612
 - projection, 509
 - pseudo-differential, 391, 392
 - Stokes, 33, 392
 - trace class, 391, 615
- Orbit
 - heteroclinic, 684
 - homoclinic, 687
 - periodic, 57
- Ordinary differential equation (ode), 139
- Orientable, 94
- Orientation, 49
- Orthant, 417
- Ortho Normalized System (ONS), 85, 106, 270, 393, 396, 397, 613
 - basis, 448
 - solenoidal, 480
- Orthogonal, 140
- P**
- Parabolic fde, 116
- Parity, 77, 515
- Parity conditions, 75, 76, 78, 458
 - scalar, 458
 - vector, 468
- Partial differential equation (pde), 2
 - Euler, 20, 26
 - Navier–Stokes, 26
- Particles, 1
- Pathline, 443
- Peclet
 - number, 2
- Percolation, 346
- Periodicity, 514
- Perry, A.E., 301
- Phase space, 3, 20, 57, 66, 67, 73, 384
- Physical dimension, 10
- Piola
 - transform, 41, 45
- Piola–Kirchhoff stress tensor
 - first, 43, 44
- Pipe
 - semi-infinite, 80
- Pipe flow, 343
- Pipeline, 343
- Point

- accumulation, 389
 critical, 39
- Poisson, 132
 PoissP0, 128
- Polynomial
 Jacobi, 76, 83, 87, 89, 452, 454, 462, 464, 476, 477, 481
 transformed, 472
- Laguerre, 80
- Pope, S.B., 6, 42, 108, 179, 189, 203
- Positive, 40, 116, 124, 153
- Potential, 38, 59, 60, 696
- Prandtl, 373, 374, 541, 549, 551
 number, 2, 22, 185
- Pre-fractal, 66
- Preimage, 278
- Pressure, 55, 76, 82, 181
 basic, 536
 gradient, 556
 Green's function, 132, 507, 537
 harmonic, 132, 507, 537
- Probabilistic, 7
- Probability density function (Pdf), 6, 196, 203, 442
 conditioned, 189
 Gaussian, 109, 206
- Process
 stochastic, 124
- Product
 scalar, 454, 467, 509
- Product measure, 700
- Product space, 700
- Profile
 composite, 556
- Projection, 78, 106, 120
 Leray, 392
 operator, 96
- Proper Orthogonal Decomposition (POD), 76, 301
- Properties
 asymptotic, 66
- Pseudo-vector, 34
- Puff, 345, 346, 350
- Pullin, D.I., 307, 316
- Pure, 3, 21, 125, 160, 182, 186, 187, 189, 191, 193
- Push-forward, 102
- Q**
 QK flow, 67, 94
- R**
 Radius, 7, 75, 150, 151
- Radon–Nikodym
 derivative, 404
- Radon–Nykodym
 theorem, 403
- Random, 4, 8, 55
- Range, 55, 68, 74, 85, 115, 199
- RANS, 6
- Rate of strain, 4, 34
- Realization, 6
- Reflection, 295
- Regularity, 20, 29
 asymptotic, 32
 conditions, 524
- Relation
 constitutive, 18
 Gibbs, 61
 recursive, 112
 thermodynamic, 18, 21, 44
- Reynolds
 number, 2, 19, 20, 29, 32, 33, 36, 42, 55, 59, 61, 63, 66–68, 75, 280, 289, 292, 303, 309, 315, 336, 349, 359, 364, 373, 375, 508, 515, 547
 critical, 346
- Reynolds, O., 4, 5, 20, 322
- Riemann
 integral, 394
- Riemann, B., 406, 428, 429
 Darboux integral, 405
 integral, 429
 series theorem, 57
- Roshko
 number, 39
- Rotation, 17, 33, 44, 60, 295
- Roughness, 344
 height, 173, 373
- S**
 Scalar
 basis, 462
 field, 2, 76, 463, 469
 product, 11
- Scale, 17, 301
 length, 19
 velocity, 19
- Schmidt
 number, 2
- Second law, 21
- Self-adjoint, 433
- Semi-group, 33

- Sensitivity, 56, 59
Separable, 109, 391
Series
 conditionally convergent, 57
 harmonic
 alternating, 57
 Mercator, 57
 Taylor, 458, 485, 691, 692
Set
 absorbing, 105
 singular, 63
Sgs
 stress, 361
Shear, 374
 flow, 61, 285, 308
 layer, 85
 stress, 59, 373
Shift, 404
Shock
 wave, 47, 56, 309
Signature, 352
Simon, B., 121
Simple, 21
Singular, 9, 62
Singularity, 4, 49, 62, 63, 344, 371
 finite time, 322
 order, 62
 second order, 62, 369
 vorticity, 364
SI system, 10
Slug, 346, 350
Smits, A.J., 373, 374
Smooth
 boundary, 28
 field, 18
Smoothness, 9
 lack of, 371
 term, 379
Solenoidal, 29, 34, 35, 47, 49, 58, 76–79, 95, 96, 125, 128
Solution, 203
 complementary, 129, 517
 spatial
 statistical, 125
 strong, 29, 31, 32
 weak, 29, 30, 63, 361, 362, 371
Solvability, 101, 137, 341, 490
Sound, 22, 374
Space, 1, 203
 Banach, 57, 58, 73, 95, 108, 115, 387, 401, 402
 separable, 429
 dual, 105
 Euclidean, 73, 312, 382, 383, 390, 394
 infinite dimension, 428
 finite dimensional, 404
 Hilbert, 30, 58, 95, 387, 454, 470, 509
 separable, 74
 Hölder, 66, 389
 infinite dimensional, 428
 linear, 404
 locally convex, 402
 nuclear, 389
 Polish, 109
 Sobolev, 62, 95, 387, 389, 393, 400
Spalart, P.R., 29
Specific heat, 21
Spectral
 space, 269
Spectrum, 68, 287, 289, 292
 energy, 290
Sphere, 7, 290, 394, 395, 404, 428
Spin, 60
Squire–Long, 322
Stability, 5, 321, 346, 470
State
 asymptotic, 94, 344
Statistics
 Gaussian, 221
Streamfunction, 319, 320, 322, 674, 676
Streamlines, 320, 321, 328
Strong
 form, 43
Strouhal
 number, 40
Structure, 2–4, 42, 62, 68, 103, 115, 182, 196, 197, 199, 204, 251, 254, 258, 277, 315
 coherent, 307, 313
 hairpin, 307
 micro, 293
Sturm–Liouville, 110, 537
 ode, 110, 131, 513, 517, 518, 524
 operator, 110, 513, 514
Subcovering, 381
Subcritical, 346
 transition, 67
Subset, 1, 280
 dense, 74
Subsonic, 2
Subspace, 404
Substance, 21, 375
Summation convention, 402
Supersonic, 2
Support, 49, 84
 compact, 371

Surface, 48, 55, 120, 130

area, 7, 59

ball, 150

closed, 75

differential, 41, 43

orientable, 47, 185

parameter, 41

propagating, 310

Symbol, 74, 116

Symmetry, 22

T

Target space, 209

Taylor, G.I., 63

Taylor series, 307, 386, 403

Temperature, 2, 17, 21, 47, 55, 359, 374, 375

Theorem, 30, 31, 36, 43, 96, 106, 111, 121, 142, 144, 429

Beale–Kato–Majda, 62

binomial, 605

Bochner–Minlos, 104, 119, 121, 124, 206, 237

extension, 104, 107, 109

Gauss, 673

Green, 524

Helmholtz, 310

Kolmogorov, 104

Lie, 23

Picard–Lindelöf, 443

Riesz, 105

Threshold, 278

Time, 1, 7, 10, 18, 20, 30, 31, 33, 40–42, 65

derivative, 18

interval, 31, 32, 42, 62, 66, 140

reference, 40

turn-over, 302

Topological, 49, 56, 63, 75, 105

Topologically, 10

Topological space, 381

Torus, 74, 75

Trace, 140, 154, 612

class, 153, 433, 612

Traceless, 50, 141, 328, 646

Transfer

function, 288

Transform

wavelet, 269

Transformation, 3, 17, 22, 40, 41, 43, 44, 47

inverse, 45, 271

nonlinear, 2

Transition, 5, 64, 66, 277, 346

Triad interaction, 273

Trkal V., 35

Tsinober, A, 9, 307

Turbulence, 2, 4, 8, 17, 55, 58, 59, 63, 101

2-d, 31

definition, 65

homogeneous, 203, 295

isotropic, 295

isotropic, 161, 220

Turbulent, 1, 2, 4, 5, 20, 31, 33, 37, 50, 55,

58, 59, 200, 277, 278, 285, 315, 360,

362, 367, 372, 382, 541

combustion, 187

U

Uniqueness, 28, 29

Unit normal vector, 47

Unit vector, 402

Unstable, 39, 61, 198

Unsteady, 39, 55, 271

V

Variable, 1

probabilistic, 7

Vassilicos, J.C., 286

Vector

Beltrami, 35

field, 695

related to vorticity, 362

Trkalian, 35

flexion, 34, 37

Lamb, 38, 39

surface, 317

Trkalian, 35

Velocity, 18, 30, 34, 36, 40, 44, 47, 48, 58, 61

bulk, 75, 349

Cartesian, 78

gradient, 17, 49

initial, 31, 102

material, 40, 48

mean, 102, 103

norm, 31, 42

scale, 68

spatial, 40

wall shear, 349

Viscosity, 17, 19, 27, 59, 60

dynamic, 18

kinematic, 68, 75, 132

Viscous, 18, 59, 63, 68, 132, 285, 302, 321

Viscous term, 132, 272, 274, 363, 538

Visualization, 2

- Volume, 7, 10, 18, 29, 42, 59, 68, 75, 130, 132, 182, 279, 280, 309–312
ball, 120
flow rate, 19, 508
Von Karman, T., 63
Vortex, 62, 70, 313, 315
dipole, 322
filament, 374
line, 39
reconnection, 308, 322
ring, 307, 314, 315, 318, 362
turbulent, 315
sheet, 62
stretching, 39, 62, 63, 69, 364, 576
tube, 62, 319, 321
Vortical, 39, 58–60, 68, 308, 319, 364
Vorticity, 4, 17, 33–37, 44, 58, 60–62, 321, 328, 362, 470, 560
Beltrami, 44
equation, 62
material, 44, 45
divergence, 46
norm, 62
spatial, 33, 34, 45
- W**
Wake, 80, 85, 277, 549, 554
- Wall, 59, 75, 82, 307, 334
boundary, 68, 82, 102, 308
pipe, 132
shear velocity, 355, 546
smooth, 75
velocity, 59
Wall stress, 372, 522, 523
Wang, X., 149, 405, 413
Wave, 2, 220, 243, 313
Wavelet, 76, 269
Wavy, 315
Weak, 30, 32, 230, 322, 553
Weierstrass function, 369
Weierstrass, K., 369
Weight function, 76, 78, 81, 83, 452, 454, 459, 467, 476, 482, 487, 489, 509
Wray, A.A., 167, 307, 470, 472
- Z**
Zero, 1, 7, 24
Zone, 59, 684
flame, 47, 310, 313
non-turbulent, 277, 279
recirculation, 684
turbulent, 279